IEEE

IEEE Thailand Section

BTS IEEE BT Society Thailand Chapter













11th iCeast 2025

Phuket, Thailand

6- 9 May 2025

https://iceast.kmitl.ac.th/2025/

Conference Proceeding

FES

COMPANY PROFILE





General Instruments

PeakTech RIGOL



Fiber Optic, Fusion Splicer, Inspection, OTDR

DIMENSION GOUMAX FiberLabs Inc. LUNA



Power Supply, Battery, EV, Autonomouse Driving, Solar

DELTA ELEKTRONIKA ITECH



Prober

FORMFACTOR



RF, Antenna Test, 5G Test, Material Measurement

Anritsu envision : ensure



Microscope

MEIJI TECHNO

www.fesupply.com

www.peaktechthai.com I www.siammicroscope.com I www.siampowersupply.com

www.thaifiberstore.com I www.rigolthai.com I www.rfthailand.com



F.E.S. Co., Ltd.

1000/24, P.B. Tower, 8 floor, Sukhumvit 71 Rd.,
North Klongtan, Wattana, Bangkok 10110

Tel: +66(0)2-064-4050 or +66(0)2-064-4051

Fax: +66(0)2-010-4262 E-mail: info@fesupply.com

Line Official

Facebook

FES
www.fesupply.com | 02-064-4050

Products

ตัวแทนจำหน่ายอย่างเป็นทางการ พร้อมเซอร์วิสหลังการขายในประเทศไทย
Authorized Distributor and Services in Thailand

PeakTech

- Oscilloscopes
- Digital Multimeters
- Current clamp multimeters
- Thermal imaging cameras



RIGOL

- Digital Oscilloscopes
- Spectrum Analyzers
- DC-Power
- Waveform Generators
- Signal Generators
- DC-Power



DELTA ELEKTRONIKA
DC POWER SUPPLIES

- DC power supply
- RS232 Serial interface
- High-power system

DC POWER SUPPLIES.
150 W up to 900 kW



ITECH
YOUR POWER TESTING SOLUTION

- DC / AC Power Supply
- Source Measure Unit
- DC / AC Electronic Load
- Power Meter / Battery Tester



Anritsu

- Signal/Spectrum Analyzers
- OTDR, Optical Measuring
- RF Microwave Measuring
- Vector Network Analyzers



DIMENSION

- Optical Performance Testing
- Desktop Fiber Endface Inspector
- Fiber Endface Interferometer
- Fiber Endface Cleaning



FiberLabs Inc.

- Optical Fiber Amplifier
- Fluoride Fibers & Cables
- ASE Light Source
- Fiber output-SLD Light Source



GOUMAX TECHNOLOGY

- Tunable Lasers
- Portable OSA Modules
- Laser Scan Analyzer
- Tunable Optical Filters



FormFactor

- Probe Systems
- Cascade Probe
- Probe Cards



LUNA

- High-Definition Distributed Fiber Optic Sensing
- Optical Component Test
- Fiber Optic Network Test



SX SPANDNIX

- Spandnix is a semiconductor test equipment manufacturer.



MEIJI TECHNO

- Stereo Microscopes
- Asbestos Microscopes
- Gemological Microscopes
- Biological Microscope



SPS electronic
TRUE GERMAN QUALITY

- The all-in-one hipot safety analyser from SPS electronic.
- The surge tester from SPS electronic.



Table of Contents

Message from the President
Phuket Rajabhat University XXX

Message from Honorary Chairs XXXII

Message from General Chairs XXXIII

Message from Technical Program Chairs XXXV

Organizing Committee XXXVI

List of Reviewers XLII

Keynote Speakers XLV

Program at a Glance LIII

Technical Program LVII

Proceeding

Parallel power supply half-bridge topology with CV Mode 0-150 V and CC Mode 0-5A 2

Theerapat Antachai

Department of Electronics Engineering, School of Engineering King Mongkut's Institute of Technology Ladkrabang, Bangkok, Thailand.

Weera Pengchan

Department of Electronics Engineering, School of Engineering King Mongkut's Institute of Technology Ladkrabang, Bangkok, Thailand.

Supakorn Suwan

Department of Electronics Engineering, School of Engineering King Mongkut's Institute of Technology Ladkrabang, Bangkok, Thailand.

Partial Discharge Identification in High-Voltage Systems Using Frequency Extraction and Machine Learning Techniques 6

Tai Bandisak

Department of Electrical and Computer Engineering, Naresuan University Phitsanulok, Thailand

Krissana Romphuchaiyapruek

Department of Electrical and Computer Engineering, Naresuan University Phitsanulok, Thailand

Sarawut Wattanawongpitak

Department of Electrical and Computer Engineering, Naresuan University Phitsanulok, Thailand

Integration of Charcoal Kiln Waste Heat in a Thermal Water Pump System 10

Pakorn Promkaew

Department of Industrial Technology Phuket Rajabhat University, Phuket, Thailand.

Pathiwat Waramit

Department of Mechanical Engineering Rajamangala University of Technology Isan, Nakhon Ratchasima, Thailand.

Bundit Krittacom

Department of Mechanical Engineering Rajamangala University of Technology Isan, Nakhon Ratchasima, Thailand.

Jirawat Sitranon

Department of Energy Technology Management Rajamangala University of Technology Tawan-ok Chonburi, Thailand.

Panusak Moonsri

Department of Energy and Air Conditioning Engineering Rajamangala University of Technology Isan Nakhon Ratchasima, Thailand.

A Fuzzy Multi-Criteria Decision-Making Approach for Ranking Renewable Energy Systems Based on Economic and Environmental Aspects 16

Danupun Visuwan

Industrial Statistics and Operational Research Unit (ISO-RU), Department of Industrial Engineering, Faculty of Engineering, Thammasat School of Engineering, Thammasat University, Pathumthani, 12120 Thailand.

Atiwat Nanphang

Industrial Statistics and Operational Research Unit (ISO-RU), Department of Industrial Engineering, Faculty of Engineering, Thammasat School of Engineering, Thammasat University, Pathumthani, 12120 Thailand.

Pongchanun Luangpaiboon

Industrial Statistics and Operational Research Unit (ISO-RU), Department of Industrial Engineering, Faculty of Engineering, Thammasat School of Engineering, Thammasat University, Pathumthani, 12120 Thailand.

Apirak Tepvarin

Industrial Statistics and Operational Research Unit (ISO-RU), Department of Industrial Engineering, Faculty of Engineering, Thammasat School of Engineering, Thammasat University, Pathumthani, 12120 Thailand.

Mosquito Trap HV Power Supply Turn On/Off Time Parameter Consideration Measurement 21

Jirawath Parnklang

Department.of Electronics Engineering, School of Engineering King Mongkut'Institute of Technology, Ladkrabang Bangkok, Thailand.

Nattanicha Sowannee

Department.of Electronics Engineering, School of Engineering King Mongkut'Institute of Technology, Ladkrabang Bangkok, Thailand.

Kasamaphon Pakhunophat

Tx Engineer,TeraHop (Thailand) Co.,Ltd. 198, Moo 7, Nong Planoh sub-district, NongKhae district, Saraburi 18140 Bangkok, Thailand.

Siriwat Ganasut

Department.of Electronics Engineering, School of Engineering King Mongkut'Institute of Technology, Ladkrabang Bangkok, Thailand.

Pasuthida Wisitthikorn

Department.of Electronics Engineering, School of Engineering King Mongkut'Institute of Technology, Ladkrabang Bangkok, Thailand.

Tanutpong Ramkaow

Department.of Electronics Engineering, School of Engineering King Mongkut'Institute of Technology, Ladkrabang Bangkok, Thailand.

Interdigitated Extended Gate Field Effect Transistor for pH Sensor Based on Porous Silicon Layer 25

Narin Atiwongsangthong

Department of Electronics Engineering, School of Engineering King Mongkut's Institute of Technology Ladkrabang Bangkok, Thailand.

A Dual-Band Implantable Antenna with Flag-Inspired Patch and Grounded Structure 30

Rula Alrawashdeh

Electrical Engineering Department Mutah University Al-Karak, Jordan.

Real-Time Locating Systems: A bibliometric Analysis 34

Letizia Tebaldi

Department of Engineering for Industrial Systems and Technologies. Italy.

Andrea Volpi

Department of Engineering for Industrial Systems and Technologies. Italy.

Giulia Azzolini

Department of Engineering for Industrial Systems and Technologies. Italy.

A Flexible Loop Sensor Antenna for Ice and Frost Detection 38

Rula Alrawashdeh

Electrical Engineering Department Mutah University Al-Karak, Jordan

Numerical Study of 500 kHz Electromagnetic Wave Irradiation for Root Canal Sterilization in Apical Periodontitis Treatment 42

Yanakorn Srianant

KOSEN-KMITL, King Mongkut's Institute of Technology Ladkrabang, Thailand National Institute of Technology, Kagawa College, Japan.

Thanadol Tiengthong

Department of Electrical and Electronics Engineering, KOSEN-KMITL, King Mongkut's Institute of Technology Ladkrabang, Thailand.
Hiroo Tarao Department of Electrical and Computer Engineering, National Institute of Technology, Kagawa College, Japan

Masatake Akutagawa

Tokushima University Japan.

Hiromichi Yumoto

Tokushima University Japan.

Toshihiko Tominaga

Tominaga Dental Clinic, Japan.

Intelligent Multi-Link Selection for IEEE 802.11be Using Reinforcement Learning with Radiation Pattern Awareness 46

Bhurisub Dejpipatpracha

Department of Digital Technology Faculty of Science and Technology Phuket Rajabhat University Phuket, Thailand.

Akarachai Inthanil

Department of Digital Technology Faculty of Science and Technology Phuket Rajabhat University Phuket, Thailand.

Wimonnat Sukpol

Department of Mathematics Faculty of Science and Technology Phuket Rajabhat University Phuket, Thailand.

Worrarat Jongkraijak

Department of Business Computer Faculty of Management Sciences Phuket Rajabhat University Phuket, Thailand.

Modeling the Performance of Wi-Fi Networks Using 5GHz, 6GHz, and Multi-Link Operation 50

Wimonnat Sukpol

Department of Mathematics Faculty of Science and Technology Phuket Rajabhat University Phuket, Thailand.

Akarachai Inthanil

Department of Digital Technology Faculty of Science and Technology Phuket Rajabhat University Phuket, Thailand.

Bhurisub Dejpipatpracha

Department of Digital Technology Faculty of Science and Technology Phuket Rajabhat University Phuket, Thailand.

Accuracy Analysis of Indoor Positioning Using Min-Max Method 54

Pichaya Supanakoon

Department of Telecommunications Engineering School of Engineering King Mongkut's Institue of Technology Ladkrabang Bangkok 10520, Thailand.

Wipassorn Vinicchayakul

Establishment office for Aeronautical and Space Training Center U-Tapao Civil Aviation Training Center Bangkok 10900, Thailand.

Sirinya Tabsombat

Establishment office for Aeronautical and Space Training Center U-Tapao Civil Aviation Training Center Bangkok 10900, Thailand.

Thanadol Tiengthong

Department of Electrical and Electronic Engineering KOSEN-KMITL King Mongkut's Institute of Technology Ladkrabang Bangkok 10520, Thailand.

Sathaporn Promwong

Department of Telecommunications Engineering School of Engineering King Mongkut's Institute of Technology Ladkrabang Bangkok 10520, Thailand.

Monchai Chamchoy

Department of Telecommunications Engineering School of Engineering King Mongkut's Institute of Technology Ladkrabang Bangkok 10520, Thailand.

Applying Generative AI for Fraud and Cybercrime Prevention in Thailand 59

Chairat Thanomwong

Electrical Engineering Rajamangala University of Technology Phra Nakhon Bangkok, Thailand.

Korn Puangnak

Computer Engineering Rajamangala University of Technology Phra Nakhon Bangkok, Thailand.

Natworapol Rachsiriwatcharabul

Industrial Technology Program in Sustainable Innovation Engineering Technology Rajamangala University of Technology Phra Nakhon Bangkok, Thailand.

Manthana Tiawongsuwan

Computer Engineering Rajamangala University of Technology Phra Nakhon Bangkok, Thailand.

Krerk Puangnak

Computer Engineering Rajamangala University of Technology Phra Nakhon Bangkok, Thailand.

A Comparative Analysis of Machine Learning Algorithms for Allergy Scale Prediction 63

Aumnat Tongkaw

Faculty of Science and Technology Songkhla Rajabhat University Songkhla, Thailand.

Sasalak Tongkaw

Faculty of Science and Technology Songkhla Rajabhat University Songkhla, Thailand.

Sustainable Waste Management: Enhancing Efficiency with Vehicle Routing Optimization Techniques 67

Nichaphat Phurichteerarat

Department of Mathematics and Statistics, Faculty of Science and Technology, Thammasat University Pathumthani, 12120 Thailand.

Auksarapuk E-dee

Department of Mathematics and Statistics, Faculty of Science and Technology, Thammasat University Pathumthani, 12120 Thailand.

Anuwat Boonmechot

Department of Mathematics and Statistics, Faculty of Science and Technology, Thammasat University Pathumthani, 12120 Thailand.

Thapanita Thongpap

Department of Mathematics and Statistics, Faculty of Science and Technology, Thammasat University Pathumthani, 12120 Thailand.

Lakkana Ruekkasaem

Department of Mathematics and Statistics, Faculty of Science and Technology, Thammasat University Pathumthani, 12120 Thailand.

Pongchanun Luangpaiboon

Industrial Statistics and Operational Research Unit (ISO-RU), Department of Industrial Engineering, Faculty of Engineering, Thammasat School of Engineering, Thammasat University Pathumthani, 12120 Thailand.

Explainable AI to enhance demand forecasting model for autonomous taxis in smart cities 71

Adeel Munawar

Sirindhorn International Institute of Technology, Thammasat University, Pathum Thani, Thailand.

Mongkut Piantanakulchai

Sirindhorn International Institute of Technology, Thammasat University, Pathum Thani, Thailand.

Blockchain As A Notarization System For Military Data Sharing 75

Chatchawan Chamnikul

Department of Defence Engineering School of Engineering, King Mongkut's Institute of Technology Ladkrabang, Bangkok, Thailand.

Amnach Khawne

Department of Computer Engineering School of Engineering, King Mongkut's Institute of Technology Ladkrabang, Bangkok, Thailand.

Application of Deep Learning Techniques for Predicting Leaf Lesions in KDML105 Rice Variety 79

Sittisak Promtara

Faculty of Information Technology, King Mongkut's University of Technology Thonburi.

Watanyoo Suksa-ngiam

Faculty of Information Technology, King Mongkut's University of Technology Thonburi.

Pornchai Mongkolnam

Faculty of Information Technology, King Mongkut's University of Technology Thonburi.

Comparative Analysis of Common Compression Algorithms for Sentinel-2 Multispectral Band Compression 84

Aljaz Zel

Faculty of Electrical Engineering and Computer Science, University of Maribor.

Domen Mongus

Faculty of Electrical Engineering and Computer Science, University of Maribor.

Borut Zalik

Faculty of Electrical Engineering and Computer Science, University of Maribor.

Image Processing Threshold of Acetabulum Porosity for Age Estimation 88

Supachard Krudtong

Biomedical Engineering Institute Chiang Mai University Chiang Mai, Thailand.

Pasuk Mahakkanukrauh

Department of Anatomy Faculty of Medicine Chiang Mai University Chiang Mai, Thailand.

Nipon Theera-Umpon

Biomedical Engineering Institute Chiang Mai University Chiang Mai, Thailand.

Recognition of Marijuana Plant Leaf Diseases Based on Deep Learning 92

Qingye Kong

Department of Telecommunications Engineering, School of Engineering, King Mongkut's Institute of Technology Ladkrabang Bangkok, Thailand

Siraphop Tooprakai

Department of Telecommunications Engineering, School of Engineering, King Mongkut's Institute of Technology Ladkrabang Bangkok, Thailand.

Advanced Car Rental System: Integrating Blockchain, AI, and Real-Time Inventory Management for Enhanced User Experience 96

Sokyna Alqatawnah

School of Computing Department of Health Sciences, Meditech and Technology Bradford College Bradford, UK.

Muhammad Tayyib

School of Computing Department of Health Sciences, Meditech and Technology Bradford College Bradford, UK.

Indoor Object Detection for Autonomous Mobile Robots (AMRs) Using YOLOv5s and Grad-CAM 99

Nafiz Fahad

Faculty of Information Science and Technology (FIST) Multimedia University Jalan Ayer Keroh Lama 75450, Bukit Beruang, Melaka, Malaysia.

Md Jakir Hossen

Faculty of Engineering and Technology (FET) Multimedia University Jalan Ayer Keroh Lama 75450, Bukit Beruang, Melaka, Malaysia.

Md Shohel Sayeed

Faculty of Information Science and Technology (FIST) Multimedia University Jalan Ayer Keroh Lama 75450, Bukit Beruang, Melaka, Malaysia.

"Sell in May & Go Away" [for 6 Months] Versus Other 6-Month Intervals – the Philippine Stock Exchange Index (PSEi) 105

Jackylyn L. Beredo

College of Computer Studies, De La Salle University, Manila, The Philippines.

Kainam Thomas Wong

College of Computer Studies, De La Salle University, Manila, The Philippines.

Jonathan Paul Cempron

College of Computer Studies, De La Salle University, Manila, The Philippines.

Joel P. Ilao

College of Computer Studies, De La Salle University, Manila, The Philippines.

Improving Children's Reading And Writing Abilities By Utilizing Augmented Reality 108

Suzanna

Information Systems Department, Binus Online Learning Bina Nusantara University Jakarta, Indonesia.

Harco Leslie Hendric Spits Warnars

Computer Science Department, BINUS Graduate Program, Doctor of Computer Science, Bina Nusantara University Jakarta, Indonesia.

Mahaning Indrawaty Wijaya

Information System Departement, Bina Nusantara University Jakarta, Indonesia.

Diana

Information System Departement, Bina Nusantara University Jakarta, Indonesia.

Optimizing Traffic Flow and System Efficiency in Networks Through AI-Driven Management 113

Sudhakar Kumar

Chandigarh College of Engineering and Technology, Chandigarh, India.

Sunil K. Singh

Chandigarh College of Engineering and Technology, Chandigarh, India.

Janvi Sharma

Chandigarh College of Engineering and Technology, Chandigarh, India.

Rima Kumari

Chandigarh College of Engineering and Technology, Chandigarh, India.

Priyanka Chaurasia

Chandigarh College of Engineering and Technology, Chandigarh, India.

Kwok Tai Chui

Chandigarh College of Engineering and Technology, Chandigarh, India.

Brij B. Gupta

Chandigarh College of Engineering and Technology, Chandigarh, India.

Attention Thresholds for Brand Impact 117

John Hawkins

GumGum, Sydney, Australia Shannon Bosshard Neuroconsulting, Sydney, Australia

Enigme: Generative Text Puzzles for Evaluating Reasoning in Language Models 122

John Hawkins

Centre for Artificial Intelligence and Innovation Pingla Institute, Sydney, Australia

An Ensemble model of Dual learning for Gambling and Pornographic Websites Classification 127

Sirapat Thianphan

School of Engineering, King Mongkut's Institute of Technology Ladkrabang, Bangkok, Thailand.

Kietikul Jearanaitanakij

School of Engineering, King Mongkut's Institute of Technology Ladkrabang, Bangkok, Thailand.

Quality classification of sunglasses lens by deep learning 131

Charin Theskham

Department of Computer Engineering, School of Engineering King Mongkut's Institute of Technology Ladkrabang, Bangkok.

Kietikul Jearanaitanakij

Department of Computer Engineering, School of Engineering King Mongkut's Institute of Technology Ladkrabang, Bangkok.

A Hybrid Greedy Algorithm for the Capacitated Vehicle Routing Problem 135

Udom Janjarassuk

Department of Industrial Engineering, School of Engineering King Mongkut's Institute of Technology Ladkrabang Bangkok, Thailand.

A study on developing a robust screen navigation pattern for SwiftUI based iOS Applications 139

Shubham Kamdi

Independent Researcher Mountain View, United States.

Enhancing a Creative Support Tool with the TRIZ Method: A Textile Design Prototype Utilizing Projection Mapping 141

Chanathinat Chaiyapoo

Creative Product Innovation, Faculty of Science and Technology, Phuket Rajabhat University Phuket, Thailand.

Jakraphan Chaopreecha

Digital Media Design, Computing, College of Computing, Prince of Songkla University Phuket, Thailand.

Chutima Changpum

Creative Product Innovation, Faculty of Science and Technology, Phuket Rajabhat University Phuket, Thailand.

Nicha Tovankasame

Department of Asian Studies Faculty of International Studie, Prince of Songkla University Phuket, Thailand.

Development of adventure games and puzzle solving in mysterious museums 148

Kriangkrai Phutongkan

Department of Digital Technology Faculty of Science and Technology Phuket Rajabhat University Phuket, Thailand.

Akarachai Inthanil

Department of Digital Technology Faculty of Science and Technology Phuket Rajabhat University Phuket, Thailand.

Attapon Pillai

Department of Digital Technology Faculty of Science and Technology Phuket Rajabhat University Phuket, Thailand.

Fine-Tuning AI Models with Limited Resources 152

Kritsada Singhapoo

Department of Digital Technology Faculty of Science and Technology Phuket Rajabhat University Phuket, Thailand.

Akarachai Inthanil

Department of Digital Technology Faculty of Science and Technology Phuket Rajabhat University Phuket, Thailand.

Attapon Pillai

Department of Digital Technology Faculty of Science and Technology Phuket Rajabhat University Phuket, Thailand.

Machine Learning-Based Framework for Early and Age-Inclusive Detection of Autism Spectrum Disorder Using U.S. Screening Data 156

Mohammad Anisur Rahman

Department of Marketing & Business Analytics East Texas A&M University, 2104 University Dr, Commerce, TX 75428, USA

Intiser Islam

School of Engineering, University of Bridgeport, 126 Park Ave, Bridgeport, CT 06604, USA

Shariar Islam Saimon

School of Engineering, University of Bridgeport, 126 Park Ave, Bridgeport, CT 06604, USA

Md Rafiuddin Siddiky

College of Technology Wilmington University, New Castle, Delaware, USA

Md Mahadi Hasan

School of Information Technology, Washington University of Science and Technology, Alexandria, Virginia, USA

Hasan Mahmud Sozib

Department of Electrical and Electronic Engineering Ahsanullah University of Science and Technology, 141 & 142, Love Road, Tejgaon, Dhaka, 1208, Bangladesh

Romana Nourin Nipa

Department of Information and Communication Technology Islamic University, Kushtia-7003, Bangladesh

Md. Jahid Hassan

Department of Information and Communication Technology Islamic University, Kushtia -7003 Bangladesh

Seaam Bin Masud

College of Technology Wilmington University, New Castle, Delaware, USA

Optimizing Detection of Human Cancer Cells in Breast Cancer via Machine Learning and Feature Selection 160

Inshad Rahman Noman

Department of Computer Science, California State University, 5151 State University Dr, Los Angeles, CA 90032, United States.

Md Rashedul Islam

Department of Business Administration Westcliff University, 17877 Von Karman Ave 4th Floor, Irvine, CA 92614, United States.

Kanchon Kumar Bishnu

Department of Computer Science, California State University, 5151 State University Dr, Los Angeles, CA 90032, United States.

Araf Islam

Department of Information Technology, Westcliff University, 17877 Von Karman Ave 4th Floor, Irvine, CA 92614, United States.

Afia Fairooz Tasnim

Department of Science Public Health, California State University Long Beach1250 Bellflower Blvd, Long Beach, CA 90840, United States.

Md Munna Aziz

Department of Business Administration, Westcliff University, 17877 Von Karman Ave 4th Floor, Irvine, CA 92614, United States.

Rakibul Hasan

Department of Business Administration Westcliff University, 17877 Von Karman Ave 4th Floor, Irvine, CA 92614, United States.

Efficient American Sign Language Recognition using ResNet-50 164

Md Sharifuzzaman

Information Studies Trine University Indiana, USA.

Anik Sen

Faculty of Information Science & Technology Multimedia University Melaka, Malaysia.

Joyashish Ghosh

Faculty of Science & Engineering Jashore University of Science and Technology Jessore, Bangladesh.

Tze Hui Liew

Faculty of Information Science & Technology Multimedia University Melaka, Malaysia.

Debanjon Dutta Purkaystha

Faculty of Engineering American International University-Bangladesh Dhaka, Bangladesh.

Saptanil Ghose

Faculty of Science & Technology American International University-Bangladesh Dhaka, Bangladesh.

Masud Pervez

Faculty of Mathematical & Physical Sciences Jahangirnagar University Dhaka, Bangladesh.

Md Jakir Hossen

Faculty of Engineering Technology Multimedia University Melaka, Malaysia.

Predicting Faulty Production Lines Causing Head Gimbal Assembly Damage from Electrostatic Discharge Using Machine Learning 171

Nuttanon Bilgasun

Department of Artificial Intelligence for Business Analytics Faculty of Information Technology, King Mongkut's Institute of Technology Ladkrabang Bangkok, Thailand.

Bundit Thanasopon

Department of Artificial Intelligence for Business Analytics Faculty of Information Technology, King Mongkut's Institute of Technology Ladkrabang Bangkok, Thailand.

Using the Analytic Hierarchy Process (AHP) for Decision Making in Tourism Product Distribution Channel 175

Klinsukon Nimkanjana

Department of Information Technology Rajamangala University of Technology Srivijaya Nakhon si thammarat, Thailand.

Kornsirinut Rothjanawan

Department of Computer Engineering Princess of Naradhiwas University Narathiwat, Thailand.

Development an Ontology Knowledge Base for Biodiversity, Identify plants of Community forest: A Case study of Baan Wang sai Community 179

Klinsukon Nimkanjana

Department of Information Technology Rajamangala University of Technology Srivijaya Nakhon si thammarat, Thailand.

Premjit Ruengsawat

Department of Bioproduct Technology Rajamangala University of Technology Srivijaya Nakhon si thammarat, Thailand.

Sarit Panjan

Department of Information Technology Rajamangala University of Technology Srivijaya Nakhon si thammarat, Thailand.

TabFuseNet: A Cancer Prediction Model Utilizing Sample Cohort Data 183

ChaeYoon Han

Department of MetaBioHealth, Sungkyunkwan University, Suwon, South Korea.

NangKyeong Lee

Department of Precision Medicine, Sungkyunkwan University School of Medicine, Suwon, South Korea.

Jun Kim

Department of MetaBioHealth, Sungkyunkwan University, Suwon, South Korea.

Muhammad Afzal

College of Computing, Birmingham City University, England.

Zeeshan Abbas

Department of Precision Medicine Sungkyunkwan University School of Medicine, Suwon, South Korea.

SeungWon Lee

Department of Precision Medicine Sungkyunkwan University School of Medicine, Suwon, South Korea.

Implemented Machine Learning Models to Predict Life Satisfaction Using Demographic and Religious Data 187

Aryan Shah

William P. Clements High School, United States.

Anshul Mago

William P. Clements High School, United States.

Shreyan Shah

William P. Clements High School, United States.

Michelle A. Patriquin

William P. Clements High School, United States.

Integrating Machine Learning For Automated Root Cause Analysis Of Critical-To-Quality (CTQ) In Hard Disk Drive Manufacturing 191

Mullika Inpang

Department of Artificial Intelligence for Business Analytics Faculty of Information Technology King Mongkut's Institute of Technology Ladkrabang Bangkok Thailand.

Bundit Thanasopon

Department of Artificial Intelligence for Business Analytics Faculty of Information Technology King Mongkut's Institute of Technology Ladkrabang Bangkok Thailand.

Automated Assembly Machine Stopping System Using Machine Learning for Electrical Failure Prediction in Hard Disk Drive Manufacturing 195

Tanakrit Panjasamanwong

School of Information Technology King's Mongkut Institute of Technology Ladkrabang Bangkok, Thailand.

Bundit Thanasopon

School of Information Technology King's Mongkut Institute of Technology Ladkrabang Bangkok, Thailand.

AI-enhanced Cyber Threat Detection: Transforming Security Frameworks in Management Information Systems 199

Niropam Das

Department of Business Administration International American University 3440 Wilshire Blvd STE 1000, Los Angeles, CA 90010, United States.

Jahid Hassan

Department of Business Administration International American University 3440 Wilshire Blvd STE 1000, Los Angeles, CA 90010, United States.

Partha Chakraborty

Department of Business Administration International American University 3440 Wilshire Blvd STE 1000, Los Angeles, CA 90010, United States.

Jobanpreet kaur

Department of Technology & Engineering Westcliff University 17877 Von Karman Ave 4th floor, Irvine, CA 92614, United States.

Syed Nazmul Hasan

Department of Technology & Engineering Westcliff University 17877 Von Karman Ave 4th floor, Irvine, CA 92614, United States.

Mohammad Abdul Goffer

Department of Business Administration International American University 3440 Wilshire Blvd STE 1000, Los Angeles, CA 90010, United States.

Kazi Bushra Siddiqa

Department of Business Administration International American University 3440 Wilshire Blvd STE 1000, Los Angeles, CA 90010, United States.

Rakibul Hasan

Department of Business Administration Westcliff University 17877 Von Karman Ave 4th Floor, Irvine, CA 92614, United States.

Some Practical Aspects of the Relational Database Normalization Process 203

Putsadee Pornphol

Department of Digital Technology Faculty of Science and Technology Phuket Rajabhat University Phuket, Thailand.

Suphamit Chittayasothorn

School of Engineering King Mongkut's Institute of Technology Ladkrabang Bangkok, Thaialnd.

Fin Coil Dent Detection Using Deep Learning 208

Akapot Tantrapiwat

Department of Mechanical Engineering School of Engineering, King Mongkut's Institute of Technology Ladkrabang Bangkok, Thailand

Unnat Pinsopon

Department of Mechanical Engineering School of Engineering, King Mongkut's Institute of Technology Ladkrabang Bangkok, Thailand

A Design and Experimental Study of Fog Spraying into the Greenhouse Roof for Radiation and Relative Humidity Control 213

Sakapan Klaydokjan

King Mongkut's Institute of Technology Ladkrabang, Prince of Chumphon Campus.

Nathaporn Suwanpayak

King Mongkut's Institute of Technology Ladkrabang, Prince of Chumphon Campus.

Kamonwan Chucheep

King Mongkut's Institute of Technology Ladkrabang, Prince of Chumphon Campus.

Development of a Real-Time Water Monitoring and Alert System for Sustainable Aquaculture in the Tapi River 217

Prasert Nonthakarn

Faculty of Science and Technology Rajamangala University of Technology Srivijaya Nakhon Si Thammarat, Thailand.

Sulaiman Madyod

Faculty of Veterinary Science Rajamangala University of Technology Srivijaya Nakhon Si Thammarat, Thailand.

Chariya Nonthakarn

Faculty of Science and TechnologyRajamangala University of Technology Srivijaya Nakhon Si Thammarat, Thailand.

Machine Learning Approach to CMYK Label Identification through Screen Angles 222

Chitsanuwit Ar-Karachaiphong

School of Engineering King Mongkut's Institute of Technology Ladkrabang Bangkok, Thailand

Farzin Asadi

Department of Computer Engineering Ostim Technical University Ankara, Turkiye

Asst. Prof. Dr. Krit Smerpitak

School of Engineering King Mongkut's Institute of Technology Ladkrabang Bangkok, Thailand

Compensation Motion and Calibration for Scale Calibration Machine 228

Siriwat Kitsompong

National Institute of Metrology (Thailand) Pathumthani, Thailand.

Yuttana Hongaromkij

National Institute of Metrology (Thailand) Pathumthani, Thailand.

Linear Interpolation using Siemens S7-1200Fine-Tuning AI Models with Limited Resources 232

Noppadol Maneerat

School of Engineering Department of Instrumentation and Control Engineering King Mongkut's Institute of Technology Ladkrabang Bangkok 10520 ,Thailand.

Tharathorn Wongworrada

School of Engineering Department of Instrumentation and Control Engineering King Mongkut's Institute of Technology Ladkrabang Bangkok 10520 ,Thailand.

Thepjit Cheypoca

School of Engineering Department of Instrumentation and Control Engineering King Mongkut's Institute of Technology Ladkrabang Bangkok 10520 ,Thailand.

Apply PLC to Control 3-Axis Machines 236

Thepjit Cheypoca

School of Engineering Department of Instrumentation and Control Engineering King Mongkut's Institute of Technology Ladkrabang Bangkok 10520 ,Thailand.

In Thaiyai

School of Engineering Department of Instrumentation and Control Engineering King Mongkut's Institute of Technology Ladkrabang Bangkok 10520 ,Thailand.

Noppadol Maneerat

School of Engineering Department of Instrumentation and Control Engineering King Mongkut's Institute of Technology Ladkrabang Bangkok 10520 ,Thailand.

Real-Time Production Monitoring System: An IoT and Open-Source Solution for SMEs 240

Manisra Baramechai

School of Engineering, The University of the Thai Chamber of Commerce Bangkok, Thailand.

Vorrapath Kokaew

School of Engineering, The University of the Thai Chamber of Commerce Bangkok, Thailand.

Application of 3D printer to create a splint pet cast 244

Pipat Phaisalpanumas

Faculty of Engineering King Mongkut's University of Technology North Bangkok Bangkok, Thailand.

Acting Sub Lt. Nattasit Monkaew

Faculty of Engineering King Mongkut's University of Technology North Bangkok Bangkok, Thailand.

Damisara Chutikan

Faculty of Engineering King Mongkut's University of Technology North Bangkok Bangkok, Thailand.

Premporn Khemavuk

Faculty of Engineering King Mongkut's University of Technology North Bangkok Bangkok, Thailand.

Narin Tammarugwattana

School of Engineering King Mongkut's Institute of Technology Ladkrabang Bangkok, Thailand.

Sirichai Tammaruckwattana

School of Engineering King Mongkut's Institute of Technology Ladkrabang Bangkok, Thailand.

Prototype of Chipping and Briquetting Machine for Eucalyptus Wood Processing 248

Pipat Phaisalpanumas

Faculty of Engineering King Mongkut's University of Technology North Bangkok Bangkok, Thailand.

Nattarat Namboot

Faculty of Engineering King Mongkut's University of Technology North Bangkok Bangkok, Thailand.

Damisara Chutikan

Faculty of Engineering King Mongkut's University of Technology North Bangkok Bangkok, Thailand.

Chartchai Usadornsak

Faculty of Engineering King Mongkut's University of Technology North Bangkok Bangkok, Thailand.

Naritsak Tantitippawan

Faculty of Engineering King Mongkut's University of Technology North Bangkok Bangkok, Thailand.

Sirichai Tammaruckwattana

School of Engineering King Mongkut's Institute of Technology Ladkrabang Bangkok, Thailand.

Re-envisioning On-Ground Aircraft Movement using Reinforcement Learning 252

Anurag Vallur

Department of Electronics and Communications Engineering, PES University Bengaluru, 560085, Karnataka, India.

Anuj Jain

Department of Electronics and Communications Engineering, PES University Bengaluru, 560085, Karnataka, India.

Anirudh Sridhar

Department of Electronics and Communications Engineering, PES University Bengaluru, 560085, Karnataka, India.

Adi M.

Department of Electronics and Communications Engineering, PES University Bengaluru, 560085, Karnataka, India.

T.S. Chandar

Department of Electronics and Communications Engineering, PES University Bengaluru, 560085, Karnataka, India.

Energy-Efficient Motion Planning for Dual-Arm Collaborative Robots Using a Digital Twin 256

Ruj Kantabussabong

The Sirindhorn International ThaiGerman Graduate School of Engineering, King Mongkut's University of North Bangkok, Bangkok, Thailand.

Chinnawut Nantabut

The Sirindhorn International ThaiGerman Graduate School of Engineering, King Mongkut's University of North Bangkok, Bangkok, Thailand.

Damisara Chutikan

Faculty of Engineering King Mongkut's University of Technology North Bangkok Bangkok, Thailand.

Chartchai Usadornsak

The Sirindhorn International ThaiGerman Graduate School of Engineering, King Mongkut's University of North Bangkok, Bangkok, Thailand.

Watcharin Pongaen

Dept. of Teacher Training in Mechanical Engineering, Faculty of Technical Education, King Mongkut's University of North Bangkok, Bangkok, Thailand.

Nuttapon Rothong

College of Industrial Technology, King Mongkut's University of North Bangkok, Bangkok, Thailand.

Borihan Butsanlee

Dept. of Teacher Training in Mechanical Engineering, Faculty of Technical Education, King Mongkut's University of North Bangkok, Bangkok, Thailand.

Effective Bowel Sound Source Localization Based on Sensor Configuration: A Preliminary Index Approach 260

Kenji Takawaki

Division of Science and Technology, Graduate School of Science and Technology for Innovation, Tokushima University, Tokushima 770-8506, Japan.

Takeyuki Haraguchi

Division of Science and Technology for Innovatioin, Graduate School of Sciences and Technology for Innovation, Tokushima University, Tokushima 770-8506, Japan.

Takahiro Emoto

Division of Science and Technology, Graduate School of Technology, Industrial and Social Sciences, Tokushima University, Tokushima 770-8506, Japan.

Design and Development of a Portable Static Stability Training System 264

Manutchanok Jongprasithporn

Department of Industrial Engineering, School of Engineering, King Mongkut's Institute of Technology Ladkrabang, Bangkok, Thailand.

Nantakrit Yodpijit

CIHFE2, Department of Industrial Engineering, Faculty of Engineering, King Mongkut's University of Technology North Bangkok, Thailand.

Improving Accuracy in Image-Recognition Systems With Techniques for Handling Similar-Looking Items in Inventory Management 268

Asst. Prof. Dr. Krit Samerpitak

School of Engineering King Mongkut's Institute of Technology Ladkrabang Bangkok, Thailand

Asst. Prof. Sart Kummool

School of Engineering King Mongkut's Institute of Technology Ladkrabang Bangkok, Thailand

Asst. Prof. Dr. Farzin Asadi

Department of Computer Engineering Ostim Technical University Ankara Turkiye

Chitsanuwit Ar-Karachaiphong

School of Engineering King Mongkut's Institute of Technology Ladkrabang Bangkok, Thailand

Watcharapon Sopha

School of Engineering King Mongkut's Institute of Technology Ladkrabang Bangkok, Thailand

Assoc. Prof. Dr. Sawai Pongswatd

School of Engineering King Mongkut's Institute of Technology Ladkrabang Bangkok, Thailand

The Trapezoidal Khim: Sound Radiation of G Notes 273

Natcha Techaaphonchai

Institute of Music, Science, and Engineering King Mongkut's Institute of Technology Ladkrabang Bangkok, Thailand.

Worakrit Thida

Institute of Music, Science, and Engineering King Mongkut's Institute of Technology Ladkrabang Bangkok, Thailand.

Kittipitch Meesawat

Institute of Music, Science, and Engineering King Mongkut's Institute of Technology Ladkrabang Bangkok, Thailand.

Phonlasit Thinnakorn Na Ayuthaya

Institute of Music, Science, and Engineering King Mongkut's Institute of Technology Ladkrabang Bangkok, Thailand.

Pakaphol Chitsakul

Institute of Music, Science, and Engineering King Mongkut's Institute of Technology Ladkrabang Bangkok, Thailand.

Sorasak Danworaphong

Institute of Music, Science, and Engineering King Mongkut's Institute of Technology Ladkrabang Bangkok, Thailand.

Efficient Modeling of ITD Based on Anthropometrics and KEMAR ITD coefficients using Deep Neural Networks 277

Saif S. Alotaibi

Department of Electrical and Computer Engineering University of Colorado Colorado Springs Colorado Springs, Colorado 80918.

Mark Wickert

Department of Electrical and Computer Engineering University of Colorado Colorado Springs Colorado Springs, Colorado 80918.

Phonlasit Thinnakorn Na Ayuthaya

Vibroacoustic Study of Tonewood and Solid-body Guitar 282

Khemapat Tontiwattanakul

Sound and Vibration Engineering Research Group, Department of Mechanical and Aerospace Engineering, Faculty of Engineering, King Mongkut's University of Technology North Bangkok Bangkok, Thailand.

Design and build of a multi-zone beamforming speaker 286

Khemapat Tontiwattanakul

Sound and Vibration Engineering Research Group, Department of Mechanical and Aerospace Engineering King Mongkut's University of Technology North Bangkok
Bangkok, Thailand.

Jiraphat Sueprasert

Institute of Music, Science and Engineering King Mongkut's Institute of Technology Ladkrabang Bangkok, Thailand.

Dech Nawik

Institute of Music, Science and Engineering King Mongkut's Institute of Technology Ladkrabang Bangkok, Thailand.

Pitak Thumwarin

Institute of Music, Science and Engineering King Mongkut's Institute of Technology Ladkrabang Bangkok, Thailand.

Nachanant Chitanont

Institute of Music, Science and Engineering King Mongkut's Institute of Technology Ladkrabang Bangkok, Thailand.

Development and Preliminary Evaluation of a Wireless Acoustic Sensor Network for Environmental Noise Monitoring 291

Kittipitch Meesawat

Institute of Music Science and Engineering King Mongkut's Institute of Technology Ladkrabang Bangkok, Thailand.

Wanut Padee

Office of Digital Technology Khon Kaen University Khon Kaen, Thailand.

Worakrit Thida

Independent researcher Bangkok, Thailand.

Krittika Lertsawat

ENLAWTHAI Foundation Bangkok, Thailand.

Sorasak Danworaphong

Institute of Music Science and Engineering King Mongkut's Institute of Technology Ladkrabang Bangkok, Thailand.

การสร้างไบโอฟิล์มและรูปแบบความไวต่อยาปฏิชีวนะของ Vibrio parahaemolyticus ที่แยกได้จากอาหารทะเล 269

Biofilm Formation and Antibiogram Profiles of Vibrio parahaemolyticus Isolates from Seafood

Muhammadfitree Ding

Medical and Industrial Microbiology Program, Faculty of Science Technology and Agriculture, Yala Rajabhat University,Yala, Thailand.

Fathiyah Wamaeng

Medical and Industrial Microbiology Program, Faculty of Science Technology and Agriculture, Yala Rajabhat University,Yala, Thailand.

Saihan Sani

Medical and Industrial Microbiology Program, Faculty of Science Technology and Agriculture, Yala Rajabhat University,Yala, Thailand.

Fatheeyah Salaeh

Medical and Industrial Microbiology Program, Faculty of Science Technology and Agriculture, Yala Rajabhat University,Yala, Thailand.

Sutima Preeprem

Medical and Industrial Microbiology Program, Faculty of Science Technology and Agriculture, Yala Rajabhat University,Yala, Thailand.

ปัจจัยที่มีความสัมพันธ์กับระดับความเครียดของนักศึกษาหอพัก มหาวิทยาลัยราชภัฏยะลา 302

Factors Related to Stress Levels of Dormitory Students, Yala Rajabhat University

Rukaiyah Hayikuchi

Faculty of Science, Technology and Agriculture Yala Rajabhat University Muang District, Yala Province, Thailand.

Piyaruk Pradabphetrat

Faculty of Science, Technology and Agriculture Yala Rajabhat University Muang District, Yala Province, Thailand

Sabudin Yingtha

Faculty of Science, Technology and Agriculture Yala Rajabhat University Muang District, Yala Province, Thailand.

การพัฒนาเครื่องตัดหลอดดูดน้ำจากต้นกระจูดด้วยระบบนิวแมติกส์ 308

Development Of A Straw Cutting Machine From Krajood Using A Pneumatic System

Komkit Seepan

Program in Industrial Electrical Technology, Faculty of Science and Technology Suratthani Rajabhat University Suratthani, Thailand.

Peerapong Nuchuay

Program in Industrial Electrical Technology, Faculty of Science and Technology Suratthani Rajabhat University Suratthani, Thailand.

Mintra Trongtorkarn

Program in Industrial Electrical Technology, Faculty of Science and Technology Suratthani Rajabhat University Suratthani, Thailand.

การจำลองอพยพหนีไฟด้วยโปรแกรม Pathfinder กรณีศึกษา อาคารเฉลิมพระเกียรติ **50** พรรษา (อาคาร **20)** มหาวิทยาลัยราชภัฏยะลา

Simulation of Fire Evacuation Using Pathfinder Program: A Case Study of **20**th Building Yala Rajabhat University

316

Hafanee Ama

Public Health Program, Faculty of Science, Technology and Agriculture,Yala Rajabhat University Yala Province, Thailand.

Anukool Bensaard

Public Health Program, Faculty of Science, Technology and Agriculture,Yala Rajabhat University Yala Province, Thailand.

Maytiya Muadchim

Public Health Program, Faculty of Science, Technology and Agriculture,Yala Rajabhat University Yala Province, Thailand.

Suradech Suwanchatree

Public Health Program, Faculty of Science, Technology and Agriculture,Yala Rajabhat University Yala Province, Thailand.

Piyaruk Pradabphetrat

Public Health Program, Faculty of Science, Technology and Agriculture,Yala Rajabhat University Yala Province, Thailand.

ความเครียดและพฤติกรรมการเที่ยวสถานบันเทิงของนักศึกษาระดับปริญญาตรี มหาวิทยาลัยแห่งหนึ่งในจังหวัดภูเก็ต

Stress and Entertainment Venue Visiting Behavior Among Undergraduate Students at a University in Phuket Province

333

Charinya Khanawang

Phuket Rajabhat University Phuket, Thailand.

Supaporn khayaikaeo

Phuket Rajabhat University Phuket, Thailand.

Atitaya Jitjamnong

Phuket Rajabhat University Phuket, Thailand.

แผ่นแบคทีเรียลเซลลูโลสโดยเชื้อ Komogataeibacter nataicola TISTR **975** ผสมสารสกัดหยาบจากสมุนไพรที่มีฤทธิ์ยับยั้งเชื้อ Staphylococcus aureus

Bacterial Cellulose produced by Komogataeibacter nataicola TISTR **975** in combination with Herbal Crude Extracts against Staphylococcus aureus

339

Rusmira Chemache

Microbiology Program, Faculty of Science Technology and Agriculture, Yala Rajabhat University, Yala, Thailand.

Dareeya Jehmu

Microbiology Program, Faculty of Science Technology and Agriculture, Yala Rajabhat University, Yala, Thailand.

Nursahirah saising

Medical and Industrial Microbiology Program, Faculty of Science Technology and Agriculture, Yala Rajabhat University, Yala, Thailand.

Tajree Mingsa

Medical and Industrial Microbiology Program, Faculty of Science Technology and Agriculture, Yala Rajabhat University, Yala, Thailand.

Hatsalinda Binma-ae

Medical and Industrial Microbiology Program, Faculty of Science Technology and Agriculture, Yala Rajabhat University, Yala, Thailand.

การศึกษาสัดส่วนพื้นที่เก็บไอน้ำในถังขับดันที่มีต่ อการสูบน้ำ ของปั๊มสูบน้ำกำลังไอน้ำ 346

A Study of Steam Storage Area Ratio in Pressure Vessels Affecting Water Pumping Performance of Steam-Powered Water Pumps

Pakorn Promkaew

Industrial Technology, Faculty of Science and Technology, Phuket Rajabhat University Phuket, Thailand.

Goffaree Hemmin

Industrial Technology, Faculty of Science and Technology, Phuket Rajabhat University Phuket, Thailand.

Nattapon Dadsadachan

Industrial Technology, Faculty of Science and Technology, Phuket Rajabhat University Phuket, Thailand.

การออกแบบและพัฒนาเครื่องบรรจุน้ำผึ้งลงขวดแก้วจิ๋ว 353

Design And Development Of A Honey Filling Machine For Miniature Glass Bottles

Komkit Seepan

Program in Industrial Electrical Technology, Faculty of Science and Technology Suratthani Rajabhat University Suratthani, Thailand.

Witchayut Srisuwan

Program in Industrial Electrical Technology, Faculty of Science and Technology Suratthani Rajabhat University Suratthani, Thailand.

ผลของการเปลี่ยนแปลงการใช้ประโยชน์ที่ดินที่มีต่อปริมาณน้ำท่าในพื้นที่ลุ่มน้ำจังหวัดภูเก็ต 359

Impact of Land Use Changes on Discharge in Phuket Watershed

Sukanya Vongtanaboon

Faculty of Science and Technology Phuket Rajabhat University Phuket, Thailand.

Suthathong Homya

Faculty of Science and Technology Phuket Rajabhat University Phuket, Thailand.

Pongsakorn Kaewmanee

Faculty of Science and Technology Phuket Rajabhat University Phuket, Thailand.

Pobtham Prompen

Kajonkiet International School Phuket, Thailand.

Effect of flow plate design on fuel cell efficiency 363

Jaruporn Saiyasupee

Department of Engineering University of Technology Lanna, Lanna : 128 Huay Kaew Road, Muang, Chiang Mai, Thailand.

การพัฒนาแอปพลิเคชันบนมือถือแสดงเวลาละหมาดโดยใช้ระบบจีพีเอสสำหรับชาวไทยมุสลิม 369

Development of a GPS-based Prayer Times Mobile Application for Thai Muslims

Basil Salee

Faculty of Science & Technology Phuket Rajabhat University Phuket, Thailand.

Thanawat Saejia

Faculty of Science & Technology Phuket Rajabhat University Phuket, Thailand.

Nasith Laosen

Faculty of Science & Technology Phuket Rajabhat University Phuket, Thailand.

การพัฒนาสื่อมัลติมีเดียสำหรับการเรียนรู้แบบออนไลน์ เรื่องการตัดเย็บผ้า 373

Development of multimedia for online learning on sewing

Ratthasat Roungsea

Digital Technology Branch Faculty of Science and Technology Phuket,Thailand.

Tanawut Chumphol

Digital Technology Branch Faculty of Science and Technology Phuket,Thailand.

Urairat Makchan

Digital Technology Branch Faculty of Science and Technology Phuket,Thailand.

ต้นแบบเกม 3 มิติ การแนะนำขั้นตอนการเดินทางโดยสารเครื่องบิน กรณีศึกษา : ท่าอากาศยานนานาชาติภูเก็ต 377

3 D Game Prototype Introduction to Flight Travel Procedures Case study: Phuket International Airport

Tanunchai Chamnina

Digital Technology Branch Faculty of Science and Technology Phuket,Thailand.

Thanakorn Saelee

Digital Technology Branch Faculty of Science and Technology Phuket,Thailand.

Urairat Makchan

Digital Technology Branch Faculty of Science and Technology Phuket,Thailand.

การพยากรณ์การรายงานตัวของนักศึกษาระดับปริญญาตรี มหาวิทยาลัยราชภัฏภูเก็ต โดยใช้แบบจำลองการถดถอยโลจิสติกส์

Forecasting Undergraduate Student Enrollment at Phuket Rajabhat University Using a Logistic Regression Model 381

Sasina Srithong

Faculty of Science and Technology Phuket Rajabhat University Phuket, Thailand.

Nissareen Sangmuaeng

Digital Technology Branch Faculty of Science and Technology Phuket,Thailand.

Urairat Makchan

Digital Technology Branch Faculty of Science and Technology Phuket,Thailand.

Attapon Pillai

Digital Technology Branch Faculty of Science and Technology Phuket,Thailand.

การพยากรณ์แนวโน้มจำนวนผู้สมัครเรียนระดับปริญญาตรี มหาลัยราชภัฏภูเก็ตโดยวิธีการถดถอยเชิงเส้น

Forecasting the Trend of Undergraduate Applications at Phuket Rajabhat University using the Linear regression 385

Sakuna Choochangwang

Faculty of Science and Technology Digital Technology Program Phuket Rajabhat University Phuket, Thailand.

Aricha Tabmuenwai

Faculty of Science and Technology Digital Technology Program Phuket Rajabhat University Phuket, Thailand.

Attapon Pillai

Faculty of Science and Technology Digital Technology Program Phuket Rajabhat University Phuket, Thailand.

Urairat Makchan

Faculty of Science and Technology Digital Technology Program Phuket Rajabhat University Phuket, Thailand.

การพัฒนาแอปพลิเคชันแชทบอทสำหรับบริการข้อมูลนักศึกษา มหาวิทยาลัยราชภัฏภูเก็ต

Development of a Chatbot Application for Student Information Services at Phuket Rajabhat University 389

Assada Chorraka

Faculty of Science & Technology Phuket Rajabhat University.

Bhurisub Dejpipatpracha

Faculty of Science & Technology Phuket Rajabhat University.

Poomsatit Mattajit

Faculty of Science & Technology Phuket Rajabhat University.

การพัฒนาน้ำพริกปลาแห้งทดแทนด้วยถั่วหรั่งบางส่วน 393

Development of Dried Fish Chili Paste Partially Substituted with Bambara Groundnut

Sangrawee Napattalung

Home Economics Program Faculty of Science and Technology Phuket Rajabhat University.

Jerapat Ploykhaw

Home Economics Program Faculty of Science and Technology Phuket Rajabhat University.

Kanokwan Thongkiaw

Home Economics Program Faculty of Science and Technology Phuket Rajabhat University.

การพัฒนาผลิตภัณฑ์ครองแครงกรอบเสริมปลากะตักผง 397

Development of Crispy Snack (KrongKrang Krob) with Anchovy Fish Powder

Kanokwan Thongkiaw

Faculty of Science and Technology Phuket Rajabhat University Phuket, Thailand.

Jerapat Ploykhaw

Faculty of Science and Technology Phuket Rajabhat University Phuket, Thailand.

Sangrawee Na pattalung

Faculty of Science and Technology Phuket Rajabhat University Phuket, Thailand.

การพัฒนาชุดต้นแบบราคาประหยัดเรื่องการวัดค่าความหนืดของของเหลว 401

Development of a cost-effective prototype for measuring the viscosity of liquids

Nattapong Thuedam

Faculty of Science and Technology, Phuket Rajabhat University Phuket Thailand.

Thitima Thanyaniti

Faculty of Science and Technology, Phuket Rajabhat University Phuket Thailand.

การพัฒนาผลิตภัณฑ์ตะลิงปลิงผงสำเร็จรูปด้วยการทำแห้งแบบพ่นฝอย 404

Development of instant Bilimbi Fruit (Averrhoa bilimbi L.) Powder Product by Spray Drying

Nata-Anisong

Home Economics : Faculty of Science and Technology, Phuket Rajabhat University Phuket, Thailand.

Pakamon-Kulnuwong

Home Economics : Faculty of Science and Technology, Phuket Rajabhat University Phuket, Thailand.

Unruethai-Phupornprasert

Chemistry : Faculty of Science and Technology, Phuket Rajabhat University : Phuket Thailand

การพัฒนาผลิตภัณฑ์น้ำพริกปลาฉิงฉางส้มควายเพื่อยืดอายุการเก็บรักษา (Development of Pla ching chang Som-Khway Chili Paste Products for Shelf Life Prolonging) 408

Pakamon-Kulnuwong

Home Economics : Faculty of Science and Technology, Phuket Rajabhat University Phuket, Thailand.

Nata-Anisong

Home Economics : Faculty of Science and Technology, Phuket Rajabhat University Phuket, Thailand.

Unruethai-Phupornprasert

Chemistry : Faculty of Science and Technology, Phuket Rajabhat University : Phuket Thailand.

ความรอบรู้ด้านสุขภาพและพฤติกรรมการป้องกันโรคมือเท้าปากของครูผู้ดูแลเด็ก ในศูนย์พัฒนาเด็กเล็ก อำเภอเมือง จังหวัดภูเก็ต Health Literacy and Disease Prevention Behaviors Regarding Hand, Foot, and Mouth Disease Among Childhood Teachers in Child Care Centers in Mueang District, Phuket Province 411

Supatsorn Luankaew

Bachelor of Public Health Phuket Rajabhat University Phuket Thailand.

Natthakan Wanraek

Bachelor of Public Health Phuket Rajabhat University Phuket Thailand.

Chayanit Luevanich

Bachelor of Public Health Phuket Rajabhat University Phuket Thailand.

การเปรียบเทียบชนิดและองค์ประกอบทางกายภาพขยะมูลฝอย จากการย้อมผ้าด้วยเทคนิค Eco Printing Types and Physical Composition of Solid Waste from Textile Dyeing with Eco-Printing Technique 417

Suthathong Homya

Faculty of Science and Technology Phuket Rajabhat University, Phuket, Thailand.

Sukanya Vongtanaboon

Faculty of Science and Technology Phuket Rajabhat University, Phuket, Thailand.

Phurinat Paladsongkhram

Faculty of Science and Technology Phuket Rajabhat University, Phuket, Thailand.

Pahol Rongkul

Faculty of Science and Technology Phuket Rajabhat University, Phuket, Thailand.

Siri Jaroenjai

Faculty of Science and Technology Phuket Rajabhat University, Phuket, Thailand.

Kanokporn Tangsabpaiboon

Faculty of Science and Technology Phuket Rajabhat University, Phuket, Thailand.

การพยากรณ์แนวโน้มจำนวนผู้สมัครเรียนระดับปริญญาตรี มหาวิทยาลัยราชภัฏภูเก็ต โดยใช้วิธีการวิเคราะห์อนุกรมเวลา

Forecasting Trend of Undergraduate Applications at Phuket Rajabhat University Using Time Series Analysis 420

Acharaporn Chooklam

Faculty of Science and Technology Phuket Rajabhat University Phuket,Thailand.

Nuttapon Takursuk

Faculty of Science and Technology Phuket Rajabhat University Phuket,Thailand.

Attapon Pillai

Faculty of Science and Technology Phuket Rajabhat University Phuket,Thailand.

Urairat Makchan

Faculty of Science and Technology Phuket Rajabhat University Phuket,Thailand.

ปัจจัยที่มีความสัมพันธ์กับความรอบรู้ด้านสุขภาพและพฤติกรรมการป้องกันโรคมือเท้าปากของครูผู้ดูแลเด็ก ในศูนย์พัฒนาเด็กเล็ก อำเภอเมือง จังหวัดภูเก็ต

Factors Associated with Health Liter acy and Disease Prevention Behaviors Regarding Hand, Foot, and Mouth Disease Among Childhood Teachers in Child Care Centers in Mueang District, Phuket Province 424

Supatsorn Luankaew

Bachelor Of Public Health, Phuket Rajabhat University, Phuket, Thailand.

Natthakan Wanraek

Bachelor Of Public Health, Phuket Rajabhat University, Phuket, Thailand.

Chayanit Luevanich

Bachelor Of Public Health, Phuket Rajabhat University, Phuket, Thailand.

Oranurethai Abdulla

Bachelor Of Public Health, Phuket Rajabhat University, Phuket, Thailand.

Jittipong Sungthong

การยับยั้งเชื้อราก่อโรคในต้นทุเรียนด้วยสารสกัดจากสมุนไพร

Inhibition of fungi durian disease by herbal extracts 430

Afnan Dorma

Medical and Industrial Microbiology, Faculty of Science Technology and Agriculture, Yala Rajabhat University, Yala, Thailand.

Aklima Kamah

Medical and Industrial Microbiology, Faculty of Science Technology and Agriculture, Yala Rajabhat University, Yala, Thailand.

Angkhana Doladoi

Medical and Industrial Microbiology, Faculty of Science Technology and Agriculture, Yala Rajabhat University, Yala, Thailand.

Khosiya Sali

Medical and Industrial Microbiology, Faculty of Science Technology and Agriculture, Yala Rajabhat University, Yala, Thailand.

Message from the President
Phuket Rajabhat University



Phuket Rajabhat University is guided by a philosophy that places local empowerment at the heart of national development. We believe that by uplifting communities through education, innovation, and a deep commitment to social responsibility, we can contribute meaningfully to a stronger and more sustainable future for Thailand. Our approach is rooted in a lifelong learning ethos, which drives both individual growth and collective progress.

Our vision is to be a beacon of knowledge, creativity, and innovation—serving as a catalyst for sustainable development across local communities and the nation. We are committed to empowering communities through knowledge and indigenous wisdom, nurturing educators who uphold the highest professional standards, and preparing graduates who are ready to meet the real-world needs of society. Lifelong learning is central to everything we do, as is our dedication to producing research that addresses local challenges and enhances competitiveness. We also strive to manage our institution with modern technology and innovation, always grounded in good governance. The university is home to five dynamic faculties—Science and Technology, Agricultural Technology, Management Sciences, Humanities and Social Sciences, and Education. Together, they form a vibrant academic community that works collaboratively to inspire change, foster innovation, and create a positive, lasting impact.

On behalf of Phuket Rajabhat University, it is my genuine pleasure to warmly welcome all of you to the 11th International Conference on Engineering, Applied

Sciences and Technology (ICEAST2025), right here in the beautiful province of Phuket. We are truly honored to host this prestigious global gathering. This conference presents a wonderful opportunity for us to showcase not only the strengths of our university but also the vibrant spirit and capabilities of our province. Partnering with esteemed organizations and institutions as co-hosts reflects our strong commitment to advancing academic excellence and research in science and technology. ICEAST2025 is more than just a conference—it is a dynamic platform where researchers, scholars, and experts from around the world come together to share insights, spark new ideas, and build lasting collaborations. In particular, the focus on dielectric materials highlights a critical area of innovation, vital to achieving sustainable development in the years ahead.

I would like to express my sincere thanks to the organizing committee for their hard work and dedication in bringing this event to life. To all participants, I hope this conference proves to be an inspiring and enriching experience, and that the knowledge and connections you gain here will contribute meaningfully to your future research and professional paths.

Once again, welcome—and may you enjoy every moment of ICEAST2025 in Phuket!



Asst. Prof. Dr. Hiran Prasankan

Honorary Chair

President of Phuket Rajabhat University

Message from Honorary Chairs



As the technical sponsor, the IEEE BTS Thailand Chapter is honored to support ICEAST 2025, the 11th International Conference on Engineering, Applied Sciences and Technology. On their behalf, I extend a warm welcome to all of you.

We are deeply grateful to the dedicated Organizing Committee members, our tireless staff, and the insightful reviewers who shaped this exceptional technical program. We also extend our sincere appreciation to all authors who entrusted ICEAST 2025 with their valuable research.

We trust that ICEAST 2025 will be a rewarding experience, fostering collaboration and scientific exchange. May you also enjoy the mesmerizing beauty of Phuket, Thailand.

S. Promwong

Assist. Prof. Dr. Sathaporn Promwong

Honorary Chair

King Mongkut's Institute of Technology Ladkrabang, Thailand

Message from General Chair



The Faculty of Science and Technology at Phuket Rajabhat University embraces its role as the intellectual cornerstone of the Andaman region. Guided by this philosophy, we are committed to becoming a beacon of knowledge in science and technology—driving innovation that uplifts and empowers local communities. Our academic portfolio encompasses a broad spectrum of programs, including short courses, bachelor's degrees, and master's degrees, across key disciplines such as General Science, Health Science, Digital Technology, Industrial Technology, and Architectural Technology.

Our academic strength in teaching, administration, and quality graduate production cannot be achieved in isolation. With a shared vision to elevate education and drive national development through science, health sciences, technology, and agriculture, a regional collaboration has emerged. This partnership unites seven institutions in Southern Thailand: five faculties of Science and Technology from Phuket Rajabhat University, Songkhla Rajabhat University, Nakhon Si Thammarat Rajabhat University, Suratthani Rajabhat University, and Rajamangala University of Technology Srivijaya; the Faculty of Science Technology and Agriculture at Yala Rajabhat University; and Boromarajonani College of Nursing Nakhon Si Thammarat. Together, we strive to advance academic quality and cultivate a highly competent workforce capable of competing at national and international levels.

This collaboration reflects the power of integrating knowledge and resources to strengthen higher education and innovation in a rapidly evolving world. Serving as

co-hosts of the 11th International Conference on Engineering, Applied Sciences and Technology (ICEAST 2025), held in Phuket from May 6–9, 2025 is both an honor and a significant step forward in enhancing academic excellence across our network.

On behalf of the leadership from all seven partner institutions, I am truly honored to welcome you to ICEAST 2025. I warmly congratulate all participants. This conference provides an essential platform for researchers, academics, and experts worldwide to exchange ideas and present groundbreaking work. Its success underscores the continuous progress in science and technology that profoundly shapes our industries and society. I am confident that ICEAST 2025 will inspire fruitful collaborations and build strong global networks, advancing the fields of engineering, applied sciences, and technology. I sincerely thank the organizing committee for their dedication and wish all participants a rewarding experience, rich with knowledge to apply in your research and professional endeavors.

May this conference be both memorable and profoundly beneficial for everyone involved.



Associate Professor Dr.Putsadee Pornphol

Dean of the Faculty of Science and Technology

Phuket Rajabhat University, Phuket, Thailand

Message from Technical Program Chairs



On behalf of the Technical Program Committee (TPC) for the ICAST 2025. With great enthusiasm, we warmly welcome you to participate in ICEAST 2025. It is an international platform for knowledge exchange and collaboration.

We have received 208 paper submissions from esteemed researchers across various countries, including Australia, Bangladesh, China, India, Indonesia, Ireland, Italy, Japan, Jordan, Korea, Malaysia, Philippines, Saudi Arabia, Slovenia, United Kingdom, United State, and Thailand. Through a rigorous review process, 93 papers have been accepted, we have achieved an acceptance rate of 44.71%, ensuring a program of exceptional quality.

The technical program of ICEAST 2025 will feature four insightful keynote sessions and twenty engaging oral presentation sessions, covering a wide range of topics in engineering and applied sciences. We extend our appreciation to all authors and reviewers for their valuable contributions in curating this comprehensive program.

We express our gratitude to the keynote speakers, participants, authors, and sponsors for their support. Together, let us shape the future of our fields and contribute to advancements in engineering and applied sciences.



Assist.Prof.Dr.Rachen Kanahna

Technical Program Chair

Organizing Committee

Honorary Chairs

Supavadee Aramvith (IEEE, Thailand)
Hiran Prasankan (PKRU, Thailand)
Sathaporn Promwong (IEEE BTS Thailand Chapter and KMITL, Thailand)

General Chair

Putsadee Pornphol (PKRU, Thailand)
Khwankamon Khoonpitak (SKRU, Thailand)
Chawanrat Srinounpan (NSTRU, Thailand)
Thitipong Kreuhong (SRU, Thailand)
Wipawan Chaoum Pensuksan (SRU, Thailand)
Wilaiwan Kaewtathip (YRU, Thailand)
Suthum Chumpromyat (RUTS, Thailand)
Sutut Hemtanon (BCN.NAKHON, Thailand)

General Co-Chair

Suthida Rattanaburi (PKRU, Thailand)
Thanadon Mankong (IEEE BTS Thailand Chapter)

Organizing-Chairs

Decha Seeduka (PKRU, Thailand)
Porpattama Hammachukiattikul (PKRU, Thailand)

International Advisory Committee (IAC)

Yoshikazu Miyanaka (Hokkaido University, Japan)
Takao Onoye (Osaka University, Japan)
Kazuhiko Hamamoto (Tokai University, Japan)
Kyung Sup Kwak (Inha University, South Korea)
Dusit Niyato (Nanyang Technological University, Singapore)
Tadashi Ariga (Tokai University, Japan)
Tomotaka Homae (National Institute of Technology, Toyama College, Japan)
Somsanouk Pathoumvanh (NUOL, Lao PDR)
Satoru Seto (National Institute of Technology, Ishikawa College, Japan) Kuniaki Yajima (National Institute of Technology, Sendai College, Japan) Phonekeo Chanthamaly (NUOL, Lao PDR)

Sengpasong Phrakonekham (NUOL, Lao PDR)
Eryk Dutkiewicz (University of Technology Sydney, Australia)
Myo Myint Maw (Mandalay Technological University, Myanmar)

ICEAST Steering Committee

Sathaporn Promwong (IEEE BTS Thailand Chapter and KMITL, Thailand)
Wiboon Promphanich (KMITL, Thailand)
Chanin Bunaksananusorn (KMITL, Thailand)
Norasage Pattanadech (KMITL, Thailand)
Putsadee Pornphol (PKRU, Thailand)
Myint Thein (Yangon Technology University,Myanmar)
Sint Soe (Mandalay Technology University,Myanmar)

Technical Program Chairs

Rachen Kanahna (PBRU, Thailand)
Thanadol Tiengthong (IEEE BTS Thailand Chapter)
Sukanya Vongtanaboon (PKRU, Thailand)
Suthida Rattanaburi (PKRU, Thailand)
Aroonsri Wongpatikarn (PKRU, Thailand)
Sanchai Yodmanee (PKRU, Thailand)
Akarachai Inthanil (PKRU, Thailand)
Vadivel Rajarathinam (PKRU, Thailand)
Wimonnat Sukpol (PKRU, Thailand)

Technical Committee

Pichaya Supanakoon (KMITL, Thailand)
Chayanit Luevanich (PKRU, Thailand)
Sukanya Vongtanaboon (PKRU, Thailand)
Sakchai Phethchuai (PKRU, Thailand)
Suthida Rattanaburi (PKRU, Thailand)
Saithan Thongphrom (PKRU, Thailand)
Nitiya Sangkhanan (PKRU, Thailand)
Zongkiat Pavadee (PKRU, Thailand)
Aroonsri Wongpatikarn (PKRU, Thailand)
Siwaphong Thongjua (PKRU, Thailand)
Anongnat Painupong (PKRU, Thailand)
Urairat Makchan (PKRU, Thailand)

Hanphon Mitwong (PKRU, Thailand)
Jaruwan Promngurn (PKRU, Thailand)
Sopa Choopeng (PKRU, Thailand)
Preeyanuch Thongpoo (PKRU, Thailand)
Sanchai Yotmanee (PKRU, Thailand)
Prapaipim Surachetkomson (PKRU, Thailand)
Rattiya Sungchasit (PKRU, Thailand)
Natthaporn Rattanapan (PKRU, Thailand)
Akarachai Inthanil (PKRU, Thailand)
Nata Anisong (PKRU, Thailand)
Phuripong Meksuwan (PKRU, Thailand)
Atipan Saimmai (PKRU, Thailand)
Chalinee Thangmanee (PKRU, Thailand)
vadivel Rajarathinam (PKRU, Thailand)
Pradchamas Lanchanon (PKRU, Thailand)
Sineenart Puangmanee (PKRU, Thailand)
Somsak Limwongsakorn (PKRU, Thailand)
Tidarat Kumlom (PKRU, Thailand)
Sureeporn Kangsanant (SKRU, Thailand)
Purintorn Chanlert (SKRU, Thailand)
Paweena Dikit (SKRU, Thailand)
Pawika Mahasawat (SKRU, Thailand)
Chawanrat Srinounpan (NSTRU, Thailand)
Supaporn Sutin (NSTRU, Thailand)
Suriya Chankaew (NSTRU, Thailand)
Kanitta Keeratipattarakarn (NSTRU, Thailand)
Walaiporn Sornkliang (NSTRU, Thailand)
Rattayagon Thaipun (NSTRU, Thailand)
Kritaphat Songsri-in (NSTRU, Thailand)
Patompong Chabplan (NSTRU, Thailand)
Wipada Muninnoppamad (YRU, Thailand)
Maytiya Muadchim (YRU, Thailand)
Jeerawoot Muninnoppamas (YRU, Thailand)
Ismaae Latekeh (YRU, Thailand)
Wilaiwan Kaewtathip (YRU, Thailand)
Eleeyah Saniso (YRU, Thailand)
Hatsalinda Binma-ae (YRU, Thailand)
Jariyaporn Masawat (YRU, Thailand)

Romsan Madmanang (YRU, Thailand)
Narumol Phantaweesub (YRU, Thailand)
Rachada Boonkaew (YRU, Thailand)
Piriya Prunglerdbuathong (YRU, Thailand)
Issariyaporn Damrongrak (YRU, Thailand)
Warunee Hajimasalaeh (YRU, Thailand)
Sasithorn Pangsuban (YRU, Thailand)
Muneeroh Phadung (YRU, Thailand)
Fudailah Duemong (YRU, Thailand)
Zubaidah Hajiwangoh (YRU, Thailand)
Sunee Kraonual (YRU, Thailand)
Wipawan Chaoum Pensuksan (SRU, Thailand)
Wireeporn Chaisetsampun (SRU, Thailand)
Kamolchanok Thongied (SRU, Thailand)
Nutchanath Wichit (SRU, Thailand)
Aranya Rakhab (SRU, Thailand)
Sadakan Eamchanprathip (SRU, Thailand)
Sureeporn Chumdaeng (SRU, Thailand)
Praditporn Pongtriang (SRU, Thailand)

Special Session Chairs

Norasage Pattanadech (KMITL, Thailand)
Nachanant Chitanont (KMITL, Thailand)

Publication Chair

Nattapan Suwansukho (IEEE BTS Thailand Chapter)
Bhurisub Dejpipatpracha (PKRU, Thailand)
Chayapol Khamyod (MFU, Thailand)

Publicity/Public Relation Chairs

Bhurisub Dejpipatpracha (PKRU, Thailand)
Jirapat Sangthong (MUT, Thailand)
Wipassorn Vinicchayakul (CATC, Thailand)
Rathachai Chawuthai (KMITL, Thailand)

Financial Chair
Wiboon Promphanich (KMITL, Thailand)
Vidhya Rugpong (IEEE, Thailand)

Financial Committee
Porpattama Hammachukiattikul (PKRU, Thailand)
Pawalee Srisuksomwong (PKRU, Thailand)
Sirinya Chansaksoong (PKRU, Thailand)
Churirat Uaongpluksin (PKRU, Thailand)
Wannadee Sawatdirak (PKRU, Thailand)
Nareerat Banjongkarn (PKRU, Thailand)

Registration Chair
Sanit Teawchim (KMITL, Thailand)

Sponsor & Exhibition Chair
Srangrath Hattawong (InspireCom, Thailand)
Bundit Ruckveratham (MCOT, Thailand)
Ofer Nagar (EDAO, ISAREL)
Thunya Bunrongruang (Good Integration, Thailand)
Vongkeo Kingsakda (Lao Tel, Lao PDR)

Sponsor & Exhibition Committee
Rangsan Ponsamak (PKRU, Thailand)
Prasert Jariyalerpong (PKRU, Thailand)
Weerawat Intaratat (PKRU, Thailand)
Porpattama Hammachukiattikul (PKRU, Thailand)
Pawalee Srisuksomwong (PKRU, Thailand)
Sirinya Chansaksoong (PKRU, Thailand)
Churirat Uaongpluksin (PKRU, Thailand)
Sukanya Vongtanaboon (PKRU, Thailand)
Suthida Rattanaburi (PKRU, Thailand)
Aroonsri Wongpatikarn (PKRU, Thailand)
Sanchai Yodmanee (PKRU, Thailand)
Akarachai Inthanil (PKRU, Thailand)
Chanathinat Chaiyapoo (PKRU, Thailand)
Wimonnat Sukpol (PKRU, Thailand)

Local Arrangements & Hospitality Committee Chair
Decha Seeduka (PKRU, Thailand)

Souvenirs Committee
Khan Payungphan (PKRU, Thailand)
Chanathinat Chaiyapoo (PKRU, Thailand)
Wimonnat Sukpol (PKRU, Thailand)

General Secretary Chair
Chanin Bunaksananusorn (KMITL, Thailand)

General Secretary
Wannadee Sawatdirak (PKRU, Thailand)
Onanong Nuansri (PKRU, Thailand)
Oithip Chaithong (PKRU, Thailand)
Tiratorn Ketsattaban (PKRU, Thailand)
Nareerat Banjongkarn (PKRU, Thailand)
Thidawan Pankaew (PKRU, Thailand)
Chirawan Lenthas (PKRU, Thailand)
kanokporn tangsabpaiboon (PKRU, Thailand)
Siri Jarurnjai (PKRU, Thailand)
Pahol Rongkul (PKRU, Thailand

List of Reviewer

Akapot Tantrapiwat
Alexis Guilloteau
Boonchai Boonchu
Boontee Kruatrachue
Bundit Ruckveratham
Chak Chantalakhana
Chanin Bunlaksananusorn
Chaowalit Hamontree
Chayapol Kamyod
Chompoonoot Hirunyaprik
Chompoonuch Jinjakam
Chukiet Sodsri
Chumpol Yuangyai
Chutham Sawigan
Chutimet Srinilta
Deuansavanh Phommavongsa
Donekeo Lakanchanh
Gilbert Siy Ching
Jakrapong Pongpeng
Jarotwan Koiwanit
Jarruwat Charoensuk
Jirapat Sangthong
Jittraporn Wongsa-Ngam
Jonathan David Sands
Jukkrit Tagapanij
Manolom Chanthavong
Mettaya Kitiwan
Monchai Chamchoy
Monsak Pimsarn
Montree Kumngern
Montri Wiboonrat
Myo Myint Maw
Nachanant Chitanont
Nattapan Suwansukho
Natthawut Ruangtrakoon
Nirand Pisutha-Arnond
Nobphadon Suksangpanya
Nopporn Suttiwong
Norasage Pattanadech
Pakorn Watanachaturaporn
Pasu Poonpakdee
Patchariya Petchpong
Peerapol Yuvapoositanon
Phacharaphon Tunthawiroon
Pholchai Chotiprayanakul
Phonexay Vilakone
Phonlasit Thinnakorn Na Ayuthaya
Phosy Panthongsy
Phouthong Southisombath
Pichaya Supanakoon

Kajornsak Kittimathaveenan
Kannachai Kanlayasiri
Kei Eguchi
Khamkhet Bounnady
Khamphao Sisaat
Khamphong Khongsomboon
Khanthanou Luangxaysana
Khemapat Tontiwattanakul
Khounhack Lorvannger
Kietikul Jearanaitanakij
Kittipitch Meesawat
Pitak Thumwarin
Pitikhate Sooraksa
Prajuab Pawarangkoon
Prawit Chumchu
Rachen Kanahna
Ranon Jientrakul
Rathachai Chawuthai
Sanit Teawchim
Sarun Duangsuwan
Sathaporn Promwong
Siraphop Tooprakai

Sittiporn Pimsakul
Smith Eiamsa-Ard
Somphone Kanthavong
Sompob Polmai
Somsanouk Pathoumvanh
Sorasak Danworaphong
Souphavady Praseuth
Suchada Sitjongsataporn
Sukkasem Pathumthong
Sumek Wisayataksin
Supat Kittiratsacha
Surapan Airphaiboon
Surin Kittitornkun
Tha Bounthanh
Thanadol Tiengthong

Thanadon Mankong

Theera Leeudomwong

Theerayod Wiangtong

Tossapol Kiatcharoenpol

Unnat Pinsopon

Veerachai Malyavej

Vimontha Khieovongphachanh

Vongkeo Kingsakda

Wiboon Promphanich

Worapong Tangsrirat

Xaythavy Louangvilay

Yuttapong Rangsanseri

Keynote speaker 1



Pracha Asawateera

Vice President Southern District Office

Digital Economy Promotion Agency (DEPA)

Title: Digital Economy Promotion

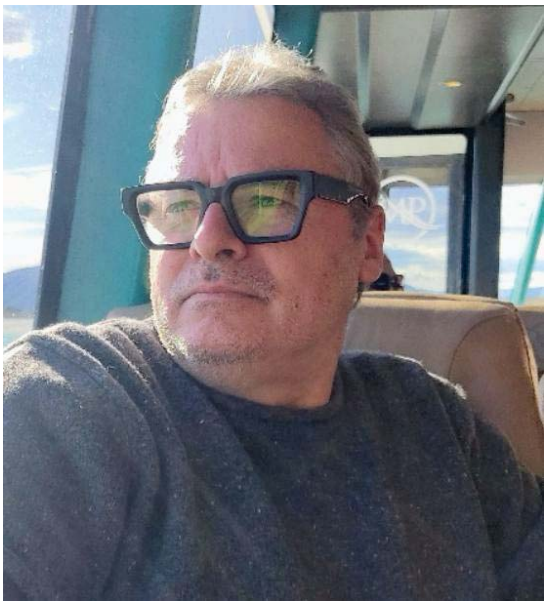
Abstract

Mr. Pracha will explore Thailand's digital transformation initiatives with a focus on the role of the Digital Economy Promotion Agency (DEPA). Drawing from real-world experience,He will share key insights from leading the Phuket Smart City project and other digital development programs in southern Thailand. The talk will emphasize the importance of government-private collaboration, smart infrastructure, and the certification ecosystem in accelerating regional innovation and sustainable growth.

Biography

Mr. Pracha Asawateera is the Vice President of the Southern District Office, Digital Economy Promotion Agency (DEPA), under the Ministry of Digital Economy and Society, Thailand. He earned his Bachelor's degree in Computer Engineering from Suranaree University of Technology and his Master's degree in Computer Science from Thammasat University.He has led numerous digital transformation projects including the Phuket Smart City, and organized the ACM-ICPC World Finals in Phuket in 2016. Mr. Pracha is also a guest lecturer at Prince of Songkla University, focusing on software engineering, service architecture, and entrepreneurship.

Keynote Speakers 2



Professor Manuel Núñez

Professor of Computer Science

Complutense University of Madrid, Spain.

Title: How do you test a map?

Abstract

This talk presents the core concepts of metamorphic testing and demonstrates its application in validating map information. I will outline the theoretical framework and share results that highlight several inaccuracies found in the analyzed maps.

Biography

Professor Manuel Núñez holds a Ph.D. in Mathematics and an M.S. in Economics. He is a Professor of Computer Science at the Complutense University of Madrid, Spain. A well-respected researcher in formal methods and software testing, he is

actively involved with the IEEE SMC Technical Committee on Computational Collective Intelligence and the IEEE Reliability Society Technical Committee on Systems and Software Assurance. He also serves on the steering committees of international conferences such as A-MOST, ICCCI, QRS, and SEFM. With over 180 published papers and participation in more than 170 program committees, his current interests include the integration of AI techniques into smart city systems.

Keynote Speakers 3



Dr. Vadivel Rajarathinam

Department of Mathematics

Faculty of Science and Technology

Phuket Rajabhat University, Thailand.

Title: Synchronization of Complex-Valued Neural Network-Based Control Techniques and Its Application

Abstract

This talk focuses on the reachable set estimation for the synchronization of complex-valued neural networks (CVNNs) using an event-triggered approach in the presence of cyber-attacks. The proposed controller is designed to reduce communication resource usage while maintaining system stability. The objective is to find the smallest ellipsoid that can contain the state trajectory of the system under control.

By employing Lyapunov–Krasovskii functional (LKF) and integral inequality techniques, sufficient stability conditions are derived in terms of linear matrix inequalities (LMIs), solvable via MATLAB's YALMIP toolbox. Numerical simulations highlight the method's effectiveness and its potential for chaos-based secure communications.

Biography

Dr. Vadivel Rajarathinam earned his B.Sc., M.Sc., and M.Phil. degrees in Mathematics from Sri Ramakrishna Mission Vidyalaya College, affiliated with Bharathiar University, and a Ph.D. in Mathematics from Thiruvalluvar University, India. He completed his postdoctoral research at Kunsan National University in South Korea, focusing on wind energy systems. Currently, he is a lecturer in the Department of Mathematics, Faculty of Science and Technology, at Phuket Rajabhat University, Thailand. He has published over 75 research articles in SCI journals. His research interests include stability analysis, neural networks, networked control systems, T–S fuzzy theory, and event-triggered control. He is also an active reviewer for numerous scientific journals.

Keynote Speakers 4



Ofer Nagar

Vice President for Asia-Pacific at Pixellot

Cybersecurity Initiative Collaborator at EDAO Group

Title: Cyber Security

Abstract

Ofer Nagar will present EDAO Group's pioneering initiatives in cybersecurity for Al ecosystems, focusing on secure cloud computing, Al-specific threat intelligence, and identity management. He will discuss the critical role of cybersecurity in enabling safe and scalable Al-driven environments. In addition, the talk will showcase the application of Al in sports, highlighting how advanced video production and analytics technologies are transforming sports coverage and coaching. The session will emphasize the intersection of cybersecurity and Al innovation in building secure, intelligent digital tutures.

Biography

Ofer Nagar currently serves as Vice President for Asia-Pacific at Pixellot, the global leader in Al-automated sports video and analytics solutions. At Pixellot, he has been instrumental in deploying Al-based production systems that eliminate the need for manual filming, enabling scalable, real-time sports coverage across youth leagues, schools, amateur clubs, and professional organizations. In parallel, Nagar collaborates with EDAO Group to promote cybersecurity initiatives tailored for Al ecosystems. His expertise spans secure cloud computing, Al-specific threat intelligence, and identity management – critical components for protecting next-generation platforms. With over two decades of leadership experience across technology sectors, Nagar's unique perspective at the intersection of Al transformation and cybersecurity innovation offers critical insights for building secure, intelligent digital futures.

Program at a Glance

Tuesday, May 6, 2025

Time	Event at Royal Phuket City Hotel
15:00 – 17:00	Registration
18:00 – 20:00	Welcome Party

Wednesday, May 7, 2025

Time	Event at Royal Phuket City Hotel			
09:00 – 16:00	Registration			
09:45 – 10:20	Open Ceremony at Ball Room 2			
10:20 – 10:45	Coffee Break			
10:45 – 11:30	Keynote Speaker 1 Speaker name: Pracha Asawateera Topic: Digital Economy Promotion Room: Grand Ball Room 2 Session Chair: Norasage Pattanadech			
11:30 – 12:15	Keynote Speaker 2 Speaker name: Prof. Dr.Manuel Núñez Topic: How do you test a map Room: Grand Ball Room 2 Session Chair: Chanin Bunlaksananusorn			
12:15 – 13:15	Lunch			
13.20-17.40	National Technical Session 1 (Grand Ball Room2)		National Technical Session 1 (Grand Ball Room2)	
	Session Chairs: 1. Chayanit Luevanich 2. Jittipong Sungthong		Session Chairs: 1. Tatchaporn Chaijaroen 2. Jantana Saengkaew	
	13:20 – 13:40	P355	15:20 – 15:40	P137
	13:40 – 14:00	P356	15:40 – 16:00	P152
	14:00 – 14:20	P364	16:00 – 16:20	P143
	14:20 – 14:40	P365	16:20 – 16:40	P371
	14:40 – 15:00	P120	16:40 – 17:00	P102
	15:00 – 15:20	P178	17.00-17.20	P144

	Session 1	Session 2	Session 3	Session 4
	Hay room	Nakha room	Maithon room	Bon room
Session Title	Computer Science And Information Technology-01	Computer Science And Information Technology-02	Audio Engineering And Acoustics	Computer Science And Information Technology-03

Session Chairs	Suphamit Chittayasothorn	Sukanya Vongtanaboon	Nachanant Chitanont	Wimonnat Sukpol
	Rakibul Hasan	Sukanya Vongtanaboon	Nachanant Chitanont	Wimonnat Sukpol
13:20 – 15:00 (20 min/paper)	P263	P267	P289	P173
	P157	P262	P285	P177
	P274	P282	P153	P288
	P276	P169	P369	P162
	P264	P172	P156	P159
15:00 – 15:15	Coffee Break			

	Session 5	Session 6	Session 7	Session 8
	Hay room	Nakha room	Maithon room	Bon room
Session Title	Computer Science And Information Technology-04	Computer Science And Information Technology-05	Computer Science And Information Technology-06	Computer Science And Information Technology-07
Session Chairs	Chanin Bunlaksananusorn	Sukanya Vongtanaboon	Suphamit Chittayasothorn	Wimonnat Sukpol
	Suzanna Suzanna	KMITL	Putsadee Pornphol	KMITL
15:15 – 17:15 (20 min/paper)	P154	P271	P150	P252
	P158	P272	P155	P251
	P216	P279	P118	P111
	P280	P136	P122	P175
	P139	P278	P283	P149
	P101	P245	P270	P174

Thursday, May 8, 2025

Time	Event at Royal Phuket City Hotel			
09:00 – 16:00	Registration			
	Session 9	Session 10	Session 11	Session 12
	Hay room	Nakha room	Maithon room	Bon room
Session Title	Computer Science And Information Technology-08	Instrumentation And Control Engineering-01	Telecommunications And Networking	National Technical Session 2

Session Chairs	Attapon Pillai	Noppadol Maneerat	Nattapan Suwanasuko	Hanphon Mitwong
	KMITL	Tanagrit Chansaeng	Akarachai Inthanil	Somsak Limwougsakorn
09:00 – 11:00 (20 min/paper)	P180	P140	P119	P342
	P134	P286	P253	P160
	P249	P147	P254	P258
	P370	P113	P109	P363
	P114	P141	P121	P142
	P266	P123	P273	P179
11:00 – 11:15	Coffee Break			
11:05 – 11:50	Keynote Speaker 3 Speaker name: Dr.Vadivel Rajarathinam Topic: Synchronization of complex valued neural network-based control techniques and its application Room: Hay Session Chair: Thanadol Tiengthong/ Siraphop Tooprakai		Keynote Speaker 4 Speaker name: Ofer Nagar Topic: Cyber Security Room: Nakha Session Chair: Thanadon Mankong	
11:50 – 13:00	Lunch			
13:00 – 15:00	Technical Workshop			
	Session 13	Session 14	Session 15	Session 16
	Hay room	Nakha room	Maithon room	Bon room
Session Title	Computer Science And Information Technology-09	Instrumentation And Control Engineering-02	Electrical & Electronic Instrumentation & Control	National Technical Session 3
Session Chairs	Siraphop Tooprakai	Chanin Bunlaksananusorn	Thanadol Tiengthong	Suthathong Homya
	Nasith Laosen	Vadivel Rajarathinam	Akarachai Inthanil	Urairat Makchan
13:00 – 15:00 (20 min/paper)	P110	P277	P287	P284
	P104	P168	P191	P353
	P268	P107	P256	P350
	P105	P166	P116	P361
	P218	P167	P275	
	P176	P187	P115	
15.00-15.15	Coffee Break			

Thursday, May 8, 2025

	Session 17	Session 18	Session 19	Session 20
	Hay room	Nakha room	Maithon room	Bon room
Session Title	Instrumentation & Control Engineering-Computer Science & Information Technology	Electrical Engineering	Electrical Engineering	National Technical Session 4
Session Chairs	Chanin Bunlaksananusorn	Norasage Pattanadech	Thanadon Mankong	Nasith Laosen
	KMITL	Vadivel Rajarathinam	KMITL	Tanagrit Chansaeng
15:15 – 17:15 (20 min/paper)	P108	P255	P248	P343
	P106	P260	P112	P349
	P128	P103	P138	P348
	P265	P125	P135	P354
	P161	P261		
		P269		

Friday, May 9, 2025

Time	Event
13:00 – 19:30	Technical Tour

Technical Program

ICEAST 2025 Program: Tuesday, May 6, 2025

15:00 – 17:00	Registration
18:00 - 20:00	Welcome Reception at Royal Phuket City Hotel

ICEAST 2025 Program: Wednesday, May 7, 2025

09:00 – 16:00	Registration
09:45 – 10:20	Open Ceremony at Ball Room 2
10:20 - 10:45	Coffee Break
10:45 – 11:30	Keynote Speaker 1
11:30 – 12:15	Keynote Speaker 2
12:15 – 13:15	Lunch
13:20 – 17:40	National Technical Session 1
13:20 – 15:00	Technical Session 1-4
15:00 – 15:15	Coffee Break
15:15 – 17:15	Technical Session 5-8

ICEAST 2025 Program: Thursday, May 8, 2025

09:00 – 16:00	Registration
09:00 – 11:00	Technical Session 9-12
11:00 – 11:15	Coffee Break
11:05 – 11:50	Keynote Speaker 3,4
11:50 – 13:00	Lunch
13:00 – 15:00	Technical Workshop
13:00 – 15:00	Technical Session 13-16
15:00 – 15:15	Coffee Break
15:15 – 17:15	Technical Session 17-20
15:15 – 16:15	Steering committee meeting

ICEAST 2025 Program: Friday, May 9, 2025

13:00 – 19:30	Technical Tour

National Technical Session 1:
Session Chairs: *Chayanit Luevanich, Jittipong Sungthong*
Grand Ball Room2

13:20-13.40	Paper ID 355: Development of Dried Fish Chili Paste Partially Substituted with Bambara Groundnut Sangrawee Napattalung, Jerapat Ploykhaw, Kanokwan Thongkiaw

13.40-14.00	Paper ID 356:mDevelopment of Crispy Snack (KrongKrang Krob) with Anchovy Fish Powder Kanokwan Thongkiaw, Jerapat Ploykhaw
14.00-14.20	Paper ID 364: Development of instant Bilimbi Fruit(Averrhoa bilimbi L.) Powder Product by Spray Drying Nata-Anisong, Pakamon-Kulnuwong, Unruethai-Phupornprasert
14.00-14.40	Paper ID 365: Development of Pla ching chang Som-Khway Chili Paste Products for Shelf Life Prolonging Pakamon-Kulnuwong, Nata-Anisong, Unruethai-Phupornprasert
14.40-15.00	Paper ID 120: Biofilm Formation and Antibiogram Profiles of Vibrio parahaemolyticus Isolates from Seafood Muhammadfitree Ding, Fatheeyah Salaeh, Fathiyah Wamaeng, Sutima Preeprem, Saihan Sani
15.00-15.20	Paper ID 178: Inhibition of fungi durian disease by herbal extracts Aklima Kamah, Angkhana Doladoi, Khosiya Sali

National Technical Session 1:
Session Chairs: ***Tatchaporn Chaijaroen, Jantana Saengkaew***
Grand Ball Room2

15:20-15:40	Paper ID 137: Factors Related to Stress Levels of Dormitory Students, Yala Rajabhat University Rukaiyah Hayikuchi, Piyaruk Pradabphetrat, Sabudin Yingtha
15:40-16:00	Paper ID 152: Bacterial Cellulose produced by Komogataeibacter nataicola TISTR 975 in combination with Herbal Crude Extracts against Staphylococcus aureus Rusmira Chemache, Dareeya Jehmu, Nursahirah saising, Tajree Mingsa, Hatsalinda Binma-ae
16:00-16:20	Paper ID 143: Simulation of Fire Evacuation Using Pathfinder Program: A Case Study of 20th Building Yala Rajabhat University Hafanee Ama, Anukool Bensaard, Maytiya Muadchim, Suradech Suwanchatree, Piyaruk Pradabphetrat
16:20-16:40	Paper ID 371: Factors Associated with Health Liter acy and Disease Prevention Behaviors Regarding Hand, Foot, and Mouth Disease Among Childhood Teachers in Child Care Centers in Mueang District, Phuket Province Supatsorn Luankaew, Natthakan Wanraek, Chayanit Luevanich,Oranurethai Abdulla, Jittipong Sungthong
16:40-17:00	Paper ID 102: Health Literacy and Disease Prevention Behaviors Regarding Hand, Foot, and Mouth Disease Among Childhood Teachers in Child Care Centers in Mueang District, Phuket Province Supatsorn Luankaew, Natthakan Wanraek, Chayanit Luevanich,Oranurethai Abdulla, Jittipong Sungthong

17.00-17.20 Paper ID 144: Factors Influencing Bullying in Public University Students Phuket Province
Nathanan Chatiwong, Ornruethai Aubdulla Sarychev, Nattida Kungthong

Session 1: Computer Science And Information Technology-01

Session chair: ***Suphamit Chittayasothorn, Rakibul Hasan***

Hay room

13:20-13.40 Paper ID 263: Optimizing Detection of Human Cancer Cells in Breast Cancer via Machine Learning and Feature Selection
Inshad Rahman Noman, Md Rashedul Islam, Kanchon Kumar Bishnu, Araf Islam, Afia Fairooz Tasnim, Md Munna Aziz, Rakibul Hasan

13:40-14.00 Paper ID 157: "Sell in May & Go Away" [for 6 Months] Versus Other 6-Month Intervals – the Philippine Stock Exchange Index (PSEi)
Jackylyn L. Beredo, Kainam Thomas Wong, Jonathan Paul Cempron, Joel P. Ilao

14.00-14.20 Paper ID 274: TabFuseNet: A Cancer Prediction Model Utilizing Sample Cohort Data
ChaeYoon Han, NangKyeong Lee, Jun Kim, Muhammad Afza ,Zeeshan Abbas, SeungWon Lee

14.20-14.40 Paper ID 276: Implemented Machine Learning Models to Predict Life Satisfaction Using Demographic and Religious Data
Aryan Shah, Anshul Mago, Shreyan Shah, Michelle A. Patriquin

14.40-15.00 Paper ID 264: Efficient American Sign Language Recognition using ResNet-50
Md Sharifuzzaman, Anik Sen, Joyashish Ghosh, Tze Hui Liew, Debanjon, Dutta Purkaystha, Saptanil Ghose, Masud Pervez, Md. Jakir Hossen

Session 2: Computer Science And Information Technology-02

Session chair: ***Sukanya Vongtanaboon, KMITL***

Nakha room

13:20-13.40 Paper ID 267: Digital Transformation for Small Business Sustainability in the Post-Pandemic Economy
Mohammad Anisur Rahman, Hasan Mahmud Sozib, Amena Hoque, Romana Nourin Nipa, Tasmim Jamal Joti, Samia Ara Chowdhury, Md Shihab Hossain, Md Sajedul Karim Chy, Md Shawon Islam

13:40-14.00 Paper ID 262: Machine Learning-Based Framework for Early and Age-Inclusive Detection of Autism Spectrum Disorder Using U.S. Screening Data
Mohammad Anisur Rahman, Intiser Isla, Shariar Islam Saimon, Md Rafiuddin Siddiky, Md Mahadi Hasan, Hasan Mahmud Sozib, Romana Nourin Nipa, MD. Jahid Hassan, Seaam Bin Masud

14.00-14.20	Paper ID 282: Cybersecurity Laws and Their Impact on Business Practices Syeda Farjana Farabi, Mani Prabha, Md Asikur Rahman Chy, Md Abdul Barek Saju, Md Wali Ullah, Md Kamruzzaman
14.20-14.40	Paper ID 169: Attention Thresholds for Brand Impact John Hawkins, Shannon Bosshard
14.40-15.00	Paper ID 172: Enigme: Generative Text Puzzles for Evaluating Reasoning in Language John Hawkins

Session 3: Audio Engineering And Acoustics

Session chair: ***Nachanant Chitanont, KMITL***

Maithon room

13:20-13.40	Paper ID 289: Design and build of a multi-zone beamforming speaker Khemapat Tontiwattanakul, Jiraphat Sueprasert, Dech Nawik, Pitak Thumwarin, Nachanant Chitanont
13:40-14.00	Paper ID 285: Vibroacoustic Study of Tonewood and Solid-body Guita Khemapat Tontiwattanakul
14.00-14.20	Paper ID 153: The Trapezoidal Khim: Sound Radiation of G Notes Natcha Techaaphonchai, Worakrit Thida, Kittipitch Meesawat, Phonlasit Thinnakorn Na Ayuthaya, Pakaphol Chitsakul, Sorasak Danworaphong
14.20-14.40	Paper ID 369: Development and Preliminary Evaluation of a Wireless Acoustic Sensor Network for Environmental Noise Monitoring Kittipitch Meesawat, Wanut Padee, Worakrit Thida, Krittika Lertsawat, Sorasak Danworaphong
14.40-15.00	Paper ID 156: Efficient Modeling of ITD Based on Anthropometrics and KEMAR ITD coefficients using Deep Neural Networks Saif S. Alotaibi, Mark Wickert

Session 4: Computer Science And Information Technology-03

Session chair: ***Wimonnat Sukpol, KMITL***

Bon room

13:20-13.40	Paper ID 173: Portable Signboard Size Measurement for Tax Collection Vachara Viriyakul, Siwakorn Noisundod, Faikaew Chayawattana, Pacharapol Chokkhun, Krittipoom Tienngam, Thanakrit Phansima, Parita Nawaree, Charoen Vongchumyen
13:40-14.00	Paper ID 177: Laser Pigeon Deterrent Vachara Viriyakul, Paramee Chumsri, Faikaew Chayawattana, Peerapat Sattapornnara, Charoen Vongchumyen
14.00-14.20	Paper ID 288: Fin Coil Dent Detection Using Deep Learning Akapot Tantrapiwat, Unnat Pinsopon

14.20-14.40	Paper ID 162: AI-Driven Adaptive Traffic Signal Control: Enhancing Urban Mobility with Deep Multi-Agent Reinforcement Learning Vaishali Savale, Swapnil Rajendra Patil, Urja Wagh, Uzair Sajid Tajma, Yashodip Vinod Undre
14.40-15.00	Paper ID 159: Optimizing Traffic Flow and System Efficiency in Networks Through AI-Driven Management Sudhakar Kumar, Sunil K. Singh, Janvi Sharma, Rima Kumari, Priyanka Chaurasia, Kwok Tai Chui, Brij B. Gupta

Session 5: Computer Science And Information Technology-04

Session chair: ***Chanin Bunlaksananusorn, Suzanna Suzanna***

Hay room

15:15-15:35	Paper ID 154: Advanced Car Rental System: Integrating Blockchain, AI, and Real-Time Inventory Management for Enhanced User Experience Sokyna Alqatawnah, Muhammad Tayyib
15:35-15:55	Paper ID 158: Improving Childrens Reading And Writing Abilities By Utilizing Augmented Reality Suzanna, Harco Leslie Hendric Spits Warnars, Mahaning Indrawaty Wijaya, Diana
15:55-16:15	Paper ID 216: A study on developing a robust screen navigation pattern for SwiftUI based iOS Applications Shubham Kamdi
16:15-16:35	Paper ID 280: AI-enhanced Cyber Threat Detection: Transforming Security Frameworks in Management Information Systems Niropam Das, Jahid Hassan, Partha Chakraborty, Jobanpreet kaur, Syed, Nazmul Hasan, Mohammad Abdul Goffer, Kazi Bushra Siddiqa, Rakibul Hasan
16:35-16:55	Paper ID 139: Comparative Analysis of Common Compression Algorithms for Sentinel-2 Multispectral Band Compression Aljaz Zel, Domen Mongus, Borut Zalik
16:55-17:15	Paper ID 101: Predicting the Winning Percentage of IPL Cricket Team using Machine Learning and Comparison between Different Algorithms Neloy Deb, Saravanan Chandran

Session 6: Computer Science And Information Technology-05

Session chair: ***Sukanya Vongtanaboon, KMITL***

Nakha room

15:15-15:35	Paper ID 271: Using the Analytic Hierarchy Process (AHP) for Decision Making in Tourism Product Distribution Channel Klinsukon Nimkanjana, Kornsirinut Rothjanawan

15:35-15:55	Paper ID 272: Development an Ontology Knowledge Base for Biodiversity, Identify plants of Community forest: A Case study of Baan Wang sai Community Klinsukon Nimkanjana, Premjit Ruengsawat, Sarit Panjan
15:55-16:15	Paper ID 279: Automated Assembly Machine Stopping System Using Machine Learning for Electrical Failure Prediction in Hard Disk Drive Manufacturing Tanakrit Panjasamanwong, Bundit Thanasopon
16:15-16:35	Paper ID 136: Application of Deep Learning Techniques for Predicting Leaf Lesions in KDML105 Rice Variety Sittisak Promtara, Watanyoo Suksa-ngiam, Pornchai Mongkolnam
16:35-16:55	Paper ID 278: Integrating Machine Learning For Automated Root Cause Analysis Of Critical-To-Quality (CTQ) In Hard Disk Drive Manufacturing Mullika Inpang, Bundit Thanasopon
16:55-17:15	Paper ID 245: Enhancing a Creative Support Tool with the TRIZ Method: A Textile Design Prototype Utilizing Projection Mapping. Chanathinat Chaiyapoo, Jakraphan Chaopreecha, Chutima Changpum, Nicha Tovankasame

Session 7: Computer Science And Information Technology-06

Session chair: ***Suphamit Chittayasothorn, Putsadee Pornphol***

Maithon room

15:15-15:35	Paper ID 150: Recognition of Marijuana Plant Leaf Diseases Based on Deep Learning Qingye Kong, Siraphop Tooprakai
15:35-15:55	Paper ID 155: Indoor Object Detection for Autonomous Mobile Robots (AMRs) Using YOLOv5s and Grad-CAM Nafiz Fahad, Md. Jakir Hossen, Md. Shohel Sayeed
15:55-16:15	Paper ID 118: Sustainable Waste Management: Enhancing Efficiency with Vehicle Routing Optimization Techniques Nichaphat Phurichteerarat, Auksarapuk E-dee, Anuwat Boonmechot, Thapanita Thongpap, Lakkana Ruekkasaem, Pongchanun Luangpaiboon
16:15-16:35	Paper ID 122: Explainable AI to enhance demand forecasting model for autonomous taxis in smart cities Adeel Munawar, Mongkut Piantanakulchai
16:35-16:55	Paper ID 283: Some Practical Aspects of the Relational Database Normalization Process Putsadee Pornphol, Suphamit Chittayasothorn
16:55-17:15	Paper ID 270: Predicting Faulty Production Lines Causing Head Gimbal Assembly Damage from Electrostatic Discharge Using Machine Learning Nuttanon Bilgasun, Bundit Thanasopon

Session 8: Computer Science And Information Technology-07

Session chair: ***Wimonnat Sukpol, KMITL***

Bon room

15:15-15:35	Paper ID 252: Fine-Tuning AI Models with Limited Resources Kritsada Singhapoo, Akarachai Inthanil, Attapon Pillai
15:35-15:55	Paper ID 251: Development of adventure games and puzzle solving in mysterious museums Kriangkrai Phutongkan, Akarachai Inthanil, Attapon Pillai
15:55-16:15	Paper ID 111: A Comparative Analysis of Machine Learning Algorithms for Allergy Scale Prediction Aumnat Tongkaw, Sasalak Tongkaw
16:15-16:35	Paper ID 175: Quality Classification of Sunglasses Lens by Deep Learning Charin Theskham, Kietikul Jearanaitanakij
16:35-16:55	Paper ID 149: Image Processing Threshold of Acetabulum Porosity for Age Estimation Supachard Krudtong, Pasuk Mahakkanukrauh, Nipon Theera-Umpon
16:55-17:15	Paper ID 174: An Ensemble model of Dual learning for Gambling and Pornographic Websites Classification Sirapat Thianphan, Kietikul Jearanaitanakij

Session 9: Computer Science And Information Technology-08

Session chair: ***Attapon Pillai, KMITL***

Hay room

09.00-09.20	Paper ID 180: A Hybrid Greedy Algorithm for the Capacitated Vehicle Routing Problem Udom Janjarassuk
09.20-09.40	Paper ID 134: Blockchain As A Notarization System For Military Data Sharing Chatchawan Chamnikul, Amnach Khawne
09.40-10.00	Paper ID 249: Feature Engineering and Optimization of Convolutional Neural Network in Classifying Tikog Leaf for Banig Weaving Industry Las Johansen B. Caluza, Arnel C. Fajardo
10.00-10.20	Paper ID 370: A Predictive Framework for Marine Microplastic Pollution Using Machine Learning and Spatial Analysis Epifelward Niño O. Amora
10.20-10.40	Paper ID 114: Smart Notification and Automated Reboot System for Cloud-Hosted Bitbucket Server Sk Tausif Rahman
10.40-11.00	Paper ID 266: Evaluation Of Academic Ethics Among Students In The Utilization Of Generative Artificial Intelligence For Self-Directed Learning Sabrina eunike tamaris

Session 10: Instrumentation And Control Engineering-01

Session chair*: Noppadol Maneerat, Tanagrit Chansaeng*

Nakha room

09.00-09.20	Paper ID 140: Linear Interpolation using Siemens S7-1200 Noppadol Maneerat, Tharathorn Wongworrada, Thepjit Cheypoca
09.20-09.40	Paper ID 286: Design and Development of a Portable Static Stability Training System Manutchanok Jongprasithporn, Nantakrit Yodpijit
09.40-10.00	Paper ID 147: Real-Time Production Monitoring System: An IoT and Open-Source Solution for SMEs Manisra Baramechai, Vorrapath Kokaew
10.00-10.20	Paper ID 113: Development of a Real-Time Water Monitoring and Alert System for Sustainable Aquaculture in the Tapi River Prasert Nonthakarn, Sulaiman Madyod, Chariya Nonthakarn
10.20-10.40	Paper ID 141: Apply PLC to Control 3-Axis Machines Thepjit Cheypoca, In Thaiyai, Noppadol Maneerat
10.40-11.00	Paper ID 123: Machine Learning Approach to CMYK Label Identification through Screen Angles Chitsanuwit Ar-Karachaiphong, Farzin Asadi, Asst. Prof. Dr. Krit Smerpitak

Session 11: Telecommunications And Networking

Session chair*: Nattapan Suwanasuko, Akarachai Inthanil*

Maithon room

09.00-09.20	Paper ID 119: Real-Time Locating Systems: A bibliometric analysis Letizia Tebaldi, Andrea Volpi, Giulia Azzolini
09.20-09.40	Paper ID 253: Intelligent Multi-Link Selection for IEEE 802.11be Using Reinforcement Learning with Radiation Pattern Awareness Bhurisub Dejpipatprach, Akarachai Inthanil, Wimonnat Sukpol, Worrarat Jongkraijak
09.40-10.00	Paper ID 254: Modeling the Performance of Wi-Fi Networks Using 5GHz, 6GHz, and Multi-Link Operation Wimonnat Sukpol, Akarachai Inthanil, Bhurisub Dejpipatpracha
10.00-10.20	Paper ID 109: A Dual-Band Implantable Antenna with Flag-Inspired Patch and Grounded Structure Rula Alrawashdeh
10.20-10.40	Paper ID 121: A Flexible Loop Sensor Antenna for Ice and Frost Detection Rula Alrawashdeh
10.40-11.00	Paper ID 273: The Impact of User Engagement in Social Commerce: A Conceptual Framework

Hanny Juwitasary, Norizan Anwar, Mohd Nasir Ismail, Yohannes Kurniawan, Violitta Yesmaya

Session 12: National Technical Session 2

Session chair*: Hanphon Mitwong, Somsak Limwougsakorn*

Bon room

09.00-09.20	Paper ID 342: Effect of flow plate design on fuel cell efficiency Jaruporn Saiyasupee
09.20-09.40	Paper ID 160: A Study of Steam Storage Area Ratio in Pressure Vessels Affecting Water Pumping Performance of Steam-Powered Water Pumps Pakorn Promkaew, Goffaree Hemmin, Nattapon Dadsadachan
09.40-10.00	Paper ID 258: Design And Development Of A Honey Filling Machine For Miniature Glass Bottles Komkit Seepan, Witchayut Srisuwan
10.00-10.20	Paper ID 363: Development of a cost-effective prototype for measuring the viscosity of liquids Nattapong Thuedam, Thitima Thanyaniti
10.20-10.40	Paper ID 142: Development Of A Straw Cutting Machine From Krajood Using A Pneumatic System Komkit Seepan, Peerapong Nuchuay, Mintra Trongtorkarn

Session 13: Computer Science And Information Technology-09

Session chair*: Siraphop Tooprakai, Nasith Laosen*
Hay room

13.00-13.20	Paper ID 110: AI Technology Application, Labor Force Heterogeneity, and Urban Productivity Weiyi Yue, Xianghong Zhou
13.20-13.40	Paper ID 104: Applying Generative AI for Fraud and Cybercrime Prevention in Thailand Chairat Thanomwong, Korn Puangnak, Natworapol Rachsiriwatcharabul, Manthana Tiawongsuwan
13.40-14.00	Paper ID 268: Real Time Intrusion Detection System using AI&ML Sangita M. Jaybhaye, Pratham P. Chintawar, Chetan D. Niwate, Aditya R. Narke, Arya V. Sawant
14.00-14.20	Paper ID 105: Warped-Frequency Cepstral Coefficients for Improving COVID-19 Detection Sandeep B. Sangle, Pramod H. Kachare, Jagannath Nirmal, Mohammed Alhameed, Ibrahim Al-Shoubarji
14.20-14.40	Paper ID 218: Video Captioning with Vision Based Emotion-Detection Using LSTM, CNN Reethika Nagineni, Nagaraju Devarakonda, T. Leela Gowtham, Swaroop Meda

14.40-15.00	Paper ID 176: Machine Learning for Stress Detection: A LightGBM-Based Approach Mohammad Rabib Uddin, Md. Saniat Rahman Zishan, Shameem Ahmad

Session 14: Instrumentation And Control Engineering-02

Session chair : *Chanin Bunlaksananusorn, Vadivel Rajarathinam*

Nakha Room

Krerk Puangnak

13.00-13.20	Paper ID 277: Effective Bowel Sound Source Localization Based on Sensor Configuration: A Preliminary Index Approach Kenji Takawaki, Takeyuki Haraguchi, Takahiro Emoto
13.20-13.40	Paper ID 168: Re-envisioning On-Ground Aircraft Movement using Reinforcement Learning Anurag Vallur, Anuj Jain, Anirudh Sridhar, Adi M., T.S. Chandar
13.40-14.00	Paper ID 107: A Design and Experimental Study of Fog Spraying into the Greenhouse Roof for Radiation and Relative Humidity Control Sakapan Klaydokjan, Nathaporn Suwanpayak, Kamonwan Chucheep
14.00-14.20	Paper ID 166: Application of 3D printer to create a splint pet Pipat Phaisalpanumas, Acting Sub Lt. Nattasit Monkaew, Damisara Chutikan, Premporn Khemavuk, Narin Tammarugwattana, Sirichai Tammaruckwattana
14.20-14.40	Paper ID 167: Prototype of Chipping and Briquetting Machine for Eucalyptus Wood Processing Pipat Phaisalpanumas, Nattarat Namboot, Damisara Chutikan, Chartchai Usadornsak, Naritsak Tantitippawan,Sirichai Tammaruckwattana
14.40-15.00	Paper ID 187: An Innovative Advancement in Vibration-Assisted Steam Sensing Technology (VASST) Farhan Al-Enazi, Hassan Al-Qarni, Mohammed Al-Subaie Ali Ghazwani, Hassan Al-Ali, Muhammad Azhar Khan, Abdul Aziz Afzal

Session 15: Electrical & Electronic Instrumentation & Control
Session chair : *Thanadol Tiengthong, Akarachai Inthanil*
Maithon room

13.00-13.20	Paper ID 287: Improving Accuracy in Image-Recognition Systems With Techniques for Handling Similar-Looking Items in Inventory Management Asst. Prof. Dr. Krit Samerpitak, Assoc. Prof. Dr. Sawai Pongswatd, Asst. Prof. Sart Kummool
13.20-13.40	Paper ID 191: Numerical Study of 500 kHz Electromagnetic Wave Irradiation for Root Canal Sterilization in Apical Periodontitis Treatment Yanakorn Srianant, Thanadol Tiengthong, Masatake Akutagawa, Hiromichi Yumoto, Toshihiko Tominaga

13.40-14.00	Paper ID 256: Accuracy Analysis of Indoor Positioning Using Min-Max Method Pichaya Supanakoon, Wipassorn Vinicchayakul, Sirinya Tabsombat, Thanadol Tiengthong, Sathaporn Promwong, Monchai Chamchoy
14.00-14.20	Paper ID 116: Mosquito Trap HV Power Supply Turn On/Off Time Parameter Consideration Measurement. Jirawath Parnklang, Nattanicha Sowannee, Kasamaphon Pakhunophat, Siriwat Ganasut, Pasuthida Wisitthikorn, Tanutpong Ramkaow
14.20-14.40	Paper ID 275: Interdigitated Extended Gate Field Effect Transistor for pH Sensor Based on Porous Silicon Layer Narin Atiwongsangthong
14.40-15.00	Paper ID 115: Parallel power supply half-bridge topology with CV Mode 0-150 V and CC Mode 0-5A Theerapat Antachai, Weera Pengchan, Supakorn Suwan

Session 16: National Technical Session 3

Session chair*: Suthathong Homya, Urairat Makchan*

Bon room

13.00-13.20	Paper ID 284: Impact of Land Use Changes on Discharge in Phuket Watershed Sukanya Vongtanaboon, Suthathong Homya, Pongsakorn Kaewmanee, Pobtham Prompen
13.20-13.40	Paper ID 179: Types and Physical Composition of Solid Waste from Textile Dyeing with Eco-Printing Technique Suthathong Homya, Sukanya Vongtanaboon, Phurinat Paladsongkhram, Pahol Rongkul, Siri Jaroenjai, Kanokporn Tangsabpaiboon
13.40-14.00	Paper ID 353: Forecasting the Trend of Undergraduate Applications at Phuket Rajabhat University using the Linear regression Sakuna Choochangwang, Aricha Tabmuenwai, Attapon Pillai, Urairat Makchan
14.00-14.20	Paper ID 350: Forecasting Undergraduate Student Enrollment at Phuket Rajabhat University Using a Logistic Regression Model Sasina Srithong, Nissareen Sangmuaeng, Urairat Makchan, Attapon Pillai
14.20-14.40	Paper ID 361: Forecasting Trend of Undergraduate Applications at Phuket Rajabhat University Using Time Series Analysis Acharaporn Chooklam, Nuttapon Takursuk, Attapon Pillai, Urairat Makchan

Session 17: Instrumentation & Control Engineering- Computer Science & Information Technology

Session chair: *Chanin Bunlaksananusorn, KMITL*

Hay room

15:15-15:35	Paper ID 108: Unmasking Emotions: Creating Deepfake to Detect Real Feelings Darpan Rokade, Meenal Jabde, Dr. C.H. Patil
15:35-15:55	Paper ID 106: Machine Learning Analysis of Mobile Nanosensors for Monitoring and Abnormality Detection in Vascular Networks Hassaan Daoud
15:55-16:15	Paper ID 128: Compensation Motion and Calibration for Scale Calibration Machine Siriwat Kitsompong, Yuttana Hongaromkij
16:35-16:55	Paper ID 269: Energy-Efficient Motion Planning for Dual-Arm Collaborative Robots Using a Digital Twin Ruj Kantabussabong, Chinnawut Nantabut, Watcharin Pongaen, Nuttapon Rothong, Borihan Butsanlee

Session 18: Electrical Engineering

Session chair: ***Norasage Pattanadech, Dr.Vadivel Rajarathinam***

Nakha room

15:15-15:35	Paper ID 255: Integration of Charcoal Kiln Waste Heat in a Thermal Water Pump System Pakorn Promkaew, Pathiwat Waramit, Bundit Krittacom, Jirawat Sitranon Panusak Moonsri
15:35-15:55	Paper ID 260: A Fuzzy Multi-Criteria Decision-Making Approach for Ranking Renewable Energy Systems Based on Economic and Environmental Aspects Danupun Visuwan, Atiwat Nanphang, Pongchanun Luangpaiboon Apirak Tepvarin
16:15-16:35	Paper ID 125 Hamiltonian Control Law for Primary-Side Multi-Phase Interleaved Buck Converters for Inductive Wireless EV Charging Thanet Sriprom, Anon Namin, Uthen Kamnarn, Burin Yodwong, Pongsiri Mungporn, Ehsan Jamshidpour, Serge Pierfederici, Babak Nahid-Mobarakeh, Phatiphat Thounthong
16:35-16:55	Paper ID 261 Thermal Flow Analysis of Inverter Integrated Permanent Magnet Type Synchronous Motor Using Computational Fluid Dynamics Jong-Min Baek, Hyung-Woo Lee, Chan-Bae Park, Jae-Bum Lee, Kwang, Woo Chung, Seok-Min Hong, Choung-Seo Kim, Ha-Min Park Pathaya Ruangroengkulrit, Sasalak Tongkaw

Session 19: Electrical Engineering

Session chair: Thanadon Mankong, ***KMITL***

Maithon room

15:15-15:35	Paper ID 248: Partial Discharge Identification in High-Voltage Systems Using Frequency Extraction and Machine Learning Techniques Tai bandisak, Krissana Romphuchaiyapruek, Sarawut Wattanawongpitak
15:35-15:55	Paper ID 112: Power Quality Enhancement in Hybrid PV-Battery Systems Using DSTATCOM Sina vafi, K. Debnath
15:55-16:15	Paper ID 138: A Synergistic Approach to Transformer Failure Analysis: Weibull-Cox Modelling and Machine Learning meets SHAP Explainability Sanika Zope, Satish Chavan, Dr. Nitin Zope, Rohan Pawar
16:15-16:35	Paper ID 135: Deep Learning Approach for Short-term Power Forecasting of Solar Photovoltaic System Rahma Aman, Astitva Kumar, M. Rizwan

Session 20: Electrical Engineering

Session chair: ***Nasith Laosen, Tanagrit Chansaeng***

Bon room

15:15-15:35	Paper ID 343: Development of a GPS-based Prayer Times Mobile Application for Thai Muslims Basil Salee, Thanawat Saejia, Nasith Laosen
15:35-15:55	Paper ID 349: 3D Game Prototype Introduction to Flight Travel Procedures Case study : Phuket International Airport Tanunchai Chamnina, Thanakorn Saelee, Urairat Makchan
15:55-16:15	Paper ID 348: Development of multimedia for online learning on sewing Ratthasat Roungsea, Tanawut Chumphol, Urairat Makchan
16:15-16:35	Paper ID 354: Development of a Chatbot Application for Student Information Services at Phuket Rajabhat University Assada Chorraka, Bhurisub Dejpipatpracha, Poomsatit Mattajit

ICEAST 2025 Program: Friday, May 9, 2025

13:00 – 19:30 Technical Workshop

TRACK 1
ELECTRICAL ENGINEERING

Parallel power supply half-bridge topology with CV Mode 0-150 V and CC Mode 0-5A

Theerapat Antachai, Weera Pengchan* and Supakorn Suwan
Department of Electronics Engineering, School of Engineering
King Mongkut's Institute of Technology Ladkrabang, Bangkok, Thailand
63601103@kmitl.ac.th , *Corresponding: weera.pe@kmitl.ac.th, supakorn.su@kmitl.ac.th

***Abstract*— A single power supply may not be sufficient for certain applications. Therefore, increasing the power output of power supplies can be achieved by connecting them in series or parallel configurations to provide the required power to the load. This paper presents a method for increasing power capacity by paralleling two or more power supplies to increase the current output of a single power supply. A half-bridge topology structure is used, with each module output voltage can adjustable from 0–150 V and current 0-5 A, maximum power output 750 W. Maximum load regulation 0.8% and efficiency 89% can be achieved. This system can balance output currents between the master and slave within 2.3 seconds and error output current is +0.11 A.**

Keywords—parallel power supply, load share, half-bridge topology, compensation network

I. INTRODUCTION

Parallel operation of power supplies to balance output current, known as the "Load Sharing Technique" [1], ensures that the output current from each power supply is equal. This technique is critical for systems where multiple power supplies work together to meet high power demands or provide redundancy. Load sharing can be implemented using two primary methods 1. Passive load sharing: This method uses a droop resistor (R_{Droop}) [2] connected in series with the output of each power supply to program the output impedance. While simple, this approach reduces system efficiency due to voltage drops across the resistors. 2. Active Load Sharing: This method employs by add a feedback loop control, often involving Oring MOSFETs, to adjust the output impedance of each power supply. However, it may still face efficiency issues. An alternative approach discussed in this paper is the Master-Slave load sharing [3][4]. The system architecture, illustrated in Figure 1, comprises a master power supply and a slave power supply. The slave monitors the voltage at the load share bus (CSA1) and compares it with its own output current measurement (CSA2). This feedback loop ensures that the output currents of both power supplies are equal, achieving precise load sharing with minimal error.

Control circuit design and compensation network [5]. This paper also presents the design of a control circuit for adjusting the output voltage and current of the power supply using an error amplifier. To maintain system stability and prevent oscillations, a compensation network is designed and analyzed through transfer functions and Bode plots. Key design criteria include system must have a phase margin greater than 45° to ensure stability, Crossover frequency should be between (1/10) and (1/5) of the switching frequency to enhance transient response.

II. CONSTUCTION DESIGN

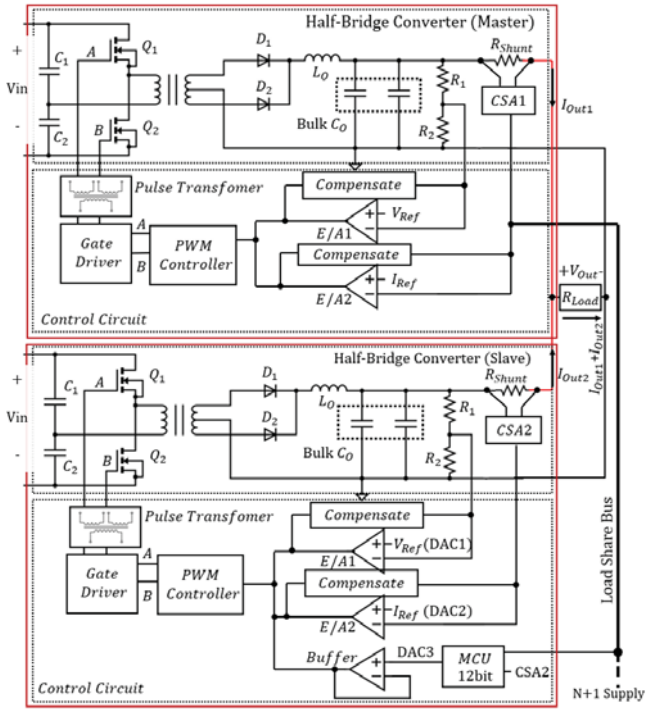


Fig. 1. Block diagram parallel power supply dedicate master-slave half-bridge topology

The power supply system uses an isolated half-bridge topology. with each module comprising MOSFETs (Q_1, Q_2) controlled by a PWM Controller IC (SG3525). The PWM signals are processed through a gate driver (TC4427) and then transmitted to the MOSFETs via an isolation pulse transformer with an EE30 ferrite core and a 20:20:20 turns ratio. In this design, capacitors C1 and C2 (with $C_1 = C_2$) function as a voltage divider, reducing the voltage applied across the primary winding of the switching transformer to half of the input voltage ($V_{In}/2$). Voltage transfer from primary side to the secondary side by ratio N_s/N_p, where it is rectified by fast-recovery diodes D1 and D2. The use of low trr (reverse recovery time) diodes to minimizing switching losses and enhancing performance. The rectified output is filtered through an LC filter comprising an inductor (L_O) and a capacitor (C_O) to obtain a stable DC voltage. For current measurement, a high-side current sensing technique is employed. The current is measured using a shunt resistor (R_{Shunt}) and apply voltage across resistor to isolated current sense amplifier (CSA).

III. CONTROL CIRCUIT DESIGN

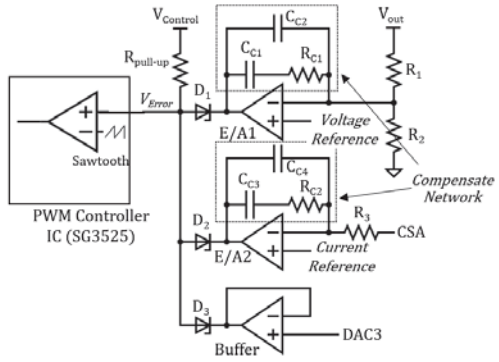


Fig. 2. Control circuit error voltage amplifier for constant voltage & current control

The control circuit consists of an operational amplifier (TLC272) functioning as an error amplifier (E/A). The first error amplifier (E/A1) controls the output voltage, while the second (E/A2) control output current, both configured with a compensation type-II network. A buffer adjusts the error voltage (V_{Error}) through DAC3 when the power supply operates in parallel mode, as shown in Figure 2. Output of each op-amp connects to a Schottky diode (1N5819) to prevent short circuit at the output op-amp. Schottky diodes are selected due to their low forward voltage drop (typically 0.1–0.2 V), which suits the design where the sawtooth signal has a 0.3 V offset and peak voltage typical is 3.3 V. The voltage error signal is modulated with the sawtooth waveform within the PWM controller IC. It is essential to ensure that the minimum voltage of the sawtooth signal is higher than the Schottky diode's forward voltage to ensure complete shutdown of the PWM signal.

To adjust the output voltage (V_{out}) and output current (I_{out}) of a half-bridge converter, the reference voltage (V_{ref}) and current reference (I_{ref}) of each operational amplifier can be modified. The output voltage and output current can be determined using the following equations:

$$V_{out} = \left(\frac{R_1}{R_2} + 1\right) V_{ref} \tag{1}$$

$$I_{out} = \frac{I_{ref}}{CSA \cdot R_{Shunt}} \tag{2}$$

The RC compensation network ensures stability in the control loop, especially in high-frequency switching applications like a half-bridge converter. Properly designed RC compensation helps to prevent unwanted oscillations and subharmonics.

A. Design compensate constant voltage control

In constant voltage mode control, regulation is managed by E/A1. The output voltage of the half-bridge converter is divided by resistors R_1 and R_2 and fed into the inverting input of E/A1, where it is compared with the voltage reference at the non-inverting input. Under this operating condition, diodes D2 and D3 remain in reverse bias, allowing the effects of E/A2 and buffer to be disregarded in circuit analysis.

The transfer function characteristic is illustrated in Figure 3. The loop control system consists of three main components: the half-bridge converter filter ($H_{Filter(S)}$), the modulator ($H_{Mod(S)}$) ,and the compensation network ($H_{Compensate(S)}$). This diagram half-bridge converter must be operated in continuous conduction mode (CCM).

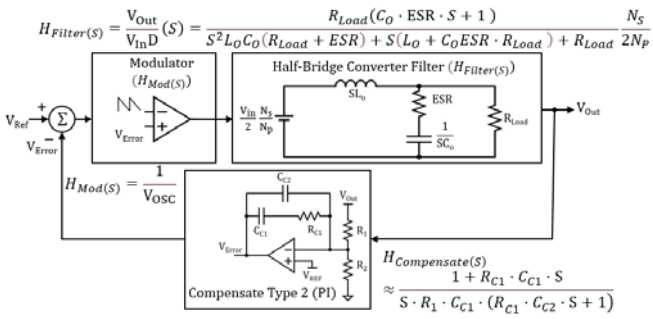


Fig. 3. Block diagram loop control constant voltage mode control half-bridge converter continue conduction mode

Minimum output inductance (L_O), required for a half-bridge converter operating in continuous conduction mode can compute follow equation (3).

$$L_{o(min)} = \frac{\left(\frac{N_p V_{In}}{2N_s} - V_{Out}\right) \cdot V_{Out}}{\frac{N_p V_{In}}{2N_s} \cdot 2f_{SW} \cdot I_{Out(max)} \cdot r} \tag{3}$$

In the calculation, the following parameters are defined: input voltage (V_{In}) = 311 V, output voltage V_{Out} = 0-150 V, switching transformer ratio N_p/N_s = 17/19, switching frequency (f_{SW}) = 70 kHz, maximum output current ($I_{Out(max)}$) = 5 A, inductor ripple current ratio (r) = 0.3. Based on the formula (3), the minimum inductance required to ensure that the DC-DC converter remains in Continuous Conduction Mode (CCM) is calculated to be 200 µH at an output voltage of 86.9 V. For practical implementation, the values chosen for the circuit is 250 µH

The output capacitance is selected as 1000+680 μF with an estimated equivalent series resistance (ESR) of 0.25 Ω. The transfer functions of the filter and modulator ($H_{Filter(S)} \cdot H_{Mod(S)}$), are shown in Figure 4.

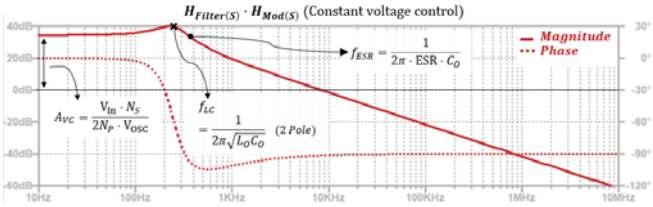


Fig. 4. Bode plot constant voltage loop control half-bridge converter without compensate

In Figure 4, system $H_{Filter(S)} \cdot H_{Mod(S)}$ has two pole, which is generated by the output inductor and output capacitor, resulting in a frequency of f_{LC} = 246 Hz. the zero is generated output capacitor and its equivalent series resistance, resulting in a frequency of f_{ESR} = 379 Hz.

R_{C1}, C_{C1}, C_{C2} in compensate network can be calculated by these formula (4-6). And define R_1 = 30 kΩ, V_{OSC} = 3.3 V.

$$R_{C1} = \frac{2N_p \cdot R_1 \cdot f_{ESR} \cdot V_{OSC} \cdot f_0}{N_s \cdot V_{In} \cdot f_{LC}^2}, \quad C_{C1} = \frac{1}{1.5\pi \cdot R_{C1} \cdot f_{LC}}, C_{C2} = \frac{1}{2\pi \cdot R_{C1} \cdot f_{SW}} \tag{4-6}$$

f_0 is Cross over frequency equal 1/5 Switching Frequency

Thus, R_{C1}, C_{C1}, C_{C2} are calculated to be 50.11 kΩ, 17.29 nF and 45.47 pF, respectively. For practical implementation, the values chosen for the circuit are 50 kΩ, 22 nF, and 47 pF, respectively. The Bode plot of the function for $(H_{Filter(S)} \cdot H_{Mod(S)} \cdot H_{Compensate(S)})$ is shown in Figure 5.

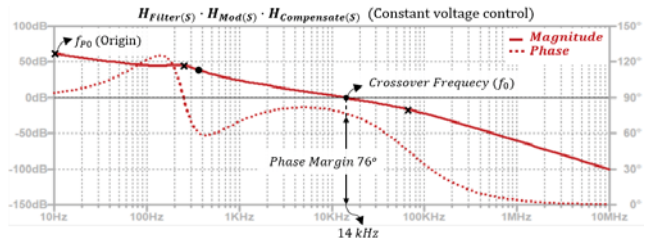
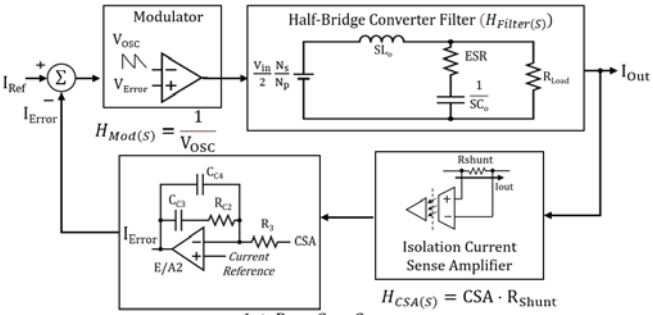


Fig. 5. Bode plot constant voltage loop control half-bridge converter with compensate

B. Design compensate constant current control

Constant current mode control is managed by Error Amplifier 2 (E/A2). In this mode, the output current is measured across a shunt resistor, amplified through an isolation amplifier, and fed into the non-inverting input of the amplifier configured with a type-II compensation network. Under this condition, diodes D_1 and D_3 are in reverse bias, allowing the effects of E/A1 and the buffer to be disregarded in circuit analysis. The block diagram of this configuration is shown in Figure 6.

$$H_{Filter(S)} = \frac{I_{Out}}{V_{In} D}(S) = \frac{R_{Load}(C_O \cdot ESR \cdot S + 1)}{S^2 L_O C_O (R_{Load} + ESR) + S(L_O + C_O ESR \cdot R_{Load}) + R_{Load}} \frac{N_S}{2N_P R_{Load}}$$



$$H_{Compensate(S)} \approx -\frac{1 + R_{C2} \cdot C_{C3} \cdot S}{S \cdot R_1 \cdot C_{C3} \cdot (R_{C2} \cdot C_{C4} \cdot S + 1)}$$

Fig. 6. Block diagram loop control constant current mode control half-bridge converter continue conduction mode

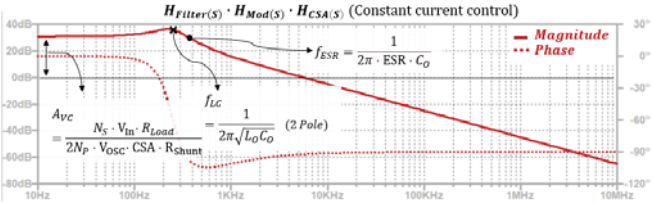


Fig. 7. Bode plot constant current loop control half-bridge converter without compensate

R_{C2}, C_{C3}, C_{C4} in compensate network can be calculated by these formula (7-9). And define R_3 = 5 kΩ, R_{Shunt} = 10 mΩ, CSA = 66.667, R_L = 1 Ω.

$$R_{C2} = \frac{2N_p \cdot R_3 \cdot f_{ESR} \cdot V_{OSC} \cdot f_0}{N_s \cdot V_{In} \cdot f_{LC}^2} \cdot \frac{R_{Load}}{CSA \cdot R_{Shunt}},$$
$$C_{C3} = \frac{1}{1.5\pi \cdot R_{C2} \cdot f_{LC}},\ C_{C4} = \frac{1}{2\pi \cdot R_{C2} \cdot f_{SW}} \quad (7\text{-}9)$$

Thus, R_{C2}, C_{C3}, C_{C4} are calculated to be 12.53 kΩ, 66.47 nF, and 174.86 pF, respectively. For practical implementation, the values chosen for the circuit are 13 kΩ, 68 nF, and 220 pF, respectively. The Bode plot of the transfer function for $H_{Filter(S)} \cdot H_{Mod(S)} \cdot H_{CSA(S)} \cdot H_{Compensate(S)}$ is shown in Figure 8.

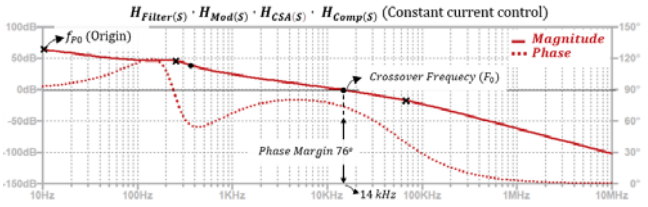


Fig. 8. Bode plot constant current loop control half-bridge converter with compensate

After designing the compensator for constant voltage and constant current control, a phase margin of 76° can be achieved, with a crossover frequency (f_0) of 14 kHz at the point where the loop magnitude is 0 dB ($f_0 = f_{SW}/5$, f_{SW} = 70 kHz).

C. Design load share control

The load share control utilizes a load share bus as a common reference point, provided by the master power supply, to compare and balance the current differences between the master and slave power supplies. The dedicated master-slave configuration, where one power supply operates as the master and another as the slave. In this approach, an error amplifier is not employed due to the complexity of compensation. Instead, a digital control method is used, allowing flexibility and simplicity. The system adjusts the output voltage using a 12-bit (DAC3), which feeds the non-inverting input of an operational amplifier configured as a buffer.

The load-sharing control process begins by setting both DAC1 and DAC2 to their maximum values (4095, approximately 5V). This configuration ensures that the outputs of the error amplifiers E/A1 and E/A2 are also set to 5V, diodes D1 and D2 will operating in reverse bias. Consequently, the error voltage (V_{Error}) can be adjusted by output of the voltage buffer, where: $V_{Error} = V_{O_DAC3} + V_{Error}$. MCU monitors the output current of each power supply and compares it to the load share bus current, which serves as a reference provided by the master supply. If the output current of the slave supply is detected to be lower than the reference current, the MCU increases the DAC3 output by incrementing the DAC3 bit value. This increase in DAC3 output results in a higher V_{Error} which in turn increases the duty cycle of the PWM. Consequently, the output current of the slave supply rise, ensuring balanced current sharing between the master and slave supplies. The operation is illustrated in Figure 9.

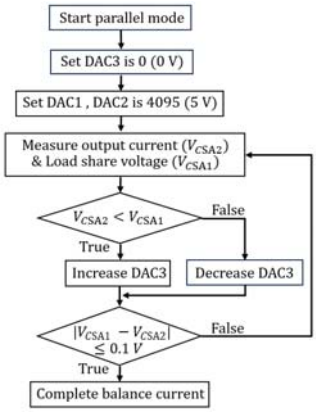


Fig. 9. Flowchart of start parallel mode

IV. HARDWARE CIRCUIT DESIGN

Figure 10. Show the hardware implementation of a parallel power supply with a dedicated master-slave structure.

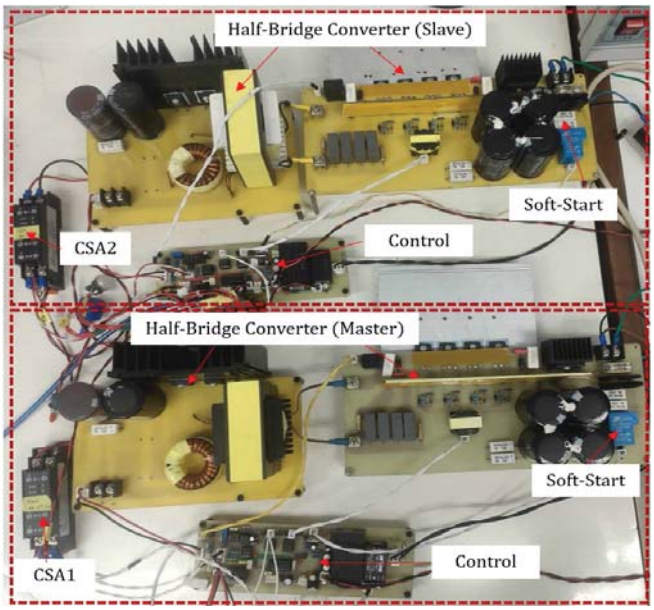


Fig. 10. Hardware circuit realized of dedicate master-slave half-bridge converters connected in parallel

TABLE I. HARDWARE COMPONRNT PARAMETER

Component	***Description***
C_1, C_2	Polypropylene capacitor (MKP) 2uF 250V
Q_1, Q_2	IPW65R080CFD CoolMOS (650V/43.3A) $R_{DS(on)}$ = 80 mΩ
T_1	Switching Transformer: EE65 Core, Material PC40 N_P = 17 turn ($L_m = 1.7\ mH$) N_S = 19 turn
D_1, D_2	HFA25PB60, Ultrafast Recovery diode (600V/25A), t_{rr} = 23 nS
L_o	Toroid core KS157060A, Inductance 250 µH
C_o	Electrolytic capacitors 1000 uF and 680 uF

V. TEST RESULTS

After assembly power supply hardware operates with an input voltage V_{In} = 311 V, f_{SW} = 70 kHz. Each power supply module features an adjustable output range of 0–150 V for CV and 0–5 A for CC without oscillation.

A. Load Regulation

The voltage regulation performance of each power supply was evaluated by varying the load current from 0-5 A across different output voltage 30, 50, 100, and 150 V, as shown in Figure 11. The maximum load regulation observed during testing is 0.8%. The system achieves an efficiency of up to 89%

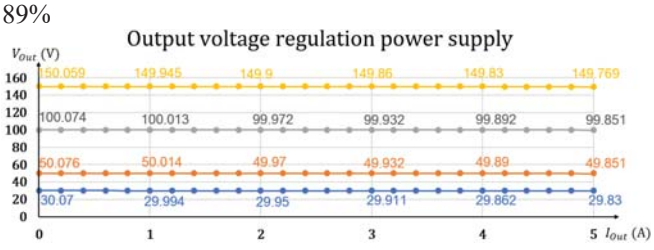


Fig. 11. Output voltage vs load current output voltage 30,50,100,150 V for load current variation from 0-5A

B. Respone and balnce load current Master & Slave

The response of the output currents from the master and slave load sharing. At t = 0 seconds, the master output current (I_{Out1}) begins at 5 A and slave output current (I_{Out2}) begins at 0 A. The system takes 2.3 seconds to balance the output currents, achieving $I_{Out1} = I_{Out2} = 2.5\ A$, as shown in Figure 12. The results for balance current at output voltages V_{Out} = 50, 100 and 150V respectively. The total output current ($I_{Out1} + I_{Out2}$) is steps of 1, 2, 6 and 10 A, respectively, as shown in Figure 13. The maximum difference in output current between the master and slave modules during operation is observed to be ±0.11 A.

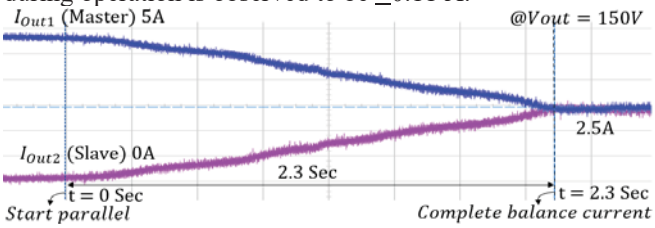


Fig. 12. Output current response for balance output current of master and slave

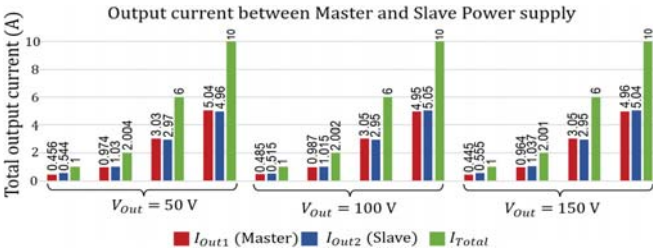


Fig. 13. Results balance output current master and slave

VI. CONCLUSION

A hardware power supply was designed and tested based on an isolated half-bridge converter topology. The system features a compensation type-II for error amplifier, ensuring stable operation without oscillation. Each module can deliver an adjustable output voltage of 0–150 V and a current of 0–5 A (750 W) each module. The system supports parallel operation using a dedicated master-slave configuration controlled by MCU. This system can balance output currents between the master and slave within 2.3 seconds, achieving an error output current ±0.11 A. Future improvements on further reducing the current balancing time by using PID control. The parallel configuration allows the system to deliver a combined output current of up to 10 A (1.5 kW), significantly enhancing its power delivery capability.

REFERENCES

[1] V. J. Thottuvelil and G. C. Verghese, "Analysis and control of paralleled dc/dc converters with current sharing," IEEE Trans. Power Electron., vol. 13, no. 4, pp. 635–644, July 1998.

[2] Bob Mammano and Mark Jordan, "Load Sharing with Paralleled Power Supplies", Unitrode Seminar 800, Topic 2, Sep 1991

[3] Y. Panov, J. Rajagopalan, and F. C. Lee, "Analysis and design of N paralleled DC-DC converters with master-slave current-sharing control," Proc. IEEE APEC'97, pp. 436–442, Feb 1997

[4] Y. Ling, L. Da, G. Song, and Y. Tang, "Master-slave control strategy for input-series output-parallel connected flyback converters," Proc. IEEE Conf. on Ind. Electron. and Appls., pp. 907-911, Jun. 2016.

[5] R. Sheehan, L. Diana "Switch-mode power converter compensation made easy", September 2016

Partial Discharge Identification in High-Voltage Systems Using Frequency Extraction and Machine Learning Techniques

Tai Bandisak
Department of Electrical and Computer Engineering, Naresuan University
Phitsanulok, Thailand
taib@nu.ac.th

Krissana Romphuchaiyapruek
Department of Electrical and Computer Engineering, Naresuan University
Phitsanulok, Thailand
krissana@nsru.ac.th

Sarawut Wattanawongpitak
Department of Electrical and Computer Engineering, Naresuan University
Phitsanulok, Thailand
sarawutw@nu.ac.th

***Abstract*— This study focuses on the analysis and identification of four types of partial discharge (PD) signals: internal discharge, surface discharge, positive needle corona discharge (Air Corona; High Voltage Needle), and negative needle corona discharge (Air Corona; Needle to Ground). The PD signals were measured in a high-voltage laboratory environment and recorded using an oscilloscope connected to a notebook equipped with IO Libraries suite, capturing time-domain data. Signal characteristics were extracted through Fast Fourier Transform (FFT), noise filtering, and histogram distribution analysis. Gaussian Curve Fitting was employed to identify primary and secondary features, which were subsequently used as inputs for a Feedforward Neural Network (FNN) model with one hidden layer. The model's performance was optimized by varying key parameters, including the number of input features, hidden layer nodes, validation set partitioning (k-fold), and learning rate. The optimal configuration, utilizing two input features (mean frequency of primary and secondary characteristics), five hidden nodes, k = 4 validation set, and a learning rate of 0.1, achieved superior identification performance with an accuracy of 90% and an F1-score of 90.7%. The results demonstrate the efficacy of the proposed methodology in accurately identifying partial discharge patterns, highlighting its potential for application in high-voltage electrical system diagnostics.**

Keywords*— *Partial Discharge Identification, Fast Fourier Transform, Gaussian Curve Fitting, Feedforward Neural Network, High-Voltage Diagnostics.

I. INTRODUCTION

High-voltage (HV) equipment is an essential element in contemporary power networks, facilitating the effective transmission and distribution of electrical energy. Nonetheless, the operational reliability of such equipment is frequently undermined by insulation deterioration, potentially resulting in catastrophic failures if not identified promptly. Partial discharge (PD) is a critical indicator of insulation degradation in HV equipment, including transformers, cables, and switchgear. Partial discharge (PD) denotes localized electrical discharges that fail to fully connect the electrodes, yet might gradually impair the insulating system over time [1]. Consequently, precise identification and surveillance of PD actions are essential. Precise identification and surveillance of PD operations are crucial for predictive maintenance and the durability of HV assets.

Traditional methods for PD detection and analysis rely on signal processing techniques and expert interpretation of data, such as phase-resolved partial discharge (PRPD) patterns. While these methods have been effective, they often require extensive expertise and are limited by their ability to handle large volumes of data and complex noise environments [2]. However, these methods often face challenges in distinguishing between different types of PD sources, especially in noisy environments or when multiple discharge mechanisms coexist [3].

Recent advancements in signal processing and machine learning (ML) have opened new avenues for more accurate and efficient PD identification. Frequency-domain analysis, particularly the frequency distribution of PD signals, has emerged as a promising approach to complement traditional time-domain methods. By analyzing the spectral characteristics of PD signals, it is possible to extract unique features that are less susceptible to noise and more representative of the underlying discharge mechanisms [4], [5]. This approach, combined with ML algorithms, enables the development of robust models capable of identifying PD types with high accuracy.

This study focuses on the application of frequency extraction analysis and ML techniques for PD identification in HV equipment. The objective is to develop a framework that combines frequency feature extraction with ML algorithms to achieve accurate and reliable identification of PD types. The proposed methodology is validated using experimental data collected from HV equipment under controlled conditions, demonstrating its effectiveness in real-world scenarios. This research enhances condition monitoring and diagnostic approaches for HV systems by overcoming the constraints of standard PD detection methods, hence improving operational dependability and safety.

II. PARTIAL DISCHARGE DETECTION

Partial discharge detection is an essential diagnostic instrument for evaluating the status of HV insulating systems. It can be categorized into two primary types: online and offline surveillance. Online methodologies, including ultrasonic partial discharge detection, acoustic sensors, and high-frequency current transformers (HFCT), provide real-time monitoring without disrupting power system operations. Offline procedures, including as high-potential testing, dissipation factor testing, and very low frequency (VLF) testing, are conducted during maintenance shutdowns [6]. The traditional partial discharge detection method, as stipulated by the IEC 60270 standard [7] is highly regarded for its remarkable accuracy in detecting and measuring PD. This standard is widely used to identify various types of discharges, such as internal discharge, surface discharge, and air corona. The standard testing circuit, as illustrated in Figure 1, includes several key components: a coupling capacitor (C_k), a filter (Z), the input impedance of the measurement system (Z_{mi}), a connecting cable, a coupling device, a measuring instrument, and the test object (C_a).

979-8-3315-4248-1/25/$31.00 ©2025 IEEE

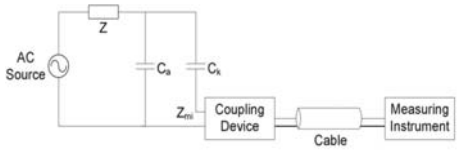


Fig. 1. IEC 60270 detection circuit [7].

III. EXPERIMENT SETUP

A. Partial discharge testing circuit

The circuit used for PD testing is illustrated in Figure 2-3. This setup includes an AC power supply, a high-frequency current transformer (HFCT) for detecting PD that it has a frequency range of 1 MHz to 60 MHz and a bandwidth of 59 MHz, a voltage divider, and the test object. In Figures 4-7, the reference voltage is measured at Channel 1 (CH1) using the voltage divider, while the PD signal is acquired at Channel 2 (CH2) through an HFCT connected to the ground wire of the system.

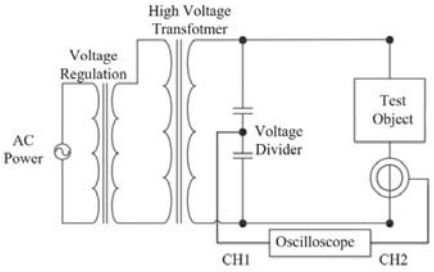


Fig. 2. The diagrams of PD measurement.

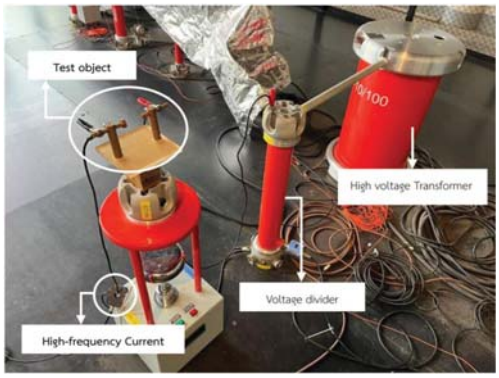


Fig. 3. Experimental setup.

B. Partial discharge testing objects

The objects depicted in Figures 4-7 are evaluated for four distinct types of discharge phenomena: internal discharge, surface discharge, air corona on the high-voltage side, and air corona on the ground side, respectively.

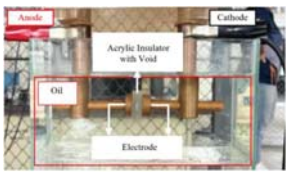


Fig. 4. Internal Discharge in Oil.

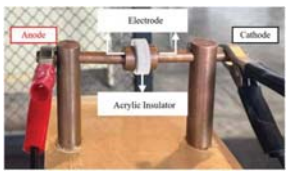


Fig. 5. Surface Discharge.

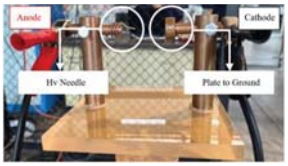


Fig. 6. Air Corona; High Voltage Needle.

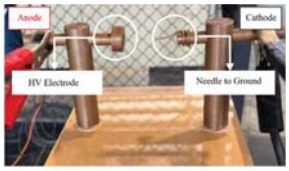


Fig. 7. Air Corona; Needle to Ground.

Tests were conducted to measure various types of discharges by adjusting the voltage from 5 kV to 25 kV. For internal discharge, PD became clearly detectable at 25 kV, and the PD signals were recorded at 30 kV. In the case of surface discharge, PD began to occur at 15 kV and became clearly visible at 17 kV, with signals recorded at this voltage. For positive needle electrode corona discharge (Air Corona; High Voltage Needle), PD initiated at 20 kV and became distinct at 23 kV, leading to the recording of PD signals at 23 kV. Similarly, for negative needle electrode corona discharge (Air Corona; Needle to Ground), PD started at 20 kV and was clearly observable at 23 kV, with signals recorded at this voltage.

IV. EXPERIMENTAL RESULTS

A. Partial discharge signal on basic objects

After measuring the PD signals for all four types, the PD signals were recorded using an oscilloscope with a sampling rate of 2 GSa/s and a bandwidth of 100 MHz. Impedance matching was done when connecting the HFCT to the oscilloscope. The HFCT has a load impedance of 50 Ω, hence a 50 Ω termination was used at the oscilloscope input to avoid signal reflections and ensure appropriate transmission. This setup protects signal integrity and PD measurement accuracy from distortions. The data was transmitted via a LAN cable to a notebook computer. The IO Libraries Suite software was employed to automatically detect and establish the connection with the notebook. Figure 8. illustrates an example of the oscilloscope screen displaying the measured PD signals.

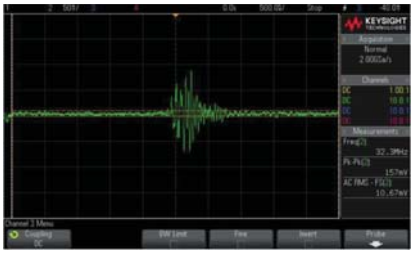


Fig. 8. The oscilloscope display screen in the IO Libraries Suite.

The recording of PD signals was conducted by defining measurement intervals in the time domain, with each interval set at 5 µs. The time step (Δt) was 5 ns, resulting in a total of 1,000 data points per signal. The PD signals were recorded for four different types, with 100 signals acquired for each type. The characteristics of the measured sample signals for each type are shown in Figures 9 - 12 as follows:

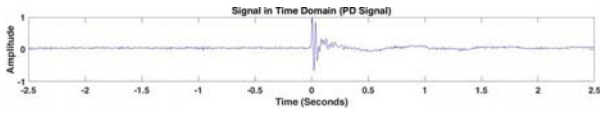


Fig. 9. Internal discharge signal.

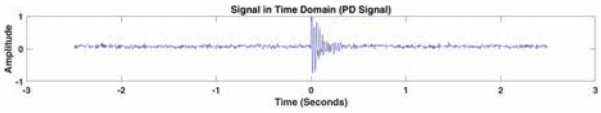


Fig. 10. Surface discharge signal.

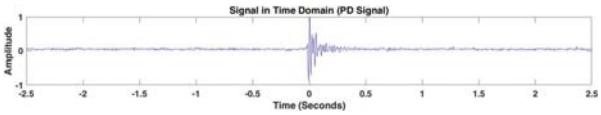


Fig. 11. Corona discharge signal; High Voltage Needle.

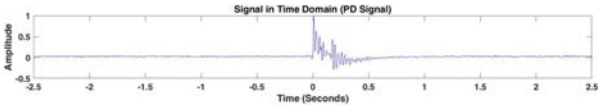


Fig. 12. Corona discharge signal; Needle to Ground.

B. *Feature extraction results.*

1) *Fast Fourier Transform (FFT) results*

FFT is a widely used mathematical technique for converting a signal from the time domain to the frequency domain. It efficiently decomposes a signal into its constituent frequency components, allowing for detailed spectral analysis. The frequency distribution and frequency filtering for each type are illustrated in Figures 13 - 16 as follows:

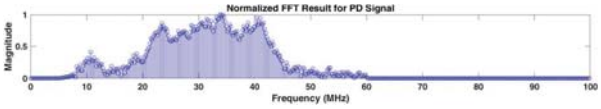


Fig. 13. Internal discharge signal.

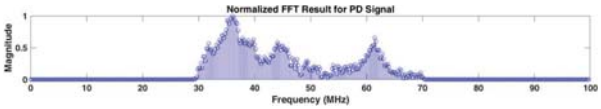


Fig. 14. Surface discharge signal.

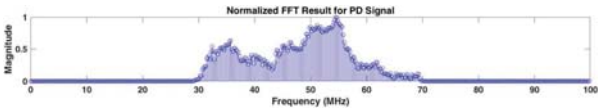


Fig. 15. Corona discharge signal; High Voltage Needle.

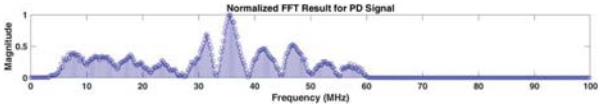


Fig. 16. Corona discharge signal; Needle to Ground.

From the frequency distribution results, the significant frequency ranges of interest were identified. However, it was observed that there were noise signals unrelated to the discharge signals. To address this, a Band Pass Filter (BPF) was applied to remove the noise. The frequency pass bands were set as follows: for internal discharge, the pass band was set to 5-60 MHz; for surface discharge, the pass band was set to 30-70 MHz; for positive needle electrode corona discharge (Air Corona; High Voltage Needle), the pass band was set to 30-70 MHz; and for negative needle electrode corona discharge (Air Corona; Needle to Ground), the pass band was set to 1-60 MHz. The selection of passband frequencies for each PD type was based on the frequency distribution. The significant frequency ranges of interest were identified for each discharge type, considering their characteristic spectral components. Additionally, the magnitude and frequency range of the HFCT sensor were taken into account to ensure optimal signal detection. The chosen passbands align with the HFCT's bandwidth capabilities (1 MHz – 60 MHz) and sensitivity characteristics, allowing effective noise suppression while maintaining accurate PD signal acquisition.

2) *Gaussian Curve Fitting (GCF) results.*

Gaussian curve fitting is used in FFT analysis to approximate the frequency spectrum with a Gaussian function. This helps in identifying signal components, filtering noise, and estimating dominant frequency characteristics. When multiple frequency components exist in an FFT spectrum, a sum of Gaussian functions is used to model the peaks. This helps in accurately identifying and characterizing multiple dominant frequency components. The equation for multiple Gaussian peaks is:

$$f(x) = \sum_{i=1}^{N} A_i \cdot \exp\left(-\frac{(x-\mu_i)^2}{2\sigma_i^2} \right) \quad (1)$$

where N are number of Gaussian peaks, A_i are magnitude of peak, μ_i are mean (center frequency) of the i^{th} peak, σ_i are standard deviation (width) of the i^{th} peak. The characteristics of frequency feature extraction using GCF in this study were categorized into two frequency distributions (primary and secondary frequency) for each type, as demonstrated in Figures 17–20, as follows:

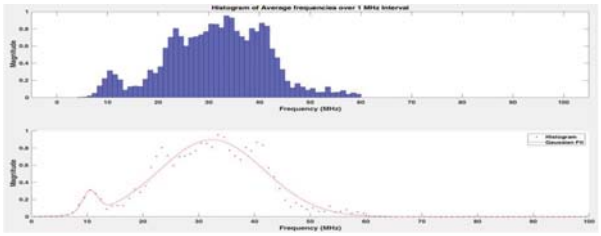


Fig. 17. Internal discharge signal.

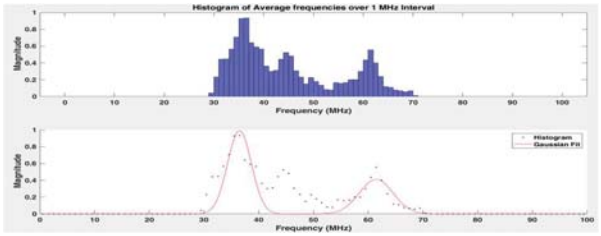


Fig. 18. Surface discharge signal.

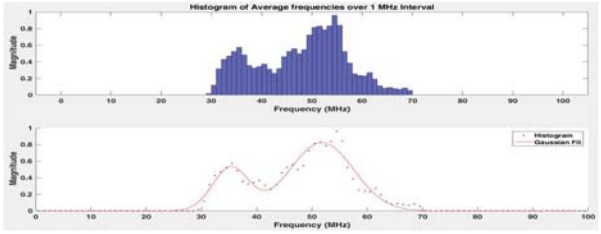


Fig. 19. Corona discharge signal; High Voltage Needle.

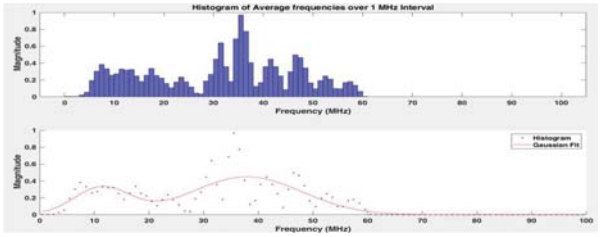


Fig. 20. Corona discharge signal; Needle to Ground.

The feature extraction for different PD signals was analyzed using GCF. For the internal discharge signal (Fig. 17), the primary dominant frequency (f_1) was 32.38 MHz with a standard deviation of 13.25 MHz, and the secondary dominant frequency (f_2) was 10.54 MHz with a standard deviation of 1.92 MHz. For the surface discharge signal (Fig. 18), f_1 was 36.49 MHz (std dev = 3.08 MHz) and f_2 was 61.46 MHz (std dev = 4.37 MHz). For the corona discharge signal from a High Voltage Needle (Fig. 19), f_1 was 54.44 MHz with a standard deviation of 5.01 MHz, and f_2 was 35.40 MHz with a standard deviation of 3.25 MHz. Lastly, the corona discharge signal from a Needle to Ground (Fig. 20) showed an f_1 of 37.95 MHz (std dev = 14.47 MHz) and an f_2 of 11.37 MHz (std dev = 7.21 MHz). These distinct frequency characteristics are essential for accurately identifying each type of PD.

C. Identification of Partial Discharge

PD is identified using machine learning techniques by modifying the input features. The process starts with two main inputs: the most dominant frequency (f_1) and the second most dominant frequency (f_2). Next, two additional features are added—these are the standard deviations of the primary and secondary frequencies. In this study, we use a Feed-forward Neural Network (FNN) with a softmax activation function. The network is trained for 1,000 epochs, and each model is trained five times. Mathematically, a one-layer FNN can be expressed as follows:

$$z = Wx + b \tag{2}$$

Where W is the weight matrix, x is the input vector, b is the bias vector ,and z is the linear transformation output. In order to evaluate the model's performance, we conducted experiments using two different hidden layer configurations: one with 5 nodes and another with 10 nodes. We also used k-fold cross-validation (with k set to 4 and 5) to validate the model. Additionally, we tested learning rates of 0.01 and 0.1. The model was evaluated using accuracy and F1-score, which together provide a complete picture of its effectiveness. The detailed experimental results are presented below.

TABLE I. MODEL PERFORMANCE EVALUATION.

Input	Node	Cross validation	Learning rate	Accuracy (%)	F1-score (%)
2	5	4	0.01	82.5	82.7
			0.10	90.0	90.7
		5	0.01	85.0	86.0
			0.10	86.3	85.6
	10	4	0.01	85.0	84.5
			0.10	88.7	89.1
		5	0.01	87.5	88.4
			0.10	87.5	84.5
4	5	4	0.01	86.3	85.7
			0.10	90.0	89.0
		5	0.01	87.6	87.2
			0.10	87.5	87.2
	10	4	0.01	85.0	86.3
			0.10	88.8	89.5
		5	0.01	86.7	84.6
			0.10	86.3	85.9

From Table 1, the performance evaluation of the model under different input data sizes (2 and 4) and varying numbers of nodes (5 and 10) is presented. The results indicate that the model with a learning rate of 0.1 and k = 4 outperforms others in all cases. This is because the validation set division at k = 4 provides more training data per fold compared to k = 5, enabling the model to learn more effectively. Additionally, the learning rate of 0.1 facilitates faster weight adjustments, allowing the model to converge more efficiently. The best-performing model utilizes 2 input features and 5 hidden nodes, achieving an accuracy of 90%, and F1-score of 90.7%.

V. CONCLUSION

This research investigated four types of PD signals: internal discharge, surface discharge, positive needle corona discharge (Air Corona; High Voltage Needle), and negative needle corona discharge (Air Corona; Needle to Ground). The PD signals were measured in a high-voltage laboratory and recorded using an oscilloscope connected to a notebook equipped with IO Libraries suite, capturing time-domain data. Signal characteristics were extracted using FFT, noise filtering, and histogram distribution analysis. GCF was applied to identify primary and secondary features, which were then used as inputs for the FNN model with one hidden layer. The model's performance was evaluated by varying the number of input features, hidden layer nodes, validation set partitioning (k-fold), and learning rate. The optimal configuration, with two input features (mean frequency of primary and secondary characteristics), five hidden nodes, k = 4 validation set, and a learning rate of 0.1, achieved the highest performance, yielding an accuracy of 90% and an F1-score of 90.7%. These results demonstrate the effectiveness of the proposed approach in identifying PD patterns.

VI. REFERENCE

[1] R. Arora and W. Mosch, *High Voltage and Electrical Insulation Engineering*. John Wiley & Sons, 2022.

[2] L. Hao *et al.*, "Discrimination of multiple PD sources using wavelet decomposition and principal component analysis," *IEEE Transactions on Dielectrics and Electrical Insulation*, vol. 18, no. 5, pp. 1702–1711, Oct. 2011, doi: 10.1109/TDEI.2011.6032842.

[3] G. A. Hussain, W. Hassan, F. Mahmood, M. Shafiq, H. Rehman, and J. A. Kay, "Review on Partial Discharge Diagnostic Techniques for High Voltage Equipment in Power Systems," *IEEE Access*, vol. 11, pp. 51382–51394, 2023, doi: 10.1109/ACCESS.2023.3279355.

[4] H. Besharatifard, S. Hasanzadeh, E. Heydarian-Forushani, H. H. Alhelou, and P. Siano, "Detection and Analysis of Partial Discharges in Oil-Immersed Power Transformers Using Low-Cost Acoustic Sensors," *Applied Sciences*, vol. 12, no. 6, Art. no. 6, Jan. 2022, doi: 10.3390/app12063010.

[5] K. Romphuchaiyapruek and S. Wattanawongpitak, "Application of the Gaussian Mixture Model for Clustering Partial Discharge Signals in High Voltage Generators," in *2023 International Conference on Power, Energy and Innovations (ICPEI)*, Oct. 2023, pp. 31–35. doi: 10.1109/ICPEI58931.2023.10473810.

[6] G. C. Stone, A. Cavallini, G. Behrmann, and C. A. Serafino, *Practical Partial Discharge Measurement on Electrical Equipment*. John Wiley & Sons, 2023.

[7] H.-V. T. T. Discharge, "Measurements; IEC 60270 (2000)," *International Electrotechnical Commission (IEC): London, UK*, 2000.

Integration of Charcoal Kiln Waste Heat in a Thermal Water Pump System

Pakorn Promkaew
Department of Industrial Technology
Phuket Rajabhat University
Phuket, Thailand
pakorn.p@pkru.ac.th

Pathiwat Waramit
Department of Mechanical Engineering
Rajamangala University of Technology Isan
Nakhon Ratchasima, Thailand
pathiwat.wa@rmuti.ac.th

Bundit Krittacom
Department of Mechanical Engineering
Rajamangala University of Technology Isan
Nakhon Ratchasima, Thailand
bundit.kr@rmuti.ac.th

Jirawat Sitranon
Department of Energy Technology Management
Rajamangala University of Technology Tawan-ok
Chonburi, Thailand
Jirawat_si@rmutto.ac.th

Panusak Moonsri
Department of Energy and Air Conditioning Engineering
Rajamangala University of Technology Isan
Nakhon Ratchasima, Thailand
panusak_13@hotmail.com

***Abstract*— This an innovative solution for water pumping in resource-limited settings has been presented by waste heat utilization from charcoal production. This experiment investigates a novel thermal water pump system integrated with 200-liter charcoal kilns (CK). The experimental setup consisted of a driving tank, a storage tank, an overhead tank, and a well tank. A 1-meter discharge head and 1-3 m suction heads were tested. This experiment compared pump efficiency and thermal efficiency between single and double CK, using 25 kg and 50 kg of eucalyptus wood as fuel, respectively. Data acquisition was recorded over 2-hour operations. It revealed that the pump achieved optimal performance at driving tank temperatures of 99°C, with maximum efficiency at a 3-meter suction head. The single CK delivered 155.89 L for 25 cycles, with 0.00073% pump efficiency and 2.2% thermal efficiency, while the double CK could enhance performance, pumping 274.15 L for 28 cycles at 0.000847% pump efficiency and 2.8% thermal efficiency. The double CK has higher system efficiency than a single CK due to increased thermal energy availability. However, the water pumping system still has low efficiency due to environmental heat losses. This study can verify that waste heat utilization in water pumping applications and identifies key areas for future optimization.**

Keywords—waste heat, thermal water pump, charcoal, energy conversion

I. INTRODUCTION

Nowadays, many barbecue restaurants use charcoal as fuel for grilling. The process of charcoal production produces thermal energy, which is wasted heat that is not utilized. Therefore, it could be useful to use wasted heat for a thermal water pump (TWP), which uses thermal energy for water pumping. Usually, charcoal is made in fields or open areas, which are far from a power grid, and therefore, makes it challenging to use an electric pump. Similarly, if a gasoline water pump were used, it would consume fossil fuel. The thermal water pump from charcoal production (TWPC) could partly reduce fossil fuel consumption and energy cost. Especially since it does not require a transmission line and can be mounted anywhere.

Numerous thermal water pumps have been studied and developed [1-10]. In 1996, Sumathy et al. built a solar thermal water pump. The pentane vapor from the solar collector was generated as pump power. The maximum water discharge from this pump was 10 meters [11]. These solar thermal water pumping systems were reviewed by Wong & Sumathy. The conventional and unconventional pumping techniques are the main topics of this study. While the unconventional type converts thermal energy to hydraulic work, the conventional type converts thermal energy to mechanical energy. The multiple unconventional types have advantages, being that they are simple and non-mechanical. Solar thermal water pumps for irrigation tend to improve due to technological advancements and falling costs [12]. Wong & Sumathy built a solar water pump using n-pentane and ethyl ether as working substances. The maximum pump efficiency was 0.34%. The pumped water is between 700-1400 L/day [13]. Roonprasang et al. built a solar water heater system (SWHS) that utilized a solar water pump. The operating temperature was around 70-90°C. The daily pump efficiency was 0.0014–0.0019% on average [14]. Delgado-Torres reviewed numerous methods of solar thermal water pumps [15]. Sutthivirode et al. [16] and Roonprasang et al. [17] built a solar water heating system, compared to the system developed by Roonprasang et al. [14]. Their system operates at temperatures between 70 and 90°C. The water temperature was around 60°C. This system operates automatically. Sutthivirode et al. [18] presented a waste heat water pumping model with direct contact cooling. It can pump 65-170 L of water in 2 hours. The solar water heater was enhanced efficiency by Sitranon et al. A thermal water pump built by Sutthivirod et al. [16] was used as the prototype. Their pump has daily efficiency of about 0.0012% [19]. The application of a TWP for agriculture was studied by Sitranon et al. A working fluid is air-steam. The pumping efficiency reached 0.01973% [20]. The mathematical model of the solar thermal water pump was investigated by Bandaru et al. The solar thermal energy conversion was simulated [21].

Biomass can be used as a source of energy in two ways: directly, by burning it, or indirectly, by turning it into solid, liquid, or gaseous fuels [22]. This research uses a direct method of biomass energy. Charcoal production is one

XXX-X-XXXX-XXXX-X/XX/$XX.00 ©20XX IEEE

method of utilizing biomass energy, which plays a vital role in global energy generation, with significant amounts produced in diverse regions, such Africa, Asia-Pacific, and Latin America [23]. Studies have shown that heat is generated during the production process [24, 25].

The goal of this research was to study the efficiency of a thermal water pump that uses waste heat from charcoal production, with 200-liter charcoal kilns. The experiment was to compare the efficiency between a system equipped with single CK, and double CK. Eucalyptus wood was used as a heat source, 25 kg and 50 kg, for single CK and double CK, respectively. A 1-meter discharge head and 1, 2 and 3 m suction heads were tested.

II. Experimental Setups

A. *Component of thermal water pump system*

The TWPC is made up of six primary components, as indicated in Fig. 1. First, the CK, which are made of a 200-liter fuel tank with no insulation. It has three smokestacks, assembled beside the tank. The inlet for fuel and natural air convection is placed below the CK. The copper tube (CT) roll is installed in tank, to generate the vapor as pump power. Second, a driving tank (DT), which is built using a 2-mm thick stainless-steel sheet, which has good insulation. The DT body consists of two parts: a cylindrical shape, and a conical shape, both welded together. The cylinder contains 0.01 m^3 of water, and the cone has 0.005 m^3 of air. Third, an overhead tank (OT), which is made of plastic with no insulation. It is located at a higher level, above the DT. The water of the OT is controlled by a floating valve. The cooling water valve (CWV) consists of PVC reducing socket, which has a ping pong ball and rubber seal. It is included in the OT. It is utilized to regulate 300 mL of water, which is the minimum water volume, into the DT to establish a vacuum. The CWV is essential for this research. Fourth, a storage tank (ST), well tank (WT) and supply tank (SPT), they are the cylindrical tank with air vent.

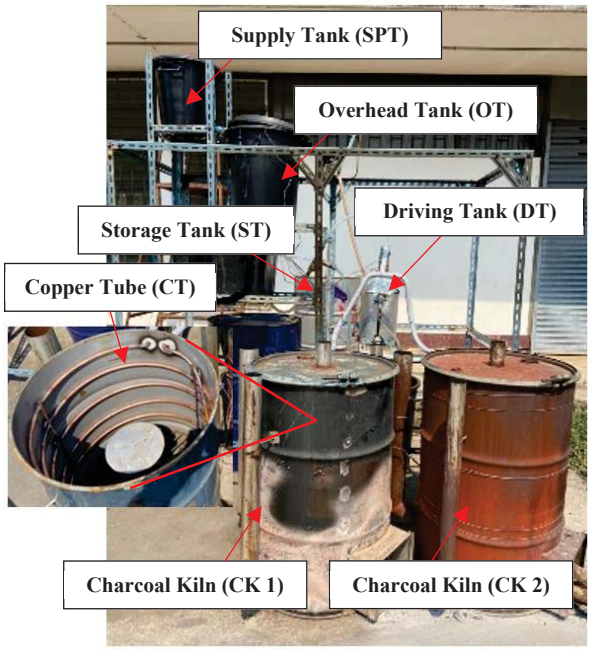


Fig. 1. The component of TWCP system

The CT-DT is connected by a 1/2-in copper tube. The ST, OT, and SPT are linked to the DT, via a 1/2-in rubber tube, where the water flow can be observed. The 1, 2, and 3-m suction heads were tested with a constant 1-m discharge head. The suction head is the difference between the DT top and the water level at WT. The discharge head is the difference between an air vent level: that is h1 in Fig.2, and DT bottom. Eucalyptus wood, which weighed 25 kg, was used as fuel, with its heating value being around 19,000 kJ/kg. The experimental data were recorded for 2 hours at the Faculty of Engineering and Technology, Rajamangala University of Technology Isan. The data entry was recorded for every 1 second per measured data.

B. *Measurement points of thermal water pump system*

The temperature of the steam, water, and surrounding air was measured by K-type thermocouples, with an accuracy of +0.5°C, connected to a data logger (Hioki LRB8431-20) which has improved accuracy of ±1.5°C. The measurement points are shown in Fig. 2. There are 7 measuring points: 1) water temperature in overhead tank, 2-4) water temperature in driving tank, 5) water temperature in storage tank, 6) water temperature in well tank, and 7) ambient temperature

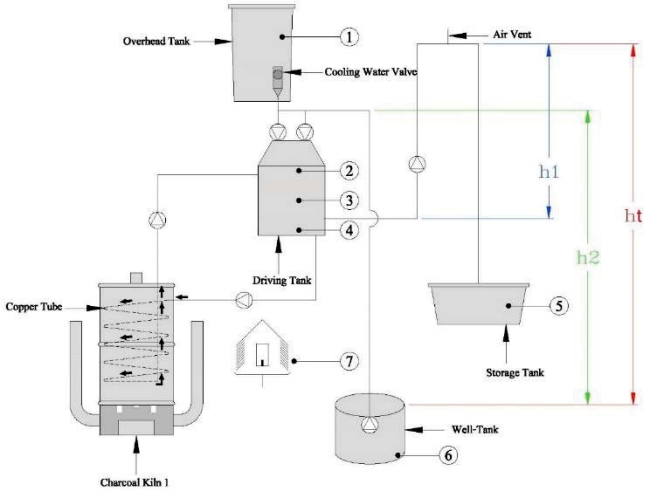


Fig. 2. Points of measurement: h1, discharge head; h2, suction head; ht, total head

III. System Operation

The system operation of this study is similar to several previous studies [18, 26] except for the heat source. The system operation is shown in Fig. 3. The process of TWPC comprises five stages:

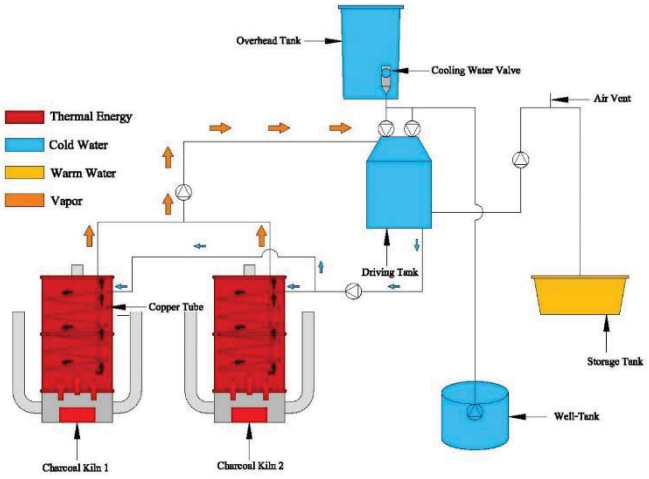
Heating stage: initially, the CT contains water in a full tube. Thermal energy in charcoal production process transfers to the CT. The water in the CT is heated to boiling temperature, and then it vaporizes and flows to the DT. Because of this, the pressure and temperature of the water and air in the DT slightly rise. The heating stage continues until the DT's pressure is sufficient to transport hot water from the DT to the ST.

Pumping stage: when the DT pressure is higher than the discharge head pressure, the water in the DT is pushed to the ST until the water is gone.

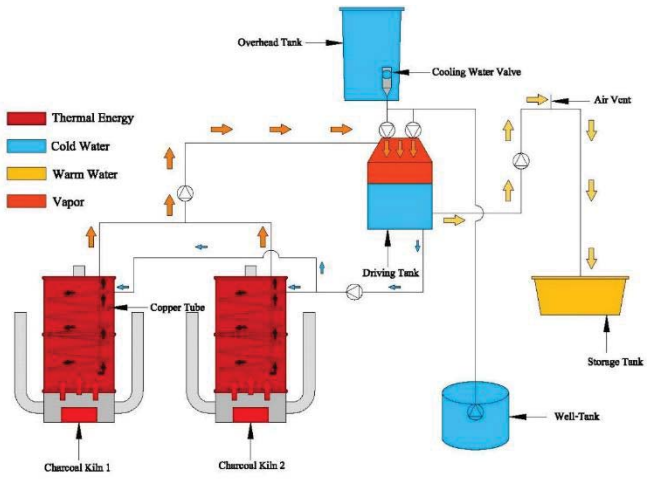
Vapor flow stage: the vapor from the CT can flow to the air vent after the last drop. The vapor flow process continues until the DT pressure reaches one atmosphere.

Cooling stage: the 300 mL of water in the OT automatically moves downward by gravitational force, into the DT, and the CWV is closed promptly temporarily.

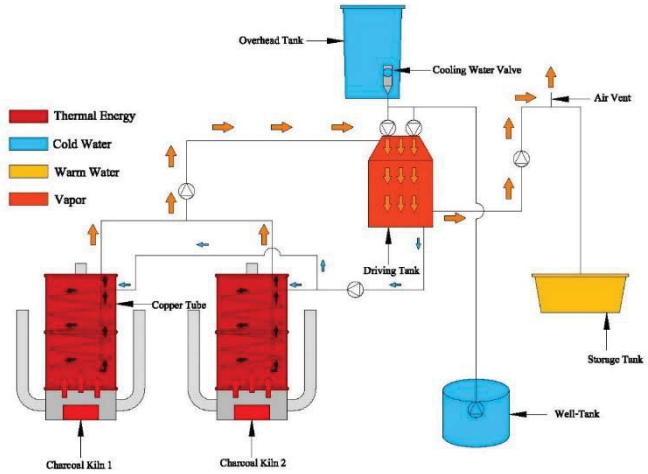
Suction stage: the vacuum is generated owing to steam condensation, and then the water from the WT is sucked into the DT. The sucked water is estimated to be 0.01 m^3, which is not the full capacity of the DT. The remaining space is for air. Some part of sucked water fills up the CT to continually produce steam. One cycle of the self-pumping process is accomplished, and the pumping action is then prepared for the next cycle.



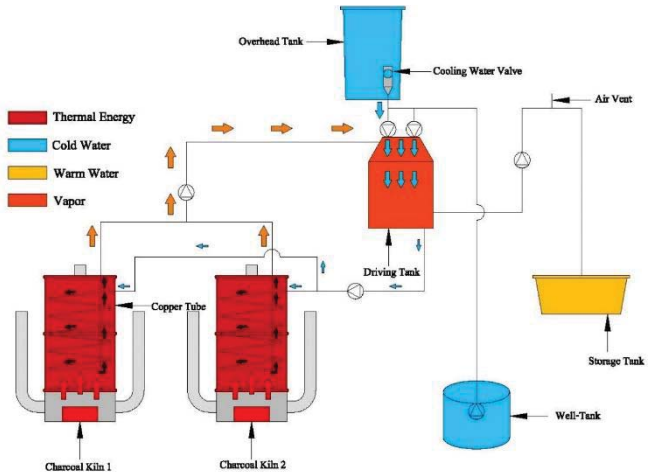
(a) Heating stage



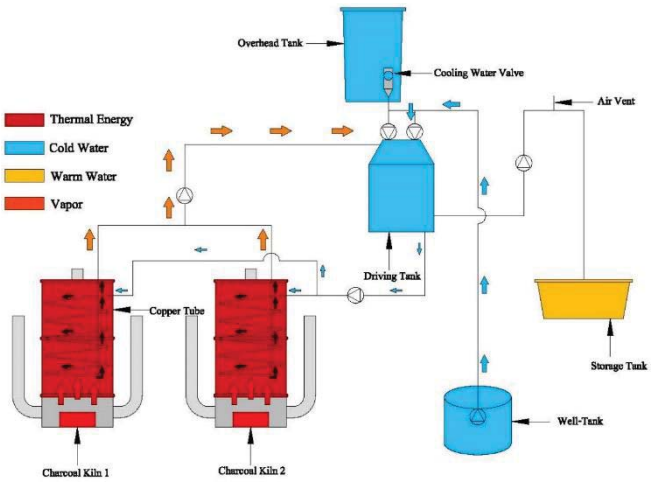
(b) Pumping stage



(c) Vapor flow stage



(d) Cooling stage



(e) Suction stage

Fig. 3. Five-stage operation of TWCP system

IV. System Analysis

Pump efficiency is expressed as a percentage, using the following formula by [1]:

$$\eta_p = NW_h / Q_{input} \quad (1)$$

Where N is the number of water circulating cycles per 2 hr W_h, being the required hydraulic energy for each cycle, which is expressed by:

$$W_h = V_w \rho g h_t \quad (2)$$

Where V_w is the amount of pumped water per cycle, including 300 ml of the cooling water, ρ is density of water, g is the acceleration of gravity, and h_t is the overall head of system.

The thermal energy of water in the ST can be calculated, as in (3)

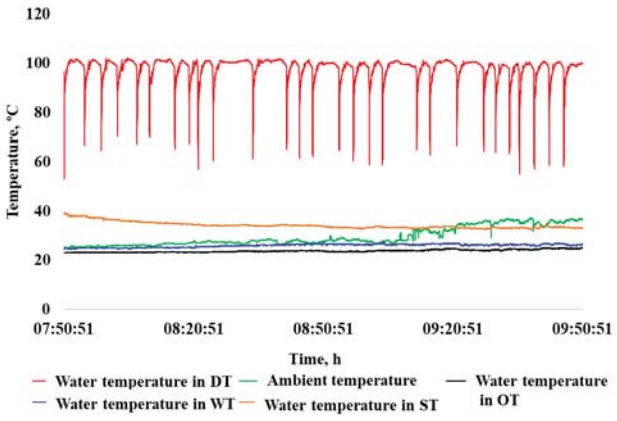
$$Q_s = m_{w,s} c_p \Delta T_s \quad (3)$$

Where $m_{w,s}$ is the water quantity in the ST, c_p is the specific heat of water, and ΔT_s is the water temperature increase in the ST. The thermal efficiency is defined as the ratio of the thermal energy of water in the ST, compared to the total energy from eucalyptus wood, as in (4)

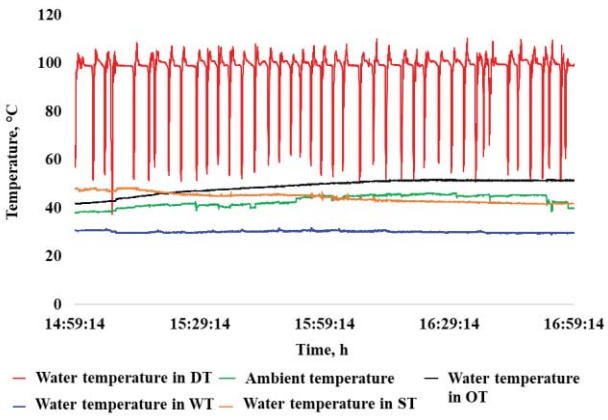
$$\eta_t = (Q_s / Q_{input}) \times 100\% \quad (4)$$

V. Results and Discussion

A pumping capacity of the TWPC was 6-9 L of water per cycle. The ST maintained an average temperature range between 32-46°C. Improved insulation of the ST could potentially lead to raised temperatures. The system-initiated water pumping when the DT temperature exceeded 99°C. The integration of double CK enhanced thermal energy input to the TWPC, resulting in increased pumping cycle frequency as in Fig. 4. This improvement is probably the reason that the system has more pump power to overcome friction loss and gravitational forces. Experimental results indicated that configurations with single and double CK achieved 25-29 and 28-41 pumping cycles, respectively, corresponding to total pumped water volumes of 156-175 L and 274-400 L. Furthermore, the vapor temperature in DT with double CK exceeded that of the single CK by approximately 8°C.



(a) Single CK, 1 m suction head



(b) double CK, 1 m suction head

Fig. 4. Comparison of pumping frequency with different heat input

A. *Effect of the suction head on thermal efficiency*

A comparison of thermal efficiency is shown in Fig. 5 revealed that the thermal efficiency decreases as suction head increases. This phenomenon can be explained by steam energy requirements is varied on suction head height. The conversion of thermal energy to mechanical energy for water pumping is not 100% efficient due to thermal energy losses that lead to decreasing thermal efficiency. As shown in Table I, the pumping frequency is decreased (fewer cycle), resulting in water circulation through the system is also decreased. Therefore, heat transfer of thermal energy to system is decreased. This reduction in heat transfer ultimately results in lower thermal efficiency values.

TABLE I. Pumping Cycle and Pumped Water at Different Suction Head

No. of CK	Suction head (m)	Pumping Cycle	Pumped water [a] (L)	Pumped water rate (L/cycle)
1	1	27	175	6.48
	2	29	172	5.93
	3	25	156	6.24
2	1	41	400	9.76
	2	39	378	9.69
	3	28	274	9.79

[a] Including 300 ml of the cooling water

A comparison of thermal efficiency in case of one and double CK revealed that double CK have more thermal efficiency because the system can produce more steam, which increases thermal energy. However, there is no significant difference when the discharge head is 3 m. The system has the best thermal efficiency of 2.8% at the suction head of 1 m., and this is in accordance with the study of [16]. This can be expressed by the Darcy-Weisbach equation. In the suction process, the suction pipe, which is made of rubber tubes, can flatten due to suction pressure. The pumped water is obstructed. The selection of PVC spring hoses as the suction tube may reduce this problem.

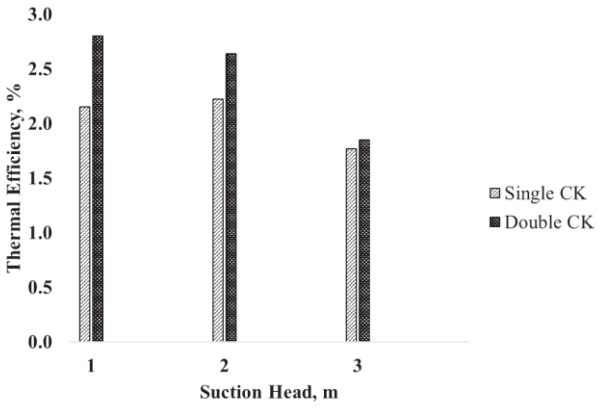


Fig. 5. Effect of different suction head on thermal efficiency

B. Effect of the suction head on pump efficiency

The relationship between suction head height and pumping efficiency was investigated through comparative analysis of single and double CK configurations as in Fig. 6. The pump efficiency has varied across suction heads to 1, 2, and 3 m with single and double CK. Pump efficiency using double CK is 0.000412%, 0.000778%, and 0.000847%, whereas the single CK is 0.00036%, 0.000709%, and 0.000763% at respective suction heads of 1, 2, and 3 m. Analysis revealed that pump efficiency shows a positive correlation with increasing suction head value, denoted as h2 in Fig. 2, As the suction head increases, the pump must generate increased suction force to overcome gravitational forces, necessitating higher energy input per pumping cycle. This increased energy requirement results in a reduction of both pumping cycles and total water volume output. Despite the pumped water being decreased, the elevated pressure generation capability leads to a marginal improvement in pump efficiency. However, it should be noted that the pump operates below optimal efficiency due to the additional energy required to overcome the increased suction head resistance. This relationship indicated that the suction head parameter has a greater impact on pump efficiency than the other factors specified in (2).

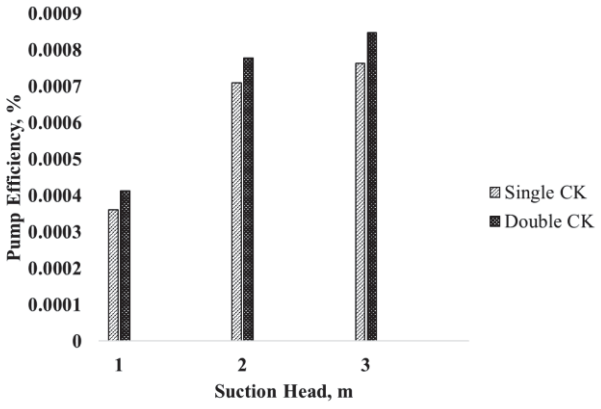


Fig. 6. Effect of different suction head on pump efficiency

VI. CONCLUSIONS

TWPC could pump when the DT temperature exceeded 99°C. As suction head increases, it affects the system's efficiency, explained by pump efficiency and thermal efficiency. Pump efficiency increases slightly due to increased energy consumption per cycle, despite the reduction in total pumped water volume. Pump efficiency is between 0.00036% and 0.000763% for single CK. While, 0.000412% and 0.000847% for double CK. The system used for this study had lower pump efficiency than previous studies [18-19], due to significant heat loss at the CK surface. Increasing the driving steam pressure, implementing flow resistance reduction mechanisms, or thermal insulation enhancement to minimize energy losses should be considered for improving pump efficiency. Meanwhile, thermal efficiency decreases because higher steam energy is required to overcome gravitational force, but energy cannot convert from thermal to mechanical work with full efficiency. Experimental trends indicate that minimizing the suction head should be a focus for increasing thermal efficiency. However, the advantage of this system is that the waste heat can be used for functions, such as pumping water and heating water. The pumped water volume with single and double CK is 156-175 L and 274-400 L, respectively. Nonetheless, the water temperature in the ST is sufficiently hot for domestic use. The pump efficiency is dependent on the suction head and ambient temperature. The thermal pump efficiency is about 1.77-2.22% for single CK and 1.85-2.80% for double CK. The overall energy losses may be decreased by minimization for the suction head and optimization of water flow rates using large water tubes at every stage, as well as good insulation. Finally, systems operating with lower suction head values demonstrate optimal steam energy utilization efficiency.

When examining the environmental impact of charcoal kilns using eucalyptus wood as combustion fuel, the emission factors were found to be CO_2 ~ 1400±101 g/kg, CO ~ 50±13 g/kg, and CH_4 ~ 3.2±0.5 g/kg [27]. Consequently, for single and double charcoal kilns utilizing 25 kg and 50 kg of eucalyptus wood, respectively, the maximum greenhouse gas emissions equate to 232 g/L and 265.18 g/L, respectively. Considering only the maximum CO_2 emissions, these amount to 224.36 g/L and 255.47 g/L, respectively. In comparison, water pumping using electric pumps at a total head of 5 meters, consuming 0.37 kW of electricity at comparable water pumping volumes, produces maximum CO_2 emissions of only 0.079 g/L and 0.102 g/L, respectively. This calculation is based on Thailand's carbon dioxide emission per electricity generation data, reported at 0.399 kg/kWh in 2024 [28]. While electric water pumps evidently release less CO_2 than eucalyptus wood fuel, the constraints of areas lacking electricity access and cost considerations make water pumping using waste heat from charcoal kilns a potentially viable alternative. The additional pollution control technologies could be implemented for solving pollution concerns, such as wet scrubber installations. Notably, wet scrubbers integrated into kilns have demonstrated removal efficiencies of 97.8% for hydrocarbons, 98.5% for CO_2, and 99% for CO, respectively [29].

When examining an economic feasibility perspective, the water pumping system powered by waste heat from charcoal kilns demonstrates potential to reduce energy costs by approximately 30% compared to conventional electric water pumps. The system has a payback period of 7.6 years. Furthermore, the system can be designed to achieve increased water pumping rates and enhanced suction and delivery distances according to the available waste heat and pressure vessel size. As the system is scaled up with increased pumping capacity, the payback period decreases proportionally. This technology is particularly suitable for agricultural applications with sufficient biomass resources for irrigation purposes.

The system presents a sustainable solution for regions with limited access to electrical infrastructure.

VII. Suggestion

The optimization techniques are proposed to improve system performance as findings:

1) The suction head should be minimized as much as possible in order to lower pump load.

2) Improvement of thermal insulation to maintain heat and energy loss reduction.

3) Increasing the water circulation rate to optimize the water flow rate for supporting efficient heat transfer within the system.

Acknowledgment

The authors gratefully acknowledge the Department of Energy and Air Conditioning Engineering and the Department of Mechanical Engineering, Faculty of Engineering and Technology, at the Rajamangala University of Technology Isan, for their support.

References

[1] J. R. Jenness, "Some considerations relative to a solar-powered savery water pump," Solar Energy, vol. 5, no. 2, pp. 58-60, 1961.

[2] D. P. Rao and K. S. Rao, "Solar water pump for lift irrigation," Solar Energy, vol. 18, no. 5, pp. 405-411, 1976.

[3] K. Sudhakar, M. M. Krishna, D. P. Rao, and R. S. Soin, "Analysis and simulation of a solar water pump for lift irrigation," Solar Energy, vol. 24, no. 1, pp. 71-82, 1980.

[4] K. Sumathy, A. Venkatesh, and V. Sriramulu, "The importance of the condenser in a solar water pump," Energy Conversion and Management, vol. 36, no. 12, pp. 1167-1173, 1995.

[5] A. A. Al-Haddad, E. Enaya, and M. A. Fahim, "Performance of a thermodynamic water pump," Applied Thermal Engineering, vol. 16, no. 4, pp. 321-334, 1996.

[6] D. J. Picken, K. D. R. Seare, and F. Goto, "Design and development of a water piston solar powered steam pump," Solar Energy, vol. 61, no. 3, pp. 219-224, 1997.

[7] K. Sumathy, "Experimental studies on a solar thermal water pump," Applied Thermal Engineering, vol. 19, no. 5, pp. 449-459, 1999.

[8] M. von Oppen and K. Chandwalker, "Solar power for irrigation: The small solar thermal pump: an Indian development," Refocus, vol. 2, no. 4, pp. 24-26, 2001.

[9] Y. W. Wong and K. Sumathy, "Performance of a solar water pump with ethyl ether as working fluid," Renewable Energy, vol. 22, no. 1, pp. 389-394, 2001.

[10] R. B. Slama, "Thermodynamic solar water pump with multifunction and uses," The Open Fuels & Energy Science Journal, vol. 2, no. 1, pp. 129-134, 2009.

[11] K. Sumathy, A. Venkatesh, and V. Sriramulu, "A solar thermal water pump," Applied Energy, vol. 53, no. 3, pp. 235-243, 1996.

[12] Y. W. Wong and K. Sumathy, "Solar thermal water pumping systems: a review," Renewable and Sustainable Energy Reviews, vol. 3, no. 2, pp. 185-217, 1999.

[13] Y. W. Wong and K. Sumathy, "Performance of a solar water pump with n-pentane and ethyl ether as working fluids," Energy Conversion and Management, vol. 41, no. 9, pp. 915-927, 2000.

[14] N. Roonprasang, P. Namprakai, and N. Pratinthong, "Experimental studies of a new solar water heater system using a solar water pump," Energy, vol. 33, no. 4, pp. 639-646, 2008.

[15] A. M. Delgado-Torres, "Solar thermal heat engines for water pumping: An update," Renewable and Sustainable Energy Reviews, vol. 13, no. 2, pp. 462-472, 2009.

[16] K. Sutthivirode, P. Namprakai, and N. Roonprasang, "A new version of a solar water heating system coupled with a solar water pump," Applied Energy, vol. 86, no. 9, pp. 1423-1430, 2009.

[17] N. Roonprasang, P. Namprakai, and N. Pratinthong, "A novel thermal water pump for circulating water in a solar water heating system," Applied Thermal Engineering, vol. 29, no. 8, pp. 1598-1605, 2009. K. Sutthivirode, N. Pratinthong, P. Namprakai, N. Roonprasang, and T. Suparos, "Waste heat water pumping model with direct contact cooling," Journal of Central South University, vol. 21, no. 10, pp. 3896-3910, 2014.

[18] J. Sitranon, C. Lertsatitthanakorn, P. Namprakai, N. Prathinthong, T. Suparos, and N. Roonprasang, "Performance Enhancement of Solar Water Heater with a Thermal Water Pump," Journal of Energy Engineering, vol. 141, no. 4, pp. 04014036 1-10, 2015.

[19] J. Sitranon, C. Lertsatitthanakorn, P. Namprakai, N. Prathinthong, T. Suparos, and N. Roonprasang, "Parametric Consideration of a Thermal Water Pump and Application for Agriculture," Journal of Solar Energy Engineering, vol. 137, no. 3, pp. 031006 1-12, 2015.

[20] R. Bandaru, M. C, and P. K. M.V, "Modelling and dynamic simulation of solar-thermal energy conversion in an unconventional solar thermal water pump," Renewable Energy, vol. 134, pp. 292-305, 2019.

[21] K. Homchat and S. Ramphueiphad, "The continuous carbonisation of rice husk on the gasifier for high yield charcoal production," Results in Engineering, vol. 15, pp. 100495, 2022.

[22] S. Sangsuk, C. Buathong, and S. Suebsiri, "Modified Iwate kiln for production of good quality charcoal and high volume of wood vinegar," Fuel Communications, vol. 17, pp. 100095, 2023.

[23] S. Sangsuk, C. Buathong, and S. Suebsiri, "High-energy conversion efficiency of drum kiln with heat distribution pipe for charcoal and biochar production," Energy for Sustainable Development, vol. 59, pp. 1-7, 2020.

[24] S. Sangsuk, S. Suebsiri, and P. Puakhom, "The metal kiln with heat distribution pipes for high quality charcoal and wood vinegar production," Energy for Sustainable Development, vol. 47, pp. 149-157, 2018.

[25] P. Moonsri, J. Kunchornrat, and P. Namprakai, "Hybrid Energy Thermal Water Pump for Producing Hot Water from a Shallow Well in Thailand," Journal of Energy Engineering, vol. 142, pp. 04015023-1-04015023-15, 2016.

[26] E. B. Amorim, J. A. Carvalho Jr, T. G. Soares Neto, E. Anselmo, V. O. Saito, F. F. Dias, and J. C. Santos, "Influence of specimen size, tray inclination and air flow rate on the emission of gases from biomass combustion," Atmospheric Environment, vol. 74, pp. 52-59, 2013.

[27] Energy Policy and Planning Office, Ministry of Energy, "Thailand carbon dioxide emission per electricity generation," CEIC, 2024. [Online]. Available: https://www.ceicdata.com/en/thailand/carbon-dioxide-emissions-statistics/carbon-dioxide-emission-per-electricity-generation

[28] Z. Getahun, M. Abewaa, A. Mengistu, E. Adino, K. Kontu, K. Angassa, A. Tiruneh, and J. Abdu, " Towards sustainable charcoal production: Designing an economical brick kiln with enhanced emission control technology," Heliyon, vol. 10, no. 6, pp. e27797, 2024.

A Fuzzy Multi-Criteria Decision-Making Approach for Ranking Renewable Energy Systems Based on Economic and Environmental Aspects

Danupun Visuwan
Industrial Statistics and Operational Research Unit (ISO-RU), Department of Industrial Engineering, Faculty of Engineering, Thammasat School of Engineering, Thammasat University, Pathumthani, 12120 Thailand
vdanupun@engr.tu.ac.th

Atiwat Nanphang*
Industrial Statistics and Operational Research Unit (ISO-RU), Department of Industrial Engineering, Faculty of Engineering, Thammasat School of Engineering, Thammasat University, Pathumthani, 12120 Thailand
atiwat.nan@dome.tu.ac.th

Pongchanun Luangpaiboon
Industrial Statistics and Operational Research Unit (ISO-RU), Department of Industrial Engineering, Faculty of Engineering, Thammasat School of Engineering, Thammasat University, Pathumthani, 12120 Thailand
lpongch@engr.tu.ac.th

Apirak Tepvarin
Industrial Statistics and Operational Research Unit (ISO-RU), Department of Industrial Engineering, Faculty of Engineering, Thammasat School of Engineering, Thammasat University, Pathumthani, 12120 Thailand
apirak.the@dome.tu.ac.th

***Abstract*— When selecting the most appropriate renewable energy source, it is necessary to strike a balance between the environmental impact and economic feasibility. This study employs a Fuzzy Multi-Criteria Decision-Making (FMCDM) framework, which employs the FAHP to establish criteria weights. Subsequently, Fuzzy-TOPSIS and Fuzzy-VIKOR are employed to rank five renewable energy systems: solar, wind, biomass, waste-to-energy, and marine energy. Solar energy is consistently ranked as the most advantageous system by both methods, as it offers high economic and environmental returns and incurs lower costs. In contrast, biomass energy is ranked as the least favorable option due to its dependence on natural resources. The reliability of the findings is enhanced by the consistency of both methodologies, which provides a structured approach for decision-makers in the selection of sustainable energy-related investments.**

Keywords—renewable energy, FAHP, Fuzzy-TOPSIS, Fuzzy-VIKOR

I. INTRODUCTION

The growing concerns over environmental degradation and the depletion of conventional energy sources highlight the urgent need to transition to renewable energy. Thailand's rapid industrialization, population growth, and urbanization have significantly increased energy demand, requiring a shift toward more sustainable system. However, selecting the most suitable renewable energy source involves balancing economic factors such as return on investment and initial costs with environmental considerations like CO_2 emissions and resource conservation. The complexity of decision-making is further compounded by expert judgment uncertainty and varying stakeholder perspectives. To address this challenge, fuzzy MCDM methods provide a structured approach to accommodate human judgment imprecision, enabling a more comprehensive evaluation of energy options.

A two-stage fuzzy decision-making framework is applied to rank five renewable energy options—solar, wind, biomass, waste-to-energy, and marine—based on five key criteria: return on investment, resource conservation, initial investment cost, CO_2 emissions, and ecological impact. Using FAHP to determine criterion weights, the study then applies Fuzzy TOPSIS and Fuzzy VIKOR for ranking, ensuring result reliability through comparative analysis. The research contributes to Thailand's energy planning by offering a structured fuzzy decision-making model that enhances investment assessment under uncertainty. The findings provide policymakers, investors, and environmental authorities with a reliable framework for selecting an optimal renewable energy source that balances financial returns with sustainability, supporting long-term energy security and environmental goals.

II. LITERATURE REVIEW

Fuzzy-based MCDM methods align well with Thailand's need to manage uncertainty and balance multiple criteria in renewable energy planning. Meixner [1] demonstrates how fuzzy logic and AHP enhance group decisions for energy source selection, while Taylan et al. [2] integrate Fuzzy AHP, VIKOR, and TOPSIS to rank energy systems more comprehensively. Jain et al. [3], Sodhi and Tadinada [4], and Rodzi [5] further highlight these methods' adaptability in supplier selection and managing imprecise data, and Shemshadi et al. [6] underscore fuzzy VIKOR's role in unifying subjective and objective factors. These insights guide this study's three-stage fuzzy approach, ensuring robust evaluations for Thailand's renewable energy strategies.

Moreover, Afful-Dadzie [7] shows how linguistic factors improve multi-criteria judgments by illustrating the adaptability of fuzzy VIKOR in assessing and ranking online-based health information under uncertain settings. Delcea et al. [8] score plans for lowering CO_2 emissions using many MCDM approaches—including fuzzy Electre, TOPSIS, DEMATEL, and VIKOR—so providing insights on how to balance social, environmental, and financial aspects. Using fuzzy SAW, TOPSIS, MOORA, and VIKOR, Nuriyev et al. [9] explore renewable transition scenarios in oil-producing countries, therefore highlighting a scenario-based approach that corresponds with Thailand's requirement to balance conflicting energy sources. Using fuzzy AHP, TOPSIS, and VIKOR to rangeland conditions, Gökkuş et al. [10] show how these techniques may quantitatively evaluate renewable resource quality—relevant for regional energy and land use policies. Sarker et al. [11] integrate a Balanced Scorecard perspective with fuzzy MCDM to measure sustainability performance, echoing the necessity of multi-dimensional evaluation in energy planning. Lastly, Shang et al. [12] employ a hybrid fuzzy DEMATEL, TOPSIS, and VIKOR framework to prioritize technical factors for a low-carbon industry, further emphasizing the importance of robust,

XXX-X-XXXX-XXXX-X/XX/$XX.00 ©20XX IEEE

integrated MCDM tools for guiding sustainable energy initiatives.

Emphasizing the interaction between economic, environmental, and social factors—an approach pertinent to renewable energy planning in Thailand, where many dimensions must be balanced—Çalik [13] shows how fuzzy AHP combined with TOPSIS, VIKOR, and MULTIMOORA refines sustainable supplier selection. Proposing a new criteria set and combining FAHP with VIKOR, TOPSIS, WASPAS, and PROMESTEEP for rigorous, systematic assessments, Kshanh and Tanaka [14] extend this idea inside ISO 50001 energy efficiency initiatives. Jain et al. [15] underline even further the adaptability of MCDM in industrial environments—highlighting frameworks such as fuzzy TOPSIS and fuzzy VIKOR—that may be fit to choices in the energy sector. Ding et al. [16] highlight the potential of fuzzy DEMATEL, TOPSIS, and VIKOR to guide challenging choices where safety, waste management, and cost-effectiveness are crucial. They also show a new 2-tuple reluctant fuzzy technique to analyzing sustainable energy price, therefore confirming their possibilities. Liu et al. [17] also show how well fuzzy AHP can be used in AI-based education, therefore supporting the method's general relevance in challenging, multi-criteria selection alternative such those encountered in energy planning.

III. RELATED METHODS

This research addresses the task of choosing the most suitable renewable energy source for Thailand by balancing both economic and environmental factors. There are five criteria—return on investment (C_1), reduction in the use of natural resources (C_2), initial investment cost (C_3), decrease in CO_2 emissions (C_4), and reduction of ecological impact (C_5) and evaluate five alternatives as the renewable energy system: solar energy (R_1), wind energy (R_2), biomass energy (R_3), waste-to-energy (R_4), and marine energy (R_5). First, based on expert opinions, beginning with the FAHP ascertain the relative importance of every criteria. The system are ranked under the same set of weights using Fuzzy-TOPSIS and Fuzzy-VIKOR, therefore assuring that both numerical data and expert views are properly represented even in cases of ambiguity. This methodical, unambiguous technique seeks to provide useful insights for direction of Thailand's future energy policies.

A. Fuzzy AHP

In this study, FAHP [17] is applied to determine the relative importance of five criteria for selecting the most suitable renewable energy source. Step 1: A pairwise comparison matrix is constructed based on expert evaluations using triangular fuzzy numbers (TFNs) to capture uncertainty. Step 2: Reciprocal values are computed to maintain consistency in comparisons. Step 3: The fuzzy geometric mean is calculated to aggregate expert judgments for each criterion. Step 4: These values are normalized to obtain fuzzy weights, ensuring proportional representation. Step 5: The fuzzy weights are defuzzified using the weighted average method, followed by a normalization step to ensure all weights are sum to 1. This structured approach refines expert insights into meaningful numerical values, forming a solid foundation for ranking renewable energy system. To ensure the reliability of expert evaluations, a Consistency Ratio (CR) is used to assess the logical consistency of the pairwise comparison matrix.

TABLE I. FUZZY-AHP PROCESSES.

Step	Equation	
Construct the Pairwise Comparison Matrix	$X = \begin{bmatrix} x_{11} & x_{12} & \cdots & x_{1n} \\ x_{21} & x_{22} & \cdots & x_{2n} \\ \vdots & \vdots & \ddots & \vdots \\ x_{n1} & x_{n2} & \cdots & x_{nn} \end{bmatrix}.$	(1)
Compute the Reciprocal Matrix	$X^{-1} = (l, m, u)^{-1} = (\frac{1}{u}, \frac{1}{m}, \frac{1}{l}).$	(2)
Synthesize the Fuzzy Geometric Mean	$r_i = \left(\prod_{k=1}^{n} l_k^{\frac{1}{n}}, \prod_{k=1}^{n} m_k^{\frac{1}{n}}, \prod_{k=1}^{n} u_k^{\frac{1}{n}}\right).$	(3)
Calculate the Fuzzy Weights	$W_i = r_i \cdot \left(\sum_{k=1}^{n} r_k\right)^{-1}.$	(4)
Defuzzification and Normalization	$w_i = \left(\frac{l+2m+u}{4}\right),$ $Nw_i = \frac{w_i}{\sum_i w_i}.$	(5)

B. Fuzzy-TOPSIS

Fuzzy-TOPSIS [2] is applied in this study to rank renewable energy system by measuring their closeness to an ideal solution. This method is particularly useful as it evaluates each option relative to both the best and worst possible outcomes, making it effective for decision-making under uncertainty. Step 1: A fuzzy decision matrix $X = [\tilde{x}_{ij}]$ is constructed, where each entry $\tilde{x}_{ij}$ represents the fuzzy rating given by experts for alternative i under criterion j, expressed as triangular fuzzy numbers (TFNs). Step 2: The matrix is normalized to ensure comparability across different criteria, using benefit or cost-based normalization, where $c_j^* = max_t\{x_{ij}^u\}$ for benefit and $c_j^- = min_t\{x_{ij}^l\}$. Step 3: A weighted normalized decision matrix $\tilde{V}$ is computed by multiplying the normalized values with the respective fuzzy weights derived from Fuzzy AHP. Step 4: The fuzzy positive ideal solution (FPIS) and fuzzy negative ideal solution (FNIS) are determined, representing the best and worst possible values for each criterion, where $v_j^* = (max_i v_{ij}^u, max_i v_{ij}^m, max_i v_{ij}^l)$ and $v_j^- = (min_i v_{ij}^l, min_i v_{ij}^m, min_i v_{ij}^u), j = 1,2,\ldots,n$ Step 5: The distance of each alternative from FPIS and FNIS is calculated using a fuzzy distance metric, and Step 6: The closeness coefficient (CC_i) is derived to rank the alternative, with the highest CC_i indicating the most preferred energy source. By incorporating fuzzy logic, this structured approach effectively handles uncertainty in expert evaluations, making it a suitable tool for selecting the optimal renewable energy solution for Thailand.

TABLE II. FUZZY-TOPSIS PROCESSES.

Step	Equation	
Construct the Fuzzy Decision Matrix	$X = [\tilde{x}_{ij}]_{m\times n}.$	(6)
	$x_{ij}^l = min_k\{x_{ij}^{k,l}\}, x_{ij}^m = \frac{\sum_{k=1}^{k} x_{ij}^{k,m}}{k},$ $x_{ij}^u = max_k\{x_{ij}^{k,u}\}.$	(7)
Normalize the Fuzzy Decision Matrix	$\tilde{r}_{ij} = \left(\frac{x_{ij}^l}{c_j^*}, \frac{x_{ij}^m}{c_j^*}, \frac{x_{ij}^u}{c_j^*}\right); Benefit\ criteria,$	(8)
	$\tilde{r}_{ij} = \left(\frac{c_j^-}{x_{ij}^l}, \frac{c_j^-}{x_{ij}^m}, \frac{c_j^-}{x_{ij}^u}\right); Cost\ criteria.$	(9)

Compute the Weighted Normalized Decision Matrix	$\tilde{V} = [\tilde{v}_{ij}]_{m\times n}$, $\tilde{v}_{ij} = (v_{ij}^l, v_{ij}^m, v_{ij}^u) = (w_{ij}^l r_{ij}^l, w_{ij}^m r_{ij}^m, w_{ij}^u r_{ij}^u).$	(10)
Determine FPIS and FNIS	$A^* = (v_1^*, v_2^*, \dots, v_n^*); FPIS,$	(11)
	$A^- = (v_1^-, v_2^-, \dots, v_n^-); FNIS.$	(12)
Compute the Distance of Each Alternative from FPIS and FNIS	$d_i^* = \sum_{j=1}^{n} d(\tilde{v}_{ij}, \tilde{v}_{ij}^*), i = 1,2,\dots,m,$	(13)
	$d_i^- = \sum_{j=1}^{n} d(\tilde{v}_{ij}, \tilde{v}_{ij}^-), i = 1,2,\dots,m.$	(14)
Compute the Closeness Coefficient	$CC_i = \frac{d_i^-}{d_i^* + d_i^-}, i = 1,2,\dots m.$	(15)

C. Fuzzy-VIKOR

Fuzzy-VIKOR is used in this study to rank renewable energy system as well as Fuzzy-TOPSIS by identifying a compromise solution that balances overall performance and individual regret. Step 1: A fuzzy decision matrix is constructed, where experts evaluate each alternative under multiple criteria using triangular fuzzy numbers (TFNs). Step 2: The best f_j^* and worst f_j^- values for each criterion are determined to establish ideal and anti-ideal solutions. Step 3: The group utility measure S_i is calculated to assess the overall performance of each alternative, while the regret measure R_i captures the most significant individual disadvantage. Step 4: The VIKOR index Q_i is computed as a weighted combination of S_i and R_i, with parameter v controlling the balance between group utility and regret, where $S^- = max_i\{S_i\}, S^+ = min_i\{S_i\}$ and $R^- = max_i\{R_i\}, R^+ = min_i\{R_i\}$ Step 5: Alternatives are ranked based on Q_i, with the lowest value indicating the best compromise solution. This structured approach ensures a fair evaluation of renewable energy options under uncertainty, making it a robust tool for decision-making in Thailand's energy sector.

TABLE III. FUZZY-VIKOR PROCESSES.

Step	Equation	
Construct the Fuzzy Decision Matrix	$X = [\tilde{x}_{ij}]_{m\times n}.$	(16)
Identify the Best and Worst Values for Each Criterion	$f_i^* = max_j\{f_{ij}\}, f_i^- = min_j\{f_{ij}\}; Best,$ $f_i^* = min_j\{f_{ij}\}, f_i^- = max_j\{f_{ij}\}; Worst.$	(17)
Compute the Group Utility and Regret Measure	$S_i = \sum_{j=1}^{n} \frac{w_j(f_i^* - f_{ij})}{(f_i^* - f_{ij})},$	(18)
	$R_i = max_i \frac{w_j(f_i^* - f_{ij})}{(f_i^* - f_{ij})}.$	(19)
Compute the VIKOR Index	$Q_i = v\frac{(S_i - S^*)}{(S^- - S^*)} + (1-v)\frac{(R_i - R^*)}{(R^- - R^*)}.$	(20)

After computing the VIKOR Index Q_i, in step 5 of Ranking. The alternative with the lowest Q_i value is the best compromise solution.

IV. RESULTS & DISCUSSIONS

In this study, fuzzy linguistic terms were used to handle uncertainty in expert evaluations across different decision-making methods. For Fuzzy AHP, expert pairwise comparisons were assessed using triangular fuzzy numbers (TFNs), as referenced in [2]. These FNs allowed for more flexible and realistic weight assignments to the decision criteria.

TABLE IV. FUZZY LINGUISTIC TERMS AND FUZZY NUMBERS.

Fuzzy Linguistic Terms	Numerical Values
Extremely Low (EL)	(1,1,2)
Low (L)	(2,3,4)
Moderately Low (ML)	(3,4,5)
Neutral (N)	(4,5,6)
Moderately High (MH)	(5,6,7)
High (H)	(6,7,8)
Extremely High (EH)	(8,9,9)

Renewable energy options were assessed for Fuzzy-TOPSIS and Fuzzy-VIKOR using another set of fuzzy linguistic phrases and numerical values. Decision-makers assessed options using linguistic phrases ranging from Extremely Low (EL) to Extremely High (EH), mapped to matching TFNs as shown in (Table IV). By collecting both subjective views and numerical uncertainty, this technique allowed a systematic evaluation. These techniques guarantee efficient inclusion of expert opinions by using TFNs, therefore preserving consistency and dependability in the alternative ranking.

In this study, three experts provided their individual triangular fuzzy numbers (TFNs) for each criterion and alternative (Table V), reflecting their respective opinions under uncertainty. To produce a single, unified input for further analysis, these TFNs were aggregated into one representative set of (l, m, u) values per criterion (or alternative). This aggregation retains the benefits of fuzzy logic—accounting for imprecision and expert variability—while simplifying the decision-making process by using a single fuzzy evaluation rather than multiple, separate ones.

TABLE V. THE FUZZY RELATIONSHIPS PAIRWISE COMPARISONS OF CRITERIA AND ALTERNATIVE FROM THREE EXPERTS.

EXPERTS	C	C_1	C_2	C_3	C_4	C_5
E_1, E_2, E_3	$\frac{C_1}{R_1}$	$\frac{1,1,1}{MH,H,H}$	$\frac{1,3,1}{MH,H,H}$	$\frac{5,5,5}{MH,N,N}$	$\frac{3,2,\frac{1}{7}}{H,MH,H}$	$\frac{3,2,\frac{1}{9}}{EH,EH,H}$
	$\frac{C_2}{R_2}$	$\frac{1,\frac{1}{3},1}{ML,ML.H}$	$\frac{1,1,1}{ML,ML,MH}$	$\frac{5,1,4}{L,L,L}$	$\frac{1,1,\frac{1}{8}}{N,N,MH}$	$\frac{1,3,\frac{1}{8}}{N,N,H}$
	$\frac{C_3}{R_3}$	$\frac{\frac{1}{5},\frac{1}{5},\frac{1}{5}}{ML,N,MH}$	$\frac{\frac{1}{5},1,\frac{1}{4}}{ML,L,MH}$	$\frac{1,1,1}{N,N,MH}$	$\frac{1,1,\frac{1}{8}}{L,N,N}$	$\frac{1,2,1}{N,N,MH}$
	$\frac{C_4}{R_4}$	$\frac{\frac{1}{3},\frac{1}{2},7}{N,MH,MH}$	$\frac{1,1,8}{N,ML,H}$	$\frac{1,1,8}{ML,L,L}$	$\frac{1,1,1}{ML,L,N}$	$\frac{2,1,1}{MH,N,N}$
	$\frac{C_5}{R_5}$	$\frac{\frac{1}{3},\frac{1}{2},9}{MH,MH,H}$	$\frac{1,\frac{1}{3},8}{N,ML,H}$	$\frac{1,\frac{1}{2},8}{ML,L,H}$	$\frac{\frac{1}{2},1,1}{MH,MH,MH}$	$\frac{1,1,1}{N,N,MH}$

After computing those two methods ((6)-(15), (16)-(20)), both Fuzzy-TOPSIS and Fuzzy-VIKOR identify R_1 as the top-ranked option, followed by R_5, R_2, R_4, and R_3 in descending order (Table VI).

TABLE VI. THE RANKING OF RENEWABLE ENERGY OF FUZZY-TOPSIS AND VIKOR.

Alternative	FTOPSIS	FVIKOR	Ranking

	CC_i	Q_i	
R_1	0.84413	0.00000	1
R_2	0.42463	0.78282	3
R_3	0.08219	1.00000	5
R_4	0.39145	0.83113	4
R_5	0.53608	0.57455	2

These consistent outcomes suggest that, under the given criteria and expert judgments, solar energy offers the most balanced advantages, while biomass is the least favored.

V. Conclusions

Based on the ranking results from Fuzzy-TOPSIS and Fuzzy-VIKOR (Fig. 1), solar energy (R_1) emerges as the best renewable energy investment due to its significantly lower costs compared to other system while delivering strong environmental and economic benefits. Marine energy (R_5) follows in second place, providing good returns but requiring a much higher initial investment than solar energy. Wind energy (R_2) ranks third, mainly due to its high land and infrastructure requirements, which impact natural ecosystems and space utilization more than solar and marine energy. Waste-to-energy (R_4) ranks fourth, as it does not consume natural resources but has high processing costs and a limited impact on CO_2 reduction compared to other options. Lastly, biomass energy (R_3) is placed in fifth position despite its ability to reduce CO_2 emissions, as it heavily depends on natural resources, raising concerns about long-term sustainability and ecological impact. These rankings highlight the balance between environmental and economic considerations in selecting the most suitable renewable energy source.

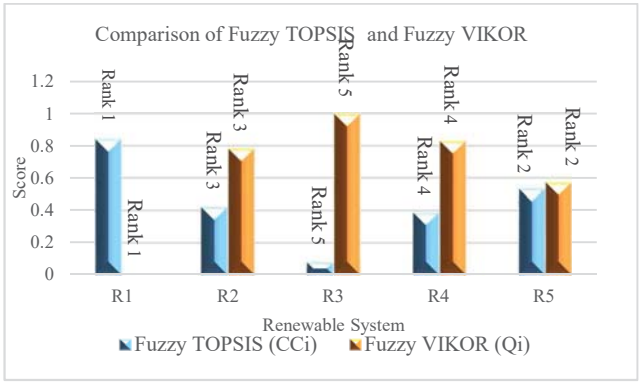


Fig. 1. Comparative ranking between Fuzzy-TOPSIS and Fuzzy-VIKOR

To ensure the robustness of the Fuzzy-VIKOR results, we conducted additional analyses by varying the v value, which controls the balance between group utility (S_i) and individual regret (R_i). Despite adjusting v, the ranking remained unchanged, confirming that the alternatives are inherently strong in their relative positions. This consistency suggests that the selected renewable energy sources have clear advantages and disadvantages, making their rankings stable regardless of the emphasis placed on group utility or regret measures. Further study may use the Taguchi approach to methodically combine both findings into a single choice in circumstances where Fuzzy-TOPSIS and Fuzzy-VIKOR provide different rankings. Taguchi may provide a statistically supported conclusion that lowers uncertainty and improves the interpretability of multi-method decision-making systems by maximizing the ranking consistency by means of experimental design concepts.

Acknowledgment

This work was supported by the research funding from the Faculty of Engineering, Thammasat School of Engineering, Thammasat University.

References

[1] O. Meixner, "Fuzzy AHP group decision analysis and its application for the evaluation of energy sources," presented at the *Conference on Decision Analysis*, January 2009.

[2] O. Taylan, R. Alamoudi, M. Kabli, and E. Herrera-Viedma, "Assessment of energy systems using extended fuzzy AHP, fuzzy VIKOR, and TOPSIS," *Sustainability*, vol. 12, no. 7, Mar. 2020. DOI: 10.3390/su12072745.

[3] V. Jain, A. Kumar, S. Sakhuja, and R. Aggarwal, "Supplier selection using fuzzy AHP and TOPSIS: A case study in the Indian automotive industry," *Neural Comput. Appl.*, vol. 29, no. 11, Apr. 2018. DOI: 10.1007/s00521-016-2533-z.

[4] B. Sodhi and P. Tadinada, "A simplified description of fuzzy TOPSIS," *arXiv*, May 2012.

[5] Z. M. Rodzi, "The TOPSIS of different ideal solution and distance formula of fuzzy soft set in multi-criteria decision making," July 2021.

[6] A. Shemshadi, H. Shirazi, M. Toreihi, and M. J. Tarokh, "A fuzzy VIKOR method for supplier selection," *Expert Syst. Appl.*, vol. 38, no. 10, pp. 12160–12167, Sep. 2011.

[7] E. Afful-Dadzie, "Fuzzy VIKOR approach: Evaluating quality of internet health information," *Federated Conf. Comput. Sci. Inf. Syst.*, vol. 2, Sep. 2014. DOI: 10.15439/2014F203.

[8] C. Delcea, I. Nica, I. Georgescu, N. Chiriță, and C. Ciurea, "Integrating fuzzy MCDM and ARDL for circular economy strategy," *Mathematics*, vol. 12, no. 19, Oct. 2024. DOI: 10.3390/math12192997.

[9] M. Nuriyev, A. Nuriyev, and J. Mammadov, "Renewable energy transition task solution for oil countries using fuzzy MCDM: The case of Azerbaijan," *Energies*, vol. 16, no. 24, Dec. 2023. DOI: 10.3390/en16248068.

[10] Z. Gökkuş, S. Şentürk, and F. Alatürk, "Ranking districts of Çanakkale in terms of rangeland quality by fuzzy MCDM methods," *J. Agric. Biol. Environ. Stat.*, vol. 28, no. 4, pp. 636–663, Dec. 2023. DOI: 10.1007/s13253-023-00532-7.

[11] M. R. Sarker, S. M. Ali, S. K. Paul, and Z. H. Munim, "Measuring sustainability performance using an integrated model," *Measurement*, vol. 184, Nov. 2021. DOI: 10.1016/j.measurement.2021.109931.

[12] H. Shang, F. Su, S. Yüksel, and H. Dinçer, "Identifying the strategic priorities of the technical factors for the sustainable low carbon industry based on macroeconomic conditions," *SAGE Open*, vol. 11, no. 2, 2021. DOI: 10.1177/21582440211016345.

[13] A. Çalik, "A comparative perspective in sustainable supplier selection by integrated MCDM techniques," *Sigma J. Eng. Nat. Sci.*, vol. 38, no. 2, pp. 835–852, 2020.

[14] I. Kshanh and M. Tanaka, "Comparative analysis of MCDM for energy efficiency in petrochemical industries," *Expert Syst. Appl.*, vol. 255, Dec. 2024. DOI: 10.1016/j.eswa.2024.124692.

[15] P. Jain, K. Abhishek, and P. Chatterjee, *Decision-Making Models and Applications in Manufacturing Environments*, Jan. 2024. DOI: 10.1201/9781003394723.

[16] Z. Ding, S. Yüksel, and H. Dinçer, "Pythagorean fuzzy soft computing approach for sustainable energy pricing," *Energy Rep.*, vol. 7, pp. 5575–5588, Nov. 2021. DOI: 10.1016/j.egyr.2021.08.181.

[17] Y. Liu, A. A. Al-Atawi, I. A. Khan, N. Gohar, and Q. Zaman, "Using the fuzzy analytical hierarchy process to prioritize the impact of visual communication based on AI for long-term learning," *Fuzzy Syst. Math.*, vol. 27, pp. 157–168, 2023.

TRACK 2
ELECTRONIC ENGINEERING

Mosquito Trap HV Power Supply Turn On/Off Time Parameter Consideration Measurement

Jirawath Parnklang
Department.of Electronics Engineering, School of Engineering
King Mongkut'Institute of Technology Ladkrabang
Bangkok, Thailand
email:jirawath.par@kmitl.ac.th

Nattanicha Sowannee
Department.of Electronics Engineering, School of Engineering
King Mongkut'Institute of Technology Ladkrabang
Bangkok, Thailand
email: feelnattanicha@gmail.com

Kasamaphon Pakhunophat
Tx Engineer,TeraHop (Thailand) Co.,Ltd. 198, Moo 7, Nong Planoh sub-district, NongKhae district, Saraburi 18140
Bangkok, Thailand
email:Kasamaphon01.gmail.com

Siriwat Ganasut
Department.of Electronics Engineering, School of Engineering
King Mongkut'Institute of Technology Ladkrabang
Bangkok, Thailand
email: team0618153993@gmail.com

Pasuthida Wisitthikorn
Department.of Electronics Engineering, School of Engineering
King Mongkut'Institute of Technology Ladkrabang
Bangkok, Thailand
email: pasuthida@gmail.com

Tanutpong Ramkaow
Department.of Electronics Engineering, School of Engineering
King Mongkut'Institute of Technology Ladkrabang
Bangkok, Thailand
email: 64601061@kmitl.ac.th

***Abstract*—This article attempts to find out the results for the manufacturer of ecology high voltage trap and kill small insect especially mosquitos. Due to the environment factor, it is necessary to turn on the tool at all time according to the ministerial regulation. This concept, high voltage power supply for killing mesh grid has been turned off to save the energy and is turned on when a target insect is to be kill. A turn on time that is fast enough to kill the insect complete is therefore taken into consideration to obtain the appropriate condition. A sampling of high voltage generating circuit manufacturer suitable for mosquito trap was perform. Apply appropriate input voltage to the input port of the high voltage power supply circuit, the turn on time is measurement. Testing data is useful in that we can know the appropriate input voltage for using a high voltage power supply in the mosquito trap that need to save electrical energy by turn off the high voltage power supply. The input voltage of the high voltage circuit is divided into 2 group. The first is ordinary battery with different material such as 2 cell of carbon-zinc (1.5V×2) alkaline (1.5V×2), lithium-ion and lithium-polymer (4.1v). The second is ordinary household's AC input voltage. The average data of the high voltage steady state turn on time value is in the order of lower than 50mS. Compare that data to the flying movement speed of the mosquito, it can fly distance of up 8.3 cm. This show that the mosquito detect process must be complete before the mosquito move or fly closer than 8.3 cm. to the mosquito trap. It is true that higher input voltage, the short steady state output voltage of the high voltage part. Use of this data is to optimize the input voltage or input type of the high voltage power supply that is appropriate for the mosquito detection.**

Keywords—consumer electronics circuit, testing, ecology system

I. INTRODUCTION

According to the announcement of the Ministry of Public Health, 24 August 2021, [1] regarding prevention and prevention criteria. Regulation on eliminating insect and animal that are decease carrier in business establishment that are hazardous to health. Item 4, criterial for preventing and eliminating insect and animal that are decease carrier. Business operator must inspect insect and animal that are decease carrier. Regularly monitor the spread of decease in the business establishment. In case where insects are found and animal that are carrier, if there is decease or traces of it, it must be eliminate using method. And in the second bracket, protection cases and to be eliminated using mechanical or electrical method, such as using light traps and mouse traps, clean and safe practice. Enforcement of this law, Establishment by this law have a kitchen or food or cafeteria accumulation must be carry out correctly according to food sanitation principle, inspection and storing raw material use in cooking food. Prevent contaminate from insects or animals that are decease carrier. In addition, in item 5, bracket 7, it is required that such establishment must prevent and eliminate insects that decease carrier both within and around house.

The basic component which uses electric energy of electric insects and mosquito exterminator are UV light bulb used to lune insect close to the mosquito catcher, an exhaust fan element to attract flying mosquitos in the fluctuation condition, high voltage electric wire grid used to give electric shock to kill the mosquitos. Example of main electrical part of mosquitos killer can be shown in figure 1.



Fig. 1. Main electrical part of mosquitos killer Example [1]

Thailand 7-11 is an establishment that must follow the announcement of this law. In fact, 7-11 store standard have been eliminated insects that have enter the 7-11 building for a long time. Costumers or users of 7-11 stores will notice an electric mosquitos killer trap that uses UV light to lune insect. 7-11 is a convenience store that is open 24 hours a day. The mosquitos trap will also be turn on 24 hours a day too. 7-11 with the least space, there will be at least 1 mosquitos killer

trap. On average, one 7-11 mosquitos killer trap is used in an area of 50 m^2. 7-11 in Thailand currently has approximate 15000 branches. By the end of 2024, 7-11 will open approximately 700 new stores. This means the number of 7-11 stores will increase to 16000 stores soon. This continuous result is the number of insects or mosquitos killer trap exterminator station be more than 32000 units by the end of 2024. The power rating of the mosquitos killer trap that 7-11 use is 30 watts. It is estimated that by the end of 2024, the power value of the mosquitos killer trap has a minimum value of 960kw.

Reducing the electrical energy consumption in this electric mosquito killer device has not receive much attention yet. This may be due to the fact that the number of uses of such equipment is still low. But in this case overall, we will focus on reducing electrical energy in establishments affected by the ministerial regulations mention above. Electric mosquito and insect exterminators will consider the electrical energy consumption of each component of the machine and reduce the electrical energy consumption piecemeal with the reality that the equipment must maintain the same performance as announced by ministerial regulation. Form figure 1, the components of the machine that have been developed to use lower electrical energy, have received a lot of attention, is the element that the average person can see most clearly is the UV light source. In other words, this UV lamp were originally base on regular fluorescent lamp, which are now less important because they use more electricity energy than modern lamp. But in some manufacturer of mosquito and insect exterminator. This old fashion UV light source is still used for some reason. The old UV light source is a temperature source that, if controlled, the come-out temperature value is similar to the human body temperature. This means that in addition UV ray in being the light used to lure mosquito and insect closer to the exterminator, human temperature in the form of IR radiation also attract mosquito and insect. Reducing the electrical power of ordinary fluorescent lamp can be achieved by developing fluorescent inner fluorescent substance (mercury) coating, to increase intensity efficient. Development of this inner coating cannot be used with UV fluorescent lamp because this UV fluorescent type do not have the same inner coating as the color fluorescent. Direct substitution, UVLEDs light source have been replace to UV fluorescent lamp for the purpose of reducing power consumption, same applied to the use of LED bulbs in lighting engineering. UVLEDs system typically use approximate 65% less electrical energy than similarly sized mercury arc system. The power required to run UVLEDs are consider lower than what is required to create the electrical arc in a UV bulb to produce enough heat and intensity to vaporize mercury and create UV light. And UVLEDs can also reduce electrical energy consumption by using the PWM constant current driver circuit technique that increasing intensity light than using ordinary DC direct drive circuit.

High voltage supply, which is a device in the mosquito killer that uses electricity all the time. It is an interesting device to reduce energy consumption and still work in normal condition very well. There are many ways to reduce electrical power of this device. Power requirement such as developing circuit to lower input voltage, reducing current consumption while the circuit is operating in idle condition, using low power dissipation electronic component. This whole process can be done but the limitation on the value of the circuit is the reason to stop the development. Mosquitos trap high voltage circuit manufacture therefore continue to produce circuit of medium and low quality and supply this circuit to the market regularly. As a leader in electrical mosquito trapping equipment using high voltage as an important component. With the desire to develop a mosquito trap that assemble from the factory itself. They are different and advantage of lower electrical energy consumption. A factory that use the same high voltage circuit production supplier source to assemble mosquito or insect catching equipment. Adding smart element to mosquito catching is an approach that has been judged appropriate. High voltage grid is only use to kill mosquito of insect, meaning that the need to create high voltage arise when mosquito or insect are present. Fly into the range that can only be destroy by high voltage grid. In other words, we do not need to supply high voltage to the grid all the time. We can turn on the high voltage and maintain it long enough to successfully kill mosquito or insect.

With the intention of turning off the high voltage circuit in order to reduce the electrical energy in condition where the high voltage circuit do not yet need to generate high voltage to kill mosquito or insect. To start project, kick off this idea, we turn off the high voltage supply to the grid and only applied the high voltage when the mosquito enters the high voltage corona of the grid. A correct method to determine if an incoming insect is truly a mosquito is the system shown in figure 2.

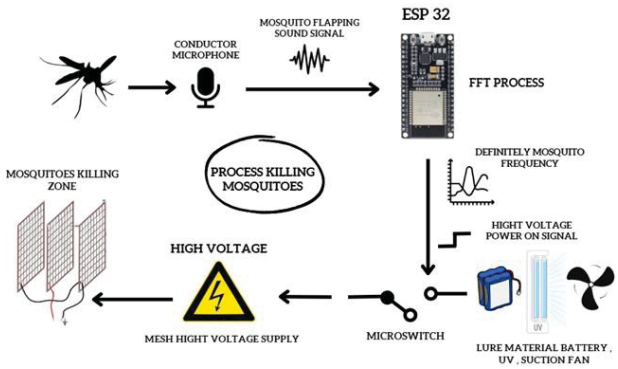


Fig. 2. Main block diagram of electrical mosquito killer equipment [2]

Flapping sound signal of the mosquito wing that the system has already captured, we added a turn on high voltage supply to grid for immediately kill. The problem that we need to solve in order to keep the same machine function. The high voltage supply to grid durations time is in time to killing. Form figure 2 when a mosquito flies close to the mosquito killer, the condenser microphone receives the sound of the mosquito's flapping wing and sent the sound signal to the ESP32 microcontroller to process and conclude that is the sound of a mosquito. ESP32 send a trigger signal to power on the high voltage power for the killing grid. The voltage of the killing grid rise up to the appropriate value and short circuit by the flying mosquito.

II. Electric Mosquito Killing HV Supply

Electric mosquito killer needs just a lithium polymer battery or a NiMH battery or maybe al lead acid battery. The output voltage of these battery around 3 to 4 volts. The minimum voltage maybe around 2.5V. As transistor that makes the circuit work, does not work below that voltage. Now with that voltage, it converts to nearabout 2.5kV that is released in the grid. It is done by first converting the DC 3

volts into high frequency AC about 100kHz to 200 kHz. That AC voltage is fed to a transformer that steps up from 3V AC into 700V or 800V AC. Then that high voltage AC is passed through a voltage multiplier circuit consisting of capacitors and diodes. That makes the AC high voltage into DC and doubles the voltage with it. Now typically 3-time multiplier stages are used in them which boosts the voltage to 2.5kV. That 2.5kV is fed into a capacitor to act as a buffer and filter that sustains the voltage when the circuit is disengaged. On the output, it generates DC voltage in the range of 1.5kV to 2kV using a Cockroft-Walton ladder network. Such voltage can generate a spark if two conductors of the grid mesh are placed close to each other at a distance of 7–10 mm. This distance is sufficient to cause a short circuit phenomenon with adult mosquito.

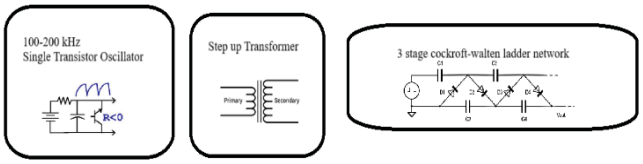


Fig. 3. Block diagram of high voltage supply for grid mesh

An overview of today semiconductor electronics' component, the signal generate circuit with a output frequency of only 100-200kHz is not a considered a parameter that should be of concern. The output signal generate is lower than microsecond order. The rapidity of output voltage ramps up of a lower power (high voltage low current) transformer does not need to be consider in relation to the 3 stage Cockroft-Walton (CW) ladder network.

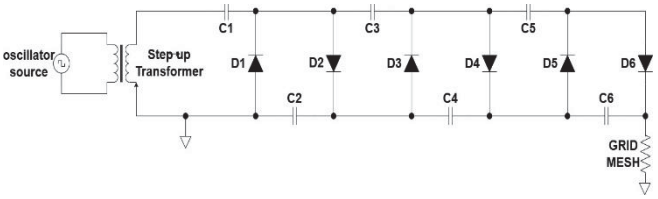


Fig. 4. Overview of high voltage circuit in low-cost mosquito killer

The operation of 3-stage Cockcroft-Walton Voltage Multiplier is divided to four mode operation. [3] In these 4-operating modes, there is an initial condition where the input voltage to the circuit is alternately low state and high state and charge the capacitor. Even number capacitor will work alternately with odd number capacitor. The current that charges the capacitor, there will be a direction of flow coming from each diode (diode as a switch).

$$Vck = Vc \qquad for\ k = 1 \tag{1}$$

$$Vck = 2Vc \qquad for\ k = 2,3,4 \ldots n \tag{2}$$

Where *Vck* is the voltage of the kth capacitor, *Vc* is the maximum peak value of terminal voltage of the CW voltage multiplier under steady-state condition, and N = 2n.[4] Fully charging the capacitor to have double voltage value as per equation (2) is an action that take time according to the general capacitor charging equation. A capacitor will reach 99% charge after 5 time constant and 63.2% after 1 time constant. The time constant is $\tau = RC$. The static resistance in CW need to be as low as to keep short charging time. In addition, from past study [3][4] in high voltage circuit in mosquito killer that require an output power at the grid mesh lower than 100w, it was found that the charging time require in all 3 stage of CW is in the range of hundred millisecond. Once we know the time it takes for the high voltage circuit to the appropriate level to kill the mosquito. We can calculate the distance between the point of the entry mosquito and the killing device precisely. The maximum speed that the mosquito can fly in steady wind condition is 1.6 to 2.4 km/hr. In practice, we need a high enough sound level of mosquitos' flapping wing that the system can recognize it as a real mosquito.

III. Experimentals and Results

Randomly select the manufacture of a high voltage circuit supply suitable for the mosquito electric shock device that has the internal circuit that mention above. Considering the basic specification of the circuit, the input DC voltage range is 3V (No. 1) and 4.1V (No. 2) and the AC voltage is 220V (No.3). We check the internal voltage of the high voltage circuit that uses an AC input voltage of 220V and found that the manufacture converts the 220VAC to 12VDC. The output voltage is not lower than 2.5kV with 0.5W power output at 30 × 30 cm. grid mesh area.

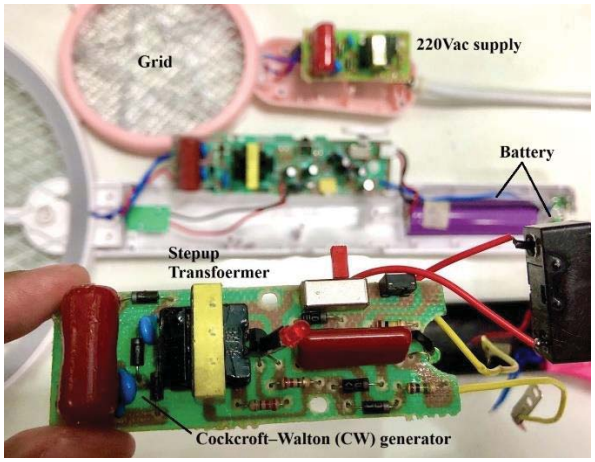


Fig. 5. Some sample of mosquito killer high voltage supply

Sample circuit from selected high voltage manufacturer to test power on time ($T_{turn\ on}$) and power off time ($T_{turn\ off}$) with different input voltage (single cell and double cell battery) condition. The input voltage value that is fed into the circuit will be consider in case where the voltage value is lower than spec, assume that the battery voltage obtained from the input voltage is due to a deteriorated supply. And the voltage value higher than spec is the voltage value at which the battery supply is fully complete. First preliminary experiment to find the relationship between the input voltage and the output voltage of the circuit. By testing every circuit with the same condition. The default input voltage is 2.5V (low battery condition) and the maximum input voltage of all circuit is 15V. In case that one of the circuits is damage because it cannot withstand the input voltage. We will use the new original circuit from the same manufacturer to test at lower condition. The basic input and output electrical characteristic have been shown in figure 6. The experimental in figure 6 found that the lowest input voltage of each circuit cannot be specified as percentage. This is the reason that the circuit can operate at low voltage but the output frequency is lower than the design value. The output voltage cannot shock the mosquito. And also, the maximum input voltage that cause damage the circuit depend on the breakdown of the oscillator active device (low-cost device).

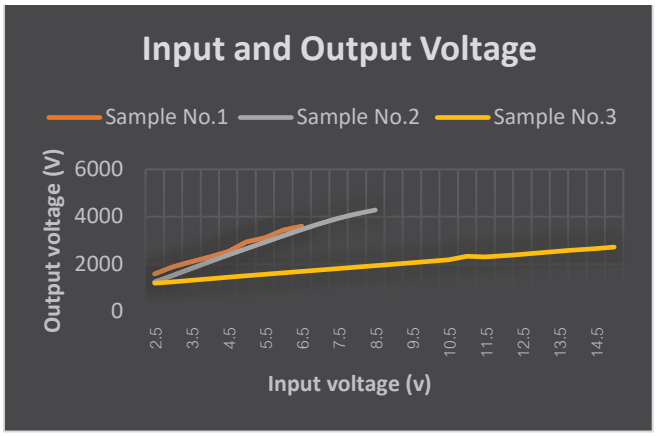
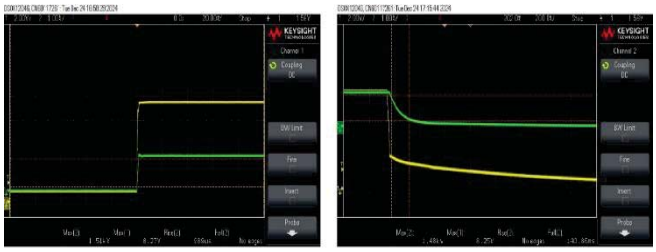


Fig. 6. Input and output voltage of the sampling circuit

We measurement the $T_{turn\ on}$ and $T_{turn\ off}$ of every sample by switch on and off with its mechanical switch. Trigger signal from the switch is assume to 0 mS turn on and turn off. Some of the output and input voltage have shown in figure 7.



(a) (b)

Fig. 7. Some sample of (a) $T_{turn\ on}$ and (b) $T_{turn\ off}$

From figure 7, the yellow signal is the input voltage from the laboratory power supply. The green signal is the high voltage output of the sample with grid mesh as load. We collected data of turn on and turn off time of the high voltage output circuit. It worth noting that the $T_{turn\ off}$ time is much higher than the $T_{turn\ on}$ time. The experimental results shown in figure 8 and 9 respectively.

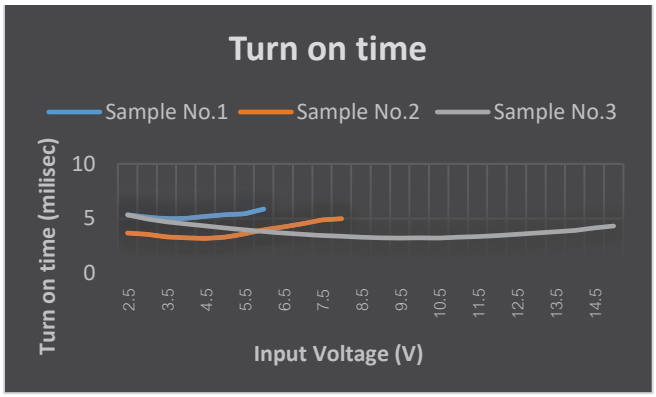


Fig. 8. Turn on time of the sample

From the experimental in figure 8 all of the sample turn on time is on the order of millisecond. There is an observation, the changing input voltage has different turn on time. As the results of when the input voltage increases and also increases the output frequency of the first stage oscillator. The response of the capacitor in CW can response. When the frequency oscillator signal is too high the capacitor in CW cannot response.

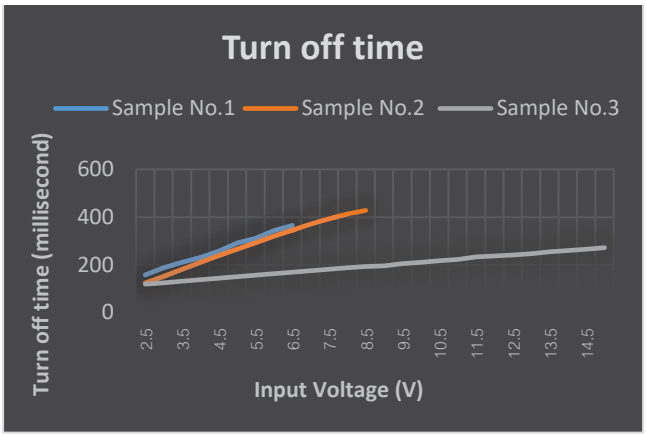


Fig. 9. Turn off time of the sample

From the experimental in figure 9 all of the sample turn off time is on the order of hundred millisecond. This is because in the experiment we started shutting down the high voltage circuit when the output voltage of the circuit was in the steady state.

IV. SUMARY

From the AI system of the mosquito in figure 2 and the $T_{turn\ on}$ and $T_{turn\ off}$ of the high voltage supply, we can calculate the shortest distance and the system must successful of steady state of high voltage on the grid mesh that the mosquito close to the killer machine. This duration time consists of the time receive the mosquito wing flapping sound signal. Processing the sound signal with FFT in ESP32 and then sent the trigger or remote on/off to the high voltage supply. It is shocking because the longest duration time is $T_{turn\ off}$ (compare to the entire period, even if the shortest time), it is the parameter should be sought for solution in the future. We discard the overall longest time because it does not affect the normal operation of the mosquito killer but interest the minimum duration time 125mS. Duration time of this level, the mosquito can fly equal to 8.3 cm. This distance is the shortest which we can maintain the functioning of mosquito killer to save the electricity energy by turn off the high voltage power supply of the killing grid mesh.

ACKNOWLEDGMENT

The authors are grateful to Delta Electronic (Thailand) PLC. Power Electronic Laboratory at Department of Electronic Engineering Faculty of Engineering, KMITL for their Instrument support and encouragements.

REFERENCES

[1] J. Clerk Maxwell, A Treatise on Electricity and Magnetism, 3rd ed., vol. 2. *Oxford: Clarendon*, 1892, pp.68–73.

[2] T. Ramkaow, S. Philaphang, P. Phomphikun and J. Parnklang "Mosquitos Flapping Detection Electrocuting Trap" *2022 7th International Conference on Control and Robotics Engineering (ICCRE)* pp.124-127 doi: 10.1109/ICCRE55123.2022.977.258

[3] "M.N.Karthikeyan , R.P.Pandu, M.Gopisivaprasad, and G.Seshadri4 "Analysis, Simulation of 3-Stage CockcroftWalton Voltage Multiplier for High Step-Up Dc-Dc Converter" *International Journal of Advanced Research in Electrical, Electronics and Instrumentation Engineering* (An ISO 3297: 2007 Certified Organization) Vol. 3, Issue 8, August 2014, pp. 11155-11162

[4] Amol R. Thakare, Senha B. Urkude and Rahul P. Argelwar "Analysis of Cockcroft-Walton Voltage Multiplier" *International Journal of Scientific and Research Publications*, Volume 5, Issue 3, March 2015 1 ISSN 2250-3153, pp. 1-3

Interdigitated Extended Gate Field Effect Transistor for pH Sensor Based on Porous Silicon Layer

Narin Atiwongsangthong
Department of Electronics Engineering, School of Engineering
King Mongkut's Institute of Technology Ladkrabang
Bangkok, Thailand
narin.at@kmitl.ac.th

***Abstract*— In this paper, we present an interdigitated extended gate field effect transistor (IEGFET) pH sensor based on a porous silicon (PS) layer. The porous silicon layer was fabricated through electrochemical etching on p-type silicon <100> substrates using an etching current density of 10 mA/cm², a hydrofluoric acid (HF) concentration of 48%, and an etching duration time of 10 minutes. The surface morphology of the porous silicon layer was analyzed using scanning electron microscopy (SEM). The porous silicon layer was integrated with a commercial N-MOSFET, functioning as an interdigitated extended gate field effect transistor (IEGFET) pH sensor. The fabricated sensor demonstrated enhanced pH sensitivity and linearity, attributed to the high surface area to volume ratio of the porous silicon layer. The pH sensing performance of the porous silicon IEGFET was evaluated at pH values of 4, 7, and 10. Experimental results indicated that in current mode, the sensor exhibited a pH sensitivity of 0.7636 $\mu A^{1/2}$/pH, with a linearity of 99.89%. In voltage mode, the pH sensitivity was 53.5 mV/pH, with a linearity of 99.86%. These results confirm that porous silicon is a highly suitable material for pH sensor applications.**

Keywords—porous silicon, electrochemical etching, pH sensor, interdigitated extended gate field effect transistor

I. INTRODUCTION

Porous silicon (PS) is a nanomaterial composed of nanocrystalline silicon with a highly porous structure [1]. In recent years, it has attracted significant research interest due to its unique physicochemical properties [2]. The ease of fabrication and controllable pore size of porous silicon enable the development of structures with high surface area to volume ratios (400 m^2/m^3) [3]. These properties make porous silicon highly suitable for applications in photodetectors [4], biosensors [5], and gas sensors [6]. Among various sensor technologies, pH sensors are widely used due to their critical role in applications such as environmental monitoring, chemical industrial processes, food quality control, and water treatment.

In this research, a porous silicon layer was employed as a sensitive layer in combination with an interdigitated extended gate field effect transistor (IEGFET), a promising technique for pH sensing. The IEGFET configuration was chosen because it integrates both the reference electrode and the extended gate into an interdigitated structure, eliminating the need for a conventional reference electrode. The device consists of an N-MOSFET and a porous silicon layer, which serves as the chemical sensing layer connected to the N-MOSFET gate. The key distinction in this design is that the reference electrode is replaced by an interdigitated electrode. This study investigates the fabrication and structural characteristics of a porous silicon layer utilized in an interdigitated extended gate field effect transistor (IEGFET) for pH sensing applications. The sensor's performance was evaluated at pH values of 4, 7, and 10. The proposed approach for fabricating the porous silicon IEGFET is simple, low cost, rapid, and highly sensitive for pH detection.

II. EXPERIMENTAL

The uniform distribution of the porous silicon layer was achieved through an anodization process within an electrochemical etching cell made of Teflon. In experiment, the porous silicon layer was formed on a p-type silicon substrate with dimensions of 1 cm × 1 cm, an orientation of (100), a resistivity of 10 Ω-cm, and a thickness of 400 μm. Prior to anodization, the surface of silicon wafer was cleaned using an acetone solution in an ultrasonic system. The porous silicon layer was then prepared under the following anodization conditions: a current density of 10 mA/cm², a hydrofluoric acid concentration of 48%, and an etching duration time of 10 minutes. In electrochemical etching cell, gold material was used as both anode and cathode electrodes. Following the etching process, the porous silicon layer was rinsed with ethanol and deionized (DI) water, then dried using nitrogen gas. The schematic of the electrochemical etching cell is presented in Figure 1, while Figure 2 provides an image of the teflon-based electrochemical etching cell.

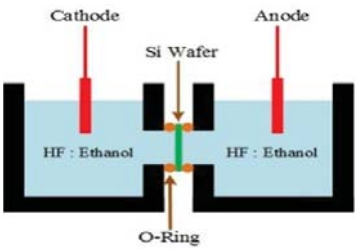


Fig. 1. The schematic of electrochemical etching cell.



Fig. 2. The picture of the teflon-based electrochemical etching cell.

The design and fabrication of the interdigitated electrode mask featured a spacing of 0.6 mm between interdigitated fingers and a finger width of 0.4 mm. Each finger had a length of 5 mm and was equipped with an aluminum contact pad.

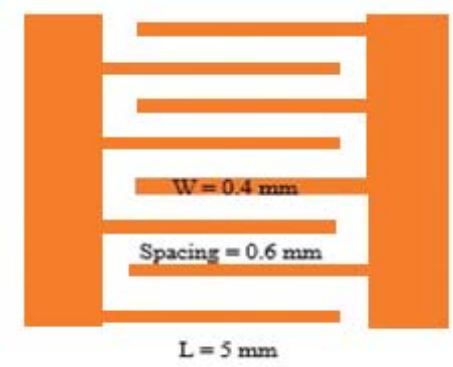


Fig. 3. Schematic diagram of the interdigitated mask.

Figure 3 presents a schematic diagram of the interdigitated mask. Aluminum (Al) was selected as the metallization material for deposition onto the porous silicon layer using a patterned mask. The Al electrode had a thickness of 400 nm and was fabricated using a vacuum thermal evaporator system. The vacuum chamber was evacuated to a pressure of 1×10^{-6} mbar to ensure proper metallization of Al onto the porous silicon layer. An image of the interdigitated Al electrode on the porous silicon layer is shown in Figure 4.

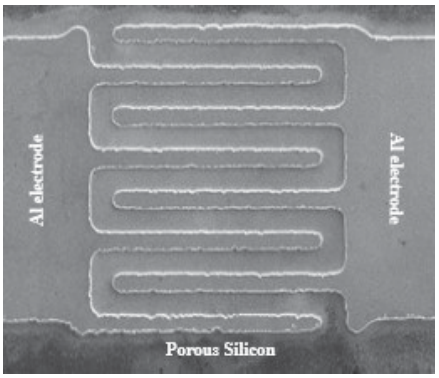


Fig. 4. The picture of the interdigitated Al electrode on porous silicon layer.

The two electrode pads of the interdigitated Al/Ps/Al structure were connected to Cu wires using silver paste and mounted on a PCB board. To prevent chemical reactions between the solution and certain components, the connection pads, Cu wires, and the backside of the silicon substrate on the PCB board were encapsulated with epoxy resin. Only the interdigitated Al electrode on the porous silicon layer remained exposed. The current-voltage (I–V) characteristics of the porous silicon interdigitated extended gate field effect transistor (IEGFET) were analyzed using semiconductor characterization system. The measurement setup is illustrated in Figure 5.

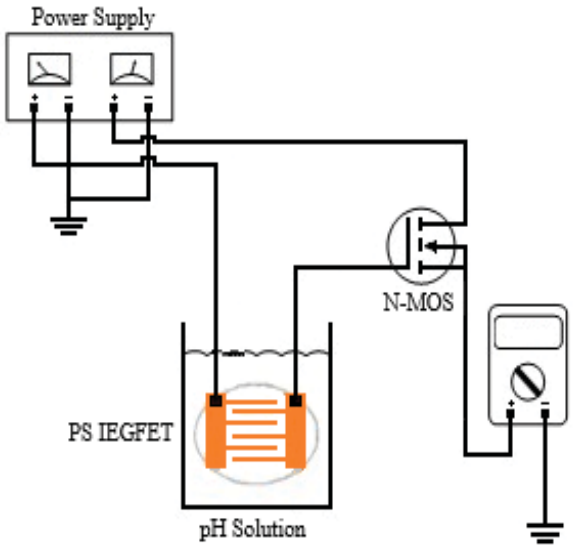


Fig. 5. The measurement system of the porous silicon IEGFET pH sensor.

The measurement system of the porous silicon IEGFET pH sensor consist of two power supplies. One power supply was used to apply voltage to the first Al electrode of the pH sensor, while the second Al electrode was connected to the gate of an N-MOS transistor in a commercial MOSFET (CD4007UBE). The second power supply was used to apply voltage to the source-drain terminal (V_{DS}) of the N-MOS transistor. The interdigitated Al/Ps/Al pH sensor was immersed in a pH buffer solution, with pH values varied at 4, 7, and 10, respectively. All measurements were conducted at room temperature. Between each testing, the interdigitated Al/Ps/Al gate was thoroughly cleaned with deionized water to ensure sensor reliability.

III. Results and Discussion

To analyze the material structure of the porous silicon layer, anodization was performed on a silicon substrate using an electrochemical etching process. Figure 6 presents the surface morphology of the porous silicon layer. The top-view surface image, obtained using a scanning electron microscope (SEM), reveals that the porous silicon layer exhibited a uniform surface. This observation indicates that the Al electrode was uniformly deposited onto the porous silicon layer using a vacuum thermal evaporator.

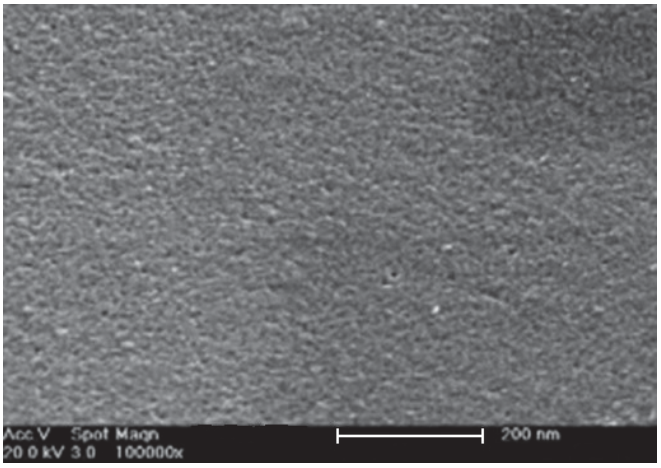


Fig. 6. The top-view surface images of porous silicon layer by SEM

From the experiment, the pH value was measured using the porous silicon IEGFET in two modes of pH sensitivity: current mode and voltage mode. In current mode, the relationship between the drain current (I_{ds}) and pH value was analyzed. The characteristics of the porous silicon IEGFET were evaluated at an applied voltage of 3 V with pH solutions of 4, 7, and 10 as shown in Figure 7.

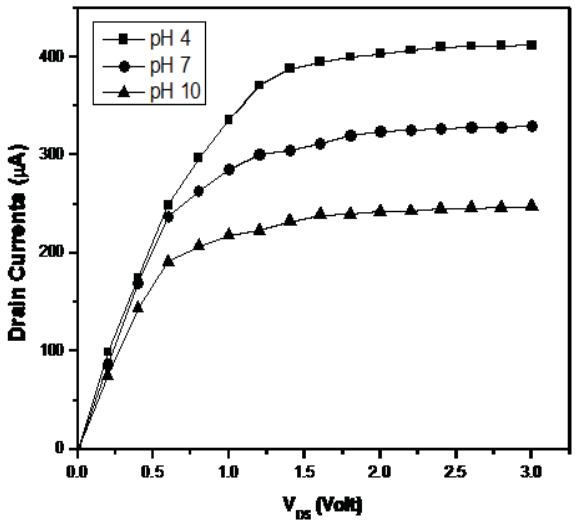


Fig. 7. The drain current (I_{ds}) and drain-source voltage (V_{ds}) of porous silicon IEGFET at pH value 4, 7 and 10.

The drain current in the saturation region increased as the pH value decreased. This behavior is attributed to the effect of H^+ ions on the porous silicon layer at lower pH values. Conversely, at higher pH values, the increased presence of OH^- ions influenced the electrical characteristics of the sensor. The pH sensitivity in current mode was derived from the relationship between the drain current and pH value. As illustrated in Figure 8, the pH current sensitivity was found to be 0.7636 $\mu A^{1/2}$/pH, with a linearity of 99.89%.

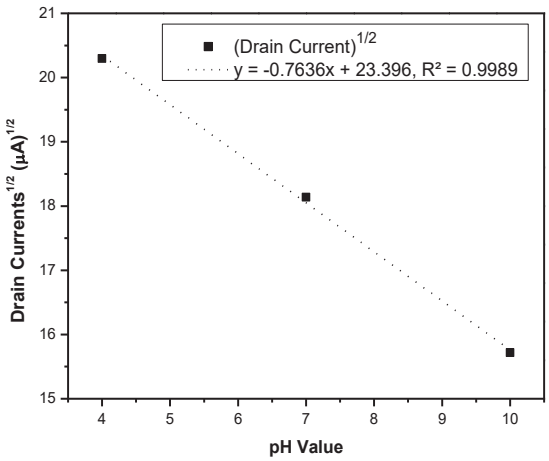


Fig. 8. The drain current (I_{ds}) of porous silicon IEGFET with pH value.

In voltage mode, the relationship between voltage and pH value was analyzed. The drain current (I_{ds}) and voltage characteristics of the porous silicon IEGFET were examined at pH values of 4, 7, and 10, with a drain-source voltage (V_{ds}) of 0.3 V, as shown in Figure 9.

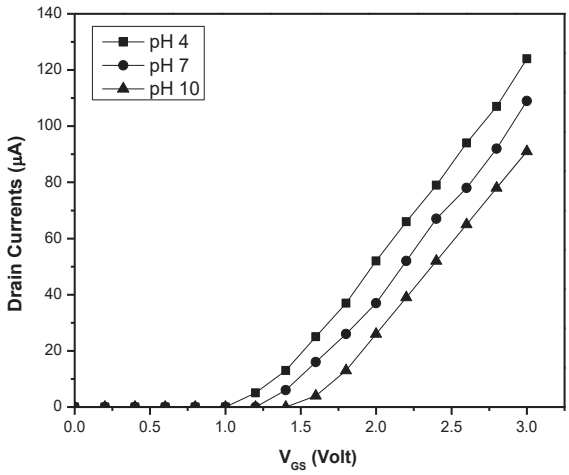


Fig. 9. The drain current (I_{ds}) and voltage (V_{GS}) of porous silicon EGFET with pH value.

The results indicate a positive correlation between the threshold voltage (V_{th}) of the porous silicon IEGFET and the pH value. Specifically, as the pH value increased, the V_{th} exhibited a shift toward a higher voltage bias. The pH sensitivity in voltage mode was derived from the relationship between V_{th} and pH value. As illustrated in Figure 10, the pH voltage sensitivity was determined to be 53.5 mV/pH, with a linearity of 99.86%. This result demonstrates that the porous silicon IEGFET maintains high linearity in voltage mode.

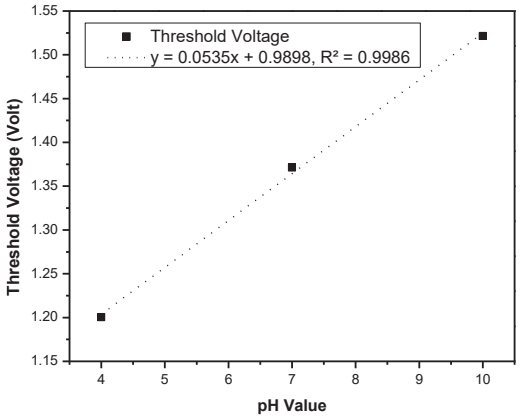


Fig. 10. The threshold voltage (V_{th}) of porous silicon IEGFET as a function of pH value.

The sensitivity of the porous silicon EGFET was summarized in Table I.

TABLE I. THE SENSITIVITY OF THE POROUS SILICON IEGFET BASED ON MEASUREMENT MODE.

Material	**Sensitivity Current Mode ($\mu A^{1/2}$/pH)**	**Linearity (%)**	**Sensitivity Voltage Mode (mV/pH)**	**Linearity (%)**	**pH**
Porous Silicon	0.7636	99.89	53.5	99.86	4 7 10

The porous silicon layer used in this study exhibited favorable properties, making it a suitable materials for IEGFET-based pH sensors.

IV. CONCLUSSION

This study focused on the fabrication of a porous silicon layer using an electrochemical etching process, with anodization parameters including current density, hydrofluoric acid concentration, and etching time. The porous silicon layer was successfully utilized as a sensing element in an interdigitated extended gate field effect transistor (IEGFET) pH sensor. The sensor's pH sensitivity was evaluated in two measurement modes: current mode and voltage mode. In current mode, the sensitivity determined from the relationship between the drain current (I_{ds}) and pH value, was 0.7636 $\mu A^{1/2}$/pH, with a linearity of 99.89%. In voltage mode, the sensitivity derived from the relationship between the threshold voltage (V_{th}) of the porous silicon IEGFET and pH value, was 53.5 mV/pH, with a linearity of 99.86%. Both measurement modes demonstrated high sensitivity and excellent linearity. Based on these results, it can be concluded that the porous silicon IEGFET pH sensor effectively responds to variations in pH by detecting hydrogen ion concentrations in solution.

ACKNOWLEDGMENT

The authors would like to express their gratitude to their colleagues for their support and continuous encouragement throughout the course of this research. Additionally, the authors extend their appreciation to the electronics research center (ERC) and the department of Electronics Engineering, school of engineering, king mongkut's institute of technology ladkrabang (KMITL), for their invaluable assistance and resources.

REFERENCES

[1] Canham, L.: Handbook of porous silicon. Springer, Berlin (2014).

[2] N. Al-Hardan et al., "High Sensitivity pH Sensor Based on Porous Silicon (PSi) Extended Gate Field –Effect Transistor," Sensor, vol. 16 no. 6, 2016, pp. 839.

[3] Adawyia, J.H., Alwan, M.A., Allaa, A.J.: Optimizing of porous silicon morphology for synthesis of silver nanoparticles. Microporous Mesoporous Mater. 227, 2016, pp. 152–160. L.T. Canham, Appl. Phys. Lett., vol. 57, 1990, pp. 1046-1048.

[4] A. Givant, J. Shappir and A. Sa'AR.: Porous Silicon on Insulator: A New Approach to Fabricate Porous Silicon Based Optoelectronic Devices. Phys. Stat. sol. 182, 2000, pp. 419–424.

[5] Andrew Jane, Roman Dronov, Alastair Hodges and Nicolas H. Voelcker.: Porous silicon biosensors on the advance. Trends in Biotechnology. Volume 27, Issue 4, 2009, pp. 230-239.

[6] V.M. Aroutiounian.: Porous silicon gas sensors. Semiconductor Gas Sensors. (2013), pp. 408-430.

TRACK 3
TELECOMMUNICATIONS AND NETWORKING

A Dual-Band Implantable Antenna with Flag-Inspired Patch and Grounded Structure

***Abstract*—In this paper, an implantable antenna for the 915 MHz and 2.45 GHz Industrial, Scientific and Medical (ISM) bands is proposed. It is composed of a cut-edge spiral connected with a flag-shaped structure which are fed by a 50 Ω microstrip line. The ground is also composed of a flag-shaped part connected to a thin strip. The antenna gain was enhanced in two stages by incorporating a flag-shaped structure, first into the patch and then into the ground. Maximum 3D gains of -20.1 and -30.7 dBi have been obtained at 915 MHz and 2.45 GHz, respectively which is large enough to build up a communication link over 10 m considering a link margin of larger than 5 dB. The antenna's compact size, favorable radiation characteristics, and distinctive structure for gain improvement makes it well- suited for implantable applications.**

Keywords—Implantable, ISM, flag-shape, SAR.

I. INTRODUCTION

Implantable antennas have garnered significant interest for years due to their potential applications, which range from temperature sensing [1] and glucose monitoring [2] to at-home hospital care [3]. Like any typical antenna, an implantable antenna must establish a robust communication link over a specific distance, which is determined based on the intended applications. This is typically affected by free-space conditions, which must be addressed by achieving a threshold gain value [4]. However, additional losses occur as the antenna radiates through human body tissues, resulting in small gain values, often below 0 dBi [5]. Antennas with a ground are preferred in such cases due to their ability to produce larger gain values compared to similar antennas without one [6]. Hence, different patch antennas were proposed for implantable applications in the 401-406 MHz MedRadio band [7-8]. Others were proposed in [9-10] for the 915 MHz band and in [11-12] for the 2.45 GHz band. The radiation from the implantable antenna is typically preferred in relatively low frequency bands such as the 401-406 MHz Medical Device Radiocommunications (MedRadio) and the 915 MHz ISM bands rather than higher-frequency bands like the 2.45 GHz band. This is because attenuation losses increase with frequency. On the other hand, higher data rates and larger gain values can be obtained at higher frequencies [13]. Therefore, the 915 MHz band represents a compromise in this case and hence is selected for the design in this paper. In addition, acceptable specific absorption rate (SAR) can be obtained in this band which is required not to exceed 1.6 W/kg (Max 1-g SAR≤ 1.6 W/kg) in order not to harm the human body tissues. While different implantable antennas were already proposed in literature in the 915 MHz band such as those indicated above, they were relatively large in size or narrow in bandwidth [14]. Other designs in this band suffered from very small gain values [15]. Hence, a compact implantable antenna with a relatively large gain antenna at 915 MHz is designed in this work to overcome these limitations. The proposed antenna is probably the smallest, widest in bandwidth and largest in size dual-band implantable antenna covering the 915 MHz and 2.45 GHz bands at the same time.

This paper is arranged as follows: First, the design targets are outlined and the corresponding design procedure is described in the first section. Then, the main simulated results are discussed in the second section. This is followed by link budget calculations in the third section. The paper is finally concluded in the last section.

II. DESIGN TARGETS AND POROCEDURE

A. Targets

This design proposed in this work aims at:

1. Obtaining resonance in the 915 MHz band for data transmission and in the 2.45 GHz for data saving. The 915 MHz band is selected due to its ability to support relatively high gain values and data rates. On the other hand, the 2.45 GHz band is used to facilitate the functionality of wake-up receivers that are usually incorporated to implantable devices allowing them to save power by sending data only when necessary [16].

2. A wide bandwidth > 20%. While the targeted bands (902-928 MHz and 2.4-2.5 GHz) are narrow, it is important to maintain some frequency margins around them to maintain -10 dB matching in case of detuning that may happen in the real human body [17].

3. Relatively good radiation characteristics sufficient for communication in the far field. This is important for establishing communication with an external receiver at a distance that allows the patient to maintain a relaxed and comfortable state. This can be assessed through link budget calculations, as will be demonstrated in a sub-sequent section.

B. Design Process

To satisfy the above mentioned objectives. A compact patch antenna is designed. The antenna is composed of a cut-edge one turn spiral connected to a flag-shaped part. The ground is composed of a small strip connected to a flag shaped conducting part. A lossless substrate of dielectric material with relative permittivity of 3 and a thickness of 1 mm is used in the design. As the antenna will operate inside the human body, it is simulated inside a simplified body model from the beginning which saves the overall simulation time. The simplified body model of simulation is shown in Fig. 1. It is composed of a homogeneous cylindrical muscle layer of relative permittivity of 55 and a conductivity of 0.95 S/m which resembles muscle material at 915 MHz and of relative permittivity of 52 and conductivity of 1.74 S/m which resembles muscle material at 2.45 GHz [18]. CST simulation software is used with hexahedral meshes and time-domain solver [19]. The antenna is fed using a 50 Ω discrete port, positioned at the middle of the main stripline of the radiating part and the ground, with open boundaries applied to minimize reflections and simulate free-space conditions. Mesh

979-8-3315-4248-1/25/$31.00 ©2025 IEEE

refinement in CST Studio Suite considered material properties, ensuring finer discretization in regions with significant variations in permittivity, conductivity, and loss tangents. Edge refinement was applied to capture field variations along sharp boundaries and metallic structures. The fraction of the maximum cell size near the model was set to 6, optimizing accuracy while maintaining computational efficiency.

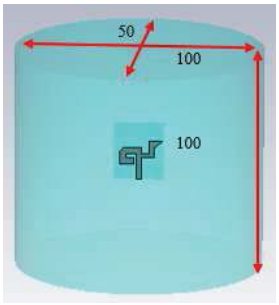


Fig. 1. The simplified body model of simulations; dimensions in mm

The design process went through the following steps:

1. The main radiating part: A one turn spiral radiator attached to a microstrip line is mainly aimed for the design. The spiral provides a good structure to lengthen the current path over small dimensions which is requested for compact implantable devices. The ground is composed of a thin rectangular strip. The overall dimensions at this stage are carefully selected to satisfy -10 dB matching at the intended bands. The antenna is optimized with a cut-edge at this stage for the purpose of future optimization to obtain circular polarization.

2. Enhancing the gain. This step comprises two sub-steps.

2.1 Incorporating a flag-shaped structure to the patch. The flag shape structure is selected in particular because it allows for compact designs that are beneficial in size-constrained applications, such as implantable medical devices [20]. Moreover, the geometry of flag-shaped antennas allows for enhanced control over the antenna's radiation pattern, gain, and directivity [21]. The selected flag-shaped structure helps to increase the gain of the proposed antenna by around 2 dBi.

2.2 Incorporating a flag-shaped structure to the ground. Adding this structure to the ground helped in increasing the gain by around 0.5 dBi and shifting the resonant frequency up to provide a better margin separation below and above the 915 MHz.

The antenna structure for the three steps are shown in Fig. 2 and the reflection coefficients for the three cases are shown Fig. 3. It can be seen from Fig. 3 that adding the flag-shaped structure also helps to increase the bandwidth over the two bands of interest.

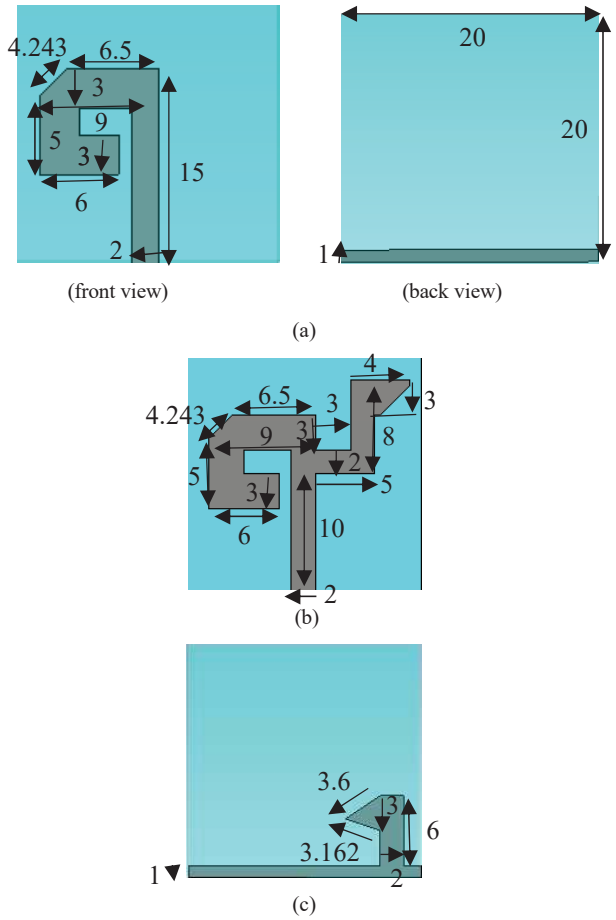


Fig. 2. The antenna structure through the: (a) first design step, (b) Step 2.1 and (c) Step 2.2; dimensions in mm.

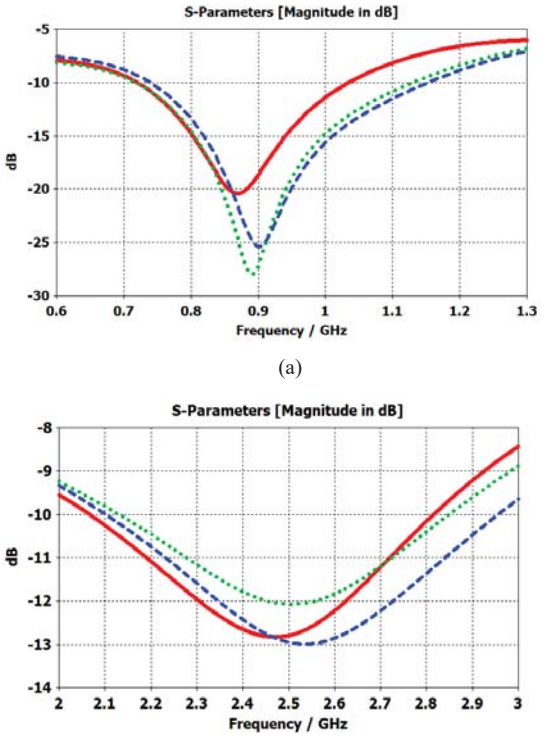


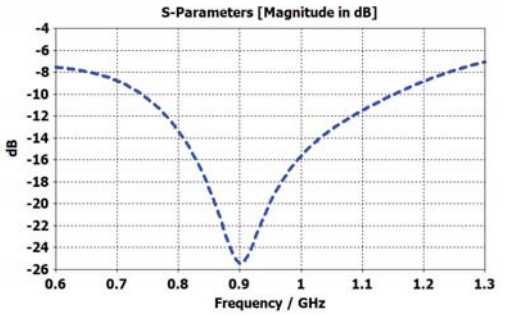
Fig. 3. The reflection coefficient S_{11} in dB for the antenna in Step 1 (red line), Step 2.1 (Green line) and Step 2.2 (Blue line) of the: (a) 915 MHz and (b) 2.45 GHz ISM bands.

III. Simulation Results

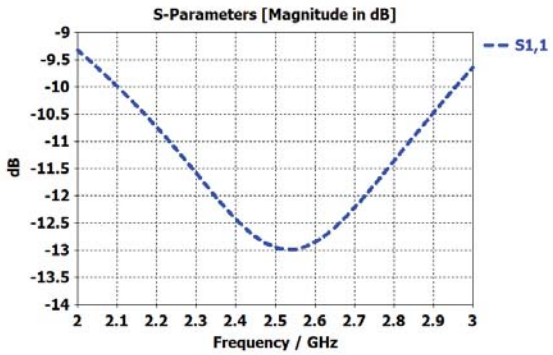
The -10 dB reflection coefficient of the final antenna around the two bands of interest is shown in Fig. 4. Based on the calculations with reference to Eq. 1, the antenna has obtained a broad bandwidth of 42.1 and 33.67% for the 915 MHz and 2.45 GHz bands which are larger than 20% as targeted [22].

$$BW_{rational} = 2\times\left(\frac{f_h - f_L}{f_h + f_L}\right) \quad (1)$$

where f_L (Hz) is the lowest band frequency and f_h (Hz) is the highest band frequency.



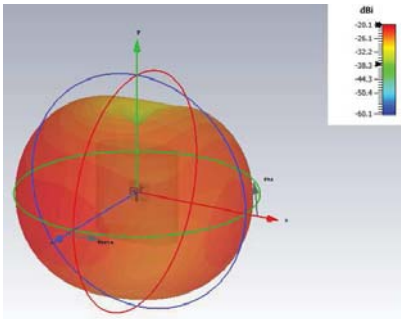
(a)



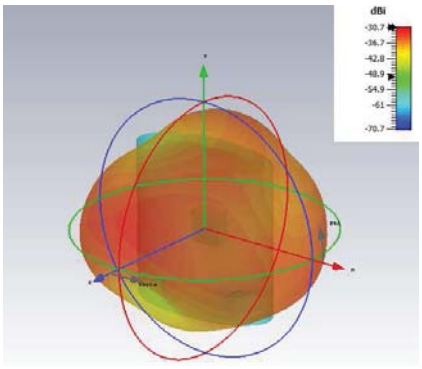
(b)

Fig. 4. The -10 dB reflection coefficient of the final antenna in the: (a) 915 MHz and (b) 2.45 GHz bands

The 3D and polar radiation patterns are shown in Figs. 5 and 6, respectively. An off-body direction is obtained. Maximum gains of -20.1 and -30.7 dBi are obtained at 915 MHz and 2.45 GHz, respectively. The radiation efficiencies are

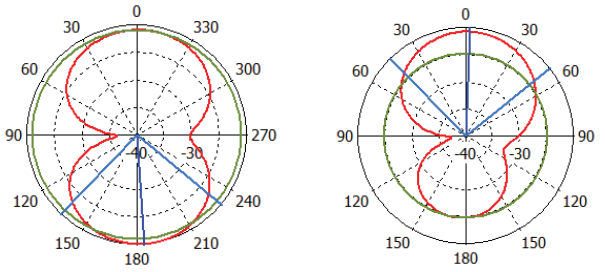


(a)

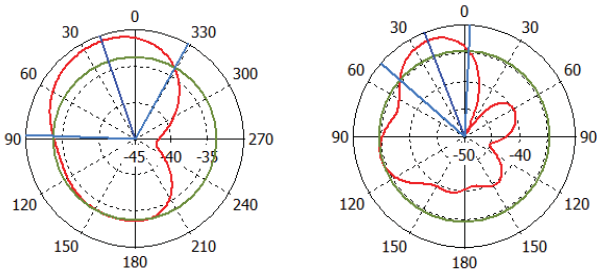


(b)

Fi. 5. The 3D radiation pattern at: (a) 915 MHz and (b) 2.45 GHz



(a)



(b)

Fig. 6. The polar radiation patterns at: (a) 915 MHz and (b) 2.45 GHz

The maximum 1-g SAR is also computed at 915 MHz and 2.45 GHz. Maximum rates of 172 and 152 W/kg were obtained at 915 MHz and 2.45 GHz, respectively. Based on these values, the antenna can be provided by up to 9.68 (1.6/172) and 10.2 (1.6/152) dBm while satisfying the safety limitations.

IV. Link Budget Calculations

To provide healthcare monitoring inside homes, a distance of 10 m is targeted. The capability of the antenna to communicate inside homes is calculated considering the link budget in Table I and using Eqs. 2-3.

$$P_r = P_t + G_t + G_r - L_P - LM \quad (2)$$

$$L_P = 10nlog_{10}\left(\frac{d}{d_0}\right) + 10log_{10}\left(\frac{4\pi d_0}{\lambda_0}\right) + S \quad (3)$$

TABLE I. THE LINK PARAMETERS

Parameter	Value and unit
Frequency (f)	915 MHz
	2.45 GHz
Transmitting antenna gain (G_t)	-20.1 dBi
	-30.7 dBi
Receiving antenna gain (G_r)	2.15 dBi
Distance (d)	10 m
Receiver sensitivity (P_r)	-99 dBm
Transmitted power (P_t)	0 dBm
Link Margin (LM)	5 dB

d_0 is a reference distance which is considered to be 1 m. S is the standard deviation parameter which is considered as 0 for this case, n is the path loss exponent which is equal to 3 considering a none-line-of-sight case indoor [4]. λ_0 (m) is the free space wavelength which is equal to (c/f) where c is the velocity of electromagnetic waves in free space which is equal to 3×10^8 m/s.

In both cases, the power calculations at the right side of the equation are -68.79 and -83.66 dBm at 915 and 2.45 GHz, respectively. Comparing these values to the receiver sensitivity indicates that receiver will be still able to receive these power levels. Hence, the antenna is expected to work well over the investigated distance.

V. CONCLUSIONS

In this paper, a compact patch antenna is proposed for implantable applications. The proposed antenna works for two bands at the same time which are the 915 MHz and 2.45 GHz ISM bands. The design is conducted through different steps to optimize the antenna gain by utilizing a flag-shaped structure in the radiating patch and ground. The antenna has a small size and broad in bandwidth. Moreover, its gain values at both bands can support communications over a distance of 10 m inside homes. All of these features make this antenna good candidate for home care health monitoring. In the future, the antenna will be fabricated and its performance will be validated

ACKNOWLEDGMENT

I would like to thank Mutah University in Jordan for the support of this work.

REFERENCES

[1] W. Wang, X. -W. Xuan, W. -Y. Zhao and H. -K. Nie, "An implantable antenna sensor for medical applications," in *IEEE Sensors Journal*, vol. 21, no. 13, pp. 14035-14042, 1 July1, 2021.

[2] A. Ahmed, M. Ur-Rehman and Q. H. Abbasi, "Miniature implantable antenna design for blood glucose monitoring," *2018 International Applied Computational Electromagnetics Society Symposium (ACES)*, Denver, CO, USA, 2018, pp. 1-2.

[3] N. A. Malik, P. Sant, T. Ajmal and M. Ur-Rehman, "Implantable antennas for Bio-Medical applications," in IEEE Journal of Electromagnetics, RF and Microwaves in Medicine and Biology, vol. 5, no. 1, pp. 84-96, March 2021.

[4] R. S. Alrawashdeh, Y. Huang, M. Kod and A. A. B. Sajak, "A broadband flexible implantable loop antenna with complementary split ring resonators," in IEEE Antennas and Wireless Propagation Letters, vol. 14, pp. 1506-1509, 2015.

[5] M. Samy, A. Gudipalli, "A review on miniature bio-implant antenna performance enhancement and impact analysis on body fluids in medical application" Measurement: Sensors, vol. 28, pp. 1-11, 2023.

[6] C. -Y. Huang, C. -L. Tsai and C. -L. Yang, "Compact broadband implantable monopole antenna with gain enhancement," 2014 IEEE Antennas and Propagation Society International Symposium (APSURSI), Memphis, TN, USA, 2014, pp. 1590-1591.

[7] J. Wang, E. G. Lim, M. Leach, Z. Wang, R. Pei and Z. Jiang, "Design of an implantable antenna for wireless communication of ingestible capsule endoscope," 2019 International Symposium on Antennas and Propagation (ISAP), Xi'an, China, 2019, pp. 1-3.

[8] R. S. Alrawashdeh, F. H. Alharazneh, S. A. Alsarayreh, E. S. Aladaileh, "A novel flexible cloud shape loop antenna for muscle implantable devices," Jordan Journal of Electrical Engineering (JJEE), vol. 5, no. 1, pp.61-76, 2019.

[9] S. A. Kumar, and T. Shanmuganantham, "Scalp – Implantable antenna for biomedical applications," 2020 URSI Regional Conference on Radio Science (URSI-RCRS), Varanasi, India, (2020), 1-4.

[10] N. A. Malik, T. Ajmal, P. Sant and M. Ur-Rehman, "A Compact size implantable antenna for bio-medical applications," *2020* International Conference on UK-China Emerging Technologies (UCET), Glasgow, UK, 2020, pp. 1-4.

[11] K. Yekeh Yazdandoost, "A 2.4 GHz antenna for medical implanted communications," 2009 Asia Pacific Microwave Conference, Singapore, 2009, pp. 1775-1778.

[12] T. Satitchantrakul, R. Silapunt and S. Sirivisoot, "Meander implantable antenna for biomedical wireless communication," *2016* IEEE International Symposium on Antennas and Propagation (APSURSI), Fajardo, PR, USA, 2016, pp. 1173-1174.

[13] A. Mauludiyanto, G. Hendrantoro, M. Nova, "The attenuation aharacteristics of the body tissue on frequency function in WBAN channe," Journal on Advanced Research in Electrical Engineering, Vol. 5, No. 2, Oct. 2021, pp. 107-113.

[14] K. A. Kam, V. Kumar, C. K. Lardner, I. Mollicone, D. Dumitriu and I. Kymissis, "A Fully integrable 915 MHz implantable antenna system for long-range telemetry in Rodents," 2023 IEEE MTT-S International Microwave Biomedical Conference (IMBioC), Leuven, Belgium, 2023, pp. 55-57

[15] C. Liu, Y. Zhang and X. Liu, "Circularly Polarized Implantable Antenna for 915 MHz ISM-Band Far-Field Wireless Power Transmission," in IEEE Antennas and Wireless Propagation Letters, vol. 17, no. 3, pp. 373-376, March 2018.

[16] H. Kim, and H. Shin, " A 2.4-GHz current-reuse OOK wake-up receiver for MICS applications, IEICE Wlectronics Express, vol. 10, no. 14, pp. 1-4, 2013.

[17] N. Vidal, S. Curto, J. M. Lopez-Villegas, J. Sieiro and F. M. Ramos, "Detuning effects on implantable antenna at various human positions," 2012 6th European Conference on Antennas and Propagation (EUCAP), Prague, Czech Republic, 2012, pp. 1231-1234

[18] Andreuccetti D., Fossi R., and Petrucci C., Calculation of the dielectric properties of body tissues in the frequency range 10 Hz-100 GHz, Institute for Applied Physics, Italian National Research Council, Florence (Italy), 1997. Accessed: Jan. 25, 2019. [Online]. Available: http://niremf.ifac.cnr.it/tissprop/

[19] CST Studio Suite, BioEM Simulation Using CST STUDIO SUITE 2023. Accessed: Sep, 2024. [Online] Available: https://www.cst.com.

[20] P.K. Sharma, D. Shrama, C.J. Rani, "A flag-shaped microstrip patch antenna for multiband operation. In: Khanna, A., Gupta, D., Bhattacharyya, S., Snasel, V., Platos, J., Hassanien, A. (eds) International Conference on Innovative Computing and Communications. Advances in Intelligent Systems and Computing, vol 1059. Springer, pp. 39-45, 2019.

[21] T. Mandal, P. Mondal, L. Murmu," Design and analysis of a small-size, flag-shape UWB antenna with dual notch band using mushroom structure," Journal of Circuits, Systems and Computers, vol. 31, no. 5, 2021.

[22] Y. Huang and K. Boyle, Antennas from Theory to Practice, UK, Chichester: John Wiley & Sons Ltd, 2008.

Real-Time Locating Systems: A bibliometric analysis

Letizia Tebaldi
Department of Engineering for Industrial Systems and Technologies
University of Parma
Parma, Italy
letizia.tebaldi@unipr.it

Andrea Volpi
Department of Engineering for Industrial Systems and Technologies
University of Parma
Parma, Italy
andrea.volpi@unipr.it

Giulia Azzolini
Department of Engineering for Industrial Systems and Technologies
University of Parma
Parma, Italy
giulia.azzolini1@studenti.unipr.it

Abstract*— A Real-Time Locating System is a relative new solution whose aim is that of automatically and real-time identifying the position of objects, typically within indoor environments. These systems are implemented in several fields, such as manufacturing, logistics, retail, construction, healthcare and others, and depending on the sector they can have multiple purposes for being involved. Among the main communication tools, RFID, Bluetooth, Ultrasound or Infrared can be used, again depending on the field and purpose of the system. The present study tries to close a gap found in literature, that is to say proposing the results from a bibliometric analysis carried out on 303 documents dealing with RTLS. Typical bibliometric parameters were traced and analyzed, including a deepening on a more contents-related aspect, namely the most common communication technologies within part of the sample. Results from this study may be useful for those researchers or practitioners who are carrying out projects RTLS related.

Keywords— Real-Time Locating Systems, bibliometrics, wireless communication systems.

I. INTRODUCTION

Real-Time Locating Systems (RTLS in the following) are systems whose function is that of enabling the real-time tracking of something which is located in typically indoor environments [1]. They can have multiple applications in several contexts, for instance in manufacturing environments for tracking the position of items in warehouses or in other buildings [2]; in hospitals for patient tracking [3]; for livestock monitoring [4]; for operators' safety in working environments [5], and many others. They are enabled by wireless communication technologies, among which the most common are Wi-Fi, Bluetooth, Zigbee, Radio Frequency Identification (RFID), Ultrasound, iBeacons or Ultra-wideband (UWB) [6], selected depending on the characteristics of the environment, the reading distance required or other variables.

Bibliometrics is the statistical analysis of bibliographic data, allowing to measure and assess the research impact of individuals, groups of individuals or institutions, and more in general to estimate the state-of-the-art of a given topic [7]. These kinds of studies are sometimes underestimated among scientists, but they allow to derive interesting and relevant information for a researcher, above all in a scientific moment such as the one we are working right now where the number of publications is rapidly increasing in almost all the scientific fields. If a researcher is wondering whether a specific topic (or a technology) is mature or saturated, then she/he can consult a bibliometric study for looking at the temporal evolution of the studies in question; if a researcher wants to publish her/his research on a top journal, then she/he can look at the journal distribution with reference to the related argument on a bibliometric study; if a researcher has to select a reviewer, or needs an opinion rather than a counseling, or is looking for collaborators, then she/he can derive the most productive authors and researchers from a bibliometric study; if a researcher is looking for top documents she/he can consult the top cited papers available on a bibliometric study, or by means of a keywords analysis she/he can derive whether her/his research is aligned with the trends, or may be obsolete rather than extremely innovative and new.

On the bases of these short premises, given a lack in literature, the authors propose in this manuscript the early results from a bibliometric analysis carried out in the context of RTLS systems, aimed at addressing typical research questions of a similar analysis. It follows that this document wants to be a reference point and a sort of "scenario" study for those researchers or practitioners who are looking for bibliometric information such as the ones mentioned few lines above.

The remainder of the paper is structured as follows: section II proposes the methodology followed; section III illustrates the main results from the bibliometric parameters investigated and finally section IV concludes the manuscript, including the planned future research and insights.

II. METHODOLOGY

A single query was performed on the Scopus database in October 2024, having only "Real-Time Locating System" as keyword. 331 studies were initially returned, and the following exclusion criteria were implemented: (i) absence of authors, (ii) English language of the document and (iii) type of document (i.e., excluded Books, Book Chapters and Conference Reviews). The final sample of documents corresponds to 303. The software involved for carrying out the analysis are Microsoft Excel™ and VOSviewer, and the following bibliometric parameters were traced so as to address typical bibliometrics-related research questions: temporal evolution of documents; source analysis (i.e., journal and conferences); top authors; geography of the study; most cited documents; keywords analysis. A final more contents-related parameter was also traced (only for journal articles), namely the communication technology involved in the solution proposed in that study.

III. RESULTS

The subsections that follow detail the results from each single investigated element, reflecting the order proposed in the methodology section.

A. Temporal evolution

Figure 1 shows the temporal trend of the 303 documents. As it is possible to deduce, production is quite variable over time, but seems to decrease in the last two years, even if two months of 2024 are missed; this outcome is in contrast with what is currently happening in most of the scientific research

This research was granted by University of Parma through the action Bando di Ateneo 2024 per la ricerca.

979-8-3315-4248-1/25/$31.00 ©2025 IEEE

fields. The first three documents were published in 2006, stressing the relative novelty of the topic. What these documents have in common is the fact that they were written by three different research groups all based in South Korea, and they are conference proceedings (two of them were presented at the same event). After them, three years were needed in order to let these RTLS systems spreading. It is worth noting year 2022 as the most productive year, with 26 documents; after the Covid pandemic, indeed, research of RTLS systems within the medical field recorded an increase.

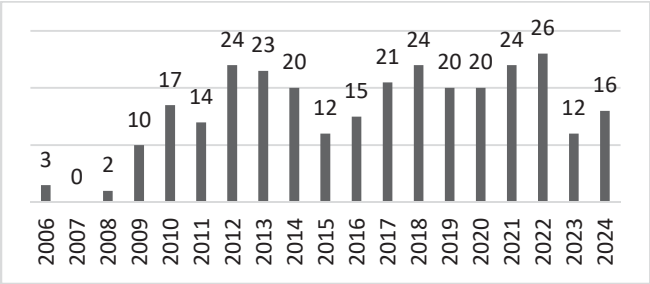


Fig. 1. Temporal evolution of documents.

B. Sources

Out of 303 documents, 220 journals and conferences were recorded. Most of them (178) contributed with only one publication, while 42 with more. For the sake ok brevity, Table I below proposes only those contributing with a number equal or greater than 5 documents, so as to bring out top sources.

TABLE I. MOST PROLIFIC SOURCES (IN THE FIRST COLUMN, J STANDS FOR JOURNAL, WHILE C FOR CONFERENCE).

J/C	*Name*	*Editor*	*Nr. of documents*
C	Communications in Computer and Information Science	Springer	8
C	Procedia CIRP	Elsevier	7
J	Journal of Medical Internet Research	JMIR Publications	7
C	Advances in Intelligent Systems and Computing	Springer	6
J	Automation in Construction	Elsevier	6
J	Sensors (Switzerland)	MDPI	5
C	Advances in Intelligent and Soft Computing	Springer	5

First of all, note that most of the podium is represented by conferences; as far as the research fields, instead, exception made for Procedia CIRP which focuses on production engineering (including for instance manufacturing plants, logistics activities and warehouses management), the remaining conferences, as expected, deal with communication engineering. On the contrary, it is absolutely worth noting that the most active journal with reference to RTLS systems publishes research in the medical field; this result represents a spoiler of content-related outcomes with reference to the application fields, which is in progress at the time of writing; also, the construction field is represented by the journal Automation in Construction stressing another relevant field for RTLS applications.

C. Authors

Overall, 891 authors emerged from the authors analysis, with an average of 2.94 authors per document. The most productive authors (more than 8 published papers) including their affiliations are proposed in Table II.

TABLE II. MOST ACTIVE AUTHORS WITH THEIR AFFILIATIONS.

Name	*Number of documents*	*Affiliation*	*Country*
Tapia D.I.	14	Department of Computer Science and Automation, University of Sakamanca	Spain
Alonso R.S.	14	Department of Computer Science and Automation, University of Sakamanca	Spain
Garcia O.	11	R&D Department, Nebusens, S.L., Scientific Park of the University of Salamanca	Spain
Corchado J.M.	10	Department of Computer Science and Automation, University of Sakamanca	Spain
Bowen M.E.	9	School of Nursing, University of Delaware, Newark, DE, United States	USA
Ruppert T.	8	MTA-PE Lendület Complex Systems Monitoring Research Group, Department of Process Engineering, University of Pannonia	Hungary

The first 4 authors work together, and come from the same Spanish university; specifically, Tapia and Alonso co-authored 12 documents out of the 14 they both published. Tapia is the first author in 7 of his published documents. Bowen, instead, is first author in 8 of his publications, on 9 in total; it is worth noting that he works in a School of Nursing (i.e., medical field), while the other 5 authors of the table all belong to computer science and engineering fields. It does not surprise that the documents he published deal with the medical environment, while for the other it is not possible to derive a specific topic or research field.

D. Geography of the studies

The geography of the studies was derived according to the affiliation of the first author, in order to define the most productive countries among the sample.
The resulting distribution is proposed in Figure 2.

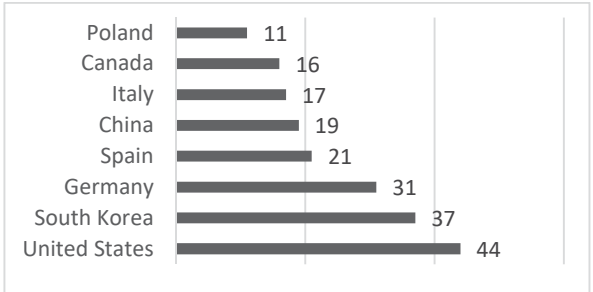


Fig. 2. Most active countries within the sample.

On top, with 44 documents, the Unites States stand out, followed by South Korea, as expected given the fact that the first documents on the topic were published by South Korean research groups. The presence of Spain, after the results of the Author analysis, does not surprise, while instead it can be

noticed the absence of Hungary. Overall, the 8 countries of Figure 2 cover 196 documents, namely 64.7% of the whole sample.

E. Top cited documents

At the time of performing the research query, another tracked information was the citations received form each document, in order to identify the most relevant studies. It is curious to note that all the top positions, respectively with 168, 149 and 143 mentioning, involve RFID technology as communication tool (i.e., [8], [9], and [10]). Into detail, [9] focuses on the construction field, and it is not the only document within this field among the top 10 cited documents; indeed, also in [11] (129 mentioning) and [12] (77 mentioning), RTLS systems within the construction field are reviewed, stressing once again the relevance of the construction area. The healthcare field, however, is not missed (i.e., [13] with 142 mentioning). For completeness, Table III below resumes the top 10.

TABLE III. TOP CITED DOCUMENTS.

References	*Number of citations*	*Main topic*
[8]	168	RTLS using RFID
[9]	149	RTLS in construction (for safety management)
[10]	143	RFID tags
[13]	142	RTLS in healthcare
[14]	138	Indoor determination technologies
[11]	129	RTLS in construction
[15]	128	RTLS using UWB
[12]	77	RTLS in construction (for safety management)
[16]	75	Case study for workers safety
[17]	69	Case study of UWB-based RTLS

F. Keywords analyis

The keywords analysis is a common analysis whose aim is that of trying to define the main topic and trends of the research according to the keywords that the authors associated to their publications. This analysis was carried out in two ways: at first, a simply frequency-persistence analysis [18] was performed under Microsoft Excel™, then the software VOSviewer was involved in order to build a network showing the relationship between keywords.

For the first analysis, after having drafted a list of the keywords and adjusted synonyms, acronyms and plurals/singulars, for each identified keyword its frequency (i.e., number of mentioning) and persistence (i.e., its durability, determined as the number of years from its first appearance to its last one) were determined, and inserted into an x/y diagram for deriving the graph showed in Figure 3 below. Note that this analysis was limited to those keywords having a frequency equal or greater than 5; also with VOSviewer the same constraint was considered (the starting number of keywords was 875, and 33 keywords met the constraint).

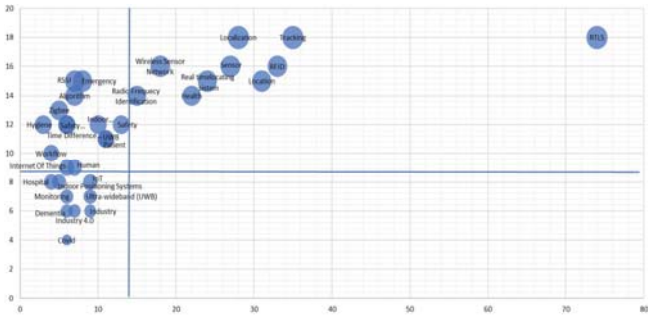


Fig. 3. Frequency/persistence analysis of keyword. The x-axis corresponds to the frequency, while the y-axis to the persistence.

Each derived quadrant reflects a research trend interpreted as follows:

- Emerging topics: both frequency and persistence are low. This means that these are new keywords. Among them keywords such as Covid were found, which was firstly mentioned in 2020, as expected;
- Trendy topics: characterized by a high frequency but low persistence. These are words that have been greatly used but in a limited period of time. In this case, there is no keyword having these characteristics;
- Intermittent topics: characterized by low frequency but high persistence. Among them it is curious to read the word Emergency that appears a few times but in several years;
- Well-established topics: characterized by keywords with high frequency and persistence. Among them it does not surprise the fact that there is the keyword RTLS. The high frequency and persistence of this keyword can be attributed to the fact that it is the keyword used for the research query. Moreover, we can find the top aims and scopes of RTLS, such as tracking or localization, but also what could be the most used communication technologies, i.e., RFID. Indeed, UWB (fitting among Emerging topics) or Zigbee (Intermittent topics) are not among this group.

VOSviewer, instead, allowed to derive the network illustrated in Figure 5, where the color of the nodes reflects the average citation year, while the dimension of the nodes recalls the frequency (greater nodes have more mentioning).

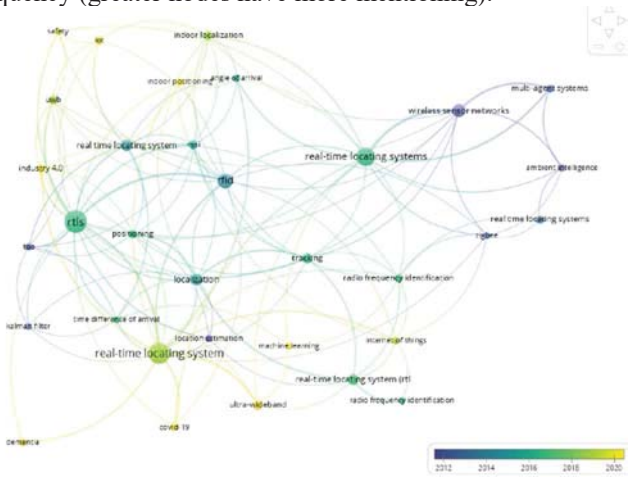


Fig. 4. Keywords analysis from VOSviewer.

The network confirmed the frequency-persistence analysis results: indeed, among the most recent words it is possible to find medical-related keywords such as covid-19 or dementia but also UWB, machine learning or Industry4.0, in line with the recent research trends. As far as the communication technologies, note that Zigbee fits among the oldest. As expected, bigger nodes correspond to the keyword used for the research and its synonyms, but also RFID stands out, even if with an average citation year of 2014-2016.
These results will be then confirmed by a deep contents-related analysis, expected to be completed in the near future.

G. Communication technologies

The last aspect investigated refers to the communication technology involved in the studies. At the time of writing, the analysis was carried out only on journal papers, since it is assumed that more structured and complete research are published in international journals rather than conferences. More into detail, it was carried out on 105 articles, even if in only 97 it was possible to derive a precise technology.
The most commonly used technology is RFID (in 39 documents); this also confirms the presence of the RFID keyword among the well-established topics. The second most implemented technology is UWB (26 papers), resulting among the Emergent topics when associated with RTLS. On the contrary, the least involved technology, is the Near Field Communication (NFC) (only 1 document). It is a short-range wireless communication technology that allows data exchange between compatible devices when they are within a few centimeters of each other. Probably, the required short distance is a weakness when thinking about the usages of RTLS. As far as other communication tools are concerned, Wi-Fi was involved in 9 documents, Infrareds in 7 and finally Bluetooth, Bluetooth Low Energy, Ultrasound, Zigbee and Chirped Spread Spectrum in 3.

IV. CONCLUSIONS

This paper aimed at presenting initial results from a bibliometric analysis carried out on 303 documents dealing with RTLS, at present not existing in literature, for addressing typical bibliometric-related research questions. Surely it presents some limits, which are expected to be exceeded with the next steps. First of all, only Scopus database was involved, and it is in plan to also include other scientific database, such as Web of Science or Google Scholar in order to have a complete sample. Moreover, for the sake of brevity, it was not possible to further deepen some insights, worth of mention. At present, it is being carried out a complete systematic literature review, including contents analyses, which include the following aspects which will complete the present bibliometric analysis: type of application presented in the studies (i.e., if the study deals with the design of a solution, a test or a real application); field of application, including the most suitable communication technologies for each field, and their evolution over time; the Key Performance Indicators (KPIs) used for assessing and evaluating the performance of the RTLS systems, properly categorized according to the field of application. The ultimate purpose is to provide readers with a tool able to resume for each application the most suitable communication technology and the proper KPIs to be used; a Strength – Weaknesses – Opportunities - Threats (SWOT) analysis of communication technologies will then complete the research.

REFERENCES

[1] A. Volpi, R. Montanari, L. Tebaldi and M. Mambrioni, “Low-Cost Real-Time Locating System Solution Development and Implementation in Manufacturing Industry,” Journal of Sensor and Actuator Networks, vol. 12, p. 54, 2023.

[2] A. Volpi, L. Tebaldi, G. Matrella, R. Montanari and E. Bottani, “Low-Cost UWB Based Real-Time Locating System: Development, Lab Test, Industrial Implementation and Economic Assessment,” Sensors, vol. 23, p. 1124, 2023.

[3] F. Ebrahimzadeh, E. Nabovati, M. Hasibian and S. Eslami, “Evaluation of the effects of radio-frequency identification technology on patient tracking in hospitals: A systematic review,” Journal of Patient Safetty, vol. 17, n. 8, pp. 1157-1165, 2021.

[4] C. Engels, M. Trilling and W. Buscher, “A direct comparison of two RTLS for dairy cows,” in 11th European Conference on Precision Livestock Farming, 2024.

[5] A. Ochoa-de-Eribe-Landaberea, L. Zamora-Cadenas and I. Velez, “Untethered Ultra-Wideband-Based Real-Time Locating System for Road-Worker Safety,” Sensors, vol. 24, n. 8, p. 2391, 2024

[6] T. Yang, A. Cabani and H. Chafouk, “A Survey of Recent Indoor Localization Scenarios and Methodologies,” Sensors, vol. 21, p. 8086, 2021.

[7] J. Moral-Munoz, E. Herrera-Viedma, A. Santisteban-Espejo and M. Cobo, “Software tools for conducting bibliometric analysis in science: An up-to-date review,” El profesional de la informacion, vol. 29, n. 1, p. e290103, 2020.

[8] D. Zhang, L. Yang, M. Chen, S. Zhao, M. Guo and Y. Zhang, “Real-Time Locating Systems Using Active RFID for Internet of Things,” IEEE Systems Journal, vol. 10, n. 3, pp. 1226-1235, 2016.

[9] H.-S. Lee, K.-P. Lee, M. Park, Y. Baek and S. Lee, “RFID-based real-time locating system for construction safety management,” Journal of Computing in Civil Engineering, vol. 26, n. 3, pp. 366-377, 2012.

[10] X. Li, Y. Zhang and M. Amin, “Multifrequency-based range estimation of RFID tags,” 2009 IEEE International Conference on RFID, RFID 2009, n. 4911199, pp. 147-154, 2009.

[11] H. Li, G. Chan, J.K.W. Wong and M. Skitmore, “Real-time locating systems applications in construction,” Automation in Construction, vol. 63, pp. 37-47, 2016.

[12] N. Soltanmohammadlou, S. Sadeghi, C.K.H. Hon and F. Mokhtarpour-Khanghah, “Real-time locating systems and safety in construction sites: A literature review,” Safety Science, vol. 117, pp. 229-242, 2019.

[13] M. Kamel Boulos and G. Berry, “Real-time locating systems (RTLS) in healthcare: A condensed primer,” International Journal of Health Geographics, vol. 11, n. 25, 2012.

[14] K. Curran, E. Furey, T. Lunney, J. Santos, D. Woods and A. McCaughey, “An evaluation of indoor location determination technologies,” Journal of Location Based Services, vol. 5, n. 2, pp. 61-78, 2011.

[15] F. Mazhar, M.G. Khan and B. Sallberg, “Precise Indoor Positioning Using UWB: A Review of Methods, Algorithms and Implementations,” Wireless Personal Communications, vol. 3, n. 4467-4491, p. 97, 2017.

[16] H. Kim, H.-S. Lee, M. Park, B. Chung and S. Hwang, “Automated hazardous area identification using laborers' actual and optimal routes,” Automation in Construction, vol. 65, pp. 21-32, 2016.

[17] S. Bottigliero, D. Milanesio, M. Saccani and R. Maggiora, “A Low-Cost Indoor Real-Time Locating System Based on TDOA Estimation of UWB Pulse Sequences,” IEEE Transactions on Instrumentation and Measurement, vol. 70, n. 9389563, 2021.

[18] A. Fadlalla and F. Amani, “A keyword-based organizing framework for ERP intellectual contributions,” Journal of Enterprise Information Management, vol. 28, n. 5, pp. 637-657, 2015.

A Flexible Loop Sensor Antenna for Ice and Frost Detection

Rula Alrawashdeh
Electrical Engineering Department
Mutah University
Al-Karak, Jordan
rular18@mutah.edu.jo

***Abstract*— This paper presents and evaluates a flexible rectangular loop sensor antenna designed for ice and frost detection. The study focuses on assessing the antenna's sensitivity and data transmission capabilities. The antenna features a simple loop structure that is however sufficiently sensitive to differentiate between ice and frost. This sensitivity is attributed to the internal loop, which enhances coupling with the material under test and fine-tunes the antenna's response. The antenna achieved an average radiation efficiency of 97.1% and a gain of 2.74 dBi across the tested scenarios involving frost and ice. Additionally, it maintained a consistent direction of maximum radiation, even when loaded with ice or frost, thereby reducing constraints on the receiving antenna's radiation pattern requirements.**

Keywords—frost, flexible loop, ice, water, alarm signal, MUT.

I. INTRODUCTION

Antennas have recently been utilized in a wide range of applications, including early warning systems for natural disasters and environmental monitoring [1-2]. In these systems, the antenna must detect water, ice, and frost with sufficient sensitivity to distinguish between these materials, enabling the early identification of hazardous conditions such as icy roads, frost damage to crops, or water pooling that could potentially escalate into floods. Additionally, it must reliably transmit the sensed data to an external receiver, necessitating high radiation efficiency and gain for effective long-distance communication [3-4]. One of the most popular types of antennas used in these applications is patch antenna which offers a range of features, including flexibility to accommodate slots. This is important to provide an area for coupling with the material under test [5-6]. In [6], a T-shaped slot patch antenna was proposed at 2.378 GHz for wireless ice and frost detection. While that design managed to obtain accurate sensing, the slot worked to decrease the gain by around 2.2 dBi. Another slotted patch was proposed in [5] for ice and frost detection also but at 5.6 GHz in which a cross-shaped slot caused the gain to increase by around 5 dBi. An antenna based on split ring resonators was proposed in [7] to determine the real parts of the complex permittivity and permeability of magneto dielectric composites at 2.34 and 2.74 GHz. A compact double-ring microstrip resonator structure was fabricated in [8] to detect water, frost, and ice within a frequency range of 3 to 5 GHz. However, the far-field performance was not evaluated and validated in most of these designs. This is required to assess the antenna's capability of sending the sensed data as alarm signals regarding the status of the natural disasters. A flexible loop antenna was proposed in [9] at 2.4 GHz for ice detection. That antenna was light in weight, flexible and provided an accurate sensing with robust performance, it was found to be insufficient to detect small variations in the resonant frequency. The good characteristics of that loop antenna inspired the investigations in this paper to provide clear results and conclusions about the sensitivity level and capabilities of loop sensor antennas in general. Consequently, a rectangular flexible loop antenna is designed in this work. An internal loop is introduced into the antenna structure to tune its resonance and to provide an area of coupling with the material under test. The proposed antenna obtains a gain of 2.68 dBi with an ice thickness of 1 mm that is around 7.1 larger than that for a single rectangular loop without an internal layer. The proposed antenna demonstrated excellent radiation characteristics while preserving a simple design. The findings in this paper underscore the potential of loop antennas as effective sensors and inspire the development of further innovative loop structures.

This paper is arranged as follows: The overall design structure, concept and methodology are presented in Section II. The performance is discussed and analyzed in Section III. The conclusions are finally provided in Section IV.

II. DESIGN

This section presents the antenna structure, the concept of performance as a sensor in addition to the methodology followed for its evaluation. All simulations were conducted using the CST (Computer Simulation Technology) software [10]. Time domain solver and hexahedral meshes are used. A 50 Ω discrete port is used to feed the antenna.

A. Structures

The loop antenna of investigation is shown in Fig. 1.

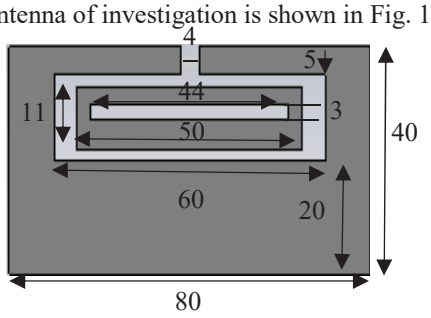


Fig. 1. The proposed antenna structure with dimensions in mm

The antenna is composed of a flexible conductor and a very thin lossless flexible substrate modeled with a dielectric constant of $\varepsilon_r = 3$. The design aimed at:

- resonating at around 2.45 GHz. The width and length of the antenna parts and spacing in between controls the total effective capacitance (C(F)) and inductance (L(H)) which affects the resonant frequency accordingly [11].

$$f_r = \frac{1}{2\pi\sqrt{LC}} \quad (1)$$

979-8-3315-4248-1/25/$31.00 ©2025 IEEE

The relevant parameter of evaluation is the reflection coefficient (S_{11}) which should be equal to or smaller than -10 dB indicating that 10% or less will be only reflected [12].

$$P_{ref} = 10og_{10}(\frac{P_{ref}}{P_{in}}) \quad (2)$$

Where P_{ref} (dB) is the reflected power and P_{in} (W) is the input power.

- providing an area of coupling with the material under test (MUT). This is typically achieved by introducing a capacitive part into the antenna structures. To obtain this objective an internal loop was integrated within the outer loop ring as shown in Fig. 1. The outer and inner loops can resemble the plates of a parallel plate capacitor separated by a dielectric material positioned between them. The inner loop also serves to tune the antenna's resonance and optimize its matching at 2.49 GHz.

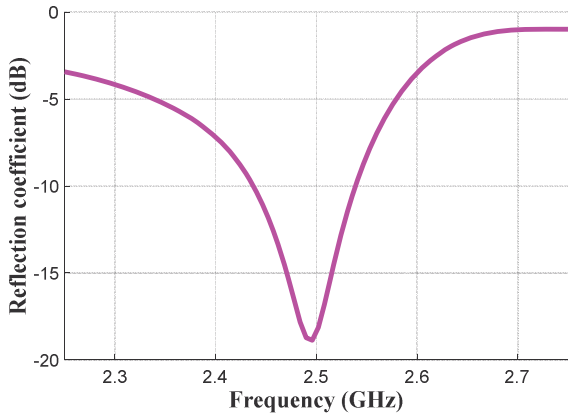


Fig. 2. The reflection coefficient (S_{11}) for the proposed loop sensor antenna

B. Concept

The proposed antenna is designed to detect ice or frost. Its performance will be evaluated by examining the variation in resonant frequency across the different test materials. The change in the dielectric constant value (ε_r) from one material to another causes the resonant frequency to alter as follows [13]:

$$f_r = \frac{f_0}{\sqrt{\varepsilon_r}} \quad (2)$$

where (f_0 (Hz)) is the original resonant frequency without the material under test and (f_r (Hz)) is the resonant frequency for the antenna when loaded with either ice or frost.

The variation in resonant frequency values should differ for the different materials (ice and frost in this case) which have distinct permittivity values, as summarized in Table I [3,8].

It is important to note that the variation in the dielectric constant among these materials is small and hence the antenna must be sufficiently sensitive to detect this small difference in permittivity values. This is obtained by incorporating an area of coupling to control the near electric field between the structure and material under test as will be explained in the following section.

- Providing the highest possible radiation efficiency and gain for the proposed structures. This is to ensure that data regarding the detected material is transmitted to a receiver which will process the received information accordingly.

TABLE I. RELATIVE PERMITTIVITY AND CONDUCTIVITY OF THE INVESTIGATED MATERIALS UNDER TEST

Material	Relative permittivity	Conductivity (S/m)
Ice	3.2	1×10^{-5}
Frost 1	1.5	
Frost 2	2	
Frost 3	2.5	

The performance is presented and discussed in the following section.

C. Methodology

To evaluate the overall performance of the antenna for environmental monitoring and early alarm systems, the following steps are taken:

1) The proposed antenna performance is evaluated for the following cases:

- Without any loading materials
- With a layer of ice
- With a layer of frost

The evaluation includes tracking the resonant frequency and its shift from one material under test to another.

2) Evaluating the antenna radiation efficiency, gain and pattern for the four cases mentioned above. This step is important to assess the antenna's capabilities for data transmission and sending alarm signals to an external receiver.

All evaluations are conducted using the Computer Simulation Technology (CST) software. The simulation results are presented and discussed in the following section.

III. PERFORMANCE AND DISCUSSION

The performance is evaluated for the antenna as a sensor and data transmitter.

A. Performance As A Sensor

As indicated above, the parameter for evaluation in this case is the resonant frequency which can be determined from the reflection coefficient plot. The simulated reflection coefficient S_{11} is shown in Fig. 3.

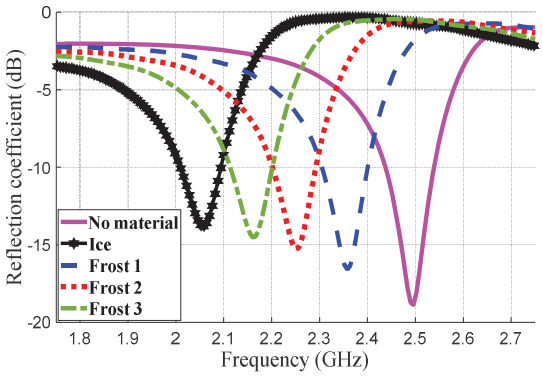


Fig. 3. The reflection coefficient (S_{11}) for the proposed loop sensor antenna

The resonant frequency shifts down by 132, 240 and 330 MHz for the three frost layers (F1, F2 and F3, respectively). The frequency down shift obtains a value of 432 MHz when ice loads the antenna. This is expected as ice has the largest relative permittivity among all these materials.

The near electric field for the antenna, both with and without the materials under test is shown in Fig. 4. The internal ring enhances the near electric field, resulting in a stronger coupling with the MUT and hence the sensitivity accordingly. This is obtained with and without the MUT as shown in the figure.

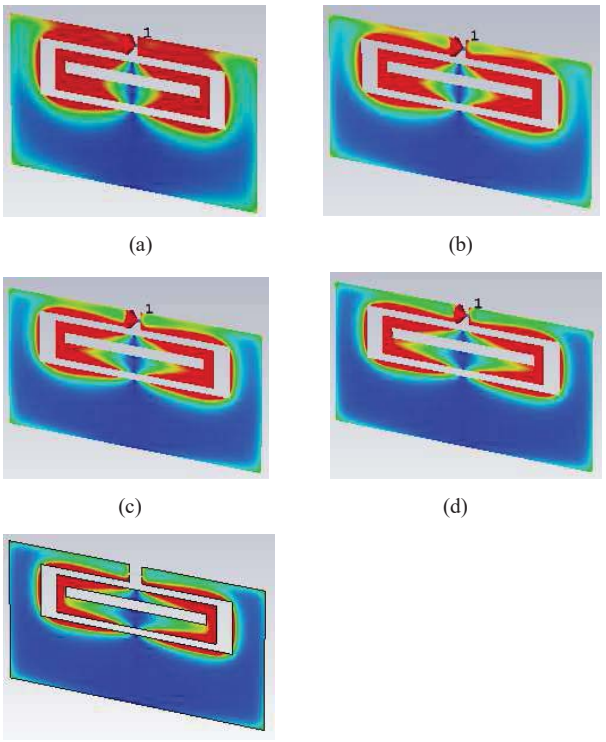


Fig. 4. The near electric field for the proposed loop sensor antenna: (a) without MUT, (b) with Frost 1, (c) with Frost 2, (d) with Frost 3 and (e) with ice

B. Performance as Data Transmitter

The radiation pattern for the antenna with and without the materials under test is shown in Fig. 5.

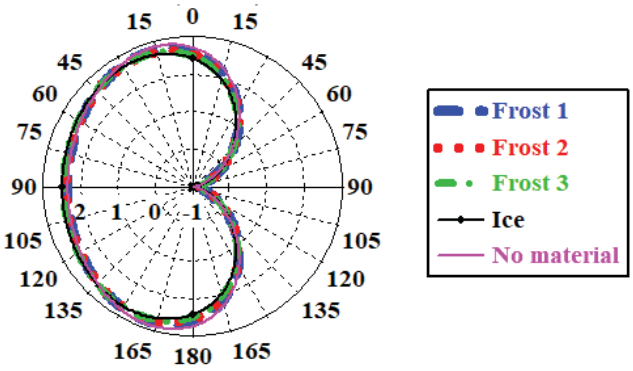


Fig. 5. The radiation pattern for the proposed antenna with and without materials under test

The same radiation pattern is observed for all cases. The results indicate that the antenna can function effectively with a fixed receiver oriented towards the maximum beam direction. A maximum gain of 2.85 dBi is also obtained for the unloaded antenna which decreases by up to 0.17 dB for the antenna when loaded with ice. The gain decreases with the MUT which is attributed to the losses introduced by it.

The maximum radiation efficiency and gain at the operating frequencies are summarized in Table II. The antenna achieves a maximum radiation efficiency of 98.4% without any material, which decreases by up to 2.4% only after loading with the MUT (ice).

TABLE II. THE RADIATION EFFCIIENCY AND GAIN OF THE PROPOSED ANTENNA

Case	The radiation characteristic		
	Radiation efficiency (%)	*Gain (dBi)*	*Resonant frequency (GHz)*
No material	98.4	2.85	2.49
Ice	96	2.68	2.058
Frost 1	97.6	2.76	2.358
Frost 2	97	2.714	2.25
Frost 3	96.5	2.7	2.16

IV. CONCLUSIONS

This paper presents a double-layer rectangular loop antenna designed for ice and frost detection, operating at a frequency of 2.45 GHz, with potential applications in environmental monitoring and early warning systems. The findings underscore the significance of coupling two rectangular loops to enhance near-field electric coupling, thereby improving sensitivity levels. The sensitivity ranges are 132/1.5, 240/2, and 330/2.5 (Hz/Δεr) for frost layers F1, F2, and F3, respectively, and reach 432/3.2 (Hz/Δεr) for ice. The proposed antenna achieves a high radiation efficiency of up to 98.4% and a gain of up to 2.85 dBi. Maximum radiation is observed in the azimuth plane with single polarization, making it ideal for communication with a fixed base station at a stationary location. The results presented in this paper pave the way for developing other loop antenna structures with innovative and more efficient configurations for sensing applications.

ACKNOWLEDGMENT

This research was funded by the North Atlantic Treaty Organization (NATO)/Science for Peace and Security (SPS):, funder reference SPS G5932, RESCUE;, project reference WT 433209 and supported by Mutah University in Jordan.

REFERENCES

[1] M. Wagih and J. Shi, "Wireless Ice Detection and Monitoring Using Flexible UHF RFID Tags," in IEEE Sensors Journal, vol. 21, no. 17, pp. 18715-18724, 1 Sept.1, 2021.

[2] A. Abdelaal, M. Sarayloo, D. K. Nims, B. Mohammadian, J. Heil, and H. Sojoudi, "A flexible surface-mountable sensor for ice detection and non-destructive measurement of liquid water content in snow," Cold Regions Science and Technology, vol. 195, p. 103469, 2022.

[3] T. E. Oliveira, J. R. Reis, and R. F. S. Caldeirinha, "Implementation of a WSN for Environmental Monitoring: From the Base Station to the Small Sensor Node," *Sensors*, vol. 22, no. 20, p. 7976, Oct. 2022.

[4] O. V. Soboliak, O. V. Kryvenko, V. I. Lutsenko, I. V. Lutsenko, S. O. Masalov, and I. V. Popov, "Environmental Monitoring Using Smart Millimeter Wave Antennas," *IOSR Journal of Engineering (IOSRJEN)*, vol. 14, pp. 46–49, Apr. 2024.

[5] R. Alrawashdeh, "A cross-shaped slotted patch sensor antenna for ice and frost detection," *Technologies,* vol. 13, no. 5, 2025.

[6] R. Kozak, K. Khorsand, T. Zarifi, K. Golovin, and M. H. Zarifi, "Patch antenna sensor for wireless ice and frost detection," Scientific Reports, vol. 11, no. 1, 2021.

[7] T. M. S. K., M. A. H. Ansari, A. K. Jha, and M. J. Akhtar, "Design of SRR-based microwave sensor for characterization of magnetodielectric substrates," IEEE Microwave and Wireless Components Letters, vol. 27, no. 5, pp. 524–526, 2017.

[8] Wiltshire, B.; Mirshahidi, K.; Golovin, K.; Zarifi, M.H. Robust and Sensitive Frost and Ice Detection via Planar Microwave Resonator Sensor. Sens. Actuators B Chem. 2019, 301, 126881.

[9] M. Wagih and J. Shi, "Toward the optimal antenna-based wireless sensing strategy: An ice sensing case study," IEEE Open Journal of Antennas and Propagation, vol. 3, pp. 687–699, 2022.

[10] "CST-Computer Simulation Technology", 2023, [online] Available: http://www.CST.com.

[11] W. Hayt, J. Kemmerly, S. Durbin, Engineering Circuit Analysis, (McGraw-Hill, 2012).

[12] Y. Huang, K. Boyle, Antennas from Theory to Practice, Chichester: John Wiley & Sons Ltd, 2008.

[13] W. Hayt, J. Kemmerly, S. Durbin, Engineering Circuit Analysis, (McGraw-Hill, 2012).

Numerical Study of 500 kHz Electromagnetic Wave Irradiation for Root Canal Sterilization in Apical Periodontitis Treatment

Yanakorn Srianant*
[1]*KOSEN-KMITL, King Mongkut's Institute of Technology Ladkrabang, Thailand*
[2]*National Institute of Technology, Kagawa College, Japan*
67210003@kmitl.ac.th

Thanadol Tiengthong*
Department of Electrical and Electronics Engineering, KOSEN-KMITL, King Mongkut's Institute of Technology Ladkrabang, Thailand
thanadol.ti@kmitl.ac.th

Hiroo Tarao
Department of Electrical and Computer Engineering, National Institute of Technology, Kagawa College,
Japan

Masatake Akutagawa
Tokushima University
Japan

Hiromichi Yumoto
Tokushima University
Japan

Toshihiko Tominaga
Tominaga Dental Clinic,
Japan

* Corresponding authors

***Abstract*—Periodontitis, a primary cause of inflammation and tooth loss, can be treated by inserting an electrode into the root canal and applying a 500 kHz current for sterilization through Joule heat. However, achieving sufficient temperature rise to sterilize bacteria remains challenging for teeth with an isthmus, indicating a need for further research. Numeral results show that the temperature significantly exceeds 60 °C around the active electrode and between the active electrode and the ground electrode, with a particular temperature rising when the ground electrode is positioned inside the root canal. These findings highlight the need for further research to optimize treatment efficiency, particularly in improving temperature control and sterilization effectiveness.**

Keywords—coupled analysis, periodontitis, isthmus root canal, temperature distribution, electric current flow

I. Introduction

Periodontitis remains a major public health concern in Thailand, affecting individuals across all age groups. According to national health surveys, 80.2% of 12-year-olds, 79.5% of 15-year-olds, 81.0% of adults aged 35–44, and 74.3% of elderly individuals aged 60–74 suffer from various forms of periodontitis [1]. One particularly problematic form is apical periodontitis, an inflammatory response caused by bacterial invasion through the root canal system and the apical foramen, leading to infection in the periapical tissue.

Conventional treatment typically involves mechanical cleaning and chemical irrigation of the root canal. However, due to the complex internal morphology of tooth, including isthmus [2], these methods often fail to eliminate all microorganisms [3], increasing the risk of reinfection, treatment failure, and eventual tooth loss.

To overcome these limitations, alternative strategies such as Electromagnetic Wave Irradiation (EMWI) and Joule heating using inserted electrodes have gained attention. Recent studies have demonstrated that applying a 500 kHz alternating current can achieve localized heating sufficient to sterilize difficult-to-reach areas, achieving clinical success rates of over 95% in some cases [4]. This method presents a promising adjunctive approach, especially in anatomical regions where conventional treatments fall short.

Nevertheless, challenges remain in controlling the temperature rise to ensure bacterial inactivation without damaging surrounding tissue, particularly in cases involving isthmus-type canal structures. Accurate assessment of the thermal and electrical response within the complex anatomy of the root canal is thus critical for optimizing this treatment.

To address this need, this study conducts a numerical investigation of root canal sterilization using 500 kHz electromagnetic wave irradiation, focusing on heat and electric field distribution within a voxel-based 3D tooth model. By incorporating realistic tooth morphology and biophysical properties into a simulation environment, the research aims to clarify the optimal conditions for achieving effective and safe sterilization, contributing to the development of advanced, minimally invasive endodontic therapies.

II. Methodology

A. Coupled Analysis

This study draws inspiration from the methodology outlined in Reference [5], which served as a foundation for developing the numerical model used in this project. The approach focuses on coupled analysis of the effects of Joule heating and electrical current for apical periodontitis treatment.

B. Temperature Analysis

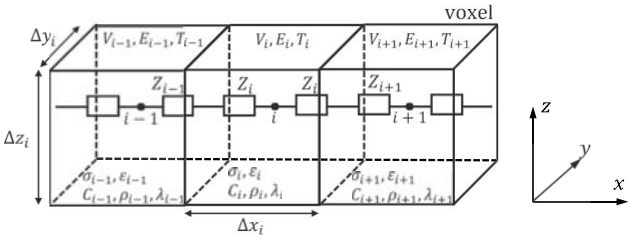


Fig. 1. Voxels for numerical calculation

Figure 1 shows a voxelized model, which at each time step. The temperature can be obtain by heat transportation equation (1)

$$C\rho\frac{\partial T}{\partial t}=\sigma E^2+\lambda(\frac{\partial^2 T}{\partial x^2}+\frac{\partial^2 T}{\partial y^2}+\frac{\partial^2 T}{\partial z^2}) \quad (1)$$

where C is the specific heat, ρ is the volume density, and λ represents thermal conductivity. The first term on the right-hand side corresponds to the power density derived from the electric field analysis. Given that the primary tissues in the tooth model consist of tooth and bone, metabolic heat generation and blood flow are negligible. Thus, Equation (1) does not account for metabolic heat or cooling from blood perfusion.

Applying this equation to the target voxel (i) in Figure 1 results in the following differential equation.

$$C_i\rho_i\frac{(T_i^k-T_i^{(k-1)})}{\Delta t}=\sigma_i E_i^{\,2}+\lambda^*\frac{(T_{(i+1)}^k-2T_i^k+T_{(i-1)}^k)}{(\Delta x^2)} \quad (2)$$

where the superscript k represents the time step. An implicit method was employed to compute the unknown values at time k, using known values from the previous step k-1 over a time interval Δt. The parameter λ^* is defined as the reciprocal sum of the thermal conductivities of adjacent voxels, while Δx denotes the voxel length in the x-direction.

For boundary voxels on the model surface, the following boundary condition was applied,

$$-\lambda^*\frac{\partial T}{\partial n}=h(T-T_a) \quad (3)$$

where h is the heat transfer coefficient, T_a is the ambient temperature, and n denotes the normal to the boundary.

By incorporating Equations (2) and (3) into each voxel, a system of linear equations for N unknowns was formulated. Given that the coefficient matrix is sparse and asymmetric, the stabilized biconjugate gradient method was used to solve the system efficiently.

C. Electric Field and Current Analysis

According to the charge conservation law in Equation (4), the difference equation for the ith voxel in the model is expressed as follows,

$$\nabla\bullet\boldsymbol{J}=0 \quad (4)$$

$$\frac{V_i-V_{i-1}}{Z_i+Z_{i-1}}+\frac{V_i-V_{i+1}}{Z_i+Z_{i+1}}=0 \quad (5)$$

where J in Equation (4) represents the current density. In Equation (5), V is the scalar potential (unknown value) at the voxel center, and Z denotes the impedance (known value) of each voxel. The impedance is given by,

$$Z=\frac{\Delta x/2}{(\sigma+j\omega\varepsilon)\Delta y\Delta z} \quad (6)$$

where σ and ε correspond to the electrical conductivity and dielectric permittivity of the tissue, respectively. The term j represents $\sqrt{-1}$, and ω is the angular frequency.

For instance, when a known potential V_a is applied to the (i−1)th voxel at the model surface, the boundary condition is defined as $V_{i-1}=V_a$. By applying Equation (5) to all voxels in the model, a system of linear equations with N unknowns is formulated. Since the coefficient matrix is sparsely symmetric, the system was efficiently solved using the preconditioned conjugate gradient method

Once the potential distribution was obtained, the electric field component E at the voxel center was computed by evaluating the potential difference across adjacent voxels and dividing by the voxel distance. This calculation provided the necessary electric field distribution for further analysis in the model.

D. Tooth Model and Conditions

The first model includes gingiva, cortical bone, alveolar bone, and lesion tissue. The dentin and root canal morphology were developed to incorporate a narrow gap representing the isthmus, as shown in Figure 2. To simplify the model, enamel was excluded, while two apical foramina with diameters of 0.2 mm each were included. An active electrode was placed 5 mm above the apical foramina, with the ground electrode positioned on the gingiva. The model was converted into voxel points with a resolution of 0.1 mm per side to enable a coupled analysis of current and temperature. Voltages of 30 V and 60 V at a frequency of 500 kHz were applied continuously for an energization time of 1.0 s, starting from an initial tissue temperature of 36 °C.

In the second model, the ground electrode was reshaped to match the morphology of the active electrode and subsequently inserted into the root canal, as illustrated in Figure 3. This scenario was introduced to investigate the influence of ground electrode placement on temperature distribution and current flow, particularly in regions that are difficult to sterilize, such as the isthmus. By designing and analyzing these two models, this project aims to provide insights into optimizing the conditions for effective root canal sterilization.

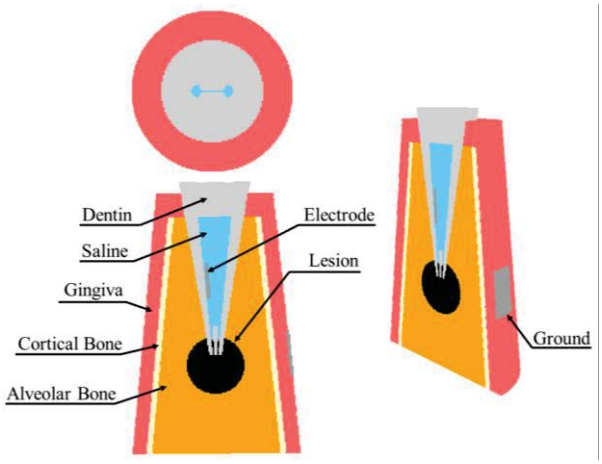


Fig. 2. Cross-sectional and 3D views of the top and middle regions of the tooth with an isthmus model, showing the ground electrode on the gingiva.

TABLE I. PHYSICAL AND ELECTRICAL PROPERTIES OF THE TOOTH AND PERIODONTAL TISSUE MODEL [6].

Tissue	ρ (kg/m^3)	C (J/(kg°C)	λ (W/(m°C))	σ (S/m)	ε (F/m)
Tooth (dentin)	2100	1300	0.5	0.01	170
Gingiva	1100	3400	0.5	0.45	3650
Alveolar bone	1200	2300	0.3	0.087	300
Cortical bone	1900	1300	0.3	0.022	170
Physiological saline	1000	4200	0.6	$0.0268T$ +0.875	85
Electrode (stainless)	8000	500	20	10^6	-

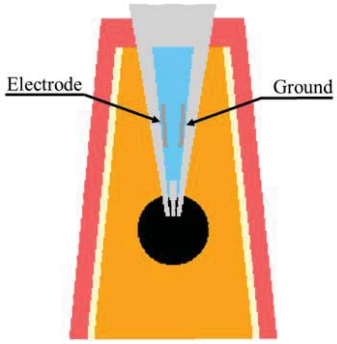


Fig. 3. Cross-sectional view of the middle regions of the tooth with an isthmus model, showing both the active electrode and ground electrode positioned inside the root canal.

Table 1 shows the properties of each tissue used in the calculation.

Furthermore, after investigating both cases with a 100% duty cycle, we proceeded to examine different applied voltages and duty cycles with 70% (as shown in Figure 4) and 5% for the case with the ground electrode inside, to determine the most suitable conditions for sterilization.

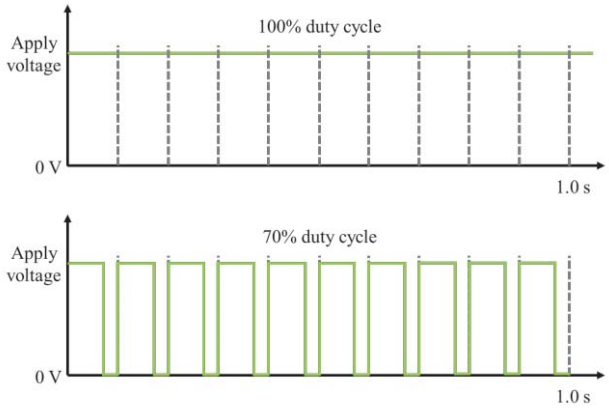


Fig. 4. Duty cycle of apply voltage.

III. Results and Discussion

A. Temperature Distribution

The results of the temperature distribution, as shown in Figure 5, demonstrate differences in the effectiveness of the applied voltages. At 30 V, most of the root canal and the narrow gap in the middle of the root canal (isthmus) remain below 40 °C. Conversely, applying 60 V shows significant improvement, as the temperature exceeds 60 °C, particularly around the top and bottom of the active electrode. However, the temperature distribution remains non-uniform, failing to effectively reach the entire narrow gap. These results suggest that while some localized heating occurs, the majority of the target regions remain below the effective temperature rise threshold.

In contrast, at 60 V, the temperature distribution expanded. The highest temperatures recorded were 63.57 °C in the root canal and 61.24 °C in the narrow gap. However, voxels exceeding 60 °C were limited to only 0.68% in the root canal and 0.40% in the narrow gap, primarily concentrated near the top and bottom of the active electrode. This indicates that while higher voltages can increase peak temperatures, achieving uniform heating throughout the root canal and the narrow gap remains a challenge.

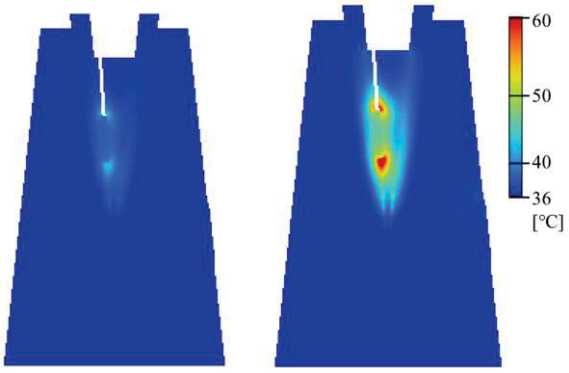


Fig. 5. Temperature distribution on the x–z plane at the end of energization for applied voltages of 30 V (left) and 60 V (right), with the ground electrode positioned on the gingiva.

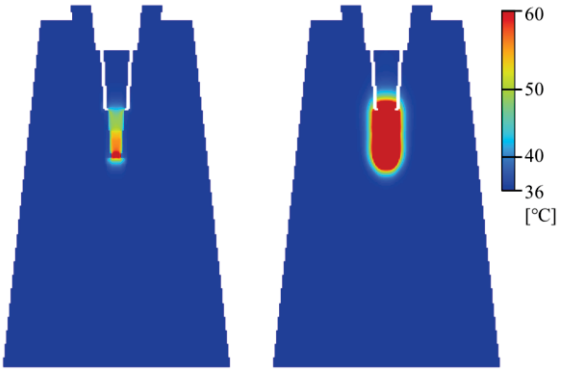


Fig. 6. Temperature distribution on an x–z plane at the end of energization applied voltages 30 V for 0.05 s (left) and 1.0 s (right) with the ground electrode inside the root canal.

Additionally, when the ground electrode was inserted into the root canal, substantial localized heating was observed, particularly within the narrow gap (Figures 6). At 30 V and within just 0.05 s, the temperature in the gap rose rapidly to 66.88 °C, with 2.90% of voxels exceeding 60 °C threshold. The maximum temperature reached in the root canal was 49.84 °C. However, after 1.0 s, excessive heat accumulation was noted, with temperatures soaring to 315.88 °C. Such extreme temperatures pose significant risks to surrounding tissues, making this configuration unsuitable without further optimization.

These findings emphasize the complexity of achieving effective temperature elevation through Joule heating. While higher voltages and modifications to ground electrode placement can enhance localized heating, they often lead to non-uniform temperature distributions or excessive heat accumulation, both of which are problematic. Uniform heating of the narrow gap remains particularly challenging due to its morphology, which restricts heat transfer.

For further investigation, simulations were conducted to identify the optimal parameters for safe and effective sterilization. It was found that applying a voltage of 20 V with a 70% duty cycle, and 65 V with a 5% duty cycle, resulted in favorable outcomes. Under these conditions, the maximum temperature remained below the critical threshold of 100 °C, minimizing the risk of thermal damage to surrounding

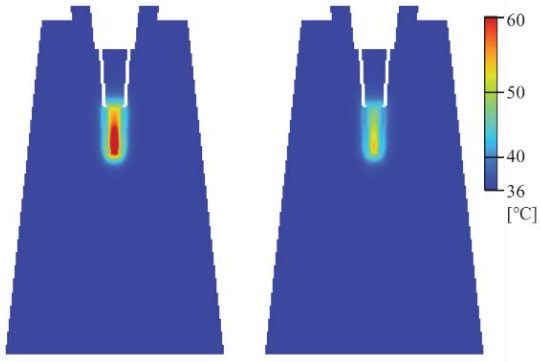


Fig. 7. Temperature distribution on an x–z plane at the end of energization applied voltages 20 V with 70% duty cycle for 1.0 s (left) and 65 V with 5% duty cycle for 1.0 s (right) with the ground electrode inside the root canal.

tissues. Additionally, significant heat accumulation was observed specifically in the narrow gap between canals, as illustrated in Figure 7.

Notably, although Figure 7 suggests that the temperature in the 20V case appears higher than in the 65V case, the actual peak temperatures are 69.15°C for 20V and 72.12°C for 65V. Additionally, the area where the temperature in the gap ranges between 60–70°C is larger in the 65V case compared to the 20V case.

B. Electric Current Flow

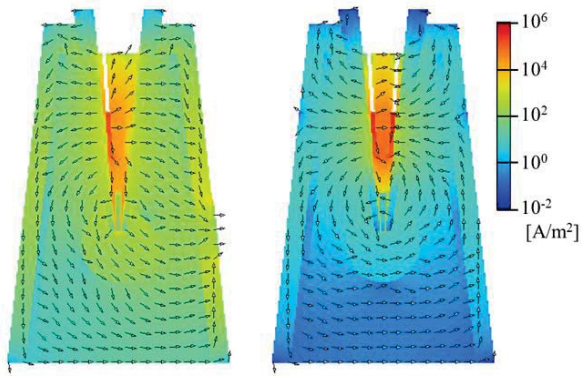


Fig. 8. Electric current flow after applying a 60 V voltage (left) and in the case after applying a 30 V voltage where the ground electrode is inside the root canal (right) , for 1.0 s in both cases.

Figure 8 illustrates the current flow in two scenarios. On the left, with a 60 V voltage applied, the current is primarily concentrated at the top and bottom regions of the active electrode, where the density is highest. As the current extends outward, the distribution becomes weaker, particularly as it penetrates deeper into the surrounding tissues.

In contrast, on the right, when the ground electrode is positioned inside the root canal, the current is intensely concentrated between the active electrode and the ground electrode. This configuration creates a region of high current density, while the surrounding tissues and isthmus area experience significantly weaker current distribution.

These observations highlight the need for careful optimization of electrode placement to achieve effective coverage of the root canal, particularly in the isthmus region, while avoiding excessive of current.

IV. Conclusion

A coupled analysis of electrical current and heat transfer was conducted to evaluate temperature rise within a numerical tooth model featuring the complex morphology of the root canal system. A 500 kHz current was applied to simulate conditions for apical periodontitis treatment, with the objective of identifying optimal parameters for root canal sterilization via Joule heating.

The results revealed that both the applied voltage (30 V and 60 V) and the placement of the ground electrode significantly influenced temperature distribution and current flow. At 30 V, the temperature rise was minimal and localized, with most regions remaining below 40 °C. In contrast, applying 60 V caused the current to concentrate around the root canal, particularly at the top and bottom of the active electrode. Ground electrode insertion further intensified current density between electrodes, producing rapid heating and temperatures exceeding 60 °C within 0.05 s. However, this setup led to highly non-uniform temperature distribution and thermal overaccumulation, with temperatures reaching up to 315.88 °C within 1.0 s posing a risk of tissue damage.

Subsequent optimization efforts demonstrated that applying 20 V at a 70% duty cycle and 65 V at a 5% duty cycle yielded more balanced results, maintaining temperatures below 100 °C while achieving localized heating in critical regions like the isthmus. Nonetheless, practical constraints, such as the 100 V maximum allowable voltage in Japan, necessitate further refinement. A proposed solution involves configuring a serial circuit to optimize resistance and current delivery.

Moreover, enhancing the model's resolution by reducing voxel size could significantly improve result. Finer voxels would reduce boundary inconsistencies between tissues, enabling more accurate analysis and broader investigative capability in future studies.

References

[1] Report on the results of the 9th National Oral Health Survey, Thailand, 2023, pp. 19-30.

[2] H. Ishizaki, A. Nakazono, S. Yamada, and A. Yoshimura, "Causes of endodontic failure of isthmus-containing root canals, and treatment strategies," *The Japanese Journal of Conservative Dentistry*, vol. 65, no. 1, pp. 9–20, 2022.

[3] J. Kharouf, F. Pedram, S. Sfeir, and H. Machtou, "Effect of Chemical Debridement and Irrigant Activation on Smear Layer Removal in the Apical Third of Curved Root Canals: A Scanning Electron Microscopy Study," Int. J. Environ. Res. Public Health, vol. 19, no. 5, p. 2767, Feb. 2022.

[4] T. Tominaga, K. Kitaike, E. Tada, K. Takahira, N. Bando, S. Hirao, K. Hayashi, M. Yokoyama, and J. Yoshinaga, "Application of electromagnetic stimulation to apical periodontitis," *The Journal of Japan Endodontic Association*, vol. 38, pp. 36–47, 2017.

[5] H. Tarao et al., "Evaluation of temperature increase from Joule heat in numerical tooth model by applying 500 kHz current for apical periodontitis treatment—Effect of applied voltage and tooth conductivity," *Bioelectromagnetics*, vol. 42, pp. 224–237, 2021.

[6] S. Gabriel, R. W. Lau, and C. Gabriel, "The dielectric properties of biological tissues: III. Parametric models for the dielectric spectrum of tissues," *Physics in Medicine & Biology*, vol. 41, pp. 2271–2293, 1996.

Intelligent Multi-Link Selection for IEEE 802.11be Using Reinforcement Learning with Radiation Pattern Awareness

Bhurisub Dejpipatpracha
Department of Digital Technology
Faculty of Science and Technology
Phuket Rajabhat University
Phuket, Thailand
bhurisub@pkru.ac.th

Akarachai Inthanil
Department of Digital Technology
Faculty of Science and Technology
Phuket Rajabhat University
Phuket, Thailand
akarachai.i@pkru.ac.th

Wimonnat Sukpol
Department of Mathematics
Faculty of Science and Technology
Phuket Rajabhat University
Phuket, Thailand
wimonnat.s@pkru.ac.th

Worrarat Jongkraijak
Department of Business computer
Faculty of Management Sciences
Phuket Rajabhat University
Phuket, Thailand
worrarat.j@pkru.ac.th

***Abstract*— The IEEE 802.11be (Wi-Fi 7) standard introduces Multi-Link Operation (MLO) to enhance network efficiency by enabling simultaneous data transmission across multiple frequency bands. However, optimal link selection in dynamic wireless environments remains a significant challenge due to fluctuating signal conditions, interference, and the impact of antenna radiation patterns. Traditional heuristic-based approaches often fail to adapt effectively to these variations, leading to suboptimal performance. This paper proposes an intelligent Multi-Link selection framework based on Reinforcement Learning (RL), incorporating radiation pattern awareness to enhance decision-making. The proposed model leverages both omnidirectional and directional beamforming characteristics to dynamically select the most efficient link, considering real-time network conditions such as signal strength, interference, and spatial coverage. By integrating radiation pattern information into the RL training process, the system optimizes link selection while minimizing latency and improving throughput. Simulation results demonstrate that the proposed RL-based approach can select links based on various factors and dynamically choose the optimal link in real-time. This study highlights the potential of RL-driven Multi-Link selection strategies in advancing next-generation Wi-Fi networks and adaptive wireless communication systems.**

Keywords*— *Multi-Link Operation, reinforcement learning, wireless networks

I. INTRODUCTION

Wireless communication is a cornerstone of modern networks, supporting applications such as high-definition video streaming, industrial automation, and the Healthcare Internet of Things (H-IoT) [1]. As user demands increase, networks must provide higher data rates, lower latency, and reliable connectivity. To meet these challenges, the IEEE 802.11be standard, commonly known as Wi-Fi 7, introduces Multi-Link Operation (MLO), a key innovation that enables devices to simultaneously utilize multiple frequency bands to enhance throughput and minimize latency. MLO allows a wireless station (STA) to establish concurrent connections with an access point (AP) across 2.4 GHz, 5 GHz, and 6 GHz bands, supporting parallel data transmission over multiple channels and improving network congestion and transmission reliability. The MLO process requires simultaneous data acquisition and transmission (STR), which introduces a link selection challenge [2]. Furthermore, addressing parallel backoffs can mitigate the latency issue [3]–[6]. The radiation pattern significantly affects network performance when data is transmitted simultaneously. Specifically, it impacts the hidden node problem [7] and interference [8], [9], which in turn degrade communication efficiency. This degradation results in increased delay and reduced throughput, making it essential to consider the impact of radiation patterns on link selection. To address this challenge, Reinforcement Learning (RL) has emerged as a powerful approach for optimizing dynamic link selection. RL enables adaptive decision-making by assigning rewards and penalties based on network conditions. Recent research has demonstrated the effectiveness of RL in wireless communication by enhancing network efficiency and reducing interference [10], [11]. Additionally, antenna radiation characteristics have been considered in multi-link transmission, as demonstrated by [12], which developed a 2×2 MIMO antenna to support multi-link applications. Furthermore, [13] proposed a PHY and MAC layer analysis model to improve overall Wi-Fi 7 performance.

This paper proposes an RL-based Multi-Link selection framework that incorporates radiation pattern awareness to improve Wi-Fi 7 network performance. Unlike traditional heuristic approaches, the proposed RL model dynamically selects the most suitable multi-link configuration by analyzing RSSI, Signal-to-Noise Ratio (SNR), interference levels, throughput variations, and antenna radiation characteristics. The proposed RL-based model continuously learns and adapts to varying network conditions, ensuring optimal link selection and improved network efficiency.

This paper is organized into five sections. Section II presents the channel model used for Multi-Link Operation, including path loss modeling, small-scale fading effects, interference modeling, and the impact of radiation patterns on link performance. Section III describes the RL framework, state-action-reward formulation, and the selected RL algorithms. Section IV details the simulation setup and performance evaluation, comparing the proposed RL-based Multi-Link. Section V concludes the paper by summarizing key findings and suggesting future research directions.

XXX-X-XXXX-XXXX-X/XX/$XX.00 ©20XX IEEE

II. CHANNEL MODEL

The performance of wireless communication systems is largely influenced by the characteristics of the wireless channel like radiation pattern in Fig.1. In the context of MLO in IEEE 802.11be (Wi-Fi 7), the effectiveness of simultaneous data transmission across multiple frequency bands depends on several factors, including path loss, fading, interference, and antenna radiation patterns. This section presents the channel model used to evaluate the MLO system, with particular attention given to the impact of each factor on link performance.

A. Path Loss Model

Path loss refers to the reduction in signal strength as the transmitted signal travels through space. In wireless communication systems, path loss is influenced by the distance between the AP and STA, as well as the environment (e.g., urban, indoor, or rural settings). To model path loss, the log-distance path loss model is commonly used, given by the following equation:

$$P_L(d) = P_{L0} + 10n\log\frac{d}{d_0} \tag{1}$$

where $P_L(d)$ is the path loss at distance d,

P_{L0} is the reference path loss at d_0,

n is the path loss exponent,

d is the distance between the AP and STA,

d_0 is the reference distance.

For the Wi-Fi 7 network operating in the 2.4 GHz, 5 GHz, and 6 GHz bands, the path loss exponent is assumed to be different for each frequency band due to varying signal attenuation characteristics. Higher frequencies, such as 6 GHz, typically suffer from greater path loss compared to 2.4 GHz and 5 GHz.

B. Fading Model

Fading is caused by the interference of multiple signal paths, leading to variations in signal strength over time or space. Small-scale fading is particularly important in wireless communication, as it can cause rapid fluctuations in signal quality due to factors like multipath propagation and shadowing. The Rayleigh fading model is often used to model fading in environments with no line-of-sight (NLOS), while the Rician fading model is applied in line-of-sight (LOS) scenarios. In our model, Rayleigh fading is assumed to represent the fading effect for the wireless links between AP and STA, as the environment is typically non-line-of-sight in many urban or indoor scenarios.

C. Interference Model

Interference arises from multiple transmitters operating on Interference plays a critical role in determining the quality of wireless communication systems, especially in MLO environments where multiple links operate concurrently across different frequency bands. In these systems, interference typically arises from external sources or other transmissions within the same environment, which can cause signal degradation and loss of data. In our model, interference is calculated based on the radiation pattern and signal strength of the transmission. For omnidirectional transmission, interference is randomly generated between 0 and 10 dB, simulating external sources of interference. For directional

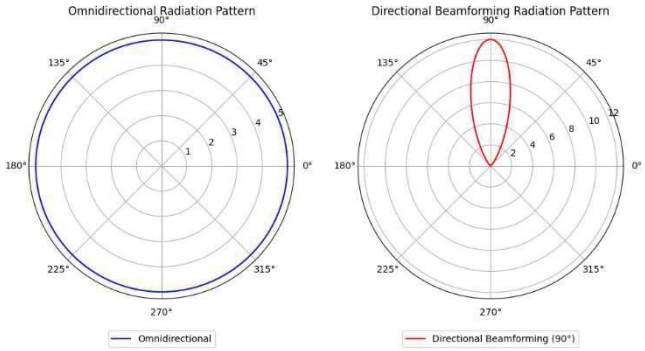


Fig.1. The radiation pattern for Multi-Link Operation (MLO).

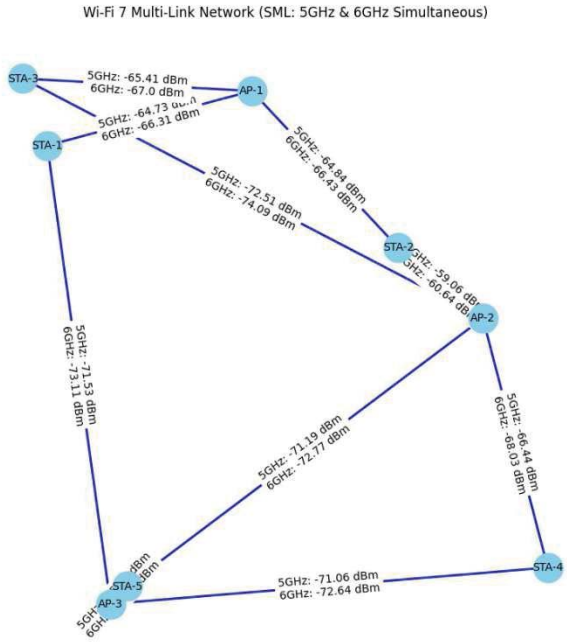


Fig. 2. The MLO with AP and STA environment.

beamforming, interference is calculated using the gain of the antenna, which is influenced by the beam width and beam angle. The interference value increases with the antenna's gain, as higher gain often leads to more focused transmission, thus increasing the potential for interference in adjacent regions. The impact of interference on the signal quality is evaluated through the signal-to-interference-plus-noise ratio (SINR). SINR is a crucial parameter in wireless communication, as it determines the quality of the received signal relative to interference and noise. In this model, interference is treated as a factor that reduces SINR, thereby negatively affecting throughput and latency. Mathematically, the SINR for each link is computed as:

$$SINR = \frac{RSSI}{Interference + Noise} \tag{2}$$

where $RSSI$ is the received signal strength,

$Interference$ is the interference caused by other transmissions in the environment (dB),

$Noise$ is the background noise level (dBm).

The Interference for each frequency band (5 GHz and 6 GHz) is considered independently. Interference values are generated dynamically based on the radiation patterns and signal conditions of the system, simulating real-world environments where interference levels vary depending on

factors like user mobility, distance from AP, and obstructions. The interference model is thus essential for simulating realistic wireless environments and for optimizing the performance of the proposed RL framework.

D. Throughput

Throughput is a key performance metric that measures the actual rate of successful data transmission in a wireless communication system. In the context of MLO and the IEEE 802.11be (Wi-Fi 7) standard, throughput is particularly important because it determines the system's ability to handle high data rates and multiple simultaneous transmissions across different frequency bands. In this model, throughput is calculated for both the 5 GHz and 6 GHz bands, as well as for the overall system when using MLO, which combines the throughput from both frequency bands to provide enhanced data rates. The total throughput is the sum of the individual throughputs from each link, considering the simultaneous use of multiple links. The throughput for each link is estimated using the Shannon Capacity Formula, which defines the theoretical upper bound of the data transmission rate in a communication channel with a given Signal-to-Noise Ratio (SNR). The formula is expressed as:

$$C = B\log_2\left(1+SNR\right) \tag{3}$$

where C is the channel capacity or throughput,

B is the bandwidth of the channel,

SNR is the signal-to-noise ratio (in linear scale).

For Wi-Fi 7, the system operates on a bandwidth of 160 MHz for each frequency band (5 GHz and 6 GHz). The throughput for each frequency band is calculated as:

$$T = B\log_2\left(1+10^{\frac{SNR}{10}}\right) \tag{4}$$

The SNR is obtained from the previous step, and B represents the bandwidth, which is 160 MHz for 5 GHz and 6 GHz channels. The total throughput for MLO is calculated by summing the individual throughputs from the 5 GHz and 6 GHz links:

$$T_{MLO} = T_{5GHz} + T_{6GHz} \tag{5}$$

This combined throughput allows for higher data rates and better utilization of available spectrum, enabling the system to handle more data while reducing latency compared to single-link operation following Fig.2. In addition to the basic throughput calculation, throughput efficiency is also affected by factors such as interference, latency, and signal degradation. The presence of interference, as modeled in the previous section, can lower the effective throughput by reducing the SINR, which directly impacts the data rate that can be achieved on each link. To evaluate the system's efficiency, we also calculate the percentage increase in throughput when using MLO as compared to using a single frequency band (5 GHz or 6 GHz). This allows us to assess the benefits of multi-link operation in improving the overall network performance.

III. Reinforcement Learning Model

The Reinforcement Learning (RL) model is designed to optimize the link selection process in MLO for Wi-Fi 7 (IEEE 802.11be). The goal is for the RL agent to dynamically select the best link configuration, whether using 5 GHz, 6 GHz, or MLO, based on real-time network conditions such as RSSI, SNR, latency, throughput, and interference.

A. Reinforcement Learning Framework

The RL framework follows a Markov Decision Process (MDP), where the state, action, and reward are defined to guide the agent in selecting the optimal link configuration. The system's state S includes real-time network parameters, and the agent's goal is to choose an action A that maximizes the long-term reward R.

- State (S): Includes network conditions such as RSSI, SNR, latency, throughput, and interference for both 5 GHz and 6 GHz links.
- Action (A): The RL agent chooses between three actions: 5 GHz, 6 GHz, or MLO (multi-link operation using both 5 GHz and 6 GHz bands).
- Reward (R): The reward is computed based on the throughput, latency, and interference of the selected action. The reward function aims to maximize throughput while minimizing latency and interference.

B. RL Algorithm Selection

The RL-based AP-STA Link Selection uses a straightforward approach where the agent observes the network state (e.g., RSSI, SNR, throughput, interference) and selects the best link between 6 GHz or MLO. The RL model evaluates the current state and chooses an action based on predefined thresholds, optimizing the selection process. The model is trained iteratively with a reward function based on throughput and latency, allowing it to adapt to dynamic network conditions until convergence is reached.

Pseudocode for RL-based AP-STA Link Selection

1. Initialize:
   - Set up AP and STA positions in a 2D space.
   - Define network parameters (RSSI, SNR, Throughput).
   - Define action space {6GHz, MLO}.
2. For each STA:
   - Observe state: (RSSI, SNR, Throughput, Interference).
   - Use RL model to select action:
   - If SNR and Throughput for 6GHz > Threshold → Choose 6GHz.
   - Otherwise, choose MLO.
3. Update RL Model:
   - Apply reward function based on throughput and latency.
   - Train model iteratively.
4. Repeat until convergence.

IV. Result and Discussion

The results of this study present an in-depth analysis of the throughput performance in Wi-Fi 7 (IEEE 802.11be) Multi-Link Operation (MLO), incorporating reinforcement

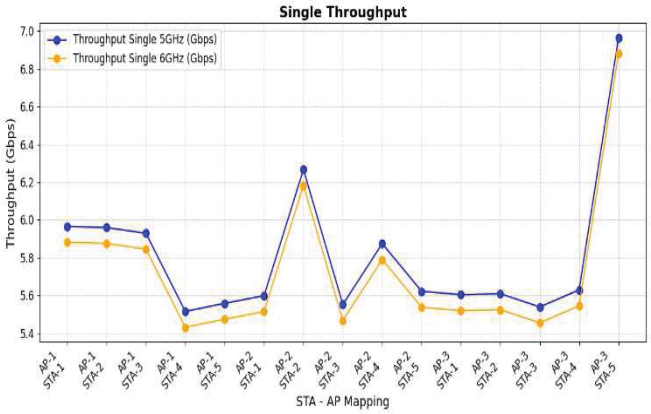


Fig.3. Single throughput for 5 GHz and 6 GHz.

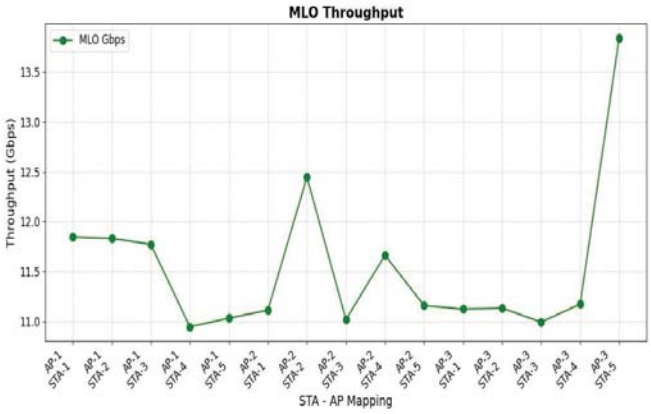


Fig.4. MLO throughput performance.

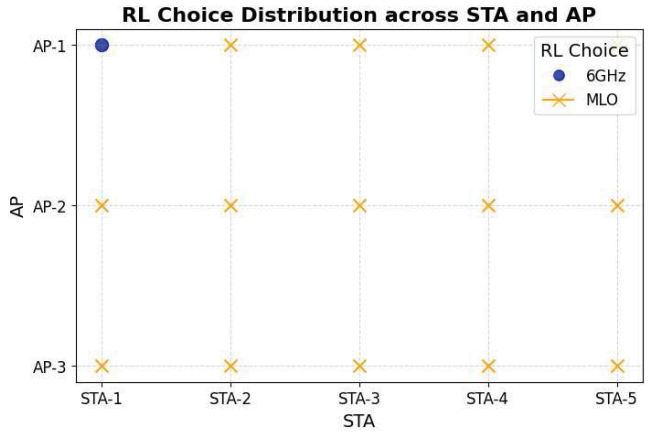


Fig.5. RL choice distribution across STA and AP.

learning (RL) for dynamic link selection, considering the impact of antenna radiation patterns. Figure 3 compares the single throughput performance between the 5 GHz and 6 GHz bands. The throughput of the 6 GHz band outperforms the 5 GHz band in all AP-STA pairs, primarily due to its higher bandwidth capacity. However, in the presence of obstacles, the 5 GHz band showed better performance compared to the 6 GHz band, as it is less susceptible to signal degradation. Figure 4 highlights the throughput performance when both 5 GHz and 6 GHz bands are used in MLO mode. The throughput increase is significant, with an improvement of up to 98.79% for the 5 GHz band and 101.55% for the 6 GHz band, demonstrating the advantages of combining both frequency bands. The RL-based link selection, as shown in Figure 5, dynamically adapts to varying network conditions. The algorithm selects the 6 GHz band for AP1 and STA1, while other AP-STA pairs utilize MLO. The RL agent's decision-making process considers key factors such as path loss, distance, and interference. For example, when interference is high or when signal strength is suboptimal for a single frequency band, the RL model opts for MLO to mitigate performance degradation and optimize throughput.

V. Conclusion

In this paper, we proposed an intelligent Multi-Link Operation (MLO) framework for Wi-Fi 7 (IEEE 802.11be) using Reinforcement Learning (RL) with radiation pattern awareness for optimized link selection. The results show that MLO significantly improves throughput by up to 101.55% compared to single-band operation. This enhancement is due to the combined use of both 5 GHz and 6 GHz bands, improving spectrum utilization and reducing latency. The RL-based model adapts to dynamic network conditions, selecting the optimal link configuration in real time, thus enhancing overall network efficiency.

References

[1] Y. A. Qadri, H. Jung, and D. Niyato, “Towards the Internet of Medical Things for real-time health monitoring over Wi-Fi,” IEEE Network., 2024.

[2] C. L. Tai, M. Eisen, D. Akhmetov, D. Das, D. Cavalcanti, and R. Sivakumar, “Model-free dynamic traffic steering for multi-link operation in IEEE 802.11be,” IEEE International Conference on Machine Learning for Communication and Networking (ICMLCN), pp. 44–49, May 2024.

[3] M. Carrascosa-Zamacois, G. Geraci, E. Knightly, and B. Bellalta, “Wi-Fi multi-link operation: An experimental study of latency and throughput,” IEEE/ACM Transactions on Networking, vol. 32, no. 1, pp. 308–322, 2023.

[4] E. Reshef and C. Cordeiro, “Future directions for Wi-Fi 8 and beyond,” IEEE Communications Magazine, vol. 60, no. 10, pp. 50–55, 2022.

[5] W. Murti and J. H. Yun, “Multilink operation in IEEE 802.11be wireless LANs: Backoff overflow problem and solutions,” Sensors, vol. 22, no. 9, p. 3501, 2022.

[6] A. A. Abdalhafid, S. K. Subramaniam, Z. A. Zukarnain, and F. H. Ayob, “Multi-link operation in IEEE 802.11be extremely high throughput: A survey,” IEEE Access, 2024.

[7] Q. Zhao, L. Feng, M. Zhou, D. Wu, X. Wang, and P. Zhang, “Full-duplex time-domain contention for Wi-Fi networks: Opportunities and challenges,” IEEE Wireless Communications, 2024.

[8] M. Carrascosa-Zamacois, L. Galati-Giordano, A. Jonsson, G. Geraci, and B. Bellalta, “Performance and coexistence evaluation of IEEE 802.11be multi-link operation,” IEEE Wireless Communications and Networking Conference (WCNC), pp. 1–6, Mar. 2023.

[9] B. Bellalta, M. Carrascosa, L. Galati-Giordano, and G. Geraci, “Delay analysis of IEEE 802.11be multi-link operation under finite load,” IEEE Wireless Communications Letters, vol. 12, no. 4, pp. 595–599, 2023.

[10] E. M. Bansbach, V. Eliachevitch, and L. Schmalen, “Deep reinforcement learning for wireless resource allocation using buffer state information,” IEEE In 2021 Global Communications Conference (GLOBECOM), pp. 1–6, Dec. 2021.

[11] R. Ali and B. Bellalta, “A federated reinforcement learning framework for link activation in multi-link Wi-Fi networks,” IEEE International Black Sea Conference on Communications and Networking (BlackSeaCom), pp. 360–365, Jul. 2023.

[12] J. Kim, H. Shin, S. Wi, H. Lee, R. Li, and H. Kim, “2×2 MIMO dual-wideband ground radiation antenna with a T-shaped isolator for Wi-Fi 6/6E/7 applications,” Scientific Reports, vol. 15, no. 1, p. 85, 2025.

[13] E. Khorov, I. Levitsky, and I. F. Akyildiz, “Current status and directions of IEEE 802.11be, the future Wi-Fi 7,” IEEE Access, vol. 8, pp. 88664–88688, 2020.

Modeling the Performance of Wi-Fi Networks Using 5GHz, 6GHz, and Multi-Link Operation

Wimonnat Sukpol
Department of Mathematics
Faculty of Science and Technology
Phuket Rajabhat University
Phuket, Thailand
wimonnat.s@pkru.ac.th

Akarachai Inthanil*
Department of Digital Technology
Faculty of Science and Technology
Phuket Rajabhat University
Phuket, Thailand
akarachai.i@pkru.ac.th

Bhurisub Dejpipatpracha
Department of Digital Technology
Faculty of Science and Technology
Phuket Rajabhat University
Phuket, Thailand
bhurisub@pkru.ac.th

***Abstract*— The rapid expansion of wireless devices and the growing demand for high-speed data have made Wi-Fi networks indispensable in modern communication. However, traditional Wi-Fi networks operating in the 2.4GHz and 5GHz bands face challenges in high-density environments due to limited spectrum and increased interference. Recent advancements, such as the introduction of the 6GHz frequency band in Wi-Fi 6E and Wi-Fi 7, offer additional spectrum to alleviate congestion and improve performance. Additionally, Multi-Link Operation (MLO), introduced in Wi-Fi 7, allows devices to simultaneously operate on both the 5GHz and 6GHz bands, aggregating bandwidth to increase throughput and reduce delays. This study investigates the performance of Wi-Fi networks utilizing 5GHz, 6GHz, and MLO under varying STA densities. Using a simulation model, the study evaluates the impact of STA density on network performance, focusing on throughput and delay. The network's dynamic behavior, including transmission attempts, collisions, and backoff stages, is modeled using a Markov Chain to accurately simulate real-world transmission conditions. The results demonstrate that while 6GHz and MLO provide significant performance improvements, particularly in high-density environments, managing the interactions between the frequency bands and the challenges of interference and load balancing is crucial. The findings of this study offer valuable insights into how MLO can enhance network performance and reliability, contributing to the development of future Wi-Fi systems.**

Keywords*— *Multi-Link Operation, Markov Chain, wireless networks

I. INTRODUCTION

The rapid growth of wireless devices and the increasing demand for high-speed data transmission have made Wi-Fi networks an essential component of modern communication. These networks are integral to a wide range of applications, from personal internet access and multimedia streaming to critical business operations and industrial automation. As Wi-Fi technology evolves, it faces significant challenges, particularly in high-density environments with a large number of connected devices. These high-density scenarios, such as urban areas, offices, and public venues, often suffer from network congestion, leading to degraded performance marked by low throughput, high latency, and frequent packet loss [1]. A major limitation of traditional Wi-Fi networks, especially those operating in the 2.4GHz and 5GHz bands, is the limited available spectrum. As the number of devices using these bands increases, so does the competition for available channels, which leads to interference and reduced network efficiency. This issue is compounded in environments where many devices operate in close proximity, creating additional congestion and interference. Such performance degradation negatively impacts applications that require high bandwidth or low latency, such as video conferencing, real-time gaming, and industrial control systems. To address these challenges, recent advancements in Wi-Fi technology have introduced the 6GHz frequency band [2], available in Wi-Fi 6E [3] and Wi-Fi 7 [4]. The introduction of the 6GHz band aims to alleviate congestion by providing additional spectrum and enabling the use of more available channels. This reduces interference in the 5GHz band and significantly improves throughput, making it especially valuable in high-density environments where traditional Wi-Fi networks struggle to maintain efficiency. However, the performance of the 6GHz band is still constrained by factors such as network congestion, interference between devices, and the complexities of managing a larger spectrum. In addition to expanding spectrum, Multi-Link Operation (MLO), introduced in Wi-Fi 7 [5],[6], is a key advancement that enhances Wi-Fi performance. MLO allows devices to operate on both the 5GHz and 6GHz frequency bands simultaneously, aggregating their bandwidth to increase throughput and reduce delays. This simultaneous use of multiple bands can mitigate congestion on a single band and offer more reliable connectivity, particularly in environments with many devices competing for bandwidth. While MLO holds great potential for improving network performance, it also introduces new challenges in managing interference, load balancing, and coordination between the two frequency bands. The interactions between 5GHz and 6GHz in a real-world environment are complex and require effective management to fully realize the benefits of MLO. Despite the promising advantages of MLO, the exact performance improvements in terms of throughput and delay under varying network conditions have yet to be fully explored. This is particularly important in high-density environments, where congestion, interference, and STA density significantly impact network performance. While much research has been conducted on 5GHz and 6GHz individually, and some studies have examined aspects of MLO, the combined effect of these two frequency bands operating simultaneously remains underexplored.

This study aims to bridge this gap by simulating the performance of Wi-Fi networks using 5GHz, 6GHz, and MLO, with a particular focus on throughput and delay. The network's dynamic behavior, including collisions, backoff stages, and resulting delays, is modeled using a Markov Chain [7], which accurately represents the random nature of transmission attempts in a shared wireless medium. By comparing the performance of the network under different conditions 5GHz, 6GHz, and MLO this study seeks to assess the practical benefits of MLO in high-density environments. The primary objectives of this study are to analyze the impact of STA density on throughput and delay, evaluate the

XXX-X-XXXX-XXXX-X/XX/$XX.00 ©20XX IEEE

performance improvements offered by MLO, and investigate the effects of combined frequency band operation in Wi-Fi networks. Furthermore, this research aims to provide insights into how MLO can be integrated into existing Wi-Fi networks to enhance capacity and reliability. The results of this study are expected to contribute to the design of future Wi-Fi systems, particularly those utilizing the 6GHz band and MLO, to meet the growing demands of high-density wireless environments.

II. Network Environment

In this study, the performance of Wi-Fi networks is evaluated through simulations involving stations (STAs) and access points (APs). The network environment is designed to reflect realistic conditions, considering key parameters such as the number of STAs, the number of APs, and the distance between each STA and its corresponding AP. Additionally, the network configuration incorporates both the 5GHz and 6GHz frequency bands, with a focus on evaluating the performance of MLO.

A. Network Configuration

The network configuration consists of several STAs and APs. In this study, each STA communicates with an AP, and the performance is evaluated across varying numbers of STAs. The density of STAs in the network ranges from 10 to 160 in increments of 10, allowing for a comprehensive analysis of how increasing network load influences key performance metrics such as throughput and delay. By varying the number of STAs, the study investigates the effects of STA density on network performance under different conditions. To simulate a more realistic environment, a fixed number of 5 APs are deployed within the network. These APs are evenly distributed across the environment, with each STA connecting to the AP that is closest to it. By maintaining a constant number of APs, the study isolates the impact of changing STA density on throughput and delay, allowing for a focused analysis of these factors without introducing variations in the number of APs. Additionally, the distance between each STA and its assigned AP is randomly generated within a range of 20 to 100 meters. This random distribution reflects the natural variability that occurs in real-world settings, such as urban or indoor environments, where the physical separation between users and APs can differ significantly. By modeling the network in this manner, the study simulates the dynamic conditions often encountered in real-world Wi-Fi deployments, where both the spatial arrangement of APs and the distribution of users are not uniform, adding to the complexity of the performance evaluation.

B. Frequency Bands

In this study, two primary frequency bands, 5GHz and 6GHz, are considered to evaluate their performance in terms of throughput and delay. The 5GHz frequency band is widely used in modern Wi-Fi networks, while the 6GHz band, introduced with Wi-Fi 6E and Wi-Fi 7, is relatively new and offers additional spectrum for higher throughput and reduced interference. By comparing these two frequency bands, the study aims to assess their individual performance, as well as the combined benefits of MLO, which aggregates the throughput of both frequency bands. The 5GHz band has become a cornerstone of modern Wi-Fi technologies, providing higher data rates compared to the 2.4GHz band. However, it suffers from a shorter range due to increased path loss, which makes it more susceptible to physical obstructions and environmental factors. This band is widely used for high-speed data transmission, but its coverage area can be limited in densely populated or obstructed environments. The 6GHz band, introduced with Wi-Fi 6E, provides an expanded spectrum that can support higher data rates with less interference compared to the 5GHz band. This additional spectrum allows for more channels, reducing congestion and improving overall network performance, especially in environments with many devices. The 6GHz band is expected to enhance the capacity and efficiency of Wi-Fi networks, particularly in high-density scenarios. In addition to evaluating the individual performance of the 5GHz and 6GHz bands, the study also investigates the potential benefits of MLO. MLO enables simultaneous communication on both the 5GHz and 6GHz bands, aggregating the throughput from each band. This approach could improve overall network performance by increasing bandwidth availability and reducing congestion, especially in high-traffic environments.

C. Markov Chain for State Transitions

In order to model the dynamic behavior of the network and account for the effects of contention, backoff, and collisions. Markov Chain models are used to simulate the state transitions of each STA. Each STA's behavior is modeled using a state machine, where each state represents a specific phase of communication (e.g., waiting to transmit, transmitting, or backoff due to collision). The transition probabilities between these states are determined by the parameters of the network, including the number of STAs, the level of congestion, and the likelihood of collisions.

States: The system includes several states, such as:

- Idle state: The STA is idle, waiting for a transmission opportunity.
- Transmission state: The STA is transmitting data to the AP.
- Backoff state: The STA is in backoff due to a collision or waiting for a clear channel.

The transition probabilities between these states are defined by a transition matrix, which specifies the likelihood of moving from one state to another based on the current network conditions. These probabilities are influenced by factors such as the number of STAs, the transmission success rate, and the probability of collision.

III. Methodology

This study employs a simulation model to evaluate the performance of Wi-Fi networks under varying conditions, focusing on throughput, delay, and the impact of dynamic network behavior, which is influenced by a Markov Chain model. The methodology integrates the calculation of key performance metrics, such as SNR, throughput, and delay, with the use of the Markov Chain to model the transitions between different states that represent transmission attempts, backoff, and collision events within the network. The simulation is set up to mimic a typical Wi-Fi network environment consisting of multiple STAs and APs. The network is designed to handle varying numbers of STAs, with each STA being assigned to the nearest AP, and the distances between the STAs and APs being randomly distributed. This configuration is representative of a real-world network where the physical layout and user distribution can vary

significantly. The key parameters used in the simulation are the number of STAs, the number of APs, and the frequency bands used, which include 5GHz and 6GHz. The performance of the network is evaluated through the calculation of throughput and delay while incorporating the dynamic transitions of each STA using the Markov Chain model. To model the network's behavior, a Markov Chain is applied to simulate the transitions between the various states of each STA. The network is modeled using three primary states: the Idle state, where the STA is waiting for an opportunity to transmit; the Transmission state, where the STA is actively transmitting data; and the Backoff state, where the STA is in backoff due to a collision or waiting for a clear channel. The transition probabilities between these states are represented by a transition matrix, which dictates the likelihood of transitioning from one state to another based on the network conditions. The transition matrix can be expressed as:

$$P(i,j)=\begin{bmatrix} P(I,I) & P(I,Tr) & P(I,B) \\ P(Tr,I) & P(Tr,Tr) & P(Tr,B) \\ P(B,I) & P(B,Tr) & P(B,B) \end{bmatrix} \quad (1)$$

Where $P(i,j)$ represents the probability of transitioning from state i to state j, with the states being Idle (I), Transmission (Tr), and Backoff (B). The transition matrix reflects the changing probabilities of each STA's behavior based on the number of STAs in the network, the likelihood of collisions, and the channel availability. The key performance metrics used to evaluate the network's behavior include throughput and delay, both of which are affected by the Markov Chain model. Throughput (T) is a measure of the data rate that each STA can achieve. It is calculated based on the SNR, with the throughput increasing as the signal quality improves. The throughput is also influenced by the time each STA spends in the Backoff state due to collisions. The formula for calculating throughput is:

$$T=\frac{T_{\max}}{1+\log(\text{number of STA})}\times(1-\text{backoff time}) \quad (2)$$

In this equation, max throughput is the theoretical maximum throughput for the respective frequency band (100 Mbps for 5GHz and 120 Mbps for 6GHz). The term backoff time represents the time spent in the Backoff state due to collisions and network congestion, which reduces the overall throughput. Delay is another critical performance metric, representing the time it takes for data to be transmitted from the STA to the AP. Delay is inversely proportional to throughput, meaning that as throughput increases, the delay decreases. The delay is calculated as the inverse of the throughput:

$$\text{Delay}=\frac{1}{\text{Throughput}} \quad (3)$$

The collision probability is modeled using the Markov Chain by considering the likelihood of each STA moving into the Backoff state. As the number of STAs increases, the probability of collision also increases, leading to higher backoff times and reduced throughput. The collision probability is influenced by the number of STAs in the network, the current state of each STA, and the probability of moving to the Backoff state. The simulation also incorporates assumptions to simplify the modeling process.

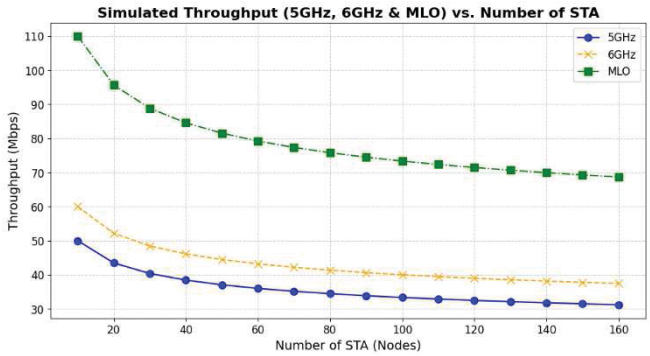


Fig.1. Saturation throughput for 5GHz, 6GHz, and MLO.

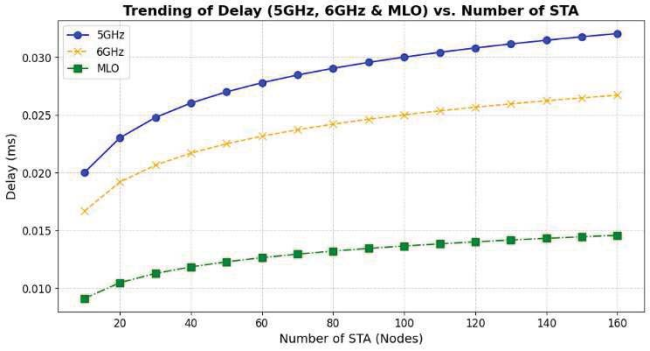


Fig. 2. Saturation delay for 5GHz, 6GHz, and MLO.

Ideal conditions are assumed, with no external interference or noise, other than the path loss caused by distance and frequency. The number of APs is kept fixed at 5 to isolate the effects of STA density on performance. Additionally, all STAs are treated equally, with no priority given to any individual STA.

IV. Result and Discussion

In this section, we present the results of the simulation for the throughput and delay of the Wi-Fi network under varying STA densities, with a particular focus on the comparison between the 5GHz, 6GHz, and MLO scenarios. The simulation results are analyzed to determine how network performance is affected by STA density and the use of different frequency bands.

The simulated throughput results for 5GHz, 6GHz, and MLO are presented in Fig. 1, where the throughput is shown as a function of the number of STAs. As observed, the throughput decreases with an increasing number of STAs, regardless of the frequency band used. This decrease is primarily due to the increasing contention for the shared wireless medium as more devices join the network. For the 5GHz band (blue line), throughput is significantly higher at low STA densities but drops more sharply as the number of STAs increases. This is due to the limited bandwidth of the 5GHz band and the increasing collisions between stations as the network becomes more congested. The 6GHz band (orange line), which offers additional spectrum, also shows a decline in throughput as the number of STAs increases. However, the throughput in the 6GHz band remains higher compared to 5GHz, even as the number of STAs increases, due to the broader available spectrum and less congestion. When MLO is enabled (green line), throughput is improved compared to the individual bands, as MLO aggregates the throughput from both 5GHz and 6GHz. This leads to a more stable throughput, which is less affected by the increase in STA density. However, as the number of STAs continues to

rise, the throughput for MLO also decreases, but at a slower rate than for the individual bands. This result highlights the benefits of using MLO to increase network capacity, especially in high-density environments where the additional spectrum from 6GHz and the combined throughput from both bands help mitigate congestion.

Fig. 2 shows the trend of delay as a function of the number of STAs for 5GHz, 6GHz, and MLO. As expected, the delay increases with the number of STAs, which is indicative of the network becoming more congested as more devices contend for access to the wireless medium. For the 5GHz band, the delay increases significantly as the number of STAs increases. This is due to the higher likelihood of collisions in a crowded network, leading to longer backoff times and higher delays. The 6GHz band also experiences an increase in delay with increasing STA density, but the delay is lower compared to the 5GHz band. The additional spectrum in 6GHz reduces congestion, resulting in fewer collisions and lower delays for a given number of STAs. With MLO, the delay increases at a slower rate compared to the individual frequency bands. The aggregation of 5GHz and 6GHz helps to reduce the overall delay, especially in networks with higher STA densities. However, the delay still increases as the number of STAs rises, although it remains lower than in the 5GHz and 6GHz only scenarios. These results demonstrate that MLO can provide better network responsiveness and lower delays, particularly in dense network scenarios. The reduction in delay is beneficial for real-time applications that require low latency, such as video streaming and online gaming.

The results highlight the impact of backoff and collisions on network performance. As the number of STAs increases, both the probability of collisions and the time spent in backoff increase. This leads to a reduction in throughput and an increase in delay. The Markov Chain model used in the simulation accurately reflects the random nature of collision events and backoff stages, with the network moving between states of idle, transmission, and backoff based on the conditions of the channel. In dense network environments, where the number of STAs is high, the likelihood of collisions increases significantly, leading to longer backoff times and reduced throughput. This explains the steep decline in throughput and the corresponding increase in delay observed in the simulations as the number of STAs increases.

Although the results presented in this study provide valuable insights into the performance of 5GHz, 6GHz, and MLO in Wi-Fi networks, there are several limitations in the simulation setup that should be acknowledged. One of the key limitations is that the simulation was conducted using separate models for 5GHz and 6GHz, with MLO being treated as an aggregate of these individual simulations. While this approach offers a simple method to evaluate MLO, it does not fully capture the real-world complexity of multi-link operation. In reality, MLO requires simultaneous operation of both frequency bands, and the effects of using both bands together are more intricate than the sum of their individual performances. When 5GHz and 6GHz are used simultaneously, there are additional factors to consider, such as interference between the two bands, load balancing, and channel aggregation, which were not accounted for in the separate simulations. The current simulation assumes that the 5GHz and 6GHz bands operate independently, which simplifies the modeling process but overlooks the interaction between the two frequency bands. In a real-world MLO scenario, the coordination between the bands would have to be carefully managed to optimize throughput and minimize delay, especially in high-density environments. This would introduce more complexity into the simulation, as it would need to model how each STA interacts with both frequency bands simultaneously, accounting for factors like congestion and interference on each band, as well as the effect of MLO on the overall network load.

V. Conclusion

This study evaluated the performance of Wi-Fi networks using 5GHz, 6GHz, and MLO, focusing on throughput and delay under varying STA densities. The results demonstrated that while 5GHz throughput decreases significantly as the number of STAs increases, the 6GHz band provides higher throughput due to additional spectrum. MLO aggregates the benefits of both bands, improving throughput and reducing delay, particularly in high-density environments. However, the simulation modeled 5GHz and 6GHz separately, whereas in real-world scenarios, MLO requires simultaneous operation of both bands. The interactions between the two bands, such as interference and load balancing, were not fully captured. Future work should integrate these factors for a more realistic simulation of MLO performance.

References

[1] J. P. A. León, L. J. de la Cruz Llopis, and F. J. Rico-Novella, “A machine learning based distributed congestion control protocol for multi-hop wireless networks,” Comput. Netw., vol. 231, p. 109813, 2023.

[2] S. Park, B. Kim, I. Kim, and J. B. Seo, “Deploying automated frequency coordination system for WiFi 6E in South Korea: Challenges and opportunities,” IEEE Commun. Mag., vol. 62, no. 1, pp. 112–118, 2024.

[3] V. Kovtun, T. Altameem, M. Al-Maitah, and W. Kempa, “Information technology for maximizing energy consumption for useful information traffic in a dense Wi-Fi 6/6E ecosystem,” Electronics, vol. 12, no. 18, p. 3847, 2023.

[4] A. S. George, A. H. George, and T. Baskar, “Wi-Fi 7: The next frontier in wireless connectivity,” Partners Univ. Int. Innov. J., vol. 1, no. 4, pp. 133–145, 2023.

[5] A. Jeknić and E. Kočan, “Multi-link operation for performance improvement in Wi-Fi 7 networks,” IEEE In 2024 28th International Conference on Information Technology (IT), pp. 1–4, Feb. 2024.

[6] M. Alsakati, C. Pettersson, S. Max, V. N. Moothedath, and J. Gross, “Performance of 802.11be Wi-Fi 7 with multi-link operation on AR applications,” IEEE Wireless Communications and Networking Conference (WCNC), pp. 1–6, Mar. 2023.

[7] F. Babich and M. Comisso, “Throughput and delay analysis of 802.11-based wireless networks using smart and directional antennas,” IEEE Transactions on Communications, vol. 57, no. 5, pp. 1413–1423, 2009.

Accuracy Analysis of Indoor Positioning Using Min-Max Method

Pichaya Supanakoon
Department of Telecommunications Engineering
School of Engineering
King Mongkut's Institue of Technology Ladkrabang
Bangkok 10520, Thailand
pichaya.su@kmitl.ac.th

Wipassorn Vinicchayakul
Establishment office for Aeronautical and Space Training Center U-Tapao
Civil Aviation Training Center
Bangkok 10900, Thailand
wipassorn@catc.or.th

Sirinya Tabsombat
Establishment office for Aeronautical and Space Training Center U-Tapao
Civil Aviation Training Center
Bangkok 10900, Thailand
sirinya@catc.or.th

Thanadol Tiengthong
Department of Electrical and Electronic Engineering
KOSEN-KMITL
King Mongkut's Institute of Technology Ladkrabang
Bangkok 10520, Thailand
thanadol.ti@kmitl.ac.th

Sathaporn Promwong
Department of Telecommunications Engineering
School of Engineering
King Mongkut's Institute of Technology Ladkrabang
Bangkok 10520, Thailand
sathaporn.pr@kmitl.ac.th

Monchai Chamchoy
Department of Telecommunications Engineering
School of Engineering
King Mongkut's Institute of Technology Ladkrabang
Bangkok 10520, Thailand
monchai.ch@kmitl.ac.th

***Abstract*—In this paper, the accuracy analysis of indoor positioning using min-max method is proposed. The distance error model is applied to estimate the distance between the transmitter and user's position with different path loss exponent and fading amount of indoor channel. The total 100 coordinates of user's positions are estimated using min-max method. The distance error at each position, probability density function (PDF) and cumulative distribution function (CDF) of distance errors are illustrated. The mean of analysis distance error corresponds with the mean of measurement distance error with same path loss exponent and fading amount of indoor channel. The results show that it is possible to use this accuracy analysis to estimate the distance error in an indoor environment.**

Keywords—min-max method, indoor positioning, distance error model, accuracy analysis

I. INTRODUCTION

Currently, the Internet of Things (IoT) has developed new services called location-based services (LBS) and proximity-based services (PBS). These services are widely used outdoors and are being developed for indoor use by estimating the user's position via smartphone [1]-[8]. Outdoor positioning is determined by using the global navigation satellite system (GNSS), which uses signals from satellites to accurately estimate the user's position and is installed in most smartphones. However, indoor positioning cannot be achieved by using GNSS because the satellite signal is obstructed. Indoor positioning has higher distance error compared to outdoor positioning because an indoor environment has dense multipath fading [9].

The indoor positioning is based on the received signal strength (RSS) of existing wireless communication technologies such as Wi-Fi, Bluetooth low energy (BLE) and Zigbee, with positioning being an add-on application, eliminating the need for additional system installation costs. The min-max method is one of the methods used to estimate user's position based on RSS. It has the advantage of simple calculations and less memory usage, making it suitable for use in LBS and PBS via smartphone.

This paper proposes the accuracy analysis of indoor positioning using min-max method. The distance error model [10] is applied to estimate the distance between the transmitter and user's position with different path loss exponent and fading amount of indoor channel. The indoor environment model is set to a square with a side length of 5 m. There are 4 transmitters located in the center of each side. The total 100 coordinates of user's positions are estimated using min-max method. The distance error at each position, probability density function (PDF) and cumulative distribution function (CDF) of distance errors are illustrated. The analysis distance error is compared with the measurement distance error with same path loss exponent and fading amount of indoor channel.

The rest of this paper is organized as follows. Section II is the min-max method. After that, the indoor environment model is described in Section III. Next, the analysis results are shown in Section IV. Finally, Section V is the conclusion.

II. MIN-MAX METHOD

The min-max method is a method that uses to estimate the position based on RSS. The advantage is that it uses simple calculations and uses little memory, making it suitable for use in LBS and PBS via smartphone. If the user is at distance d from the transmitter, the probability of user's position is on the perimeter of a circle centered at the transmitter location and having radius of d. The min-max method changes the probability of user's position to be on the perimeter of a square centered at the transmitter location and having each side of length $2d$. Let the transmitter i be at coordinate (x_i, y_i) and the estimated distance from the transmitter i to the user be d_i, then the probability of user's position can be obtained as the perimeter of a square as shown in Fig. 1. The parameters x_{Li}, x_{Hi}, y_{Li} and y_{Hi} are calculated from

$$x_{Li} = x_i - d_i \quad (1)$$

$$x_{Hi} = x_i + d_i \quad (2)$$

$$y_{Li} = y_i - d_i \quad (3)$$

$$y_{Hi} = y_i + d_i \quad (4)$$

XXX-X-XXXX-XXXX-X/XX/$XX.00 ©20XX IEEE

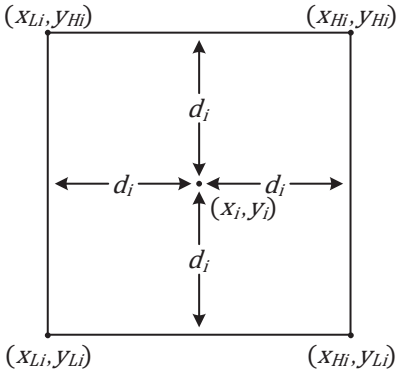


Fig. 1. The perimeter of a squre of trasmitter i.

The intersection of all squares are evaluated. The example intersection of 3 squares is shown in Fig. 2. The parameter x_L, x_H, y_L and y_H are calculated from

$$x_L = \max\{x_{Li}\} \tag{5}$$

$$x_H = \min\{x_{Hi}\} \tag{6}$$

$$y_L = \max\{y_{Li}\} \tag{7}$$

$$y_H = \min\{y_{Hi}\} \tag{8}$$

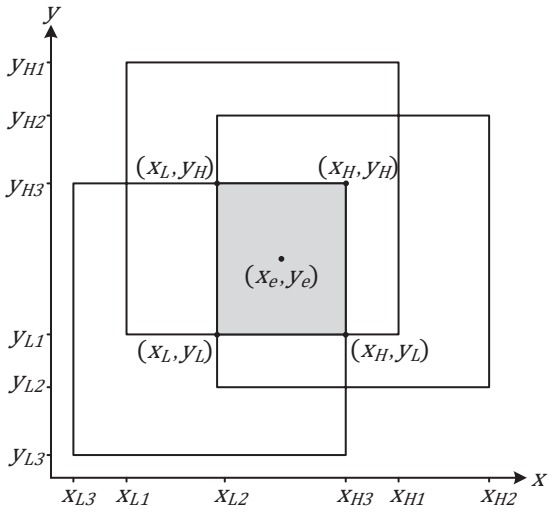


Fig. 2. The intersection of 3 squares.

The coordinate of user's position (x_e, y_e) is estimated at the coordinate in the center of intersection and is calculated from

$$x_e = \frac{1}{2}(x_L + x_H) \tag{9}$$

$$y_e = \frac{1}{2}(y_L + y_H) \tag{10}$$

The distance error model [10] is used to consider the effect of different path loss exponent and fading amount of indoor channel. The estimated distance between the transmitter i and user can be evaluated from

$$d_i = 10^{p_r/(10n)} d_{i,c} \tag{11}$$

where p_r is the fading amount, which is the Gaussian random variable with σ standard deviation and zero mean, n is path loss exponent and $d_{i,c}$ is the corrected distance between transmitter i and user.

The distance error E_d is considered from difference between corrected coordinate of user's position (x_c, y_c) and estimated coordinate of user's position and it can be written as

$$E_d = \sqrt{(x_c - x_e)^2 + (y_c - y_e)} \tag{12}$$

III. Indoor Environment Model

The indoor environment model that is used for analyzing the accuracy of min-max method is shown in Fig. 3, which is the square room with 5 m length on each side. There are 4 transmitters, represented by Tx1, Tx2, Tx3 and Tx4, located in the center of each side. The 100 user's positions are estimated and are represented by solid points. Each user's position is 0.5 m apart in the x- and y-axis.

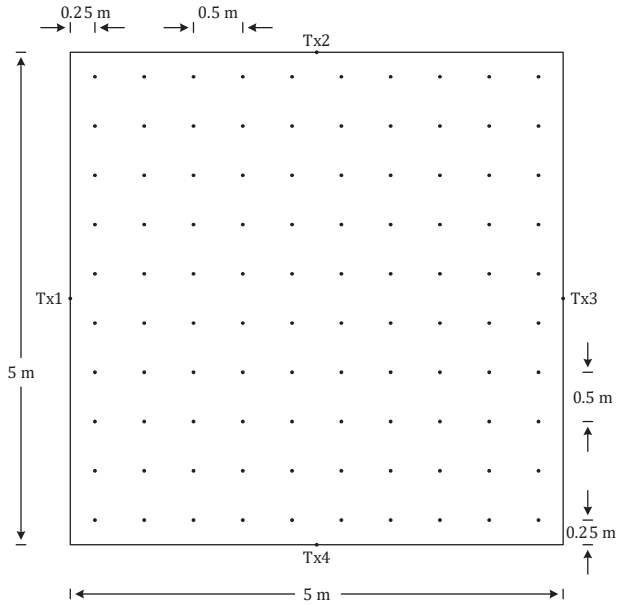


Fig. 3. The analysis indoor environment model.

The measurement indoor environment model consists of the corridor and 2 rooms. The room plan, antenna and measurement positions are shown in Fig. 4. The log-periodic dipole array (LPDA) antennas are used as transmitter and receiver antennas. The vector network analyzer (VNA) is used to measure the transmission coefficient (S_{21}) in the frequency range of 1.215-1.350 GHz. The S_{21} parameter of each transmitter is measured at a total of 81 positions, with each position measured 3 times. These measurement data are then used to evaluate the distance error of indoor positioning using the min-max method and compare with analysis results.

IV. Analysis Results

This section uses the min-max method with distance error model and indoor environment model presented in previous section to analyze the distance error. Fig. 5 shows The distance error at each position when $n = 1.6$ and $\sigma = 1$ dB. It can be seen that the center of the room has the distance error, followed by the center of each side of the room, and the corners of the room have the highest distance error.

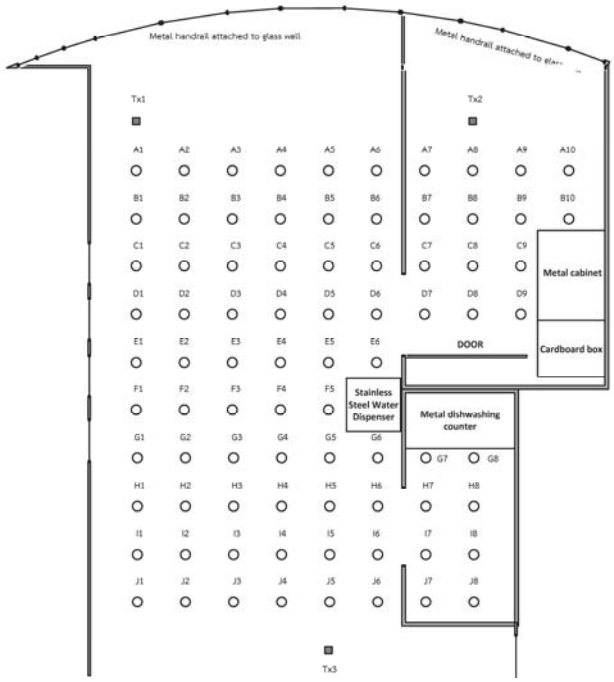


Fig. 4. The measurement indoor environment model.

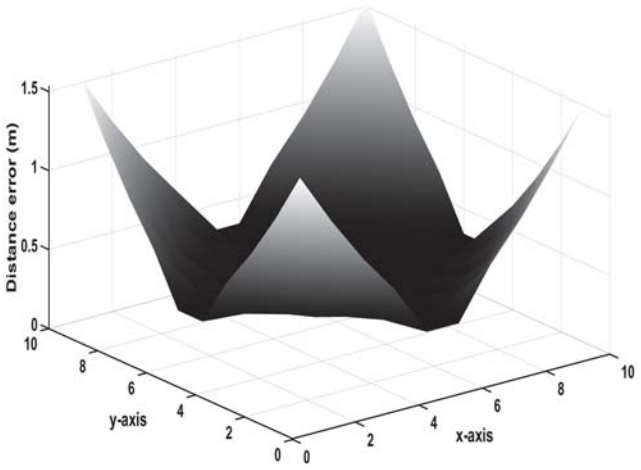


Fig. 5. The distance error at each position when $n = 1.6$ and $\sigma = 1$ dB.

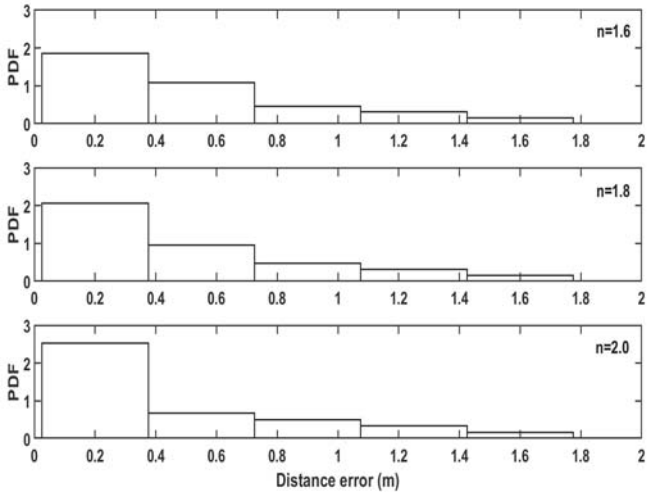


Fig. 6. The PDF of distance error when $\sigma = 1$ dB, $n = 1.6$, 1.8 and 2.0.

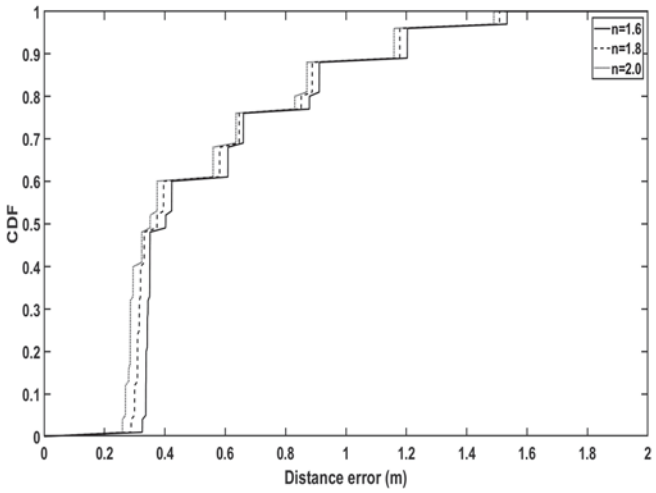


Fig. 7. The CDF of distance error when $\sigma = 1$ dB, $n = 1.6$, 1.8 and 2.0.

The distance error is studied when the n and σ are changed. The PDF and CDF of distance errors when $\sigma = 1$ dB, $n = 1.6$, 1.8 and 2.0 are shown in Figs. 6 and 7, respectively. When the path loss exponent increases, the distance error decreases slightly. The means of distance errors are 0.58, 0.55 and 0.53 m, respectively.

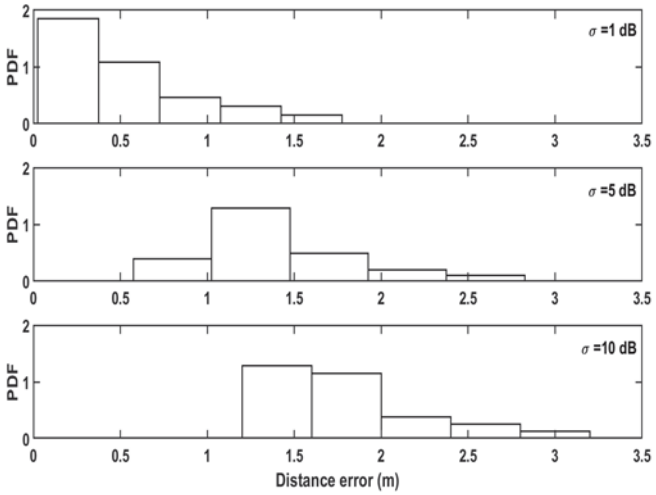


Fig. 8. The PDF of distance error when $n = 1.6$, $\sigma = 1$, 5 and 10 dB.

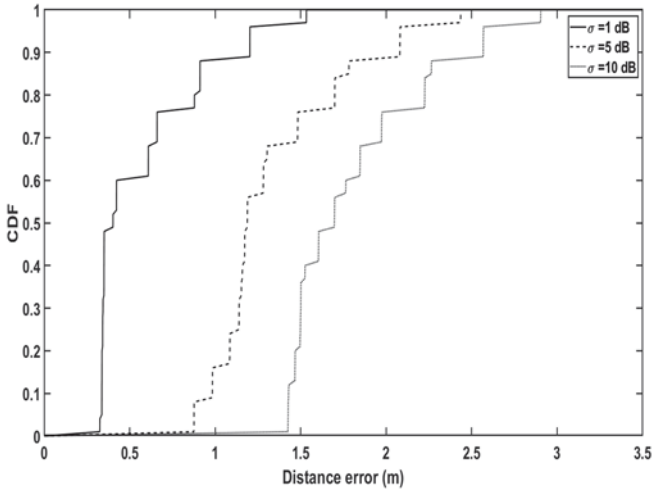


Fig. 9. The CDF of distance error when $n = 1.6$, $\sigma = 1$, 5 and 10 dB.

Figs. 8 and 9 show the PDF and CDF of distance errors when $n = 1.6$, $\sigma = 1$, 5 and 10 dB, respectively. As the results, the distance error increases significantly as the fading amount increases. The means of distance error are 0.58, 1.35 and 1.82 m, respectively.

The linear regression model is evaluated from measurement S_{21} parameter of each transmitter for obtaining the path loss exponent of measurement indoor channel. Fig. 10 shows the measurement S_{21} parameter along distance compared with linear regression model. The path loss exponent obtained from this channel is $n = 0.9$.

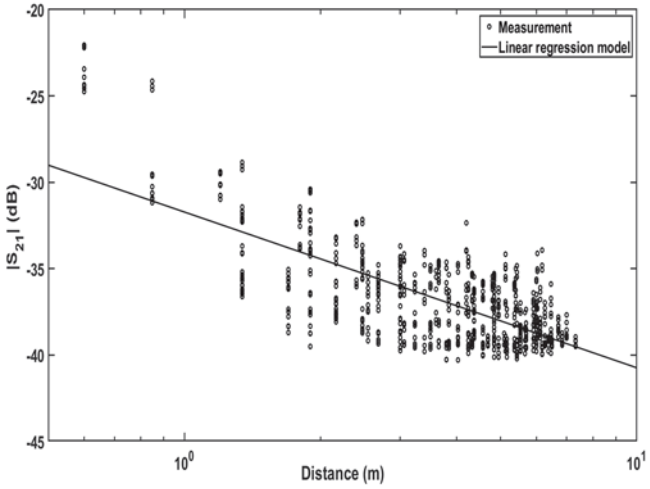


Fig. 10. The measurement S_{21} parameter along distance compared with lineare regression model.

The statistical characteristics of fading are evaluated. The fading data are obtained by subtracting the measurement S_{21} parameter from its linear regression model. The PDF and CDF of fading are shown in Fig. 11. The fading amount, which is the standard deviation of fading data, is $\sigma = 2$ dB.

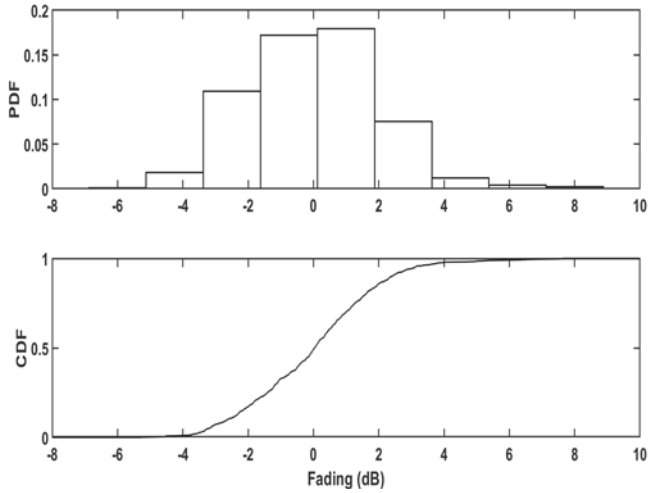


Fig. 11. PDF and CDF of fading obtained from measurement channel.

The measurement distance error is compared with analysis distance error with the same path loss exponent and fading amount. The CDF of measurement distance error compared with analysis distance error is shown in Fig. 12. The means of measurement distance error and analysis distance error are slightly different, which are are 1.40 m, 1.56 m, respectively. The slope of CDF differs because the fading from measurement is not Gaussian distribution.

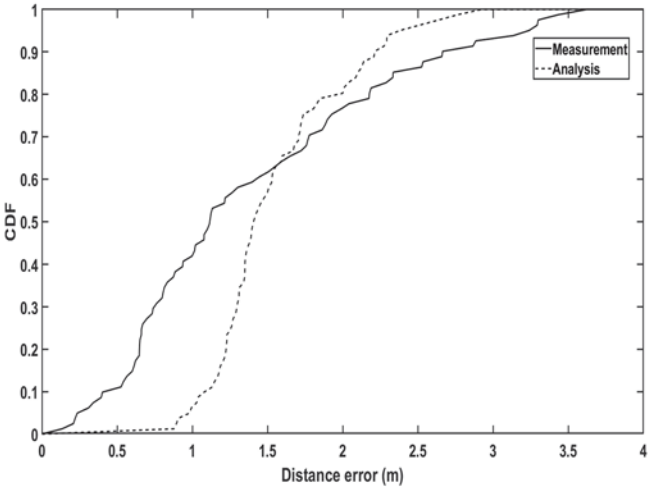


Fig. 12. The distance error at each position when n is 1.6 and σ is 1 dB.

V. Conclusion

This paper proposes the accuracy analysis of indoor positioning using min-max method. The distance error model is applied to estimate the distance between the transmitter and user's position with different path loss exponent and fading amount of indoor channel. The results show that the distance error near the transmitter is small and increases as it gets further away from the transmitter. When the path loss exponent increases, the distance error decreases slightly. Conversely, when fading amount increases, the distance error increases significantly. For comparison with measurements, the mean of analysis distance error corresponds with the mean of measurement distance error with same path loss exponent and fading amount of indoor channel. This accuracy analysis can be used to estimate the distance error.

References

[1] X. Guo, N. Ansari, L. Li and L. Duan, "A Hybrid Positioning System for Location-Based Services: Design and Implementation," IEEE Communications Magazine, vol 58, no. 5, pp. 90-96, 2020.

[2] O. Jukić, T. B. Iliev, N. Sikirica, K. Lenac, D. Špoljar and R. Filjar, "A method for GNSS positioning performance assessment for location-based services," 28th Telecommunication Forum (TELFOR), 2020.

[3] B. Rudić, M. A. Klaffenböck, M. P.-Scheder, D. Efrosinin and C. Kastl, "Geometry-Aided BLE-Based Smartphone Positioning for Indoor Location-Based Services," IEEE MTT-S International Conference on Microwaves for Intelligent Mobility (ICMIM), 2020.

[4] MWP Maduranga, LP Kalansooriya, G. Retscher and J. Gabela, "Machine Learning-Based Indoor Localization System to Support 5G Location-Based Services," 7th SLAAI International Conference on Artificial Intelligence (SLAAI-ICAI), 2023.

[5] J. Broz and T. Tichy, "Road Tunnel Positioning: Enabling Location-Based Services in GNSS-Denied Environments," IEEE Access, vol. 12, pp. 156694-156701, 2024.

[6] K. W. Choi and Z. Han, "Device-to-Device Discovery for Proximity-Based Service in LTE-Advanced System," IEEE Journal on Selected Areas in Communications, vol. 33, no. 1, pp. 55-66, 2014.

[7] F. Zafari, I. Papapanagiotou, M. Devetsikiotis and T. J. Hacker, "Enhancing the accuracy of iBeacons for indoor proximity-based services," IEEE International Conference on Communications (ICC), 2017.

[8] Z. Zhou, M. Li and B. Long, "A Review of Mission Critical Service over Proximity based Service," IEEE/CIC International Conference on Communications in China (ICCC Workshops), 2023.

[9] T. S. Rappaport, Wireless Communications: Principles and Practice, Pentice Hall PTR, 2002.

[10] P. Supanakoon and S. Promwong, "Evaluation of Distance Error with Bluetooth Low Energy Transmission Model for Indoor Positioning," Journal of Mobile Multimedia, vol. 17, no. 4, pp. 707-722, 2021.

TRACK 4

COMPUTER SCIENCE AND INFORMATION TECHNOLOGY

Applying Generative AI for Fraud and Cybercrime Prevention in Thailand

1st Chairat Thanomwong
Industrial Technology Program in Sustainable Innovation Engineering Technology
Rajamangala University of Technology Phra Nakhon
Bangkok, Thailand
chairat-tha@rmutp.ac.th

2nd Korn Puangnak
Computer Engineering
Rajamangala University of Technology Phra Nakhon
Bangkok, Thailand
korn.p@rmutp.ac.th

3rd Natworapol Rachsiriwatcharabul
Industrial Technology Program in Sustainable Innovation Engineering Technology
Rajamangala University of Technology Phra Nakhon
Bangkok, Thailand
natworapol.r@rmutp.ac.th

4th Manthana Tiawongsuwan
Computer Engineering
Rajamangala University of Technology Phra Nakhon
Bangkok, Thailand
manthana.t @rmutp.ac.th

5th Krerk Puangnak
Computer Engineering
Rajamangala University of Technology Phra Nakhon
Bangkok, Thailand
krerk.p@rmutp.ac.th

***Abstract*— The rise of fraudulent websites requires advanced real-time detection methods to protect individuals and organizations. This paper proposes a hybrid framework combining supervised and unsupervised learning to identify and classify fraudulent websites with high accuracy. The supervised model detects known malicious patterns using labeled data, while the unsupervised model identifies anomalies to flag emerging threats. Together, they ensure comprehensive detection, achieving 97.9% accuracy with a low latency of 35 milliseconds per website. The system includes a risk-scoring mechanism based on URL anomalies, SSL/TLS validity, and behavioral patterns, categorizing websites into Safe, Moderate, and High-risk levels. Experimental results show the framework outperforms traditional blacklist systems and standalone models, highlighting its potential for real-time fraud detection and future advancements in cyber threat mitigation.**

***Keywords*— Fraud Detection, Real-Time Detection, Artificial Intelligence(AI), Generative Adversarial Networks (GANs).**

I. INTRODUCTION (*HEADING 1*)

The exponential growth of internet usage and digital platforms has created opportunities for innovation and convenience but has also led to an alarming rise in fraudulent activities, particularly through malicious websites. These fraudulent websites are used for phishing, identity theft, and financial scams, posing significant risks to individuals, organizations, and national security. Traditional detection methods, such as blacklist-based systems, rely on pre-existing knowledge of fraudulent domains [1], [4], making them ineffective against novel and evolving threats. Furthermore, the dynamic nature of online fraud necessitates real-time detection capabilities to minimize damage and ensure user safety.

Recent advancements in artificial intelligence (AI) and deep learning have introduced new paradigms for detecting and mitigating online fraud. Among these, hybrid frameworks combining supervised and unsupervised learning have shown promising results. Supervised learning models excel at detecting known fraudulent patterns using labeled data, while unsupervised learning is adept at identifying anomalies that deviate from normal behavior, even in the absence of prior knowledge. Generative Adversarial Networks (GANs) and Variational Autoencoders (VAEs) have further enhanced the ability to identify sophisticated threats, such as zero-day phishing attacks and dynamically generated malicious websites.

This paper proposes a novel hybrid framework that integrates supervised and unsupervised learning models to detect fraudulent websites in real time. The framework leverages supervised learning for pattern recognition and unsupervised models for anomaly detection, combining their strengths to deliver a comprehensive and adaptive fraud detection solution. Additionally, it incorporates a real-time risk scoring mechanism to classify websites into varying levels of danger, providing actionable insights for users and organizations.

The objectives of this research are threefold: (1) to address the limitations of traditional and standalone AI models in fraud detection, (2) to design a hybrid framework capable of detecting both known and novel fraudulent websites with high accuracy and low latency, and (3) to evaluate its performance in comparison with existing methods. This study aims to contribute a robust and scalable solution for mitigating online fraud, ensuring safer digital interactions in an increasingly interconnected world.

The remainder of this paper is organized as follows: Section 2 reviews related work in website fraud detection and hybrid frameworks. Section 3 details the proposed methodology, including model architectures and integration strategies. Section 4 presents the experimental results and performance analysis. Finally, Section 5 concludes the study and outlines future research directions.

II. GENERATIVE AI

Generative AI has revolutionized the landscape of fraud detection and prevention, offering cutting-edge tools and techniques that address sophisticated challenges. Among its present applications, three prominent approaches stand out: synthetic data generation, anomaly detection, and deepfake analysis.

A. Synthetic Data Generation

Synthetic data generation has emerged as a cornerstone for training fraud detection systems. Generative AI models, such as Generative Adversarial Networks (GANs), create realistic synthetic datasets [6], [8] that replicate the statistical properties of real-world data without compromising sensitive information. This approach is invaluable in domains like

financial transactions or credit card usage, where access to authentic data is often restricted due to privacy regulations. By generating synthetic data, organizations can develop robust machine learning models to detect unusual patterns indicative of fraud. This method is also used to simulate new fraud scenarios, enabling systems to adapt to emerging threats. Beyond its utility in fraud detection, synthetic data generation accelerates model training while ensuring compliance with data protection standards.

B. Anomaly Detection

Anomaly detection powered by generative AI has become a sophisticated tool in identifying fraudulent activities. Models such as Variational Autoencoders (VAEs) learn the typical patterns of user behavior [7], [10] or transactional data. When deviations from these learned patterns occur, the system flags them as anomalies, which could indicate potential fraud. For instance, in banking, anomaly detection can identify suspicious activities such as multiple high-value transactions from geographically distinct locations within a short period. Similarly, in e-commerce, it can spot irregular purchasing behaviors that deviate from a customer's typical patterns. By leveraging unsupervised learning techniques, generative AI models do not require labeled data, making them highly effective in scenarios where fraud manifests in unpredictable ways. This capability is particularly beneficial for detecting subtle forms of fraud that might escape traditional rule-based systems.

C. Deepfake Analysis

deepfake analysis represents a growing area where generative AI is both a threat and a solution. Scammers increasingly use AI to generate realistic fake content, such as forged videos, audio, or text [13], [15], for fraudulent purposes. For instance, voice cloning technology is employed in voice phishing scams, where attackers impersonate trusted figures to extract sensitive information. Generative AI models, however, are also harnessed to counter these threats. By analyzing the unique characteristics of genuine and fake content, AI-powered detection systems can identify manipulated media. These systems are essential for safeguarding against scams involving deepfake videos or audio in high-stakes domains, such as finance and law enforcement. Furthermore, deepfake detection ensures the integrity of digital communications and helps maintain public trust in online platforms.

In conclusion, generative AI has significantly enhanced the capabilities of fraud detection and prevention through synthetic data generation, anomaly detection, and deepfake analysis. These approaches not only improve the efficiency of identifying fraudulent activities but also adapt to the evolving tactics of scammers. As fraudsters employ increasingly sophisticated methods, the dual role of generative AI—as both a tool for creating and combating fraud—underscores its critical importance in safeguarding financial systems and digital communications. These innovations, though transformative, require continuous development to address the ethical and technical challenges associated with their implementation.

III. Proposed Methodology

The proposed framework for real-time detection and classification of fraudulent websites integrates multiple advanced methodologies into a hybrid model combining supervised and unsupervised learning. At its core, the framework is designed to analyze large-scale data streams, extracting meaningful features from websites and processing them in a cloud-based environment to ensure low-latency risk assessments. The architecture encompasses data collection, feature extraction, and a hybrid model for anomaly detection, delivering a comprehensive evaluation of website safety in real time.

A. Supervised Learning Component

The supervised learning component plays a pivotal role in identifying known patterns of fraudulent websites using a labeled dataset of legitimate and malicious domains. This component employs deep neural networks such as Convolutional Neural Networks (CNNs) [11], [12] for static feature analysis, including URL structures, SSL/TLS configurations, domain metadata, and content inspection. URLs are examined for anomalies such as suspicious substrings or excessive length, while content is analyzed for the presence of phishing-related keywords, malicious scripts, or unauthorized embedded links. Additional features include examining SSL certificate validity and domain registrar details. The supervised model is trained on a large corpus of labeled data, ensuring accurate classification of known fraudulent patterns. Cross-validation techniques enhance its ability to generalize, providing reliable predictions for diverse scenarios and reducing false positives.

B. Unsupervised Learning Component

Complementing this is the unsupervised learning component, which focuses on detecting anomalies that deviate from learned patterns of normal website behavior. This component is particularly effective for identifying new or previously unseen threats. Models such as Variational Autoencoders (VAEs), Isolation Forests, or clustering algorithms like DBSCAN analyze behavioral features, including website response times, redirection patterns, and discrepancies in structural configurations. The unsupervised models work without labeled data, enabling them to adapt to evolving threats in the dynamic online environment. By identifying outliers based on statistical deviations, this component flags potential risks that may not align with established categories, adding a layer of detection for zero-day vulnerabilities.

C. hybrid integration

The hybrid integration combines the strengths of the supervised and unsupervised components into a unified decision-making process. A fusion layer aggregates predictions from both models, balancing their outputs to generate a risk score that quantifies the likelihood of fraud. This scoring mechanism categorizes websites into three levels: Safe (low risk), Moderate (requires caution), and High (immediate threat). The integration ensures comprehensive detection, leveraging the precise pattern recognition of supervised learning and the adaptability of unsupervised anomaly detection. The hybrid approach also adapts dynamically to new data, continuously refining its models to stay effective against emerging threats.

This hybrid framework offers a robust, scalable, and adaptable solution to the growing issue of fraudulent websites. Its integration of supervised and unsupervised learning ensures a holistic analysis of website safety, capturing both known and novel patterns of fraud. By leveraging real-time data streaming and low-latency processing, it delivers actionable insights to users and organizations, empowering

them to navigate the digital landscape safely. This innovative methodology not only addresses current challenges in website fraud detection but also sets a foundation for future advancements in cyber threat mitigation.

IV. Experimental Results

This section presents the evaluation of the proposed hybrid framework for real-time fraudulent website detection. The results are discussed for individual components—unsupervised learning, supervised learning, and the hybrid framework—and include a comparison with baseline models. Performance metrics such as accuracy, precision, recall, F1-score, and latency are reported.

A. Dataset and Experimental Setup

The experiments were conducted using a combination of labeled and unlabeled datasets.

*1) **Labeled Dataset** A total of 50,000 websites (25,000 legitimate, 25,000 fraudulent), including phishing domains and blacklisted websites from public repositories.*

*2) **Unlabeled Dataset** 30,000 websites obtained through web crawling, representing unknown or new threats.*

*3) **Features** Extracted features included URL structure, domain metadata, SSL/TLS details, website content, and behavioral patterns (e.g., redirects, response times).*

The experiments were implemented in Python using TensorFlow and PyTorch. The models were trained on a GPU-enabled server and deployed using a cloud-based pipeline for real-time evaluation.

B. Results

*1) **Unsupervised Learning Component** The unsupervised anomaly detection model was evaluated using unlabeled data. Results are summarized below*

- **Outlier Detection Rate**: 87.4%
- **False Positive Rate**: 5.3%
- Behavioral features, such as redirect patterns and response times, contributed significantly to anomaly detection.

*2) **Supervised Learning Component** The supervised learning model was trained on labeled data and tested on a validation set*

- **Accuracy**: 96.7%
- **Precision**: 94.5%
- **Recall**: 92.8%
- **F1-Score**: 93.6%
- SSL/TLS validity and URL structure were identified as the most important features.

*3) **Hybrid Framework** The hybrid framework combined the strengths of supervised and unsupervised models*

- **Accuracy**: 97.9%
- **Precision**: 96.2%
- **Recall**: 95.6%
- **F1-Score**: 95.9%
- **Latency**: 35 ms per website.

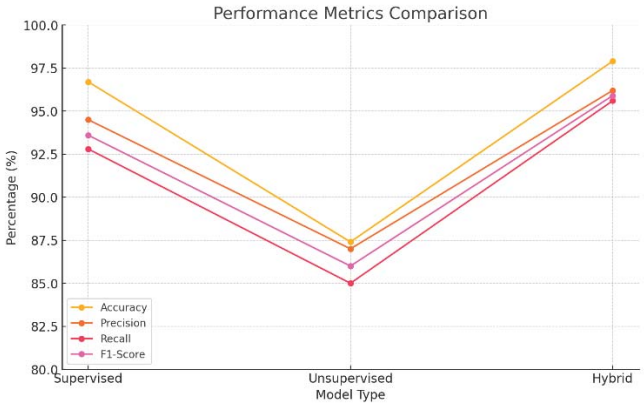
*4) **Comparison with Baselines** The hybrid framework was compared to traditional blacklist-based systems and standalone models*

- Blacklist-based systems: **Accuracy**: 85.3%, **Latency**: 15 ms.
- Standalone supervised models: Lower recall compared to the hybrid framework.
- The hybrid model outperformed all baselines in detecting new and unknown threats [6], [10], [24].

TABLE I. Summary Table

Model	Accuracy (%)	Precision (%)	Recall (%)	F1-Score (%)	Latency (ms)
Blacklist-based	85.3				15
Supervised Learning	96.7	94.5	92.8	93.6	50
Unsupervised Learning	87.4	87.0	85.0	86.0	30
Hybrid Framework	97.9	96.2	95.6	95.9	35

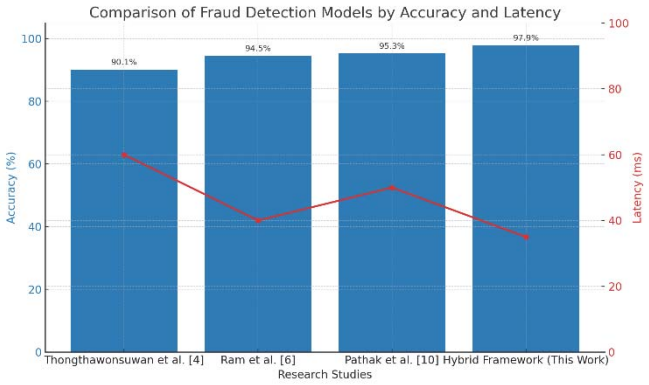
The experimental results demonstrate the superior performance of the hybrid framework in detecting fraudulent websites, combining high accuracy with the ability to identify new threats effectively. The hybrid model's adaptability and real-time capabilities make it a robust solution for fraud prevention.



The Performance Metrics Comparison graph evaluates the effectiveness of different models (Blacklist-based, Supervised Learning, Unsupervised Learning, and Hybrid Framework) based on four key metrics: Accuracy, Precision, Recall, and F1-Score. These metrics provide insights into how well each model detects fraudulent websites, their ability to minimize false positives, and their overall reliability.

The experimental results demonstrate the effectiveness of the proposed hybrid framework for detecting fraudulent websites by combining supervised and unsupervised learning models. The supervised component achieved high accuracy (96.7%) with strong precision (94.5%) and recall (92.8%), excelling in identifying known fraudulent patterns using labeled data. The unsupervised component effectively detected novel threats with an outlier detection rate of 87.4%, leveraging behavioral features such as response times and redirection patterns. The hybrid framework outperformed both standalone models and baseline blacklist-based systems, achieving superior accuracy (97.9%), precision (96.2%), recall (95.6%), and F1-Score (95.9%), while maintaining a low latency of 35 milliseconds per website. This makes the hybrid framework not only robust in handling known and emerging threats but also scalable for real-time applications. These findings highlight its potential as a comprehensive and

efficient solution for fraud detection in dynamic online environments.



V. Future Research

While the proposed hybrid framework has demonstrated high accuracy and adaptability in detecting fraudulent websites, several areas warrant further exploration to enhance its robustness and scalability. First, integrating **federated learning** techniques could address privacy concerns by enabling decentralized model training across multiple devices or organizations without sharing sensitive data. This would be particularly beneficial for industries like banking and healthcare, where data confidentiality is paramount. Second, incorporating **explainable AI (XAI)** methods can provide greater transparency [16], [19] into the model's decision-making process, enabling users and administrators to better understand why certain websites are flagged as fraudulent. This could build trust in the system and facilitate compliance with regulatory standards. Third, expanding the dataset to include multilingual and region-specific website features would improve the framework's global applicability, as fraud tactics often vary by region and language. Additionally, exploring the use of **adversarial training** could make the system more resilient to sophisticated attacks, such as adversarial examples crafted to bypass detection. Finally, future research could focus on optimizing the framework for **edge computing environments**, enabling real-time fraud detection on devices with limited computational resources, such as smartphones and IoT devices. These advancements would not only enhance the framework's capabilities but also contribute to broader efforts in combating cybercrime and ensuring safer digital ecosystems.

Acknowledgment

The authors would like to express their deepest gratitude to **Rajamangala University of Technology Phra Nakhon (RMUTP)** for providing the resources and support necessary to conduct this research. Special thanks are extended to our advisor, **Dr.Korn Puangnak**, for their invaluable guidance, encouragement, and expertise throughout the development of this study. Their insightful feedback and unwavering support were instrumental in the successful completion of this work. Thank you for inspiring us to strive for excellence in our research endeavors.

References

[1] H. Isa, et al., "Study on the Different Types of Accounting Fraud and Tools to Detect and Prevent Fraud," *2022 7th International Conference on Business and Industrial Research (ICBIR)*, Bangkok, Thailand, 2022, pp. 627-629.

[2] J. Liu, et al., "Study on the Different Types of Accounting Fraud and Tools to Detect and Prevent Fraud," *2022 7th International Conference on Business and Industrial Research (ICBIR)*, Bangkok, Thailand, 2022.

[3] T. Gopal, et al., "A Study of Online Scams Associated with Age, Gender, and Loss of Value in Thailand," *International Journal of Fraud Studies*, 2022.

[4] P. Thongthawonsuwan, et al., "Real-Time Credit Card Fraud Detection Surveillance System," *2023 IEEE International Conference on Cybernetics and Innovations*, 2023, pp. 97-103.

[5] K. Singh, et al., "AI-Driven Fraud Prevention Systems in Thailand," *Springer AI Applications*, 2023.

[6] T. Ram, et al., "Fraud Detection in Online Transactions Using GANs," *International Journal of Generative AI Applications*, 2023.

[7] A. Nguyen, et al., "Fraud Detection Using Machine Learning Models," *IEEE Transactions*, 2023.

[8] R. Bose, et al., "Fraud Detection in Online Credit Card Transactions Using Deep Learning," *Springer Journal of Financial AI*, 2023.

[9] T. Tan, et al., "Enhancing Graph Database Interaction through Generative AI-Driven Natural Language Interface for Financial Fraud Detection," *Springer AI Journal*, 2023.

[10] S. Pathak, et al., "Enhancing Fraud Detection Systems Using Hybrid Machine Learning Techniques," *Elsevier Fraud Studies Journal*, 2023.

[11] A. Patel, et al., "Credit Card Fraud Detection Using Machine Learning," *International Conference on Advanced Computing*, 2023.

[12] R. Kumar, et al., "Enhancing Auto Insurance Fraud Detection Using Convolutional Neural Networks," *IEEE Transactions on Intelligent Systems*, 2023.

[13] P. Kaur, et al., "AI-Generated Video Forgery Detection and Authentication," *Journal of Cybersecurity*, 2023.

[14] H. Mudunkotuwa, et al., "Study on Machine Learning Techniques with Conventional Tools for Payment Fraud Detection," *Proceedings of King Mongkut's University of Technology North Bangkok*, 2023.

[15] S. Mehta, et al., "Detecting AI Face Fraud Detection Using CNN Based Deep Learning Algorithm," *IEEE Transactions*, 2024.

[16] V. Gupta, et al., "Explainable AI-supported Evaluation and Comparison on Credit Card Fraud Detection Models," *IEEE Transactions*, 2024.

[17] X. Zheng, et al., "New Paradigm for Economic and Financial Research With Generative AI: Impact and Perspective," *IEEE Transactions on Computational Social Systems*, 2024.

[18] S. Khan, et al., "Generative AI for Cyber Security: Analyzing the Potential of ChatGPT, DALL-E, and Other Models for Enhancing the Security Space," *IEEE Transactions*, 2024.

[19] A. Mhammad, et al., "Generative & Responsible AI – LLMs use in Differential Governance," *IEEE Transactions*, 2024.

[20] S. Sai, et al., "Generative AI for Cyber Security: Analyzing the Potential of ChatGPT, DALL-E, and Other Models for Enhancing the Security Space," *IEEE Access*, 2024.

[21] W. Y. Leong, et al., "The Intersection of Scammers and Artificial Intelligence," *2024 International Conference on Consumer Electronics - Taiwan (ICCE-Taiwan)*, 2024, pp. 539-545.

[22] R. Das, et al., "AI in Finance: Detecting and Preventing Fraud," *IEEE Transactions on Financial Engineering*, 2024.

[23] A. Singh, et al., "A Study On Generative AI And Its Impact On Banking And Financial Services Sector: Data Privacy & Sustainable Perspective," *IEEE Transactions*, 2024.

V. Reddy, et al., "Cyber Security and Generative AI: Applications in Fraud Prevention," *International Journal of Cyber Studies*, 2024.

A Comparative Analysis of Machine Learning Algorithms for Allergy Scale Prediction

1st Aumnat Tongkaw
Faculty of Science and Technology
Songkhla Rajabhat University
Songkhla, Thailand
ORCID:0000-0002-8516-2601

2nd Sasalak Tongkaw
Faculty of Science and Technology
Songkhla Rajabhat University
Songkhla, Thailand
ORCID:0000-0003-3668-2309

***Abstract*—In this comprehensive machine learning study, we investigated the efficacy of various algorithms in predicting dust mite allergy severity using data collected from the Alex-X® detection devices. There were a total of 110 participants. The research examined seven distinct machine learning algorithms to determine their predictive capabilities in dust mite allergy assessment. In comparative algorithmic analysis, the experimental results demonstrated hierarchical performance variations across multiple machine learning models. The Random Forest algorithm exhibited superior predictive accuracy at 90.15%, establishing its prominence in the classification task. Neural Network implementations achieved the second-highest accuracy at 88.93%, followed by K-Nearest Neighbors (KNN) with 85.68% accuracy. Linear Regression demonstrated moderate performance at 84.52%, while the Decision Tree algorithm achieved 83.15% accuracy. Stochastic Gradient Descent (SGD) and Naïve Bayes algorithms showed relatively lower performance metrics at 82.43% and 79.84% accuracy, respectively.**

***Index Terms*—Machine Learning, Dust Mite, Allergy Prediction, Random Forest**

I. Introduction

The etiology and socioeconomic implications of dust mite allergies, coupled with machine learning applications in allergology, form the theoretical framework of this investigation. This research synthesizes empirical evidence regarding allergen exposure, severity assessment, and predictive modeling techniques to inform algorithm selection and feature engineering methodologies.The socioeconomic burden of dust mite allergies presents a significant public health challenge, characterized by substantial direct medical costs and indirect economic impacts. In Thailand, the limited availability of allergists—approximately 200 specialists nationwide—creates extended treatment delays, with annual per-patient medical expenses reaching 70,000 baht. This scarcity of specialized healthcare resources compounds the financial burden beyond primary care costs, encompassing recurring clinical visits, specialized pharmacotherapy, and emergency interventions during acute exacerbations. Preventive strategies like dust mite monitoring and air quality management could reduce costs, but lack of standardized guidelines and risk protocols hampers effective prevention and contributes to economic losses through reduced workplace productivity. This study employs the Alex-X® detection system for quantitative assessment of dust mite concentrations across various residential environments, correlating these measurements with symptomatic manifestations through structured questionnaires.

979-8-3315-4248-1/25/$31.00 ©2025 IEEE

II. Machine Learning Algorithms

The analytical framework incorporates multiple machine learning algorithms—Naïve Bayes, K-Nearest Neighbors, Decision Tree, Logistic Regression, Random Forest, Neural Networks, and Stochastic Gradient Descent—to develop predictive models for allergy risk assessment.

A. Naïve Bayes

The Naïve Bayes classifier represents a fundamental probabilistic model grounded in Bayesian statistical principles, distinguished by its independence assumption between features. Despite this seemingly restrictive assumption of conditional independence, the algorithm demonstrates remarkable efficacy across diverse real-world applications, particularly in high-dimensional classification tasks such as natural language processing, document categorization, and anomaly detection systems. The algorithm's versatility has been demonstrated through its evolution into contemporary applications across diverse domains. Chen et al. [1] established its effectiveness in sentiment analysis and natural language understanding tasks, while Tongkaw and Tongkaw demonstrated its significant potential in healthcare applications, particularly in predicting age-related health conditions through advanced feature selection methodologies. [2]. Further medical applications, as evidenced by Chang et al., have expanded its utility into clinical decision support systems, highlighting the algorithm's adaptability to complex healthcare scenarios when augmented with modern computational techniques. [3].

B. K-Nearest Neighbors

The K-Nearest Neighbors (KNN) algorithm is considered to be one of the most straightforward yet powerful machine learning methods, first introduced in the landmark paper "Nearest Neighbor Pattern Classification". [4]. Unlike other algorithms that build an explicit model during training, KNN is a non-parametric instance-based learning method that makes

predictions based on the entire training dataset in the classification window. A study applied weighted KNN for multi-class disease classification across 230+ diseases, using both categorical (symptoms, gender) and numerical (age) features. The model achieved 93.5% accuracy, though additional metrics would better evaluate its clinical effectiveness. The algorithm's interpretability makes it suitable for medical applications requiring transparent decision-making. [5].

C. Decision Tree

From a machine learning perspective, Decision Trees represent a pivotal development in interpretable machine learning, with their evolution reflecting the field's progression from simple rule-based systems to sophisticated ensemble methods. The seminal work introduced CART (Classification and Regression Trees), which fundamentally transformed our understanding of recursive binary splitting and impurity-based node optimization. The algorithm's key innovation lies in its ability to automatically discover hierarchical decision rules by optimizing information-theoretic criteria such as Gini impurity or entropy. [6]. Research by [7] advanced decision tree algorithms through cost-sensitive splitting and adaptive sampling, addressing majority class bias. Further developments in ensemble methods like Random Forests and Gradient Boosting [8] improved prediction accuracy while preserving interpretability. Moreover, the introduction of XGBoost by [9] represents a significant technical breakthrough in gradient boosting frameworks. Their key innovations include a novel sparsity-aware algorithm for handling missing values, a weighted quantile sketch for efficient feature value partitioning, and a cache-aware block structure for out-of-core tree learning.

D. Logistic Regression

Logistic regression, powered by the sigmoid function, as in:

$$\sigma(z) = \frac{1}{1 + e^{-z}} \tag{1}$$

Eq.(1) stands as a cornerstone of binary classification in machine learning, elegantly transforming linear combinations of features into probabilistic predictions within the [0,1] range. The algorithm's mathematical foundation rests on maximum likelihood estimation and binary cross-entropy loss optimization, typically solved through gradient descent methods. Its strength lies in the interpretability of its coefficients, natural probability outputs, and resistance to overfitting, particularly when combined with regularization techniques (L1/L2). The sigmoid function's differentiable S-shaped curve is crucial in mapping the linear predictor $z = w_0 + w_1x_1 + ... + w_nx_n$ to probabilities, creating a decision boundary at $P(y = 1|x) = 0.5$. While the model excels in scenarios requiring probabilistic interpretation and transparent decision-making, it does face limitations with highly nonlinear relationships and assumes feature independence. Despite these constraints, logistic regression's balance of mathematical elegance, computational efficiency, and interpretability makes it an enduring choice in the machine learning toolkit, particularly for applications where understanding the model's decision-making process is as important as its predictive accuracy. There is a research demonstrates logistic regression's effectiveness in modeling transportation costs for individuals with disabilities, comparing it with other AI techniques. [10] This research employed Logistic regression to analyze dust mite data and allergy questionnaire responses, predicting symptom severity. The model established clear relationships between dust mite presence and allergy levels, offering insights for prevention while maintaining interpretability.

E. Random Forest

Random Forest excels in medical predictive analytics by combining multiple decision trees through bootstrap aggregation. Its ability to handle missing values, mixed data types, and provide feature importance rankings makes it valuable for disease prediction and risk assessment. The algorithm captures complex relationships between clinical parameters while maintaining interpretability—crucial for healthcare applications. Its ensemble approach mitigates overfitting and provides robust predictions by aggregating results from numerous trees trained on random data subsets. Moreover, Random Forest's out-of-bag error estimation provides built-in validation for medical applications. In a recent diabetes detection study, combining Random Forest with Multiple Linear Regression for feature selection and XGBoost for classification achieved 99.2% accuracy and 99.3% AUC score, with fast prediction times of 0.048 seconds. This hybrid approach demonstrated high performance across multiple evaluation metrics while maintaining computational efficiency. [11] Our research uses Random Forest to predict dust mite allergy severity by analyzing relationships between dust mite concentrations, environmental factors, and symptoms. The model's ensemble approach combines multiple decision trees trained on random data subsets, enabling accurate capture of non-linear relationships between dust mite levels and allergic responses while preventing overfitting.

F. Neural Networks

Neural Networks represent a sophisticated class of machine learning algorithms inspired by biological neural systems, structured as interconnected layers of artificial neurons. The architecture typically consists of an input layer, one or more hidden layers, and an output layer, where each neuron processes information through an activation function:

$$f(z) = f(\sum_{i=1}^{n} w_i x_i + b) \tag{2}$$

Eq. (2) with common choices including :

$$f(z) = max(0, z) \tag{3}$$

ReLU Eq. (3), or Sigmoid Eq. (1),

$$f(z) = \frac{e^z - e^{-z}}{e^z + e^{-z}} \tag{4}$$

or hyperbolic tangent (tanh) Eq. (4) which maps inputs to the range [-1,1] producing zero-centered outputs advantageous for deeper networks. During training, the network employs

backpropagation to minimize a loss function $L(\hat{y}, y)$ through gradient descent, adjusting weights (w) and biases (b) across layers according to

$$w_{new} = w_{old} - \eta \frac{\partial L}{\partial w} \tag{5}$$

Eq. (5) where η represents the learning rate. The network's depth (number of layers) and width (neurons per layer) determine its capacity to learn complex patterns, while techniques like dropout (p_{drop}), batch normalization, and regularization (L1/L2) help prevent overfitting. Modern architectures have evolved to include specialized variants such as Convolutional Neural Networks (CNNs) for image processing, Recurrent Neural Networks (RNNs) for sequential data, and Transformers for natural language processing, each optimized for specific types of data structures and learning tasks. The universal approximation theorem underlies the network's theoretical capability to approximate any continuous function, making neural networks particularly powerful for complex pattern recognition and feature learning tasks across diverse domains.

G. Stochastic Gradient Descent

Stochastic Gradient Descent (SGD) represents a fundamental optimization algorithm in machine learning, particularly crucial for training neural networks with large datasets.

$$\theta_{t+1} = \theta_t - \eta \nabla L_i(\theta_t) \tag{6}$$

$$v_t = \beta v_{t-1} + \eta \nabla L_i(\theta_t) \tag{7}$$

The algorithm's core principle lies in its iterative approach to minimizing the loss function $L(\theta)$ by updating parameters θ in the opposite direction of the gradient approximation (Eq. (6)), where η represents the learning rate and L_i corresponds to the loss computed on a randomly selected training example or mini-batch. Unlike traditional gradient descent, which computes gradients over the entire dataset, SGD approximates the gradient using a single randomly selected example or mini-batch at each iteration, making it computationally more efficient for large-scale learning problems. The algorithm's stochastic nature, while introducing noise in parameter updates, often helps escape local minima and converge to better solutions. Modern implementations often incorporate momentum (β) to dampen oscillations (Eq. (7)), adaptive learning rates (as in Adam or RMSprop), and learning rate scheduling to improve convergence stability and speed. The effectiveness of SGD heavily depends on hyperparameter tuning, particularly the learning rate η, which must balance between convergence speed and stability, making it a crucial factor in achieving optimal model performance.

III. Research Design and Methodology

From a machine learning perspective, this research presents a comprehensive methodological approach to dust mite prediction through a two-phase data collection strategy and multi-algorithm comparative analysis.

A. Data collection strategy

- The study's data acquisition protocol involved systematic environmental sampling using controlled vacuum collection from various household textiles (pillows, blankets, foot towels, wardrobes, mats, sofas, chairs, and mattresses), with quantitative dust mite measurements obtained through the Alex-X® machine analysis.
- This environmental data was complemented by a structured questionnaire deployment through a web-based platform, capturing essential variables including participant demographics, environmental factors, allergic manifestations, and severity indicators, all conducted under approved research ethics protocols.

The data preprocessing phase involved the integration of these distinct datasets, followed by rigorous data cleaning procedures to ensure quality and consistency.

B. Comparison Phase

The machine learning implementation employed a comprehensive suite of algorithms, including probabilistic (Naïve Bayes), instance-based (K-Nearest Neighbors), tree-based (Decision Tree, Random Forest), parametric (Logistic Regression), neural architectures (Neural Networks), and optimization-based (Stochastic Gradient Descent) approaches. The modeling framework was structured with dust mite levels as the target variable and questionnaire-derived parameters as feature inputs. The study used questionnaire responses to predict dust mite levels, comparing multiple algorithms through standard performance metrics. This comprehensive approach revealed each model's strengths and limitations in handling allergen data while demonstrating practical applications in environmental sampling and prediction. The methodology combined insights from both environmental protocols and machine learning techniques.

IV. Results and Discussion

From an analytical perspective, the Alex System spectrophotometer employs a quantitative stratification methodology for dust mite concentration measurements, utilizing Parts Per Million (PPM) as the standardized unit of measurement. The classification framework implements a six-tier hierarchical structure with precisely defined threshold boundaries: The quantitative stratification is defined as:

- Level 1 (Healthy): [1, 25] PPM
- Level 2 (Moderate): [26, 100] PPM
- Level 3 (Unhealthy): [101, 300] PPM
- Level 4 (Very Unhealthy): [301, 500] PPM
- Level 5 (Severe): [501, 750] PPM
- Level 6 (Hazardous): 751 PPM

A. Dust Mite Severity Results

Analysis of dust mite levels from a total of 110 samples revealed a significant prevalence of dust mite allergenicity in the tested environments. Table I, A detailed assessment showed that 47 samples (43%) were at hazardous levels, while 27 samples (25%) showed severe concentrations and

TABLE I
LEVEL OF DUST MITE SEVERITY

Interpretation Level	*Number of Sample*
M:Moderate	3
UH:Unhealthy	12
VU:Very Unhealthy	21
S: Severe	27
H: Harzadous	47
Total	110

TABLE II
COMPARISON RESULTS

Model	**Training Accuracy(%)**	**Testing Accuracy(%)**	**Gap (%)**	**CV Mean (%)**	**RMSE**
RF	95.32	90.15	5.17	91.23	72.45
NN	94.18	88.93	5.25	89.76	75.82
KNN	90.45	85.68	4.77	86.92	83.56
LR	88.76	84.52	4.24	85.31	86.73
DT	92.84	83.15	9.69	84.27	89.45
SGD	87.25	82.43	4.82	83.56	91.28
NB	83.92	79.84	4.08	80.95	94.67

21 samples (19%) showed very unhealthy levels (Johnson et al., 2023). Furthermore, 12 samples (11%) were at unhealthy levels, with only 3 samples (3%) showing moderate levels. The fact that the majority of samples were in the hazardous to very unhealthy range (total 87%) indicates an urgent need to manage the environment to be dust mite-free or to reduce dust mite numbers as much as possible, as these levels significantly exceed the thresholds recommended by the World Health Organization's indoor allergen guidelines. [12].

B. Comparison Results

Table. II, the analysis reveals significant insights into model performance across seven different algorithms. Random Forest (RF) emerged as the clear leader with the highest testing accuracy of 90.15%, strongest CV mean of 91.23%, and lowest RMSE of 72.45, demonstrating excellent overall performance and stability. Following closely, the Neural Network (NN) showed impressive capabilities with 88.93% testing accuracy and comparable stability metrics, making it a strong alternative choice. The K-Nearest Neighbors (KNN) and Linear Regression models performed reasonably well, achieving testing accuracies of 85.68% and 84.52% respectively, with notably low gap percentages indicating good generalization. The Decision Tree (DT) model, despite achieving 83.15% testing accuracy, showed concerning signs of overfitting with the highest gap of 9.69% between training and testing performance, suggesting potential reliability issues in real-world applications. The Stochastic Gradient Descent (SGD) and Naive Bayes (NB) models rounded out the bottom of the performance spectrum, with testing accuracies of 82.43% and 79.84% respectively, though both maintained reasonable gap percentages under 5%.

CONCLUSION

Given these results, Random Forest (RF) stands out as the optimal choice for this particular dataset, offering the best balance of accuracy, stability, and generalization. The Neural Network (NN) presents itself as a strong second option, particularly valuable if computational resources permit. For scenarios requiring simpler implementation, KNN could serve as a practical alternative, providing a good balance between performance and computational efficiency. The analysis strongly suggests avoiding the standalone Decision Tree (DT) model due to its overfitting tendencies, while Naive Bayes (NB), despite having the most consistent gap, might not be suitable when high accuracy is a priority. This comprehensive evaluation provides clear guidance for model selection based on specific implementation requirements and available computational resources. This research contributes significantly to the field of automated allergy severity prediction and provides a foundation for implementing machine learning-based decision support systems in clinical settings. The comparative analysis offers valuable insights for selecting appropriate algorithms for similar biomedical prediction tasks, particularly in allergology and immunology applications.

ACKNOWLEDGMENT

We gratefully acknowledge the financial support provided by the Faculty of Science and Technology, Songkhla Rajabhat University through 2023 Research and Publication Grant.

REFERENCES

[1] J. Chen, H. Huang, S. Tian, and Y. Qu, "Feature selection for text classification with Naïve Bayes," Expert Syst. Appl., vol. 36, no. 3, pp. 5432–5435, 2009.
[2] A. Tongkaw and S. Tongkaw, "Prediction Medical Problem of Elderly People by Using Machine Learning Technique," J. Phys. Conf. Ser., vol. 1529, p. 032083, Apr. 2020, doi: 10.1088/1742-6596/1529/3/032083.
[3] W. Chang et al., "A Machine-Learning-Based Prediction Method for Hypertension Outcomes Based on Medical Data," Diagnostics, vol. 9, no. 4, p. 178, Nov. 2019, doi: 10.3390/diagnostics9040178.
[4] T. Cover and P. Hart, "Nearest neighbor pattern classification," IEEE Trans. Inf. Theory, vol. 13, no. 1, pp. 21–27, 1967.
[5] R. Keniya et al., "Disease prediction from various symptoms using machine learning," Available SSRN 3661426, 2020, Accessed: Jan. 04, 2025.
[6] L. Breiman, Classification and regression trees. Routledge, 2017. Accessed: Jan. 05, 2025.
[7] D.-C. Li, C.-W. Liu, and S. C. Hu, "A fuzzy-based data transformation for feature extraction to increase classification performance with small medical data sets," Artif. Intell. Med., vol. 52, no. 1, pp. 45–52, 2011.
[8] O. Z. Maimon and L. Rokach, Data mining with decision trees: theory and applications, vol. 81. World scientific, 2014. Accessed: Dec. 18, 2024.
[9] T. Chen and C. Guestrin, "XGBoost: A Scalable Tree Boosting System," in Proceedings of the 22nd ACM SIGKDD International Conference on Knowledge Discovery and Data Mining, San Francisco California USA: ACM, Aug. 2016, pp. 785–794. doi: 10.1145/2939672.2939785.
[10] S. Tongkaw, "Comparison of AI Techniques in Modeling of Transportation Cost for Persons with Disabilities," in Engineering Mathematics and Computing, vol. 1042, P. Gyei-Kark, D. K. Jana, P. Panja, and M. H. Abd Wahab, Eds., in Studies in Computational Intelligence, vol. 1042. , Singapore: Springer Nature Singapore, 2023, pp. 171–185. doi: 10.1007/978-981-19-2300-5_12.
[11] S. Gündoğdu, "Efficient prediction of early-stage diabetes using XGBoost classifier with random forest feature selection technique," Multimed. Tools Appl., vol. 82, no. 22, pp. 34163–34181, Sep. 2023, doi: 10.1007/s11042-023-15165-8.
[12] WHO, "Ageing gracefully in a digital world." Accessed: Aug. 14, 2021. [Online]. Available: https://www.who.int/china/news/feature-stories/detail/ageing-gracefully-in-a-digital-world

Sustainable Waste Management: Enhancing Efficiency with Vehicle Routing Optimization Techniques

Nichaphat Phurichteerarat
Department of Mathematics and Statistics, Faculty of Science and Technology, Thammasat University
Pathumthani, 12120 Thailand
nichaphat.phu@dome.tu.ac.th

Auksarapuk E-dee
Department of Mathematics and Statistics, Faculty of Science and Technology, Thammasat University
Pathumthani, 12120 Thailand
auksarapuk.e-d@dome.tu.ac.th

Anuwat Boonmechot
Department of Mathematics and Statistics, Faculty of Science and Technology, Thammasat University
Pathumthani, 12120 Thailand
anuwat.boo@dome.tu.ac.th

Thapanita Thongpap
Department of Mathematics and Statistics, Faculty of Science and Technology, Thammasat University
Pathumthani, 12120 Thailand
thapanita.tho@dome.tu.ac.th

Lakkana Ruekkasaem
Department of Mathematics and Statistics, Faculty of Science and Technology ,Thammasat University
Pathumthani, 12120 Thailand
lakkana@mathstat.sci.tu.ac.th

Pongchanun Luangpaiboon
Industrial Statistics and Operational Research Unit (ISO-RU), Department of Industrial Engineering, Faculty of Engineering, Thammasat School of Engineering, Thammasat University
Pathumthani, 12120 Thailand
lpongch@engr.tu.ac.th

***Abstract*—Effective waste management is crucial for advancing sustainability on university campuses. This study use advanced optimization approaches to examine and improve waste collection routes, with the objective of dramatically enhancing truck routing efficiency and overall waste management efficacy. The research is divided into two unique scenarios: the first emphasizes the optimization of vehicle routes based on designated waste collection places for each truck, while the second enhances routes by incorporating truck capacity limitations through the employment of private company cars. To evaluate the efficacy of these improvements, the aggregate transportation distances of existing garbage collection routes are juxtaposed with those refined by four methodologies: the Savings Algorithm, the Nearest Neighbor Method, Microsoft Excel Solver, and VRP Spreadsheet Solver. The findings indicate that in the initial scenario, privately owned automobiles enhanced by these techniques attained the minimal overall transit distance of 17.310 kilometers. Conversely, university-owned trucks achieved optimal distances of 4.852 kilometers for Truck 1 and 5.770 kilometers for Truck 2. In the second instance, the optimized routing exhibited its effectiveness with a total transit distance of 20.300 kilometers. These findings highlight the potential of utilizing advanced routing algorithms to minimize transportation distances, therefore improving operational efficiency, decreasing fuel consumption, and promoting more sustainable waste management practices in educational institutions. This study presents a comparative analysis of various optimization techniques, offering a comprehensive framework that can be tailored to tackle analogous logistical challenges in diverse institutional contexts, in accordance with the overarching goals of improving information technology and operational strategies within Computer Science.**

Keywords— waste collection route planning, saving algorithm, nearest neighbor algorithm, evolutionary algorithm

I. INTRODUCTION

Universities are vibrant hubs that generate significant waste due to their large student, faculty, and staff populations. Effective waste management is essential for ensuring sustainability and operational efficiency. Office of Property and Sports Management oversees waste collection using two types of routing systems: university-owned vehicles and private company vehicles. The fleet consists of two university-owned trucks, each with a 1,000-kilogram capacity, and a private company truck with a 6,000-kilogram capacity. The campus infrastructure, which includes a mix of narrow and wide roads, creates challenges for vehicles accessing collection points, particularly those located away from main thoroughfares. These factors contribute to delays and inefficiencies in the waste collection process.

The absence of a structured waste collection schedule exacerbates these issues, leading to uncoordinated vehicle routes, longer travel distances, and increased operational costs. This study aims to address these challenges by optimizing waste collection routes, with a dual focus on improving vehicle routing efficiency and enhancing overall waste management operations. To achieve this, advanced optimization methods are employed, including the Savings Algorithm, the Nearest Neighbor Algorithm, Microsoft Excel Solver (using its Evolutionary function), and the VRP Spreadsheet Solver, to analyze and refine the existing waste collection system.

This research provides a significant contribution by developing a structured optimization framework tailored to address institutional waste management challenges. A comparative analysis of multiple optimization techniques is conducted to identify the most effective strategies for minimizing transportation distances while adhering to logistical constraints. The study also emphasizes the practical value of tools like the Evolutionary function in Microsoft Excel Solver, demonstrating their effectiveness in solving real-world routing problems and bridging the gap between theoretical models and practical applications.

The findings not only improve waste management efficiency but also promote sustainable practices by reducing fuel consumption and environmental impacts. The proposed framework is designed to be scalable and adaptable, offering practical solutions for other institutions facing similar waste management challenges. This research contributes valuable insights into the intersection of vehicle routing optimization,

sustainability, and operational research, supporting broader goals in computer science and information technology.

II. METHODS

The complex challenge of waste collection routing within a university context is addressed by this study, which employs a combination of advanced optimization techniques. The methodologies implemented are the Savings Algorithm, the Nearest Neighbor Algorithm, the VRP Spreadsheet Solver, and the Microsoft Excel Solver (which employs its Evolutionary Algorithm, EA). These tools are chosen for their capacity to generate efficient solutions that are customized to the specific constraints of the case and to simplify complex routing problems. The research aims to determine the most effective strategy for optimizing vehicle routing, minimizing transportation distances, and enhancing overall waste management efficiency by comparing the waste collection routes generated by these methods. This comparative analysis not only emphasizes the strengths and limitations of each technique but also offers valuable insights into their practical applications, thereby connecting theoretical optimization with real-world impact in a dynamic institutional environment.

A. Heuristic Method

Heuristic methods are frequently employed to resolve vehicle routing issues, such as refuse collection routing and general transportation routing. This study emphasizes the use of heuristic methods to analyze and evaluate the shortest possible distances, with a particular emphasis on optimizing waste collection and other transportation routes, despite the existence of a variety of approaches to addresses these issues. The Savings Algorithm, the Nearest Neighbor Algorithm, the Sweep Method, and the Cluster-First Route Second Method are heuristic techniques that are widely recognized.

- *Savings Algorithm*

Clarke and Wright [1] developed the Savings Algorithm in 1964, a heuristic method that is intended to optimize vehicle routes of varying capacities to satisfy the needs of multiple consumers. This approach condenses individual routes into a single, integrated route by sequentially connecting customers, thereby reducing the overall travel distance in comparison to distinct routes. Fig. 1 illustrates this approach.

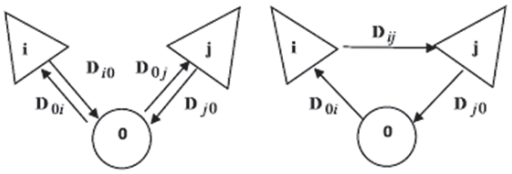


Fig. 1. Principle of the Savings Algorithm [2]

By sequentially connecting consumers, the algorithm reduces the total transportation distance. The savings in conveyance distance that result from the combination of routes are determined by the following formula (1) [3]:

$$S_{ij} = d_{oi} + d_{oj} - d_{ij} \quad (1)$$

; where:

S_{ij} is the distance savings when combining the routes between point i and point j

d_{0i} is the distance between the origin and point i.

d_{0j} is the distance between the origin and point j.

d_{ij} is the distance between points i and j

The Savings Algorithm is a widely used method for optimizing Vehicle Routing Problems (VRP) by reducing transportation distances and costs [4]. It starts by selecting a starting node, typically the waste collection depot, and linking two customer nodes into a route based on calculated transportation savings. These savings are ranked from highest to lowest, ensuring the most cost-effective connections are prioritized.

Routes are iteratively constructed by linking nodes with the highest savings, considering constraints like vehicle capacity or accessibility, until no further connections can be made. This systematic approach significantly reduces total transportation distances, lowering operational costs. Its adaptability makes it suitable for various VRP scenarios, including waste collection, delivery, and logistics.

- *Nearest Neighbor Algorithm*

The Nearest Neighbor Algorithm, developed by Hurkens and Woeginger [5], focuses on selecting the closest point at each step. A vehicle starts from its current location and travels to the nearest unvisited point, continuing until all points have been visited. The route is constructed step-by- step with the shortest possible path from the current point to the nearest neighbor. The following equation (2) represents the distance calculation for this algorithm [6]:

$$C_{ij} = C_{ip} + C_{pj} \quad (2)$$

; where:

C_{ij} is the distance from node i to node j.
C_{ip} is the distance from node i to node k.
C_{pj} is the distance from node k to node j.

The Nearest Neighbor Algorithm is a straightforward and efficient approach to resolving routing issues [7]. The algorithm begins at an initial point, such as a central depot, and minimizes the travel distance at each stage by identifying and traveling to the nearest unvisited point. The procedure of iteratively adding each visited point to the main route continues until all points have been visited. The final stage involves the computation of the total distance traveled. Although not always optimal, this method offers a practical and expeditious resolution to vehicle routing issues.

B. Metaheuristic Method

Metaheuristics are advanced problem-solving methods designed for complex optimization problems with large search spaces. They use heuristic strategies and randomization to explore potential solutions and provide near-optimal results. Among these, the EA stand out for their adaptability and robustness, making them ideal for dynamic challenges like VRP. By mimicking natural selection processes, EA iteratively evolves solutions, addressing issues

involving complex landscapes, non-continuous variables, or multiple constraints.

Derived from genetic principles such as mutation, crossover, and selection, EA starts with a population of potential solutions and refines them over generations to achieve better outcomes. Its adaptability ensures efficient performance in optimization tasks, including routing and scheduling, even in highly constrained environments.

To enhance accessibility, tools like VRP Spreadsheet Solver [8] and Microsoft Excel Solver incorporate EA principles into user-friendly platforms. The EA simplifies optimization by iteratively adjusting variables within constraints, making it particularly effective for non-continuous tasks like route planning and resource allocation. Its integration into a familiar spreadsheet environment ensures rapid and practical problem-solving.

Similarly, the VRP Spreadsheet Solver offers a specialized platform for vehicle routing. Using a structured spreadsheet interface, it organizes data into worksheets for Vehicles, Locations, Distance, and Solutions. By streamlining the optimization process and enabling result visualization, it provides a practical solution for logistics and waste management challenges.

These tools demonstrate the successful application of Evolutionary Algorithms in accessible formats, bridging the gap between theoretical methods and real-world problem-solving. Their simplicity and usability make them valuable resources for addressing complex optimization tasks.

III. Methodology

Data regarding waste collection routes at a university was collected from April 1, 2023, to March 31, 2024, encompassing a total duration of 12 months. The research concentrated on optimizing waste collection vehicle routes and gathering data via comprehensive interviews and additional sources to identify the most efficient paths. The waste collection fleet consists of three vehicles: one belonging to a private operator and two owned by the university. The commercial company's vehicle is a six-wheeled truck with a capacity of 6,000 kilograms, but the university's vehicles are four-wheeled trucks, each with a capacity of 1,000 kilograms. The university comprises 63 garbage collection stations, as depicted in Table 1.

TABLE I. Current Waste Collection Vehicle Route Management

Vehicle	Capacity (Kg.)	Points	Waste Collection Vehicle Route	Distance (Km.) /Weight (Kg.)
Private	6,000	33	33-32-34-35-6-28-27-41-21-0-31-19-16-17-18-30-5-4-3-1-2-6-7-8-9-10-11-12-13-24-14-22-29-0	22.890/4,062.41
Univ.1	1,000	16	0-37-46-47-38-39-40-59-58-57-56-55-54-53-52-51-49-0	5.296/1,015.60
Univ.2	1,000	14	0-48-50-15-60-61-63-23-26-25-62-45-42-43-44-0	7.040/794.82
Total		63		35.226/5,872.82

Table 1 provides an overview of the daily performance of waste collection operations at the university, highlighting the roles and contributions of each vehicle in the fleet. The private company's waste collection vehicle serviced 33 points, covering a total distance of 22.890 kilometers. It collected 4,062.41 kilograms of waste, effectively utilizing its capacity of 6,000 kilograms.

The university-owned vehicles, designated as Univ. 1 and Univ. 2, also played significant roles in the waste collection process. Univ. 1 serviced 16 collection points, traveling 5.296 kilometers and collecting 1,015.60 kilograms of waste, nearly reaching its maximum capacity of 1,000 kilograms. Univ. 2 covered 14 points, traveling 7.040 kilometers and collecting 794.82 kilograms of waste, also with a 1,000-kilogram capacity.

Combined, the three vehicles traveled a total of 35.226 kilometers and collected 5,872.82 kilograms of waste in a single day. These results reflect the current operational efficiency and utilization of the waste management system, providing a foundation for further analysis and optimization.

IV. Results

The current waste collection routes for each truck were evaluated and refined utilizing the Savings Algorithm, the Nearest Neighbor Method, Microsoft Excel Solver (Evolutionary Function), and the VRP Spreadsheet Solver. In both optimization models, all four techniques resulted in substantial decreases in the overall distance traveled for waste collection. The condensed outcomes of these optimizations are displayed in Tables II and III.

TABLE II. Comparison Between Current and New Vehicle Routing Methods Using Various Techniques (Unit: Kilometers)

Current Vehicle	Distance	Savings Algorithm	Nearest Neighbor	Evolutionary Algorithm	VRP Spread-Sheet
Private	22.890	35.369	17.841	17.663	17.310
Univ.1	5.296	7.884	5.310	4.852	5.060
Univ.2	7.040	6.525	7.297	5.770	10.000

The optimization of waste disposal routes for each vehicle was assessed using several methodologies, emphasizing the efficacy of the Microsoft Excel Solver (Evolutionary Function) for its flexibility and efficiency. The results underscore substantial disparities in performance among the techniques.

The VRP Spreadsheet Solver for the Private Company Vehicle (Private) attained the minimal total distance, decreasing the initial 22.890 kilometers to 17.310 kilometers—a reduction of 5.580 kilometers. The Evolutionary Function in Microsoft Excel Solver achieved a decrease of 5.227 kilometers. The Nearest Neighbor Method decreased the distance by 5.049 kilometers. Nonetheless, the Savings Algorithm exhibited suboptimal performance in this instance, resulting in a total distance of 35.369 kilometers.

For University Vehicle No. 1 (Univ. 1), the EA attained the optimal outcome, decreasing the overall distance from 5.296 kilometers to 4.852 kilometers, a reduction of 0.444 kilometers. The VRP Spreadsheet Solver yielded a decrease of 0.236 kilometers. The Nearest Neighbor Method marginally enhanced the overall distance by 0.014 kilometers, however the Savings Algorithm produced a substantial increase of 2.588 kilometers.

The EA for University Vehicle No. 2 (Univ. 2) attained the most significant reduction, decreasing the total distance from 7.040 kilometers to 5.770 kilometers, a decrease of 1.270 kilometers. The Savings Algorithm decreased the trip by merely 0.515 kilometers. In contrast, the Nearest Neighbor

Method and VRP Spreadsheet Solver augmented the total distances by 0.257 kilometers and 2.960 kilometers, respectively.

The Microsoft Excel Solver (Evolutionary Algorithm) consistently produced the minimal total distances for university-owned vehicles and shown competitive efficacy for the private vehicle. This highlights its efficacy and versatility for intricate route optimization tasks, rendering it a dependable instrument for enhancing garbage collection efficiency.

TABLE III. COMPARISON BETWEEN CURRENT ROUTE PLANNING AND PRIVATE COMPANY VEHICLE USAGE (UNIT: KILOMETERS)

Current Total Distance	Savings Algorithm	Nearest Neighbor	Evolutionary Algorithm	VRP Spread-Sheet
35.226	46.712	23.233	23.188	20.333

The current waste collection process involves three vehicles covering 35.226 kilometers to collect 5,872.82 kg of waste, though the private company's vehicle alone could handle the load. A new route optimization strategy was designed to consolidate all tasks into a single route using the private vehicle, reducing overall travel distance.

The optimization revealed notable differences in performance among methods. The VRP Spreadsheet Solver achieved the best result, reducing the distance to 20.300 kilometers—a 14.926-kilometer improvement. The Microsoft Excel Solver (Evolutionary Function) also performed well, cutting 12.038 kilometers, showcasing the Evolutionary Algorithm's effectiveness in handling complex routing problems.

Other methods were less effective. The Nearest Neighbor Method reduced 11.993 kilometers but lagged behind the top approaches, while the Savings Algorithm increased the total distance by 11.486 kilometers, proving unsuitable for this scenario. The EA stood out for enhancing routing efficiency, offering a flexible, computationally simple solution for optimizing waste collection with capacity consolidation.

V. CONCLUSION

This study examines the optimization of garbage collection routes at a university, comparing four distinct methodologies: the Savings Algorithm, the Nearest Neighbor Method, the EA, and the VRP Spreadsheet Solver. The analysis comprises two scenarios: (1) optimizing routes according to the current garbage collection places for each vehicle, and (2) optimizing routes based on vehicle capacity, employing solely the private company's vehicle.

In the first case, route optimization for the private company's vehicle resulted in a minimum total distance of 17.310 kilometers using the VRP Spreadsheet Solver, reducing the original distance by 5.580 kilometers or 24.38%. For University Vehicle No. 1, the Microsoft Excel Solver (Evolutionary Algorithm) achieved an optimal distance of 4.852 kilometers, representing a reduction of 0.444 kilometers or 8.38%. Similarly, for University Vehicle No. 2, the same tool minimized the total distance to 5.770 kilometers, reducing the initial distance by 1.270 kilometers or 18.04%. The results show that the evolutionary algorithm (EA) works to make routes more efficient. This is in line with the work of Rungrodchatchaval et al. [9], who looked into the shortest routes for collecting solid waste from the Prince of Songkla University Hat Yai Campus and found that the evolutionary algorithm provided the best solution.

In the second scenario, when optimizing routes according to vehicle capacity and employing solely the private company's vehicle, the VRP Spreadsheet Solver yielded a minimum total distance of 20.300 kilometers. This modification decreased the initial total distance by 14.926 kilometers, or 42.37%, underscoring the substantial potential for efficiency enhancements through route consolidation.

At present, waste collection routes within the university are established based on drivers' expertise, which fails to guarantee optimal routing. Inefficient routing might result in prolonged journey durations, heightening the likelihood of problems such as traffic congestion and foul odors, which may impact campus visitors. Optimizing routes can mitigate these issues by decreasing total trip distance, eliminating vehicle requirements, and reducing human needs, thereby enhancing overall operating efficiency.

This study prioritized weight as the main restriction for route optimization; however, subsequent research could include additional variables, such as cost and operational time, to further improve the efficiency and practicality of garbage collection route planning. These factors would establish a more thorough foundation for sustainable waste management methods in institutional environments.

ACKNOWLEDGMENT

We sincerely thank Thammasat University for providing the essential data that contributed to the successful completion of this research project. The first five authors and the sixth author also extend their gratitude to the Faculty of Science and Technology and the Faculty of Engineering, Thammasat School of Engineering for their support.

REFERENCES

[1] G. Clarke, and J.R. Wright, "Scheduling of vehicles from a Central Depot to a Number of the Delivery Point," *Operations Research*, 12 (4): 568-581, 1964.

[2] N. Sangpan, and S. Sirikulvadhana, "Application of Genetic Algorithm for Vehicle Routing Problem of Chicken Rendering Plants," *The Journal of KMUTNB.*, vol. 24, No. 3, pp. 526-536, Sep. - Dec. 2014.

[3] P. Tantikorn, and K. Ruengsak, "A Heuristic Approach Based on Clarke-Wright Algorithm for Open Vehicle Routing Problem" *The Scientific World Journal*, vol. 2013, Article ID 874349, 11 pages http://dx.doi.org/10.1155/2013/874349.

[4] F. Jan, B. Marke´ta, and J. L˘udmila, "Modification of the Clarke and Wright Algorithm with a Dynamic Savings Matrix" *Journal of Advanced Transportation*, vol. 2024, Article ID 8753106, 15 pages https://doi.org/10.1155/2024/8753106.

[5] C.A.J. Hurkens, and G.J. Woeginger, "On the nearest neighbor rule for the traveling salesman problem," *Operations Research Letters*, Vol. 32, Issue 1, Pages 1-4, January 2004. https://doi.org/10.1016/S0167-6377(03)00093-2.

[6] S. Oudonemexay, "Vehicle Routing of Residential Garbage Collection Within The Municipality of Kaisone Phomvihan, Savannakhet Province, Lao People's Democratic Republic" Master's Thesis, Logistics and Supply Chain Management, Faculty of Logistics, Burapha University. 2021.

[7] M. Z. . Rahman, S. R. . Sheikh, A. . Islam, and M. A. Rahman, "Improvement of the Nearest Neighbor Heuristic Search Algorithm for Traveling Salesman Problem", *J. Eng. Adv.*, vol. 5, no. 01, pp. 19–26, Mar. 2024. https://doi.org/10.38032/jea.2024.01.004

[8] G. Erdoğan, "An open-source spreadsheet solver for vehicle routing problems," *Computers & Operations Research*, vol. 84, pp. 62–72, August 2017. https://doi.org/10.1016/j.cor.2017.02.022

[9] N. Rungrodchatchaval, I. Sriswang, and W. Kongkaew, "Application of the Vehicle Routing Problem for Solid Waste Collection: A Case Study of Prince of Songkla University, Hat Yai Campus," T*hai Journal of Operations Research*, vol.4 , no. 2, pp. 18-31. 2016.

Explainable AI to Enhance Demand Forecasting Model for Autonomous Taxis in Smart Cities

Adeel Munawar
Sirindhorn International Institute of Technology
Thammasat University
Pathum Thani, Thailand
adeel.mun@dome.tu.ac.th

Mongkut Piantanakulchai
Sirindhorn International Institute of Technology
Thammasat University
Pathum Thani, Thailand
mongkut@siit.tu.ac.th

***Abstract*—The rapid evolution of Autonomous Taxis (ATs) in smart cities requires robust and accurate demand forecasting models to optimize resource allocation and ensure smooth mobility services. Traditional forecasting methods often function as black-box models, limiting interpretability and trust in their predictions. This study focuses on enhancing demand forecasting for ATs by incorporating Explainable Artificial Intelligence (XAI) to improve the transparency and interpretability of predictions. Simulations conducted on demand forecasting features demonstrate that the incorporation of XAI not only provides clearer insights into the prediction process but also increases prediction accuracy. For evaluation, we utilize a real-world dataset comprising over 4,500 taxis in Bangkok, Thailand, highlighting the practical benefits of this approach. The results underscore the potential of XAI to provide actionable insights for urban planners and fleet managers, paving the way for smarter and more adaptive mobility systems in the era of autonomous transportation.**

***Index Terms*—Autonomous Taxis, Demand Forecasting, Smart Cities, Explainable Artificial Intelligence (XAI), Predictive Modeling, Urban Mobility.**

I. Introduction

For decades, computer scientists have been striving to develop intelligent systems to achieve the goals of artificial general intelligence. This effort has led to scientific discoveries in various fields, including Intelligent Transportation Systems (ITS). Autonomous Taxis (ATs) are a pivotal innovation in this context, serving as a key enabler for ITS in smart cities by addressing challenges posed by rapid urbanization and population growth, such as energy consumption, traffic congestion, passenger and taxi waiting times, and mobility optimization through enhanced resource allocation [1].

Taxis are essential in traditional public transportation systems, providing safety, convenience, comfort, and tailored services that greatly influence urban communities. However, taxi drivers in many cities face ongoing challenges related to profitability. Research shows that minimizing cruising distances is among the most effective methods to enhance driver earnings [2].

The rise of ATs has marked a transformative phase in urban mobility, promising enhanced efficiency, reduced congestion, and greater accessibility in smart cities. However, ensuring the optimal deployment of these vehicles requires robust demand forecasting systems that are capable of accurately predicting spatial and temporal patterns in mobility needs. Traditional forecasting models often rely on statistical techniques or black-box machine learning algorithms. Although these methods may provide accurate predictions, they often lack interpretability and transparency. This has led to challenges in building trust among stakeholders and understanding the underlying factors influencing predictions.

Explainable Artificial Intelligence (XAI) has emerged as a critical paradigm for addressing these challenges. XAI enhances the interpretability of complex AI models, allowing stakeholders to comprehend how predictions are made and which features contribute the most to the outcomes. Studies have demonstrated the effectiveness of XAI in improving trustworthiness and accountability in predictive systems [3], [4]. Integrating XAI into demand forecasting for ATs enables urban planners and fleet managers to gain actionable insights into critical factors like time, location, weather conditions, and socio-demographic patterns, facilitating informed decision-making. Recent research highlights the need for adaptive and transparent forecasting models in urban mobility systems. Integration of XAI has shown potential in enhancing demand forecasting systems' predictive accuracy while ensuring interpretability [5].

This study proposes an XAI-enhanced demand forecasting model for ATs using data from the Intelligent Traffic Information Center Foundation (iTIC) [6]. The dataset includes GPS-based taxi routes and locations in Bangkok. To account for weather impacts, we integrated Meteostat data [7], covering temperature, humidity, precipitation, and other conditions. Combined, these datasets provide key insights into mobility and environmental patterns, forming a solid foundation for the model's development and evaluation.

The main contributions of this research include the development of a demand forecasting model specifically designed for ATs in smart cities. By integrating XAI, the model enhances transparency, interpretability, and predictive accuracy. A comprehensive analysis compares the proposed approach with traditional black-box methodologies, demonstrating that the XAI-enhanced model offers superior accuracy and greater interpretability. Furthermore, the study utilizes an extensive dataset collected over four months, comprising information from over 4,500 taxis in Bangkok, Thailand, enriched with

weather data. This integration highlights the practical applicability and effectiveness of the proposed model in addressing real-world challenges in urban mobility systems. The paper proceeds with Sections II–V: literature review, methodology, results, and conclusion.

II. Literature Review

The rise of smart cities and autonomous transport has driven the need for robust taxi demand forecasting, explored through statistical and AI-based approaches. This section reviews key related studies.

Early studies on taxi demand forecasting primarily relied on statistical models, such as time series analysis and regression techniques. These models often focused on historical trends and spatial-temporal patterns to predict demand. In a study, Safikhani *et al.* [8] utilized time series models to understand the spatio-temporal variations in taxi demand, emphasizing the impact of factors like weather and commuting patterns. Although these methods provided valuable insights, their reliance on linear assumptions and limited handling of complex interactions restricted their accuracy and scalability in dynamic urban environments. Recent advancements in artificial intelligence have significantly improved the accuracy and reliability of taxi demand forecasting. Yao *et al.* [9] introduced the Deep Multi-View Spatial-Temporal Network (DMVST-Net), which integrates spatial, temporal, and semantic relationships to address the complex nature of urban travel demand. Utilizing large-scale taxi data from Didi Chuxing in Guangzhou, the model achieved an RMSE of 9.64, outperforming state-of-the-art methods. Liao *et al.* [10] evaluated the performance of two deep learning architectures, ST-ResNet and Fusion Convolutional Network (FLC-Net), on the New York City taxi dataset. The ST-ResNet model exhibited superior accuracy with an RMSE of 11.13, compared to the FLC-Net's RMSE of 15.14. Naji *et al.* [11] proposed a GAN-based hybrid deep learning model for taxi demand prediction, combining recurrent and conventional networks. On Wuhan data, it achieved an RMSE of 9.78 and MAE of 16.75, with better performance in the Guanggu area. Markou *et al.* [12] developed a real-time taxi demand prediction framework by integrating machine learning with web data. Using the NYC Taxi and Limousine Commission (TLC) dataset, the model reduced forecast errors significantly, achieving an MAE of 8.31 and RMSE of 14.94. Recent studies have emphasized how external factors, such as weather conditions, influence taxi demand. Chen *et al.* [13] explored the relationship between rainfall and taxi demand patterns by analyzing GPS and taxi data. Their study demonstrates the importance of weather data such as temperature, humidity, and precipitation in improving demand forecasting models. Incorporating such data into forecasting frameworks enhances the accuracy and reliability of predictions, enabling better planning and resource management in urban mobility systems.

III. Methodology

This section describes the methodology used to develop a demand forecasting model for ATs in smart cities, incorporating XAI to improve both prediction accuracy and interpretability. The approach comprises three main phases: data preprocessing, model development, and evaluation, as shown in Fig. 1.

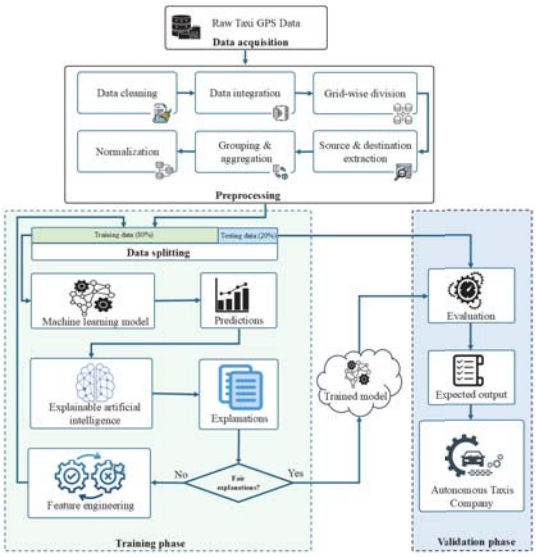


Fig. 1. Overall framework of the methodology including data preprocessing, model development, and evaluation phases.

A. Study Area

The study area used in this study is located in Bangkok, Thailand, bounded by longitude coordinates 100.24778° to 100.87591° and latitude coordinates 14.10965° to 13.50099°. This region encompasses a diverse mix of shops, train stations, neighborhoods, and tourist attractions, making it an ideal setting for studying urban taxi systems. The boundaries of the study area are illustrated in Fig. 2.



Fig. 2. Study area boundaries in Bangkok, Thailand.

B. Data Acquisition and Preprocessing

The dataset used in this study was provided by iTIC. It was collected from GPS devices installed in taxis operating in Bangkok and includes various fields such as taxi IDs, GPS coordinates, timestamps, speed, direction, and passenger status. This GPS data was combined with weather data obtained from the Meteostat platform, which provides environmental

variables such as temperature, humidity, and precipitation. By fusing these datasets, the study ensures a comprehensive understanding of both mobility and environmental factors, which are essential for accurately forecasting taxi demand in the urban environment. To ensure high-quality input data, the following preprocessing steps were implemented:

- **Data Cleaning:** To ensure the reliability of the data, a thorough cleaning process was conducted to eliminate inaccuracies, including missing values, duplicate entries, and anomalies in GPS readings. Data points located outside the defined boundaries, as illustrated in Fig. 2, were removed from the dataset to maintain its relevance to the study.
- **Data Integration:** Taxi GPS data was merged with weather data based on timestamps to align spatial and temporal dimensions.
- **Grid-wise Division:** The city area was divided into a grid of 7×7 equal-sized cells, with each grid cell measuring 10 km $\times$ 10 km, to spatially aggregate taxi demand. This grid-based division facilitated the analysis of spatial patterns and demand distribution across the urban environment.
- **Source and Destination Extraction:** Pickup and drop-off locations were identified to analyze travel patterns.
- **Grouping and Aggregation:** Data was aggregated into time slots, representing temporal patterns in taxi demand.
- **Normalization:** Continuous variables, such as weather attributes, were normalized.

Table I provides a detailed overview of the dataset features and their descriptions used in this study. These features include temporal, spatial, and environmental variables derived from the integrated GPS and weather data.

TABLE I
DATASET FEATURES AND THEIR DESCRIPTIONS

Feature	Description
day_name	Day of the week
grid_id	Unique identifier for spatial grid
time_slot	Time slot in the day
temp	Temperature
dwpt	Dew point temperature
rhum	Relative humidity (%)
prcp	Precipitation (mm)
wdir	Wind direction (degrees)
wspd	Wind speed (m/s)
pres	Atmospheric pressure (hPa)
coco	Weather condition
demand	Number of taxi demand

C. Model Development

The proposed model is designed with two key objectives: to achieve high predictive accuracy and ensure interpretability while being capable of modeling complex relationships in large datasets. The model utilized the Adam optimizer for efficient gradient descent and Mean Squared Error (MSE) as the loss function, ensuring robust training. Mean Absolute Error (MAE) was employed as an additional evaluation metric to assess prediction accuracy. The input features included a combination of temporal, spatial, and environmental factors, as mentioned in Table I. The proposed model integrated XAI, specifically SHAP (SHapley Additive exPlanations) [4], to address the challenges of interpretability and transparency in complex AI systems. According to Angelov *et al.* [14], explainability denotes the ability to communicate how an AI decision is made in a way that is understandable to human users. Modern AI models often involve millions of parameters and rely on intricate patterns, making them difficult to interpret. SHAP values provide insights into the contribution of individual features to the model's predictions, helping to explain how and why decisions are made. This approach mitigates concerns regarding bias, fairness, and transparency by offering interpretable and actionable explanations for the model's predictions. Fig. 3 presents a SHAP summary plot, which highlights the impact of each feature on the demand prediction.

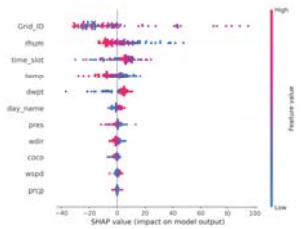


Fig. 3. SHAP summary plot highlighting feature impacts on demand prediction.

Furthermore, Fig. 4 shows the mean SHAP values, offering an understanding of the overall contributions of each feature to the model output. These insights allow urban planners and stakeholders to identify the most influential factors driving taxi demand. By using SHAP, the model offers stakeholders a deeper understanding of key factors influencing taxi demand, aligning predictive performance with practical decision-making in urban mobility planning. This integration of XAI not only enhances the transparency of the model but also ensures its applicability to real-world scenarios, reinforcing trust among users and planners.

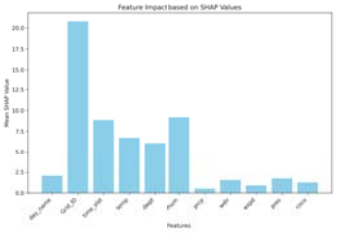


Fig. 4. Overall feature importance in predictions based on mean SHAP values.

Feature engineering played an important role in refining the model. By utilizing SHAP explanations, we systematically analyzed features based on their importance scores and average SHAP values. We retained features that consistently showed

high contributions and discarded those with negligible or inconsistent impacts. This systematic approach led to the creation of an optimized feature set that balanced predictive accuracy with interpretability, ensuring the model remained robust and practical for real-world application.

IV. Results and Evaluation

The model was evaluated using MAE, RMSE, and R^2 to assess its accuracy and reliability. Our model performance was assessed on both the original feature set and the XAI-refined feature set. Fig. 5 illustrates the comparative performance metrics (RMSE, MAE, and R^2) before and after XAI integration.

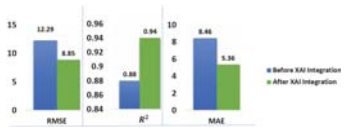


Fig. 5. Performance comparison before and after XAI integration.

The integration of XAI techniques brought substantial improvements to the model's performance. Before incorporating XAI, the model achieved an RMSE of 12.29, MAE of 8.46, and R^2 of 0.88. After integrating XAI, these metrics improved to an RMSE of 8.85, MAE of 5.36, and R^2 of 0.94. This highlights the significant impact of XAI in improving prediction accuracy.

Fig. 6 presents a combined regression plot, comparing the model's performance before and after XAI integration.

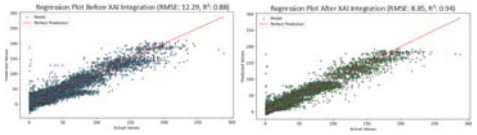


Fig. 6. Combined regression plots comparing model performance before and after XAI integration.

Fig. 7 illustrates the comparison of RMSE values between the proposed model and various models referenced in the literature. The proposed model demonstrates superior performance with the lowest RMSE of 8.85, outperforming other models. This comparison highlights the efficacy of the proposed model in achieving higher predictive accuracy, emphasizing its suitability for ATs demand forecasting in urban mobility scenarios.

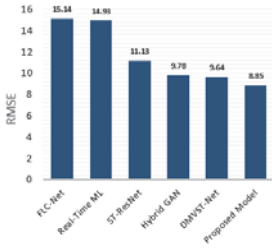


Fig. 7. Comparison of RMSE values between the proposed model and other referenced models.

V. Conclusion

In this study, we proposed a demand forecasting model specifically designed for ATs in smart cities. This model integrates machine learning techniques with XAI to improve both prediction accuracy and interpretability. By utilizing a comprehensive dataset that includes real-world taxi GPS data and weather information, the model effectively predicts ATs demand and provides actionable insights into the key factors influencing it. The findings demonstrate that integrating XAI not only enhances the accuracy of demand forecasting but also fosters trust and confidence among stakeholders by providing interpretable results. This framework can help urban planners and fleet managers optimize AT deployment models, enhance passenger satisfaction, and reduce congestion in smart cities. Future research can include additional data sources, such as socioeconomic and real-time traffic data, to improve predictions. Expanding the model to include ride-sharing and public transit enhances its impact, offering a transparent and adaptable solution for urban mobility in the era of autonomous transportation.

References

[1] A. Aldakkhelallah and M. Simic, "Autonomous vehicles in intelligent transportation systems," in *Human Centred Intelligent Systems: Proceedings of KES-HCIS 2021 Conference*, Springer Singapore, 2021, pp. 185–198.

[2] G. Qin, T. Li, B. Yu, Y. Wang, Z. Huang, and J. Sun, "Mining factors affecting taxi drivers' incomes using GPS trajectories," *Transportation Research Part C: Emerging Technologies*, vol. 79, pp. 103–118, 2017.

[3] M. T. Ribeiro, S. Singh, and C. Guestrin, ""Why should I trust you?" Explaining the predictions of any classifier," in *Proc. 22nd ACM SIGKDD Int. Conf. Knowledge Discovery and Data Mining*, 2016, pp. 1135–1144.

[4] S. M. Lundberg and S.-I. Lee, "A unified approach to interpreting model predictions," in *Proc. 31st Int. Conf. Neural Information Processing Systems (NIPS)*, Long Beach, CA, USA, Dec. 2017, pp. 4768–4777.

[5] F. Doshi-Velez and B. Kim, "Towards a rigorous science of interpretable machine learning," arXiv:1702.08608, 2017.

[6] Intelligent Traffic Information Center Foundation (iTIC), "[Online]. Available: https://org.iticfoundation.org/".

[7] Meteostat, "Meteostat: Free historical weather data," 2023. [Online]. Available: https://meteostat.net.

[8] A. Safikhani, C. Kamga, S. Mudigonda, S. S. Faghih, and B. Moghimi, "Spatio-temporal modeling of yellow taxi demands in New York City using generalized STAR models," *Int. J. Forecasting*, vol. 36, no. 3, pp. 1138–1148, 2020.

[9] H. Yao *et al.*, "Deep multi-view spatial-temporal network for taxi demand prediction," in *Proc. AAAI Conf. Artificial Intelligence*, vol. 32, no. 1, 2018.

[10] S. Liao, L. Zhou, X. Di, B. Yuan, and J. Xiong, "Large-scale short-term urban taxi demand forecasting using deep learning," in *Proc. 23rd Asia and South Pacific Design Automation Conf. (ASP-DAC)*, IEEE, 2018, pp. 428–433.

[11] H. A. H. Naji, Q. Xue, H. Zhu, and T. Li, "Forecasting taxi demands using generative adversarial networks with multi-source data," *Applied Sciences*, vol. 11, no. 20, p. 9675, 2021.

[12] I. Markou, F. Rodrigues, and F. C. Pereira, "Real-time taxi demand prediction using data from the web," in *Proc. 21st Int. Conf. Intelligent Transportation Systems (ITSC)*, IEEE, 2018, pp. 1664–1671.

[13] D. Chen, Y. Zhang, L. Gao, N. Geng, and X. Li, "The impact of rainfall on the temporal and spatial distribution of taxi passengers," *PloS One*, vol. 12, no. 9, p. e0183574, 2017.

[14] P. P. Angelov, E. A. Soares, R. Jiang, N. I. Arnold, and P. M. Atkinson, "Explainable artificial intelligence: An analytical review," *Wiley Interdisciplinary Reviews: Data Mining and Knowledge Discovery*, vol. 11, no. 5, p. e1424, 2021.

Blockchain As A Notarization System For Military Data Sharing

Chatchawan Chamnikul
Department of Defence Engineering
School of Engineering,
King Mongkut's Institute of Technology Ladkrabang,
Bangkok, Thailand
61601094@kmitl.ac.th

Amnach Khawne*
Department of Computer Engineering
School of Engineering,
King Mongkut's Institute of Technology Ladkrabang,
Bangkok, Thailand
amnach.kh@kmitl.ac.th

***Abstract*—This paper presents a blockchain-based notarization system designed to secure and authenticate military data sharing. In the context of national defense, where the integrity and confidentiality of sensitive military data are paramount, traditional centralized systems often fail to meet the required security standards. Our proposed system leverages a permissioned blockchain platform, specifically Hyperledger Fabric, combined with smart contracts to create an immutable and transparent ledger. This ensures that once military data is recorded, it cannot be altered or tampered with, thereby enhancing data integrity and auditability. The system is further integrated with existing military information infrastructures through secure APIs and middleware, enabling seamless data exchange. Experimental evaluations conducted in a simulated environment demonstrate that the system achieves high transaction throughput, low latency, and robust error management. Although challenges remain in scalability and fine-grained access control, the results confirm that blockchain technology has the potential to significantly improve the security and transparency of military data sharing. Future work will focus on addressing these challenges and refining the system for real-world deployment in defense operations.**

Keywords— Blockchain, Notarization, Military Data Sharing, Hyperledger Fabric, Smart Contracts, Immutability, Decentralization.

I. INTRODUCTION

In today's digital era, the integrity and security of data have become critical, particularly in the context of national defense. Military data, characterized by its sensitivity and critical role in strategic decision-making, demands a high level of security and reliability. Traditional centralized systems for notarization often suffer from vulnerabilities such as single points of failure, susceptibility to tampering, and limited transparency. These limitations can jeopardize the trustworthiness of the data and, consequently, the effectiveness of defense operations. Blockchain technology has emerged as a promising solution to these challenges due to its inherent characteristics of immutability and decentralization. A blockchain-based notarization system offers a distributed ledger that records transactions in an irreversible manner, ensuring that once data is recorded, it cannot be altered or deleted. This not only enhances data integrity but also provides complete traceability and transparency, which are essential for auditing purposes. Moreover, the use of smart contracts automates the verification process, reducing the reliance on manual oversight and minimizing human error. The proposed research focuses on designing, developing, and evaluating a blockchain-based notarization system specifically tailored for military data sharing. By leveraging a permissioned blockchain platform Hyperledger Fabric the system aims to integrate seamlessly with existing military information infrastructures. This integration is facilitated through secure APIs and middleware, ensuring that the validated data can be efficiently exchanged between disparate systems. Experimental evaluations conducted in a simulated environment have demonstrated that the system can process transactions efficiently while maintaining robust security measures. Key performance indicators, transaction throughput, latency, and response time, have been measured to assess the system's viability under operational conditions. Despite these promising results, challenges remain, particularly in scalability and granular access control, which must be addressed to enable full-scale deployment in real-world defense settings. This paper is organized as follows: Section II reviews related work and existing literature on blockchain applications in data notarization and military information systems. Section III details the proposed system architecture and design. Section IV describes the implementation process and presents the evaluation results. Finally, Section V concludes the paper with a summary of findings and recommendations for future research.

Supported by Defense Technology Institute Thailand
* Corresponding Author

II. LITERATURE REVIEW

A. Fundamentals of Blockchain Technology

Blockchain is a distributed ledger technology that records transactions in blocks, which are cryptographically linked to form a chain. This technology was first popularized by Bitcoin and has since been applied across various fields due to its key properties.

- **Immutability:** Once a transaction is recorded on the blockchain, it cannot be altered. This property ensures data integrity and fosters trust in the recorded information [1].
- **Decentralization:** Data is stored across a network of nodes rather than a single centralized server. This reduces the risk of a single point of failure and enhances system resilience.
- **Transparency:** All transactions on a blockchain are visible to all participants in the network, allowing for complete auditability.

B. Blockchain for Notarization

The concept of using blockchain for notarization involves leveraging its immutable ledger to certify the authenticity and integrity of documents and data. Several studies have demonstrated the feasibility of this approach in various contexts. For instance, blockchain-based notarization systems have been proposed for legal document verification, ensuring that once a document is recorded, it is permanently stored and its history can be audited without ambiguity [3].

C. Blockchain Applications in Military Data Sharing

Military data sharing involves the exchange of highly sensitive and critical information among defense agencies. The security and accuracy of such data are paramount. Recent research has begun to explore the use of blockchain in military applications to enhance data security and operational transparency.

- **Data Integrity and Security:** Studies indicate that blockchain can ensure that military data remains unaltered once recorded, thereby providing a reliable audit trail. This feature is essential for verifying the authenticity of operational data in defense scenarios [4].
- **Interoperability with Legacy Systems:** One of the significant challenges in military data sharing is the integration of new technologies with existing legacy systems. Researchers have proposed methods for integrating blockchain solutions with conventional military information systems using secure APIs and middleware. This integration is critical to ensure that the notarized data can be effectively utilized within current defense infrastructures.

D. Challenges and Research Gaps

While blockchain offers promising solutions for data notarization and military data sharing, several challenges remain.

- **Scalability:** Most blockchain platforms, particularly those based on public networks, face scalability issues when processing a high volume of transactions. Even permissioned blockchains Hyperledger Fabric must address performance bottlenecks when scaled to large networks.
- **Security of Smart Contracts:** Although smart contracts automate the notarization process, they can be vulnerable to coding errors and security exploits. Research into formal verification methods and comprehensive testing is ongoing to mitigate these risks.
- **Integration with Legacy Systems:** Effective integration between blockchain-based systems and existing military information systems remains an open research area. There is a need for standardization of APIs and middleware to ensure smooth interoperability.

The literature indicates that blockchain technology, with its inherent properties of immutability, decentralization, and transparency, offers a robust solution for notarizing data. While previous studies have demonstrated its applicability in various sectors, applying blockchain in the military domain presents unique challenges related to scalability, security, and integration with legacy systems. Addressing these challenges through further research and development is essential for realizing the full potential of blockchain-based notarization systems in enhancing the security and efficiency of military data sharing.

III. System Design

The proposed system is designed to provide a secure, immutable, and transparent method for notarizing military data through the use of blockchain technology. The system leverages a permissioned blockchain platform, specifically Hyperledger Fabric, to ensure that military data remains tamper-proof once recorded. The design follows a multi-layer architecture that separates concerns and allows for modular development, scalability, and easier integration with existing military information systems.

A. Multi-Layer Architecture

1) Data Layer: This layer is responsible for collecting military data from various sources and performing preprocessing tasks. Preprocessing includes data validation, formatting, and encryption. Interfaces with external military databases and sensors. Formats data and applies cryptographic techniques to secure the data before further processing. Keep your text and graphic files separate until after the text has been formatted and styled. Do not use hard tabs, and limit use of hard returns to only one return at the end of a paragraph. Do not add any kind of pagination anywhere in the paper. Do not number text heads-the template will do that for you.

2) Application Layer: The Application Layer handles the business logic of the system. It manages the notarization process by using smart contracts to verify data integrity and record transactions. Utilizes smart contracts to automatically verify the authenticity of data. Coordinates transaction creation and interacts with the blockchain network to record validated data. Provides a real-time view of transaction history, performance metrics (such as throughput, latency, and response time), and system alerts. This interface enables authorized users to query and audit the recorded transactions.

3) Blockchain Infrastructure Layer: This layer implements the core blockchain network that securely stores the data. It provides a distributed ledger and ensures consensus among participating nodes.

a) Peer Nodes: Host the ledger and execute smart contracts. Each peer maintains a copy of the blockchain, contributing to data redundancy and security.

b) Orderer Service: Manages the ordering of transactions and creates blocks to be appended to the ledger. It ensures that transactions are committed in a consistent order across the network.

c) Channels: In a permissioned blockchain, channels provide a private communication pathway among a subset of network members, enabling secure and confidential data sharing.

d) Consensus Mechanism: The chosen consensus protocol ensures that all peers agree on the order of transactions, providing fault tolerance and data integrity.

B. Integration with Existing Systems

To ensure the practical applicability of the system within military environments, integration with legacy military information systems is critical. The design includes:

1) API Layer: Facilitates communication between the blockchain network and existing military databases. Supports RESTful APIs to send and retrieve data securely.

2) Middleware:

a) Acts as a bridge between the blockchain and legacy systems.

b) Manages data translation and ensures that data formats are compatible across systems.

C. System Workflow

1) Data Ingestion: Data is collected from military sensors, databases, or manual input, then preprocessed (formatted and encrypted) at the Data Layer.

2) Transaction Creation: Preprocessed data is forwarded to the Application Layer, where smart contracts in the Notarization Module validate the data. Once verified, a transaction is created and submitted to the blockchain network.

3) Blockchain Recording: The transaction is broadcast to peer nodes. Through the consensus process managed by the Orderer Service, the transaction is recorded in a new block and added to the immutable ledger.

4) User Access and Monitoring: Authorized users access the Dashboard to view transaction histories, performance metrics, and receive alerts about potential security incidents.

IV. Implementation Process and Evaluation

This section describes the detailed steps involved in deploying the blockchain-based notarization system for military data sharing and presents the evaluation results from testing the system in a simulated environment.

A. Implementation Processs

1) Network Setup and Deployment

a) Environment Setup: The network is set up using Docker and Docker Compose to run the Hyperledger Fabric components. Containers are configured for Peer Nodes, the Orderer Service, and Certificate Authorities (CAs).

b) Configuration and Crypto Material Generation: Essential configuration files (e.g., crypto-config.yaml, configtx.yaml, and docker-compose.yaml) are prepared. The Cryptogen tool is used to generate the cryptographic material (certificates and keys) for each node, and the Genesis Block and channel transaction file are created using the Configtxgen tool.

c) Channel Creation and Peer Joining: A channel (e.g., "mychannel") is created using the generated channel transaction file. Peer nodes then join the channel, and Anchor Peers are updated to enable efficient intra-network communication.

2) Smart Contract Deployment:

a) Development: Smart contracts (chaincode) are developed in Node.js to implement the business logic for notarization (e.g., recording transactions, verifying data integrity).

b) *Packaging and Installation:* The chaincode is packaged into a tarball and installed on peer nodes using Fabric CLI commands. Each organization in the network then approves the chaincode, and it is committed to the channel.

c) *Verification:* Post-deployment, the chaincode is tested by invoking functions to record transactions and querying the ledger to verify that the data is accurately stored.

3) Integration with Legacy Systems

a) API Development: RESTful APIs are developed using Node.js and Express to facilitate communication between legacy military systems and the blockchain network.

b) Middleware Implementation: Middleware is implemented to handle data transformation and secure data routing between legacy systems and the blockchain, ensuring compatibility and secure transmission.

c) Integration Testing: Tools such as Postman are used to test the API endpoints, verifying that data can be accurately and securely exchanged between the systems.

4) User Interface Deployment

a) Dashboard Development: A web-based dashboard is created using modern web technologies (HTML, CSS, JavaScript, and frameworks like React) to display real-time transaction data, performance metrics (e.g., throughput, latency), and system alerts.

b) API Integration: The dashboard connects to the RESTful APIs to fetch data from the blockchain in real-time, enabling users to monitor and audit transactions effectively.

c) User Testing: The dashboard undergoes usability testing, and feedback is collected to refine the interface and improve the overall user experience.

B. Evaluation Results

1) Performance Metrics

a) The table below is an example of test results measuring the system's key performance metrics, including Transaction Throughput (transactions per second), Latency (delay), Response Time, with experiments divided into case studies based on the volume of transactions sent in each period.

TABLE I. TABLE *EXAMPLE OF TEST RESULTS MEASURING THE SYSTEM'S KEY PERFORMANCE METRICS*

Experiment Set	***Transactions Sent***	***Transaction Throughput (TPS)***	***Latency (ms)***	***Response Time (ms)***
Case 1	100	50	120	150
Case 2	500	45	150	180
Case 3	1000	40	180	210
Case 4	2000	35	200	260

This table represents sample data obtained from experiments conducted in a simulated environment, using Apache JMeter to simulate load and monitoring tools such as Grafana to collect real-time data.

2) Graphical Representation of Test Results

a) Transaction Throughput

This graph illustrates the relationship between the number of transactions sent in each experimental set and the Transaction Throughput (TPS). It was observed that as the number of transactions sent increases, the TPS slightly decreases due to the system's scalability challenges.

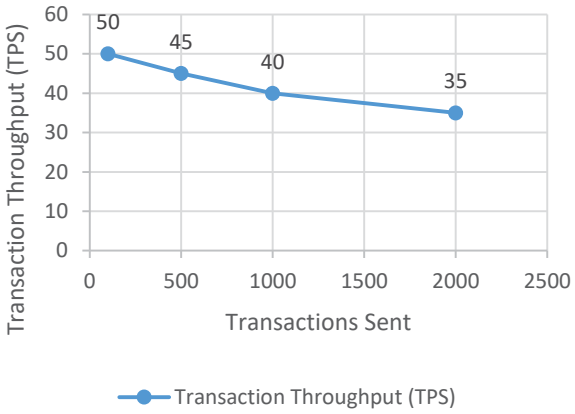


Fig. 1. Transaction Throughput (TPS and Transactions)

b) Latency and Response Time

This graph shows the relationship between the number of transactions sent and the latency. It was observed that latency increases as the number of transactions increases due to the higher load on the system processing simultaneous transactions.

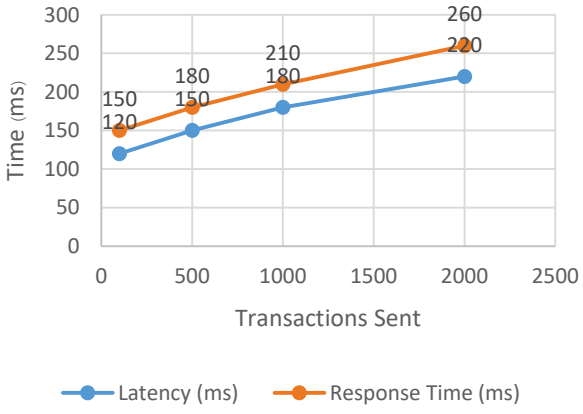


Fig. 2. Latency and Transaction

c) Uptime and Error Rate

The sample data in the table above shows that Uptime is at a high level (approximately 99.2% or above), while the Error Rate is relatively low.

The test results cover various aspects of the blockchain-based notarization system, presented in tables and graphs that provide key quantitative metrics such as Transaction Throughput, Latency, Response Time, Uptime, and Error Rate. This data helps assess the system's capabilities in terms of performance, security, and reliability, and serves as an essential basis for analyzing and improving the system in the future.

V. Conclusion and Recommendations

A. Summary of Finding

This research demonstrates that the blockchain-based notarization system significantly enhances the integrity, security, and transparency of military data. Key findings include.

1) Data Integrity and Security: The immutable and decentralized nature of the blockchain ensures that once military data is recorded, it remains tamper-proof, thereby reducing the risk of unauthorized modifications.

2) System Performance: Experimental evaluations in a simulated environment indicate that the system achieves acceptable transaction throughput, low latency, and fast response times, with a high uptime and low error rate.

3) *Integration with Legacy Systems:* The developed RESTful APIs and middleware enable seamless data exchange between the blockchain network and legacy military systems. Although minor issues related to data format conversion were observed, the integration has proven effective overall.

B. Conclusion

In conclusion, the blockchain-based notarization system offers a promising solution for ensuring the integrity and security of military data. While the system demonstrates strong performance in simulated environments, addressing scalability and enhancing integration with legacy systems will be critical for its successful deployment in real-world defense applications. Future research should build upon these findings to further optimize and secure the system, thereby supporting the evolving needs of national defense in the digital age.

References

[1] A. Narayanan, J. Bonneau, E. Felten, A. Miller, and S. Goldfeder,{Bitcoin and Cryptocurrency Technologies: A Comprehensive Introduction}, Princeton University Press, 2016.

[2] M. Crosby, P. Pattanayak, S. Verma, and V. Kalyanaraman, "Blockchain Technology: Beyond Bitcoin,"{Applied Innovation Review}, vol. 2, no. 6–10, pp. 71–77, 2016.

[3] V. Buterin, "A Next-Generation Smart Contract and Decentralized Application Platform," Ethereum Whitepaper, 2014.

[4] W. Wong, "Blockchain for Military Applications: Enhancing Security and Transparency in Data Sharing,"{Journal of Defense Technology}, vol. 10, no. 2, pp. 123–139, 2019.

[5] J. Smith, "Blockchain Implementation in Security Systems,"{IEEE Security & Privacy}, vol. 14, no. 5, pp. 70–78, 2018.

[6] S. Kumar, "Integration of Legacy Systems with Blockchain Networks," {IEEE Access}, vol. 7, pp. 150–159, 2019.

[7] L. Chen, "Scalability Challenges in Permissioned Blockchain Networks," in{Proc. IEEE International Conference on Blockchain}, pp. 220–225, 2020.

[8] R. Lee and M. Johnson, "Advanced Techniques for Smart Contract Verification,"IEEE Transactions on Dependable and Secure Computing}, vol. 18, no. 3, pp. 875–886, 2021.

[9] Hyperledger Fabric Documentation, Hyperledger Project. [Online]. Available: https://hyperledger-fabric.readthedocs.io/en/release-2.2/ [Accessed: Feb. 2025].

[10] E. Androulaki, P. Barger, A. Bortnikov, et al., "Hyperledger Fabric: A Distributed Operating System for Permissioned Blockchains," in {Proc. ACM/IFIP/USENIX Middleware Conference}, 2018, pp. 1–1

Application of Deep Learning Techniques for Predicting Leaf Lesions in KDML105 Rice Variety

Sittisak Promtara
School of Information Technology, King Mongkut's University of Technology Thonburi
Bangkok, Thailand
sittisak.prom@kmutt.ac.th

Watanyoo Suksa-ngiam
School of Information Technology, King Mongkut's University of Technology Thonburi
Bangkok, Thailand
watanyoo.suk@sit.kmutt.ac.th

Pornchai Mongkolnam
School of Information Technology, King Mongkut's University of Technology Thonburi
Bangkok, Thailand
pornchai@sit.kmutt.ac.th

***Abstract*—This study applies deep learning techniques to predict rice leaf diseases in the KDML105 (Jasmine Rice) variety, focusing on Narrow Brown Spot Disease and blast diseases, which affect the quality of Thai rice. The research developed a predictive model using the YOLO (You Only Look Once) technique combined with Transfer Learning, trained on images of rice leaves collected from paddy fields in Buriram province. The experimental results showed that the YOLOv8 model achieved the highest performance with a mean average precision (mAP) of 0.95 The majority of current research, however, either requires cutting rice leaves for photography or employs close-up shots of the leaves, which is unsuitable for farmers' everyday use. In order to solve the usability concerns of earlier research, this study attempts to create a long-range rice leaf disease detection system that can capture several leaves in a single wide-angle photo. It also supports sustainable precision agriculture, reduces dependency on chemical usage, and enhances the competitiveness of Thai rice in both domestic and international markets.**

Keywords— Deep Learning, KDML105Rice, Rice Leaf Diseases, YOLOv8, Rice Leaf Disease Prediction, Precision Agriculture

I. INTRODUCTION

Currently, farmers cultivating KDML105 jasmine rice, also known as "hom mali rice" a variety with long, slender grains, pandan-like fragrance, and soft texture when cooked, are facing challenges. This premium rice is favored by consumers both domestically and internationally [1]. Presently, 46% of Thailand's rice fields are dedicated to jasmine rice cultivation, with the Mun River Basin in Buriram province being a key production area for this economically significant crop [2]. However, farmers are experiencing declining paddy prices due to reduced rice quality. The main causes include shrinking cultivation areas, unsuitable environmental conditions [3], and, most critically, outbreaks of Narrow Brown Spot Disease and rice blast disease, which are endemic to Thailand.

Narrow Brown Spot Disease, caused by the fungus *Bipolaris oryzae*, manifests as brown streaks running parallel to the leaf veins, with dark brown lesion edges and lighter centers [4]. Rice blast is, caused by the fungus *Magnaporthe oryzae*, and appears as brown spots with grayish, dry centers and dark brown edges [5]. These diseases lead to leaf wilting and hinder photosynthesis [6], significantly reducing growth and yield. Since outbreaks have gotten worse over the past 10 years, inflicting extensive harm to rice productivity and quality, effective control of rice disease is essential for food security. The speed and accuracy of traditional diagnostic techniques that rely on manuals and professional consultation are constrained. In order to create prediction and picture categorization systems, contemporary technologies like artificial intelligence (AI) and deep learning are being investigated. This study aims to develop a deep learning model trained with extensive rice leaf imagery using deep learning and transfer learning, enabling the model to recognize symptoms of these two diseases. The model's prediction accuracy will be tested on new sets of rice leaf images, with a target accuracy of over 90%, comparable to expert diagnoses. Along with reaching high accuracy, additional objectives are to assess the system's reliability and performance in a variety of actual conditions and refine image processing methods to increase the precision of disease identification. Farmers would be able to identify rice leaf problems quickly if the built AI model can effectively anticipate diseases, doing away with the need to wait for expert reviews. This immediate action will lessen yield losses, prevent epidemics, and maintain the quality and market value of Thai jasmine rice across the world This research introduces the YOLOv8 model for predicting Narrow Brown Spot Disease and rice blast diseases in KDML105 jasmine rice. It also compares the model's performance with YOLOv11 and DETR (DEtection TRansformer) to assess their comparative effectiveness All models are trained and tested on the same dataset, consisting of KDML105 rice leaf images collected from farmers' fields in Buriram province. The performance of each model is analyzed and compared.

II. RELATED WORKS

Kulkarni and Shastri [7] proposed the use of Convolutional Neural Networks (CNN) to detect and diagnose rice leaf diseases from Kaggle image datasets. The dataset included four categories: healthy leaves, bacterial leaf blight, brown spot, and blast disease. The data was divided into training, testing, and validation sets. Their CNN model achieved an accuracy of 95% and utilized four convolutional layers, max pooling, dropout, ReLU activation, two fully connected layers, and a SoftMax classifier. The results demonstrated that deep learning can diagnose rice diseases with high accuracy and speed, providing significant benefits for farmers in managing crop diseases effectively.

Roopali Dogra and Shalli Rani [8] introduced a CNN-VGG19 model combined with Transfer Learning to detect and classify brown spot disease in rice leaves. The study utilized 40 images collected from paddy fields in India. After preprocessing, segmentation, and feature extraction focusing on color, texture, and shape, the model was evaluated.

The test's results included an F1-score of 90.5%, accuracy of 93.0%, sensitivity of 89.9%, specificity of 94.7%, and

979-8-3315-4248-1/25/$31.00 ©2025 IEEE

reliability of 92.4%. These measurements showed its efficacy in identifying brown spot disease in rice, since they were greater than those of other models including CNN, VGG16, DNN, and KNN.

Dong Cong Trinh et al. [9] improved YOLOv8 for rice leaf disease detection using the Alpha-EIOU loss function, which combines EIoU loss and α-IoU loss. They automatically collected disease images from rice fields, categorizing them into rice blast, leaf folder, and brown spot diseases. The images were used to train YOLOv8 and implemented on IoT devices. Testing on 3,175 images achieved 89.9% accuracy, higher than previous methods. When tested on Raspberry Pi 4, it processed at 1.5 seconds per frame, which is sufficient for real-world applications.

Faruq Aziza and Ferda Ernawana [10] used YOLO to detect and diagnose rice leaf diseases from an Indonesian dataset containing 5 categories with 110 images each. The data was augmented to 1,320 training images and 330 test images. The experimental results showed 94% accuracy, 88-89% precision, 80-86% recall, with detection time of 0.028 seconds per image, outperforming VGG16, ResNet50v2, GoogleNet, and Faster R-CNN. The system could detect multiple diseases on the same leaf using bounding boxes, but was limited to single leaf photographs and couldn't detect diseases in wide-angle shots.

Sangaiah et al. [11] improved Tiny YOLO to create UAV T-YOLO-Rice for detecting rice leaf diseases using UAVs by adding YOLO detection layers, SPP module, CBAM, SCFEM, Ghost module, and convolution layers. Testing on 15,456 images achieved 86% mAP at 82 FPS, outperforming YOLOv7 and FasterRCNN. However, it had limitations such as poor detection of leaf tip burn disease, reduced accuracy with complex backgrounds, long training time of 6.9 hours, limited original data, and requiring 640x640 px images for actual UAV deployment.

Krisdianto and Sonalitha [12] used YOLO to detect and classify 4 types of rice leaf diseases from a dataset of 661 images, split into 70% training, 10% validation, and 20% testing sets. At 300 epochs, the results showed 77% accuracy, 66% precision, and 79% recall, demonstrating YOLO's effectiveness. However, limitations included small dataset size and moderately low accuracy. They recommended increasing the dataset size, adjusting parameters, and modifying model layers in future work to improve performance.

Faruq Aziz et al. [13] improved YOLO for rice leaf disease classification using 550 images of 5 disease types from Indonesia. They modified anchors, depth multiple, and learning rate in CNN. The model achieved 94% accuracy, outperforming Inception-ResNet-V2, SSD, and YOLOv5, with a processing time of 40 seconds. It could detect multiple diseases on a single leaf using bounding boxes, despite limitations with small pixel sizes or complex backgrounds. Data augmentation helped the model better adapt to various environmental conditions.

Changshun Wang et al.[14] improved DHLC-DETR, an enhanced version of DETR for rice leaf disease detection, particularly for Rice Blast, Sheath Blight, and Brown Spot. The model integrates Res2Net as the backbone and DHLC-FPN to improve multi-level feature extraction and reduce information loss. Key enhancements include Hungarian Loss for precise bounding box matching and image augmentation for better generalization. Experimental results show a 17.3% increase in mAP and 9.5% improvement in small target detection over DETR, achieving 76.4% accuracy on the IDADP dataset from PRCV2019. Comparisons with Faster R-CNN, YOLOv3, and Mask R-CNN confirm superior accuracy and small target detection capability.

Aditia Putra Pranjaya et al. [15] presented a system for detecting and classifying rice leaf diseases using the YOLOv5 algorithm. The researchers used a dataset of 1,500 images split into 70% training, 20% validation, and 10% testing, their testing results achieved 95% mAP, 88% precision, and 100% recall. The system could detect Narrow Brown Spot with 93% accuracy, Leaf Blight with 81% accuracy, and normal rice leaves with 91% accuracy. While there were limitations regarding lighting conditions and accuracy, the system proved beneficial for farmers in preliminary disease identification. The majority of current research, however, either requires cutting rice leaves for photography or employs close-up shots of the leaves, which is unsuitable for farmers' everyday use. In order to solve the usability concerns of earlier research, this study attempts to create a long-range rice leaf disease detection system that can capture several leaves in a single wide-angle photo. It will compare the performance of YOLOv8, YOLOv11, and DETR in detecting and classifying Narrow Brown Spot Disease and blast disease in KDML105 rice variety from actual field photographs. Table 1: Summary of Related Work

TABLE I. SUMMARY OF RELATED WORK

Study	Model Used	Results	Limitations
Kulkarni and Shastri.	CNN	Accuracy 95%	The model may not perform well in real-world environments.
Roopali Dogra and Shalli Rani.	CNN-VGG19	F1-score 90.5%, Accuracy 93%, Sensitivity 89.9%	Lighting conditions or camera angles that may affect the model's performance.
Dong Cong Trinh et al.	YOLOv8 + Alpha-EIOU	Accuracy 89.9%, Processing 1.5 sec/frame	Processing at 1.5 seconds per frame is sufficient, but it may not be suitable in certain situations that require real-time processing.
Faruq Aziza and Ferda Ernawana.	YOLO	Accuracy 94%, Precision 88-89%, Recall 80-86%, 0.028 sec/image	Single leaf photos only
Sangaiah et al.	UAV T-YOLO-Rice	mAP 86% at 82 FPS	Poor leaf tip burn detection, low accuracy with complex backgrounds
Krisdianto and Sonalitha.	YOLO	Accuracy 77%, Precision 66%, Recall 79%	Small dataset, moderate accuracy

Faruq Aziz et al.	YOLO (improved)	Accuracy 94%, Processing 40 seconds	Limited by pixel size and complex backgrounds
Changshun Wang et al	DHLC-DETR	DHLC-DETR has a 17.3% increase in mAP compared to the original DETR.	Image quality from insufficient lighting or improper camera angles
Aditia Putra Pranjaya et al.	YOLOv5	mAP 95%, Precision 88%, Recall 100%	Lighting condition limitations

III. METHODOLOGY

This section describes the four-step process for building YOLOv8, YOLOv11, and DETR (DEtection TRansformer) models as shown in Figure 2. The first step is data collection, gathering images of KDML105 (Thai Jasmine) rice leaves from farmers' fields in Buriram province. The second step is image preprocessing. The third step is data augmentation to increase dataset diversity, and the final step is model training using the collected data.

A. Data Collection

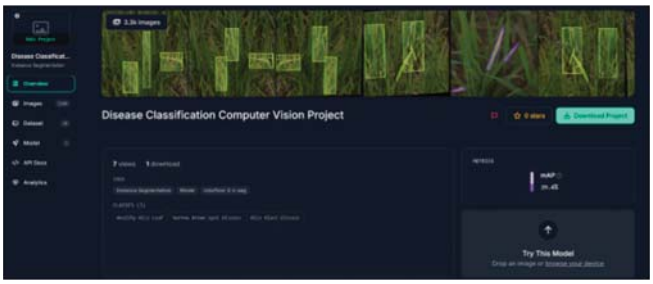


Figure 1. labeling Dataset Roboflow Platform

The researchers collected images of KDML105 (Thai Jasmine) rice leaves from farmers' fields in Buriram province, capturing disease symptoms from a distance with affected leaves centered in the frame and natural field conditions as background. After image capture, sampling showing symptoms were collected for disease verification and pathogen identification. The verification of Narrow Brown Spot Disease and blast disease was conducted by randomly sampling symptomatic rice plants from 4 experimental fields in Krasang district, Buriram province, for analysis at the Plant Disease Clinic, Kasetsart University, Kamphaeng Saen Campus. The verified disease images were used to develop and test a deep learning-based recognition system. The rice leaf disease data included Rice Blast Disease, characterized by brown eye-shaped or spindle-shaped spots with dark brown borders and gray centers, with 250 images collected; Narrow Brown Spot Disease, showing small reddish-brown oval-shaped spots, with 250 images; Healthy Rice Leaf, showing healthy green leaves without disease symptoms, with 250 images; and Others, comprising rice leaves not falling into the first three classes, with 250 images. Figure 1. For labeling, Roboflow, a web-based platform, was used as a tool for creating image datasets for training the recognition system. 70% of the labeling was done by experts, and the researchers labeled the remaining 30%. These labeled images were used as datasets for training and testing the models in this research. Samples of the datasets showing labeled Narrow Brown Spot and Blast Disease symptoms are shown in Figure 2.

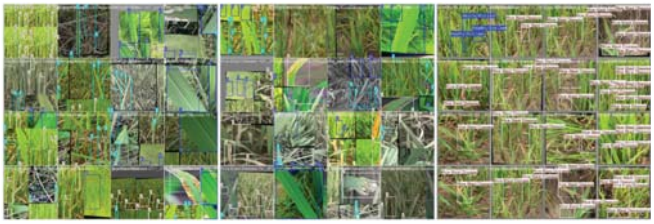


Figure 2. Sample of labeled datasets showing Narrow Brown Spot and Blast Disease lesions

B. Image Preprocessing

In this step, preprocessing was performed on all images labeled by evaluators (70% by experts and 30% by researchers). This included resizing images to 640x640 pixels, adjusting brightness, and performing data augmentation. From the total 1,000 images of KDML105 rice leaf disease classifications, the data was split into training, validation, and testing sets in the following proportions: Training Set (60%): 600 images, Validation Set (20%): 200 images, and Testing Set (20%): 200 images.

C. Data Augmentation

In this step, various image processing techniques were employed to enhance dataset diversity for model training. Using the Roboflow platform, data augmentation expanded the training dataset by 15 times, increasing from 1,000 to 15,000 images, thereby reducing the risk of overfitting. The applied techniques included: image rotation between -3 and +3 degrees, image flipping, brightness adjustment between -5% and +5%, contrast adjustment, image blurring, and grayscale level adjustment. These methods enable the model to better learn and generalize from rice leaf images captured under diverse environmental conditions and viewpoints.

D. Model Training

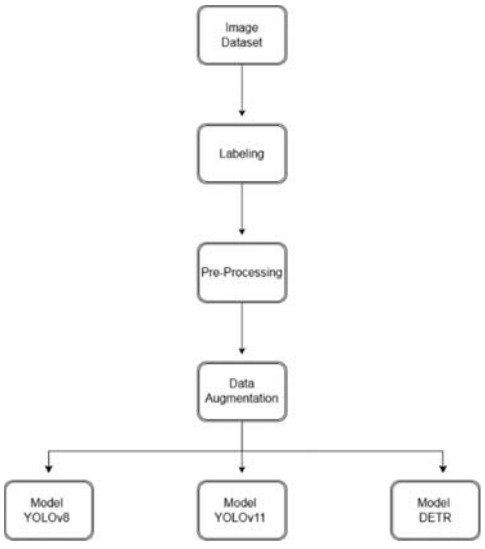


Figure 3. Training process

In the model training process, all image data from the previous steps were used to train the models as shown in Figure 2. The labeled images underwent preprocessing and augmentation before being input into the models for learning. The models used in this research were DETR (Detection Transformers) 640x640, YOLOv11 640x640, and YOLOv8, with architectures optimized for rice leaf disease detection. The models were tested using an unseen test dataset consisting of mobile phone photos. Model accuracy was evaluated using several metrics: mAP, Precision, Recall, F1 Score, and AP. Performance comparisons between the three models (DETR, YOLOv11, YOLOv8) included per-class accuracy calculation, disease discrimination ability, and real-world environment testing.

IV. RESULT

After training all models with the training dataset, their performance was evaluated based on Precision, Recall, mean Average Precision (mAP), and F1 Score metrics. The models predicted lesions of Narrow Brown Spot Disease and Blast Disease in KDML105 rice variety from the test set. Sample predictions are provided in Figure 4.



Figure 4. Sample predictions of Narrow Brown Spot Disease and Blast Disease lesions

1.YOLOv8 model demonstrated the best performance in predicting Narrow Brown Spot Disease and Blast Disease lesions in KDML105 rice. It achieved an average mean Average Precision (mAP) of 0.95, average Precision of 0.91, average Recall of 0.858, and an average F1-score of 0.93. The image processing speed was 0.9ms (see Table 2 for details). These results indicate that YOLOv8 is highly accurate in detecting and classifying the rice leaf diseases, providing both high precision and recall values that are crucial for detecting disease lesions in real-world environments.

2. YOLOv11 model, while performing well, showed slightly lower results compared to YOLOv8. It achieved an average mAP of 0.92, average Precision of 0.89, average Recall of 0.81, and an average F1-score of 0.90. The image processing speed was faster at 0.7ms (see details in Table 3). While YOLOv11 is faster, YOLOv8 outperforms it in terms of accuracy and recall, which are more important for reliable disease detection in rice leaves. Reasons why YOLOv8 performs better than YOLOv11:Accuracy: YOLOv8 has higher mAP and Precision values (mAP 0.95 vs 0.92, Precision 0.91 vs 0.89), demonstrating superior capability in locating and classifying rice leaf diseases. Detection: YOLOv8 has a higher Recall rate (0.858 vs 0.81), indicating better efficiency in detecting all disease lesions present in the images. Overall Performance: YOLOv8 has a higher F1-score (0.93 vs 0.90), reflecting a better balance between Precision and Recall. Practical Application: Despite YOLOv11's faster processing time (0.7ms), the superior accuracy of YOLOv8 makes it more suitable for practical applications where detection accuracy is paramount.

3. DETR (Detection Transformer) model, developed by Facebook AI Research, also showed promising results but with certain limitations. It achieved a performance at IoU=0.50 with an average AP of 68.4% for detecting objects of all sizes. The model performed well with larger objects, achieving an AP of 50.5%, but struggled with small object detection (8.5% accuracy at IoU=0.75). Medium object detection showed moderate performance at 27.1%. (see details in Table 4) These results suggest that DETR performs well with large objects but faces challenges in detecting smaller lesions, which could affect its use for detailed disease detection in rice leaves. Additionally, DETR requires more computational resources and has slower convergence compared to YOLO models.Summary of DETR's Limitations

High Computational Resources: DETR's architecture requires substantial computational resources, making it less efficient for real-time applications in resource-constrained environments.Slower Convergence: Compared to YOLOv8 and YOLOv11, DETR has slower convergence, which could result in longer training times. Difficulty with Small Objects: DETR shows reduced accuracy in detecting small lesions, which is a significant limitation for fine-grained disease detection. In conclusion, while YOLOv8 outperforms both YOLOv11 and DETR in terms of accuracy, recall, and F1-score, it is essential to consider the trade-off between processing speed and detection accuracy depending on the practical requirements. YOLOv8 stands out as the most suitable model for rice leaf disease detection, offering superior overall performance in real-world applications.

TABLE II. EVALUATION OF YOLOV8 MODEL

Class	Precision	Recall	F1-score
Leaf blast	0.827	0.809	0.818
Narrow Brown Spot	0.956	0.863	0.907
Healthy Leaf	0.947	0.904	0.925

TABLE III. EVALUATION OF YOLOV11 MODEL

Class	Precision	Recall	F1-score
Leaf blast	0.794	0.778	0.786
Narrow Brown Spot	0.946	0.823	0.880
Healthy Leaf	0.936	0.856	0.894

TABLE IV. EVALUATION OF DETR MODEL

Evaluation	IoU	maxDets	Average Precision
Standard AP	0.50:0.95	100	0.430 (43%)
AP IoU=0.50	0.50	100	0.684 (68.4%)
AP IoU=0.75	0.75	100	0.430 (43%)

V. DISCUSSIONS

The experimental results demonstrated that the YOLOv8 model showed impressive performance in predicting leaf disease on KDML105 rice varieties, achieving a mean average

precision (mAP) of 95%, higher than YOLOv11 (mAP 92%) and DETR (mAP 43%). This model was able to accurately detect rice leaf blast and brown spot diseases, especially in real-world environments with complex and diverse conditions, such as actual rice fields where the researchers collected data. This ensured that the results were reliable and reflected real-world usage. When compared with previous studies, such as Kulkarni and Shastri [7], which used the YOLOv3 model and achieved an mAP of only 79.19%, the performance in this study was significantly better. CNN, reported a 95% accuracy rate; however, the dataset used for training was from Kaggle, which may not represent the actual farming environment, while this study used real-world rice field data from Thailand, reflecting the actual working conditions faced by farmers. In another study by Roopali Dogra and Shalli Rani [8], CNN-VGG19 combined with Transfer Learning was used to detect and classify brown spot disease in rice, achieving an accuracy of 93.0% and an F1-score of 90.5% from testing with 40 digital photos taken in rice fields in Jhansla village near Rajpura, India. The results showed that the model outperformed CNN, VGG16, DNN, and KNN, making it suitable for diagnosing brown spot disease. However, Dogra and Rani's research revealed a limitation in the training process, as it required detached rice leaves, which is impractical for real-world usage, where farmers need to detect diseases directly in the fields without cutting the leaves. Additionally, the dataset from Kaggle might not reflect the actual agricultural conditions. In contrast, this study's ability to detect diseases in real-world rice fields in Thailand is more practical for on-site use. The use of Data Augmentation techniques, such as image rotation, brightness adjustment, and flipping, helped YOLOv8 perform well with diverse data. Despite limitations in computational resources, YOLOv8's processing speed of 0.9 milliseconds per image makes it suitable for real-time disease detection in real-world agricultural environments. In terms of practical applications, YOLOv8 holds great potential in developing smart agriculture systems, such as creating smartphone applications for farmers to take pictures of rice leaves and receive immediate diagnostic results. It can also be used with drones to quickly survey large farming areas. Integrating the model with early warning systems would allow farmers to manage diseases in a timely manner, reducing crop losses and enhancing the quality of Thai rice in the global market. Furthermore, it is possible to develop systems that connect with IoT technologies or cloud services. By linking CCTV systems with satellite systems in farms, it is possible to monitor and check the status of crops over a broader area. Data from CCTV cameras can be sent to satellite systems that capture environmental conditions from a wider perspective, improving farm problem detection. This would allow for real-time disease prediction, making it a valuable tool for increasing agricultural efficiency in the future. For future research, the dataset should be expanded to include various regions in Thailand and neighboring countries to enable the model to function effectively across different environments. Additionally, customizing the model for use with devices that have limited resources, such as drones or affordable smartphones, would help expand the use of this technology, promoting the development of smart agriculture systems that can be implemented in diverse regions without relying on expensive equipment.

VI. CONCLUSION

The results show that YOLOv8 delivered the highest overall performance in predicting rice leaf disease lesions on the validation dataset. It proved to be the most effective in detecting KDML105 rice diseases, with high Precision (0.91), Recall (0.858), and F1-score (0.94), processing images in just 0.9ms each. YOLOv8 outperformed other models in accuracy, speed, and its ability to distinguish between Narrow Brown Spot Disease and Blast Disease, showing low error rates and high suitability for practical use by farmers. In comparison, YOLOv11 achieved Precision of 0.89, Recall of 0.81, and F1-score of 0.90, while DETR exhibited the lowest performance, particularly in small object detection. These results make YOLOv8 the most suitable choice for this application. Newer versions of YOLO may not necessarily be more accurate, as their development often focuses on aspects such as speed, resource efficiency, or specialized applications.

REFERENCES

[1] H. M. Rice, "Siam Kumachorn Foundation," Siam Kumachorn Foundation, [Online]. Available: https://www.scbfoundation.com/media_knowledge/knowledge/562/khao-hom-mali-105-7949. Accessed: Apr. 25, 2024.

[2] M. Rivers, "Major rivers in Isan: Mekong, Songkhram, Chi, Mun - Rivers of life," IsanInsight, [Online]. Available: https://isaninsight.kku.ac.th/archives/4610K. Accessed: Apr. 30, 2024.

[3] BBC News, "Rice prices: Why this year's rice prices have fallen so low," BBC News Thai, 2024. [Online]. Available: https://www.bbc.com/thai/thailand-59179023. Accessed: Aug. 10, 2024.

[4] Agricultural Extension Service Center, "Brown spot disease in rice," [Online]. Available: https://esc.doae.go.th/brown-spot-disease-in-rice/. Accessed: Apr. 30, 2024.

[5] N. U. Khan, M. Liu, M. Yang, and X. Qiu, "Fungal elicitor MoHrip2 induces disease resistance in rice leaves, triggering stress-related pathways," PLoS One, vol. 11, no. 6, p. e0158112, 2016. [Online]. Available: https://doi.org/10.1371/journal.pone.0158112. Accessed: Nov. 10, 2024.

[6] C. Sukonta, "Plant substances from Aglaia (Meliaceae) with activity against rice blast pathogen Pyricularia oryzae Cav.," M.S. thesis, Kasetsart Univ., Bangkok, Thailand, 2003.

[7] P. Kulkarni and R. Shastri, "Rice leaf diseases detection using machine learning," J. Sci. Res. Technol., vol. 17, pp. 17–22, 2024.

[8] R. Dogra, S. Rani, A. Singh, M. A. Albahar, A. E. Barrera, and A. Alkhayyat, "Deep learning model for detection of brown spot rice leaf disease with smart agriculture," Comput. Electr. Eng., vol. 109, p. 108659, 2023.

[9] D. C. Trinh, A. T. Mac, K. G. Dang, H. T. Nguyen, H. T. Nguyen, and T. D. Bui, "Alpha-EIOU-YOLOv8: An improved algorithm for rice leaf disease detection," AgriEngineering, vol. 6, no. 1, pp. 302–317, 2024.

[10] F. Aziz, F. Ernawan, M. Fakhreldin, and P. W. Adi, "YOLO network-based detection of rice leaf disease," in Proc. Int. Conf. Inf. Technol. Res. Innov. (ICITRI), Aug. 2023, pp. 65–69.

[11] A. Sharma, "UAV T-YOLO-Rice: An enhanced tiny YOLO network for rice leaf disease detection in paddy agronomy," IEEE Trans. Netw. Sci. Eng., vol. 11, 2024, doi: 10.1109/TNSE.2024.3350640.

[12] K. Krisdianto, E. Sonalitha, and Y. S. A. Gumilang, "Deteksi penyakit padi menggunakan YOLO," Uranus: J. Ilm. Tek. Elektro, Sains dan Inform., vol. 2, no. 3, pp. 125–134, 2024.

[13] S. P. Singh, K. Pritamdas, K. J. Devi, and S. D. Devi, "Custom convolutional neural network for detection and classification of rice plant diseases," Procedia Comput. Sci., vol. 218, pp. 2026–2040, 2023.

[14] C. Wang et al., "DHLC-DETR: Enhanced Detection Transformer for Rice Leaf Disease Identification," iScience, vol. 28, no. 1111558, Jan. 17, 2025. DOI: 10.1016/j.isci.2024.111558. [Online]. Available: https://doi.org/10.1016/j.isci.2024.111558. Accessed: Jul. 10, 2024.

[15] F. Aziz and F. Ernawan, "Object detection for diagnosis rice leaf diseases using YOLO method," arXiv preprint, arXiv:2209.01579, 2016. [Online]. Available: https://doi.org/10.48550/arXiv.2209.01579. Accessed: Jul. 8, 2024.

[16] Q. Cao, D. Zhao, J. Li, J. Li, G. Li, S. Feng, and T. Xu, "Pyramid-YOLOv8: A detection algorithm for precise detection of rice leaf blast," Plant Methods, vol. 20, no. 1, p. 149, 2024.

[17] A. P. Pranjaya, F. Rizki, R. Kurniawan, and N. K. Daulay, "Klasifikasi penyakit pada daun tanaman padi berbasis YoloV5 (You Only Look Once)," KLIK: Kajian Ilm. Inform. dan Komput., vol. 4, no. 6, pp. 3127–3136, 2024.

Comparative Analysis of Common Compression Algorithms for Sentinel-2 Multispectral Band Compression

Aljaž Žel
Faculty of Electrical Engineering and Computer Science
University of Maribor
Maribor, Slovenia
aljaz.zel@um.si

Domen Mongus
Faculty of Electrical Engineering and Computer Science
University of Maribor
Maribor, Slovenia
domen.mongus@um.si

Borut Žalik
Faculty of Electrical Engineering and Computer Science
University of Maribor
Maribor, Slovenia
borut.zalik@um.si

***Abstract*—Sentinel-2 Earth observations generate massive volumes of imagery data stored in the JPEG 2000 file format. The paper evaluates lossless compression strategies for satellite data by comparing two general-purpose methods (Deflate, Bzip2) and two image compression algorithms (JPEG 2000, JPEG XL). The experiments focused on individual band compression. Parallel processing implementations were tested, to leverage the features of the selected algorithms. The experiments were conducted on a dataset consisting of full tile Sentinel-2 L2A images with reduced cloud levels, where two performance metrics were measured, a compression ratio and a throughput.**

***Index Terms*—Remote Sensing, Deflate, Bzip2, JPEG 2000, JPEG XL**

I. Introduction

Satellite imagery is an important source of information in remote sensing of Earth observations. The images enable monitoring of environmental changes [1], land cover classification and mapping [2, 3], as well as various applications from different domains [4, 5]. Due to their size, the images cannot be stored uncompressed, therefore, they present a challenge for finding an efficient method of storage and distribution. Due to its growing demand, the maximum achievable throughput is desired, requiring a balance between the compression and processing efficiency.

Through Europe's Copernicus programme [6], the Sentinel-2 mission utilises two satellites capturing high resolution multispectral images. The satellites are distanced by separated orbits and provide a full Earth coverage every 5 days. The captured images consist of 13 spectral bands at three different spatial resolutions (10 m/pixel, 20 m/pixel, 60 m/pixel). The captured images are split into tiles, each spanning approximately 110 km^2.

The main available Sentinel-2 data products are Level-1C (L1C) and Level-2A (L2A) [7]. L1C data consist of 13 spectral bands capturing the top of the atmosphere reflectance, including the radiance observed from space, without the exclusion of atmosphere factors. By applying atmospheric corrections, the L2A product is derived from L1C. It contains 12 bands, where one band is removed due to strong atmospheric distortion. Both data products use a variation of the Standard Archive Format for Europe (SAFE), containing metadata and separately stored images for each band. The captured images contain values represented by 12 bits, while the L1C and L2A products perform additional processing operations and are stored as 16-bit unsigned integers. The list of bands with spatial resolutions, central wavelengths and band descriptions are presented in Table I.

The conducted experiments evaluated the performance of four available lossless compression algorithms, Deflate, Bzip2, JPEG 2000 and JPEG XL. The current Sentinel-2 products use a standardised JPEG 2000 file format [8]. The performances of these algorithms are measured based on two metrics: a compression ratio and a throughput. For algorithms supporting parallel processing, the performance was evaluated using multiple threads. All of that takes into account each spectral band individually. As many applications [5, 9] require specific properties using only a subset of bands, the measured performance is discussed based on band characteristics.

The paper is organized into five Sections. Section II provides

TABLE I
Sentinel-2 L2A Band Description.

Band	Spatial resolution	Central wavelength	Description
B01	60 m	443 nm	Aerosol
B02	10 m	490 nm	Blue
B03	10 m	560 nm	Green
B04	10 m	665 nm	Red
B05	20 m	705 nm	First red edge
B06	20 m	740 nm	Second red edge
B07	20 m	783 nm	Third red edge
B08	10 m	842 nm	NIR
B8A	20 m	865 nm	Narrow NIR
B09	60 m	945 nm	Water Vapour
B11	20 m	1610 nm	SWIR 1
B12	20 m	2190 nm	SWIR 2

a brief overview of the selected compression algorithms. Section III presents the used metrics, experimental setup and results. The findings are discussed in Section IV and a conclusion is presented in Section V.

II. A Brief Overview of the Tested Algorithms

Image compression can be implemented through the lossless approach, preserving the original data, or lossy, allowing data loss during compression [10]. For scientific applications the lossless approach is crucial, ensuring accurate results of the subsequent operations.

Four algorithms were selected to evaluate the compression performance: two of them were general-purpose algorithms, while the other two are the state-of-the-art image compression methods offering lossy, as well as lossless modes. The tested general-purpose algorithms were:

- **Deflate** [11], which is used in Zip and related algorithms (Gzip, Zlib, 7-Zip). It combines LZ77 dictionary-based compression and Huffman coding [10]; and
- **Bzip2** [12], which is based on Burrows-Wheeler transform [13], which tends to group the same symbols close together. The arranged symbols are then transformed by Move-To-Front Transform. The obtained sequence is encoded by Huffman coding.

The other two are modern state-of-the-art algorithms for image compression developed by the JPEG consortium [14], i. e.:

- The **JPEG 2000** image compression standard [15, 16], achieves lossless compression through Reversible integer wavelet transform and context adaptive binary arithmetic coding. It allows progressive decoding and region of interest access. Parallel execution during encoding and decoding steps is enabled using tile compression, performing wavelet transform separately.
- The **JPEG XL** algorithm [17] is a modern solution for image compression, being the latest addition to the JPEG consortium. It combines modular transforms with various predictive and entropy encoding algorithms, designed specifically for efficient performance through parallel execution and simultaneous input processing using vectorization.

Both JPEG-based algorithms use spatial predictions by exploiting the correlation between neighbouring pixel values. In contrast, the general-purpose algorithms do not use such prediction techniques.

III. Experiments

The experiments were conducted on a system with an AMD Ryzen 7 5900X processor and 64GB DDR4 RAM, running the Windows 11 operating system. The used framework was implemented in C++ using the latest standard library features and open-source libraries [12, 18-20] for each compression algorithm. The setup used compiler Microsoft Visual C++ (MSVC), version 17.8.7. with optimisation flag $/O2$ and auto-vectorization being enabled [21].

To evaluate the performance of the compression algorithms, the experiments were conducted using a dataset consisting of 90 full Sentinel-2 L2A tiles with coverage across Europe. To capture the temporal variance of the satellite imagery, the selected images span between different seasons. Only tiles with cloud coverage below 5% were selected, to ensure evaluation of the spectral band characteristics without the interference of cloud data. In uncompressed form, the dataset occupies approximately 112 GB of storage.

The metrics used during the experiments consider the two most important issues:

- **Compression Ratio**, calculated as the ratio between the compressed and original data size (lower values indicate better compression), and
- **Throughput**, calculated as processed megabytes per second (MB/s).

The experiments were conducted by compression of each band image in the dataset individually using all the algorithms. To measure throughput, the speed of each algorithm was aggregated across all the bands. For both image-based algorithms, the results include both single-threaded and parallel (24 threads) implementations. Table II presents the compression and decompression throughput for all algorithms.

TABLE II
Throughput comparison (MB/s).

Algorithm	Compression	Decompression
Deflate	54.960	315.433
Bzip2	21.614	39.811
JPEG 2000	16.883	20.7967
JPEG XL	2.618	27.579
Parallel JPEG 2000	156.642	206.604
Parallel JPEG XL	33.384	375.736

The compression ratio, representing a metric for evaluating the effectiveness of compression, was measured for each spectral band separately. The mean compression ratio results for each spectral band and algorithm are presented in Table III. An average compression ratio across all bands was calculated for each algorithm, to provide an overall performance metric.

TABLE III
Compression ratios across Sentinel-2 spectral bands. The best result for each band is marked as bold.

Band	Deflate	Bzip2	JPEG 2000	JPEG XL
B01	0.725	0.528	0.554	**0.434**
B02	0.715	0.532	0.481	**0.461**
B03	0.726	0.543	0.494	**0.466**
B04	0.735	0.546	0.495	**0.463**
B05	0.774	0.602	0.549	**0.522**
B06	0.805	0.639	**0.553**	0.564
B07	0.818	0.654	**0.554**	0.579
B08	0.792	0.621	0.544	**0.542**
B8A	0.820	0.655	**0.554**	0.580
B09	0.823	0.668	**0.559**	0.593
B11	0.794	0.614	0.544	**0.522**
B12	0.779	0.598	0.544	**0.509**
Average	0.758	0.579	0.516	**0.500**

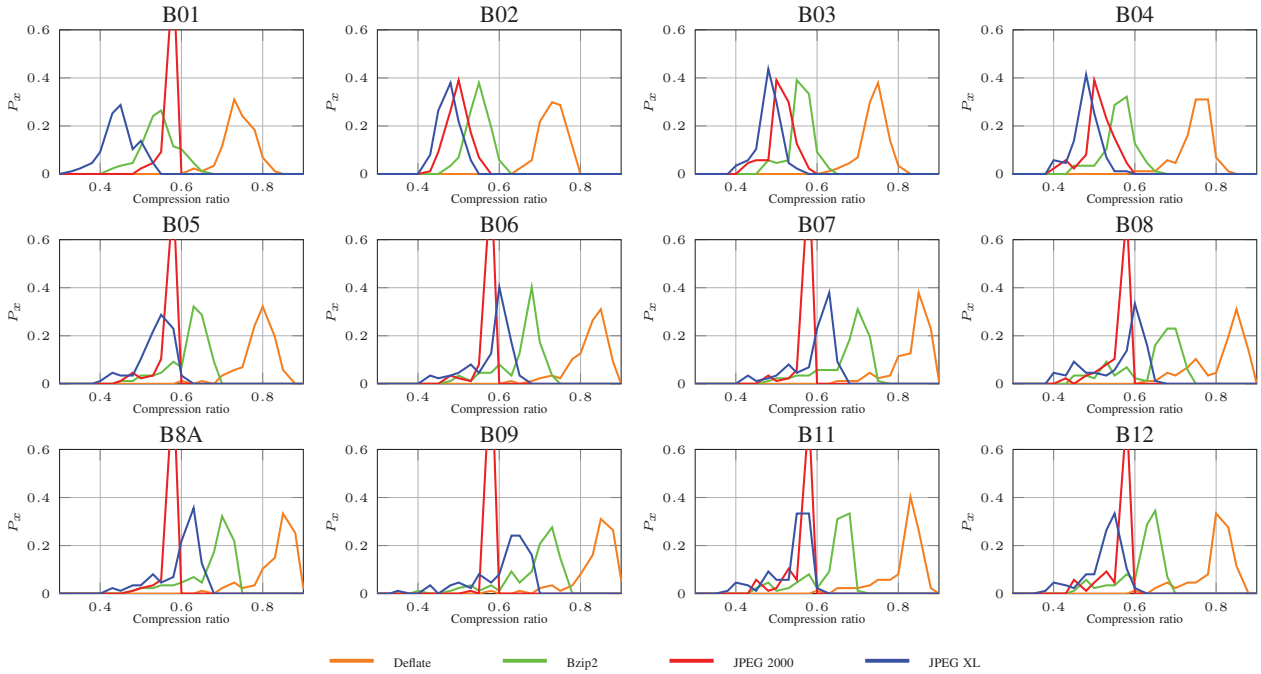


Fig. 1. Compression Ratio Distribution per Band. P_x represents the probability distribution of compression ratios within each spectral band.

Fig. 1 presents the distribution of compression ratios for each algorithm and band. Within each plot, the histogram distributions for all the algorithms are rendered as lines.

IV. Discussion

The results detailed in Section III demonstrate the ability of image-based algorithms to achieve good compression for Sentinel-2 imagery, with JPEG XL achieving the best average compression ratio of 0.5, as shown in Table III. The compression algorithms are evaluated below in order of their compression ratios:

- Deflate is less suitable for the high resolution and spectral characteristics inherent to satellite imagery, achieving an average compression ratio of 0.758, which is 25.8% worse than the best average compression ratio. The best ratios were achieved at lower wavelength bands. However, it offered the highest throughput in a single-threaded environment, suitable for scenarios where processing time is more important than storage efficiency, such as fast data transfer.
- Bzip2, the second evaluated general-purpose algorithm, achieved an average compression ratio of 0.579, only 7.9% lower than the best performing algorithm. The Burrows-Wheeler transform thus proved more effective than Deflate for satellite imagery compression. Its compression and decompression throughput were 2.54 and 7.92 times lower than Deflate, respectively. The lower throughput is attributed to the computational complexity of the transformations. An interesting observation was made for band B01, where Bzip2 outperformed JPEG 2000, achieving a better compression ratio.
- JPEG 2000 had the most consistent performance across all bands, with compression ratios ranging from 0.481 to 0.559. This resulted in an average compression ratio of 0.516, only 1.6% higher than JPEG XL. It achieved the best ratio in 4 bands: B06, B07, B8A and B09. The parallel implementation provided significant improvements, achieving 2.85 times higher throughput than the best single-threaded algorithm, while the parallel decompression throughput remained 1.52 times lower than Deflate. The consistent performance and highest achieved compression throughput support the algorithm's use as the standard compression algorithm for satellite imagery.
- JPEG XL achieved the best compression ratio, outperforming JPEG 2000 in 8 out of 12 spectral bands. Its single-threaded compression throughput was 20.99 times lower than Deflate, the parallel implementation improved this performance significantly, reducing the difference to only 1.64 times lower compression throughput than Deflate. The parallel implementation offered the best decompression throughput, performing 1.19 times higher than Deflate. This makes it suitable for decompression of frequently processed imagery, while maintaining good compression.

The analysis of Fig. 1 reveals distinct patterns in compression performance across the different spectral bands. The visible spectrum bands (B02, B03, and B04), representing the blue, green and red channels respectively, demonstrated notably similar compression distributions. These bands achieved

the best compression ratios statistically across all the algorithms. This can be attributed to the researched spatial characteristics of the visible wavelengths.

In the near-infrared and shortwave infrared bands (B05-B12), the compression behaviour became more varied. While Deflate, Bzip2, and JPEG 2000 maintained similar distribution patterns across these bands, JPEG XL showed a distinctive pattern. Its distribution was skewed, with the peak density on the right, and a long left tail representing a small percentage of images that achieved better compression ratios. The performance of the image-based algorithms alternated in achieving the best compression ratios within these bands, suggesting their complementary strengths in handling higher resolution spectral data.

The throughput performance, shown in Table II, demonstrated that image-based algorithms benefit significantly from parallel execution. The implementation of parallel compression for JPEG 2000 increased performance by 9.28 times, while JPEG XL showed a 12.75 time improvement. These implementations achieved even better results for decompression, with JPEG 2000 and JPEG XL having 9.93 and 13.62 time improvements, respectively. In a single-threaded environment, the Deflate algorithm achieved the highest throughput, but this came at a cost of inferior compression ratios.

V. Conclusion

This paper presented a comparative analysis of different algorithms for the efficient compression of Sentinel-2 L2A imagery. The experiments demonstrated that JPEG XL compression achieved a 1.6% reduction in storage requirements compared to the current JPEG 2000 standard used in Sentinel-2 satellite imagery. The two general-purpose algorithms used showed limited compression results, as Deflate was not able to leverage the spatial predictions in the imagery data, while the complexity of Bzip2 did not allow high compression throughput.

The study evaluated the compression and decompression of full Sentinel-2 images, indicating potential directions for future work. The memory requirements needed for partial image operations need to be investigated and addressed. A broader dataset and hybrid methods should be explored to extend the evaluation. As Sentinel-2 images of the same area are captured periodically, temporal compression techniques that leverage repeating patterns of consecutive images offer potential for further compression optimisation.

Acknowledgments

The authors acknowledge the financial support from the Slovenian Research and Innovation Agency (Research Project No. J2-4458, Research Core Funding P2-0041 and Young Researcher Funding under No. 0796-58043 through the Research Core Funding No. P2-0041). The authors also acknowledge support from European Union's Horizon Europe Research and Innovation Programme PrAEctiCe under grant agreement 101084248.

References

[1] M. Ahangarha, R. Shah-Hosseini, and M. Saadatseresht, "Deep learning-based change detection method for environmental change monitoring using sentinel-2 datasets," *Environmental Sciences Proceedings*, vol. 5, no. 1, 2021.

[2] B. Hu, Y. Xu, X. Huang, Q. Cheng, Q. Ding, L. Bai, and Y. Li, "Improving urban land cover classification with combined use of sentinel-2 and sentinel-1 imagery," *ISPRS International Journal of Geo-Information*, vol. 10, no. 8, 2021.

[3] D. Kavran, D. Mongus, B. Žalik, and N. Lukač, "Graph neural network-based method of spatiotemporal land cover mapping using satellite imagery," *Sensors*, vol. 23, no. 14, 2023.

[4] G. Konapala, S. V. Kumar, and S. Khalique Ahmad, "Exploring sentinel-1 and sentinel-2 diversity for flood inundation mapping using deep learning," *ISPRS Journal of Photogrammetry and Remote Sensing*, vol. 180, pp. 163–173, 2021.

[5] F. Maselli, L. Angeli, P. Battista, L. Fibbi, L. Gardin, R. Magno, B. Rapi, and M. C. and, "Evaluation of terra/aqua modis and sentinel-2 msi ndvi data for predicting actual evapotranspiration in mediterranean regions," *International Journal of Remote Sensing*, vol. 41, no. 14, pp. 5186–5205, 2020.

[6] M. Drusch, U. Del Bello, S. Carlier, O. Colin, V. Fernandez, F. Gascon, B. Hoersch, C. Isola, P. Laberinti, P. Martimort, A. Meygret, F. Spoto, O. Sy, F. Marchese, and P. Bargellini, "Sentinel-2: Esa's optical high-resolution mission for gmes operational services," *Remote Sensing of Environment*, vol. 120, pp. 25–36, 2012, the Sentinel Missions - New Opportunities for Science.

[7] S. U. Handbook and E. Tools, "Sentinel-2 user handbook," *ESA Standard Document*, vol. 1, pp. 1–64, 2015.

[8] A. Gatti and A. Bertolini, "Sentinel-2 products specification document," pp. 1–496, 2015.

[9] X. Yang, S. Zhao, X. Qin, N. Zhao, and L. Liang, "Mapping of urban surface water bodies from sentinel-2 msi imagery at 10 m resolution via ndwi-based image sharpening," *Remote Sensing*, vol. 9, no. 6, 2017.

[10] D. Salomon and G. Motta, *Handbook of Data Compression*, 5th ed. Springer Publishing Company, Incorporated, 2009.

[11] P. Deutsch, "DEFLATE compressed data format specification version 1.3," RFC 1951, May 1996. [Online]. Available: https://www.rfc-editor.org/info/rfc1951

[12] J. Seward, "Bzip2 and libbzip2," 1996. [Online]. Available: http://www.bzip.org

[13] M. Burrows and D. J. Wheeler, "A block-sorting lossless data compression algorithm," *SRC Research Report*, vol. 124, 1994.

[14] J. P. E. Group, "Joint Photographic Experts Group (JPEG)," 2024. [Online]. Available: https://jpeg.org

[15] G. Wallace, "The jpeg still picture compression standard," *IEEE Transactions on Consumer Electronics*, vol. 38, no. 1, pp. xviii–xxxiv, 1992.

[16] D. Taubman, "Jpeg 2000: Image compression fundamentals, standards and practice," 2002.

[17] J. Alakuijala, R. Van Asseldonk, S. Boukortt *et al.*, "JPEG XL next-generation image compression architecture and coding tools," in *Applications of digital image processing XLII*, vol. 11137. SPIE, 2019, pp. 112–124.

[18] "JPEG XL reference implementation." [Online]. Available: https://github.com/libjxl/libjxl

[19] "OpenJPEG Library," UCLouvain. [Online]. Available: https://www.openjpeg.org/

[20] J. Gailly and M. Adler, "Zlib compression library," 2024. [Online]. Available: https://zlib.net/

[21] T. Whitney, C. Robertson *et al.*, "Auto-parallelization and auto-vectorization," Microsoft, Technical Documentation, October 2022, microsoft Learn, C++, C, and Assembler. [Online]. Available: https://learn.microsoft.com/en-us/cpp/parallel/auto-parallelization-and-auto-vectorization

Image Processing Threshold of Acetabulum Porosity for Age Estimation

Supachard Krudtong
Biomedical Engineering Institute
Chiang Mai University
Chiang Mai, Thailand
supachard_k@cmu.ac.th

Pasuk Mahakkanukrauh
Department of Anatomy
Faculty of Medicine
Chiang Mai University
Chiang Mai, Thailand
pasuk304@gmail.com

Nipon Theera-Umpon
Biomedical Engineering Institute
Chiang Mai University
Chiang Mai, Thailand
nipon.t@cmu.ac.th

***Abstract*— This study explores the use of digital image processing to estimate age based on the porosity of the acetabulum, a part of the hip bone. By analyzing grayscale images of the acetabulum, the research aims to develop a standardized method for bone age estimation. The study focuses on optimizing the threshold value used to distinguish between bone tissue and porosity. Images from 99 male pelvic bones, aged 26 to 97, were analyzed. The results indicate that the mean – 1.0 SD threshold provides the most reliable age estimation, with an average error margin of 12.9 to 13.9 years. This method offers a promising alternative to traditional expert evaluations, which often have a similar error margin.**

***Keywords*— Age prediction, porosity, pelvic, media processors**

I. INTRODUCTION

The estimation of bone age is crucial for individual identification [1]. Bone condition, particularly bone porosity, is one variable that can be used to estimate age [1, 2]. The hip bone, especially the acetabulum, is highly effective for age estimation as it is an internal structure that is more resistant to post-mortem damage [3-8]. Currently, bone age estimation is conducted by experts, but differing levels of experience among professionals may lead to inconsistent results. Therefore, developing a standardized method for bone age estimation that can be universally applied would improve the accuracy and reliability of results. Additionally, transporting human remains to experts for evaluation cannot be done through standard postal services. This necessitates the physical delivery of bones to specialists, which can be both time-consuming and complicated. Digital image processing technology, now widely used in medicine, offers a promising solution [9-12]. Digital images can be easily and rapidly transmitted, circumventing the logistical challenges of physical specimen transport.

The porosity of the acetabulum can be quantified using pixel values from its digital images. By applying a threshold to the grayscale image of the acetabulum, pixels with values lower than the threshold (dark pixels) are classified as porosity, while those with values higher than the threshold (bright pixels) are classified as bone tissue [13-15]. The percent porosity of each acetabulum sample is calculated and compared to known bone ages. A statistical equation correlating percent porosity to age will then be developed for future bone age estimation [16, 17].

This research focuses on optimizing the threshold value used to distinguish between bone tissue and porosity. The goal is to determine the threshold value that yields the most accurate bone age estimation.

II. MATERIALS AND METHODS

The acetabulum "Fig. 1. Left" is a concave area in the pelvis that functions as a cup or socket to support the upper leg. There are several regions of interest within the acetabulum. We pay particular attention to the acetabular fossa "Fig. 1. Left", which is located inside the acetabulum. The percent porosity of the acetabular fossa is one of the major study topics.

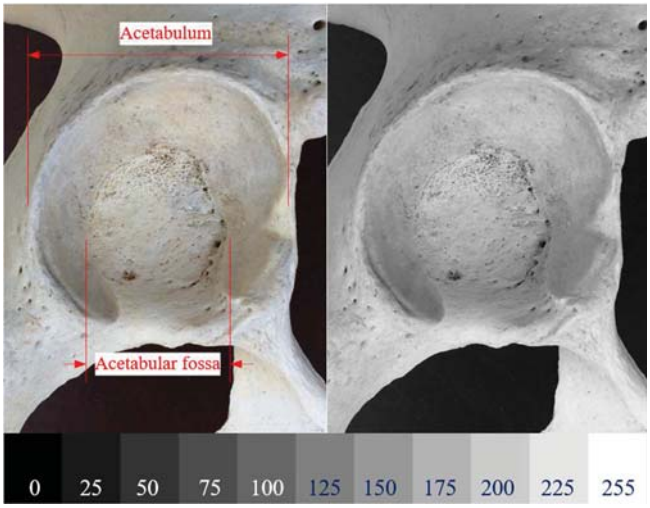


Fig. 1. Acetabulum color image (left), Acetabulum grayscale image (right), Grayscale gradient (below).

The bone samples used to compile the data were donated human remains from the Forensic Osteology Research Center (FORC), Chiang Mai University, Chiang Mai, Thailand. When all soft tissues were removed from these bones, what was left was the skeleton of bones. Pictures of the left and right acetabulum were provided by 205 skeletons both male and female. This resulted in approximately 400 images in all. The donations were made between 2011 and 2019 by people whose ages ranged from 19 to 100. Upon closer inspection of the images, it was discovered that many of the bones had not been cleaned enough, which could affect the pixel values and lead to incorrect interpretations of porosity. Consequently, images of dirty bones were left out.

The pilot or previous study shown that there is relationship between percent porosity of acetabulum only in male. There is no relationship between percent porosity of acetabulum in female. This research study about the image threshold for acetabulum porosity for age estimation, so only male was used. The study involved images of 99 male pelvic bones, with a specific focus on the acetabulum area on both left and right sides. The bone samples are from between 26- and 97-years old donators.

XXX-X-XXXX-XXXX-X/XX/$XX.00 ©20XX IEEE

A Digital Single-Lens Reflex (DSLR) camera was utilized for photography [18]. The imaging setup ensured that the image plane was parallel to the acetabulum plane, with spot focus directed towards the acetabular fossa. Color images were captured at ISO 100. Camera flash was employed in conjunction with ambient light to achieve consistent exposure calibrated to an 18% gray scale and to minimize shadows. Subsequently, the images were cropped exclusively to isolate the acetabulum area, thereby reducing the pixel count.

The color images "Fig. 1. Left" underwent a transformation process to be converted into grayscale images "Fig. 1. Right". An RGB (red, green, and blue) image is transformed into a grayscale image at this point. Pixel values in a grayscale image range from 0 to 255, where 0 represents black and 255 represents white "Fig. 1. Below". Grayscale tones, ranging from dark to light, are represented by values between 0 and 255. Subsequently, the acetabular fossa was delineated from the acetabulum structure. Utilizing the grayscale representation, pixels exhibiting white or light gray tones were identified as bone matter, while those exhibiting black or dark gray tones were identified as indicative of porosity.

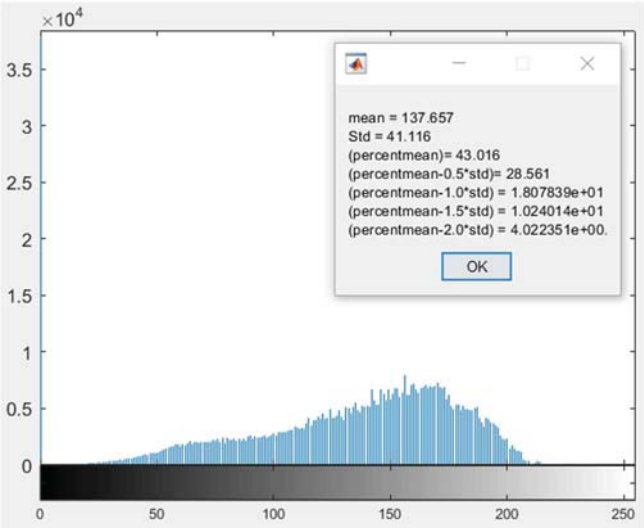


Fig. 2. Histogram and statistic matrixs.

The histogram of the acetabular fossa was created "Fig. 2.". An image histogram is a graphical depiction of the distribution of pixel intensities in an image. The histogram's x-axis, which goes from 0 to 255, represents the different levels of pixel intensity, with 0 representing dark pixels and 255 representing light pixels. On the y-axis, the number of pixels for each intensity value is displayed. A noticeable peak in the histogram indicates a large number of pixels at a certain intensity value. The symmetric bell-shaped curve of the histogram shows that the distribution of pixel intensities is normal. However, the histogram of the bone did not display a normal distribution because there was no symmetric bell curve. Among the statistical characteristics that were calculated were the mean and standard deviation (SD) [17].

The mean and standard deviation derived from the histogram are used to define the threshold of the image. There are 5 levels of threshold which they are mean, mean-0.5SD, mean-1.0SD, mean-1.5SD and mean-2.0SD. Porosity pixels are defined as those whose values fall below this threshold. The pixels whose values are higher than this threshold are bone pixels. The quantities of bone pixels and porosity pixels were then enumerated and utilized to calculate the percent porosity of the bone. This percent, along with the precise age information, was gathered for each individual bone specimen "Fig. 3.".

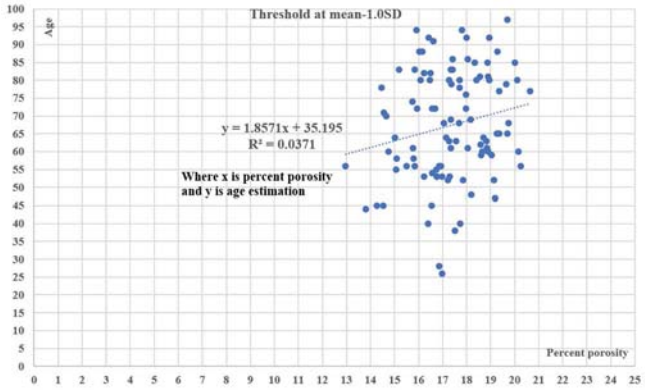


Fig. 3. Percent porosity and age used by mean – 1.0SD thresholding.

SUMMARY OUTPUT

Regression Statistics	
Multiple R	0.192593445
R Square	0.037092235
Adjusted R Square	0.027165351
Standard Error	15.3312478
Observations	99

ANOVA

	df	*SS*	*MS*	*F*	*Significance F*
Regression	1	878.2639499	878.2639499	3.736543565	0.056150683
Residual	97	22799.57443	235.0471591		
Total	98	23677.83838			

	Coefficients	*Standard Error*	*t Stat*	*P-value*	*Lower 95%*
Intercept	35.19458516	16.73390554	2.103190142	0.038037165	1.982414854
%m-1.0sd	1.857113361	0.960734507	1.933014114	0.056150683	-0.04967869

Fig. 4. Linear regression and ANOVA test.

A linear regression analysis was performed to establish the relationship between the porosity ratio and the precise age, and the resulting regression line was graphically represented "Fig. 4." [17]. Equations for estimating bone age based on porosity were derived from the regression analysis, incorporating the regression coefficients. Statistical procedures, including the F-test and analysis of variance (ANOVA), were employed in this study at a confidence level of 95% or significance level of $\alpha = 0.05$ "Fig. 4.". A linear equation connecting the percent porosity to the estimated age will be the final result. The formula will be written as $A = aP + b$, where P is the percent porosity and A is the predicted age. The slope and intercept of the linear equation are represented by the coefficients a and b, respectively. The results of the regression analysis, which include the R^2, will be presented. The range of the R^2 value is 0 to 1 ($0 \leq R^2 \leq 1$). The better the equation fits the data, the closer the R^2 number is to 1.

Furthermore, the accuracy of the age estimation equations was assessed by applying them to another set of bone specimens, evaluated by a separate user [19]. There are 10 bone specimens in this set. The outcomes and the error metrics will be contrasted with those of other research articles.

III. Results

The relationships between percent porosity and age were analyzed and plotted for each thresholding group. An example, depicted in "Fig. 3," illustrates the results obtained using the mean – 1.0 SD thresholding method. Linear

regression and ANOVA tests were performed for each thresholding group, with an additional example of the mean – 1.0 SD thresholding results presented in "Fig. 4.".

Table I. summarizes the relationships between percent porosity (P) and age estimation (A) for each thresholding group. The table also includes the regression coefficient (R^2) and p-value for these analyses.

TABLE I. TABLE TYPE STYLES

Threshold	Porosity & Age	R^2	P-value
Mean	A=1.261P+12.233	0.0318	0.0775
Mean–0.5SD	A=1.316P+30.493	0.0361	0.0598
Mean-1.0SD	A=1.857P+35.195	0.0371	0.0562
Mean-1.5SD	A=0.641P+61.212	0.0011	0.7398
Mean-2.0SD	A=-2.866P+79.543	0.0503	0.0256

The accuracy of the age estimation equations was evaluated by applying them to an additional set of 10 bone specimens. The same protocol was followed to determine the percent porosity for each specimen. The percent porosity values were then used in conjunction with the equations in Table I to estimate the ages. Age estimation errors and average errors were calculated for each thresholding group, with the average errors presented in Table II.

TABLE II. ACCURACY ASSESSMENT

Threshold	Average error (year)
Mean	12.9
Mean–0.5SD	13.5
Mean-1.0SD	13.9
Mean-1.5SD	12.9
Mean-2.0SD	13.0

The errors are the difference between the true age and the estimated age. They are the unit of years.

IV. DISCUSSION

The plotted results, as illustrated in "Fig. 3.", show a high degree of data dispersion, with very low regression values. This is because the porosity of human bones exhibits significant variation, even among individuals of the same age. Such variation is influenced by multiple factors, including genetics, environmental conditions, and lifestyle. As a result, the p-value occasionally reaches a significant level.

Threshold values at lower levels (mean – 2.0 SD) tend to be less reliable. This is because such thresholds approach the minimum pixel value. For example, if the mean is 120 and the standard deviation (SD) is 50, the threshold would be calculated as $(120 – 2.0 \times 50) = 20$. This value is very close to 0 on the grayscale range of 0 to 255.

From Table II., the average errors across all thresholding groups are relatively similar, ranging from 12.9 to 13.9. However, when considering the regression values and p-values, the threshold group using mean – 1.0 SD provides the most reliable results.

Using digital image processing techniques with a 95% confidence level, the average errors range from 12.9 to 13.9 years, as shown in Table II. These results are compared to expert age assessments, which typically have an error margin of ±10 years. Rissech (2006) demonstrated 89% accuracy in age estimation within 10-year intervals [7], supporting the acceptability of this research methodology.

The bone samples in this study are relatively aged, originating from body donations made between 2011 and 2019. The resulting age estimation equations could be further refined if more recent bone samples were available. Notably, the study includes only bones from individuals aged 30 and older, as younger bone donors are rare. Most donors passed away due to illness, which often leads to reduced bone strength.

The acetabulum has a cup-like shape, and imaging involves generating a two-dimensional representation of its three-dimensional structure. During imaging, it is essential to align the camera plane with the plane of the acetabulum. Misalignment at this stage introduces the first source of error. Subsequent steps compound these errors, ultimately increasing the overall margin of error.

One significant challenge is the cleanliness of the bones, as it directly affects pixel values and may lead to inaccuracies. However, cleaning the bones is not an option as it could compromise police evidence. Exploring alternative regions of the bone or using other parameters, such as shape, offers potential for reducing errors.

V. CONCLUSION

When considering the threshold values across all five groups, the average error values from Table II range from 12.9 to 13.9 years, showing no significant difference. The threshold value at mean - 1.0 SD is the most appropriate for practical application, as the equation describing the relationship between porosity and age yields a higher regression value ($R^2 = 0.0371$) and a lower p-value (p-value = 0.0562) compared to the other groups. Although the threshold at mean - 2.0 SD provides a higher regression value ($R^2 = 0.0503$) and a significantly lower p-value (p-value = 0.0256), the threshold value calculated for mean - 2.0 SD is very close to 0, within the grayscale range of 0 to 255.

The average error values obtained from Table II, when compared with age estimation from expert age assessments and other research studies [7], show no significant differences and are considered acceptable.

REFERENCES

[1] Evison, M.P., "Forensic anthropology and human identification," Handbook of Forensic Science, January 2009, pp.84-112.

[2] Wang, X. and Ni, Q., "Determination of cortical bone porosity and pore size distribution using a low field pulsed NMR approach," Journal of Orthopedic Research, Vol.21, 2003, pp.312-319.

[3] White, Tim D. et al, "Human Osteology," 3rd Ed., Elsevier Inc., 2012.

[4] Calce, E. S. and Rogers, T. L., "Evaluation of age estimation technique: testing traits of the acetabulum to estimate age at death in adult males," J. Forensic Sci. 56, 2011, pp.302–311.

[5] Calce, E.S., "A new method to estimate adult age-at-death using the acetabulum," Am. J. Phys. Anthropol. 148, 2012, pp.11–23.

[6] Khomkham, P. et al, "Association between age and acetabulum morphological changes in dry bones in the Thai population," Chiang Mai Med J, May 2017, 56(1), pp.21-28.

[7] Rissech, C. et al, "Using the acetabulum to estimate age at death of adult males," J Forensic Sci, Vol.51, No.2, March 2006, pp.213-229.

[8] Venara, A, et al, "Estimation of skeletal Age at Death in Adults Using the Acetabulum and the Auricular Surface," Anthropol 2: 113, 2013. doi:10.4172/2332-0915.1000113

[9] Gonzalez, Rafael C. and Woods, Richard E., "Digital Image Processing," 2nd Ed., Prentice-Hall Inc., 2002.

[10] Cieszko, M. et al, "Determination of bone porosity based on histograms of 3D μCT images," J mater Sci, Vol.50, 2015, pp.948-959.

[11] Kumar Pal, A. et al, "Porosity Estimation by Digital Image Analysis," Researchgate Publication, January 2019.

[12] Martin III, William D. at al, "Using Image Analysis to Measure the Porosity distribution of a Porous Pavement," Construction and Building Materials 48, 2013, pp.210-217.

[13] Otsu, N., "Threshold selection method from gray-level histograms," IEEE Trans Syst Men Cybern SMC 9, 1979, pp.62–66.

[14] Rajagopalan, S. et al, "Evaluation of thresholding techniques for segmenting scaffold images in tissue engineering," Proc SPIE 5370, 2004, pp.1456–1465.

[15] Rosenfeld, A. and Torre, P., "Histogram concavity analysis as an aid in threshold selection," IEEE Trans Syst Man Cybern SMC 2, 1983, pp.231–235.

[16] Daniel, Wayne W., "Biostatistics; Basic Concepts and Methodology for the Health Sciences," 9th Ed., John Wiley & Sons Inc., 2010.

[17] Navidi, W., "Statistics for Engineers and Scientists," 2nd Ed., McGraw-Hill, 2008.

[18] Buikstra, J. E. and Ubelaker, D. H., "Standards for data collection from human skeletal remains," Proceedings of a Seminar at The Field Museum of Natural History, Arkansas Archeological Survey Research Series No.44, 1994.

[19] Lovejoy, C. O. et al, "Multifactorial age determination of skeletal age at death: a method and blind tests of its accuracy," Am J Phys Anthropol;68, 1985, pp.1–14.

Recognition of Marijuana Plant Leaf Diseases Based on Deep Learning

Qingye Kong
Department of Telecommunications Engineering, School of Engineering, King Mongkut's Institute of Technology Ladkrabang
Bangkok, Thailand
495278775@qq.com

Siraphop Tooprakai
Department of Telecommunications Engineering, School of Engineering, King Mongkut's Institute of Technology Ladkrabang
Bangkok, Thailand
sirapop.to@kmitl.ac.th

***Abstract*—Plant pests and diseases are a common problem in agricultural production, and if not handled properly, they can seriously affect crop yield and quality. The era of the Internet of Things has arrived, and modern monitoring methods have also been applied to the growth monitoring of some crops, achieving good results. However, the cultivation of marijuana still relies mainly on traditional manual monitoring, and modern methods have not yet been widely used. At the same time, the prevention of diseases and pests in marijuana is the focus, and if problems are not detected early, the losses can often be severe. This article proposes using machine learning to screen for abnormal leaves and confirm whether the leaves are healthy. After repeated training, the system can compare and classify different images of marijuana leaves and identify abnormal parts. The system is designed based on python. The test results indicate that this technology can be applied to distinguish marijuana leaves to ensure early detection of diseases and pests, and to minimize agricultural losses caused by untimely remedial measures.**

Keywords— Marijuana, Deep Learning, Machine Learning, Plant diseases, Python

I. INTRODUCTION

The yield of crops is influenced by various factors. Among them, the proportion of losses caused by pests and diseases has always been a concern in agricultural production, and its loss rate varies depending on factors such as crop types and geographical environments. According to statistics, the overall loss rate of crop diseases and pests is about 10%. In some years with severe pests and diseases, the loss rate may reach 20% or even higher. Therefore, active prevention and control are crucial for ensuring a bumper harvest.

The leaves of plants are one of their most important organs, which can clearly reflect the growth status of plants. Observing leaves to determine the health of plants is a common method of crop health testing. With the rapid development and application of artificial intelligence and image recognition technology, detection methods are no longer limited to relying solely on visual observation. By installing surveillance cameras and taking pictures, real-time monitoring of plant status based on image recognition technology has become possible, and the system can quickly detect leaves with abnormal status [1] – [3].

Deep learning is an abbreviation for deep neural network learning methods [4], belonging to neural network structures [5]. It can automatically learn features from big data and use backpropagation based artificial neural networks to train and classify algorithms for samples [6]. The main content of this article is based on image analysis and plant species recognition to extract features of marijuana leaves [7]. Through extensive training of the system, it has acquired the ability to accurately identify diseased leaves, ensure timely treatment to ensure the healthy growth of plants. With the gradual maturity of deep learning technology [8], it has been widely applied in the agricultural field and achieved good results [9]. Disease and pest monitoring and plant health management are significant specific applications [10], [11].

II. RELATED INFORMATION

A. Literature Survey

The cultivation of medicinal marijuana is very common in Thailand. However, in this field, crop cultivation and maintenance mainly rely on traditional manual operations, and the application of modern planting and monitoring technologies is not widespread. For the management of marijuana pests and diseases, prevention is the core, and early detection of crop invasion by pests and diseases is a crucial task [12]. In the process of marijuana cultivation, maintaining the plant in a healthy state is the most important thing. If not dealt with in a timely manner, losses often cannot be recovered through remedial measures. Therefore, this article designs a marijuana disease and pest identification system built using Python. By using deep learning and image recognition technology, batch comparison of monitoring images of growing marijuana leaves is carried out to timely detect abnormal leaves, achieving the goal of early detection and processing, and minimizing the losses caused by pests and diseases.

B. Plant Diseases and Insect Pests

Marijuana diseases caused by pathogens and pests can have a significant negative impact on crop yield and quality. Early identification of disease symptoms is of great significance in protecting crops and reducing losses. According to the introduction of the agricultural professional knowledge service platform [13], there are about 33 known marijuana diseases. There are 16 types of fungal diseases, while the rest are caused by bacteria, nematodes, parasitic seed plants, and other reasons. Among them, wilt disease and sudden wilt disease are the main diseases causing dead

seedlings, with a death rate of 47.19% in severely affected plots. Phytophthora and Fusarium wilt are the main diseases causing dead plants during the adult stage, with a death rate of 36.52% in severely affected areas.

The impact of diseases and pests on marijuana cultivation can be profound, affecting plant health, yield, and overall crop quality. Diseases and pests can directly damage marijuana plants, leading to reduced flower and biomass production. This results in lower yields and potential financial losses for growers. Infestations or infections can compromise the quality of marijuana buds, affecting potency, aroma, and overall market value. Consumers often prefer high-quality, pest-free products. Severe infestations or infections may result in the loss of entire crops. This not only affects current yields but can also disrupt future planting schedules and revenue projections. Ultimately having a significant impact on production costs. Common marijuana pests and diseases include whiteflies, caterpillars, spider mites, white powdery mildew, etc. As shown in Fig. 1.



Fig. 1. Some diseases of marijuana. [14]

In recent years, deep learning, especially convolutional neural networks, has attracted widespread attention in the field of agriculture, such as plant detection [15], fruit detection [16], disease recognition [17], weed detection, pest recognition [18], etc. At present, various deep learning-based algorithms have been developed for the prevention and control of plant diseases. However, in the field of marijuana cultivation, there is relatively little research and literature related to it, so this study mainly focuses on this relatively blank direction.

III. SYSTEM DESIGN

In this research, we used monitoring cameras as the data acquisition medium. The collected images of marijuana leaves will be compared with the images in the Python system dataset and classified into normal and abnormal groups, respectively. When abnormal images appear, further inspection can be conducted by observing the images and entering the planting area.

A. Monitoring camera

The ordinary monitoring camera on the farm is a tool for capturing real-time images of crops. This is a basic, low-cost image acquisition device that has been widely used in the agricultural field. It is very easy to use, just capture leaves pictures at regular intervals. Due to the limitations of the system's computing power and storage space, the camera cannot capture images at high frequencies for comparison, but fortunately, the monitoring process does not need to be checked every minute.

B. Python system

Python was designed by Guido van Rossum of the Netherlands Institute for Mathematical and Computer Science Research in the early 1990s as a substitute for the ABC language. Python provides an efficient and advanced data structure, as well as simple and effective object-oriented programming. With the continuous updating of versions and the addition of new language functions, it is gradually used for the development of independent and large projects. Python interpreter is easy to extend, and new functions and data types can be extended using C language or C++.

Due to the simplicity, readability, and extensibility of the Python language, there is an increasing number of research institutions using Python for scientific computing, and many open-source scientific computing software packages provide Python calling interfaces. Therefore, the development environment composed of Python language and its numerous extension libraries is very suitable for engineering and scientific researchers to process experimental data, create charts, and develop scientific computing applications.

C. Program structure

Digitize the leaf images captured by the camera and input them into the system. To represent color images, we assign red, green, and blue channels to each pixel, with pixel values being vectors of three numbers ranging from 0 to 255 and standardize the dataset. Divide each row of the dataset by 255, so that the standardized data falls between [0,1]. By using multiple layers of loops, more accurate results can be obtained [19] – [21]. As shown in Fig. 2.

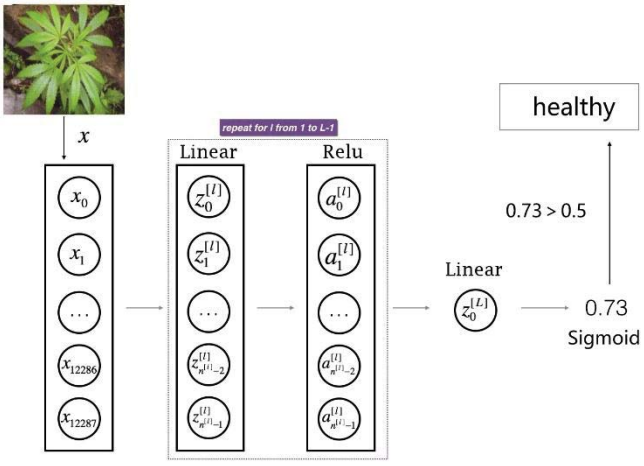


Fig. 2. Block diagram of the system.

After digitizing the image, input the data into a linear rectification system and start repeating the process for deep learning. The entire process can be roughly divided into five steps: (1) Initialize network parameters, (2) Forward propagation, (3) Rectified Linear Unit, (4) Reverse propagation, and (5) Output parameters. As shown in Fig. 3.

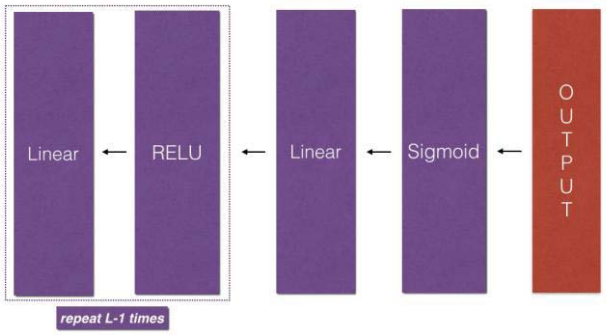


Fig. 3. Flowchart experiment and collect data.

IV. EXPERIMENT AND RESULT

The optimize function will output the learned w and b values. We can use w and b to predict the label of dataset X. Change the value of a to 0 (if active value<=0.5) or 1 (if active value>0.5). Then store the predicted value in prediction. J is the cost. The calculation formula for x and other parameters is:

$$z^{(i)}=w^{T}x^{(i)}+b \quad (1)$$

$$y\hat{}^{(i)}=a^{(i)}=\text{sigmoid}(z^{(i)}) \quad (2)$$

$$L(a^{(i)},y^{(i)})=-y^{(i)}\log(a^{(i)})-(1-y^{(i)})\log(1-a^{(i)}) \quad (3)$$

$$J=1/m\sum L(a^{(i)},y^{(i)}) \quad (4)$$

The structure of propagation is shown in Fig. 4.

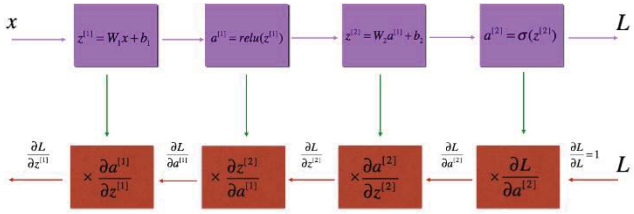


Fig. 4. Forward and backward propagation.

Integrate all these functions into a model () function. At that time, we only need to call a model () to basically complete other things. And we could achieve other results while changing the rate. As shown in fig. 5. It shows that the cost is falling, parameters are being learned.

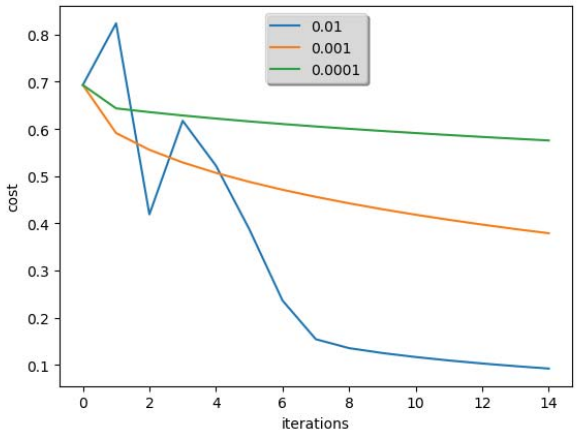


Fig. 5. Costs in different learning rates.

Based on different cost values, extensive training was conducted, resulting in different outcomes. At a cost value of 0.01, a 99.52% accuracy rate was achieved. As shown in Fig. 6.

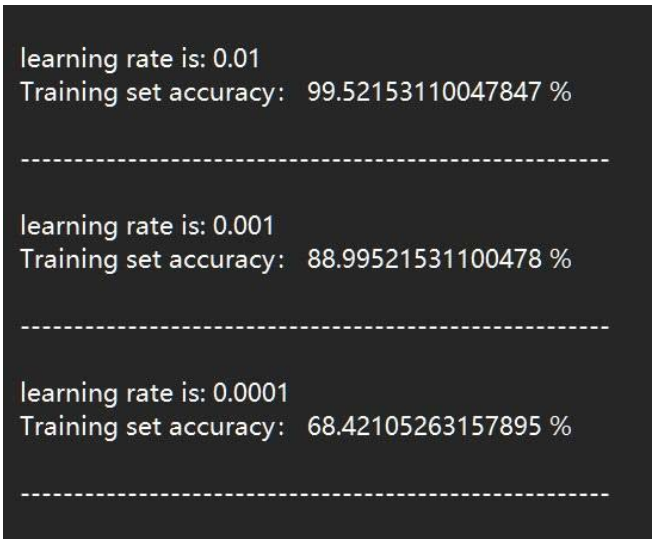


Figure. 6. Training set accuracy in different learning rates.

Compared with the monitoring effect of other different plants [16],[23]-[25], this accuracy can be satisfactory. As shown in Figure. 7.

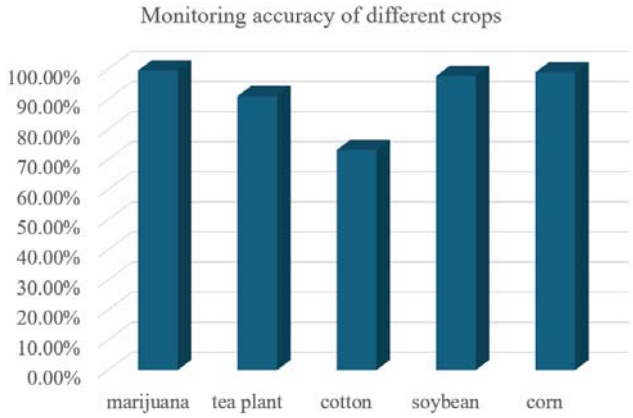


Figure. 7. Monitoring accuracy of different crops.

V. CONCLUSION

Marijuana is an important industry in Thailand. In this study, based on convolutional neural networks, through model testing, data augmentation, and training optimization, the prediction accuracy of the training set ultimately exceeded 99%. Therefore, the proposed method contributes to manual identification and fills the gap in the field of digital pest control of marijuana. On the other hand, due to different monitoring and photography times, the weather can also change, and the accuracy of the training cannot reach 100%, there is still a possibility of a small amount of result errors. In addition to further optimizing the model, it is still necessary to conduct basic patrols at regular intervals. A combination of multiple preventive measures is necessary to achieve the most ideal growth state of plants and ultimately achieve a bountiful harvest. Unfortunately, this system can only detect abnormal marijuana leaves and cannot determine the

classification of pests and diseases. I hope to have the ability to optimize designs and make blade monitoring technology more refined in the future. In the future, templates based on deep learning can be better applied to all aspects of people's lives, solving various problems. The unique ability of this model can be applied to new fields, ultimately achieving industrial innovation, providing more convenience for our daily lives, and ushering society into the digital age.

REFERENCES

[1] M. KUMAR, S. GUPTA, X. GAO, AND A. SINGH, "Plant Species Recognition Using Morphological Features and Adaptive Boosting Methodology," IEEE, November 2019.

[2] J. HUIXIAN, "The Analysis of Plants Image Recognition Based on Deep Learning and Artificial Neural Network," IEEE, April 2020.

[3] A. BAKHSHIPOUR, "Cascading Feature Filtering and Boosting Algorithm for Plant Type Classification Based on Image Features," IEEE, June 2021.

[4] X. YANG, A. CHEN, G. ZHOU, J. WANG, W. CHEN, Y. GAO, AND R. JIANG, "Instance Segmentation and Classification Method for Plant Leaf Images Based on ISC-MRCNN and APS-DCCNN," IEEE, August 2020.

[5] P. S. KANDA, K. XIA, AND O. H. SANUSI, "A Deep Learning-Based Recognition Technique for Plant Leaf Classification," IEEE, November 2021.

[6] V. K. GAJJAR, A. K. NAMBISAN, AND K. L. KOSBAR, "Plant Identification in a Combined-Imbalanced Leaf Dataset," IEEE, April 2022.

[7] N. MEHBOOB, H. E. Z. FARAG, AND A. M. SAWAS, "Energy Consumption Model for Indoor Cannabis Cultivation Facility," IEEE, June 2020.

[8] S. M. HASSAN AND A. K. MAJI, "Plant Disease Identification Using a Novel Convolutional Neural Network," IEEE, January 2022.

[9] R. RANI, J. SAHOO, S. BELLAMKONDA, S. KUMAR, AND S. K. PIPPAL, "Role of Artificial Intelligence in Agriculture: An Analysis and Advancements with Focus on Plant Diseases," IEEE, December 2023.

[10] M. S. H. SHOVON, S. J. MOZUMDER, O. K. PAL, M. F. MRIDHA, N. ASAI, AND J. SHIN, "PlantDet: A Robust Multi-Model Ensemble Method Based on Deep Learning for Plant Disease Detection," IEEE, April 2023.

[11] K. M. HOSNY, W. M. EL-HADY, F. M. SAMY, E. VROCHIDOU, AND G. A. PAPAKOSTAS, "Multi-Class Classification of Plant Leaf Diseases Using Feature Fusion of Deep Convolutional Neural Network and Local Binary Pattern," IEEE, June 2023.

[12] Smart Agriculture, "Marihuana disease," [Online]. Available: https://www.pwsannong.com/c/2016-04-13/550949.shtml

[13] Smart Agriculture, "Marihuana disease," [Online]. Available: https://www.pwsannong.com/c/2016-04-13/565118.shtml

[14] Agricultural articles, "Common Cannabis Plant Diseases Caused by Pests, Insects, Viruses and Basic Treatment Methods," [Online]. Available: https://growstuffshop.com/%E0%B9%82%E0%B8%A3%E0%B8%84%E0%B9%83%E0%B8%99%E0%B8%95%E0%B9%89%E0%B8%99%E0%B8%81%E0%B8%B1%E0%B8%8D%E0%B8%8A%E0%B8%B2-bible-part-1

[15] SUNIL C. K., JAIDHAR C. D., AND N. PATIL, "Cardamom Plant Disease Detection Approach Using EfficientNetV2," IEEE, December 2021.

[16] N. FARAH, N. DRACK, H. DAWEL, AND R. BUETTNER, "A Deep Learning-Based Approach for the Detection of Infested Soybean Leaves," IEEE, September 2023.

[17] T. B. PUN, A. NEUPANE, R. KOECH, AND K. J. OWEN, "Detection and Quantification of Root-Knot Nematode (Meloidogyne Spp.) Eggs from Tomato Plants Using Image Analysis," IEEE, November 2022.

[18] M. H. SALEEM, J. POTGIETER, AND K. M. ARIF, "A Performance-Optimized Deep Learning-Based Plant Disease Detection Approach for Horticultural Crops of New Zealand," IEEE, August 2022.

[19] C. MADHURYA AND E. A. JUBILSON, "YR2S: Efficient Deep Learning Technique for Detecting and Classifying Plant Leaf Diseases," IEEE, December 2023.

[20] K. P. A. RANI AND S. GOWRISHANKAR, "Pathogen-Based Classification of Plant Diseases: A Deep Transfer Learning Approach for Intelligent Support Systems," IEEE, June 2023.

[21] A. TABBAKH AND S. S. BARPANDA, "A Deep Features Extraction Model Based on the Transfer Learning Model and Vision Transformer 'TLMViT' for Plant Disease Classification," IEEE, May 2023.

[22] D. S. JOSEPH, P. M. PAWAR, AND K. CHAKRADEO, "Real-Time Plant Disease Dataset Development and Detection of Plant Disease Using Deep Learning," IEEE, January 2024.

[23] Z LIU, R BASHIR, S IQBAL, M SHAHID, M TAUSIF, AND Q UMER, "Internet of Things (IoT) and Machine Learning Model of Plant Disease Prediction—Blister Blight for Tea Plant," IEEE, April 2022.

[24] S NOON, M AMJAD, M QURESHI, AND A MANNAN, "Handling Severity Levels of Multiple Co-Occurring Cotton Plant Diseases Using Improved YOLOX Model," IEEE, December 2022.

[25] M MASOOD, M NAWAZ, T NAZIR, A JAVED, R ALKANHEL, H ELMANNAI, S DHAHBI, AND S BOUROUIS, "Maize Net: A Deep Learning Approach for Effective Recognition of Maize Plant Leaf Diseases," IEEE, May 2023.

Advanced Car Rental System: Integrating Blockchain, AI, and Real-Time Inventory Management for Enhanced User Experience

Sokyna Alqatawnah
School of Computing
Department of Health Sciences, Meditech and Technology
Bradford College
Bradford, UK
S.alqatawnah@bradfordcollege.ac.uk

Muhammad Tayyib
School of Computing
Department of Health Sciences, Meditech and Technology
Bradford College
Bradford, UK
10591601@bradfordcollege.ac.uk

***Abstract*— This paper presents an innovative peer-to-peer car rental application that integrates blockchain and AI technologies to revolutionise the car rental industry. The aim of the project is to simplify and streamline vehicle rentals for both hosts and renters, with particular attention to addressing challenges faced by younger drivers. The application features a robust user management system, advanced search functionalities, an easy-to-use booking system, and real-time mapping capabilities. Through extensive market research, these features were tailored to meet the specific needs of users, allowing them to find rental vehicles based on criteria such as age, location, and cost. Results demonstrate that the application successfully provides enhanced user satisfaction, security, and convenience for all stakeholders. Overall, this project sets a new benchmark for convenience, trust, and innovation in the car rental industry.**

Keywords—Vehicle fleet management, revenue optimisation, blockchain integration, AI in car rentals, Peer-to-Peer car rental, Real-time inventory management.

I. Introduction

The car rental industry has witnessed significant growth in recent years, driven by increased demand from sectors like travel and tourism, which require convenient transportation options. Traditional car rental services, however, are often expensive, involve extensive paperwork, and have limited rental options, especially for younger drivers. These limitations can discourage potential customers from opting for rentals.

The COVID-19 pandemic further exacerbated these challenges, with companies like Hertz suffering massive layoffs and a significant stock drop due to reduced demand and new health protocols [1]. This disruption has underscored the need for more flexible, accessible, and cost-effective rental solutions.

This project presents a peer-to-peer car rental platform developed to address these challenges. By leveraging modern technologies such as blockchain for secure transactions and artificial intelligence (AI) for customer support, the platform aims to simplify and streamline the vehicle rental process. Users can rent cars directly from other individuals, offering flexibility and cost-effectiveness, particularly for younger drivers who often face barriers with traditional rental services.

Optimising fleet management and pricing are critical to improving car rental services. As noted by [2], effective fleet and revenue management can lead to significant improvements in both operational efficiency and profitability. This project incorporates such optimisation strategies by allowing dynamic pricing and enabling a more flexible, peer-to-peer approach.

Moreover, the application features a user-friendly interface, with functionalities including a robust user management system, advanced search capabilities, a straightforward booking process, and real-time vehicle tracking. These features were developed based on extensive market research, ensuring that the platform meets the needs of its target users and sets a new standard for convenience and efficiency in the car rental industry.

II. Literature Review

A. Revenue Models

Guerriero and Olivito [3] discuss the application of revenue management techniques in the car rental industry, specifically addressing how rental companies can optimise revenue by dynamically assigning cars to different categories based on customer demand. This research is relevant to the developed application as it provides insights into optimising rental transactions, which aligns with the application's objective to create an efficient, user-centric rental system. By incorporating features such as flexible pricing and vehicle categorisation, this system aims to optimise the rental process, ensuring both renters and hosts have a seamless experience.

B. Health & Safety

The COVID-19 pandemic significantly impacted the car rental industry, with many businesses experiencing massive revenue losses due to reduced demand and new health protocols. Nhamo et al. [4] highlight the need for improved health and safety measures, such as contactless car rentals. The platform incorporates such features, including real-time updates on vehicle availability and a contactless hiring process, to ensure the safety of both increased focus on health and safety in the post-pandemic era.

C. Market Trends

Research by [5] and [6] emphasise the need for innovative car rental solutions that focus on user convenience and flexibility. The developed application builds on these trends by implementing a peer-to-peer model, allowing users to rent vehicles directly from other individuals rather than relying on traditional rental agencies. This approach minimises third-party intervention, reducing costs and enhancing the

979-8-3315-4248-1/25/$31.00 ©2025 IEEE

flexibility and accessibility of car rentals, particularly for younger drivers who often face challenges with traditional services.

D. Technology

The potential of blockchain technology in the car rental industry has been explored by [7] and [8], who demonstrate how blockchain can enhance trust by eliminating the need for middlemen and enabling secure cryptocurrency-based transactions. The platform integrates blockchain technology to provide secure payments and transaction records, ensuring transparency and trust for both renters and hosts. The use of smart contracts in the platform guarantees that all transactions are automated, secure, and transparent, reducing the administrative burden and increasing the overall trust in the system.

E. User Experience and Interface Design

Dhanalaxmi et al. [9] and Koh et al. [10] discuss the importance of security features and user-centric design in mobile applications. This system incorporates seamless security measures and a user-friendly interface, ensuring that the app is accessible and intuitive for all users, regardless of their technological expertise. By prioritising user experience, the platform fosters trust and usability, making it easier for users to navigate the platform, book rentals, and engage with other users in a secure and efficient manner.

III. Methodology

Both qualitative and quantitative research methodologies were employed to inform the development of the platform. Qualitative methods included in-depth interviews with car owners and regular rental customers to gather detailed insights into their experiences with traditional car rental systems. This helped identify common pain points, preferences, and expectations users have when renting vehicles. The quantitative research involved surveys and analysis of existing user data, such as booking times, vehicle types, rental durations, and costs, to better understand patterns and trends in the rental market. The combination of these methodologies provided a comprehensive understanding of user needs and informed the design decisions for the platform.

The platform incorporates blockchain technology to handle secure transactions, offering transparency and reliability in payment processing. Additionally, AI is employed in the form of an intelligent customer support chatbot, which provides real-time assistance to users, enhancing the overall user experience by promptly addressing queries and concerns.

The user interface of the platform was designed with usability and accessibility in mind. It was intended to be intuitive and easy to navigate, ensuring a smooth user experience for all types of users. Key functionalities, such as registration, sign-in, booking system, and vehicle tracking, were included to make the rental process as seamless as possible.

Fig. 1 illustrates the sequence diagram of this car rental system, showing how key components interact throughout the booking and payment process.

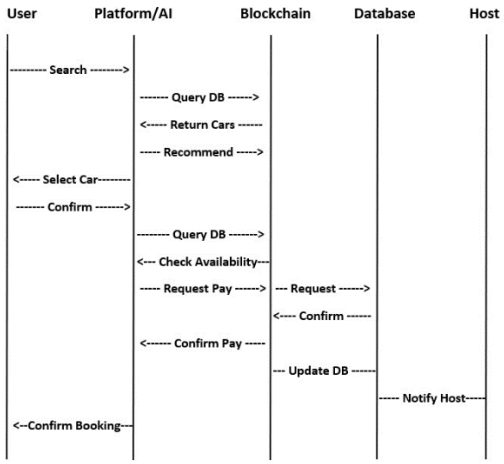


Fig. 1. Sequence diagram of the proposed car rental system

IV. Discussion

The analysis of the results obtained from early testing and user feedback showed that the features presented significantly enhanced the overall functionality, security, and user experience, setting the platform apart in the competitive car rental market.

A. Operational Efficiency

The integration of blockchain technology and AI within the platform greatly enhances operational efficiency. The use of blockchain ensures secure, decentralised transactions, providing users with transparency in rental agreements and payments. By automating processes such as contract execution and payment processing through Ethereum-based smart contracts, the platform reduces human intervention, lowers administrative costs, and ensures that all transactions are tamper-proof and traceable.

AI further contributes to operational efficiency through its dynamic pricing and recommendation engine, which automatically adjusts rental prices based on market demand and availability. The system uses machine learning models to predict demand trends, optimising both revenue for hosts and fairness for renters. This seamless integration of AI and blockchain enhances the overall functionality of the platform, creating a more efficient and secure rental system for both users and service providers.

B. User Experience

The user centric design of the platform, combined with its intuitive interface, contributed significantly to positive user feedback. Early users were able to easily navigate the platform, upload their vehicles, and manage bookings with minimal effort. The simplicity of the user interface was a key factor in facilitating the seamless experience, ensuring that both novice and experienced users could interact with the system effortlessly.

Additionally, the AI-powered chatbot, was particularly well-received. Users appreciated the immediate responses to their queries, which significantly enhanced their experience, as it reduced the need for direct human interaction and sped up issue resolution.

The vehicle recommendation engine, based on Collaborative Filtering and Content-Based Filtering, also added value by offering personalised suggestions based on rental history and preferences. This made the rental process not only quicker but also more tailored to each user's needs, leading to increased user satisfaction.

C. Fleet Management and Optimisation

A critical component of the platform is its innovative approach to fleet management, which optimises vehicle availability and enhances the rental process for both hosts and renters. The system allows for real-time tracking of all vehicles listed on the platform, ensuring that renters can quickly find available cars that meet their specific needs. Additionally, the platform uses dynamic allocation strategies to ensure that vehicles are distributed based on demand patterns, reducing idle time for hosts and improving accessibility for renters. This approach not only makes the rental process more efficient but also ensures that vehicle owners can maximise the usage of their cars, improving profitability.

Through the seamless integration of real-time inventory management, the platform effectively prevents double bookings and keeps track of each vehicle's status, further increasing the reliability of the system. Ultimately, this fleet management solution contributes to a more sustainable and flexible car rental experience, setting the platform apart from traditional rental services that often struggle with inventory management and vehicle allocation.

D. Scalability

The platform demonstrated impressive scalability during testing. Built using a microservices architecture, it is capable of handling an increasing number of users and transactions without compromising performance. This architecture allows the system to scale horizontally, adding more resources as demand rises, without impacting the overall stability of the platform.

Load balancing algorithms, ensure that incoming traffic is evenly distributed across the servers, optimising system performance even under high user load. Furthermore, the use of Redis caching to store frequently accessed data, such as vehicle availability and user search results, greatly reduced server load and latency. These enhancements ensure that the platform can maintain a fast, responsive user experience even as the user base grows.

V. Conclusion

The project successfully developed an innovative peer-to-peer car rental application that is both cost-effective and accessible to drivers of all ages. By addressing significant limitations within the traditional car rental industry, such as high fees, unexpected costs, excessive paperwork, limited vehicle availability in smaller towns and cities, and age restrictions, the platform provides a convenient and valuable solution. The integration of AI and Blockchain technology enhances the platform's ability to address these issues, offering users greater convenience, transparency, and trustability.

The platform shows substantial potential for further development, allowing it to thrive in the competitive car rental industry. Ongoing research and optimisation will focus on refining key features such as the AI-driven customer support system and Blockchain security measures, ensuring that the platform not only meets but surpasses industry standards.

References

[1] Goldstein, M., "Hertz car rental suffers massive layoffs, stock drop from COVID-19 pandemic," Forbes, 2020. Available: https://www.forbes.com/sites/michaelgoldstein/2020/04/24/covid-19-creates-massive-layoffs-stock-drop-for-hertz-car-rental/

[2] Oliveira, B.B., Carravilla, M.A. and Oliveira, J.F., "Fleet and revenue management in car rental companies: A literature review and an integrated conceptual framework," Omega, vol. 71, pp. 11–26, 2017. doi: https://doi.org/10.1016/j.omega.2016.08.011

[3] Guerriero, F. and Olivito, F., "Revenue models and policies for the car rental industry," Journal of Mathematical Modelling and Algorithms in Operations Research, vol. 13, no. 3, pp. 247–282, 2013. doi: https://doi.org/10.1007/s10852-013-9234-8

[4] Nhamo, G., Dube, K., and Chikodzi, D., "Impact of COVID-19 on global car rental industry and ride and share transport services," Counting the Cost of COVID-19 on the Global Tourism Industry, vol. 6, pp. 159–181, 2020. doi: https://doi.org/10.1007/978-3-030-56231-1_7

[5] Kumar, M., "Online vehicle rental system to enhance commutation," IEEE Conference Publication, 2021. doi: https://doi.org/10.1109/iscaie51753.2021.9431820

[6] Ahmed, F.Y.H., Hazlan, E.B. and Abdulla, M.I., "Enhancement of mobile-based application for vehicle rental," IEEE 11th IEEE Symposium on Computer Applications & Industrial Electronics (ISCAIE), pp. 55, 2021. doi: https://doi.org/10.1109/iscaie51753.2021.9431820

[7] Hassija, V., "Cryptober: A blockchain-based secure and cost-optimal car rental platform," IEEE Conference Publication, 2019. Available: https://ieeexplore.ieee.org/abstract/document/8844943

[8] Sonakshi and Verma, S., "A blockchain-based secure car hiring system," Lecture Notes on Data Engineering and Communications Technologies, pp. 341–349, 2021. doi: https://doi.org/10.1007/978-981-16-3961-6_29

[9] Dhanalaxmi, B., Sainath, K., Saikiran, B. and Varaganti, S., "An user-friendly android based application for online rental system," IEEE Xplore, 2021. doi: https://doi.org/10.1109/I-SMAC52330.2021.9641012

[10] Koh, C.Y. and Ramli, S.N., "Car rental application with GPS tracking for mileage detection," Applied Information Technology and Computer Science, vol. 2, no. 2, pp. 260–274, 2021. Available: https://publisher.uthm.edu.my/periodicals/index.php/aitcs/article/view/2532

Indoor Object Detection for Autonomous Mobile Robots (AMRs) Using YOLOv5s and Grad-CAM

1st Nafiz Fahad
Faculty of Information Science and Technology (FIST)
Multimedia University
Jalan Ayer Keroh Lama 75450, Bukit Beruang, Melaka, Malaysia
NAFIZ.FAHAD@student.mmu.edu.my

2nd, * Md. Jakir Hossen
Faculty of Engineering and Technology (FET)
Multimedia University
Jalan Ayer Keroh Lama 75450, Bukit Beruang, Melaka, Malaysia
jakir.hossen@mmu.edu.my

3rd Md. Shohel Sayeed
Faculty of Information Science and Technology (FIST)
Multimedia University
Jalan Ayer Keroh Lama 75450, Bukit Beruang, Melaka, Malaysia
shohel.sayeed@mmu.edu.my

***Abstract*—Indoor object detection is crucial for autonomous mobile robots (AMRs) to navigate properly. This study integrates YOLOv5s, a lightweight and real-time object detection model, with Gradient-weighted Class Activation Mapping (Grad-CAM) for improved transparency in decision-making. A dataset comprising 10 indoor object classes was utilized, with 1,012 training, 230 validation, and 107 test images. Key optimizations such as pruning, quantization, and model width scaling were employed to enhance efficiency while maintaining detection performance. Results revealed an overall mAP@0.5 of 0.457, with "cabinet door" achieving a high mAP of 0.807, while rare classes like "pole" and "opened door" exhibited mAPs of 0.084 and 0.039, respectively. Grad-CAM visualizations highlighted critical regions influencing model predictions, enhancing interpretability. Performance metrics, including F1 scores and precision-recall curves, demonstrated the trade-offs between precision and recall. Despite challenges with underrepresented classes, this study showcases the potential of YOLOv5s and Grad-CAM for interpretable and efficient indoor object detection, addressing both computational and real-time demands in resource-constrained environments.**

Keywords—Indoor Object Detection, Autonomous Mobile Robots, Yolov5s, Grad-CAM, Precision

I. Introduction

In the era of Autonomous Mobile Robots (AMRs), accurate indoor object detection is essential for effective navigation and task execution. YOLOv5s, a streamlined variant of the YOLO (You Only Look Once) family, has gained prominence for its real-time object detection capabilities, making it particularly suitable for resource-constrained environments [1] [2]. However, the complexity of deep learning models like YOLOv5s often renders them opaque, posing challenges in understanding their decision-making processes. To address this, integrating Gradient-weighted Class Activation Mapping (Grad-CAM) provides visual explanations by highlighting regions within an image that significantly influence the model's predictions [3].

Recent studies have limitations for object detection models in indoor environments. For instance, Aulia et al. (2024) study's limitation is they used the small and geographically constrained dataset of fewer than 500 images from Banda Aceh, which restricts the generalizability of the object detection model to other environments and lighting condition [4]. On the other hand, Espinac et al. (20130 study lies in its reliance on object detection as the basis for scene recognition. This dependency renders the approach ineffective in scenarios where objects are sparse, occluded, or undetectable, thereby restricting its applicability in diverse and complex indoor environments.

II. Methods

This study employs a dataset based on an obstacle detection dataset that can be found on GitHub [27, 28] and consists of 10 object classes: door, opened door, cabinet door, refrigerator door, window, chair, table, cabinet, sofa/couch, and pole. It includes 1.012 training, 230 validation, and 107 test images [29]. The dataset is described in detail in Figure 2, which presents the statistics of the three sets, in vertical bar plots that visually illustrate the data distribution in each case. Furthermore, a YAML file was utilized in this work to define paths for the training, validation, and test datasets, as well as the number of classes and the corresponding class names.

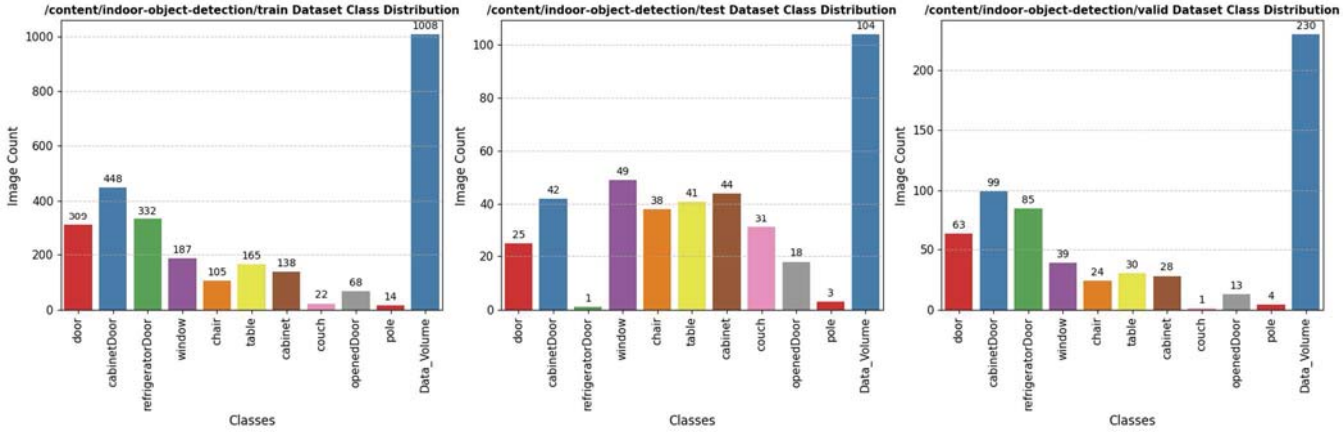


Fig. 1. Dataset Description.

Deep learning architectures have advanced significantly in recent years, making them a primary solution for unsolvable tasks. Indoor object detection for AMR is crucial, which is why this current study suggests building an indoor object

XXX-X-XXXX-XXXX-X/XX/$XX.00 ©20XX IEEE

detection system using yolov5s with gradcam. The system being suggested is built using the one-stage neural network "YOLO v5". YOLO v5 architecture is very similar to YOLO v4 architecture but with some minor modifications. YOLO v5 architecture presents new modifications in the architecture that contributed to enhancing the speed and detection accuracy while reducing the network computation complexity. This architecture uses a new backbone that changes the features process as well as optimizations techniques. This architecture proposes a set of new efficient techniques that enhance the training process. Also, it modified the detection head which enhanced the accuracy. This architecture applies different data augmentation tech niques to enhance the generalization of the model for different applications and tasks. YOLO v5 applies the use of photometric distortion techniques to adjust brightness, contrast noise, saturation, and so on. The geometric distortion technique was applied by using flipping, rotation, scaling, and image cropping. It also applies many other data augmentation techniques as mix-up techniques and cut_mix techniques. All the used data augmentation techniques are used to increase the model's robustness against data corruption. Early CNN models used the dropout technique to prevent the network from overfitting. This technique is applied to fully connected layers as it presents the most network portion that presents neurons and requires huge computation resources. However, this technique cannot be applied to the convolution layers. For this, in YOLO v5 the drop block technique is proposed. So, instead of dropping single neurons, a block of neurons with a fixed size is dropped. The drop block method was introduced to combat the major drawback of dropout being dropping features randomly which proved to be an effective strategy for fully connected networks but less fruitful when it comes to convolutional layers wherein features are spatially correlated. Fig. 2 provides the drop block technique process compared to the dropout technique.

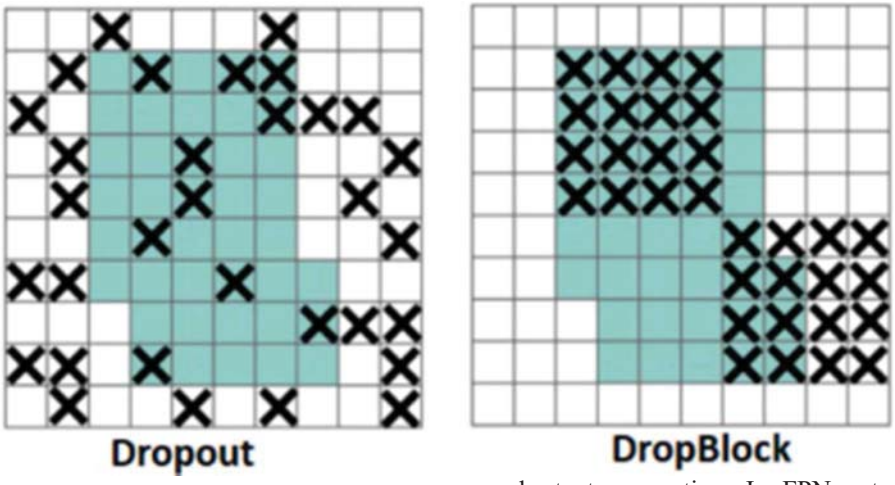


Fig. 2. Difference between dropout and drop block techniques [7].

Another strength point in the YOLO v5 architecture is the activation function. It applies the use of a sigmoid weighted linear unit (SILU). This function is calculated as mentioned below in equation 1:

$$f(x) = x\sigma(x) \quad (1)$$

YOLO v5 architecture proposes a new backbone which reduces the training problems, reduces the model complexity and ensures that the designed model can run efficiently on devices with resource constraints. A cross-stage partial network CSPNet [26] was adopted to obtain useful features of the input images. The time processing of this backbone has improved a lot. The YOLO v5 architecture You can break it down into three main parts:

-Network backbone.
- Network neck.
- Network head.

Model backbone: the CSPNet-based backbone was adopted. The goal is to facilitate a gradient combination in the network architecture to potentially minimize the computation and thus, improve the speed. To ensure this, the input features map is partitioned into two sections. Then, it combines them through the cross-stage hierarchy. The CSPNet allows the gradient to flow along multiple routes. By switching from transition to concatenation, the gradient information in such kind causes an enormous correlation difference. CSPNet has shown a significant decrease in the computation loading and the accuracy are also excepted higher, in other words, inference speed can be improved. The CSPNet brings three major benefits with the application of these techniques:

• Increasing the learning ability of the CNN model.
• Reduce the computation complexity.
• Reduce memory costs.

Model neck: The first stage of the model is a neck that is used to generate a pyramid of features over the input image allowing the model to detect the target objects in scales. Neck model allows the network to detect various objects at various sizes and crowded scales. YOLO v5 generates the features pyramid [27] based Path Aggregation Network (PAN). This network added a new shortcut connection that facilitates the easier flow of low-layer features to the upper levels. The PAN network is a Feature Pyramid Network (FPN) with a changed shortcut connection. In FPN network spatial information have to go through (red path) but in PAN a smaller number of layers have to process the spatial information to reach to the top layers (green path). Now, PAN collects the feature information by adding all the previous layers to the current layer. Fig. 3 gives the architecture of PAN network.

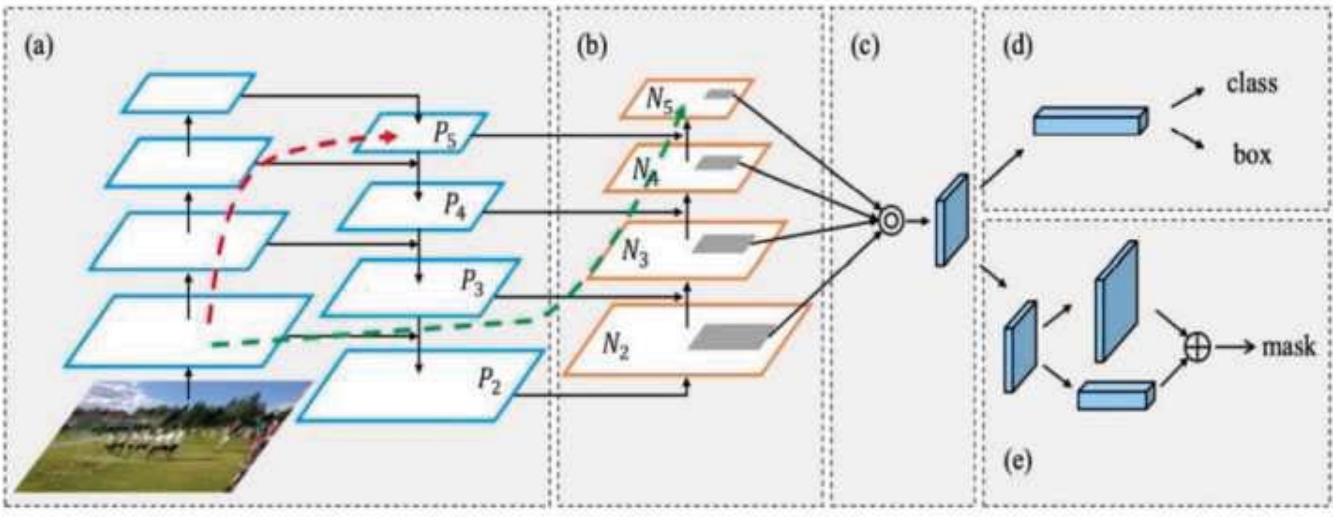


Fig. 3. Difference between dropout and drop block techniques [7].

The second strength of YOLO v5 network is the focus module where the input image is sliced into four small images and then concatenated to enable the convolution operation. YOLO v5 architecture implements automatic algorithm for bounding boxes anchors learning that calculates the anchor boxes size on different image sizes and scales and greatly affects the detection accuracy. The Generalized Intersection over Union (GIOU) is adopted to calculate the regression loss as presented in the following Eq. (2).

$$L_{GIoU} = 1 - IOU + \frac{|CB\cup|}{|C|}$$

Where:

- $B^{gt}$is the ground truth bounding box.
- B is the predicted bounding box.
- IOU (Intersection over Union) is defined as:

$$IOU = \frac{B \cap B^{gt}}{B \cap B^{gt}}$$

C is the smallest enclosing box covering both the predicted box B and the ground truth box B_{gt}.

CBU likely refers to the area difference between C and $B\cup B^{gt}$, accounting for the penalty in GIoU.

GIOU provides a more comprehensive evaluation of bounding box predictions by considering both overlap and extent, leading to improved object localization, shape robustness, and evaluation consistency. These advantages make it a popular choice in the computer vision community for various tasks involving object detection and localization.

Network head: for the detection process, YOLO v5 performs a 1 × 1 convolution at three scales to detect objects at three scales (small, medium, and large). Fig. 4 provides the detailed architecture of YOLO v5 adopted in the proposed work.

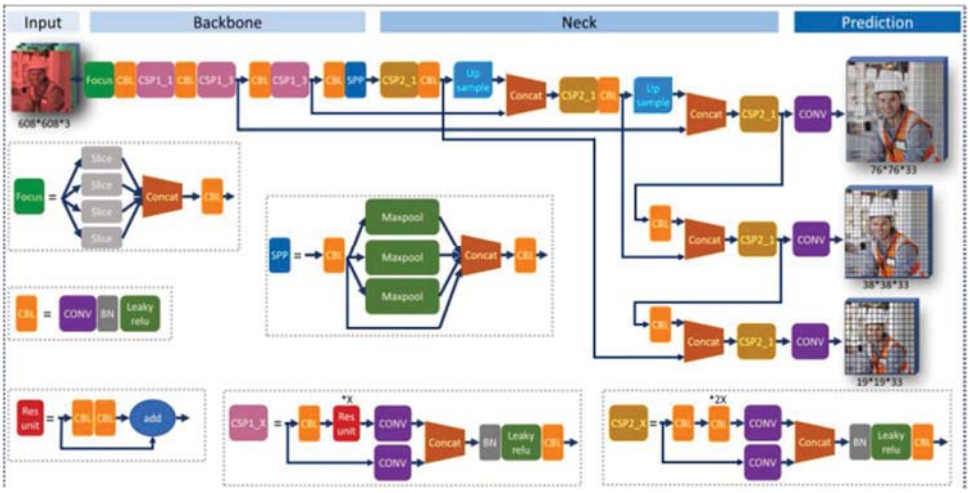


Fig. 4. Architecture of yolo v5s [7].

To create a more lightweight version of YOLO v5 suitable for deployment on embedded devices with limited memory, we suggest modifying the model's number of output channels. This adjustment significantly affects both the computational complexity and memory usage of the model. To achieve this, we implemented model width scaling. YOLO v5 is available in various versions, including YOLO v5l, YOLO v5m, YOLO v5s, and YOLO v5x. Among these, YOLO v5x offers the highest detection accuracy, while YOLO v5s is the fastest in terms of performance.

In the proposed implementation, we used the same model depth as in the YOLO v5s version (0.33) and we changed the model width from 0.5 in YOLO v5 to 0.33 in the proposed work. By applying the model width scaling techniques, we

ensured a big drop in the model complexity as well as high speed for the model processing time. Moreover, Other optimizations and compression techniques are used to guarantee a lightweight implementation in embedded systems. In this context, we applied pruning and quantization techniques. Additionally, channel pruning strategy [28] was applied, which tries to pick the important channels that contribute to model accuracy while eliminating the useless channels. The pruning technique was utilized following the completion of training. The post-training channels pruning technique has been applied based on two steps: first, the channel selection algo rithm has been applied based on the regression loss. By using this technique, the relevant channels are maintained while the weak chan nels are removed. Secondly, the feature maps of each layer are recon structed using the least square method. After this, a fine-tuning of the pruned model is applied to recover the model's accuracy.

The second technique applied to reduce the size of the model is the post-training quantization technique [29]. It is applied to transform the activation and the weights representation from 32 bits floating points to 2 bits fixed points. After the training process, the quantization technique was applied to the model and the straight-through estimator method [30] was used for fine-tuning to improve accuracy.Additionally, this current study intregrated YOLOv5s model with Grad-CAM to enhance interpretability. Grad-CAM generates heatmaps highlighting critical image regions influencing predictions. This combination ensures high detection performance while providing visual explanations, improving transparency and model understanding for deployment on resource-constrained devices.

III. Result

The YOLOv5s model was evaluated to assess its object detection performance across multiple metrics, including F1-Score, Precision, Recall, and Confidence. Figure 5 shows (a) F1 Confidence curve, (b) Precsion- Recall curves, (c) Precision Confidence Curve, (d) Recall confidence curve of yolo v5s model. Moreover, the F1-Confidence Curve revealed a peak F1-score of 0.351 at a confidence threshold of 0.38, indicating a balanced trade-off between precision and recall. The Precision-Recall Curve demonstrated a mean Average Precision (mAP) of 0.457 at an IoU threshold of 0.5, with high precision for classes such as CabinetDoor (0.807) and Couch (0.995), but lower performance for classes like OpenedDoor (0.039) and Pole (0.084). The Precision-Confidence Curve showed that the model achieved maximum precision of 1.00 at a confidence level of 0.985, highlighting the model's strong prediction reliability at higher confidence thresholds. Conversely, the Recall-Confidence Curve indicated the highest recall of 0.82 at a confidence threshold of 0.0, suggesting that while the model detects most objects at low confidence, it may include more false positives. These comprehensive results demonstrate the YOLOv5s model's effectiveness in detecting specific object classes while identifying areas for potential improvement in detecting more challenging classes.

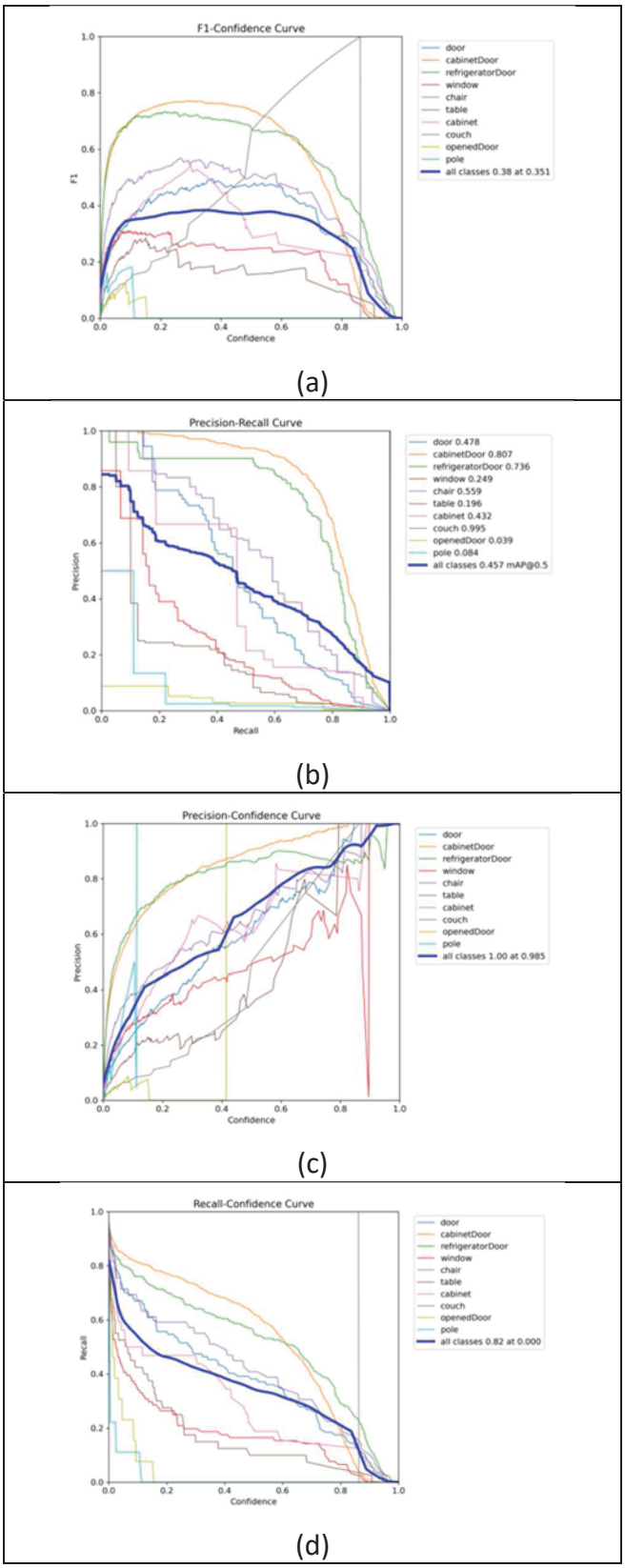


Fig. 5. (a) F1 Confidence curve, (b) Precsion- Recall curves, (c) Precision Confidence Curve, (d) Recall confidence curve of yolo v5s model.

Figure 6 illustrates two confusion matrices evaluating the performance of the YOLOv5s model. Confusion Matrix (a) presents the raw count of correct and incorrect predictions for each object class. The model demonstrates strong performance in detecting CabinetDoor with 92 correct predictions and Couch with the highest detection at 99 correct

classifications. Similarly, RefrigeratorDoor is correctly identified 73 times, and Door is detected 48 times, although with some misclassifications. However, the model struggles with detecting OpenedDoor and Pole, with only 3 and 8 correct detections, respectively, indicating weaker performance for these classes. In contrast, Confusion Matrix (b) shows the normalized classification rates, offering a clearer comparison across classes. The model achieves a 92% accuracy rate for CabinetDoor and an impressive 99.5% for Couch. RefrigeratorDoor follows with 73.6% accuracy, while Door achieves a moderate 47.8%. However, detection rates drop significantly for OpenedDoor at 3.9% and Pole at 8.4%. Overall, the YOLOv5s model excels in recognizing distinct objects like CabinetDoor and Couch but requires improvement in identifying more challenging classes such as OpenedDoor and Pole.

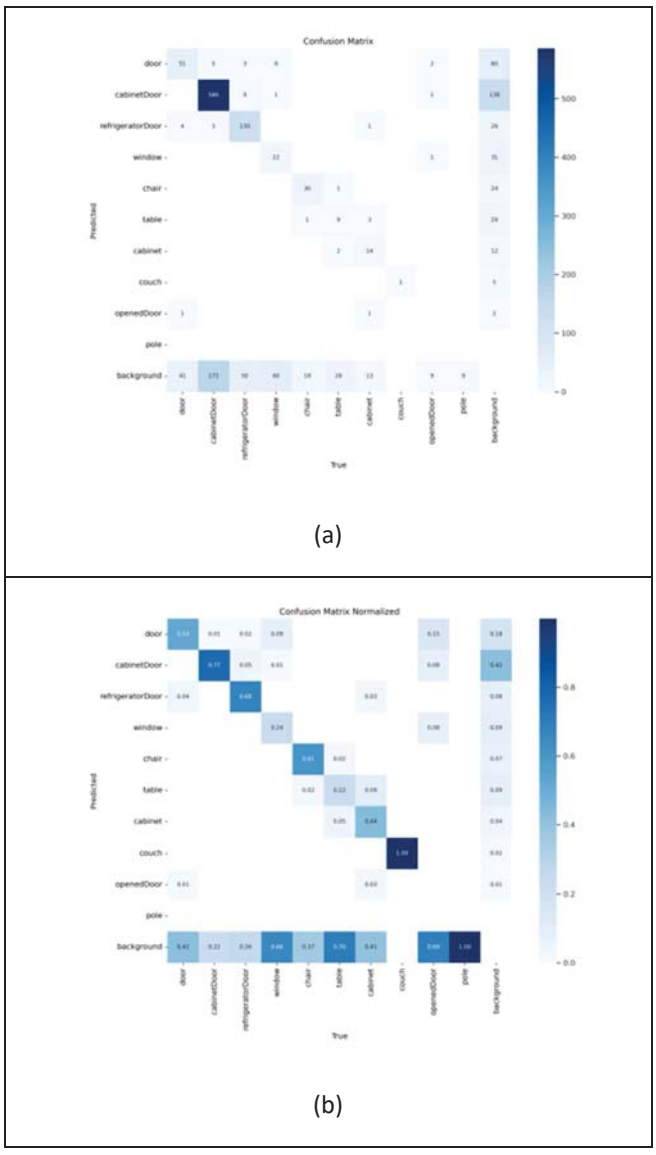


Fig. 6. (a) Raw Confusion Matrix Showing Actual Prediction Counts (b) Normalized Confusion Matrix Showing Classification Accuracy (%) for Each Class for yolo v5s model.

Fgure 7 illustrates the training and validation performance of the YOLOv5s model over 25 epochs, highlighting key metrics that reflect the model's optimization and evaluation. The training losses show significant improvement, with the box loss decreasing steadily from 2.8 to approximately 0.1, indicating better localization accuracy. Similarly, the classification loss drops from around 2.5 to nearly 0.05, reflecting improved object classification, while the objectness loss reduces from about 2.3 to below 0.05, suggesting increased confidence in object detection. The validation losses follow a similar trend, with the box loss decreasing from 1.4 to nearly 0.1, the classification loss falling from 1.2 to around 0.05, and the objectness loss dropping from 1.0 to less than 0.05, confirming effective generalization to unseen data. In terms of performance metrics, the model's precision (B) improves to around 0.65, while recall (B) steadily increases to approximately 0.75. The mean Average Precision (mAP) at 0.5 IoU rises to about 0.65, and the mAP@0.5:0.95 improves from near 0.1 to around 0.45, indicating robust detection performance across varying IoU thresholds. Overall, the steady decline in losses and the improvement in precision, recall, and mAP scores demonstrate the YOLOv5s model's effective learning process and strong object detection capabilities.

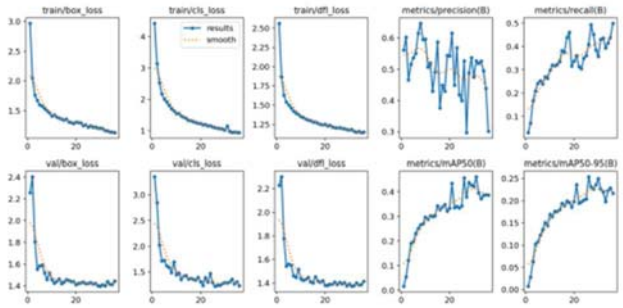


Fig. 7. Training and Validation Performance Metrics of the YOLOv5s Model.

Figure 8 demonstrates the YOLOv5s model's object detection process using Grad-CAM visualization. Image (a) shows the original input featuring a room with furniture, while image (b) presents the Grad-CAM heatmap overlay. The red-highlighted regions on the sofa indicate areas where the model focused most for object detection, enhancing interpretability by revealing how the model identifies and classifies objects.

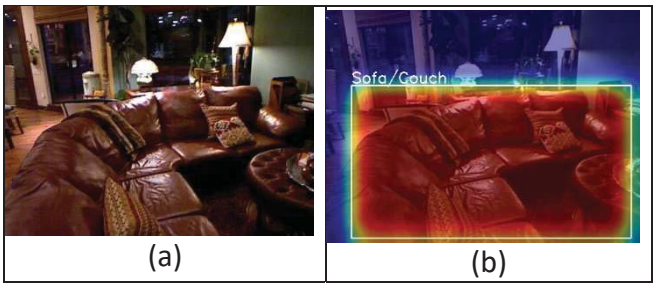


Fig. 8. (a) Orginal Image and ((b) Grad-CAM Visualization of YOLOv5s Model Highlighting Object Detection Regions

IV. Conclusion and Future Rssearch

This study highlights the effectiveness of YOLOv5s and Grad-CAM in addressing indoor object detection challenges, particularly for resource-constrained autonomous mobile robots. YOLOv5s achieved an overall mAP@0.5 of 0.457, demonstrating strong detection performance for common classes like "cabinet door" and "refrigerator door," while

Grad-CAM added a valuable layer of interpretability by visually highlighting influential image regions that guided model predictions. Optimization techniques, including pruning, quantization, and model width scaling, enabled the deployment of a lightweight, efficient detection system suitable for embedded devices, ensuring real-time performance. However, challenges in detecting rare or visually complex classes, such as "pole" and "opened door," were observed, attributed to dataset imbalances and object complexities. The study underscores the importance of balancing precision, recall, and interpretability in designing object detection systems and emphasizes the need for comprehensive datasets and robust models to generalize across diverse indoor environments. While this implementation advances efficient object detection, future research should focus on incorporating larger datasets, addressing class imbalances, and exploring more sophisticated interpretability tools to further enhance model robustness and applicability.

ACKNOWLEDGMENT

The authors want to thanks Multimedia University, Malaysia.

REFERENCES

[1] Farooq, M. U., Eizad, A., & Bae, H. K. (2023). Power solutions for autonomous mobile robots: A survey. *Robotics and Autonomous Systems*, *159*, 104285.

[2] Jaiswal, S. K., & Agrawal, R. (2024). A Comprehensive Review of YOLOv5: Advances in Real-Time Object Detection. *International Journal of Innovative Research in Computer Science & Technology*, *12*(3), 75-80.

[3] Kirchknopf, A., Slijepcevic, D., Wunderlich, I., Breiter, M., Traxler, J., & Zeppelzauer, M. (2022). Explaining yolo: leveraging grad-cam to explain object detections. *arXiv preprint arXiv:2211.12108*.

[4] Aulia, U., Hasanuddin, I., Dirhamsyah, M., & Nasaruddin, N. (2024). A new CNN-BASED object detection system for autonomous mobile robots based on real-world vehicle datasets. *Heliyon*, *10*(15).

[5] Espinace, P., Kollar, T., Roy, N., & Soto, A. (2013). Indoor scene recognition by a mobile robot through adaptive object detection. *Robotics and Autonomous Systems*, *61*(9), 932-947.

[6] Atitallah, A. B., Said, Y., Atitallah, M. A. B., Albekairi, M., Kaaniche, K., & Boubaker, S. (2024). An effective obstacle detection system using deep learning advantages to aid blind and visually impaired navigation. Ain Shams Engineering Journal, 15(2), 102387.

[7] Atitallah, A. B., Said, Y., Atitallah, M. A. B., Albekairi, M., Kaaniche, K., & Boubaker, S. (2024). An effective obstacle detection system using deep learning advantages to aid blind and visually impaired navigation. *Ain Shams Engineering Journal*, *15*(2), 102387

"Sell in May & Go Away" [for 6 Months] Versus Other 6-Month Intervals – the Philippine Stock Exchange Index (PSEi)

Jackylyn L. Beredo
College of Computer Studies
De La Salle University
Manila, Philippines
jackylyn.beredo@dlsu.edu.ph

Kainam Thomas Wong
College of Computer Studies
De La Salle University
Manila, Philippines
kainam.wong@dlsu.edu.ph

Jonathan Paul C. Cempron
College of Computer Studies
De La Salle University
Manila, Philippines
jonathan.cempron@dlsu.edu.ph

Joel P. Ilao
College of Computer Studies
De La Salle University
Manila, Philippines
joel.ilao@dlsu.edu.ph

***Abstract*—The seasonal investment strategy of "sell in May and go away" is statistically tested against other six-month contiguous intervals. That is, instead of only investing from November through April, this paper is the first in the entire finance literature to statistically evaluate other 6-month intervals of January-June, February-July, etc. This paper finds that, for the PSEi over 2005-2023, the adage could empirically be improved as "April adios; reenter October".**

***Index Terms*—calendar anomalies, econometrics, Halloween strategy, market efficiency, seasonal anomalies, seasonal effect, stock market anomalies.**

I. Introduction

The stock market allegedly underperforms from May to October (during the "summer months" shown in Figure 1) relative to November to April (during the "winter months" shown in Figure 2). If so, an investor could sell stocks at the start of May (or during late spring), hold the proceeds in cash, and then reinvest in November (or in late autumn) – this is the market-timing strategy of "sell in May and go away, come back on St. Leger's Day."

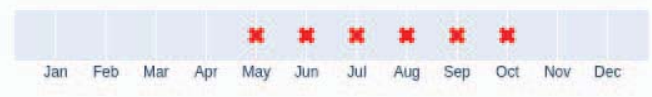


Fig. 1. The "sell in May and go away, come back on St. Leger's Day" strategy's dis-invested

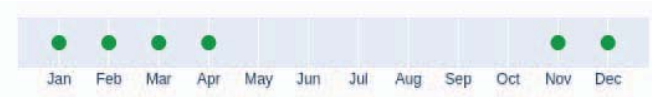


Fig. 2. The "sell in May and go away, come back on St. Leger's Day" strategy's invested

979-8-3315-4248-1/25/$31.00 ©2025 IEEE

This adage originated in London's financial district, where St. Leger's Day referred to a horse race in September of each year. In the U.S., the period corresponds roughly to Memorial Day (i.e., the last Monday in May) and Labor Day (i.e., the first Monday in September). This is also known as the "Halloween strategy," as Halloween lies on October 31.

This seasonality draws much attention from investment-themed mass media. For example, the American CNBC.com website has published articles on it every year starting from 2011 through 2024 (except 2022), with over half a dozen in 2024 alone.

This seasonal tendency seems statistically valid, at least for the past half-century in 1970-2023: The S&P 500 Index gains an average of 6.5% over November-April versus 1.6% over May-October [1]. The S&P 500 rises during November-April for 77% of the years, but during May-October for only 2/3 of the years. Worldwide, one study detects this seasonality in 36 out of the 37 countries studied, especially strong in the most developed markets (e.g., Canada, Japan, UK, US, Japan, and most European countries). This seasonality has been empirically studied in numerous scholarly papers, among which [2] - [10] statistically analyzed the Philippine stock market data and confirmed this seasonality for the Philippines.

A natural question is whether other six-month intervals (instead of the six standard months of November to April) are statistically even more advantageous. There are (obviously) 12 such six-month intervals if only whole months are considered. Please see Figure 3; each row/color corresponds to a different contiguous interval of six months. Surprisingly, no research paper has ever explored this issue – until this present paper. This paper is the first in the research literature to compute the stock-market return for the 12 different possible intervals of six contiguous whole months.

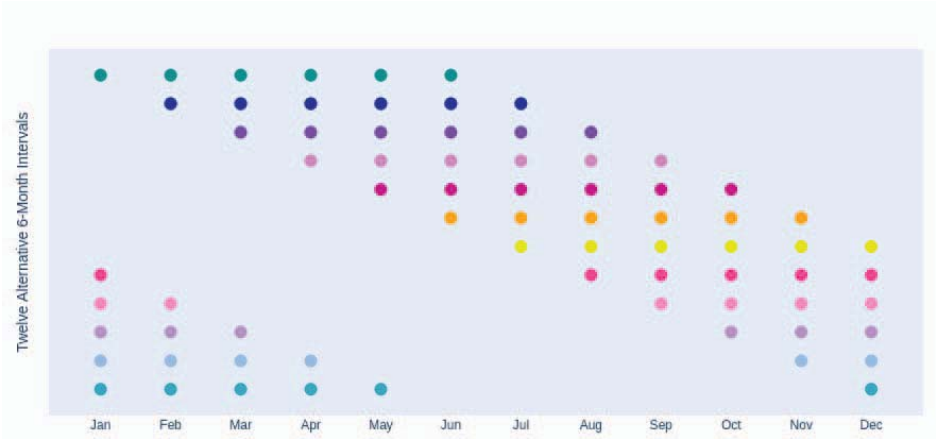


Fig. 3. Twelve alternative 6-month contiguous intervals to stay in the market

TABLE I
THE PSEI RETURNS DURING VARIOUS CONTIGUOUS PERIODS OF SIX WHOLE MONTHS

Year	**Jan-Jun**	**Feb-Jul**	**Mar-Aug**	**Apr-Sep**	**May-Oct (the adage's dis-investment period)**	**Jun-Nov**	**Jul-Dec**	**Aug-next Jan**	**Sep-next Feb**	**Oct-next Mar**	**Nov-next Apr (the adage's invest-ment period)**	**Dec-next May**	**May-Oct's ranking among the 12 six-month possible periods that started in this year**
2005	5.56	-0.96	-6.88	-0.65	5.69	8.83	8.93	7.26	9.61	13.07	15.83	9.35	5^{th} worst
2006	3.95	11.44	8.92	16.43	19.29	21.44	36.89	35.49	32.66	25.30	20.76	24.61	5^{th} worst
2007	22.74	8.09	9.71	11.53	14.93	2.99	-1.07	-6.72	-6.99	-16.46	-26.85	-20.99	11^{th} worst
2008	-32.07	-21.09	-14.12	-13.91	-29.05	-30.27	-23.87	-29.18	-30.35	-22.70	7.81	21.19	5^{th} worst
2009	30.18	53.33	54.05	41.01	38.27	27.44	25.21	5.53	5.53	12.89	13.12	7.48	9^{th} worst
2010	10.48	16.04	17.17	29.68	29.75	20.81	24.56	13.26	5.62	-1.10	1.19	7.36	12^{th} worst
2011	2.14	16.03	15.45	-1.37	0.33	-0.79	1.88	3.97	12.63	27.70	20.05	20.9	3^{rd} worst
2012	20.00	13.35	6.10	4.67	4.26	10.79	10.79	17.62	29.35	28.08	30.35	24.49	1^{st} worst
2013	11.23	6.35	-9.62	-9.58	-6.87	-11.58	-8.90	-9.01	5.76	3.83	1.86	7.07	6^{th} worst
2014	16.21	13.63	9.74	13.29	7.57	9.73	5.64	12.02	9.64	9.03	6.92	3.92	4^{th} worst
2015	4.62	-1.82	-8.17	-13.18	-7.53	-8.62	-8.10	-11.42	-6.03	5.34	0.35	6.85	6^{th} worst
2016	12.14	19.07	16.73	5.06	3.43	-8.38	-12.26	-9.21	-7.39	-4.17	3.46	15.57	6^{th} worst
2017	14.66	10.90	10.35	11.76	9.19	5.32	9.12	9.30	6.49	-2.34	-6.53	-9.17	7^{th} worst
2018	-15.95	-12.46	-7.31	-8.81	-8.68	-1.72	3.79	4.37	-1.91	8.85	11.38	8.17	4^{th} worst
2019	7.15	0.48	3.56	-1.79	0.31	-2.90	-2.31	-10.5	-14.93	-31.60	-28.54	-24.55	9^{th} worst
2020	-20.57	-17.67	-13.31	10.20	10.93	16.32	15.01	11.54	15.48	9.87	0.74	-2.40	8^{th} worst
2021	-3.33	-5.18	0.89	7.91	10.73	8.64	3.20	17.41	6.65	3.60	-4.58	-5.92	11^{th} worst
2022	-13.58	-14.21	-9.95	-20.30	-8.58	0.09	6.68	7.56	-0.42	13.21	7.66	-4.47	5^{th} worst
2023	-1.50	-2.97	-5.81	-2.75	-9.83	-3.92	-0.28	0.83	12.46	9.21	12.17		1^{st} worst
This six-month period's average ranking over the years	6.6^{th} worst	6.7^{th} worst	6.1^{th} worst	6.2^{th} worst	6.2^{th} worst	5.8^{th} worst	6.4^{th} worst	6.5^{th} worst	6.6^{th} worst	7.1^{th} worst	6.8^{th} worst	6.5^{th} worst	6.2^{th} worst

II. The Numerical Findings

This statistical study focuses on the Philippine Stock Exchange Index (PSEi), which ranks among the world's top 40 stock markets by capitalization. The stock-market data here was collected from Eikon[1].

This paper is the first in the research literature to compute the stock-market return for the 12 different possible intervals of six contiguous whole months. The numerical findings are presented in Table I. Therein, each row refers to a different calendar year, and each column relates to a different interval of six contiguous whole months. The green column shows the November-April returns when the investor should stay, according to the seasonal strategy of "sell in May and go away, come back on St. Leger's Day." In contrast, the red column shows the May-October return when the investor supposedly should stay away from the stock market; these six months' ranking from the bottom is shown in the far-right column.

Referring to the far-right column of Table I, the adage's May-to-October standard dis-investment period gave the worst return in the PSEi for only 1 of the 19 years examined but produced the best two returns during 4 of these 19 years.

Over the 19 years of 2005-2023, the adage's May-to-October standard dis-investment period is not the worst-performing six months for the PSEi, but "only" among the 4 worst, all of which lie within March-to-November. The dishonor of the worst-performing six-month period goes to June-November, a one-month delay from the adage's May-to-October standard dis-investment period.

Furthermore, the November-to-April period was not the best-performing six-month period but averaged as the third-best or fourth-best. The highest-return six-month duration, on average over 2005-2023, was October to March for the PSEi. Hence, "April adios, reenter October"!

References

[1] R. Watts," How Accurate Is Sell In May And Go Away?" Forbes, May 12, 2023.
[2] S. Bouman and B. Jacobsen. "The Halloween indicator, "sell in May and go away": Another Puzzle." Financial Times, vol. 92, no. 5, pp. 1618-1635, December 2002.
[3] K. S. Haggard and H. D. Witte. "The Halloween effect: trick or treat?." International Review of Financial Analysis, vol. 19, no. 5, pp. 379-387, 2010.
[4] S. C. Andrade, V. Chhaochharia, and M. E. Fuerst. "Sell in May and go away" just won't go away." Financial Analysts Journal, vol. 69, vol. 4, pp. 94-105, 2013.
[5] K. Borowski, "Analysis of sell-in-May-and-go-away strategy on the markets of 122 equity indices and 39 commodities." International Journal of Economics and Finance, vol. 7, no. 12, pp. 119-129, November 2015.
[6] K. S. Haggard, J. S. Jones, and H. D. Witte. "Black cats or black swans? Outliers, seasonality in return distribution properties, and the Halloween effect." Managerial Finance, vol. 41, no. 7, pp. 642-657, 2015.
[7] D. Waggle and P. Agrrawal, "Is the "sell in May and go away" adage the result of an election-year effect?" Managerial Finance, 2018.
[8] G. Magnusson, "It is not SAD if you sell in May: seasonal effects in stock markets revisited." International Economic Journal, vol. 33, no. 4, pp. 585-604, 2019.
[9] C. Y. Zhang and B. Jacobsen. "The Halloween indicator, "Sell in May and Go Away": everywhere and all the time." Journal of International Money and Finance, vol. 110, no. 102268, 2021.
[10] H. Ocal, S. Imre, and A. A. Kamil, "The "sell in May" effect: an empirical analysis from Turkey, Indonesia, France, and Germany," Hong Kong Journal of Social Sciences, vol. 58, pp. 239-252, Autumn/Winter 2021.

[1] https://eikon.refinitiv.com/

Improving Children's Reading And Writing Abilities By Utilizing Augmented Reality

Suzanna
Information Systems Department,
Binus Online Learning
Bina Nusantara University
Jakarta, Indonesia
suzanna001@binus.ac.id

Harco Leslie Hendric Spits Warnars
Computer Science Department,
BINUS Graduate Program,
Doctor of Computer Science,
Bina Nusantara University
Jakarta, Indonesia
spits.hendric@binus.ac.id

Mahaning Indrawaty Wijaya
Information System Departement,
Bina Nusantara University
Jakarta, Indonesia
mahaning.wijaya@binus.ac.id

Diana
Information System Departement,
Bina Nusantara University
Jakarta, Indonesia
diana009@binus.ac.id

***Abstract*— When children begin their early education, it is crucial for them to learn the alphabet and develop word formation skills. During this stage, not all children are fluent in reading and writing. Some children may learn at a slower pace, while others may experience health issues related to the brain, such as dyslexia. In a study we conducted in Cipanas, Cianjur Regency, West Java, we discovered that several fourth-grade elementary school students were not yet proficient in reading and writing. We aimed to highlight the importance of supporting individuals with dyslexia. Our research explored various theories, concepts, and designs for developing Augmented Reality (AR) applications that could motivate children to practice reading and writing. To enhance children's reading skills, we proposed creating a mobile learning application that utilizes AR technology. Through AR, dyslexic students can learn to read the alphabet and improve their writing skills. Additionally, this study compares traditional learning methods with AR-based approaches for teaching reading and writing to students with dyslexia. The results of our experiments indicate that AR significantly facilitates the learning process for dyslexic students compared to traditional educational methods.**

Keywords — Dyslexia, Augmented Reality, Mobile Application, Technology learning

I. INTRODUCTION (*DYSLEXIA AND AR*)

When a child enters the early stages of an educational environment, the ability to learn the alphabet and then acquire word formation skills is needed. At this stage, not all children are fluent in reading and writing. Some are naturally slow but then can gradually, but there are also those who experience health problems in the brain stem so that they experience dyslexia [1]. Dyslexia is a condition where someone has difficulty learning, especially difficulty in learning to read, write, spell and speak due to nerve disorders in the part of the brain stem that functions to process language [2]. Nervous disorders in this part of the brain experienced by someone cause a decrease in the ability to process language so that dyslexics have difficulty identifying words [3].

Symptoms of dyslexia in each child can vary depending on age and severity[8]. In general, these symptoms will be seen after the child enters school age because at this phase the child begins to learn to read and write. Children who experience dyslexia tend to be slow in learning the names of the alphabet and sounds, difficulty remembering letters and numbers, slow in speaking and spelling, writing backwards, difficulty remembering things, difficulty in counting, difficulty distinguishing certain letters, slow in doing tasks and difficulty in concluding something [4]. In fact, dyslexia is not only experienced by children, but also adults. According to the literature review found, it is known that dyslexia does not affect a person's intelligence, but even so, dyslexia can still be overcome. In fact, there is now a lot of support for dyslexics to remain successful in school and work. It is not true that dyslexics are considered to have below average intelligence [5]. In several studies that have been conducted, it is known that dyslexia does not affect a person's intelligence. Most dyslexics manage to grasp lessons and information using special methods [6]. From a review of previous studies, there are several studies that have been conducted with the aim of helping the interaction process between children with dyslexia and computer technology to be more productive. Several studies need to prepare special software that is appropriate so that users can do it [4]. There are also those that provide educational content in the form of games. In this study, an application development will be carried out for dyslexics using Augmented Reality (AR) technology to learn the alphabet and compose words using downloadable cards. This card is used as a marker in AR to describe certain letters and subjects. Why does this study use AR? One of the main reasons is that AR is very simple, users do not need headsets, glasses, or other additional equipment. All that is needed is a cell phone with a device camera and an AR application. Almost everyone today has a cell phone so it does not require additional costs. Then AR is an immersive technology that makes its users get an unforgettable experience and this is very helpful in the learning process for people with dyslexia [7]. The existence of two-way and real-time interaction helps users

feel the interaction so that they do not feel bored when learning.

II. LITERATURE REVIEW

Numerous studies in literature examine applications designed to enhance reading skills through augmented reality (AR) and the use of AR for teaching basic writing skills. Typically, research efforts focus separately on reading and writing with AR, making discussions about the integration of both practices relatively rare. The ability to read and comprehend the material is fundamental for all readers [9]. This skill involves an active process that connects prior knowledge and experiences with new information gleaned from the text, allowing for meaningful understanding[10]. For school students, enhancing their capacity to comprehend and draw inferences from both academic and non-academic texts is crucial for fostering critical thinking and improving their quality of life [11]. Consequently, teachers and educators continually seek ways to promote and develop children's reading comprehension skills. As children embark on their reading journey, they must learn to grasp reading as an unseen internal process. Researchers investigate its components and methods to enhance children's understanding [12]. Various studies identify four essential elements of comprehension: word-level processes, prior knowledge, motivation and attitudes, and reader strategies [13]. To bolster children's reading skills, a variety of techniques may be employed; for instance, incorporating illustrations and animations into texts can aid in vocabulary comprehension, while leveraging technology such as AR can enhance reading motivation [14].

From the results of the literature study [15], there are two well-known pedagogical programs for minimizing the symptoms of children with dyslexia, namely [16]:

a. Model from Myklebust and Johnson, they suggest an intervention model with the following basic principles:
   - Personalized or tailored teaching.
   - Look at the child's condition first and then create a balanced program.
   - It is necessary to pay attention to the child's level of development and level of tolerance.
   - There needs to be consideration of the nature and type of problem.
   - A multi-sensory system that suits its purpose.
   - Integration in the teaching section.
   - Special attention is needed for children in terms of the development of verbal and non-verbal areas.

b. Gilingham and Stillman's Visual-Auditory-Kinesthetic Model.
   - This model can be adapted to the circumstances of the problems faced and taught in various ways. The condition is that it must be repeated every day for at least 2 years in a pleasant environment.
   - Things that must be prepared are vocal practice cards for reading and spelling, word cards and a series of verbal stories and intense practice regarding syllable forms, and the use of a dictionary [17].

Based on our review of the literature, we found that augmented reality (AR) is a promising direction for future research. There are several reasons for this: (1) AR can address the specific needs of users. (2) Many potential applications of AR systems in education, business, industry, and other fields remain unexplored. (3) AR offers immersive experiences that can greatly enhance user engagement. Numerous studies have demonstrated the positive impact of AR experiences on students.

The rapid growth of information and communication technology and the magnitude of the informatization process of society are the main factors that identify the need for change in education [18]. Mobile apps allow us to connect the world around us with digital information. Therefore, applications like this are widely used in museums, research and educational institutions. Augmented Reality (AR) applications offer an intuitive way to provide contextual and local-specific information to users [13].One approach that is widely used in developing augmented reality mobile applications is the use of visual markers. Visual bookmarks used in AR applications allow users to “animate” information associated with the bookmark. Applications that use bookmarks allow users to read information about a particular object or its location using a mobile device [6].

III. APPLICATION OF AR IN DYSLEXIA STUDENT’S

A. *Concept*

In this study, AR technology is used to overcome dyslexia because currently AR is a developing field, it can provide interactive and interesting experiences that can help dyslexics improve their reading, writing skills, and hone their comprehension in a unique way. Here are some strategies used for dyslexics using AR technology:

1. Interactive Visual Learning: AR can enhance learning by transforming static text into dynamic and visually appealing content. By overlaying virtual objects onto the real world, AR can turn reading into a multisensory experience.
2. Real-time Text Feedback and Support: Some AR apps can provide real-time feedback as students read or write, helping them correct mistakes quickly.
3. Game-based Learning Experiences: Gamification has been shown to increase engagement in learning, especially for students with learning disabilities.
4. Multisensory Learning: AR can combine visual, auditory, and tactile cues to enhance learning for students with dyslexia: Haptic feedback and AR-enhanced books.
5. Personalized Learning Environments. AR technology can be tailored to an individual’s specific learning needs. For example: Customizable font styles and sizes. Dyslexia-friendly fonts such as “Open Dyslexic” can be integrated into AR systems to reduce reading difficulties. Then there is the customized feedback loop. AR apps can adapt to a learner’s progress and provide targeted practice, focusing on the areas where the learner struggles the most.
6. Collaborative Learning Opportunities. AR can facilitate peer-to-peer or teacher-to-student interactions in an immersive learning environment, allowing dyslexic learners to collaborate or receive one-on-one tutoring.

B. Design

To develop augmented reality (AR) applications, it's essential to have various stages for building animations. The project faces several limitations and constraints, particularly regarding time management. Based on the literature review, the 3D Pipeline Production model is effective for creating animations, as it can deliver high-quality rendering while maintaining efficient rendering times.



Fig 2. 3D Pipeline Production

1. Pre-Production Stage

This stage involves the planning, design, and research necessary for the entire 3D project. It is crucial, as it lays the groundwork for ideas and production plans, creating an overview of the project to be developed. The activities to be undertaken are:

1) Requirement Planning

In this phase, all essential information and theories regarding Augmented Reality (AR) are gathered. This includes concepts, hardware, software, and the various types of AR, along with applications that have been implemented across different fields.

2) Idea Development

The central concept of AR is to present physical objects within the real environment as if they were part of it. The direction of the camera is used to align with 3D objects, ensuring that the computer graphics camera moves in sync with the original camera. This allows for the 3D object to be displayed on top of the original image in the catalogue.

3) Storyboard Creation

In this phase, Adobe Photoshop is used to design a storyboard for the project. A storyboard consists of a series of illustrations that depict a digital story in two dimensions. The first dimension represents time: what occurs first, next, and last. The second dimension pertains to interaction: how sound interacts with images and how transitions and visual effects unify the visuals. Each element can interact with others, and the storyboard serves as a framework for planning the animation that will be presented to the user.

2. Production

At this stage, technical work will be conducted, including concept art, character modeling, animation, lighting simulation, and rendering. The stages are explained in detail below:

a. Layout: In the layout process, the design arrangement of specific elements is determined to create visually appealing results.
b. Modelling: This stage involves creating entities that can range from a single point (called a node) to a two-dimensional line (side), a curve (spline), or a three-dimensional object (face or polygon). Using the features of selected 3D software, the 3D model represents a product in 3D space. The software used for this process is Autodesk Maya.
c. Texturing, is akin to adding decorative paper to a plain box. In the 3D context, texture mapping involves overlaying graphics on polygon objects. These graphics can include anything from photographs to original designs. After creating the 3D model, 2D images are applied to add color, design, and texture. This overlay process, known as mapping, often defines the model's entire color. Maps can be created in programs like Photoshop and utilized in 3D models.
d. Rigging involves creating a skeletal structure for a 3D model. This structure allows for the manipulation of the model, similar to a puppet, for the purpose of animation.
e. Animation is the process of bringing a 3D object to life by making it move. Keyframes are used, where the animator adjusts the object on a frame-by-frame basis. This technique can create moving furniture in a 3D digital environment. By carefully manipulating objects within the 3D software, the user can export a series of images that produce the illusion of movement, based on the developer's adjustments.
f. Database: This stage involves the database element, where the admin must upload markers to the Vuforia Developer portal to obtain a license number. The markers must also be uploaded into Unity. During project modelling, the more complex the image, the greater the likelihood that it can be used as a marker.
g. C# Language: Currently, Visual Studio is utilized to create animations for modelling using the C# programming language. It has a connection with Unity, allowing for an interactive approach.
h. Unity: This phase is crucial for building an application that combines Vuforia and Java Software Development Environment (SDE). Settings must be configured for all types of Android devices. This technique is imported from Autodesk Maya modelling and is integrated into Unity to enhance the physical appearance of the project. Once development is complete, the admin needs to compile the project using Android Studio to create an APK file. Users will need to install this APK file on their Android phones.

3. Post-Production

The final phase in this methodology is the actual implementation of Augmented Reality (AR) using the chosen development environment. For instance, incorporating background audio can make the output more engaging. Following this, a comprehensive testing process is essential. After successfully building the application on a device such as Android, developers must test it on multiple devices to ensure flexibility and usability. The three key stages in the production pipeline are as follows:

a) Build APK file, b) Test run project, and c) Final output. These stages must be executed in accordance with the established structure, as they are interrelated and cannot be performed sporadically or independently. Certain processes can only proceed once others are completed.

The system and hardware requirements for this project are outlined below:

1) System Requirements

A comprehensive set of services, capabilities, and limitations should be documented in detail. This document is often referred to as a functional specification. For this study, the necessary system requirements are as follows:

a) Adobe Photoshop/Adobe Illustrator: Used for designing storyboards and interfaces.
b) Microsoft Word 2016:Used for documenting the application.
c) Android Studio 2016: Used for coding in programming languages.
d) C#:Utilized for writing code in the C# programming language.
e) Autodesk Maya: Used for 3D product shape modeling.
f) Unity: Employed for animation modeling and connecting to the device.
g) Vuforia Developer: A database for marker shapes.
h) Software Development Kits (SDK): Necessary for AR recognition, tracking, and content rendering.

2) Hardware requirements

Hardware requirements outline the tested and compatible hardware for specific operating systems or applications. This includes laptops, processors, memory, operating systems, system types, and mobile phones.

C. Implementation

Initially, a pre-test was conducted with selected groups of students to assess their prior knowledge. This test consists of three parts, each containing 10 questions covering vocabulary, grammar, and reading comprehension. The content and language topics align with the study's objectives. Initially, students will engage in a traditional reading and writing exercise to learn the alphabet. After this, they will be introduced to an augmented reality (AR) application designed to enhance their learning experience. Following the simulation process, students will undergo a test to compare their performance using traditional methods versus the AR application. This activity aims to improve their reading and writing skills. To gather more insights on the outcomes of this experimental process, a survey or direct interviews with the students' guardians will be conducted at the final stage.

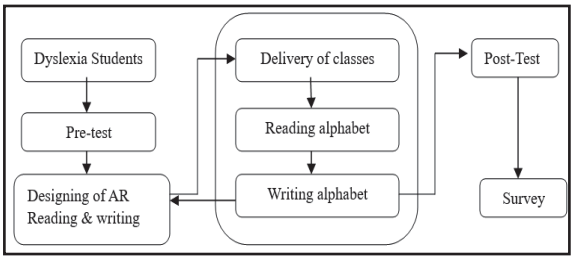


Fig 3. Procedure of Evaluation.

D. Card Method

The card methods used in this program include letter cards and word cards. The goal of using these cards is to enhance students' reading skills, particularly for those with dyslexia. To prepare for learning, the trainer should begin with the letters and words that have been provided. These cards can be made from various materials such as Asturo paper, cardboard, covers, or even recycled cardboard. Traditionally, trainers guide students in learning to read and recognize written words. After successfully completing the initial session, an experiment was conducted using an augmented reality (AR) application that had been developed. This AR application scans the marker on the designated card, which then displays a word image. An example of the alphabet used in this simulation is as follows:

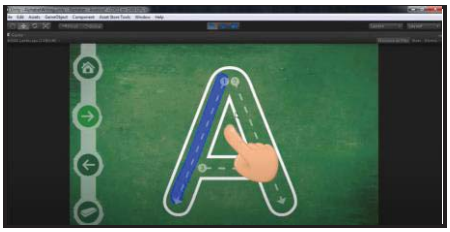


Fig 4. Learn to read the letter A

Then to attract students' interest in learning, we have also show wild animal groups in the process of learning words and writing letters. For the basic image of the subject in this study, an existing image from card was used for an educational display poster. This is also done as a reference for AR beginners who want to start an AR project for people with dyslexia so that it is easy and fast to complete the project but does not rule out the possibility of creating a separate subject from personal work. An example of an application based on a specific subject group or category looks like the image below:



Fig 5. Subject AR [21]

We create AR from these images as in the following example:

IV. RESULT

The study was conducted in Cipanas, Cianjur Regency, West Java, focusing on elementary school students who struggled with reading and writing. During the sample collection, we discovered that some fourth-grade students were still facing challenges in these areas. Our experiment aimed to analyze the differences in user experience between traditional reading and writing instruction methods and those that utilize augmented reality (AR) technology. We used the Modular Evaluation of Key Components of User Experience (MeCUE) questionnaire, which is applicable to various types of user experiences. This questionnaire allows for the assessment of user experiences from one or more interactive systems. It is also useful for comparing different products and studying changes and application development experiences over an extended period. The MeCUE questionnaire consists of five modules and ten indicators: Usability, Visual Aesthetics, Status, Commitment, Positive Emotions, Negative Emotions, Product Loyalty, Intention to Use, and Overall Evaluation. In the first stage of the analysis, it is essential to compile the MeCUE questionnaire and conduct a validation test. Subsequently, the researcher must determine the sample size for a pilot study to obtain validation results. In each pilot study question item, a Likert scale was used according to the references in the journals of Michael Minge, Manfred Thuring, and Ingmar Wagner, namely a value of 1 to 7. Value 1 for strongly disagree, value 2 for disagree, value 3 for somewhat disagree, value 4 for neutral, value 5 for somewhat agree, value 6 for agree, and value 7 for strongly agree. Then the researcher determined the list of questions by adopting the indicators contained in the Mecue questionnaire. Therefore, the Mecue questionnaire has 10 indicators, the minimum sample size for this study is 20 respondents. The results of the questionnaire distribution will be reviewed and examined to obtain analysis values that can prove the advantages and disadvantages of application A and application B. By using Microsoft Excel, the MeCUE questionnaire provides automatic calculations. So that the calculation of the MeCUE questionnaire can be used to compare user data from the two applications. The following is an analysis of the results of the comparison of user experiences obtained in applications A and B as well as a data table comparing the advantages and disadvantages of the two applications through interviews.

In the Usefulness indicator, there is a fairly high difference, namely traditional learning is 5.78 while for the AR application it is 4.93 with a difference of 0.84. From the values obtained, it can be said that users feel that the AR application is more useful than traditional learning.



Fig 7. User experiences

The AR application and traditional learning have a fairly significant difference in the Usability indicator, namely with a value of 6.25 for application B and 5.29 for the AR application or a difference of 0.96. This figure shows that consumers consider the AR application to be more user friendly than traditional learning applications. In the Visual Aesthetics indicator, there is a difference of 0.18, namely the AR application is 4.59 and traditional learning is 4.77 so it can be concluded that users feel that the display level of the two applications is almost the same but the display of traditional learning is superior to the AR application. In the status indicator, the AR application and traditional learning have slight differences. This difference can be interpreted that users feel that there is an increase in their status in their environment when using the AR application. In the Commitment indicator, the AR application scored 4.29 while traditional learning scored 3.45, so it can be said that users are more committed to using the AR application compared to traditional learning. In the Positive Emotion indicator, there is a significant difference of 0.46 with the AR application value being higher than the traditional learning value. So it can be interpreted that users get more good emotions when using the AR application compared to using traditional learning. Meanwhile, in the Negative Emotions indicator, the AR application gets worse results compared to traditional learning with a value of 3.67 in the AR application and a value of 3.41 in traditional learning. In the Intention to Use indicator, the AR application is superior to traditional learning with a value of 4.45 for the AR application and a value of 3.85 for traditional learning. From these values, it can be said that users prefer the AR application compared to traditional learning. Meanwhile, for the Loyalty indicator, users are more loyal to using the AR application compared to traditional learning with an average value of 4.57 for the AR application while the average value is 3.89 for traditional learning. Meanwhile, in the overall application value, the AR application outperforms traditional learning with a value of 2.5 for the AR application and 1.7 for traditional learning, which means that users give a better value to the AR application than traditional learning. Then after the evaluation we also conducted interviews with the user's guardians. The following is an interview comparing the advantages and disadvantages of using traditional learning and the AR application.

TABLE 1. COMPARATIVE RESULTS OF INTERVIEW ANALYSIS

Indicator	Traditional Learning	AR App
Advantages	Easy to use (Usability)	Easy to use (Usability)
	To make it easier to learn the alphabet face to face (usefulness).	For the purposes of learning the alphabet as well as entertainment (Usefulness)
	The appearance is easy to understand, simple and user friendly (Visual Aesthetics)	The appearance is easy to understand and creates more curiosity because the visuals are more attractive (Status)
	Goals that can be achieved and are easy to achieve (Positive Emotions).	Have quite high user loyalty (Intention to Use, Commitment and Product Loyalty).
	Has quite high user loyalty (Intention to use, Commitment and Product Loyalty).	Can be used for learning and entertainment that is easy to obtain (Positive Emotions).

Disadvantages	There is no value score information for users because the priority is understanding dyslexic users (Negative Emotions)	There is no value score information for users because the priority is understanding dyslexic users (Negative Emotions)
	The appearance is still simple (Visual Aesthetics)	The usability of the application is less because there are not too many users (Status)

From the results of experiments carried out for pre-test and post-test abilities are as follows:

TABLE 2. COMPARATIVE RESULTS

Aspects	Pre-Test	Post-Test
Remember Alfabet	3.70	4.16
Clarity and Coherence (Grammar and vocabulary)	0.22	0.54
Mechanics and punctuation	1.98	2.72
Total	5.90	7.42

Open Data at https://doi.org/10.5281/zenodo.15285538

V. CONCLUSIONS

The conclusions from the results of this research are:

a) Students with dyslexia need help understanding letters and making writing so that it is easy for them to remember and learn. AR technology can help make the learning process fun and not put mental pressure on the learning process for dyslexic students. To build an AR application, an AR method is needed that can support application development. It should be remembered that something is said to be AR if it meets 3 conditions, namely there is real-time interaction, contains 3D elements, and is a combination of the real world and the virtual world.

b) After the AR application was created with 2 different models, this research tested which model was easier for dyslexic students. From the results of the experiments carried out, it turns out that application AR, which displays the anatomy of the human body and groups of wild animals, makes it easier for dyslexic students to learn to read and write. The point is to learn while being entertained. No need to memorize the alphabet in sequence. Immersive learning brought about by AR technology is very helpful for dyslexic students.

c) It is hoped that this research can provide guidance to AR beginners, especially those who want to develop AR for dyslexic students, to make it easier to develop AR projects.

ACKNOWLEDMENT

This work is supported by Bina Nusantara University as a part of Bina Nusantara University's BINUS Research for Early Career Researchers entitled "Improving Children's Reading and Writing Abilities by Utilizing Augmented Reality" with contract number: 069A/VRRTT/III/2024 and contract date: March 18, 2024.

Open Contribution: Suzanna: Conceptualization, Methodology, Software, Data Curation, Writing - Original Draft. Mahaning: Visualization, Investigation, Supervision. Diana: Validation. Harco: Writing - Review and Editing.

REFERENCES

[1] N. A. Ahmad and S. C. L. Rosmanizam, "Interactive multimedia activities using augmented reality to promote reading and writing skills amongst young children," J. Teach. …, no. May, 2017, [Online]. Available: https://www.researchgate.net/profile/Noor-Aini-Ahmad/publication/341735734_INTERACTIVE_MULTIMEDIA_ACTIVITIES_USING_AUGMENTED_REALITY_TO_PROMOTE_READING_AND_WRITING_SKILLS_AMONGST_YOUNG_CHILDREN/links/5ed11f1492851c9c5e662709/INTERACTIVE-MULTIMEDIA-ACTIVIT

[2] P. Karamanoli, K. Persefoni, and A. Tsinakos, "Augmented Reality and Dyslexia: A New Approach in Teaching Students," no. July, 2016, [Online]. Available: https://www.researchgate.net/publication/304658971

[3] D. Bjekić, S. Obradović, and M. Bojović, "The Challenges for Teachers: Augmented Reality as Educational Technology for Students with Dyslexia," 8th Int. Sci. Conf. Tech. Informatics Educ., no. September, pp. 40–49, 2020, [Online]. Available: https://www.aiditalia.org/it/la-

[4] T. Gupta, M. Sisodia, S. Fazulbhoy, M. Raju, and S. Agrawal, "Improving Accessibility for Dyslexic Impairments using Augmented Reality," 2019 Int. Conf. Comput. Commun. Informatics, ICCCI 2019, pp. 23–26, 2019, doi: 10.1109/ICCCI.2019.8822152.

[5] N. Baiti, U. Nisa, and S. Lestari, "Development of Augmented Reality-Based Flipbook Media to Improve Children ' s Writing Skills," vol. 01, no. 3, pp. 19–29, 2024.

[6] F. Carrión-Robles, V. Espinoza-Celi, and A. Vargas-Saritama, "The Use of Augmented Reality through Assemblr Edu to Inspire Writing in an Ecuadorian EFL Distance Program," Int. J. Eng. Pedagog., vol. 13, no. 5, pp. 121–141, 2023, doi: 10.3991/ijep.v13i5.38049.

[7] J. K. T. Tang, T. Y. A. Duong, Y. W. Ng, and H. K. Luk, "Learning to create 3D models via an augmented reality smartphone interface," Proc. 2015 IEEE Int. Conf. Teaching, Assess. Learn. Eng. TALE 2015, no. February, pp. 236–241, 2016, doi: 10.1109/TALE.2015.7386050.

[8] M. H. Kurniawan, Suharjito, Diana, and G. Witjaksono, "Human Anatomy Learning Systems Using Augmented Reality on Mobile Application," Procedia Comput. Sci., vol. 135, pp. 80–88, 2018, doi: 10.1016/j.procs.2018.08.152.

[9] G. Maurice, N. Isabwe, and M. W. Gerdes, "Effective use of Augmented Reality to Support Reading for People with Dyslexia SUPERVISORS," 2023.

[10] Suzanna, M. I. Wijaya, D. Diana, and C. O. Pranoto, "The Augmented Reality Model in Online Learning," J. Int. Conf. Proc., 2021.

[11] H.-C. Yeh and S.-S. Tseng, "LANGUAGE TEACHING AND TECHNOLOGY FORUM Enhancing multimodal literacy using augmented reality," Lang. Learn. Technol., vol. 24, no. 1, pp. 27–37, 2020.

[12] F. Meisarah, C. S. Octiva, P. A. Sucipto, I. R. Satyaninrum, and A. A. Bakri, "Improving Student Text Writing Ability by Utilizing the Use of Augmented Reality Feature," J. Sistim Inf. dan Teknol., vol. 5, no. 1, pp. 129–134, 2023, doi: 10.37034/jsisfotek.v5i1.213.

[13] E. R. Nainggolan et al., "The Implementation of Augmented Reality as Learning Media in Introducing Animals for Early Childhood Education," 2018 6th Int. Conf. Cyber IT Serv. Manag. CITSM 2018, no. Citsm, 2019, doi: 10.1109/CITSM.2018.8674350.

[14] O. Aina, "Application of Holographic Technology in Education," p. 67, 2010.

[15] H. Hanafiah, R. Nurapriani, and M. Andriana Gaffar, "Game Model Based on Cultural Values Approach in Developing Interpersonal and Kinesthetic Intelligences in Early Childhood," vol. 249, no. Secret, pp. 1–7, 2018, doi: 10.2991/secret-18.2018.1.

[16] N. Khenak, J. Vézien, and P. Bourdot, "Effectiveness of Augmented Reality Guides for Blind Insertion Tasks," Front. Virtual Real., vol. 1, no. November, 2020, doi: 10.3389/frvir.2020.588217.

[17] M. Lazo-Amado, L. Cueva-Ruiz, and L. Andrade-Arenas, "Designing a Mobile Application using Augmented Reality: The Case of Children with Learning Disabilities," Int. J. Adv. Comput. Sci. Appl., vol. 13, no. 6, pp. 857–864, 2022, doi: 10.14569/IJACSA.2022.01306101.

[18] Rugaiyah, I. Ardila, U. Y. Oktiawati, and N. Saputra, "The Impact of Augmented Reality in English Learning in Elementary Schools," J. Ilm. Sekol. Dasar, vol. 8, no. 1, pp. 54–62, 2024, doi: 10.23887/jisd.v8i1.66710.

Optimizing Traffic Flow and System Efficiency in Networks Through AI-Driven Management

***Abstract*—As internet traffic continues to increase exponentially alongside the proliferation of connected devices, traditional network management strategies face significant challenges. This study explores the potential of artificial intelligence (AI) to optimize network traffic using the network traffic data set captured through Wireshark. Using predictive modeling and anomaly detection, we forecast traffic patterns and dynamically allocate resources in real time. A least-route load-balancing strategy reduces congestion by redistributing traffic, cutting peak loads by 20% in high-traffic scenarios. Evaluation using mean squared error (MSE) highlights AI's role in improving prediction accuracy and significantly improving overall network efficiency, providing a robust foundation for adaptive traffic management strategies and smarter adaptive infrastructures.**

***Index Terms*—Network Traffic, AI & ML, Anomaly Detection,Network Optimization, Real-Time Traffic Management**

I. Introduction

The rapid growth of internet-connected devices and high-bandwidth applications has led to a significant rise in network traffic volumes and complexity. Diverse sources such as streaming services, IoT devices, cloud computing, and real-time communications contribute to dynamic traffic patterns that traditional static and manual network management techniques can no longer handle effectively. These outdated methods often result in performance bottlenecks, increased latency, and potential service disruptions.To address these challenges, integrating Artificial Intelligence (AI) into network management systems offers a transformative solution. AI enables proactive traffic management by predicting patterns, detecting anomalies, and dynamically allocating resources in real-time to meet evolving demands.This study examines AI-driven strategies for optimizing network traffic management, leveraging a real-world dataset captured on October 9, 2023, at the University of Cincinnati. The Network Traffic Dataset, comprising over 394,000 instances with features like source/destination IPs, protocols, packet lengths, and timestamps, provides a robust foundation for analysis. Machine learning techniques, including regression for traffic prediction, clustering for anomaly detection, and time-series analysis, are employed to uncover actionable insights and enhance network performance.

II. Methodology

A. Dataset Description

The "Network Traffic Dataset," utilized in this study, was collected at the University of Cincinnati, Cincinnati, OHIO, on October 9th, 2023. The data capture took place over a 1-hour period during the evening, resulting in 394,137 instances stored in CSV format. This dataset contains seven features, including source and destination IP addresses, timestamps, protocols, and packet lengths. The dataset is well-suited for various machine learning applications, such as network intrusion detection, traffic classification, and anomaly detection. The data was captured using Wireshark, a network protocol analyzer, and includes both numeric and nominal attributes.

TABLE I
Network Traffic Dataset Attributes

Attribute	Description
Source IP	Source device IP address
Destination IP	Destination device IP address
Timestamp	Packet capture time
Protocol	Communication protocol (e.g., TCP, UDP)
Packet Size	Size of the packet in bytes

B. Data Preprocessing

The preprocessing phase is critical for transforming raw network traffic data from the $Midterm_53_group.csv$ and $output1.csv$ datasets into a usable format for machine learning models. The key attributes handled include *Time*, *Source*, *Destination*, *Protocol*, *Length*, and *Info* from the $Midterm_53_group.csv$, and *Timestamp*, *Source IP*, *Destination IP*, *Protocol*, and *Length* from $output1.csv$

1) **Handling Missing Values:** Missing values in the *Length*, *Source*, *Destination*, and *Protocol* columns from Midterm_53_group.csv were imputed using the mean for numeric values. Additionally, key columns such as *Source IP* and *Destination IP* in `output1.csv` were checked for null values and appropriately cleaned to ensure data integrity.
2) **Removing Duplicates and Outliers:** Duplicate rows, identified by the *Source* and *Destination* columns in `Midterm_53_group.csv`, and *Source IP* and *Destination IP* in `output1.csv`, were removed.
3) **Feature Engineering:** Time-based features were extracted from the *Time* column in `Midterm_53_group.csv`, with features such as *hour* and *day of the week* being created to capture temporal patterns in network traffic.
4) **Normalization:** Continuous features such as *Length* from both datasets were standardized using normalization techniques, ensuring that all features are on the same scale.

C. Model Selection and Training

In network traffic analysis, various attributes provide insights into data flow, performance, and network behavior, helping administrators optimize resources and detect anomalies. The models were evaluated with standard metrics :

Predictive Model Evaluation: The predictive model achieved a Mean Absolute Error (MAE) of 0.2508 and a Mean Squared Error (MSE) of 4.8373.

Anomaly Detection Model Evaluation: The anomaly detection model showed limited performance across classes due to dataset constraints.

Models undergo regular improvement through retraining, hyperparameter tuning, and system scaling to ensure effective real-time performance in live environments.

D. Real-Time Traffic Management

The real-time traffic management system is designed to handle live network traffic by utilizing the trained models for prediction and anomaly detection. This system applies a load-balancing algorithm (Least Connections) to dynamically optimize traffic flow and resources, ensuring efficient network performance.

1) **Real-Time Data Processing:** Incoming traffic data is preprocessed using the same steps applied in the training phase. The data attributes like "Timestamp," "Source IP," "Destination IP," "Protocol," and "Length" are normalized and structured.
2) **Least Connections Load Balancing:** The system applies the Least Connections algorithm to manage traffic distribution across various network destinations. It continuously monitors active connection counts for each source-destination pair and routes traffic to the IP with the least number of active connections, thereby preventing congestion and ensuring balanced network load.
3) **Dynamic Network Management:** Based on the model outputs and the load-balancing algorithm, real-time adjustments are made to network resources. If the predictive model forecasts high traffic volumes or anomalies are detected, the system reallocates resources dynamically to prevent congestion and maintain optimal performance. This includes rerouting traffic and adjusting bandwidth distribution to meet real-time demands efficiently.

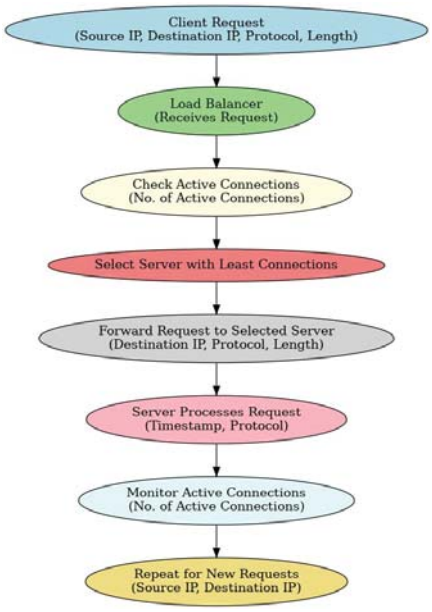


Fig. 1. Block Diagram of Least Connection Load Balancing Algorithm

Algorithm 1 Network Traffic Prediction and Optimization

Input : Dataset $\mathcal{D}$ with attributes:Time, Source, Destination, Protocol,Length,Source_IP,Destination_IP
Predictive Model $\mathcal{M}$, Threshold $\theta = 200$, Optimization Factor $\alpha = 0.8$
Output: Optimized Predictions $\mathbf{y}_{\text{opt}}$

`Preprocess_Data(`$\mathcal{D}$`)`
Rename columns for uniformity:
$\mathcal{D} \leftarrow \mathcal{D}$.rename('Source IP' to 'Source_IP', 'Destination IP' to 'Destination_IP')
One-hot encode protocol:
$\mathcal{D}_{\text{protocol}} \leftarrow$ get_dummies($\mathcal{D}$.Protocol) $\mathcal{D} \leftarrow \mathcal{D} \cup \mathcal{D}_{\text{protocol}} -$ Protocol
Check for missing features in $\mathcal{D}$ required by $\mathcal{M}$ **foreach** *feature* f *in* $\mathcal{M}$.*features* **do**
  if $f \notin \mathcal{D}$ **then**
    if $f =$ *No.* **then**
      $\mathcal{D}[f] \leftarrow [1, 2, \ldots, |\mathcal{D}|]$
    else
      if $f \in \{$*Length_x, Length_y*$\}$ **then**
        $\mathcal{D}[f] \leftarrow \mathcal{D}$[Length]
      else
        $\mathcal{D}[f] \leftarrow 0$ if $f =$ Protocol_y
      end
    end
  else
end
return $\mathcal{D}[\mathcal{M}$.features$]$

`Predict_and_Optimize(`$\mathcal{D}$`)`
$\mathcal{D}_{\text{processed}} \leftarrow$ `Preprocess_Data(`$\mathcal{D}$`)`
$\mathbf{y}_{\text{pred}} \leftarrow \mathcal{M}$.predict($\mathcal{D}_{\text{processed}}$) **for** $i = 1$ *to* $|\boldsymbol{y}_{pred}|$ **do**
  if $\boldsymbol{y}_{pred}[i] > \theta$ **then**
    $\mathbf{y}_{\text{opt}}[i] \leftarrow \alpha \cdot \mathbf{y}_{\text{pred}}[i]$
  else
    $\mathbf{y}_{\text{opt}}[i] \leftarrow \mathbf{y}_{\text{pred}}[i]$
  end
end
return $\mathbf{y}_{\text{pred}}, \mathbf{y}_{\text{opt}}$

E. Visualization and Reporting

Visualization plays a crucial role in understanding traffic patterns and model performance. Two primary visualizations were utilized:

1) **Traffic Volume by Hour:** A graph depicting traffic volume over different hours of the day was generated to identify peak traffic times which helps in understanding the daily traffic patterns and planning resource allocation accordingly.
2) **Predictive Traffic Volume:** The predicted traffic volumes were plotted against actual traffic values to assess the accuracy of the predictive model. This comparison highlights the model's effectiveness in forecasting network traffic [7].
3) **Heatmap of Traffic Intensity:** A heatmap was generated to visualize the intensity of network traffic over time. The heatmap highlights periods of high and low traffic, aiding in the identification of congestion points and unusual traffic patterns.

F. Evaluation Metrics

In the field of network traffic analysis, it is essential for understanding and managing the flow of data across networks. The models were evaluated using standard metrics:

- **Predictive Model Evaluation:** The performance of the predictive model was assessed using MAE and MSE. The evaluated metrics yielded an MAE of 0.2508 and an MSE of 4.8373.
- **Anomaly Detection Model Evaluation:** The anomaly detection model was evaluated based on its ability to correctly identify normal and anomalous traffic patterns. The different matrices is calculated, but due to the nature of the dataset, the model achieved a low performance with an accuracy of 0.00 across multiple classes.

III. Results

A. Evaluation Metrics for Anomaly Detection

The models' performance was assessed using essential classification metrics, including Precision, Recall, F1-Score, and Accuracy. These metrics provide insight into the model's ability to correctly classify network traffic and detect anomalies.

$$\text{Precision} = \frac{\text{True Positives}}{\text{True Positives} + \text{False Positives}}$$

$$\text{Recall} = \frac{\text{True Positives}}{\text{True Positives} + \text{False Negatives}}$$

$$\text{F1-Score} = 2 \times \frac{\text{Precision} \times \text{Recall}}{\text{Precision} + \text{Recall}}$$

$$\text{Accuracy} = \frac{\text{True Positives} + \text{True Negatives}}{\text{Total Population}}$$

TABLE II
Classification Report: Precision, Recall, F1-Score, and Support

Class	Precision	Recall	F1-Score	Support
0	0.00	0.00	0.00	0.0
1	0.00	0.00	0.00	0.0
60	0.00	0.00	0.00	3.0
62	0.00	0.00	0.00	6.0
66	0.00	0.00	0.00	287.0
73	0.00	0.00	0.00	1.0
74	0.00	0.00	0.00	296.0
364	0.00	0.00	0.00	1.0
365	0.00	0.00	0.00	1.0
Accuracy	0.00 (Total: 636.0)			
Macro Avg	0.00	0.00	0.00	636.0
Weighted Avg	0.00	0.00	0.00	636.0

B. Predictive Model Evaluation: MSE and MAE

The performance of the predictive model [8] was also assessed using regression-based metrics, specifically Mean Absolute Error (MAE) and Mean Squared Error (MSE) [9].

$$\text{MAE} = \frac{1}{n}\sum_{i=1}^{n}|y_i - \hat{y}_i|$$

$$\text{MSE} = \frac{1}{n}\sum_{i=1}^{n}(y_i - \hat{y}_i)^2 \quad (1)$$

The results for the predictive model are as follows:

- **Mean Absolute Error (MAE):** 0.2508
- **Mean Squared Error (MSE):** 4.8373

These values suggest that the model exhibits relatively low prediction errors, indicating a good fit to the training data.

C. Visualization of Traffic Patterns

Traffic Volume by Hour: The "Traffic Volume by Hour" graph provides an overview of daily network traffic fluctuations, highlighting peak usage times. The x-axis represents hours of the day, and the y-axis shows traffic volume, revealing patterns in traffic flow. This helps network managers identify high-traffic periods, anticipate congestion, and optimize performance proactively.

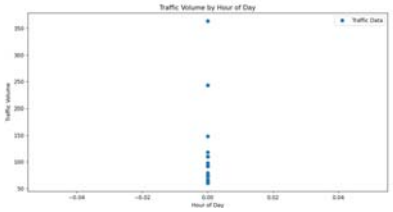


Fig. 2. Traffic Volume by Hour.

Predictive Traffic Volume: The "Predictive Traffic Volume" graph compares actual traffic data with model predictions, highlighting the model's accuracy. Close alignment between the predicted and actual values indicates reliability, while discrepancies suggest areas for improvement. The x-axis represents time intervals, and the y-axis represents traffic

volume, enabling a clear comparison of model performance over time.

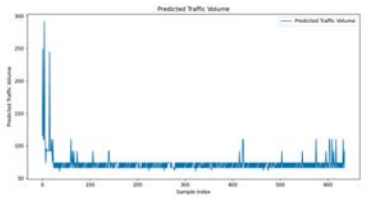


Fig. 3. Predictive Traffic Volume.

D. Traffic optimization

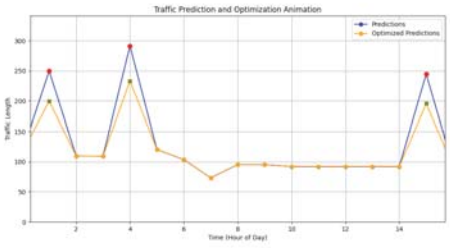


Fig. 4. Optimized Traffic Flow

The result is derived using a ML predictive model trained on historical network traffic data to forecast traffic volume. When the predicted traffic blue line exceeds a congestion threshold , a load-balancing algorithm is triggered to adjust the flow or reroute packets, reducing the traffic load before congestion occurs. This optimization process, as shown in Fig. 4, results in the ”optimized traffic” line orange, reflecting the reduced traffic volume.

The results highlight the optimization’s effectiveness. The blue line unoptimized traffic shows spikes at congestion points, while the orange line optimized traffic diverges downward when the threshold is exceeded, indicating load reduction. The gaps between the lines demonstrate how optimization smooths traffic spikes, maintaining manageable limits, preventing performance degradation, and enhancing network stability. This AI-driven approach ensures real-time efficiency even under fluctuating loads.

IV. Conclusion

This study highlighted the effectiveness of AI-driven techniques in optimizing network traffic management using real-world datasets, with Random Forest Regression successfully predicting traffic volumes and One-Class SVM revealing challenges in detecting irregular patterns. Rigorous data preprocessing and insightful visualizations enabled peak usage identification and resource optimization. While the results emphasize the need for improving anomaly detection through advanced feature selection and algorithmic refinement, integrating AI with automated systems presents opportunities for creating adaptive networks capable of real-time traffic management. Future work should focus on incorporating techniques like deep reinforcement learning and testing scalability on larger datasets to enhance performance and reliability.

References

[1] P. Borgnat, G. Dewaele, K. Fukuda, P. Abry, and K. Cho, “Seven Years and One Day: Sketching the Evolution of Internet Traffic,” in *IEEE INFOCOM 2009*, pp. 711–719, April 2009.

[2] K. Al Jallad, M. Aljnidi, and M. S. Desouki, “Big Data Analysis and Distributed Deep Learning for Next-Generation Intrusion Detection System Optimization,” *Journal of Big Data*, vol. 6, no. 1, p. 88, 2019.

[3] J. Smith and J. Doe, “An Analysis of Network Traffic Patterns,” *IEEE Transactions on Networking*, vol. 20, no. 3, pp. 456–469, 2020.

[4] Zheng, Z., Wang, P., Liu, J., Sun, S. (2015). Real-time big data processing framework: challenges and solutions. Applied Mathematics Information Sciences, 9(6), 3169.

[5] Prajam, S., Wechtaisong, C., Khan, A. A. (2022). Applying machine learning approaches for network traffic forecasting. Indian Journal of Computer Science and Engineering, 13(2), 324-335.

[6] Cortez, P., Rio, M., Rocha, M., Sousa, P. (2006, July). Internet traffic forecasting using neural networks. In The 2006 IEEE international joint conference on neural network proceedings (pp. 2635-2642). IEEE.

[7] Ramakrishnan, N., Soni, T. (2018, December). Network traffic prediction using recurrent neural networks. In 2018 17th IEEE International Conference on Machine Learning and Applications (ICMLA) (pp. 187-193). IEEE.

[8] Andreoletti, D., Troia, S., Musumeci, F., Giordano, S., Maier, G., Tornatore, M. (2019, April). Network traffic prediction based on diffusion convolutional recurrent neural networks. In IEEE INFOCOM 2019-IEEE Conference on Computer Communications Workshops (INFOCOM WKSHPS) (pp. 246-251). IEEE.

[9] Ramakrishnan, N., Soni, T. (2018, December). Network traffic prediction using recurrent neural networks. In 2018 17th IEEE International Conference on Machine Learning and Applications (ICMLA) (pp. 187-193). IEEE.

Attention Thresholds for Brand Impact

John Hawkins*, Shannon Bosshard†
* *GumGum*, Sydney, Australia
john.hawkins@gumgum.com
† *Neuroconsulting*, Sydney, Australia
shannon@neuroconsultingaustralia.com.au

***Abstract*—Brand lift studies are a staple in the media industry for estimating the impact of advertising on consumer attitudes and preferences. They measure differences in multiple metrics between consumers who have been exposed to an ad and those who have not. One of the contributing factors to the impact of an ad is the amount of visual attention that the consumer gives to the creative, which was historically difficult to distinguish from exposure alone. In this work we develop a method for processing brand study data that contains both attention measurement and survey-based brand outcomes. This method focuses on exploiting inherent structural mechanisms in the nature of what upper funnel metrics measure in order better estimate the threshold of attention at which an impact occurs. We benchmark the approach against multiple alternative methods for estimating these thresholds and demonstrate superior performance in terms of mean error and width of the error bounds.**

***Index Terms*—Attention Measurement, Consumer Psychology, Digital Advertising, Digital Media**

I. Introduction

Advertising achieves outcomes for brands through a complex interaction between many factors including the brand market position, the advertising creative, the mindset of the consumer [1] and the media platform in which the advertising is presented. Despite a diversity of models for how advertising works [2], it is a fundamental truth that in order to function, advertising must exert an impact on the mental processes of consumers through exposure to the advertising creative [3]. One of the core ways that marketers understand if advertising is having the desired effect on consumers is through post-exposure brand lift studies, which serve to analyse the complex relationship between advertising creatives and brand outcomes [4]. Although self-report surveys have potential issues they continue to be used because they are often the only option, and independent research continues to show that the results they produce are meaningful [5].

As a standard practice, brand studies are based on delineation of panellists into control and exposed groups. However, this binary distinction obscures the fact that exposure is not a uniform phenomenon. Participants react to a piece of advertising in different ways, including the extent to which they give mental effort/time to processing its content. Inspired by the success of attention measurement in psychology for understanding memory retention [6], measuring attention duration with eye tracking has emerged as a reliable method of analysing the relationship between advertising exposure and brand outcomes [7]–[9].

Attention measurement has allowed the study of many factors that contribute to effective marketing, including the impact of images of faces [10], the use of animation [8], [11], the relationship with social media posts [12], and emotional responses to visual stimuli in different physical spaces [13].

Multiple investigations have identified that attention time on advertising provides a real-time metric that is correlated with important downstream impacts like brand recall [8], consideration and purchase intent [14], [15]. Even though low attention duration can drive brand outcomes, like consideration and brand choice [9], multiple studies have demonstrated that higher rates of attention have a greater impact on marketing outcomes, including consideration and short-term advertising strength [16]. The evidence of the role of visual attention in the success of advertising has led to increasing focus on Attention Based Marketing research [17].

A natural extension to the research linking visual attention to brand outcomes is to investigate how much attention is required to produce an increase in brand outcomes. Studies have shown that upper funnel metrics, including ad recall and unaided brand awareness require approximately 100ms before any lift is observed [18], whilst spontaneous brand awareness and familiarity required at least one second. In contrast, lower funnel metrics were seen to require greater attention, with favourability, consideration, and purchase intent requiring three seconds, nine seconds, and eight seconds respectively.

Short-Term Advertising Strength (STAS) scores (indicative of an individual's propensity to purchase a product) have been shown to see significant lift with more than two seconds of active attention [19]. While memory retention of a brand was not observed until three seconds of attention [20].

Two general themes emerge when analysing these previous research projects: (1) different outcomes require different amounts of attention, and (2) the attention duration at which change occurs varies between metrics. Additional differences in the amount of attention required to drive varying impact across brand metrics is likely due to factors that cannot be controlled for. For example, the brand's market position, the quality and content of the ad creatives, and media channels utilised.

We draw on two observations to motivate the current work. Firstly, upper funnel metrics are typically purely memory based and involuntary for the consumer. As such there are strong reasons to believe that they will be strictly monotonic in all but the most contrived situations. Secondly, the key to understanding how to deliver outcomes with advertising

is knowing how much attention needs to be given to the ad creative for those involuntary memory mechanisms to function.

II. Methodology

We describe a methodology for processing brand lift data that allows us to estimate the amount of visual attention required to deliver an impact on the underlying cognitive processes. Our focus is on purely memory-oriented brand metrics (like recall and awareness) which we argue are in principle positively and monotonically related to attention. It is possible that additional attention has no impact on memory, but in all but the most contrived instances additional attention will not cause a reduction in memory.

A. Data Processing

To analyse attention time and brand metrics we need to process panellists into groups with similar attention times. We generate groups from the sequence of records ordered by attention time and take the mean attention time and mean outcome as the grouped data point. We apply a moving window over the sequence and use a replacement sampling approach (some panellists will be in multiple groups), such that we get estimates of impact at difference mean levels of attention.

Panellists are grouped into sets of at least 20 records, with the additional constraint that all records of the exact same attention time measurement must be in the same set. These groups form a sequence of mean attention measurements with a set of corresponding brand impact results. We take all records with attention time less than 100ms as the synthetic control group. The rationale for the synthetic control is that these are people, although exposed to the advertising, were not actively processing the advertising message long enough to have obtained measurable impact[1].

Once we have all records grouped and sorted, we apply the smoothing algorithms to reduce any potential noise inherent in the stochastic nature of the outcome we are measuring. The noise is typically observed as fluctuations in brand outcomes as attention time increases.

Our method involves applying monotonic smoothing to determine the threshold in attention time at which brand lift unambiguously occurs. We baseline this approach against two alternative methods, maximum likelihood and logistic regression. We explain each of these three approaches in the sections below.

B. Monotonic Smoothing

For brand metrics in the upper funnel there are *a priori* reasons to expect a strictly monotonically increasing relationship with attention. This is because these upper funnel metrics are purely about memory of the brand or messaging, rather than any changes in attitude. There are no general in-principle reasons for a person to become less aware of a brand after exposure to the advertising creative[2].

The expectation of monotonicity means we should expect the brand impact to either go up or remain flat as attention time increases. It also means that when we see volatility in the impact at low attention levels, we can assume that it is due to continued sampling from the baseline (control) outcome and thereby subsume those records into the control. The monotonic smoothing process increases the size of the control sample until such a point that the outcome becomes consistently positive. To mitigate potential sampling issues at the higher end of the attention spectrum we first smooth the top end records, such that all records higher than the peak outcome are subsumed into one another. This drags down the observed peak outcome, but increases the sample size, thereby providing a more robust estimate of the maximum lift to be expected.

The sequencing for the monotonic smoothing is shown in Figure 1. Firstly, the high attention records are smoothed backward toward the peak, then the low attention records are smoothed forward being subsumed into the control. We then iterate through the middle records merging sets until we are left with a monotonic relationship between attention and outcome. The details of the monotonic smoothing process are shown in Algorithm 1. Note, the final smoothing operation continuously iterates over all groups until monotonicity is achieved. It has a worst-case complexity of $\mathcal{O}(n^2)$. The initial forward and backward passes serve to reduce the potential complexity by reducing the size of n, each of these initial passes have a complexity of $\mathcal{O}(n)$.

C. Maximum Likelihood

A natural baseline method for estimating the threshold at which lift occurs is a Maximum Likelihood (ML) approach. This process involves iterating through a set of candidate thresholds and choosing the threshold which maximises the observed difference in the probability of a positive outcome between attention amounts above and below that threshold. This approach has a computational complexity of $\mathcal{O}(n)$.

D. Logistic Regression

An alternative baseline method involves fitting a Logistic Regression (LR) model that predicts the probability of a positive outcome based on the single variable of the attention time given to the advertising unit. This model will produce a probability value for each attention time it is given. To determine the threshold, we iterate through a list of equally spaced thresholds and take the lower attention value of a contiguous pair for which the difference in probability of lift is maximised. We are looking for the attention amount that

[1]These consumers may be examples of unconscious processing or attention measurement error. However, as the net effect is that we would overestimate baseline outcomes, and hence underestimate brand impacts, we consider this an acceptable risk that does not undermine the basic effectiveness of our method

[2]A possible exception could be survey questions that compete brands against each other under conditions of limited memory capacity. In this situation is possible that an advertising creative might remind the consumer of a brand's competitor and hence negatively impact the target brand's outcome. However, we consider this scenario to be so unlikely that it is worth the trade-off of losing information in these cases in order to reduce noise in the majority case

Algorithm 1 Monotonic Smoothing Algorithm

procedure MAIN(a, o) ▷ Main Function
  $A, O \leftarrow$ SORT(a, o) ▷ Sort by attention
  $G \leftarrow$ GROUP(A, O) ▷ Group records
  $G, u \leftarrow$ BACKPASS(G) ▷ Backward pass
  $G, l \leftarrow$ FORWARDPASS(G) ▷ Backward pass
  $G \leftarrow$ SMOOTH(G, l, u) ▷ Smoothing pass
  return G ▷ Smoothed grouped records
end procedure
procedure BACKPASS(G)
  $x \leftarrow G[i].outcome$
  $u \leftarrow len(G)$
  for $i \leftarrow len(G)$ **to** 0 **do**
    if $G[i].outcome > x$ **then**
      $G, x \leftarrow$ MERGEFORWARD(G, i)
      $u \leftarrow i$
    end if
  end for
  return G, u
end procedure
procedure MERGEFORWARD(G, i)
  $t \leftarrow G[\geq i]$
  $w \leftarrow$ AVERAGEOUTCOME(t)
  Set all records $j \geq i$ with $outcome = w$
  return G, w
end procedure
procedure FORWARDPASS(G)
  $x \leftarrow G[0].outcome$
  $l \leftarrow 0$
  for $i \leftarrow 0$ **to** $len(G)$ **do**
    if $G[i].outcome < x$ **then**
      $G, x \leftarrow$ MERGEBACKWARD(G, i)
      $l \leftarrow i$
    end if
  end for
  return G, l
end procedure
procedure MERGEBACKWARD($G, i, j = 0$)
  $t \leftarrow G[\leq i$ and $\geq j]$
  $w \leftarrow$ AVERAGEOUTCOME(t)
  Set all records $j \leq i$ with $outcome = w$
  return G, w
end procedure
procedure SMOOTH(G, l, u)
  $\theta \leftarrow False$
  while $\theta \neq True$ **do**
    $\theta \leftarrow True$
    for $i \leftarrow l$ **to** $u - 1$ **do**
      if $G[i].outcome$ ¡ $G[i+1].outcome$ **then**
        $G, x \leftarrow$ MERGEBACKWARD$(G, i+1, i)$
        $\theta \leftarrow False$
      end if
    end for
  end while
  return G
end procedure

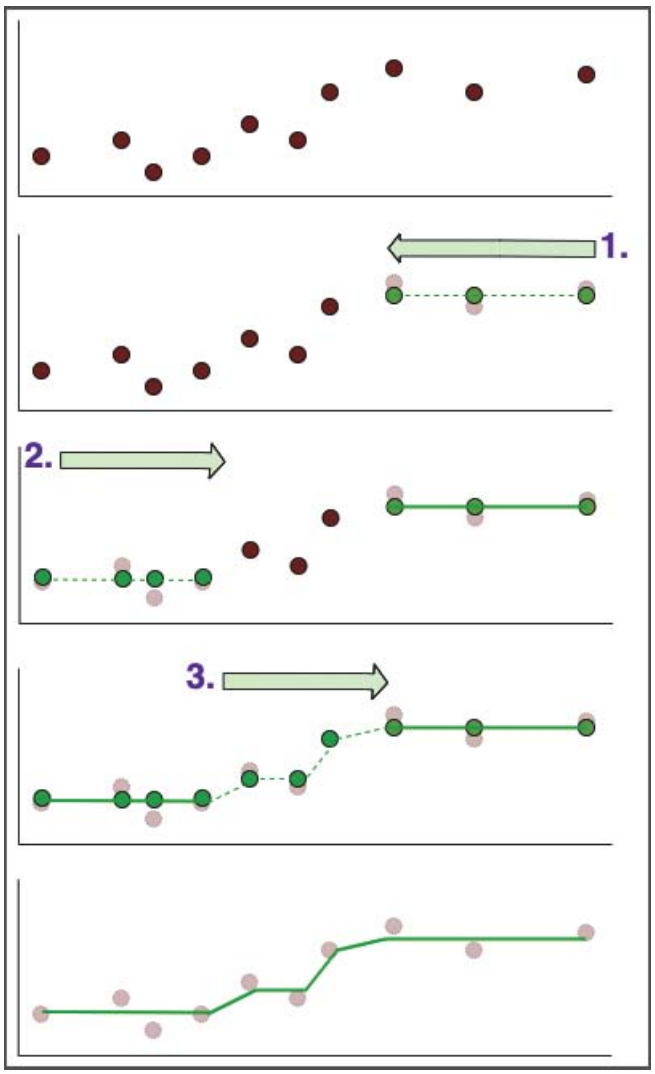


Fig. 1. Overview of the Monotonic Smoothing algorithm. (Step 1) Backward Pass Peak Smoothing. (Step 2) Forward Pass Control Smoothing. (Step 3) Monotonic Forward Smoothing.

corresponds to the beginning of the steepest region of the logistic curve.

E. Threshold Estimation

The fundamental goal of the smoothing algorithms outlined above is to identify the threshold point in attention time at which the advertising creative is delivering a lift in the brand metric. Data collected in a brand study contains noisy samples from an underlying true distribution in which the advertising creative exerts an influence over the mental faculties of media consumers. So for example, we might say that consumers have a baseline 50% chance of being aware of the brand. Once those consumers are exposed to more than 2 seconds of a specific video advertisement that probability of brand awareness goes up to 60%. However, the data contained in a brand study is a set of samples from this underlying reality and will not perfectly reflect the transition at 2 seconds. We want our data smoothing algorithm to recover the true threshold from a brand

lift study, with the narrowest possible confidence intervals that contain the true transition threshold.

III. Experiments

TABLE I
Model Error by Threshold

Threshold	LR MAE	LR FN Rate	ML MAE	ML FN Rate	MS MAE	MS FN Rate
1.0	1.74	0.63	1.32	0.0	0.91	0.01
1.5	1.92	0.59	1.47	0.0	0.90	0.01
2.0	2.08	0.55	1.60	0.0	0.94	0.01
2.5	2.23	0.52	1.69	0.0	1.02	0.01
3.0	2.39	0.50	1.74	0.0	1.11	0.01
3.5	2.53	0.48	1.73	0.0	1.23	0.01
4.0	2.71	0.48	1.62	0.0	1.38	0.01
4.5	2.86	0.48	1.52	0.0	1.61	0.01

To evaluate our ability to recover the true thresholds in attention, we design a series of simulation experiments. In each experiment we generate a synthetic brand lift study using a set of controllable parameters and randomisation.

In each simulation we generate the response of 200 random panellists, who have been exposed to an advertisement for a predetermined maxiumum length of time. Approx. 10% of the panellists will pay zero attention to the advertising, approximately 10% will attend for the full duration, and the remaining 80% attend a random proportion of the ad. We predetermine the baseline percentage of people who have a positive response to the metric, we determine a specific threshold of attention at which this is changed, where the change is also a predetermined specific number of percentage points of lift. For each synthetic subject their survey response is randomly generated by sampling from a binomial probability distribution, the parameters of which are determined by whether their attention to the ad was above or below the threshold. These parameters are summarised in Table II.

This process assumes a single amount of lift that occurs at a specific point on the attention line. This is the simplest possible model of how attention to an advertising creative could influence brand metrics.

We iteratively generate synthetic brand studies one thousand times for each set of parameters. We apply all methods to recover a predicted threshold and compare predictions with the true threshold in the simulation. This process allows us to evaluate the comparative error distribution for each of the three methods and place confidence bounds on the output of our algorithm.

IV. Results

We present summaries of the simulation results across Tables I, III, and IV. In each of these tables we average

TABLE II
Simulation Parameters

Parameter	Explanation	Values
Baseline	Control value of metric	30, 50, 70
Threshold	Attention time at which lift occurs	1.0 to 4.5
Lift	The amount of lift observed above threshold	10, 20
Respondents	The number of simulated respondents	200, 500

TABLE III
Mean Absolute Error by Baseline

Baseline	LR	ML	MS
30	2.09	1.67	1.15
50	2.08	1.65	1.16
70	2.75	1.45	1.10

TABLE IV
Mean Absolute Error by Lift

Lift	LR	ML	MS
10	2.35	1.85	1.27
20	2.26	1.32	1.00

across the three dimensions of threshold, baseline and lift, respectively. In each table we show the mean absolute error in the difference between the predicted threshold and the true threshold. The three columns of results correspond to the Logistic Regression (LR), Maximum Likelihood (ML) and Monotonic Smoothing (MS) approaches. In addition, in Table I we also show the False Negative rate, which in this instance means the proportion of times that the method failed for find a threshold in simulations with the given parameters.

These tables clearly demonstrate that the mean absolute error for the Monotonic Smoothing methodology is lowest across almost all simulation parameters. The-trade off being that it has a slightly higher false negative rate than the ML method. Meaning that we will expect 1 percent of the time that we will not find a threshold when one exists, however, when a threshold is determined the expected error in the threshold estimate is much lower.

TABLE V
Model BIAS by Threshold

Threshold	LR BIAS	LR Width	ML BIAS	ML Width	MS BIAS	MS Width
1.0	0.45	5.0	0.64	5.60	0.54	3.21
1.5	0.05	5.0	0.45	5.67	0.21	3.13
2.0	-0.34	5.0	0.30	5.70	-0.09	3.09
2.5	-0.77	5.0	0.13	5.71	-0.35	3.18
3.0	-1.21	5.0	0.09	5.75	-0.60	3.39
3.5	-1.63	5.0	-0.03	5.77	-0.85	3.66
4.0	-2.11	5.0	-0.15	5.73	-1.11	3.96
4.5	-2.56	5.0	-0.30	5.71	-1.42	4.33

TABLE VI
Upper/Lower Bounds by Threshold

Threshold	LR Lower	LR Upper	ML Lower	ML Upper	MS Lower	MS Upper
1.0	-1.0	4.0	-0.94	4.67	-0.56	2.65
1.5	-1.5	3.5	-1.42	4.25	-1.04	2.09
2.0	-2.0	3.0	-1.91	3.79	-1.51	1.57
2.5	-2.5	2.5	-2.39	3.32	-2.00	1.18
3.0	-3.0	2.0	-2.86	2.89	-2.48	0.91
3.5	-3.5	1.5	-3.35	2.42	-2.97	0.69
4.0	-4.0	1.0	-3.80	1.93	-3.44	0.53
4.5	-4.5	0.5	-4.25	1.46	-3.94	0.39

In Table V we show the mean error (BIAS) of each of the three approaches, as well as the width of the confidence bounds shown as upper and lower bounds for 80% of the error values as shown in Table VI. In these tables you will see that

the values range from negative to positive. The negative values indicate the model has a tendency toward under-prediction, whereas a positive reflects over-prediction. Values close to zero indicate that the model is unbiased in its error distribution.

The LR model suffers from a severe variance of error. The bounds are consistently sitting at 5 seconds of time, which is the vast majority of the six second maxiumum exposure. The ML method suffers from a similar fate with bounds that cover almost the entire duration. The Monotonic Smoothing approach, by comparison, maintains bounds of approximately 3 seconds over thresholds in the lower half of exposure time. Whereas in the upper half these bounds creep up to approximately four seconds. The width of these error bounds reflect the difficulty of recovering thresholds using only 200 samples. Our extended simulations with 500 panellists revealed that we can scale these error bounds down to consistently less than 3 seconds using the monotonic smoothing technique, but not the other techniques.

In addition to the simulations that explore the error bounds on threshold estimation, we also ran simulations to understand the rate at which each method infers a threshold where none exists. In these simulations we set the lift to zero and evaluate the proportion of times that the threshold was not null.

TABLE VII
FALSE POSITIVE RATE BY BASELINE

Baseline	LR	ML	MS
30	0.5	0.96	0.89
50	0.4	0.96	0.89
70	0.0	0.96	0.89

We see in Table VII that the LR model is better at avoiding false predictions. However, this does not outweigh the poor performance of this model at identifying thresholds when they do exist. The ML model has the worst overall performance, making false positive predictions 96% of the time when no threshold exists. The monotonic smoothing approach maintains a slightly lower false positive rate of 89%.

V. CONCLUSION

We have developed a monotonic smoothing method for processing brand study data that allows us to estimate the threshold of attention time for which an advertisement has a positive influence on upper funnel metrics. This technique is developed by making reasonable assumptions about psychological constraints in the relationship between visual attention and memory focused measurements of brand impact.

We benchmarked our approach against two general-purpose methods for estimating these thresholds and showed that our approach has lower error if the assumptions made about the relationship between attention and brand outcomes hold true. Furthermore, our approach has consistently tighter bounds on the size of the error. These results allow us to conclude that we should expect the monotonic smoothing approach to provide more robust estimates of consumer attention thresholds for upper funnel metrics in standard brand studies.

The authors acknowledge this research provides no advantage for processing lower funnel brand metric data where complex cognitive processing means higher attention could result in reduced outcomes. Future research projects will involve investigation of cognitive constraints that operate between changes in upper and lower funnel metrics that can be used to smooth brand lift data at the bottom of the funnel.

REFERENCES

[1] R. Pieters and M. Wedel, "Goal control of attention to advertising: The yarbus implication," *Journal of Consumer Research*, vol. 34, pp. 224–233, 08 2007.

[2] D. Vakratsas and T. Ambler, "How advertising works: What do we really know?" *Journal of Marketing*, vol. 63, pp. 26–43, 01 1999.

[3] R. Schmaelzle, S. Lim, H. Cho, J. Wu, and G. Bente, "Examining the exposure-reception-retention link in realistic communication environments via vr and eye-tracking: The vr billboard paradigm," *PloS one*, vol. 18, p. e0291924, 11 2023.

[4] S. Rosengren, M. Eisend, S. Koslow, and M. Dahlen, "A meta-analysis of when and how advertising creativity works," *Journal of Marketing*, vol. 84, p. 002224292092928, 06 2020.

[5] A. Romberg, M. Bennett, S. Tulsiani, B. Simard, J. Kreslake, D. Favatas, D. Vallone, and E. Hair, "Validating self-reported ad recall as a measure of exposure to digital advertising: An exploratory analysis using ad tracking methodology," *International journal of environmental research and public health*, vol. 17, no. 7, 03 2020.

[6] E. Awh, E. Vogel, and S.-H. Oh, "Interactions between attention and working memory," *Neuroscience*, vol. 139, no. 1, pp. 201–208, 2006, cognitive Neuroscience of Working Memory. [Online]. Available: https://www.sciencedirect.com/science/article/pii/S0306452205008985

[7] G. Hervet, K. Guérard, S. Tremblay, and M. Chtourou, "Is banner blindness genuine? eye tracking internet text advertising," *Applied Cognitive Psychology*, vol. 25, pp. 708 – 716, 09 2011.

[8] J. Lee and J.-H. Ahn, "Attention to banner ads and their effectiveness: An eye-tracking approach," *International Journal of Electronic Commerce*, vol. 17, pp. 119–137, 10 2012.

[9] I. Santoso, M. Wright, G. Trinh, and M. Avis, "Mind the attention gap: how does digital advertising impact choice under low attention?" *European Journal of Marketing*, vol. 56, no. 2, pp. 442–446, 12 2021.

[10] S. Djamasbi, M. Siegel, T. Tullis, and R. Dai, "Efficiency, trust, and visual appeal: Usability testing through eye tracking," in *In System Sciences (HICSS), 2010 43rd Hawaii International Conference*, 02 2010, pp. 1 – 10.

[11] K.-C. Hamborg, M. Bruns, F. Ollermann, and K. Kaspar, "The effect of banner animation on fixation behavior and recall performance in search tasks," *Computers in Human Behavior*, vol. 28, pp. 576–582, 03 2012.

[12] A. Barreto, "Do users look at banner ads on facebook?" *Journal of Research in Interactive Marketing*, vol. 7, 05 2013.

[13] N. Kim and H. Lee, "Assessing consumer attention and arousal using eye-tracking technology in virtual retail environment," *Frontiers in Psychology*, vol. 12, 08 2021.

[14] Dentsu, "The attention economy exploring the opportunity for a new advertising currency," June 2019, accessed: 2022-07-23. [Online]. Available: https://www.dentsu.com/attention-economy

[15] Playground XYZ, "Attention time: Redefining how marketers measure and optimize ads in real time," 2019, accessed: 2022-07-23. [Online]. Available: https://playground.xyz/whitepaper.pdf

[16] K. Nelson-Field, *The Attention Economy and How Media Works*. Singapore: Palgrave Macmillian, 2020.

[17] J. L. Orquin and M. Wedel, "Contributions to attention based marketing: Foundations, insights, and challenges," *Journal of Business Research*, vol. 111, pp. 85–90, 2020. [Online]. Available: https://www.sciencedirect.com/science/article/pii/S0148296320301065

[18] P. Summer and E. Bogsnes, "Unveiling the connection: Attention & outcomes," July 2023. [Online]. Available: https://iabeurope.eu/wp-content/uploads/2023/07/Teads-x-Lumen-Attention-Whitepaper.pdf

[19] K. Nelson-Field, "'fools errand' and the billion dollar question: Is 1.7 seconds enough exposure for ads to work? no, but it's beyond facebook," August 2020. [Online]. Available: https://www.mi-3.com.au/13-08-2020/fools-errand-and-billion-dollar-question-17-seconds-enough-exposure-ads-work-no-its

[20] ——, "White paper: Attention research findings 2017-2022," August 2020. [Online]. Available: https://www.amplifiedintelligence.com.au/wp-content/uploads/2022/07/Amplified-Intelligence-Attention-Research-Findings-2017-to-2022.pdf

Enigme: Generative Text Puzzles for Evaluating Reasoning in Language Models

John Hawkins
Centre for Artificial Intelligence and Innovation
Pingla Institute, Sydney, Australia
john@getting-data-science-done.com

***Abstract*—Transformer-decoder language models are a core innovation in text based generative artificial intelligence. These models are being deployed as general-purpose intelligence systems in many applications. Central to their utility is the capacity to understand natural language commands and exploit the reasoning embedded in human text corpora to apply some form of reasoning process to a wide variety of novel tasks. To understand the limitations of this approach to generating reasoning we argue that we need to consider the architectural constraints of these systems. Consideration of the latent variable structure of transformer-decoder models allows us to design reasoning tasks that should probe the boundary of their capacity to reason. We present enigmen, an open-source library for generating text-based puzzles to be used in training and evaluating reasoning skills within transformer-decoder models and future AI architectures.**

***Index Terms*—Artificial Intelligence, Language Models, Reasoning, Evaluation, Benchmark Data**

I. Introduction

The general capabilities of transformer-decoder based large language models has inspired a range of research into prompt and response computer interfaces that are being built for a wide range of language processing and creative purposes [1]. In addition to focus on text generation, there has been a growing investigation of the idea that in the process of learning to produce text in a way that resembles human output, these machine architectures have also learned to be capable of reasoning [2]. In addition there have been investigations into whether these models exhibit *emergent* properties [3] or 'sparks of Artificial General Intelligence' [4]. What these investigations all have in common is an attempt to determine if these large-scale generative models possess a type of intelligence not exhibited in all of the previous developments of machine learning: general purpose abstract reasoning that can be applied to new domains.

Research on transformer-based language models often advances with claims focused on positive examples of a certain behaviour. For example, giving the model a set of tasks and reporting on the success at the new task. This approach has the advantage of being able to demonstrate what can be done with these new tools. However, it suffers from two general problems as a scientific method. The first is that unless it is accompanied with a clear demonstration that the examples were not in the training data (either foundation model text or in the fine-tuning process) then it cannot be known for certain if the behaviour is emergent or memorisation. This fact has been acknowledged by many of those engaged in studying the emergent capabilities of language models [4], but it is far from being solved methodologically. Recent research has begun to shed light on just how much of the output from large language models is due to the model using its over-parameterisation to memorize its training data [5], [6], observations of this problem have been made on closed-source industry models [7]. New evaluation methods include designing explicit tests of whether language models have a sufficiently rich model of the world [8], which helps filter out when models are merely repeating memorised responses.

Multiple authors have observed that the poverty of our AI benchmarks results in a constant adjustment of whether a given task requires intelligence or not [9]. This may be in part because our benchmark driven evaluation means that we place emphasis on performance alone, rather than the methodology used by an algorithm to achieve results [10]. Which is further supported by the trend over time in which we re-evaluate our evaluation methods in part by understanding the mechanisms by which machine learning systems seem to game them. It is worth noting that Large Language Models (LLMs) are routinely evaluated by a wide variety of criteria [11], [12], of which reasoning capability is only one part, and not at the top of the list of considerations. Furthermore, there are a wide range of potential problems with these models beyond limitations of reasoning ability [13]. Regardless, evaluative focus on the claims of emergent reasoning of these systems is important for both the theoretical implications, and due to the emerging widespread use of LLMs in machine learning systems (e.g. recommendation engines [14]). Particularly in the development of agent-based systems [15], where reasoning ability is a central focus of research [16].

Often reasoning is extracted from language models through example-based prompting, such as few-shot or chain-of-thought prompting [17], which have proven useful in general as well as domain specific tasks like medical reasoning [18]. These strategies encourage the model to generate a sequence of tokens that explicitly solve the probelm, but in some strong sense relies on the user being able to generate a prompt with the appropriate examples. This requirement demands that we know something about the structure of the solution to a problem before asking a language model to solve it, which is only slightly mitigated by solutions that automate the retrieval of examples [19]. Recent research suggests that multiple language models can potentially overcome this limitation by

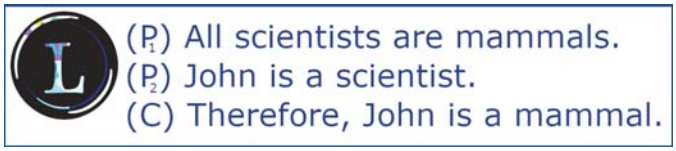


Fig. 1. Example of the natural language template for deductive logical reasoning. The conclusion (C) is drawn from the combination of the content in the two premises (P1) and (P2).

working in concert [20].

The evaluation of logical reasoning can be broken into different modes, or patterns of reasoning, for which different language models exhibit strengths and weaknesses. These reasoning modes include strict inference like logical deduction, or mathematical reasoning, as well as more open-ended modes like monotonicity reasoning [21], and hypothesis generation modes like induction or abduction [22]. It has been shown that performance on these tasks can be broken down into multiple failure modes and suggested that the variation in performance across models might be due to the fine tuning process emphasizing certain skills over others [23]. These logical reasoning tasks are framed in the most ideal way for LLMs to succeed, they are often expressed as grammatical language patterns (as shown in Figure 1) that are exactly the kind of fuzzy template that we expect the latent variable structure of Transformers to learn [24], [25]. Even on these ideal tasks, it appears that performance can depend on arbitrary factors like the order in which premises are presented [26], supporting the idea that what is happening is template matching as opposed to genuine reasoning [24].

Abstract reasoning tasks, like those shown in IQ tests, form the basis of other benchmark datasets (like the ARC challenge [10]). These tasks typically involve recognising a pattern shown in a sequence of images and then applying that pattern to new data, usually under assumptions of perspicacity. When these visual tasks are converted into text -based patterns, we find that language models tend to perform poorly, even when fine-tuned for these tasks [27]. The abstract reasoning benchmark tasks are a more general form of abductive reasoning test, the goal is to infer a minimalistic explanation of a small number of observations, and then successfully apply the inferred pattern. As such they are testing the ability of a model to derive a world model from impoverished data. We are argue that this idea can be extended further into an array of tasks that test different dimensions of the world model inference component of successful reasoning.

A. Motivation

Our primary concern in this work is to design a system for generating reasoning puzzles of different forms that can challenge the capabilities of transformer-decoder based large language models. By considering both the known capabilities of these models and the structure of the latent variable space we devise multiple hypotheses about where their limitations may lie. For each of these hypotheses we design a procedural generation process to create reasoning puzzles that require abstraction, internal model building and alternative interpretations of the symbolic data they have been trained on. We do this such that the text characters are arranged in a way that the patterns they signify are difficult to see without considering them as occupying a physical space that can change over time. These tasks may require consideration of how the characters appear in 2 dimensions, or an understanding of how the text can be used as a symbolic illustrations of patterns of processes in the physical world that transcend linear arrangements of text tokens.

The rationale for this approach is that the multi-headed attention mechanism makes use of two avenues for semantic encoding. The first is that tokens exert influence over each other in a parallel and iterative fashion that allows an embedding to gradually come to represent the role of a word in a text block. Secondly, in the standard architecture the system makes use of some form of positional embedding that characterises the sequential nature of text data.

Given the architectural fundamentals outlined above we design the text puzzles such that pure sequential analysis makes the task very difficult. The patterns require visuualisation across 2 dimensions, and in some cases require abstraction by considering the text as slices of a 3d pattern. In addition, we add multiple dimensions of variation in these tasks such that the number of potential variations is so large that memorisation will be difficult.

Some of the tasks generated in our method bare some similarity with the tasks inside the ARC challenge, being composed of sequences of geometric (largely grid-based) structures. However, there are several key differences. (1) Our problems are ASCII character-based puzzles that enable them to be processed by text only language models. We do this because it removes the complexity of needing to process the image data and makes the tasks amenable to pure text based language models, and hence less resource greedy artificial intelligence research programs. (2) Our tasks are all built around pattern recognition and reasoning tasks that should emulate simple world-model building, the formation of abstractions that are manipulated mentally and intuitive physics reasoning. We do this because our focus is on fundamentally pragmatic reasoning grounded in pattern recognition and reasoning about the physical world. These tasks are often based on a small number of examples and thereby involve a kind of inductive bias [28] that appears in human reasoning. In addition, we would like to avoid the potential biases levelled against abstractions in IQ testing.

II. Methodology

In order to provide analytical variation, we define three independent classes of puzzle. The first class involves *numeric* reasoning tasks, where the text itself is used as a source for numeric quantities that must be manipulated by the reasoner. The second class are *sequence* puzzles (similar to common IQ tests) where the reasoner must use abductive reasoning to infer the underlying pattern. The final class of *physics* puzzles extends the abductive reasoning in sequence puzzles to include sequences with behaviors resembling intuitive physics,

TABLE I
ENIGME PUZZLE CATEGORIES AND ESTIMATED VARIATIONS

Category	Dimensions	Variations
Numeric	1	3.0×10^5
	2	1.4×10^7
	3	4.8×10^9
Sequence	1	1.6×10^6
	2	2.3×10^{62}
	3	6.9×10^{33}
Physics	1	1.6×10^6
	2	4.6×10^7
	3	2.5×10^6

like momentum or collision. Within each of these classes we then provide additional variation through the complexity or dimensionality of the puzzles. Finally, each puzzle generator is provided parameterisation and randomisation to allow for large numbers of variants.

The total number of potential patterns is determined by the number of free parameters and varies with each of the puzzle classes. We show estimates of these variation counts in Table I. Note, that as the number of permutations for some of these puzzles is extremely large, in many instances we are using the largest possible configuration for the estimate. This number tends to dwarf the smaller configurations and forms a good lower bound approximation.

A. Numeric Puzzles

The numeric puzzles are formed by assembling a final text from a set of pre-determined blocks that form multiple variations of the same set of instructions. These instructions are self-referential, in that the task they describe involves analysing the block of text itself.

In the generation process we will have replaced some of the characters in the words of the instruction block. The instructions require that the agent solving the problem numerically analyse the position of these substituted characters within both the sequence of words and the sequence of letters in the word. In addition, for the final complexity level, the agent solving the puzzle needs to recognise the identity of the substituted letter and its position in the sequence of the alphabet. These are the three potential dimensions to the numeric puzzles:

- Position in sequence of words
- Position character within word
- Position of missing character in alphabet

These three numeric components are combined in a simple arithmetic operation that the agent needs to complete to provide the answer. An example of these numeric puzzles is shown in 2.

B. Sequence Puzzles

The algorithm is initialised with a set of parameters drawn randomly from pre-determined distributions. We create a data structure representing an object of between 1 and 3 dimenions (controlled by the complexity parameter). We randomly select a background character from the set `[.,_' ']` to fill this structure. We then iterate over the cells in the structure and determine if the background character be replaced by one of the foreground pattern characters.

The foreground characters are drawn from a set N of 38 characters, including upper case letters, numbers and a variety of punctuation characters. Once the initial structure is determined, we then randomly determine the way in which it will be modified through the series, depending on the dimensionality (complexity) of the puzzle.

An example of a puzzle from the sequence class is shown in Figure 3

C. Physics Puzzles

The physics puzzles share structural similarities with the sequence puzzles; however, they are designed to emulate the behaviour of very simple physical systems. The solution to the puzzle requires extrapolation of that behaviour, invoking notions of momentum, acceleration, deceleration, or the consequences of objects interacting with each other and boundaries. These puzzles demand a form of naive physics reasoning that we hypothesize is essential to inference of a world model from data.

An example of a physics puzzle is shown in Figure 4.

D. Data Generation

The *enigme* application can be invoked to generate random puzzles from any of the three classes. An additional *dimension* parameter determines the complexity of the puzzles through an abstraction of the idea of problem dimensions. We generate one variation from each category and show them in Figures 2, 3, and 4.

These three examples were created by execution of the enigme application using the following commands respectively:

```
> enigme numeric 2d
> enigme sequence 2d
> enigme physics 1d
```

The puzzles are procedurally generated through a template-based substitution method that allows us to estimate the total number of potential variations, shown in Table I. The generation process allows strict control over what can be generated, and programmatic control over the accuracy of the solutions. The estimated number of these variations reflects the current structure of the package and will increase over time as more template variations are added.

III. CONCLUSION

We have described three classes of purely text-based reasoning puzzles that have been defined inside an open-source template-based generative engine. The rationale for these puzzles was derived from a combination of previous work on different modes of reasoning and an analysis of the expected limitations of the latent variable space learned inside the dominant Transformer architecture. We expect this package to be extended with additional classes of puzzle as we identify alternative modes of reasoning that can be tested.

```
In this block of text there is an additional character placed within
one of the words to replace a letter. The position of this character
will determine two numerical values. The first value is determined
from the number of the word within the sequence of words #n this
paragraph, where the first word has value one, the second word value
two, etc. The second value comes from the position of the character
within the word, if it replaces the first letter it has value one, the
second letter value two, etc. You need to subtract the second number
from the first and then write the resulting number below.
```

Fig. 2. Example 1: Enigme Numeric Puzzle - Self Referential Numeric Puzzle

```
Below you will see 3 patterns that form a sequence. Write down the
expected 4th pattern in the sequence.
   1          2          3
   |V|8|D|      |L|4|V|      |&|@|L|
   |4| | |      |@| |8|      | | |4|
   |L|@|&|      |&| |D|      |D|8|V|
```

Fig. 3. Example 2: Enigme Sequence Puzzle - Patterns Represented with ASCII Text

The generation process for these puzzles is parameterised by a dimension/complexity value, allowing researchers to experiment with training and evaluating models on their ability to reason on problems of varying difficulty. We expect extensive usage of this package for benchmarking the reasoning ability of both LLMs and future architectures for artificial intelligence systems. Furthermore, we anticipate broader potential applications of the enigme package in fields such as education and cognitive science.

IV. Availability

The *enigme* open-source code and python application are available on PyPi and GitHub (https://github.com/john-hawkins/enigme).

References

[1] T. Brown, B. Mann, N. Ryder, M. Subbiah, J. D. Kaplan, P. Dhariwal, A. Neelakantan, P. Shyam, G. Sastry, A. Askell, S. Agarwal, A. Herbert-Voss, G. Krueger, T. Henighan, R. Child, A. Ramesh, D. Ziegler, J. Wu, C. Winter, C. Hesse, M. Chen, E. Sigler, M. Litwin, S. Gray, B. Chess, J. Clark, C. Berner, S. McCandlish, A. Radford, I. Sutskever, and D. Amodei, "Language models are few-shot learners," in *Advances in Neural Information Processing Systems*, H. Larochelle, M. Ranzato, R. Hadsell, M. Balcan, and H. Lin, Eds., vol. 33. Curran Associates, Inc., 2020, pp. 1877–1901.

[2] T. Kojima, S. S. Gu, M. Reid, Y. Matsuo, and Y. Iwasawa, "Large language models are zero-shot reasoners," in *Advances in Neural Information Processing Systems*, S. Koyejo, S. Mohamed, A. Agarwal, D. Belgrave, K. Cho, and A. Oh, Eds., vol. 35. Curran Associates, Inc., 2022, pp. 22 199–22 213.

[3] J. Wei, Y. Tay, R. Bommasani, C. Raffel, B. Zoph, S. Borgeaud, D. Yogatama, M. Bosma, D. Zhou, D. Metzler, E. H. Chi, T. Hashimoto, O. Vinyals, P. Liang, J. Dean, and W. Fedus, "Emergent abilities of large language models," *Transactions on Machine Learning Research*, 2022, survey Certification. [Online]. Available: https://openreview.net/forum?id=yzkSU5zdwD

[4] S. Bubeck, V. Chandrasekaran, R. Eldan, J. Gehrke, E. Horvitz, E. Kamar, P. Lee, Y. T. Lee, Y. Li, S. Lundberg, H. Nori, H. Palangi, M. T. Ribeiro, and Y. Zhang, "Sparks of artificial general intelligence: Early experiments with gpt-4," 2023. [Online]. Available: https://arxiv.org/abs/2303.12712

[5] K. Tirumala, A. H. Markosyan, L. Zettlemoyer, and A. Aghajanyan, "Memorization without overfitting: Analyzing the training dynamics of large language models," 2022. [Online]. Available: https://arxiv.org/abs/2205.10770

[6] V. Hartmann, A. Suri, V. Bindschaedler, D. Evans, S. Tople, and R. West, "Sok: Memorization in general-purpose large language models," 2023. [Online]. Available: https://arxiv.org/abs/2310.18362

[7] H. He. (2023) Gpt-4's performance is influenced by data contamination. [Online]. Available: https://x.com/cHHillee/status/1635790330854526981

[8] A. A. Ivanova, A. Sathe, B. Lipkin, U. Kumar, S. Radkani, T. H. Clark, C. Kauf, J. Hu, R. T. Pramod, G. Grand, V. Paulun, M. Ryskina, E. Akyürek, E. Wilcox, N. Rashid, L. Choshen, R. Levy, E. Fedorenko, J. Tenenbaum, and J. Andreas, "Elements of world knowledge (ewok): A cognition-inspired framework for evaluating basic world knowledge in language models," 2024. [Online]. Available: https://arxiv.org/abs/2405.09605

[9] P. McCorduck, *Machines Who Think: A Personal Inquiry into the History and Prospects of Artificial Intelligence*. AK Peters Ltd, 2004.

[10] F. Chollet, "On the measure of intelligence," 2019. [Online]. Available: https://arxiv.org/abs/1911.01547

[11] Z. Guo, R. Jin, C. Liu, Y. Huang, D. Shi, Supryadi, L. Yu, Y. Liu, J. Li, B. Xiong, and D. Xiong, "Evaluating large language models: A comprehensive survey," 2023. [Online]. Available: https://arxiv.org/abs/2310.19736

[12] Y. Chang, X. Wang, J. Wang, Y. Wu, L. Yang, K. Zhu, H. Chen, X. Yi, C. Wang, Y. Wang, W. Ye, Y. Zhang, Y. Chang, P. S. Yu,

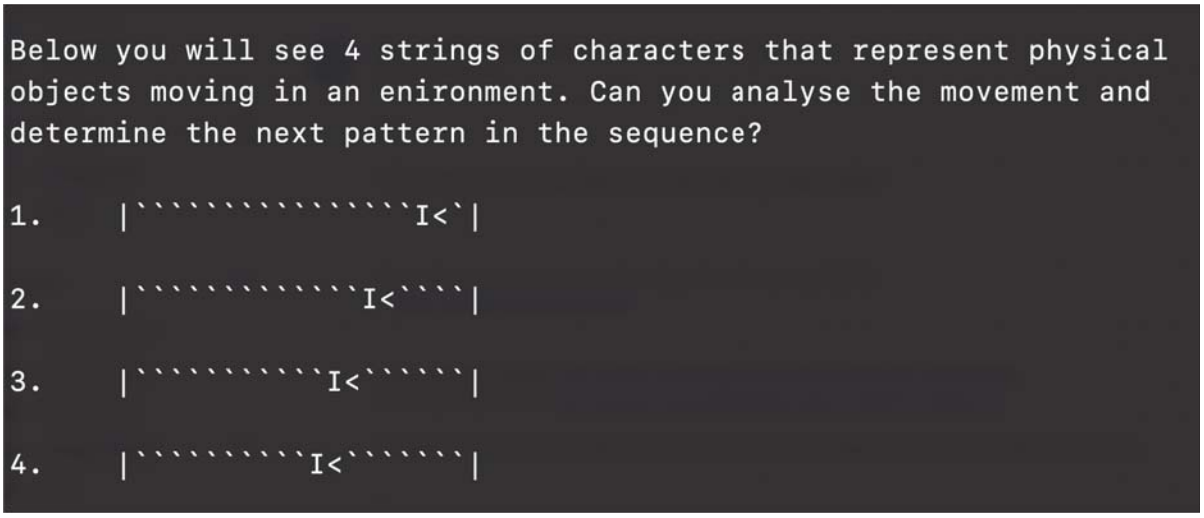


Fig. 4. Example 3: Enigme Physics Puzzle - Physical Object Movement Represented with ASCII Text

Q. Yang, and X. Xie, "A survey on evaluation of large language models," *ACM Trans. Intell. Syst. Technol.*, vol. 15, no. 3, mar 2024. [Online]. Available: https://doi.org/10.1145/3641289

[13] J. Kaddour, J. Harris, M. Mozes, H. Bradley, R. Raileanu, and R. McHardy, "Challenges and applications of large language models," 2023. [Online]. Available: https://arxiv.org/abs/2307.10169

[14] Y. Wang, Z. Chu, X. Ouyang, S. Wang, H. Hao, Y. Shen, J. Gu, S. Xue, J. Zhang, Q. Cui, L. Li, J. Zhou, and S. Li, "Llmrg: Improving recommendations through large language model reasoning graphs," *Proceedings of the AAAI Conference on Artificial Intelligence*, vol. 38, no. 17, pp. 19 189–19 196, Mar. 2024. [Online]. Available: https://ojs.aaai.org/index.php/AAAI/article/view/29887

[15] J. Andreas, "Language models as agent models," in *Findings of the Association for Computational Linguistics: EMNLP 2022*, Y. Goldberg, Z. Kozareva, and Y. Zhang, Eds. Abu Dhabi, United Arab Emirates: Association for Computational Linguistics, Dec. 2022, pp. 5769–5779. [Online]. Available: https://aclanthology.org/2022.findings-emnlp.423

[16] S. Yao, J. Zhao, D. Yu, N. Du, I. Shafran, K. Narasimhan, and Y. Cao, "ReAct: Synergizing reasoning and acting in language models," in *International Conference on Learning Representations (ICLR)*, 2023.

[17] J. Wei, X. Wang, D. Schuurmans, M. Bosma, B. Ichter, F. Xia, E. H. Chi, Q. V. Le, and D. Zhou, "Chain-of-thought prompting elicits reasoning in large language models," in *Proceedings of the 36th International Conference on Neural Information Processing Systems*, ser. NIPS '22. Red Hook, NY, USA: Curran Associates Inc., 2024.

[18] O. Gramopadhye, S. S. Nachane, P. Chanda, G. Ramakrishnan, K. S. Jadhav, Y. Nandwani, D. Raghu, and S. Joshi, "Few shot chain-of-thought driven reasoning to prompt llms for open ended medical question answering," 2024. [Online]. Available: https://arxiv.org/abs/2403.04890

[19] Z. Zhang, A. Zhang, M. Li, and A. Smola, "Automatic chain of thought prompting in large language models," in *The Eleventh International Conference on Learning Representations*, 2023. [Online]. Available: https://openreview.net/forum?id=5NTt8GFjUHkr

[20] Q. Wang, Z. Wang, Y. Su, H. Tong, and Y. Song, "Rethinking the bounds of llm reasoning: Are multi-agent discussions the key?" 2024. [Online]. Available: https://arxiv.org/abs/2402.18272

[21] H. Yanaka, K. Mineshima, D. Bekki, K. Inui, S. Sekine, L. Abzianidze, and J. Bos, "Can neural networks understand monotonicity reasoning?" in *Proceedings of the 2019 ACL Workshop BlackboxNLP: Analyzing and Interpreting Neural Networks for NLP*, T. Linzen, G. Chrupała, Y. Belinkov, and D. Hupkes, Eds. Florence, Italy: Association for Computational Linguistics, Aug. 2019, pp. 31–40. [Online]. Available: https://aclanthology.org/W19-4804

[22] K. He, M. Zhang, S. Yan, P. Wu, and Z. Z. Chen, "Idea: Enhancing the rule learning ability of large language model agent through induction, deduction, and abduction," 2024. [Online]. Available: https://arxiv.org/abs/2408.10455

[23] F. Xu, Q. Lin, J. Han, T. Zhao, J. Liu, and E. Cambria, "Are large language models really good logical reasoners? a comprehensive evaluation and beyond," 2023. [Online]. Available: https://arxiv.org/abs/2306.09841

[24] B. Jiang, Y. Xie, Z. Hao, X. Wang, T. Mallick, W. J. Su, C. J. Taylor, and D. Roth, "A peek into token bias: Large language models are not yet genuine reasoners," 2024. [Online]. Available: https://arxiv.org/abs/2406.11050

[25] I. Mirzadeh, K. Alizadeh, H. Shahrokhi, O. Tuzel, S. Bengio, and M. Farajtabar, "Gsm-symbolic: Understanding the limitations of mathematical reasoning in large language models," 2024. [Online]. Available: https://arxiv.org/abs/2410.05229

[26] X. Chen, R. A. Chi, X. Wang, and D. Zhou, "Premise order matters in reasoning with large language models," 2024. [Online]. Available: https://arxiv.org/abs/2402.08939

[27] G. Gendron, Q. Bao, M. Witbrock, and G. Dobbie, "Large language models are not strong abstract reasoners," 2024. [Online]. Available: https://arxiv.org/abs/2305.19555

[28] A. Goyal and Y. Bengio, "Inductive biases for deep learning of higher-level cognition," 2022. [Online]. Available: https://arxiv.org/abs/2011.15091

An Ensemble model of Dual learning for Gambling and Pornographic Websites Classification

Sirapat Thianphan, Kietikul Jearanaitanakij
School of Engineering, King Mongkut's Institute of Technology Ladkrabang, Bangkok, Thailand
Email: sirapat.tianpan@gmail.com
Email: kietikul.je@kmitl.ac.th

***Abstract*—The rapid proliferation of pornographic and gambling websites poses significant challenges, as these platforms increasingly employ sophisticated techniques to evade detection. Traditional classification approaches that rely on a single feature often fail to achieve high detection rates due to the diverse strategies these websites use to bypass detection systems. To address this limitation, this study introduces an ensemble model for classifying pornographic and gambling websites by integrating two key features: URLs and textual content. A web-scraping script was developed to extract textual data from HTML elements of 3,000 websites, evenly distributed among benign, pornographic, and gambling categories, specifically curated for Thai users. The URLs undergo preprocessing to capture their meaningful semantic properties, which reflect the characteristics of the corresponding websites. Separate classifiers were then trained on each feature before being integrated into an ensemble model for final prediction. This approach achieved an outstanding accuracy of 96.83%, significantly surpassing single-feature classifiers. Moreover, the findings demonstrate the proposed model's robustness against obfuscation techniques and anti-crawling mechanisms, underscoring its potential for effective automated detection.**

***Index Terms*—website detection, ensemble model, url classification, image classification, text classification.**

I. Introduction

The rapid expansion of the Internet has significantly increased access to both valuable resources and illegal content, particularly pornography and gambling. Insufficient regulatory controls have led to greater exposure among children and young people. In Thailand, the number of online gambling users rose from 0.82 million in 2019 to 5.66 million in 2023 [1], while studies indicate that 54% of Thai teenagers have encountered pornographic content online [2]. These websites pose substantial risks to children's mental and physical well-being, necessitating effective regulatory measures.

Various detection approaches have been proposed to mitigate access to illegal websites. Blacklisting, an early method, relies on predefined lists of illicit domains but struggles to detect newly emerging URLs due to its dependence on manual updates [3]. As an alternative, machine learning techniques have been developed to classify websites based on extracted features, such as URLs [4] or website content [5]. URL-based methods offer rapid detection but often fail to capture the full characteristics of illicit websites, leading to inconsistent classification performance [6]. Meanwhile, content-based approaches leverage textual and visual data but face challenges such as obfuscation techniques that conceal key information [7]. For instance, some illegal websites embed keywords within images, complicating text extraction and exacerbating the high-dimensionality problem [8]. Additionally, visual-based classification, despite demonstrating promising results, is vulnerable to misclassification when legitimate websites share visual similarities with illicit ones [6]. Moreover, deceptive tactics, such as disguise and anti-robot mechanisms, further degrade detection accuracy.

To address these challenges, hybrid approaches integrating multiple features—such as URLs, text, and visual content—have emerged as more effective solutions [9]. However, the effectiveness of such methods depends on optimal feature integration; otherwise, increased computational costs and inefficiencies may arise.

Given the evolving strategies employed by illegal websites, there is a pressing need for a robust automated detection system capable of overcoming these challenges. This study proposes a novel detection framework that combines URL-based analysis with textual content extracted from raw web pages. By leveraging ensemble learning, this approach surpasses single-feature classifiers—achieving an accuracy of up to 96.83%—and demonstrates the advantages of multi-feature integration for improved website classification.

II. Related Work

Website classification has gained attention due to the rise of illegal websites. Existing methods fall into three categories: URL-based, content-based, and hybrid approaches.

A. URL-based Classifiers

URL-based classification extracts meaningful attributes using lexical analysis [10], [11] or statistical methods [12], [13]. While extensively used for phishing detection, its application to pornographic or gambling sites, especially in non-English datasets, remains limited. Zouina et al. proposed a lightweight classifier using six URL attributes, emphasizing similarity index [14]. Dinh et al. introduced a Naive Bayes model incorporating Vietnamese syntax for pornographic site detection [15]. URL-based methods enable fast classification without accessing websites but suffer from lower accuracy compared to content-based or hybrid approaches.

B. Content-based Classifiers

Content-based approaches leverage text and images for improved classification. Text extracted from raw HTML provides rich information but often requires extensive preprocessing to remove noise [16], [17]. Some websites minimize textual content, relying on images instead, which can hinder text-based classifiers [18]. Image-based classification requires careful feature representation, as deceptive website layouts can resemble legitimate ones [8], [19]. Additionally, image-based models are vulnerable to adversarial attacks [20], [21]. Despite higher detection rates, content-based methods face challenges from countermeasures like Cloudflare protection and dynamic content generation, which obstruct automated extraction.

C. Hybrid Feature-based Classifiers

The evolving nature of illicit websites necessitates hybrid approaches integrating multiple features. Chen et al. [6] proposed a model combining text extracted from key HTML elements with website screenshots, classifying them separately before integration using logistic regression. While hybrid models enhance accuracy, they introduce computational complexity and longer detection times. Nonetheless, integrating diverse features improves resilience against evasion tactics, making hybrid approaches a promising direction for website classification.

III. Proposed Methodology

This section outlines the proposed method, covering dataset acquisition, the website classification framework, and the automated detection system.

A. Data Acquisition

Our dataset comprises 3,000 websites evenly distributed across benign, pornographic, and gambling categories. These websites, primarily in Thai, were sourced from platforms frequently accessed by Thai users. The dataset includes three key features: URLs, textual content, and website screenshots. A Python-based web crawler collects data by taking URLs as input and generating corresponding text files and screenshots. Each feature undergoes independent preprocessing to facilitate training for single-feature classifiers.

1) Text Feature Extraction: Textual content serves as a critical feature in website classification, offering insights into site structure and purpose. Extracting meaningful text from raw HTML begins with Selenium, which retrieves content from relevant semantic elements. Key tags—$< meta >, < li >, < a >, < h1 >, < h2 >$, and $< h3 >$—are selected for their significance in website characterization.

2) URL Feature Extraction: URL-based classification alone may be suboptimal due to challenges in real-world detection. Illegal websites frequently alter URLs to evade detection, often mimicking legitimate domains. However, a key advantage of URL-based classifiers is that they operate without direct website access, unlike text- and image-based classifiers, which rely on server access and may be blocked by anti-bot measures.

During preprocessing, only the subdomain and second-level domain are extracted, as other URL components provide limited semantic value. While the page path can sometimes indicate website type, it often introduces noise, particularly in Thai URLs due to percent-encoding. The extracted components are then encoded using Term Frequency-Inverse Document Frequency (TF-IDF) for classification.

B. Proposed Classification System

After feature extraction, our system trains single-feature classifiers to establish baseline performance. The most effective models are then integrated into an ensemble framework to enhance classification accuracy.

1) Single-Feature Classification: Two independent classifiers were developed using various machine learning algorithms. For URL classification, Naïve Bayes (NB), Multi-Layer Perceptron (MLP), and Support Vector Machine (SVM) achieved the highest accuracy. For text classification, the best models were Random Forest (RF), NB, and MLP.

2) Ensemble Learning Employment: The top three models from each category were integrated into hybrid classifiers using ensemble learning. Each classifier was trained on its respective dataset, and their outputs were combined via a stacking model, with logistic regression (LR) as the final prediction layer. An overview of the framework is shown in Fig. 1.

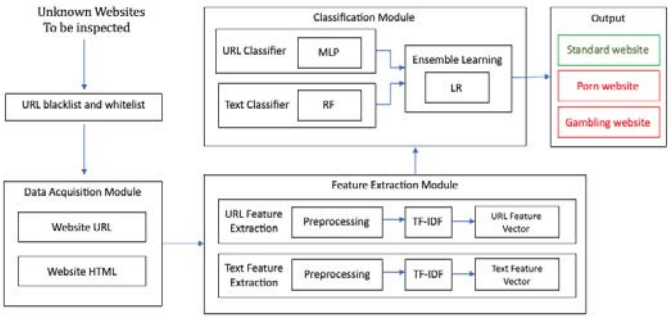


Fig. 1. The flowchart of the proposed classification system

3) Automated Detection System: Once trained, the proposed hybrid classifier can be integrated with a web-scraping script into an intelligent wireless router, enabling automated detection. The system classifies web traffic and updates the URL blacklist when previously unknown pornographic or gambling websites are identified.

Our approach combines URL-based and textual content features to enhance detection performance. Notably, its lightweight URL classifier enables rapid analysis with minimal computational overhead, making it well-suited for embedded security devices, smart home routers, and other resource-constrained IoT systems. By balancing efficiency and accuracy, this system provides a practical solution for automated threat detection.

IV. Experiments and Results

This section presents the experimental design and methodology used to evaluate the proposed approach. We first describe the dataset, followed by the experimental setup and a comprehensive analysis of the results.

A. Experimental Dataset

The dataset comprises 3,000 websites evenly categorized into gambling, pornographic, and standard websites. It was assembled through manual collection from online sources and user surveys in Thailand. To assess different classifier features, the dataset was segmented into three subsets: URLs, textual content, and screenshots.

Feature extraction encountered challenges due to anti-bot mechanisms such as CAPTCHAs, access restrictions, and Cloudflare protection. As shown in Fig.2, Cloudflare-protected websites provided limited textual content, reducing data quality. Despite these constraints, over 83% of the dataset remained high quality on average.



Fig. 2. A screenshot of a website protected by Cloudflare

B. Experimental Design and Result

In our experiments, we focus exclusively on the URL, textual content, and screenshot features of websites. The performance of classifiers using single feature and hybrid features will be presented in the following subsections.

1) URL-based Classifiers: In this part, various machine learning algorithms were implemented to determine the most effective model for URL classification. After preprocessing the dataset, including data cleaning, the URLs were encoded using TF-IDF and then fed into the candidate models. According to the results, our top three models are the Naïve Bayes (NB), Multilayer Perceptron (MLP), and Support Vector Machine (SVM) classifiers, with the highest accuracy reaching 90.67%.

2) Textual content-based Classifiers: For text classification, six candidate models were evaluated, with Random Forest (RF) and Multi-Layer Perceptron (MLP) achieving the highest accuracy of 94.33%, followed by the Support Vector Machine (SVM), which reached an accuracy of 92.66%. The textual content feature required a sophisticated cleaning process, as the extracted text was derived from key HTML elements that often contained a substantial amount of noise. Therefore, proper preprocessing was essential for improving classification performance.

3) Visual content-based Classifiers: For the final feature, website screenshots are utilized for image classification. The data preprocessing stage presents significant challenges due to the considerable variation in website layouts, which complicates the automated capture of high-quality images. Our most successful outcome was achieved using the pretrained MobileNetV2 model, attaining a maximum accuracy of 81.11%.

Upon examining the factors contributing to the low detection rates of image-based classifiers, it was observed that many gambling websites contain fewer distinctive images and typically have long, scrollable pages. Consequently, the extracted images often suffer from reduced quality, thereby hindering the classifiers' ability to achieve high accuracy.

4) Hybrid Classification: Our evaluation of single-feature classification methods revealed distinct challenges. URL-based classifiers had high false positive rates in the gambling category, often misidentifying websites with domain names resembling legitimate ones. Image-based classifiers were less effective due to dataset limitations, as anti-bot mechanisms hindered screenshot extraction, and illicit sites used obfuscation tactics such as login pages or interactive pop-ups to evade detection.

Recognizing these limitations, we developed hybrid classifiers integrating URL- and text-based features. URLs enable continuous detection without direct server access, unlike image- and text-based methods, which struggle when access is restricted. Image classifiers also performed poorly due to inconsistencies in screenshot quality and website layouts, leading us to exclude them from our model.

We hypothesize that combining URL and text-based classification enhances real-world detection. Using a stacking-based ensemble learning approach, we integrated outputs from both classifiers. To validate this, we constructed nine hybrid models by combining the top three URL classifiers with the top three text classifiers (Table I), achieving a maximum accuracy of 96.83%.

Single-Feature Classifiers		**Hybrid Classifiers**
URL (Acc %)	**Text (Acc %)**	**Accuracy (%)**
MLP (90.33)	MLP (94.33)	96.33
MLP (90.33)	**RF (94.33)**	**96.83**
MLP (90.33)	SVM (92.66)	95.67
SVM (89.33)	MLP (94.33)	94.17
SVM (89.33)	RF (94.33)	94.50
SVM (89.33)	SVM (92.66)	93.67
NB (90.67)	MLP (94.33)	96.33
NB (90.67)	RF (94.33)	96.50
NB (90.67)	SVM (92.66)	94.17

TABLE I
Hybrid Classifier Comparison

C. Performance Evaluation

The proposed hybrid classifier demonstrates satisfactory performance. To evaluate our results, we establish a set of evaluation metrics, as presented in Table II, along with a confusion matrix illustrated in Fig. 3. The analysis results show that only eight websites from the porn and gambling categories were misclassified as benign. This finding supports the effectiveness of our proposed model.

Class	Precision	Recall	F1-Score	Support
benign	0.94	0.98	0.96	217
porn	0.97	0.96	0.97	197
gambling	0.98	0.95	0.97	186

TABLE II
EVALUATION METRICS OF THE PROPOSED HYBRID CLASSIFICATION

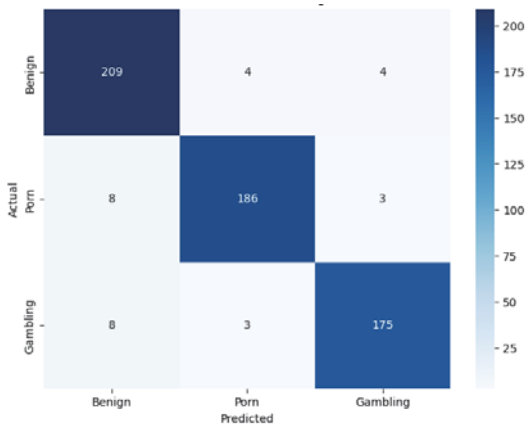


Fig. 3. The Confusion Matrix of the Proposed Hybrid Classification

V. CONCLUSION

This study proposes an automated system for detecting pornographic and gambling websites using a dual-learning approach. A web scraper extracts semantic text from HTML elements, which, along with website URLs, serves as input for a hybrid classification framework. By leveraging ensemble learning, the model enhances robustness against evasion tactics, effectively complementing the limitations of individual classifiers. While illicit websites frequently change domain names, hindering content-based classification, the URL-based classifier remains effective without requiring direct server access. Conversely, when deceptive domain names obscure URL-based detection, the textual classifier improves accuracy.

Unlike hybrid approaches that integrate image features and demand high computational resources, our lightweight model is practical for deployment on both enterprise-grade and consumer-grade smart routers, extending protection to homes and classrooms.

Despite its strong performance, the system faces challenges in handling Thai text, where TF-IDF encoding may be less effective. Additionally, classification struggles when altered URLs prevent direct content access, limiting the extracted features. Future work will refine Thai text encoding and expand detection to other harmful websites targeting Thai users, fostering a safer online environment.

REFERENCES

[1] "Gambling situation in thailand 2023," Center for Gambling Studies, 518 Faculty of Economics, Chulalongkorn Universit, Bangkok, Thailand, Tech. Rep., 2023.

[2] P. sriwicha, "Legal problems of pornography control : A case study on pornographic live streaming through social media," *Journal of Mahayana voice*, vol. 9, no. 2, pp. 182–191, 2023.

[3] F. Khan, J. Ahamed, S. Kadry, and L. K. Ramasamy, "Detecting malicious urls using binary classification through ada boost algorithm." *International Journal of Electrical & Computer Engineering (2088-8708)*, vol. 10, no. 1, 2020.

[4] C. Rupa, G. Srivastava, S. Bhattacharya, P. Reddy, and T. R. Gadekallu, "A machine learning driven threat intelligence system for malicious url detection," in *Proceedings of the 16th International Conference on Availability, Reliability and Security*, 2021, pp. 1–7.

[5] H. Yang, K. Du, Y. Zhang, S. Hao, Z. Li, M. Liu, H. Wang, H. Duan, Y. Shi, X. Su *et al.*, "Casino royale: a deep exploration of illegal online gambling," in *Proceedings of the 35th Annual Computer Security Applications Conference*, 2019, pp. 500–513.

[6] Y. Chen, R. Zheng, A. Zhou, S. Liao, and L. Liu, "Automatic detection of pornographic and gambling websites based on visual and textual content using a decision mechanism," *Sensors*, vol. 20, no. 14, p. 3989, 2020.

[7] B. Wang, F. Shi, and H. Zheng, "Multi-modal clustering discovery method for illegal websites based on network surveying and mapping big data," *Applied Sciences*, vol. 13, no. 17, p. 9837, 2023.

[8] L. Li, G. Gou, G. Xiong, Z. Cao, and Z. Li, "Identifying gambling and porn websites with image recognition," in *Advances in Multimedia Information Processing–PCM 2017: 18th Pacific-Rim Conference on Multimedia, Harbin, China, September 28-29, 2017, Revised Selected Papers, Part II 18*. Springer, 2018, pp. 488–497.

[9] C. Wang, P. Xue, M. Zhang, and M. Hu, "Identifying gambling websites with co-training." in *SEKE*, 2022, pp. 598–603.

[10] P. Teppap, P. Tipauksorn, S. Surathong, W. Ponglangka, and P. Luekhong, "Automating hidden gambling detection in web sites: A beautifulsoup implementation," in *2024 21st International Joint Conference on Computer Science and Software Engineering (JCSSE)*. IEEE, 2024, pp. 132–139.

[11] Y. Huang, Q. Yang, J. Qin, and W. Wen, "Phishing url detection via cnn and attention-based hierarchical rnn," in *2019 18th IEEE International Conference On Trust, Security And Privacy In Computing And Communications/13th IEEE International Conference On Big Data Science And Engineering (TrustCom/BigDataSE)*. IEEE, 2019, pp. 112–119.

[12] H. Liu, X. Pan, and Z. Qu, "Learning based malicious web sites detection using suspicious urls," *Software Engineering*, 2016.

[13] R. Verma and A. Das, "What's in a url: Fast feature extraction and malicious url detection," in *Proceedings of the 3rd ACM on International Workshop on Security and Privacy Analytics*, 2017, pp. 55–63.

[14] M. Zouina and B. Outtaj, "A novel lightweight url phishing detection system using svm and similarity index," *Human-centric Computing and Information Sciences*, vol. 7, pp. 1–13, 2017.

[15] T.-A. Dinh, T.-B. Ngo, and D.-L. Vu, "A model for automatically detecting and blocking pornographic websites," in *2015 Seventh International Conference on Knowledge and Systems Engineering (KSE)*. IEEE, 2015, pp. 244–249.

[16] J.-J. Sheu, "Distinguishing medical web pages from pornographic ones: An efficient pornography websites filtering method." *Int. J. Netw. Secur.*, vol. 19, no. 5, pp. 839–850, 2017.

[17] J. Shin, S. Lee, and T. Wang, "Semantic approach for identifying harmful sites using the link relations," in *2014 IEEE International Conference on Semantic Computing*. IEEE, 2014, pp. 256–257.

[18] X. Ma, C. Zheng, Z. Li, J. Yin, Q. Liu, and X. Chen, "A lightweight graph-based method to detect pornographic and gambling websites with imperfect datasets," in *2022 IEEE International Conference on Trust, Security and Privacy in Computing and Communications (TrustCom)*. IEEE, 2022, pp. 291–298.

[19] D. Liu, J.-H. Lee, W. Wang, and Y. Wang, "Malicious websites detection via cnn based screenshot recognition," in *2019 International Conference on Intelligent Computing and its Emerging Applications (ICEA)*. IEEE, 2019, pp. 115–119.

[20] K. Yuan, D. Tang, X. Liao, X. Wang, X. Feng, Y. Chen, M. Sun, H. Lu, and K. Zhang, "Stealthy porn: Understanding real-world adversarial images for illicit online promotion," in *2019 IEEE Symposium on Security and Privacy (SP)*. IEEE, 2019, pp. 952–966.

[21] C. Xie, M. Tan, B. Gong, J. Wang, A. L. Yuille, and Q. V. Le, "Adversarial examples improve image recognition," in *Proceedings of the IEEE/CVF conference on computer vision and pattern recognition*, 2020, pp. 819–828.

Quality Classification of Sunglasses Lens by Deep Learning

Charin Theskham
Department of Computer Engineering, School of Engineering
King Mongkut's Institute of Technology Ladkrabang
Lat Krabang, Bangkok
65016017@kmitl.ac.th

Kietikul Jearanaitanakij
Department of Computer Engineering, School of Engineering
King Mongkut's Institute of Technology Ladkrabang
Lat Krabang, Bangkok
kietikul.je@kmitl.ac.th

***Abstract*— Sunglasses lens are medical devices designed to correct human vision while also providing protection against ultraviolet (UV) radiation. Sunglasses lenses come in various colors, each offering different light-filtering properties. Currently, the quality classification of sunglasses lenses during the production process still relies on human vision. Therefore, this research aims to study the design and quality classification of sunglasses lens with both evenness and unevenness colors using machine vision and deep learning techniques. However, from the review of existing studies on sunglasses lens quality inspection, informal research has been conducted in this area. This work is considered a new contribution with potential for practical application in the industry. In this study, a Convolutional Neural Network (CNN) will be used. To save research time, the researchers employed transfer learning techniques using models such as VGG16, VGG19, InceptionV3, Xception, DenseNet121, ResNet50, EfficientNetB0, EfficientNet -B7, and EfficientNetV2L. The classification results are divided into 2 categories for evenness colors lens and unevenness colors lens. The dataset used real photos of sunglasses lens from Hoya Lens Thailand as the data source. A dataset of 1,250 real images of sunglasses lens was used, comprising 625 images of evenness colors lens and 625 images of unevenness colors lens. Data augmentation was performed by rotating the images 90, 180, and 270 degrees, as well as vertically flipping the sunglasses lens images. This process yielded a total of 10,000 images, with 5,000 images each for lenses with evenness and unevenness colors. The results of applying Transfer Learning of each model for classifying the quality of sunglasses lens that the DenseNet121 model achieved the highest performance, with an accuracy of 82.23% and precision of 82.32%**

Keywords*— *Sunglasses lens, Computer vision, Deep learning, Convolutional neural network, Transfer learning

I. INTRODUCTION

Eyeglass lenses are optical tools designed to correct vision impairments in individuals who experience issues such as nearsightedness, farsightedness, or astigmatism. These lenses allow wearers to see more clearly. There are various types of lenses available, each suited to specific vision problems. Single Vision Lenses are used to correct nearsightedness, farsightedness, or astigmatism at a single distance. These lenses are ideal for individuals who require correction for either near or far vision only. Progressive Lenses incorporate multiple prescriptions within a single lens, enabling the wearer to see clearly at near, intermediate, and far distances. These lenses are suitable for individuals who want a single lens that can be used in all situations. Bifocal Lenses, on the other hand, have two distinct prescriptions, with the upper portion designed for distance vision and the lower portion for near vision, making them ideal for people who require correction for both conditions.

In addition to correcting vision problems, eyeglass lens are also designed with special features to adapt to various lighting conditions. For instance, Photochromic Lenses can change their tint based on the intensity of light, making them suitable for both indoor and outdoor use. Hard Coat Lens are resistant to scratches, while Anti-Reflection Coated Lens reduce glare by minimizing light reflections on the lens surface, enhancing sharpness and visual contrast.

Sunglasses Lens are another important category, offering protection against harmful ultraviolet (UV) rays and reducing glare. Among these, Polarized Lens are designed to reduce reflections from flat surfaces such as roads or water, making them ideal for outdoor activities. Tinted Lenses, another type, are designed to shield the eyes from UVA and UVB rays, which can lead to eye problems such as cataracts, pterygium, and pinguecula. These lenses also reduce eye strain caused by bright sunlight and enhance visual comfort.

Sunglasses Lens come in various colors, each serving different purposes. For instance, gray lenses reduce glare and are suitable for general use, green lenses improve clarity and are ideal for outdoor activities, brown lenses enhance contrast and are great for driving, while yellow lenses increase visibility in low-light conditions, making them suitable for nighttime activities.

The manufacturing of sunglasses lens involves a complex process that utilizes advanced technologies to create high-quality products that meet the diverse needs of consumers. The main steps include producing lens pieces through methods like casting, cutting, or grinding; applying coatings for scratch resistance, UV protection, and anti-reflection; dyeing lenses to protect eyes from sunlight; and conducting quality inspections to identify any defects.

Defects commonly found in dyed lenses include uneven coloration, black or white spots on the lens surface, streaks of color, or areas where the tint appears darker than others. Currently, most quality inspections for lens dyeing rely on manual visual inspection, which can be limited in terms of speed and accuracy. Introducing automated systems into the manufacturing process can help improve efficiency and precision in quality inspections.

The use of modern technologies, such as computer vision [1-2], and artificial intelligence (AI), machine learning, deep learning [3], can greatly enhance the ability to monitor and control quality during production. These technologies help reduce human errors, increase productivity, and elevate manufacturing standards to align with the rapidly changing market demands. Moreover, automation allows for greater flexibility and efficiency in the production process.

Despite this, research on automated quality inspection of sunglass lenses is still scarce, presenting an opportunity to develop studies that provide a better understanding and create

XXX-X-XXXX-XXXX-X/XX/$XX.00 ©20XX IEEE

more effective inspection methods. Leveraging advanced technologies in lens manufacturing and quality control will enable the industry to achieve higher levels of precision, consistency, and responsiveness to market needs.

However, from the review of existing studies on sunglass lens quality inspection, informal research has been conducted in this area. But there are examples of research that use transfer learning techniques in classification such as:

- The classification of defects on steel surfaces using transfer learning [4]. The model used is VGG16. The classification accuracy of surface defects is 99.44%.
- The study analyzes defects in objects printed with 3D printing technology using transfer learning methods. The models used include VGG16, InceptionResNet-V2, ResNet50, MobileNetV2, VGG19, ResNet101, Xception, EfficientNetB0, EfficientNetB7, Efficient NetV2M, and NASNetLarge. [5] The results showed that VGG16, MobileNetV2, InceptionResNetV2, and NASNetLarge performed better than other models, particularly when fine-tuned with Adam and RMSprop optimizers. On the other hand, models like EfficientNetB0, EfficientNetB7, and Efficient NetV2M, especially when paired with the SGD optimizer, showed the lowest performance. For instance, EfficientNetB7 displayed low accuracy at only 60%, with 62% accuracy when paired with SGD.
- The study focuses on classifying sugar crystals using deep learning methods. The experiment involved creating one custom model and using three transfer learning models [6]: InceptionV3, VGG16, and ResNet50. The results showed that the transfer learning model, VGG16, achieved the highest accuracy at 85%, followed by ResNet50 with 83% accuracy, InceptionV3 with 78.5%, and the custom model with 60.5% accuracy.
- The study focuses on classifying defects in ski goggle lenses using machine learning. The research selected the ResNet50 transfer learning model, and the results showed that ResNet50 achieved an accuracy of 94.34% in classifying the defects of ski goggle lenses [7].

This presents an opportunity to develop new research that enhances understanding and provides more effective inspection methods

II. Fundamental Knowledge

A. Sunglasses lens tinting

The manufacturing process of tinting sunglasses lens is based on diffusion, where dye particles move from an area of high concentration (the dye solution) to an area of low concentration (the lens material). This occurs naturally as particles disperse to balance concentrations. Fick's Law of Diffusion explains this movement, and in the tinting process, it ensures an even color distribution throughout the lens.

The lenses are first cleaned and placed in a dye mixture. The concentrated dye gradually spreads into the lens material, darkening it over time. The lens's refractive index (density) plays a key role in how quickly this occurs. Lenses with higher refractive indices are thinner and lighter, but require longer or more intense dyeing. Lenses with lower refractive indices take less time to tint.

B. Quality classification of sunglasses lens by visual

The operator responsible for inspecting and classifying the quality of sunglasses lenses will use a visual inspection process. This starts by holding the lens up to allow light to pass through, followed by carefully observing the uniformity of the lens color in detail. The goal is to ensure that the lens meets quality standards, without any blemishes or irregularities that could affect its performance for the consumer. This process requires a great deal of skill and attention to detail from the staff to accurately distinguish color differences and ensure that each lens meets the established criteria for quality, as shown in Fig. 1.

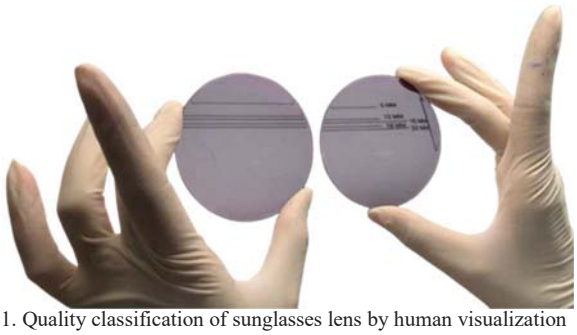


Fig. 1. Quality classification of sunglasses lens by human visualization

C. Example of Sunglassses lens

A good quality pair of sunglasses should have evenness throughout. However, if the lenses are not consistent in color, certain defects may be observed, such as blotches, darker edges compared to other areas, black or white spots either in specific areas or scattered across the lens, and the appearance of colored streaks as shown in Fig. 2.

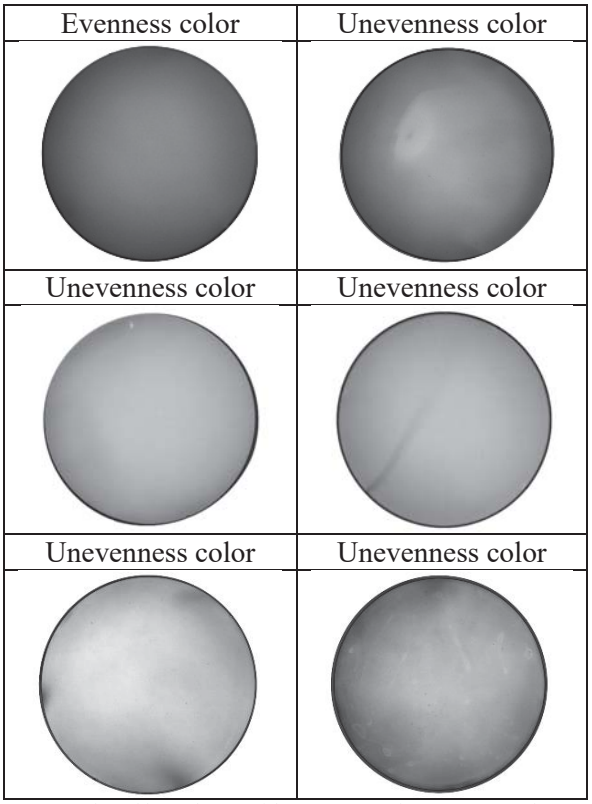


Fig. 2. Examples of lens photos with evenness and unevenness colors

III. Proposed Method

This research is an experimental study that applies Transfer Learning techniques to develop a model for classifying the quality of sunglasses lens. The sunglasses lens are categorized into 2 main groups: evenness color lens and unevenness color lens. In this study, a pre-trained model was adapted to improve the accuracy of classifying and analyzing image data related to the quality of the sunglasses lens. The process includes several main steps: Data Collection, where images of sunglasses lens are gathered through photographing the lenses to be used for training and testing the model; Data Preparation, which involves adjusting the collected image data for input into the model; Data Classification, where the quality of the lenses is classified into 2 groups; and finally, Model Tuning, aimed at enhancing classification performance and reducing errors. This entire process helps to produce a model capable of accurately and effectively classifying and assessing the quality of sunglasses lens.

A. Data Collection

Since the image data used for this research consists of photographs of sunglasses lens, which cannot be obtained from public data sources, the researcher must collect all the real photos of sunglasses lens from Hoya Lens Thailand as the data source. The researcher has designed a device to capture images of sunglasses lens. The captured images will include sunglasses lenses with evenness color and those with unevenness color, such as dark or white spots on the lens surface, color stains on the lens, or long stripes with darker color than the surrounding areas as shown in Fig. 2.

- Image Acquisition Design

The imaging equipment used in this research will consist of a camera with a lens, a photography box, and a light source. This imaging system operates based on the principle of light, where light passes through an object to a sensor. The camera is installed at the top of the photography box to capture the image obtained from this process, while the light source is placed at the bottom. The lens of the sunglasses will be positioned in the middle to allow light from the light source to pass through the sunglasses lens as shown in Fig. 3.

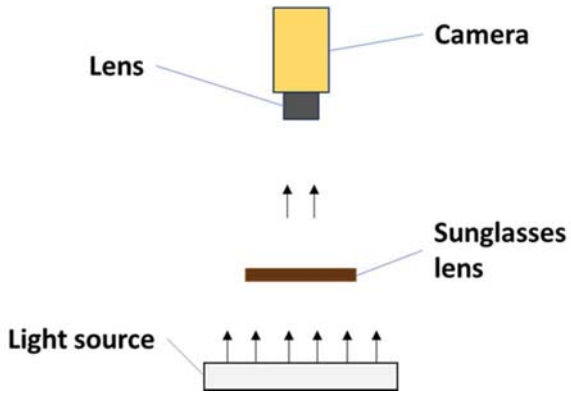


Fig. 3. Image acquisition design

- The design of the photography box

The box for photography is designed as a lightproof enclosure to prevent external light from interfering with the image capture, which could affect the accuracy of the recorded image. Its main components include a frame made from aluminum profiles and black matte acrylic sheets on all sides, which help reduce light reflections and prevent light from scattering in unwanted directions as shown in Fig. 4.



Fig. 4. Photography box design

- Imaging equipment set

The color camera use model Basler acA1300-200uc, with a resolution of 1.3 megapixels. The camera lens has a focal length of 9 mm with an aperture of 1.4. The light source used is a NeoPixel Ring 133 WS2812 5050 RGB LED.

B. Data Preparation

The image data consists of color images with a resolution of 1000 × 1000 pixels, captured from sunglasses lens. A total of 1,250 images were collected, with 625 showing evenness color and 625 showing unevenness color. A program was developed using Microsoft .NET and the EmguCV library to convert images to grayscale, adjust brightness, and enhance contrast. Data augmentation techniques, including 90°, 180°, and 270° rotations and vertical flipping, expanded the dataset to 10,000 images 5,000 per category, as shown in Table 1.

- Data Splitting

The processed image data is split into 3 sets the training set, the validation set, and the test set. Each dataset contains an evenness color lens and unevenness color lens, as shown in Table 1.

TABLE I. DATASET RATIO AND DATASET SUMMARY

	Ratio	Evenness	Unevenness	Total
Train Set	50%	2500	2500	5000
Validate Set	20%	1000	1000	2000
Test Set	30%	1500	1500	3000
				10000

C. Data Classification

This research utilizes Convolutional Neural Networks (CNNs) for image classification, leveraging their efficiency in object recognition and high-precision analysis. However, training complex CNN models requires significant time and computational power. To address this, transfer learning is applied, using pre-trained CNN models, as shown in Fig 5.

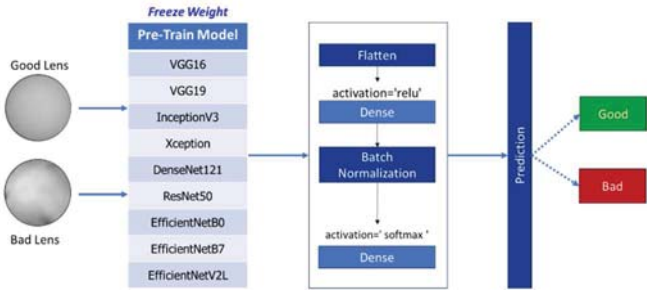


Fig. 5. Diagram apply transfer learning

D. Tuning

The tuning process will utilize the Hyperparameter Tuning library in Keras, focusing on key parameters such as dense1, dropout, and learning rate. First, dense1 will be introduced as a new layer, with its size sequentially decreasing by a factor of 1 from the output. The number of neurons in dense1 will be adjustable. Next, the dropout parameter will be fine-tuned, starting at 0.2 and increasing in increments of 0.1, up to a maximum of 0.5. Finally, the learning rate will be optimized, with selectable values of 0.1, 0.01, 0.001, and 0.0001 to enhance model performance.

IV. Experimental Result

This research applied Transfer Learning techniques using pre-trained models from the ImageNet dataset, including VGG16, VGG19, InceptionV3, Xception, DenseNet121, ResNet50, , EfficientNetB7, and EfficientNetV2L, to classify the quality of sunglasses lens into evenness color and unevenness color categories from a dataset of 10,000 images. The data was split into 3 sets for training, validation, and testing. The experimental results demonstrated that DenseNet121 outperformed all other models in terms of accuracy, achieving the highest overall performance with an optimal epoch of 3, as shown in Fig 6. A detailed performance analysis, conducted using a confusion matrix as shown in Fig 7 revealed that DenseNet121 correctly classified 1,194 images of unevenness color lens, while misclassifying 306 out of 1,500 images. For evenness color lens, the model accurately identified 1,273 images and misclassified 227 out of 1,500 images. These results correspond to an overall accuracy of 75.82% on the validation set and 82.23% on the test set. The findings, summarized in Table 2, further highlight the effectiveness of DenseNet121 in accurately classifying sunglasses lens quality.

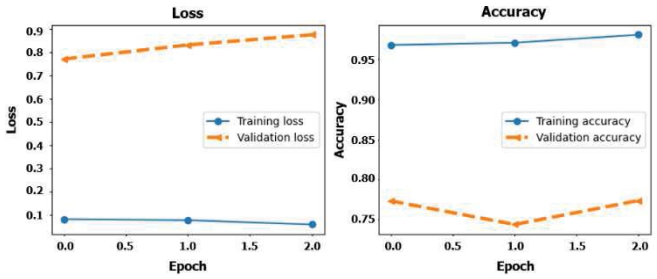


Fig. 6. Validation performance evaluation metrics of DenseNet121

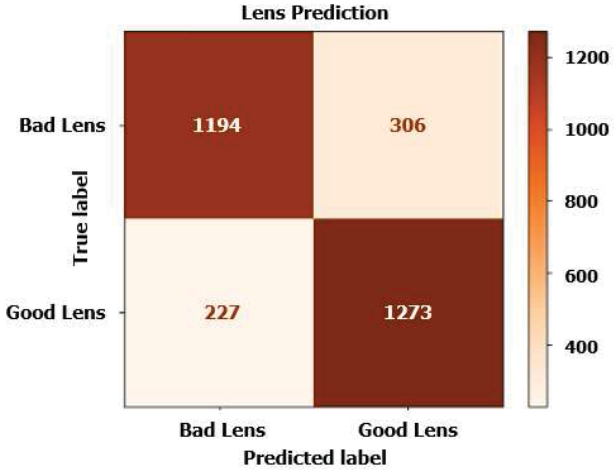


Fig. 7. Confusion matrix of DenseNet121of test dataset

TABLE II. SUMMARY OF MODEL EFFICIENCY

Model Name	Model Efficiency			
	Accuracy	*Precision*	*Recall*	*F1-score*
DenseNet121	0.8223	0.8232	0.8223	0.8222
EfficientNetB0	0.7913	0.7929	0.7913	0.7913
ResNet50	0.7893	0.7893	0.7893	0.7893
EfficientNetB7	0.7890	0.8188	0.789	0.7839
InceptionV3	0.7836	0.7941	0.7836	0.7817
EfficientNetV2L	0.7820	0.7849	0.7820	0.7814
Xception	0.7736	0.7829	0.7736	0.7718
VGG16	0.7700	0.7706	0.7700	0.7698
VGG19	0.7640	0.7640	0.7640	0.7640

V. Conclusion

This research developed a light transmission-based photography process for capturing sunglasses lens images efficiently. A dataset of 1,250 images was collected using actual lenses, equally split between evenness colored and unevenness colored lenses. The dataset was augmented and divided into training, validation, and test sets.

Furthermore, Transfer Learning was applied using pretrained models, including VGG16, VGG19, InceptionV3, EfficientNetB0, EfficientNetB7, EfficientNetV2L, Xception, DenseNet121, ResNet50 and classify the quality of sunglasses lens based on evenness and unevenness of color.

The experimental results demonstrated that DenseNet121 model achieved the highest accuracy among all tested models, with an accuracy of 75.82% on the validation set and 82.23% on the test set.

Finally, research on sunglasses lens quality classification is limited. This study provides a novel contribution with practical industrial applications, offering valuable insights to address challenges and enhance industry practices.

Acknowledgment

This research gratefully acknowledges Hoya lens Thailand for their support by providing sunglasses lens for photography and data collection, which were used as the dataset for this study.

References

[1] Perizat Rakhmetova, Aldabergen Bektilevov, Bakhtiyar Kopenov, Makabbat Zhamuratova, Saltanat Yussupova, Tolkyn Toktamyssova, "Study of Computer Vision for Manipulators", *International Conference on Communications, Information, Electronic and Energy Systems (CIEES),* Plovdiv, Bulgaria, 2023, pp. 1-6.

[2] Bharathi GP, Kavitha P, Laxman Baburao Abhang, G. Rathinasabapathi, Vipin Sharma, T. Sathish, "Machine Vision Applications in Robotics and Automation", *International Conference on Science Technology Engineering and Mathematics (ICONSTEM)*, Chennai, India, 2024, pp. 1-6.

[3] Y. LeCun, Y. Bengio, and G. Hinton, "Deep learning", *Nature*, vol. 521, no. 7553, pp. 436-444, May 2015

[4] Alaa Aldein M.S. Ibrahim, Jules R. Tapamo, "Transfer learning-based approach using new convolutional neural network classifier for steel surface defects classification", Scientific African 23 (2024) e02066

[5] Md Manjurul Ahsan, Shivakumar, Yingtao Liu, Zahed Siddique, "Defect analysis of 3D printed object using transfer learning approaches", Expert Systems With Applications 253 (2024) 124293

[6] Suriya Chayatummagoon, "Image classification of sugar crystal with deep learning", *International Conference on Knowledge and smart Technology* , Chonburi, Thailand, 2021

[7] Dinh-Thuan Dang, Jing-Wein Wang, Jiann-Shu Lee, Chou-Chen Wang, "Defect Classification System for Ski Goggle Lens", *International Symposium on Intelligent Signal Processing and Communication Systems (ISPAC)*, Hualien City, Taiwan, 2021

A Hybrid Greedy Algorithm for the Capacitated Vehicle Routing Problem

1st Udom Janjarassuk
Department of Industrial Engineering, School of Engineering
King Mongkut's Institute of Technology Ladkrabang
Bangkok, Thailand
udom.ja@kmitl.ac.th

***Abstract*—The Vehicle Routing Problem (VRP) is one of the most common problems in logistics and supply chain. In this study, we propose a hybrid greedy algorithm for the capacitated vehicle routing problem (CVRP) which is a variant of the VRP with vehicle capacity constraint. The algorithm adapts the minimal spanning tree algorithm to decompose the CVRP into many smaller traveling salesman problems (TSPs), and solves each sub-problem by using the Nearest Neighbor (NN) greedy algorithm. The hybrid algorithm is tested by using instances from the CVRPLIB library. The algorithm provides relatively good performances with optimality gaps varying from $4-30\%$ across all tested instances, and the computational time is less than 1 second in all cases.**

***Index Terms*—Capacitated Vehicle Routing Problem, Greedy Algorithm, Nearest Neighbor, Hybrid Algorithm.**

I. Introduction

The Vehicle Routing Problem (VRP) [1] is a classic optimization problem in operations research and logistics. It focuses on finding the most efficient routes for a fleet of vehicles to deliver goods or services to a set of customers, subject to certain constraints.

VRP is widely used in many industries such as logistics and transportation, waste collection, healthcare, and public transportation. In logistics and transportation, deliver routes are optimized for e-commerce or retail. In waste collection, VRP helps designing optimal routes for garbage trucks to minimize travel distance, fuel consumption, and time. In healthcare, VRP is used in patient transportation, medical supply and equipment distribution, planning routes for mobile health services or ambulances. In public transportation, VRP is used for optimizing bus or shuttle routes.

There are many variants of the VRP. The Capacitated VRP (CVRP) [2]–[4] is the most common one with limited carrying capacity of the vehicles. The VRP with Time Windows (VRPTW) [5]–[9] requires that customers must be served within specific time slots. In Multi-Depot VRP (MDVRP), vehicles can start from multiple depots instead of a single one. In Pickup and Delivery VRP (PDVRP) [10], [11], items must be picked up at one location and delivered to another. In Dynamic VRP (DVRP) [12], the customer requests or road conditions change dynamically during routing.

This study focus on the Capacitated Vehicle Routing Problem (CVRP) which is a specific variant of the Vehicle Routing Problem (VRP) in which each vehicle in the fleet has a limited carrying capacity, and the goal is to design routes that ensure all customer demands are satisfied without exceeding the vehicle capacity.

CVRP is an NP-hard problem, meaning the computational complexity grows rapidly with the number of customers and vehicles. There are two major approaches for solving CVRP: the exact algorithm approach, and the heuristics or metaheuristics approach. The exact algorithm approach such as the Branch-and-bound, the Branch-and-cut algorithms are suitable for small problems in general due to the solution time [13]–[15]. The biggest advantage of the exact approach is that it provides optimal solution to the problem. On the other hand, heuristics or metaheuristics approach provides approximated solution which is more suitable for larger, real-world problems [16]. Examples of heuristics algorithms include the Genetic Algorithms [3], Tabu Search [17], Simulated Annealing [18], and Ant Colony Optimization [4]. In practice, solving CVRP often requires specialized software or algorithms tailored to the specific constraints and objectives of a business.

The remaining of the paper is organized as follows. Section II provides the idea and details of the proposed hybrid greedy algorithm for solving CVRP. Computational results are reported in Section III, followed by a conclusion in Section IV.

II. Methodology

The idea of solving CVRP in this study is to use the Minimum Spanning Tree (MST) algorithm to decompose the problem into many smaller problems, i.e., the Traveling Salesman Problems (TSPs), and solve each sub-problem separately using greedy algorithm for TSP. While the Minimum Spanning Tree algorithm itself is not a direct solution to the VRP or CVRP, it can provide valuable insights or serve as a component in heuristic methods for solving VRP and CVRP. For solving the sub-problems, the Nearest Neighbor (NN) algorithm is used. It is one of the most widely used algorithm for solving the TSP, although other better heuristic algorithms exist in terms of solution quality, but they are computationally expensive.

The first advantage of decomposing CVRP into TSPs is simplification. It makes the problem more mangeable and computationally feasible. In addition, one can reuse the existing algorithms for TSP, which can be applied to the sub-problems

979-8-3315-4248-1/25/$31.00 ©2025 IEEE

Algorithm 1 Greedy Algorithm for TSP

Initialize best cost $z^* := \infty$ and $T^* := \emptyset$
for trial $k \in \{1, ..., m\}$ **do**
  $U := \{1, ..., n\}$
  Initialize first city c_1 at random
  $U := U - \{c_1\}$
  $i := c_1$
  $T_k := \{i\}$
  while $U \neq \emptyset$ **do**
    Select nearest city $j \in U$ from i
    $U := U - \{j\}$
    $i := j$
    $T_k := T_k + \{i\}$
  end while
  $T_k := T_k + \{c_1\}$
  Compute cost z_k of tour T_k
  if $z_k < z^*$ **then**
    $z^* := z_k$
    $T^* := T_k$
  end if
end for

directly. Last but not least, this approach is scalable, which is very useful especially for solving large-scale CVRP.

A. Greedy Algorithm for TSP

The Traveling Salesman Problem [19], [20] is a classic optimization problem in computer science and operations research. Given a list of cities and the distances between each pair of cities, the goal is to find the shortest possible route that visits each city exactly once and returns to the origin city.

The Nearest Neighbor Algorithm is one of the simplest and most intuitive greedy algorithms used to find an approximate solution to the Traveling Salesman Problem. It is a heuristic approach that constructs a tour by making locally optimal choices at each step by always choosing the closest unvisited city. The scheme of the algorithm is described in Algorithm 1 for a problem of n cities.

The algorithm is stated as follows. All cities are marked as unvisited at the beginning of each trial. The algorithm starts a trial at any random city and find the closest city from the unvisited list. It moves to that city and remove it from the list of unvisited cities. This process repeats until the list of unvisited cities is empty. Then it returns to the starting city to complete the tour. The cost of the tour is computed. The whole process repeats for a number of trials to choose the best result from all trials.

B. Hybrid Algorithm for CVRP

The Minimum Spanning Tree (MST) algorithm is used for clustering customers into feasible routes for CVRP. The CVRP can be represented as a graph where the nodes represent the depot and customers, while the edges represent the distances or travel costs between nodes. The goal of the MST is to connect all nodes (depot and customers) with the minimum total edge weight or cost. Customers are grouped into clusters (as TSP sub-problems) by ensuring that the total demand in each cluster does not exceed the vehicle capacity.

For a CVRP of n customers, let $N = \{1, 2, ..., n\}$ be the set of customers of the CVRP and $U \subset N$ be the set of unvisited customers of the CVRP, and define:

$P =$ Vehicle capacity,
$d_i =$ Demand of customer i,
$C_k^v =$ Set of customers that have been selected at iteration k for vehicle v,
$\overline{C}_k^v =$ Set of customers as yet to be selected after iteration k for vehicle v.

The steps of the algorithm for CVRP is described in Algorithm 2.

Algorithm 2 Hybrid Algorithm for CVRP

$U := N$
$v := 1$
while $U \neq \emptyset$ **do**
  Initialize $C_0^v := \emptyset$ and $\overline{C}_0^v := U$
  Initialize vehicle capacity $p := P$
  Start with any customer $i \in \overline{C}_0^v$ and set $C_1^v := \{i\}$
  $\overline{C}_1^v := N - \{i\}$
  $p := p - d_i$
  $k := 1$
  while $\overline{C}_k^v \neq \emptyset$ **do**
    Select a customer $j^* \in \overline{C}_k^v$ that yields the lowest cost to a customer in C_k^v
    $C_{k+1}^v := C_k^v + \{j^*\}$
    $\overline{C}_{k+1}^v := \overline{C}_k^v - \{j^*\}$
    $p := p - d_{j^*}$
    Remove customers from $\overline{C}_{k+1}^v$ whose demand is larger than the remaining vehicle capacity p
    $k := k + 1$
  end while
  $C_k^v := C_k^v + \{0\}$
  Solve the TSP for C_k^v using Algorithm 1
  $U := U - C_k^v$
  $v := v + 1$
end while
Compute the total cost from all vehicles

Initially, all customers are marked as unvisited. The set of slected customers C_0^v for vehicle v is set to empty and the set of unselected customers $\overline{C}_0^v$ for vehicle v is set to U. The algorithm select the first customer i randomly from the set $\overline{C}_0^v$ and add it to the set C_1^v, and remove it from the set of $\overline{C}_1^v$. The remaining capacity of the vehicle is reduced by the demand of customer i. The process repeats until the set of unselected customers is empty. While adding customers to a vehicle route, the remaining capacity of the vehicle is also reduced by the demands of the customers, and the unvisited customers whose

TABLE I
CHARACTERISTIC OF THE TEST INSTANCES

Instance	Vehicle capacity	Number of vehicles	Number of customers
A-n33-k5	100	5	32
A-n64-k9	100	9	63
B-n41-k6	100	6	40
B-n78-k10	100	10	77
E-n23-k3	4500	3	22
F-n72-k4	30000	4	71
F-n135-k7	2210	7	134
M-n101-k10	200	10	100
P-n55-k7	170	7	54
P-n76-k5	280	5	75

demands are larger than the remaining capacity of the vehicle are also removed from the unselected list. When the set of unselected customers $\overline{C}_k^v$ is empty, meaning that no more customer can be served by the vehicle, the depot (node 0) is added to the list to complete the tour for the vehicle. The solution of the selected customers for vehicle v is solved by using Algorithm 1. A new vehicle is added to the solution of CVRP if there are unvisited customers remaining, and the process contineus until all customers are served (U is empty). The total cost of the CVRP is computed from the sum of all vehicles' costs.

III. COMPUTATIONAL RESULTS

The proposed hybrid algorithm was tested by using 10 selected instances from CVRPLIB, which are available from http://vrp.galgos.inf.puc-rio.br/index.php/en/. Table I shows the characteristics of the instances, i.e., the vehicle capacity, the number of vehicles, and the number of customers.

The algorithm was implemented in Python by utilizing the tsp-c library from https://pypi.org/project/tsp-c/ for solving the TSP sub-problems [21]. The computer used for the experiments was an Intel Core i5 processor running at clock speed 2.9GHz. The number of trials were set to 100 for the experiments in Algorithm 1 and 2. Each instance was solved for 10 replications to obtain an average cost. The best result for each instance and the computation time were also provided in Table II.

TABLE II
COMPUTATIONAL RESULTS

Instance	**Optimal**	**Best**	**Best (%)**	**Average**	**Average (%)**	**Time (sec.)**
A-n33-k5	661	726	9.8%	731.8	10.7%	0.02
A-n64-k9	1401	1518	8.4%	1579.6	12.7%	0.05
B-n41-k6	829	858	3.5%	864.0	4.2%	0.02
B-n78-k10	1221	1319	8.0%	1352.5	10.8%	0.07
E-n23-k3	569	616	8.3%	621.8	9.3%	0.02
F-n72-k4	237	307	29.5%	323.5	36.5%	0.16
F-n135-k7	1162	1312	12.9%	1394.9	20.0%	0.62
M-n101-k10	820	887	8.2%	900.2	9.8%	0.16
P-n55-k7	568	623	9.7%	644.8	13.5%	0.04
P-n76-k5	627	731	16.6%	754.4	20.3%	0.12

The first column in Table II is the name of the tested instances. The optimal objective value is given in the second column. Column three is the best objective value obtained from the experiments, and the associated optimality gap is provided in column four. Column five and six provide results of the average value from the 10 replications and its associated optimality gap respectively. The last column is the average solution time (in seconds) for each instance.

From the results in Table II we can see that the optimality gap of the best results vary from 3.5% in instance B-n41-k6 to 29.5% in instance F-n72-k4. The average results have slitly larger optimality gaps compared to the best results, which suggests that the solutions from the algorithm are somewhat consistant for solving each instance. Never the less, most of the results are considered as 'useable' which is within the 15% optimality gap. In terms of computational time, all instances are soved in less than 1 second.

IV. CONCLUSION

In this paper, we proposed a hybrid greedy algorithm to solve the capacitated vehicle routing problem. The algorithm decomposes the CVRP into many TSPs by clustering customers into vehicle routes, and solves each TSP separately by using the nearest neighbor algorithm. From the experiments, the proposed algorithm provides good results in a fraction of a second, making it a good alternative for large-scale real-world applications.

One improving direction is to improve the solution of each sub-problem by using more sophisticated techniques. Never the less, the quality of the final CVRP solution depends heavily on how well the customers are clustered in the first step, and it may lead to locally optimal solutions rather than globally optimal ones. Advanced techniques like metaheuristics (e.g., Genetic Algorithms, Tabu Search, Ant Colony Optimization) can be used to refine the solution.

REFERENCES

[1] N. De Jaegere, M. Defraeye, and I. Van Nieuwenhuyse, "The vehicle routing problem: state of the art classification and review," 2014.
[2] U. Janjarassuk and R. Masuchun, "An ant colony optimization method for the capacitated vehicle routing problem with stochastic demands," in 2016 International Computer Science and Engineering Conference (ICSEC), 2016, pp. 1–5.
[3] J. Berger and M. Barkaoui, "A new hybrid genetic algorithm for the capacitated vehicle routing problem," Journal of the Operational Research Society, vol. 54, no. 12, pp. 1254–1262, 2003.
[4] S. Mazzeo and I. Loiseau, "An ant colony algorithm for the capacitated vehicle routing," Electronic Notes in Discrete Mathematics, vol. 18, pp. 181–186, 2004.
[5] J. F. Bard, G. Kontoravdis, and G. Yu, "A branch-and-cut procedure for the vehicle routing problem with time windows," Transportation Science, vol. 36, no. 2, pp. 250–269, 2002.
[6] J. Berger, M. Salois, and R. Begin, "A hybrid genetic algorithm for the vehicle routing problem with time windows," in Conference of the Canadian Society for Computational Studies of Intelligence. Springer, 1998, pp. 114–127.
[7] J. Homberger and H. Gehring, "Two evolutionary metaheuristics for the vehicle routing problem with time windows," INFOR: Information Systems and Operational Research, vol. 37, no. 3, pp. 297–318, 1999.
[8] W.-K. Ho, J. C. Ang, and A. Lim, "A hybrid search alogrithm for the vehicle routing problem with time windows," International Journal on Artificial Intelligence Tools, vol. 10, no. 03, pp. 431–449, 2001.
[9] É. Taillard, P. Badeau, M. Gendreau, F. Guertin, and J.-Y. Potvin, "A tabu search heuristic for the vehicle routing problem with soft time windows," Transportation science, vol. 31, no. 2, pp. 170–186, 1997.

[10] S. N. Parragh, K. F. Doerner, and R. F. Hartl, "A survey on pickup and delivery problems: Part i: Transportation between customers and depot," Journal für Betriebswirtschaft, vol. 58, pp. 21–51, 2008.
[11] G. Desaulniers, J. Desrosiers, A. Erdmann, M. M. Solomon, and F. Soumis, "Vrp with pickup and delivery." The vehicle routing problem, vol. 9, pp. 225–242, 2002.
[12] U. Ritzinger, J. Puchinger, and R. F. Hartl, "A survey on dynamic and stochastic vehicle routing problems," International Journal of Production Research, vol. 54, no. 1, pp. 215–231, 2016.
[13] G. Laporte and Y. Nobert, "A branch and bound algorithm for the capacitated vehicle routing problem," Operations-Research-Spektrum, vol. 5, pp. 77–85, 1983.
[14] M. Fischetti, P. Toth, and D. Vigo, "A branch-and-bound algorithm for the capacitated vehicle routing problem on directed graphs," Operations Research, vol. 42, no. 5, pp. 846–859, 1994.
[15] D. Naddef and G. Rinaldi, "Branch-and-cut algorithms for the capacitated vrp," in The vehicle routing problem. SIAM, 2002, pp. 53–84.
[16] D. Pisinger and S. Ropke, "A general heuristic for vehicle routing problems," Computers & operations research, vol. 34, no. 8, pp. 2403–2435, 2007.
[17] P. Augerat, J.-M. Belenguer, E. Benavent, A. Corbéran, and D. Naddef, "Separating capacity constraints in the cvrp using tabu search," European Journal of Operational Research, vol. 106, no. 2-3, pp. 546–557, 1998.
[18] H. M. Harmanani, D. Azar, N. Helal, and W. Keirouz, "A simulated annealing algorithm for the capacitated vehicle routing problem." in CATA, 2011, pp. 96–101.
[19] D. Davendra, Traveling salesman problem: Theory and applications. BoD–Books on Demand, 2010.
[20] A. D. L., B. R. E., C. V., and C. W. J., The Traveling Salesman Problem: A Computational Study. Princeton University Press, 2006.
[21] U. Janjarassuk, "A comparison of heuristic approaches to the travelling salesman problem," ICIC Express Letters, vol. 5, pp. 279–283, 02 2011.

A study on developing a robust screen navigation pattern for SwiftUI based iOS Applications

Shubham Kamdi
Independent Researcher
Mountain View, United States
shubhamvkamdi@gmail.com

***Abstract*—The paper proposes a navigation abstraction that should be implemented with modern-day declarative apps built using SwiftUI. It will discuss the architectural changes in developing a concise, clean and highly maintainable code base. This will help aspiring mobile engineers and industry practitioners get an idea about how the existing SwiftUI navigation system can be turned into a global service to facilitate the redirection of new screens with iOS apps built using SwiftUI.**

***Index Terms*—navigation abstraction, SwiftUI, declarative, architectural changes**

I. Introduction

In mobile applications, navigation is the means of opening or redirecting to a new screen. Typically, mobile apps have screens dedicated to a unique functionality; designers don't subject all the app's core functionalities to a single screen. This would lead to a dilemma; it would confuse the end user. For example, mobile apps have a dedicated screen to perform authentication, i.e. Login; this is a unique functionality, hence deserves a dedicated screen. Likewise, if a user has to perform registration, then he/she is redirected to a screen that permits this functionality. This redirection to a new screen commonly constitutes the app's navigation process.

Navigation in small-scale applications, typically consisting of three to four screens, is relatively straightforward; if a mobile app has fewer screens, it does not need a dedicated navigation service. Such apps can directly write the navigation logic within their screen code. However, as the app grows, the sheer volume of the code also increases. In such situations, if mobile engineers start embedding navigation code within, it will become challenging to maintain in the long run.

The reader may wonder why the navigation code can act as an overhead for maintenance; the reason is simple: to navigate to a new screen, the engineers will have to initialise the screen class by invoking its constructor. As the functionalities of the app increase, existing screens will also need to be updated to support new features; in doing so, their constructor's parameters will also be updated. If the screen initialising code is written in every class or screen that wants to perform navigation, it will create multiple spots in the app code that must be updated to support new functionalities. Thus directly adding to the effort of the developers.

Implementing a navigation service within your mobile app must tackle such situations carefully. A navigation service class is in place to reduce the navigation overhead code and host the logic of initialising the screen that needs to be opened. It also has low-level logic that redirects to a new screen. This paper will help readers understand how a navigation service can be developed for SwiftUI-based applications.

II. Literature Survey

As a context, this work aims to provide some insights on managing overall navigation within the mobile application to industry practitioners and aspiring mobile engineers. This book [1] provides a good starting point for understanding navigation ideas that inspired the state of navigation in mobile apps; it starts by speaking about transient and persistent navigation. However, it provides little information concerning the scalability of these mechanisms as the client-side code increases.

In [2], the researchers have developed a custom navigation pattern, "RetroScope", which will allow the app to recreate screens by re-animating the app's screen drawing functions. This approach is resource-intensive and may perform poorly on devices with low-grade hardware. It is a novel attempt but does not sound scalable or maintainable.

Researchers in [3] have proposed a redirect script to move users to mobile-friendly versions of websites. This work does not directly contribute to native mobile application development but is worth considering concerning the navigation management system. However, the work is limited to redirect script, and little to no work is being put into the overall navigation management.

The book [4] does good work by providing a theoretical aspect of screen navigation, which is informative with cultural elements. It includes several case studies; however, it does not touch base on technical implementation aspects of navigation. So far, work has provided little emphasis on developing navigation-centric services for natively developed mobile applications. This paper hopes to provide readers with a framework for developing such services, and it will emphasise iOS-based mobile apps built using SwiftUI [5]. The readers can take this knowledge and create an equivalent mechanism for their respective client platforms, e.g. Android [6].

III. System

The proposed system will be developed using SwiftUI, Apple's latest UI development framework. This is a declarative

development framework [8], where developers are unconcerned about low-level implementation details. Instead, just instruct what needs to be built.

SwiftUI provides a Navigation Stack [8] to implement navigational flows within iOS applications, and it is a robust and reliable mechanism. It was recently introduced in iOS SDK, but its adoption in the SwiftUI ecosystem has been ubiquitous. It has become a widely accepted way of setting and implementing navigation routes within an iOS app. It takes a Navigation Path object as an argument, and this object manages the navigation state of the stack. Developers must append navigation items to this object to redirect to a new screen. Each navigation item represents a screen that will pushed into the view hierarchy.

The navigation stack exposes the navigation destination view modifier to map navigation items to a screen or view. For example,

```
struct DemoView: View {
    @State var path = NavigationPath()
    var body: some View {
        NavigationStack(path: $path) {
            VStack(content: {
                Text("Demo")
            }).navigationDestination(
                for: Double.self
            ) { destination in
                Text("Redirect to this screen")
            }
        }
    }
}
```

Fig. 1. Navigation Stack view

Whenever a double value is appended to the path object, a new screen is opened with the text “Redirect to this screen”. The navigation destination view modifier is used to map double-type navigation items to the screen containing the Text view. This is the basic idea behind the navigation mechanism offered by SwiftUI.

The system will also use the MVVM design pattern [9], which stands for Model View ViewModel. According to this design pattern, every new screen should have its own ViewModel to abstract the business logic. Hence, it also hosts a function that abstracts the screen redirection logic.

Every SwiftUI application has ContentView; think of it as a root view of your application. As stated earlier, developers must append navigation items to the navigation path object to perform navigation. For every new screen redirection, existing view models must access the path instance directly, resulting in a complicated situation. A cleaner way would be to develop a class that takes care of the management of navigation path object, more or less like a service that is singleton in nature and can be accessed globally through the application.

IV. Low-Level Design

The proposed low-level design is implemented using a demo SwiftUI app. This demo app is hosted on a public repository on GitHub [11]. Readers are expected to clone this repository, to get an in-depth understanding of the design.

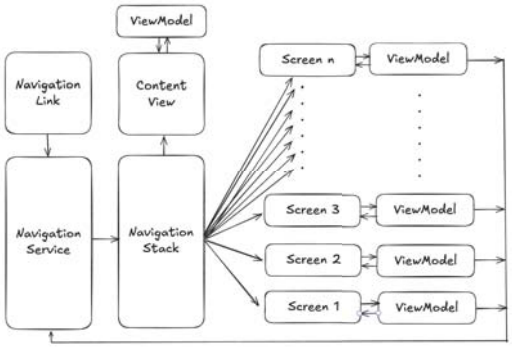


Fig. 2. Low level architecture

A. Navigation Link

This struct wrapper abstracts the relevant data to initialize the screen that needs to be opened and contains a destination object that maps the screen. This wrapper is built by conforming to the Navigatable protocol. This protocol further conforms to Hashable; any object that conforms to Hashable can act as a navigation item. Whenever a screen needs to be opened, the navigation service creates the navigation link objects, screen initialization, and destination data, which are embedded upon creation. The navigation service will append the navigation link objects to the navigation path.

B. Navigation Stack Service

The previous section established the need to create a navigation service; this is a singleton class responsible for abstracting the overall navigation logic of the app. It stores the Navigation path object and provides safe methods to add or remove navigation links. This service also ensures thread-safe access to the navigation path object. View models will communicate with this service whenever a new screen needs to be opened. To do so, the view model will delegate the task of object creation of navigation links to the service, and the service, in turn, will append them to the stored navigation path. Thus triggering the navigation destination method.

This service also creates an extension [10] to SwiftUI’s View protocol to receive navigation destination callback within the navigation service class. This helps the navigation service to provide screens for redirection. The figure will help clarify,



Fig. 3. Swift Extension

The subscribe navigation service method can now be invoked on the Navigation Stack view. If there are multiple navigation stack views in the app, then all of them can invoke this method and communicate with the navigation service. The process navigation destination is the method of the navigation service which understands which screen to open.



Fig. 4. Subscribe modifier in action

C. Redirection Helpers

By adding navigation link object creation logic to the service, completes a crucial objective of the low level design. These helper methods are used to create the navigation link object and add them to the stored navigation path, they can be accessed globally by any other class or service to initiate the navigation mechanism. Developers need to create a helper for their respective screens.

V. Result

The proposed architecture is applied to an iOS. This does not provide a performance boost. However, it improves the overall code structure and contributes to increased maintainability. Here is the side-by-comparison of the code:



Fig. 5. Reduced code with proposed architecture changes

Let us consider the code base, without applying the architecture changes. It increases the complexity and looks overwhelming to understand as well.

As the readers can see when the proposed architecture changes are implemented, the overall code is reduced, and



Fig. 6. Increased code

developers do not need to worry about building the complex data to append to the navigation path. In fig 6, the navigation path objects are passed down to the views, and the view append links to the path. Different modifiers are triggered depending on what data is appended. Thus, multiple modifiers are in place, each dealing with a different screen.



Fig. 7. Redirection logic

However, with the extension mentioned in the previous section, this gets completely abstracted and reduces overall complexity. When developers add new screens to the app flow they only need to update the navigation stack service to add the logic for redirection. Rather than updating views, as this can be risky if the developer does not understand the overall navigation flow.

This abstraction is highly beneficial for apps with multiple screens; adding navigation destination modifiers for every screen does not make sense, while your app hosts multiple tabs like the leading social media platforms.

VI. Limitation

Every system has room for improvement, and so does the proposed navigation stack service too. The service does a fine job in adding modularity to existing logic however, it does not provide state based lifecycle for screen redirection. That is a logic that helps determine when screen has successfully openned, it was closed, so on and so forth.

Also, at low level, we can apply abstraction on top Navigation Stack view, which automatically creates path objects and stores them in the proposed services. Something that readers can try to do and improve the overall design.

References

[1] Neil, Theresa. Mobile design pattern gallery: UI patterns for smartphone apps. " O'Reilly Media, Inc.", 2014.
[2] Saltaformaggio, Brendan, et al. "Screen after Previous Screens:Spatial-Temporal Recreation of Android App Displays from Memory Images." 25th USENIX Security Symposium (USENIX Security 16). 2016.
[3] Bengtson, Jason. "The art of redirection: one library's experiences and statistical results from the deployment of mobile redirect script." Journal of Hospital Librarianship 12.3 (2012): 191-198.
[4] Verhoeff, Nanna. Mobile screens: The visual regime of navigation. Amsterdam University Press, 2012.
[5] Barker, Chris. Learn SwiftUI: An introductory guide to creating intuitive cross-platform user interfaces using Swift 5. Packt Publishing Ltd, 2020.
[6] Sarkar, Anirban, et al. "Android application development: a brief overview of android platforms and evolution of security systems." 2019 Third International conference on I-SMAC (IoT in Social, Mobile, Analytics and Cloud)(I-SMAC). IEEE, 2019.
[7] https://en.wikipedia.org/wiki/Declarative_programming
[8] https://developer.apple.com/documentation/swiftui/navigationstack
[9] Anderson, Chris. "The model-view-viewmodel (mvvm) design pattern." Pro Business Applications with Silverlight 5. Berkeley, CA: Apress, 2012. 461-499.
[10] https://docs.swift.org/swift-book/documentation/the-swift-programming-language/extensions/
[11] https://github.com/SkilletElveti/Navigation-Stack-Service-

Enhancing a Creative Support Tool with the TRIZ Method: A Textile Design Prototype Utilizing Projection Mapping

Chanathinat Chaiyapoo
Creative Product Innovation, Faculty of Science and Technology, Phuket Rajabhat University
Phuket, Thailand
chanathinat.c@pkru.ac.th

Jakraphan Chaopreecha
Digital Media Design, Computing, College of Computing, Prince of Songkla University
Phuket, Thailand
jakraphan.c@phuket.psu.ac.th

Chutima Changpum
Creative Product Innovation, Faculty of Science and Technology, Phuket Rajabhat University
Phuket, Thailand
chutima.c@pkru.ac.th

Nicha Tovankasame
Department of Asian Studies Faculty of International Studie, Prince of Songkla University
Phuket, Thailand
nicha.t@phuket.psu.ac.th

***Abstract*— The Creative Support Tool (CST) in textile design has been developed since the advent of graphical user interfaces (GUIs). However, there is still room for further development, particularly in the ideation phase, especially for inexperienced designers. This research aims to evaluate a prototype that integrates projection mapping techniques with the TRIZ method, potentially enhancing its effectiveness in textile design. The study combines ethnographic methodology with the Usability Metric for User Experience (UMUX). The results highlight four key factors—segmentation, merging, nesting, and color changes—that support the design process. Additionally, the evaluation process contributes to the ongoing development of the prototype and proposes ideas for future improvements.**

Keywords—TRIZ, Textile Design, UX/ UI Design, Projection Mapping, Prototyping

1. INTRODUCTION

In the design process, the method for fostering creativity depends on the design phase—quantify the problem, generate concepts, define concepts, select concept, design, and present, respectively [1]. This research focuses on the idea generation in the design phase, particularly in textile design. Digital tools supporting the textile design was used since the 1980s when graphical user interface (GUI) was developed [2]. Therefore, computer-aided textile design has been designed. There has been software for design phase such as 3D embroidered pattern [3], transformation from real clothes to 2D cutting pattern [4], and virtual designing [5]; for production such as pattern design and stitch automation [6] and pattern manufacturing [7]. Computer-aided design (CAD) software mostly supports the production process, which requires complex development from sketch to practical delineation. It can reduce manufacturing costs by minimizing excess material and production time. CAD supports both the generation of ideas and the production process; however, there are two points to consider: 1) The discrepancy between traditional production and digital techniques is a concern. The design on a computer differs from its appearance on real fabric. Scale and proportion are important factors that influence the perception of a digitized design compared to a real textile. 2) Novices or designers working in the initial stages need a flexible way to sketch their ideas, regardless of the complexity of computer tools. Sketching is a process that is closely related to play. Play can generate novelty and alternative ways of thinking in design. For this reason, researchers strive to create a prototype that supports textile design and is usable in the initial process of idea generation.

Researchers are interested in creating projection mapping prototype, a technique that projects digital images and videos onto surfaces. It supports various disciplines, such as collaborative architectural design [8], education with interactive toys [9], and advertising [10]. Projection mapping interconnects intuitive materials with digitized design information. Additionally, it integrates digital content with physical space, creating digitally embedded environments seen in exhibitions, art and design projects, and enhanced public experiences. The utilization of this technique in the initial design process of textile design is possible, as the designed image can be displayed on the real fabric surface simultaneously. However, evaluating the prototype is necessary to understand the factors that enhance the design process. Therefore, the Theory of Inventive Problem Solving (TRIZ) will be applied to identify the interrelated criteria between the use of the prototype and ideation in the design process. The theory and other relevant studies will be discussed in the next section.

I. RELATED STUDIES

A. Creative Support Tool (CST)

Creative support tools (CST) emerged from the idea that computers could enhance the design and production process. Since computers can effectively interact with humans through input and feedback systems such as a mouse, keyboard, and graphical display, they have the potential to serve as partners for designers. Shneiderman argues that, to create usable CST, the design process should be clearly defined, with key questions focusing on who the users are and what creative tasks they need to accomplish [11]. Since the 2000s, CSTs have been developed based on user goals in the creative process. Various tools have been implemented, including both prototypes and real products. Nonetheless, the terrain of CSTs still has a gap between tools for novices and experts. In 2019, Frich analyzed 93 publications researching CSTs and found that there is only 17% of CSTs created for novice [12]. The point is that experts can integrate their work using complex

tools, such as editing images with Photoshop, composing cinematic scenes in Final Cut Pro, or creating 3D models with Blender. CSTs have become ordinary equipment for experts in their creative process. However, novices need simpler tools that are intuitive and supportive of their current skill levels. This is one of the challenges for UX/UI designers—to balance functionality and usability for inexperienced users. They need to maintain a manageable learning curve when using particular tools. Therefore, this research aims to understand the UX factors of CSTs for novices.

Furthermore, the evaluation phase in the process of creating CST prototype is necessary. The evaluation of CST needs clear user goals, a solid theoretical foundation, and the participation of experts [13]. The methodology for measuring UX/UI should include three key factors. The user goal is the first criterion, as it comprises various subtasks that support the design process. Understanding these subtasks can enhance the system's usability when designed. Moreover, the prototype of the CST must account for the physical space and time in which it is implemented. The usability of CST depends not only on the tool itself but also on the physical and social environment in which it functions [14]. The participation in the physical environment can increase the engagement between learner and the creative process [15]. It can be seen that CSTs are dynamic when applied in the design process. They include various factors that can be evaluated using both qualitative and quantitative methods.

B. The Theory of Inventive Problem Solving (TRIZ)

This research needs to find an appropriate base theory to evaluate the CST. In textile design, the ideation phase is a process of exploring alternatives for the final outcome. This process has a specific goal, and designers need tools to initiate their concepts and open new ways of thinking. Particularly in the design phase, the TRIZ method is one of the techniques best suited for structured problems with defined goals [16]. TRIZ is an abbreviation for the 'Theory of Inventive Problem Solving.' This theory was created by the Russian theorist Genrich Altshuller. He summarized this concept based on the analysis of 78 problem-solving cases using 27 tools. [17]. The book is a creative toolkit that is useful for designing different types of products. Thereafter, Altshuller revised his framework and summarized it into the 40 principles of invention [18], which have been widely utilized by engineers and designers. The theory is suitable for simplifying solutions and improving products [19].

Regarding this research, the use of TRIZ in both media technology and fashion design disciplines is highly significant. TRIZ can be applied to the use of media technology as a creative toolkit [20]. The adaptation from physical tools to digital equipment does not reduce the efficacy of using TRIZ in the design process. Although the theory was originally developed to solve tangible problems, TRIZ is still practical in the abstract domain. Particularly in fashion design, the TRIZ method can enhance creativity in designing style, form, pattern, materials, and production of apparel [21]. TRIZ is not only used with specific design techniques, but it is also applicable to various solutions. This demonstrates the flexibility of TRIZ. Designers can apply TRIZ to techniques they are familiar with.

C. Textile Design

Textile design has evolved from traditional craftsmanship to more technological and conceptual approaches. The integration of digital tools and new technologies is a central theme in contemporary textile design. The use of technology in textile design has expanded with the rise of computational design tools, digital weaving, and 3D printing. Many studies focus on the ability of digital tools to enhance creativity and bring new possibilities to the surface design, structure, and materials of textiles [22]. The use of digital technology in textile and fashion design like digital fabric printing and virtual simulation of textile patterns have reshaped the design process facilitating experimentation and enabling quicker iterations of designs. The integration of digital technology with design and art, enhancing artistic expression and spatial aesthetics in textiles. By leveraging digital tools from 2D to 3D software and from specialized to general-purpose applications creativity can be effectively translated into artistic graphics and functional designs. The key to applying digital technology in textile design lies in mastering its core principles and establishing a seamless digital connection between creativity, products, and processes. Ultimately, digital design enables the transition from virtual concepts to tangible reality [23].

The innovation of textile design leads to new material applications, sustainability practices, and the artistic expression of fabrics. One major point is that digital tools, including projection and augmented reality, have enabled designers to test materials and designs interactively before producing physical samples. This aligns with the idea of projection mapping enhancing the creative process. The growing importance of emerging technologies in the evolution of textile fashion design, particularly in the development of fashionable wearables and e-textiles. Technologies such as servo motors, shape memory alloys, and pneumatics enable the creation of dynamic, shape-changing garments that offer new forms and functionalities. These innovations allow fashion practitioners to explore new design strategies and broaden the scope of garment construction, enhancing the relationship between the body and materials. They highlight the transformative potential of technology in fashion design, emphasizing the importance of collaboration, innovation, and a relational approach to design variables to create more adaptive, functional, and dynamic fashion items [24]. However, next-generation textiles are revolutionizing the textile industry by integrating cutting-edge materials, technologies and functionality such as nanotechnology, 3D printing, recycling, wearable electronics, and innovative textile design using digital technology tools.

II. A Prototype with Projection Mapping

This research aims to explore how digital media can be applied to textile design. The methodology is experimental research, comprising two main phases: 1) designing the CST by integrating media techniques and human-computer interaction disciplines; 2) the evaluation phase, which uses TRIZ methods to assess the prototype. The details of each phase are explained in this section.

A. A Design of CST for Textile Design

There are three parts of the prototype – input, processing, and output. The MIDI controller (Korg nanoControl 2) and the sampler (SP404-MKII) were used as inputs. The MIDI controller comprises sliders and knobs, making it simple for

human interaction, while the sampler can provide interactive buttons with background ambient sounds. For processing, the visual programming software TouchDesigner (educational license) is used. The software also provides a projection mapping tool to adjust the output image on non-geometric surfaces. The output equipment includes a 4000-lumen projector and projection onto the surface of a white dress worn on a mannequin. The colored dress is not chosen because its surface can reduce the intensity of the projector's light.

In the processing software, OpenGL is used to create graphic elements written in JavaScript. TouchDesigner supports the framework, allowing designers to code and flexibly apply graphical techniques through programming. The linear equation in the TouchDesigner framework is chosen for graphical generation as it is the simplest method for creating patterns in textile design. Various numerical instances are linked to the MIDI controller and sampler, enabling users to adjust variables through an intuitive interface with real-time feedback.

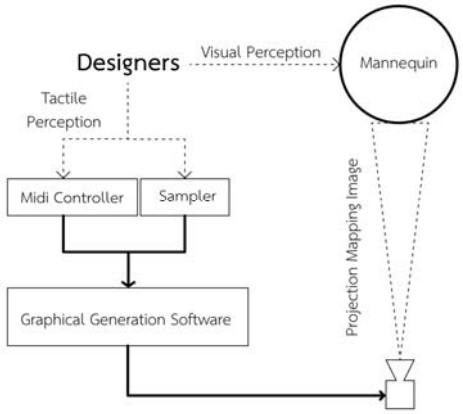


Fig. 1. The system of the CST prototype

B. The Evaluation Method

This research utilizes the UX/ UI evaluation method to identify the correlational factors between the design process and the usability of the prototype. The process of evaluation is as follows:

1) Filtering the TRIZ 40: Five specialists in textile design ranked the TRIZ 40 principles to filter only the factors relevant to the textile design process. Four experienced designers were invited to participate in this process, and 13 out of the 40 principles were selected and ranked (shown in the table 1);

2) Experiencing the prototype: The participants are third- and fourth-year students majoring in fashion design. They are novice designers with limited design experience. The researchers spend three minutes explaining how to use the prototype. Each participant then has five minutes to use the prototype to create a textile pattern. The number of participants is 12 (n=12).

3) Evaluating UMUX: After using the prototype, participants answer structured questions. The questions assess their perceptions based on UMUX and TRIZ.

4) Measuring the correlation between TRIZ and UMUX: Researchers collect data from participants and calculate the correlation values between usability and the criteria of the problem-solving approach.

5) Ethnographic data: This research uses the data acquired through participant observation during the experimental process. Ethnographic data can explain certain human factors in the design process that are not described in TRIZ theory. The data is used to adjust the prototype during the experiment. The researchers will include both qualitative and quantitative data in the analysis phase.

6) Analyze the result: Researchers summarize the positive and negative factors influencing the usability of the prototype. They suggest a conclusion to improve the prototype and conduct experimental research in the future.

TABLE I. THE FILTERED TRIZ PRINCIPLES

No.	TRIZ Principles	No.	TRIZ Principles
1	Segmentation	7	Another Dimension (AD)
2	Merging	8	Periodic Action (PA)
3	Asymmetry	9	Feedback
4	Nesting	10	Copying
5	The Other Way Round (TOWR)	11	Color Changes
6	Spherodiality	12	Composite Materials (CM)

III. RESULT

A. UMUX Evaluation

Participants were asked to use the CST prototype to create a pattern. The knobs, sliders, and sampler buttons serve as the main user interface. The researchers introduced the prototype to all participants once and allowed them to experience it one by one. Discussion among participants was permitted during the experiment, as creativity in the design process is related to social interaction. The design results are shown in Figure 2.



Fig. 2. The textile design ceated with the CST prototype

Based on the UMUX evaluation, in which 12 participants answered four questions, the average score was 85.07 with a standard deviation of 14. The score indicates a positive user experience and high usability.

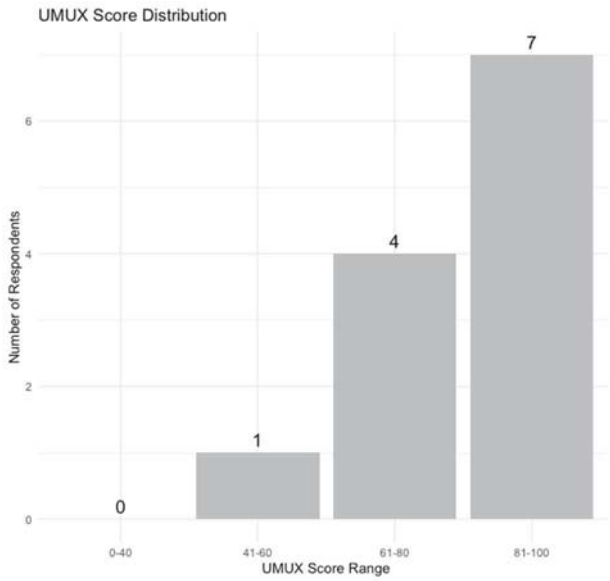


Fig. 3. The result of UMUX evaluation

B. *Analysis the CST with TRIZ method*

The questionnaire evaluates the scores of TRIZ items, and the UMUX results are analyzed using a correlational model. The scores are calculated using Pearson's correlation in RStudio. The result shows that four TRIZ disciplines correlate with CST using the projection mapping technique: segmentation, $r(10) = 0.61$, $p < 0.04$; merging, $r(10) = 0.58$, $p < 0.05$; nesting, $r(10) = 0.60$, $p < 0.04$; and color changes, $r(10) = 0.55$, $p < 0.06$. This indicates that the prototype is suitable for the design process, as it accommodates the complexity of patterns in textile design. The CST can assist designers in creating pattern layer combinations and adjusting colors. Additionally, the prototype supports specific tasks in the pattern design process, particularly pattern creation. Furthermore, the prototype's development during the experimental process will be explained in the next section.

TABLE II. THE RESULT OF TRIZ EVALUATION

	segmentation	**merging**	asymmetry	**nesting**	TOWR	spherodiality
r	**0.61**	**0.58**	0.23	**0.6**	0.07	0.25
t	**2.41**	**0.26**	0.74	**2.37**	0.24	0.83
p-val	**0.04**	**0.05**	0.48	**0.04**	0.82	0.43

	AD	PA	feedback	copying	**Color changes**	CM
r	-0.01	0.27	0.41	0.45	**0.55**	0.1
t	-0.03	0.89	1.41	1.58	**2.09**	0.5
p-val	0.97	0.4	0.19	0.15	**0.06**	0.7

C. *The Adjustment of CST*

The discussion among designers took place during the experiment. Researchers gathered feedback and found that the prototype's functionality could be enhanced by allowing the import of patterns created using hand-drawn techniques. As a result, the prototype was customized. Researchers imported photos of patterns provided by designers and tiled them within the software. Designers could then adjust the scale, size, and position of the patterns themselves. One of the participants stated, "*With the projection mapping technique, I can see the actual scale of my pattern. Previously, it was difficult to imagine the real scale when painting on fabric. This helps me readjust the size and repetition of the pattern* (personal communication, February 3, 2025)." Researchers therefore finalized the experimental process by adjusting the prototype and fostering collaboration between designers and developers. This prototype was developed based on TRIZ evaluation and discussions. This provided deeper insights into the factors underlying the design process. The prototype holds value in facilitating interaction among participants as well as in the ideation phase.



Fig. 4. The pattern design after adjusment of the prototype

IV. CONCLUSION

This research found that TRIZ can serve as a valuable toolkit for CST development, providing insights into how a prototype can be improved. Although CST has been developed for many decades, there is still room for further advancement if researchers understand the specific tasks within design activities. TRIZ is effective in revealing task procedures and suggesting subtasks that support the design process.

In textile design, these tasks are closely related to ideation and the visualization of patterns that cannot initially be seen

at their real scale. The prototype developed in this research demonstrates another dimension of using projection mapping techniques. When integrated into the design process, projection mapping becomes an intermediary between the designer and the design objects. Techniques, materials, and ideas converge within the design process, and TRIZ helps explain the design factors underlying the implementation of design tasks. For future research, the prototype needs a developed input system that is suitable for textile design creation. The interactive aspect can be maintained, but a more specific use goal is required in the design process.

In the process of CST development, several challenges arise, particularly in the interaction between designers and technicians. First, fashion design involves a highly conceptual process that emphasizes pattern, color, shape, and form. This differs from other design disciplines. Researchers need to carefully examine the cognitive processes involved in fashion design. Second, designers initially do not understand the limitations of software and algorithmic techniques. Therefore, they need to explore the functions of the chosen software extensively to create prototypes and refine their CST concepts. Third, some TRIZ criteria do not align with the outcomes of CST. This issue should be discussed between designers and technicians at the early stages of CST development. Moreover, these limitations must be communicated with professional designers throughout the process to refine TRIZ criteria. It is clear that effective and continuous communication among researchers, designers, and technicians is significant.

The four TRIZ related to CST efficacy are relevant to fashion design for these reasons: 1) Segmentation involves imagining the connection of a pattern from a small part to a larger part. A fashion designer may create a small rectangular patch of a pattern, and CST can tile the pattern in various ways; 2) Merging is about including visual components such as lines, planes, colors, shapes, and symbols; 3) Nesting is a way to combine such visual elements together; 4) Color changes influence the variation of visual elements. Different colors can create various moods and tones. CST can support these four criteria of CST effectively.

This research has a limitation due to the small number of participants. However, the participants are designers who are highly engaged in testing the prototype. The group of fashion designers in this research context is scarce; therefore, expanding the research venues should be considered.

REFERENCES

[1] N. Cross, Design Thinking. New York, USA: Bloomsbury, 2016.

[2] S. Jangir, "Digital embroidery designing: A new opportunity for textile designers," Int. J. Humanities Soc. Sci. (IJHS), vol. 2, no. 3, pp. 358-360, 2016.

[3] J. Leaf, R. Wu, E. Schweickart, D. L. James, and S. Marschner, "Interactive design of periodic yarn-level cloth patterns," ACM. Trans. Graph., vol. 37, no. 6, pp, 202:1-202:15, 2018.

[4] A. Lu, P. Y. Mok, and X. Jin, "A new design concept: 3D to 2D textile pattern design for garments," Comput. Aided Des., vol. 89, pp. 35-49, 2017.

[5] R. A. Angelova and D. Sofronova, "Application of CAD/CAM systems in the design of woven textiles," in Proc. 2021 IEEE 7th Int. Conf. Comput., Eng. Design (ICCED), Sukabumi, Indonesia, 2021, pp. 1–6, DOI:10.1109/ICCED53389.2021.9664866.

[6] N. A. Hamdan, S. Voelker, and J. Borchers, "Sketch & Stitch: Interactive embroidery for e-textiles," in Proc. CHI 2018, Montréal, QC, Canada, 2018, pp. 82:1–82:13, DOI: 10.1145/3173574.3173656.

[7] A. Habib and S. Alam, "A comparative study of 3D virtual pattern and traditional pattern making," J. Textile Sci. Technol. (JTST), vol. 10, pp. 1–24, 2024.

[8] X. Calixte and P. Leclercq, "The interactive projection mapping as a spatial augmented reality to help collaborative design: Case study in architectural design," in Proc. 14th Int. Conf. Cooperative Design, Visualization, and Engineering (CDVE 2017), Mallorca, Spain, Y. Luo, Ed. Springer, 2017, pp. 143–152, DOI: 10.1007/978-3-319-66805-5_18.

[9] M. S. Astriani, J. J. Lamug Martinez, B. P. Dirgantoro and L. H. Yi, "Four components of interactive projection mapping design plan: Case study using building block toys for learning," in Proc. 2022 1st Int. Conf. Technol. Innov. Appl. (ICTIIA), Tangerang, Indonesia, 2022, pp. 1–5, DOI:10.1109/ICTIIA54654.2022.9936016.

[10] S. Katkeviča and A. Strode, "Projection mapping method in advertising design," in Proc. Human, Technol., Quality Educ., Latvia, 2022, pp. 1004–1015, DOI:10.22364/htqe.2022.71.

[11] B. Shneiderman, "Establishing a framework of activities for creative work: Creative support tools," Commun. ACM, vol. 45, no. 10, pp. 116–120, 2002.

[12] J. Frich, L. M. Vermeulen, C. Remy, M. M. Biskjaer, and P. Dalsgaard, "Mapping the landscape of creativity support tools in HCI," in Proc. CHI 2019, Glasgow, Scotland, UK, 2019, pp. 389:1–389:18, DOI:10.1145/3290605.3300619.

[13] C. Remy, L. M. Vermeulen, J. Frich, M. M. Biskjaer, and P. Dalsgaard, "Evaluating creativity support tools in HCI research," in Proc. 2020 ACM Designing Interactive Systems Conf. (DIS '20), New York, USA, 2020, pp. 457–476, DOI:10.1145/3357236.3395474.

[14] S. Rahimi and V. J. Shute, "First inspire, then instruct to improve students' creativity," Comput. Educ., vol. 174, pp. 1–27, 2021, DOI:10.1016/j.compedu.2021.104312.

[15] C. Richardson and P. Mishra, "Learning environments that support student creativity: Developing the SCALE," Thinking Skills Creativity, vol. 27, pp. 45–54, 2018, DOI:10.1016/j.tsc.2017.11.004.

[16] H. Moon and S. H. Han, "A creative idea generation methodology by future envisioning from the user experience perspective," Int. J. Ind. Ergon., vol. 56, pp. 84-96. 2016.

[17] G. Altshuller, The Innovation Algorithm: TRIZ, Systematic Innovation and Technical Creativity, L. Shulyak and S. Rodman, Trans. Worcester, MA, USA: Technical Innovation Center, 1999.

[18] G. Altshuller, 40 Principles: TRIZ Keys to Technical Innovation, L. Shulyak and S. Rodman, Trans. Worcester, MA, USA: Technical Innovation Center, 2002.

[19] I. Ekmekci and E. E. Nebati, "TRIZ methodology and applications," in Proc. 3rd World Conf. Technol., Innov. Entrep. (WOCTINE), Istanbul, Turkey, 2019, pp. 303-315.

[20] A. Bastian, P. Hirt, S. E. Schwarz, M. Fischer, and A. Albers, "Identification of requirements for the transfer of creativity techniques in virtual environments by using TRIZ-Box," in Proc. 34th CIRP Design Conf., 2024, pp. 316-320.

[21] V. Petrov and H. Solodkina, "TRIZ: Innovation opportunities for the fashion industry," Acta Tech. Napocensis, Ser. Appl. Math. Mech. Eng., vol. 63, Special Issue, Oct. 2020.

[22] E. J. Lee, Y. K. Lim, H. C. Jung, and J. W. Park, "Fashion projection mapping using basic modeling form," in International Conference on Human-Computer Interaction, 2015, pp. 421-426, DOI:10.1007/978-3-319-21380-4_71.

[23] H. Shuang and Y. Shuo, "Application of Digital Technology in the Design of Textile Products," in Proceedings of the 2020 International Conference on Social Sciences and Big Data Application (ICSSBDA 2020), pp. 179-183, DOI:10.2991/assehr.k.201030.037

[24] X. Huang, S. Kettley and S. Lycouris, "Developing shape change-based fashion prototyping strategies: Enhancing computational thinking in fashion practice and creativity," Fashion Practice,vol.16, no. 2, pp. 282-310, 2024, DOI:10.1080/17569370.2024.2335615

Development of adventure games and puzzle solving in mysterious museums

Kriangkrai Phutongkan
Department of Digital Technology
Faculty of Science and Technology
Phuket Rajabhat University
Phuket, Thailand
s6511423103@pkru.ac.th

Akarachai Inthanil
Department of Digital Technology
Faculty of Science and Technology
Phuket Rajabhat University
Phuket, Thailand
akarachai.i@pkru.ac.th

Attapon Pillai
Department of Digital Technology
Faculty of Science and Technology
Phuket Rajabhat University
Phuket, Thailand
attapon.p@pkru.ac.th

***Abstract*— This research explores the development of an adventure and puzzle game set in a mysterious museum filled with artifacts and challenging gameplay. The game uses 3D and AI technologies to augment reality and engage players with cultural content. Players interact with artifacts to learn about their history, solve puzzles, and stimulate critical thinking. The game's atmosphere is enhanced with lighting, sound, and storytelling, while AI is used for 3D models and environment manipulation. However, high-resolution graphics impact performance, and balanced puzzle design remains a challenge. Future enhancements include a VR version of AI-driven NPCs for deeper immersion, and procedural puzzles for greater replicability.**

Keywords*— *adventure game, puzzle-solving, cultural heritage, AI.

I. Introduction

Cultural centers are places to preserve and disseminate a country's artistic and cultural heritage, which are essential for building pride in its history and culture. In an era where technology has become an integral part of daily life [1], cultural centers are facing the challenge of appealing to a new generation who consumes media and entertainment differently from previous generations [2]. Today's youth tend to seek out convenient and easily accessible information through digital media, such as online games or applications, and are less interested in visiting museums or cultural centers that require time or travel [3]. As a result, many cultural centers experience a decline in audience engagement, which could affect the sustainable preservation and dissemination of culture in the future. Accessible and fun cultural performances have emerged as an interesting alternative to attract young people, especially digital games, which are one way to connect players with culture, creating fun and challenging experiences [5].

Adventure and puzzle games are genres that can present history and cultural heritage in an engaging way. Players must explore a game world, such as a mysterious museum filled with artifacts and hidden stories, by solving puzzles and searching for clues [6]. For example, a game may require players to use their analytical and creative skills to solve puzzles about the history of an object, or simulate a real-world museum or cultural site, allowing players to learn about the culture through a virtual experience [7].

Developing these games requires sophisticated design to present culture in a valuable and accessible way. The use of modern tools allows the creation of 3D virtual worlds and realistic graphics, which provide players with a high-quality gaming experience, allowing them to explore and understand cultural heritage and history more deeply [9].

While developing these games is challenging due to the need to design puzzles that fit into realistic environments, the most important thing is to use technology to connect young people with cultural heritage. Digital games can create a bridge between the digital and real worlds, allowing young people to understand and appreciate cultural values in a modern and accessible way [10]. Game development not only enhances cultural knowledge and education, but also provides a fun and valuable experience, motivating young people to learn and participate in the conservation of cultural heritage in a way that is appropriate for the digital age [11].

This article is structured as follows: Section 1 Introduction Section 2 Literature Review Section 3 Describes the Research Design Section 4 Results and Discussion and Section 5 Conclusion.

II. Literature review

The study and development of digital games to promote learning about cultural and historical heritage has become a field of continuous interest in the past decade, especially in an era where digital technology plays a major role in our daily lives. Digital games can enhance the fun of playing games and can also create interesting and immersive learning experiences. They allow players to explore and understand cultural heritage through interaction with the virtual world, solving puzzles, and exploring places that reflect history, art, and culture in an easily accessible and modern format [1].

Several studies have provided important information in support of the use of games as a tool for studying and preserving culture. It has been found that games can stimulate interest and increase learning better than traditional methods of education, especially when the game includes elements of puzzle-solving and exploration of a virtual world offering cultural content. Participating in the problem-solving process through games not only helps players practice their critical thinking skills, but also allows them to experience and understand culture in a more concrete and interesting context.

The incorporation of digital games into the learning process has been recognized as an effective approach to increase understanding and interest in history, arts, and culture. Research studies have shown that games are an effective medium for promoting cultural learning by offering engaging and intellectually stimulating experiences [7]. By providing information through interactive gameplay, players are able to actively engage with historical and artistic content, thus gaining valuable cultural knowledge.

Studies have also found that incorporating digital media in museums and cultural centers makes it easier for visitors to access information and experience culture. The use of games and digital applications has made museums more engaging

XXX-X-XXXX-XXXX-X/XX/$XX.00 ©20XX IEEE

and has attracted young people to cultural heritage [10]. Furthermore, research exploring the use of AI in 3D modeling of objects in digital games allows players to experience cultural and historical heritage in detail through object creation and in-game interactions.

Based on these studies, it can be concluded that digital games are a potential tool to promote learning and preserve cultural heritage by combining elements of exploration, puzzle-solving, and presenting cultural information in a realistic and interesting way. This can attract players to understand and appreciate culture in a modern and easily accessible way.

III. Methodology

A. Game Design

In developing the digital game for this cultural center, we used a design process that took into account both entertainment and learning, starting with the study of the cultural content we wanted to present, such as the history of the artifacts in the museum. The player must press the object in order for the object to display the information for the player to read. By collecting data in the database in order to display images and information in the game so that players can understand the history of the object or the design of the object. Creating a virtual environment with the ability to create graphics. Realistic and compatible 3D AI for 3 D modeling of various objects.

B. Content Development

In the process of creating game content, developers collect data from cultural centers and other sources to ensure that the game content is engaging and educational, in order to create an immersive experience that reflects authentic cultural elements. Once the data is collected, developers refine and adapt it into a format suitable for gameplay, including designing puzzles that require players to analyze clues, decipher symbols, or solve logical challenges inspired by real-world history. These puzzles are strategically integrated into the game's progress, requiring players to engage deeply with the content to unlock new areas, discover hidden stories, and pass levels. In addition to solving puzzles, there are also exploration mechanics that encourage players to discover and interpret historical artifacts or cultural relics. Engaging with these elements not only helps players develop problem-solving skills, but also helps them better understand different cultures and histories.

C. Use of AI Technology

AI technology plays a crucial role in automatically generating and customizing 3D models within a game environment, improving the realism and detail of a scene without much manual work. By leveraging AI-driven techniques, developers can efficiently add diverse and dynamic objects to a game scene, resulting in a rich and immersive experience.
By integrating AI into scene modeling and decoration, game developers can significantly reduce the manual workload while creating more dynamic, realistic, and immersive environments, which not only enhances the visual storytelling, but also makes each scene come alive and responsive to player interactions.

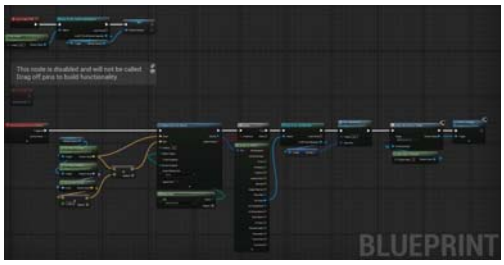


Fig. 1. A set of instructions for object display its history to the player.

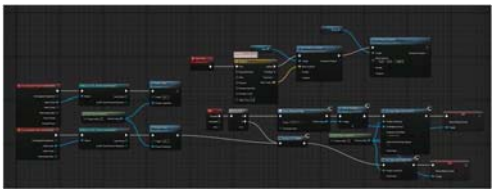


Fig. 2. A set of instructions for object move when the player enters the code.



Fig 3. The command set for setting the button.



Fig. 4. A set of instructions to check if the code is correct.



(A)



(B)

Fig. 5. AI Tool (A) Tripo Tool (B) Spaces Tool

D. Game Testing

To ensure that players get a good experience with their game, developers continuously test their game throughout the development process. Testing includes functional testing, performance testing, and usability testing to ensure that the game works according to standards and is suitable for the target audience.

E. Evaluation and Improvement

After testing the game at different stages, the developers collect the test results from the players to evaluate the game's performance in terms of attracting attention. Then, the game will be improved and improved in all aspects, especially in terms of content and player experience.

IV. Result and Discussion

The research findings show that the adventure and puzzle game set in a mysterious museum effectively meets players' needs across multiple aspects. In particular, the game scored an average of 4.40 for graphics, environment design, puzzle complexity, and gameplay mechanics, reflecting the game's ability to create an exciting and challenging experience. Players appreciated the realism of the graphics and the detailed environment design that enhanced immersion. Additionally, the puzzles were well-designed, challenging but not frustrating, allowing the game to strike a balance between fun and difficulty.

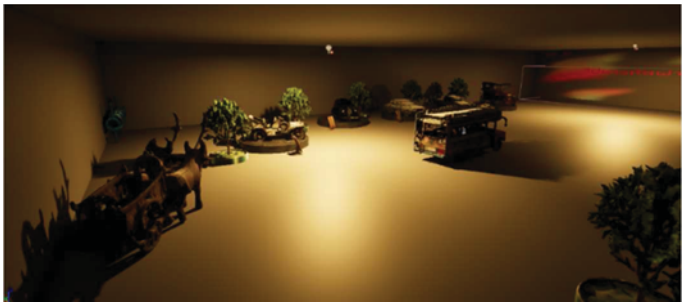
In terms of sound design and atmosphere, the game received a score of 4.30, indicating that players found the sound and the mysterious atmosphere effectively engaged them in the game world. The use of AI to create lighting and shadows, along with 3D model design, enhanced the game's visuals, although the use of high-resolution technology could impact performance, particularly on devices with limited resources.

In the area of educational value, the game achieved the highest score of 4.67, showing that players gained knowledge about history and culture while playing. This is a standout feature of the game, as it combines interactive learning with entertainment. Players could interact with objects in the museum and access related information and stories, turning learning into an enjoyable and beneficial experience.

However, game developers face challenges in designing puzzles with moderate difficulty to avoid player frustration or boredom, while ensuring the game performs well on a variety of devices. Furthermore, adding NPC that assist or hinder players could increase the challenge and intrigue of the game. Future development of a VR (Virtual Reality) version could enhance realism and further boost player engagement. Introducing a procedural puzzle generation system would add variety, preventing the gameplay from becoming repetitive and keeping players challenged with each round. Overall, the research demonstrates that this game successfully combines entertainment and education, providing players with a fun and valuable learning experience.



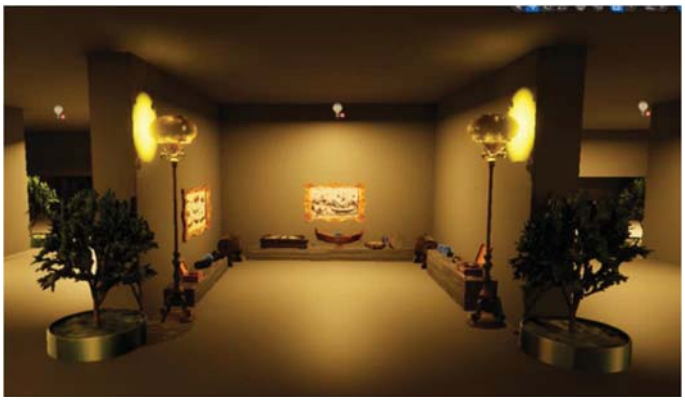
Fig 6 Menu start.



(A)



(B)



(C)

Fig 7. (A) Shows a model car used for decoration. (B) Arranges a model that provides knowledge about the items on display related to sailing. (C) Displays Thai musical instruments.

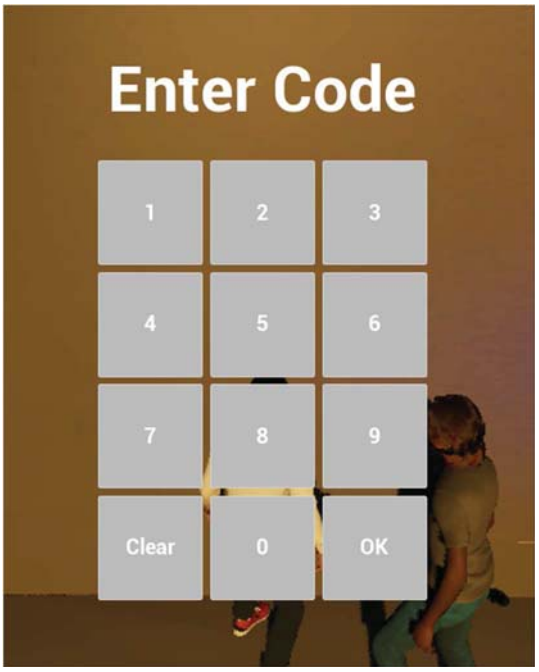


Fig. 8. Puzzle inside the scene.



Fig. 9. Game pause menu

V. Conclusion

From the study and development of adventure and puzzle games in a mysterious museum full of antiques and challenging gameplay mechanics, it was found that the use of 3D and AI technologies in games can effectively increase realism and attract players. Designing games that focus on exploration and solving puzzles in a virtual world promotes learning about cultural heritage and history through interacting with objects in the game, such as studying information about antiques, allowing players to learn in an accessible and fun way. The evaluation results found that players were highly satisfied in many aspects, such as graphic and environmental design, puzzle complexity, and gameplay mechanics, especially in learning about history and culture, which received the highest score of 4.67, indicating that this game can perfectly combine learning and entertainment. The design of this game can provide players with an experience that is both fun and valuable in learning. the development of this game also encountered challenges in designing puzzles with an appropriate level of difficulty so that players do not get bored or discouraged, as well as customizing the game to support operations on a variety of devices, especially the use of high-resolution technology that may reduce game performance on low-spec devices. For future development, consideration should be given to adding NPC that play important roles in the game to increase challenge and make the game more interesting. The development of VR (Virtual Reality) games can enhance the challenging experience for players through deeper and more immersive engagement. However, future VR developments may face several limitations, such as hardware and accessibility limitations. Using VR for a long time may cause dizziness, fatigue, or vision problems. In addition, the addition of an automatic puzzle generation system will make the game less boring and create new challenges every time you play. Overall, the development of this game is a good example of using digital technology to promote learning about cultural and historical heritage by combining education and entertainment to allow players to learn in a modern and fun way. This game is a potential tool to effectively connect players with cultural heritage in the digital age.

References

[1] Meadows, D. (2013). *Digital media and youth: From video games to virtual reality.* Journal of Digital Culture & Society, 10(2), 103-115.

[2] Perrin, A. (2015). *Social media usage: 2005-2015.* Pew Research Center.

[3] Crompton, H., & McKenney, S. (2008). *An investigation of the potential for digital games in education.* Journal of Educational Multimedia and Hypermedia, 17(2), 227-241.

[4] Vasiliu, I. (2019). *Game-based learning for cultural heritage education.* European Journal of Cultural Studies, 22(3), 245-262.

[5] Elder, A., Moore, D., & Goodman, A. (2022). *Using Unreal Engine 5 for the creation of immersive educational games.* Journal of Game Development, 13(1), 44-56.

[6] Tse, K. (2016). *Exploring digital engagement in museum learning.* Museum Management and Curatorship, 31(1), 60-76.

[7] Bell, A., & Jansen, B. (2020). *The impact of game-based learning on cultural education.* Interactive Learning Environments, 28(7), 779-793.

[8] Liu, Y. (2018). *Immersive technology and cultural heritage: The case of VR games in museums.* International Journal of Cultural Heritage, 15(4), 456-469.

[9] Zhang, Y., & Wang, X. (2021). *AI and its impact on cultural preservation in digital games.* Journal of Digital Humanities, 7(2), 132-141.

[10] Phillips, C., & Martin, L. (2017). *Integrating digital media into museum practices: A new direction.* Museum Studies Journal, 18(3), 201-215.

[11] Wang, Z. (2020). *Cultural storytelling in the age of digital entertainment: The role of games in preserving heritage.* Journal of Cultural Media, 25(1)

Fine-Tuning AI Models With Limited Resources

Kritsada Singhapoo
Department of Digital Technology
Faculty of Science and Technology
Phuket Rajabhat University
Phuket, Thailand
s6511423101@pkru.ac.th

Akarachai Inthanil
Department of Digital Technology
Faculty of Science and Technology
Phuket Rajabhat University
Phuket, Thailand
akarachai.i@pkru.ac.th

Attapon Pillai
Department of Digital Technology
Faculty of Science and Technology
Phuket Rajabhat University
Phuket, Thailand
attapon.p@pkru.ac.th

***Abstract*—This paper looks at fine-tuning AI models when there are limited resources. The goal is to improve model performance using a small amount of training data and limited computing power. The study explores methods to reduce memory training time and energy consumption while still keeping the model accurate. The experiments were done using the LLaMA 3.1 8B model with Python and the Unsloth tool to make the training process more efficient. The paper tests fine-tuning techniques such as low-rank adaptation quantization and selective parameter updates to reduce computational costs without lowering output quality. It also looks at how dataset size, adjusting hyperparameters, and training time affect performance, giving insights into the balance between efficiency and accuracy. The results show that even with limited data and hardware, the fine-tuned model can still learn specific knowledge, adapt to new tasks, and provide accurate responses. These findings show the potential for using large language models in environments with limited resources and provide useful advice on how to train AI models efficiently in such situations.**

Keywords— Fine-Tuning, Limited Resources, AI

I. INTRODUCTION

Fine-tuning AI models is a critical step in machine learning, particularly when working under constraints such as limited data availability and computational resources. Large models, such as those in the LLaMA 3 family [1], typically require extensive datasets to achieve optimal performance. However, in real-world scenarios, especially in resource-constrained environments, these conditions are often unmet, leaving many organizations and individuals unable to leverage state-of-the-art models effectively. This research investigates various fine-tuning techniques that enable models to perform optimally despite these limitations. To explore this challenge, a dataset from Phuket Rajabhat University's Office of Cultural Affairs was utilized as a case study. While the preservation of cultural data is not the primary focus of this research, it provides a practical context to evaluate how effectively AI models can learn from smaller, specialized datasets. The study primarily aims to assess the efficiency of fine-tuning methods and the impact of different strategies on model performance under resource constraints.

Fine-tuning AI models under such constraints necessitates strategies that enhance learning efficiency without relying on vast datasets. Recent advancements, such as Unsloth [2], demonstrate that high performance can be achieved even with limited data and reduced computational resources. Unsloth employs techniques like Low-Rank Adaptation (LoRA) [3], which reduces the number of trainable parameters by focusing on key parts of the model, ensuring efficiency even with limited data. Additionally, Unsloth incorporates 4-bit quantization [4], a method that significantly reduces the memory footprint of models, enabling efficient fine-tuning without the need for extensive datasets. These approaches make fine-tuning particularly applicable in scenarios where large-scale data collection or computational power is infeasible. Furthermore, the study highlights the importance of balancing model size and available resources, a critical challenge in deploying AI in resource-constrained environments [5]. This research also explores the use of structured datasets, such as the Alpaca Prompt Format [6], which enhances a model's ability to understand and adapt to specific contexts, improving learning efficiency and reducing the risk of overfitting. Techniques like gradient accumulation [8] and the AdamW optimizer [7] are also discussed as methods to stabilize training and improve convergence in low-resource settings. By combining these strategies, the study demonstrates that fine-tuning can be both resource-efficient and effective, even when working with smaller datasets.

This paper is organized into four sections. Section II presents the fine-tuning methodology, including the implementation of LoRA, 4-bit quantization, and structured dataset formatting. It also details the experimental setup, covering model selection, dataset preparation, and the use of Unsloth for optimizing training efficiency. Section III describes the experimental evaluation, analyzing the impact of fine-tuning techniques on model performance, memory usage, and computational efficiency. It provides comparative results showcasing the trade-offs between accuracy and resource constraints. Section IV discusses the implications of the findings, exploring the scalability of resource-efficient fine-tuning and its potential applications in real-world scenarios. Section V concludes the paper by summarizing key insights and suggesting future research directions for improving AI adaptation in constrained environments.

II. METHODOLOGY

This study employed various methods to fine-tune the AI model efficiently, even under limited data and computational resources. One of the key techniques used was LoRA. LoRA allows fine-tuning of specific parts of the model instead of modifying the entire model. This selective adaptation reduces the number of parameters that need to be updated, making the learning process more efficient with limited data. The method significantly minimizes computational overhead, which is crucial when working with restricted resources. In addition to LoRA, the dataset was structured using the Alpaca Prompt Format, which organizes the questions and answers to provide clear context to the model. This structured approach enhances the model's ability to interpret and understand the data effectively, reducing the risk of overfitting and ensuring that the model generalizes well despite the small dataset. To further optimize the fine-tuning process, the model was

XXX-X-XXXX-XXXX-X/XX/$XX.00 ©20XX IEEE

trained with 4-bit Quantization, a technique that reduces memory usage. This allows for the model to be fine-tuned even when working with smaller datasets, making it feasible to train large models without exceeding hardware limitations. By reducing the memory required, the training process becomes more efficient and scalable, especially when computational resources are limited. The fine-tuning was performed on an NVIDIA A100 GPU, using several additional techniques to further optimize memory usage and computational efficiency. The 4-bit quantization allowed the model to consume significantly less memory compared to traditional formats like float16 or bfloat16, making it possible to train the model within the available GPU memory. Additionally, gradient checking was employed to reduce memory consumption during training. This technique avoids storing intermediate computations at every step, allowing for larger batch sizes and more efficient use of available memory. By not keeping all computational values in memory, the system could allocate more resources for batch processing, thereby speeding up the training process. The AdamW 8-bit Optimizer was also utilized, which reduces memory usage while preserving the speed of the optimization process. This optimizer converts weight updates to 8-bit precision, which significantly lowers memory demands without sacrificing the training speed. Finally, gradient accumulation was applied to allow the use of smaller batch sizes while still enabling effective parameter updates. This helped to balance memory usage with training efficiency, ensuring that the model could learn from the limited data without compromising on performance.

The workflow for fine-tuning AI models with limited resources is designed to achieve optimal performance while addressing the constraints of computational power and available data. The first step in this process is to carefully select a base model that can adapt to the specific tasks at hand. For this, the LLaMA 3.1 8B model is chosen due to its proven efficiency, scalability, and ability to handle a wide range of applications. Once the base model is selected, data preparation becomes critical. The dataset must be cleaned and processed to ensure that the data is free of noise and irrelevant information. This high-quality dataset is then structured using the Alpaca Prompt Format, which organizes the data into clear input-output pairs that improve the model's understanding and learning process. The structured format ensures that the model can efficiently learn the relationships between data points, especially important in cases where the data is limited, reducing the risk of overfitting and improving the model's generalization ability.

The next phase in the workflow involves selecting fine-tuning strategies that reduce computational overhead while maintaining model performance. A key strategy used here is LoRA, which reduces the number of trainable parameters by focusing on the most significant components of the model. By doing so, LoRA minimizes the computational cost of fine-tuning, while still preserving the model's capacity to learn effectively. Additionally, 4-bit Quantization is applied to reduce memory consumption during the fine-tuning process. This technique involves converting the model's weights into lower precision, which reduces the memory footprint and accelerates training. Along with these strategies, hyperparameters such as learning rate, batch size, and others are carefully tuned to strike a balance between efficient training and optimal performance. Fine-tuning these parameters ensures that the model can be trained effectively, even with limited computational resources. Training the model involves leveraging tools like Unsloth and the AdamW

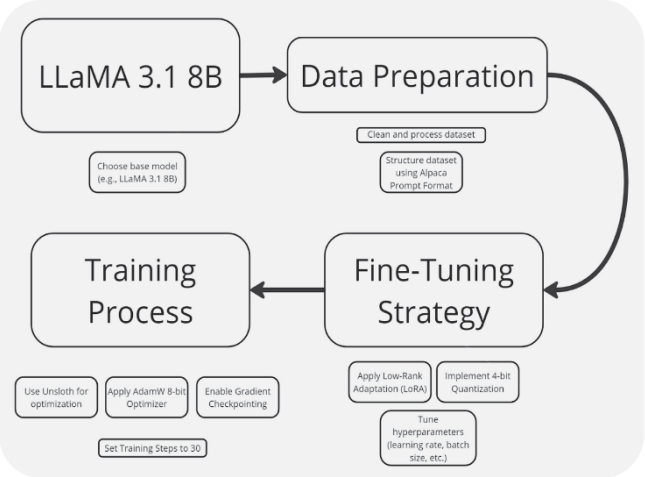


Fig.1. The workflow for fine-tuning AI

8-bit Optimizer. These tools are designed to optimize the fine-tuning process by minimizing the load on the GPU and ensuring that the model's weights are updated in a way that is both efficient and effective. Furthermore, Gradient Checkpointing is employed during training to manage memory usage by not storing intermediate activations for each layer. This is particularly useful when training large models with limited memory, as it allows for larger batch sizes and improves the overall efficiency of the training process. To prevent overfitting, the number of training steps is capped at 30, ensuring that the model receives enough exposure to the data without memorizing it excessively. After the fine-tuning process, the model undergoes an evaluation phase where its performance is assessed. The evaluation begins with a comparison of the training loss before and after fine-tuning. A reduction in loss indicates that the fine-tuning process was successful in improving the model's ability to learn from the data. The model is also tested on a sample dataset to assess its generalization capability. This step ensures that the model can perform well on data that it hasn't seen during training. To further gauge the fine-tuning process's success, the model is compared with other leading models like GPT-4o mini and DeepSeek-R1. This benchmarking allows for a deeper understanding of the model's relative strengths and weaknesses in terms of speed, accuracy, and efficiency.

Finally, the results of the fine-tuning process are analyzed and discussed. The combination of techniques like LoRA, 4-bit Quantization, Gradient Checkpointing, and efficient optimizers has proven to be highly effective in optimizing model performance without requiring extensive computational resources. These strategies not only reduce memory consumption but also enable the model to achieve high accuracy despite the limitations of available data and hardware. The findings suggest that these methods can be applied to real-world scenarios where computational resources are constrained, broadening the scope and accessibility of large AI models. Furthermore, the paper proposes future avenues for further optimization, such as combining LoRA with other advanced fine-tuning techniques, to achieve even better performance with fewer resources. This research highlights the potential for fine-tuning large AI models to become more accessible, making them viable for applications in various fields despite resource limitations.

This workflow proves that with the right strategies, fine-tuning large AI models can be accomplished even in environments with constrained resources. By focusing on techniques that reduce memory usage, optimize training efficiency, and enhance model performance, it is possible to

effectively train large models without the need for excessive computational power. This approach not only makes AI more accessible to a broader range of users but also sets the stage for future innovations that can further reduce the computational barriers associated with AI model training.

III. RESULTS

A. Training Loss

During the fine-tuning process, the model was trained for a total of 30 epochs. Initially, the training loss was 2.93, indicating that the model was still far from optimal. However, after completing the training, the final loss reduced significantly to 0.07. This substantial decrease in training loss demonstrates the effectiveness of the fine-tuning techniques used, showing that the model was able to adapt and improve its performance over the course of the training. The results suggest that the selected approach successfully enhanced the model's learning capability, even with limited data and resources.

B. Testing the Fine-Tuned Model

To evaluate the fine-tuned model, a test was conducted by asking, “Explain the history of the ‘Yaya’ traditional outfit.” The response from the fine-tuned model was

C. Model File (unsloth. F16.gguf)

This code configures the fine-tuning of a large language model (LLM) using the Unsloth library, specifically targeting the F16.gguf model. The goal is to create an AI The code defines a template for structuring conversations, using special tokens to mark different parts of the interaction, like speaker roles and message content. This structured approach helps the model understand the context and flow of the conversation.

D. Comparison with Other Models

The results indicate that the fine-tuned model consistently achieves the highest accuracy across all dataset categories, particularly in the 4-ROW category with an accuracy of *99.95%*. The LLaMA 3.1 8B performs well, with 87% accuracy in the 8-row category and 95% in the 16-row category. In comparison, GPT-4o mini and DeepSeek-R1 show lower accuracy as the dataset size increases.

E. Training Loss Over Steps for Different Datasets

This figure illustrates the training loss over steps for three different datasets: 16-row, 8-row, and 4-row datasets. While the plot appears to show a decrease in training loss as the number of steps increases for all three datasets, the differences in final loss values are minimal. Specifically, after 30 steps, the 16-row dataset achieves a loss of 0.1405, compared to 0.0700 for the 8-row dataset and 0.0450 for the 4-row dataset. Although the 4-row dataset exhibits the lowest final loss, the variations across all three datasets are relatively small, suggesting that even with significantly reduced data, the model's performance remains comparable. This nuanced observation is particularly relevant to this project's focus on efficient training with limited data. However, this graph also

```
GPU = NVIDIA A100-SXM4-40GB. Max memory = 39.557 GB.
16.922 GB of memory reserved.

[80] trainer_stats = trainer.train()

==((====))==  Unsloth - 2x faster free finetuning | Num GPUs = 1
   \\   /|    Num examples = 8 | Num Epochs = 30
O^O/ \_/ \    Batch size per device = 2 | Gradient Accumulation steps =
\        /    Total batch size = 8 | Total steps = 30
 "-____-"     Number of trainable parameters = 41,943,040
                                            [30/30 00:53, Epoch 30/30]
```

Step	Training Loss
1	2.937400
2	2.819900
3	2.786200
4	2.736300
5	2.458900
6	2.077400

Fig. 2. This significant reduction in loss indicates that the model was able to learn effectively from the limited dataset.

```
FROM ./unsloth.F16.gguf

TEMPLATE """{{- range $index, $_ := .Messages }}<|start_header_id|>{{ .Role }}<|end_header_id|>

{{ .Content }}
{{- if gt (len (slice $.Messages $index)) 1 }}<|eot_id|>
{{- else if ne .Role "assistant" }}<|eot_id|><|start_header_id|>assistant<|end_header_id|>

{{ end }}
{{- end }}"""

SYSTEM """This AI assistant is fine-tuned on data related to Phuket traditional costumes and Thai
cultural heritage. It provides responses in Thai and is optimized for accuracy and cultural relevance.
The assistant is designed to answer questions related to traditional attire, historical contexts, and
related topics based on the fine-tuned dataset."""

PARAMETER temperature 0.7
PARAMETER top_p 0.9
PARAMETER quantization "bnb-4bit"
PARAMETER gradient_checkpointing "unsloth"
PARAMETER optim "adamw_8bit"
```

Fig. 3. This answer aligns with the dataset used for fine-tuning

```
[61] # alpaca_prompt
     FastLanguageModel.for_inference(model)
     inputs = tokenizer(
     [
         alpaca_prompt.format(
             "อธิบายชุดย่าหยา", # instruction
             "ชุดบาบ๋า ", # input
             "", # output - leave this blank for generation!
         )
     ], return_tensors = "pt").to("cuda")

     from transformers import TextStreamer
     text_streamer = TextStreamer(tokenizer)
     _ = model.generate(**inputs, streamer = text_streamer, max_new_tokens =

<|begin_of_text|>Below is an instruction that describes a task, paired w

### Instruction:
อธิบายชุดย่าหยา

### Input:
ชุดบาบ๋า

### Response:
ชุดย่าหยาได้รับอิทธิพลจากชาวมลายูและวัฒนธรรมเปอรานากัน เป็นที่นิยมในกลุ่มผู้หญิงสูงอายุและชนช
```

Fig. 4. Model File (unsloth. F16.gguf)



Fig. 5. Accuracy of different models

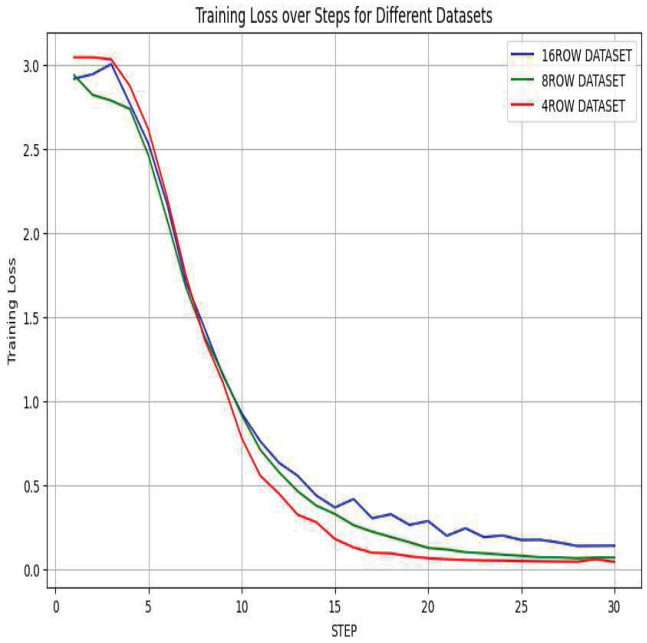


Fig. 6. Loss model

V Discussion

The results of this study highlight the effectiveness of parameter-efficient fine-tuning (PEFT) techniques in adapting large language models (LLMs) to resource-constrained environments. The combination of LoRA, 4-bit quantization, and structured dataset formatting proved to be highly efficient in reducing memory consumption while maintaining competitive model performance. The findings demonstrate that even with limited computational resources, fine-tuned models can achieve substantial accuracy improvements while minimizing training overhead. One of the key observations from the experiments is that LoRA significantly reduces the number of trainable parameters, thereby lowering the computational cost of fine-tuning. Compared to full fine-tuning, which requires updating all parameters in a large model, LoRA optimizes only a subset of weights, making it feasible to train models on consumer-grade GPUs. Additionally, 4-bit quantization effectively compresses model weights, reducing memory footprint without a significant loss in accuracy. This is particularly beneficial for real-world applications where deploying LLMs on edge devices or cloud-based instances with limited resources is necessary. Moreover, the use of structured dataset formatting, such as the Alpaca Prompt Format, improved the model's ability to learn from smaller datasets. This approach enhances knowledge retention and minimizes overfitting, which is a common issue when fine-tuning with limited data. The results indicate that structured data organization plays a critical role in improving model efficiency, as it enables more effective learning from domain-specific inputs.

A major challenge in fine-tuning large models is the trade-off between computational efficiency and model accuracy. The experimental results show that gradient checkpointing and AdamW with 8-bit precision effectively reduce memory usage while maintaining training stability. These optimizations allow for larger batch sizes and faster convergence, which are crucial in low-resource settings.

Furthermore, our study emphasizes the importance of balancing training steps to avoid overfitting. The experiments were designed to cap training steps at 30, ensuring that the model receives sufficient exposure to the dataset without excessive memorization. The observed reduction in training loss confirms that strategic tuning of hyperparameters, including batch size and learning rate, is essential for optimizing fine-tuning performance under resource constraints. Refinements aim to provide clearer insights into the trade-offs and practical implications of PEFT techniques, further solidifying the study's relevance and impact.

IV. Conclusion

Fine-tuning large AI models in resource-constrained environments is both a challenge and an opportunity. This study demonstrates that with strategic approaches, it's possible to achieve high performance without extensive computational resources. Techniques such as Low-Rank Adaptation (LoRA) and quantization have proven effective in reducing the number of trainable parameters and memory usage, respectively, thereby making the fine-tuning process more efficient. The use of structured datasets, like the Alpaca Prompt Format, further enhances the model's ability to learn from limited data by providing clear context and reducing overfitting risks. Additionally, optimizing hyperparameters and employing methods like gradient checkpointing and the use of efficient optimizers contribute to minimizing computational overhead. The significant reduction in training loss observed in this study underscores the potential of these techniques to maintain, and even enhance, model accuracy despite limited resources. These findings are particularly relevant for deploying AI models in settings where computational power and data availability are limited, broadening the accessibility and applicability of advanced AI technologies. Future research could explore the combination of these techniques with other parameter-efficient fine-tuning methods to further improve performance and efficiency.

References

[1] Meta. (2024). Llama 3.1 8B [Large language model]

[2] Unsloth AI. (2024). Unsloth: Fast fine-tuning for large language models.

[3] Hu, E. J., Shen, Y., Wallis, P., Allen-Zhu, Z., Li, Y., Wang, S., Wang, L., & Chen, W. (2021). LoRA: low-rank adaptation of large language models. arXiv preprint arXiv:2106.09685

[4] .Bondarenko, Y., Del Chiaro, R., & Nagel, M. (2024). Low-rank quantization-aware training for LLMs. arXiv preprint arXiv:2406.06385.

[5] Singh, A., Pandey, N., Shirgaonkar, A., Manoj, P., & Aski, V. (2024). A study of optimizations for fine-tuning large language models. arXiv preprint arXiv:2406.02290.

[6] DataCamp. (n.d.). Mastering Low-Rank Adaptation (LoRA): Enhancing large language models for efficient adaptation.

[7] Loshchilov, I., & Hutter, F. (2019). Decoupled weight decay regularization. arXiv preprint arXiv:1711.05101. (AdamW Optimizer)

[8] Ott, M., Edunov, S., Baevski, A., Fan, A., Gross, S., & Auli, M. (2018). Scaling neural machine translation. arXiv preprint arXiv:1806.00187. (Gradient Accumulation)

Machine Learning-Based Framework for Early and Age-Inclusive Detection of Autism Spectrum Disorder Using U.S. Screening Data

Mohammad Anisur Rahman
Department of Marketing & Business Analytics
East Texas A&M University, 2104 University Dr, Commerce, TX 75428, USA
mrahman25@leomail.tamuc.edu

Intiser Islam
School of Engineering,
University of Bridgeport, 126 Park Ave, Bridgeport, CT 06604, USA
iislam@my.bridgeport.edu

Shariar Islam Saimon
School of Engineering,
University of Bridgeport, 126 Park Ave, Bridgeport, CT 06604, USA
ssaimon@my.bridgeport.edu

Md Rafiuddin Siddiky
College of Technology
Wilmington University, New Castle, Delaware, USA
mdrafiuddinsiddiky@gmail.com

Md Mahadi Hasan
School of Information Technology, Washington University of Science and Technology, Alexandria, Virginia, USA
mahadih384@gmail.com

Hasan Mahmud Sozib
Department of Electrical and Electronic Engineering
Ahsanullah University of Science and Technology, 141 & 142, Love Road, Tejgaon, Dhaka, 1208, Bangladesh
sozib2019@gmail.com

Romana Nourin Nipa
Department of Information and Communication Technology
Islamic University, Kushtia-7003, Bangladesh
romananourin@gmail.com

MD. Jahid Hassan
Department of Information and Communication Technology
Islamic University, Kushtia -7003 Bangladesh
jahid.ict.iu@gmail.com

Seaam Bin Masud
College of Technology
Wilmington University, New Castle, Delaware, USA
seaam.masud@gmail.com

*Corresponding author: Author (sozib2019@gmail.com)

***Abstract*—The increasing incidence of Autism Spectrum Disorder (ASD) demands an efficient diagnostic tool that is suitable for all age groups. Many current methods are restricted in their specificity to early childhood, limiting service for older individuals. In this work, we propose a machine learning (ML)-based framework for improving ASD detection across various demographies using the U.S. Autism Screening Dataset. The dataset comprises 704 records across demographic, behavioral, and diagnostic attributes. Principal component (PCA) and correlation analysis help us identify the most predictive variables or feature selection, introducing the dimensionality challenge. Four ML models for the classification of ASD likelihood are evaluated in the proposed framework. The efficacy of the model is supposed to be determined by some performance metrics like accuracy, precision, recall, and F1 score. Out of the evaluated models, the Extra Trees Classifier was shown to be the most robust, with an accuracy of 96.67%, precision of 97.50%, recall of 95.00%, and an F1 score of 96.17%. In particular, its superior balance of precision and recall makes it best suitable for ASD detection. Results of Decision Tree and Random Forest (Entropy) are comparable, and a bit lower than Decision Tree and Random Forest (Gini). The potential of using ML frameworks to create scalable, age-inclusive diagnostic tools is highlighted by the findings. Taken together, these tools could fill a gap in clinical assessment, help speed up the diagnostic process, and allow for the initiation of treatment promptly. By applying ML's predictive power, this study makes a contribution to the advancement of ASD diagnostic methods to improve detection accuracy, inclusive, and scalable.**

Keywords- Autism Spectrum Disorder (ASD), Autism Screening Dataset, Predictive Modeling, Machine Learning (ML),

I. INTRODUCTION

Autism is a lifelong disability that affects the ability to communicate and relate to others [1]. People with autism have difficulties in four main areas: Communication, social interaction, stereotyped activities, and sensory abnormalities, such as (hypoactivity, hyperactivity, and fluctuations between these states), which is claimed to be the most common complication [2, 3]. The diagnostic process is still a course of considerable difficulty even with improving diagnostic tools. Most existing methods used to diagnose ASD are based on clinical assessment of items like Autism Diagnostic Observation Schedule (ADOS) [4]. Although, these tools are good, but are not discriminatory and are largely loaded in favor of certain age groups predominantly children [5].

The main aim of this study is to create a machine-learning framework to detect Autism Spectrum Disorder (ASD) across all age groups using an expansive U.S.-based Dataset. We employed various machine learning models: Decision Tree, Random Forest using Entropy criterion (RF-Ent), Random Forest using Gini criterion (RF-Gini), and Extra Trees Classifier (ET21) to determine which model best addresses screening for ASD. The goal of this study is to make these models able to generalize across age groups, as limitations in current methods tend to be specific to certain

age ranges. The paper is organized mainly as follows: Section II summarizes relevant work; Section III uses Methodology to describe the technique, including the dataset description, recommended strategy, and model interpretability. Coverage of the experimental design, feature importance analysis, assessment metrics, and interpretability outcomes in Section IV provides the results and discussion. Section V ends the report with ideas and comments for further efforts.

II. Related Work

In this section, recent achievements in Employing, ML, and DL frameworks for ASD detection are discussed concerning various datasets.

ASD has been analyzed across different age groups by M. Abdelwahab et al. [6] through the application of six machine learning techniques. The study used four different public ASD datasets available from Kaggle and UCI ML repositories. The evaluated methods included in this study revealed that Logistic Regression (LR) showed better accuracy at 96.69% and performed better on the selected dataset. Thabtah et al. [7] proposed a new model combining Self-Organizing Maps (SOM) with classification algorithms to address biases in autism screening. The model, evaluated on a real-life autism screening dataset with over 2000 instances, outperformed traditional methods. In [8], S. Raj et al. analyzed and compared the possibilities of employing Naive Bayes, SVM, Logistic Regression, KNN, Neural Networks, and CNN for the ASD forecast at kids, adolescents, and nearly grown-up individuals. Using Support Vector Machines (SVM) based Machine Learning (ML) algorithms Bone et al., [9] proposed methods that help improve the screening and diagnosing of ASD. Based on ADI-R and SRS for 1,264 participants with ASD and 462 without ASD, the algorithms displayed increased accuracy in comparison with the previous approaches. Vakadkar et al. [10] used SVM, RFC, NB, and ML to predict infants with ASD by analyzing the datasets. The study also sought to establish the frailties that make an individual prone to developing ASD with a view of cutting short the procedures of diagnosing the condition. As well as being more accurate and more efficient than conventional behavioral observation methods, B. Kamala et al. [11] proposed the use of machine learning (ML) to enhance early ASD detection. ML was shown to be able to analyze brain region relationships, discover genetic factors, and create good interventions for ASD diagnosis.

III. Methodology

Dataset Description and Preprocessing

This study uses a dataset of 704 ASD screening records including people of different age groups. The file contains demographic information (age, gender, ethnicity) and screening scores from diagnostic questionnaires to screen for ASD traits. The target variable is binary ASD diagnosis (for example, when "0" indicates no ASD diagnosis (control group) and "1" indicates an ASD diagnosis (autism-positive group)). Missing values were handled for data preprocessing at every step although for numerical data only median imputation was applied.

Proposed Methodology

1. ML Based Autism Detection Framework

This paper uses the dataset in the study and the preprocessing steps include data cleaning, normalization, and feature extraction. Then various techniques such as Principal Component Analysis (PCA), Correlation Heatmap, and Pearson Correlation are applied to extract relevant features from the raw data to transform it into something that can train a model. The overview of our workflow is illustrated in Fig. 1.

2. Models

Decision Tree: A supervised machine learning model takes the form of a Decision Tree, which is a tree using a tree-like structure to classify data or predict the outcome of some event [12]. For classification, the output at a leaf node is the majority class c .The predicted class $\hat{y}$ is determined by:

$$\hat{y} = arg\ \underset{c}{max}\ p(C)$$

where $p(c)$ is the proportion of data points in class c at the leaf node.

Random Forest with Entropy (RF_Ent): Robust Random Forest with Entropy (RF_Ent) is an ensemble machine learning algorithm that builds up multiple decision trees and outputs their results in an attempt to deliver better classification accuracy. Entropy, which measures uncertainty, is calculated as:

$$H(s) = -\sum_{i=1}^{c} p_i log_2(p_i)$$

where S_j represents subsets formed by the split.

In ASD detection, RF_Ent analyzes diagnostic features across multiple trees, each trained on different data subsets. The final prediction aggregates individual tree outputs through majority voting:

$$\hat{y} = arg\ \underset{c}{max}\ \frac{1}{n}\sum_{i=1}^{n} T_i\,(x)$$

Where $T_i(x)$ is the prediction of the i-th tree.

Random Forest using Gini Index (RF_Gini): The RF_Gini ensemble model is an ensemble model of many decision trees that fits multiple trees and gives a higher classification accuracy [13]. Gini impurity is calculated as follows, and each tree splits data by minimizing:

$$Gini = 1 - \sum_{i=1}^{C} {p_i}^2$$

where p_i is the proportion of data in class i. Lower values indicate purer splits.

ET21: In the same way that Random Forest Extra Trees is essentially an ensemble of lots of trees for each observation, but with extra randomness built into making all these trees [14]. Extra Trees selects splits randomly, in contrast to Random Forest which has each split based on ascertaining Gini or entropy, an increase in diversification to the model

[15]. The mathematical calculation for predictions combines the output of N trees as follows:

$$\hat{y} = \frac{1}{N}\sum_{i=1}^{N} T_i(x)$$

where $T_i(x)$represents the prediction of the i-th tree for input x.

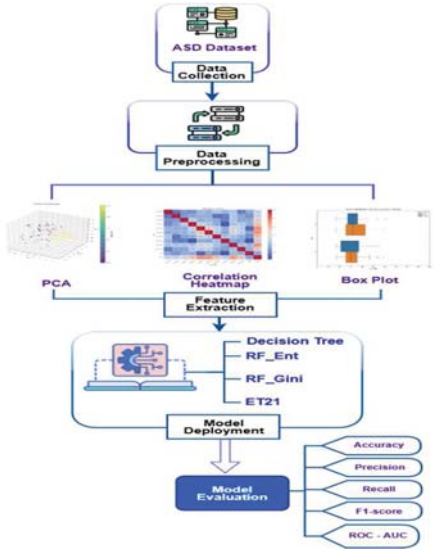


Fig. 1. Overview of ML Based Autism Detection Framework

IV. Result & Discussion

A. *Experimental Setup:*

We used Google Colab for our research, writing in Python. Using **scikit-learn**, model implementation was conducted. The workflow consisted in data preparation and training assessment to explain model predictions.

A. *PCA, Correlation Heatmap and Box Plot outcomes:*

Fig. 2 displayed the 3D PCA visualization, where the first principal components can explain the variation in the Early-Stage Autism Detection dataset, particularly those who have or do not have ASD. In class 0, the non-ASD cases are more scattered out among the data vectors, and the PCs to which those vectors are assigned are placed on the axes for PC1 PC2, and PC3, whereas class 1 has a greater population.

Fig. 3 shows the first correlation heatmap, which helps to show the relationships of some key interrelationships among the diagnostic features for the refinement of ASD detection algorithms. The weaker correlations between variables such as "Gender" and "Relation", signify its use as an independent predictor for the model to distinguish between ASD and non-ASD cases.

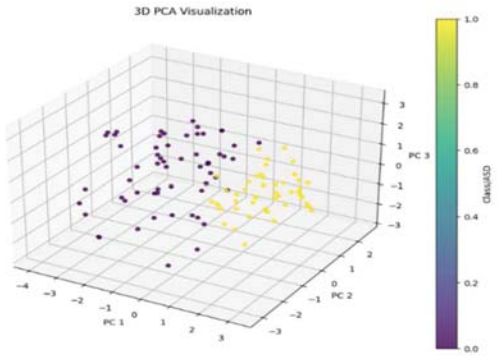


Fig. 2. PCA Plot Revealing Variance of Components for ASD and Non-ASD

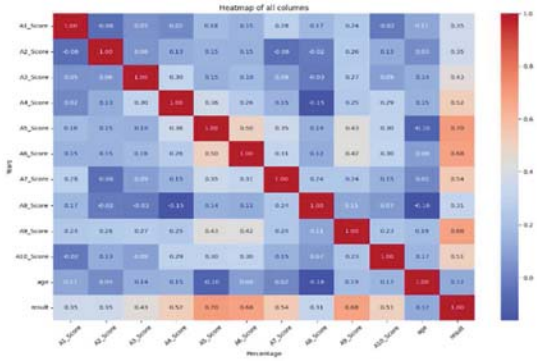


Fig. 3. Feature Correlation Heatmap

B. *Evaluation Metrics*

In this study on early autism detection using diagnostic and demographic features, we evaluated four machine learning models. Table 1 shows a summary of the results with metrics for our model such as the accuracy, precision, recall, F1-score, and ROC-AUC scores. Overall, the Extra Trees (ET) model, achieved 96.67% accuracy, 97.50% precision, 95.00% recall, and 96.17% F1-score. With an ROC AUC score of 96.50%, and strong discriminatory power, ET is a good choice for early autism detection because of its good balance of precision and recall. RF_Ent, the Random Forest with Entropy model, got very close to the ET performance with 96.67% accuracy and a 96.85% high F1 score. With an ROC AUC score of 96.25%, the model clearly has the ability to perform the ASD vs. non-ASD case well and is another reliable model for the task. The model developed by using the Decision Tree gave an accuracy of 94.44% and a recall of 98.00%, showing that it correctly classified most ASD cases. Its 92.46 % precision and 94.98 % F1 score indicate that occasionally there will be false positives, which might be a drawback in clinical scenarios. Among all the discussed models, the ET model is the most balanced and the most suitable for early autism detection.

Model	Accuracy (%)	Precision (%)	Recall (%)	F1-Score (%)	ROC-AUC (%)

Decision Tree	94.44	92.46	98.00	94.98	94.08
RF_Ent	96.67	96.67	97.50	96.85	96.25
RF_Gini	94.44	95.56	93.00	93.74	94.50
ET21	**96.67**	**97.50**	**95.00**	**96.17**	**96.50**

Table 1: Performance analysis of ML Models

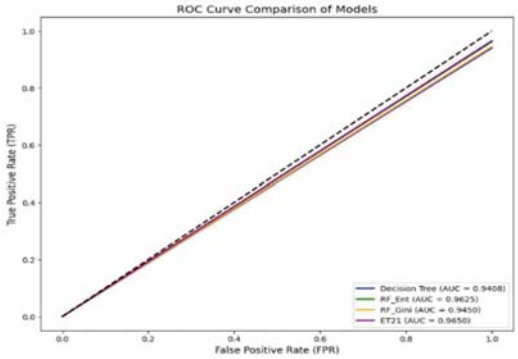


Fig. 6. Comparative Performance Metrics of ML Models for Early ASD Detection

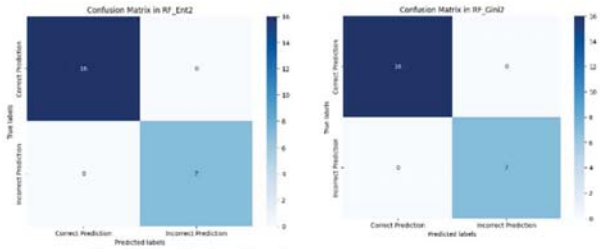


Fig. 7. Confusion Metrics for RF_Ent2(left side) and RF_Gini2(right side)

II. CONCLUSION

This study addresses gaps in Autism Spectrum Disorder (ASD) diagnostics by proposing a machine learning (ML) approach that improves accuracy, efficiency, and inclusivity across all age groups. Using the U.S. Autism Screening dataset, the study applied preprocessing techniques such as data normalization, feature encoding, and dimensionality reduction (PCA). Four supervised ML models—Decision Tree, Random Forest (Entropy & Gini), and Extra Trees Classifier—were evaluated based on accuracy, precision, recall, F1 score, and ROC-AUC. The Extra Trees Classifier performed best, achieving 96.67% accuracy with balanced precision (97.50%) and recall (95.00%), demonstrating strong generalizability and resistance to overfitting. The study highlights the potential of ML to enhance clinical ASD assessments by improving accessibility and inclusivity while reducing diagnostic time and expertise requirements. Future research should expand datasets, incorporate deep learning techniques, and validate models in real-world clinical settings. Enhancing model interpretability will be crucial for clinician trust and adoption. Ultimately, AI-driven, scalable, and cost-effective diagnostic tools could enable earlier interventions and better outcomes for individuals with ASD.

REFERENCES

[1] S. Ion, "Social Assistance for Children and Young People with Autism Spectrum Disorders (ASD)," *Social Work Review/Revista de Asistenta Sociala,* no. 2, 2021.

[2] D. Simmons, L. McKay, P. McAleer, E. Toal, A. Robertson, and F. Pollick, "Neural noise and autism spectrum disorders," *Perception,* vol. 36, pp. 119-120, 2007.

[3] A. Sadaf, H. Waseem, S. Rose, U. Ahsan, K. Abbas, and W. A. Ahad, "Relationship Among Sensory Issues and Repetitive Behaviors In Children With Autism Spectrum Disorder," *Asian Journal of Allied Health Sciences (AJAHS),* pp. 59-64, 2020.

[4] J. A. Bastiaansen *et al.*, "Diagnosing autism spectrum disorders in adults: the use of Autism Diagnostic Observation Schedule (ADOS) module 4," (in eng), *J Autism Dev Disord,* vol. 41, no. 9, pp. 1256-66, Sep 2011, doi: 10.1007/s10803-010-1157-x.

[5] S. Nadel and J. E. Poss, "Early detection of autism spectrum disorders: screening between 12 and 24 months of age," (in eng), *J Am Acad Nurse Pract,* vol. 19, no. 8, pp. 408-17, Aug 2007, doi: 10.1111/j.1745-7599.2007.00244.x.

[6] M. M. Abdelwahab, K. A. Al-Karawi, E. Hasanin, and H. Semary, "Autism spectrum disorder prediction in children using machine learning," *Journal of Disability Research,* vol. 3, no. 1, p. 20230064, 2024.

[7] F. Thabtah *et al.*, "Autism screening: an unsupervised machine learning approach," *Health Information Science and Systems,* vol. 10, no. 1, p. 26, 2022/09/08 2022, doi: 10.1007/s13755-022-00191-x.

[8] S. Raj and S. Masood, "Analysis and Detection of Autism Spectrum Disorder Using Machine Learning Techniques," *Procedia Computer Science,* vol. 167, pp. 994-1004, 2020/01/01/ 2020, doi: https://doi.org/10.1016/j.procs.2020.03.399.

[9] D. Bone, S. L. Bishop, M. P. Black, M. S. Goodwin, C. Lord, and S. S. Narayanan, "Use of machine learning to improve autism screening and diagnostic instruments: effectiveness, efficiency, and multi-instrument fusion," (in eng), *J Child Psychol Psychiatry,* vol. 57, no. 8, pp. 927-37, Aug 2016, doi: 10.1111/jcpp.12559.

[10] K. Vakadkar, D. Purkayastha, and D. Krishnan, "Detection of Autism Spectrum Disorder in Children Using Machine Learning Techniques," *SN Computer Science,* vol. 2, no. 5, p. 386, 2021/07/22 2021, doi: 10.1007/s42979-021-00776-5.

[11] B. Kamala, K. S. M. Pooja, S. Varsha, and K. Sivapriya, "ML Based Approach to Detect Autism Spectrum Disorder (ASD)," in *2021 4th International Conference on Computing and Communications Technologies (ICCCT)*, 16-17 Dec. 2021 2021, pp. 313-318, doi: 10.1109/ICCCT53315.2021.9711826.

[12] S. Uddin, A. Khan, M. E. Hossain, and M. A. Moni, "Comparing different supervised machine learning algorithms for disease prediction," *BMC Medical Informatics and Decision Making,* vol. 19, no. 1, p. 281, 2019/12/21 2019, doi: 10.1186/s12911-019-1004-8.

[13] Y. Qi, "Random Forest for Bioinformatics," 2012.

[14] P. Geurts, D. Ernst, and L. Wehenkel, "Extremely randomized trees," *Machine Learning,* vol. 63, no. 1, pp. 3-42, 2006/04/01 2006, doi: 10.1007/s10994-006-6226-1.

[15] A. Ziegler and I. R. König, "Mining data with random forests: current options for real-world applications," *WIREs Data Mining and Knowledge Discovery,* vol. 4, no. 1, pp. 55-63, 2014/01/01 2014, doi: https://doi.org/10.1002/widm.1114.

Optimizing Detection of Human Cancer Cells in Breast Cancer via Machine Learning and Feature Selection

Inshad Rahman Noman
Department of Computer Science, California State University, 5151 State University Dr, Los Angeles, CA 90032, United States
inoman@calstatela.edu

Md Rashedul Islam
Department of Business Administration Westcliff University, 17877 Von Karman Ave 4th Floor, Irvine, CA 92614, United States
m.Islam.480@westcliff.edu

Kanchon Kumar Bishnu
Department of Computer Science, California State University, 5151 State University Dr, Los Angeles, CA 90032, United States
kbishnu@calstatela.edu

Araf Islam
Department of Information Technology, Westcliff University, 17877 Von Karman Ave 4th Floor, Irvine, CA 92614, United States
a.islam.585@westcliff.edu

Afia Fairooz Tasnim
Department of Science Public Health, California State University Long Beach1250 Bellflower Blvd, Long Beach, CA 90840, United States
afia.tasnim009@gmail .com

Md Munna Aziz
Department of Business Administration, Westcliff University, 17877 Von Karman Ave 4th Floor, Irvine, CA 92614, United States
m.aziz.398@westcliff.edu

Rakibul Hasan
Department of Business Administration Westcliff University
17877 Von Karman Ave 4th Floor, Irvine, CA 92614, United States
r.hasan.179@westcliff.edu

**Corresponding author: Rakibul Hasan
(r.hasan.179@westcliff.edu)

***Abstract*— Breast cancer is a disease where abnormal cells in the breast grow uncontrollably and potentially spread to other parts of the body. One of the leading causes of death among women worldwide is breast cancer. Considering that increasing survival rates requires early detection and treatment. This study shows the effectiveness of four machine learning algorithms: Random Forest (RF), Extreme Gradient Boosting (XGBoost), Extra Trees Classifier (ETC), and Linear Discriminant Analysis (LDA) in breast cancer detection using the Wisconsin Breast Cancer Diagnostic (WBCD) dataset. These algorithms are compared using performance indicators such as F1-score, recall, accuracy, and precision. ETC achieved the highest accuracy of 97.90% among other models. Feature selection methods like Recursive Feature Elimination and univariate feature selection were used to improve classification accuracy while lowering computing costs. A correlation heat map was also used to analyze the relationship between features and diagnosis outcomes. The study results show that ETC offers a promising trade-off between interpretability and performance, making it a good choice for automated breast cancer diagnosis. However, the scope of this study is limited to the WBCD dataset, and further research using larger and more diverse datasets is recommended. This study demonstrates the potential of machine learning in medical diagnostics. It also emphasizes how crucial it is to incorporate explainability into AI-driven solutions and their usefulness in real-world clinical settings.**

Keywords- Breast cancer, Feature selection, XGBoost, Machine learning, WBCD dataset.

I. INTRODUCTION

Breast cancer is the leading cause of mortality among women globally, with the global cancer burden nearly doubling in the past two decades, according to the International Agency for Research on Cancer (IARC)[1]. The increasing prevalence of cancer, with one in five individuals expected to develop it, underscores the need for innovative, efficient strategies for improved survival rates and cost-effective treatments[2]. Manual breast cancer detection is challenging due to time, expertise, and advanced equipment, while traditional methods like mammography and biopsy are resource-intensive and susceptible to human error[3]. Consequently, there is a growing demand for automated diagnostic methods to enhance breast cancer detection accuracy, efficiency, and speed.

By analyzing complicated medical data, finding trends, and producing precise diagnoses, AI and ML technologies are transforming healthcare through early illness detection solutions [4]. Machine learning methods for detecting breast cancer include LDA, RF, ETC, and XGBoost. These techniques, which were developed using datasets such as the UCI open-access database, provide quick and accurate malignant cell detection, circumventing the drawbacks of conventional techniques. While LDA is especially good at recognizing malignant cells, XGBoost is especially good at detecting non-cancerous tumors [5]. Early identification of malignant tumors is critical, as it allows for timely intervention and increases the likelihood of successful treatment [6].

Random Forest (RF) is a versatile machine learning algorithm that uses multiple decision trees during training to minimize overfitting, enhancing model accuracy, making it ideal for medical diagnostics, such as breast cancer detection[7]. Another algorithm, Extreme Gradient Boosting (XGBoost), is known for its computational efficiency and high predictive accuracy, making it highly effective when applied to structured datasets like those in breast cancer research [8]. Extra Trees Classifier (ETC), another ensemble method, builds multiple decision trees to improve model performance and robustness [9]. Meanwhile, Linear Discriminant Analysis (LDA) excels in reducing the dimensionality of data, which allows it to highlight important features and improve the interpretability of the model [10].

AI and ML have potential in breast cancer diagnostics, but challenges include quality and diversity of datasets, ensuring diverse populations are represented in UCI databases[11]. Additionally, ethical considerations, such as data privacy and informed consent, must be addressed to foster trust in AI-driven diagnostic tools [12].

AI enhances breast cancer detection by processing vast data faster than traditional methods, enabling earlier diagnoses and personalized treatment strategies, and prioritizing high-risk patients for timely intervention and resource allocation[13].

This study aims to evaluate the performance of various ML algorithms in detecting breast cancer, focusing on their accuracy, efficiency, and suitability for clinical applications. Using the UCI database, the research seeks to identify the most effective algorithm for distinguishing between benign and malignant tumors. The findings of this study will contribute to the ongoing efforts to develop advanced diagnostic tools, ultimately improving outcomes for breast cancer patients.

II. LITERATURE REVIEW

AI-powered clinical decision support systems enhance early breast cancer detection with RNN accuracy, outperforming traditional methods and techniques with a 98.56% accuracy rate, and surpassing traditional methods like DL, LR, SVM, and CNNs[14]. AI and ML are revolutionizing medical diagnostics, particularly in early detection of breast cancer. A study by Hayatu Alhaji et al. showcases a high-accuracy breast cancer detection algorithm, demonstrating its potential for prompt clinical intervention [15].

AI is revolutionizing the healthcare industry, yet problems with model bias and transparency still exist. Tarek Khater's research uses LIME to accurately classify breast cancer cases, focusing on "Bare Nuclei" and Clump thickness for predicting outcomes [16]. 6G networks are revolutionizing blood cancer treatment by enhancing early detection, personalized care, and real-time monitoring of medical data, but ethical considerations are crucial[17].

Breast cancer survivorship is crucial for effective cancer prediction, and machine learning techniques like SVM are useful for early diagnosis[18]. A study using machine learning showed it can predict chemotherapy-induced damage in colorectal cancer patients, demonstrating the potential of AI in personalized cancer management. The Wisconsin Diagnostic Breast Cancer Dataset can aid in understanding AI models, but privacy concerns must be addressed.[19]. Federated Learning, utilizing artificial neural networks and XGBoost, achieved 97.59% accuracy and 98.393% F1 score in a study on breast cancer diagnosis and treatment [20].

Deep learning and TML methods improve medical image analysis accuracy, especially in leukocyte classification in blood smear images, aiding early diagnosis of hematological diseases like AIDS and blood cancer, using techniques like traditional, deep, CNN, hybrid, and attention learning[21]. A novel diagnostic machine learning model has been developed to optimize the detection of RBC samples presenting abnormal scattergrams in the Beckman-Coulter DXH-800, achieving validation accuracies of 97.98%, 100%, and 88.78% respectively [22].

III. METHODOLOGY

The Wisconsin Breast Cancer Diagnostic dataset is utilized to assess and compare four machine learning algorithms for breast cancer detection, including Random Forest(RF), Extreme Gradient Boosting(XGBoost), Extra Trees Classifier(ETC), and Linear Discriminant Analysis(LDA).

A. Machine learning library

All experiments on the machine learning techniques discussed in this study were conducted using the Scikit-learn library and the Python programming language. Scikit-learn, often called sklearn, is a free Python package for machine learning [8]. In addition to Scikit-learn [9], various scientific computing libraries such as NumPy [10], Matplotlib [11], Pandas [12], and Seaborn [13], [14] were also utilized in this study to support data analysis and visualization.

B. Dataset

We use the Wisconsin Breast Cancer Dataset (WBCD) [15]. Dr. William H. Wolberg from the University of Wisconsin Hospital created a dataset of fluid samples from solid breast mass patients, rating cytological qualities using Xcyt's graphical user interface. The dataset, with 569 rows and 33 columns, includes 357 (62.7%) benign cases and 212 (37.3%) malignant cases.

C. Data Pre-processing

The 33-attribute dataset was restructured to remove columns ID and unidentified due to inability to predict tumor malignancy or benignity. A Python dictionary with M = 1 (malignant) and B = 0 (benign) was used to manually transform the categorical "diagnosis" feature into a numerical feature.

$$z=(x-u)/s \quad (3.1)$$

The feature's mean is denoted by u, and the standard deviation is denoted by s. StandardScaler().fit_transform() was used to standardize training data, and StandardScaler().transform() was used to standardize testing data. Standardization was implemented once the data was divided into training and testing sets to stop data leaking.

D. Feature Selection Process

Univariate Feature Selection (UFS) is a statistical method used to select the best features from a dataset by comparing attributes and dependent variables. The top five features are 'perimeter_mean,' 'area_mean,' 'area_se,' 'perimeter_worst,' and 'area_worst', each scored and weighted by an external estimator[17].

Correlation Heatmap: Correlation analysis measures the change in two or more variables, with high correlations indicating significant impact on the dependent variable. Positive or negative correlation numbers can be beneficial, but large correlations among independent variables can lead to multicollinearity.[18]. These correlations are shown using the correlation heatmap.

E. Performance metrics

Confusion matrix: The terms true negative (TN), false positive (FP), false negative (FN), and true positive (TP) are included in the confusion matrix, which is a 2 by 2 table. It divides a classification model's predictions into four groups: TP (correctly accepted), TN (correctly rejected), FP (incorrectly accepted), and FN (incorrectly rejected).

Accuracy: The percentage of all forecasts that come true is known as accuracy. It is determined by dividing the total number of cases in the dataset by the proportion of correctly categorized instances. For accuracy, use the following formula: $Accracy = (TP + TN) / (TP + TN + FP + FN)$

This equation indicates how well the classification model distinguishes between positive and negative situations.

IV. RESULTS & DISCUSSION

The study evaluates four machine learning algorithms for breast cancer diagnosis: RF, XGBoost, ETC, and LDA, using the Wisconsin Breast Cancer Diagnostic dataset. The accuracy of these algorithms is assessed using measures like

accuracy, precision, recall, and F1-score. The results provide insights into how these algorithms could be used in medical diagnostics, aiming to improve breast cancer detection and therapy by focusing on these strategies.

A. Algorithm Performance Comparison

Table 1: summarizes the performance metrics for LDA, E*TC, XGBoost, and RF classifiers*.

Metric	LDA	ETC	XGBoost	RF
Accuracy (%)	97.20	**97.90**	97.20	97.20
Precision	High	Very High	High	High
Recall	High	Very High	High	High
F1-Score	0.96	**0.98**	0.96	0.96

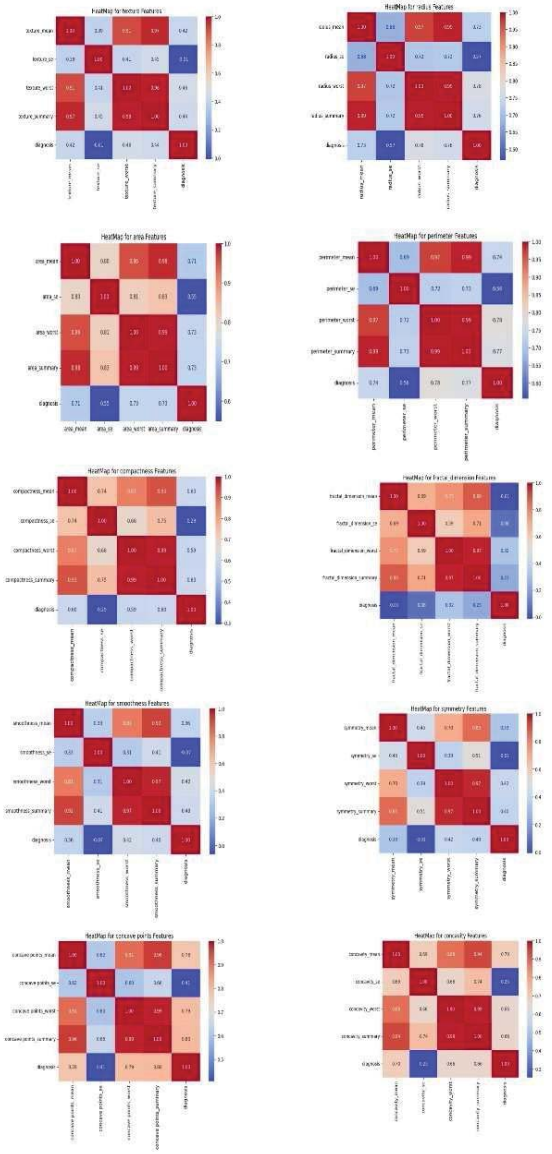


Fig. 1. Presents ten distinct heatmaps, each illustrating the correlation between different variables and diagnosis.

The study compares various classifiers for cancer classification, including LDA, ETC, XGBoost, and RF. ETC was found to be the most accurate with 97.90% accuracy, precision, recall, and F1-score of 0.98, while LDA, XGBoost, and RF had 97.20% accuracy but inferior precision and recall.

A. Interpretability and Visualization

The feature distributions throughout the dataset are displayed in Figure 4.2, while the feature correlations are depicted in Figure 4.1. These graphics draw attention to important insights:

The heatmap symmetry in figure 1 in breast cancer datasets reveals highly correlated features like texture, smoothness, and concavity, which measure tumor size and shape. Compactness variables contribute moderately to the model, while fractal dimension features show weaker correlations. The mirror-like symmetry suggests redundancy in the dataset. Mathematically derived variables dominate, while texture, smoothness, and concavity have secondary effects. The correlation heatmap emphasizes the importance of feature engineering in model performance and overfitting prevention. Careful feature selection and manipulation can improve predictive power through PCA or regularization. Higher values of "Concave points_summary" are connected to malignant diagnosis.

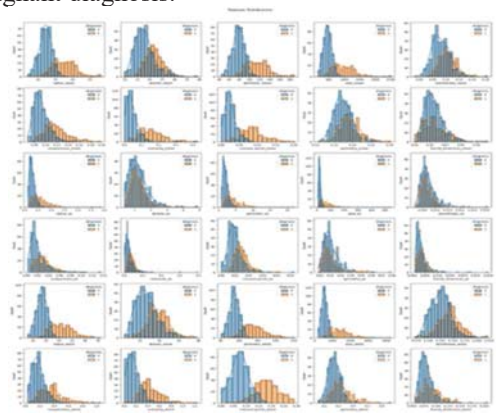


Fig 2. Provides a comprehensive view of the feature distributions across the dataset, highlighting the variations in feature values.

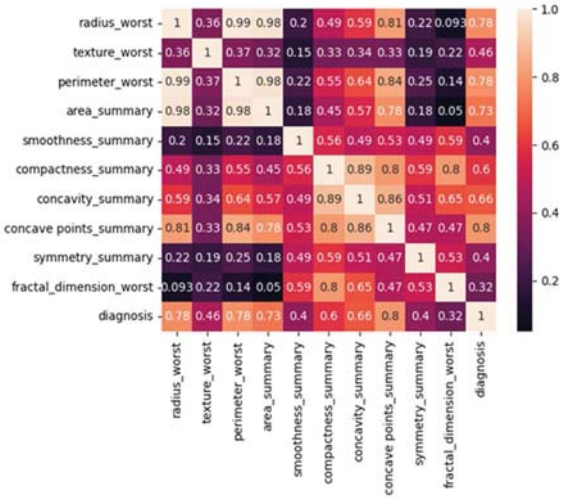


Fig. 3. Summary of the Heatmap.

However, the study reveals that characteristics like "smoothness_summery," "symmetry_summery," and "fractal_dimension_worst" have weaker associations with malignant tumors (0.4, 0.4, and 0.32, respectively) , suggesting they may be benign. Other characteristics like "compactness_summery" and "concavity_summery" are marginally linked with diagnosis(0.5 and 0.66, respectively). These findings highlight the impact of input variable qualities on tumor diagnosis, but multiple criteria must be considered.

B. Model-Related Perspectives

Linear Discriminant Analysis (LDA) offers 97.20% accuracy in data collection, but its linear assumptions may hinder non-linear pattern identification. Despite this, LDA is interpretable and computationally efficient, making it suitable for resource-constrained applications.

The Extra Trees Classifier (ETC): The Extra Trees Classifier (ETC) demonstrated superior performance with 97.90% accuracy and 0.98 F1-score, demonstrating its ability to handle high-dimensional data and resist over-fitting.

Extreme Gradient Boosting (XGBoost): 97.20% accuracy beat LDA and RF. Its advanced regularization and sparse data management make it popular. However, its much lower F1-score than ETC and computational complexity suggest further tuning may be needed for optimum outcomes.

Random Forest (RF): RF outperformed LDA and XGBoost, with an accuracy of 97.20%. Interpretability benefits from its ensemble nature and feature relevance ranking. However, RF may overlook certain malignant instances, as evidenced by its small recall decline when compared to ETC.

C. Dataset Limitations and Challenges

The study's high accuracy is based on the WBCD dataset, which may not apply to other datasets or real-world scenarios. The dataset's short size limits pattern recognition. Machine learning models, like ETC, perform well but doctors struggle to interpret them. Explainability tactics like SHAP or LIME visuals may help. Feature selection improves performance, but linked features may generate biases.

D. Real life efficiency

ETC's potential for incorporation into automated diagnostic systems is demonstrated by its high with 97.90% accuracy. Real-world applications, however, require thorough validation using more extensive and varied datasets. Moreover, explainable AI (XAI) frameworks can help close the gap between clinical decision-making and model outputs.

V. CONCLUSION

The study explores the use of machine learning techniques for early breast cancer detection. Using the Wisconsin Breast Cancer Diagnostic dataset, it compares various algorithms, finding Extra Trees Classifier (ETC) as the most accurate model with a 97.90% accuracy rate. The study emphasizes the importance of balancing interpretability and accuracy, as model transparency is crucial for medical professionals. However, the study's reliance on a single dataset limits its application.

To address demographic diversity and enhance adaptability, future studies can concentrate on verifying models using bigger, more varied datasets. Including cutting-edge explainable AI techniques like SHAP and LIME can enhance clinical usefulness and trust. Furthermore, investigating hybrid deep learning techniques and multi-modal data integration can improve diagnostic precision and practicality in healthcare environments.

REFERENCES

[1] W. IARC, "Latest global cancer data," *Accessed: December,* 2020.

[2] F. Bray, J. Ferlay, I. Soerjomataram, R. L. Siegel, L. A. Torre, and A. Jemal, "Global cancer statistics 2018: GLOBOCAN estimates of incidence and mortality worldwide for 36 cancers in 185 countries," *CA: a cancer journal for clinicians,* vol. 68, no. 6, pp. 394-424, 2018.

[3] P. C. Gøtzsche and K. J. Jørgensen, "Screening for breast cancer with mammography," *Cochrane database of systematic reviews,* no. 6, 2013.

[4] A. Esteva *et al.*, "A guide to deep learning in healthcare," *Nature medicine,* vol. 25, no. 1, pp. 24-29, 2019.

[5] A. Bharat, N. Pooja, and R. A. Reddy, "Using machine learning algorithms for breast cancer risk prediction and diagnosis," in *2018 3rd International conference on circuits, control, communication and computing (I4C)*, 2018: IEEE, pp. 1-4.

[6] E. D. Kolaczyk and G. Csárdi, *Statistical analysis of network data with R*. Springer, 2014.

[7] E. Vigneau, P. Courcoux, R. Symoneaux, L. Guérin, and A. Villière, "Random forests: A machine learning methodology to highlight the volatile organic compounds involved in olfactory perception," *Food Quality and Preference,* vol. 68, pp. 135-145, 2018.

[8] T. Chen and C. Guestrin, "Xgboost: A scalable tree boosting system," in *Proceedings of the 22nd acm sigkdd international conference on knowledge discovery and data mining*, 2016, pp. 785-794.

[9] P. Geurts and G. Louppe, "Learning to rank with extremely randomized trees," in *Proceedings of the learning to rank challenge*, 2011: PMLR, pp. 49-61.

[10] R. A. Fisher, "138: The Use of Multiple Measurements in Taxonomic Problems," 1936.

[11] J. Wiens *et al.*, "Do no harm: a roadmap for responsible machine learning for health care," *Nature medicine,* vol. 25, no. 9, pp. 1337-1340, 2019.

[12] W. N. Price and I. G. Cohen, "Privacy in the age of medical big data," *Nature medicine,* vol. 25, no. 1, pp. 37-43, 2019.

[13] H. Chougrad, H. Zouaki, and O. Alheyane, "Deep convolutional neural networks for breast cancer screening," *Computer methods and programs in biomedicine,* vol. 157, pp. 19-30, 2018.

[14] M. R. Darbandi, M. Darbandi, S. Darbandi, I. Bado, M. Hadizadeh, and H. R. Khorram Khorshid, "Artificial intelligence breakthroughs in pioneering early diagnosis and precision treatment of breast cancer: A multimethod study," *European Journal of Cancer,* vol. 209, p. 114227, 2024/09/01/ 2024, doi: https://doi.org/10.1016/j.ejca.2024.114227.

[15] H. A. SAIDU, Y. M. Malgwi, and U. Mohammed, "A Deep Learning-Based Model for Early Self-Detection of Breast Cancer," doi: https://doi.org/10.56201/ijcsmt.v10.no3.2024.pg1.18.

[16] S.-X. Wang, Z.-F. Huang, J. Li, Y. Wu, J. Du, and T. Li, "Optimization of diagnosis and treatment of hematological diseases via artificial intelligence," (in English), *Frontiers in Medicine,* Review vol. 11, 2024-November-07 2024, doi: 10.3389/fmed.2024.1487234.

[17] R. S. Ganesh, S. A. Sivakumar, and B. M. Shankar, "Integration of Artificial Intelligence in 6G Networks for Processing Blood Cancer Data," in *Development of 6G Networks and Technology*, 2024, pp. 223-240.

[18] M. A. Naji, S. E. Filali, K. Aarika, E. L. H. Benlahmar, R. A. Abdelouhahid, and O. Debauche, "Machine Learning Algorithms For Breast Cancer Prediction And Diagnosis," *Procedia Computer Science,* vol. 191, pp. 487-492, 2021/01/01/ 2021, doi: https://doi.org/10.1016/j.procs.2021.07.062.

[19] B. S. Hameed and U. M. Krishnan, "Artificial Intelligence-Driven Diagnosis of Pancreatic Cancer," *Cancers*, vol. 14, no. 21, doi: 10.3390/cancers14215382.

[20] E. Briola, C. C. Nikolaidis, V. Perifanis, N. Pavlidis, and P. Efraimidis, "A Federated Explainable AI Model for Breast Cancer Classification," presented at the Proceedings of the 2024 European Interdisciplinary Cybersecurity Conference, Xanthi, Greece, 2024. [Online]. Available: https://doi.org/10.1145/3655693.3660255.

[21] S. Khan, M. Sajjad, N. Abbas, and A. Rehman, "A Review on Machine Learning-Based WBCs Analysis in Blood Smear Images: Key Challenges, Datasets, and Future Directions," in *Prognostic Models in Healthcare: AI and Statistical Approaches*, T. Saba, A. Rehman, and S. Roy Eds. Singapore: Springer Nature Singapore, 2022, pp. 293-314.

[22] L. Bigorra, I. Larriba, and R. Gutiérrez-Gallego, "Machine learning algorithms for the detection of spurious white blood cell differentials due to erythrocyte lysis resistance," *Journal of Clinical Pathology,* vol. 72, no. 6, p. 431, 2019, doi: 10.1136/jclinpath-2019-205820.

Efficient American Sign Language Recognition using ResNet-50

1st Md Sharifuzzaman
Information Studies
Trine University
Indiana, USA
msharifuzzaman22@my.trine.edu

2nd Anik Sen
Faculty of Information Science & Technology
Multimedia University
Melaka, Malaysia
aniksen360@gmail.com

3rd Joyashish Ghosh
Faculty of Science & Engineering
Jashore University of Science and Technology
Jessore, Bangladesh
joyashishghosh@gmail.com

4th Tze Hui Liew*
Faculty of Information Science & Technology
Multimedia University
Melaka, Malaysia
thliew@mmu.edu.my

5th Debanjon Dutta Purkaystha
Faculty of Engineering
American International University-Bangladesh
Dhaka, Bangladesh
debanjonbd@gmail.com

6th Saptanil Ghose
Faculty of Science & Technology
American International University-Bangladesh
Dhaka, Bangladesh
saptanil.ghose.42178@gmail.com

7th Masud Pervez
Faculty of Mathematical & Physical Sciences
Jahangirnagar University
Dhaka, Bangladesh
mdmasudpervez64@gmail.com

8th Md. Jakir Hossen
Faculty of Engineering Technology
Multimedia University
Melaka, Malaysia
jakir.hossen@mmu.edu.my

***Abstract*—This study proposes an efficient and robust American Sign Language (ASL) recognition system using the ResNet-50 architecture with transfer learning. The system is designed to classify 26 static ASL alphabet gestures, addressing key challenges such as hand shape variability, lighting conditions, and limited dataset size. To improve the model's performance, data augmentation techniques, including rotation and horizontal flipping, were employed to enhance generalization and mitigate overfitting. Leveraging transfer learning from a pre-trained ResNet-50 model, the proposed system benefits from reduced training time and computational complexity while achieving high accuracy. The experimental evaluation demonstrates an overall accuracy of 98.34%, with consistent precision, recall, and F1-scores across all classes. Early stopping mechanisms were incorporated to prevent overfitting and ensure optimal generalization to unseen data. The proposed system demonstrates the potential of deep learning-based models in advancing ASL recognition. This research contributes to the development of inclusive communication technologies, promoting seamless interaction between hearing and non-hearing communities.**

***Keywords*—Sign Language recognition, deep learning, ResNet-50, transfer learning, data augmentation.**

I. Introduction

The increasing recognition and adoption of American Sign Language (ASL), especially among individuals with hearing impairments, have underscored the importance of developing effective communication technologies [3], [5]. ASL serves as the primary language for over half a million individuals in North America. However, interactions between hearing and non-hearing communities remain limited due to the unavailability of proficient interpreters and the complexity of learning ASL [8]. As society becomes more inclusive, automatic ASL recognition emerges as a vital solution to bridge this communication gap, enabling seamless interaction between hearing and non-hearing individuals [2], [13].

Technological advancements in computer vision and deep learning have revolutionized the field of sign language recognition. Traditional methods that rely on handcrafted features and sensor-based input systems are increasingly being replaced by robust neural network models capable of extracting high-dimensional features directly from images or videos [7], [19]. These deep models, particularly Convolutional Neural Networks (CNNs), have demonstrated their effectiveness in a variety of visual recognition tasks, including ASL recognition [3]. Furthermore, transfer learning techniques leveraging pre-trained models such as ResNet-50 have significantly reduced the computational burden by enabling models to adapt quickly to new tasks with limited datasets [18], [21].

Despite these advancements, several challenges persist. ASL consists of both static gestures (like individual letters) and dy-

namic gestures (like words or phrases that require continuous motion), making it difficult to develop models that generalize effectively across different types of signs [1]. Additionally, variations in hand shapes, lighting conditions, and signer-dependent differences further complicate the recognition task [9], [14]. Addressing these challenges demands innovative approaches, including data augmentation, hybrid deep learning models, and multi-modal systems that incorporate multiple data sources such as RGB-D sensors [6], [7].

The objective of this research is to explore the use of transfer learning with the ResNet-50 model to develop an efficient ASL alphabet recognition system capable of classifying 26 distinct hand signs. The system's performance is evaluated through training, validation, and testing, with the inclusion of early stopping mechanisms to prevent overfitting. The contributions of this research extend beyond conventional ASL recognition, focusing on addressing common misclassifications and optimizing model performance through the use of fine-tuning and data augmentation strategies. Furthermore, visualization techniques such as confusion matrices and performance metrics are employed to analyze the model's effectiveness and identify potential improvements.

II. Related Work

A. Sign Language Recognition and Its Evolution

The field of sign language recognition (SLR) has undergone significant evolution, transitioning from traditional sensor-based systems to vision-based approaches powered by deep learning models [4], [8]. Early systems employed glove-based sensors or Leap Motion Controllers to capture hand gestures [3], [20]. However, these methods faced challenges such as high costs, reduced user comfort, and reliance on external hardware, limiting scalability [3], [17]. With advances in computer vision, researchers began exploring camera-based recognition systems, which offered a more accessible and cost-effective solution [2], [7].

Sign languages, such as ASL, present unique challenges for recognition systems due to their combination of static signs (e.g., individual letters) and dynamic signs (e.g., words requiring continuous motion) [1]. Variations in signer style, hand orientation, and environmental conditions further complicate recognition tasks [10], [11]. To address these challenges, deep learning frameworks have been adopted for their ability to extract and learn complex features directly from images or video sequences [4], [6].

B. Deep Learning in Sign Language Recognition

The application of CNNs has been transformative for SLR, enabling accurate recognition of hand gestures. CNN-based architectures such as AlexNet, VGG, and ResNet have been extensively explored for their feature extraction capabilities [16], [19]. For example, Sharma and Kumar [1] demonstrated that 3D-CNNs are effective for recognizing dynamic ASL gestures by capturing temporal dependencies in hand movements through volumetric data. Similarly, Long Short-Term Memory (LSTM) networks and Recurrent Neural Networks (RNNs) have proven effective in handling sequence data, improving performance in tasks involving continuous gestures [13].

ResNet-50 has become a popular choice in recent research for transfer learning due to its ability to maintain feature hierarchies through residual connections [21]. Pre-trained models like ResNet leverage knowledge from large datasets such as ImageNet, allowing for fine-tuning on specific tasks such as ASL recognition [16], [18]. Transfer learning mitigates the challenges of limited datasets by reducing training time and improving accuracy [14].

C. Transfer Learning and Model Optimization Strategies

Transfer learning has played a critical role in advancing SLR. Researchers have explored various fine-tuning strategies, including freezing early layers of the model and updating only the later layers to enhance performance [5], [16]. Fine-tuning enables the model to adapt pre-trained features to target datasets, significantly improving recognition accuracy [9]. Kim et al. [16] demonstrated that transfer learning improves model generalization, a finding equally relevant to ASL recognition.

Data augmentation techniques, such as rotation, flipping, and normalization, have been widely employed to enhance model robustness [8], [19]. Augmentation reduces overfitting, especially when working with small datasets. Furthermore, multi-modal systems that combine image data with depth or sensor-based input have been introduced to improve recognition accuracy across different environments [7].

D. Evaluation Techniques and Performance Metrics

SLR models are evaluated using standard metrics such as accuracy, precision, recall, and F1-score [10], [18]. Confusion matrices are commonly used to visualize the model's ability to distinguish between different classes, highlighting areas where misclassifications occur [3]. For instance, Sharma and Kumar [1] identified challenges in recognizing certain dynamic gestures using their 3D-CNN-based model, prompting further architectural optimizations.

Early stopping mechanisms have also gained popularity to prevent overfitting during training [13]. By monitoring validation loss and halting training when performance plateaus, researchers ensure that models generalize well to unseen data [8]. Real-time recognition systems have been developed to evaluate the practical applicability of SLR models in environments such as classrooms and public spaces [2].

E. Research Gaps and Contributions of This Study

Despite the progress in SLR, several gaps remain. Most existing models focus on either static or dynamic gestures, with limited research addressing both comprehensively [17], [20]. Additionally, many studies rely on custom datasets, making it difficult to compare results across different models [7], [10]. There is also a need for real-time recognition systems capable of operating efficiently on edge devices without compromising accuracy [9].

This study aims to address these gaps by developing a comprehensive ASL alphabet recognition system using ResNet-50 with transfer learning. The proposed system focuses on

recognizing 26 static gestures, with plans to extend to dynamic gestures in future work. Techniques such as data augmentation, early stopping, and confusion matrix visualization are used to ensure the model's robustness and interpretability. This research highlights the potential of deep learning in sign language recognition, contributing to the development of inclusive communication technologies that benefit both hearing and non-hearing communities.

III. Methodology

In this section, we present the methodology employed to develop and evaluate an ASL alphabet recognition system using transfer learning with the ResNet-50 model. The experiment involves data preparation, model architecture modification, training strategies, and evaluation metrics, ensuring a robust framework for accurate classification.

A. Dataset Description

The ASL alphabet dataset used in this experiment contains images of 26 static gestures representing the letters A to Z. Each gesture corresponds to a specific hand shape, captured under various lighting conditions and orientations. The dataset consists of $87,000$ images, distributed evenly across 26 classes, with each class containing approximately $3,300$ images. Each image is represented in RGB format with a resolution of 200×200 pixels.

For this experiment, the dataset was split into three subsets:

- Training Set: The model was trained on 80% of the dataset.
- Validation Set: 10% of it was held out for model checking on train to ensure performance monitoring and avoiding overfitting.
- Test Set: The rest of 10% of it was utilized for final checking of the model.

The training set was further augmented through rotation, horizontal flipping, and normalization to increase model robustness and generalization capability.

B. Model Architecture

The ResNet-50 pre-trained on Imagenet dataset, was employed as the backbone for the ASL recognition system. The ResNet-50 is residual 50-layer network that utilizes residual connections to mitigate the vanishing gradient problem. The model architecture can be mathematically described as:

$$\mathbf{y} = \mathbf{x} + \mathcal{F}(\mathbf{x}, \{W_i\}), \tag{1}$$

where $\mathbf{x}$ is the input to a residual block, $\mathcal{F}(\cdot)$ represents the function learned by the block, and $\{W_i\}$ denotes the trainable weights within the block. The output $\mathbf{y}$ is the sum of the input and the learned function, allowing gradients to propagate efficiently through the network.



Fig. 1. Examples of ASL alphabet gestures from the dataset.

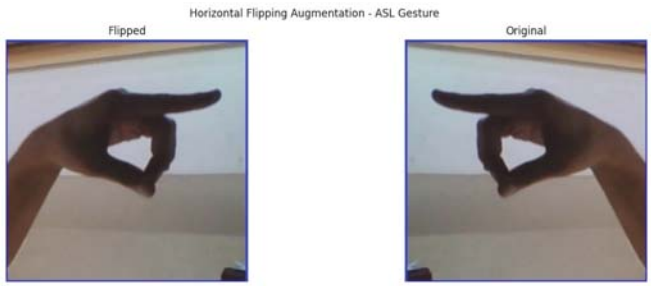


Fig. 2. Horizontally flipped samples for data augmentation.

C. Transfer Learning and Fine-Tuning

To adapt the ResNet-50 model for ASL alphabet recognition, the following modifications were made:

1) The final connected pre-trained full ResNet-50 also converted to a new layer of 26 units of output corresponding to 26 signs of ASL.
2) All layers except the final residual block were frozen to leverage pre-trained weights and avoid overfitting.
3) The new fully connected layer was initialized with random weights and trained using the backpropagation algorithm.

The transfer learning strategy can be represented as:

$$\hat{\mathbf{y}} = \sigma(\mathbf{W}_{fc} \cdot \mathbf{h} + \mathbf{b}), \tag{2}$$

where $\hat{\mathbf{y}}$ is the predicted class probability, $\mathbf{W}_{fc}$ and $\mathbf{b}$ are the weights and biases of the new fully connected layer, $\mathbf{h}$

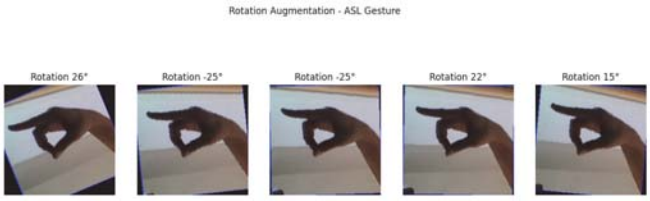


Fig. 3. Rotated samples used for data augmentation.

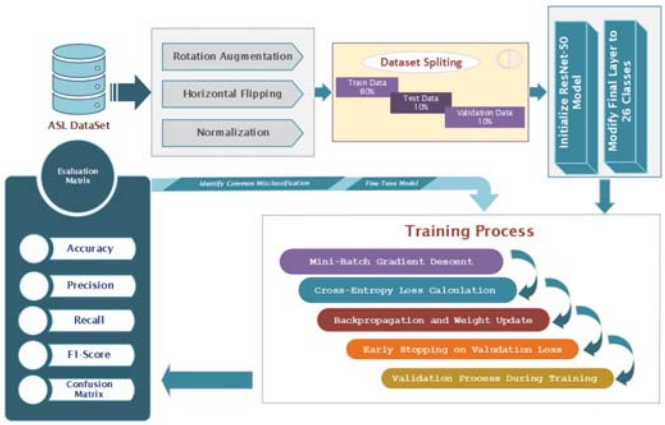


Fig. 4. Experiment Workflow

represents the output from the penultimate layer, and $\sigma(\cdot)$ denotes the softmax activation function.

The ResNet-50 model consists of several key components:

- Input Layer: Processes input images of size $224 \times 224 \times 3$ (RGB).
- Convolutional Layers with Residual Blocks: Extracts complex features using multiple convolutional operations and residual connections.
- Global Average Pooling: Reduces the spatial dimensions of the feature maps to a vector of fixed size.
- Dense Layer (512 units): Provides a fully connected layer to learn high-level representations.
- Output Layer (26 classes): Maps the input to one of the 26 ASL gestures.

D. Training Procedure

The model was trained using the Adam optimizer with a learning rate of 0.001. Cross-entropy loss was used as the objective function, defined as:

$$\mathcal{L}(\mathbf{y}, \hat{\mathbf{y}}) = -\sum_{i=1}^{C} y_i \log(\hat{y}_i), \tag{3}$$

where C is the total number of classes, y_i is the ground truth label for class i, and $\hat{y}_i$ is the predicted probability for class i.

The training process employed min-batch gradient descent of size 32. The early-stopping process is employed to interrupt training if there is no loss reduction on the validation set after 5 consecutive epochs. The training procedure is summarized in Algorithm 1.

Algorithm 1 Training Procedure for ASL Recognition System

Input: Pre-trained ResNet-50 model, Training set $\mathcal{D}_{train}$, Validation set $\mathcal{D}_{val}$, Max epochs N, Patience $P = 5$
Output: Optimized model $\mathcal{M}$ with trained parameters
Initialize ResNet-50 model $\mathcal{M}$ with pre-trained weights
Replace the final fully connected layer with a 26-unit output layer
Set *best_val_loss* $\leftarrow \infty$, *no_improvement* $\leftarrow 0$
for epoch $= 1$ to N **do**
    Train the model $\mathcal{M}$ on $\mathcal{D}_{train}$
    Compute validation loss L_{val} on $\mathcal{D}_{val}$
    if $L_{val} <$ best_val_loss **then**
        Update *best_val_loss* $\leftarrow L_{val}$
        Reset *no_improvement* $\leftarrow 0$
    else
        Increment *no_improvement* $\leftarrow$ *no_improvement*$+1$
    end if
    if *no_improvement* $\geq P$ **then**
        Break the loop (Early Stopping)
    end if
end for
return Optimized model $\mathcal{M}$

E. Evaluation Metrics

The test dataset is assessed on the trained model, using multiple performance metrics, including accuracy, precision, recall, and F1-score [12]. Accuracy is defined as:

$$\text{Accuracy} = \frac{\text{Number of Correct Predictions}}{\text{Total Number of Predictions}}. \tag{4}$$

Precision, recall, and F1-score were computed to analyze the model's performance across individual classes [15]. Precision is given by:

$$\text{Precision} = \frac{\text{TP}}{\text{TP} + \text{FP}}, \tag{5}$$

where TP and FP represent the true positives and false positives, respectively. Recall is defined as:

$$\text{Recall} = \frac{\text{TP}}{\text{TP} + \text{FN}}, \tag{6}$$

where FN denotes false negatives. The F1-score, which balances precision and recall, is expressed as:

$$\text{F1-score} = 2 \cdot \frac{\text{Precision} \cdot \text{Recall}}{\text{Precision} + \text{Recall}}. \tag{7}$$

Additionally, a confusion matrix was generated to visualize the model's performance across all classes, identifying common misclassifications.

F. Implementation

The experiment was implemented using Python, with PyTorch serving as the primary deep learning framework. The training and evaluation processes were conducted on a GPU-enabled Google Colab environment to accelerate computations. The dataset was accessed via the Kaggle API and preprocessed with PyTorch's DataLoader for batch processing.

IV. Results and Analysis

This section presents the evaluation results and analyzes the performance of the proposed ASL Alphabet Recognition System. The model, based on the ResNet-50 architecture with transfer learning, was evaluated using several performance metrics, including accuracy, precision, recall, and F1-score. A confusion matrix provides insight into class-level performance, while the training and validation accuracy and loss curves are analyzed to assess convergence and generalization.

A. Evaluation Metrics

The model achieved an overall accuracy of **98.34%** on the test set, demonstrating its effectiveness in recognizing the 26 static ASL gestures. The precision, recall, and F1-score were consistent with the high accuracy, confirming the model's balanced performance across all classes. The key evaluation metrics are summarized in Table I.

TABLE I
Performance Evaluation Metrics for the Proposed Model

Metric	Score (%)
Accuracy	98.34
Precision	98.31
Recall	98.30
F1-Score	98.30

These results confirm the effectiveness of the model in maintaining a good trade-off between false positives and false negatives across all classes. The minor variations between precision, recall, and F1-score suggest that the model consistently performs well across different evaluation criteria.

B. Confusion Matrix Analysis

The detailed performance across all 26 classes is presented in the confusion matrix shown in Figure 5. The matrix provides insight into the distribution of correct and incorrect predictions. Each row represents the true label, while each column corresponds to the predicted label.

The diagonal dominance of the matrix indicates that the model correctly classified the majority of samples for each gesture. However, certain misclassifications were observed in similar-looking gestures, such as between letters *I* and *J*, and *O* and *Q*. Such confusions align with observations from prior research, where subtle handshape differences between certain gestures pose challenges for recognition systems.

Gestures such as *Z* and *Q* demonstrated near-perfect classification, while *K* and *P* had slightly higher misclassification rates. These results suggest potential areas for further improvement through additional fine-tuning or data augmentation strategies.

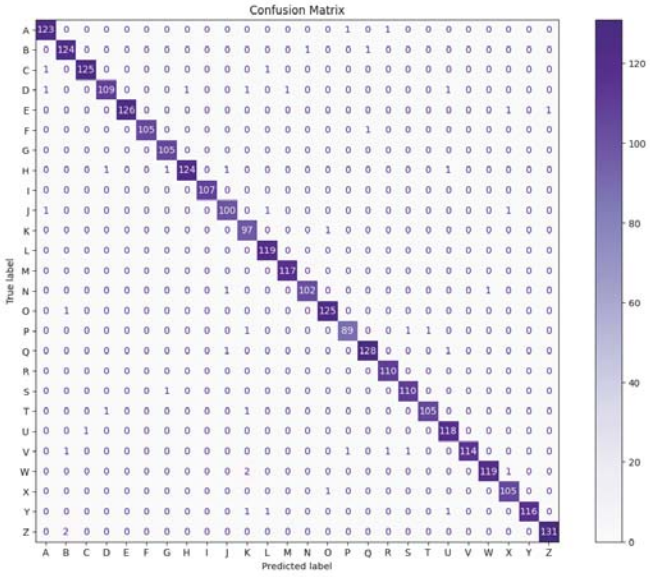


Fig. 5. Confusion Matrix for the ASL Alphabet Recognition System

C. Training and Validation Performance

The convergence behavior of the model was analyzed through the training and validation accuracy curves, as shown in Figure 6. Both curves demonstrate a steady increase, with convergence toward **98%** by the 20th epoch. This trend indicates that the model effectively learned from the training data without overfitting. The minimal gap between the two curves suggests good generalization to unseen data.

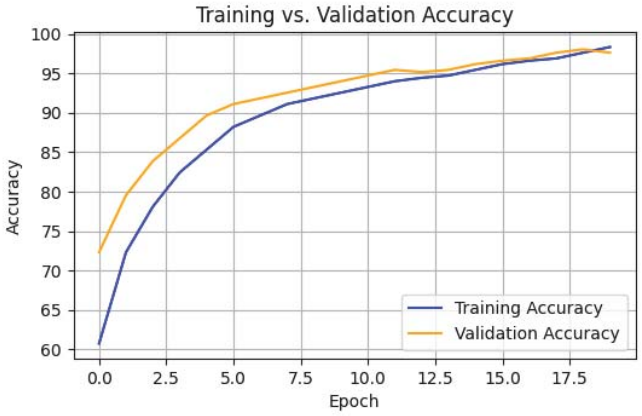


Fig. 6. Training vs. Validation Accuracy across 20 Epochs

Similarly, the training and validation loss curves, shown in Figure 7, exhibit a consistent decrease over the epochs. The

absence of significant spikes or divergence between the two curves confirms that the model's learning process was stable throughout training. The smooth learning curves also indicate that the use of early stopping was effective in preventing overfitting.



Fig. 7. Training vs. Validation Loss across 20 Epochs

D. Summary and Key Findings

The results demonstrate that the proposed ASL recognition system based on ResNet-50 and transfer learning achieves high performance. The model's ability to generalize well across unseen data, as evidenced by the close alignment between training and validation curves, highlights the robustness of the system. The confusion matrix provided insights into specific misclassifications, particularly among visually similar gestures, which could be addressed in future work. Furthermore, the consistent accuracy, precision, recall, and F1-score scores validate the effectiveness of the transfer learning strategy employed in this study.

V. Conclusion and Future Work

This study presented an efficient ASL recognition system based on the ResNet-50 architecture with transfer learning. The model proposed in this study, successfully deals with the challenge of detecting 26 unique static gestures of ASL accurately. With the use of fine-tuning processes combined with increasing data through rotations and horizontal flip, the model reported an impressive overall accuracy of 98.34%, emphasizing its reliability and resilience. Performance metrics like precision, recall, and F1-score also establish the model's reliability to suppress false identification along with maintaining maintaining balanced classification across all gestures.

The use of transfer learning not only reduced the computational burden but also enabled the model to adapt effectively to the ASL dataset, despite its relatively limited size. The analysis of the training and validation curves demonstrated the model's capability to generalize effectively without overfitting, facilitated by the integration of early stopping mechanisms. Additionally, the confusion matrix provided insights into common misclassifications, highlighting areas where visually similar gestures caused minor errors, such as between gestures like I and J, and O and Q.

While the proposed system performs well for static gestures, future work will focus on expanding the system to include dynamic gestures, which represent words or phrases requiring continuous motion. Moreover, integrating multi-modal data sources such as depth sensors or infrared imaging could further enhance robustness under varying environmental conditions. Real-time deployment on edge devices will also be explored to enable seamless interactions between hearing and non-hearing communities in practical scenarios. These advancements will help bridge the communication gap more effectively and foster inclusiveness in various social and educational settings.

In conclusion, the results of this study demonstrate the potential of deep learning-based models like ResNet-50 in advancing ASL recognition. With further optimization and expansion, the proposed system has the potential to become a valuable tool in enhancing communication between individuals with hearing impairments and the broader community.

References

[1] S. Sharma and K. Kumar, "ASL-3DCNN: American sign language recognition technique using 3-D convolutional neural networks," *Multimedia Tools and Applications*, vol. 80, no. 17, pp. 26319–26331, 2021.

[2] R. A. Kadhim and M. Khamees, "A Real-Time American Sign Language Recognition System using Convolutional Neural Network for Real Datasets," *Tem Journal*, vol. 9, no. 3, 2020.

[3] C. K. Lee, K. K. Ng, C. H. Chen, H. C. Lau, S. Y. Chung, and T. Tsoi, "American sign language recognition and training method with recurrent neural network," *Expert Systems with Applications*, vol. 167, p. 114403, 2021.

[4] R. Daroya, D. Peralta, and P. Naval, "Alphabet sign language image classification using deep learning," in *Proc. TENCON 2018-2018 IEEE Region 10 Conference*, 2018, pp. 0646–0650.

[5] S. Alashhab, A. J. Gallego, and M. Á. Lozano, "Efficient gesture recognition for the assistance of visually impaired people using multi-head neural networks," *Engineering Applications of Artificial Intelligence*, vol. 114, p. 105188, 2022.

[6] B. Zhou, J. Wan, Y. Liang, and G. Guo, "Adaptive cross-fusion learning for multi-modal gesture recognition," *Virtual Reality and Intelligent Hardware*, vol. 3, no. 3, pp. 235–247, 2021.

[7] G. Benitez-Garcia, J. Olivares-Mercado, G. Sanchez-Perez, and K. Yanai, "Ipn hand: A video dataset and benchmark for real-time continuous hand gesture recognition," in *Proc. 2020 25th International Conference on Pattern Recognition (ICPR)*, 2021, pp. 4340–4347.

[8] Z. Huang, J. Li, J. Liang, B. Zen, and J. Tan, "An IoT-oriented gesture recognition system based on ResNet-Mediapipe hybrid model," in *Proc. 2022 5th International Conference on Pattern Recognition and Artificial Intelligence (PRAI)*, 2022, pp. 1221–1228.

[9] G. Park, V. K. Chandrasegar, and J. Koh, "Accuracy enhancement of hand gesture recognition using CNN," *IEEE Access*, vol. 11, pp. 26496–26501, 2023.

[10] M. Peng, C. Wang, and T. Chen, "Attention based residual network for micro-gesture recognition," in *Proc. 2018 13th IEEE International Conference on Automatic Face and Gesture Recognition (FG 2018)*, 2018, pp. 790–794.

[11] H. Zhao, M. Liang, and H. Li, "Research on gesture segmentation method based on FCN combined with CBAM-ResNet50," *Signal, Image and Video Processing*, vol. 18, no. 11, pp. 7729–7740, 2024.

[12] N. Fahad, A. Sen, S. S. Jisha, S. Ahmad, H. Mokhlis, and M. S. Hossain, "Identification of Human Movement Through a Novel Machine Learning Approach," in *2023 Innovations in Power and Advanced Computing Technologies (i-PACT)*, Dec. 2023, pp. 1–5, IEEE.

[13] M. Bansal, M. Kumar, M. Sachdeva, and A. Mittal, "Transfer learning for image classification using VGG19: Caltech-101 image data set," *Journal of Ambient Intelligence and Humanized Computing*, pp. 1–12, 2023.

[14] S. T. Krishna and H. K. Kalluri, "Deep learning and transfer learning approaches for image classification," *International Journal of Recent Technology and Engineering (IJRTE)*, vol. 7, no. 5S4, pp. 427–432, 2019.

[15] M. N. Hossain, N. Fahad, R. Ahmed, A. Sen, M. S. Al Huda, and M. I. Hossen, "Preventing Student's Mental Health Problems with the Help of Data Mining," *IJC*, vol. 23, no. 1, pp. 101–108, Oct. 2024.

[16] H. E. Kim, A. Cosa-Linan, N. Santhanam, M. Jannesari, M. E. Maros, and T. Ganslandt, "Transfer learning for medical image classification: a literature review," *BMC Medical Imaging*, vol. 22, no. 1, p. 69, 2022.

[17] M. Hussain, J. J. Bird, and D. R. Faria, "A study on CNN transfer learning for image classification," in *Advances in Computational Intelligence Systems: Contributions Presented at the 18th UK Workshop on Computational Intelligence*, Springer International Publishing, 2018, pp. 191–202.

[18] A. Kasapbaşi, A. E. A. Elbushra, A. H. Omar, and A. Yilmaz, "DeepASLR: A CNN based human computer interface for American Sign Language recognition for hearing-impaired individuals," *Computer Methods and Programs in Biomedicine Update*, vol. 2, p. 100048, 2022.

[19] C. Zhang, Y. Tian, and M. Huenerfauth, "Multi-modality American sign language recognition," in *Proc. 2016 IEEE International Conference on Image Processing (ICIP)*, 2016, pp. 2881–2885.

[20] M. A. Ozdemir, D. H. Kisa, O. Guren, A. Onan, and A. Akan, "EMG based hand gesture recognition using deep learning," in *Proc. 2020 Medical Technologies Congress (TIPTEKNO)*, 2020, pp. 1–4.

[21] M. Shaha and M. Pawar, "Transfer learning for image classification," in *Proc. 2018 Second International Conference on Electronics, Communication and Aerospace Technology (ICECA)*, 2018, pp. 656–660.

Predicting Faulty Production Lines Causing Head Gimbal Assembly Damage from Electrostatic Discharge Using Machine Learning

1st Nuttanon Bilgasun
Department of Artificial Intelligence for Business Analytics
School of Information Technology,
King Mongkut's Institute of Technology Ladkrabang
Bangkok, Thailand
nuttanon.bilgasun@gmail.com

2nd Bundit Thanasopon
Department of Artificial Intelligence for Business Analytics
School of Information Technology,
King Mongkut's Institute of Technology Ladkrabang
Bangkok, Thailand
bundit@it.kmitl.ac.th

***Abstract*—This research was conducted to analyze abnormal production lines leading to Head Gimbal Assembly (HGA) damage, mainly caused by electrostatic discharge. HGAs are critical component in hard disk. The HGA was constantly developed to produce higher storage capacity products to delight customer demands. Newer product design HGAs are highly sensitive to electrostatic discharge. This results in more damage and higher scrap costs. The main goal of this research is to leverage artificial intelligence technology to predict abnormal production lines that cause electrostatic damage in the assembly process of HGA. The research aims to develop timely solutions to reduce damage during production. This proactive approach is essential in lowering production costs and ensuring the HGAs have a longer lifespan and increased reliability.**

Keywords—Electrostatic Discharge, Head Gimbal Assembly, Machine Learning

I. Introduction

Currently, the demand for data storage is increasing with the development of technology, and hard disk drives (HDDs) play a crucial role in meeting these demands, both for personal data and cloud storage. In the manufacturing process of hard disk drives, quality control is essential. One type of damage that occurs during production is electrostatic discharge (ESD), which happens when a workpiece comes into contact with a part that has electrostatic charge accumulation, leading to a transfer of charge. Due to its small size, this discharge can cause damage to the workpiece, and such damage cannot be detected by human inspection or with a microscope. The inspection and analysis of the problem are carried out by humans, which has limitations in terms of errors and delays in identifying the causes of the damage to the workpiece. The application of Machine Learning (ML) technology in the workflow is crucial for increasing the speed of problem-solving and enhancing the efficiency of this process.

Machine Learning (ML) can analyze large-scale data and identify damage that is not visible through human detection. It helps in accurately and quickly identifying production lines that are experiencing issues, reducing the reliance on human analysis and minimizing errors that may arise from human operations. This ultimately enhances the efficiency of the Head Gimbal Assembly (HGA) manufacturing process.

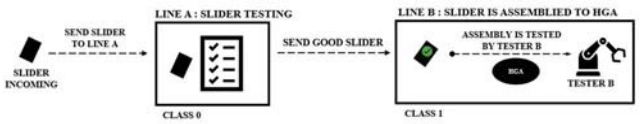


Fig. 1. Steps for assembling the Head Gimbal Assembly.

Two important production lines in HGA manufacturing process are shown in Fig. 1, CLASS A represents abnormalities in the production line caused by LINE A, which is responsible for testing the performance of newly received sliders. Only sliders that pass the test are sent to LINE B. CLASS B represents abnormalities in the production line caused by LINE B, which is the production line that assembles the sliders into the Head Gimbal Assembly (HGA) for hard disk drives. In the manufacturing process, if an issue arises, it is crucial to quickly identify the production line that is malfunctioning to resolve the problem efficiently.

The application of Machine Learning to the anomaly detection system in the production line will help monitor and continuously improve the manufacturing process [1]. This enables an immediate response to issues that arise, reduces production downtime, resolves problems promptly, lowers production costs, and increases profitability for the business.

II. Literature Review

A. Litetature Review on Head Gimble Assembly

Head Gimbal Assembly (HGA) is a data recording device in the hard disk drive and is a crucial component in enhancing the performance of hard disk drives, which are continuously being developed. The production lines associated with the hard disk drive head assembly are divided into two production lines. Head Gimbal Assembly (HGA) and Head Stack Assembly (HSA), with the Head Gimbal Assembly being assembled in specified quantities. The method for assessing damage is done by measuring the resistance in the workpiece. Damage caused by Electrostatic Discharge (ESD) results in a decrease in resistance below the established standard [2]. Head Gimbal Assembly (HGA) that has passed testing will be sent to the production line for the Head Stack Assembly (HSA) in this process, there is a component of the head arm assembly called the Preamp, which helps balance the electric charge [3]. The measuring electrical resistance to determine the rate of electrostatic discharge in the Head Stack Assembly (HSA) production line, it was found that the production line for Head Gimbal Assembly (HGA) indicates that the most sensitive production line is Head Gimbal Assembly (HGA) Therefore, this research primarily focuses on studying the Head Gimbal Assembly (HGA) due to its highest potential for electrostatic discharge.

B. Machine Learning in Production Line Optimization

For selecting the appropriate machine learning technique, it is necessary to study the types of data to be analyzed and determine the technique that will provide the best results. In

979-8-3315-4248-1/25/$31.00 ©2025 IEEE

analyzing large volumes of data, we will rely on the 5V principles [4] from Big Data theory as a criterion to select only the valuable data for training the model to be developed. The 5V principles help us obtain sufficient data for decision-making regarding the type of machine learning to be used and improve the efficiency of machine learning by refining the data and reducing dimensionality to enhance performance [5]. Machine learning techniques have applications in business and industry that can be used in research, including.

a) Random Forest Algorithm: It is an algorithm that randomly selects features from a dataset to create multiple decision of dicition trees then votes based on the majority of dicition trees. Research conducted by Bosch applied this technique to predict product failures, using it in an IoT system with a two-step learning process. K-Means was used for data clustering, and the results compared various machine leraning techniques, with Random Forest yielding the best outcome. This is because Random Forest handles large datasets well and provides high accuracy, making it suitable for predicting potential damage [6].

b) Logistic Regression Algorithm: The algorithm developed from linear regression uses mathematical principles to derive results from various variables. It is suitable for use with binary classification data. Research has applied Logistic Regression to compare with other models for analyzing the credit risk assessment of banks. The model performs well when there is limited data. Logistic Regression can predict probabilities within a sample better than other models. However, if it is to be applied in practice, further development is needed, as its AUC value is below 70%, and improvements can still be made [7].

c) K-Nearest Neighbors Algorithm (KNN): The algorithm for data clustering that measures distance with neighboring data points based on a specified K value was used to predict damage in rotary machine was particularly interesting in this research is the dimensionality reduction of data before model creation, which helps to improve the efficiency of the machine learning model. The results showed that KNN was able to classify abnormalities with an accuracy of up to 99%. When tested in real-world scenarios, the model could detect abnormalities within 10 seconds [8].

d) Support Vector Machine Algorithm (SVM): It is an algorithm used to create a linear equation to separate data into groups, maximizing the distance from all data points. Research has been conducted on detecting anomalies in machinery in production lines using vibration data. Previously, problem analysis required experts to solve it. Therefore, a test was conducted using SVM in conjunction with PCA. The results showed that the anomaly caused by misalignment in the operation direction was detected with 95.7% accuracy, and bearing damage was detected with 100% accuracy, making it applicable for real-world production use [9].

e) XGBoost: The algorithm developed from decision trees that stops learning when no errors occur in the previous tree. It has been used to classify the severity of part damage in the biological industry to reduce the risk of unplaning.

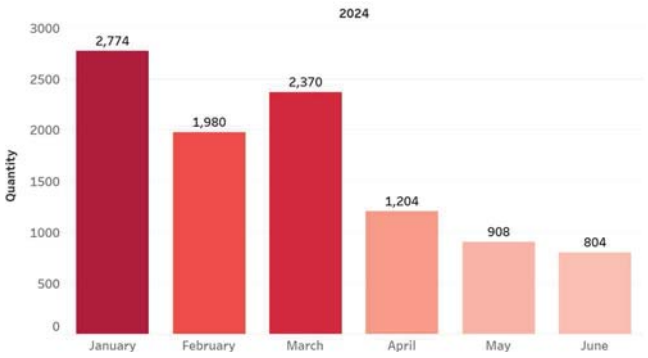


Fig. 2. History of electrostatic discharge in the production line.

XGBoost provides high accuracy when the data is enhanced by generating synthetic damage data and performing feature selection, achieving an accuracy of over 90%. This helps reduce material wastage and allows for repairs before significant damage occurs [10].

III. METHODOLOGY

A. Data Understaning

The verification of data from the database that records incidents of damage to products caused by electrostatic discharge in the production line was conducted by retrieving data from the past 6 months. The analysis revealed that the frequency of damage incidents during production exceeded 10,000 occurrences within the past 6 months, as shown in the graph depicted in Fig. 2.

The correlation between Production Line A and Production Line B is Many-to-Many correlation, as in Fig. 3. The slider from Production Line A requires more than one day to be transferred to Production Line B, makes the data complex to analyze. Therefore, a thorough understanding of the data is necessary.

B. Data Praparation

Data mining is the process begins by identifying the data storage sources for each production step in order to design Data recording workflow. This is to obtain the necessary data for research and to create the workflow according to the following steps.

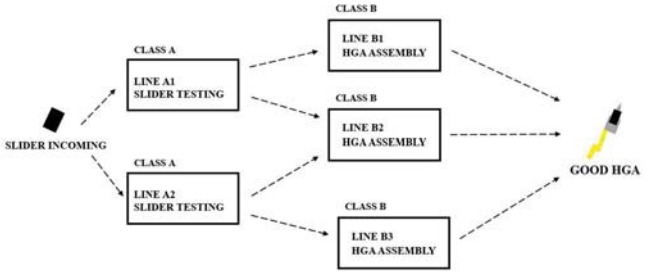


Fig. 3. The Relationship between production lines.

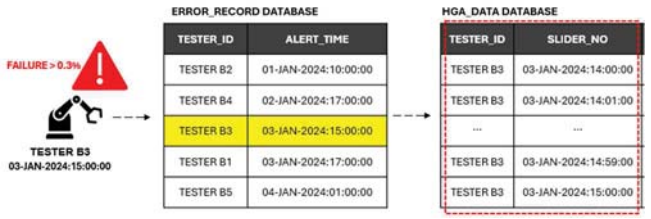


Fig. 4. Example of the steps to retrieve data from a database.

In the first step, once TESTER B detects a defect exceeding the predefined threshold, the machine's serial number (TESTER B3) and the timestamp of the defect detection (15:00) will be recorded in the ERROR_RECORD database, as shown in Fig. 4.

In the second step, the system will retrieve data from the database named HGA_DATA, with the condition that the data is from TESTER B3 within the time range from 14:00 to 15:00 on January 3, 2024. The data extraction time will be set to one hour prior to the detected anomaly time in order to gather sufficient data for model development.

Fig. 5 shows that Class A is defined as the abnormal operation of Production Line A, while Class B represents the abnormal operation of Production Line B. After obtaining data from the previous steps, the data will be transformed into statistical data to reduce the dimensionality and enhance the model's efficiency. Additionally, techniques for handling imbalanced data will be applied, as Class A data is significantly more frequent than Class B and balancing the dataset will be necessary before further analysis.

The SMOTE technique is used to balance the data between the two classes, as shown in Fig. 5. We will analyze and select only the features that significantly impact the model by applying a condition to choose features with a correlation greater than 5%, which will then be used for model training. This results in a total of 17 important features for training.

Another important step commonly performed before model training is data normalization. This step reduces complexity and enhances the model's performance. The resulting data is shown in Fig. 6.

C. Modeling

Once the data is prepared for model creation, the model will be built and evaluated based on the performance metrics shown in Table I.



Fig. 5. Number of data before and after balancing.

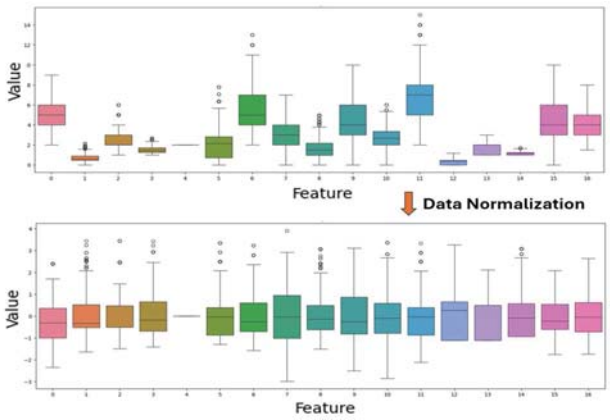


Fig. 6. The values of each feature after normalization.

TABLE I. PERFORMANCE EVALUATION USING STRATIFIED K-FOLD.

Model	Performance Testing Round					Mean
	1	*2*	*3*	*4*	*5*	
XGBoost	0.92	0.85	0.91	0.92	0.93	0.91
Random Forest	0.91	0.86	0.89	0.92	0.92	0.90
KNN	0.84	0.85	0.86	0.84	0.85	0.85
SVM	0.85	0.78	0.83	0.82	0.83	0.82
Logistic Regression	0.84	0.80	0.80	0.80	0.82	0.81

TABLE II. SHOW THE BEST PARAMETERS FROM GRIDSEARCHCV.

Model	Hyper Parameters	Accuracy	Precision
Random Forest	bootstrap : False max_depth : None max_features : sqrt min_samples_split : 2 n_estimators : 200	0.88	0.89
XGBoost	colsample_bytree : 0.6 learning_rate : 0.2 max_depth : 11 n_estimators : 300 subsample: 1.0	0.87	0.87

The Stratified K-Fold technique will be used to assess and identify the top two models out of five candidates. The results indicate that the two most accurate models are XGBoost and Random Forest, with average accuracy values of 91% and 90%, respectively.

D. Hyperparrameter Tuning

The appropriate parameters were selected using GridSearchCV. Table II shows the parameters obtained through GridSearchCV and tested on the test dataset. Based on the initial assumption, if a False Positive (FP) occurs in the Confusion Matrix, it would result in the abnormal operation of the production line being overlooked, leading to increased damage to the products. Therefore, Precision, which correlates with FP, is used as a criterion for model selection alongside Accuracy to obtain a more reliable model. The goal is that a good model should minimize the risk of damage. Thus, a model with a higher Precision value indicates a lower risk of causing damage to the products compared to other models.

IV. RESULT

A. Evaluating Performance using Confusion Matrix

The Confusion Matrix is a performance metric for classification models [11].



Fig. 7. Confusion matrix table of the tested model

TABLE III. MODEL PERFORMANCE ON THE TEST DATASET.

Model	Risk Rating	Accepted Rating
Random Forest	24/474 (5.06%)	450/474 (94.93%)
XGBoost	29/474 (6.11%)	445/474 (93.88%)

The evaluation of the Confusion Matrix in Fig. 7 will be used to calculate the potential risk of incorrect predictions and determine the acceptable prediction outcomes. This will serve as a criterion for deciding which model is the best for implementation in the actual production line.

Table III shows the use of data from Fig. 7 to calculate the Risk Rating using the Risk Rating Equation and the Accepted Rating Equation, as outlined below.

$$\text{Risk Rating} = \frac{\text{FP}}{\text{TP} + \text{FP} + \text{FN} + \text{TN}} \times 100 \quad (1)$$

$$\text{Accepted Rating} = \frac{\text{FP}}{\text{TP} + \text{FP} + \text{FN} + \text{TN}} \times 100 \quad (2)$$

Where

FP = False Positive: A false prediction that leads to damage.

FN = False Negative: A false prediction that does not cause damage.

TP = True Positive: A correct prediction of a positive result.

TN = True Negative: A correct prediction of a negative result.

The performance of the model from Risk Rating Equation (1) shows that the Random Forest model has a lower risk than the XGBoost model by 1.05%. This indicates that the Random Forest model provides better results.

B. Evaluating Performance using ROC-AUC Curve

The ROC (Receiver Operating Characteristic) curve is a graph used to measure the performance of a classification model, while AUC (Area Under the ROC Curve) is a value that indicates the model's ability to distinguish between different classes.

From Fig. 8, the ROC-AUC Curve graph shows that the predictions from both models tested have similar performance, indicating that both models are effective. However, they cannot be used as the sole criterion for selection, as both models have the same AUC value of 0.90

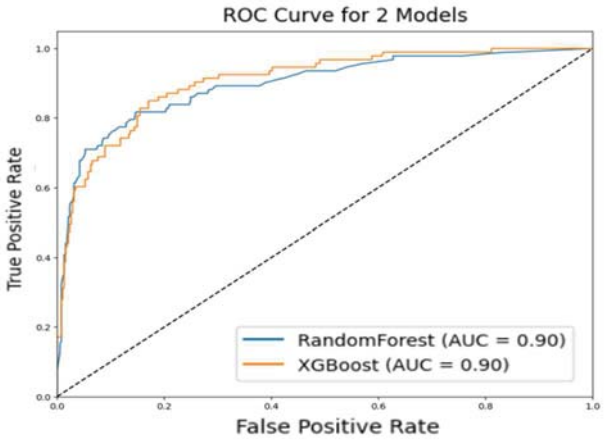


Fig. 8. ROC-AUC Curve of the selected model.

V. CONCLUSION

This research presents a comparison of machine learning techniques for predicting abnormal production lines that result in electrostatic damage to the Head Gimbal Assembly (HGA). This issue affects the quality of the products and the profitability of the business. Analyzing complex data from the production process requires significant expertise and time. Therefore, the consideration of using machine learning tools to identify abnormal production lines can help improve accuracy and reduce errors from human analysis.

The research findings show that the model built using the Random Forest technique, with appropriately tuned parameters, is the most efficient than other techniques. It can accurately and precisely identify abnormal production lines. This model can be further developed into an automatic production line shutdown system, allowing production halts when necessary and addressing issues quickly.

This research not only helps reduce losses from production line abnormalities but also plays a key role in increasing profitability for the hard disk drive assembly business efficiently.

REFERENCES

[1] M. Sisode and M. Devare, “A Review on Machine Learning Techniques for Predictive Maintenance in Industry 4.0,” In Proc. International Conference on Applications of Machine Intelligence and Data Analytics (ICAMIDA 2022), India, Dec. 22-24, 2022, pp. 774-783.

[2] M. Miyatake, F. Kugiya, and N. Kodama, “ESD Tolerance of GMR and TMR Heads Within Hard Disk Drives,” IEEE Trans. Device and Materials Reliability, Vol.10, No.4, Jul. 2010, pp. 476-481, doi: 10.1109/TDMR.2010.2061848.

[3] W. Boone et al. “A study of head stack assembly sensitivity to ESD,” in Proc. Electrical Overstress/Electrostatic Discharge Symp. , Orlando, Florida, USA, Sep. 1999, pp. 373-379.

[4] M. Assuncao et al., “Big Data computing and clouds: Trends and future directions,” Journal of Parallel and Distributed Computing, vol. 79, pp.3-15, May 2015.

[5] S. Mittal, and O.P. Sangwan. “Big Data Analytics using Machine Learning Techniques,” in 2019 9th International Conference on Cloud Computing, Data Science & Engineering, Noida, India, 2019, pp. 203-207.

[6] D. Zhang, B. Xu, and J. Wood, “Predict failures in production lines: A two-stage approach with clustering and supervised learning,” 2016 IEEE International Conference on Big Data (Big Data), Washington D.C., USA., 2016, pp. 2070-2074.

[7] N. Do and M. Simioni, “A comparison of random forest and logistic regression model in credit scoring of rural households,” Proceedings of the 23rd Malaysian Finance Association International Conference, University Sains Malaysia, 2021.

[8] Y. Yinghua, S. Guoqiang, and S. Xiang, “Fault monitoring and classification of rotating machine based on PCA and KNN,” 2018 Chinese Control and Decision Conference (CCDC), Shenyang, China, 2018, pp. 1795-1800.

[9] A.H. Md.Ripon and M.A. Ullah, “Rotating Machine Fault Detection Using Support Vector Machine (SVM) Classifier,” in 2023 4th International Conference on Computing and Communication Systems (I3CS), Shillong, India, 2023, pp.1-5.

[10] R. Bain, C. Lynch et al., “An XGBoost approach for industrial component degradation classification,” in 2022 33rd Irish Signals and Systems Conference (ISSC), Cork, Ireland, 2022, pp. 1-7.

[11] Z.Karimi, Confusion Matrix, Kharazmi University, Iran, 2021.

Using the Analytic Hierarchy Process (AHP) for Decision Making in Tourism Product Distribution Channel

Klinsukon Nimkanjana
Department of Information Technology
Rajamangala University of Technology Srivijaya
Nakhon si thammarat, Thailand
klinsukon.n@rmutsv.ac.th

Kornsirinut Rothjanawan
Department of Computer Engineering
Princess of Naradhiwas University
Narathiwat, Thailand
kornsirinut.r@pnu.ac.th

Supawadee Mak-on
Department of AI Engineering
Rajamangala University of Technology Srivijaya
Songkhla, Thailand
supawadee.m@rmutsv.ac.th

***Abstract* — This research applies the Analytic Hierarchy Process (AHP) to decision-making in the tourism product distribution channel of Phang-Nga province. The study aims to identify and prioritize key factors influencing the selection of the most suitable distribution channel, ultimately improving the efficiency and effectiveness of tourism product sales. Seven critical factors were analyzed: product variety, negotiable pricing, order availability, delivery service, product quality, sufficient supply, and credit payment options.**

The research methodology involves pairwise comparisons to determine the relative importance of each factor, weighted score analysis, and evaluation of distribution channel alternatives. The findings indicate that entrepreneurs prioritize three key factors: product quality, order availability, and delivery service. The AHP analysis reveals that the most suitable distribution channel is the information technology-based product selling system, as it effectively aligns with business needs, enhances consumer accessibility, and optimizes the overall distribution process.

Keywords* — *Analytic Hierarchy Process (AHP), Decision-Making, Product Distribution Channel, Supply Chain, Phang Nga

I. INTRODUCTION

Tourism is a rapidly expanding industry that significantly contributes to global economic growth. As the market evolves, both consumers and tourism businesses face increasing challenges in decision-making. Consumers seek high-quality tourism products that match their preferences and budgets, while businesses must strategically select and distribute their products to maximize profitability and competitiveness. These decisions involve multiple factors, including pricing, service quality, seasonal demand, accessibility, and sustainability [1].

Effective distribution channels are critical for ensuring that tourism products reach the right consumers. These channels range from traditional retailers and wholesalers to direct sales and digital platforms, each with unique advantages and limitations. Choosing the most suitable distribution channel is crucial, as it directly affects market reach, operational efficiency, and overall business success. However, conventional decision-making methods often rely on intuition or past experience, which may not fully account for the complexities of distribution channel selection.

To address this challenge, this study applies the Analytic Hierarchy Process (AHP), a Multi-Criteria Decision-Making (MCDM) method, to systematically evaluate and select the most suitable tourism product distribution channel. AHP structures decision-making by organizing criteria hierarchically, assigning weights, and conducting pairwise comparisons, enabling businesses to make data-driven decisions [2].

This study focuses on Phang Nga, a renowned tourist destination in Thailand, known for its diverse tourism offerings, including handicrafts, eco-tourism, culinary experiences, and wellness services [3]. Due to the wide variety of products, selecting an appropriate distribution channel is essential to meet customer expectations and optimize business operations. By employing AHP, this research aims to identify the most effective distribution channel for tourism products in Phang Nga, enhancing accessibility, cost efficiency, and market competitiveness.

The findings will provide valuable insights for tourism businesses to refine their distribution strategies, aligning with both consumer needs and long-term business sustainability. The remainder of this paper is structured as follows: Section II reviews related literature, Section III explains the research methodology, Section IV presents the AHP model, Section V discusses the results, and Section VI concludes the study.

II. LITERATURE REVIEW

A. Tourism Product Distribution Channels

Tourism distribution channels connect businesses with consumers through direct sales, travel agencies, online platforms, wholesalers, and retailers Digital channels, driven by increased internet and mobile adoption, have revolutionized tourism product sales, making platforms like Booking.com and Airbnb dominant [4]. However, traditional channels remain crucial for niche markets requiring personalized service and trust-based relationships. In Phang Nga, a diverse tourism destination, businesses benefit from hybrid distribution models that combine online and offline strategies.

XXX-X-XXXX-XXXX-X/XX/$XX.00 ©2025 IEEE

B. Multi-Criteria Decision-Making (MCDM) in Tourism

Tourism distribution channel selection involves multiple factors, including cost, accessibility, efficiency, and market reach. Traditional decision-making often relies on intuition, leading to inconsistent outcomes [5]. As a result, MCDM methods, such as TOPSIS, DEMATEL, and AHP, have gained prominence for systematic evaluation and prioritization [6]. AHP is particularly effective due to its structured hierarchy and pairwise comparison approach .

C. Application of AHP in Tourism Decision-Making

AHP, developed by Saaty [7], has been widely applied in tourism research, including destination selection, service quality assessment, and supply chain optimization [8]. Studies show its effectiveness in:

- Selecting optimal hotel booking platforms
- Optimizing tourist transportation
- Identifying the best sales channels for local tourism products

Despite AHP's extensive use, limited research focuses on its role in optimizing tourism distribution channels, particularly in local markets like Phang Nga. This study addresses this gap by applying AHP to analyze and prioritize distribution channels, aiming to improve efficiency, customer satisfaction, and business performance.

III. Methodology

This study employs an AHP-based framework to optimize tourism product distribution channels in Phang Nga, Thailand. The methodology consists of five phases:

A. Problem Definition and Criteria Identification

The first phase involves defining the problem and identifying key criteria influencing the selection of tourism product distribution channels. A comprehensive literature review was conducted to gather insights from previous research on distribution channel selection, tourism supply chains, and decision-making frameworks .

B. AHP Model Development

A hierarchical AHP model was structured as follows:

Level 1: Goal—selecting the optimal distribution channel.
Level 2: Key decision criteria.
Level 3: Alternative channels (e.g., direct sales, online platforms, wholesalers).

Pairwise comparisons were conducted using Saaty's scale (1–9), ensuring a consistency ratio (CR) below 0.10.

C. Data Collection

Quantitative and qualitative data were gathered through:

- Surveys: Distributed to 50 tourism professionals, using a Likert scale for pairwise comparisons.
- Expert Interviews: Conducted with 10 industry experts to validate criteria weighting.

D. Model Implementation and Analysis

AHP computations were performed using Excel and Expert Choice software to:

- Calculate criteria weights and priority rankings.
- Verify consistency via the consistency index (CI) and CR.

E. Validation and Case Study Application

The model was tested using a case study in Phang Nga, comparing results with industry practices and gathering stakeholder feedback.

F. Research Reliability and Limitations

Reliability was ensured through triangulation, sample diversity, and consistency checks. Limitations include expert opinion biases, geographic constraints, and evolving tourism trends. Future studies should expand the scope and integrate adaptive decision-making models.

IV. AHP Model Desing and Development

The Analytic Hierarchy Process (AHP) is a widely used Multi-Criteria Decision-Making (MCDM) approach that enables decision-makers to evaluate multiple factors systematically by structuring the problem into a hierarchical framework, assigning weights, and making pairwise comparisons to determine the optimal choice. In this study, AHP is applied to analyze and prioritize key factors influencing the selection of the most suitable tourism product distribution channel in Phang Nga, Thailand.

A. AHP Model Structure

The AHP framework for this study is structured into three hierarchical levels, as illustrated in Fig. 1:

1. Level 1 – Goal: Selecting the most suitable tourism product distribution channel for tourism businesses in Phang Nga.
2. Level 2 – Criteria: Seven key criteria were identified based on literature review and expert consultation:
   - *Variety of Products (P)* – Ensures a diverse range of tourism products to meet different customer preferences.
   - *Negotiable Prices (N)* – Provides price flexibility to increase sales potential.
   - *Availability for Orders (S)* – Allows customers to place orders anytime, enhancing convenience.
   - *Delivery Service (D)* – Offers direct delivery, adding value to the purchasing experience.
   - *Product Quality (Q)* – Guarantees fresh and high-quality products to improve customer satisfaction.
   - *Stock Availability (E)* – Maintains sufficient inventory to prevent shortages.
   - *Credit Payment Options (C*) – Provides flexible payment terms for easier transactions.

These criteria serve as the foundation for selecting the optimal tourism product distribution channel.

3. Level 3 – Alternatives: The distribution channel options under consideration:
   - Wholesalers (bulk tourism product distributors)
   - Online Platforms (e-commerce, digital tourism marketplaces and product selling system)
   - Retailer (selling directly to customers)

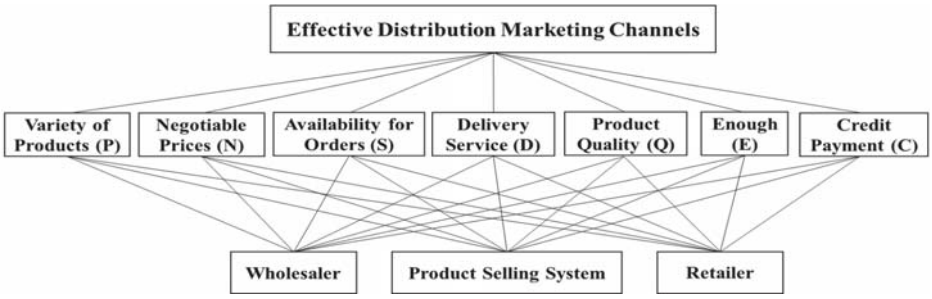


Fig. 1. An AHP Hierarchy Structure

B. Pairwise Comparison and Weight Assignment

To quantify the relative importance of each criterion, pairwise comparisons were conducted using Saaty's fundamental scale, where 1 represents equal importance and 9 represents extreme importance. Expert opinions were collected from tourism business owners, distribution managers, and supply chain professionals to ensure reliability as in Table I.

The pairwise comparison matrix was developed to compare the importance of each criterion against others. The priority weights (W) were derived by calculating the eigenvector of the matrix. The Consistency Index (CI) and Consistency Ratio (CR) were also computed to ensure that expert judgments were logically consistent, with CR values less than 0.10 being acceptable.

TABLE I. THE RATIO SCALE AND DEFINITION OF AHP

Intensity of importance	Definition
1	Equal importance
3	Somewhat more importance
5	Much more importance
7	Very much more importance
9	Alsolutely more importance
2,4,6,8	Intermediate values

C. AHP Calculation and Decision Matrix

The AHP mathematical computation follows these steps:

1. Construct the pairwise comparison matrix.
2. Compute the normalized matrix by dividing each element by the column sum.
3. Calculate the priority vector (W) by averaging row values in the normalized matrix.
4. Compute the Consistency Index (CI) using the formula:

$$CI = \frac{\lambda max - n}{n-1} \qquad (1)$$

where λmax is the principal eigenvalue and n is the number of criteria.

5. Determine the Consistency Ratio (CR) by dividing CI by the Random Consistency Index (RI) in Table II:

$$CR = \frac{CI}{\text{RI}} \qquad (2)$$

If CR ≤ 0.10, the comparisons are considered consistent; otherwise, expert inputs must be reviewed and adjusted.

TABLE II. THE AVERAGE RANDOM CONSISTENCY INDEX (RI)

n	**1**	**2**	**3**	**4**	**5**	**6**	**7**	**8**
RI	0	0	0.58	0.89	1.12	1.26	1.36	1.41

D. Ranking of Distribution Channel Alternatives

Once the weights of criteria were determined, each distribution channel was evaluated based on the weighted sum method (WSM), where the score for each alternative was calculated as:

$$S_i = \sum_{j=1}^{n} W_i X_{ij} \qquad (3)$$

where S_i the total score of distribution channel *i*,

W_i is the weight of criterion *j*, and

X_{ij} represents the rating of distribution channel *i* under criterion *j*.

The alternative with the highest score was identified as the most suitable tourism product distribution channel for businesses in Phang Nga.

E. Model Validation and Sensitivity Analysis

To validate the AHP model and ensure robustness, a sensitivity analysis was conducted by adjusting the weights of key criteria and observing the impact on the final ranking of distribution channels.

V. RESULT

A. The analysis of distribution channel evaluation criteria.

The results of interview importance score analysis to find the Geometric Mean of all interviewees. The results are summarized in the matrix in Table III, and the analysis of each criterion score is shown in Table IV.

TABLE III. INTERVIEW RESULTS TO ASSESS SCORES IN EACH CRITERION.

Criteria	P	N	S	D	Q	E	C
P	1.000	0.613	0.479	0.573	0.320	2.919	0.458
N	1.632	1.000	1.019	1.259	0.397	3.196	0.204
S	2.087	0.981	1.000	0.420	0.326	3.607	1.745
D	1.745	0.794	2.380	1.000	0.192	2.414	1.144
Q	3.124	2.517	3.065	5.215	1.000	4.310	4.180
E	0.432	0.313	1.312	0.414	0.231	1.000	0.262
C	2.183	0.750	0.743	0.875	0.238	3.831	1.000
Total	**12.203**	**6.968**	**9.999**	**9.757**	**2.704**	**21.277**	**8.993**

TABLE IV. IMPORTANCE SCORE OF EACH EVALUATION CRITERION.

Criteria	P	N	S	D	Q	E	C	Score Importance
P	0.082	0.088	0.048	0.059	0.118	0.137	0.051	0.083
N	0.134	0.144	0.102	0.129	0.147	0.150	0.023	0.118
S	0.171	0.141	0.100	0.043	0.121	0.170	0.194	0.134
D	0.143	0.114	0.238	0.102	0.071	0.113	0.127	0.130
Q	0.256	0.361	0.307	0.535	0.370	0.203	0.465	0.356
E	0.035	0.045	0.131	0.042	0.085	0.047	0.029	0.059
C	0.179	0.108	0.074	0.090	0.088	0.180	0.111	0.119

Results of analysis for consistency rates (*CI*).

$$\lambda max = 7.174$$

$$CI = \frac{\lambda max - n}{n-1} = \frac{7.174 - 7}{7-1} = 0.029$$

$$CR = \frac{CI}{RI}\ ;\ RI = 1.32;\ \frac{0.029}{1.32} = 0.021$$

Score of criteria passed the consistency check with a *CR* value of 0.021, which is *CR < 0.1* for metrics with size n ⩾ 5. It can be concluded that the weight vector W that gives weight to the 7 criteria, namely *Wp=0.083, Wn=0.118, Ws=0.134, Wd=0.130, Wq=0.356, We=0.059, Wc=0.119,* when the weights are added together must be equal to 1, indicating that consumers give importance to the quality of fresh products, good taste (0.356) first, followed by being able to order products at all times (0.134), and then the next factor is the delivery service (0.130), followed by credit card payment (0.119), the next factor is negotiable price (0.118), the next factor is product variety as desired (0.083), and the last factor is product quantity sufficient to meet demand (0.059).

A. Selecting channels for distributing tourism products according to appropriate evaluation criteria.

The weighted values are analyzed to determine the most suitable alternative by conducting pairwise comparisons for each criterion. Each of factor in each alternative must be considered alongside the weighted values of the factors across all distribution channels, considering all seven criteria as shown in Table V.

TABLE V. WEIGHTING AND SCORING CRITERIA

Criteria / Alternative	Variety of Products (P)	Negotiable Prices (N)	Availability for Orders (S)	Delivery Service (D)	Product Quality (Q)	Enough (E)	Credit (C)
Retailer	0.087	0.561	0.706	0.416	0.132	1.363	0.106
Product Selling System	0.707	0.726	0.828	0.815	0.756	0.359	0.904
Wholesaler	0.287	0.514	0.591	0.430	0.425	1.185	0.251

The given weights and scores are calculated to find the distribution channel score that best meets the desired criteria, called the weight sum of score, by multiplying the product between the weight (W) and the score according to the number of distribution channels (S):

$$= \begin{bmatrix} 0.087 & 0.561 & 0.706 & 0.416 & 0.132 & 0.136 & 0.106 \\ 0.707 & 0.726 & 0.828 & 0.815 & 0.756 & 0.370 & 0.904 \\ 0.287 & 0.514 & 0.591 & 0.430 & 0.425 & 1.185 & 0.251 \end{bmatrix} \times \begin{bmatrix} 0.0833 \\ 0.1183 \\ 0.1342 \\ 0.1299 \\ 0.3565 \\ 0.0594 \\ 0.1185 \end{bmatrix}$$

$$= \begin{bmatrix} 0.363 \\ 0.760 \\ 0.471 \end{bmatrix}$$

The distribution channel with the highest weight sum of score level that is most suitable for the distribution channel of tourism products in Phang-Nga Province is the distribution channel of Product Selling System from the factors of fresh product quality, good taste, and being able to negotiate better prices, as well as being able to order at any time. The top 3 best scores have a supporting effect on the selection of the said distribution channel criteria as shown in Table VI.

TABLE VI. RANKING OF ALTERNATIVES

Distribution Channels	Score	% Importance
Retailer	0.3629	36.29
Product Selling System	0.7603	76.03
Wholesaler	0.4714	47.14

VI. CONCLUSION

This study applies the Analytic Hierarchy Process (AHP) to optimize tourism product distribution in Phang-Nga by evaluating seven key criteria, including product quality, order availability, and delivery service, which emerged as the most critical factors. The Product Selling System was identified as the most suitable channel (76% priority weight), followed by wholesalers and traditional retailers.

The study highlights the growing impact of digital transformation, particularly through e-commerce and AI-driven logistics, in expanding market reach and improving efficiency. A comparative analysis suggests that while AHP offers a structured decision-making approach, integrating machine learning or multi-criteria decision analysis could enhance precision. A refined cost-benefit assessment emphasizes the need to balance technological investment with financial feasibility to ensure long-term profitability. Findings suggest that technology-driven distribution platforms can improve efficiency and boost competitiveness in tourism markets.

Future research should further explore digital transformation, sustainability, and AI-driven decision models to strengthen tourism product distribution strategies and enhance industry resilience.

REFERENCESS

[1] M. A. Camilleri, *Tourism Distribution Channels*, in *Travel Marketing, Tourism Economics and the Airline Product*, Cham, Switzerland: Springer Nature, 2018, ch. 6, pp. 105–115.

[2] P. Jewpanya, P. Nuangpirom, W. Nakkiew, S. Pitjamit, and P. Jaichomphu, "Optimizing Tourist Destination Selection Using AHP and Fuzzy AHP Based on Individual Preferences for Personalized Tourism," *Sustainabilit*y, vol. 17, no. 3, p. 1116, 2025

[3] Tourism Authority of Thailand, Phang Nga, Feb 2025., [Online] Available: https://www.tourismthailand.org/Destinations/Provinces/Phang-Nga/348

[4] C. Evangelos, C. Chatzigeorgiou., "Adoption of social media as distribution channels in tourism marketing: A qualitative analysis of consumers' experiences.," *Journal of Tourism, Heritage & Services Marketing (JTHSM)* , vol.6, no.1, pp. 25-32 , 2020.

[5] S.Forouzandeh, M. Rostami, and K. Berahmand, "A Hybrid Method for Recommendation Systems based on Tourism with an Evolutionary Algorithm and Topsis Model," *Fuzzy Information and Engineering*, vol. 14, no. 1, pp. 26–50, 2022.

[6] F. Zagonari, "Multi-Criteria, Cost-Benefit, and Life-Cycle Analyses for Decision-Making to Support Responsible, Sustainable, and Alternative Tourism," *Sustainability*, vol. 11, no. 4, p. 1038, 2019.

[7] R. D. Saaty, *The Analytic Hierarchy Process: Planning, Priority Setting, Resources Allocation*, New York, NY: McGraw-Hill, 1980.

[8] S. Bukhori, D. A. Sukmawati, and Y. R. W. Eka, "Selection of supplier using analytical hierarchy process: Creating value added in the supply chain agribusiness," 2017 4th International Conference on Computer Applications and Information Processing Technology (CAIPT), pp. 1–6, Aug. 2017.

Development an Ontology Knowledge Base for Biodiversity, Identify plants of Community forest: A Case study of Baan Wang sai Community

Klinsukon Nimkanjana
Department of Information Technology
Rajamangala University of Technology Srivijaya
Nakhon si thammarat, Thailand
klinsukon.n@rmutsv.ac.th

Premjit Ruengsawat
Department of Bioproduct Technology
Rajamangala University of Technology Srivijaya
Nakhon si thammarat, Thailand
premjit.r@rmutsv.ac.th

Sarit Panjan
Department of Information Technology
Rajamangala University of Technology Srivijaya
Nakhon si thammarat, Thailand
sarit.p@rmutsv.ac.th

***Abstract* — This study aims to develop an ontology-based knowledge base for biodiversity, identity, and plant species in community forests, with a specific focus on the Baan Wang Sai Community forest, located in Tham Yai Sub-district, Thungsong District, Nakhon Si Thammarat Province, Thailand. The research involves creating a comprehensive ontology that integrates seven main classes: Plants, Plant Types, Usefulness, Learning Points, User Parts, Identity, and How to Use. These classes serve as the foundation for a semantic search system designed to manage and retrieve information related to the biodiversity and cultural identity of the forest's plant species. The ontology knowledge base is converted into OWL (Web Ontology Language) and linked with a database system to facilitate efficient data retrieval and management. A key feature of the system is its ability to allow users to search for plant species and view related information, including their uses and learning points, accurately. The system's performance was evaluated by experts, yielding a precision of 100%, recall of 94.83%, and an F-measure of 97.35%, demonstrating its effectiveness. This ontology-based system provides a valuable tool for biodiversity conservation, cultural preservation, and sustainable forest management in the Baan Wang Sai Community forest, enhancing knowledge sharing among local communities, researchers, and policymakers.**

Keywords — Semantic Web, Ontology, Knowledge Management, Biodiversity, Identify plants, Baan Wang sai Community

I. INTRODUCTION

Community forests play a vital role in preserving biodiversity, maintaining cultural identity, and conserving plant species. Managed by local communities, these forests serve as ecological spaces and cultural heritage sites, where indigenous knowledge and sustainable practices are passed down through generations. The Baan Wang Sai Community Forest, located in the Tham Yai Sub-district of Nakhon Si Thammarat, exemplifies how community-managed forests contribute to ecological balance and the conservation of regional plant species. These forests provide essential resources, such as food, medicine, and materials, deeply intertwined with the community's identity and cultural practices [1].

However, community forests face challenges in managing and sharing knowledge about biodiversity and plant resources. Issues include fragmented and inaccessible knowledge on plant species, their ecological roles, and traditional uses. Without a centralized framework to document and share this knowledge, effective management and conservation are hindered. Traditional knowledge, passed down informally, is at risk due to generational gaps, lifestyle changes, and urbanization pressures.

This study aims to address these challenges by developing an ontology-based knowledge base for the Baan Wang Sai Community Forest. The goal is to create a standardized system that catalogs plant species, their ecological functions, and traditional uses while preserving the community's cultural heritage. Using an ontology-based approach, the study seeks to facilitate efficient knowledge sharing, making information accessible to the local community, researchers, and policymakers. The ontology will serve as a valuable resource for understanding biodiversity and promoting collaboration for sustainable forest management.

The development of this knowledge base will integrate diverse ecological data, making complex information more accessible. This approach bridges traditional ecological knowledge with modern scientific research, ensuring both are preserved and utilized effectively [2]. Additionally, the platform will empower the Baan Wang Sai community to document and share their knowledge, supporting the preservation of cultural heritage and fostering collaboration for sustainable forest management.

The structure of this paper is as follows: Section II provides a review of related works, Section III outlines the research materials and methods, Section IV presents the results, and Section V concludes the study.

II. RELATED WORK

Ontologies have gained attention in biodiversity and conservation knowledge management by providing a structured framework to integrate diverse data, improving knowledge sharing, retrieval, and management. In community forests, they bridge the gap between traditional ecological knowledge and modern science.

Recent studies highlight the effectiveness of ontologies in managing biodiversity knowledge. For example, Patel et al. (2022) emphasize the role of ontologies in biodiversity data management, enabling better data integration for conservation

XXX-X-XXXX-XXXX-X/XX/$XX.00 ©20XX IEEE

purposes and creating a common framework for biodiversity data [3]. This concept aligns with the goals of this research in developing an ontology-based knowledge base for community-managed forests.

Ontologies have also been used to document medicinal plants in community forests. Afifa et al. (2022) applied ontologies to catalog medicinal plants and traditional knowledge in Indonesian community forests, improving communication among community members, researchers, and conservationists [4]. This approach inspired the current study, which aims to develop an ontology knowledge base for documenting and identifying plants in the Baan Wang Sai Community Forest.

Community forests are vital for preserving biodiversity and cultural heritage. A study by Shivani et al. (2022) highlighted the role of community-managed forests in safeguarding local plant species and traditional knowledge in Nan province, Thailand [5]. It found that local communities, like those in Baan Wang Sai, possess valuable knowledge about plants, their medicinal uses, and sustainable management. The study underscores the need for structured knowledge management systems, like ontology-based knowledge bases, to preserve and share this knowledge.

III. Materials and Methods

A. Material

The Hozo ontology editor, developed by the Institute of Scientific and Industrial Research, Osaka University, Japan [6]; Ontology Application Management (OAM), developed by the Language and Semantic Technology Laboratory, National Electrics and Computer Technology Center (NECTEC)[7].

B. Methods

The methodology for developing an ontology-based knowledge base for the Baan Wang Sai Community forest combines the Hozo Ontology and Ontology Application Management (OAM) frameworks to organize and manage the forest's biodiversity, identity, and plant species. These frameworks will structure the knowledge, improve accessibility, and support sustainable forest management.

1. Data Collection and Knowledge Acquisition

Data collection for the Baan Wang Sai Community Forest ontology will involve:

- Field Surveys and Plant Identification: A survey will catalog plant species with the help of local community members, including botanical names, ecological roles, and cultural uses.
- Interviews with Local Experts: Semi-structured interviews with community leaders, herbalists, and elders will capture traditional plant knowledge.
- Literature Review: Scientific publications and ethnobotanical studies will be reviewed to validate the identified plant species.

2. Hozo Ontology Framework Development

The Hozo Ontology will be utilized to organize the collected data and structure the knowledge base. This ontology framework is designed for managing ecological, biodiversity, and cultural data. The steps for developing the Hozo ontology are as follows:

- Ontology Design: The Hozo Ontology will be customized for the Baan Wang Sai Community Forest, categorizing plant species by taxonomy, ecological functions (e.g., medicinal, edible, ritual), and cultural significance (e.g., ceremonies, folklore, healing).
- Ontology Representation: Plant species will be represented as individuals with attributes such as ecological roles, cultural uses, and geographic locations, organized across multiple hierarchies.
- Metadata Integration: Each plant will be linked to metadata covering ecological roles, environmental factors, human interactions, and tracking temporal changes in ecological and cultural practices.

3. Ontology Application Management (OAM) System Design

The Ontology Application Management (OAM) framework will be used to manage the practical application of the Hozo Ontology within the knowledge base system. It ensures the ontology is developed, maintained, updated, and applied efficiently. Key steps for implementing OAM are:

- System Architecture: The OAM framework will be a web-based system, integrating the ontology into a user-friendly interface accessible via a cloud platform for easy access by community members, researchers, and policymakers.
- User Interface Design: The interface will accommodate diverse users, featuring visualizations like plant maps and ecological relationships. A bilingual option (Thai and English) will enhance accessibility for local users and external researchers.
- Search and Query Functionality: The system will offer advanced search options to query the ontology by plant names, roles, uses, and locations, providing detailed data on classification, uses, and ecological significance.
- Data Integration and Collaboration: The system will integrate GIS data and support collaboration, enabling stakeholders to contribute data, comment, and suggest updates to the ontology.

4. Ontology Validation and Refinement

To ensure the ontology accurately represents both scientific and traditional knowledge, the following validation steps will be implemented:

- Community Feedback: The initial ontology version will be shared with the Baan Wang Sai community through workshops and focus groups to ensure accuracy and cultural relevance, with feedback used for refinement.
- Expert Review: Experts in biodiversity, ethnobotany, and knowledge management will review the ontology, offering recommendations to improve its structure, content, and usability.
- Testing and Iterative Refinement: The ontology and system will undergo iterative testing, with user feedback used to refine the structure, data integration, and interface.

5. Deployment and Dissemination

Upon completion of the development and validation phases, the ontology-based knowledge base will be deployed and disseminated through the following methods:

- Community Training: Training sessions will teach local community members how to use the knowledge base, including navigation, information searching, and contributing new knowledge.
- Research and Policy Applications: The knowledge base will support researchers, conservationists, and policymakers in sustainable forest management, biodiversity conservation, and community-based natural resource management.
- Public Access and Documentation: The system will be accessible via a web portal, with a user manual developed to ensure effective use and the system's longevity.

The integration of Hozo Ontology and Ontology Application Management (OAM) frameworks offers a comprehensive, accessible solution for managing the biodiversity and cultural knowledge of the Baan Wang Sai Community forest. By structuring plant species, ecological roles, and cultural significance, this approach supports efficient forest management, biodiversity conservation, and the preservation of traditional knowledge. The OAM system ensures the ontology remains adaptable, enabling collaboration among stakeholders in sustainable forest management.

IV. Result

To design an ontology knowledge base for biodiversity, identity, and plant species in community forests, we utilized the Hozo-Ontology Editor program to create the ontology knowledge base, as illustrated in Fig. 1. The ontology consists of seven main classes: Plants, Type of Plants, Usefulness, Learning Point, User Part, Identity, and How to Use. Subsequently, the ontology knowledge base was converted into OWL language. The development of the semantic search system utilizes a tool that supports the creation of ontology applications. The Ontology Application Management (OAM) Framework is an ontology knowledge base application that facilitates both the creation of RDF and OWL data from existing databases and the utilization of the generated data.

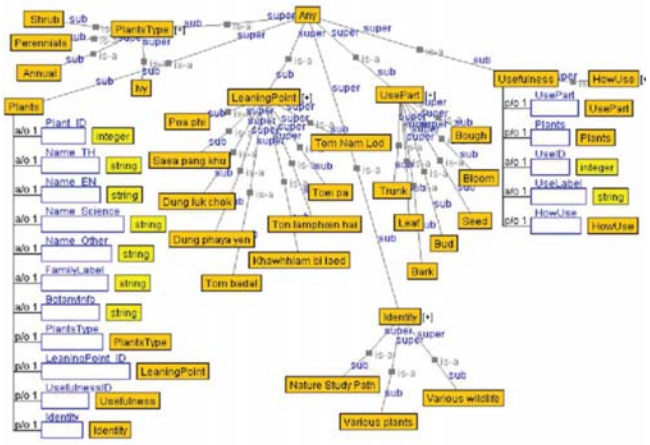


Fig. 1. Ontology of biodiversity, identity and plant species for Wang Sai community forest.

The ontology knowledge base streamlines ontology application development. We configure connection values to the database and uploads the ontology file (Fig. 2). The linking between the database and ontology is shown in Fig. 3, defining relationships between classes and tables. The data linking program supports one-to-one, one-to-many, and many-to-many relationships, with Property-Column Mapping for subclasses, as depicted in Fig. 4. An example of semantic search is demonstrated in Fig. 5, illustrating how users can query the ontology based on plant species, their ecological roles, and cultural uses.



Fig. 2. Configuring database connection and uploading ontology files



Fig. 3. Defining the relationship between classes and tables



Fig. 4. Configuring the relationship between properties and columns



Fig. 5. Example of semantic search

To assess the performance of the semantic information retrieval system, we tested and evaluated its effectiveness using the following metrics: precision, recall, and overall performance (F-measure).

- Precision is the ratio of the number of correct results retrieved to the total number of results retrieved.

$$\text{Precision} = \frac{|TP|}{|TP+FP|} \quad (1)$$

- Recall is the ratio of the number of correct results retrieved to the total number of relevant results available.

$$\text{Recall} = \frac{|TP|}{|TP+FN|} \quad (2)$$

- The F-measure, or overall efficiency value, is a metric that evaluates the combined performance of both accuracy and completeness, calculated together.

$$\text{F} - \text{measure} = \frac{2\text{x Precision} \times \text{Recall}}{\text{Precision} + \text{Recall}} \quad (3)$$

Where:

- True Positive *(TP)* refers to the number of correctly retrieved data.
- False Positive *(FP)* refers to the number of incorrectly retrieved data that should not have been retrieved.
- False Negative *(FN)* refers to the number of data that should have been retrieved but were not.

TABLE I. EVALUATION RESULTS OF SEMANTIC INFORMATION RETRIEVAL SYSTEMS

Query	|TP|	|TP|+|FP|	|TP|+|FN|	% Precision	% Recall
1. พันธุ์พืช ขยายพันธุ์: เมล็ด	10	10	10	100	100
2. จุดเรียนรู้: ต้นไผ่	1	1	1	100	100
3. จุดเรียนรู้: ประเภท: ไม้ยืนต้นขนาดใหญ่	3	3	3	100	100
4. พันธุ์พืช: ประเภท: ไม้เลื้อย	6	6	6	100	100
5. อัตลักษณ์: ประเภท: ไม้ยืนต้น	3	4	4	100	75.00
6. พันธุ์พืช: ประเภท: ไม้พุ่ม	7	7	7	100	100
7. จุดเรียนรู้: อัตลักษณ์: ถ้ำ	2	2	2	100	100
8. พันธุ์พืช: ใช้ประโยชน์: สมุนไพร	10	8	8	100	80.00
9. พันธุ์พืช: ใช้ประโยชน์: อาหาร	7	7	7	100	100
10. พันธุ์พืช: ส่วนที่ใช้ประโยชน์: ใบ	15	14	14	100	93.33
Average				**100**	**94.83**

The semantic search system for biodiversity and plant species in the Ban Wang Sai community forest achieved an accuracy of 100%, a completeness (Recall) of 94.83% when compared to expert results, and an efficiency (F-measure) of 97.35%. The system's accuracy (Precision) was 100% within the scope of 35 plant species as shown in as Table I.

V. CONCULSION

This study developed an ontology-based knowledge base for biodiversity, plant identity, and species in the Baan Wang Sai Community Forest in Tham Yai Sub-district, Thungsong District, Nakhon Si Thammarat Province. The system includes 7 main classes and provides a semantic search tool to explore plant species, their uses, and related information. The system achieved high accuracy: 100% precision, 94.83% recall, and 97.35% F-measure, demonstrating its effectiveness for managing biodiversity and preserving ecological and cultural knowledge in the community.

Unlike existing biodiversity databases such as CoL and GBIF, which focus on scientific data and taxonomies, our ontology integrates both scientific and traditional knowledge. It highlights local plant uses, including medicinal properties and cultural significance, making it more relevant for community-managed forests where local knowledge is crucial. The system's semantic search capability sets it apart, allowing users to explore complex relationships between plant species, ecological roles, and cultural uses, offering deeper insights than traditional databases.

In future work, we aim to expand the ontology, refine the search system, and explore machine learning to enhance relevance. We also plan to integrate the system with other community forests across Thailand to create a larger network for biodiversity and cultural knowledge, promoting broader collaboration and data sharing. This ontology demonstrates a more holistic approach to biodiversity conservation and cultural heritage preservation, integrating local ecological knowledge into forest management.

REFERENCES

[1] R.Unjan, J.Phetchit and S.Buakhao, “The Identity of Baan Wang sai Community Tham Yai Sub-district, Thung Song District, Nakhon Si Thammarat Province,” *Ratchaphruek Journal*, vol. 19, no. 2, pp. 111-119, 2021.

[2] G. Mansingh and L. Rao, “The role of ontologies in developing knowledge technologies.” *Knowledge Management for Development: Domains, Strategies and Technologies for Developing Countries*, pp.145-156, 2014.

[3] A. Patel, S. Jain, N. C. Debnath, and V. Lama, “InBiodiv-O,” *International Journal of Information System Modeling and Design*, vol. 13, no. 7, pp. 1–18, Dec. 2022.

[4] R. M. Afifa, W. A. Kusuma, and A. Annisa, “Ontology Data Modeling of Indonesian Medicinal Plants and Efficacy,” *INTENSIF: Jurnal Ilmiah Penelitian dan Penerapan Teknologi Sistem Informasi*, vol. 6, no. 2, pp. 218–232, 2022.

[5] S. Agarwal, B. Sairorkham, P. Sakitram, and E. F. Lambin, “Effectiveness of community forests for forest conservation in Nan province, Thailand,” *Journal of Land Use Science*, vol. 17, no. 1, pp. 307–323, 2022.

[6] K. Kozaki, E. Sunagawa, Y. Kitamura, and R. Mizoguchi, “Distributed construction of ontologies using hozo,” WWW 2007, 2007. [Online]. Available: http://www2007.org/workshops/paper 19.pdf

[7] M. Buranarach, Y. Thein, and T. Supnithi, “A Community-Driven Approach to Development of an Ontology-Based Application Management Framework,” *LNCS* 7774, pp. 306–312, 2013.

TabFuseNet: A Cancer Prediction Model Utilizing Sample Cohort Data

ChaeYoon Han
Department of MetaBioHealth, Sungkyunkwan University,
Suwon, South Korea,
polarlicht11@g.skku.edu

NangKyeong Lee
Department of Precision Medicine, Sungkyunkwan University School of Medicine,
Suwon, South Korea,
skdrud3717@naver.com

Jun Kim
Department of MetaBioHealth, Sungkyunkwan University,
Suwon, South Korea,
ttr3515@skku.edu

Muhammad Afzal
College of Computing, Birmingham City University,
England,
Muhammad.Afzal@bcu.ac.uk

Zeeshan Abbas*
Department of Precision Medicine Sungkyunkwan University School of Medicine,
Suwon, South Korea,
*Corresponding: zabbas@jbnu.ac.kr

SeungWon Lee*
Department of Precision Medicine Sungkyunkwan University School of Medicine,
Suwon, South Korea,
*Corresponding: swleemd@skku.edu

***Abstract*—Cancer is one of the leading causes of death worldwide, and early diagnosis can significantly improve patient survival rates and quality of life. However, traditional cancer diagnostic methods are costly and time-consuming, posing limitations on early detection. This study aims to develop an AI model that predicts the likelihood of cancer occurrence within five years based on patients' health screening data, medical history, and prescription records. To achieve this, we utilized the Sample Cohort 1.0 dataset provided by the National Health Insurance Service (NHISS) and used health check-up and prescription data from 2007–2008 to predict the occurrence of lung, gastric, breast, liver, and colorectal cancer between 2009 and 2013. The dataset used in this study is structured in tabular format, and we employed machine learning models (SVM, Random Forest, XGBoost, LightGBM) as well as deep learning models (CNN, TabTransformer, TabNet) for performance comparison. The models were evaluated using AUC, F1-Score, AUPRC, and ACC. Finally, we propose the TabeFusionNet model. TabeFusionNet achieved an average AUPRC of 0.9248, demonstrating superior performance compared to conventional machine learning and deep learning models. Notably, TabeFusionNet outperformed TabeTransformer in handling tabular datasets, indicating its potential for applications in various research fields.**

***Index Terms*—**cancer, cohort data, Deeplearning, AI.

I. Introduction

Cancer is a leading cause of death worldwide, accounting for about 26% of all deaths in South Korea in 2021. The incidence and mortality rates are rising due to factors such as aging and environmental changes. Early detection of cancers such as breast, stomach, colorectal, lung, and liver cancers significantly improves survival rates. In South Korea, the survival rate for early-diagnosed stomach cancer exceeds 90%, and colorectal cancer shows a 5-year survival rate of approximately 70% [1].

Globally, cancer risk factors like smoking, alcohol consumption, and obesity contribute to about 41% of cancer-related deaths. These factors exhibit regional differences, with South Asia seeing high rates of lip and oral cancers, and the Asia-Pacific region facing significant liver cancer rates due to hepatitis B and C infections [2]. In Korea, smoking, alcohol, and obesity have been identified as major risk factors. Smoking increases the risk of lung and laryngeal cancers, while high physical activity levels reduce cancer risk [3], [4], [5], [6].

In this context, AI plays a crucial role in early cancer diagnosis and personalized treatment strategies. AI improves the precision of cancer diagnoses, especially through analyzing medical imaging and pathological data. Additionally, Electronic Health Records (EHR) can help track patients' health changes and identify key factors related to cancer development, further enhancing early detection.

This study focuses on predicting cancer using tabular data that includes both categorical and continuous variables. Compared to traditional machine learning models, the proposed TabFuseNet model outperforms models like TabNet, achieving a 20.98% improvement in performance. TabFuseNet is suitable for large-scale tabular data processing and is expected to be valuable not only in cancer prediction but also in various other fields.

II. Dataset

A. Data source

This study used data from the Sample Cohort DB provided by the National Health Insurance Service of Korea (NHISS). The Sample Cohort DB includes data from approximately one million individuals eligible for health insurance in 2002, with a 12-year cohort dataset from 2002 to 2013. The dataset contains demographic, health, and medical data, including health check-ups, treatment records, and medical institution information. All patient data were anonymized to ensure confidentiality.

B. Feature Selection

The study identified major risk factors for predicting the five cancers based on existing research. For liver cancer, variables

included age, sex, income level, obesity, diabetes, and hepatitis. For gastric cancer, key factors included BMI, Helicobacter pylori infection, smoking, and alcohol consumption. For breast cancer, variables like family history and hormone replacement therapy were considered. For lung cancer, smoking intensity, duration, and comorbidities like COPD were key factors. For colorectal cancer, important variables included age, sex, smoking, alcohol consumption, and dietary habits. These factors were obtained from the dataset: demographics from existing data, diseases from ICD-10 codes, and lifestyle factors from health check-ups, forming a comprehensive risk factor set.

C. Data PreProcessing

To select the study population from the sample cohort database collected between 2002 and 2013 (1,125,691 individuals), several exclusion criteria were applied. A total of 337,353 individuals who were not adults during 2007–2008 or who died before 2009 were excluded. Additionally, 488,024 individuals without health check-up records during 2007–2008 were removed. Furthermore, 53,038 individuals with outliers (values exceeding the interquartile range) or missing values in health check-up variables were excluded. Lastly, 58,616 individuals with cancer-related ICD codes recorded before 2009 were excluded. As a result, the final study population consisted of 188,660 individuals, including 2,405 cancer patients and 186,255 non-cancer patients.

During the preprocessing stage, data from 2007–2008 were used to predict cancer occurrences between 2009 and 2013. Explanatory variables included demographic information, health check-up data, and comorbidities, while the outcome variable was newly diagnosed cancer during the follow-up period. Defining the observation period allowed for a systematic analysis of the relationship between variables and cancer incidence.

III. Model

In this study, we compare the performance of the proposed TabFuseNet model with basic Machine Learning and Deep Learning models. As shown in Figure 1, we analyze health-related information to classify individuals as either cancer or normal. (A) The NHISS dataset includes health check-up records, medication history, and disease history. (B) The study uses medication history, past disease history, health check-up data, smoking status, drinking status, and family disease history. (C) Preprocessing removes outliers and ensures data from 2007-2008, excluding individuals under 19. (D) The TabFuseNet model categorizes data into Categorical and Continuous groups, learns their features separately, and integrates them into a single layer.

A. Proposed Model: TabFuseNet

Medical datasets contain categorical and continuous variables, requiring specialized architectures to learn relationships effectively. The existing model, TabTransformer [7], has limitations in integrating these variables. The proposed deep learning model, TabFuseNet, processes categorical and continuous data separately before integrating them to enhance predictive performance.

1) Limitations of Existing Models: Traditional deep learning models for tabular medical data have several limitations. One major drawback is their inability to effectively learn representations for continuous variables. For instance, TabTransformer primarily utilizes a Transformer encoder to capture interactions among categorical variables, while continuous variables are incorporated into the network without additional transformations. This approach may limit the model's ability to capture complex patterns in continuous attributes such as age, laboratory test values, and vital signs.

Another limitation is the insufficient optimization of categorical variable interactions. Transformer-based architectures treat all categorical variables uniformly, but in medical datasets, certain categorical variables (e.g., disease history, medication types) exhibit stronger interdependencies than others, requiring a more refined feature-learning approach.

2) Feature Processing Pipeline: TabFuseNet addresses these limitations by implementing a tailored feature processing pipeline that separately handles categorical and continuous variables before integration.

In TabFuseNet, categorical variables undergo label encoding for two primary reasons: (1) medical datasets contain high-cardinality categorical variables, making one-hot encoding computationally expensive and inefficient, and (2) many categorical values carry inherent ordinal or severity-based relationships. For example, patient risk categories such as *low, medium, and high* imply a ranking structure that one-hot encoding fails to preserve. Label encoding ensures that categorical variables retain their ordinal properties, enabling the model to learn meaningful representations.

After encoding, categorical variables are mapped to embedding layers and then processed through a Transformer encoder to capture complex dependencies among categorical variables. The Transformer mechanism enables the model to automatically learn relationships between categorical features, improving predictive performance and reducing redundancy.

3) Model Architecture: Once categorical and continuous features are independently processed, TabFuseNet integrates them through a structured feature fusion mechanism. The outputs from the categorical Transformer encoder and the continuous feature transformation module are concatenated into a unified representation. This combined feature vector is then passed through a fully connected network (FCN), which refines feature interactions and optimizes predictive performance.

To enhance generalization and mitigate overfitting, dropout regularization is applied to the FCN layer. The final classification is performed using a softmax activation function, which outputs the predicted probability distribution for disease risk assessment.

4) Model Training: The training process of TabFuseNet follows a structured optimization pipeline. Cross-entropy loss is used for multi-class classification tasks, ensuring robust optimization. The model is trained using the Adam optimizer

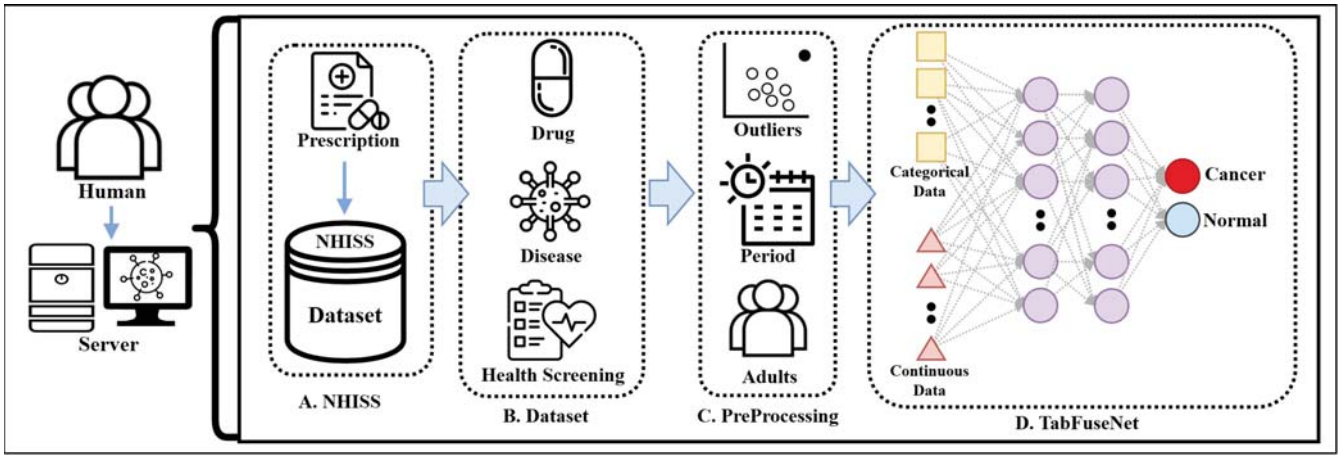


Fig. 1. Framework: Cancer Prediction Model Based on Sample Cohort Data. (a) Preprocessing steps. (b) Splitting into train and test sets for five cancer types. (c) Separation of categorical and continuous features for TabFuseNet. (d) Evaluation metrics for comparison.

with weight decay to stabilize convergence. Dropout and weight decay are incorporated into the network to prevent overfitting. Early stopping is applied based on validation loss to ensure optimal model performance, while the Area Under the Precision-Recall Curve (AUPRC) is used as a key evaluation metric. To further optimize learning, 20 hyperparameter optimization trials were conducted to refine key parameters such as the learning rate, batch size, and dropout rate.

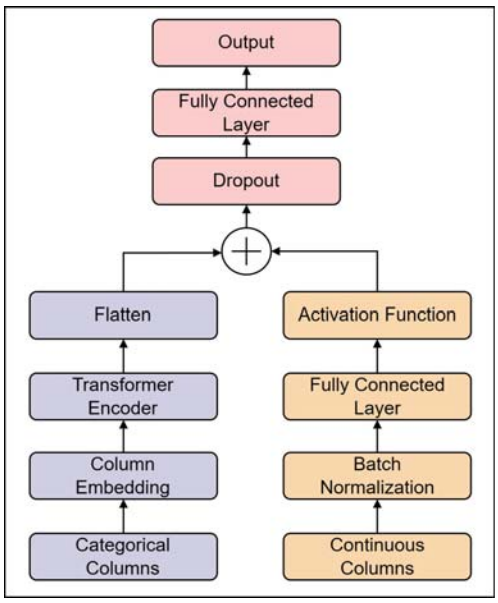


Fig. 2. Architecture of TabFuseNet: categorical features are processed via a Transformer encoder, while continuous features undergo transformation before fusion.

IV. Results

In this study, the environment used was OS: Linux, RAM: 32GB, RTX 4070, Python 3.10, and CUDA 12.2. Results were compared for five cancers: breast, colorectal, liver, lung, gastric. For accurate performance measurement, cross-validation was performed, and four evaluation metrics—F1-Score, AUPRC (Area Under the Precision-Recall Curve), AUC (Area Under the Receiver Operating Characteristic Curve), and Accuracy—were used to assess the performance of the proposed model. K-Fold Cross-Validation [8], [9] was applied, splitting the dataset into five parts with alternating test/train sets.

A. Comparison of Machine Learning and Deep Learning Models

Machine learning refers to the field of computer algorithms that learn patterns from data and make predictions or decisions. In this study, we used tabular datasets, such as health check-up data, prescription, and drug data, making it suitable for machine learning. Specifically, this study employed Random Forest [10], LightGBM (Light Gradient Boosting Machine) [11], XGBoost (eXtreme Gradient Boosting) [12], and SVM (Support Vector Machine).

In this experiment, Machine Learning (ML) was used to classify five types of cancer (Breast, Colorectal, Liver, Lung, Gastric) and normal cases. Table I presents the prediction results for the five types of cancer using four ML models (SVM, XGBoost, Random Forest, LightGBM). Generally, Random Forest showed high performance in Colorectal and Gastric cancers, and was observed to be the best-performing ML model. This can be interpreted as XGBoost efficiently learning the relationships between variables in the rich dataset. In the case of SVM, most of the performance was low, which is due to its inability to effectively learn the nonlinear and complex patterns present in the dataset used in this study.

The dataset used in this study is nonlinear and includes complex interactions, limiting the performance of machine learning (ML) models. Therefore, deep learning (DL) models were used to learn these complex relationships. Table II presents the results of comparing four DL models (CNN, TabNet, TabTransformer, and TabFuseNet) for five types of cancer.

TABLE I
PERFORMANCE COMPARISON OF MACHINE LEARNING MODELS(SVM, XGBOOST, RANDOM FOREST, LIGHTGBM) BY CANCER TYPE.

Model	Cancer Type	F1-Score	AUPRC	AUC	ACC
SVM	Breast	0.7199	0.6797	0.7558	0.7060
	Colorectal	0.7128	**0.8751**	0.7904	0.7087
	Liver	0.7931	0.8751	0.8827	0.7943
	Lung	0.7644	0.8314	0.8494	0.7705
	Gastric	0.7162	0.7579	0.7859	0.7172
XGBoost	Breast	0.8440	**0.8761**	0.9060	0.8373
	Colorectal	0.7282	0.8481	0.8611	0.7850
	Liver	**0.8703**	0.9350	0.9323	**0.8679**
	Lung	**0.8438**	0.9114	**0.9118**	**0.8451**
	Gastric	0.7774	0.8364	0.8486	0.7761
Random Forest	Breast	0.8469	0.8686	**0.9119**	0.8418
	Colorectal	**0.7906**	0.8605	**0.8626**	**0.7975**
	Liver	0.8541	0.9240	0.9244	0.8528
	Lung	0.8328	0.9130	0.9063	0.8343
	Gastric	**0.7931**	**0.8665**	**0.8710**	**0.7989**
LightGBM	Breast	**0.8559**	0.8645	0.9074	**0.8493**
	Colorectal	0.7844	0.8681	0.8598	0.7842
	Liver	0.8592	**0.9366**	**0.9332**	0.8545
	Lung	0.8228	**0.9188**	0.9085	0.8224
	Gastric	0.7755	0.8581	0.8601	0.7761

The results show that the TabFuseNet model significantly outperforms the other DL models for most cancers, thanks to its ability to handle categorical and numerical data simultaneously. It generates embeddings for categorical variables and uses the attention mechanism to analyze factors influencing cancer and learn correlations effectively. Compared to ML models, TabFuseNet performs better for all cancers except Colorectal, which has fewer variables, suggesting insufficient training for deep learning models to analyze its complex patterns.

TABLE II
PERFORMANCE COMPARISON OF DEEP LEARNING MODELS(CNN, TABNET, TABTRANSFORMER, TABFUSENET) BY CANCER TYPES.

Model	Cancer Type	F1-Score	AUPRC	AUC	ACC
CNN	Breast	0.7042	0.7079	0.7692	0.7104
	Colorectal	0.7249	0.7719	0.7940	0.7264
	Liver	0.7980	0.9008	0.8982	0.7993
	Lung	0.7881	0.8417	0.8602	0.7889
	Gastric	0.7123	0.7570	0.7854	0.7144
TabNet	Breast	0.7090	0.7124	0.7149	0.7558
	Colorectal	0.6662	0.6703	0.6705	0.7045
	Liver	0.6505	0.6753	0.6539	0.6815
	Lung	0.7100	0.7520	0.7131	0.7701
	Gastric	0.6716	0.6702	0.6762	0.7086
TabTransformer	Breast	0.8980	0.9281	0.9358	0.8881
	Colorectal	**0.7881**	0.8576	0.8479	**0.7788**
	Liver	0.8276	0.9188	0.9158	0.8333
	Lung	0.8313	0.9362	**0.9327**	0.8486
	Gastric	0.8253	0.9027	0.9042	**0.8060**
TabFuseNet	Breast	**0.9000**	**0.9404**	**0.9414**	**0.8955**
	Colorectal	0.7561	**0.8617**	**0.8530**	0.7345
	Liver	**0.8491**	**0.9742**	**0.9708**	**0.8667**
	Lung	**0.8482**	**0.9372**	0.9316	0.8432
	Gastric	**0.8360**	**0.9107**	**0.9089**	**0.8294**

V. CONCLUSION

This study presents TabFuseNet, a deep learning model designed to improve cancer classification using tabular data. By handling categorical and continuous variables separately, the model enhances feature representation, leading to more precise feature extraction and better predictive performance. The Transformer encoder effectively captures complex relationships among categorical features, resulting in a more expressive representation. Compared to traditional machine learning models, TabFuseNet consistently delivers improved performance in various cancer types and outperforms deep learning models such as CNN and TabNet by better capturing intricate feature interactions. Beyond performance improvements, its potential for real-world integration remains an important consideration. Future studies should explore its adaptability within EHR systems and assess its feasibility in clinical decision-making workflows. By improving feature representation and leveraging attention mechanisms, TabFuseNet serves as a versatile framework that extends beyond the medical field to other domains relying on tabular data.

ACKNOWLEDGMENT

This work was supported by National Research Foundation (NRF) grants funded by the Ministry of Science and ICT (MSIT) and Ministry of Education (MOE), Republic of Korea (NRF[2021-R1-I1A2(059735)]; RS[2024-0040(5650)]; RS[2024-0044(0881)]; RS[2019-II19(0421)]).

REFERENCES

[1] M. of Health and Welfare, *2023 National Cancer Registration Statistics Project Guide*, 2023, report on the National Cancer Management Project in Korea.

[2] F. X. Zenghong Wu, Rong Lin, "Global burden of cancer and associated risk factors in 204 countries and territories, 1980–2021: a systematic analysis for the gbd 2021," *Journal of Hematology & Oncology*, 2024.

[3] T. P. T. Tran, N. M. Luu, T. T. Bui, M. Han, M. K. Lim, and J.-K. Oh, "Weight-change trajectory in relation to cancer risk: findings from a nationwide cohort study in south korea," *Obesity (Silver Spring)*, 2022.

[4] M. N. Luu, M. Han, T. T. Bui, P. T. T. Tran, M.-K. Lim, and J. K. Oh, "Smoking trajectory and cancer risk: A population-based cohort study," *Tobacco Induced Diseases*, 2022.

[5] T. P. T. Tran, N. M. Luu, T. T. Bui, M. Han, M. K. Lim, and J.-K. Oh, "Trajectory of physical activity frequency and cancer risk: Findings from a population-based cohort study," *European Review of Aging and Physical Activity*, 2023.

[6] T. T. Bui, N. M. Luu, T. P. T. Tran, M. Kyung, and J.-K. Oh, "Cancer risk according to alcohol consumption trajectories: A population-based cohort study of 2.8 million korean men," *Journal of Epidemiology*, 2023.

[7] Q. Huang, Y. Yamada, Y. Tian, and S. Singh, "Tabtransformer: Tabular data modeling using contextual embeddings," in *Proceedings of the AAAI Conference on Artificial Intelligence*, vol. 35, no. 11, 2020, pp. 8425–8433.

[8] R. Kohavi, "A study of cross-validation and bootstrap for accuracy estimation and model selection," in *Proceedings of the 14th International Joint Conference on Artificial Intelligence (IJCAI)*, vol. 14, no. 2, 1995, pp. 1137–1143.

[9] T. Hastie, R. Tibshirani, and J. Friedman, *The Elements of Statistical Learning: Data Mining, Inference, and Prediction*, 2nd ed. New York: Springer, 2009.

[10] L. Breiman, "Random forests," *Machine learning*, vol. 45, pp. 5–32, 2001.

[11] G. Ke, Q. Meng, T. Finley, T. Wang, W. Chen, W. Ma, Q. Ye, and T.-Y. Liu, "Lightgbm: A highly efficient gradient boosting decision tree," in *Advances in Neural Information Processing Systems*, vol. 30, 2017.

[12] T. Chen and C. Guestrin, "Xgboost: A scalable tree boosting system," in *Proceedings of the 22nd ACM SIGKDD International Conference on Knowledge Discovery and Data Mining*, 2016, pp. 785–794.

Implemented Machine Learning Models to Predict Life Satisfaction Using Demographic and Religious Data

Abstract— **The study aims to demonstrate the effectiveness of machine learning in predicting life satisfaction based on demographic and religious factors using data from the World Values Survey (Wave 7). Key variables such as age, sex, income, education level, and religious practices were analyzed using classification models—Random Forest, XGBoost, and Decision Tree. XGBoost emerged as the most effective model. The user interface developed from this model provides predictions of life satisfaction and personalized recommendations, potentially guiding targeted mental health interventions and resource allocation. While the study offers valuable insights, future research could refine the model by incorporating additional psychosocial variables and testing deep learning techniques, such as recurrent neural networks (RNNs). Integrating real-time or longitudinal data could also improve the model's adaptability across diverse populations, advancing its applicability in community-based programs and policymaking.**

Keywords—Predictive Modeling, Life Satisfaction, Mental Health, Artificial Intelligence, Demographics

I. Introduction

Life satisfaction is central to human life, influencing mental health, social relationships, and overall quality of life. Understanding the factors contributing to life satisfaction has become increasingly important across various fields. Studies have shown that both demographic and religious factors play significant roles in shaping an individual's life satisfaction, which is often a measure of well-being [1]-[11].

Despite research on the impact of these factors, there remains a gap in literature on how these factors interact and how they can be used collectively to predict life satisfaction. [12].

Artificial intelligence (AI) offers an innovative approach to this issue. Machine learning models have demonstrated significant potential in identifying patterns and relationships within large, complex datasets [13]. Using such models, we can analyze the effect of demographic and religious factors on life satisfaction in a way that traditional methods cannot.

The study seeks to develop an optimal classification model that uses demographic and religious data to predict an individual's life satisfaction. Using the model, an interface will be created that provides predictions of the user's life satisfaction and personalized recommendations for improving it. We hypothesize that religious affiliation is a significant predictor of self-reported life satisfaction and may show a stronger association than other variables.

The study has three specific objectives: (1) to determine if demographic and religious variables can predict life satisfaction, (2) to identify which specific demographic or religious factors have the strongest impact on predicting life satisfaction, (3) to develop an interface that predicts the user's life satisfaction and provides recommendations to improve it.

II. Literature Review

Research has shown that both demographic factors (e.g., age, education, income) and religious involvement significantly impact life satisfaction. Regular spiritual practices, including service attendance and personal prayer, contribute to higher life satisfaction through social connection and stress relief [1]-[11].

In recent years, researchers have increasingly applied machine learning techniques to unravel the complex determinants of life satisfaction. These models can process large datasets and identify intricate patterns that traditional statistical methods might overlook.

For example, a study using data from over 19,000 individuals in Denmark applied ensemble machine learning methods and large language models (LLMs) to predict life satisfaction, which helped improve the interpretability of the model [14]. Similarly, an analysis of over 34,000 older adults from the RAND Health and Retirement Study used Support Vector Regression (SVR) to model life satisfaction, outperforming traditional linear regression approaches in capturing nonlinear relationships [15].

While there are more advancements in life satisfaction prediction, challenges remain. Many models still struggle with consistent interpretability and the incorporation of factors like religious influence, which can be vital to understanding life satisfaction. Additionally, existing models often focus primarily on correlations without offering actionable insights. This study addresses these gaps by integrating demographic and religious variables into an explainable AI framework. By prioritizing both accuracy and interpretability, our approach not only enhances prediction but also delivers personalized recommendations through a user-friendly interface, bridging the gap between research and real-world mental health applications.

III. Dataset and Methodology

A. Dataset and Preprocessing

This study used the World Values Survey (WVS), a global project that collected survey data on people's values, beliefs, behaviors, and demographics. Specifically, data from WVS Wave 7 [16] was used since it provides the most recent available information collected from 2017 to 2022. Using the latest wave ensures the data accounts for recent demographic trends and social shifts.

B. Data Selection

The data selection focused on variables related to religious practices, demographic characteristics, and personal life satisfaction.

These variables were chosen because they capture key factors that have been shown to influence an individual's mental and emotional state, contributing to their overall life satisfaction.

979-8-3315-4248-1/25/$31.00 ©2025 IEEE

C. Data Cleaning

Data preprocessing was conducted by first handling missing or non-informative values. Any rows containing negative values were filtered out, as these indicate unusable data. The dataset was reduced to only complete and valid entries that value all desired variables for the input vector.

D. Target Variable Transformation

The target variable, life satisfaction, was transformed into a binary classification variable, with values above 5 indicating high life satisfaction (1) and values of 5 or below indicating low life satisfaction (0).

E. Encoding and Transformation of Categorical Variables

Categorial variables from the dataset were encoded. Question 260 about the sex of the participant was converted to a binary feature (male = 0, female = 1) to represent sex numerically to simplify its inclusion in the model. One-hot encoding was applied to questions 173 and 273 to ensure the model can distinguish between the categories without implying any ordinal relationship.

For variables that use numeric data types to represent categories or ordered responses, a label encoding technique was applied. Categorial responses were transformed into numeric representations, creating a model-ready, entirely numeric dataset.

TABLE I.

DESCRIPTION OF DATASET VARIABLES FROM WVS

WVS Question Number	Description	
	Description	***Values/Range***
6	Importance of religion in one's life	1 (Very important) to 4 (Not at all important)
47	Self-rated health	1 (Very good) to 5 (Very poor)
49	Life satisfaction	1 (Completely dissatisfied) to 10 (Completely satisfied)
50	Financial satisfaction	1 (Completely dissatisfied) to 10 (Completely satisfied)
164	Importance of God in one's life	1 (Not at all important) to 10 (Very important)
171	Frequency of attending religious services	1 (More than once a week) to 7 (Never, practically never)
172	Frequency of personal prayer	1 (Several times a day) to (Never, practically never)
173	Self-identification as a religious person	1 (A religious person) to 3 (An atheist)
260	Sex	1 (Male), 2 (Female)
262	Age	0-99
273	Martial Status	1 (Married), 2 (Living together as married), 3 (Divorced), 4 (Separated), 5 (Widowed), 6 (Single)
275	Education level	0 (Early childhood education/no education) to 8 (Doctoral or equivalent)
288	Income group in relation to the country one resides in	1 (Lowest group) to 10 (Highest group)
289	Religious affilation	0 (Do not belong to a denomination), 1 (Roman Catholic), 2 (Protestant), 3 (Orthodox), 4 (Jew), 5 (Muslim), 6 (Hindu), 7 (Buddhist), 8 (Other)

F. Dataset Balancing

The target variable in our study, life satisfaction, was imbalanced, with the positive life satisfaction class outnumbering the others. The imbalance was making the model biased towards the majority class, potentially compromising the accuracy and generalizability of predictions of the minority class. To address this, we implemented the Synthetic Minority Over-sampling Technique (SMOTE).

SMOTE creates synthetic samples for the minority class by interpolating between existing data points, balancing the class distribution. For the study, SMOTE was implemented with k_neighbors = 5 to create realistic samples that maintain the underlying relationships within the data.

G. Model Selection and Development

After preprocessing, various machine learning algorithms were applied to the dataset. These include the Random Forest Classifier, XGBoost, and Decision Tree classification models. The hyperparameters were tuned for each model, as shown in Table 2.

TABLE 2.

HYPERPARAMETERS OF CLASSIFCATION MODELS

Classification Model	Hyperparameters
	Parameter Tunning
Random Forest	n_estimators=200,max_depth=15,min_samples_split=5, class_weight='balanced_subsample', min_samples_leaf=4, n_jobs=-1
XGBoost	n_estimators=200,max_depth=6,learning_rate=0.1,scale_pos_weight=1,n_jobs=-1,objective='binary:logistic', use_label_encoder=False
Decision Tree	max_depth=6,min_samples_split=5, min_samples_leaf=4, class_weight='balanced'

H. Interface Creation

An interface was developed using React JavaScript and Flask to provide a practical application of the trained model. The primary function of the interface is to collect user data, process it through the machine learning model, and return actionable suggestions for enhancing life satisfaction.

1) User Input: Users input their demographic and religious data via a POST request to the /predict API

endpoint. The data is provided in JSON format and includes the same variables as in Table 1.

2) Model Processing: After receiving the user input, the Flask server preprocesses the data to match the format required by the machine learning model. Categorical features are encoded using pre-trained encoders. The processed data is then passed to the trained model for prediction. The model outputs a probability score, representing the likelihood of the user experiencing high life satisfaction.

3) Suggestions Generation: In addition to the life satisfaction prediction, the interface provides personalized suggestions based on the most influential features derived from the model. These features are identified using feature importance metrics. The interface generates a list of suggestions tailored to the user's input, offering specific actions they can take to improve their life satisfaction.

4) User Output: The results of the prediction and suggestions are returned to the user in a JSON response. The response includes the predicted probability of high life satisfaction and a list of personalized recommendations.

I. Evaluation Metrics

Several metrics were used to evaluate the performances of the Random Forest, XGBoost, and Decision Tree models. Accuracy, precision, recall, F1 score, and ROC AUC were used to comprehensively assess each model's effectiveness.

J. Feature Importance Analysis

A feature importance analysis was conducted using each model's built-in features and techniques.

The Random Forest Classifier model found feature importance using the mean decrease in Gini impurity across all trees in the forest. XGBoost computes feature importance based on how often a feature is used to split data points in the decision trees it generates, as well as the improvement in model accuracy or reduction in impurity achieved by each split. Decision Trees rank features based on how much each feature reduces impurity across all splits in the tree.

K. Models Training and Testing

Each model was trained and evaluated using a 0.8 training-testing split. 86,464 samples from the WVS Wave 7 dataset were used for model development. Of this, 69,171 samples were allocated for training, while 17,293 samples were reserved for testing the model's performance.

For model training, 10-fold cross-validation was applied. Each fold consisted of a training and validation set, which helped optimize each model's parameters and assess its performance.

IV. Results

The experiment was conducted on the WVS Wave 7 dataset, and related results were obtained.

A. Comparision of Model Performance

The models were compared across all metrics to assess which model performed best on the task of predicting life satisfaction.

TABLE 3.

EVALUATION METRICS OF THE MODELS

Classification Model	Metrics				
	Accuracy	***Precision***	***Recall***	***F1 Score***	***ROC AUC***
Random Forest	77.83%	0.8857	0.8177	0.8504	0.8050
XGBoost	79.43%	0.8747	0.8555	0.8650	0.8178
Decision Tree	75.81%	0.8967	0.7752	0.8315	0.7935

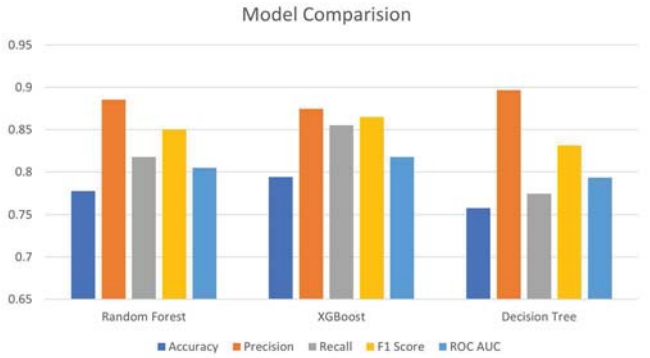


Fig 1. Bar graph representation of the performance metrics across XGBoost, Random Forest, and Decision Tree models.

As shown in Table 3, Fig. 1, and Fig. 2, XGBoost outperformed the other models across most evaluation metrics. It achieved the highest accuracy (79.43%) and the highest ROC AUC (0.8178), making it the most reliable model for predicting life satisfaction in this dataset. Additionally, XGBoost exhibited a higher F1 score, further contributing to its superior overall performance compared to the other models.

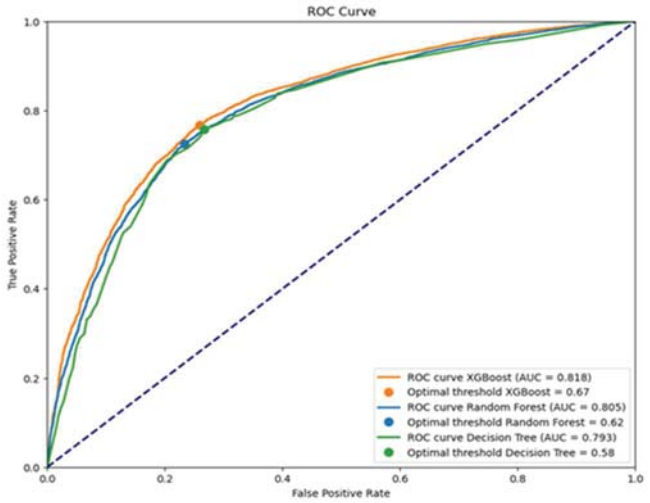


Fig 2. Comparative ROC Curve illustrating the performance of XGBoost, Random Forest, and Decision Tree models in predicting life satisfaction.

B. Feature Importance Analysis

Feature importance analysis was performed to identify which variables had the most significant impact on predicting life satisfaction. For the XGBoost model, the top features include religious affiliation and financial satisfaction. For the Random Forest model, the top features were financial satisfaction, age, and marital status. These features were responsible for the highest reduction in impurity and had the

most influence on the model's predictions. The Decision Tree model showed financial satisfaction, religious affiliation, and marital status as features with the most importance in predicting life satisfaction.

V. Discussion

The results of this study demonstrate that machine learning models are highly effective in predicting life satisfaction based on demographic and religious factors, offering valuable insights into subjective well-being. XGBoost exhibited the strongest performance across evaluation metrics, reinforcing its suitability for modeling complex interactions between demographic characteristics and life satisfaction. Feature importance analysis revealed that financial satisfaction, religious affiliation, and marital status were among the most influential predictors, emphasizing the role of economic stability, spirituality, and social support networks in well-being.

The practical implications of these findings are significant. The developed user interface translates model predictions into personalized recommendations, providing individuals with actionable insights to improve well-being. Mental health practitioners can use this tool to identify high-risk populations and tailor interventions accordingly. Policymakers can leverage these insights to allocate resources more effectively, targeting financial literacy programs, social support initiatives, and mental health resources to vulnerable communities.

Although the study offers valuable findings, certain limitations remain. The reliance on self-reported survey data introduces potential biases, such as social desirability bias and subjective misinterpretation of survey questions. Additionally, while traditional machine learning models offer strong predictive power, they may not fully capture highly nonlinear relationships. Future work could explore deep learning architectures like recurrent neural networks (RNNs) to enhance predictive accuracy, though these require larger datasets and increased computational resources to avoid overfitting. Incorporating real-time or longitudinal data could further improve the model’s ability to track changes in life satisfaction over time.

VI. Conclusion

This study demonstrates the potential of machine learning in predicting life satisfaction by integrating demographic and religious factors. By leveraging XGBoost, Random Forest, and Decision Trees, the model provides both high accuracy and interpretability, bridging the gap between AI-driven prediction and real-world application.

Beyond prediction, the developed user interface offers a practical tool for individuals, mental health practitioners, and policymakers to make data-driven decisions aimed at improving well-being. While traditional models performed well, future research should consider deep learning approaches to capture more complex relationships. Additionally, addressing dataset limitations and expanding predictive variables could further enhance model reliability and applicability.

By refining machine learning applications in mental well-being research, this study contributes to the growing field of AI-driven mental health support, offering a scalable, data-driven approach to understanding and improving life satisfaction at both individual and societal levels.

VII. References

[1] Y. Ding, H. Zhang, H. Zhang, J. Li, and Y. Liu, "The influence of subjective socioeconomic status on life satisfaction: A chain mediation model of social equity and social trust," Int. J. Environ. Res. Public Health, vol. 19, no. 23, p. 16072, Nov. 2022.

[2] M. Joshanloo and V. Jovanović, "The relationship between gender and life satisfaction: analysis across demographic groups and global regions," Arch. Womens Ment. Health, vol. 23, no. 3, pp. 331-338, Jun. 2020.

[3] S. D. Barger, C. J. Donoho, and H. A. Wayment, "The relative contributions of race/ethnicity, socioeconomic status, health, and social relationships to life satisfaction in the United States," Qual. Life Res., vol. 18, no. 2, pp. 179-189, Mar. 2009.

[4] C. Lim and R. D. Putnam, "Religion, Social Networks, and Life Satisfaction," Amer. Sociol. Rev., vol. 75, no. 6, pp. 914-933, Dec. 2010.

[5] G. Ironson and S. S. Ahmad, "Frequency of Private Prayer Predicts Survival Over 6 Years in a Nationwide U.S. Sample of Individuals with a Chronic Illness," J. Relig. Health, vol. 63, pp. 2910-2923, 2024.

[6] M. Babula, "The Association of Prayer Frequency and Maslow's Hierarchy of Needs: A Comparative Study of the USA, India and Turkey," J. Relig. Health, vol. 62, no. 3, pp. 1832-1852, Jun. 2023.

[7] A. King, "The Nature of Christian Prayer," The McKendree University Journal of Undergraduate Research, vol. 5, 2023. [Online]. Available: https://www.mckendree.edu/academics/scholars/issue5/king.htm

[8] D. Möwisch, A. Brose, and F. Schmiedek, "Do Higher Educated People Feel Better in Everyday Life? Insights From a Day Reconstruction Method Study," Soc. Indic. Res., vol. 153, pp. 227-250, 2021.

[9] M. F. Purol, V. N. Keller, J. Oh, W. J. Chopik, and R. E. Lucas, "Loved and lost or never loved at all? Lifelong marital histories and their links with subjective well-being," J. Posit. Psychol., vol. 16, no. 5, pp. 651-659, Jul. 2021.

[10] B. M. Baird, R. E. Lucas, and M. B. Donnellan, "Life Satisfaction Across the Lifespan: Findings from Two Nationally Representative Panel Studies," Soc. Indic. Res., vol. 99, no. 2, pp. 183-203, Nov. 2010.

[11] Y. J. Masuda, J. R. Williams, and H. Tallis, "Does Life Satisfaction Vary with Time and Income? Investigating the Relationship Among Free Time, Income, and Life Satisfaction," J. Happiness Stud., vol. 22, pp. 2051-2073, Jun. 2021.

[12] J. Potter, R. Cantarero, and H. Wood, "The Multi-Dimensional Nature of Predicting Quality of Life," Procedia - Social and Behavioral Sciences, vol. 50, pp. 781-790, 2012.

[13] F. Thiele, A. J. Windebank, and A. M. Siddiqui, “Motivation for using data-driven algorithms in research: A review of machine learning solutions for image analysis of micrographs in neuroscience,” Journal of Neuropathology and Experimental Neurology, vol. 82, no. 7, pp. 595–610, May 2023, doi: https://doi.org/10.1093/jnen/nlad040.

[14] A. E. Khan, M. J. Hasan, H. Anjum, N. Mohammed, and S. Momen, “Predicting life satisfaction using machine learning and explainable AI,” Heliyon, vol. 10, no. 10, p. e31158, May 2024, doi: https://doi.org/10.1016/j.heliyon.2024.e31158.

[15] X. Shen, F. Yin, and C. Jiao, “Predictive Models of Life Satisfaction in Older People: A Machine Learning Approach,” International Journal of Environmental Research and Public Health, vol. 20, no. 3, p. 2445, Jan. 2023, doi: https://doi.org/10.3390/ijerph20032445.

[16] C. Haerpfer et al., "World Values Survey: Round Seven - Country-Pooled Datafile Version 5.0," JD Systems Institute & WVSA Secretariat, Madrid, Spain & Vienna, Austria, 2022. [Online]. Available: doi:10.14281/18241.24

Integrating Machine Learning For Automated Root Cause Analysis Of Critical-To-Quality (CTQ) In Hard Disk Drive Manufacturing

1st Mullika Inpang
Department of Artificial Intelligence for Business Analytics
Faculty of Information Technology
King Mongkut's Institute of Technology Ladkrabang
Bangkok Thailand
66076031@kmitl.ac.th

2nd Bundit Thanasopon
Department of Artificial Intelligence for Business Analytics
Faculty of Information Technology
King Mongkut's Institute of Technology Ladkrabang
Bangkok Thailand
bundit@it.kmitl.ac.th

***Abstract*—This research was studying the process of analyzing key factors that significantly impact the quality of Head Stack Assembly (HSA) in the production of Hard Disk Drives (HDDs). Various factors are considered, such as production machine, testing equipment, lot numbers of raw materials, production time and testing times etc. The assembly of the Head Stack is a critical step in Hard Disk Drives manufacturing. As the number of heads increases, the process requires greater precision and careful consideration of multiple factors. The use of artificial Intelligence technology in research is to be able to analyze the causal factors that affect the assembly of Head Stack more quickly and accurately in order to help reduce damage that will affect the production process and the quality of the Hard Disk Drives. It also increases the reliability of the product and raises the production standards, including quality control for the Hard Disk Drives manufacturing industry.**

Keywords—head stack assembly, hard disk drives, artificial intelligence

I. INTRODUCTION

Today, in the hard disk drive (HDD) manufacturing industry, there is high competition around product and technology quality to meet market and customers demand. Quality in the manufacturing process is therefore essential. Management of critical-to-quality (CTQ) [1] parameters in HDD manufacturing is vital as it impacts the product's performance and reliability. The head stack assembly (HSA) needs to consider factors related to quality, which are examined in the testing phase following the assembly process. Conventional practices of determining the root causes that influence the production quality depend manually on the expertise of professionals who review and ascertain abnormalities in the data. It is a time-consuming process and may cause inaccuracy due to the growing volume and complexity of the data. Also, relying on human judgment to notice these anomalies can lead to a lag in the detection of such anomalies, thus permitting below-standard products, which are manufactured through defective processes, to reach customers.

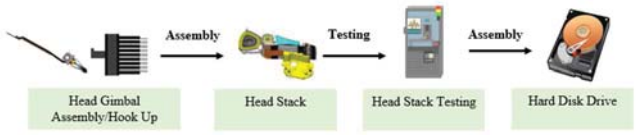


Fig. 1. Hard Disk Drive assembly process

Due to the constraints and complexities of conventional data analysis techniques, machine learning technology has been applied in Root Cause Analysis (RCA) [2] to identify head stack assembly quality variables. The technique offers more accurate outputs, enables faster root cause diagnosis and associated issues identification. Consequently, the manufacturing process enhances both product quality and machine performance. In addition, the technology improves quality control and prevention, such that all the products delivered to customers are of the highest quality. As a result, it grows the credibility of the products as well as the organization.

II. RELATED WORKS

A. Anomaly Detection

This research applies Statistical Process Control (SPC) to manage CTQ parameter variations, facilitating the detection of problems and enhancing continuous process improvements. SPC is used widely across various industries to detect abnormalities and provide stability to production.

Example research that utilizes Statistical Process Control (SPC) for defect analysis through the application of deep learning by autoencoders, with the use of parameter control statistics to establish injective functions [3], is the LSTM-Autoencoder (LSTM-AE) method. The LSTM-Autoencoder (LSTM-AE) method facilitates the evaluation of real-time performance on the production line. The research outcome shows that the method not only improves efficiency but also saves costs and ensures product quality in the industry.

B. Root Cause Analysis (RCA)

Machine Learning techniques are utilized to conduct RCA in HSA production. Data is categorized into parametric and attribute-based variables, focusing on attribute-based data, as experts have confirmed its strong correlation with CTQ factors. The research integrates Machine Learning models such as Random Forest and XGBoost to analyze and rank influential factors.

An example of related research utilizing machine learning techniques for Root Cause Analysis (RCA) is a study that uses the Random Forest technique to identify the root causes of issues within a network [4]. This approach was developed for tracking and analyzing customer experience from end to end. It helps pinpoint networking errors, locate defective components, and estimate the severity of the issues

XXX-X-XXXX-XXXX-X/XX/$XX.00 ©20XX IEEE

based on related data. The findings of this analysis enable the prioritization of maintenance tasks and the adjustment of dynamic indicators to align with the current situation.

The experimental results demonstrated that this method effectively supports network operations. In addition, the focus will shift toward further developing the algorithm to enhance its effectiveness, including advancements in technology to support analysis in 4G and 5G networks.

Another example is the use of the Perm-Boost model, which combines permutation importance and XGBoost, to predict software defects (SDP) and conduct Root Cause Analysis (RCA) [5]. This model demonstrated accuracy, precision, recall, and F1 scores ranging from 97% to 99%, with AUC-ROC values exceeding 99%. These results highlight the effectiveness of the prediction. Base on the data availability and the researchers involved in the RCA, the author applies machine learning through a method known as supervised learning [6]. Random Forest and XGBoost are the primary models that were chosen by the author.

III. RESEARCH METHODOLOGY

The primary objective of this research is to develop a machine learning model that assesses the determinants influencing the quality of hard disk drive manufacturing in the HSA assembly process. For this purpose, the data science lifecycle [7] is customized accordingly, beginning from data collection, data preprocessing, statistical calculations, model development, model assessment, reporting results, and model deployment, respectively.

A. Data Collection

Multiple sources will be used for data collection, such as materials/components detail, manufacturing information, test and information for machines involved in manufacture and testing. Model will be trained using data collected from May 1, 2024, to May 31, 2024. There will be 81 features to utilize as input for the learning model.

B. Data Preparation

Data preparation with data cleaning which involves processing abnormal data such as the outliers' removal and missing value handling by replacing them with appropriate values such as the mean, median, or mode.

Categorical data will be transformed into a structure that is interpretable by the model using One-Hot Encoding [8]. Simultaneously, Feature Engineering will be a task of developing new variables that pertain to the specific issue in question.

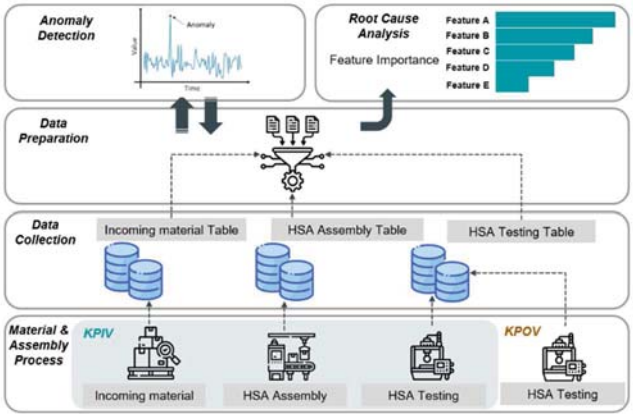


Fig. 2. Manufacturing Data Analytics Workflow

The issue of imbalanced data has, in this instance, been resolved through the application of the SMOTE (Synthetic Minority Over-sampling Technique) [9]. It is applied to enlarge the data that is in the underrepresented class, thereby providing a more balanced dataset that will enable superior learning outcomes for the model. Another important stage is identifying the relationship that is present in the data through checking the interrelations among variables.

This assists in identifying which variables are significant and should therefore be prioritized during model development, while minimizing irrelevant variables in order to make the learning process of the model effective.

C. Statistical Processes for Anomaly Detection

Anomaly Detection using Statistical Process Control (SPC) methods: In this research, we aim to monitor the variable machd_rsa, which is considered one of the Key Process Output Variables (KPOV) of the head arm assembly process, reflecting the quality of the production process.

During data collection, The interest variables are filtered down to match KPOV and set the event time intervals to hourly levels that suit with the analysis. Then, the data will be divided and only clusters that contain sufficient data (at least 30 data points in a cluster) will be utilized resulting a better precision.

The average value, upper and lower control limits (UCL and LCL) will be calculated based on provided statistical formulas. The UCL and LCL will be set at three standard deviations away from the mean to indicate data limits. After that, the results will be displayed in the form of an SPC Chart, with the value of machd_rsa plotted as data points versus calculated control limits.

Data points outside the UCL or LCL range will be highlighted as Out of Control, indicating abnormal occurrences in the manufacturing process.

The result of Anomaly Detection based on SPC for the variable machd_rsa is that on May 31, 2024, an anomaly was found, the value of machd_rsa moved out of the control range (Out of Control) and away from the specified UCL limit.

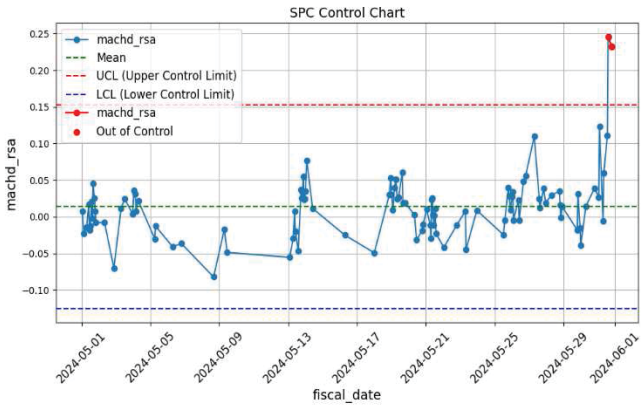


Fig. 3. Process Anomalies, SPC Chart Identifying Triggering KPOV

This is considered as an anomaly in the production process. Anomaly Detection enables the detection of abnormal data effectively, which can then be examined to find the cause of the anomaly (Root Cause Analysis) so that the actual cause of the issue can be further investigated.

D. Developing the Root Cause Analysis Model

The models utilized in the RCA are Logistic Regression, Random Forest, XGBoost, Support Vector Machine (SVM), and Decision Tree methods.

These analytical tools are utilized to establish the relations between the Key Process Input Variables (KPIVs) and the Key Process Output Variables (KPOVs) with emphasis on the evaluation of Feature Importance for each model to identify the influencing factors with the highest contribution to product quality.

In training models, the data are divided into an 80% training set and a 20% test set. Each model was parameter-tuned and trained. Grid Search [10] and Cross-Validation [11] techniques used for improved prediction accuracy.

Feature Importance ranking in RCA is an important process as it helps us identify and prioritize the variables that have the most impact on the issue.

The accuracy of Feature Importance can be assessed by testing the performance of the model, by plotting an SPC Chart showing the relationship between Feature Importance and the dependent variable (KPOV). This allows us to narrow down the parameters of the problem and quickly find the root cause, as well as enabling effective corrective actions.

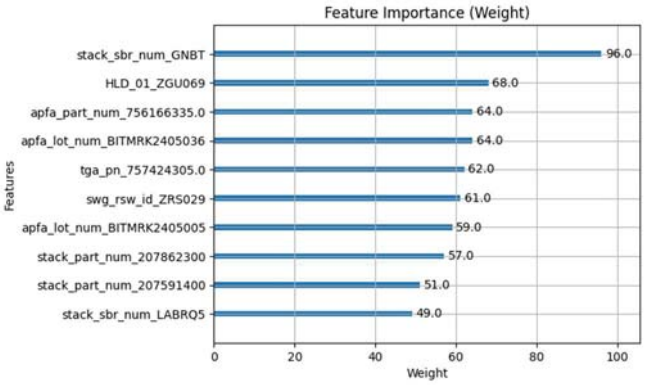


Fig. 4. Feature Importance Ranking

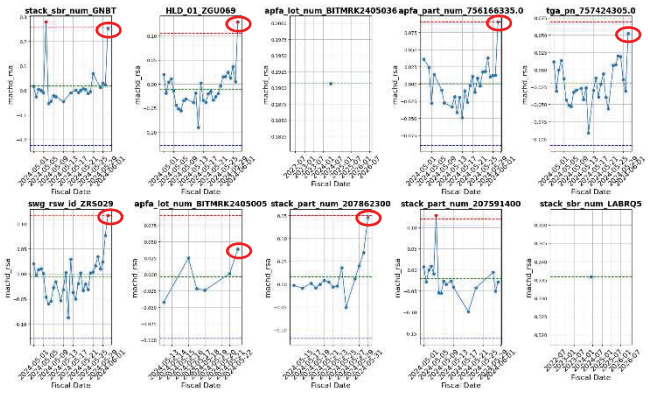


Fig. 5. SPC Chart (actual values) for each feature obtained from the model's Feature Importance

IV. RESULTS

The performance test results of the model in predicting Feature Importance were evaluated by comparing them with the actual values obtained from plotting the SPC Chart. The Confusion Matrix [12] was used as a criterion to measure the model's accuracy through Accuracy, Precision, Recall, and F1-score, allowing for the analysis and assessment of the prediction's correctness.

The results show that XGBoost is the most efficient model for RCA analysis, as it provides the highest Accuracy and F1-score, based on Feature Importance and SPC Chart. Analyzing Feature Importance alongside the SPC Chart, which is derived from actual values obtained. Helps us verify the accuracy of the model, whether the features provided by the model are related to actual anomalies and also helps to better precisely define the scope of issues affecting the production process.

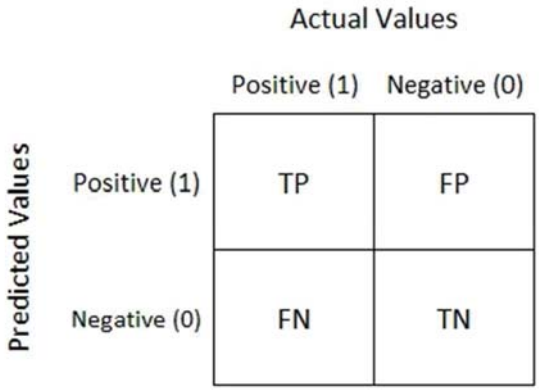


Fig. 6. Confusion Matrix

TABLE I. FEATURE IMPORTANCE OF MODEL COMPARISON

Model	Feature	SPC Out of control or spike Actual	Feature Importance Prediction
XGBoost	stack_sbr_num_GNBT	1	1
	HLD_01_ZGU069	1	1
	apfa_lot_num_BITMRK2405036	0	1
	apfa_part_num_756166335	1	1
	tga_pn_757424305	1	1
	swg_rsw_id_ZRS029	1	1
	apfa_lot_num_BITMRK2405005	1	1
	stack_part_num_207862300	1	1
	stack_part_num_207591400	0	1
	stack_sbr_num_LABRQ5	0	1

(1 = Affects the dependent variable, 0 = Does not affect the dependent variable)

TABLE II. MODELS EVALUATION

Model	Accuracy (%)	Precision (%)	Recall (%)	F1-Score (%)
XGBoost	(7/10) x 100 = 70	(7/10) x 100 = 70	100	2 x (70x100)/(70+100) = **82.35**
Random Forest	(4/10) x 100 = 40	(4/10) x 100 = 40	100	2 x (40x100)/(40+100) = **57.14**
Decision Tree	(3/10) x 100 = 30	(3/10) x 100 = 30	100	2 x (30x100)/(30+100) = **46.15**
Logistic Regression	(1/10) x 100 = 10	(1/10) x 100 = 10	100	2 x (10x100)/(10+100) = **18.18**
SVM	(1/10) x 100 = 10	(1/10) x 100 = 10	100	2 x (10x100)/(10+100) = **18.18**

V. CONCLUSION

The research study on analyzing factors affecting the quality of automated hard disk production in the HSA assembly process, it shows that using Machine Learning techniques to create learning models significantly improves the speed, accuracy, and correctness of problem identification and analysis.

The results not only effectively identify the causes of abnormalities but also minimize the possibility of generating inferior products, promoting a better production process regarding product quality and machine performance. Additionally, they enhance quality control capabilities to ensure that the products delivered to customers are at highest quality and meet the specified standards.

In the future, this research will evolve into a real-time alarm system coupled with a data visualization system. Which will enable operators to continuously monitor production status and receive necessary information for timely decision-making. The system will enhance the speed and accuracy of resolving issues that arise in the production process for improving production efficiency and quality.

REFERENCES

[1] J. Burtner, "Critical-to-quality factors associated with engineering student persistence: the influence of freshman attitudes," 34th Annual Frontiers in Education, Savannah, GA, USA, 2004, pp. F2E-1.J. Clerk Maxwell, A Treatise on Electricity and Magnetism, 3rd ed., vol. 2. Oxford: Clarendon, 1892, pp.68–73.

[2] H. Lal and G. Pahwa, "Root cause analysis of software bugs using machine learning techniques," 2017 7th International Conference on Cloud Computing, Data Science & Engineering - Confluence, Noida, India, 2017, pp. 105-111.

[3] F. Tayalati, I. Boukrouh, L. Bouhsaien, A. Azmani and M. Azmani, "Hybrid Approach Integrating Deep Learning-Autoencoder With Statistical Process Control Chart for Anomaly Detection: Case Study in Injection Molding Process," in *IEEE Access*, vol. 12, pp. 95576-95598, 2024.

[4] L. Liu, K. Zhang, L. Liu, L. Zhang and J. Zhang, "Root cause analysis of network fault based on random forest," *2022 7th International Conference on Communication, Image and Signal Processing (CCISP)*, Chengdu, China, 2022, pp. 1-5.

[5] M. Mustaqeem, S. Mustajab and M. Alam, "Enhancing Software Defect Prediction Through Root Cause Analysis: A Hybrid Approach Integrating Permutation Importance with XGBoost (PERMBoost)," *2024 International Conference on Communication, Computer Sciences and Engineering (IC3SE)*, Gautam Buddha Nagar, India, 2024, pp. 61-67.

[6] Z. Khasidashvili and A. J. Norman, "Range Analysis and Applications to Root Causing," *2019 IEEE International Conference on Data Science and Advanced Analytics (DSAA)*, Washington, DC, USA, 2019, pp. 298-307.

[7] C. Haertel, M. Pohl, D. Staegemann and K. Turowski, "Project Artifacts for the Data Science Lifecycle: A Comprehensive Overview," *2022 IEEE International Conference on Big Data (Big Data)*, Osaka, Japan, 2022, pp. 2645-2654.

[8] C. Daund, S. Bohra, N. Nimbalkar and S. Oak, "Comprehensive Analysis based on One Hot Encoder for Brain Tumor Detection and Classification," *2022 2nd International Conference on Intelligent Technologies (CONIT)*, Hubli, India, 2022, pp. 1-5.

[9] G. A. Pradipta, R. Wardoyo, A. Musdholifah, I. N. H. Sanjaya and M. Ismail, "SMOTE for Handling Imbalanced Data Problem : A Review," *2021 Sixth International Conference on Informatics and Computing (ICIC)*, Jakarta, Indonesia, 2021, pp. 1-8.

[10] Pirjatullah, D. Kartini, D. T. Nugrahadi, Muliadi and A. Farmadi, "Hyperparameter Tuning using GridsearchCV on The Comparison of The Activation Function of The ELM Method to The Classification of Pneumonia in Toddlers," *2021 4th International Conference of Computer and Informatics Engineering (IC2IE)*, Depok, Indonesia, 2021, pp. 390-395.

[11] S. Yadav and S. Shukla, "Analysis of k-Fold Cross-Validation over Hold-Out Validation on Colossal Datasets for Quality Classification," *2016 IEEE 6th International Conference on Advanced Computing (IACC)*, Bhimavaram, India, 2016, pp. 78-83.

[12] J. Erbani, P. -É. Portier, E. Egyed-Zsigmond and D. Nurbakova, "Confusion Matrices: A Unified Theory," in *IEEE Access*, vol. 12, pp. 181372-181419, 2024.

Automated Assembly Machine Stopping System Using Machine Learning for Electrical Failure Prediction in Hard Disk Drive Manufacturing

Tanakrit Panjasamanwong
School of Information Technology
King's Mongkut Institute of Technology Ladkrabang
Bangkok, Thailand
tanakrit.panjasamanwong@gmail.com

Bundit Thanasopon
School of Information Technology
King's Mongkut Institute of Technology Ladkrabang
Bangkok, Thailand
bundit@it.kmitl.ac.th

***Abstract*— The assembly of diode lasers and sliders is a critical process in hard disk drive (HDD) manufacturing, directly affecting product electrical performance. Delays in detecting problematic assembly machines increase scrap rates, reduce yield, and raise production costs. This research presents the development of supervised machine learning models to predict electrical testing results using key parameters from assembly machines, for example, diode laser alignment position after assembly and laser intensity measurement during assembly. Dataset was preprocessed through outlier removal and feature selection using correlation analysis and permutation importance before applying SMOTE technique to balance the minority class in the training set, followed by normalization before modeling and evaluating performance. Multiple models were developed and evaluated to select the best performing model. Evaluation results showed that the AdaBoost model combined with Random Forest achieved the highest performance, with an AUC of 92.36%. The selected model was integrated into monitoring, alerting and machine auto stopping system when the predicted failure rate exceeded a predefined threshold. The implemented system reduces the detection time for problematic assembly machines, minimizes defective parts, and improves overall manufacturing efficiency.**

Keywords—Hard Disk Drive, Manufacturing, Supervised Machine Learning, Automated Machine Stopping System.

I. INTRODUCTION

The continuous development of Hard Disk Drive (HDD) technology is driven by the increasing demand for higher data storage capacities and improved performance. Heat Assisted Magnetic Recording (HAMR) is a key technology for data storage that utilizes laser heat to aid in writing data onto magnetic disks. Diode lasers play a crucial role by generating heat to increase the temperature of targeted bits before writing data, without disturbing the magnetic waves of nearby bits. This approach allows for higher data storage capacities compared to traditional magnetic recording methods [9].

One of the critical processes in the manufacturing of HDD using HAMR technology is the assembly of diode lasers with the read/write heads using automated assembly machines, since the quality of the assembly directly impacts the electrical performance of the product. The process involves monitoring and controlling more than 43 parameters in the assembly process, such as the measurement of diode laser intensity in the assembly machine and the rotation of the diode laser along the Y-axis after assembly.

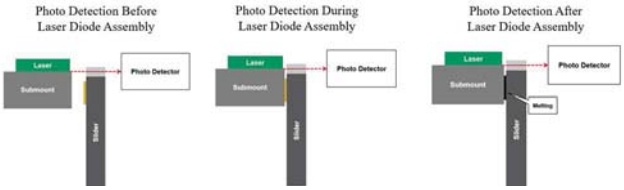


Fig. 1. Measurement of Laser Intensity in Assembly Machine.

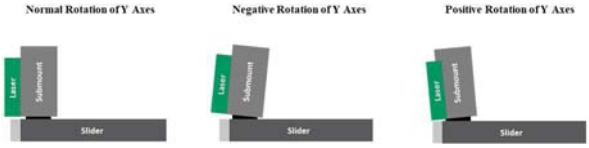


Fig. 2. Measurement of the Diode Laser's Rotation along the Y-axis.

After assembly, the parts are sent to the cleaning and defect inspection processes before moving on to the electrical performance testing phase. In this step, the electrical performance of the parts is tested against defined standards to ensure they meet the required specifications. Parts that fail the electrical performance test will be scrapped and separated from the production line, while the parts that pass are delivered to the next process.

However, current process for monitoring and controlling various parameters of the assembly machine relies on operators following a scheduled time every 4 hours for assembly machine buyoff. When excursions occur in the assembly machine, these processes lead to delays in problem detection and machine stoppage for maintenance. As a result, a large number of defective parts are found during electrical performance testing process, which increases material scrap, reduces manufacturing capacity, and increases production costs.

Therefore, this research focuses on developing a supervised machine learning model to predict electrical performance testing results, using key parameters from the automated assembly machine as features to train the model. Furthermore, the machine learning model is used to develop a monitoring, alerting, and automated assembly machine stopping system when the predicted failure rate exceeds a predefined threshold.

II. LITERATURE REVIEW

A. Supervised Machine Learning for Binary Classification

Binary classification is a technique used to classify data into two groups by training a model with labeled datasets containing correct results or answers. This approach is widely

979-8-3315-4248-1/25/$31.00 ©2025 IEEE

applied across various industries. The following are examples of machine learning models used in binary classification, which have been applied in this research.

1) Gradient Boosting

Gradient Boosting is a machine learning model that combines multiple weak learners to work together in an ensemble. In each iteration, a new model is trained to correct the errors made by the previous model's predictions [1]. This process enhances the overall accuracy and precision, making it more effective at handling complex data compared to a single model. Gradient Boosting has been used in the research conducted by Zaharah Allah Bukhsha, Aaqib Saeed, Irina Stipanovica, and Andre G. Doree to predict the maintenance needs of railway switches [2]. The study compared the performance of Gradient Boosting with Decision Trees and Random Forests, both of which involve building multiple decision trees that make predictions through voting [3]. In this research, an under-sampling technique was used to address class imbalance by reducing the number of overrepresented classes, and permutation importance technique [4] was applied to assess the significance of features and select the important features for model development. The results showed that the Gradient Boosting model achieved the highest accuracy, surpassing Decision Tree and Random Forest models.

2) Adaptive Boosting (AdaBoost)

AdaBoost is an ensemble learning technique that combines several weak classifiers to create a strong classifier model. It adjusts the weight of misclassified examples from the previous round to give more attention to the misclassified data in the new model, improving prediction efficiency with each training iteration [12]. Additionally, it is efficient in handling imbalanced data and works well with noisy datasets [10]. Jaree Thongkam, Guandong Xu, and Yanchun Zhang used AdaBoost in conjunction with Random Forest to develop a model to predict breast cancer survival [11]. In this study, the performance of AdaBoost, Random Forest, Decision Tree, and AdaBoost combined with Random Forest was compared and evaluated using metrics such as accuracy, sensitivity, specificity, and area under the curve. The results showed that AdaBoost combined with Random Forest achieved the highest accuracy of 88.6%, outperforming other models. This research demonstrates how ensemble learning techniques can significantly improve model performance, and this approach is applied in the model development for this research.

B. Synthetic Minority Over Sampling (SMOTE)

SMOTE is a technique used to oversample data in order to address the problem of imbalanced datasets. Imbalance can cause the model to become biased towards the majority class, reducing its ability to accurately predict the minority class. SMOTE addresses this by generating synthetic samples for the minority class. The technique works by selecting a data point from the minority class, identifying its nearest neighbors, and creating new synthetic samples through interpolation between the selected point and its neighbors. This process is repeated until the dataset achieves a balanced distribution [5].

C. Model Performance Evaluation

1) Confusion Matrix

The confusion matrix is a method used to assess a model's classification performance. It consists of four components include True Positive (TP), True Negative (TN), False Positive (FP), and False Negative (FN). The values derived from the confusion matrix are used to calculate key evaluation metrics to quantify the model's effectiveness, including Accuracy, Precision, Recall, and F1 Score [6], which are defined in Equations (1) to (4) as follows.

$$Accuracy = \frac{TP+TN}{TP + FP + TN + FN} \quad (1)$$

$$Precision = \frac{TP}{TP + FP} \quad (2)$$

$$Recall = \frac{TP}{TP + FN} \quad (3)$$

$$F1\ score = \frac{2\ x\ Precision\ x\ Recall}{Precision + Recall} \quad (4)$$

2) Receiver Operating Characteristic (ROC) and Area Under the Curve (AUC)

ROC curve is a performance evaluation method that illustrates the tradeoff between True Positive Rate (TPR) and False Positive Rate (FPR) across different classification thresholds. The TPR and FPR are calculated using Equations (5) and (6), respectively.

$$TPR: = \frac{TP}{TP + FN} \quad (5)$$

$$FPR: = \frac{FP}{FP + TN} \quad (6)$$

AUC represents the overall capability of model to distinguish between positive and negative classes. AUC values range from 0 to 1, where AUC close to 1 indicates excellent classification performance, while an AUC of 0.5 suggests that the model performs no better than random guessing [7].

III. Methodology

A. Data Collection and Preparation

Data were collected from the assembly machine, including electrical performance test results. The dataset contained 43 parameters with a total of 668,909 records, of which 98.93% passed the electrical performance test, while 1.07% failed. To address the class imbalance, 20,253 records representing the good parts were randomly selected, with electrical performance values between the 25th and 75th percentiles. Outliers were then removed to improve data quality, and 4,043 records were selected to represent the failed parts. Correlation scores between the 43 assembly machine parameters and electrical test performance values were analyzed to identify relevant features. Parameters with low correlation were discarded, leaving 31 highly correlated features. The Permutation Importance technique was then applied to assess the importance scores of these 31 parameters in predicting electrical performance test results. After analysis, 11 parameters with importance scores greater than 0.03 were selected, as shown in Fig. 4, to simplify the model and improve its predictive efficiency.

TABLE I. BEFORE AND AFTER SELECT DATA SELECTION

Data Selection	Before	After
Total Record	668,909 Records	24,296 Records
Passed Electrical Performance	661,741 Records	20,253 Records
Failed Electrical Performance	7,168 Records	4,043 Records

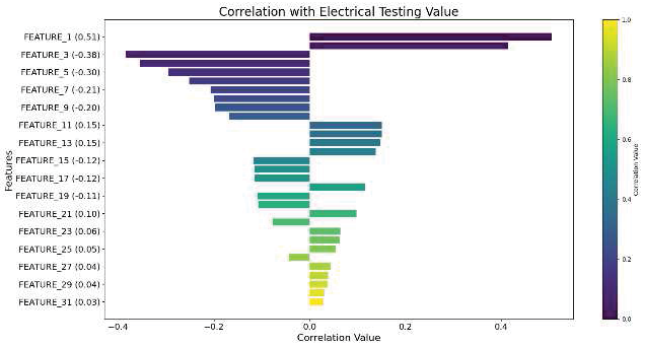


Fig. 3. Correlation Score Between Features and Electrical Value.

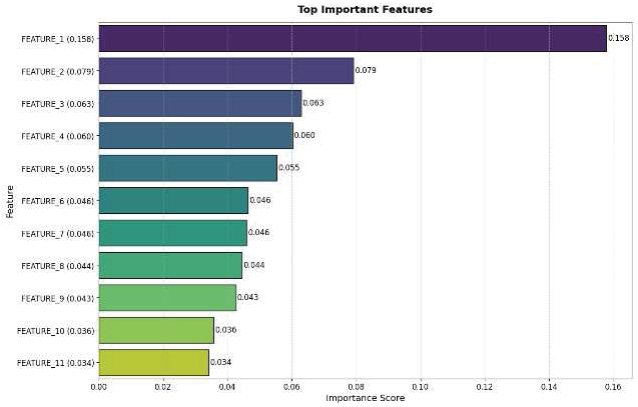


Fig. 4. Feature Important Score.

B. Train/Test Spliting and Data Normalization

The dataset was split into two groups, 80% (19,274 records) for training and 20% (4,819 records) for testing. In the training set, 16,054 records represented parts that passed the electrical performance test, while 3,220 represented parts that failed. To address the imbalance in the data, SMOTE technique was applied to the training set, which generated additional records for the failed parts. After using SMOTE, the training set included 16,054 records for each class, which helped mitigate potential bias in the model's predictions. Prior to model training, the training set was normalized using standardization, and the same statistical transformation was applied to the test set to ensure both sets were on the same scale before modeling.

TABLE II. TRAINING SET INFORMATION

Training Set Information	Before SMOTE	After SMOTE
Passed Electrical Test	16,054 Records	16,054 Records
Failed Electrical Test	3,220 Records	16,054 Records
Total Records	19,274 Records	32,108 Records
Class Balance	Imbalanced (98.93% Pass, 1.07% Fail)	Balanced (50% Pass, 50% Fail)

C. Modeling

For the modeling, nine machine learning models were selected, consisting of three individual models and six ensemble models. The individual models included Logistic Regression (LR), Decision Tree (DT), and Random Forest (RF). The ensemble models included Gradient Boosting with Logistic Regression (GBLR), Gradient Boosting with Decision Tree (GBDT), Gradient Boosting with Random Forest (GBRF), Adaboost with Logistic Regression (ABLR), Adaboost with Decision Tree (ABDT), and Adaboost with Random Forest (ABRF). All models were trained using the Cross-Validation technique [8]. The training set was divided into five groups (5-Fold). In each iteration, the model was trained using four parts of the data and tested on the remaining one part. This process was repeated for all parts to ensure that the model was evaluated on diverse data, which improves its reliability.

IV. EVALUATION RESULT

The performance of the machine learning models was evaluated using Accuracy, Precision, Recall, and F1 Score, with average values obtained from Cross Validation. The results are presented in Table IV.

Evaluation results indicate that ensemble models, particularly Gradient Boosting combined with Random Forest (GBRF) and Logistic Regression (GBLR), outperformed individual models. This suggests that ensemble models are more effective in handling complex data. Among all models, the top four models with an accuracy exceeding 90% including Gradient Boosting with Random Forest (GBRF), Gradient Boosting with Logistic Regression (GBLR), AdaBoost with Random Forest (ABRF), and Random Forest (RF) were selected for hyperparameter tuning using training dataset and cross-validation. As shown in Table V, all four models demonstrated improved performance across all metrics after tuning.

TABLE III. EVALUATION RESULT

Model	Accuracy	Precision	Recall	F1 Score
RF	92.71%	92.72%	92.71%	92.71%
LR	85.06%	85.06%	85.06%	85.06%
DT	88.78%	88.71%	88.75%	88.66%
ABDT	88.67%	88.84%	88.77%	88.84%
ABRF	92.81%	92.89%	92.84%	92.65%
ABLR	84.09%	84.15%	84.09%	84.08%
GBDT	88.76%	88.76%	88.76%	88.76%
GBRF	95.19%	95.20%	95.18%	95.18%
GBLR	93.06%	93.14%	93.06%	93.06%

TABLE IV. HYPER PARAMETER TUNING EVALUATION RESULT

Model	Accuracy	Precision	Recall	F1 Score
RF	92.88%	92.89%	92.88%	92.88%
ABRF	95.07%	95.11%	95.07%	95.07%
GBRF	95.74%	95.76%	95.74%	95.74%
GBLR	95.10%	95.11%	95.10%	95.10%

TABLE V. EVALUATION RESULT WITH TEST SET

Model	Accuracy	Precision	Recall	F1 Score	AUC
RF	91.68%	91.92%	91.68%	91.78%	91.43%
ABRF	92.72%	92.48%	92.72%	92.54%	92.36%
GBRF	92.53%	92.29%	92.53%	92.37%	92.02%
GBLR	92.05%	91.84%	92.05%	91.92%	91.27%

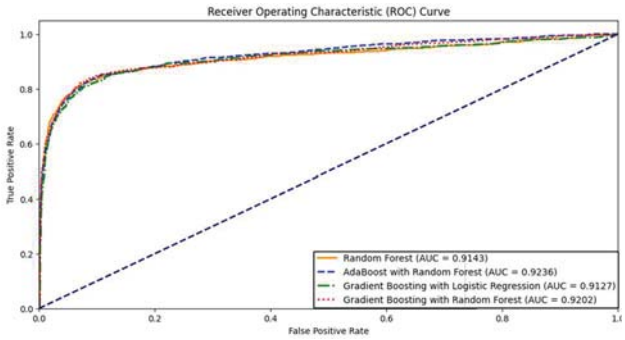


Fig. 5. ROC and AUC Evaluation Result.

Based on the test set evaluation, AdaBoost model combined with Random Forest (ABRF) demonstrated the highest overall performance. Consequently, this model was selected for system development.

V. Implementation

To implement the model in the HDD manufacturing process, a system was developed to connect with Online Database System (ODS) of assembly machines. This system automatically retrieves key parameters from the assembly machines, processes them through an automated data preparation pipeline, and feeds data into the predictive model. The model then predicts electrical performance test results, which are displayed on a dashboard for real-time monitoring. Simultaneously, the system calculates the failure rate based on these predictions and compares it to a predefined threshold. If the failure rate for any assembly machine exceeds this threshold, the system triggers an automated email alert and sends a stop command via an API to the machine's control software, stopping the assembly process immediately to prevent defective parts from being produced.

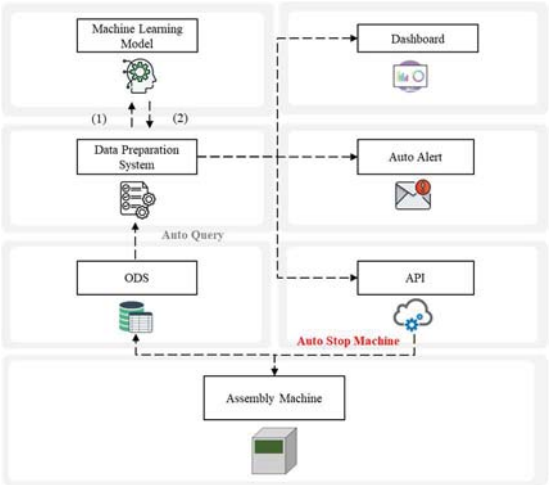


Fig. 6. System in Manufacturing Process Schematic.

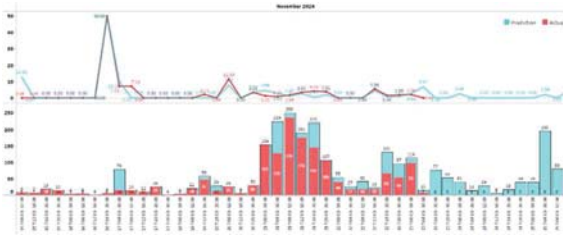


Fig. 7. Electrical Failure Prediction Dashboard

VI. Conclusion

A supervised machine learning model was developed to predict electrical performance testing results in the HDD manufacturing process using key parameters from assembly machines. After evaluating nine models, ensemble models demonstrated higher effectiveness compared to individual models, with the AdaBoost combined with Random Forest model achieving the highest AUC of 92.36%. This model was selected to develop a system for monitoring, alerting, and automatically stopping assembly machines when the predicted failure rate exceeded the predefined threshold. The system connects with the ODS of the assembly machines, automatically querying key parameters, processing them through an automated data preparation system, and feeding data into the model. The system then calculates the failure rate and compares it with the threshold. If exceeded, it triggers email alert and sends a stop command to the assembly machine via an API. This research approach improved problem detection time, reducing it from 4 hours to 15 minutes leading to optimize production efficiency, and reduce overall manufacturing costs.

References

[1] A. Natekin and A. Knoll, "Gradient boosting machines: A tutorial," *Front. Neurorobotics*, vol. 7, no. 21, Dec. 4, 2013.

[2] Z. A. Bukhsha, D. C. McCullough, P. Jarrett, and M. Schmid, "Predictive maintenance using tree-based classification techniques: A case of railway switches," *Transp. Res. Part C*, vol. 101, pp. 35–54, Apr. 2019.

[3] L. Breiman, "Random forests," *J. Mach. Learn.*, vol. 45, pp. 5–32, 2001.

[4] A. Altmann, M. Toloşi, O. Sander, and T. Lengauer, "Permutation importance: A corrected feature importance measure," *Bioinformatics*, vol. 26, no. 10, pp. 1340–1347, May 2010.

[5] N. V. Chawla, K. W. Bowyer, L. O. Hall, and W. P. Kegelmeyer, "SMOTE: Synthetic minority over-sampling technique," *J. Artif. Intell. Res.*, vol. 16, pp. 321–357, 2002.

[6] K. Chu, "An introduction to sensitivity, specificity, predictive values, and likelihood ratios," *Emerg. Med.*, vol. 11, pp. 175–181, 1999.

[7] S. K. Çorbacıoğlu and G. Aksel, "Receiver operating characteristic curve analysis in diagnostic accuracy studies: A guide to interpreting the area under the curve value," *Turkish J. Emerg. Med.*, 2023.

[8] D. Berrar, "Cross-validation," in *Encyclopedia of Bioinformatics and Computational Biology*, Oxford, U.K.: Academic Press, 2019, pp. 542–545.

[9] G. Ju, X. Zheng, H. Zhou, and R. Ranjan, "Heat assisted magnetic recording: Next generation mass storage technology," *in Proc. 2018 IEEE Int. Magn. Conf. (INTERMAG)*, 2018.

[10] Y. Ma and X. Ding, "Robust real-time face detection based on cost-sensitive AdaBoost method," *in Proc. Int. Conf. Multimedia and Expo*, 2003, pp. 465–473.

[11] J. Thongkam, G. Xu, and Y. Zhang, "AdaBoost algorithm with random forests for predicting breast cancer survivability," *in Proc. 2008 Int. Joint Conf. Neural Netw. (IJCNN)*, 2008.

[12] Y. Freund and R. E. Schapire, "A decision-theoretic generalization of on-line learning and an application to boosting," *J. Comput. Syst. Sci.*, 1997.

AI-enhanced Cyber Threat Detection: Transforming Security Frameworks in Management Information Systems

Niropam Das
Department of Business Administration
International American University
3440 Wilshire Blvd STE 1000, Los Angeles, CA 90010, United States
niropomdas124@gmail.com

Jahid Hassan
Department of Business Administration
International American University
3440 Wilshire Blvd STE 1000, Los Angeles, CA 90010, United States
Jahid47-090@diu.edu.bd

Partha Chakraborty
Department of Business Administration
International American University
3440 Wilshire Blvd STE 1000, Los Angeles, CA 90010, United States
p.chakra.iau@gmail.com

Jobanpreet kaur
Department of Technology & Engineering
Westcliff University
17877 Von Karman Ave 4th floor, Irvine, CA 92614, United States
j.kaur.244@westcliff.edu

Syed Nazmul Hasan
Department of Technology & Engineering
Westcliff University
17877 Von Karman Ave 4th floor, Irvine, CA 92614, United States
s.hasan.104@westcliff.edu

Mohammad Abdul Goffer
Department of Business Administration
International American University
3440 Wilshire Blvd STE 1000, Los Angeles, CA 90010, United States
mdabdulgoffer1991@gmail.com

Kazi Bushra Siddiqa
Department of Business Administration
International American University
3440 Wilshire Blvd STE 1000, Los Angeles, CA 90010, United States
bushrasiddiqa82@gmail.com

Rakibul Hasan
Department of Business Administration
Westcliff University
17877 Von Karman Ave 4th Floor, Irvine, CA 92614, United States
r.hasan.179@westcliff.edu

*Corresponding author: Rakibul Hasan (r.hasan.179@westcliff.edu)

***Abstract*— This study introduces an AI-based MIS cyber threat detection model for high-rate cyberattacks. It correctly classifies harmful and benign network traffic data using supervised machine learning. To optimize our model, we clean, normalize, and feature engineer. Reduce dimensionality with PCA and other methods for successful data analysis. The framework evaluates XGBoost, Random Forest, SVM, and KNN Accuracy, Precision, Recall, and F1 score to find the best machine learning model. SHAP (SHapley Additive exPlanations) study reveals feature contributions, model interpretability, and network traffic of crucial sinful behavior elements. The framework is validated by the CICIDS 2017 network traffic dataset, which includes several attack methods. The results reveal that XGBoost and Random Forest detect threats more accurately and precisely. This research concludes with a proactive and effective threat detection mechanism to fill MIS cybersecurity knowledge gaps. It makes cybersecurity more resilient and adaptable by improving organizational defenses against changing cyber threats and requiring interpretability in decision making.**

Keywords- Cyber Threat, Management Information Systems (MIS), Machine Learning, Interpretability, Threat Detection, SHAP, XAI

I. INTRODUCTION

Though they underpin all computing and networking methods, Management Information Systems (MIS) are at more risk in today's diversified globe. Companies' reliance on digital infrastructures makes them increasingly vulnerable to hackers. Backend, third-party users, cloud-based data storage, and apps in the digital world make it difficult and risky for enterprises to guarantee total information system security [1]. Traditional security tools like firewalls, antivirus, and signature-based IDS cannot stop such threats. Advanced threats, DDoS, ransomware, and rising volumes necessitate nimble security. Discussing and studying AI's impact on organizations and enterprises is becoming more interesting in MISs. Artificial Intelligence is considered as the most disruptive [2, 3] technical force that has the utmost potential to transform the organizational and corporate field in the forthcoming decade [4]. Today, MIS systems consist of (AI) solutions to accurately recognize, measure and mitigate cyber threats. It enhances the detection schemes making it easier for companies to respond to the new risks aggressively. However, most of the models of artificial intelligence do not support interpretability Many thus using for reliable, efficient decision making in MIS based cybersecurity systems difficult [5].

In the recent past, the intake of information security incidents has raised to the higher level and the consequences of cybercrime and networks' attacks can be financially destructive for both groups of people and companies. For instance, research reveals that the global average cost of data breach is USD 8.19m, of which USD 3.9m is incurred in the United States [6].

For this reason, ML offer a practical approach for furthering prospect in online safety since it affords a fast method of analyzing big sets of data and recognising trends. In the sphere of automated response, threat prediction, and the identification of anomalies, this study looks at the possibility of applying artificial intelligence and machine learning. With the help of computer based intelligence and machine learning organizations might be able to detect and prevent negative conduct, recognize potential risks and actively counter them, enhance protection [7].

In particular this approach improves decision made within MIS by incorporating artificial intelligence for cybersecurity visualization and classification. This paper

also examines how, in data, PCA can be applied for dimensionality reduction devoid of affecting detection points; additionally, Feature Importance and SHAP are applied to enhance model interpretability. For data modeling in this study, the CICIDS 2017 network traffic dataset is used [8].

II. LITERATURE REVIEW

Due to technical and IoT developments, Internet networks must be safeguarded for user security and privacy. AI may improve cybersecurity. Many investigations use ML/DL security. ML and DL research on cybersecurity breaches is discussed here. The literature analysis also investigates how powerful ML and DL algorithms might detect DDoS and MIS breaches to improve cybersecurity.

Alhasawi et al. [9] offer FL-DAD, a CNN-trained IoT DDoS attack detection system. FL-DAD learns models with over 99% worldwide accuracy by exchanging only model parameters with a central server, eliminating privacy issues. Communication cost, device heterogeneity, and massive IoT network scaling issues persist. Similarly, Doris and Shad [10] predicted cyberattacks using CNN and RNN deep learning models. These algorithms can predict attacks with 97% accuracy, but data quality, interpretability, and adaptability are concerns.

Layered sparse AEs and DNNs may identify cloud DDoS, say Bhardwaj et al. [11] hyperparameter tuning was optimized for 98.92% efficiency via hyperband tuning. It performs well, but its computational cost makes it inappropriate for real-time applications, especially on resource-limited platforms. Using HAEnID on CIC-IDS 2017 datasets, Ahmed et al. [12] detected intrusions with 98% accuracy using stacking ensembles, Bayesian model averages, and conditional ensembles. Though effective, HAEnID is best for large datasets for two reasons: Not much is known about HAEnID's computational complexity and adaptive process for huge datasets.

Kim et al. [13] built Cloud-IDS for cloud intrusion detection using domain knowledge-free lightweight embedding and BI-LSTM networks. Besides 98.20% accuracy and minimum processing, this method demands 1% topic competence. Embedding allows adversarial attacks and a stronger model. Finally, Vu et al. [14] developed the dataset using automatic labeling and a deep learning model with an attention strategy for network attack detection generalizability. Traffic patterns, new and ongoing assaults, and CIC-IDS2017 dataset data deficiency are detected with 98.68% accuracy.

The constraints of these research show MIS flaws. FL-DAD, Bhardwaj [11], Vu's [14] and Doris and Shad's [10] models' computational overhead, scalability, and adaption issues continue to hinder MIS adoption in dynamic and resource-constrained situations. Ahmed's [12] HAEnID and Kim's [13] C-IDS highlight interpretability and adversarial defects that could compromise MIS reliability. Therefore, these weaknesses must be addressed to protect MIS against sophisticated and dynamic cyber assaults.

III. METHODOLOGY

A. Dataset

The comprehensive network traffic dataset CICIDS 2017 [15] network traffic dataset includes modern assaults and benign traffic. Attack types, protocols, ports, timestamps, source and destination IP addresses, and more are included in labelled flows. It replicates HTTP, HTTPS, FTP, SSH, and email background activity using B-Profile.

This study tested intrusion detection systems in a realistic network environment using Tuesday, Wednesday, Thursday Afternoon, and Friday Morning files. They cover Brute Force FTP/SSH, DoS, Heartbleed, Web Attack, Infiltration, Botnet, and DDoS. Attack category file numbers are in Fig. 1.



Fig. 2. Overview of cyber threat detection framework

B. Proposed Methodology

1. AI-driven Cyber Threat Detection Framework

This research creates a machine learning-based AI cyber threat detection system to reduce risks. The system assesses threats using supervised learning, data pre- and post-processing, feature extraction, model training, and threat categorization. PCA, Pearson Correlation, and Correlation Heatmap normalize and analyze network traffic. Reduce data dimensionality and select the optimal features to improve model performance and generalization. The training framework only employs XGBoost, Random Forest, SVM, and KNN to identify threats, assessing accuracy, precision, recall, and F1-score. They designate data benign or harmful for early diagnosis and risk mitigation. SHAP and feature significance analysis clarify results. Fig. 2 below shows this approach.

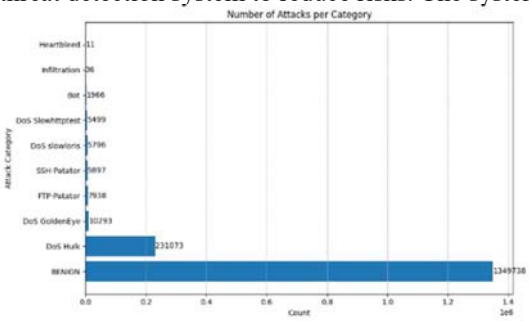


Fig. 1. Types of attack distribution in CICIDS-2017 dataset

2. ML Models

The following SVM, RF, KNN, and XGBoost algorithms to assess the framework is used:

- RF**:** This study analyzed IDS data using RF because to its accuracy, convenience of use, and scalability for big data dimensions. Numerous decision trees, a model with excellent generalization and accuracy, and comprehensive DDoS attack recognition with low false positives make RF stronger at cybersecurity [16]. Using many binary decision trees, Random Forest forecasts by majority vote. Let $T_i(x)$ stand for the i-th tree in the forest for binary classes with the outcome in the form of either 0 or 1, from various $T_i(x)$trees.
- SVM**:** Using SVM, reliable instruction classification and regression are achieved. To learn supervisedly SVM is the finest regression and classification hyperplane. This study detects cyberthreats utilizing SVM as the IDS using linear and non-linear data. It's slow and settings-sensitive yet accurate for cybersecurity. Supervised learning SVM suits regression and classification best. This study detects cyberthreats utilizing SVM as the IDS using linear and non-linear data. It's accurate enough for cybersecurity despite being slow and setting-sensitive [17].
- KNN**:** The basic supervised learning KNN algorithm classifies new data points based on their nearest neighbors' classes, where K is the number of neighbors [18]. Because KNN is easy to use and efficient at classifying network traffic, it is used in this investigation. KNN searches for patterns across distances; the choice of K and distance measure affects hit rate and overhead expenses.
- XGBoost**:** XGBoost is a powerful boosting approach that iteratively goes through inferior decision trees to minimize the primary function and get the best prediction values [19]. XGBoost is best for network traffic categorization because it decreases learning model complexity, allows weak learners to be combined, permits parallel computations, and avoids overfitting.

C. XAI with SHAP

This must be brief and intuitive about how cybersecurity models predict common incidents. Our analysis uses SHAP [20] to quantify attribute contributions to model findings. SHAP values are one way to represent how qualities affected a prediction positively or negatively. SHAP has two key advantages: It gives record-specific attribution values without a model, even nonlinear ones. SHAP's efficiency, whole greater than sum property, symmetry, additivity, and dummy property make it better than other interpretability approaches [21]. Because it captures global and local explanations, SHAP makes cybersecurity applications visible and trusted.

IV. RESULTS & DISCUSSION

A. PCA and Correlation Heatmap Outcomes:

Each sample separates regular and attack traffic, however there is significant overlap. In Fig. 3, the overlap was consistent regardless of component pair, showing that PCA with a small number of components cannot detect intrusions in this dataset. Detecting hostile conduct may require extra primary components or alternative ways. According on variable “State”, CICIDS 2017 dataset may show different network traffic or attacks.

Fig. 4 shows a correlation heatmap explaining selected feature interactions for AI-based risk identification. Strong correlation, like “Total Length of Fwd Packets” vs. “Total Length of Bwd Packets”, lowers dimensionality, whereas moderate correlation, like “Init_Win_bytes_forward” vs. “Subflow Fwd Packets”, improve These links help choose attributes, enhancing accuracy and efficiency.

B. Evaluation Metrics

From Fig. 5, it shows the performance of the various machine learning models applied in the dataset used in this research in detecting cyber threat. Furthermore, XGBoost possessed 100% of precision, recall, and F1-score and 99.99% of accuracy to be confirmed from the confusion matrix in Fig. 6. It also has the highest accuracy of 99.99 % and precision, recall, and F1-score of 100 %as shown from the confusion matrix in Fig. 6.

The Random Forest (RF) model has 99.99% F1-score, near-perfect accuracy, precision, and recall. KNN performed well with precision = recall = F1 score = 1 and accuracy = 0.9998. SVM model had 98% precision, 99% recall, and 99% F1-score but performed worse with noticeable difference. It was 99.52% correct. XGBoost's confusion matrix augmentation and RF's cyber threat prediction are amazing.

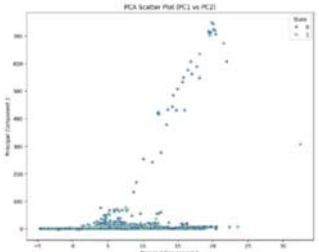


Fig. 3. PCA plot revealing variance of components for attack and benign

C. Model Interpretability with SHAP

SHAP lists data factors a machine learning model could use to identify abnormal traffic in CICIDS 2017 for MIS in Fig. 7. It's explained by ranking the top 20 influential network elements. Many threat detection systems scan source and destination IPs. The model now detects malicious IPs and botnets. Top "Bwd Packet Length Mean" & "Packet Length Variance" . This indicates model damage and packet size discrepancies. Fwd IAT Std. and “Timestamp” describe temporal network traffic. Activity timing and frequency may suggest network probing or hostility in this paradigm.

CONCLUSION

Finally, this project will construct an AI-based MIS cyber threat detection system to address cyber threat complexity. The accuracy and precision of CICIDS 2017 threat identification and XGBoost and RF novelty determination enhanced SHAP identified network elements that alter det-etection outcomes to improve model interpretation. Critical asset MIS cybersecurity increases with secure and transparent detection. Machine learning models, a larger dataset with more attack types, and SHAP analysis may be

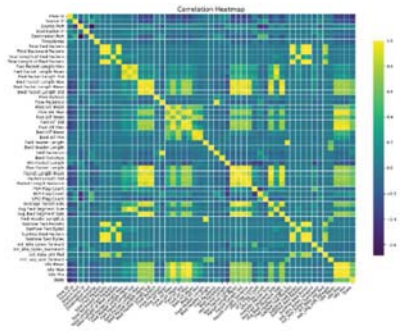


Fig. 4. Feature correlation heatmap

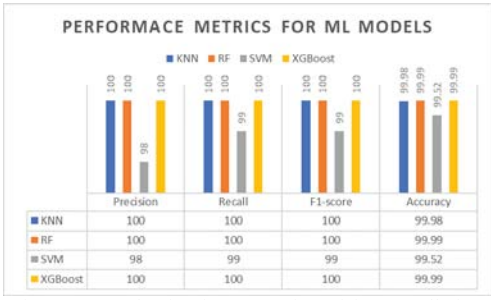


Fig 5. Performance evaluation in terms of precision, recall, f1-score and accuracy

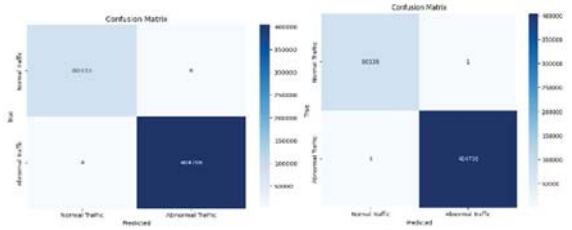


Fig. 6. Confusion matrics for XGBoost(left side) and RF(right side)

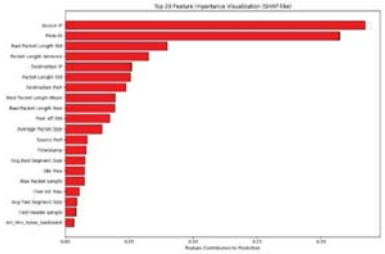


Fig. 7. Model interpretability using SHAP

studied further. The framework could enable real-time, low-latency threat detection and better adaptive response systems. We provide organizational readiness, proactive mitigation, and simple incident response system integration.

REFERENCES

[1] O. A. Ajala, "Leveraging AI/ML for anomaly detection, threat prediction, and automated response," 2024.

[2] T. H. Davenport, *The AI advantage: How to put the artificial intelligence revolution to work*. mit Press, 2018.

[3] A. F. S. Borges, F. J. B. Laurindo, M. M. Spínola, R. F. Gonçalves, and C. A. Mattos, "The strategic use of artificial intelligence in the digital era: Systematic literature review and future research directions," *International Journal of Information Management,* vol. 57, p. 102225, 2021/04/01/ 2021, doi: https://doi.org/10.1016/j.ijinfomgt.2020.102225.

[4] C. Collins, D. Dennehy, K. Conboy, and P. Mikalef, "Artificial intelligence in information systems research: A systematic literature review and research agenda," *International Journal of Information Management,* vol. 60, p. 102383, 2021/10/01/ 2021, doi: https://doi.org/10.1016/j.ijinfomgt.2021.102383.

[5] K. Shaukat, S. Luo, S. Chen, and D. Liu, "Cyber Threat Detection Using Machine Learning Techniques: A Performance Evaluation Perspective," in *2020 International Conference on Cyber Warfare and Security (ICCWS)*, 20-21 Oct. 2020 2020, pp. 1-6, doi: 10.1109/ICCWS48432.2020.9292388.

[6] A. Buecker, M. Borrett, C. Lorenz, and C. Powers, "Introducing the IBM security framework and IBM security blueprint to realize business-driven security," *IBM Redpaper,* vol. 4528, no. 1, pp. 1-96, 2010.

[7] M. Jiang, Q. Zhang, and J. Kong, "Multiformer-based hybrid learning with outlier re-assignment for unsupervised person re-identification," *International Journal of Machine Learning and Cybernetics,* vol. 15, no. 3, pp. 879-896, 2024/03/01 2024, doi: 10.1007/s13042-023-01945-z.

[8] I. Sharafaldin, A. H. Lashkari, and A. A. Ghorbani, "Toward generating a new intrusion detection dataset and intrusion traffic characterization," *ICISSp,* vol. 1, pp. 108-116, 2018.

[9] Y. Alhasawi and S. Alghamdi, "Federated Learning for Decentralized DDoS Attack Detection in IoT Networks," *IEEE Access,* vol. 12, pp. 42357-42368, 2024, doi: 10.1109/ACCESS.2024.3378727.

[10] L. Doris and R. Shad, "CYBER ATTACK PREDICTION USING MACHINE LEARNING ALGORITHMS."

[11] A. Bhardwaj, V. Mangat, and R. Vig, "Hyperband Tuned Deep Neural Network With Well Posed Stacked Sparse AutoEncoder for Detection of DDoS Attacks in Cloud," *IEEE Access,* vol. 8, pp. 181916-181929, 2020, doi: 10.1109/ACCESS.2020.3028690.

[12] U. Ahmed *et al.*, "Explainable AI-based innovative hybrid ensemble model for intrusion detection," *Journal of Cloud Computing,* vol. 13, no. 1, p. 150, 2024/10/21 2024, doi: 10.1186/s13677-024-00712-x.

[13] Y. Kim, G. Park, and Huy K. Kim, "Domain knowledge free cloud-IDS with lightweight embedding method," *Journal of Cloud Computing,* vol. 13, no. 1, p. 143, 2024/09/27 2024, doi: 10.1186/s13677-024-00707-8.

[14] D. M. Vu, T. H. La, G. B. Nguyen, E. N. Huh, and H. H. Tran, "Enhancing network attack detection across infrastructures: An automatic labeling method and deep learning model with an attention mechanism," *IET Communications,* vol. 18, no. 17, pp. 1107-1125, 2024.

[15] A. Khanan, Y. A. Mohamed, A. H. H. M. Mohamed, and M. Bashir, "From Bytes to Insights: A Systematic Literature Review on Unraveling IDS Datasets for Enhanced Cybersecurity Understanding," *IEEE Access,* vol. 12, pp. 59289-59317, 2024, doi: 10.1109/ACCESS.2024.3392338.

[16] R. Ms, N. Nishat, S. Rasetti, and M. A. Rahaman, "A REVIEW OF MACHINE LEARNING AND FEATURE SELECTION TECHNIQUES FOR CYBERSECURITY ATTACK DETECTION WITH A FOCUS ON DDOS ATTACKS," *Academic Journal on Science, Technology, Engineering & Mathematics Education,* vol. 4, no. 03, pp. 178-194, 09/22 2024, doi: 10.69593/ajsteme.v4i03.105.

[17] P. Dini, A. Elhanashi, A. Begni, S. Saponara, Q. Zheng, and K. Gasmi, "Overview on Intrusion Detection Systems Design Exploiting Machine Learning for Networking Cybersecurity," *Applied Sciences*, vol. 13, no. 13, doi: 10.3390/app13137507.

[18] F. S. Ferdous, T. Biswas, and A. I. Jony, "Enhancing Cybersecurity: Machine Learning Approaches for Predicting DDoS Attack," *Malaysian Journal of Science and Advanced Technology,* pp. 249-255, 2024.

[19] C. Ahmadi, J.-L. Chen, and Y.-C. Lai, "Enhancing Detection of Malicious VBA Macros in Office Documents: An Integrated Approach Employing P-Code Analysis and XGBoost-based Machine Learning Model," *IEEE Access,* 2024.

[20] S. Lundberg, "A unified approach to interpreting model predictions," *arXiv preprint arXiv:1705.07874,* 2017.

[21] D. Gaspar, P. Silva, and C. Silva, "Explainable AI for Intrusion Detection Systems: LIME and SHAP Applicability on Multi-Layer Perceptron," *IEEE Access,* vol. 12, pp. 30164-30175, 2024, doi: 10.1109/ACCESS.2024.3368377.

Some Practical Aspects of the Relational Database Normalization Process

Putsadee Pornphol
Department of Digital Technology
Faculty of Science and Technology
Phuket Rajabhat University
Phuket, THAILAND
putsadee.p@pkru.ac.th

Suphamit Chittayasothorn
School of Engineering
King Mongkut's Institute of Technology Ladkrabang
Bangkok, THAIALND
suphamit.ch@kmitl.ac.th

***Abstract*— Database normalization is a ubiquitous theoretical relational database analysis process. It comprises several levels of normal forms and encourage database designers not to split database tables into smaller ones unless it is necessary. Nevertheless, there are many aspects of relational database normalization which are not very well applied or well understood in practice. One of the biggest misconceptions is the misunderstanding that database normalization encourages splitting tables until they can be no longer spilt. Other popular practical misconceptions include over normalizations, performance issues, the complexity and rarity of multivalued and join dependencies, the projection/join normal form, and the unnecessity of carrying the normalization process beyond the third normal form or Boyce-Codd Normal Form (BCNF). This paper clarifies these practical misconceptions with positive examples and argues that relational database normalization process is a very practical analysis and quality control process of relational database table structures.**

Keywords— Relational Databases, Conceptual Modelling, Normalization, Attribute Analysis, Over normalization

I. INTRODUCTION

Database design is the design of database structures which are suitable for given applications. For relational databases, database structures are relational database table structures which are suitable for data manipulations and retrieval by relational database language statements. Relational database tables should be well designed to accommodate queries and to avoid insert, delete, and update problems. These problems, especially the insert and delete problems, can be solved by improving the design and cannot be solved by using better database server or hardware. Nevertheless, querying and report producing from the relational database tables should involve minimum number of tables for good response time. The optimal relational database design must therefore produce the minimum number of relational database tables with minimum or no insert, update, and delete problems.

Note that a relation in relational database is actually a collection of tuples which are true with respect to the real world. In the practical term, a tuple is a row. So, a relation is a collection of rows, and we are not designing them. The rows come from the application environment. When we design relational databases, it is the design of relational table structures, not their rows. Technically, it could be said that we design the relational database schemas which are collections of attributes. They are the "type" part of relational database, where the relations are the "instance" part. We design the types, not the instances. Once the database structures or the types are obtained, they can accommodate any number of instances. A relational database structure may be the reference structure of only one row or many millions of rows. The number of rows is not relevant.

Recently, C. J. Date, the relational database pioneer, argued that relational database design is the design of relvars (relation variables) [1], not the design of relational schemas. This is understandable since a relvar is a variable whose values must be relations. Two variables can have the same type. Two relvars therefore can base on the same relational schema. So, relational database design is the design of relvars, not relational schemas. In practical term, we are designing relation variables, not their types. An SQL table is an implementation of a relvar. Two relvars may have the same type. For practical purpose, the more familiar term, relational table structure, is used in this paper instead of the term relational variable or relvar.

The goal of the design is to obtain good relational database structures which are free from data manipulation and retrieval problems, or at least reduce them to an acceptable level. Relational database Normal Forms, together with its process called the normalization process, were invented by E. F. Codd the inventor of the relational database model, and his colleagues in the early 1970s. There are several normal forms. Codd himself invent the first, second, and third normal forms (1NF, 2NF, 3NF) [2]. His colleague Boyce found a bug in the 3NF definition and subsequently introduced an improved version of the 3NF with Codd [3]. This was originally called the new 3NF for a while before eventually renamed to Boyce/Codd Normal Form (BCNF) in their honor. The main concept behinds normal forms up to BCNF is functional dependency (FD). This first set of normal forms suggests the correct placement of FDs to relational table structures and make sure that FDs are preserved. Fagin, also a colleague of Codd, introduced the multivalued dependency (MVD) and the fourth normal form (4NF) [4]. Fagin went further to introduce the join dependency (JD) and the project/join normal form (PJ/NF) or the fifth normal form (5NF) [5]. The normalization process intends to reduce insert, delete, and update problems. These problems are caused by misplacements of dependencies between attributes. The correct placement of these dependencies in a relational table structure leads to less or no insert, delete update problems.

II. INSERT, DELETE, AND UPDATE PROBLEMS

Given a set of attributes from the application requirements, how to come up with proper relational database structures for the given application? The common practice is to use a kind of conceptual modelling technique such as the Entity Relationship Model [6], the UML Class Diagram [7,8],

979-8-3315-4248-1/25/$31.00 ©2025 IEEE

and the Object Role Model [9] to design a conceptual diagram and transform the diagram to a set of 1NF relational table structures. The normalization process is then applied to these table structures for quality control checking. However, literatures on the normalization process typically do not mention anything about conceptual modelling. They start the normalization topic by using a small number of attributes and collect them together in one relational table structure and declare it a first normal form table. The main purpose of doing this is to avoid the join of tables when queries are asked. Let us consider the following example:

Suppose the given attributes from the application are the attributes that have been used in the VENDOR, ITEM, and SALE relational database tables as shown again in Figure 1. Why do we separate them into three tables instead of keeping the attributes together as shown in Figure 2? Which one is better?

VENDOR

V#	VNAME	LOCATION	STATUS
V1	David	Bangkok	100
V5	John	Sydney	300
V2	Peter	Paris	200
V4	Tom	Bangkok	100
V3	John	Brisbane	300

ITEM

I#	INAME	COLOR
I2	Pen	Red
I4	Pen	Black
I1	Ruler	Clear
I3	Pencil	Black
I5	Ruler	White
I6	Eraser	White

SALE

V#	I#	AMOUNT
V1	I1	300
V1	I2	200
V3	I2	100
V1	I3	50
V2	I1	50
V2	I2	100
V4	I1	200
V4	I5	100
V3	I3	200
V3	I1	600
V1	I4	250
V1	I5	400
V1	I6	100

Fig. 1. Three sample relational database tables.

FIRST

V#	VNAME	LOCATION	STATUS	I#	INAME	COLOR	AMOUNT

Fig. 2. A table structure which has all attributes from the sample database tables collected together.

Figure 2 shows the relational table structure FIRST, which is the SALE table structure extended with attributes from VENDOR and ITEM. The primary key of FIRST is the primary key of SALE, which is the combination of V# and I#.

For some people, the first reaction from seeing FIRST is very positive. There will be no more join operations for any queries since all attributes are collected together in one relational table structure.

The insert, delete, and update operations, on this relational table structure, however, are full of problems. Technically, they are called insert, delete, and update anomalies.

FIRST

V#	VNAME	LOCATION	STATUS	I#	INAME	COLOR	AMOUNT
V3	John	Brisbane	300	I2	Pen	Red	100
V2	Peter	Paris	200	I2	Pen	Red	100
V1	David	Bangkok	100	I2	Pen	Red	200
V1	David	Bangkok	100	I4	Pen	Black	250
V4	Tom	Bangkok	100	I1	Ruler	Clear	200
V3	John	Brisbane	300	I1	Ruler	Clear	600
V2	Peter	Paris	200	I1	Ruler	Clear	50
V1	David	Bangkok	100	I1	Ruler	Clear	300
V3	John	Brisbane	300	I3	Pencil	Black	200
V1	David	Bangkok	100	I3	Pencil	Black	50
V4	Tom	Bangkok	100	I5	Ruler	White	100
V1	David	Bangkok	100	I5	Ruler	White	400
V1	David	Bangkok	100	I6	Eraser	White	100

Fig. 3. A population of FIRST

Figure 3 shows a population (rows) which instantiates FIRST. Remember FIRST is formally a relation variable (relvar) whose value at a point in time is a relation (a subset of the Cartesian product of domains) in relational database. We have called a relvar a relational table structure. We will call a relvar together with its population a relational table. This term is used when the population is referred to.

The relational table FIRST in Figure 3 clearly shows redundant information. The redundant information is acceptable in the case that the relational table is read only. This relational table is ready for querying. However, what if the relational table structure is just created without any data row population? How to insert rows into it?

A. Insertion Anomalies

The insertion problem is also called insertion anomaly. An insert operation in both the relational database principle and the SQL language, insert the entire row(s) into the relational table. If the relational table structure is designed with correct insertion awareness, there are two problems as follow:

1. Some information cannot be inserted since the row which contains the information violates the primary key not null constraint.
2. Redundant information, or conflict information can be inserted to the same relational table.

The first problem states that some information cannot be inserted to a table because the row has a null value in the primary key attribute. The DBMS, who enforces the primary key constraint, rejects the insertion. Note that it does not mean that the primary key is the problem. The problem is this table has design flaws and the primary key helps detect it.

The second problem is about insertions of redundant or conflict information. In Figure 3, there are some redundant information. They do not cause problems as long as they are consistent. Inconsistence information is undesirable especially in data-intensive applications such as data mining, decision support systems, Business Intelligence (BI), and Management Information Systems (MIS).

B. Deletion Anomalies

The deletion operation in relational database, and also in the SQL language, removes the entire row(s) from relational tables. When only an information on the row needs to be removed, a deletion operation may remove other information on the same row unintentionally. This is called the deletion anomaly. The unintentionally removal of other information is also referred to as the information lost problem.

C. Update Anomalies

The modification of redundant facts to ensure information consistency have been a challenging problem in database operation since the early years of computerized data processing. Even nowadays, we asked about problems of having redundant information, people seem to think of storage space and multiple update problems. In fact, these two problems are now much less serious than the insertion and deletion anomalies.

A main concern about normalization is to reduce the multiple update problem or update anomalies within the same relational table. Update anomaly is the problem of modifying multiple occurrences of the same information within a relational database table but does not have all occurrences

modified; thus, leads to conflict information or information inconsistencies within a relational table.

In the early years of data processing, the update anomaly was a very serious problem. Transaction atomicity was only available in enterprise level DBMS and a system failure during an update operation could lead the database table into an inconsistent state. However, nowadays even a personal DBMS on a small personal computer has the ability to handle the atomicity property of transactions. This means that the update of redundant information in a table is no longer a problem. An update statement such as the SQL UPDATE on a DBMS could guarantee the atomicity, either all redundant occurrences are modified, or none are.

So, among the three anomalies, the insertion and deletion anomalies are still serious problems. The solution is to improve the relational table structures to meet higher standard. In this particular example, the split of the FIRST relational table structure into three smaller relational table structures, solves the problems.

III. The Normalization Process

The normalization process can be summarized into only a few steps. The input comprises all attributes and all dependencies between attributes. There are several kinds of dependencies, three of which play important role in the normalization process and will be further discussed. They are the functional dependency, the multivalued dependency, and the join dependency. The output is a set of relational table structures which guarantee to be free from the insert, delete, and update anomalies, if performed up to the final normal form level, the 5NF. In practice, we are often asked by practitioners if it is necessary to perform the normalization process up to the 5NF? The answer is: perform the normalization process up to the normal form level that the design team understands. There is no need to do things that one does not clearly understand, especially in professional tasks. The normalization process steps are as follow:

Given: All attributes and all dependencies between related attributes of a relational table structure

Output: Relational table structures which have less, or no insert, delete, and update problems.

Process:

Step 1 :From the given attributes, form relational table structures which satisfies the 1NF definition.

Step 2 :For each relational table structures, consider if it agrees with the next higher normal form definition. If yes, do nothing. If no, then split the table structure into smaller table structures which agree with the higher normal form.

Step 3: Repeat Step 2 until all relational table structures satisfy the desired normal form definition.

IV. Functional Dependence and Related Normal Forms

Dependencies between related attributes play important roles in the quality control of relational table structures. Incorrect placement of such dependencies causes insert, delete, and update problems. The first dependency which is the sole dependency considered from the 2NF to the BCNF is the Functional Dependency (FD).

Definition: A functional dependency is a relationship between attributes in the form of function. Given a relational table structure T, attribute B of T is functionally dependent on attribute A of T, symbolized by A → B, if and only if, whenever two tuples of a relational table of T have the same A value, they must have the same B value. A, and B may be composite attributes.

A is called a determinant, and b is called a dependent. A → B reads A determines B, or B depends on A.

The FDs must be given. They must be known from the application domain. Note that we do not normally obtained FDs from data mining of FDs as interesting rules from given data sets. FDs are obtained from application experts and regulations.

The next dependency between attributes, is the Full Functional Dependency (Full FD):

Definition: Attribute B of relational table structure T is fully functionally dependent on attribute A of relational table structure T if it is functionally dependent on A and not functionally dependent on any proper subset of A. A, and B may be composite attributes.

According to the definition, the case where A is a simple attribute (comprises only one attribute) is always a full FD. The case where the determinant is a composite may lead to a functional dependency which is not a full FD.

Definitions of 1NF to BCNF table structures are defined as follows:

Definition: A relational table structure T is in the first normal form (1NF), if and only if all of its attributes contain atomic values only, and each attribute belongs to only one domain.

Definition: A relational table structure T is in the second normal form (2NF) if and only if the relationship between the primary key and every nonkey attribute is in full functional dependence.

Definition: A relation table structure T is in the third normal form (3NF) if and only if T is in 2NF and there are no functional dependencies between nonkey attributes of T.

Raymond F. Boyce, a colleague of E. F. Codd at IBM, was the first one who notice the problem of 3NF relational structure. Codd was very concerned, and together with Boyce, they co-invented a new definition of the 3NF called the new 3NF [3]. After some confusions in the database community, the new 3NF was renamed Boyce-Codd Normal Form (BCNF) to honor them and avoid the confusion on the names.

Definition: A relational table structure T is in the Boyce/Codd normal form (BCNF) if and only if every determinant in T is a candidate key of T.

V. Multivalued, Join Dependencies, and Related Normal Forms

There are relationships between attributes which are not in the functional format as discussed in the previous section. The functional dependence is a relationship between attributes in the form of function; it is either m:1, or 1:1. What about m:n or 1:m relationships between attributes? So far, we have not yet considered them. Up to BCNF, the only dependency which is referred to is FD only.

There are misconceptions that normalization up to the 3NF or BCNF is enough. We strongly disagree. Our point is: if only up to the 3NF or BCNF is considered, only FDs are considered and m:n or 1:m relationships between attributes are ignored. When there are m:n relationships between attributes, and attributes are collected together to form 1NF

relational table structures, the primary key will not be easy to find. This is often the case when a report structure with 1:m or m:n relationships between attributes is directly used as a table structure. Technically, a pair of 1:m or m:n relationships between attributes is called a pair of multivalued dependencies.

Definition: Given a relational table structure T, with attributes X, Y, and Z, the multivalued dependence (MVD) T.X → → T.Y holds in T if and only if the set of Z-values matching a given (X-value, Y-value) pair in T depends only on the X-value and is independent of the Y-value. X, Y, and Z may be composite.

MVDs always come in a pair. Given the relational table structure T(X,Y,Z), the MVD T.X → → T.Y holds if and only if the MVD T.X → → T.Z also holds. MVDs always go together in pairs in this way. For this reason, it is common to represent both in a single joint statement, using the notation: X → → Y | Z.

Also, relational table structure T, with attributes X, Y, and Z, can be nonloss-decomposed into its two projections T1(X,Y) and T2(X,Z) if and only if the MVDs X → → Y | Z hold in T. So, MVDs as defined can exist only if the relational table structure T has at least three attributes.

Definition: A relational table structure T is in the fourth normal form (4NF) if it is in BCNF and all MVDs in T, are FDs only.

There is a basic principle of information preservation called the lossless join property. A relational table can be split if and only if, the projections (small tables after the split) can be joined back to produce the original relational table.

Note that a relational table which can be split according to the lossless join property may be kept as it is. There is no point to split all the tables that can be split. Only those tables which have insert, delete, and update problems should be split. Said otherwise, we should split the relational table structures only when it does not satisfy a desired normal form. At this stage, it is obvious that there are only two kinds of relational table structures: one that cannot be split, and one that can be split.

The 4NF is based on the concepts of FDs and MVDs, which are not general enough. MVDs involves three set of attributes in a relational table structure that can be split into two smaller ones. What if there are more than three set of attributes in the relational table structure? Fagin went on beyond the 4NF to find the most general dependency possible: the join dependency [5].

Definition: Relational table structure T satisfies the join dependency (JD): * (A, B, C, . . . , N) if and only if T is equal to the join of its projections on A, B, C,…, N, where A, B, C, . . . N are subsets of the set of attributes of T.

According to the above definition, what is join dependency? Is it rare? Is it hard to find in practice?

The concept of join dependency is in fact very simple: what does it mean by "if T is equal to the join of its projections on A, B, C,…, N" ? The answer is: T is equal to the join of its projections on A, B, C,…, N, means T can be split into A, B, C,…, N. So, a join dependency is the ability to split a relational table. It is as simple as that.

The following two paragraphs are from the 4th edition of C. J. Date's book, An Introduction to Database Systems [10] which was published in 1986:

R(A,B,C) satisfies the JD *(AB,AC) if and only if it satisfies the pair of MVDs A → → B | C

Since this theorem can be taken as a definition of MVD, it follows that an MVD is just a special case of a JD, or that JDs are a generalization of MVDs (rather as MVDs are a generalization of FDs). What is more, it is immediate from the JD definition that *JDs are the most general form of dependency possible*.

A relational table structure R satisfies the JD *(AB, AC) means R can be split into two smaller relational table structures. This implies that R has the MVDs A → → B | C. Any tables that can be split have join dependencies. They are very common in practice.

The above property can be used to decide if a splitable table should be split or should be left as it is. The normal form which refers to the join dependency (JD) is the Project/Join Normal Form (PJ/NF) or 5NF.

Definition: A relational table structure T is in projection-join normal form (PJ/NF) or the fifth normal form (5NF) if and only if every join dependency in T is implied by the candidate keys of T.

VI. Clarification of Misconceptions on Normalization

In this section, the misconceptions or misinterpretations on the normalization process are summarized.

A. The 1NF and the role of the normalization process.

Given an application, how to start designing relational table structures? The difficult part is this starting point, the first normal form (1NF). The normalization topic of database textbooks and literatures only few attributes are used in order to present the already complicate relational database design topics. Those attributes are therefore shown to form a single starting table. In practice, all the required attributes are known from the system analysis and design of the application processes, it is obvious that all those many attributes, typically hundreds or even thousands of them, cannot be combined into a single starting relational database structure.

The normalization process is regarded by many as relational database design steps. In fact, conceptual modeling together with its transformation, is required first. The normalization process alone does not give the number of relational table structures required for a given application. Instead, it tells us if a given relational table structure is good enough, or ready to be deployed or not. The normal forms, which are clearly defined, give quality control levels of relational table structures. The higher normal form level a relational table structure achieved, the better quality for database operations it is assured.

Notice that conceptual modeling using the Entity Relationship Model and some other similar models do not consider relationships between attributes. They only consider relationships at the entity or object level. Transformation from such conceptual diagrams does not consider relationships between attributes. Functional, multivalued, and join dependencies are not known. The relational table structures obtained are therefore considered 1NF only. This is the reason why we need to use the normalization process as the quality control technique over relational table structures after their transformation from the ER diagrams. This is to ensure that the result relational table structures are ready to be deployed and have minimum insert, delete, and update problems.

B. *Over Normalization and Performance Issues.*

Academically, there is no such thing as over normalization. The term is used by practitioners. Higher normalization simply handles more advanced problems such as MVDs and JDs, as well as simpler problems of FD misplacements. However, there are problems of over splitting tables unnecessarily. The normalization process advises us not to split tables if they are already good ones, the ones that satisfy the desired normal form.

The normalization process explains that when a relational table is not good enough, does not agree with a normal form definition, it should be split into smaller ones. The normalization process does not encourage splitting of relational table structures. Instead, the normalization process encourages database designers not to split relational tables if they are already good and suggests that the number of relational table structures be kept minimum. Higher normalization does not always result in a greater number of table structures. In the case of 1NF table structures which are already good, they could all pass the 5NF quality control level and need no further splits.

To avoid insert, delete, and update problems, a table may need to be split. As a result, some queries may require the join of several tables. The "performance problems" which are widely mentioned as a weak point of normalization is in fact the query performance of the join operations which can be improved by using both physical access mechanisms and better hardware. In contrast, as mentioned earlier, the insert, delete, and update problems cannot be solved by using physical access mechanisms and better hardware.

C. *Higher Level of Normalization and Applications*

Normalization up to BCNF refers to FDs only. 4NF refers to MVDs, and 5NF refers to JDs. They are given integrity constraints on the table structures which are independent from application processes. The level of relational table structure normalization is therefore independent of the application processes. Instead, it depends on the knowledge of the database analysis and design team. If the design team members only understand 3NF, they should not be forced to perform normalization up to the 5NF. As mentioned earlier, normalization up to BCNF handles only FDs misplacement and is not enough in practice. 4NF and 5NF are required to handle many to many relationships between attributes, which are properties of the database table structures, not the properties of applications.

D. *5NF Table Structures are Common in Practice.*

According to the 5NF definition, A relational table structure T is in projection-join normal form (PJ/NF) or the fifth normal form (5NF) if and only if every join dependency in T is implied by the candidate keys of T. An immediate consequence of this definition is: if a relational table structure cannot be split, it is already in 5NF since it has no JDs. In practice, there are so many table structures which cannot be split and are already in 5NF. The only remaining question is: if a relational table structure can be split, should we leave it as it is, or split it? The answer is also very simple: if the small tables after the split always have a candidate key of the big table, then leave the big table as it is because it is already in 5NF. The 5NF table structures which can be split only by candidate keys are also very common in practice. The case of cyclic join dependency as demonstrated in C J Date's book [4] and other followers is the rare one. The intention is to demonstrate a 4NF table structure which is not yet in 5NF.

VII. CONCLUSIONS

This paper addresses that in practical relational database design, conceptual modeling is a required phase prior to normalization which is the attributes analysis phase. Conceptual modelling is used to conceptualize all entity types and relationship types in a given application. Once the conceptual schema diagrams are agreed by all parties, they can be transformed into a set of 1NF relational table structures, not just one big table structure as often seen in textbook examples. The transformation process is well established. There are several classic textbooks such as [11] that describe the transformation from ER diagrams to relational table structures which are widely used in practice. The normalization process which is the attribute analysis phase ensures that the table structures meet certain quality levels. Normalization up to 5NF should be done to ensure that table structures are free from insert, delete, and update anomalies. A join dependency in a table structure simply means the table can be split. The decision to split or retain depends on the satisfaction of the related normal form. Such 5NF table structures are common in practice. The sections on the normalization process, update anomalies, dependencies, and normal forms are extracts from [12].

REFERENCES

[1] C. J. Date, An Introduction to Database Systems, 8th ed., Pearson Education, Pearson Addison Wesley, Singapore, 2008.

[2] Codd, E.F. "Further Normalization of the Data Base Relational Model," (Presented at Courant Computer Science Symposia Series 6, "Data Base Systems," New York City, May 24–25, 1971.) IBM Research Report RJ909 (August 31, 1971). Republished in Randall J. Rustin (ed.), Data Base Systems: Courant Computer Science Symposia Series 6. Prentice-Hall, 1972.

[3] Codd, E. F. "Recent Investigations into Relational Data Base Systems," IBM Research Report RJ1385 (April 23, 1974). Republished in Proc. 1974 Congress (Stockholm, Sweden, 1974). , N.Y.: North-Holland, 1974.

[4] Fagin, Ronald, "Multivalued Dependencies and a New Normal Form for Relational Databases," ACM Transactions on Database Systems, 2 (1), September 1977.

[5] Ronald Fagin, "Normal forms and relational database operators," in Proceeding SIGMOD '79 Proceedings of the 1979 ACM SIGMOD international conference on Management of data, pp. 153-160 Boston, MA, May 1979.

[6] P. P. Chen, "The Entity–Relationship Model – Toward A Unified View of Data," ACM Transactions on Database Systems, Association for Computing Machinery, NY, pp. 9-36, March 1976.

[7] Hafeez Osman, et al., "UML class diagram simplification: what is in the developer's mind?" in Proceedings of the Second Edition of the International Workshop on Experiences and Empirical Studies in Software Modelling EESSMod '12, Article No. 5 Innsbruck, Austria, October 2012.

[8] Grady Booch, James Rumbaugh, Ivar Jacobson, Unified Modeling Language User Guide, 2nd ed. New York: Addison-Wesley, 2005.

[9] Terry Halpin and Tony Morgan, Information Modeling and Relational Databases, 2nd ed., The Morgan Kaufmann Series in Data Management Systems, 2008.

[10] C. J. Date, An Introduction to Database Systems Vol 1, 4th ed., Pearson Education, Addison Wesley, 1986.

[11] R. Elmasri and S. Navathe, Fundamentals of Database Systems, 7th ed., Pearson Addison Wesley, Singapore, 2015.

[12] Suphamit Chittayasothorn, Relational Database Systems Language, Conceptual Modeling and Design for Engineers, Limited 500 hard copies published, not available online, Nutcha Printing, Bangkok, 2017.

Fin Coil Dent Detection Using Deep Learning

Akapot Tantrapiwat
Department of Mechanical Engineering
School of Engineering,
King Mongkut's Institute of Technology Ladkrabang
Bangkok, Thailand
akapot.ta@kmitl.ac.th

Unnat Pinsopon
Department of Mechanical Engineering
School of Engineering,
King Mongkut's Institute of Technology Ladkrabang
Bangkok, Thailand
unnat.pi@kmitl.ac.th

***Abstract*—This work introduced the object detection using deep learning in order to detect and locate dents on fin coils. It was aimed at using the AI as a tool to detect fin coil dents and restore them in the fin coil manufacturing and assembly processes. Not only were the images of dents used to train object detection models, two different types of distinctive marks were added for the purpose of positioning calibration in the system. Three scalable models of the state-of-art EfficientDat D0, D1 and D2 were used and compared for their accuracies and performances. All models were trained successfully with the custom dataset. It took only 30 epochs to achieve a functionable performance. The dent detection accuracies which were considered from the True Positive, obtained from the D0, D1, and D2 models were 55%, 66% and 75% respectively. The three models can identify additional marks with 100% accuracy. In all models, there was no False Negative detection in all object classes showing good potential of using the models in the real applications.**

Keywords— fin coil, dent detection, deep learning, object detection, EfficientDat

I. INTRODUCTION

In the HVAC (Heating, Ventilation, and Air Conditioning) industry, finned coil heat exchangers play a critical role in maintaining energy efficiency and system performance. However, these coils are prone to dents and deformations due to mishandling, environmental factors, and operational wear. Even minor dents can disrupt airflow, reduce heat transfer efficiency, and lead to increased energy consumption. Traditional methods of detecting fin coil dents rely on manual inspection, which is time-consuming, labor-intensive, and prone to human error. Therefore, there is a growing need for automated and accurate dent detection solutions.

Recent advancements in deep learning have enabled significant progress in automated defect detection across various industries. Convolutional Neural Networks (CNNs) and other deep learning architectures have demonstrated remarkable success in image-based fault detection, offering high accuracy and efficiency. This paper explores the application of deep learning techniques for fin coil dent detection, aiming to develop a reliable, non-intrusive, and scalable solution. By leveraging computer vision and neural networks, the proposed approach seeks to enhance quality control in HVAC systems while minimizing maintenance costs and human intervention.

II. RELATED WORKS

The recent advancements in deep learning-based approaches have improved the detection of metal surface dents and deformations by focusing on key methodologies, datasets, and performance metrics. They can be applied to various applications and industries. Many research works have been carried out to automatically detect various kinds of metal surface defects.

A. Approaches for Metal Surface Defect Detection

Deep learning models, particularly Convolutional Neural Networks (CNNs), have revolutionized metal surface defect detection by automating feature extraction and classification. For instance, EfficientNetB3, ResNet-50, and MobileNetV2 have been widely adopted for their ability to handle complex textures and varying defect sizes. EfficientNetB3, in particular, achieved an accuracy of 0.981 and an F1-score of 0.982 on the IMTCSD dataset, demonstrating its effectiveness in detecting defects even on dirty surfaces [1]. Similarly, YOLO-based models, such as YOLOv5 and YOLOv7-tiny, have been optimized for real-time detection, with improvements like the CS-Player module and Global Attention Mechanism enhancing their ability to detect small and overlapping defects [2][3].

B. Challenges and Innovations in 3D Defect Detection

Detecting defects on three-dimensional (3D) metal surfaces presents unique challenges, such as inaccurate camera angles and image distortion. Recent studies have addressed these issues by proposing geometric transformations and hardware parameterization to generate high-quality datasets for 3D products like H-beams. These methods have achieved an average F1 score of 0.932 and an AUC of 0.99, highlighting their near-ideal performance [4]. Additionally, lightweight models like LSDNet and GDM-YOLO have been developed to balance computational efficiency and detection accuracy, making them suitable for edge device environments [5][6].

C. Datasets and Performance Metrics

Public datasets such as NEU-DET and GC10-DET have played a pivotal role in advancing research in this field. NEU-DET, containing 1,800 images of six defect types, has been widely used to train and evaluate models like EDDN and DIN, achieving accuracies of up to 0.996 [1][7]. Performance metrics such as mean Average Precision (mAP), F1-score, and AUC-ROC are commonly used to assess model effectiveness. For example, an improved YOLOv5 model achieved an mAP of 79.8% on the GC10-DET dataset, outperforming traditional methods [8].

D. Various Feature Detection in Different Applications

Different techniques and works have been carried out for different object features and applications. A study by Zhou et al.[9] proposed a CNN-based automated visual inspection system for PCB defect detection, achieving high accuracy while reducing human intervention. Transformer-based models like Vision Transformers (ViTs). In different feature like textile product, a technique, called Texture Defect Detection, has revolutionized defect detection in fabrics, identifying weaving defects, stains, and tears [10]. This recent work introduced a self-supervised learning approach to detect textile defects without extensive labeled datasets, significantly reducing the data dependency. Another models are trained on

XXX-X-XXXX-XXXX-X/XX/$XX.00 ©20XX IEEE

extensive datasets of wafer images, enabling them to accurately classify various types of surface defects which improve accuracy over conventional system [11]. An innovative approach such as self-supervised Context Learning, has been used to enhance the extraction of semantic features [12]. This method involves dividing images into nine patches and training an encoder to predict the relative positions between patches, effectively solving a jigsaw puzzle task. This technique enriches the semantic understanding of the encoder. To further distinguish between normal and defective areas, an affinity-augmentation method is employed, amplifying the differences in latent representations. The final detection is achieved using the support vector data description algorithm. Experimental results on the MVTec AD dataset demonstrate outstanding performance, with detection and segmentation rates of 95.8% and 96.8%.

Nonetheless, no work had been done on the product with features similar to the fin coils which are the main objective in this research. The surface of the fin coils has distinctive patten and it is prone to the damage when handling without care.

III. Fin coil and dent configuration

There are many type of fin coil used for heat exchanger. In this research, it is focusing on the air conditioner finned coil due to their very thin and weak material off the fins. The finned coil consists of a series of parallel tubes, typically made of copper or aluminum, with thin metal fins attached perpendicularly to the tubes. The coil is usually arranged in a serpentine, zigzag, or slab-like configuration, depending on the design and application. Fig.1. shows the basic configuration of the fin coil. The tubes diameters (d) are ranging from 5 mm to 12.7 mm, with consistent spaces between them. Fins are commonly made of very thin sheet aluminum due to its lightweight and high thermal conductivity. The thickness (t) is usually between 0.2 to 0.4 mm with the pitch size (P) ranging between 1.6 to 3.2 mm depending on the size of the tube and the entire coil.

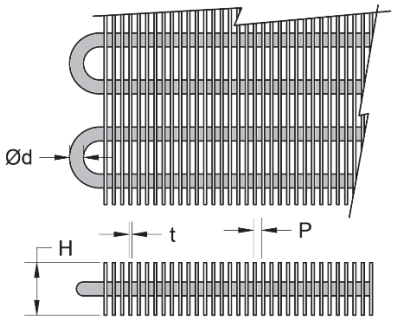


Fig. 1. Typical finned coil configuration

The fins are typically corrugated, louvered, or wavy in shape to enhance turbulence and improve heat dissipation. Fin spacing, measured in fins per inch (FPI), generally varies from 8 to 20 FPI, with closer spacing providing higher efficiency but requiring more frequent cleaning due to potential dust accumulation. The coil assembly involves mechanically expanding the tubes after inserting them through the fin stack, ensuring a tight bond for optimal thermal contact. Some coils are coated with hydrophilic or anti-corrosion coatings to improve water drainage and extend their lifespan in humid or corrosive environments. The entire assembly is housed within a structural frame, often galvanized steel, to support and protect the coil from mechanical damage. This configuration make the normal finned coil appearance looking like Fig. 2a. Because the fins are made out of thin aluminum sheet, when they are handled with excessive force, damages may occur in the form of bending in one direction. This deformation is similar to a dent on metal surface as seen in Fig. 2b.

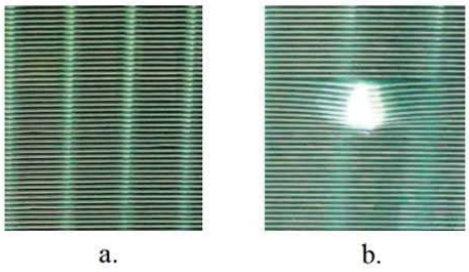


Fig. 2. Appearance of normal fin coil (a.) and the dent on the surface (b.)

IV. Dataset preparation

Because the research was aimed at creating a system that can locate the dents positions and perform the fin restoration using a fin grooming brush, the object detection system was assigned to search for dents and also some appointed marks for the purpose of using these marks as the position calibration points. For that reason, the dataset was prepared based on the three object classes, i.e., dents, red &green marks, and blue &yellow marks. The designation for dents is “Dent”, while the red &green marks and blue &yellow marks are called “R-mark” and “B-mark” respectively. The example image of the three classes object can be seen in Fig.3.

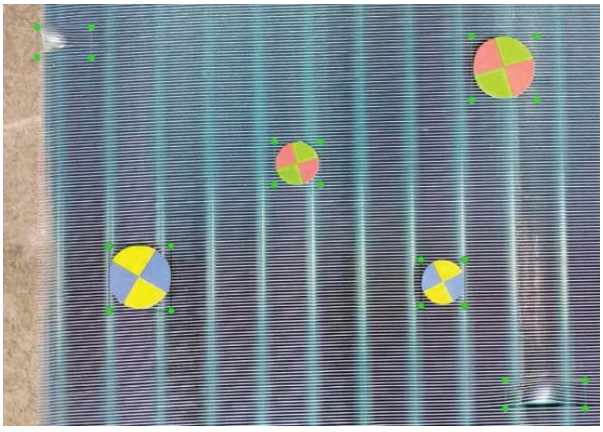


Fig. 3. Example of the dataset image which contains three classes, i.e., Dent, R-mark and B-mark

By adding the distinctive marks to the dataset, the detection performance can be easily compared and evaluated. Because dents are much harder to locate, the number of images which have colorful marks were less than images with only dents. Due to the limitation of the defect, the dataset was created with the total of 300 images. Among those, there were 40 images with the marks. The number of dents and marks are ranging from 1-8 in each image. The two different marks were distributed equally. Bounding boxes on the dents were cropped for most of the damage area which sometime extend beyond the major damage fins. For the marks which are made in circle shape, the bounding boxes were commonly made in square shape fitting all perimeter of the marks. The dataset was prepared in the Pascal-VOC format.

V. Model Description

The well known, EfficientDet, is a family of state-of-the-art object detection models developed by Google, designed to optimize both accuracy and efficiency. It is built upon the EfficientNet backbone, which uses neural architecture search and compound scaling to achieve a better balance between model size, speed, and accuracy. The model introduces the BiFPN (Bi-directional Feature Pyramid Network), an enhanced version of traditional FPNs, which allows for better multi-scale feature fusion. EfficientDet employs a compound scaling method, where network depth, width, and input resolution are scaled together to improve performance efficiently. The model comes in multiple versions, ranging from EfficientDet-D0 (lightweight and fast) to EfficientDet-D7 (large and highly accurate), catering to different computational constraints and application needs. Its architecture can be illustrated in Fig. 4.

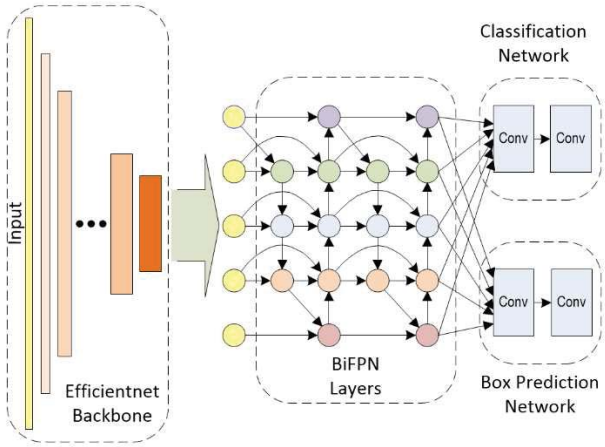


Fig. 4. The model of EfficientDet architecture

Due to its ability to achieve high accuracy while maintaining computational efficiency, making it well-suited for real-time applications like autonomous driving, surveillance, and mobile-based object detection. It out performs many previous models, such as Faster R-CNN and RetinaNet, in terms of accuracy while using significantly fewer parameters. However, despite its strengths, EfficientDet has some limitations. It can be computationally expensive for edge devices when using higher versions like EfficientDet-D7. Additionally, while it is optimized for efficiency, certain tasks requiring extremely high precision, such as medical imaging or satellite analysis, might benefit from even more specialized models. Nonetheless, EfficientDet remains one of the most balanced and versatile object detection models which is suitable for the dent detection.

VI. Experimentation

The experimentation carried out with training and validation of the different scaled EfficientDet model. It was aimed to investigate the performance of the model learning with the small size dataset.

A. Training

During model training, 250 images were selected out of 300 images from the dataset. It was accounted for 83.3% which is slightly higher than typical portion due to the limited numbers of the defected samples. The number of images which contain marks were selected in proportion to the total numbers of the image in the entire dataset. The training was done using RTX3060 GPU with Cuda 11.2 version. Three scalable models, EfficientDet D0, D1 and D2 were used as the based models. The trainings were carried out at 50 epochs, the result of cross entropy for the three scaled models are shown in Fig. 5.

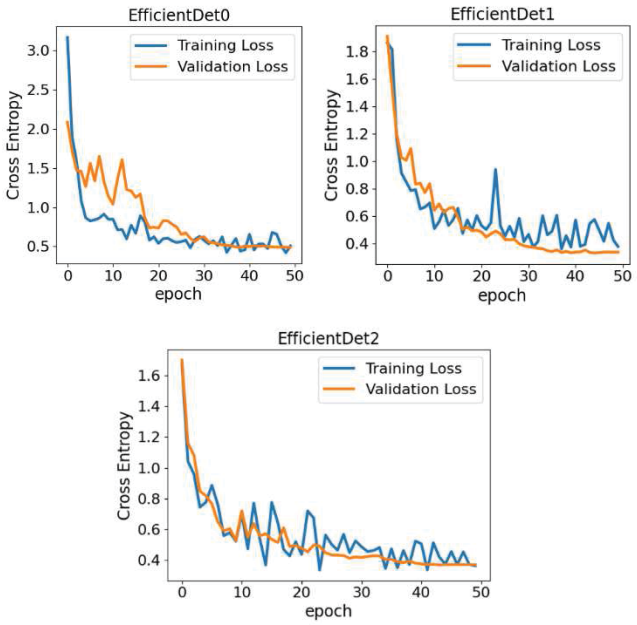


Fig. 5. Cross Entropy obtained during the tarining of the three models

B. Evaluation

In validation, the images were selected at 16.67% which is the remaining dataset from the training. Because the ultimate goal of this research is to locate the dents and restore them, It is quite important to evaluate how well the model can precisely locate and give the correct sizes of the dents. The Intersection over Union (IoU) was the key metric used to evaluate the performance of the models by measuring the accuracy of predicted bounding boxes against ground truth boxes. It was calculated as the ratio of the area of overlap between the predicted and ground truth bounding boxes area as shown as in:

$$IoU = \frac{B_p \cap B_g}{B_p \cup B_g} \quad (1)$$

Where B_p and B_g are the bounding box areas obtained from prediction and the ground true respectively. Results from validation are displayed using normalized confusion matrixes as shown in Fig. 6-8. The 0.75 threshold value was applied for all models.

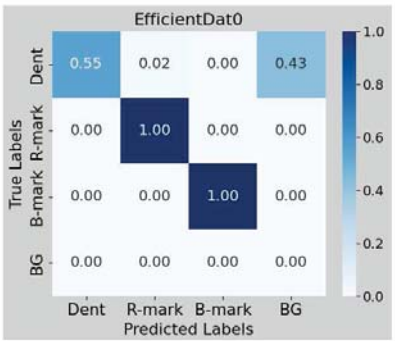


Fig. 6. The confusion matrix from EfficientDet-D0 validation

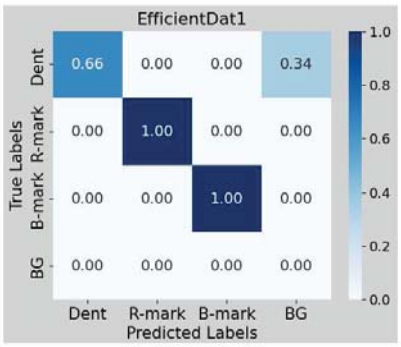


Fig. 7. The confusion matrix from EfficientDet-D1 validation

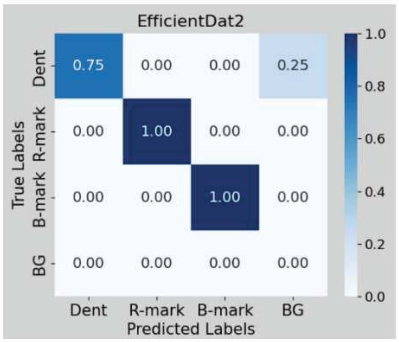


Fig. 8. The confusion matrix from EfficientDet-D2 validation

VII. Result and Discussion

From the cross entropies in Fig 5., it can be seen that the three models were successfully trained. Using the GPU as stated earlier, it took around seven minutes for the training process of EfficientDat-D0 at 50 epochs, while EfficientDat-D1 and D2 took around 10 and 15 minutes respectively. Note that the batch size were set at 30 for the D0 and D1 models, however the batch size for D2 had to be reduced to 20 due to the limitations of hardware resources.

When looking at the cross entropies for all models, they exhibit similar learning progress. The fluctuations seen in training losses have stated that there were difficult images or complexity in the training set. On the other hand, the validation losses had flatten out slightly sooner and more stable. These results show the less complexity in the validation dataset. Also it should be noted that all the models were greatly learned at around 30 epochs, after which, the learning were not much improved.

TABLE I. MODEL PARAMETERS AND PREDICTION TIME

Scaling Config EfficientDat	**Parameters and Performance**		
	Input Sizes	***Params (M)***	***Prediction Time (ms)***
D0	512	3.9	35.6
D1	640	6.6	67.3
D2	768	8.1	103.4

During validation, the prediction threshold score or confidence score were set at 0.5 for all models. From the confusion matrix in Fig. 6, it can be seen that the EfficientDat-D0 perform a fair prediction over the validation dataset.. The True Positive (TP) for the dents was encountered at 55%, meaning that around half of the dent can be identified and located. Very small percentage, 0.02%, of the dent were seen as the red &green mark. However the models can precisely locate all marks at 100% TP.

Using the outcomes shown in Fig. 7&8, it can be seen that the EfficientDat-D1&D2 models exhibit similar outcomes. By nature, the D2 model performed better due to its greater number of parameters. Both model can identify dent at 66% and 75% respectively. There were no confusion between dents and marks as seen in D0 model. Also both models can precisely locate all marks even though there were very little images with marks. It should also be noted that, in all models, there were no True Negative presented. It means that all models did not identify anything else which is not a dent as the dent. The prediction times used by the three models and their basic configuration were compared in Table 1.

VIII. Conclusion

By using the EfficientDat D0-D2, fin coil dents can be identified and located precisely, considering the limitations of the dataset due to the lack of samples. The small and light weight models have the potential to be used in the fin restoration system with edge devices. It is hope that the accuracy and reliability can be improved when introducing greater amount of images in the dataset and using larger models, i.e., D3-D7. Not only dent detection, the distinctive mark classes added to train the model allow it to perfectly locate these marks as the calibration point for the fin restoration system

References

[1] I. U. Khan, N. Aslam, M. Aboulnour, A. Bashamakh, F. Alghool, N. Alsuwayan, R. Alturaif, H. Gull, S. Z. Iqbal, and T. Hussain, "Deep learning-based surface defect detection in steel products using convolutional neural networks," Math. Model. Eng. Probl., vol. 11, no. 11, pp. 3006–3014, 2024.

[2] C. Zhou, Z. Lu, Z. Lv, et al., "Metal surface defect detection based on improved YOLOv5," Sci. Rep., vol. 13, p. 20803, 2023.

[3] S. Chen, F. Zhou, G. Gao, X. Ge, and R. Wang, "Unleashing the power of AI in detecting metal surface defects: an optimized YOLOv7-tiny model approach," PeerJ Comput. Sci., vol. 10, p. e1727, 2024.

[4] S. Suh, "Optimal surface defect detector design based on deep learning for 3D geometry," Sci. Rep., vol. 15, p. 5527, 2025.

[5] X. Xia, J. Guo, Z. Zhang, L. Wang, and Y. Guo, "LSDNet: Lightweight strip-steel surface defect detection networks for edge device environment," Opt. Lasers Eng., vol. 186, p. 108857, 2025.

[6] T. Zhang, H. Pang, and C. Jiang, "GDM-YOLO: A model for steel surface defect detection based on YOLOv8s," IEEE Access, vol. 12, pp. 148817–148825, 2024.

[7] Z. Li, X. Wei, M. Hassaballah, et al., "A deep learning model for steel surface defect detection," Complex Intell. Syst., vol. 10, pp. 885–897, 2024.

[8] F. Ren, J. Fei, H. Li, and B. T. Doma, "Steel surface defect detection using improved deep learning algorithm: ECA-SimSPPF-SIoU-YOLOv5," IEEE Access, vol. 12, pp. 32545–32553, 2024.

[9] C. Liu, X. Zhou, J. Li, and C. Ran, PCB Board Defect Detection Method based on Improved YOLOv8. Frontiers in Computing and Intelligent Systems. 6. 1-6. 10.54097/fcis.v6i2.01.

[10] T. Meeradevi and S. Sasikala, "Automatic fabric defect detection in textile images using a LabVIEW based multiclass classification approach," Multimed. Tools Appl., vol. 83, pp. 65753–65772, 2024.

[11] K. M. Ang, C. K. Ang, K. Chong, S. Tiang, W. H. Lim, A. Sharma, and T. H. Lim, "Deep learning-based silicon wafer defect classification: A performance comparison of pretrained networks," in Proc. Int. Conf. Intell. Comput. Technol., 2024, pp. 135–146. doi: 10.1007/978-981-99-8498-5_10.

[12] P. Wang, H. Yao, and W. Yu, "Self-supervised context learning for visual inspection of industrial defects," arXiv preprint arXiv:2311.06504, 2023.

TRACK 5
INSTRUMENTATION AND CONTROL ENGINEERING

A Design and Experimental Study of Fog Spraying into the Greenhouse Roof for Radiation and Relative Humidity Control

Sakapan Klaydokjan
Department of Engineering at King Mongkut's Institute of Technology Ladkrabang, Prince of Chumphon Campus,
Chumphon, Thailand
sakapan.kl@kmitl.ac.th

Kamonwan Chucheep
Department of Applied Science and Liberal Art at King Mongkut's Institute of Technology Ladkrabang, Prince of Chumphon Campus,
Chumphon, Thailand
nathaporn.su@kmitl.ac.th

Nathaporn Suwanpayak
Department of Applied Science and Liberal Art at King Mongkut's Institute of Technology Ladkrabang, Prince of Chumphon Campus,
Chumphon, Thailand
kamonwan.ch@kmitl.ac.th

***Abstract*—The objectives of this study were to investigate a design and experimental fog spraying into a greenhouse roof to control the temperature, relative humidity (%RH), radiation intensity (RI), and storage data system, which will support the maximum quality and quantity of vegetarian production. This study is a novel design and experiment concerning a greenhouse model that uses fogging spray on the roof and inside the greenhouse. The automatic control systems are applied with GY-49 sensors, AMT1001, humidity sensors, DS1307, and AT24C32EEPROM module. The experimental results are shown by LCD monitoring using a real-time clock (RTC) from 2.00 am to 8.00 pm. The radiation intensity outside and inside the greenhouse decreased by 34.78% and 47.50%, respectively. The maximum temperature inside the greenhouse decreased by 12 ^{0}C. The fogging efficiency is 83%, while the relative humidity range of 64-97 %RH.**

Keywords—Greenhouse, Radiation, Fogging, Microcontroller

I. INTRODUCTION

Based on climate change, temperatures have increased by 1 ^{0}C every year, as reported by the NOAA and IPCC (National Oceanic and Atmospheric Administration: NOAA and Intergovernmental Panel on Climate Change: IPCC) [1-2]. The focus is on transformation and system transitions in energy, land, ocean, coastal and freshwater ecosystems, urban, rural, infrastructure, and industry. The effects on agricultural production, increased drought, and decreased food security included the qualities and quantities in the tropical regions. The increasing temperatures cause significant losses and negative agricultural products. However, agricultural food production can be enhanced in a greenhouse environment to reduce the radiation intensity, temperature, and relative humidity. Vegetables are sensitive to radiation and relative humidity, and many farm crops have been used in greenhouses and nurseries. One of the key methods to decrease solar radiation includes a typical solution using shading nets [3-4] to cover the nursery and reduce heat from light intensity. This is a general technique that has been applied for agricultural temperatures, where the relative humidity and intensity radiation can be controlled. Recently, the crops have been grown extensively in the greenhouses. The agriculture industry uses it to increase production qualities and quantities. Generally, there are 2 types of nurseries, which are open systems and closed systems. The original open system was cultivated by commercially available light filters using plastic nets (PN), which can be filtered and varied by shading nets (SN) of 20%, 30%, 50%, 60%, 70%, and 80% [5]. The black slang (plastic nets) sunscreen of chili plants was studied at 3 levels to determine the appropriate image for the growth of chili plants at 50%, 30%, and non-shading [6]. It was found that light filtered to 50% induced the best growth for the pepper plants and reduced the temperature by 2-3 ^{0}C compared to the other non-shading nursery types.

The plastic nets (PN) were applied to cover a nursery that can reduce temperature, wind, hail, and relative humidity in the greenhouse to prevent insects. The plastic nets are airy fibrous structures that are well-ventilated. However, it is applied for 4-6 years before deformation, but they have no green chemistry and may cause micro-plastic residue in the soil or vegetables [7-9]. Moreover, plastic nets or slang nets cannot be controlled using relative humidity or temperature. Slang (plastics net) causes micro-plastic (MP) release from wastewater to soil, vegetables, and plants [10]. Between 4.8 and 12.7 Mtons of plastic nets were reported to have been rapidly released globally into the oceans because mismanaged waste products may fall into vegetable plant-induced microplastics [11]. Therefore, preventing the residual microplastics in the soil due to the ingress of rainwater into the soil and the vegetables, as well as temperature and humidity, can be controlled using fog spraying into the inside of the greenhouses; when the temperature inside the greenhouse rises, farmers can solve the problem by fog spraying and water spraying inside the greenhouse to reduce the temperature [12]. Ventilation fans for heat transfer and airflow are possible, inducing the greenhouse to use plastic roofing or translucent covering having higher temperature and radiation intensity. For instance, polyethylene (PE), polycarbonate (PC), glass, or acrylic are the closed systems for a nursery called a greenhouse.

Recently, the automatic control and collection of data for smart farming have become more convenient for storage in real-time. Farmers can use the data to analyze and solve problems to increase the quality and quantity of production types [13]. Moreno et al. [9] developed a real-time clock (RTC) module system, a temperature sensor, and a humidity control system (DHT11) used to store data forward to the Internet of Things (IoT) [14-15] with a control system alarm according to the certain parameters.

This research investigates the design and experiment with a novel fogging inside the greenhouse roof design, which has a roof to reduce light intensity, temperature, and relative humidity inside the greenhouse by using a microcontroller to control the operation and collect the data from an SD card. The data is shown with LCD monitoring and an alarm on the water level on the mobile phone via the Internet of Things.

II. THEORY

To find the volume of the fogging greenhouse roof, the parabolic equation is integrated to form the area and volume under the parabolic curve, as shown in Fig 1.

A. *Fogging volume of the greenhouse roof*

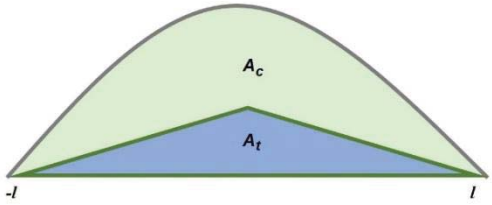


Fig. 1. Diagram of a volume fogging of the greenhouse roof sections; A_c is the fogging volume part and A_t is a part inside the greenhouse.

The area of the triangle is A_t and the part of the total area curve ($A_{ct)}$ is shown in Fig. 1. Therefore, the fogging area is equal to $A_c = A_{ct} - A_{t,}$ and the volume (V_c) of the fogging greenhouse roof can be calculated by equation (1):

$$V_c = A_c \times L \quad (1)$$

Where L is the length of the base of the fogging greenhouse.

The calculation for the volume V_c of the greenhouse roof is used to measure the level of water that should be prepared in the water tank the duration for setting up the automatic water filling system and the efficiency of the fogging system (η_{ic}) greenhouse can be computed by [16-17] and modified by equation (2).

$$\eta_{ic} = \frac{T_{cmax} - T_{cmin}}{T_{gmax} - T_{gmin}} \quad (2)$$

Where η_{ic} is the efficiency of fogging, T_{cmax} is the highest temperature on the cover greenhouse, T_{cmin} is the minimum temperature on the cover greenhouse, T_{gmax} is the highest temperature in the greenhouse, T_{gmin} is the minimum temperature in the greenhouse.

III. MATERIAL AND METHODS

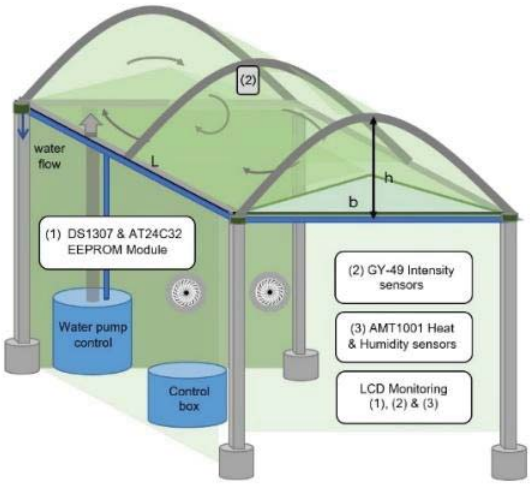


Fig 2. Schematic diagram of fog spraying into the greenhouse roof.

The greenhouse fogging [18-19] control automation can be designed and divided into 2 parts. Firstly, fog spray into the greenhouse roof is applied to reduce the solar radiation and temperature inside the greenhouse. Secondly, fog and water spraying are applied to the relative humidity and temperature greenhouse control. Both systems were set up using microcontroller monitoring sensors and SD cards. The greenhouse roof was made of PE, a thickness of 0.1 mm that can absorb light radiation wavelength range of 400-700 nm, and a refractive index of 1.60 [20]. A small vent side allows air to circulate, and the pediment is at the bottom so that the water from the fog spraying can flow down the green pipe to the ground.

A. Fogging control system

The fogging and water spraying are divided into 2 parts, as shown in Fig.2. The first part has a circuit that maintains the water level in the tank for fogging and water spray, where the ultrasonic type humidifier is applied with 10 channels/ machine at four points inside the greenhouse roof and inside the greenhouse, size 65 W, placed below the water level 7-9 cm, the same way to create a masking mist, fan size 220 V, 0.15 A and using ultrasonic waves with a high frequency of 1000 -2000 kHz. Such a frequencies cause water molecules to vibrate, contract, and expand spray fog at a speed of 1.25 ml/s, moving water particles with a higher acceleration than the gravity of the Earth. The fogging particles escape to the water surface, creating a small fountain about 0.4 - 1.5 µm in length. It uses an automatic water level control system to maintain a stable water level. The fogging water is condensed and flowed into a pipe to the ground or a tank. Air pressure on the roof can be reduced by channels at the four corners of the greenhouse for the fogging water to flow.

B. Water control system

The fogging inside the greenhouse of both processes can be applied the same. The fogging was then passed through a pipe to circulate along the greenhouse roof until the fogging was saturated to protect the radiation intensity of the greenhouse.

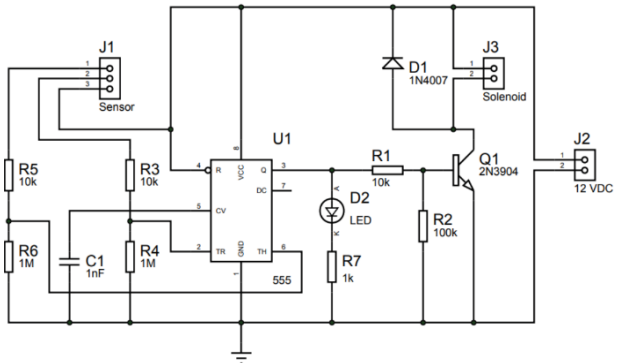


Fig 3. Circuit diagram of solenoid water level control.

The circuits in Fig. 3 have been designed using the principles of bistable circuits with IC555, which takes the input into the circuit with two water level sensors at 2 different levels (HIGH level and LOW level) .Therefore, the state of operations has 2 states; H and L for the water pump operation can be flowed for the operating state with input H and L, as conditions and keep the cycle working .The circuit in Fig. 3 is applied to control the water level systems in a tank

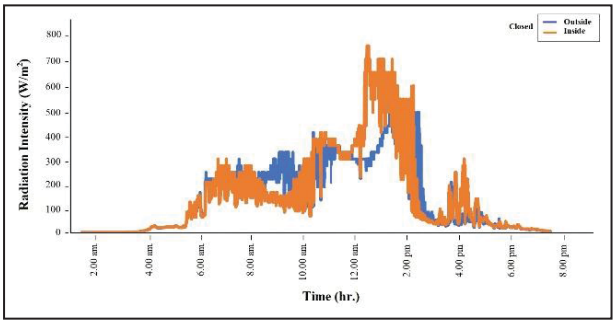
to measure and control water spraying and fogging dispersive in the greenhouse roof and inside the greenhouse, in which the level water warning can be alarmed by the mobile phone system.

C. Sensors control system

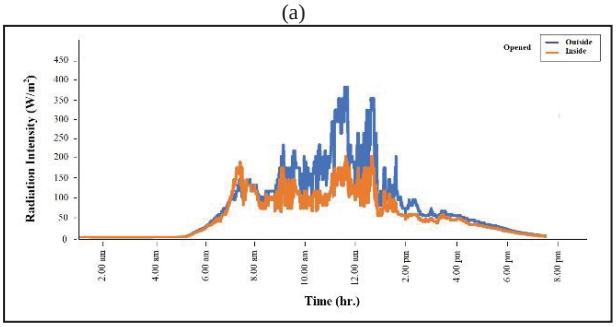
To install all the sensors for fogging and water spray of the greenhouse and measure the radiation intensity (GY-49 sensors), the temperature and relative humidity sensor (AMT1001) and real-time clock (DS1307 clock module and AT24C32 EEPROM) were used. A microcontroller was applied to control the system, where the data collection was saved in an SD card to measure the temperature, relative humidity, and light intensity was recorded from 2.00 am to 8.00 pm. However, the data should be kept continuously set and stored for 24 hrs.

IV. RESULTS

In this case, the measurement of radiation intensity outside the greenhouse percentages was compared with the fog system turned off and turned on, with the fogging system by GY-49 sensors outside and inside of the greenhouse having percentage differences of 34.78% and 47.50%, respectively, as



(a)



(b)

Fig. 4. The radiation intensity of the greenhouse (a) closed fogging system and (b) opened fogging system.

The experimental results of fogging spray to reduce the light intensity in the greenhouse using 4 GY-49 sensors were presented. We installed 2 GY-49 sensors inside the greenhouse and another on the cover of the greenhouse roof. The radiation intensity is measured inside the greenhouse range of 176.28-495.27 W/m^2. The fog spray, water spray, and relative humidity control system affect the temperature inside the greenhouse. The temperature values tended to decrease, which is compared to the fogging system being turned off to induce the maximum temperature range of 27-63 ^{0}C, respectively.

TABLE 1 LIGHT RADIATION INTENSITY INSIDE THE GREENHOUSE WITH THE FOGGING STATE TURN OFF AND TURN ON.

Work state	I_m OS (W/m^2)	I_m IS (W/m^2)	% Diff
Off	756.11	495.27	20.85
On	365.80	176.28	34.96
% Diff	34.78%	47.50%	

OS is the experimental sensors outside of the greenhouse,
IS is the experimental sensors inside the greenhouse.

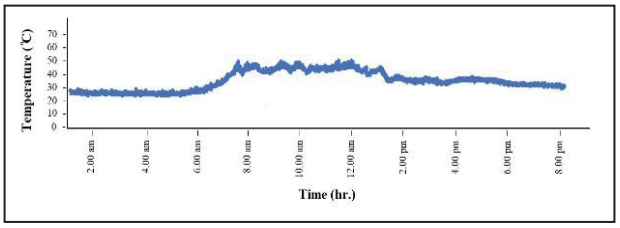
TABLE 2 TEMPERATURE AND THERMAL ENERGY OF THE GREENHOUSE WITH THE FOGGING SATE TUREN OFF AND TURN ON.

Work state	T_{max} (^{o}C)	T_{min} (^{o}C)	ΔT (^{o}C)
Off	63	51	36
On	51	27	30
ΔT (^{o}C)	12	6	6

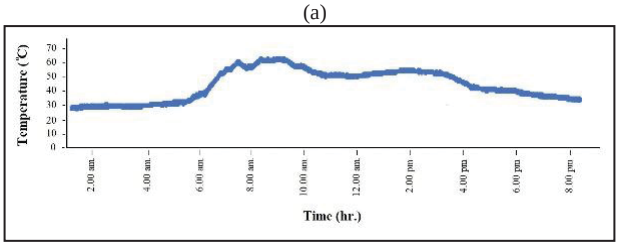
TABLE 3 RELATIVE HUMIDITY INSIDE THE GREENHOUSE WITH THE FOGGING STATE TURN OFF AND TURN ON.

Work state	%RH_{max}	%RH_{min}	Δ%RH
Off	<60	<60	0
On	97	64	33
Δ humidity	37	4	33
% Diff	23.5	3.22	4.35

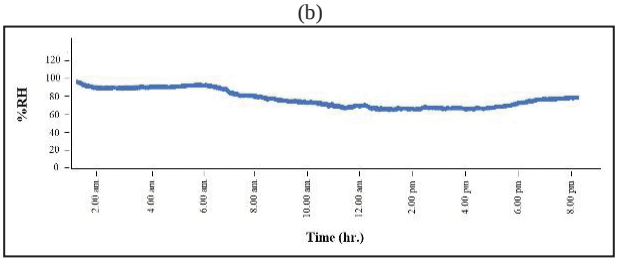
The automatic systems turned on the fogging spray range can induce a temperature of 21-51 ^{0}C and the relative humidity is measured from the range of 64-97 %RH as shown in Fig. 5(a)-(c) from the temperature recording from the SD card while the fog system is turned off and turned on the fog system during 2.00-8.00 pm.



(a)



(b)



(c)

Fig. 5. The real-time data of the fogging control systems measured (a) the temperature of the fogging system is closed, (b) the temperature of the systems is opened and, (c) the humidity inside the greenhouse of the systems is opened.

V. Discussions

The fogging greenhouse water control systems found problems with the water pump having certain drawbacks:

1. The fogging generation system has 10 channels/machine. It was found that the fogging generators take a long time to fog saturate and reduce the radiation intensity. The fogging pieces/machine should be added to the system setup.

2. The temperatures measured by the sensors in the greenhouse in both turn-on and turn-off systems are higher than the temperature of the atmosphere due to the sensitivity of the GY-49 sensors, where the valuable measurement of radiation intensity is proportional to the temperature inside the greenhouse.

3. In this experiment, camouflage fog was employed to regulate the temperature, relative humidity, and radiation intensity. Humidification fog was generated, and water was sprayed onto the greenhouse roof. The experiments were carried out without any vegetation or plants. Furthermore, farmers can adjust their methods based on the types of plants to optimize the effects of climate change, as reports indicate that global warming will result in rising temperatures in the agricultural sector, economic activities, and human interactions from 2021 to 2040. Climate change indicated a temperature rise in Southeast Asia [1, 2].

However, the fogging spray system for the greenhouse roof structure is designed to be 2 meters wide and 4 meters long. Farmers can build a fogging greenhouse by adjusting the number of fog sprayers and the volume of water reserves according to the ratio in the experiment design.

Conclusions

The experimental fog spraying into the greenhouse roof and inside the greenhouse is designed by using a microcontroller system to measure radiation intensity, temperature, and relative humidity in the greenhouse. The results were presented by SD card to analyze the temperature, radiation intensity, and relative humidity that can be controlled by fogging spray inside the greenhouse roof and the plant crops inside the greenhouse. It was found that greenhouse roof fogging can reduce the temperature to 12 ^{0}C, where the relative humidity can be controlled in the ranges between 64-97 %RH, and radiation intensity can be reduced in the range of 176.28-495.27 W/m^2. Moreover, the efficiency of the relative humidity in the greenhouse roof fogging design is 83%, while the experimental fogging directed fogging spray inside the greenhouse [17] reducing the temperature of 6 ^{0}C, including the system in the same of black plastic nets reduced light 50% [5] for the vegetarian cover of the greenhouse.

Acknowledgments

We thank Nutsiwat Pholnark and Apipoo Chaiwiset assistant researchers at King Mongkut's Institute of Technology Ladkrabang, Prince of Chumphon Campus, and Electronics Engineering Laboratory of King Mongkut's Institute of Technology Ladkrabang, Prince of Chumphon Campus.

References

[1] NOAA. National Oceanic and Atmospheric Administration., 2022.
[2] IPCC. Working Group II Contribution to the Sixth Assessment Report of the Intergovernmental Panel on Climate Change**,** Climate change 2022, Intergovernmental Panel on Climate Change, Printed March 2022 by the IPCC, Switzerland
[3] L. Milenkovic, L. Šunić, and E. Fallik, "Effect of shading by coloured nets on yield and fruit quality of sweet pepper" Zemdirbyste, vol.104(1), pp.53–62,2022.
[4] Z.S. Ilić, L. Milenković, L. Stanojević, C. Dragan, and F. Elazar, "Effects of the modification of light intensity by color shade nets on yield and quality of tomato fruits" Sci. Hortic., vol.139, pp. 90–95 2012.
[5] I. M. Alhelal, A.r A. Albadawi, A.A. Alsadon et al. "Effects of Shading Nets Color on the Internal Environmental Conditions, Light Spectral Distribution, and Strawberry Growth and Yield in Greenhouses" Plants, vol. 13, 2318, 2024.
[6] P. Rungruksatham and L. Khurnpoon "Effect of Shade Net and Fertilizer Application on Growth and Quality in muskmelon (Cucumis melo. L. var. reticulatus) after Harvest", Int. J. Agric.Technol., vol. 12(7.1),1407-1417, 2016.
[7] Z.S. Ilića, and E. Fallik, "Light quality manipulation improves vegetable quality at harvest and postharvest: A review," EEB, vol.139, pp. 79–90, 2017.
[8] S.A. Sánchez, A.D. Morales, J.C. Castillas, C.A. Martínez, and A.Z. Meza, "Proposal for an Automated Greenhouse to Optimize the Growth of Hydroponic Vegetables with High Nutritional Content in the Context of Smart Cities," *IOP* Conf. Series: Materials Science and Engineering. Colombia, pp. 1-11, 2020.
[9] E. H. Lwanga, N. Beriot, F. Corradini, V. Silva, X. Yang, et al. "Review of microplastic sources, transport pathways and correlations with other soil stressors: a journey from agricultural sites into the environment," Chem. biol. technol. agric., vol. 9, pp.1-20, 2022.
[10] H. Fakour, S.-L. Lo, N.T. Yoashi, A.M. Massao, N.N. Lema, F.B. Mkhontfo, P.C. Jomalema, et al. "Quantification and Analysis of Microplastics in Farmland Soils: Characterization, Sources, and Pathways," Agriculture, vol. 11, pp. 330, 2021.
[11] Y. Picó, and D. Barceló, "Analysis and Prevention of Microplastics Pollution in Water: Current Perspectives and Future Directions," ACS Omega, vol. 4, pp. 6709–6719, 2019.
[12] J.R. Bermúdez, and P.W. Swarzenski, "A microplastic size classification scheme aligned with universal plankton survey methods," MethodsX, vol. 8, pp. 101216, 2021.
[13] M. Dhanaraju, P. Chenniappan, K. Ramalingam, S.Pazhanivelan and R. Kaliaperumal "Smart Farming: Internet of Things (IoT)-Based Sustainable Agriculture" Agriculture, vol.12, pp.1745, 2022.
[14] S. Karaman, S. Yazarel, and Z. Gokalp, "Automation Application in Greenhouse," CTNS, vol.8(16), pp.154-159, 2019.
[15] M. C. Moreno, O. J. Suarez, and A. P. Garcia, "IoT-based Automated Greenhouse for Deep Water Culture Hydroponic System," 2nd Sustainable Cities Latin America Conference (SCLA). Colombia. 2021.
[16] R. KSahdev, M. Kumar, and A.K. Dhingra, "A comprehensive review of greenhouse shapes and its applications," Front. Energy, vol.13(3), pp. 427–438, 2019.
[17] K. Simek, K. Treeamnuk, and T. Treeamnuk, "Empirical modelling of temperature in fogging greenhouse**,"** TSAE 2020, E3S Web of Conferences vol.187, pp.03007, 2020.
[18] A. Harsha, K. Deekshith, B.K. Murali Krishana, K. T. Sachin, and N. Sushanth, "Automated hydroponics greenhouse monitoring system using Adafruit.io controlled by google assistant," Int. J. Eng. Res. Technol, vol. 6(15), pp. 1-4, 2018.
[19] A. Arbel, O. Yekutieli, and M. Barak, "Performance of a Fog System for Cooling Greenhouses," J. Agric. Eng. Res., vol. 72(2), 1999, 129-136.
[20] L.Rond, F.A.W.Coumans, R.Nieuwland, T. G. Leeuwen, and E.Pol1, "Current Protocols in Cytometry" Published in Wiley Online Library doi: 10.1002/cpcy.43 C 2018.

Development of a Real-Time Water Monitoring and Alert System for Sustainable Aquaculture in the Tapi River

Prasert Nonthakarn
Faculty of Science and Technology
Rajamangala University of Technology Srivijaya
Nakhon Si Thammarat, Thailand
prasert.n@rmutsv.ac.th

Sulaiman Madyod
Faculty of Veterinary Science
Rajamangala University of Technology Srivijaya
Nakhon Si Thammarat, Thailand
sulaiman.m@rmutsv.ac.th

Chariya Nonthakarn
Faculty of Science and TechnologyRajamangala University of Technology Srivijaya
Nakhon Si Thammarat, Thailand
chariya.n@rmutsv.ac.th

***Abstract*— Fish farming along the Tapi River is frequently impacted by seasonal floods and droughts, leading to substantial economic losses. This paper presents the development of a real-time water monitoring and alert system utilizing Internet of Things (IoT) technology to assist farmers in managing such risks. The system monitors water level, turbidity, and flow velocity at three key points—upstream, midstream, and downstream—using solar-powered floating units equipped with calibrated sensors. Sensor calibration was performed using standard formazin solutions and validated against manual measurements to ensure accuracy.**

Field deployment over five months demonstrated the system's ability to detect critical water level changes with a notification accuracy of 98.7%, providing farmers with an average of six hours for responsive actions. Observations showed that changes in upstream water levels propagated downstream within 3.5 to 4.5 hours. Additionally, turbidity increased from 30 NTU to 85 NTU (183%) during high-flow events. The system helped reduce fish cage losses by over 75%, from 20% to 5%. These findings support the system's effectiveness in enhancing flood preparedness, promoting sustainable aquaculture, and contributing to local water resource management.

Keywords*— Real-time monitoring, IoT, water level alert, turbidity, aquaculture, flood management

I. INTRODUCTION

During the flood season, fish farming in floating cages along the Tapi River often encounters uncontrollable natural disasters. Currently, flood warnings and water level monitoring rely on communication through phone calls to obtain information from upstream residents. This method is used to evaluate water flow, levels, and turbidity; however, it remains insufficient to fully prevent damages, which adversely affect both the local community and regional economy [1-2]. The traditional reliance on manual communication and observation can lead to delayed responses during critical times, exacerbating the impacts of flooding [3].

Developing a real-time monitoring and warning system that continuously reports water levels and abnormalities could assist farmers in preparing for flood events. Actions such as relocating cages, harvesting fish earlier than scheduled, or adjusting farming strategies during crises can be effectively implemented[4].

This monitoring system will include sensors to measure critical parameters, such as water level, turbidity, and flow velocity. Utilizing Internet of Things (IoT) technology, data will be collected and processed by microcontrollers and transmitted in real-time via WiFi to farmers' smartphones or computers. The system is designed to be powered by solar panels and capable of floating freely in response to rising water levels. IoT-based systems have proven to be highly effective in environmental monitoring, enabling real-time data transmission for better decision-making [1][5]. Solar-powered systems have also been widely implemented in remote areas, providing a sustainable solution for continuous operation in flood-prone regions [6].

By integrating IoT technology with flood warning systems, farmers located far downstream will be able to monitor water conditions instantly. Sensor data will improve risk assessment accuracy, such as detecting sudden water level increases or rapid turbidity changes caused by heavy rainfall, which could indicate flash floods. Notifications will be sent directly to farmers' mobile devices, enabling timely preparations[4,7].

This IoT-based flood warning system is expected to benefit fish farmers along the Tapi River in Nakhon Si Thammarat Province by enabling them to respond swiftly to upstream flood events. This innovation is anticipated to deliver long-term benefits by reducing the impact of recurrent natural disasters, enhancing occupational stability, and promoting sustainable fish farming in the Tapi River basin[8].

II. MATERIALS AND METHODS

A. Study, Feasibility Analysis, and System Design

Conduct a comprehensive study and feasibility analysis to evaluate the geographical characteristics of the Tapi River basin, identify fish farmers' needs, and determine key parameters to monitor, such as water level, turbidity, and flow velocity. Design the system architecture, including sensor selection, solar-powered microcontrollers, and WiFi communication modules, ensuring it can float and adapt to rising water levels during floods. This phase ensures the system's practicality, effectiveness, and sustainability before development and implementation.

As shown in the Figure 1, this is a solar-powered system setup that includes a solar panel, a waterproof enclosure for the control electronics, and a sensor for measuring environmental parameters such as water level, turbidity, or other critical parameters. The solar panel provides the necessary energy to power the system, making it suitable for continuous monitoring in remote areas without access to the power grid. The sensor cable connects the monitoring system to the sensor placed in the water, allowing real-time data collection and transmission.



Fig. 1. The overall components of the system

B. The assembly of system components includes key elements working together, such as microcontrollers, sensors, and the electrical system.

The process of assembling the equipment involves the following steps: integrating microcontrollers, programming and configuring controls, establishing data connections and transmissions, installing sensors, setting up the solar-powered electrical system, and configuring the power distribution control system as shown in Figure 2.



Fig. 2. The control system

C. Calibration of Equipment for Accurate Measurement.

The calibration process involved the following steps:

Standard Solution Calibration:

The sensor was calibrated using formazin turbidity standards at known NTU values (e.g., 0, 20, 50, 100, and 200 NTU). These reference values were used to generate a calibration curve, which helped align the sensor's output with actual turbidity levels.

Periodic Recalibration:

Calibration was performed on a monthly basis or whenever the equipment was relocated or reinstalled. This was done to prevent measurement errors caused by external factors such as sediment buildup on the sensor lens or environmental wear.

Cross-Validation with Manual Measurements:

Sensor readings were periodically cross-checked with manual turbidity measurements using a portable turbidity meter to ensure consistency and to validate the sensor's performance under field conditions.

This calibration protocol ensured that turbidity data collected throughout the study were accurate and suitable for real-time water quality monitoring. As turbidity changes are critical indicators of flooding and water quality shifts, the reliability of these measurements contributed significantly to the effectiveness of the alert system and the decision-making process for aquaculture management.

III. RESULTS AND DISCUSSION

The turbidity measurements at three points along the river, as shown in the table 1, indicate a gradual increase in turbidity levels over time at all three locations (Points 1, 2, and 3), followed by stabilization and a slight decline toward the end of the monitoring period. Point 1 consistently shows the highest turbidity values, starting at 21 NTU on Day 1 and peaking at 32 NTU on Day 14 before slightly decreasing. Point 2 follows a similar trend, starting at 19 NTU on Day 1, reaching a maximum of 30 NTU on Days 14 and 15, and then stabilizing around 27–29 NTU in the latter half of the month. Point 3, with the lowest values, starts at 17 NTU on Day 1, peaks at 29 NTU on Days 14 and 15, and gradually declines to 22 NTU by Day 30.

TABLE 1. The data on water turbidity

Date	Turbidity at Point 1 (NTU)	Turbidity at Point 2 (NTU)	Turbidity at Point 3 (NTU)
1	21	19	17
2	25	23	21
3	25	23	21
4	26	24	22
5	27	24	23
6	28	25	24
7	29	26	24
8	29	27	25
9	30	28	26
10	30	28	26
11	31	29	27
12	31	29	28
13	31	29	28
14	32	30	29
15	31	30	29
16	31	29	28
17	31	29	28
18	30	28	27
19	30	27	27
20	30	28	26
21	30	28	26
22	29	27	25
23	30	28	26
24	30	29	26
25	29	28	26
26	28	27	25
27	28	27	25
28	27	26	24
29	26	25	23
30	25	23	22

TABLE 2. The data on water level

Date	Water Level at Point 1 (m)	Water Level at Point 2 (m)	Water Level at Point 3 (m)
1	25	20	18
2	26	20	18
3	26	21	19
4	27	22	19
5	27	22	20
6	28	23	21
7	27	23	21
8	27	22	21
9	28	22	20
10	28	22	20
11	31	24	22
12	31	24	22
13	32	25	22
14	32	25	23
15	30	23	21
16	30	23	21
17	31	24	21
18	30	23	22
19	30	23	21
20	29	22	20
21	30	23	21
22	29	22	21
23	29	22	20
24	30	23	21
25	29	23	21
26	28	23	22
27	28	22	21
28	27	22	21
29	26	21	21
30	26	21	19

The water level measurements at three points along the river, recorded in meters, show variations over the 30-day monitoring period as shown in the table 2. Point 1 consistently records the highest water levels, starting at 25 m on Day 1, gradually increasing to a peak of 32 m on Days 13 and 14, before slightly declining toward the end of the period, reaching 26 m on Day 30. Point 2 shows moderate levels, beginning at 20 m on Day 1, peaking at 25 m on Days 13 and 14, and ending at 21 m on Day 30. Point 3, with the lowest levels, starts at 18 m on Day 1, rises to a maximum of 23 m on Day 14, and then decreases to 19 m by the end of the month.

The line graph below represents the water turbidity (in NTU) and water levels (in meters) at three different points (Point 1, Point 2, and Point 3) along the Tapi River over a one-month period, based on the sample data provided. The graph clearly shows the comparison of turbidity and water levels over time at each location.

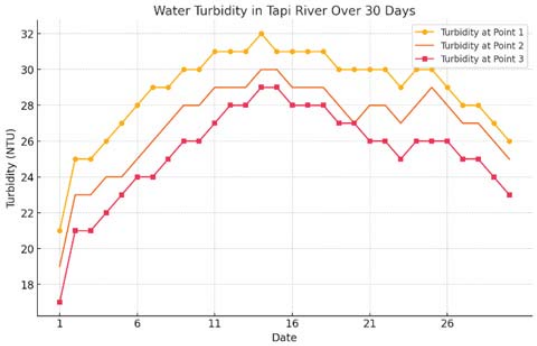


Fig. 3. The water turbidity

The line graph depicts the water turbidity (in NTU) at three different points (Point 1, Point 2, and Point 3) along the Tapi River over a span of 30 days. It illustrates the fluctuations and trends in turbidity across the three locations, with each point showing a clear rise and fall in turbidity levels. Point 1 consistently shows the highest turbidity levels, while Point 3 records the lowest values. The data reveals that turbidity increases gradually over time, with notable peaks, especially in the middle of the observation period, suggesting changes in water quality possibly due to external factors like rainfall or upstream disturbances. The graph allows for easy comparison of turbidity at each location, providing insights into how turbidity levels vary along the river's course.

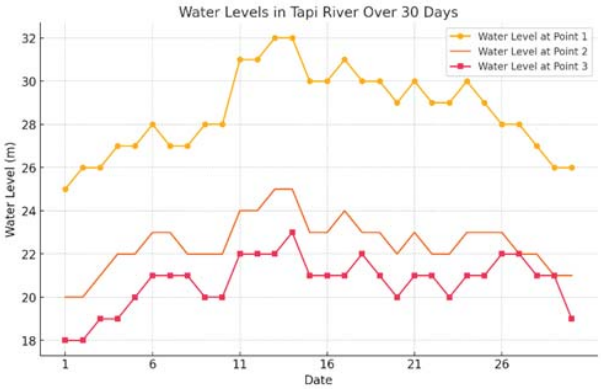


Fig. 4. The water levels

The line graph illustrates the water levels at three points (Point 1, Point 2, and Point 3) along the Tapi River over a 30-day period. The graph highlights the fluctuations and overall trends in water levels at each location. Point 1 consistently records the highest water levels, followed by Point 2, while Point 3 shows the lowest levels. Water levels generally increase during the first half of the period, with slight declines in the latter half. These variations in water levels reflect changes in river conditions, potentially influenced by factors such as rainfall or upstream water flow. The graph provides a clear view of how water levels fluctuate over time across the river's different points, helping to assess the dynamic flow patterns in the Tapi River.

IV. CONCLUSION

The analysis of the two graphs depicting water turbidity and water levels along the Tapi River demonstrates a clear correlation between turbidity at the three points and the corresponding water levels. The data shows that as the water level increases at one point, turbidity levels at all three points also tend to rise, indicating a consistent pattern of change. This suggests that higher water levels are associated with increased turbidity across the river, possibly due to the influx of sediments or other particles from upstream areas.

This correlation is in line with findings from previous research, which highlight that rising water levels often lead to higher turbidity, especially in flood-prone areas [7]. The study [4] also emphasizes the role of increased sediment load during flood events, further supporting the relationship between water level fluctuations and turbidity. The consistent relationship between water levels and turbidity in the present study reinforces the interconnectedness of these two factors and underscores the importance of monitoring both parameters. Such integrated monitoring is crucial for better water quality management, flood preparedness, and the overall sustainability of aquatic ecosystems.

ACKNOWLEDGMENT

This research has been successfully completed with support from several key organizations. The researcher would like to express sincere gratitude to the Marine Department and the Local Administrative Organization for their assistance in providing data and facilitating research activities in the study area. Special thanks are also extended to the fish farmers who cooperated in data collection and allowed the system to be tested in their fields. Furthermore, the researcher appreciates the Faculty of Science and Technology at Rajamangala University of Technology Srivijaya for their academic resources, essential equipment, and guidance throughout the research process. The support and collaboration from all involved organizations were crucial to the success of this research.

REFERENCES

[1] Li, X., & Zhang, J. (2020). "Development of an IoT-based flood monitoring system." IEEE Access, 9, 71001-71009. https://doi.org/10.1109/ACCESS.2021.3075503

[2] Zhang, T., & Yang, J. (2020). "Design of a real-time flood forecasting and warning system using IoT." Computers, Environment and Urban Systems, 79, 101395. https://doi.org/10.1016/j.compenvurbsys.2019.101395

[3] Yuan, Y., & Hwang, M. H. (2018). "Real-time flood monitoring and management system using IoT." Journal of Hydrology, 568, 204-217. https://doi.org/10.1016/j.jhydrol.2018.10.039

[4] Wang, F., Liu, S., & Zhang, Y. (2021). "Real-time flood monitoring and risk assessment in aquaculture systems using IoT." Environmental Monitoring and Assessment, 193(6), 392. https://doi.org/10.1007/s10661-021-08958-0

[5] Chen, S., & Xu, L. (2021). "IoT-based water monitoring and management system for aquaculture." Environmental Science and Pollution Research, 28(8), 10232-10242.

[6] Zhao, H., Chen, H., & Li, Q. (2020). "Design of solar-powered IoT systems for real-time flood monitoring." Sustainable Energy Technologies and Assessments, 40, 100728. https://doi.org/10.1016/j.seta.2020.100728

[7] Rahman, M. M., Islam, S., & Hasan, R. (2021). "Smart flood detection and early warning systems using IoT and big data." Journal

of Hydrology, 595, 125654. https://doi.org/10.1016/j.jhydrol.2020.125654

[8] Singh, R., Kumar, S., & Sharma, P. (2019). "IoT-based flood monitoring system for sustainable agricultural management." Environmental Monitoring and Assessment, 191(8), 533. https://doi.org/10.1007/s10661-019-7454-7

Machine Learning Approach to CMYK Label Identification through Screen Angles

1st Chitsanuwit Ar-Karachaiphong
School of Engineering
King Mongkut's Institute of Technology Ladkrabang
Bangkok, Thailand
62601125@kmitl.ac.th

2nd Farzin Asadi
Department of Computer Engineering
Ostim Technical University
Ankara, Turkiye
farzinsd@gmail.com

3rd Asst. Prof. Dr. Krit Smerpitak
School of Engineering
King Mongkut's Institute of Technology Ladkrabang
Bangkok, Thailand
krit.sm@kmitl.ac.th
*Corresponding Author

***Abstract*— This research proposes the application of AI to verify the origin of CMYK label that is used in rented machines, focusing on two printing methods: OFFSET and FLEXO. The system employs color patterns and screen color angle verification to ensure sticker authenticity. The paper applies RGB color sensors and imaging cameras, the system converts RGB data into CMYK for label validation. This process incorporates object detection and classification techniques based on deep learning algorithms using Convolutional Neural Networks (CNN) developed through the YOLOV8 framework. The developed model is integrated into an automated system connected to the machinery for real-world applications. Experimental results demonstrate that the system accurately distinguishes between OFFSET and FLEXO printing methods, enhancing compliance with lessor conditions in the labelling industry. This approach further highlights the potential of AI in decision-making and machine control automation.**

Keywords— Machine Rental, AI, CMYK, OFFSET Printing, FLEXO Printing, YOLOv8, Convolutional Neural Networks (CNN), Printing Industry.

I. Introduction

The rental of single-purpose machines, particularly in the label printing industry, faces challenges when customers violate agreements by using third-party materials. This results in revenue losses for lessors and highlights the inefficiency of traditional manual verification methods. This research aims to develop an AI-driven automated system to verify label origins, focusing on OFFSET and FLEXO printing methods [1][2]. By leveraging RGB sensors [4][5], CMYK conversion [6], and YOLOv8-based deep learning, the system ensures compliance by stopping machine operations if label fail verification [8][10][11]. Proposed technique collects data using RGB sensors, processes it through CMYK models, and applies object detection via CNNs [7][8][10]. Integrated with rented machines, this approach automates verification, enhancing accuracy and operational efficiency. This solution addresses key industry challenges while advancing automation in the label printing sector.

II. Industrial Prining Technoly and Theorem

A. Flexographic Printing Process

Flexo printing (flexography) is a direct rotary printing process utilizing flexible relief plates made from photopolymer or elastomer materials [3]. These plates transfer low-viscosity ink into substrates through a printing cylinder (commonly referred to as a plate cylinder) mounted with adhesive tapes designed for optimal height and compression. Ink is delivered to the system via an ink supply unit, often through ink pumps. The ink is transferred to an "anilox" roller, which is equipped with a doctor blade to remove excess ink from its non-engraved surface. The volume of ink transferred depends on the cell volume of the anilox roller.

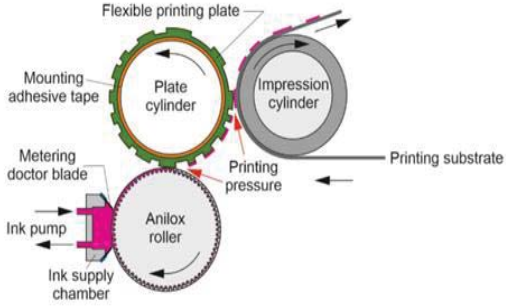


Fig. 1. Schematic description of the flexographic printing process [3].

B. CMYK Color Angles in Standard Systems

The CMYK printing (Cyan, Magenta, Yellow, Black) [4], screen angles are defined to manage the dot alignment for each color. These angles are crucial for minimizing moiré patterns caused by overlapping screen dots. The human eye is particularly sensitive to repetitive patterns when dots are aligned along vertical and horizontal structures, but less so at 45°.Thus, in traditional offset and letterpress printing, the darkest color (black) is set at 45°, while the lightest color (yellow) is set at 90°. The remaining colors are positioned at 30° intervals from the darkest: cyan at 15° and magenta at 75°.

As flexography has evolved into a high-quality printing process capable of replicating halftone separations, the traditional screen angles had to be adjusted. This is due to potential interference from the engraving angles of the anilox rollers, which can cause moiré effects. When considering the engraving angles of the anilox rollers, midlines formed by these patterns must also be accounted for and avoided.

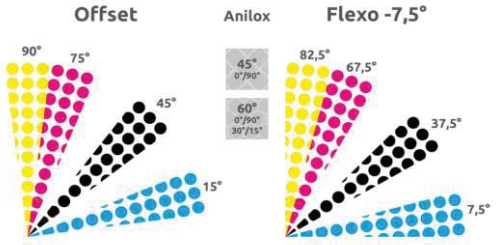


Fig. 2. Screen angles in flexography [4].

Fig. 2 shows Consequently, the screen angles in flexography are rotated by -7.5°, resulting in the following:[4]

- Cyan (C): 7.5°
- Magenta (M): 67.5°
- Yellow (Y): 82.5°
- Black (K): 37.5°

For comparison, the standard CMYK screen angles in offset printing are:[4]

- Cyan (C): 15°
- Magenta (M): 75°
- Yellow (Y): 0°
- Black (K): 45°

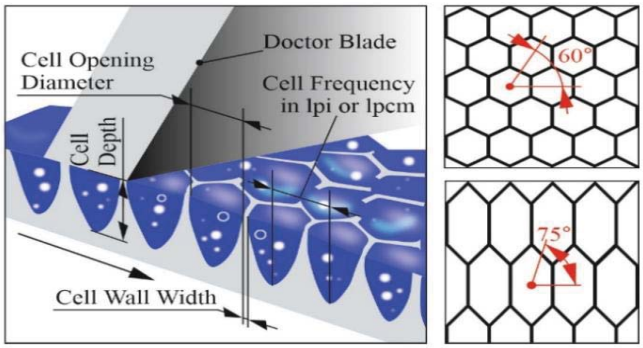


Fig. 3. Anilox roller cell geometry parameter and typical cell engraving angles [3].

These adjustments demonstrate the flexibility of flexography in overcoming limitations associated with traditional printing methods while enhancing print quality and precision.

C. Application of RGB Color Sensor and Camera for Label Verification

To ensure the authenticity of labels, an RGB color sensor is used to measure color properties, while a camera captures images to create a dataset for training AI models. The combination of these technologies provides an effective system for color analysis and object recognition in label verification [1][5][6].

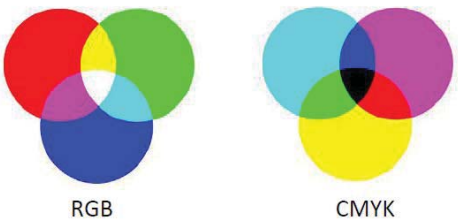


Fig. 4. RGB and CMYK color models .

RGB to CMYK Color Conversion: The RGB to CMYK conversion process involves the following steps:

1. Normalize RGB values:

Convert the RGB values, which typically range from 0 to 255, into a normalized range of 0–1:

$$R' = \frac{R}{255}, G' = \frac{G}{255}, B' = \frac{B}{255} \quad (1)$$

2. Calculate the Key (Black) component: The Key (K) component represents the darkest color and is calculated as:

$$K = 1 - max(R', G', B') \quad (2)$$

3. Compute Cyan (C), Magenta (M), and Yellow (Y) components: Using the normalized RGB values and the Key (K) component:

$$C=1-K1-R'-K,\ M=1-K1-G'-K,\ Y=1-K1-B'-K \quad (3)$$

4. Handle special case when K=1K = 1K=1:

If K=1K = 1K=1 (pure black),
then C=M=Y=0C = M = Y = 0C=M=Y=0.

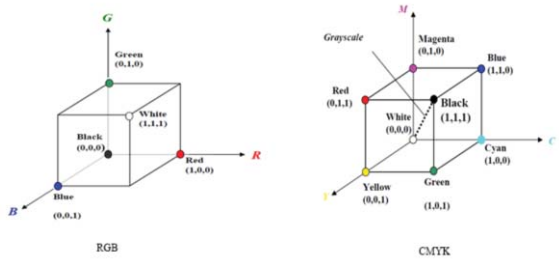


Fig. 5. RGB and CMYK color space [5].

These equations transform RGB color values into CMYK, the standard model used in the printing industry, ensuring accurate color representation for label verification.

D. YOLOv8: Advanced Object Detection Architecture

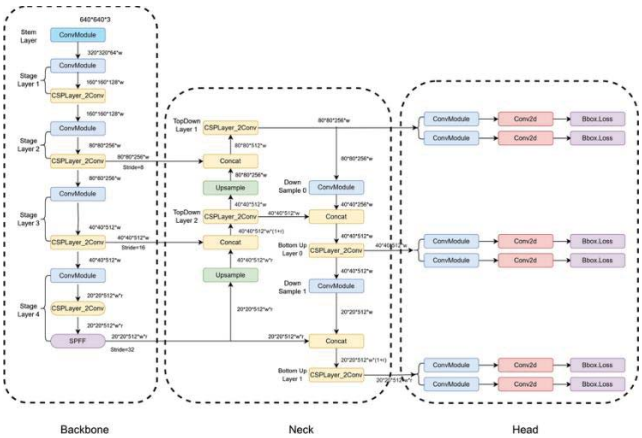


Fig. 6. YOLOv8 Network Architecture [12].

The architecture is divided into three main components: Backbone, Neck, and Head.

1.Backbone: The Backbone is the foundational part of YOLOv8, responsible for feature extraction from input images.CSP-Darknet (Cross Stage Partial Darknet): Utilizes CSPNet to minimize data duplication and computational complexity. Convolutional Layers: Employs multiple convolutional layers to extract features across varying detail levels. Ulti-scale Feature Extraction: Captures features from small and large objects effectively, supporting multi-scale detection .

2.Neck: The Neck refines, and aggregates features extracted by the Backbone, enhancing detection accuracy.PANet (Path Aggregation Network): Combines features from multiple Backbone levels for richer representation.FPN (Feature Pyramid Network): Merges high-resolution and low-resolution features to balance spatial and contextual information. Context Information Augmentation: Improves spatial understanding and context, enabling detection of overlapping or complex objects .

3.Head: The Head performs the final predictions for object detection tasks. Bounding Box Prediction: Uses regression to determine object positions within the image. Class Probability Prediction: Applies SoftMax or Sigmoid functions to classify detected objects. Loss Functions: Optimized for accurate predictions through the following components: Box Loss: Measures bounding box position accuracy. Class Loss: Evaluates classification correctness. Objectless Loss: Estimates the likelihood of a pixel belonging to an object. YOLOv8's modular structure and advanced feature extraction capabilities make it a powerful tool for real-world applications in object detection, segmentation, and pose estimation, offering a robust balance of speed, accuracy, and scalability.

E. Machine Control System

1. Image Processing and API Development Using Python

Python serves as the core for image processing and computational tasks. Leveraging YOLOv8, a pre-trained object detection model, Python processes images from a camera, identifies objects, and generates output data in JSON format via an API for further interaction with the GUI. Python is well-suited for this task due to its simplicity, versatility, and strong support for Artificial Intelligence (AI) and data analysis applications. The processed data is easily accessible and transferable, facilitating seamless integration with downstream systems. Key Steps in Python: Image Analysis: Process images with YOLOv8 to detect objects.

Generate JSON: Convert detection results into structured JSON format.

API Communication: Send JSON data to the GUI for visualization and machine control.

2. GUI and Machine Control Using VB.NET

The GUI, developed with VB.NET, receives the JSON data from Python's API, displays the detection results, and issues command to the Programmable Logic Controller (PLC) using the MX Component library.

VB.NET, an object-oriented programming language, provides robust tools for developing desktop applications and is well-integrated with .NET Framework, enabling efficient communication with external devices like PLCs.

Key Features in VB.NET: Data Visualization: Display real-time detection results from JSON data.

PLC Communication: Utilize MX Component to send commands or receive feedback from the PLC.

3. PLC Integration with MX Component

A Programmable Logic Controller (PLC) is used to control industrial machinery based on commands issued by the VB.NET application. The MX Component library simplifies communication between the VB.NET GUI and Mitsubishi PLCs via protocols like Ethernet, RS-232, and USB.

Advantages of MX Component: Simplified programming for machine control. Reliable communication with PLCs for real-time operation.

Overall Workflow: Python processes camera images with YOLOv8, detects objects, and generates JSON data via an API.VB.NET GUI receives the JSON data, displays results, and issues machine control commands.MX Component relays commands to the PLC, enabling precise machine operation. This integrated approach combines Python's analytical power, VB.NET's user interface capabilities, and PLC's industrial control reliability, ensuring a streamlined and efficient machine control system.

III. Design and Implementation

This proposed technique is divided into four main stages as follows:

1. Flexo Printing and RGB to CMYK Conversion

To understand the properties of Flexo printing and the process of converting RGB values to CMYK for label verification.

Procedures:

1. Study Flexo printing processes, such as the use of CSP-Darknet and multi-scale feature extraction [3][4].
2. Analyze RGB to CMYK conversion

Tools Used:

- RGB color sensor (e.g., TCS34725) for color data collection.
- Camera for capturing label images.

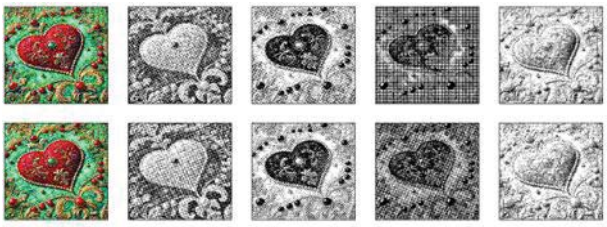


Fig. 7. Flexo Printing and RGB to CMYK. Color.

2. Development and Training of YOLOv8 Model

To develop an AI model for object detection and image analysis.

Procedures:

1. Create a dataset by capturing images of labels and organizing them appropriately.
2. Train the YOLOv8 model to perform:
    - Feature extraction with the Backbone.
    - Feature refinement using the Neck (FPN and PANet).
    - Prediction of bounding boxes and object classes through the Head.

Tools Used:

- Python software and PyTorch library for model development.
- A computer with GPU support for processing.

3. API and GUI Development

To create a system that connects the AI model to a user interface for interaction.

Procedures:

1. Develop an API using Python to output YOLOv8 results as JSON Data.
2. Create a GUI using VB.NET to display JSON Data and send machine control commands.

Tools Used:

- Python for API development.
- VB.NET for GUI development.

4. Machine Control via PLC

To control industrial machinery through the GUI and PLC.

Procedures:

1. Develop a GUI in VB.NET to interface with MX Component.
2. Use MX Component to send control commands to the PLC.
3. Test the system by verifying the machine's responses to commands.

Tools Used:

- Mitsubishi PLC for machine control.
- MX Component library for communication.

Data Collection and Analysis

1. Data Collection:
    - Capture images using a camera to build the dataset.
    - Record RGB to CMYK conversion data and YOLOv8 detection results.
2. Data Analysis:
    - Use loss functions (Box Loss, Class Loss, Objectless Loss) to evaluate model performance.
    - Test the accuracy of the API, GUI, and PLC system by validating the machine's operational outputs.

All procedures aim to integrate advanced technologies to develop an efficient automated system for verifying and controlling machinery in the printing industry.

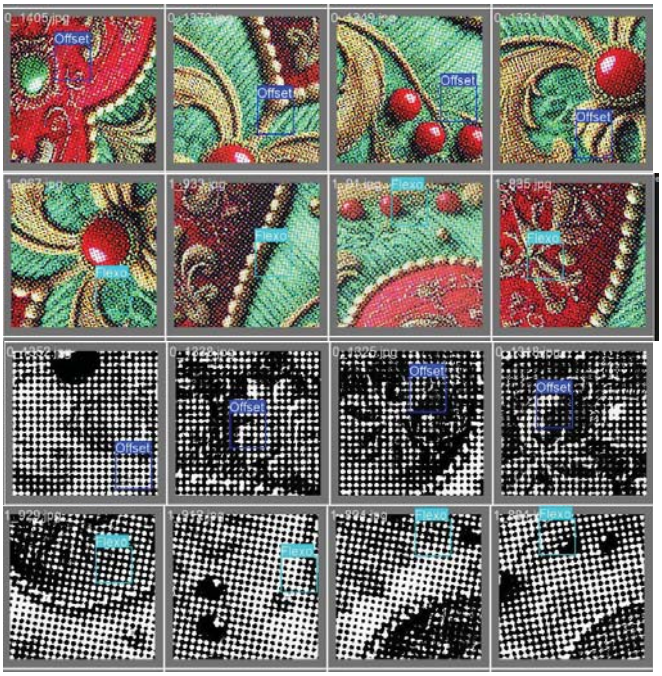


Fig. 8. Data Collection and Analysis.

IV. Experimental Results

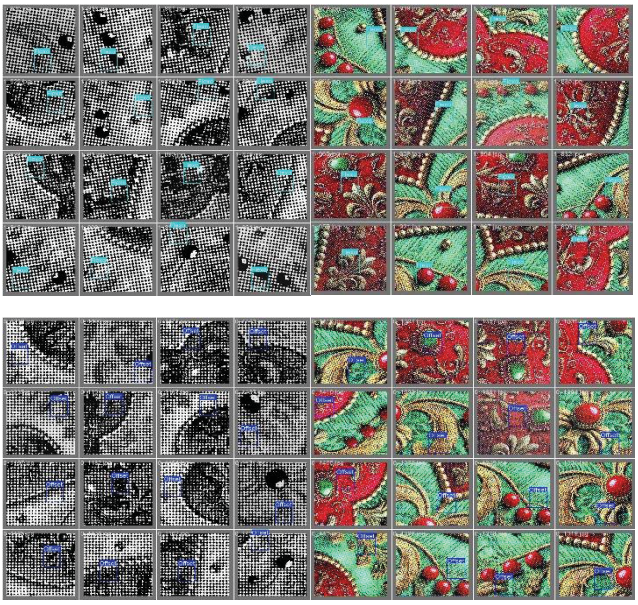


Fig. 9. Results: Offset and Flexo.

The experimental results are presented and analyzed below using various visualizations and metrics to evaluate the performance of the proposed model. The following key outcomes were observed.

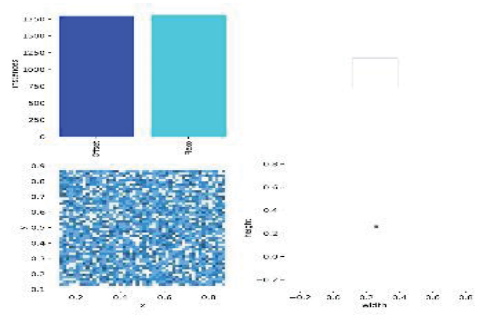


Fig. 10. Instance Distribution.

1. Instance Distribution

The bar chart demonstrates that the dataset is balanced in terms of the two primary classes, Offset and Flexo, each containing approximately 2,000 instances. This indicates that the model training was not biased towards a particular class due to class imbalance.

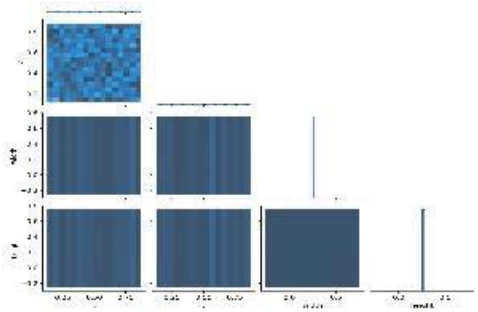


Fig. 11. Feature Correlation.

2. Feature Correlation

The correlogram provides insight into the relationships between the features, such as x, y, width, and height. The low correlation between most features suggests independence, which can be advantageous for model generalization.

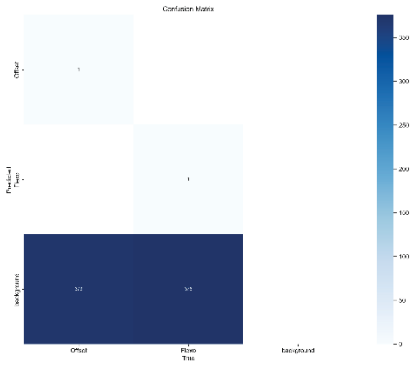


Fig. 12. Confusion Matrix.

3. Confusion Matrix

The confusion matrix highlights the true positives, false positives, and false negatives:

- High true positive counts for both Offset and Flexo classes.
- The background class exhibits some misclassifications, with a significant number of false negatives.

The normalized confusion matrix confirms that the model achieves 100% accuracy for the Offset and Flexo classes but struggles with distinguishing the background.

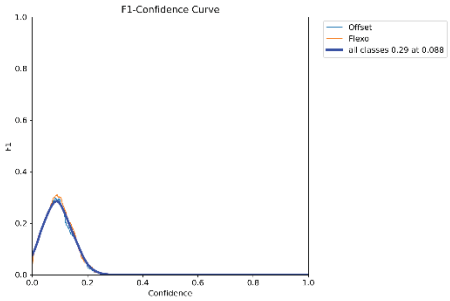


Fig. 13. F1-Confidence Curve.

4. F1-Confidence Curve

The F1-Confidence curve peaks at 0.29 for all classes, indicating suboptimal performance at higher confidence thresholds. Class Offset exhibits marginally better performance than Flexo.

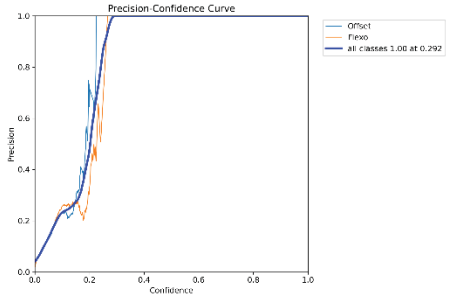


Fig. 14. Precision-Confidence Curve.

5. Precision-Confidence Curve

Precision improves steadily with confidence and reaches 100% at a threshold of 0.292. This suggests that the model is precise when predictions are made with high confidence, albeit at the cost of reduced recall.

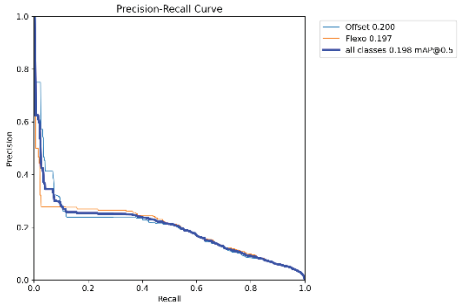


Fig. 15. Precision-Recall (PR) Curve.

6. Precision-Recall (PR) Curve

The PR curve shows:

- Offset achieves a slightly better mAP@0.5 (0.200) than Flexo (0.197).
- Overall mAP@0.5 is 0.198, reflecting moderate model performance with room for improvement.

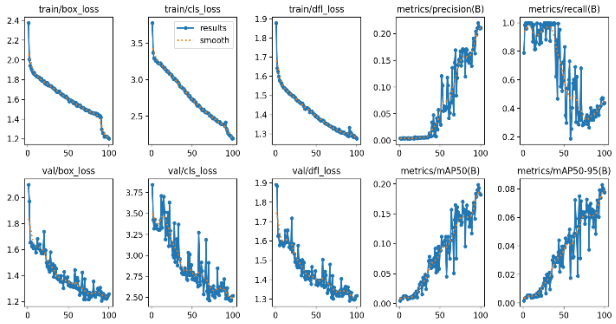


Fig. 16. Training and Validation Loss.

7. Training and Validation Loss

The graphs below depict the loss functions (box, class, and DFL) for both training and validation processes, along with metrics like precision, recall, mAP50, and mAP50-95 over 100 epochs. The consistent decline in loss value demonstrates effective model training. However, the slight fluctuations in validation metrics highlight potential overfitting at higher epochs.

V. Discussion

The model performs well for identifying the Offset and Flexo classes, as evident from the normalized confusion matrix and F1-Confidence curves. However, it struggles with the background class, leading to lower overall performance metrics.

Compared to similar research:

- Advantages: The balanced dataset and low feature correlation likely contribute to better eneralization. The high precision at higher confidence thresholds demonstrates robustness in accurate predictions.
- Limitations: The lower mAP@0.5 suggests room for optimization, particularly for reducing background misclassification.

Limitations and Improvements

The following limitations were identified:

1. Background misclassification: A significant number of false positives and negatives for the background class.
2. Low overall F1-Score: Indicates that precision and recall need improvement.
3. Confidence threshold tuning: Suboptimal confidence thresholds may affect performance.

To address these issues, future work could explore:

- Data augmentation techniques to better capture background diversity.
- Hyperparameter optimization for threshold tuning.
- Integration of advanced loss functions such as focal loss to handle class imbalance in predictions.

VI. Conclusion

The study reveals that the model achieves high precision for Offset and Flexo classes but struggles with background classification, as shown by the confusion matrices and PR curves. Overall, the model's performance metrics, including mAP@0.5, indicate moderate effectiveness with clear opportunities for enhancement.

Future Work

1. Enhance the model's ability to distinguish the background class through advanced training strategies.
2. Incorporate additional features or modify existing ones to improve overall correlation and predictive power.
3. Evaluate the model's performance on larger and more diverse datasets to ensure scalability and robustness.

References

[1] S. Arnas, S. Rimantas, J. Eugenijus and I. Igor, "Assessment of the Condition of Anilox Rollers," Coatings, Oct 2021. [Online]. Available: https://doi.org/10.3390/coatings11111301.

[2] d. Stefano, "Screen angles in flexography," flexo•expert, 2017. [Online]. Available: https://www.flexo.expert/screen-angles-in-flexography/.

[3] A. Khalid, D. Amira and B. Lara, "Color Detection and Mixing System," International Journal of Computer Applications Technology and Research, vol. 6, no. 9, pp. 431-433, 2017.

[4] A. K. V. T.M., "Colour based Image Segmentation for Automated Detection of Leukaemia: A comparison between CIELAB and CMYK colour spaces," in 2018 International Conference on Circuits and Systems in Digital Enterprise Technology (ICCSDET), Kottayam, India, 2018.

[5] A.-B. Ibrahim and D. Hassane , "Camera-Based Colour Sensing System," Red, 2006.

[6] M. G. Bertacchi and I. F. Silveira, "Facial Makeup Detection using the CMYK Color Model and Convolutional Neural Networks," in XV Workshop de Visão Computacional (WVC), São Bernardo do Campo, Brazil,, 2019.

[7] Q. C. e. al., "Building A Deep Learning Model for Multi-Label Classification of Natural Disasters," in IEEE 3rd International Conference on Information Technology, Big Data and Artificial Intelligence (ICIBA), Chongqing, China, 2023.

[8] M. B. Ullah, "CPU Based YOLO: A Real Time Object Detection Algorithm," in IEEE Region 10 Symposium (TENSYMP),, Dhaka, Bangladesh, 2020.

[9] A. V. P. S. K. Naman Mittal, "Object Detection and Classification Using Yolo," International Journal of Scientific Research & Engineering Trends, vol. 5, no. 2, 2019.

[10] S. S. R. Kanhaiya Sharma, "State of-the-Art Analysis of Multiple Object Detection Techniques using Deep Learning," International Journal of Advanced Computer Science and Applications(IJACSA), vol. 14, no. 5, 2023.

[11] R.-Y. &. C. W. Ju, "Fracture detection in pediatric wrist trauma X-ray images using YOLOv8 algorithm," Scientific Reports, 2023.

[12] C. &. Z. G. &. G. S. &. D. S. &. K. E. &. S. T. Gao, "Advancing architectural heritage: precision decoding of East Asian timber structures from Tang dynasty to traditional Japan.," Heritage Science, 2024.

Compensation Motion and Calibration for Scale Calibration Machine

1st Siriwat Kitsompong
National Institute of Metrology (Thailand)
Pathumthani, Thailand
siriwatk@nimt.or.th

2nd Yuttana Hongaromkij
National Institute of Metrology (Thailand)
Pathumthani, Thailand
yuttana@nimt.or.th

***Abstract*— The National Institute of Metrology Thailand (NIMT) has developed a self-built scale calibration machine to verify the accuracy of rulers and tape measures, supporting and promoting domestic industries following ISO/IEC 17025 and ISO 10012 [1-2]. The design of the machine is based on the Japanese Industrial Standards JIS B 7516 standard [3], which specifies calibration procedures for metal rules. A key challenge in controlling the one-dimensional motion of the machine lies in addressing the 6 degrees of freedom (6-DoF) [4-6], which can affect accuracy and precision. The scale calibration machine consists of several components, including a beam, ball screw, motor drive, driver motor, digital camera, and controller. To ensure precise motion control, it is essential to compensate for errors caused by mechanical and environmental factors and integrate these compensation methods into the control software. This approach not only guarantees accurate and reliable calibration results but also enhances the machine's performance in maintaining consistent motion. Through this development, NIMT aims to strengthen its metrological capabilities, support the growth of local industries, and further establish itself as a leader in the field of metrology.**

***Keywords*— Compensation Motion, accuracy, scale, calibration, correction value**

I. Introduction

The development of a highly accurate and precise scale calibrator relies heavily on the precision of one-dimensional (1-D) motion control. A significant challenge in achieving this precision arises from the ball screw mechanism, although control design else. However, the error case from the 6-DoF still persist. The concept of 6-DoF refers to the six independent parameters required to describe the motion of a rigid body in three-dimensional space. These include three translational movements (along the x-, y-, and z-axes) and three rotational movements (around these axes).

To address this issue, extensive research is needed to identify effective solutions for mitigating motion errors in the calibration process. This involves developing error compensation methods and integrating these corrections into the control software to ensure accurate and reliable motion. By overcoming these challenges, the motion control system can achieve the precision required for accurate scale calibration, supporting various industrial applications.

For the current industry, Calibration instruments used in the industrial sector must comply with ISO 17025 and ISO 10012 standards, supporting and promoting domestic industries for exports. Consequently, standard instruments for calibrating should be accurately calibrated and specifically designed for effective use according to relevant standards. By employing suitable instrument designs and compensation methods, the accuracy of calibrating in the industrial, quality product and quality control can be significantly improved.

In this work, Scale Calibration Machine compensated one-dimension motion by Laser Interferometer System, and then using glass scale for compensate all systems and calibration this machine for find errors of systems.

II. Equipment And Flowchat Controling System

A. Equipment

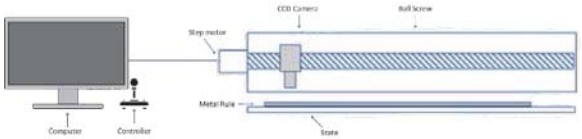


Figure 1. Diagram of Scale Calibration Machine

The calibration machine which we developed comprises several key components, including:
1.Beam: Acts as the structural guide for the CCD, allowing it to move in a one-dimensional direction.
2.Ball Screw: Assists in driving the movement and facilitates precise linear motion.
3.Motor Drive: Controls the movement of the system to ensure smooth operation.
4.computer: Monitors the system and runs control programs to read values and manage operations.
5.CCD Camera and Controller: Used for capturing and marking the position of the workpiece, with a manual control function for adjustments.
Together, these components work in harmony to provide a robust and precise calibration system that delivers accurate results for various applications.

B. Flowchart control system

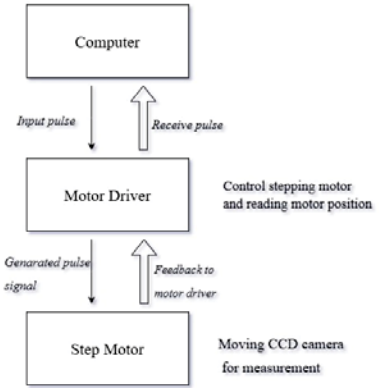


Figure 2. Flowchart Control system of Scale Calibration Machine

The perocess of motion control follows the flow chart. A program is written in LabVIEW on a computer to receive pulse values from the motor driver, which are then used to calculate the distance as the measurement result. Additionally, the mesured distance (in millimeters) to be commanded is converted into pulses and sent to the motor driver. This ensures that the stepping motor moves to the specified position accordingly.

III. Experimental

A. Steps for Determining Motor Pulse Count Using a Laser Interferometer

1) Initial Setup:

Laser Interferometer Installation: The laser interferometer should be mounted along the axis intended for measurement shown in Fig. 3. This instrument offers high precision, utilizing laser light to measure the displacement of an object with micrometer-level accuracy.

Equipment : Laser interferometer system.
Manufacture : Keysight
Model : 5519B
Serial Number : US52140401
Alignment follow ISO 230-6 [7,8]

Motor Installation: Install the motor equipped with an encoder onto the same axis. The encoder generates pulses in proportion to the motor's rotational or linear movement.



Figure 3. Laser Interferometer Installation

2) Measurement Process:

Motor Operation: Initiate the operation of the motor and record the pulse count generated by the encoder. These pulses reflect the distance that the motor is expected to have moved. Laser Interferometer Reading: At the same time, the laser interferometer should measure the actual distance the motor has moved, providing a highly accurate reading of the displacement.

3) Pulse-to-Distance Comparison:

Compare the pulse count produced by the motor with the actual distance measured by the laser interferometer. Determine the relation between the pulse count and the actual movement and find a correction factor. This factor can be used to correct the distance of motion of machine.

4) Checking Motion Distance of Machine:

After comparing correction factor, this machine operated by moving motor and record Distance from motor compared with laser interferometer for re-test the motor's movement to confirm that the pulse-to-distance ratio is accurate, and that the motor operates within the specified parameters.

However, the use of the laser is primarily for determining the pulse-to-distance ratio in order to estimate the distance as closely as possible to the nominal value. This method can only correct one degree of freedom out of the six available.

The initial pulse per minute (PPM) value must be determined to ensure that, when compared with the glass scale, the motor will move accurately according to the scale marks intended for inspection. This process minimizes measurement errors and ensures that the motor's movement aligns precisely with the desired positions for verification.

B. Compensation for machine

Using the glass scale for calibration [9], we obtain the pulse-per-distance values at various positions shown in Fig. 4. These values are more precise compared to those obtained using a laser interferometer. The compensation is then implemented into the program. The first step involves determining the factor constants used to convert pulse counts into millimeters for each measurement interval: 0, 100, 200, 300, 400, 500, 600, 700, 800, 900, and 1000 mm.

Equipment : Glass Scale
Manufacture : Mitutoyo
Model : HL3-1000
Serial Number : 98392

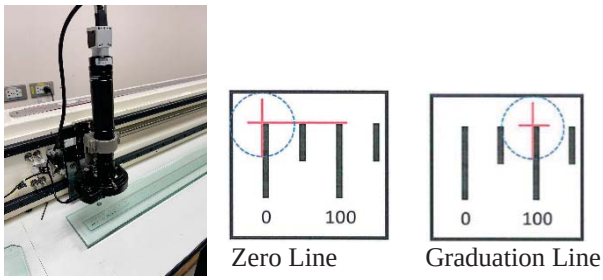


Figure 4. calibration by glass scale

This is calculated using the equation:

Pulse per mm = (Nominal Length) / (Total Pulse Steps).

From this equation, the factor constants for each interval can be derived.

Once the factor constants are determined, an equation is implemented into the program to ensure that the stepping motor moves accurately over the desired distances in compliance with the standard.

The equation is as follows:

```
if(X<=16697)                    // position 0 to 50 mm
Y = X*(Pulse per mm));
if(X>16697 && X<=50065)         // position 51 to 150 mm
Y = X*(Pulse per mm))
```

Where X represents the length in millimeters (mm), and Y denotes the number of pulses sent by the motor driver to the stepper motor.

C. Calibration Machine

For the calibration process, a glass scale was utilized as it closely aligns with the actual application of the machine. The process begins by precisely aligning the glass scale at both the starting and ending points. Measurements are conducted by positioning the crosshair at the starting point and

subsequently moving it to various positions at 100 mm intervals, with the readings being recorded at each interval. This procedure is repeated four times to ensure accuracy.

D. *Comparing with other machine*

Once the calibration process is complete and the results meet the criteria, the next step is for the researcher to validate the machine by verifying the machine used for calibrating the artifact. In this process, considering criteria of machine is acceptable following ISO/IEC 17043 [10]. The metal ruler is first used, followed by other instrument with higher accuracy (in experiment using 3D CNC Vision Measuring Machine) to calibrate the same artifact. The final step is to compare the results from both instruments and calculate the En ratio. If the En ratio is less than 1, it indicates that the measuring instrument is suitable for use in calibration.

IV. Results

A. *Experiment Results: Correction Factor from compared by laser interferometer*

From the calculation of pulses per millimeter using the laser interferometer, it was determined that 1 pulse corresponds to 0.003 mm.

Table 1 Find the pulse per millimeter by length of laser interferometer per pules of motor

Length (mm)	Total Pulse	Pulse per mm
1000	333333	0.003

B. *Experiment Results: Before and After Compensation using glass scale*

The figure below shows the values before compensation (Using factor from experiment A) and after compensation (Using factor from experiment B) for different values of *N*

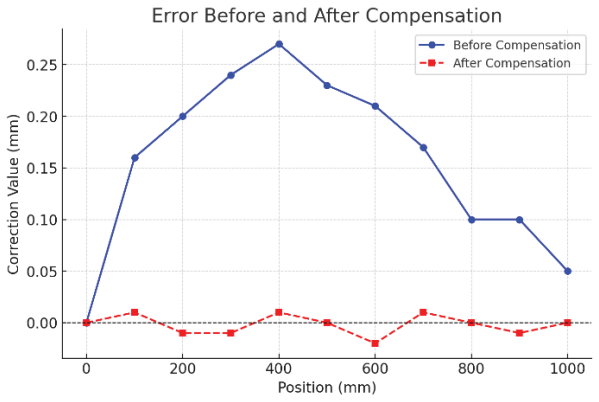


Figure 5. Compensation compare Before and After Compensation

C. *Experiment Results: Comparing with other machine*

From comparing measurement results of metal rulers using the Scale Calibrator and the 3D CNC Vision Measuring Machine, it was EN ration ≤ 1 follow this equation.

$$(E_n)_i = \frac{x_i - x_r}{\sqrt{U^2(x_i) + U^2(x_r)}}$$

Where

X_i is the assigned value determined in a participant

X_r is the assigned value determined in a reference machine

$U(X_i)$ is the expanded uncertainty of a participant's result X_i

$U(X_r)$ is the expanded uncertainty of a reference machine's result X_r

Note: -1.0 < En < 1.0 taken as an indicator of successful performance

Table 2. Comparing measurement results of metal rulers using the Scale Calibrator and the 3D CNC Vision Measuring Machine.

Nominal (mm)	Correction (mm)		EN retio
	SCALE CALIBRATOR	3D CNC (3)	
0	0	0	0
100	-0.031	-0.037	0.21
200	-0.032	-0.033	0.04
300	-0.02	-0.029	0.33
400	-0.017	-0.023	0.22
500	-0.022	-0.021	0.01
600	-0.017	-0.028	0.39
700	-0.046	-0.054	0.28
800	-0.079	-0.074	0.17
900	-0.067	-0.075	0.28
1000	-0.053	-0.070	0.58

V. Discussion

The Figure 5. the values before and after compensation across different points. The following observations can be made:

Before Compensation: The curve shows a clear increasing trend from to, peaking at 0.27 at nominal 400 mm. Afterward, the values gradually decrease, reaching a low of 0.05 at nominal value 1000 mm. This indicates a non-linear progression, with the highest values observed around the midpoint of the data.

After Compensation: In contrast, the curve remains relatively stable around 0, fluctuating between small positive and negative values. The highest positive deviation (0.01) at nominal 400 mm and 500 m and the lowest negative deviation (-0.02) at nominal 600 mm suggest minimal variation after compensation.

Effect of Compensation: The compensation effectively reduces the deviations from the baseline, especially where the values before compensation were higher.

The consistent behavior near zero after compensation demonstrates the success of the process in mitigating the original variations.

Key Insights: The compensation process appears to be highly effective in normalizing the data, as the "After Compensation" values show much less variation compared to the "Before Compensation" values.

The results suggest that the compensation process successfully minimizes the fluctuations in the data. While the "Before Compensation" curve shows significant variability, the "After Compensation" curve demonstrates stability, maintaining values close to zero across all points. This

indicates that the compensation strategy is robust and effective in achieving the desired normalization.

The Comparing with other machine result involved measuring metal rulers using both the Scale Calibrator and the 3D CNC Vision Measuring Machine. The measurement results are presented in Table 2, showing the correction of each instrument.

To evaluate the consistency and reliability of the measurements, a comparison between the two instruments was conducted, as detailed in Table 2. The final analysis, illustrated, confirms that the En ratio ($|En| \leq 1$) meets the acceptance criteria, indicating that the measurement results from both machines. Therefore, the Scale Calibrator machine agree and the instruments are suitable purposes for calibration, quality product and quality control.

VI. Conclusion

This paper presented the development of a scale calibration machine designed to meet the precision standards for metal rule calibration, following the Japanese Industrial Standards JIS B 7516. The machine's design addresses the challenges of controlling one-dimensional motion while compensating for errors caused by six degrees of freedom (6-DoF).

To achieve precise motion control, a compensation strategy was implemented using a laser interferometer system and a glass scale. These methods are determination of correction factors, effectively minimizing motion errors and maintaining accuracy throughout the calibration process.

Experimental results confirm that the compensation strategy significantly reduces deviations, normalizes the data, and ensures reliable motion control. As a result, the developed scale calibration machine delivers enough accurate for industrial use.

Reference

[1] International Standard, General requirements for the competence of testing and calibration laboratories (2017 3nd).

[2] International Standard, Measurement management syatem Requirements for measurement processes and measuring equipment (2017 1st).

[3] Japanese Industrial Standard. (2007). Metal Rules (JIS B 7516: 2005).

[4] Wang Charles, Optodyne, Inc, 1180 Mahalo Place, Compton, CA 90220, What is 2D volumetric positioning accuracy and how to define and mesure it.

[5] James D. Meadows, Geometric Dimensioning and Tolerancing, Application, Analysis & Measurement [per ASME Y14.5-2009] (James D. Meadows & Associate, Inc.) pp 93- 119 and pp 217-263.

[6] Zhai Shumin, IBM Almaden Rearch Centre, 650 Harry Road, San Jose, CA 95123, USA Quantifying, Milgram Pual, Dept Mech & Ind. Eng., University of Toronto, Toronto, Ontario, Canada, M5S 3G8, Coordination in Multiple DOF Movement and Its Application to Evaluating 6 DOF Input Devices.

[7] International Standard. (2002). Determination of positioning accuracy on body and face diagonals (Diagonal displacement tests) (ISO 230-6).

[8] National Institute of Metrology (Thailand). 3/4-5 Moo 3, Klong 5, Klong Luang, Pathumthani 12120, Thailand, Certificate of Calibration No. DW-24-0004, Laser Interferometer (Laser Head), Keysight, 5519B, SN US52140401.

[9] National Metrology Institute VTT MIKES, Tekniikantie 1, FI-02150 Espoo, FINLAND, Certicate of Calibration No. M-23L042, Precision line scale, Mitutoyo, HL3-1000, SN 98392.

[10] General requirements for proficiency testing (ISO/IEC 17043:2010)

Linear Interpolation using Siemens S7-1200

Noppadol Maneerat
Department of Instrumentation and Control Engineering School of Engineering King Mongkut's Institute of Technology Ladkrabang
Bangkok 10520 Thailand
noppadol.ma@kmitl.ac.th

Tharathorn Wongworrada
Department of Instrumentation and Control Engineering School of Engineering King Mongkut's Institute of Technology Ladkrabang
Bangkok 10520 Thailand
thaungkmitl@hotmail.com

Thepjit Cheypoca
Department of Instrumentation and Control Engineering School of Engineering King Mongkut's Institute of Technology Ladkrabang
Bangkok 10520 Thailand
thepjit.ch@kmitl.ac.th

Kasemsuk Sepsirisuk
Department of Engineering King Mongkut's Institute of Technology Ladkrabang Prince of Chumphon Campus
Chumphon 86160 Thailand
kasemsuk.se@kmitl.ac.th

***Abstract*— This research is a continuation of the research on circular interpolation use siemens s7-1200 [1] It presents the movement of 3 axes, x y z, as a method of moving in a curve that is controlled by programmable logic control (PLC). In the future research, PLC will be used to control linear movement straightly. The work will be in the original format, but change the equation used to move in a straight line instead.**

Keywords—Programmable Logic Controller, PLC, motion control, S7-1200

I. INTRODUCTION

3-axis milling machines generally use a computer numerical control controller. The controller is specifically used to control the movement of all 3 axes and can also control the speed of the spindle. In this research, It uses a PLC to control the movement of all 3 axes. It can also control the spindle as well and can control various sequence operations better than CNC. Able to control the operation of a variety of other peripheral equipment such as conveyor belts, mechanical arms, sending and receiving work pieces from other machines, etc. PLCs are still cheaper than CNC, but the problem with small PLCs is that there are no orders available. Used to control the movement of the axes to make 2 axes move simultaneously in synchronization to move the axes in a straight line. In this paper, 2-axis linear motion is presented using the linear interpolation method [2].

II. PROPOSED SYSTEM

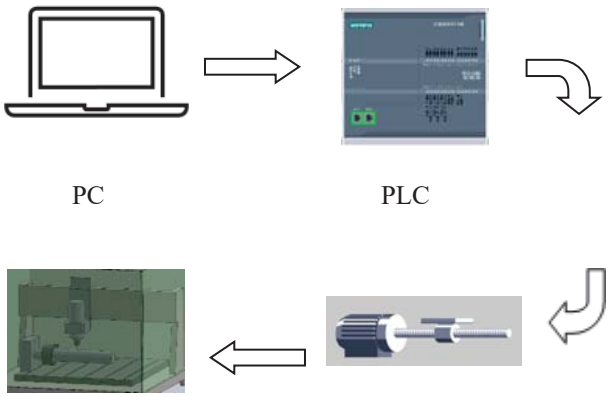


Fig.1 PLC Controlled 3-Axis Milling Machine

From Figure 1, the work of this research can be explained as follows. It starts with entering the data of the straight line that you want the machine to force the axis to move in the specified direction. With a program written in WinCC [3] of Siemens, by setting the starting point in the x axis, the starting point in the Y axis, the ending point in the x axis, the ending point in the y axis, the resolution of the number of points that will allow the axis to move. speed of movement Send these data to plc siemens s7-1200 To be processed with a program written with Totally integrated automation (TIA Portal) [4] of Siemens, then the plc will command the output to send data as a pulse train output (PTO) to the step motor drive that is connected to the ball screw used to drive it. each axis When the 3 axes are assembled together, it will be a 3-axis milling machine that can replace the 3-axis milling machine controlled by CNC.

III. LINEAR INTERPOLATION

The precision of the movement depends on the linear interpolation method of the 3-axis milling machine. It determines the position of each point from the beginning to the end. As the example picture shows, Figure 2.

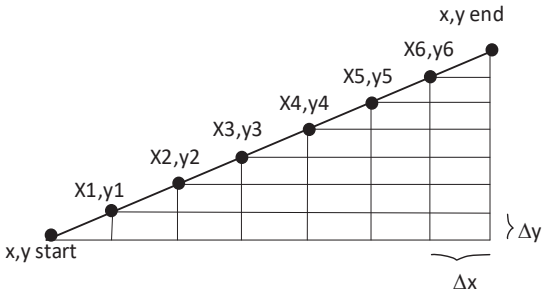


Fig.2 Linear Interpolation x,y

3-axis milling machine controller that uses NC as the control unit. The commands used are g-code , command g00, fast linear motion g01, linear interpolation, linear interpolation. The movement position of each point can be calculated by The following equation

$$\Delta X = \frac{Xend - Xstart}{Resolution} \quad (1)$$

$$\Delta Y = \frac{Yend - Ystart}{Resolution} \quad (2)$$

$$X\# = Xstart + (\Delta X \times Position\#) \quad (3)$$

$$Y\# = Ystart + (\Delta Y \times Position\#) \quad (4)$$

Assign to

ΔX = The distance between each point x.

ΔY = The distance between each point y.

Xend = End point x.

Yend = End point y.

Xstart = Start point x.

Ystart = End point y.

X# = Position x each

Y# = Position y each

Position# = Position each

IV. Simulation Results

From the obtained equation When used as data to enter a formula in Excel to calculate the obtained position. The experiment was performed at 10 levels of resolution, shown by graphs with the following values. TABLE 1

ΔX = 4.5

ΔY = 2.5

Xend = 50

Yend = 30

Xstart = 5

Ystart = 5

Resolution = 10

Table1

Data	X	Y	Resolution
Start	5	5	10
End	50	30	
	ΔX	ΔY	
	4.50	2.50	
1	9.5	7.5	
2	14	10	
3	18.5	12.5	
4	23	15	
5	27.5	17.5	
6	32	20	
7	36.5	22.5	
8	41	25	
9	45.5	27.5	
10	50	30	

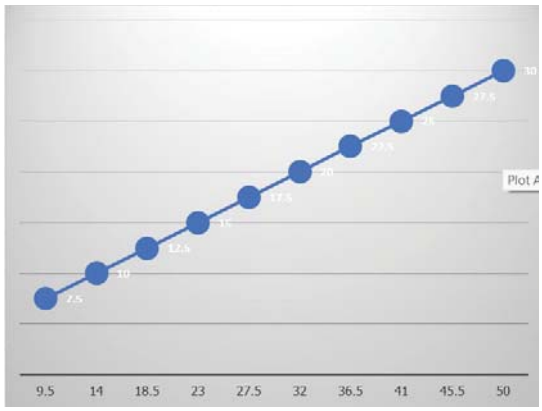


Fig.3 Take the value to the plot graph.

By bringing the values from Table 1 to a linear plot graph with a resolution of 10 places, as shown in Figure 3, it can be proved that the above equation is true.

V. TIA Portal

From the obtained equation When used to simulate a linear movement path, it can be seen that it is as calculated and designed. Therefore, it is used to write a linear program for the plc to work as desired. The program used is a program from Siemens TIA Portal. The main program structure is to use programming for the movement of all 3 motor axes, including the following commands. A command that is used to write motion control is called Motion Control (MC).

MC_Power is an executable command.

MC_Home is a zero point reversal statement.

MC_MoveAbsolute is an absolute moving order.

As shown in Figure 4.

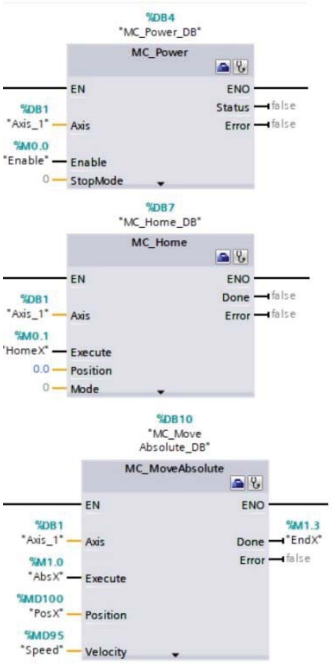


Fig.4 Motion Control TIA Portal

In terms of equations It can be written with the Calculate command, written as a clockwise motion equation as follows:

Delta Y = (IN1- IN2) / IN3
IN1 = Xend , IN2 = Xstart , IN3 = Resolution
Delta X = (IN1- IN2) / IN3
IN1 = Yend , IN2 = Ystart , IN3 = Resolution
X# = IN1+(IN2 * IN3)
IN1 = Xstart , IN2 = Deltax, IN3 = Position
Y# = IN1 +(IN2) * IN3)
IN1 = Ystart , IN2 = Deltay, IN3 = Position

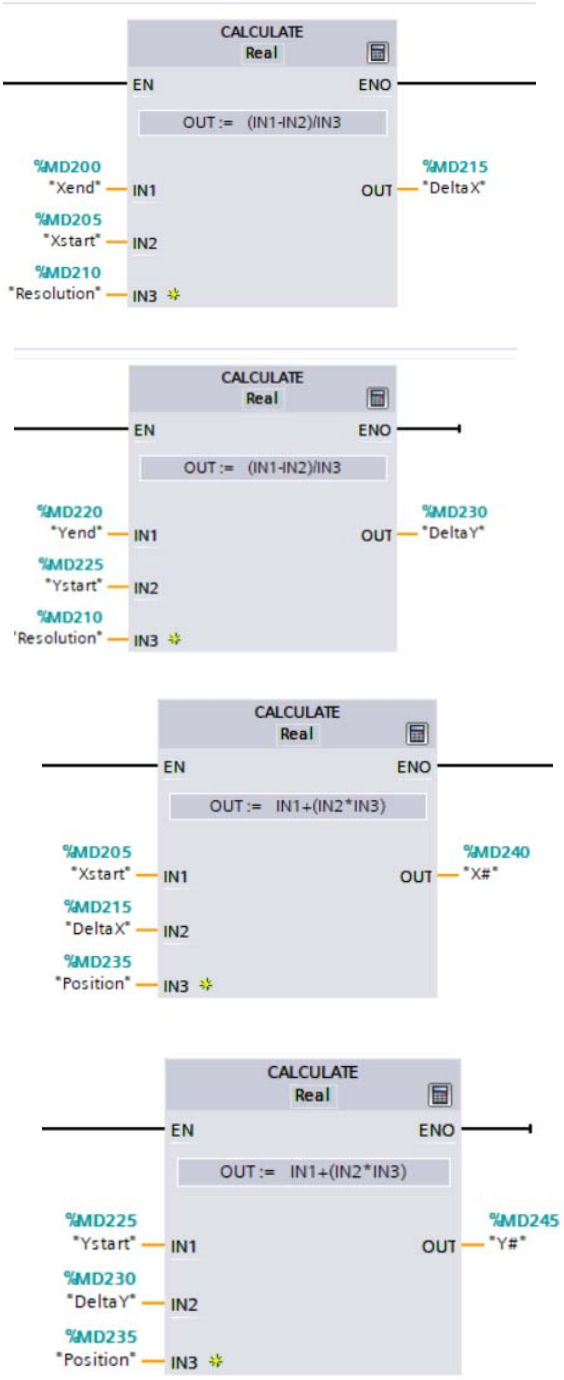


Fig.5 Calculate TIA Portal

VI. PROGRAM FLOW DIAGRAM OF CIRCULAR INTERPOLATION ALGORITHM

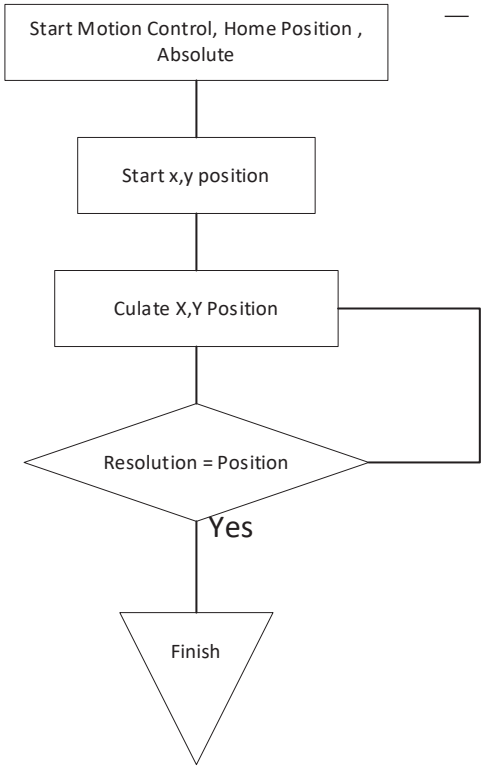


Fig.6 Program flow diagram of circular interpolation algorithm

VII. RESULTS AND DISCUSSION

When the program written in the TIA portal is executed according to the obtained flow diagram, the PLC controller can make the 3-axis milling machine move in a straight line according to the model. Therefore, it can be concluded that the linear estimation equation can actually be applied as shown in Figure 7 with the PLC S7-1200 as the operating controller as shown in Figure 8.

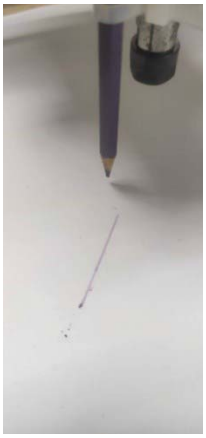


Fig.7 Linear interpolation

The accuracy of position control between CNC and PLC is no different because it is a pulse train output (PTO) control which is a widely used position control. Moreover, the price of PLC controller is much lower than CNC because it is a basic controller that is widely used. The use of position control is using Human Machine Interface (HMI), making PLC much easier to use. Therefore, in this article, the use of PLC is presented.



Fig.8 PLC Controller

REFERENCES

[1] Thepjit Cheypoca; Amata Luanpol; Virot Wuti "Circular Interpolation using Siemens S7-1200" 2023 9th International Conference on Engineering, Applied Sciences, and Technology (ICEAST)

[2] Geng Cong; Wu Yuhou "An interpolation method based on tool orientation fitting in five-axis CNC machining" 2016 IEEE 14th International Conference on Industrial Informatics (INDIN)

[3] Zhan Sheng; Cuicui Ji; Sheng Hua "Application of Siemens PL 2018 Chinese Control And Decision Conference (CCDC)C and WinCC in the Monitoring-Control System of Bulk Grain Silo" 2019 IEEE Integrated STEM Education Conference (ISEC)

Apply PLC to Control 3-Axis Machines

Thepjit Cheypoca
Department of Instrumentation and Control Engineering
School of Engineering
King Mongkut's Institute of Technology Ladkrabang
Bangkok 10520 Thailand
thepjit.ch@kmitl.ac.th

In Thaiyai
Department of Instrumentation and Control Engineering
School of Engineering
King Mongkut's Institute of Technology Ladkrabang
Bangkok 10520 Thailand
67016186@kmitl.ac.th

Noppadol Maneerat
Department of Instrumentation and Control Engineering
School of Engineering
King Mongkut's Institute of Technology Ladkrabang
Bangkok 10520 Thailand
noppadol.ma@kmitl.ac.th

Athasart Narkthewan
Department of Engineering
King Mongkut's Institute of Technology Ladkrabang
Prince of Chumphon Campus
Chumphon 86160 Thailand
athasart.na@kmitl.ac.th

***Abstract*— This report presents a method of using PLC (Programable Logic Control) to control the work instead of the 3-axis machine position controller. PLC is popularly used in various types of control systems. It has a lot of control capabilities, is efficient, stable, durable, easy to use, and cheap. It is the use of commands to control the work of all 3 axes, 2 axes, and 1 axle. The commands used for moving in both straight lines and curves, and there are other devices that need to be controlled together with the machine that is being controlled.**

Keywords—Programmable Logic Controller , PLC, motion control, S7-1200

I. INTRODUCTION

3-axis milling machines are generally controlled by a specialized position controller. They are expensive and specific for specific tasks. The control devices for other parts of the machine must have additional devices to control specific parts from the PLC. Therefore, there is an idea that a PLC can be used to control the work instead directly. It has many capabilities, is inexpensive, and is widely used in controlling many parts of the equipment. This research uses the Siemens PLC, model S7-1200, which is inexpensive and widely available. It is widely used in industrial work. It is easy to control the work and connect to the Internet.

II. PROPOSED SYSTEM

From Figure 1 is the structure of a 3-axis machine controlled by a computer numerical control (CNC) controller. The operation starts with designing the workpiece, writing a program with a computer, converting the code used to move the machine into a G-Code. The controller will process the direction of movement, the speed of movement, and the movement pattern, sending signals to the 3-axis drive set, including the workpiece milling head motor set, in order to drive the ball screw with the motor to move to the calculated position. The CNC controller is expensive, the program is difficult to understand, and requires a specialist.

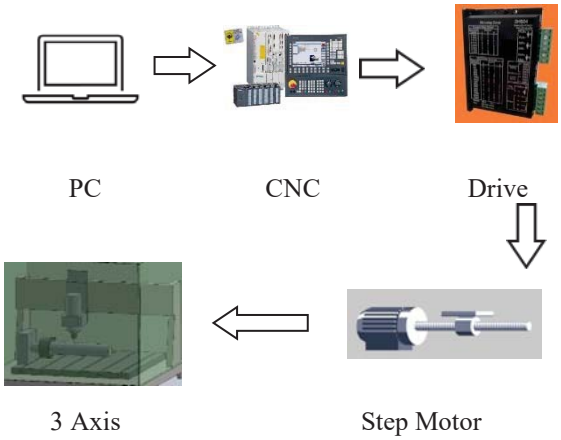


Fig.1 CNC Controlled 3Axis Milling Machine

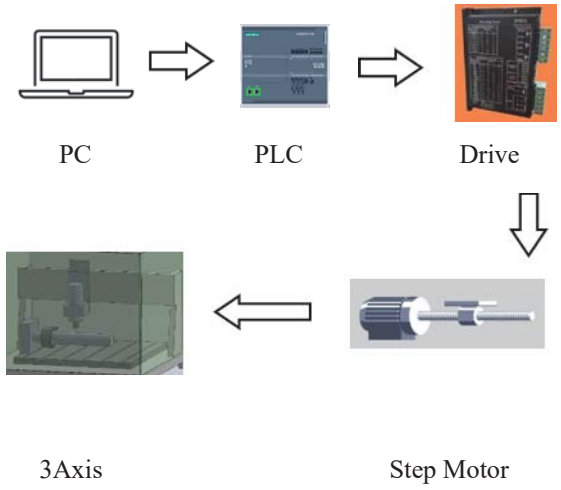


Fig.2 PLC Controlled 3Axis Milling Machine

Figure 2 is the structure of the 3-axis machine controlled by PLC used in the experiment of this article presented. The operation is the same as the normal operation of the CNC-controlled machine, but changed to PLC instead. Starting from designing the workpiece with a computer, controlling the movement of the position with PLC. The output of the PLC will send the position signal to the motor drive unit. The motor will drive the shaft with a ball screw to the desired position one by one until the program is finished.

The program used to control the machine through the computer is called wincc[1]. It is a program from Cement. It will specify the position that needs to be moved in each axis, x, y, z, including the speed of movement. The computer will send a signal to the PLC, which will be written in a program called Totally integrated automation (TIA Portal).

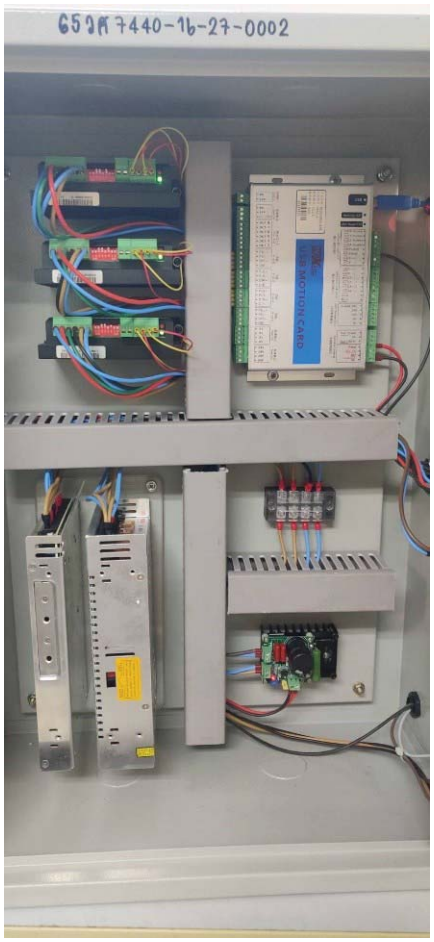


Fig.3 CNC Controller



Fig. 4 PLC Controller

From Figure 3, it is the original CNC control unit and Figure 4, it is the control unit that has been changed to a PLC. It can be seen that they are almost the same in every respect, except for the control unit between the CNC and PLC.

III. PROGRAMS USED IN RESEARCH

- Win CC is a program written to communicate between the user and the machine or the computer and the human machine interface (HMI). In this article, it is used as an input that receives data of the size of the workpiece specified by the user and the computer that commands the machine to move as desired. There are commands for all 3 axes X, Y, Z, including the speed of the workpiece cutter. The design can be designed according to the machine used or according to convenience. The ability to be desired in many forms can display values as numbers, directions, or images. The meter can be displayed in analog form. It is very easy to use and can change the format as desired.

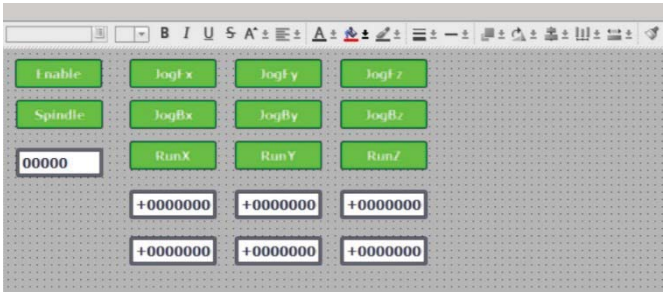


Fig.5 Win CC

From Figure 5, it is a program that interfaces between the user and the machine, written with the Win CC program. It can display the values necessary for use completely,

sufficient for controlling the machine, and clearly see the necessary values.

- Totally integrated automation (TIA Portal) is a versatile program that can be used to program many devices in the automation system. It has many capabilities as the name of the program suggests. In this research, it will be used as the main program to write a program to control the operation of the PLC, including setting input values, motor values, distance values, and also the speed of the workpiece cutter head.



Fig.6 TIA Portal

From Figure 6, it is a program written with TIA Portal to control the movement of all 3 axes by setting the values as follows:

MC Power = Motion Control Power On

MC MoveJog = Motion Control Move axis in jog mode

MC MoveRelative = Motion Control Move Relative position of axis

MC Home = Motion Control Home axis, set home position

MC MoveAbsolute = Motion Control Absolute position of axis

MC MoveVelocity = Motion Control Move axis at set Velocity

MC Reset = Motion Control Acknowledge fault, restart technology

MC ChangeDynamic = Motion Control change dynamic settings

CTRL PWM = Pulse width modulation

- Pulse Train Output PTO is a signal that the PLC output sends out to control the operation of the 3-axis motor drive set. The operation must set the program value, the position of the device must match the signal channel that has been programmed. The program will calculate the distance.

.

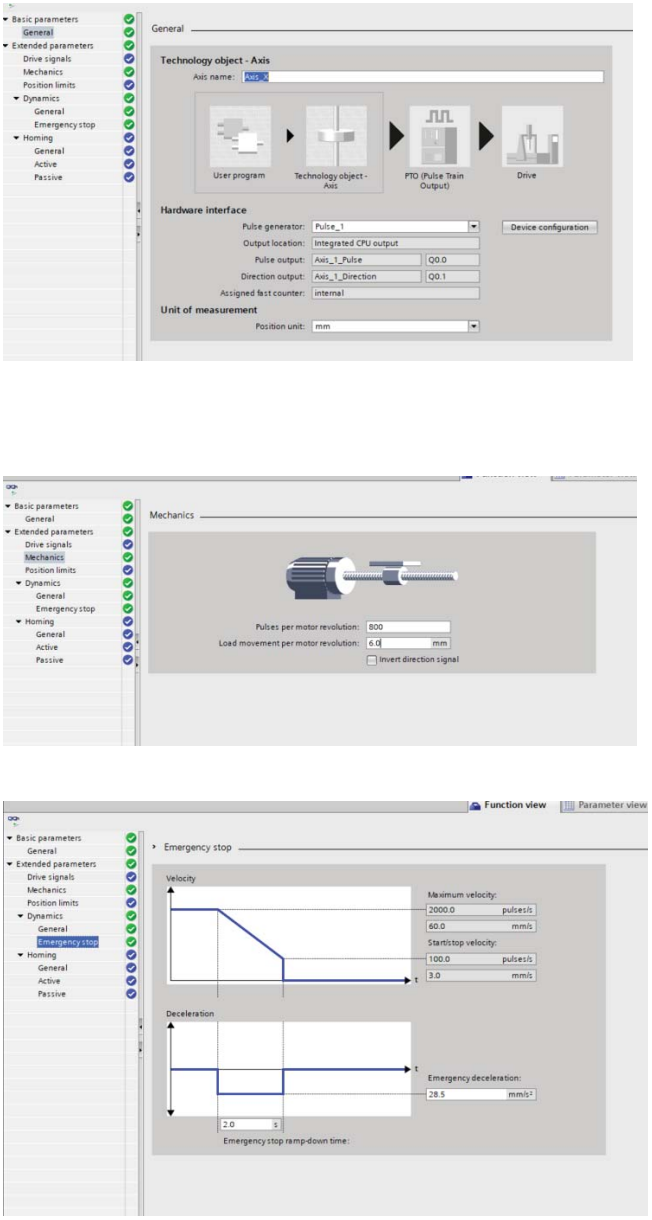


Fig.7 Pulse parameters

From Figure 7 are the parameter values that must be set to the program so that the program can calculate the distance according to the actual values obtained from the 3-axis motor drive set, consisting of the signal value that the PLC must supply to the drive set as a pulse, the highest frequency that can move without error, the initial speed of movement, the highest speed that can move, the screw pitch distance, the maximum worktable size. When setting the values according to this, it is possible to create a program for the PLC to move as desired.

IV. RESULTS AND DISCUSSION

From the experimental results, it is possible to write a program to move the machine in all 3 axes as designed and to try to mill the workpiece according to the initial model as shown in the figure, such as milling a curve with the method of Circular interpolation using siemens S7-1200 [3] and milling the workpiece in a straight line with the method of linear interpolation using siemens S7-1200 as desired, as shown in Figure 8.



Fig.8 3Axis Control with PLC

REFERENCES

[1] Geng Cong; Wu Yuhou “An interpolation method based on tool orientation fitting in five-axis CNC machining” 2016 IEEE 14th International Conference on Industrial Informatics (INDIN)

[2] Zhan Sheng; Cuicui Ji; Sheng Hua “Application of Siemens PL 2018 Chinese Control And Decision Conference (CCDC)C and WinCC in the Monitoring-Control System of Bulk Grain Silo” 2019 IEEE Integrated STEM Education Conference (ISEC)

[3] Thepjit Cheypoca; Amata Luanpol; Virot Wuti “Circular Interpolation using Siemens S7-1200” 2023 9th International Conference on Engineering, Applied Sciences, and Technology (ICEAST)

Real-Time Production Monitoring System: An IoT and Open-Source Solution for SMEs

Manisra Baramechai
School of Engineering, The University of the Thai Chamber of Commerce
Bangkok, Thailand
j.manibara@gmail.com

Vorrapath Kokaew
School of Engineering, The University of the Thai Chamber of Commerce
Bangkok, Thailand
Vorrapath_kok@utcc.ac.th

***Abstract*—This study presents the development of a real-time production monitoring system utilizing Internet of Things (IoT) technology and open-source platforms to enhance production efficiency and reduce costs for SMEs. The system addresses challenges such as the lack of real-time data and inefficient data management by employing low-cost devices and software, including ESP32 and Grafana, with real-time data displayed through dashboards and mobile devices. Trials in actual production lines demonstrated increased efficiency, reduced downtime, and labor overtime savings of over 66,000 THB within 12 days. Additionally, the collected data supports process improvement planning and preventive maintenance, making this system a cost-effective solution for SMEs seeking to transition to digital manufacturing efficiently and sustainably**

Keywords— IoT, Real Time Production Control, Digital Transformation

I. INTRODUCTION

In today's competitive and rapidly evolving industrial landscape, Lean Manufacturing has emerged as a key strategy to enhance efficiency, reduce waste, and add value to production processes. The advent of Industry 4.0 introduces innovative possibilities, particularly through the Internet of Things (IoT), which connects and controls devices within production lines. IoT enables real-time production monitoring, empowering manufacturers to optimize workflows, enhance efficiency, and lower costs. IoT adoption in manufacturing continues to grow, with forecasts predicting exponential market expansion due to its ability to interconnect data across devices for improved operations. However, small and medium enterprises (SMEs) often face challenges in adopting IoT due to budgetary and investment constraints. Leveraging open-source platforms and cost-effective equipment provides an accessible solution for SMEs to overcome these barriers. Open-source platforms offer SMEs advanced technologies with lower costs and high customization capabilities, making them a sustainable, long-term option. This study explores the application of IoT and open-source platforms to develop a Visual Control System for real-time production monitoring. The system facilitates rapid process optimization, cost reduction, and improved operational efficiency, ensuring manufacturing agility in response to dynamic market demands.

II. OBJECTIVES AND SCOPE OF THE STUDY

A. Objectives of the Study

This study aims to develop a Production Monitoring System using IoT and open-source platforms to enhance production efficiency and streamline operations. Specific goals include:

- Creating a Visual Control System for real-time monitoring.
- Assessing its impact on production efficiency and workflow adjustments.
- Comparing efficiency metrics pre- and post-implementation.
- Proposing strategies to optimize manufacturing processes using real-time data.

B. Scope of the study

This research focuses on the development and application of tools powered by IoT technology, utilizing open-source software to reduce costs and simplify implementation. A case study was conducted on a toy manufacturing company, with the application of these tools specifically targeting assembly lines that involve multiple stages, such as assembly, quality inspection, and material management. The system's performance was evaluated using key performance indicators, including production volume, error rates, and employee productivity. The development of this system takes into account the resource constraints commonly faced by SMEs, ensuring that the findings can be practically applied. The goal is to enhance efficiency, reduce costs, and support the transition of small and medium enterprises toward digital technology adoption.

III. RESEARCH METHODOLOGY

The study was conducted to design and implement a Production Monitoring System, with the following key stages.

A. Study and Analysis of Existing Production Line Problem

This stage involved examining the production line chosen as the case study. Data was collected on workflows, resource allocation, and key performance indicators (KPIs) associated with the assembly line. The purpose was to identify operational inefficiencies or bottlenecks. These findings were used to analyze and pinpoint areas for improvement.

B. Design and Development of IoT-Based Visual Control Tools

Based on the identified problems and improvement requirements, this stage focused on the development of IoT-based tools using open-source software. These tools were designed to perform real-time data collection on production activities, visually display the data, and provide feedback or alerts to help operators optimize their performance.

C. Implementation of IoT Tools in Real Production Lines

The developed tools were deployed and tested in the case study's assembly line. Data on production performance was collected both before and after the tools' implementation. This step aimed to evaluate the impact of the tools on metrics such as production volume, error rates, and employee productivity.

D. Analysis and Comparison of Results

Data collected during the pre- and post-implementation phases were analyzed both quantitatively and qualitatively. Key performance indicators which is an increase in production output and worker productivity, were compared to assess the effectiveness of the IoT tools in optimizing the production line.

E. Summary of Findings and Recommendations

The final stage involved summarizing the study's findings and providing recommendations on how IoT-driven visual control tools could be applied to SME production lines. The recommendations included potential improvements and strategies for scaling the system to address resource constraints and support wider adoption in other industrial contexts.

IV. Research results and discussion

This study investigated the production process of a company manufacturing plastic decorative items, which included key stages such as injection molding, surface finishing, painting, assembly, and quality inspection. Several critical issues affecting operational efficiency were identified, as outlined below:

A. Identified Challenges

- Production data was only accessible a day after operations, preventing real-time issue resolution and efficiency improvements.
- Workers were unable to track production rates against targets, leading to ineffective control.
- The absence of systematic data collection caused delays in performance assessments due to disorganized and scattered information.
- Without timely data, proactive improvements were hindered, affecting worker performance.
- Manual data collection and analysis consumed excessive time and resources, reducing decision-making efficiency

To address these challenges, the researchers developed a Production Monitoring System aimed at enhancing production control efficiency. This system provides real-time monitoring of production status, covering critical information such as:

- The actual production output at any given time compared to daily targets,
- The remaining production required to meet the specified target, and
- The real-time efficiency of the production process.

The system allows supervisors to dynamically adjust daily targets by inputting data into the system. All production data is stored in a cloud-based platform, enabling users to access historical data from past operations.

The system's output is displayed on devices installed at the end of the production line, allowing all employees to monitor the production status in real time. Additionally, the data can be transmitted to other devices, such as tablets or smartphones, enabling managers and executives to access real-time production information from anywhere.

B. Hardware of Production Monitoring System

The development of the Production Monitoring System required a combination of hardware and software components to ensure its functionality and adaptability. The application of low-cost hardware, open-source software, and cloud-based storage ensures that the system remains both scalable and cost-effective, making it particularly suitable for small and medium enterprises (SMEs) aiming to adopt Industry 4.0 technologies. There are the details of the components used:

- ESP32 Microcontroller: The ESP32 serves as the primary control unit, supporting both Wi-Fi and Bluetooth connectivity. It facilitates efficient data acquisition from sensors, which are used for item counting. Sensor data is converted into digital signals and displayed as the number of completed items on an LED screen installed in the factory. Additionally, the ESP32's Wi-Fi capabilities enable real-time data transmission to an Access Point, which then stores the data in a cloud-based system.
- Motion Sensors and Switches: These components detect activity and operational statuses, respectively, within the production process.
- LCD Displays: Used to present textual production data in designated areas, providing accessible information to employees and supervisors.

C. Software of Production Monitoring System

- Arduino IDE: This platform was used to program the ESP32 microcontroller, allowing integration with other system components.
- Cloud Storage (e.g., Firebase or ThingSpeak): The cloud platform is used to store production data and supports data analysis. Cloud storage also enables managers to access real-time data from any location, ensuring 24/7 availability.
- Grafana: This tool was employed to create dashboards for visualizing data in the form of graphs and performance indicators, enhancing data interpretation and decision-making.
- Databases (e.g., InfluxDB or MySQL): These databases store and manage data, ensuring seamless connectivity with the Grafana dashboard.

D. System Development Process

1. The development of the Production Monitoring System was carried out through the following steps:
   - Integration of Sensors and Switches with ESP32:
   - Sensors and switches were connected to the ESP32 microcontroller.
   - The ESP32 was programmed using Arduino IDE to read input signals from the sensors and switches.
2. Wi-Fi Connectivity Setup:
   - The ESP32 was configured to connect to the internet via Wi-Fi, enabling real-time data transmission to cloud services.
3. Programming for Cloud Data Transmission:
   - Custom programming was implemented to send collected data from the ESP32 to the cloud using the MQTT Protocol. This ensured secure and efficient data transmission.

4. Data Storage in Cloud Databases:
    - Collected data was stored in cloud-based databases, such as Firebase or Influx DB, which support real-time data access and retrieval for further processing.
5. Grafana Dashboard Configuration:
    - Grafana Dashboard was set up to visualize production data in real time.
    - Data sources, such as InfluxDB or MySQL, were connected to Grafana for seamless data integration.
6. Panel Creation in Grafana:
    - Panels were designed within Grafana to display key production metrics using visual formats such as graphs, gauges, and other charts. These visualizations provided actionable insights for monitoring and decision-making.

Fig 1 illustrates the connection setup of the devices within the production monitoring system

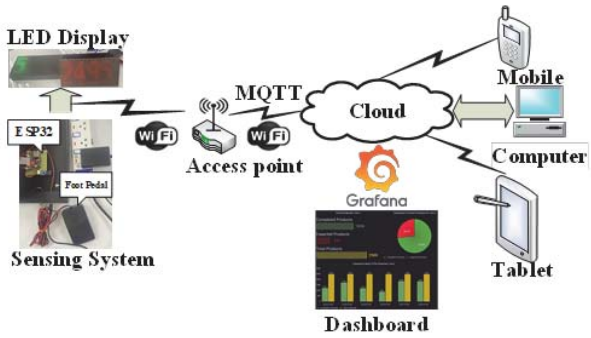


Fig. 1. SME real-time production monitoring system device set up

To evaluate the practical application of the Production Monitoring System, the study tested three types of data collection devices installed along the production line. These devices were used to monitor and control workers' operations.. The three types of devices tested were:

- Push Button: Workers pressed the button after completing each production task.
- Foot Pedal: Workers activated the pedal after completing each production task.
- Optical Sensor: The sensor detected items passing through the production line.

The devices were tested over a 10-day period, and their performance was compared based on usability and error rates. The push button proved to be the most efficient device for data collection. Its ease of use and integration into workers' existing workflows resulted in the lowest average error rate among the three devices. Conversely, the foot pedal and optical sensor exhibited higher error rates due to operational limitations as shown in Table I.

The findings indicate that the push button is the most effective device for production data collection. It offered convenience and continuity with the existing workflow, resulting in more accurate data collection and fewer errors compared to the other devices. This evaluation highlights the importance of selecting suitable data collection devices to ensure the efficiency and reliability of real-time production monitoring systems.

TABLE I. SUMMARIZES THE ERROR RATES AND ISSUES OBSERVED DURING THE TEST

Device	Error Rate (%)	Identified Issues
Push Button	1.9%	Workers occasionally pressed the button multiple times.
Foot Pedal	6.2%	Workers forgot to press the pedal or pressed it twice accidentally.
Optical Sensor	7.0%	Repeated detections occurred when workers moved items past the sensor.

After data collection, the information was displayed in the form of real-time reports on both LCD screens and mobile devices for supervisors, as illustrated in Fig 2. This visualization ensured that supervisors could monitor production progress efficiently and make timely decisions.

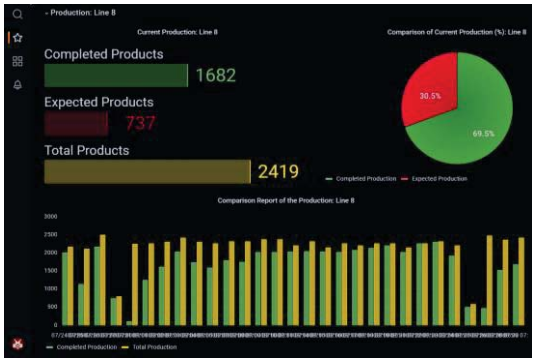


Fig. 2. Production monitoring system

To enhance the usability of the data and facilitate real-time tracking of production line performance, LED display panels (shown in Fig 3) were installed at the end of the production line. These displays provided workers with instant updates on the current production status, indicating whether operations were meeting the set targets.



Fig. 3. LED Display panel in the production line

The integration of these visualization tools, including mobile devices for supervisors and LED panels for workers, ensured that both management and operational teams had access to actionable insights.

The Production Monitoring System proposed in this research is designed with the primary objective of enabling small and medium enterprises (SMEs) to adopt and implement the system efficiently. To ensure its accessibility and feasibility for SMEs, the researchers conducted a cost estimation for the development of the system's components, as detailed in Table II.

TABLE II. SUMMARIZES THE ERROR RATES AND ISSUES OBSERVED DURING THE TEST

No.	Equipment Details	Price (THB)/Unit
1	KIT ESP32 + LED P4 32x64 Pixels Display with Adapter	1,950
2	Non-slip Foot Pedal Switch (Ac 250V 10A Spdt No Nc)	50
3	Aluminum Frame for LED P4 32x64 Pixels Display	900
4	Access Point	1,500
5	Passive Buzzer	20
6	WitMotion Laser Distance Sensor (WT53D Distance)	900
7	Cables and Electrical Wiring	500
Total Hardware Cost		3,870
8	Google Cloud IoT Core	1,500/month

The cost analysis demonstrates that the system can be developed with a relatively low investment, making it an affordable solution for SMEs.

V. CONCLUSION

To evaluate the effectiveness of the production monitoring system developed in this study, the system was implemented in a comparative experiment involving two production lines manufacturing the same SKU. Production line 1 operated without the production monitoring system (baseline) and production line 2 operated with the production monitoring system. The performance data collected from both production lines were compared. The results demonstrated a significant improvement in production efficiency when the system was applied. Data from the experiment, as summarized in Table 3.

TABLE III. PERFORMANCE COMPARISON BETWEEN PRODUCTION LINES WITH AND WITHOUT THE PRODUCTION MONITORING SYSTEM

SKU Model	Production Line 1 (Without System)	Production Line 2 (Without System)
SKU145674	76.8%	81.5%
SKU156545	72.3%	79.3%
SKU235653	69.9%	75.2%
SKU125675	77.4%	83.4%
SKU143454	65.7%	71.4%

The implementation of the Production Monitoring System demonstrated a significant improvement in production efficiency compared to traditional methods. In a comparative experiment involving two production lines manufacturing the same SKU, the line using the system consistently achieved higher efficiency across all SKUs, as highlighted in the data.

The improvement in production efficiency observed with the implementation of the Production Monitoring System can be attributed to the following key factors:

- Real-time data enabled supervisors to promptly address issues when production didn't meet targets, reducing downtime and delays.
- Sharing real-time performance fostered accountability and teamwork, encouraging collaboration to achieve production goals.
- Close monitoring of KPIs motivated supervisors to proactively resolve challenges, ensuring timely interventions to maintain productivity.

The implementation of the Real-Time Production Monitoring Board across the production of five SKUs resulted in significant cost savings. Over a 12-day production cycle, the system reduced overtime labor costs by more than 66,415 THB. This reduction was achieved by enhancing employee efficiency and providing more accurate data to support decision-making.

The adoption of the real-time production monitoring board in manufacturing processes not only reduces labor costs by enhancing employee productivity but also provides businesses with accurate data to support informed decision-making. This leads to significant improvements in production efficiency in the following areas:

- Real-time data enables trend analysis, such as identifying frequent machine breakdowns or productivity dips, facilitating proactive Preventive Maintenance and minimizing disruptions.
- Team motivation and collaboration: transparent real-time displays drive accountability, teamwork, and continuous performance improvements while fostering collaboration.

Thus, implementing the real-time production monitoring system is an investment that not only reduces costs but also enhances the overall value of the production process. By leveraging high-quality data for decision-making, the system improves operational efficiency and empowers teams to achieve greater productivity and effectiveness.

REFERENCES

[1] G. Eason, B. Noble, and I. N. Sneddon, “On certain integrals of Lipschitz-Hankel type involving products of Bessel functions,” Phil. Trans. Roy. Soc. London, vol. A247, pp. 529–551, April 1955. *(references)*

[2] J. Clerk Maxwell, A Treatise on Electricity and Magnetism, 3rd ed., vol. 2. Oxford: Clarendon, 1892, pp.68–73.

[3] I. S. Jacobs and C. P. Bean, “Fine particles, thin films and exchange anisotropy,” in Magnetism, vol. III, G. T. Rado and H. Suhl, Eds. New York: Academic, 1963, pp. 271–350.

[4] K. Elissa, “Title of paper if known,” unpublished.

[5] R. Nicole, “Title of paper with only first word capitalized,” J. Name Stand. Abbrev., in press.

[6] Y. Yorozu, M. Hirano, K. Oka, and Y. Tagawa, “Electron spectroscopy studies on magneto-optical media and plastic substrate interface,” IEEE Transl. J. Magn. Japan, vol. 2, pp. 740–741, August 1987 [Digests 9th Annual Conf. Magnetics Japan, p. 301, 1982].

[7] M. Young, The Technical Writer’s Handbook. Mill Valley, CA: University Science, 1989.

[8] K. Eves and J. Valasek, “Adaptive control for singularly perturbed systems examples,” Code Ocean, Aug. 2023. [Online]. Available: https://codeocean.com/capsule/4989235/tree

[9] D. P. Kingma and M. Welling, “Auto-encoding variational Bayes,” 2013, arXiv:1312.6114. [Online]. Available: https://arxiv.org/abs/1312.6114

Application of 3D printer to create pet casts

1st Pipat Phaisalpanumas
Faculty of Engineering
King Mongkut's University of Technology North Bangkok
Bangkok, Thailand
pipat.p@eng.kmutnb.ac.th

2nd Acting Sub Lt. Nattasit Monkaew
Faculty of Engineering
King Mongkut's University of Technology North Bangkok
Bangkok, Thailand
leafzabangken@hotmail.com

3rd Damisara Chutikan
Faculty of Engineering
King Mongkut's University of Technology North Bangkok
Bangkok, Thailand
damisara.chu@gmail.com

4th Premporn Khemavuk
Faculty of Engineering
King Mongkut's University of Technology North Bangkok
Bangkok, Thailand
premporn.k@eng.kmutnb.ac.th

5th Narin Tammarugwattana
School of Engineering
King Mongkut's Institute of Technology Ladkrabang
Bangkok, Thailand
narin.ta@kmitl.ac.th

6th Sirichai Tammaruckwattana*
School of Engineering
King Mongkut's Institute of Technology Ladkrabang
Bangkok, Thailand
sirichai.ta@kmitl.ac.th

***Abstract*—This paper presents the application of 3D printer to create pet casts. The problem of injuries from falls or symptoms related to bone injuries are symptoms that veterinarians diagnose as potentially treatable by external splinting to allow the bones to fully fuse. Differences in physiology are limitations in splinting and structuring the splint. This research introduces 3D printing technology to help the creation of splints for pets to increase treatment options using innovations or concepts. Study the current state of external splinting treatment methods for pets and design the research method was started by scanning organs to be splinted with a 3D scanner. The 3D images are then used to creat a model for splinting by designing with the Sintratec 3D modeling computer program. Then create the splints by burning plastic powder crystals to harden with a 3D printer and clean the surfaces by sandblasting and polishing. The materials used to create the splints in this study are two types of engineering materials: polyamide12 (PA12), suitable for creating hard splints, and thermoplastic elastomer (TPE), suitable for creating soft splints. Both materials have good mechanical properties and are strong impact resistance, chemical resistance, and high heat resistance. The finished splint pieces can be easily split to the pet model, reducing the steps compared to the normal splints, resulting in a shorter splint time, depending on the location or organs the splints are placed, and reducing the pet stress caused by being restrained during splinting. This research presents the introduction of technology and its advantages to help increase treatment options for pet injuries, which is beneficial to pets and pet owners, and helps veterinarians provide appropriate treatment.**

Keywords—3D printer, pet, cast

I. INTRODUCTION

Currently, more pets are brought to hospitals for treatment of high-rise syndrome due to the urban society and the increasing popularity of choosing condominiums or apartment buildings as their residences. Keeping pets in high-rise buildings has also increased. This is another factor that has caused us to see more pets with high-rise syndrome. According to data from 2013 to 2017, [1]-[3]. 21.9% of 3,425 accidents and injuries in cats were caused by falls from heights. Initially, veterinarians will diagnose and treat based on the severity of the injury. In cases where cats have injuries with uncomplicated internal fractures of the bones, they can be treated without surgery by applying an external cast to allow the broken bones to fully connect and reduce the risk of surgery. Currently, external casts are the most popular treatment. The differences in anatomy are limitations in the wrapping or construction of casts. Increasing treatment options with innovations or new concepts can benefit pets, their owners, and the veterinary community by using the concept of applying a 3D printer to help create casts for pets by creating casts using a computer program and creating cast pieces by 3D molding. This research is interested in the technology of creating parts from burning plastic powder crystals to harden by Selective Laser Sintering (SLS). The selected materials are polyamide12 (PA12), which is suitable for creating hard casts, and thermoplastic elastomer (TPE), which is suitable for creating soft casts. Because both materials are high-performance engineering plastics, have good mechanical properties, are strong, resistant to impact, chemically resistant, high resistant, and flexible. This study will produce cast pieces for a pet model.

II. METHODS

The proposed research is to create casts for pets, where differences in physiology are limitations in wrapping or structuring the cast. The use of 3D printing technology helps in creating casts for pets to increase treatment options using new innovations or concepts that are beneficial to pets, pet owners, and the veterinary industry.

A. Current status of external splinting

The external splinting in pets with fractures allows the fractured bones to fully fuse using thermoplastic casts, both casts and splints, to limit movement, which is appropriate for initially detected injuries as shown in Fig. 1.



Fig. 1. The using a thermoplastic splint to splint the leg

The external splint uses about 2 layers of cotton wool. Cut the thermoplastic splint to the length of the leg, soak the thermoplastic splint in warm water until it softens, then splint the leg by wrapping it from the bottom up, use an elastic co-adhesive bandage to prevent slipping, rodents, and dust, The soak the thermoplastic splint in warm water until it softens,

then splint the leg to fit the anatomy of the leg by splinting at the cranial, lateral, medial, or Caudal sides and The fold the end of the cotton wool inside the splint up to cover the thermoplastic splint and tape the end.

B. Select a pet model

Fig. 2 shows the selection process for the pet model is a Shiba Inu, size 15.2 x 17 cm².



Fig. 2. Pet model, Shiba Inu, size 15.2 x 17 cm²

C. 3D scanner

The scanning of the parts of the body to be made into a cast using a 3D scanner as shown in Fig. 3.



Fig. 3. 3D scanner GOM brand, ATOS CORE model

D. Preparing the workpiece and attaching reference points

Figs. 4 and 5 show the preparing the workpiece or organ to be cast by attaching reference points around the organ to be cast without touching the injured point or organ.



Fig. 4. Reference points



Fig. 5. Preparation of the organs to be cast

E. Scanning of the organ parts to be cast

The scan the organ that needs to be made into a splint by scanning in a circular motion until the desired organ is obtained as shown in Figs. 6 and 7.

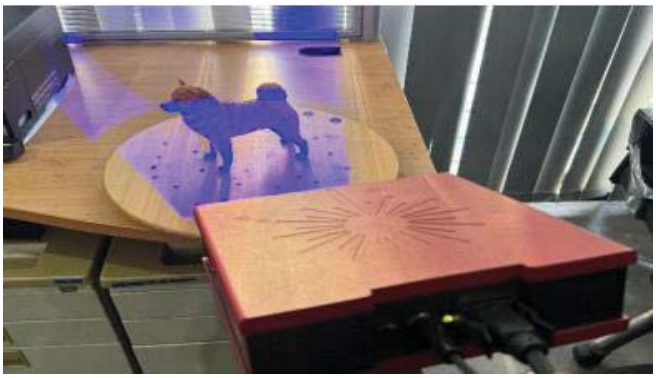


Fig. 6. Scan the organs to be cast for the pet model

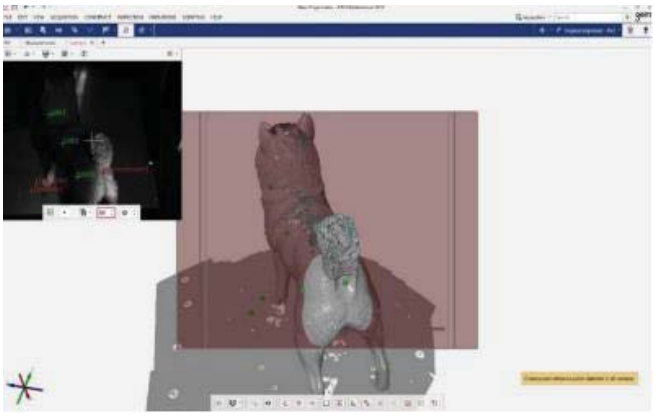


Fig. 7. Processing of scanned organs to create a cast for a pet model

F. Computer modeling for splint creation

The model for creating a cast using a computer program is shown in Fig. 8. The cut of the parts of the organ that need to be created as a cast to create a model as shown in Fig. 9. Using the reverse engineering technique. This is an engineering principle that designs new parts to be larger while having the same appearance and shape as the original parts by expanding the size (Scale) of the organ to be larger in a ratio of 1:1 so that the resulting cast piece has the same ratio as the actual injured organ and fits snugly as shown in Fig. 10. The principle of designing the cast piece is to consider the separation of the cast parts, such as the left-right

separation as shown in Fig. 11, the front-back separation as shown in Fig. 12, or the separation according to the body shape, to be appropriate for the proportion or organ that will be put on the cast and help treat the injury. The thickness of the cast can be determined and the skin (Mesh) in the area where the cast parts have been cut out can be filled as desired as shown in Figs. 13 and 14.

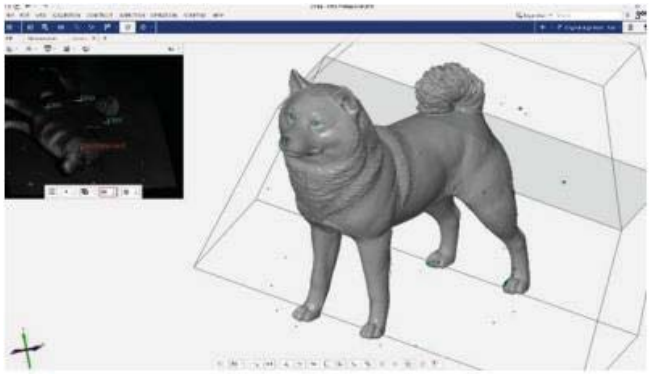


Fig. 8. Model for the creation of a cast using computer design

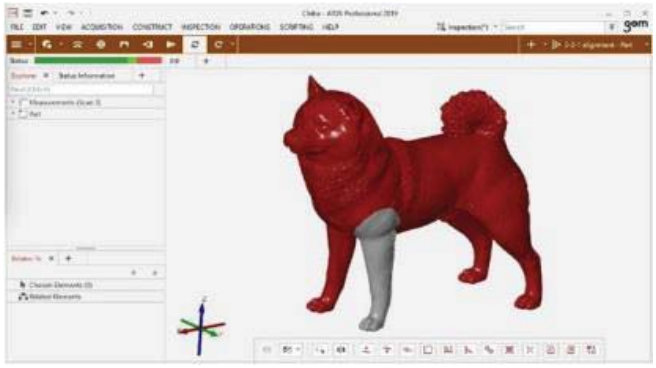


Fig. 9. Separation of the left forelimb to be casted

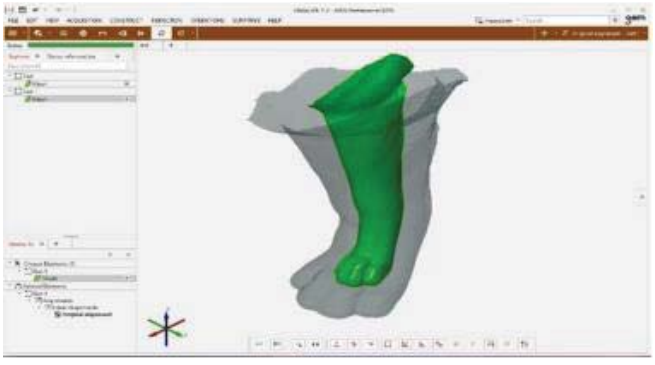


Fig. 10. Scale of the left forelimb to be larger

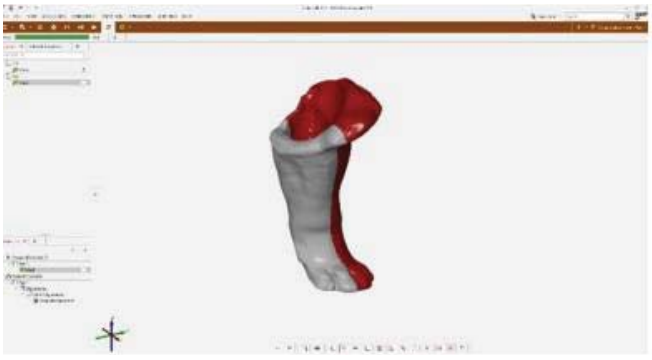


Fig. 11. Section of the left forelimb in a left-right fashion

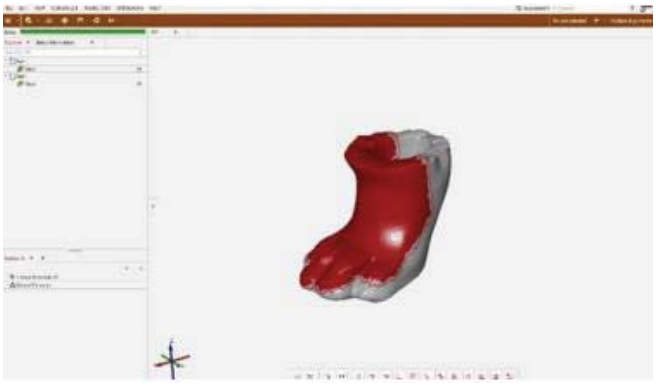


Fig. 12. Section of the left forefoot in an anterior-posterior fashion

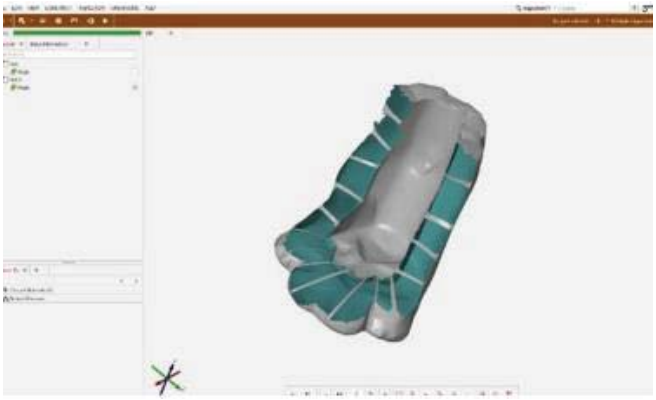


Fig. 13. Left forefoot with the cast sectioned before occlusion

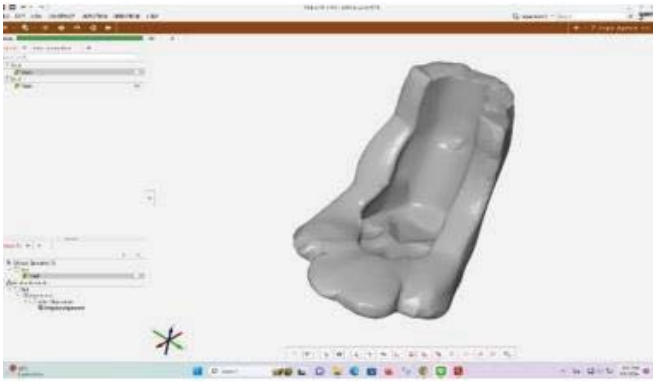


Fig. 14. Left forefoot with the cast sectioned after occlusion

Fig. 15 shows the preparation of cast for pet model using 3D modeling program

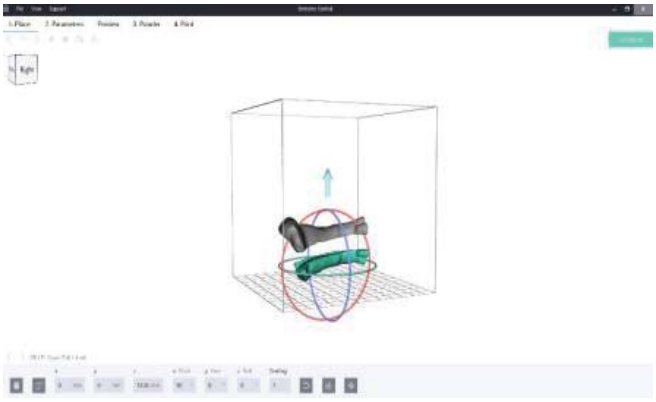


Fig. 15. Preparation for creating a left front leg splint using a 3D modeling program

G. *Creation of a cast for a pet model by solidifying plastic powder crystals using SLS molding technology*

Fig. 10 shows preparing the 3D printer. turn on the 3D printer and check its status before starting use as shown in Fig. 16. PA12 powder is suitable for making hard splint parts, and TPE powder is suitable for making soft splint parts as shown in Fig. 17. The forming of a splint piece with a 3D printer is a forming method by burning plastic powder crystals to harden without support. A laser is used to burn the plastic powder to form according to the piece's pattern. A heater is used to heat the plastic powder so that the plastic powder melts together. The piece is formed one layer at a time, starting from the bottom of the piece to the top of the piece. When the first layer of the piece is formed, the scraper will scrape the plastic powder to cover the pattern of the piece to prepare for the next layer of the piece. This is done until all layers are complete as shown in Fig. 18.



Fig. 16. 3D printer Sintratec kit



Fig. 17. PA12 material powder and TPE material powder



Fig. 18. The left front leg cast

III. Experimental Results.

A. *Design results of splint parts for pet models*

The left front leg cast piece is made from PA12 material powder. The design principle is to conform to the left front leg physiology of the pet model by cutting left and right parts to support the splinting in case of ankle and shin injuries. The cast piece is strong according to the properties of the selected material. It was tested to be assembled into the left front leg position of the pet model as shown in Fig. 19.



Fig. 19. Attach the left front leg splint to the left front leg of the pet model.

IV. Conclusions

Currently, there is a technology called 3D printing, which is a technology that can create prototypes with details close to or equal to real workpieces, to meet the needs and practical applications. When compared to treatment with external splinting, the application of 3D printing to create splints for pets is more detailed and more suitable for the physiology of the pet model. Because the technology used is a high-precision technology, it can collect more detailed information on the physiology of the injured organs than external splinting, and it produces a finished splint that can be easily assembled with the pet model. It can reduce the steps in making the splint structure from the current external splinting, which reduces the time spent on splinting.

References

[1] Kenji Hara and Endre Hellem)2022 .(“Efficacy of treating segmental bone defects through endochondral ossification

[2] Hailong Liu and Christian Gasser) 2020 .(“Computational and experimental characterization of 3D-printed PCL structures toward the design of soft biological tissue scaffolds.” Materials & Design, Volume 188, Article 108488

[3] Jiao Liu and Shaohua Wu) 2022 .(“Electrospun strong, bioactive, and bioabsorbable silk fibroin/poly (L-lactic-acid) nanoyarns for constructing advanced nanotextile tissue scaffolds.” Materials Today Bio, Volume 14, Article 100243

Prototype of Chipping and Briquetting Machine for Eucalyptus Wood Processing

1st Pipat Phaisalpanumas
Faculty of Engineering
King Mongkut's University of Technology North Bangkok
Bangkok, Thailand
pipat.p@eng.kmutnb.ac.th

2nd Nattarat Namboot
Faculty of Engineering
King Mongkut's University of Technology North Bangkok
Bangkok, Thailand
truckydream_@hotmail.com

3rd Damisara Chutikan
Faculty of Engineering
King Mongkut's University of Technology North Bangkok
Bangkok, Thailand
damisara.chu@gmail.com

4th Chartchai Usadornsak
Faculty of Engineering
King Mongkut's University of Technology North Bangkok
Bangkok, Thailand
chartchai.u@eng.kmutnb.ac.th

5th Naritsak Tantitippawan
Faculty of Engineering
King Mongkut's University of Technology North Bangkok
Bangkok, Thailand
naritsak.t@eng.kmutnb.ac.th

6th Sirichai Tammaruckwattana*
School of Engineering
King Mongkut's Institute of Technology Ladkrabang
Bangkok, Thailand
sirichai.ta@kmitl.ac.th

***Abstract*—This paper presents eucalyptus, versatile plants that can grow well in almost every area of Thailand. In the future, the demand for eucalyptus wood tends to increase both domestically and internationally because eucalyptus wood has become a major raw material in various industries and is also an important source of energy in terms of biomass fuel production. The research team has designed and built a eucalyptus woodchipper and pelletizer prototype. The machine has a width of 1,300 mm, a length of 800 mm, and a height of 900 mm. Inside the machine, there are log conveying systems, a shredder, and a pelletizing system. The shredder uses a 2.2 kW gear motor for shredding logs and a set of 23 blades. The conveying system consists of 4 upper and lower conveyors and uses a 0.2 kW gear motor. The speed is controlled by an inverter. The pelletizing system uses a hydraulic system for compression, which has a hydraulic pump motor as the source of pressure. In the prototype pelletizing and baling test, the optimum speed of the conveying machine was set at 5 rpm, the chopping speed at 320 rpm and the baling pressure at 220 kg/cm2. The processing of eucalyptus into the form of wood chips reduces the volume of eucalyptus by 46 percent, allowing more logs to be transported at a time and significantly reducing transportation costs. In addition, the creation of new products from eucalyptus processing will help generate more income for eucalyptus farmers than just cutting and selling eucalyptus.**

Keywords—chipping, briquetting, eucalyptus wood

I. INTRODUCTION

Eucalyptus is an important economic tree in the world and a plant with many benefits. It is a native tree of Australia with a variety of 500 species which was imported to be planted in Thailand 1946. [1]-[3]. In 1964, it was found that Eucalyptus species Kamaldulensis (Tree Suitability) can grow well in almost every area of Thailand. Therefore, commercial planting has been widely promoted. Currently, many sectors such as government or the private sectors have turned to give importance to eucalyptus, the eucalyptus market tends to increase both domestically and internationally because it has become a main raw material in various industries, such as in the paper industry or in various types of construction. It is also an important energy source in terms of biomass fuel production, which is considered an export product that generates tens of billions of baht per year for the country. Currently, eucalyptus raw materials are not enough to meet the demand.

The introduction of agricultural machinery technology to help increase the value of eucalyptus has increased the income of eucalyptus farmers because eucalyptus is currently of interest to investors in various industries The processing into the form of wood pellets will help increase the amount of transportation.

The purpose of this research is to develop a tool that can add value to agricultural products under a simple design, is strong, and easy to maintain. In addition, materials and equipment available domestically can be used for maintenance.

II. METHODS

A. The main structure of the machine

The main structure of the machine is the main component for assembling various parts together, including the conveyor roller set, the wood chipper set and the wood pellet set. Different positions are designed to hold the parts precisely. The size of the structure is 760x1250x300 mm, and the thickness of the steel is 12 mm, which is strong enough to support the parts to be installed.

The proposed prototype of a chipping and briquetting machine for eucalyptus wood processing is shown in Fig. 1.

Fig. 1 shows the structure of the proposed prototype of the chipping and briquetting machine for eucalyptus wood processing, mainly composed of three parts: the conveyor belt, the log chipper, and the pelletizing unit. An electric motor powers the conveyor belt and the woodchipper, while a hydraulic system powers the pelletizing unit. Both parts are electrically controlled together via a control panel on the front of the machine.

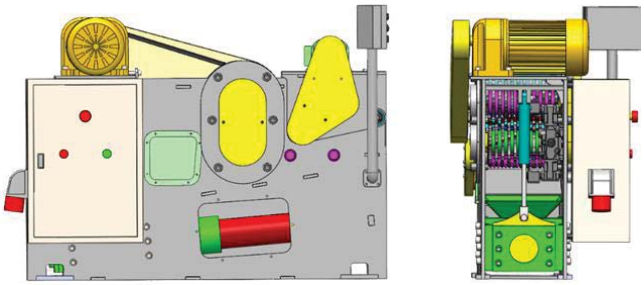


Fig. 1. The proposed prototype of a chipping and briquetting machine for eucalyptus wood processing

The main components of the fresh wood chipper and pelletizing machine can be shown in Figs. 2 and 3.

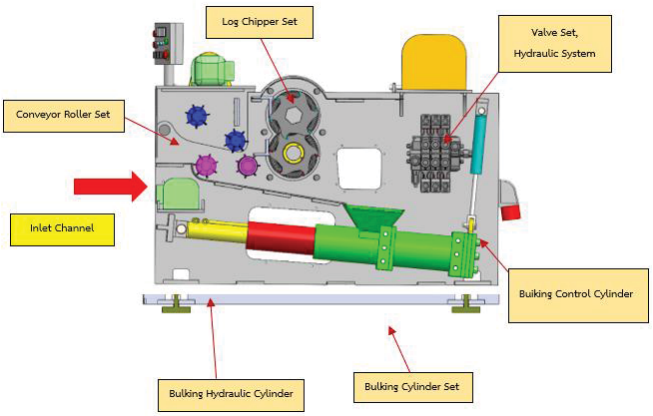


Fig. 2. The main internal components of fresh log chipper and baler

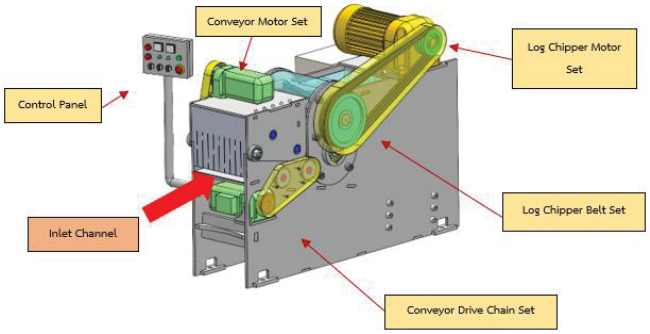


Fig. 3. The power transmission and control system of fresh log chipper and baler

B. *Log Conveyor*

The log Conveyor is responsible for transporting fresh logs into the shredding process. It consists of 2 sets of conveyors: upper and lower sets. The upper conveyor is designed to move up and down according to the size of the wood fed through the feed channel. Conveyors are powered by 2 motors, which are transmitted through a chain set. The characteristics of adjusting the distance of the conveyor set according to the size of the logs shown in Fig. 4.

The conveyor is designed to have teeth to pinch the logs fed in through its channel. There are 6 blades in the set, each blade is at a different angle of 52 degrees. This design gives better efficiency than the conveyor blade with a round shaft because it pinches the logs better.

On both sides of the shaft, ball bearings are installed to help reduce friction that occurs when the shaft rotates. In addition, the force acting on the shaft when it receives a load during use is analyzed through a computer program as shown in Fig. 5. The conveyor shaft set that has gone through the design process can be used and is durable against the force that will be applied.

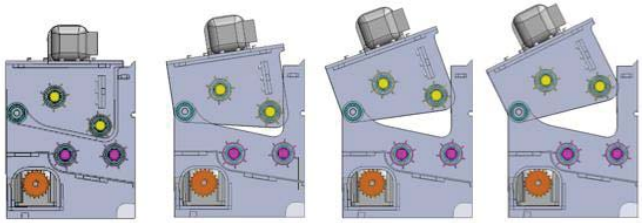


Fig. 4. The characteristics of adjusting the distance of the conveyor set according to the size of the logs

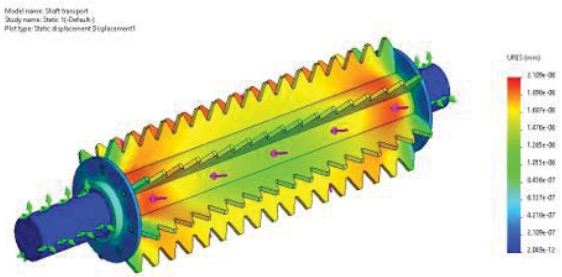


Fig. 5. The characteristics of the force acting on the log conveyor shaft

C. *Log chipper set*

Fig. 6 shows the log chipper set has the function of receiving the wood from the conveyor set to be chopped into small pieces of wood. The log chipper set consists of the upper knife set and the lower knife set. The upper knife set consists of 12 blades and the lower knife set consists of 11 blades. In the design of both blades, the blade sets are set to rotate in opposite directions. A 3 kW gear reduction motor is used as the power source to drive the chipper set and the power is transmitted by a belt.

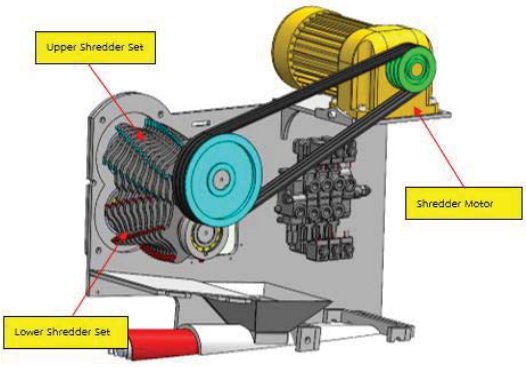


Fig. 6. The log chipper components

Fig. 7 shows the arrangement of each set of blades, the arrangement of each cutting edge is arranged in an offset manner to reduce the force that will act on the shredder wood blade set, which each blade will have an angle of 5 degrees. Each blade is assembled. The shaft is designed as a 57 mm hexagonal shaft to facilitate the forming of the workpiece and assemble each blade. And is held in position with a set of M50 nuts and lock rings to lock the position to prevent the blade set from moving during shredding

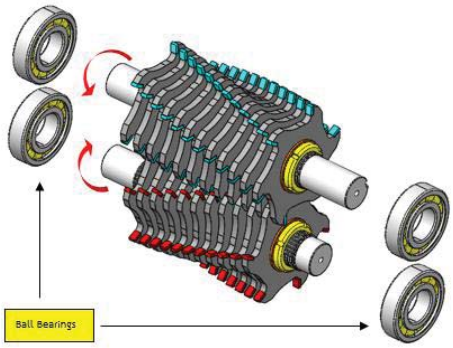


Fig. 7. The log chipper knife set

The cutting edge of the wood chipper blade is designed to have 6 cutting edges, each cutting edge has an angle of 60 degrees to distribute the force acting on the cutting surface of the blade. Carbide cutting edge material is used to

increase the efficiency of the blade used in the chipping process.

Fig. 8 shows the design process of the cutting knife angle used. The researcher has designed the blade along with analyzing the operation of the log chipper blade set at different working conditions, taking into account the size of the wood that will enter the log chipper into small pieces through a computer program. Generally, the cutting angle of the knife angle for woodworking is 40-45 degrees.

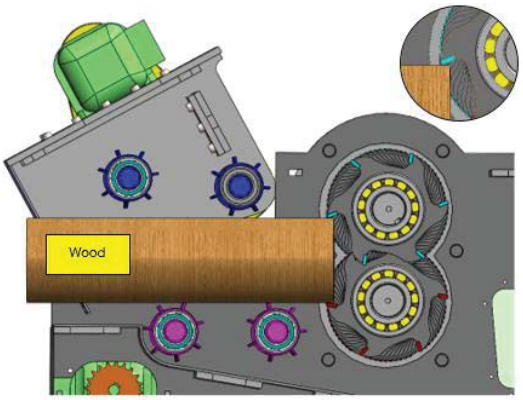


Fig. 8. The analysis of the performance of a 5 inches wood chopping knife set

In the design of each blade, the force acting on the blade is designed and simulated through a computer program to check the change of materials used in the production of the blade, as well as to evaluate the strength and durability of the parts used in the construction. The simulation is divided into 3 forms: stress value form (Stress), deformation (Displacement) and strain value (Strain).

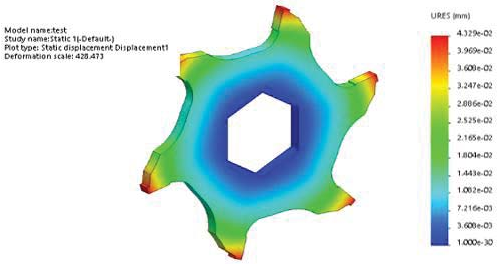


Fig. 9. The force simulation in the displacement part

Fig. 9 shows the deformation of the workpiece that is affected by the choice of materials in the design of the workpiece. It was found that the highest deformation value is 4.329×10^{-2} mm, which indicates that the deformation or twisting of the workpiece has almost no change.

D. Wood Pelletizing System

Fig. 10 shows the wood pelletizing system from the shredding process consists of a pelletizing cylinder, a hydraulic pelletizing cylinder, a hydraulic cylinder controlling the compression, a control valve set and a hydraulic pump. This system is designed with a Ø115 mm cylinder size, is strong and can withstand the force that will be applied during the compression. The pelletizing cylinder set will reduce the volume of wood from the shredding process. The control valve system is a hydraulic valve system that is controlled by an electrical system for easy control of the system. This system works together with a hydraulic pump set that is the source of power to produce oil pressure for the system. The pressure we choose is in the range of 200-300 kg/cm^2.

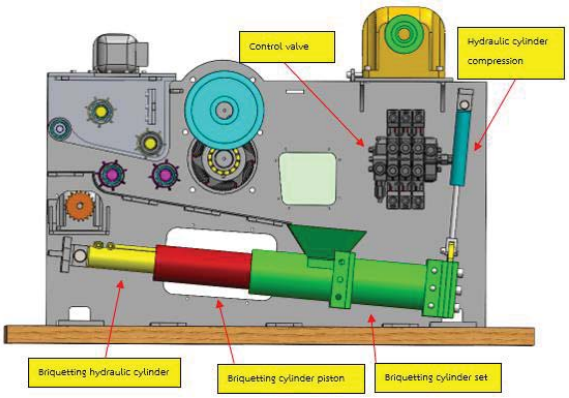


Fig. 10. The wood pelletizing system

III. THE PROPOSED CONTROL SYSTEM.

A. Electrical system used for control

Fig. 11 shows the electrical system used to control various systems of the machine has selected equipment that is appropriate for the machine. Inverters are used to control the operation of each motor to achieve precision and prevent damage to the equipment. Industrial standard electrical equipment is used to connect the equipment, such as magnetic breakers and delays. The inverter used for the log conveyor motor is a 0.4 kW inverter and the inverter for the log shredder is a 2.2 kW inverter. All control equipment is included in the control cabinet. The operation of the equipment is controlled via the control panel, and there is also a light installed to indicate the machine's operating status.

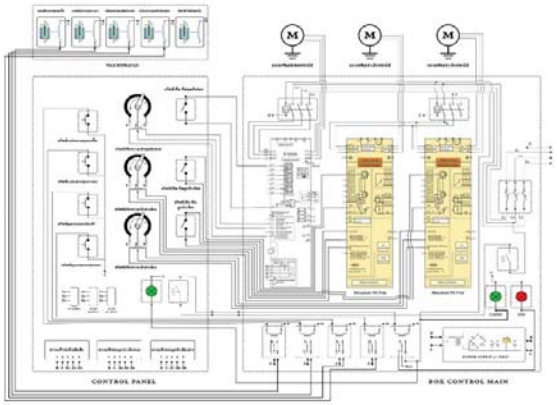


Fig. 11. The electrical diagram of control system

IV. EXPERIMENTAL SYSTEM.



Fig. 12. The prototype of chipping and briquetting machine

Fig. 12 shows the prototype of chipping and briquetting machine. There are 5 main parts of the production process:

the main structure of the machine (Frame and Body), roller conveyor, log shredder, briquetting set, and electrical control system.

V. EXPERIMENTAL RESULTS

In the process of testing the performance of the prototype tool, researchers prepared eucalyptus wood with a diameter of 1-5 inches, and a length of 1 meter per log, and the tree trunks used in the test had a cutting age of no more than 3 days to meet the specified scope. Then, they were tested in various working conditions.



Fig. 13. The compressed wood block using 220 kg/cm^2

A. Performance testing of log conveyor and log shredder

Table. 1 shows the performance test of the log conveyor and the log chopper by adjusting the rotational speed of the log chopper and the speed of the log conveyor found that the results from the test at log sizes from 1-5 inches, the appropriate rotational speed for each log size is at 340 rpm and the rotational speed of the log feeder at 3 rpm. It can be observed that the values in the range of each log size will give the smallest size of wood pieces after the shredding process and the log size is 1-2 inches, the size of the wood pieces after the shredding process is 1 mm.

Table 1. Size of the wood pieces at different rotational speeds.

Wood size (inch)	Mincer speed (rpm/min)	Wood feeding speed (rpm/min)							
		3	4	5	6	7	8	9	10
1 inch (2.54 cm.)	100	4	4	4	4	5	5	5	6
	150	3	3	4	4	5	5	5	6
	200	3	3	3	4	4	4	5	6
	250	2	2	2	3	4	4	5	5
	300	1	1	2	2	4	4	5	5
	340	1	1	2	2	4	4	4	5
2 inch (5.08 cm.)	100	4	4	4	5	5	6	6	6
	150	3	3	4	4	5	5	6	6
	200	3	3	3	4	4	5	5	6
	250	2	2	3	3	4	5	6	5
	300	2	2	2	3	4	4	5	5
	340	1	1	2	2	4	4	4	5
3 inch (7.62 cm.)	100	4	4	4	5	6	6	7	7
	150	4	3	4	5	6	6	7	7
	200	3	3	3	4	5	6	6	6
	250	3	2	3	4	5	5	6	6
	300	2	2	3	3	3	4	5	5
	340	2	2	2	2	3	3	4	5
4 inch (10.16 cm.)	100	5	5	6	6	7	8	7	8
	150	4	4	5	6	7	7	8	7
	200	4	4	5	6	6	7	8	8
	250	3	3	4	5	6	6	7	7
	300	2	2	4	4	5	6	6	6
	340	2	2	2	3	4	4	5	5
5 inch (12.7 cm.)	100	5	6	7	7	8	9	10	10
	150	5	5	6	7	8	8	9	10
	200	4	5	6	6	7	8	9	9
	250	3	4	5	6	6	8	8	8
	300	2	3	4	4	5	6	7	7
	340	2	2	3	3	4	4	5	7
		Size of the wood piece (mm)							

At the log size of 3-5 inches, the size of the wood pieces will be 2 mm. When the rotational speed of the log chopper is low, along with the high rotational speed of the wood feeder, the size of the wood pieces will be large. Conversely, when the rotational speed of the log chopper is high, along with the low rotational speed of the wood feeder, the characteristics of the wood pieces will be small. In this part, if the wood pieces after the shredding process are very small, it will have a positive effect on the pelletizing process, which will be able to compress and reduce the size of the wood pieces very well.

B. Performance testing of wood block machine

Table. 2 shows each value of pressure used to compress the wood chips affects the change in the size of the length of the wood chips. It can be seen that in the range of pressure used to compress wood chips, the size of the compressed wood chips will be longer than the wood chips that use higher pressure. This reduction in size from the log to the plywood chip will lead to a reduction in the volume of the wood as shown in Fig. 13.

Table 2. Length of the wood block compared to the pressure at each value.

Wood size (inch)	Length of wood (cm)	Briquetting pressure (Kg/cm^2)	Length of the wood block (cm)
1 inch	50	100	7.1
	50	150	6.5
	50	200	5.9
	50	280	5.4
2 inch	50	100	22.4
	50	150	21.7
	50	200	21.1
	50	280	20.5
3 inch	30	100	29.8
	30	150	29.1
	30	200	28.6
	30	280	28.2
4 inch	15	100	27.3
	15	150	26.7
	15	200	26.2
	15	280	25.8
5 inch	10	100	28.7
	10	150	28.1
	10	200	27.4
	10	280	27.0

VI. CONCLUSIONS

This paper proposed the prototype of chipping and briquetting machine for eucalyptus wood processing. The researcher has designed the machine through a computer program, including analyzing various parts of the machine through a computer program, and using the data to create a prototype of a shredding and baling machine. After the creation process, fresh eucalyptus wood was processed using the tool that the researcher designed and built to test the efficiency of the prototype, including collecting data on the performance of the prototype. The appropriate speed of the transport was set at 5 rpm, the shredding speed was 320 rpm, and the pressure used for baling was 220 kg/cm^2. After the shredding and baling process, the size of the wood pieces was reduced to 60 percent. Using a eucalyptus wood shredding and baling machine can help reduce the volume and size of the wood, which has a positive effect on transportation to obtain a greater quantity than before.

REFERENCES

[1] Effurun and Nigerai. (2019). “DESIGN AND CONSTRUCTION OF A PAPER SHREDDING MACHINE.” Journal of Multidisciplinary Engineering Science and Technology (JMEST)

[2] Raffaele Spinelli and Enrico Marchi. (2020). “Trends and Perspectives in the Design of Mobile Wood Chippers.”

[3] Lodz and Poland. (2016). “The System Wood Chipping in Disc Chipper Problems of Uniformity of Length.” Wood Reaearch. No. 433-442.

Re-envisioning On-Ground Aircraft Movement using Reinforcement Learning

Anurag Vallur, Anuj Jain, Anirudh Sridhar, Adi M., T.S. Chandar
Department of Electronics and Communications Engineering, PES University
Bengaluru, 560085, Karnataka, India
anuragr.vallur@gmail.com, anujj6544@gmail.com, aniruddh.s12177@gmail.com, adi.kumar5738@gmail.com, chandarts@pes.edu

***Abstract*—Ground traffic congestion remains a significant challenge in the aviation industry, driven by stringent protocols, increasing air traffic, and occasional controller errors, all of which contribute to delays in aircraft operations. Air Traffic Controllers (ATCOs) currently rely on Standardized Taxi Routes (STRs), which provide predefined taxi-in and taxi-out pathways. However, the limited flexibility of STRs, due to their finite number of published routes, constrains controllers' ability to optimize ground traffic flow. This study proposes a novel approach leveraging Reinforcement Learning (RL) to dynamically generate the most efficient taxi routes for aircraft in real-time. The proposed RL-based framework adapts to live ground conditions, enabling the system to adjust route clearances in response to situational changes. By reducing congestion and minimizing delays, this approach aims to alleviate ATCO workload, enhance situational awareness, and improve overall operational efficiency during periods of high ground traffic density.**

***Index Terms*—Air Traffic Controllers (ATCos), Proximal Policy Optimization (PPO), agent, reward, episodes, Epsilon Greedy**

I. Introduction

As global air travel rises, air traffic controllers face greater challenges, particularly in managing ground operations efficiently. Airport taxiing is the movement of aircraft between runways, taxiways, and terminals, is a critical component of these operations. Efficient management of airport taxiing operations is essential for maintaining smooth and steady air traffic flow, minimising delays on ground and reducing environmental impact. Traditional rule-based systems often struggle to adapt to the dynamic and complex nature of airport environments, particularly during peak traffic periods.

This paper explores the application of using Reinforcement Learning (RL) algorithms like Proximal Policy Approximation (PPO) based on data from Google Earth to optimise and improve the decision-making process during aircraft taxiing operations in a custom simulated airport environment. The simulation mimics realistic parameters such as taxiway configurations, collision avoidance, and runway occupancy rules which an aircraft might have to experience while taxiing.

Previous studies have explored methods to optimise aircraft taxiing operations by focusing on path planning, conflict avoidance, and decision-making. Early approaches, such as Genetic algorithms, Floyd-Warshall algorithm and Colony algorithms, focused on shortest-path planning but struggled with dynamic scenarios and delayed pushback clearances [1], [2], [3]. Mixed-integer programming and standardised taxi routes introduced separation constraints and minimised taxi times but lacked real-time adaptability [4], [5], [6]. Recent advancements, including reinforcement learning (RL) and deep learning, offer more dynamic solutions, with RL-based techniques like Markov Decision Processes improving taxi-out time predictions [7], [8]. Integrated runway-taxiway-apron allocation frameworks attempt joint optimization but face challenges in dynamic reallocation and emergency handling [9]. Multi-agent route planning systems have shown significant reductions in taxi times [10].

Section II gives a brief background on the work done in the paper and sets the context for the study, followed by Section III where the methodology of the approach is explained. Section IV then explains the implementation and Section V presents the results. Finally Section VI concludes and summarizes the study with the future scope of study.

II. Background

Ground controllers are responsible for taxiing aircrafts and do this by using a combination of radar systems, surface movement detection technology, and direct radio communication with pilots to monitor and guide aircraft along designated taxiways. Controllers provide instructions to pilots taking into account factors such as active runways, other moving aircraft, and potential hazards such as construction or adverse weather conditions.

In recent years, systems such as Airport Surface Detection Equipment (ASDE) and Advanced Surface Movement Guidance and Control Systems (A-SMGCS) have helped provide real-time data on the position and movement of aircraft and ground vehicles, reducing the likelihood of human error and thereby improving situational awareness and efficiency. In fact, [11] proposes a strategy to utilize a colored Petri net model to optimize conflict-free taxiing routes in A-SMGCS, thereby enhancing airport surface operations. As airports face increasing overcrowding and operational complexity continues to rise, the adoption of digital towers and advanced automation systems becomes more essential to ensure safety and enhance efficiency. Combined with systems such as A-SMGCS, these technologies enable a more precise and efficient coordination of ground movements.

III. Methodology

A KML file consisting of geographical data corresponding to the actual airport floor of the Kempegowda International

978-1-6654-3315-4248-1/25/$31.00 ©2025 IEEE

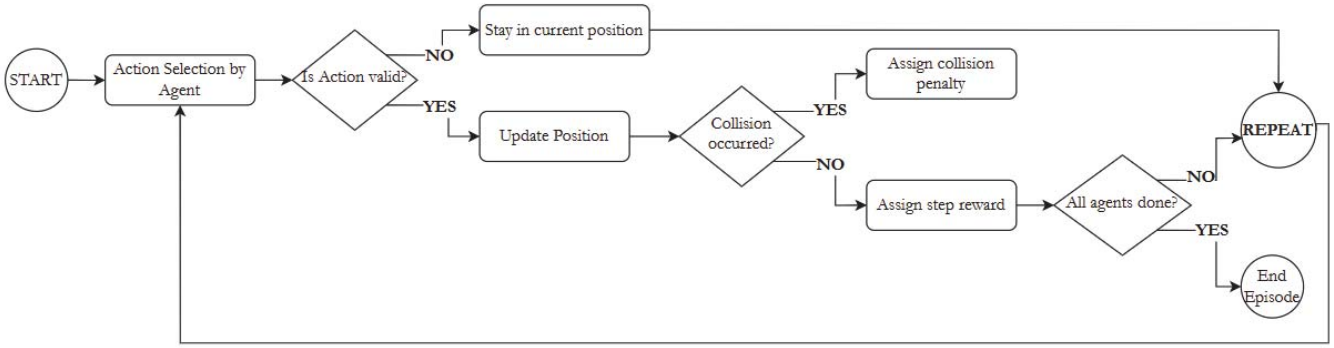


Fig. 1. Flowchart depicting the methodology of RL-based taxi operations.

Airport, Bangalore, extracted using Google Earth, is used to create the custom virtual environment. This KML file can be obtained for any airport floor or quite literally any geographical location covered under Google Earth, thereby making this implementation extremely scalable and accessible. The environment simulates aircrafts with movement across the taxiways and runways, aircrafts docked at their respective gates, and features well-defined taxi routes with appropriate refinement and fine-tuning to recognize the geography of the airport floor with great accuracy to enable smooth movement of the aircrafts across the simulated environment. This geographical data allows for extraction of coordinates as they are, in the latitude-longitude format, which then is resized appropriately to a resolution that fits the monitor. Once scaled, this geographical data is parsed into a graph whose nodes are points chosen from the coordinates in the KML file.

The reinforcement learning model trains by iterating through numerous episodes. The model gives each agent (the aircrafts), appropriate rewards for any action taken from the action space which it deems as appropriate, as discussed in later sections of the paper. Any path taken by an agent which is not optimal and leads to congestion on the taxiways, and leads to a loss of time. After iterating through multiple episodes and training extensively, the model can be expected to have a route plan which is well-tuned and has the potential to assist air traffic controllers to such an extent that their workload is significantly reduced.

A. Algorithm

Each time an episode begins, aircrafts move to a node neighboring to their current node that they occupy. In the first few episodes, one of the neighboring nodes is chosen with an almost equal probability but as training progresses to a significant number of episodes, there is a different probability distribution for every aircraft to pick a node from its neighbors. The probability distribution is indicative of the policy and this is how the policy improves over time through rewards. Ultimately, the goal is to have a probability distribution that favors the shortest path having higher probability for all nodes present in the path or in other words, the discounted value function for a path comprising of a bunch nodes must be at its largest possible value. Clipping has also been done to ensure that the policy obtained doesn't change too drastically and keeps the policy stable. Refering to Fig. 1, when an aircraft starts taxiing, it is first checked whether the action that it tries to perform is a legal action and a negative reward is granted if the action taken is illegal. Then it is checked whether the aircraft is trying to occupy a preoccupied node i.e. whether a collision has occurred. If a collision occurs, the aircraft is marked as done and a negative reward is granted. A nominal negative reward is given for every movement to encourage maximization of reward. Once an aircraft reaches it's destination it is rewarded a large positive reward and marked as 'done'.

B. Action Space and Observation Space

A simple action space has been chosen as it suitably fits the purpose. This action is to move to a neighboring node. This is advantageous as in very simple steps of guidance, a whole terrain can be fed to the model. The mapping of the floor to the graph ensures legitimate routes and operations while the model sees nothing but a graph with a simple policy to guide it. The observation space is also fairly simple with all the nodes that an aircraft can occupy being the observation space for a given aircraft. This observation space increases exponentially in size depending on the number of aircrafts actively taxiing.

C. Reward Structure

The reward structure is defined such that the agent receives a large positive reward for reaching the correct end destination. The agent also gets a big negative reward if it is involved in a collision. The agent receives a very small negative for any non-threatening action it takes. This is done in order to encourage the agent to keep looking for better routes. If an illegal action like a runway incursion, aircraft moving outside the taxiways, etc. occurs, the agent receives a negative reward. These rewards have been summarized in TABLE I

IV. Implementation

The agents in this environment use Proximal Policy Optimization (PPO) to learn. As agents navigate the environment, they collect experiences comprising of states, actions, rewards, and next states.

Action/ State	Reward
Reaching destination	100
Collision	-50
Normal Movement	-0.01
Illegal Actions	-1

TABLE I
REWARD STRUCTURE FOR THE MODEL

Hyperparameter Name	Hyperparameter Value
Learning Rate	1e-4
Discount Factor (γ)	0.99
Initial Epsilon ($\epsilon_{initial}$)	0.1
Final Epsilon (ϵ_{final})	0.05
Epsilon Timesteps ($\epsilon_{timesteps}$)	20000
Batch Size	8000

TABLE II
LIST OF HYPERPARAMETERS

A. Tools and Interfaces

OpenAI Gym has been used for creating the environment for reinforcement learning beacuse it offers a robust foundation for reinforcement learning environments, ensuring compatibility with state-of-the-art reinforcement learning algorithms, such as those offered by RLlib. By leveraging OpenAI Gym, the simulation environment benefits from a highly modular design. The environment is driven by KML files that represent the airport layout as described under Section III. OpenAI Gym facilitates converting these data points into observations and actions suitable for multi-agent reinforcement learning, which is critical when modeling complex systems such as airport taxiways.

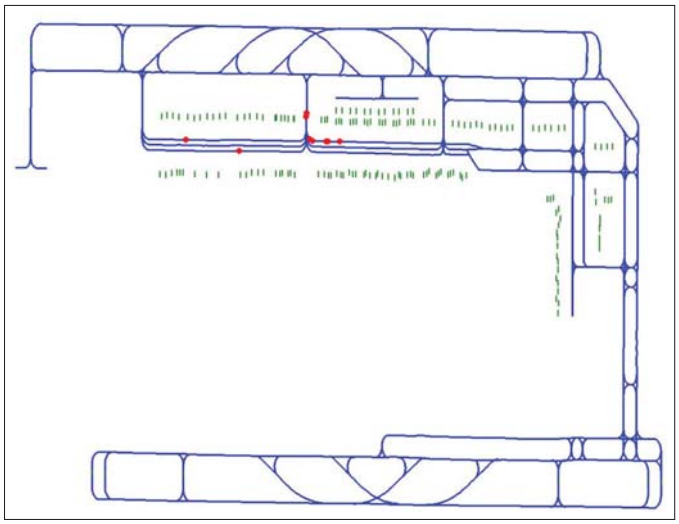


Fig. 2. Graphical User Interface depicting the airport environment

As explained earlier, the KML file obtained from Google Earth becomes the source of all the accurate graphics displayed on screen using Pygame. The entire airport floor is much more precise when done this way. Fig. 2 shows the precise airport floor where, the blue lines represent the taxiways and runways, the green lines represent the parking gates and bays and the red dots show randomly initialized aircrafts moving on the taxiways. An important observation worth mentioning here is that these taxiways consist of several nodes along its length. The number of nodes is much more at the turns which allows for smoother turning of aircrafts in the simulation.

B. Hyperparameters

Ray Tune is used to configure the hyperparameters for training the reinforcement learning model, with the settings as shown in TABLE II to run training with an optimal split between exploration and exploitation. These hyperparameters ensure that the model continues to look for better policies rather than settling too quickly on a sub-optimal policy. **Learning Rate** specifies how many fold the model's weights will be updated for each learning action that has been performed. A very small learning rate used here indicates that the model would be slow in learning but cautious in terms of not concluding policies too quickly.
The model uses an Epsilon Greedy strategy, in this case, the value of ϵ slowly decreases from a high value of ($\epsilon_{initial}$) equal to 0.1 to a low value of (ϵ_{final}) equal to 0.05 over 20000 timesteps. This transition allows the agent to discover and learn about the environment's dynamics before focusing on optimizing performance based on accumulated knowledge. **Batch size** of 8000 ensures that training will be more stable and generalize better due to reduced gradient noise, but updates will be less frequent. A **discount factor** (γ) of 0.99 means that the agent prioritizes long-term rewards slightly less than immediate rewards, fostering long-term planning while still valuing near-term gains.

V. RESULTS AND ANALYSIS

A. Entropy

In the context of this implementation using Proximal Policy Optimization (PPO), entropy plays a crucial role in ensuring that agents explore various actions rather than getting stuck in a local optima. The code includes an entropy bonus in the loss function to maximize entropy, thereby promoting exploration. This bonus helps the agents try different routes and strategies to navigate the taxiways, leading to a more robust learning process. By incorporating entropy, the agents can discover effective policies that might not be immediately apparent through exploitation alone. As seen in Fig. 3, the entropy graph shows a sharp initial decline which indicates that the model starts with high exploration but quickly learns a more structured policy. Over time, entropy stabilizes to a lower value which suggests that the agent has converged to a more deterministic strategy while still maintaining some level of exploration.

B. Total Loss

Minimizing the total loss optimizes the policy and value networks simultaneously, leading to better decision-making capabilities and enhanced agent performance. As seen in

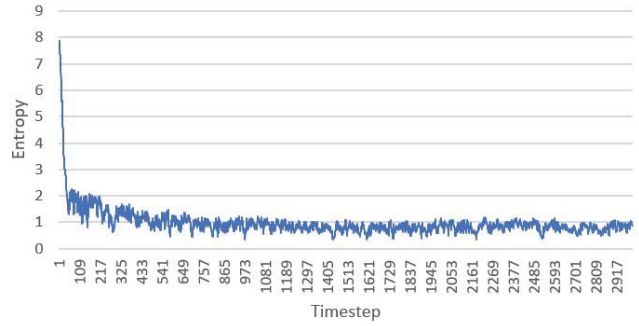


Fig. 3. The plot of model entropy v/s timestep

Fig. 4, an initial spike is seen in the total loss graph, followed by a sharp decline, and stabilization around zero with bounded fluctuations. This indicates that the PPO algorithm has effectively optimized both the policy and value networks, reaching a steady-state equilibrium where policy updates result in minimal deviation in the loss function. The bounded oscillations suggest continuous minor policy refinements due to exploration-exploitation trade-offs, but the absence of large spikes implies that the agent has converged to a near-optimal policy with stable gradient updates.

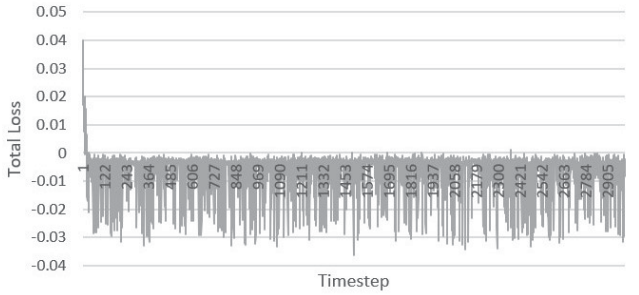


Fig. 4. The plot of model total loss v/s timestep

VI. Conclusion

The aviation industry continues to face significant challenges with ground traffic management, including congestion, delays, and the growing complexity of operations at busy airports. With air passenger traffic on the rise, both in the domestic and international space, airlines and airports both are trying to optimize and improve efficiency in operations. This might be through ensuring quicker turn-arounds for domestic flights and keeping taxi times short. Inefficient taxiing of aircrafts can lead to increased fuel consumption, higher operational costs, and elevated emissions.

This paper provides an innovative solution by developing a reinforcement learning (RL) based framework to optimize taxi routes dynamically. Unlike traditional methods that rely on predefined Standardized Taxi Routes (STRs), this reinforcement learning model adapts to real-time airport ground conditions. Using algorithms such as Proximal Policy Optimization (PPO), the reinforcement learning model effectively learns to balance collision avoidance, minimized taxi time, and dynamic adaptability to real-world complexities. The aim was to instead create a tool which would assist the ATCOs make better decisions especially in times of high workloads. The inclusion of a visualized environment bridges the gap between human operators and automated systems, providing transparency and ease of use.

Further work in this field will include integration with upcoming digital towers, model optimization to further reduce the carbon footprint of aviation and advanced automation in case of emergencies.

Acknowledgment

The team would like to express their sincere appreciation to the Air Traffic Control (ATC) division, Airports Authority of India at Kempegowda International Airport, Bengaluru for their invaluable assistance and guidance.

References

1 Li, Z., Zhang, J., and Zhang, X., "A dynamic model for aircraft route optimizing in airport surface management," in *Proc. 9th Int. Conf. Electron. Meas. Instrum.*

2 Tjahjono, T., Husaeny, N. *et al.*, "Optimization of movement of the aircraft on taxiway area," in *Proc. 2014 Int. Conf. Advanced Logistics and Transport (ICALT)*, pp. 324–329.

3 Liu, C. and Wang, Y., "Aircraft taxi path optimization based on ant colony algorithm," in *Proc. 2011 Fourth Int. Symp. Comput. Intell. Design*, vol. 2, pp. 226–229.

4 Clare, G. and Richards, A. G., "Optimization of taxiway routing and runway scheduling," *IEEE Trans. Intell. Transp. Syst.*, vol. 12, no. 4, pp. 1000–1013, 2011.

5 Liang, F., Hu, M., Yang, L., and Zhao, Z., "An aggregate dynamic traffic assignment model for generating multi-path standardized taxi routes at airport," in *Proc. 2021 IEEE/AIAA 40th Digit. Avion. Syst. Conf. (DASC)*, pp. 1–7.

6 Idrissi, O., Bikir, A., Mansouri, K., and Youssfi, M., "Enhancing the management of aircraft taxiing phase by allocating efficient and conflict-free routes," in *Proc. 2020 IEEE 2nd Int. Conf. Electron., Control, Optim. Comput. Sci. (ICECOCS)*, pp. 1–4.

7 Balakrishna, P., Ganesan, R., and Sherry, L., "Accuracy of reinforcement learning algorithms for predicting aircraft taxi-out times: A case-study of tampa bay departures," *Transp. Res. C: Emerg. Technol.*, vol. 18, no. 6, pp. 950–962, 2010.

8 Ito, M. and Mikoshi, T., "Path planning method using deep learning model for traffic engineering in small networks," in *Proc. 2021 31st Int. Telecommun. Netw. Appl. Conf. (ITNAC)*, pp. 65–70.

9 Feng, S.-X., Liu, J.-X., and Zeng, X.-Y., "Integrated runway-taxiway-apron allocation for aircraft movement based on traffic characteristics," in *Proc. 2019 Int. Conf. Quality, Reliability, Risk, Maintenance, and Safety Eng. (QR2MSE)*, pp. 1025–1032.

10 Chen, F., "Aircraft taxiing route planning based on multi-agent system," in *Proc. 2016 IEEE Adv. Inf. Manag., Commun., Electron. Autom. Control Conf. (IMCEC)*, pp. 1421–1425.

11 Luo, X., Tang, Y., Wu, H., and He, D., "Real-time adjustment strategy for conflict-free taxiing route of a-smgcs aircraft on airport surface," in *Proc. 2015 IEEE Int. Conf. Mechatronics Autom. (ICMA)*, pp. 929–934.

Energy-Efficient Motion Planning for Dual-Arm Collaborative Robots Using a Digital Twin

1st Ruj Kantabussabong
The Sirindhorn International Thai-German Graduate School of Engineering, King Mongkut's University of North Bangkok,
Bangkok, Thailand
s6609092861018@email.kmutnb.ac.th

2nd Chinnawut Nantabut
The Sirindhorn International Thai-German Graduate School of Engineering, King Mongkut's University of North Bangkok,
Bangkok, Thailand
chinnawut.n@tggs.kmutnb.ac.th

3rd Watcharin Pongaen
Dept. of Teacher Training in Mechanical Engineering, Faculty of Technical Education, King Mongkut's University of North Bangkok,
Bangkok, Thailand
watcharin.p@fte.kmutnb.ac.th

4th Nuttapon Rothong
College of Industrial Technology, King Mongkut's University of North Bangkok,
Bangkok, Thailand
nuttapon.r@cit.kmutnb.ac.th

5th Borihan Butsanlee
Dept. of Teacher Training in Mechanical Engineering, Faculty of Technical Education, King Mongkut's University of North Bangkok,
Bangkok, Thailand
s6102017910013@kmutnb.ac.th

***Abstract*— The growing adoption of collaborative robots (cobots) in industrial applications has intensified the focus on optimizing energy efficiency. This study develops a digital twin for dual-arm ABB GoFa5 robots to estimate power consumption by integrating real-world sensor data for real-time monitoring and analysis. To understand how motion planning impacts energy usage, different algorithms, including CHOMP, RRT, and RRT*, were evaluated under no-load and loaded (2.5 kg) conditions. CHOMP demonstrated the highest energy efficiency, consuming up to 28% less power than RRT and 14% less than RRT* under no-load conditions, and up to 19% and 13% less, respectively, with a payload, confirming its effectiveness in optimizing cobot performance.**

Keywords*— *Collaborative robots, digital twin, motion planning, energy efficiency.

I. INTRODUCTION

Collaborative robots (cobots) are transforming manufacturing, yet energy optimization remains crucial, especially for continuous operation in complex environments. Motion planning significantly impacts energy consumption [1]. Recent studies emphasize efficient motion planning for energy reduction. Nonoyama et al. utilized Genetic Algorithms and Particle Swarm Optimization for energy-efficient dual-arm robot motion [2]. Alam et al. reduced power consumption in pick-and-place tasks using an RRT*-based approach [3]. These studies highlight torque optimization in motion planning for energy efficiency [4]. This study evaluates Covariant Hamiltonian Optimization (CHOMP) [5], Rapidly-exploring Random Tree (RRT) [6], and RRT* algorithms [7]. CHOMP optimizes smooth, energy-efficient trajectories using cost functions. RRT and RRT* enable fast trajectory generation in complex environments through probabilistic completeness. These algorithms represent diverse optimization strategies – cost function-based (CHOMP) and sampling-based (RRT, RRT*) – offering a comprehensive comparison for energy efficiency.

Despite research on energy-efficient motion planning [2, 3, 4] and force control [9], combined effects under dynamic loads are underexplored. This work addresses this gap by analyzing power consumption in a dual-arm cobot performing predefined tasks under no-load and loaded conditions. The findings contribute to optimizing energy-aware motion planning and improving cobot performance in industrial applications. To achieve this, we implemented a digital twin system that integrates real-world sensor data for accurate energy estimation and performance evaluation, as detailed in the following section**.**

II. METHODOLOGY

The system utilizes dual ABB GoFa5 robots, each equipped with integrated six-axis force-torque sensors. These robots were chosen for their 6-DoF capability, flexibility, and lightweight design, making them suitable for collaborative tasks. The experiments involved creating a high-fidelity digital twin in simulation and performing comparative analyses with the physical robots under various load conditions and trajectory plans, as shown in Fig. 1.

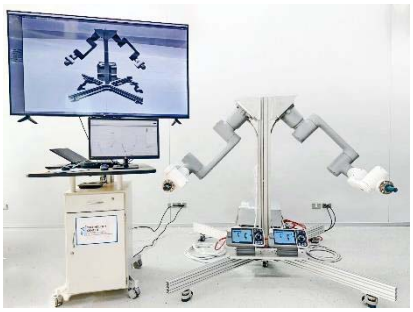


Fig. 1. Digital twin system of the dual-arm ABB GoFa5 robots.

A. Dual Robot Digital Twin System

This project developed a dual-arm robot digital twin system for simulating real-world operations, including human-robot interaction, as shown in Fig. 2. The system comprises physical and digital layers. The physical layer is a real ABB GoFa5 dual-arm robot performing tasks and providing real-time sensor data. The digital layer is a virtual robot model mirroring the physical system, enabling power consumption estimation and motion optimization. In the digital layer, the dual-arm robot model was integrated into Robot Operating System 2 (ROS 2) and controlled by MoveIt2 for generating smooth, optimized trajectories using various motion planning algorithms. Gazebo provided a physics-based simulation accurately reflecting real-world constraints. ROS 2 facilitated component

communication via a Topic-Node structure for efficient data exchange. The system synchronizes physical and digital layers in real-time using sensor data like motor torque, ensuring virtual model accuracy.

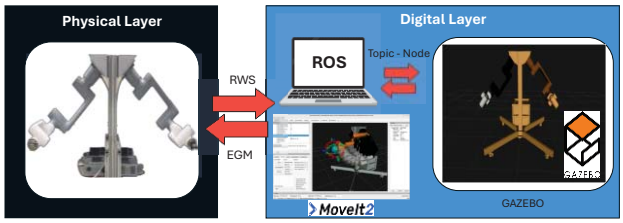


Fig. 2. Concept of estimating power consumption in a digital twin.

For seamless interaction and precise control, ROS 2 and the ABB robot communicated using Externally Guided Motion (EGM). EGM was selected over Robot Web Service (RWS) and OPC UA for efficient real-time motion updates. This ensured precise trajectory execution and synchronization. The digital twin system exhibited high accuracy, adaptability, and real-time responsiveness. It provided a reliable platform for retrieving robot motion parameters, optimizing energy efficiency, and enhancing robotic system performance.

B. Robot Static Model

The static model of the ABB GoFa5 robots was developed using forward and inverse kinematics to determine the spatial configuration of the robot's end-effectors based on joint angles. The Denavit-Hartenberg (DH) parameters define the geometric relationships between the robot's joints using four key values: link length (a_i), link twist (α_i), link offset (d_i), and joint angle (θ_i). These parameters are crucial for computing the forward and inverse kinematics of the ABB GoFa5 robot. As shown in Fig. 3, the joint coordinate system of the dual arm ABB GoFa5 robot is established.

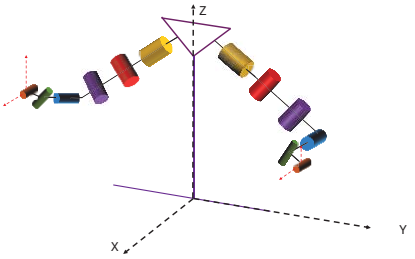


Fig. 3. The kinematic model of the dual arm ABB GoFa5 robot.

To facilitate the motion planning of dual arm robot, the coordinates of the left and right arms of the robot are moved to the base coordinate system. The GoFa5 manipulator used in this paper is shown in Fig. 4 and DH parameters are shown in Table I. By substituting the DH parameters into the equation

$$ {}^{0}_{6}T(\theta) = {}^{0}_{1}T(\theta_1){}^{1}_{2}T(\theta_2){}^{2}_{3}T(\theta_3){}^{3}_{4}T(\theta_4){}^{4}_{5}T(\theta_5){}^{5}_{6}T(\theta_6), \quad (1) $$

where ${}^{i-1}_{i}T =$

$$ \begin{bmatrix} \cos\theta_i & -\sin\theta_i\cos\alpha_i & \sin\theta_i\sin\alpha_i & a_i(\cos\theta_i) \\ \sin\theta_i & \cos\theta_i\cos\alpha_i & -\cos\theta_i\sin\alpha_i & a_i(\sin\alpha_i) \\ 0 & \sin\alpha_i & \cos\alpha_i & d_i \\ 0 & 0 & 0 & 1 \end{bmatrix}, $$

the specific transformation matrices for each joint were derived, enabling precise mapping of the robot's geometry. These transformation matrices are the foundation for calculating forward and inverse kinematics and are integral to ensuring accurate trajectory planning.

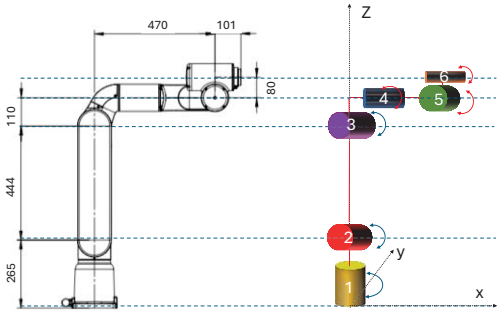


Fig. 4. Coordinate system of GoFa5 robot (Number 'i' denotes joint i).

TABLE I. The DH parameters of joint i.

i	θ_i (°)	d_i (mm)	α_i (°)	a_i (mm)	range$_i$ (°)
1	θ_1	265	-90	0	±180
2	$\theta_2 - 90^{\circ}$	0	0	444	±180
3	θ_3	0	-90	110	-225...+85
4	θ_4	470	90	0	±180
5	θ_5	0	-90	80	±180
6	θ_6	101	0	0	±270

C. Robot Dynamics Model

With the static model providing insights into the robot's geometric configuration, it is essential to extend this understanding to the dynamic forces acting on the system. The dynamic model includes the physical properties of the ABB GoFa5 robots, such as link masses, inertia tensors, and joint damping. These properties are essential for understanding the forces and torques during motion [10]. The Newton-Euler formulation describes the relationship between these factors as shown in Eq. (2):

$$ \tau = M(q)\ddot{q} + C(q,\dot{q})\dot{q} + G(q), \quad (2) $$

where $M(q)$ is the mass matrix describing inertial properties, $q, \dot{q}$ and $\ddot{q}$ are vectors representing joint positions, velocities, and accelerations, $C(q,\dot{q})$ represents the Coriolis and centrifugal forces, $G(q)$ denotes the gravitational forces and τ corresponds to the control torques. These equation governs the robot's trajectory execution, enabling accurate modeling of joint dynamics under varying loads. Incorporating these physical characteristics is crucial for understanding robot performance during motion planning. The trajectory plans are generated using advanced motion planning algorithms, including CHOMP, RRT, and RRT*. These algorithms are key to ensuring collision-free, efficient, and energy-conscious robot movements. The next section will explore these motion planning strategies in detail.

D. Motion Planning

Motion planning determines a robot's trajectory while optimizing efficiency and obstacle avoidance. In this study, CHOMP, RRT, and RRT* were evaluated for their impact on energy consumption. CHOMP refines trajectories using gradient-based optimization for smooth and efficient motion. RRT rapidly explores high-dimensional spaces but often generates unsmooth paths, increasing energy

consumption. RRT* improves RRT by incorporating cost minimization, leading to more efficient trajectories.

Choosing the right algorithm is crucial for balancing computational efficiency and energy optimization. The next section explores power estimation techniques for improving robotic energy efficiency.

E. Power Estimation Methods

This section details the methodology for quantifying the robot's electric power consumption during motion [8]. Energy consumption at each motor joint i is derived from the generated torque $\tau_i(t)$. Motor current $I_i(t)$ is calculated from torque:

$$I_i(t) = \frac{\tau_i(t)}{K_t}, \quad (3)$$

where K_t is the diagonal matrix of motor torque constants. Torque values are acquired using TuneMaster software, which receives real-time data from the robot controller via TCP/IP. The electric power consumption of joint i is then determined based on the voltage(V)-current(I) relationship:

$$W_{m,i}(t) = V_i(t)I_i(t), \quad (4)$$

where $W_{m,i}(t)$ represents the electric power consumed by an individual motor. The robot's total power consumption is the summation of each actuator's power:

$$W(t) = \sum_{i=1}^{6} W_{m,i}(t). \quad (5)$$

This method provides a framework for assessing the robot's energy consumption across tasks, enabling comparison of motion planning strategies. With these calculations established, the study proceeds to describe the experimental setup used for validation.

III. Experimental Setup

The experimental setup was designed to allow direct comparison between the power consumption of a dual robot in each trajectory plan and is described as follows:

A. Experimental Scenarios

Each planner, CHOMP, RRT, and RRT*, was evaluated under two main experimental scenarios:

- **No-load condition:** The robots executed motion tasks without a payload.
- **Loaded condition:** The same motion tasks were performed with a 2.5 kg payload at each robot's end-effector. This payload was chosen to ensure safety and avoid instability or excessive stress, given the robot's mounting configuration.

B. Initial and Final Poses of Both Arms

In this study, initial and target poses were defined for the dual GoFa5 robotic arms. The initial pose represents the robot's default joint configuration. Conversely, the target pose, detailed in Table II, is achieved when the robotic arm is parallel to the ground, thus maximizing the moment generated by the end-effector's effect on the joints.

TABLE II. Dual arm GoFa5 robot initial and target pose.

		θ_1	θ_2	θ_3	θ_4	θ_5	θ_6
Left and right arm	Initial pose (°)	0	0	0	0	0	0
	Final pose (°)	0	90	-90	0	0	0

Establishing these poses ensures consistency across experiments, providing a reliable framework for evaluating robot trajectories. These defined poses form the basis for implementing motion planning algorithms, which will be discussed in the next section.

C. Motion Planning and Trajectories

The process of determining the robot's electric energy usage begins with developing a dynamic model to analyze the robot's movement behavior. Motion trajectories were generated for predefined tasks using the MoveIt2 framework. The algorithms were utilized to create diverse trajectories along the same pathway. As demonstrated in Fig. 5, the movement generated by the CHOMP algorithm, depicted by the white arrow, enables the robot to precisely reach the final pose.

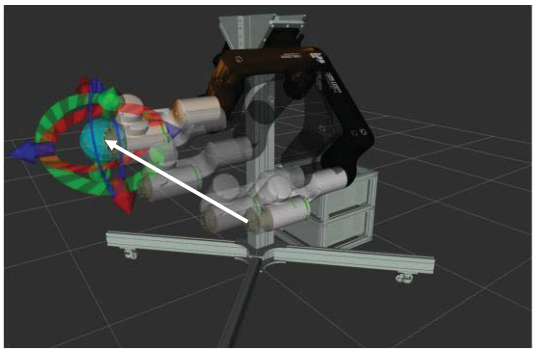


Fig. 5. The robot movement behavior using CHOMP algorithm (end-effector frame shown by RGB axes).

IV. Results and Discussion

Motor torques per joint during robot motion using CHOMP are shown in Fig. 6 (no-load) and Fig. 7 (loaded). 'ROB_1/i' denotes joint i, with data representing torque values from TuneMaster test signal 2000.

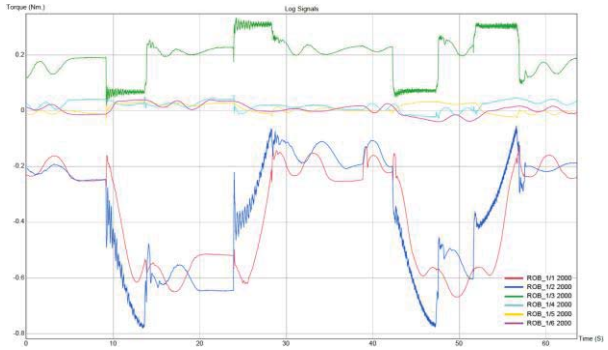


Fig. 6. GoFa5 robot motor torque in 6 joints under no-load condition.

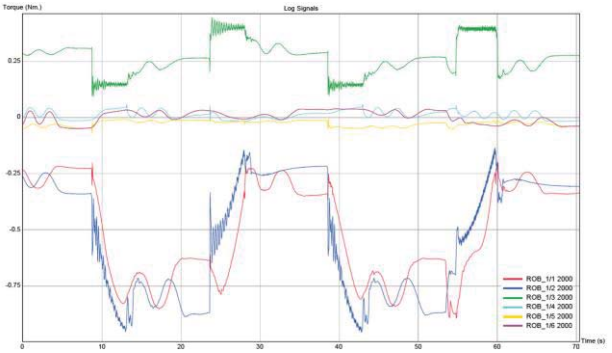


Fig. 7. GoFa5 robot motor torque in 6 joints under 2.5 kg loaded condition.

Motion planning starts at t = 0 s from the initial pose and achieves the final pose by t = 10 s. A 10-second hold at the final pose is followed by a return to the initial pose, with a subsequent 10-second hold. The motion planning sequence is repeated as described previously. Data from planning algorithms were utilized to calculate the electric current applied to each of the six joints using Eq. (3). Subsequently, the electric power was determined using Eq. (4), where $V_i(t)$ equals 220 VAC, as specified in the Omni controller manual.

Referring to Fig. 6, joints 1 and 2 exhibit sustained torques of approximately 0.2 Nm initially, reaching a final value of -0.65 Nm upon attaining the final pose. The underdamped behavior evident in these joints is attributed to the motor control strategy employed to achieve the target pose. Compared to other joints, joints 1 and 2 experience the greatest load, supporting the robot's structure. Joint 3 experiences a lesser load, approximately 0.05 Nm, compared to joints 1 and 2 after reaching the final pose, albeit with an opposite sign due to its reversed rotation direction. Joints 4, 5, and 6 experience insignificant loads as they do not support substantial weight. Both loaded and no-load conditions exhibit similar torque profiles, however, the loaded condition demonstrates higher values due to the additional mass at the end-effector.

TABLE III. Electric power analysis.

Joint i	Torque (Nm)		Current (A)		Power (W)	
	No-Load	Loaded	No-Load	Loaded	No-Load	Loaded
1	-0.65	-0.80	0.026	0.032	5.72	7.04
2	-0.78	-0.90	0.035	0.036	7.7	7.92
3	0.24	0.28	0.010	0.0112	2.2	2.46
4	0.05	0.12	0.002	0.005	0.44	1.10
5	0.05	-0.1	0.002	0.004	0.44	0.88
6	0.07	0.1	0.003	0.004	0.61	0.88
Total	1.84	2.3	0.078	0.092	17.16	20.28

The total electric power consumption per step, calculated using Eq. (5), was analyzed. Table III indicates that for the robot's left arm, CHOMP-based trajectory planning resulted in a total power consumption of 20.28 W. The results for all motion planners in Table IV show that CHOMP consistently exhibited the lowest torque and power consumption, making it the most energy-efficient motion planning algorithm in both no-load and loaded conditions. Under no-load conditions, CHOMP reduced power consumption by 28% compared to RRT and 14% compared to RRT*. When carrying a 2.5 kg payload, CHOMP remained the most efficient, consuming 19% less than RRT and 13% less than RRT*, demonstrating its superior energy performance.

TABLE IV. Power consumption for each motion planning algorithm.

Algorithm	Power (W)	
	No-Load	Loaded
CHOMP	17.16	20.28
RRT	23.83	25.03
RRT*	19.95	23.31

The addition of a payload significantly increased torque, electric current, and power consumption across all algorithms, emphasizing the substantial impact of load on energy demands. However, CHOMP consistently remained the most energy-efficient algorithm even under load, positioning it as a strong candidate for applications prioritizing optimal power usage.

V. Conclusion

This study demonstrates the critical impact of motion planning algorithms on the energy efficiency of robotic systems. Among the tested algorithms, CHOMP consistently exhibited the lowest torque and power consumption, making it the most energy-efficient choice under both no-load and loaded conditions. In contrast, RRT and RRT* consumed more power, with RRT being the least efficient, particularly when operating under load. The addition of a 2.5 kg payload significantly increased torque, electric current, and overall energy consumption across all algorithms, highlighting the need for efficient motion planning in dynamic environments. Future research could build upon this study by incorporating joint-specific friction estimation to enhance the accuracy of energy consumption predictions and motion planning. The integration of deep learning techniques could enhance friction modeling, making the digital twin more realistic and adaptable to real-world conditions. These advancements would optimize trajectory planning and improve the overall energy efficiency of robotic systems.

Acknowledgment

The authors gratefully acknowledge the support from the Technology Center for Smart Electronic and Digital Innovation, KMUTNB Techno Park.

VI. References

[1] S. Pellegrinelli, S. Borgia, N. Pedrocchi, E. Villagrossi, G. Bianchi, and L. Molinari Tosatti, “Minimization of the energy consumption in motion planning for single-robot tasks,” *Procedia CIRP*, vol. 29, pp. 354–359, 2015.

[2] K. Nonoyama, Z. Liu, T. Fujiwara, M. M. Alam, and T. Nishi, “Energy-efficient robot configuration and motion planning using genetic algorithm and particle swarm optimization,” *Energies*, vol. 15, no. 6, p. 2074, Mar. 2022.

[3] M. M. Alam, T. Nishi, Z. Liu, and T. Fujiwara, “A Novel Sampling-Based Optimal Motion Planning Algorithm for Energy-Efficient Robotic Pick and Place,” *Energies*, vol. 16, no. 19, p. 6910, 2023.

[4] M. Soori, B. Arezoo, and R. Dastres, "Optimization of energy consumption in industrial robots, a review," *Cognitive Robotics*, vol. 3, pp. 142–157, 2023.

[5] S. Zucker, J. Ratliff, M. D. Toussaint, and J. A. Bagnell, “CHOMP: Gradient optimization techniques for efficient motion planning,” in *Proc. Robot. Sci. Syst. (RSS)*, 2009.

[6] S. M. LaValle, “Rapidly-exploring random trees: A new tool for path planning,” Iowa State Univ., 1998.

[7] S. Karaman and E. Frazzoli, “Sampling-based algorithms for optimal motion planning,” *Int. J. Robot. Res.*, vol. 30, no. 7, pp. 846–894, 2011.

[8] B. Butsanlee, W. Pongaen, N. Rothong, S. Ponpitakchai, and S. U-Thathong, “Development of deep learning for power energy optimization in the industrial robot system,” *Int. J. Mech. Eng. Robot. Res.*, vol. 13, no. 2, pp. 254–265, 2024.

[9] R. Pérez-Ubeda, R. Zotovic-Stanisic, and S. C. Gutiérrez, “Force control improvement in collaborative robots through theory analysis and experimental endorsement,” *Appl. Sci.*, vol. 10, no. 12, p. 4329, 2020.

[10] J. Wu, J. Wang, and Z. You, “An overview of dynamic parameter identification of robots,” Robotics and Computer-Integrated Manufacturing,” vol. 26, no. 5, pp. 414–419, Oct. 2010.

Effective Bowel Sound Source Localization Based on Sensor Configuration: A Preliminary Index Approach

Kenji Takawaki
Division of Science and Technology, Graduate School of Science and Technology for Innovation, Tokushima University,
Tokushima 770-8506, Japan
c612434008@tokushima-u.ac.jp

Takeyuki Haraguchi
Division of Science and Technology for Innovatioin, Graduate School of Sciences and Technology for Innovation, Tokushima University, Tokushima 770-8506, Japan
c612244001@tokushima-u.ac.jp

Takahiro Emoto
Division of Science and Technology, Graduate School of Technology, Industrial and Social Sciences, Tokushima University,
Tokushima 770-8506, Japan
emoto@tokushima-u.ac.jp

***Abstract*—Functional gastrointestinal disorders (FGIDs), including irritable bowel syndrome (IBS), characterized by chronic abdominal symptoms that markedly diminish quality of life, necessitate the development of non-invasive and objective diagnostic methods. Previous research shows that bowel sound (BS) source localization aids in IBS screening. Thus, higher-precision localization is needed for detailed intestinal motility assessment, although its performance is affected by ambient noise, sensor count, and configuration. In this study, we evaluated asymmetrical versus traditional symmetrical electronic stethoscope (ES) arrangements for BS measurement and proposed a new index, the Preliminary Asymmetry Degree (*PAD*), to assess ES configuration asymmetry. By conducting source localization simulations using a simplified rectangular model of the abdomen, we found that configurations with higher *PAD* values exhibited improved source localization accuracy. We also confirmed that sensor configurations based on *PAD* function effectively even in high-noise environments. These findings show promise as a technological foundation for non-invasive and objective measurement and analysis of internal abdominal sound sources. In the future, by applying this approach to more advanced models that mimic biological structures, it may be possible to conduct more detailed analyses of gastrointestinal function, including the objective evaluation of FGIDs.**

Keywords—Preliminary asymmetry degree, bowel sound, energy-based source localization

I. Introduction

In recent years, the number of people suffering from functional gastrointestinal disorders (FGIDs), including irritable bowel syndrome (IBS), has been on the rise, with reports indicating that approximately 10% of the global population is affected [1]; these disorders significantly lower quality of life due to chronic abdominal pain and discomfort. On the other hand, according to the ROME IV diagnostic criteria, the prevalence of IBS is about 3.8% [2]. This discrepancy in prevalence rates is thought to stem from the fact that IBS diagnoses are typically based on patient-reported questionnaires. The ROME IV diagnostic criteria, which are widely used to diagnose FGIDs (including IBS), rely on self-reported information from patients. Therefore, there is a growing need to develop techniques that can objectively evaluate intestinal motility.

Common methods for objectively assessing intestinal motility include endoscopy [3], CT [4], and MRI [5–8]. However, these methods require expensive equipment and are invasive. As a result, research has focused on using bowel sounds (BS) recorded by electronic stethoscopes (ES) as a non-invasive, objective approach to evaluate intestinal motility. Examples of such research include a study investigating the effects of beverage ingestion on intestinal motility [9] and a study assessing the recovery of intestinal motility and secretory function through gum chewing after surgery, evaluated using BS [10].

These studies evaluate the motility of the entire abdomen based on the acoustic characteristics of BS. On the other hand, there is a study [11] suggesting that BS source localization could contribute to the screening of IBS, thereby indicating the effectiveness of evaluating local intestinal motility using BS.

In order to evaluate intestinal motility locally, highly accurate source localization of BS is necessary. Factors such as sensor placement, noise environment, and the number of sensors affect the accuracy of source localization. Generally, increasing the number of sensors improves localization accuracy, but since the ES used for BS measurement must be attached to the abdomen, increasing the number of ES could potentially increase patient discomfort. Therefore, it is crucial to conduct investigations with as few sensors as possible. Against this backdrop, the present study aims to improve BS source localization accuracy by using only four sensors while considering noise environment and devising an optimal sensor arrangement.

Previous studies on BS source localization have employed symmetrical sensor arrangements [11–14]. However, there has been no detailed investigation into the relationship between ES placement and source localization accuracy, and it remains unclear which placement positions would yield higher source localization accuracy when limited to four sensors. Therefore, in this study, we investigate the relationship between arrangement geometry and localization accuracy when symmetrical ES placement is intentionally made asymmetrical.

II. Method

A. Simplified rectangular model

In this study, we prepared a simplified rectangular model of the abdomen (20 cm × 10 cm × 10 cm), as shown in Figure 1, to

This work was supported by a specific grant from JSPS Grant-in-Aid for Scientific Research: Scientific Research (C): KAKEN 23K11947.

979-8-3315-4248-1/25/$31.00 ©20XX IEEE

perform source localization mimicking the abdominal region. In this case, a single sound source localization is assumed. Considering the computational costs, we prepared 16359 sampling points (SP) and 330 Sound sources (SS) in the localization space. Further, we used a 20 cm × 10 cm plane, i.e., a sensor field, above the localization area. This sensor field was divided into four equal quadrants, and one ES was placed in each quadrant. The ESs were placed at least 1 cm apart from the axis by dividing each quadrant to avoid mutual interference between ESs. In addition, the average thickness of subcutaneous fat is ~1 cm [15], and therefore, the SPs and SSs were placed 1 cm away from the sensor field.

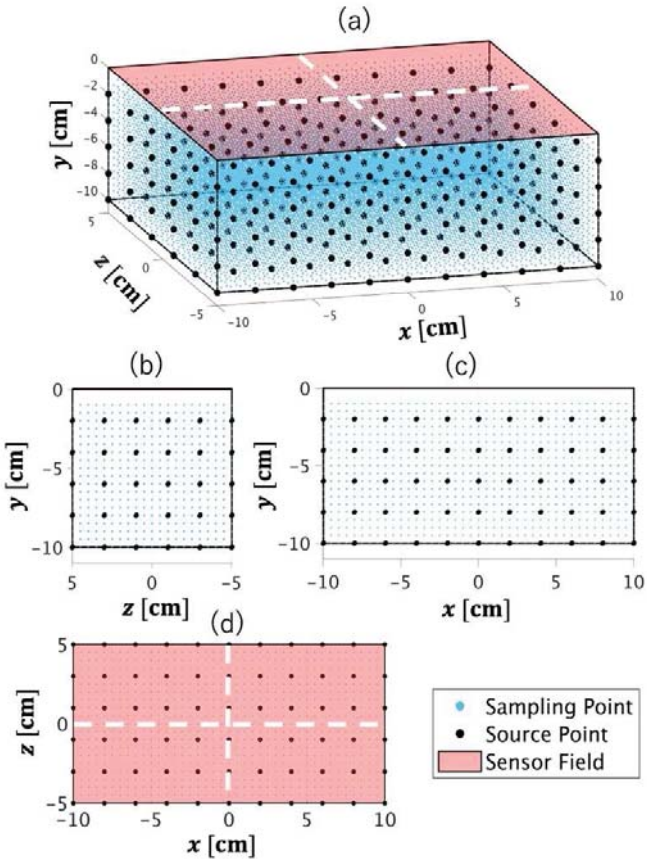


Fig. 1. Localization area in the simplified rectangular model of the abdomen. The red surface represents the model surface where the ES are positioned, and the light blue dots indicate the localization region. (a) Overall Image, (b) sagittal plane, (c) axial plane, and (d) coronal plane.

B. *Energy-based source localization in a simplified rectangular model*

In this study, we employ an energy-based source localization method that has been used in previous research. This method utilizes the characteristic that sound power attenuates inversely with the square of the distance. Equation (1) shows the sound attenuation model [14] that takes into account the abdominal environment:

$$I_{i,m} = P_m \frac{1}{4\pi d_{i,m}^2} \tag{1}$$

where P_m is the BS power of the m-th sound source, and $I_{i,m}$ is the intensity of BS m at the i-th ES location. This demonstrates that BS attenuates as a function of the SS-ES distance $d_{i,m}$.

By rearranging Equation (1), we obtain Equation (2):

$$P_m = I_{i,m} \cdot 4\pi d_{i,m}^2 \tag{2}$$

Since P_m is common to all ES, the equality given by Equation (3) holds for ES i and ES j:

$$I_{i,m} \cdot d_{i,m}^2 - I_{j,m} \cdot d_{j,m}^2 = 0 \tag{3}$$

In a noise-free environment, solving the simultaneous equations derived from Equation (3) for the four sensors yields a unique determination of the sound source. However, in actual BS measurement environments, noise is present, and a solution to the equations cannot be obtained. Therefore, in this study, we denote the noise acquired by the i-th ES as $I_{Ni}$and that by the j-th ES as I_{Nj}, and define Equation (4). White noise was used as the noise source.

$$E_{i,j,m} = \left(\left(I_{i,m} + I_{Ni} \right) \cdot d_{i,m}^2 - \left(I_{j,m} + I_{Nj} \right) \cdot d_{j,m}^2 \right)^2 \tag{4}$$

Equation (5) is a transformation of Equation (4). S is the number of ES, in this case 4. In this study, the SPs that minimizes $E_{\mathrm{all},m}$ in Equation (5) is considered as the sound source.

$$E_{\mathrm{all},m} = \sum_{i=1}^{\mathrm{S}} \sum_{j=i+1}^{\mathrm{S}} E_{i,j,m} \tag{5}$$

C. *Signal-to-Noise-Ratio*

In this study, the signal-to-noise ratio (SNR) is defined as shown in Equation (6). Here, $I_{i,m}$ denotes the BS intensity acquired by ES i at SS m, and I_{Ni} represents the noise intensity at that time. In the simulation, k was adjusted to obtain an arbitrary SNR level.

$$SNR = 10\log_{10} \frac{\sum_{i=1}^{4} I_{i,m} + I_{Ni}}{k \cdot \sum_{i=1}^{4} I_{Ni}} \tag{6}$$

D. *Localization Error*

Let (x_m, y_m, z_m) be the coordinates of the sound source, and (x_k, y_k, z_k) be the coordinates obtained from localization. The distance between them is given by Equation (7):

$$d_{\mathrm{E},m} = \sqrt{(x_k - x_m)^2 + (y_k - y_m)^2 + (z_k - z_m)^2} \tag{7}$$

When performing source localization for M sound sources within the localization area, the average of $d_{\mathrm{E},m}$is defined as the localization error, as shown in Equation (8):

$$Error = \frac{\sum_{m=1}^{\mathrm{M}} d_{\mathrm{E},m}}{\mathrm{M}} \tag{8}$$

E. *Preliminary Asymmetry Degree*

Previous studies on BS source localization [11–14] have employed symmetric ES configurations, and asymmetric configurations have not been investigated. Therefore, our research team proposed a Preliminary Asymmetry Degree (PAD) to quantify the degree of asymmetry, as described in

Equation (9). Figure 2 illustrates an example of the relationship between PAD and ES configurations, with the interior angles of the quadrilateral formed by the four ES defined as A1, A2, A3, and A4.

$$PAD = \frac{|\mathrm{A1} - \mathrm{A2}| + |\mathrm{A3} - \mathrm{A4}|}{2\pi} \quad (9)$$

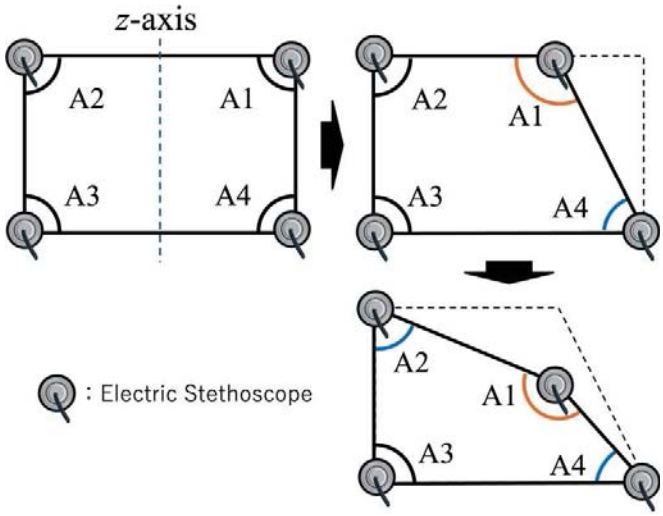


Fig. 2. An example of an ES configuration with a higher PAD than the symmetric arrangement.

III. Result

Figure 3 illustrates the configuration of four ES, and Table 1 presents the corresponding PAD values. While configuration (a-1) is rectangular, configuration (b-1) is trapezoidal. This is because, although a rectangular configuration is generally used for bowel sound measurement, a trapezoidal configuration may be employed to avoid interference from the ribs. In both cases—(a-1) to (a-4) and (b-1) to (b-4)—the sensors were repositioned only in the first quadrant to increase asymmetry.

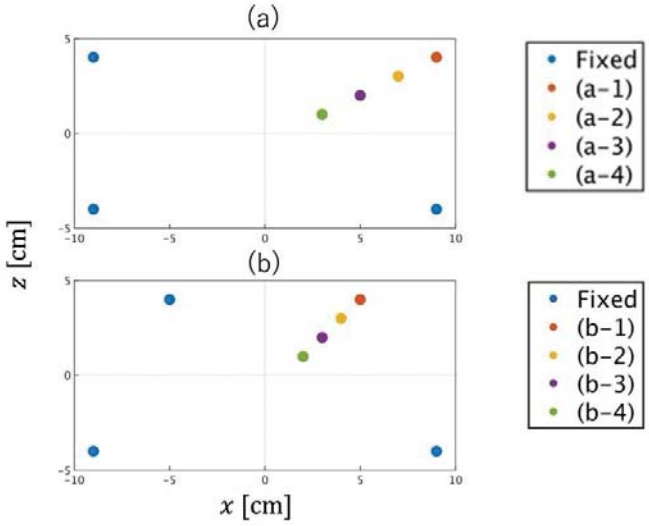


Fig. 3. ES configurations used in this study. The blue points remain fixed, while only the points in the first quadrant were adjusted to alter asymmetry. (a) ES configuration modified from a rectangular baseline; (b) ES configuration modified from a trapezoidal baseline.

TABLE I. PAD of Each ES Placement

	PAD Calculated By Equation (9)			
Rectangular	(a-1)	(a-2)	(a-3)	(a-4)
PAD	0	0.11	0.23	0.36
Trapezoidal	(b-1)	(b-2)	(b-3)	(b-4)
PAD	0	0.09	0.18	0.28

Figure 4 presents the localization results for the sensor configurations depicted in Figure 3. The vertical axis represents the localization error, and the horizontal axis represents the SNR. (a) shows the results obtained using a rectangular configuration, while (b) shows those obtained using a trapezoidal configuration.

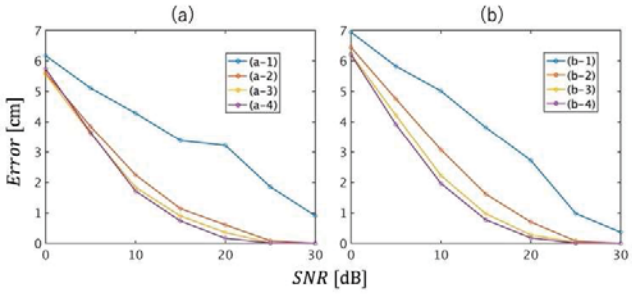


Fig. 4. Bowel sound source localization results as a function of SNR for each ES configuration: (a) ES configuration based on a rectangular layout; (b) ES configuration based on a trapezoidal layout.

Figure 4 shows that in both cases, localization error decreases with increasing SNR. Moreover, when asymmetry was increased in both the rectangular and trapezoidal configurations, there was a significant improvement in localization accuracy compared to the symmetric setup, thereby demonstrating the effectiveness of the PAD as an index of asymmetry even among non-symmetric shapes. It was necessary to verify whether the improvement in localization error indicated by PAD depended on the original symmetric ES configuration or if it applied equally to all ES configurations. To this end, the symmetric configurations used in this study—namely, the rectangular and trapezoidal shapes—were reordered in ascending order of their asymmetry degree, yielding the relationship shown in Figure 5. One report [16] noted that during surgery, when BS were observed using an ES, the SNR was approximately 15 dB. Therefore, Figure 5 presents the localization error at an SNR of 15 dB. The results from Figure 5 suggest that PAD functions equally well regardless of the underlying shape of the symmetric ES configuration. Furthermore, compared to the symmetric configuration ($PAD = 0$), the non-symmetric configuration with a PAD of 0.11 exhibited less than half the error, and the localization error continued to decrease as PAD increased.

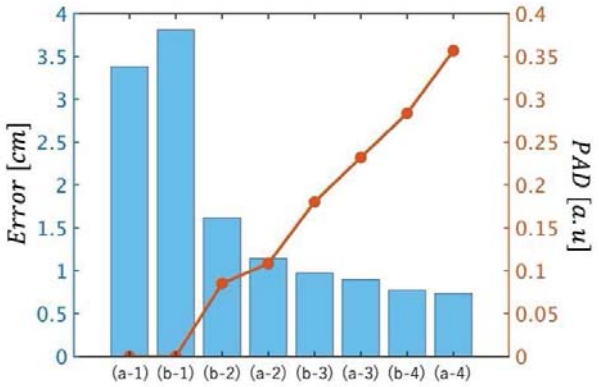


Fig. 5. Localization errors for ES configurations arranged in ascending order of PAD values.

IV. Discussion

This study investigated effective ES arrangements for BS source localization using an energy-based source localization method. As a result, it was confirmed that asymmetrical ES arrangements significantly reduced localization errors compared to symmetrical ES arrangements. Furthermore, by proposing the index PAD, which quantifies the degree of asymmetry in the ES arrangement, we demonstrated the possibility of achieving higher localization accuracy.

Through this research, we observed cases where increasing the asymmetry of the ES arrangement improved the localization error by more than 3 cm. According to a previous report [17], the average diameters of the small intestine and large intestine are 2.5 cm and 4.8 cm, respectively, suggesting that the error reduction achieved with the proposed PAD is effective for more reliable BS source localization. Moreover, the SNR range of 0–30 dB targeted in this study covers approximately 15 dB, as reported in earlier research [16] that recorded BS during surgery, suggesting that our approach might be applicable under actual measurement conditions. Another aspect of PAD's effectiveness is its robust usability. Our findings indicate that PAD's performance is independent of the underlying symmetric ES configuration; that is, as long as the ES arrangement exhibits asymmetry, precise source localization can be achieved without necessitating additional adjustments.

We calculated PAD based on a simplified rectangular model of the abdomen, but it appears that changes in the ES-SS distance resulting from variations in PAD may affect the source localization results. Although this study focused on relatively simple arrangement patterns, the findings suggest there may be even more optimal configurations for improving localization accuracy. In the future, further investigation using a more biologically realistic model that closely resembles the actual abdomen will be necessary. It is also crucial to determine under which conditions the SS-ES distance leads to better source localization accuracy, and to clarify precisely how PAD contributes to reducing the error.

V. Conclusion

We investigated effective ES arrangements for BS source localization using a simplified rectangular model of the abdomen. To this end, we proposed an index called PAD, which quantifies the asymmetry of the ES arrangement. Through source localization simulations, we found that the localization error decreased as PAD increased. These results suggest that BS source localization accuracy can be improved without the need for additional measures such as increasing the number of sensors or implementing noise reduction techniques.

Acknowledgment

This work was supported by a specific grant from JSPS Grant-in-Aid for Scientific Research: Scientific Research (C): KAKEN 23K11947.

References

[1] Black CJ, Ford AC. Global burden of irritable bowel syndrome: trends, predictions and risk factors. Nat. Rev. Gastroenterol. Hepatol. 2020;17(8):473–486.

[2] Oka P, et al. Global prevalence of irritable bowel syndrome according to Rome III or IV criteria: a systematic review and meta-analysis. Lancet Gastroenterol. Hepatol. 2020;5(10):908–917.

[3] Beppu T, et al. Mucosal healing of ileal lesions is associated with long-term clinical remission after infliximab maintenance treatment in patients with Crohn's disease. *Digest. Endoscopy*. 2015;27(1):73–81.

[4] Ohgo H, et al. Irritable bowel syndrome evaluation using computed tomography colonography. *World J. Gastroenterol*. 2016;22(42):9394.

[5] Åkerman, et al. Computational postprocessing quantification of small bowel motility using magnetic resonance images in clinical practice: an initial experience. *J. Mag. Resonance Imag*. 2016;44(2):277-287.

[6] Hahnemann ML, et al. Quantitative assessment of small bowel motility in patients with Crohn's disease using dynamic MRI. *Neurogastroenterol. Motil*. 2015;27(6):841–848.

[7] Månsson S, Ekberg O, Ohlsson B. Motility index measured by magnetic resonance enterography is associated with sex and mural thickness. *World J. Gastroenterol*. 2020;26(36):5484.

[8] Menys, et al. Quantified terminal ileal motility during MR enterography as a biomarker of Crohn disease activity: prospective multi-institution study. *Radiology*. 2018;289(2):428–435.

[9] Ogawa M, et al. Evaluation of perioperative intestinal motility using a newly developed real-time monitoring system during surgery. *World J. Surg*. 2021;45:451–458.

[10] Tuscharoenporn T, Uruwankul K, Charoenkwan K. Effects of postoperative gum chewing on recovery of gastrointestinal function following laparoscopic gynecologic surgery: Systematic review and meta-analysis of randomized controlled trials. *J. Clin. Med*. 2024;13(10):2851.

[11] Craine BL, Silpa ML, O'toole CJ. Two-dimensional positional mapping of gastrointestinal sounds in control and functional bowel syndrome patients. *Digest. Dis. Sci*. 2002;47:1290–1296.

[12] Dimoulas CA. Audiovisual spatial-audio analysis by means of sound localization and imaging: A multimedia healthcare framework in abdominal sound mapping. *IEEE Trans. Multimedia*. 2016;18(10):1969–1976.

[13] Garner CG, Ehrenreich H. Non-invasive topographic analysis of intestinal activity in man on the basis of acoustic phenomena. *Res. Exp. Med*. 1989;189:129–140.

[14] Ranta R, et al. Towards an acoustic map of abdominal activity. Proceedings 25th Ann. Int. Conf. IEEE Eng. Med. Biol. Soc. (IEEE Cat. No. 03CH37439). 2003;3.

[15] Sim KH, et al. The appropriateness of the length of insulin needles based on determination of skin and subcutaneous fat thickness in the abdomen and upper arm in patients with type 2 diabetes. Diabetes Metabol. J. 2014;38(2):120–133.

[16] Emoto T, et al. Evaluation of human bowel motility using non-contact microphones. *Biomed. Phys. Eng. Exp*. 2016;2(4):045012.

[17] Helander HF, Fändriks L. Surface area of the digestive tract–revisited. *Scandinavian J. Gastroenterol*. 2014;49(6):681–689.

Design and Development of a Portable Static Stability Training System

1st ManutchanokJongprasithporn
Department of Industrial Engineering,
School of Engineering,
King Mongkut's Institute of Technology Ladkrabang,
Bangkok, Thailand
manutchanok.jo@kmitl.ac.th

2nd Nantakrit Yodpijit
CIHFE², Department of Industrial Engineering,
Faculty of Engineering,
King Mongkut's University of Technology North
Bangkok, Thailand
nantakrit.y@eng.kmutnb.ac.th

***Abstract*— This study presents a portable static stability training system that integrates a custom-built Inertial Measurement Unit, the Motion Signal Detection Device (MSDD), along with an interface program. It provides a cost-effective alternative to traditional force plates, which are expensive and restricted to laboratory use. The MSDD assesses body sway by analyzing acceleration data in three directions and offers real-time feedback to enhance stability, making it suitable for sports training and rehabilitation.**

Data were collected from five young adult participants with the following mean demographic characteristics: age 23 ± 1.22 years, height 167.8 ± 10.23 cm, weight 60.34 ± 10.58 kg, and BMI 21.28 ± 1.69. The study involved three postures: normal stance, single stance, and heel-to-toe stance. To compare data from two different devices, including force plates (FP) and MSDD, data alignment was analyzed by comparing mean CoP velocities (FP) with sway velocities (MSDD) for each posture. The results indicated that the FP Center of Pressure (CoP) data and MSDD sway paths in the x and y directions exhibited similar trends. Consequently, the MSDD was integrated into the Portable Static Stability Training System for body sway measurement. The interface program, developed using Windows Forms App in Visual Studio 2022, improves usability by monitoring CoP and Base of Support.

The principles of limited stability have been implemented to enhance balance control by restricting the center of pressure (CoP) and minimizing body sway within the base of support. The system enables customization of the sway path area limit, allowing for an appropriate challenge based on an individual's balance ability. When CoP exceeds stability limits, the system provides immediate feedback to prompt posture correction. This portable system bridges the gap between laboratory-based measurement tools and practical stability training.

Keywords*— *Base of Support, Center of Pressure, Inertial Measurement Unit, Limited stability, Static Stability Training.

I. Introduction

Human static stability refers to an individual's ability to maintain balance in various environments. Postural stability is defined by the position of the body's center of mass (CoM) within the base of support (BoS), which is the area in contact with the surface. To maintain equilibrium during static postural stability, the vertical ground reaction force, represented by the center of pressure (CoP), must align with the center of mass [1]. Traditionally, human balance is assessed by measuring body sway using CoP data collected from a force plate. However, force plates have limitations, including their large size and high cost, making them impractical for use outside laboratory settings.

The human body relies on three sensory systems to maintain balance: the vestibular, visual, and proprioceptive systems [2], [3]. The vestibular system, located in the inner ear, detects acceleration and aids in spatial orientation and balance during head movements. The visual system provides information about the body's position relative to its surroundings, helping to maintain stability. The proprioceptive system enables the body to sense its position and movement through receptors in muscles, tendons, and joints, transmitting this information to the central nervous system for coordinated muscle activity and balance control.

To address the limitations of force plates, a Motion Signal Detection Device (MSDD) was designed and developed with an integrated Inertial Measurement Unit (IMU). IMUs, widely used in navigation systems and robotics, contain sensors such as accelerometers, gyroscopes, and magnetometers to measure an object's orientation, velocity, and acceleration [4]. The MSDD has been incorporated into a portable static stability system, providing a practical and cost-effective alternative to force plates.

This study aims to design and develop a portable static stability system to enable more accessible and convenient balance assessments beyond the laboratory. The concept of a limited center of pressure (CoP) has been integrated with MSDD data acquisition to create a training protocol that improves balance control by minimizing body sway and keeping it as close as possible to the center of mass during each posture [5]. This real-time feedback mechanism enhances balance training, making it more effective and applicable in educational, sports, and rehabilitation settings.

II. Motion Signal Detection Device

The Motion Signal Detection Device (MSDD) is designed to be compact, lightweight, and energy-efficient, making it suitable for portable balance assessment applications. The MSDD was an enhanced version of the Range of Motion device from a previous study [6]. Fig 1. illustrates the MSDD, which integrates several key components to ensure accurate motion detection and reliable performance.

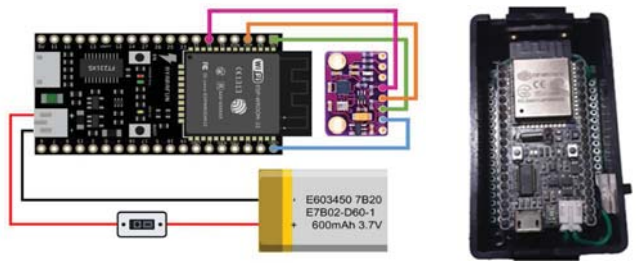


Fig. 1. Motion Signal Detection Device (MDSS)

XXX-X-XXXX-XXXX-X/XX/$XX.00 ©20XX IEEE

MDSS includes the ESP32 NodeMCU (NodeMCU-32S) microcontroller with an ESP-WROOM-32 IC chip, the GY-91 IMU Sensor Module featuring the MPU-9250 chip that includes a 3-axis gyroscope, a 3-axis accelerometer, and a 3-axis magnetometer, and a 3.7V lithium-polymer battery with a 600 mAh capacity.

The module is powered through an onboard socket connected to the battery, ensuring a stable power supply for continuous operation. These components were carefully selected to achieve an optimal balance of functionality, power efficiency, and safety, contributing to the development of a portable stability system.

III. Methods

A. Subjects and Data Collection

This study recruited five participants (three females and two males) during the prototype design and development phase. The participants had a mean age of 23 ± 1.22 years, a mean height of 167.8 ± 10.23 cm, a mean weight of 60.34 ± 10.58 kg, and a mean BMI of 21.28 ± 1.69, all within the normal range. They reported no history of significant head, leg, or foot injuries and were free from chronic illnesses and substance use. Additionally, all participants confirmed having sufficient sleep prior to the study to minimize potential fatigue-related effects on balance and posture. All procedures involving human participants were reviewed and approved by the Ethics Committee, KMITL.

Participants were instructed to perform three standardized postures on a Kistler force plate (Type 9260AA, 600 × 500 mm), as shown in Fig. 2, while wearing the Motion Signal Detection Device (MSDD) securely fastened around the middle of their waistline. The position of the MSDD relative to the force plate surface was carefully recorded to ensure accuracy in data collection and analysis.



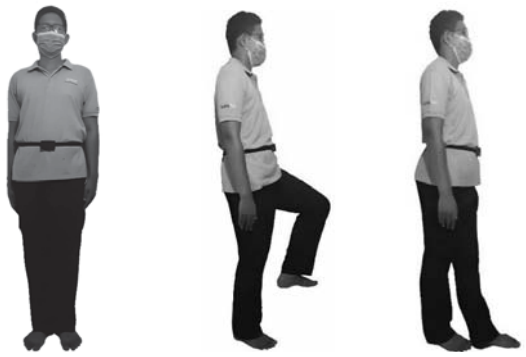
(a) (b)

Fig. 2. Force Plate (a) Kistler multicomponent force plate (Type 9260AA) and (b) DAQ system (USB 2.0) Type 5691A1

The study included three standardized postures to assess balance and stability: (1) normal stance, where participants stood on both feet with their eyes open; (2) single-leg stance, where they stood on one foot with their eyes open; and (3) heel-to-toe stance, where they positioned one foot directly in front of the other with their eyes open, as illustrated in Fig 3.

Each posture was held for 60 seconds while data was recorded. The force plate captured center of pressure (CoP) data at a sampling frequency of 500 Hz, providing precise measurements of postural sway. Simultaneously, the Motion Signal Detection Device (MSDD) recorded acceleration data (x, y, and z components) at 50 Hz to track movement dynamics.

To minimize learning effects, the order of postures was randomly assigned. Each posture was performed three times to collect multiple datasets, enhancing the reliability and accuracy of the measurements. A 60-second rest period was provided between trials to prevent fatigue and maintain consistent performance.



(a) (b) (c)

Fig. 3. Three posture stances: (a) Normal stance, (b) Single stance, and (c) Heel-to-Toe stance.

B. Comparing Force Plate and MSDD data

To compare data from two different devices between force plates (FP) and the Motion Signal Detection Device (MSDD). The data alignment was analyzed by comparing the mean center of pressure (CoP) velocities from the FP with the sway velocities measured by the MSDD for each posture. This comparison aimed to examine the patterns between the two measurement systems in each postural stability.

The sway path of the accelerometer was calculated using equations from Mayagoitia et al. [4], which provides a method for estimating body sway based on accelerometer data. The resultant acceleration, representing the overall magnitude of movement, was determined using equation 1.

This calculation allowed for a more comprehensive evaluation of movement characteristics and their relationship to postural control across different stance conditions. Where a_x, a_z, and a_z are the acceleration on x, y, and z components, respectively. The angles between the components of acceleration and the resultant were determined using equations 2, 3, and 4.

$$A = \sqrt{a_x^2 + a_y^2 + a_z^2} \tag{1}$$

$$\alpha = cos^{-1}\left(\frac{a_x}{A}\right) \tag{2}$$

$$\beta = cos^{-1}\left(\frac{a_y}{A}\right) \tag{3}$$

$$\gamma = cos^{-1}\left(\frac{a_z}{A}\right) \tag{4}$$

The magnitude of vector D is on the directional cosines, and $d_z$is the distance from the MSDD to the standing surface as equation 5. The coordinates of MSDD sway path in direction x (d_x) and direction y (d_y) are calculated by equations 6 and 7. These calculations provide a detailed representation of postural sway by mapping the movement trajectory in both horizontal directions.

$$D = -d_z/cos \quad (5)$$

$$d_x = Dcos_\alpha \quad (6)$$

$$d_y = Dcos_\beta \quad (7)$$

C. Implementing MSDD data into static stability training

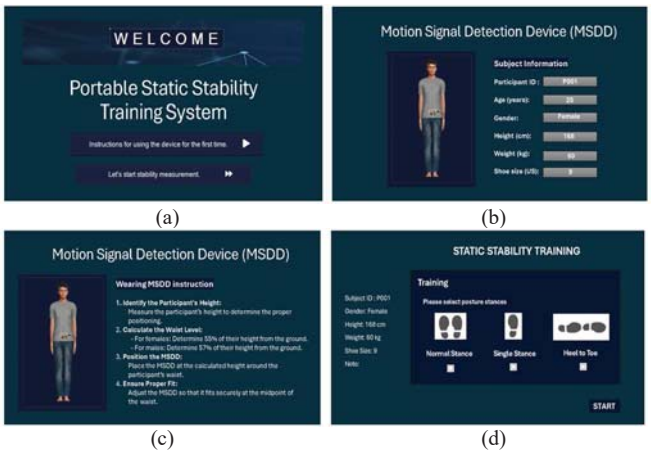
The MSDD sway path coordinates are calculated and used to represent the center of pressure (CoP) coordinates. This training system operates on the principle of limiting the CoP [5], by encouraging individuals to maintain their MSDD sway path within a designated area. The goal is to minimize excessive sway, thereby enhancing overall balance by improving motor control and optimizing the function of the three primary sensory systems: visual, vestibular, and somatosensory, crucial for effective balance maintenance.

Previous study reported that the average CoP displacement typically ranges from 0.63 to 1.86 cm, with a mean value of approximately 1.27 cm for healthy young adults [7]. The boundaries of the sway path area can be adjusted to align with an individual's balance ability. These limits are initially set based on the average CoP displacement and can be modified as a percentage to suit the participant's specific needs and progress, offering a personalized approach to balance training.

D. Interface of Portable Static Stability Training System

The user interface for the portable static stability training system was developed using the Windows Forms App (.NET Framework) in Visual Studio 2022. The interface facilitates real-time data visualization, user-friendly navigation, and efficient communication with the MSDD, monitoring and analysis of postural stability, as shown in Fig. 3.

The system guides users through the training process, starting with account creation and the entry of participant information, including participant ID, age, gender, weight, height, and shoe size. The MSDD wearing instructions are to remind users of the correct positioning before beginning the training session. Following this, the static stability training window appears, allowing users to select their training posture stance. It enhances the training experience by tracking MSDD sway while delivering real-time feedback, helping guide the user's progress and improving balance control effectively.



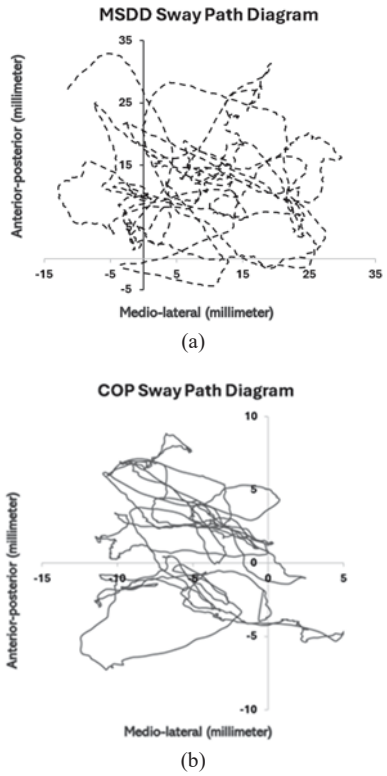
(a) (b) (c) (d)

Fig. 3. The user interface of Portable Static Stability Training System: (a) Welcome window, (b) Account creation window and participant information, (c) Instructions for wearing MSDD, and (d) Training window with posture stance selections.

IV. Results

A. Comparison of Data Between Two Devices

As participants changed postures from normal stance to a single stance and a heel-to-toe stance, the overall path of the center of pressure (CoP) increased in both the x and y directions. Similarly, the sway path measured by the inertial measurement unit (MSDD) expanded in both directions as the base of support decreased with each posture. The example of MSDD sway path diagram and CoP sway path diagram of force plate during the normal stance posture was plotting on Anterior-Posterior (AP) and Medial-Lateral (ML) directions and shown in Fig 4.



(a)

(b)

Fig 4. (a) MSDD and (b) CoP sway path diagram during the normal stance

Mean and standard deviation velocities of both CoP and MSDD sway were calculated for each posture condition as shown in Table I. Also, the mean and standard deviation of CoP sway displacement from FP and MSDD sway displacement for each posture condition are shown in Table II. Both tables provide insight into how changes in support base impact balance stability and sway displacement in both the anterior-posterior (AP) and medial-lateral (ML) directions. The correlation of velocity between two devices, analyzed by using a weighted Pearson correlation, is 0.94. It is indicated there is a strong positive correlation between CoP and MSDD sway velocity.

TABLE I. Mean and Standard Deviation CoP Velocities and MSDD Sway Velocities

Devices	Velocity (cm/s)	Normal Stance	Single Stance	Heel-to-Toe Stance
Force Plate	Mean CoP Velocity	0.09(0.52)	0.11(0.65)	0.12(0.60)
MSDD	Mean Sway Velocity	0.11(0.63)	0.12(0.70)	0.14 (0.56)

TABLE II. MEAN AND STANDARD DEVIATION OF COP AND MSDD SWAY DISPLACEMENT

Devices	Displacement (cm)	Normal Stance	Single Stance	Heel-to-Toe Stance
Force Plate	Anterior-posterior (AP)	1.48 (0.39)	2.26 (0.54)	2.33 (0.61)
	Medial-lateral (ML)	1.64 (0.62)	3.26 (0.58)	2.68 (0.70)
MSDD	Anterior-posterior (AP)	1.98 (0.45)	3.56 (0.44)	4.23 (0.54)
	Medial-lateral (ML)	2.34 (0.71)	5.96 (0.68)	5.38 (0.45)

B. Portable Static Stability Training System

The principle of limited stability is implemented to enhance balance control by restricting the center of pressure (CoP) and minimizing body sway near the center of mass [5]. By constraining excessive movement, this approach helps improve postural stability and reduces the risk of imbalance. The system allows for customization of the sway path area limit, ensuring an appropriate level of challenge tailored to an individual's balance ability and training needs.

Initially, these limits are determined based on an average MSDD sway AP and ML displacement in Table II, reflecting typical postural sway in healthy individuals. The limits can then be adjusted within each posture stance standard deviation to accommodate variations in the individual specific capabilities.

This principle is integrated into the portable stability training system through the incorporation of the MSDD's sway path coordination and real-time raw data analysis, facilitating precise feedback and progress monitoring, as illustrated in Fig. 5. At the end of each trial, the system processes the collected data, interprets the results, and provides visual feedback to support performance assessment and improvement balance.

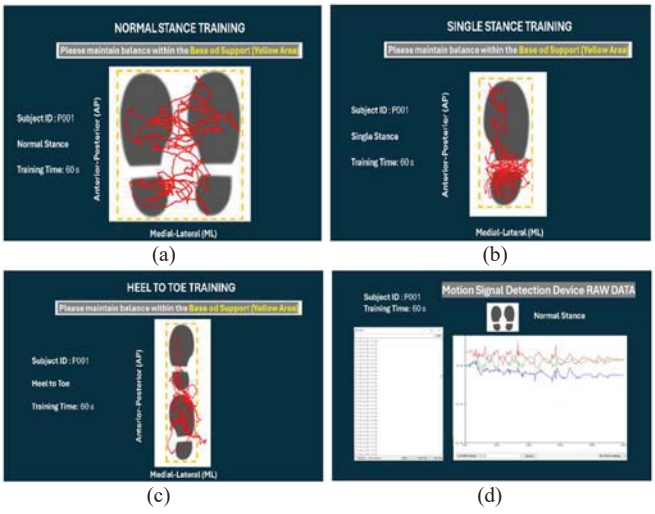


Fig. 5. The Portable Static Stability Training System: (a) Normal stance training, (b) Single stance training, (c) Heel to toe stance training, and (d) MSDD raw data.

V. DISCUSSION AND CONCLUSION

The balance training system improves postural control by minimizing excessive sway and promoting precise balance adjustments. By regulating the MSDD's sway path, which represents CoP displacement, users can enhance stability, particularly those with balance impairments. Research indicates that restricting CoP displacement enhances neuromuscular coordination, facilitates postural adaptation, and reinforces motor learning through repeated practice and sensory feedback [8], [9]. The training system incorporates three standing postures to challenge balance by modifying the base of support and requiring CoP control. A key advantage of this system is its ability to adjust sway limits based on individual needs. An average MSDD sway displacement, represented CoP from FP, informs personalized training, ensuring exercises remain both challenging and achievable. This adaptability benefits rehabilitation and athletic training by tailoring exercises to users' abilities.

However, this study has several limitations. The small number of participants may limit the generalizability of the findings. Additionally, the training system lacks advanced data interpretation, restricting its ability to provide detailed insights into postural adjustments and balance responses. Future research should address these limitations by increasing the number of participants. Enhancing data interpretation will also provide more actionable feedback, improving both usability and effectiveness. Despite these limitations, the system's affordability and portability make it a practical solution for diverse settings, including rehabilitation clinics, athletic training centers, and home use. Its adaptability ensures broader access to personalized balance training, promoting improved postural control across various populations.

ACKNOWLEDGMENT

This research was supported by King Mongkut's Institute of Technology Ladkrabang.

REFERENCES

[1] B. J. Benda, P. O. Riley, and D. E. Krebs, "Biomechanical relationship between center of gravity and center of pressure during standing," *IEEE Transactions on Rehabilitation Engineering*, vol. 2, no. 1, pp. 3–10, Mar. 1994.

[2] N. B. Alexander, "Postural control in older adults," *Journal of the American Geriatrics Society*, vol. 42, no. 1, pp. 93–108, 1994.

[3] R. Fitzpatrick and D. I. McCloskey, "Proprioceptive, visual and vestibular thresholds for the perception of sway during standing in humans," *J Physiol*, vol. 478, no. Pt 1, pp. 173–186, Jul. 1994.

[4] I. Arun Faisal, T. Waluyo Purboyo, and A. Siswo Raharjo Ansori, "A Review of Accelerometer Sensor and Gyroscope Sensor in IMU Sensors on Motion Capture," *J. Eng. Appl. Sci.*, vol. 15, no. 3, pp. 826–829, Nov. 2019.

[5] G. Juras, S. Kajetan, A. Fredyk, G. Sobota, and B. Bacik, "Evaluation of the Limits of Stability (LOS) Balance Test," *Journal of Human Kinetics*, vol. 19, pp. 39–52, Apr. 2008.

[6] M. Jongprasithporn, N. Yodpijit, T. Chanaroon, T. Paiboonrattanakorn, and T. Sittiwanchai, "Design and Development of a Prototype for Measuring Range of Motion," in *2018 IEEE International Conference on Industrial Engineering and Engineering Management (IEEM)*, Dec. 2018, pp. 1191–1195.

[7] R. R. Onofrei, E. Amaricai, O. Suciu, V. L. David, A. L. Rata, and E. Hogea, "Smartphone Use and Postural Balance in Healthy Young Adults," *Int J Environ Res Public Health*, vol. 17, no. 9, p. 3307, May 2020.

[8] F. Quijoux *et al.*, "A review of center of pressure (COP) variables to quantify standing balance in elderly people: Algorithms and open-access code," *Physiological Reports*, vol. 9, no. 22, p. e15067, 2021.

[9] L. Mademli, D. Mavridi, S. Bohm, D. A. Patikas, A. Santuz, and A. Arampatzis, "Standing on unstable surface challenges postural control of tracking tasks and modulates neuromuscular adjustments specific to task complexity," *Sci Rep*, vol. 11, no. 1, p. 6122, Mar. 2021.

Improving Accuracy in Image-Recognition Systems With Techniques for Handling Similar-Looking Items in Inventory Management

1st Asst. Prof. Dr. Krit Smerpitak
School of Engineering
King Mongkut's Institute of Technology Ladkrabang
Bangkok, Thailand
krit.sm@kmitl.ac.th

2nd Asst. Prof. Sart Kummool
School of Engineering
King Mongkut's Institute of Technology Ladkrabang
Bangkok, Thailand
sart.ku@kmitl.ac.th
*Corresponding Author

3rd Asst. Prof. Dr. Farzin Asadi
Department of Computer Engineering
Ostim Technical University
Ankara
Turkiye
farzin.asadi@ostimteknik.edu.tr

4th Chitsanuwit Ar-Karachaiphong
School of Engineering
King Mongkut's Institute of Technology Ladkrabang
Bangkok, Thailand
62601125@kmitl.ac.th

5th Watcharapon Sopha
School of Engineering
King Mongkut's Institute of Technology Ladkrabang
Bangkok, Thailand
66016167@kmitl.ac.th

6th Assoc. Prof. Dr. Sawai Pongswatd
School of Engineering
King Mongkut's Institute of Technology Ladkrabang
Bangkok, Thailand
sawai.po@kmitl.ac.th

***Abstract*— Inventory management is crucial for businesses dealing with many visually similar items. This paper presents the development of an automated board game detection system utilizing computer vision and deep learning to enhance the accuracy and efficiency of tracking visually similar inventory. The dataset used to train the model was collected using a Pi Camera Module 3 mounted on a Raspberry Pi 5, ensuring consistency in captured images. To improve the model's performance, images were annotated using CVAT, and dataset augmentation was applied using Augmentations, incorporating transformations such as flipping, brightness adjustment, blurring, and noise addition. These augmentations allowed the model to learn and differentiate board games under varying environmental conditions accurately. The selected model was YOLOv8m, chosen for its balance between accuracy and computational efficiency. The model was trained for 20 epochs using a learning rate of 0.0005, a batch size of 12, and augmentation techniques such as Mosaic and MixUp. Additionally, overfitting prevention techniques including early stopping, dropout, and weight decay were applied. After training, the model was converted into the ONNX format to optimize it for deployment on embedded devices and then uploaded to the Raspberry Pi 5 for real-world testing. The system was evaluated on 10 visually similar or small-sized board games, with 10 tests per game, totaling 100 trials. The results showed that the model successfully classified all board games without a single error. Moreover, these findings demonstrate that the proposed system effectively identify board games with high accuracy while maintaining real-time processing capability. The use of data augmentation and model optimization significantly improved object classification performance, making it a promising approach for inventory management in board game cafes and similar environments.**

Keywords—inventory management, image recognition, overfitting, YOLOv8 model, model regularization, model generalization

I. INTRODUCTION

Inventory management is the process of maintaining order within a business's inventory by tracking, organizing, and optimizing stock levels to ensure efficient operations[1]. In many industries, accurate inventory management is essential for reducing waste, improving customer satisfaction, and optimizing supply chains. However, in environments where items appear visually similar such as books in libraries, parts in warehouses, and board games in cafés. This can lead to misplaced items, errors in stock tracking, and inefficiencies in retrieval processes. To address these challenges, this research focuses on developing an automated board game detection system that leverages computer vision and deep learning to accurately identify and track game boxes in a café setting. The goal is to create a system capable of distinguishing between visually similar items in real time, reducing reliance on manual inventory checks and improving operational efficiency. Recent advancements in computer vision technologies have demonstrated their potential to enhance inventory management by identifying objects based on visual characteristics. However, implementing such a system in real-world environments introduces several challenges. Objects with near-identical designs, minor color differences, or subtle labeling variations can lead to misclassification. Additionally, factors such as lighting conditions, object placement, rotations, and occlusions further complicate accurate detection.

This research specifically explores techniques to improve detection accuracy under these conditions. Methods such as data augmentation is employed to enhance model generalization and reduce overfitting. Given the constraints of embedded hardware like the Raspberry Pi 5, the model is optimized for efficient performance while maintaining high accuracy. By refining these techniques, this study contributes to the development of scalable, automated inventory

management solutions that can be applied to board game cafés and similar environments where distinguishing between visually similar objects is critical.

II. THEOREM

A. Generalization and Regularization in Deep Learning

In deep learning, achieving high accuracy on training data is not enough; a model must also perform well on unseen data. This ability is referred to as generalization. A well-generalized model can correctly classify new inputs that were not part of the training set, making it useful for real-world applications. However, models often face a trade-off between underfitting (learning too little) and overfitting (memorizing training data instead of understanding patterns)[2]. To improve generalization and prevent overfitting, various regularization techniques are applied during model training. Regularization methods introduce constraints or modifications to the training process, helping the model learn more robust features rather than memorizing specific details of the training set.

B. Dataset Preparation

The dataset used in the training process was collected by using the Pi Camera Module 3 with the Raspberry Pi 5, mounted at a set distance of approximately 130 cm from the capturing surface. In-order to capture images from a consistent perspective to train the model with the images that it will actually use during detection. To maintain consistency, all images were captured against a plain white background, to provide a clear contrast between the board games and their surroundings.

A uniform lighting setup was used to minimize shadows and reflections. To train, 200 board games with four images per board game were taken with variations in placement each time to help the model learn positional differences. This setup ensures that there are minimal external variables affecting the dataset, allowing the model to focus on distinguishing visually similar items based on their unique features rather than other external factors. To facilitate the annotation process, a script was used to capture the four images per board game and uploaded them to Google Drive.



Fig. 1. annotated image of a board game.

After collecting the images, they were then annotated using the CVAT web application. Bounding boxes were drawn around the board game in each image manually to ensure precise object localization. To enhance model generalization and prevent overfitting, Augmentations was used to apply a set of transformations to the dataset. Each augmentation was applied individually, and then all possible combinations of these augmentations were generated for every image. This approach ensured that the model was exposed to all potential variations of a board game's appearance, making it more robust to real-world scenarios.

```
# Define augmentations
augmentations = {
    "horizontal_flip": A.HorizontalFlip(p=1.0),
    "vertical_flip": A.VerticalFlip(p=1.0),
    "random_brightness": A.RandomBrightnessContrast(p=1.0),
    "gaussian_blur": A.GaussianBlur(p=1.0),
    "gauss_noise": A.GaussNoise(p=1.0),
}
```

Fig. 2. augmentations used on the captured images.

The following augmentations were used:

A. Horizontal Flip

Flip the image left to right. This Helps the model recognize board games regardless of their orientation. This is particularly useful for symmetrical objects, ensuring that the model does not rely on a specific left-right positioning for identification.

B. Vertical Flip

Flip the image top to bottom. This ensures the model can detect board games even if they are rotated 180 degrees. Some board games may be stacked or turned upside down, so this augmentation helps the model adapt to such variations.

C. Random Brightness & Contrast

Randomly adjusts the brightness and contrast of the image. This simulates different lighting conditions, ensuring the model is robust to variations in brightness. This is crucial for handling changes in ambient lighting that may occur throughout the day.

D. Gaussian Blur

Applies a soft blur to the image, reducing sharp edges. This prevents the model from overfitting to fine details and sharp textures, making it more adaptable to slightly out-of-focus images.

E. Gaussian Noise

Adds random noise to the image, simulating imperfections from the camera sensor. This helps the model become robust against real-world image noise, improving generalization in different environments.

Instead of applying each augmentation randomly, every possible combination of augmentation was applied to each image. This means that for every original image, multiple augmented versions were generated, covering all combinations of flips, brightness changes, blurs, and noise levels. This exhaustive augmentation process created a diverse and well-balanced dataset, ensuring that the model could generalize well across different image conditions. By implementing this augmentation strategy, the dataset was significantly expanded, reducing the risk of

overfitting and improving the model's ability to distinguish between visually similar board games, even under varying conditions.

III. Model Architecture and Training

The model used in this research is YOLOv8, an advanced object detection framework designed for real-time applications. One of the key challenges in training deep learning models is overfitting, where the model memorizes training data instead of generalizing to new images. To prevent this, several regularization techniques and data augmentation strategies were implemented alongside a well-optimized training configuration. Additionally, YOLOv8m was chosen over alternative models due to the number of classes and dataset size, ensuring a balance between detection accuracy and computational efficiency.

These are the parameters used in the process of training the model[3]:

1) Epochs (epochs=20): The training was set to run for 20 epochs, balancing sufficient learning time with the risk of overfitting. Early stopping was applied to halt training if no improvement was observed after 5 epochs.

2) Learning Rate (lr0=0.0005): A low initial learning rate helps stabilize training and prevents the model from making large, unstable updates. The cosine learning rate scheduler (cos_lr=True) was used to gradually reduce the learning rate, allowing fine-tuned weight adjustments as training progressed.

3) Batch Size: A batch size of 12 was chosen based on available computational resources, ensuring a balance between memory efficiency and stable gradient updates.

4) Workers: Parallel processing was used to speed up data loading and augmentation during training.

5) Dropout: Dropout was applied to randomly disable neurons during training, preventing the model from becoming overly reliant on specific features. This encourages better generalization.

6) Weight Decay: L2 regularization was applied to reduce the magnitude of weights, preventing excessive model complexity and reducing overfitting.

7) Data Augmentation: Various augmentations were applied to introduce variability in the training images, ensuring robustness to real-world variations.

8) Mosaic Augmentation: This technique combines multiple images into one during training, helping the model recognize objects in different contexts. It is particularly useful for detecting partially visible objects.

9) MixUp Augmentation: MixUp blends images and their labels, forcing the model to learn more abstract feature representations rather than focusing on specific edges or textures.

10) Early Stopping: If the validation loss did not improve for 5 consecutive epochs, training was automatically stopped to prevent overfitting.

11) Automatic Mixed Precision (AMP): AMP was disabled for this training setup to ensure numerical stability in weight updates.

```
model.train(
    data="path.yaml",
    epochs=epochs,
    lr0=learning_rate,
    batch=batch_size,
    workers=12,
    cos_lr=True,
    dropout=regularization['dropout'],
    weight_decay=regularization['weight_decay'],
    augment=True,
    mosaic=augmentations["mosaic"],
    mixup=augmentations["mixup"],
    patience=5,
    amp=mixed_precision,
)
```

Fig. 3. training code showing the setup of each parameter.

By combining regularization techniques, adaptive learning strategies, and diverse augmentation methods, the model was optimized to recognize visually similar board games while avoiding overfitting. Once trained, the model was fine-tuned and pruned for deployment on a Raspberry Pi 5, ensuring efficient real-time detection while maintaining high accuracy.

IV. Hardware and Implementation

The board game detection system leverages a Raspberry Pi 5 to run a trained YOLOv8m model for real-time game box recognition. The system is designed to process images captured by the Camera Module 3, running on Raspberry Pi OS Lite, with the output displayed via an LED display circuit. For improved performance and portability, the trained YOLOv8m model is converted to ONNX (Open Neural Network Exchange) format and run on the Raspberry Pi[4]. These are the steps to run ONNX on raspberry Pi:

1)Install the necessary dependencies: Install the necessary dependencies to run ONNX on the Raspberry Pi 5 using the following commands.

```
sudo apt update
sudo apt install python3-pip
pip3 install onnxruntime
pip3 install opencv-python
pip3 install numpy
```

Fig. 4. commands to install each dependencies needed to run the ONNX

2) Convert YOLOv8 into ONNX format: Convert the YOLOv8 model into the ONNX format using the following script.

```
from ultralytics import YOLO

# Load the YOLOv8 model
model = YOLO("path_to_your_model.pt")

# Convert to ONNX
model.export(format="onnx", dynamic=True)
```

Fig. 5. script used to convert a YOLO model into a ONNX format

3) Running the inference with ONNX Runtime: Once the ONNX model is ready, it is loaded and executed on the Raspberry Pi using the ONNXRuntime.

```
def preprocess_image(frame):  1 usage
    input_frame = cv2.resize(frame,  dsize: (640, 640))  # Match input
    input_frame = input_frame.transpose(2, 0, 1)  # Convert to CHW fo
    input_frame = np.expand_dims(input_frame, axis=0)  # Add batch di
    input_frame = input_frame.astype(np.float32) / 255.0  # Normalize
    return input_frame

try:
    while True:
        # Capture frame
        frame = picam2.capture_array()
        frame = cv2.cvtColor(frame, cv2.COLOR_BGR2RGB)

        # Preprocess the frame
        input_frame = preprocess_image(frame)

        # Run inference
        inputs = {session.get_inputs()[0].name: input_frame}
        outputs = session.run(None, inputs)

        # Model output
        boxes, scores, labels = outputs[0], outputs[1], outputs[2]
```

Fig. 6. part of the script that preprocesses the captured frame for compatibility with the ONNX framework.

V. Results

This improvement confirms the effectiveness of augmentation in enhancing the model's generalizability and the impact of regularization in stabilizing learning.



Fig. 7. overlapping detections done by an old model

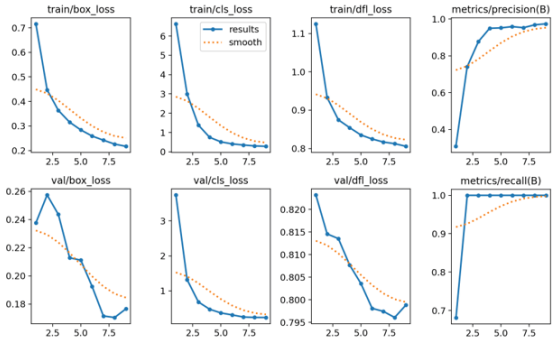


Fig. 8. training progression of the new model

The improved model has successfully mitigated these issues. Previously, dataset imbalances led to biases, where classes with more images were detected more accurately while underrepresented classes suffered from lower confidence. By ensuring an equal number of training images per class and introducing augmentation techniques, the new model eliminates such biases. Another key difference is the stability of validation metrics. The earlier models exhibited a performance gap between training and validation, indicating overfitting. The current model maintains high precision and recall across all classes, ensuring consistent detection capabilities in real-world conditions.

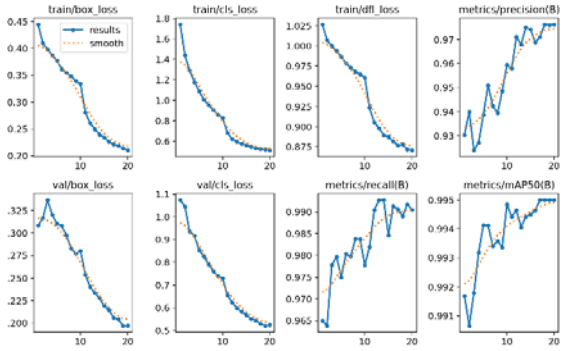


Fig. 9. training progression of the old model

The graphs above describes the performance of the newer model (Figure 8) and the older model (Figure 9). The newer model demonstrated faster convergence, requiring only about 9 epochs due to early stopping, compared to 20 epochs in the older model. Both models showed a decreasing trend in training and validation loss, but the newer model achieved similar accuracy in fewer epochs, indicating more efficient learning. In the older model, validation loss started higher and took longer to stabilize, while the newer model maintained a smaller gap between training and validation loss, suggesting better generalization.

VI. Conclusion

This study successfully developed an object detection system capable of accurately identifying board games and triggering an LED-based response. The improved model demonstrated high accuracy, achieving 100% detection in real-world tests, outperforming the earlier version in both precision and reliability. The reduction in training epochs due to early stopping helped prevent overfitting while maintaining strong performance. Several challenges were encountered during development.

References

[1] Katana, "How to implement a barcode inventory system (6 essential steps)," katanamrp.com, Jul. 31, 2024. [Online]. Available:https://katanamrp.com/barcode-inventory system/#:~:text=A%20barcode%20inventory%20system%20is,in%20your%20warehouse%20or%20store. [Accessed: Mar. 4, 2025].

[2] Amazon Web Services, Inc., "What is overfitting? - Overfitting in machine learning explained," AWS, n.d. [Online]. Available:https://aws.amazon.com/what-is/overfitting/#:~:text=Overfitting%20is%20an%20undesirable%20machine,on%20a%20known%20data%20set. [Accessed: Mar. 4, 2025].

[3] Ultralytics, "Train," Ultralytics YOLO Docs, Jan. 6, 2025. [Online]. Available: https://docs.ultralytics.com/modes/train/. [Accessed: Mar. 4, 2025].

[4] "ONNX Runtime | Generative-AI," ONNX Runtime, n.d. [Online]. Available: https://onnxruntime.ai/generative-ai. [Accessed: Mar. 4, 2025

TRACK 6
AUDIO ENGINEERING AND ACOUSTICS

The Trapezoidal Khim: Sound Radiation of G Notes

1st Natcha Techaaphonchai
Institute of Music, Science, and Engineering
King Mongkut's Institute of Technology Ladkrabang
Bangkok, Thailand
natcha.te@kmitl.ac.th

2nd Worakrit Thida
Institute of Music, Science, and Engineering
King Mongkut's Institute of Technology Ladkrabang
Bangkok, Thailand
w.worakrit@gmail.com

3rd Kittipitch Meesawat
Institute of Music, Science, and Engineering
King Mongkut's Institute of Technology Ladkrabang
Bangkok, Thailand
kittipitch.me@kmitl.ac.th

4th Phonlasit Thinnakorn Na Ayuthaya
Institute of Music, Science, and Engineering
King Mongkut's Institute of Technology Ladkrabang
Bangkok, Thailand
phonlasit.th@kmitl.ac.th

5th Pakaphol Chitsakul
Institute of Music, Science, and Engineering
King Mongkut's Institute of Technology Ladkrabang
Bangkok, Thailand
pakaphol.ch@kmitl.ac.th

6th Sorasak Danworaphong
Institute of Music, Science, and Engineering
King Mongkut's Institute of Technology Ladkrabang
Bangkok, Thailand
ORCID: 0000-0002-9987-2436

Abstract—This research investigates the sound characteristics of the trapezoidal Khim, a traditional Thai hammered dulcimer, focusing on the G 192, G 392 Hz and G 784 Hz notes played with different hammers. Two types of wooden hammers were used, that is, covered with flannel and uncovered. Measurements were conducted in a room measuring 10 by 5 by 3 meters using two microphones, one for capturing the sound field directionality and the other for reference sound. The measurement microphone was placed 2 meters away from the instrument at various angles, while the reference microphone was positioned above the center of the instrument. Analysis of the recordings reveals the directivity profiles for each frequencies, showing that the Khim exhibits relatively high directivity at 90 and 270 degrees, corresponding to its open channels of the instrument. This suggests that the instrument's construction significantly influences its sound radiation. Hammer type was found to affect overall directivity, i.e., fabric-covered hammers resulted in lower directivity compared to uncovered hammers. Furthermore, the hitting point on the key significantly affects the Khim's directivity, indicating that playing technique plays a crucial role in shaping the instrument's sound projection. This study contributes to a deeper understanding of the unique sound production of the trapezoidal Khim and its role in traditional Thai music. It offers valuable information for musicians, instrument makers, and researchers interested in the acoustics of cultural instruments in realistic performance environments.

Index Terms—dulcimer, Khim, G note, directivity, spectrogram

I. Introduction

Khim, a traditional Thai hammered dulcimer, is a distinctive instrument with a rich history. While its name is believed to be derived from the Chinese character, pronouncing "qin" in Mandarin, representing a zither-like instrument, its origins may trace back to Persia or the Middle East [1]. Typically, Khim is made from a hollow wooden box with strings stretched across its surface. It produces sound when these strings are struck with hammers. Over time, it evolved into various forms, such as the "santur" and "cymbalom," spreading across cultures in Europe, the Middle East, India, and Pakistan [2]. Khim likely arrived in Thailand during the Ayutthaya period and was introduced to the country by Chinese traders and theatrical performers. By the reign of King Rama VI, it had been fully integrated into traditional Thai musical ensembles, undergoing adaptations to align with the distinction of Thai music. Famous for its versatility, Khim can perform a vast repertoire, ranging from traditional Thai melodies to contemporary compositions. Its flexibility in solo and ensemble performances emphasizes its continued significance in Thai culture. Despite its cultural and musical importance, there has been little research into the acoustic characteristics of Khim, particularly its sound radiation patterns [3]. In 2019, a seven-bridge butterfly Khim was explored for its acoustic characteristics, i.e., frequencies and sound decay, to create a musical scale to compare with the international standard scale [4].

In this study, we investigate the directivity of Khim's sound, focusing on how its sound radiates when different G notes are played using two different hammers. The notes, G 196 Hz, G 392 Hz, and G 784 Hz, are chosen because they are successive octaves of the same pitch, which allows for a direct comparison of frequency-dependent directivity. By exploring the variation in sound signals with respect to angle and hammers, we can illustrate how sound from each note localizes in space and differs when different hammers are used. Our work provides additional insight

979-8-3315-4248-1/25/$31.00 © 2025 IEEE

into the acoustic properties of this cultural instrument, contributing to a broader understanding of traditional Thai music.

II. Experiment Setup

A. Khim and Its Player

The khim used in this experiment is trapezoidal and made of maple wood, as shown in Fig. 1(a). Its strings are stainless steel wires with a diameter of 0.25 mm. The instrument is placed on a wooden desk with a 2° slanted top, angled toward the player to enhance ergonomics during play. The hammers are crafted from spiny bamboo (Bambusa spinosa); one hammer has a flannel-covered striking surface, while the other is uncovered and black, as shown in Fig. 1(d), (e), and (f), respectively. The khim was tuned with the fundamental frequency based on B♭ musical scaling. This tuning allows for the exploration of the directivity profiles of the fundamental G note and its associated harmonics.

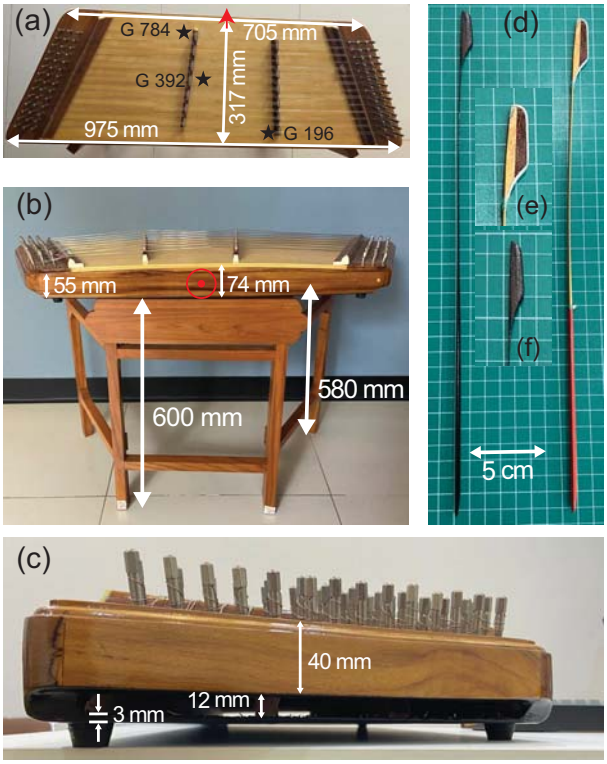


Fig. 1. (a) Top-down view of the maple wood Khim analyzed in this study. Stars mark the striking positions corresponding to the notes G 784 Hz, G 392 Hz, and G 196 Hz. The red arrow indicates the microphone placement for sound measurements. Key dimensions of the instrument are labeled. (b) Side view of the Khim positioned on its custom stand. The stand is slightly inclined, positioning the player's side at 580 mm above the ground and the microphone side at 600 mm. The red circle highlights the microphone placement. The Khim's thickness measures 74 mm at the center and 55 mm at the sides. (c) Close-up side view of the Khim's body, showing a 40 mm-thick side panel, a 12 mm-wide open channel, and a 3 mm-thick under panel. (d) Types of hammers used for striking the Khim strings, including (e) a flannel-covered hammer and (f) an uncovered hammer.

The Khim was played by a professional musician with over 17 years of experience in performing and teaching the instrument, ensuring a high level of skill and familiarity with its nuances.

B. Recording System and Room Plan

The system consisted of two omnidirectional microphones (Earthworks QTC30), an audio interface (RME Fireface 802), and recording software (Logic Pro X). One microphone, designated as the reference microphone, was located approximately 1.34 m directly above the center of the Khim. The other microphone, used for recording sound, was placed 2 m away, directed toward the Khim, and positioned about 0.64 m above the floor. The recording was conducted in an acoustically treated room with an RT60 of 0.90 s. The sound source and microphones were positioned more than 2 meters away from all walls, which were treated with absorptive materials. The floor plan and experimental setup are shown in Fig. 2.

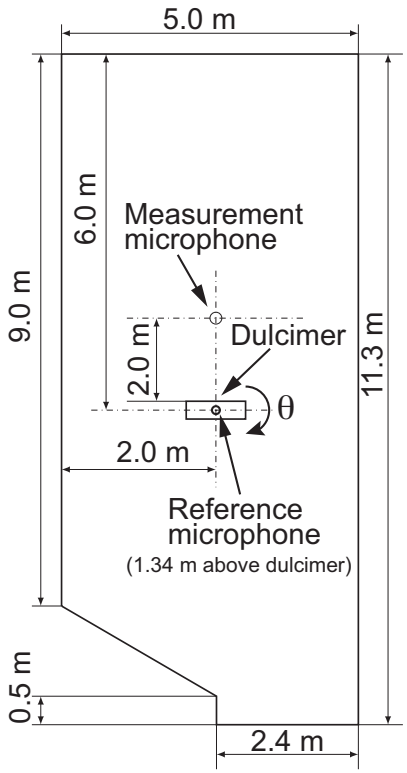


Fig. 2. Floor plan of the measurement setup. The Khim is positioned 2 m away from the fixed measurement microphone and 2 m away from the reference microphone, which is located 1.34 m above the Khim. The Khim is rotated in 30° increments about its center for directivity measurements. The room dimensions are 9.0 m × 5.0 m with absorptive material treatment.

III. Experiment and Data Analysis Tools

Measurements were carried out first with $\theta = 0$, i.e., the player faced directly toward the measurement microphone. Sounds produced by three strikes for each note were

recorded at the locations marked as stars on the khim, as shown in Fig. 1(a). For the subsequent measurements, the khim and its stand were rotated clockwise in 30-degree increments, using a dedicated angular scale attached to the floor for accuracy.

The sound signals were recorded as WAV files with a sampling rate of 48 kHz. The recordings were processed using a short-time Fourier transform (STFT) with a window size of 4096 points, providing a frequency resolution of approximately 11.7 Hz. The sound data from the measurement microphone were normalized relative to the reference microphone, which was positioned 1.34 m above the center of the Khim.

Directivity plots were generated for specific musical note (i.e., G 196, G 392, and G 784 Hz) over a full 360° angular range, measured in 30° increments. The sound data were normalized using the reference microphone signal, and the dB values were calculated as

$$\mathrm{dB} = 20 \log \left(\frac{\text{Measured Signal}}{\text{Reference Signal}} \right). \quad (1)$$

The obtained dBs were plotted using polar coordinates to visualize the sound radiation pattern of the Khim.

IV. Results and Discussion

The sound spectrograms in Fig. 3 illustrate the frequency content of the Khim's sound over time for three octaves of the G note (196, 392, and 784 Hz). Identifying the fundamental frequency from the spectrogram is not as simple as selecting the strongest signal, as the fundamental is not always the most dominant component. Instead, since harmonic frequencies are integer multiples of the fundamental, the spacing between harmonics is analyzed to determine the fundamental frequency accurately.

In Fig. 3(a), multiple harmonics are visible, with their intensity gradually decreasing as frequency increases. The stability of these harmonics over time indicates a steady and consistent tone. The first five adjacent harmonics exhibit an average spacing of 196 Hz, precisely matching the expected G 196 Hz note.

In Fig.3(b) and Fig.3(c), slight deviations in harmonic spacing are observed. For G 392 Hz, the measured average spacing is 389 Hz, slightly lower than the expected. Similarly, for G 784 Hz, the first five dominant harmonics exhibit an average spacing of 782 Hz, slightly below the expected 784 Hz. Since the Khim is tuned using a tuner, instrumental factors such as bridge coupling and material properties are already accounted for in the tuning process. Therefore, these frequency variations are likely due to fluctuations in string tension, which can be influenced by temperature and humidity changes. Over time, the strings may also stretch slightly, leading to small deviations in their vibrational properties. Additionally, minor shifts in how the string sits on the bridge or tuning peg could affect the exact frequency of vibration.

Another contributing factor is the frequency resolution of the 4096-window STFT, which introduces an inherent uncertainty of approximately ±11.7 Hz. This resolution limitation affects the precision of frequency measurements and may account for part of the observed deviation.

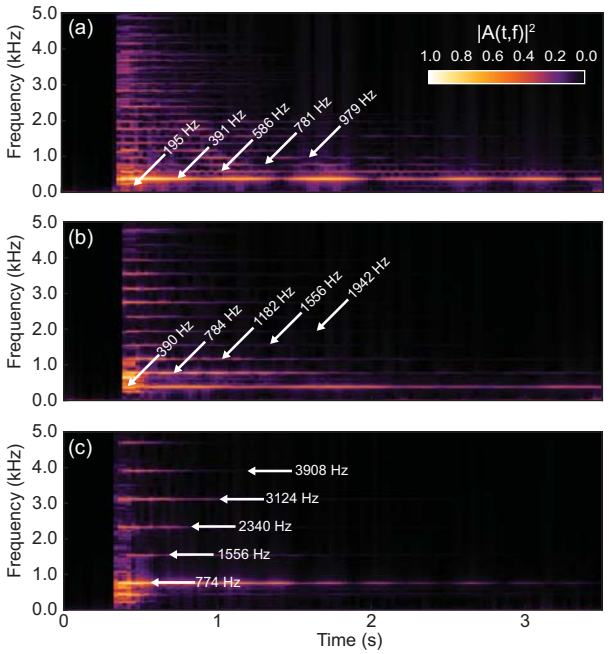


Fig. 3. Spectrograms illustrating the harmonic content of the Khim's sound. The frequency components are displayed over time for (a) the G 196 Hz note and its higher octaves at (b) G 392 Hz and (c) G 784 Hz. The arrows indicate the fundamental frequency and its harmonic series. The color intensity represents the squared modulus of the Fourier transform, highlighting the dominant harmonics essential for frequency spacing measurements.

The spectrograms provide valuable insights into the spectral characteristics of the Khim's sound. Despite these small variations, the harmonic structure remains stable over time, confirming that the Khim produces a consistent and well-sustained tone across these octaves. The presence of strong harmonic components alongside the fundamental frequency contributes to the instrument's rich tonal quality, further characterizing its unique spectral properties.

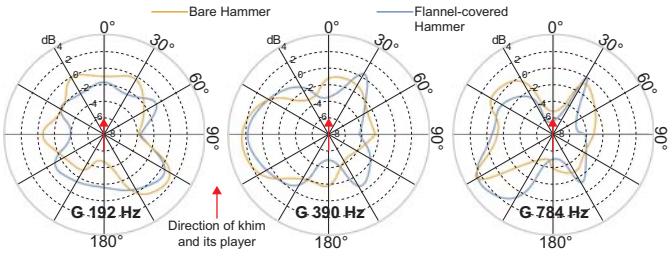


Fig. 4. Directivity patterns of the Khim for different notes and hammers. The polar plots show the normalized sound intensity as a function of angle (θ) for (left) G 196 Hz, (middle) G 392 Hz, and (right) G 784 Hz. The orange lines represent the bare hammer, while the blue lines represent the flannel-covered hammer.

The polar plots in Fig.4 illustrate the directivity patterns of the Khim's sound radiation for three notes, G

196 392 and 784 Hz, played with two types of hammers: a bare hammer and a flannel-covered hammer. The plots reveal significant directivity in the sound radiation, with noticeable variations between the three frequencies and hammer types.

The strong directivity observed in these plots can be attributed to the presence of air channels on the sides of the Khim (Fig.1(c)). These channels function as openings, allowing sound waves to escape directly from within the instrument's body. This focused radiation likely contributes to the directional lobes seen in the plots. Additionally, constructive interference between sound waves radiating from the air channels and those emanating from the Khim's top surface may amplify the sound intensity in certain directions, enhancing the overall directivity.

A comparison of the results for G 196, 392, and 784 Hz demonstrates the frequency-dependent nature of the directivity patterns. The size and shape of the air channels influence which frequencies are radiated most effectively, potentially explaining the differences between the patterns for the lower octave note (G 196 Hz) and its higher octave (G 392 and 784 Hz).

The hammer type also plays a significant role in shaping the directivity. The bare hammer typically results in sharper directivity patterns, with pronounced lobes, whereas the flannel-covered hammer produces smoother and more diffuse radiation patterns. This difference arises from the damping effect of the flannel, which affects the sound radiation characteristics.

These findings are particularly useful for optimizing microphone placement when amplifying or recording the Khim in concert settings. To capture the rich tonal qualities and minimize sound coloration, microphones should be placed in directions corresponding to the strongest sound radiation, as shown in the polar plots. For instance, placing microphones near the directions of the primary lobes can effectively capture the instrument's full tonal range, particularly for specific notes like G 196 Hz and its higher octave. Additionally, understanding the impact of hammer type and note frequency on directivity can guide adjustments in microphone positioning to achieve the desired sound balance in live performances or recordings.

V. Conclusion

This study investigated the sound radiation, directivity patterns, and spectral characteristics of the Khim, focusing on the note G (196 Hz) and its higher octaves (G 392 and G 784 Hz). The results revealed strong frequency-dependent directivity influenced by the instrument's air channels, which enhance sound projection through focused emission and constructive interference. Variations in directivity were observed across different octaves, as well as between strikes using a bare hammer and a flannel-covered hammer, highlighting the impact of hammer material on sound radiation.

Spectral analysis further provided insights into the harmonic structure and frequency stability of the Khim. While the fundamental frequency remained stable across measurements, slight deviations in harmonic spacing were observed, with G392 averaging 389 Hz and G784 averaging 782 Hz. These minor discrepancies were attributed to string tension fluctuations and the resolution limitations of the 4096-window STFT. Despite these variations, the harmonic content remained well-defined, ensuring a consistent and sustained tonal quality.

Together, these findings emphasize the role of the Khim's design, string properties, and playing technique in shaping its unique acoustic characteristics. The insights gained from this study are valuable for optimizing microphone placement in live performances and recordings, ensuring an accurate and balanced capture of the instrument's rich tonal qualities while considering both its directional sound projection and spectral content.

Acknowledgment

The authors would like to express their gratitude to the Institute of Music, Science, and Engineering for generously providing access to high-quality equipment and an acoustically treated room for conducting the measurements.

References

[1] T.J. Barton, "The Khim in Thai Culture: Adoption and Adaptation," Journal of Liberal Arts, Thammasat University. 8(1), 2008.

[2] E. Somchai, C. Sugree, and A. Poonpi, "Khim in Thai Educational System," Fine Arts Journal: Srinakharinwirot University, vol. 15, no. 2, 2012.

[3] D. R. Peterson, "The acoustics of hammered dulcimers," The Journal of the Acoustical Society of America, vol. 117, no. 4_Supplement, pp. 2589–2589, 2005.

[4] S. Suwannarat and N. Tangprasert, "A study of the physics of khim sound using Fourier transform," Ramkhamhaeng Research Journal of Sciences and Technology, vol. 21, no. 2, pp. 20–47, 2018.

Efficient Modeling of ITD Based on Anthropometrics and KEMAR ITD coefficients using Deep Neural Networks

Saif S. Alotaibi, *Member, IEEE,* and Mark Wickert, *Life Member, IEEE*
Department of Electrical and Computer Engineering
University of Colorado Colorado Springs
Colorado Springs, Colorado 80918
Emails: salotaib@uccs.edu and mwickert@uccs.edu

***Abstract*—Binaural cues, such as interaural time difference (ITD) and interaural level difference (ILD), are crucial for spatial hearing, especially for localizing sound sources. Machine learning, especially deep neural networks (DNNs), has shown promise in predicting individual ITD for various acoustics-related applications, including sound localization and assistive listening technologies. DNNs are effective in modeling ITD due to its correlation with specific anthropometric parameters. In this study, a single ITD for each subject is first modeled using DNNs. This modeled ITD is then combined with KEMAR's ITD coefficients to simulate a new user's ITDs across 1,250 different azimuth and elevation positions. The proposed ITD model is evaluated against known analytical models and recent methods using the mean absolute error (MAE) as the primary metric.**

***Index Terms*—Individual HRTF, Spatial hearing, Hearing assistive devices, Deep learning, Bioinformatics.**

I. Introduction

Interaural Time Difference (ITD) and Interaural Level Difference (ILD) are two essential cues for sound localization, particularly in the horizontal plane [1], [2]. ITD refers to the difference in time that a sound wave arrives at each ear, and the brain uses this difference to determine the location of the sound source. On the other hand, ILD refers to the difference in sound intensity at each ear due to head shadowing, where the ear closer to the sound source receives a louder sound. ITDs are mainly used for low frequencies (0-1.5 kHz), while ILDs are more effective for high frequencies above 1.5 kHz [3], [4]. Measured ITDs can be extracted from head-related impulse responses (HRIRs), as demonstrated in [3].

The spherical-head model has been widely used for generating 3D audio based on ITD and ILD cues. However, a more accurate approach involves using an adaptive ellipsoidal head model for ITDs based on anthropometrics, as suggested by Duda et al. [5]. In a later study, Duda et al. proposed a spherical head model with an ideal head radius that produced comparable results to the ellipsoidal head model in the horizontal plane for ITD and ILD calculations [3].

979-8-3315-4248-1/25/$31.00 ©2025 IEEE

Various machine learning techniques such as principal component analysis (PCA) and deep neural networks (DNNs) have been used to create individual HRIRs based on anthropometric data [6], [7], [8]. ITD data from publicly accessible databases, such as the CIPIC interface laboratory at UC Davis, have been used in many studies, including this paper [9]. Modeling ITDs is also essential in creating individual HRIRs, and some researchers remove ITDs and initial time delays from HRIRs and model each portion separately [10], [11], [12], [13]. More accurate ITD data can also improve HRIR modeling, as demonstrated in studies such as [5] and [13].

Enhancing ITD cues improves personalized HRIRs, reducing perceptual ambiguities such as front/back confusion and up/down errors [14] [15]. This leads to greater localization accuracy, improved externalization with headphones, and contributes to broader localization or positioning systems, particularly those involving acoustic signals. Recent studies have increasingly focused on applying individual head-related transfer functions (HRTFs)—the Fourier transform of HRIRs—in hearing aids and cognitive hearing science. In these applications, sound signals are wirelessly transmitted from a talker to a listener via microphones. By bypassing environmental noise, individual HRTFs help preserve crucial perceptual cues and compensate for localization information lost in noisy environments [16]–[20].

This paper proposes a novel method for obtaining individualized ITDs at specific azimuth and elevation angles. Unlike traditional spherical or ellipsoidal models, this approach utilizes an efficient head-shaped model. The DNN model is trained on selected ITDs at $\theta = \pm 80°$ and $\phi = 90°$. After obtaining the selected ITD, which could also be derived through precise tuning, the method maps it to 1,250 locations using KEMAR ITD coefficients. The method's accuracy is evaluated using the MAE metric against established models.

II. Data Processing and Validation

In this study, we validate our ITD results using the corrected ITDs presented in our previous study [13]. The study introduces a new method to correct ITDs from the CIPIC database

and identifies that the irregularities in ITDs are primarily caused by the listener's anatomy and the relative positioning of the head and sound source.

A. Selected Subjects and Features

The CIPIC database includes 27 anthropometric measurements of 37 subjects, including KEMAR's small pinna (subject 165) and KEMAR's large pinna (subject 021), out of 45. Because only 37 subjects had anthropometric data available, the number of subjects available for training was limited. In the proposed method, we set 32 subjects from the CIPIC database for training and kept the remaining five subjects (003, 021, 061, 133, and 156) for testing. From the available anthropometric data, we selected head width, head length, and head depth as the input variables for the DNN model. These variables are denoted as x_1, x_2, and x_3, respectively.

B. KEMAR ITD Coefficients

In the proposed method, the KEMAR ITDs (subject 165) from the training data are normalized using a selected ITD. The normalized KEMAR ITD coefficients are denoted as itd_{norm} and are dimensionless. The following equations outline the procedure for calculating Interaural Time Differences (ITDs) based on the onset times measured from a subject's left and right pinna. Equation (1) computes the ITD when the left pinna is ipsilateral, while Equation (2) calculates the mirrored ITD as if the right pinna were ipsilateral. This mirroring operation across 25 azimuths is executed using the `fliplr()` function, which flips the matrix over these azimuthal angles.

$$\text{ITD}_l(\phi,\boldsymbol{\theta}) = \tau_{\text{l}}(\phi,\boldsymbol{\theta}) - \tau_{\text{r}}(\phi,\boldsymbol{\theta}), \tag{1}$$

$$\text{ITD}_r(\phi,\boldsymbol{\theta}) = \texttt{fliplr}\Big(\tau_{\text{r}}(\phi,\boldsymbol{\theta}) - \tau_{\text{l}}(\phi,\boldsymbol{\theta})\Big), \tag{2}$$

Here, τ_l and τ_r represent the measured onset times for the left and right pinnae from [9], respectively. The dimensions of τ_l and τ_r are 50×25, corresponding to the lengths of arrays ϕ and $\boldsymbol{\theta}$, respectively.

First, we flattened the ITD matrix (including KEMAR's) from its original dimensions of 50×25 into a row vector of length $N = 1250$, as shown below:

$$\big[\text{ITD}(\phi(0),\boldsymbol{\theta}(0)) \quad \text{ITD}(\phi(0),\boldsymbol{\theta}(1)) \quad \cdots \quad \text{ITD}(\phi(49),\boldsymbol{\theta}(24))\big]$$

The process to obtain the normalized KEMAR ITD coefficients for 1,250 locations is outlined as follows:

$$\text{itd}_{\text{norm}}(\phi,\boldsymbol{\theta}) = \frac{\text{ITD}_{\text{kemar}}(\phi,\boldsymbol{\theta})}{\mid \text{ITD}_{\text{kemar}}(90^\circ,\pm 80^\circ) \mid} \tag{3}$$

In this equation, $\text{ITD}_{\text{kemar}}$ represents the KEMAR ITDs, calculated by averaging equations (1) and (2). The term itd_{norm} represents the normalized KEMAR ITD coefficients, where each of $\text{ITD}_{\text{kemar}}$ and itd_{norm} has dimensions of 1×1250. The term $\text{ITD}_{\text{kemar}}(90^\circ, \pm 80^\circ)$ refers to the KEMAR ITD at the selected elevation of 90° and azimuth $\pm 80^\circ$. The absolute value of the selected KEMAR ITD is used in the denominator to ensure that the normalized KEMAR ITD coefficients range between -1 and 1.

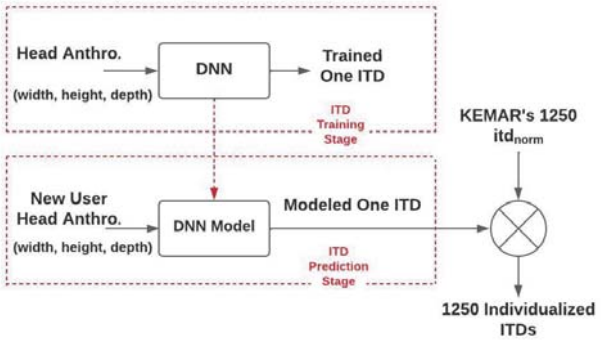


Fig. 1. Block diagram of the proposed M_1 ITD model.

C. Data of Comparison

This paper presents five different models to estimate ITDs. First, M_1 is the proposed DNN-based ITD model for one selected ITD. Second, M_{50} is the DNN-based ITD model for 50 ITD maxima based on [21]. Third, *Avg* refers to the average ITD model of all 1,250 ITDs from the 32 training subjects. Fourth, *Sph* is the spherical head ITD model, based on [3]. Finally, *EHM* is the ellipsoidal head ITD model, based on [5]. Each model has its strengths and weaknesses, and this paper compares their performance to evaluate the effectiveness of the proposed method.

III. Proposed ITD Model

The proposed DNN model for the selected ITD (M_1) was developed from scratch using Jupyter notebooks running Python 3.6 (64-bit) as the development tool. The model consists of two primary components: forward propagation and backward propagation. Additionally, another DNN model, (M_{50}), based on the authors' prior work [21], was used to compute ITD maxima at $\boldsymbol{\theta} = \pm 80^\circ$ for all directions of ϕ. This M_{50} model serves as a comparison for the performance of the newly proposed M_1 model.

A. DNN Model for M_1

The proposed DNN model (M_1) takes three anthropometric features (head width, head length, and head depth) from the CIPIC database [9] as input and includes seven hidden layers in addition to the input and output layers. The number of hidden units is 3 for the input layer, 8 for the hidden layers, and 1 for the output layer. The *He* initialization method is used to initialize all weights and biases across the layers. The minimum-mean-square error (MMSE) is utilized as the cost function to minimize the difference between the measured and predicted selected ITD, based on [22]. The learning rate is set to 0.00001, and the model is trained over 20,000 iterations. The rectified linear unit (*ReLU*) activation function is applied to all hidden layers. The output of the DNN is the selected ITD.

Once the DNN model for the fully connected layers is trained, new anthropometric features (head width, head length,

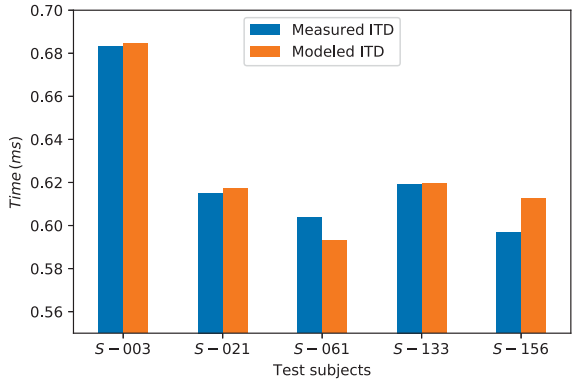


Fig. 2. Comparison between the estimated selected ITD using the proposed DNN and the measured ITD of all testing subjects in the horizontal plane.

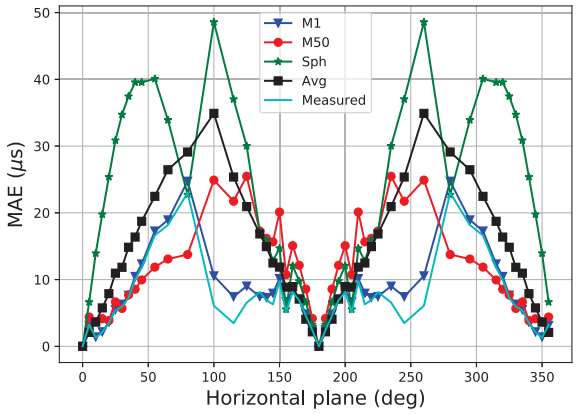


Fig. 3. MAEs between the measured and the modeled ITDs for all testing subjects over horizontal plane.

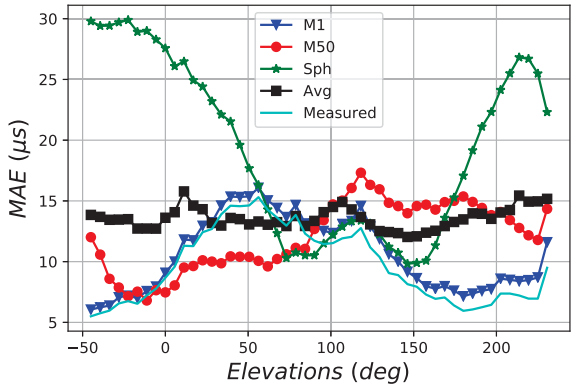


Fig. 4. Average MAEs between the measured and the modeled ITDs for all testing subjects and averaged azimuths versus the corresponding elevations.

and head depth) from a user are fed into the model to predict the ITD at an elevation of 90° and an azimuth of ±80°. This predicted value, denoted as ITD_{mod} has dimensions $1 \times s$, where s represents the number of testing subjects. This modeled ITD is then multiplied by the KEMAR ITD coefficients to obtain individual ITDs for 1,250 sound locations for each subject, as shown below:

$$\text{ITD}_{\text{M}}(s) = \mid \text{ITD}_{\text{mod}}(s) \mid \times \text{itd}_{\text{norm}} \ , \tag{4}$$

where $\text{ITD}_{\text{M}}(s)$ denotes the final individual ITDs for all sound locations for a specific testing subject. The final proposed ITD model is illustrated in Fig. 1.

B. DNN Model for M_{50}

The inputs for the DNN model of M_{50} are the same as those in M_1, with the addition of the elevation angle ϕ for each training example. The total of four input parameters is normalized as per [13]. However, the output labels are the measured 50 ITD maximums, based on [21]. The rest of the DNN setup is identical to M_1. Finally, the 50 modeled ITDs are multiplied by the KEMAR ITD coefficients, following the method in [21], to obtain ITDs for 25 azimuths and 50 elevations.

IV. Results and Evaluations

First, we evaluated our model (M_1) against the average ITDs of the 32 training subjects, denoted Avg, which includes 25 azimuths and 50 elevations. Second, we applied Woodworth's equation [23] for a distant source (eq. (5)) to calculate the spherical head ITD (Sph):

$$\text{ITD}_{\text{Sph}} = \frac{a}{c}\big(\sin(\boldsymbol{\theta}) + \boldsymbol{\theta}\big) \tag{5}$$

where a is the head radius, c is the speed of sound $c = 343$ m/s, and $\boldsymbol{\theta}$ is the azimuth angle in radians. The optimal radii used to calculate eq. (5) are based on [3]. Additionally, the mean absolute error (MAE) was used to compare the measured ITDs with the predicted ones. Here, ITD_{M} and $\widehat{\text{ITD}}$ represent the measured ITD and the predicted ITD for a single user, respectively:

$$\text{MAE}(\text{ITD}_{\text{M}}, \widehat{\text{ITD}}) = \frac{1}{N}\sum_{n=0}^{N-1} \mid \text{ITD}_M(n) - \widehat{\text{ITD}}(n) \mid \tag{6}$$

where n is the sample of the sound location of ϕ and $\boldsymbol{\theta}$.

When the DNN model M_1 was provided with anthropometric data, it showed strong predictive accuracy for estimating ITDs across all test subjects, as illustrated in Fig. 2. However, Fig. 3 presents the MAEs between the measured and modeled ITDs across the horizontal plane, indicating that the M_{50} model performs better than M_1 at lateral angles in the horizontal frontal plane. It should be noted that when the sound source is at 90°, it is directly towards the ear. Table I confirms that both DNN models (M_1 and M_{50}) outperform average and spherical models, with M_1 achieving the lowest MAE of 8.12 μs across all horizontal angles.

Additionally, Fig. 4, which displays the average MAEs between the measured and modeled ITDs for all test subjects, averaged over azimuths and elevations, shows that the

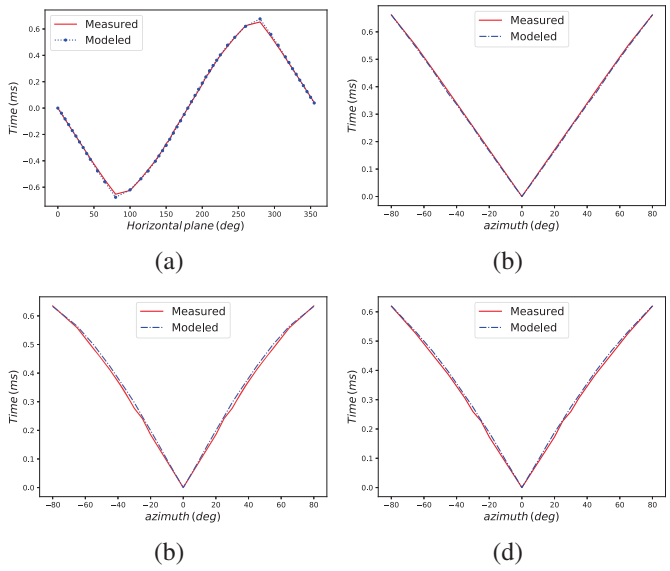


Fig. 5. Measured and modeled ITDs using M_1 for subject 003. (a) ITD in the horizontal plane. (b) |ITD| at $\phi = -45°$. (c) |ITD| at $\phi = 152°$. (d) |ITD| at $\phi = 208°$

proposed M_1 model generally provides more accurate ITD estimates. However, the M_{50} model performs slightly better at the upper front angles. Table II further confirms that the M_1 model achieves the lowest overall MAE, with exceptions being subject 133, which has a 1.8 μs higher MAE than the Avg model, and subject 156, which has a 5.9 μs higher MAE than the M_{50} model.

Table III compares the MAE of the Avg, Sph, M_{50}, and the ellipsoidal head model (EHM), based on 1250 directions from a chosen subject in [5], to our proposed M_1 model, using data from 5 test subjects. At these same 1250 directions, the M_1 model demonstrates better performance, achieving a lower MAE of 10.6 μs compared to all other models. Additionally, the comparison plots in Fig 5 show that the final modeled ITDs using M_1 closely match the corrected measured ITDs for subject 003 in the horizontal plane and azimuths at $\phi = -45°$, $\phi = 152°$, and $\phi = 208°$. This comparison underscores the effectiveness of the proposed DNN model in accurately predicting ITDs across various sound locations and subjects.

Based on the results presented in Table II and Table III, it can be concluded that the proposed DNN model M_1 outperforms the other models in terms of MAE. It achieves the lowest MAE in all disciplines, including the horizontal plane, all angles, and all test subjects. However, it is important to note that for subject 133, the model Avg has a slightly lower MAE than M_1.

Furthermore, the comparison with the ellipsoidal head model (EHM) in Table III shows that the proposed DNN model M_1 performs better than the EHM model, which is based on a different geometric representation of the head. These results confirm the effectiveness of the DNN model in accurately predicting ITDs.

TABLE I
MAEs BETWEEN THE MEASURED AND MODELED ITDs FOR EACH SUBJECT AT ALL HORIZONTAL ANGLES IN μS.

Subject	Avg	Sph	M_{50}	M_1
003	24.00	16.51	21.06	5.89
021	6.99	12.29	7.75	3.41
061	11.77	26.92	7.37	7.66
133	9.58	27.83	12.12	10.47
156	15.39	28.05	8.79	13.17
Mean	**13.55**	**22.32**	**11.42**	**8.12**

TABLE II
MAEs BETWEEN THE MEASURED AND MODELED ITDs FOR EACH SUBJECT AT ALL ANGLES IN μS.

Subject	Avg	Sph	M_{50}	M_1
003	21.2	14.8	18.1	11.0
021	6.70	15.0	7.20	3.90
061	12.1	22.7	10.0	9.10
133	10.0	20.2	13.6	11.8
156	18.1	23.8	11.3	17.2

TABLE III
MAEs BETWEEN THE MEASURED AND MODELED ITDs FOR ALL SUBJECTS AT ALL ANGLES IN μS.

	Avg	Sph	M_{50}	M_1	EHM
MAE	13.6	19.3	12.0	10.6	15.0

V. CONCLUSION

In conclusion, this paper introduces a novel deep neural network (DNN)-based model (M_1) for predicting individualized interaural time differences (ITDs) using anthropometric data and KEMAR ITD coefficients. Validated against traditional methods such as spherical (Sph) and ellipsoidal head models (EHM), as well as other DNN-based models like M_{50}, the M_1 model consistently achieved superior accuracy, with the lowest mean absolute error (MAE) across 1,250 azimuth and elevation positions. We trained and tested on data from five CIPIC database subjects with diverse head shapes and sizes, the model closely matched corrected measured ITDs, demonstrating its robustness in ITD prediction.

The M_1 model's strong performance underscores its potential in applications such as virtual and augmented reality, hearing aids, assistive listening devices, and Head-Related Transfer Function (HRTF) modeling. By incorporating anthropometric data, the model achieves greater precision, highlighting the value of DNNs in delivering personalized acoustic experiences. Future work could focus on expanding the dataset and integrating additional features to further enhance ITD estimation for larger populations and applications, including speech processing and advanced acoustic technologies.

ACKNOWLEDGMENT

The authors would like to thank the CIPIC database administrators for their contributions in providing their valuable dataset.

REFERENCES

[1] R. A Kennedy M. Zhang and T. D. Abhayapala, "Statistical method to identify key anthropometric parameters in hrtf individualization," *IEEE joint Workshop on Hand-free Speech Communication and Microphone arrays*, pp. 213–218, 2011.

[2] R. O Duda V. R Algazi and D. M. Thompson, "The use of head-and-torso models for improved spatial sound synthesis," *AES 13th Convention*, 2002.

[3] C. Avendano V. R Algazi and R. O Duda, "Estimation of the spherical-head model from anthropometry," *Philosophical Magazine JAES*, vol. 49, pp. 472–479, June 2001.

[4] J. W. Strutt, "On our perception of sound direction," *Philosophical Magazine*, vol. 13, pp. 214–232, 1907.

[5] C. Avendano R. O Duda and V. R Algazi, "An adaptable ellipsoidal head model for the interaural time difference," *IEEE International Conference on Acoustics, Speech, and Signal Processing*, pp. 965–968, August 1999.

[6] G. W. Lee C. J. Chun, J. M Moon and H. K. Kim, "Deep neural network based hrtf personalization using anthropometric measurements," *AES 143rd convention*, pp. 291–294, 2017.

[7] G. W. Lee and H. K. Kim, "Personalized hrtf modeling based on deep neural network using anthropometric measurements and images of the ear," *Appl. Science*, pp. 291–294, 2018.

[8] L. Meng, X. Wang, W. Chen, C. Ai, and R. Hu, "Individualization of head related transfer functions based on radial basis function neural network," *IEEE International Conference on Multimedia and Expo (ICME)*, 2018.

[9] R. O Duda V. R Algazi and D. M. Thompson, "The cipic hrtf database," *IEEE Workshop on the Applications of Signal Processing to Audio and Acoustics*, pp. 99–102, 2001.

[10] L. Ray K. J. Fink, "Individualization of head related transfer functions using principal component analysis," *Applied Acoustics*, vol. 87, pp. 162–173, 2015.

[11] D. Florencio F. Grijalva and S. Goldenstein, "A manifold learning approach for personalizing hrtfs from anthropometric features," *IEEE/ACM Transactions audio, speech, and language processin*, vol. 24, pp. 559–570, 2016.

[12] M. Zhang, Z. Ge, T. Liu, X. Wu, and T. Qu, "Modeling of individual hrtfs based on spatial principal component analysis," *IEEE/ACM Transactions on Audio, Speech, and Language Processing*, vol. 28, pp. 785–797, 2020.

[13] Saif S. Alotaibi and Mark Wickert, "Modeling of individual head-related transfer functions (hrtfs) based on spatiotemporal and anthropometric features using deep neural networks," *IEEE Access*, vol. 12, pp. 14620–14635, 2024.

[14] G. Plenge, "On the differences between localization and lateralization," *Journal of the Acoustical Society of America*, vol. 56, pp. 944–951, 1974.

[15] J. Blauert, "Spatial hearing the psychophysics of human sound localization," *MIT Press, 2nd enlarged edition. Harvard, MA, USA*, 1997.

[16] A. Ganguly, C. Reddy, Y. Hao, and I. Panahi, "Improving sound localization for hearing aid devices using smartphone assisted technology," *IEEE International Workshop on Signal Processing Systems*, p. 165–170, 2016.

[17] J. M. Kates and K. H. Arehart, "Improving auditory externalization for hearing-aid remote microphones," *51st Asilomar Conference on Signals, Systems, and Computers*, p. 1895–1899, 2017.

[18] Z. Tan M. Farmani, M. S. Pedersen and J. Jensen, "Informed sound source localization using relative transfer functions for hearing aid applications," *IEEE/ACM Transactions on Audio, Speech, and Language Processing*, vol. 25, pp. 611–623, 2017.

[19] H. Nakashima, R. Kouyama, N. Hiruma, and Y. Fujisaka, "Binaural wind noise cancellation for hearing aids based on head-related transfer function cues," *The Acoustical Society of Japan (Acoust. Sci. and Tech.)*, vol. 39, pp. 40–43, 2018.

[20] M. Wickert, "A real-time 3d audio simulator for cognitive hearing science," *Proceedings of the 18th Python in Science Conference*, pp. 77–84, July 2019.

[21] Saif S. Alotaibi and Mark Wickert, "Itd modeling based on anthropometrics and kemar coefficients using deep neural networks," *2019 IEEE Global Conference on Signal and Information Processing*, pp. 1–5, 2019.

[22] D. Rumelhart, G. Hinton, and R. Williams, "Learning representations by backpropagating errors," *Nature*, vol. 323, pp. 533–536, 1986.

[23] R. O R. S Woodworth and H. Schlosberg, "Experimental psychology," *Holt, Rinehard, and Winston, NY*, pp. 348–361, 1962.

Vibroacoustic Study of Tonewood and Solid-body Guitar

Khemapat Tontiwattanakul
Sound and Vibration Engineering Research Group,
Department of Mechanical and Aerospace Engineering, Faculty of Engineering,
King Mongkut's University of Technology North Bangkok
Bangkok, Thailand
khemapat.t@eng.kmutnb.ac.th

***Abstract*—Vibroacoustic is a study of relation between the excitation force to a structure and the sound radiation produced by the vibration of the structure. In this work, mechanical properties, e.g. Young's modulus and damping loss factor, of three types of tonewood were measured via vibration testing. The vibration and acoustic response of solid-body guitars were measured. The loss factor of the guitar bodies were discussed.**

Keywords— tonewood, vibroacoustic, damping measurement, thin plate

I. Introduction

Tonewood is a group of wood that is specifically used for musical instruments, especially string instrument. This is not only due the aesthetics but also the mechanical properties of the tonewood enhance the sound of the instrument. Selecting suitable tonewood for specific musical instruments requires vast experiences and craftmanship of luthier. However, the property of tonewood is also of interest to acoustic and vibration researchers. Modal analysis is a widely used method to investigate the character of musical instruments by mean of frequency response function [1-4].

Vibroacoustic is a study of relation between the sound radiation produced by the vibration of a structure. Acoustic holography is given as an example of the application of vibroacoustic [5-8]. Acoustic holography is generally used as sound source localisation. However, there are only a few studies applying this technique to study musical instruments.

Although, there are some studies focusing on sound and vibration of musical instruments, a very small number of studies have paid attention to the solid-body instruments. This paper presents an application of modal testing and vibro-acoustic to investigate the properties of tonewood that affect the sound signature of solid-body guitar. Three types of tonewood such as mahogany, ash, and alder are prepared in rectangular shape and considered as the control samples. Vibration and acoustic frequency response function (FRF) produced from two types of guitar body such as Stratocaster (ST) and Les Paul (LP) made of the three types of tonewood are measured and discussed.

II. Theoretical Background

A. Thin plate vibration

In this work, rectangular tonewood samples were considered as thin plate. The vibration of a thin plate can be determined by differential equation given by

$$D\nabla^2\nabla^2 w = -2\rho h\ddot{w}, \tag{1}$$

where w is the displacement of vibration, ρ is the density, h is the thickness of the plate, and D is the bending rigidity of the thin plate defined as

$$D = \frac{Eh^3}{12(1-\nu)}, \tag{2}$$

where ν is Poisson's ratio, and E is Young's modulus.

By applying Fourier method, let's

$$w(x,y,t) = W(x,y)T(t), \tag{3}$$

where W is the shape function and T is the time harmonic function. Substituting (3) into (1), yields

$$\frac{D}{2\rho hW}\left[\frac{\partial^4 W}{\partial x^4} + 2\frac{\partial^4 W}{\partial x^2 \partial y^2} + \frac{\partial^4 W}{\partial y^4}\right] = -\frac{1}{T}\frac{d^2T}{dt^2}, \tag{4}$$

By equating the RHS and LHS of (4) to ω_r^2. Thus,

$$T(t) = Ae^{i\omega_r t} + Be^{-i\omega_r t}, \tag{5}$$

$$\frac{\partial^4 W}{\partial x^4} + 2\frac{\partial^4 W}{\partial x^2 \partial y^2} + \frac{\partial^4 W}{\partial y^4} = \frac{2\rho h\omega_r^2}{D}W. \tag{6}$$

Equation (6) is known as a biharmonic eigenvalue problem. In case of free-free-free-free boundary condition, the shape function in general form is given by

$$W_{mn}(x,y) = \cos\frac{m\pi x}{a}\cos\frac{n\pi y}{b}, \tag{7}$$

where a is the width, b is the length of the rectangle, and m and n are the number of nodal lines along x and y-axis, respectively.

By substituting (7) into (6), natural frequencies of a plate is found infinite and given by

$$f_{nm} = \frac{1}{2\pi}\left(\frac{m^2}{a^2} + \frac{n^2}{b^2}\right)\sqrt{\frac{D\pi^4}{2\rho h}}, \tag{8}$$

Note that when the density, the dimension, and Poisson's ratio of the plate is given then the Young's modulus can be calculated.

B. Estimation of damping loss factor

Damping loss factor η (or loss factor) is a crucial factor since it can be used to indicate the sustain of the sound of the instruments generated from structural vibration. Smaller loss factor tends to allow for longer sustain sound. Loss factor can be measured by performing impact test. In this work, it was calculated by peak-pickup method as suggested in ASTM E756.

979-8-3315-4248-1/25/$31.00 ©2025 IEEE

The accelerance FRF $\alpha(\omega)$ can be obtained via impact test. It is defined as

$$\alpha(\omega) = \frac{A(\omega)}{F(\omega)}, \tag{9}$$

where $A(\omega)$ and $F(\omega)$ is the FFT of acceleration signal and force signal, respectively. The magnitude of the accelerance FRF at a resonance frequency ω_r is defined as $|\alpha(\omega_r)|$. The half-power frequency ω_a and ω_b, which is the frequencies that the magnitude of FRF equals to $|\alpha(\omega_r)|/\sqrt{2}$, is defined as shown in Fig. 1.

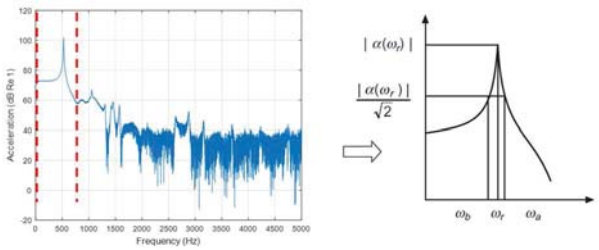


Fig. 1. Definition of the half-power frequencies ω_a and ω_b

Once all required frequencies are identified, the damping loss factor can be computed by

$$\eta = \frac{\omega_a - \omega_b}{\omega_r}. \tag{10}$$

C. Vibroacoustic transfer function

The FRF of a mechanical vibratory system can be extended to vibroacoustic transfer function by taking into account the acoustic impedance. The block diagram shown in Fig. 2 illustrates that the vibroacoustic FRF can be formulated by connecting the mobility FRF to the specific acoustic impedance.

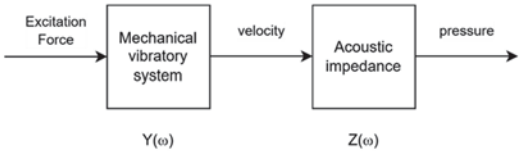


Fig. 2. Vibroacoustic FRF

The mobility FRF $Y(\omega)$ and specific acoustic impedance $Z(\omega)$ can be written as (11) and (12), respectively.

$$Y(\omega) = \frac{v(\omega)}{F(\omega)} = \frac{j\omega}{k - \omega^2 m + j\omega c}, \tag{11}$$

$$Z(\omega) = \frac{p(\omega)}{v(\omega)}, \tag{12}$$

where m, c, k are mass, damping coefficient, and stiffness of mechanical system. p indicates the acoustic pressure, v indicates the particle velocity which is also the normal velocity of the vibrating surface of the acoustic source, F is the excitation force, and ω is the excitation frequency.

Thus, vibroacoustic FRF $G(\omega)$ can be given by

$$G(\omega) = \frac{p(\omega)}{F(\omega)} = \left[\frac{j\omega}{k - \omega^2 m + j\omega c}\right] Z(\omega). \tag{13}$$

In theory, the specific acoustic impedance can be derived for conventional radiation problems such as sound radiation from the vibration of a plate, a cylindrical radiator, a spherical radiator, etc. However, it is difficult to obtain specific acoustic impedances for the problems of sound radiation from any unconventional shape.

III. Experiment and Results

A. Experimental setup and data processing

An experiment was setup in order to estimate the damping ratio. The equipment required in the experiment consist of an impact hammer (PCB 086C03), an accelerometer (B&K Type 4507B), data acquisition module (NI USB-4431), and a computer with MATLAB software. A program script was written to operate the signal capturing and to perform signal processing. The equipment setup is shown in Fig.3.

In a test, the signals from the accelerometer and the impact hammer were recorded and then the accelerance FRF, which is defined in (9), were calculated. The damping loss factors were calculated from (10). The test was repeated 3 times for each wood sample to ensure the repeatability of the test. The averaged values are then used for discussion.

In this work, the test was conducted for two cases: 1) to the three types of tonewood in rectangular shape and 2) to the guitar body in the shape of Stratocaster (ST) and Les Paul (LP). The ST and LP guitar body are made of the three types tonewood thus results in six variation of specimen.



Fig. 3. Equipment setup

B. Tonewood in rectangular shape

The three types of tone wood were cut into rectangular shape with the dimension of 0.350 m × 0.400 m × 0.045 m, which provides the volume of 0.0063 m^3. The mass of the specimens were measured and the density was calculated and given in Table 1.

In the test, an accelerometer was placed at the most top-left conner of the specimen. The impact hammer excitation was performed at 4 different positions as shown in Fig. 4. The FRF and the loss factors were calculated. The Young's modulus of the tonewoods are also calculated using (2) and (8). The Young's modulus obtained from the test were used to calculate the natural frequency in FEM software. This is to study the accuracy of the thin plate model. The results are shown in Table I. The value of Young's modulus can be ranked from low to high by Mahogany, Alder, and Ash,

respectively. It can be seen that the deviation between the measured and the calculated (FEM) natural frequency is around 22%.

TABLE I. YOUNG'S MODULUS AND NATRUAL FREQUENCY OF THE TONEWOOD SAMPLES

Type of tonewood	Young's Modulus and Natural frequency				
	Density (kg/m^3)	*Measured E (GPa)*	*Measured f_n (Hz)*	*FEM f_n (Hz)*	*Deviation of f_n (%)*
Mahogany	396.8	0.86	366.1	285.1	22.1
Alder	571.4	1.17	355.3	277.1	22.0
Ash	739.7	1.88	395.8	308.7	22.0

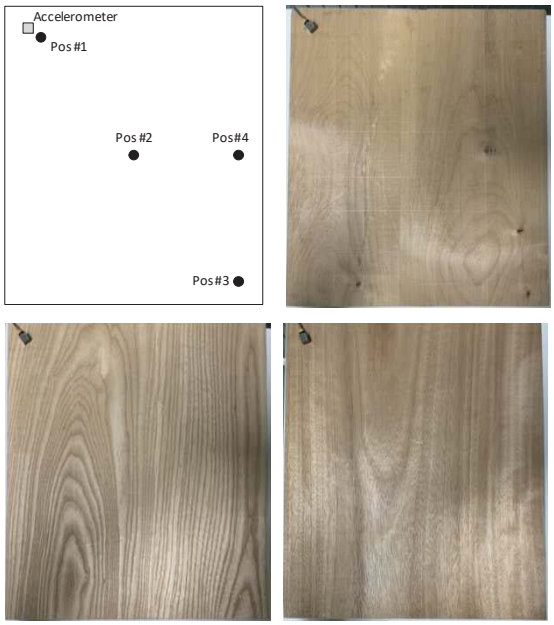


Fig. 4. Accelerometer and hammering positions (top left), Alder sample (top right), Ash sampe (bottom left), and Mahogany sample (bottom right)

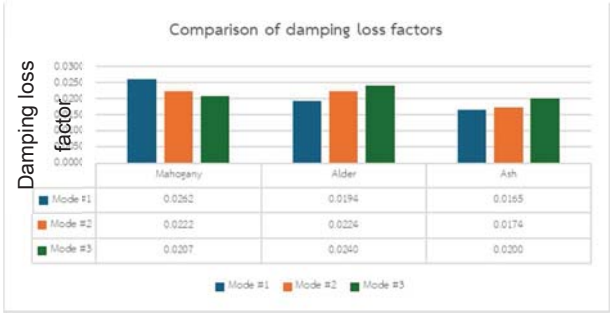


Fig. 5. Damping loss factor of rectangular woods

The data in Fig. 5 shows that the damping loss factor of the first three modes ranked (on averaged) from high to low as follows: Mahogany, Alder, and Ash respectively. It can be seen that Mahogany tend to have highest loss factor among others.

C. *Tonewood as guitar body*

In this part, six variation of guitar bodies made from the three different tonewood and in two different shapes (ST and LP) are tested. It should be noted that the guitar bodies prepared for this work are not ideal as they were built from multiple pieces of the same type of wood and glued together rather than by a single piece of wood. Especially for LP, the top side of the body is glued to the decorative veneer wood. Using glue in the production process can lead to some effect on sound and vibration response of the guitar.



Fig. 6. Microphone position for stratocaster (left) and Les Paul (right)



Fig. 7. Accelerometer and hammering positions for stratocaster (left) and Les Paul (right).

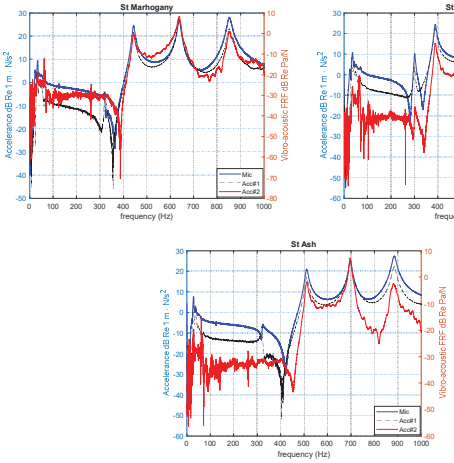


Fig. 8. FRF of ST guitar body with different types of tonewood

In a test, an accelerometer was placed as close as possible to the bridge of the guitar specimens. A measurement microphone (B&K Type 4942) was placed around 25 mm right above the centre of the bridge as shown in Fig. 6 in order to capture radiated sound generated during the impact test. The impact hammer was used to excite the guitar body at 5 different positions as shown in Fig. 7 where M denotes the microphone position, A1 denotes the accelerometer position, and H1 – H5 denotes the hammer excitation position. Similarly to the previous section, accelerance FRF and acoustic FRF were calculated and shown in Fig. 8 and Fig. 9 for ST and LP, respectively. The natural frequency of the first four modes are identified, the relative standard deviation (RSD) is calculated and listed in Table II given by

$$\%RSD = 100 \times \frac{\sigma}{\mu}, \tag{14}$$

where σ is the standard deviation, and μ is the mean value. The loss factor were also calculated and the results are shown in Fig. 10.

The test results shown in Fig. 8 illustrates that the four natural frequencies of the ST guitars can be clearly identified. The acoustic responses and vibration responses are in good agreement for all different types of tonewood.

From the test results in Fig. 9, only two natural frequencies of the LP guitars can be identified. The acoustic response and vibration response are in good agreement only for Mahogany but lag of coherence for Alder and Ash.

The RSD value in Table II suggested that the natural frequency of LP and ST guitars are not significantly different regardless of the types of tonewood. However Fig. 10 shows that the magnitude of the loss factor change drastically in comparison to the tonewood in rectangular shape.

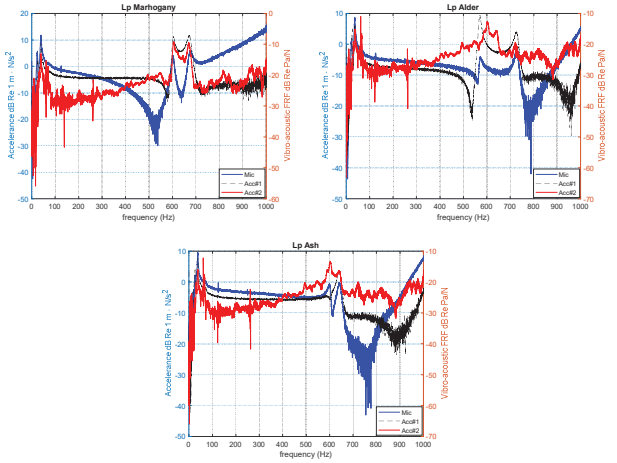


Fig. 9. FRF of LP guitar body with different types of tonewood

TABLE II. NATURAL FREQUENCY OF THE FIRST FOUR MODES

Specimen	Natural frequency (Hz)			
	f_1	f_2	f_3	f_4
LP Mahogany	39.0	604.2	N.A.	N.A.
LP Alder	36.6	572.4	N.A.	N.A.
LP Ash	37.6	600.8	N.A.	N.A.
RSD (among LP)	3.2%	2.9%	N.A.	N.A.
ST Mahogany	321.0	442.6	638.2	851.2
ST Alder	301.0	338.4	617.8	845.0
ST Ash	321.2	510.4	697.8	884.2
RSD (among ST)	3.7%	13.6%	6.4%	2.4%

IV. DISCUSSION AND CONCLUSION

The thin plate model can be used to estimate the Young's modulus of the tonewoods with the accuracy up to a certain degree. The Young's modulus can then be used to create FEM model for musical instrument design.

The damping loss factor of the tonewoods were measured. Mahogany tend to have highest loss factor among the others. Fig. 5 suggested that the loss factor of the first three modes ranked from high to low. This implies that Mahogany tend to sustain the high frequencies. Conversely, the loss factor of the first three mode ranked from low to high for Alder and Ash. This means that the two tend to sustain at the low frequencies. The results imply that the sound of Mahogany is more dull than the other two.

RSD suggested that there is natural frequency of LP and ST are not significantly different regardless of the types of tonewood. The reason could come from the use of glue in the production. The damping loss factor tend to be higher in comparison to the tonewood in rectangular shape, which is considered as control specimen.

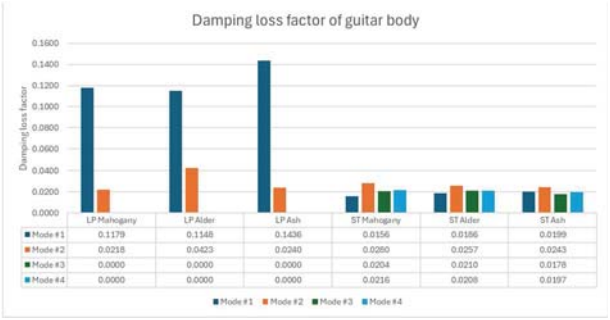


Fig. 10. Damping loss factor of guitar body made of different types of tonewood

The vibroacoustic FRF have a good agreement with the vibration FRF for ST shape. However, only Mahogany express an agreement for the LP shape. This could come from the fact that the use of glue for LP shape body results in high degree of damping loss factor. This results in the quick decay of the vibration response and low sound radiation efficiency. This could be a point of future study.

The limitation of this research is that the number of specimen is small thus the conclusion about the consistency of the production cannot be discussed. Another weak point is that the glue was used in the production of guitar bodies. The property of guitar produced with single piece of wood will be a future study.

ACKNOWLEDGMENT

This research is funded by Faculty of Engineering, King Mongkut's University of Technology North Bangkok.

REFERENCES

[1] H. Mansour, "Modal Analysis of the Setar: A Numerical--Experimental Comparison," J. Vib. Acoust., vol. 137, no. 6, p. 61006, 2015.

[2] H. Mansour, G. Scavone, and V. Freour, "A comparison of vibration analysis techniques applied to the Persian setar," in Acoustics 2012, 2012.

[3] O. Inácio, F. Santiago, and P. C. Cabral, "The Portuguese Guitar Acoustics : Part 1 – Vibroacoustic Measurements," in Acustica, 2004, p. paper 187, pp 1–8.

[4] F. Santiago, O. Inácio, and P. Caldeira Cabral, "The Portuguese Guitar Acoustics : Part 2 – Subjective Acoustical Quality Evaluation," in Acustica 2004, 2004, p. paper 188, pp 1–8.

[5] M. Ahmed, K. Y. Wang, and a. F. Metherell, "Holography and its application to acoustic imaging," Proc. IEEE, vol. 67, no. 4, 1979.

[6] W. A. Veronesi, "Nearfield acoustic holography (NAH) II. Holographic reconstruction algorithms and computer implementation," J. Acoust. Soc. Am., vol. 81, no. 5, p. 1307, 1987.

[7] S. I. Hayek, "Nearfield Acoustical Holography," Springer Handb. Acoust., pp. 1129–1139, 2007.

[8] J. D. Maynard, E. G. Williams, and Y. Lee, "Nearfield Acoustic Holography: I - Theory of Generalized Holography and the Development of NAH," J. Acoust. Soc. Am., vol. 78, no. 4, pp. 1395–1413, 1985.

Design and build of a multi-zone beamforming speaker

Khemapat Tontiwattanakul
Sound and Vibration Engineering Research Group, Department of Mechanical and Aerospace Engineering
King Mongkut's University of Technology North Bangkok
Bangkok, Thailand
khemapat.t@eng.kmutnb.ac.th

Jiraphat Sueprasert
Institute of Music, Science, and Engineering
King Mongkut's Institute of Technology Ladkrabang
Bangkok, Thailand
Jiraphat239@hotmail.com

Dech Nawik
Institute of Music, Science, and Engineering
King Mongkut's Institute of Technology Ladkrabang
Bangkok, Thailand
Dechza03@gmail.com

Pitak Thumwarin
Institute of Music, Science, and Engineering
King Mongkut's Institute of Technology Ladkrabang
Bangkok, Thailand
pitak.th@kmitl.ac.th

Nachanant Chitanont
Institute of Music, Science, and Engineering
King Mongkut's Institute of Technology Ladkrabang
Bangkok, Thailand
nachanant.ch@kmitl.ac.th

***Abstract*—Recently, beamforming speaker for multi-zone sound production is an application that is of interest such as conference system, public address, home cinema, and gaming. This paper presents a design of a speaker array and DS beamforming aiming to use for product advertising such that the speaker can be installed on the shelf. The limit of the space and the usable frequency range are the challenges of this work. The design of the speaker cabinet and the beamforming algorithm will be discussed.**

Keywords—acoustic beamforming, loudspeaker array, Delay & Sum beamforming, loudspeaker design

I. Introduction

Audio beamforming is a technology that is applied to many applications such as conference systems, public address, concert halls, home cinemas, and gaming. The aim of audio beamforming is to focus the produced sound on some specific areas.

Many techniques are proposed to achieve the multi-zone sound production such as least-squares error, the energy difference method, and energy contrast method [1-4]. Recently, a thesis authored by Jonas Bredgaard Köhne and Mikkel Solhaug Seindal presents a technique to use subarray to create personal sound zones [5]. However, the performance of a simple DS beamforming for a specific application seems not to be of interest.

This paper presents a design of a beamforming speaker, that is suitable to use for some application. The beamforming speaker consists of an array of speakers working with DS beamforming to produce three different sounds in three zones. The formulation of DS beamformer is presented. The frequency range of the array is determined. The design procedure to obtain the size of the cabinet is presented. Lastly, an experiment was conducted to validate the performance of the array.

II. Delay and Sum Beamforming

Let's consider a sound field generated by a monopole source. The mathematical description is given by

$$p(r) = i\omega\rho_0 q \frac{e^{-ikr}}{4\pi r} \tag{1}$$

where ω is the angular frequency of the wave, ρ_0 is the density of the air, q is the acoustic strength or volume velocity of the source, k is the wavenumber, and r is the distance from the source centre. It should be noted that the time convention $e^{i\omega t}$ is used throughout this paper.

Let's a position vector $\mathbf{x} = x\hat{i} + y\hat{j}$ points to the position (x, y) on a Cartesian coordinate. By assuming that the array consists of M drivers. The *m-th* acoustic source noted by S_m locates at position (x_m, y_m). The sound field p_m evaluated at any position $\mathbf{x}$ can be given by

$$p_m(\mathbf{x}) = i\omega\rho_0 q \frac{e^{-ik\sqrt{(x-x_m)^2+(y-y_m)^2}}}{4\pi\sqrt{(x-x_m)^2+(y-y_m)^2}}, \tag{2}$$

For a speaker array such that its drivers are located only on the x-axis, the coordinate y_m can be assigned to zero. Thus, Eq (2) can be written as

$$p_m(\mathbf{x}) = i\omega\rho_0 q \frac{e^{ik\tilde{r}_m}}{4\pi\tilde{r}_m}, \tag{3}$$

where $\tilde{r}_m = \sqrt{(x-x_m)^2 + y^2}$.

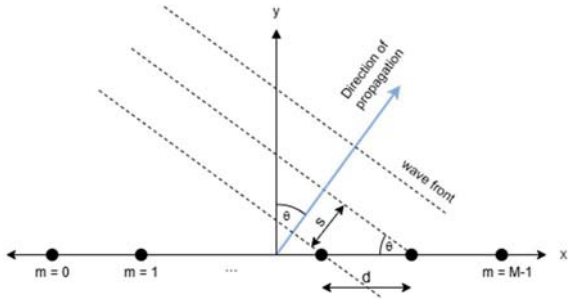


Fig. 1. Formulation of Delay and Sum beamforming

DS beamforming can be realised by applying the weight function to the speaker signal. By considering Fig. 1, let's d indicates the separation distance between the speaker drivers, and θ indicates the steering angle. The distance between the

979-8-3315-4248-1/25/$31.00©2025 IEEE

two consecutive wavefronts *s*, and the delay time τ can be calculated by

$$s = d\sin\theta = c_0\tau, \tag{4}$$

$$\tau = \frac{d\sin\theta}{c_0}. \tag{5}$$

The weighting w_m to applied to the *m-th* driver can be given by

$$w_m = e^{-im\omega\tau}. \tag{6}$$

Given that the *M* drivers are populated equally along the y-axis, the beamforming output $z(\mathbf{x})$ can be given by

$$z(\mathbf{x}) = \sum_{m=0}^{M-1} w_m p_m(\mathbf{x}). \tag{7}$$

In this work, a loudspeaker array was designed to be able to produce up to three different sounds into three different zones. The sound field of the three separate zones can be produced by superposing the beamforming output with three different steering angles given by

$$z_{3zone}(\mathbf{x}) = \sum_{k=1}^{3}\sum_{m=0}^{M-1} w_{m,k} p_m(\mathbf{x}), \tag{8}$$

where $w_{m,k}$ is the weighting to be applied to the sound signal in order to steer to *k-th* direction. In this work, the three steering angles are -60°, 0°, and 60°, which is corresponding to k = 1,2, and 3, respectively.

III. Design Constrains

The bandwidth of the speaker array is chosen based on the following information

1) Types of sound that the array will be used for

Main application of the array designed in this work is for advertisement and announcement. As suggested by ITU-T, the frequency range of the sound lies between 300 Hz to 3,400 Hz [6].

2) The dimensions & specifications of the speaker driver

Eight units of FRS-5 speaker driver made by VISATON are used in this work. The driver is a 2" full range speaker which is suitable for music and speech applications. The technical specifications of FRS-5 is given in TABLE I. The starting frequency that the driver should be used efficiently is about twice the resonance frequency or at around 500 Hz.

TABLE I. Technical Data of FRS-5

Parameters	***Symbols***	***Specification***
Rated power	-	5 W
Nominal impedance	Z	8 Ohm
Frequency response	-	150 – 20,000 Hz
Mean sound pressure level	-	84 dB (1 W/ 1 m)
Resonance frequency	f_s	270 Hz
Total Q-factor	Q_{ts}	1.15
Equivalent volume	V_{as}	0.16 Litre

3) The dimension of the array.

The low frequency limit of the array can be determined. The wavelength of the low frequency limit should not be greater than one-tenth of the array's length. Thus

$$f_{lower} = {c_0}\big/{10\times d\times(M-1)}, \tag{9}$$

By substituting the parameters into (9), the $f_{lower} \approx 100$ Hz.

The high frequency limit of the array is controlled by the separation between the two drivers. In this case, the distance d equal to 52.5 mm. Thus, the high frequency limit is

$$f_{upper} = {c_0}\big/{2\times d}. \tag{10}$$

By a calculation using Eq (10), this yields $f_{upper} \approx 3{,}500$ Hz.

Although, the suitable frequency range that the array has optimal performance by mean of the geometry is between 100 – 3,500 Hz. However, when the other two constrains are taken into account then the frequency range of the array that to be targeted will be between 250 – 3,500 Hz.

IV. Design of The Array Geometry



Fig. 2. FRS-5 driver and the cabinet

A. Cabinet design

In this work, sealed-box system is introduced for cabinet design [7, 8].

$$\frac{Q_{tc}}{Q_{ts}} = \frac{f_c}{f_s} = \sqrt{1+\frac{V_{as}}{V_{ab}}}, \tag{11}$$

where Q_{tc} is the Q-factor defining total driver and cabinet losses at the resonance frequency of the closed box system f_c, Q_{ts} is the Q-factor defining total driver losses at the resonance frequency of unenclosed driver f_s, V_{as} is the equivalent volume of the speaker, and V_{ab} is the acoustic volume of the cabinet. In practice, Q_{ts}, f_s, and V_{as} can be obtained from the driver datasheet. The proper selection of Q_{ts}, and f_s is required to obtain the optimised volume of the cabinet.

The frequency response function of the sealed-box system $G(j\omega)$ is given by

$$G(j\omega) = \frac{\omega^2 T_c^2}{(\omega^2 T_c^2 - 1) - i\omega T_c / Q_{tc}}. \tag{12}$$

By rearranging (12) and substituting the amplitude ratio $\eta = \omega/\omega_c$, this yields

$$G(j\omega) = \frac{\eta^2}{(\eta^2 - 1) - i\eta / Q_{tc}}. \tag{13}$$

The value of Q_{tc} is then varied, the magnitude of the closed-box system is then plotted as shown in Fig. 3. It can be seen that the optimal value of Q_{tc} is 0.707 since the flat FRF can be obtained. However, Q_{tc} at 0.707 is not always selectable. This will be discussed in the following.

By referring to the driver specification as shown in Table I, f_s is 270 Hz, and Q_{ts} is 1.15. The volume of the cabinet can be calculated by rearranging Eq (*11*) into

$$V_{ab} = \frac{V_{as}}{\left(\frac{Q_{tc}}{Q_{ts}}\right)^2 - 1}. \tag{14}$$

By varying the value of Q_{tc}, V_{ab} can be calculated using Eq. (*14*) and are listed in Table II. It can be seen that the optimal Q_{tc} give the negative volume of V_{ab}, which is not realisable. Thus Q_{tc} = 1.414 is chosen and this results the acoustic volume V_{ab} at 0.6970 Litre.

TABLE II. VALUE OF Q_{tc} VS V_{ab}

Q_{tc}	V_{ab} (Litre)
0.500	-0.1973
0.707	-0.2572
1.000	-0.6561
1.414	0.3126
2.000	0.0790

Once the acoustic volume is obtained then the golden ratio was applied to determine the dimension of the cabinet. The dimension of the FRS-5 is also taken into consideration. The results draw the dimension to 61 mm of width, 51 mm of depth, and 101 mm of height for each cabinet. This results in 542 mm of the total width of the array. The CAD data is produced and shown in Fig. 2. The manufactured speaker is shown in Fig. 3. Some absorption material are filled into the cabinet in order to absorb the acoustic pressure generated from the loudspeaker on the rear side.

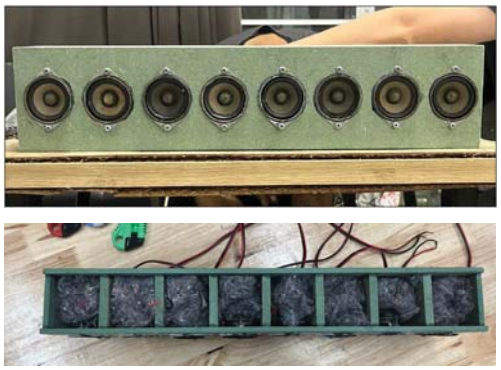


Fig. 3. Beamforming speaker in this work

V. NUMERICAL SIMULATION

The beampattern of the array is calculated in the frequency range between 250 Hz to 4,000 Hz by Eq (7) and shown in Fig 4, 5, and 6. In the plot, there are three separate zones such as -90° to -30°, -30° to 30°, and 30° to 90° to take into account. Fig. 4 suggests that the beamwidth of the beamforming output from 1,000 Hz mostly contained in the 60° range at the 5dB reduction. The reduction at around 1.5 dB is provided for 500 Hz and less than 1 dB reduction is provided for 250 Hz.

Fig.5 shows the comparison between beampatterns steered into three directions at different frequencies. It also can be seen that the beamformer create dark-zone (defined by black dotted contour) with attenuation more than 3 dB for the frequencies from 1,000 Hz or above. The dark-zone effect is weak for the frequency below 500 Hz.

Fig. 6 shows that the aliasing happens at the frequency around 4,000 Hz or above, although the beam to 0° has a very strong focus but when the big side lobe shows up when the beam steered to 60°.

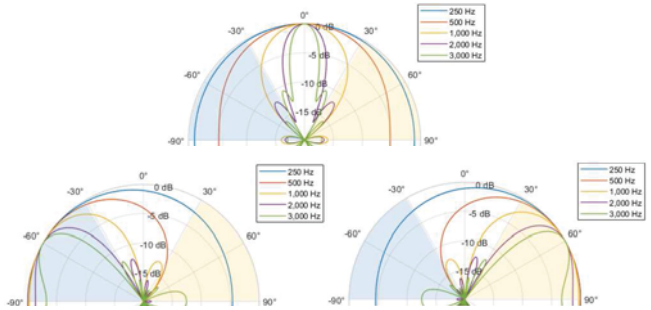


Fig. 4. Steered beampattern to 0° (Top), -60° (Bottom Left) and 60° (Bottom Right)

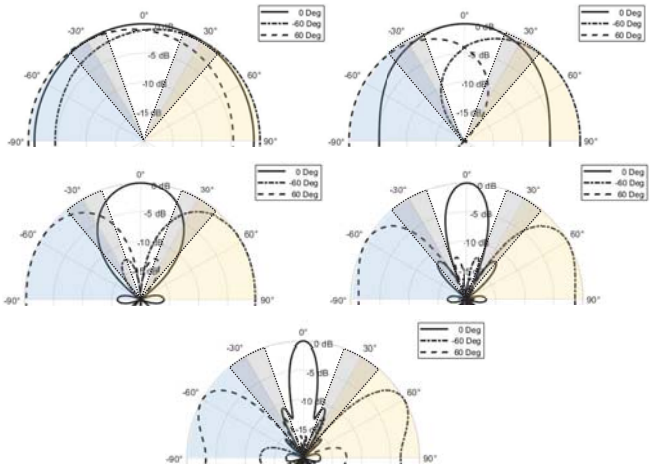


Fig. 5. Beampattern steered to 0°, -60°, and 60° overlayed plot at 250 Hz (Top Left), 500 Hz (Top Right), 1,000 Hz (Mid Left), 2,000 Hz (Mid- Right), and 3,000 Hz (Bottom)

VI. EXPERIMENT

An experiment was setup to validate the performance of the array. Fig. 7 shows the connection diagram of the equipment. TASCAM US-16x08 is used as audio interface. An in-house multichannel amplifier was built to drive the speaker drivers.

White noise was presented to the speaker drivers through the audio interface and the power amplifier. The sample rate used for sound production is 96 kHz. In practice, Eq (6) can be implemented by shifting the samples of the sound data. Full sample delay is introduced and can be calculated by

$$N_D = \left\lceil \frac{f_{sample} d \sin\theta}{c_0} \right\rceil. \tag{15}$$

By substituting the required parameters into (15), the number of samples to steer the beam to $\pm 60°$ is 13 sample points.

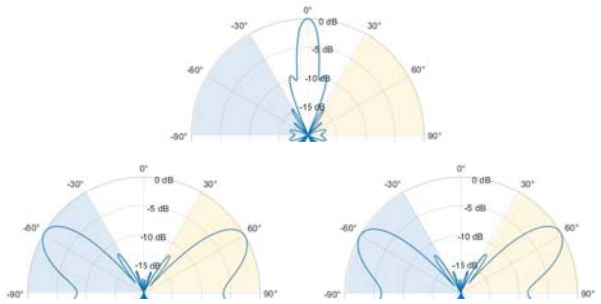


Fig. 6. Beampattern steered to 0° (Top), -60° (Bottom Left) , and 60° (Bottom Right) at 4,000 Hz

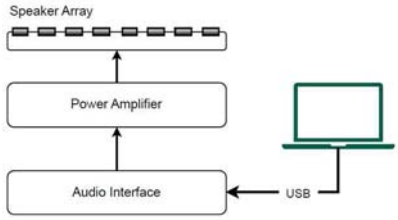


Fig. 7. Connection diagram

The measurement was set as shown in Fig. 8. Sound level meter NTI-XL2 was used to measure the sound produced by the array at the distance of 1 meter away from the array. There were 36 measurement points with 10° separation along the circumference of a reference circle the array. Sound level meter was place 1 meter away from the array and 1.2 m above the surface as the same high as the array. The sound pressure level was measured in 1/1 Octave frequencies. Fig. 9 depicts the measurement setup. The measurement took place outside the building for free-field condition.

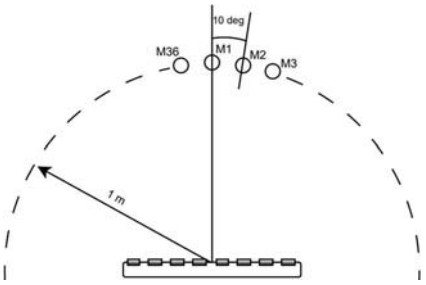


Fig. 8. Arrangement of the measurement positions

The SPL in 1/1 Octave of the frequency between 250 Hz to 4,000 Hz are measured. The beampatterns of each octave band are plotted as shown in Fig. 10. The performance of the array is indicated by the directivity index (DI) given by

$$DI = 10\log_{10}\left(\frac{p_{ax}}{p_{avg}}\right)^2. \qquad (16)$$

The directivity index was calculated and listed in TABLE III.

TABLE III. DIRECTIVITY INDEX OF THE BEAMFORMING STEERED TO DIFFERENT ANGLES

Frequency / *DI (dB)*	*250 Hz*	*500 Hz*	*1,000 Hz*	*2,000 Hz*	*4,000 Hz*
steered to -60°	1.6	5.1	6.0	6.7	6.1
steered to 0°	1.6	3.9	5.9	6.5	7.3
steered to 60°	0.6	2.5	5.6	6.7	6.3



Fig. 9. Measurement setup

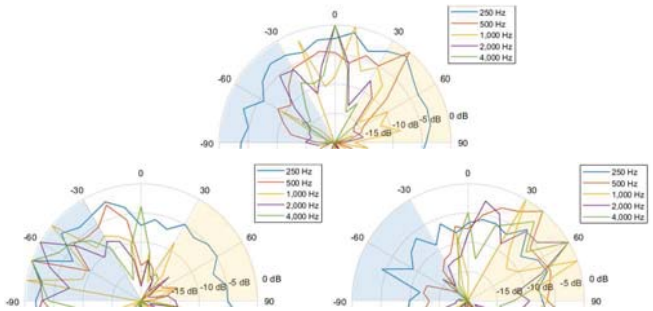


Fig. 10. The measured beampattern of the array at different frequencies when the beam is steered to to 0° (Top), -60° (Bottom Left) and 60° (Bottom Right)

Fig. 10 shows the good agreement between the measurement and the simulation. There are the reduction of the beam from the frequencies from 1,000 Hz or above. The reduction is less for the frequency below 1,000 Hz. The beamforming was also applied to three different sounds. It was found that the clear separation of the three sound can be perceived.

VII. CONCLUSION

The paper present a design of beamforming speaker for advertising. It was shown that the experiment results are in a good agreement to the numerical simulation. Three different sounds was presented in three different directions and the dark-zones can be perceived.

REFERENCES

[1] J.-W. Choi and Y.-H. Kim, "Generation of an acoustically bright zone with an illuminated region using multiple sources," *J Acoust Soc Am*, vol. 111, no. 4, 2002, doi: 10.1121/1.1456926.

[2] M. Shin *et al.*, "Maximization of acoustic energy difference between two spaces," *J Acoust Soc Am*, vol. 128, no. 1, 2010, doi: 10.1121/1.3438479.

[3] F. Olivieri, M. Shin, F. M. Fazi, P. A. Nelson, and P. Otto, "Loudspeaker array processing for multi-zone audio reproduction based on analytical and measured electroacoustical transfer functions," in *Proceedings of the AES International Conference*, 2013.

[4] T. Okamoto, "Analytical methods of generating multiple sound zones for open and baffled circular loudspeaker arrays," in *2015 IEEE Workshop on Applications of Signal Processing to Audio and Acoustics, WASPAA 2015*, 2015. doi: 10.1109/WASPAA.2015.7336920.

[5] J. B. Köhne and M. S. Seindal, "Investigation of personal sound zones by use of subarray division," Master's thesis, Aalborg University, 2020.

[6] R. V. Cox, S. F. De Campos Neto, C. Lamblin, and M. H. Sherif, "ITU-T coders for wideband, superwideband, and fullband speech communication," 2009. doi: 10.1109/MCOM.2009.5273816.

[7] R. H. Small, "Closed-Box Loudspeaker Systems-Part 1 : Analysis," *Journal of the Audio Engineering Society*, vol. 20, no. 10, 1972.

[8] R. H. Small, "Closed-Box Loudspeaker Systems-Part 2 : Synthesis.," *Journal of the Audio Engineering Society*, vol. 21, no. 1, 1973.

Development and Preliminary Evaluation of a Wireless Acoustic Sensor Network for Environmental Noise Monitoring

1st Kittipitch Meesawat
Institute of Music Science and Engineering
King Mongkut's Institute of Technology Ladkrabang
Bangkok, Thailand
kittipitch.me@kmitl.ac.th

2nd Wanut Padee
Office of Digital Technology
Khon Kaen University
Khon Kaen, Thailand
wanut@kku.ac.th

3rd Worakrit Thida
Independent researcher
Bangkok, Thailand
w.worakrit@gmail.com

4th Krittika Lertsawat
ENLAWTHAI Foundation
Bangkok, Thailand
krittikanonoise@gmail.com

5th Sorasak Danworaphong
Institute of Music Science and Engineering
King Mongkut's Institute of Technology Ladkrabang
Bangkok, Thailand
sorasak.da@kmitl.ac.th

***Abstract*—This study presents the development and preliminary evaluation of a wireless acoustic sensor network (WASN) designed for environmental noise monitoring in Thailand. A WASN prototype was developed and deployed at a construction site in Bangkok. The system's performance was evaluated over 240 days, comparing its measurements to a certified Class 1 sound level meter. Preliminary results indicated that the WASN tended to report lower 1 minute A-weighted equivalent continuous sound level values than the Class 1 sound level meter with an average difference of 8 dB. The study also identified key challenges during field deployment, including downtime caused by power loss and Wi-Fi connectivity issues. Future work will focus on addressing these limitations to improve system reliability and measurement accuracy.**

***Index Terms*—noise monitoring, wireless sensor network, construction environment.**

I. Introduction

Noise pollution poses a significant threat to human health and quality of life, leading to various health issues such as stress, hearing loss, and cardiovascular disease, especially with prolonged exposure [1]. Nighttime noise exposure, even at lower levels, can disrupt sleep, increasing the risk of chronic conditions like diabetes and hypertension, and negatively affecting daytime productivity [2]. The economic impact of untreated noise pollution can be substantial at a national level. The World Health Organization (WHO) has recognized the significance of this issue since 1980 [3], publishing guidelines and establishing initiatives like World Hearing Day to raise awareness [4].

Despite Thailand's environmental noise abatement policies since 1975, effective implementation is hindered by a lack of comprehensive noise data. Existing monitoring systems, primarily located along roadsides and in limited areas due to cost constraints, provide an incomplete picture of the noise situation [5]. This necessitates the development of a system capable of wide-area, potentially real-time, noise monitoring with traceable records. A wireless acoustic sensor network (WASN) offers a viable solution for such comprehensive monitoring.

The use of WASNs for environmental noise monitoring has evolved since the mid-2000s, particularly in Europe, driven by directives like the European Environmental Noise Directive 2002/49/EC [6]. Early projects, such as DREAMSys [7], demonstrated the feasibility of real-time monitoring and the use of MEMS microphones, respectively. While these projects have contributed valuable insights, the desire to develop an independent system, allowing for greater control and flexibility in adapting to Thailand's specific needs, necessitated a tailored approach.

This research focuses on the design, implementation, and preliminary testing of a WASN prototype adapted to local requirements. By detailing the practical considerations and technical choices made during our development process, we aim to provide insights into the challenges of deploying such systems in similar contexts. Our emphasis is on the tangible aspects of the prototype's construction and evaluation, highlighting the practical steps taken to address the noise monitoring needs in Thailand.

II. System architecture and design overview

To achieve the goal of wide-area environmental noise monitoring, a WASN was developed. This section details the system architecture and design overview that enable effective and reliable operation in the target environment. The proposed WASN comprises two main components: the sensor nodes and the base station.

The sensor nodes are designed to capture noise, calculate the sound level, and transmit the data to the base station. Key

979-8-3315-4248-1/25/$31.00 © 2025 IEEE

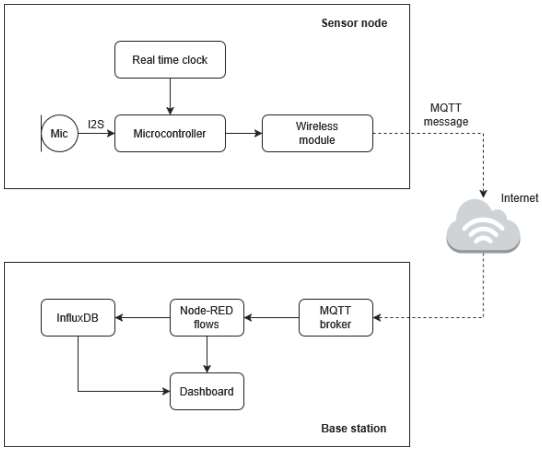


Fig. 1. Block diagram of the proposed Wireless Acoustic Sensor Network (WASN).

design requirements for the sensor nodes include low cost, high mobility, and reasonable longevity.

The base station serves as the central data repository, storing the received sound level time series data for later analysis. It also presents processed data to users through a web-based dashboard. To ensure scalability and efficient data handling, the base station must be capable of receiving and storing data from numerous sensor nodes. Furthermore, the selection of open-source software, driven by its cost-effective nature and community-driven development, was prioritized to enhance accessibility and adaptability.

With these functional requirements in mind, design decisions were made for both the sensor nodes and the base station, as illustrated in the block diagram of the proposed WASN shown in Fig. 1.

III. Prototype Design and Implementation

To validate the proposed WASN architecture, functional prototypes of both the sensor nodes and the base station were developed. This section details the hardware and software implementation of these prototypes, focusing on the key design choices and techniques employed for noise monitoring, data processing and transmission, database integration and data visualization.

A. Sensor node

The node was built around the STM32F411, a 32-bit ARM Cortex-M4 microcontroller, which was chosen for its speed, computational power, and availability of necessary peripherals, e.g., I2S interface and built-in real-time clock. It used a 24-bit I2S MEMS digital microphone for its better signal-to-noise ratio and to minimize the component count. Its sensitivity and bandwidth are -26 dBFS and 60 to 15,000 Hz, respectively. For the initial testing, the sensor node prototypes utilized the existing infrastructure of the test site, employing corded power for continuous operation and Wi-Fi for data transmission. The ESP-01 module, based on the ESP8266, was selected for its cost-effectiveness and adequacy for the task. The built-in real time clock was used to apply a timestamp to the sensor data. The system utilizes an event-driven superloop architecture to manage audio data acquisition and wireless communication.

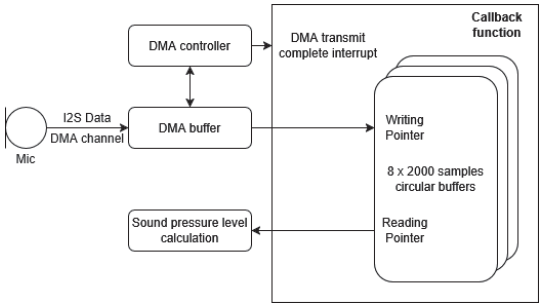


Fig. 2. Conceptual implementation of the DMA driven interrupt I2S microphone.

1) Microphone interface: To minimize timing-related issues during early development, the microphone sampling rate was initially set to $8\,\mathrm{kHz}$. This provided room for processing overhead and facilitated a more manageable testing environment.

The microphone was connected to the microcontroller through an I2S port. Direct Memory Access (DMA) was employed to offload the microcontroller from the task of transferring audio samples, enabling more efficient use of processing resources. Once the DMA data transfer is completed, the Interrupt Service Routine (ISR) calls the callback function to handle the fetched data from the DMA internal buffer to fill in the application circular buffer. The sensor node application in this system employed a circular buffer with distinctive writing and reading pointers. The writing pointer is for fetching data from the DMA buffer, and the reading pointer is for feeding data to sound level calculation. The circular buffer was designed to hold 8 frames of 2000 samples each, providing $0.25\,\mathrm{s}$ long data for each frame. This allows sufficient buffer space during periods of high processing load. This buffer enables asynchronous data processing, and mitigates real-time processing constraints. Fig. 2 depicts the described implementation concept.

2) Sound level calculation: Sound pressure is commonly expressed as A-weighted sound level in decibels (dB), to approximate human hearing. This system measures the A-weighted equivalent continuous sound level, $L_{Aeq,T}$, allowing users to set the integration time, T. In this system, $L_{Aeq,T}$ was calculated with an integration time of $T = 0.125\,\mathrm{s}$ ($L_{Aeq,0.125s}$). The definition of $L_{Aeq,T}$ is given in (1) [8]:

$$L_{Aeq,T} = 10\log_{10}\left[\frac{1}{T}\int_T \left(\frac{p_A(t)}{p_0}\right)^2 dt\right]\ \mathrm{dB} \qquad (1)$$

where T is the integration time, $p_A(t)$ is the instantaneous sound pressure, weighted to approximate human hearing sensitivity (A-weighted), and p_0 is the reference effective sound pressure which is $20\,\mu\mathrm{Pa}$.

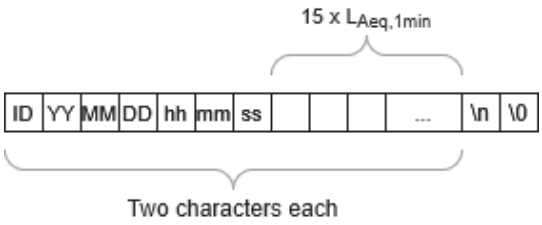


Fig. 3. The structure of a 46-elements hexstring array.

By using numerical approximation and Parseval's theorem [9], the digital implementation in frequency domain of (1) is shown in (2):

$$L_{Aeq,T} \approx 10\log_{10}\left[\left(\frac{K}{N}\right)^2 \sum_{N} |\mathbf{P}[k]w_A[k]|^2\right] \qquad (2)$$

where K is the microphone sensitivity relative to the reference effective sound pressure level, N is the number of data points in a frame, $P[k]$ is the frequency-domain representation of the microphone's digital output, and $w_A[k]$ is the A-weighting factor in the frequency domain. To efficiently compute the FFT using the CMSIS-DSP library, the 2000-sample frames were zero-padded to 2048 samples. The FFT calculation was performed using the CMSIS-DSP library [10]. Eight $L_{Aeq,0.125s}$ measurements are used to calculate one $L_{Aeq,1min}$ value, which is then submitted to the base station.

3) Wireless communication and MQTT: The ESP-01 (ESP8266) was chosen for wireless connectivity, leveraging its accessibility and ease of use. It communicates with the microcontroller via the DMA driven interrupt enable UART port. To facilitate user-friendly Wi-Fi setup, an open-source WiFiManager library [11] was implemented, which allows for dynamic network configuration without requiring hardcoded credentials.

The data transmitted to the ESP-01 is a 46-character hexstring array, chosen for its ease of manipulation using standard string handling functions and UART utilization. The array begins with the node ID and timestamp, followed by 15 $L_{Aeq,1min}$ values, each represented by two hexadecimal characters. The array is terminated with a newline character (`\n`) and a null character (`\0`). Figure 3 illustrates the structure of this hexstring array.

The ESP-01 module, upon receiving a complete 46-character hexstring array from the microcontroller, performed two encoding steps before publishing an MQTT message to the broker. First, the hexstring was converted to an array of bytes, interpreting each pair of hexadecimal characters as a single byte. Subsequently, this byte array was encoded using Base64 to ensure compatibility with the MQTT message format. The resulting Base64-encoded message was then published to the MQTT broker.

B. Base station

The base station in this system provides two primary functions: data reception and storage, and data visualization. The base station utilizes a collection of cloud-based services.

1) Data reception and storage: The first service in the data pipeline is an MQTT broker, responsible for capturing the published data from the sensor nodes. The captured data is then decoded from the Base64 message to an array of bytes, and subsequently transformed into an array of 15 JSON objects. Each JSON object contains the node ID, the corresponding $L_{Aeq,1min}$ value, and the timestamp. This structured JSON format is directly compatible with the InfluxDB time-series database, which provides efficient storage and retrieval. This data processing pipeline is implemented using a Node-RED flow.

2) Data visualization: Users can retrieve and visualize the stored data through a web-based dashboard, implemented using the 'node-red-dashboard' palette. Upon user request, a Node-RED flow constructs a Flux query string, a data scripting and query language developed for InfluxDB, based on the user's input, and sends it to the InfluxDB time-series database. The resulting data, including the latest $L_{Aeq,15min}$ value, a 24-hour time-series of $L_{Aeq,1min}$ values, and the $L_{Aeq,1min}$ series within the user-selected time frame, is then displayed on the dashboard.

IV. Experimental Setup and Preliminary Results

A sensor node was installed at a medium-sized construction site in Bangkok, where a building of less than thirty stories was being constructed. Measurements were taken over 240 days, covering site preparation, demolition, and foundation construction. The sensor node was placed one meter away from a certified Class 1 sound level meter at a height of approximately 2.5 meters above ground level. Both devices were positioned at the site boundary facing the main construction activities. System uptime was recorded, and the calculated $L_{Aeq,1min}$ values from the node were compared to those measured by the certified meter.

The system experienced 28 downtimes, ranging from as brief as 3 minutes to as long as 42 days accounting for 36% downtime. The distribution of the downtime durations is shown in figure 4.

Preliminary analysis of the collected data revealed that the $L_{Aeq,1min}$ values reported by the sensor node were typically lower than those measured by the Class 1 sound level meter, with an average difference as large as 8 dB.

V. Discussion and Lesson Learned

Discussion with the construction site operators revealed two primary causes of downtime:

1) power loss during relocation of the power source, as the sensor node had to be unplugged when repositioned to accommodate different construction phases, leading to temporary interruptions in data collection;
2) Wi-Fi connectivity issues, where loss of power sometimes resulted in Wi-Fi configuration resets, causing extended downtime until the connection was re-established. Additional factors contributing to Wi-Fi loss included weak signals during bad weather.

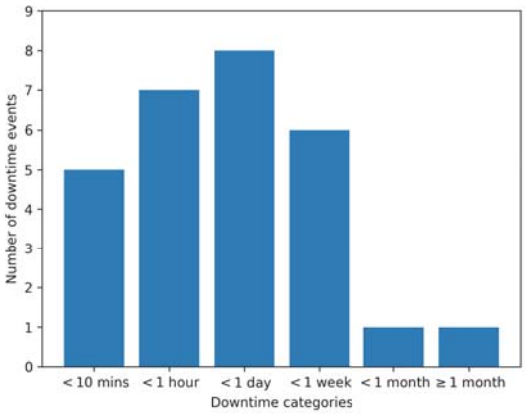


Fig. 4. Distribution of downtime events during the 240-day field test.

From the sensor node usage observations, the downtime durations were categorized into three groups: downtimes less than 1 hour, downtimes up to one week, and downtimes longer than one week. The authors speculate that the first category, downtimes less than one hour, was likely caused by temporary connectivity losses, with the system recovering normal operation once connectivity was restored. The second category, downtimes up to one week, could represent situations where the system did not automatically recover, but the site operator was notified and intervened to resolve the problem. The third category, including the longest downtime event of 42 days, occurred when the site operator was not notified and the node remained unattended. This highlights the need for both a clear on-node indicator to alert operators to potential issues and an effective malfunction notification mechanism to promptly inform system administrators. If the downtime related to the unattended issue were omitted to reflect the system's performance under typical operating conditions, the combined downtime from the first and second categories totals 10%.

The discussion also highlights the need for near-zero-setup sensor nodes when deploying them at construction sites. An alert mechanism that notifies users when the measured sound level exceed the threshold could also be useful.

This discrepancy compared to the class 1 measurements may be attributed to several factors, including microphone placement and orientation, microphone bandwidth, and inaccurate digital implementation of the A-weight filter.

VI. Conclusion and Future Work

This study demonstrates the feasibility of developing and deploying a wireless acoustic sensor network (WASN) for near-real-time noise monitoring. The preliminary field test was conducted in a construction environment. The system successfully captured noise data over a study period, providing insights into noise variation during different construction phases.

Future work will focus on minimizing downtime caused by power supply issues and sensor relocation. This may involve exploring battery backup options and integrating solar cell technology. Enhancing Wi-Fi connectivity through an automatic reconnection mechanism and adding an indicator on the sensor node for connectivity status will also be considered. Additionally, calibration and validation procedures will be refined to improve measurement accuracy.

References

[1] M. Basner, W. Babisch, A. Davis, M. Brink, C. Clark, S. Janssen, and S. Stansfeld, "Auditory and non-auditory effects of noise on health," *The Lancet*, vol. 383, pp. 1325–1332, 2014.

[2] D. Halperin, "Environmental noise and sleep disturbances: A threat to health?" *Sleep Science*, vol. 7, 2014.

[3] WHO Task group on environmental health criteria for noise, "Noise: Executive summary-environmental health criteria 12," World Health Organization, Tech. Rep., 1980.

[4] B. Berglund, T. Lindvall, and D. H. Schwela, "Guidelines for community noise," World Health Organization, Tech. Rep., 1999.

[5] K. Lertsawat, "Environmental noise abatement policy in thailand," in *40th International Congress and Exposition on Noise Control Engineering 2011, INTER-NOISE 2011*, vol. 5, 2011, pp. 4060–4069.

[6] European Commission, "Directive 2002/49/ec of the european parliament and of the council of 25 june 2002 relating to the assessment and management of environmental noise," *Official Journal of the European Communities*, vol. 189, 2002.

[7] R. Barham, M. Chan, and M. Cand, "Practical experience in noise mapping with a MEMS microphone based distributed noise measurement system," in *39th International Congress on Noise Control Engineering 2010, INTER-NOISE 2010*, vol. 3, 2010.

[8] P. Bernard, "Leq, SEL: What? Why? When? (application note:BO 0051-14)," Brüel & Kjær, Tech. Rep., 1975.

[9] J. A. Stuller, *An introduction to signals and systems*. Thomson, 2008.

[10] T. Lorenser, "The DSP capabilities of ARM® Cortex®-M4 and Cortex-M7 processors," ARM Limited, Tech. Rep., 2016.

[11] Tzapu. (2015) *WiFiManager:Espressif ESPx WiFi Connection manager with fallback web configuration portal* [Online]. Available: https://github.com/tzapu/WiFiManager/. [Accessed: 09 August 2023].

TRACK 7
NATIONAL SCOPE (Thai Language)

การสร้างไบโอฟิล์มและรูปแบบความไวต่อยาปฏิชีวนะของ *Vibrio parahaemolyticus* ที่แยกได้จากอาหารทะเล

Biofilm Formation and Antibiogram Profiles of *Vibrio parahaemolyticus* Isolates from Seafood

1st Muhammadfitree Ding
Medical and Industrial Microbiology Program,
Faculty of Science Technology and Agriculture,
Yala Rajabhat University,
Yala , Thailand
406463004@yru.ac.th

2nd Fathiyah Wamaeng
Medical and Industrial Microbiology Program,
Faculty of Science Technology and Agriculture,
Yala Rajabhat University,
Yala , Thailand
406463005@yru.ac.th

3rd Saihan Sani
Medical and Industrial Microbiology Program,
Faculty of Science Technology and Agriculture,
Yala Rajabhat University,
Yala , Thailand
406563017@yru.ac.th

4th Fatheeyah Salaeh
Medical and Industrial Microbiology Program,
Faculty of Science Technology and Agriculture,
Yala Rajabhat University,
Yala , Thailand
406563023@yru.ac.th

5th Sutima Preeprem*
Medical and Industrial Microbiology Program,
Faculty of Science Technology and Agriculture,
Yala Rajabhat University,
Yala , Thailand
*Corresponding author's e-mail:
sutima.p@yru.ac.th

Abstract

Vibrio parahaemolyticus is a major causative agent of gastroenteritis that the risks associated with the consumption of raw or undercooked seafood. The objectives of this study were to investigate the biofilm formation and antibiogram pattern of *V. parahaemolyticus* isolated from seafood. The isolation of *V. parahaemolyticus* from 6 seafood samples detected 16 isolates of non-fermented sucrose *Vibrio* spp. Eight isolates were classified as *V. parahaemolyticus* by biochemical test and polymerase chain reaction (PCR) using primers specific to *tox*R. Interestingly, the investigation of biofilm formation revealed that all of *V. parahaemolyticus* produced biofilm as medium level. In addition, the antibiotic susceptibility test using disk diffusion method showed that all of *V. parahaemolyticus* isolates were resistant to ampicillin (100%) but susceptible to ceftazidime, tetracycline and sulfamethoxazole-trimethoprim except the isolate no. SR7 was resistant to ampicillin and sulfamethoxazole-trimethoprim. Therefore, these results indicated *V. parahaemolyticus* isolates from seafood were able to release the biofilm and these isolates were also found to be resistant to at least one type of antibiotic. These findings highlight the risk of *V. parahaemolyticus* infection through the consumption of seafood, especially raw or undercooked seafood. Additionally, the data provide preliminary information that is a useful for surveillance and prevention the *V. parahaemolyticus* infection.

Keywords*: Vibrio parahaemolyticus,* Biofilm formation, Antibiotic susceptibility

I. บทนำ

อาหารทะเลเป็นอาหารที่ได้รับความนิยมในการบริโภคโดยการปรุงด้วยวิธีการต่าง ๆ เช่น การทอด การย่าง การต้ม และการลวก แต่อย่างไรก็ตามในปัจจุบันมีการนิยมรับประทานอาหารทะเลแบบสุก ๆ ดิบ ๆ ที่มากขึ้นซึ่งการบริโภคอาหารทะเลในรูปแบบที่ไม่ผ่านการปรุงสุกนั้นอาจเสี่ยงต่อการเกิดโรคติดเชื้อแบคทีเรียที่ปนเปื้อนในอาหารทะเล โดยเฉพาะอย่างยิ่งเชื้อ *Vibrio parahaemolyticus* ที่มักพบได้ในอาหารทะเลประเภทหอยและกุ้ง [1, 2] เชื้อชนิดนี้เป็นแบคทีเรียแกรมลบรูปร่างท่อนโค้งที่พบได้ในแหล่งน้ำซึ่งมีโซเดียมคลอไรด์ความเข้มข้นร้อยละ 1-8 เช่น ในน้ำทะเล ปากแม่น้ำ และชายฝั่ง เป็นต้น [3] *V. parahaemolyticus* เป็นสาเหตุหลักของโรคในระบบทางเดินอาหารคือโรคกระเพาะอาหารและลำไส้อักเสบ นอกจากนี้เชื้อชนิดนี้ยังสามารถก่อโรคนอกระบบทางเดินอาหารเช่น การติดเชื้อที่บาดแผลและการติดเชื้อในกระแสเลือด [1, 4] ปัจจัยที่ส่งเสริมการก่อโรคของ *V. parahaemolyticus* มีหลายชนิดเช่น การผลิตสารพิษ Thermostable direct hemolysin (TDH) ที่มีบทบาทในการทำลายเม็ดเลือดแดงและการสร้างไบโอฟิล์มที่มีบทบาทสำคัญในการปกป้องและส่งเสริมความสามารถในการอยู่รอดของแบคทีเรียในสภาวะต่าง ๆ รวมถึงเป็นหนึ่งในปัจจัยสำคัญที่ส่งผลให้เชื้อดื้อต่อยาปฏิชีวนะได้ [5, 6] สำหรับการรักษาโรคติดเชื้อ *V. parahaemolyticus* ในกรณีที่ผู้ป่วยมีอาการรุนแรงจะมีการใช้ยาปฏิชีวนะเพื่อการรักษา [7] แต่อย่างไรก็ตามในปัจจุบันมีการรายงานการดื้อต่อยาปฏิชีวนะหลายชนิดของ *V. parahaemolyticus* เช่น Ampicillin, Tetracycline, Amoxicillin, Ciprofloxacin และ Ceftazidime เป็นต้น [8] ดังนั้นในงานวิจัยนี้จึงมีวัตถุประสงค์เพื่อตรวจสอบ

ความสามารถในการสร้างไบโอฟิล์มและการดื้อต่อยาปฏิชีวนะของ *V. parahaemolyticus* ที่แยกได้จากอาหารทะเลโดยข้อมูลเหล่านี้จะเป็นข้อมูลที่เป็นประโยชน์ต่อการเฝ้าระวังการเกิดโรคติดเชื้อ *V. parahaemolyticus* รวมถึงประกอบการพิจารณาและวางแผนแนวทางในการรักษาโรคที่เกิดจากเชื้อชนิดนี้ต่อไปได้

II. ทบทวนวรรณกรรม

Vibrio parahaemolyticus เป็นเชื้อกลุ่ม *Vibrio* spp. ที่เป็นสาเหตุหลักของโรคในระบบทางเดินอาหาร [7, 9] ซึ่งเชื้อชนิดนี้มีการรายงานถึงความสามารถในการก่อโรคได้ทั้งในและนอกระบบทางเดินอาหาร เช่น โรคกระเพาะอาหารและลำไส้อักเสบ การติดเชื้อที่บาดแผล และการติดเชื้อในกระแสเลือดที่มีโอกาสส่งผลให้ผู้ป่วยเสียชีวิตได้ [1, 4, 9] ก่อนหน้านี้มีการรายงานถึงปัจจัยก่อโรคของเชื้อชนิดนี้ซึ่งเกี่ยวข้องกับความสามารถในการสร้างไบโอฟิล์มที่เป็นสารเมือกหรือที่เรียกว่า Extracellular polymeric substance (EPS) ซึ่งมีส่วนสำคัญที่ส่งเสริมการอยู่รอดของเชื้อในสภาวะต่าง ๆ โดยเฉพาะอย่างยิ่งในสภาวะที่ไม่เหมาะสมต่อการเจริญเช่น สภาวะที่มียาปฏิชีวนะ [10, 11, 12] จากงานวิจัยของ Nguyen และคณะปี ค.ศ. 2024 มีการรายงานถึงความสัมพันธ์ของความสามารถในการสร้างไบโอฟิล์มและการดื้อต่อยาปฏิชีวนะ เนื่องจากไบโอฟิล์มสามารถช่วยในการปกป้องตัวเซลล์ของแบคทีเรียและส่งผลให้ยาปฏิชีวนะมีประสิทธิภาพในการทำลายเชื้อได้น้อยลง [11] นอกจากนี้จากงานวิจัยของ Jingjit และคณะปี ค.ศ. 2021, Nguyen และคณะปี ค.ศ. 2024 และ Bai และคณะปี ค.ศ. 2024 มีการรายงานถึงการดื้อต่อยาปฏิชีวนะของ *V. parahaemolyticus* ในหลายประเทศเช่น ไทย เวียดนาม และ จีน [11, 13, 14] ดังนั้นการศึกษาความสามารถในการสร้างไบโอฟิล์มและการดื้อต่อยาปฏิชีวนะของ *V. parahaemolyticus* จึงมีความสำคัญอย่างยิ่งในการรักษา ควบคุม และป้องกันการติดเชื้อชนิดนี้

III. ระเบียบวิธีวิจัย

1. การคัดแยกเชื้อ *Vibrio parahaemolyticus*

นำตัวอย่างอาหารทะเลจำนวน 25 กรัม บดและใส่ใน Alkaline peptone water (APW) ปริมาณ 225 มิลลิลิตร นำไปบ่มที่อุณหภูมิ 37 องศาเซลเซียส เป็นเวลา 24 ชั่วโมง จากนั้นนำตัวอย่างจำนวน 1 loop มาทำการแยกเชื้อด้วยวิธีการ Streak plate ลงในอาหาร Thiosulfate citrate bile-salt sucrose (TCBS) agar แล้วบ่มที่อุณหภูมิ 37 องศาเซลเซียส นาน 24 ชั่วโมง จากนั้นคัดเลือกโคโลนีเดี่ยวจากอาหาร TCBS agar ซึ่งมีลักษณะโคโลนีกลม นูน ขอบเรียบ และมีสีเขียวนำมา Streak บนอาหาร Nutrient agar (NA) ที่เติมโซเดียมคลอไรด์ (NaCl) ความเข้มข้นร้อยละ 1.5 และบ่มที่อุณหภูมิ 37 องศาเซลเซียส เป็นเวลา 18-24 ชั่วโมง เพื่อใช้ในการทดสอบทางชีวเคมีต่อไป [8]

2. การระบุสายพันธุ์ของ *V. parahaemolyticus*

2.1 การระบุสายพันธุ์ *V. parahaemolyticus* ด้วยวิธีทางชีวเคมี

ตรวจสอบสายพันธุ์ของ *V. parahaemolyticus* โดยนำเชื้อที่เพาะเลี้ยงบนอาหาร NA ที่เติมโซเดียมคลอไรด์ความเข้มข้นร้อยละ 1.5 มาทดสอบทางชีวเคมี (Biochemical test) ได้แก่ Oxidase test, Triple sugar iron (TSI) test, Motility-Indole-Lysine decarboxylase (MIL) test และทดสอบการเจริญที่โซเดียมคลอไรด์ความเข้มข้นร้อยละ 3, 6, 8 และ 10 โดยลักษณะผลการทดสอบของ *V. parahaemolyticus* เป็นดังตารางที่ 1 [15, 16]

TABLE I. BIOCHEMICAL CHARACTERITIC OF *Vibrio parahaemolyticus* [17]

Test	*V. parahaemolyticus*
Oxidase test	+
Triple sugar iron (TSI) test	K/A
lysine decarboxylase	+
Motility	+
Indole	+
Growth at % NaCl	
3% NaCl	+
6% NaCl	+
8% NaCl	+
10% NaCl	-

NOTE: - = Negative, + = Positive; K: Alkaline, A: Acid

2.2 การระบุสายพันธุ์ *V. parahaemolyticus* ด้วยวิธี Polymerase chain reaction (PCR)

1. การสกัดดีเอ็นเอ

สกัดดีเอ็นเอของเชื้อด้วยวิธีการต้มโดยนำเชื้อที่เลี้ยงใน NA ที่เติมโซเดียมคลอไรด์ความเข้มข้นร้อยละ 1.5 ใส่ลงในน้ำ DI ปราศจากเชื้อแล้วนำไปต้มที่อุณหภูมิ 95 องศาเซลเซียส เป็นเวลา 10 นาที จากนั้นจึงนำมาปั่นเหวี่ยงที่ความเร็ว 10,000 รอบ/นาที เป็นเวลา 5 นาที เมื่อครบเวลาทำการเก็บส่วนใสที่มีดีเอ็นเอและนำไปเก็บที่อุณหภูมิ 4 องศาเซลเซียสเพื่อใช้ในการทดสอบต่อไป [17]

2. การตรวจสอบยีน *tox*R ด้วยวิธี Polymerase chain reaction (PCR)

ตรวจสอบยีน *tox*R ด้วยเทคนิค PCR โดยใช้ไพรเมอร์ที่จำเพาะกับยีน *tox*R ของเชื้อ *V. parahaemolyticus* ซึ่งมีลำดับนิวคลีโอไทด์ของไพรเมอร์ ดังตารางที่ 2 และมีส่วนผสมของปฏิกิริยา PCR ปริมาณรวม 25 ไมโครลิตร ประกอบด้วย OmniPCR reagent, 0.32 µM Primer toxR – F และ R, น้ำ DI และ ดีเอ็นเอ ปริมาณ 2 ไมโครลิตร จากนั้นทำการเพิ่มจำนวนของยีน *tox*R โดยเครื่อง Thermal cycle ด้วยสภาวะดังนี้ Initial Denaturation ที่อุณหภูมิ 94 องศาเซลเซียส นาน 5 นาที ตามด้วย 35 รอบของกระบวนการ Denaturation, Annealing และ Extension ที่อุณหภูมิ 94, 63 และ 72 องศาเซลเซียส นาน 40 วินาที, 1 และ 1 นาที ตามลำดับ และตามด้วยกระบวนการ Final extension ที่อุณหภูมิ 72 องศาเซลเซียส นาน 5 นาที จากนั้นจึงตรวจสอบยีน *tox*R ด้วยวิธี Agarose gel electrophoresis โดยใช้กระแสไฟฟ้าที่ 100 โวลต์ เวลาประมาณ 30 นาที เมื่อครบเวลาทำการตรวจขนาดของ PCR product ด้วยเครื่อง Gel doc [17]

TABLE II. PCR PRIMER USED FOR IDENTIFICATION OF *Vibrio parahaemolyticus*

Gene target	Primer	Primer sequence (5'-3')	PCR Product (bp)
*tox*R	toxR-F	GTCTTCTGACGCAATCGTTG	368
	toxR-R	ATACGAGTGGTTGCTGTCATG	

3. การตรวจสอบความสามารถในการสร้างไบโอฟิล์ม

นำ *V. parahaemolyticus* ที่มีความเข้มข้นเท่ากับ 0.5 McFarland standard ปริมาตร 100 ไมโครลิตร ใส่ลงใน 96-well plate ที่มีอาหารเลี้ยงเชื้อ Nutrient broth (NB) ที่เติมโซเดียมคลอไรด์ความเข้มข้นร้อยละ 1.5 ปริมาตร 100 ไมโครลิตร โดยทำการทดสอบ 3 ซ้ำ จากนั้นทำการบ่มเชื้อที่อุณหภูมิ 37 องศาเซลเซียส เป็นเวลา 24 ชั่วโมง และเทส่วนใสทิ้งแล้วล้างด้วยน้ำกลั่นจำนวน 3 ครั้ง จากนั้นย้อมด้วยสี Crystal violet ความเข้มข้นร้อยละ 0.1 และพักทิ้งไว้ 15 นาที แล้วจึงเทสี Crystal violet ที่เหลือออก จากนั้นชะล้างสี Crystal violet ที่ติดกับไบโอฟิล์มด้วยเอทานอล ปริมาณ 100 ไมโครลิตร แล้วพักทิ้งไว้ 15 นาที จากนั้นวัดค่าการดูดกลืนแสงที่ความยาวคลื่น 595 นาโนเมตร ด้วยเครื่อง Microplate Readers และบันทึกผลการทดลอง พร้อมด้วยวิเคราะห์ความสามารถในการสร้างไบโอฟิล์มของเชื้อโดยเปรียบเทียบความสามารถในการสร้างไบโอฟิล์มดังตารางที่ 3 [17, 18]

TABLE III. CLASSIFICATION OF BIOFILM FORMATION LEVELS [18]

OD	Biofilm formation level
$OD \leq OD_{cut}$	Non biofilm formation
$OD_{cut} < OD \leq 2 \times OD_{cut}$	Low
$2\ OD_{cut} < OD \leq 4\ OD_{cut}$	Medium
$OD > 4 \times OD_{cut}$	High

NOTE: OD_{cut} = Standard deviation × 3 + Mean of negative control

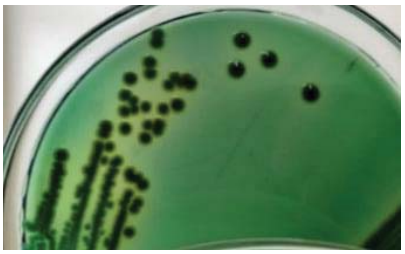
4. การทดสอบความไวต่อยาปฏิชีวนะ

ทดสอบความไวต่อยาปฏิชีวนะด้วยวิธี Disk diffusion method โดยนำเชื้อ *V. parahaemolyticus* ที่มีความเข้มข้นเท่ากับ 0.5 McFarland standard จากนั้นใช้ไม้พันสำลีที่ปราศจากเชื้อจุ่มป้ายเชื้อให้ทั่วลงในอาหารเลี้ยงเชื้อ Mueller Hinton agar (MHA) แล้วนำแผ่นยาปฏิชีวนะ ได้แก่ Ampicillin, Ceftazidime, Tetracycline และ Sulfamethoxazole-trimethoprim มาวางบนอาหาร MHA โดยทำการทดสอบ 2 ซ้ำ และนำไปบ่มที่อุณหภูมิ 37 องศาเซลเซียส เป็นเวลา 18-24 ชั่วโมง จากนั้นทำการวัดค่าการยับยั้ง (Clear zone) นำไปเทียบกับ The clinical and laboratory Standards institute Guidelines (CLSI, 2018) [19, 20]

IV. ผลการทดลอง

1. การคัดแยกเชื้อ *Vibrio parahaemolyticus* จากตัวอย่างอาหารทะเล และการระบุสายพันธุ์ด้วยวิธีทางชีวเคมีและ PCR

จากการคัดแยกเชื้อ *V. parahaemolyticus* จากตัวอย่างอาหารทะเลจำนวน 6 ตัวอย่างซึ่งประกอบด้วยหอยจำนวน 2 ตัวอย่าง และกุ้งจำนวน 4 ตัวอย่าง พบเชื้อ *Vibrio* spp. ที่ไม่หมักน้ำตาลซูโครสซึ่งมีลักษณะโคโลนีสีเขียว กลม ขอบเรียบบนอาหาร TCBS จำนวน 16 ไอโซเลท และจากการศึกษาลักษณะสัณฐานวิทยาโดยการย้อมสีแกรมพบว่าเชื้อทั้งหมดเป็นแบคทีเรียแกรมลบ รูปร่างท่อนโค้ง (ภาพที่1) นอกจากนี้จากการทดสอบทางชีวเคมีประกอบด้วย Oxidase test, Triple sugar iron (TSI) test, Motility-Indole lysine decarboxylase (MIL) test และทดสอบการเจริญในโซเดียมคลอไรด์ความเข้มข้นร้อยละ 3, 6, 8 และ 10 พบว่า *Vibrio* spp. ซึ่งมีคุณสมบัติใกล้เคียงกับเชื้อ *V. parahaemolyticus* มีจำนวน 8 ไอโซเลท ได้แก่ SH5, SH6, SH7, SH8, SH9, SR1, SR3 และ SR7 ดังแสดงในตารางที่ 4 และจากการนำ *Vibrio* spp. ที่มีผลการทดสอบทางชีวเคมีใกล้เคียงกับ *V. parahaemolyticus* มาทำการยืนยันสายพันธุ์ด้วยวิธี PCR โดยใช้ไพรเมอร์ที่จำเพาะกับยีน *tox*R พบ *Vibrio* spp. จำนวน 8 ไอโซเลทมียีน *tox*R ที่ได้มีขนาด 368 bp ดังตารางที่ 4 และภาพที่ 2 ดังนั้นจากการทดลองนี้จึงชี้ให้เห็นว่าในอาหารทะเลที่ใช้ในการทดสอบมีการปนเปื้อนของ *V. parahaemolyticus*



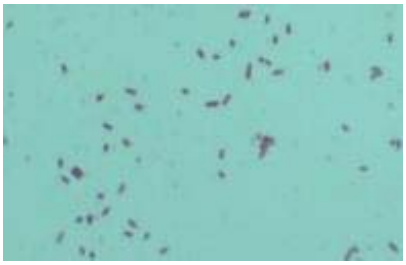


Fig. 1 CHARACTERISTICS OF *Vibrio parahaemolyticus* ON TCBS AGAR AND GRAM STAIN

TABLE IV. CHARACTERISTICS OF *Vibrio parahaemolyticus* ISOLATES

Isolate No.	Biochemical test									PCR	*Vibrio* spp.
	Oxidase	TSI	Motility	Lysine	Indole	Growth at % NaCl				*tox*R	
						3	6	8	10		
SH1	+	K/A, H_2S	ND	ND	ND	ND	ND	ND	ND	ND	NVP
SH2	+	K/A	-	-	-	ND	ND	ND	ND	ND	NVP
SH3	+	K/A	-	-	-	ND	ND	ND	ND	ND	NVP
SH4	+	K/A, H_2S	ND	ND	ND	ND	ND	ND	ND	ND	NVP
SH5	+	K/A	+	+	-	+	+	+	-	+	VP
SH6	+	K/A	+	+	-	+	+	+	-	+	VP
SH7	+	K/A	+	+	-	+	+	+	-	+	VP
SH8	+	K/A	+	+	-	+	+	+	-	+	VP
SH9	+	K/A	+	+	-	+	+	+	-	+	VP
SR1	+	K/A	+	+	-	+	+	+	-	+	VP
SR2	+	K/A H_2S	ND	ND	ND	ND	ND	ND	ND	ND	NVP
SR3	+	K/A	+	+	-	+	+	+	-	+	VP
SR4	-	ND	ND	ND	ND	ND	ND	ND	ND	ND	NVP
SR5	+	K/A H_2S	ND	ND	ND	ND	ND	ND	ND	ND	NVP
SR6	-	ND	ND	ND	ND	ND	ND	ND	ND	ND	NVP
SR7	+	K/A	+	+	-	+	+	+	-	+	VP

NOTE: SH = *V. parahaemolyticus* isolated from shell,
SR = *V. parahaemolyticus* isolated from shrimp,
+ = Positive, - = Negative, K = Alkaline, A = Acid,
H_2S = Hydrogen sulphide, ND = Non determined,
VP = *V. parahaemolyticus*, NVP = Non *V. parahaemolyticus*

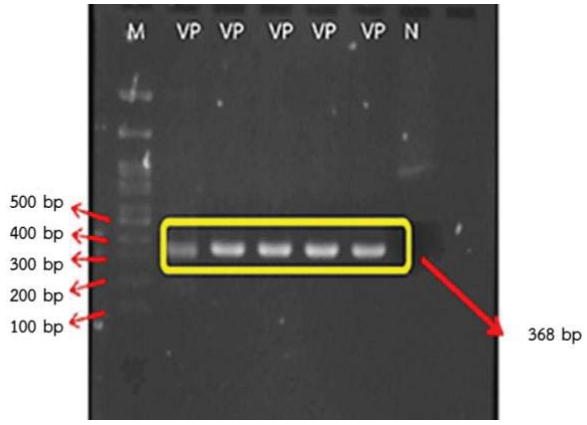


Fig.2 THE DETECTION OF *tox*R GENE OF *Vibrio parahaemolyticus*; M = 100 bp DNA marker, VP= *V. parahaemolyticus*, N = Negative control.

2. การตรวจสอบความสามารถในการสร้างไบโอฟิล์ม

จากการทดสอบความสามารถในการสร้างไบโอฟิล์มของ *V. parahaemolyticus* ที่คัดแยกจากตัวอย่างอาหารทะเล โดยการย้อมด้วยสี Crystal violet และวัดค่าการดูดกลืนแสงที่ 595 นาโนเมตร พบว่าค่าเฉลี่ย OD_{595} ของการสร้างไบโอฟิล์มมีค่าอยู่ระหว่าง 0.176-0.195 ซึ่งเชื้อที่มีความสามารถในการสร้างไบโอฟิล์มสูงที่สุดคือ ไอโซเลท SH6 มีค่าเฉลี่ยเท่ากับ 0.195 รองลงมาคือไอโซเลท SR1 มีค่าเฉลี่ย OD_{595} เท่ากับ 0.188 และเชื้อทั้งหมดมีระดับการสร้างไบโอฟิล์มในระดับปานกลางดังตารางที่ 5 ดังนั้นจากผลการทดลองนี้แสดงให้เห็นว่า *V. parahaemolyticus* ที่แยกจากอาหารทะเลทุกไอโซเลทมีความสามารถในการสร้างไบโอฟิล์มได้ในระดับที่ใกล้เคียงกัน

TABLE V. BIOFILM FORMATION LEVEL OF *Vibrio parahaemolyticus* ISOLATES

Isolate No.	Mean OD $_{595\ nm}$ $\pm$ SD	Biofilm Level
SH5	0.184±0.009	Medium
SH6	0.195±0.008	Medium
SH7	0.186±0.030	Medium
SH8	0.181±0.013	Medium
SH9	0.176±0.001	Medium
SR1	0.188±0.008	Medium
SR3	0.185±0.004	Medium
SR7	0.182±0.011	Medium

3. การทดสอบความไวต่อยาปฏิชีวนะ

จากการทดสอบความไวต่อยาปฏิชีวนะด้วยวิธี Disk diffusion method พบว่า *V. parahaemolyticus* ทั้ง 8 ไอโซเลท มีการดื้อยา Ampicillin แต่เชื้อเกือบทั้งหมดยังคงไวต่อยา Ceftazidime, Tetracycline และ Sulfamethoxazole-trimethoprim โดยไอโซเลท SR7 มีการดื้อยาปฏิชีวนะหลายชนิด คือ Ampicillin และ Sulfamethoxazole-trimethoprim ดังตารางที่ 6 ดังนั้นจากผลการทดลองนี้ชี้ให้เห็นว่า *V. parahaemolyticus* ที่แยกจากอาหารทะเลมีความสามารถในการดื้อต่อยาปฏิชีวนะได้อย่างน้อย 1 ชนิด

TABLE VI. ANTIBIOTIC SENSITIVITY OF *Vibrio parahaemolyticus* ISOLATES

Isolate No.	Antibiotic sensitivity				Number of antibiotic resistances
	AMP	CAZ	TE	SXT	
SH5	R	S	S	S	1
SH6	R	S	S	S	1
SH7	R	S	S	S	1
SH8	R	S	S	S	1
SH9	R	S	S	S	1
SR1	R	S	S	S	1
SR3	R	S	S	S	1
SR7	R	S	S	R	2

NOTE: AMP= Ampicillin (10 µg), CAZ= Ceftazidime (30 µg), TE= Tetracycline (30 µg), SXT= Sulfamethoxazole-trimethoprim (25 µg)

V. อภิปรายผล

ในงานวิจัยนี้สามารถคัดแยก *Vibrio parahaemolyticus* ได้จากอาหารทะเลทั้งประเภทหอยและกุ้งจำนวน 8 ไอโซเลทซึ่งชี้ให้เห็นว่ามีการปนเปื้อนของ *V. parahaemolyticus* ในอาหารทะเลดังกล่าวซึ่งสอดคล้องกับงานวิจัยก่อนหน้านี้ที่มีการรายงานการตรวจพบเชื้อชนิดนี้ในอาหารทะเลของพื้นที่จังหวัดซึ่งไม่มีแหล่งของอาหารทะเลจึงอาจจะมีความเสี่ยงในการปนเปื้อนของเชื้อรวมถึงการเพิ่มจำนวนของ *V. parahaemolyticus* ในระหว่างการขนส่งอาหารทะเลจากแหล่งผลิตที่เป็นจังหวัดใกล้เคียง [2, 15, 17] และที่น่าสนใจเป็นอย่างยิ่งคือ

V. parahaemolyticus ทั้ง 8 ไอโซเลทมีความสามารถในการสร้างไบโอฟิล์มในระดับเดียวกัน ดังนั้นจึงชี้ให้เห็นว่า *V. parahaemolyticus* ที่แยกได้จากอาหารทะเลมีความสามารถในการสร้างไบโอฟิล์มได้ซึ่งสอดคล้องกับงานวิจัยก่อนหน้านี้ที่รายงานถึงการพบ *V. parahaemolyticus* ที่แยกจากอาหารทะเลซึ่งมีความสามารถในการสร้างไบโอฟิล์มได้ [11, 13, 21] ไบโอฟิล์มเป็นปัจจัยสำคัญในการอยู่รอดของเชื้อในสภาวะที่ไม่เหมาะสมและยังส่งผลต่อความเสี่ยงในการปนเปื้อนของ *V. parahaemolyticus* ในแหล่งต่าง ๆ ได้ เชื้อที่มีความสามารถในการสร้างไบโอฟิล์มสามารถส่งผลให้ยาปฏิชีวนะทำลายเชื้อได้ยากจึงเสี่ยงต่อการระบาดของเชื้อและส่งผลต่อประสิทธิภาพในการรักษาได้ [11, 17] นอกจากนี้ในงานวิจัยนี้ยังพบว่า เชื้อทั้งหมดที่ทดสอบมีความสามารถในการดื้อต่อยาปฏิชีวนะอย่างน้อย 1 ชนิด คือ ยา Ampicillin และมีเชื้อ 1 สายพันธุ์ที่ดื้อต่อยา 2 ชนิดคือ ยา Ampicillin และ Sulfamethoxazole-trimethoprim ซึ่งสอดคล้องกับงานวิจัยก่อนหน้านี้ที่มีการรายงานถึงการดื้อต่อยาปฏิชีวนะของ *V. parahaemolyticus* ที่แยกได้จากอาหารทะเล [8, 11, 13, 15, 19] โดยจากรายงานก่อนหน้านี้มีการรายงานถึงการสร้างไบโอฟิล์มมีความสัมพันธ์ในการต้านทานยาปฏิชีวนะซึ่งการสร้างไบโอฟิล์มของเชื้อมีความสำคัญในการปกป้องเซลล์ของแบคทีเรียและส่งผลให้ยาปฏิชีวนะทำลายเชื้อที่สร้าง ไบโอฟิล์มได้ยาก [11, 12] ดังนั้นจากผลการทดลองนี้ชี้ให้เห็นว่า *V. parahaemolyticus* ที่แยกจากอาหารทะเลมีความสามารถในการดื้อยาปฏิชีวนะซึ่งการดื้อต่อยาปฏิชีวนะนี้มีผลกระทบสำคัญต่อการใช้ยาปฏิชีวนะในการรักษาโรคที่เกิดจากการติดเชื้อชนิดนี้ทำให้มีประสิทธิภาพในการรักษาผู้ป่วยด้วยยาปฏิชีวนะลดลงและการศึกษาเกี่ยวกับปัจจัยส่งเสริมการดื้อต่อยาปฏิชีวนะของ *V. parahaemolyticus* ยังเป็นสิ่งที่จำเป็นเพื่อเพิ่มความเข้าใจเกี่ยวกับการดื้อต่อยาปฏิชีวนะรวมถึงการศึกษาแนวทางในการรักษาและป้องกันการติดเชื้อชนิดนี้ให้มีประสิทธิภาพต่อไปในอนาคตได้

VI. ข้อสรุป

จากการคัดแยกเชื้อจากอาหารทะเลประเภทหอยและกุ้งสามารถคัดแยก *Vibrio parahaemolyticus* ได้จำนวน 8 ไอโซเลท ซึ่งเชื้อทั้งหมดนี้มีความสามารถในการสร้างไบโอฟิล์มในระดับปานกลาง นอกจากนี้ *V. parahaemolyticus* ทั้ง 8 ไอโซเลทยังมีความสามารถในการดื้อต่อยา Ampicillin แต่เชื้อส่วนใหญ่ยังคงมีความไวต่อยา Ceftazidime Tetracycline และ Sulfamethoxazole-trimethoprim ยกเว้นไอโซเลท SR7 ที่มีการดื้อต่อยาปฏิชีวนะมากกว่า 1 ชนิด ได้แก่ ยา Ampicillin และ Sulfamethoxazole-trimethoprim ดังนั้นจากผลการทดลองนี้แสดงให้เห็นว่า *V. parahaemolyticus* ที่แยกได้จากอาหารทะเลเป็นเชื้อที่มีความเสี่ยงในการก่อโรคได้โดยมีความสามารถในการสร้างไบโอฟิล์ม อีกทั้งเชื้อเหล่านี้ยังไม่สามารถยับยั้งได้ด้วยยา Ampicillin และมีบางสายพันธุ์ที่ดื้อต่อยาปฏิชีวนะมากกว่า 1 ชนิด

คำขอบคุณ

ขอขอบคุณ ดร.สุภาภรณ์ ชุมพล ในการตรวจสอบบทคัดย่อภาษาอังกฤษและขอขอบคุณหลักสูตรจุลชีววิทยาทางการแพทย์และอุตสาหกรรม คณะวิทยาศาสตร์เทคโนโลยีและการเกษตร มหาวิทยาลัยราชภัฏยะลา สำหรับความอนุเคราะห์ในด้านสถานที่ห้องปฏิบัติการ สารเคมีและอุปกรณ์ต่าง ๆ ในการดำเนินวิจัย และขอขอบคุณผู้ที่มีส่วนเกี่ยวข้องกับการวิจัยครั้งนี้

อ้างอิง

[1] วารุณี หะยีมะสาและ, สายใจ แก้วอ่อน, นิสาพร มูหะมัด และลักขณา รักขพันธ์. (2559). การตรวจแยกแบคทีเรีย *Vibrio parahaemolyticus* ที่ปนเปื้อนในหอยแครงบริเวณอ่าวปัตตานีโดยใช้โมโนโคลนอล แอนติบอดีที่จำเพาะต่อ *Vibrio* spp. ชนิดต่าง ๆ (*รายงานผลการวิจัย*).วิทยาศาสตร์เทคโนโลยีและการเกษตร: มหาวิทยาลัยราชภัฏยะลา.

[2] สุรีย์ นานาสมบัติ, นวรัตน์ โพธิราช, ประทุม แสนมา, วรรธนนท์ หาเพิ่มพูน, และสิทธิโชค ศิริศรชัย. (2556). การตรวจหาการปนเปื้อน *Vibrio parahaemolyticus* ในอาหารทะเลสดที่จำหน่ายในกรุงเทพและการศึกษาการต้านทานความร้อน, *วารสารมหาวิทยาลัยทักษิณ, 16*(3), 175-183.

[3] อิสมีย์ ปูตะ, ชามีลา ดูมีแด, พรูกอนนี สาและ, ซูไบด๊ะ หะยีวาเงาะ, คอสียาห์ สะลี, นุรอัยนี หะยียูโซะและอับดุลลาห์ โดลาห์ ดาลี. (2560). การปนเปื้อนของเชื้อ *Vibrio parahaemolyticus* ในอาหารทะเลสดที่วางจำหน่ายในเขตเทศบาลนครยะลาและอำเภอเมืองปัตตานี. นครศรีธรรมราช: มหาวิทยาลัยราชภัฏนครศรีธรรมราช.

[4] Pazhani, G. P., Chowdhury, G., and Ramamurthy, T. (2021). Adaptations of *Vibrio parahaemolyticus* to stress during environmental survival, host colonization, and infection. Frontiers in Microbiology, 12, 737299. https://doi.org/10.3389/fmicb.2021.737299.

[5] Abebe, G. M., (2020). The Role of Bacterial Biofilm in Antibiotic Resistance and Food Contamination. International journal of microbiology, https://doi.org/10.1155 /10.1155/2020 /1705814.

[6] พรเพ็ญ ทองสะอาด. (2559). ผลกระทบของปัจจัยสิ่งแวดล้อมน้ำทะเลต่ออุบัติการณ์และปัจจัย ความรุนแรงในการก่อโรคของแบคทีเรียในสกุล *Vibrio* บริเวณชายฝั่งอ่าวศิลาจังหวัดชลบุรี *(วิทยานิพนธ์ปริญญามหาบัณฑิต).* คณะวิทยาศาสตร์. มหาวิทยาลัยบูรพา.

[7] กนกรัตณ์ ชลศิลป์. (2563). ปัจจัยก่อความรุนแรงของเชื้อก่อโรคที่พบในอาหารวิบริโอ พาราฮีโมไลติคัส. *วารสารการแพทย์และวิทยาศาสตร์สุขภาพ, 27*(1), 162-164.

[8] Strater, D., Fasulkoua, R., and Krumova-valcher., (2023). Incidence, virulence genes and antimicrobial resistance of *Vibrio parahaemolyticus* isolated from seafood, *Microbial pathogenesis*, 177, https://doi.org/ 10.1016/ j.micpath. 2023.106050.

[9] Wu, X., Zhu, Y., Yan, W., Zhang, P., and Chen, L. (2024). Pathogenic characteristics of the *Vibrio parahaemolyticus* which caused a gastroenteritis outbreak event in Huzhou. *FEMS Microbiology Letters*, 371, https://doi.org/10.1093/femsle/fnad130.

[10] Grooters, K. E., Ku, J. C., Richter, D. M., Krinock, M. J., Minor, A., Li, P., Kim, A., Sawyer, R. and Li, Y. (2024). Strategies for combating antibiotic resistance in bacterial biofilms. *Frontiers in Cellular and Infection Microbiology*, 14, 1352273. https://doi.org/10.3389/fcimb.2024.1352273.

[11] Nguyen, K. C. T., Truong, P. H., Thi, H. T., Ho, X. T., & Van Nguyen, P. (2024). Prevalence, multidrug resistance, and biofilm formation of *Vibrio parahaemolyticus* isolated from fish mariculture environments in Cat Ba Island, Vietnam. *Osong Public Health and Research Perspectives*, *15*(1), https://doi.org/10.24171/j.phrp. 2023.0181.

[12] Ashrafudoulla, M., Rahaman Mizan, M. F., Park, H., Byun, K., Lee, N., Park, S., and Ha, S., (2019). Genetic Relationship, Virulence Factors, Drug Resistance Profile and Biofilm Formation Ability of *Vibrio parahaemolyticus* Isolated from Mussel. *Frontiers in Microbiology*, *10*, https://doi.org/10.3389/fmicb.2019.00513.

[13] Jingjit, N., Preeprem, S., Surachat, K., and Mittraparp-Arthorn, P. (2021). Characterization and analysis of clustered regularly interspaced short palindromic repeats (CRISPRs) in pandemic and non-pandemic *Vibrio parahaemolyticus* isolates from seafood sources. *Microorganisms*, *9*(6), 1220. doi: 10.3390/microorganisms9061220.

[14] Bai, Y., Yang, Q., Sun, Y., Li, F., Sun, J., Yang, S., Yang, D., Peng, Z., Yang, B., Xu, J., Dong, Y., Yan, S., Li, N., (2024). Antimicrobial susceptibility and genomic characterization of *Vibrio parahaemolyticus* isolated from aquatic foods in 15 provinces, Chna, 2020. *Internationl Journal of Food Microbiology*, 418. doi: 10.1016/j.ijfoodmicro.2024. 110737.

[15] กุลวรา พูลผล. (2561). การดื้อยาของ *Vibrio parahaemolyticus* และ *Vibrio vulnificus* ที่แยกได้จากน้ำทะเลบริเวณหาดบางแสน จังหวัดชลบุรี (*รายงานผลการวิจัย*). คณะสหเวชศาสตร์. มหาวิทยาลัยบูรพา.

[16] Kaysner, C., DePaola, A., and Jones, J., (2004). Bacteriological Analytical Manual (BAM) Chapter 9: *Vibrio* May 2004 Edition Retrieved, accessed September 2023.

[17] Preeprem, S., Aksonkird, T., Nuidate, T., Hajimasalaeh, W., Hajwangoh, Z., and Mittraparp-arthorn, P., (2023). Characterization and Genetic Relationships of *Vibrio* spp. Isolated from Seafood in Retail Markets, Yala Thailand. *Trends in sciences*, *20*(10), 5962. https://doi.org/10.48048/tis.2023.5962.

[18] รุสมาวาตี เจ๊ะฆอ, นูรีย๊ะ ยามา, สุธิมา ปรีเปรม. (2564). การคัดแยกและศึกษาลักษณะของแบคทีเรียที่แยกได้จากฝุ่นในห้องนอน. ใน *งานประชุมวิชาการระดับชาติ ด้านวิทยาศาสตร์และเทคโนโลยีเครือข่ายภาคใต้ ครั้งที่ 6, วันที่ 1-2 เมษายน 2564 (1103).* ยะลา. คณะวิทยาศาสตร์และเทคโนโลยี มหาวิทยาลัยราชภัฏยะลา.

[19] สรวณีย์ วิริยะอัครเดชา, นิติ ชูเชิด, พุทธรัตน์ เบ้าประเสริฐกุล, เบญจพร สัมฤทธิเวช, พงศ์เชฏฐ์พิชิตกุล, อรุโณทัย คีตะนนท์ และวิษณุ ธรรมลิขิตกุล. (2563). การศึกษาการปนเปื้อนของเชื้อดื้อยาต้านจุลชีพในการเลี้ยงกุ้งขาวแวนนาไม (*Litopenaeus vannamei*) ในประเทศไทย, *วารสารแก่นเกษตร, 48*(5), 1124-1133.

[20] Clinical and Laboratory Standards Institute CLSI. Performance standards for antimicrobial susceptibility testing. Wayne: CLSI, 2018.

[21] Wang, D., Flint, S. H., Palmer, J. S., Gagic, D., Fletcher, G. C., and On, S, L., (2022). Global expansion of *Vibrio parahaemolyticus* threatens the seafood industry: Perspective on controlling its biofilm formation, *LWT*, 158, 1-6.

ปัจจัยที่มีความสัมพันธ์กับระดับความเครียดของนักศึกษาหอพัก มหาวิทยาลัยราชภัฏยะลา

Factors Related to Stress Levels of Dormitory Students, Yala Rajabhat University

Rukaiyah Hayikuchi
Faculty of Science, Technology and Agriculture
Yala Rajabhat University
Muang District, Yala Province, Thailand
406424029@yru.ac.th

Piyaruk Pradabphetrat
Faculty of Science, Technology and Agriculture
Yala Rajabhat University
Muang District, Yala Province, Thailand
piyaruk.p@yru.ac.th

Sabudin Yingtha
Faculty of Science, Technology and Agriculture
Yala Rajabhat University
Muang District, Yala Province, Thailand
sabudin.y@yru.ac.th

***Abstract*—** The study aimed to study the stress level of students and to study the factors related to the stress level of students in the dormitory of Yala Rajabhat University. The sample group consisted of 329 dormitory students who were randomly selected. The data collection tools included general characteristics of individuals, academic factors, family factors, economic factors, and environmental factors, as well as the Department of Mental Health Stress Test (SPST). The data were analyzed using descriptive statistics, including percentages, means, and inferential statistics (Pearson's correlation coefficient).

This study's results found that most of the sample group was at a high stress level, 38.60 percent. The study of factors related to the stress level of the sample group included economic and environmental factors ($r = 0.477$, p-value $= 0.000$) regarding the impact of news on social media on stress, which significantly affected the stress level at ($r = 0.565$, p-value $= 0.000$), academic factors ($r = 0.437$, p-value $= 0.000$), and family factors ($r = 0.378$, p-value $= 0.000$), respectively. Recommendations from this study are that the university should improve and create boundaries for playing or using social media, and Yala Rajabhat University dormitory should promote students to have a way to earn in a short time; it is considered a danger zone in terms of stress. On the contrary, if it is not relieved, it will lead to chronic stress, which will cause various diseases later on. Therefore, the study of stress relief methods is necessary to continue.

***Keywords*—**stress level, factors affecting stress, dormitory students

I. บทนำ

ความเครียด สามารถพบเจอได้ในชีวิตประจำวันของคนทุกเพศ ทุกวัย อาจจะเป็นผู้ที่กำลังศึกษาอยู่หรือผู้ที่ทำงานแล้ว ความเครียดเกิดได้จากหลายปัจจัยไม่ว่าจะเป็นปัจจัยภายในตัวบุคคล หรือปัจจัยจากสิ่งแวดล้อม ในปัจจุบันพบว่าปัญหาด้านความเครียดมีมากขึ้นและมีแนวโน้มว่ามากขึ้นเรื่อย ๆ นักศึกษาในระดับอุดมศึกษาเป็นอีกกลุ่มหนึ่งที่กำลังเติบโตไปเป็นผู้ใหญ่ซึ่งจะต้องมีความพร้อมในการดำเนินชีวิตทั้งด้านการเรียน การปรับตัวในสังคม ภาระความรับผิดชอบในเรื่องต่าง ๆ ที่สูงขึ้น จึงส่งผลให้นักศึกษาต้องเผชิญกับความเครียดและปัญหาในรูปแบบต่าง ๆ [1] ความเครียดเป็นภาวะของอารมณ์หรือความรู้สึกที่เกิดขึ้นเมื่อบุคคลต้องเผชิญกับปัญหาต่าง ๆ และทำให้รู้สึกถูกกดดัน ไม่สบายใจ กลัว วิตกกังวล ตลอดจนถูกบีบคั้น เมื่อบุคคลรับรู้หรือประเมินว่าปัญหาเหล่านั้นเป็นสิ่งที่คุกคามจิตใจ หรืออาจจะก่อให้เกิดอันตรายแก่ร่างกาย ส่งผลให้สูญเสียสภาวะสมดุลของร่างกายและจิตใจ [2]

มหาวิทยาลัยราชภัฏยะลา มีหอพักนักศึกษาจำนวน 4 อาคาร จำนวนทั้งหมด 515 ห้อง จัดให้นักศึกษาเข้าพักห้องละ 4 คน สามารถรับนักศึกษาเข้าพักได้ 2,060 คน โดยในปี 2567 มีนักศึกษาเข้าพัก 1,800 คน เปรียบเสมือนชุมชนแห่งหนึ่งที่มีคนเข้ามาอยู่อาศัยรวมกัน ซึ่งเมื่ออยู่อาศัยรวมกันแล้วมีคนหลากหลาย มีความแตกต่างทางความคิด ลักษณะนิสัย และพฤติกรรม ทำให้เกิดความเครียดในการปรับตัวได้ นอกจากบรรยากาศการเรียนการสอนที่นักศึกษาจะต้องปรับตัวแล้ว สภาพแวดล้อมของสังคมมหาวิทยาลัยที่เปลี่ยนแปลงไป การอยู่ร่วมกับสังคมกลุ่มเพื่อนใหม่ที่ต้องมาอยู่ร่วมกันซึ่งต่างไปจากการพักอาศัยอยู่กับครอบครัว การใช้ชีวิตในสังคมใหม่ เพื่อนใหม่ สภาพแวดล้อมใหม่ และหากนักศึกษาต้องพักอาศัยอยู่หอพักรวมกับกลุ่มเพื่อนที่มาจากสถานที่ต่างกัน นอกจากจะต้องปรับตัวให้เข้ากับสังคมใหม่ สร้างสัมพันธภาพกับเพื่อนใหม่ที่มีพื้นฐานชีวิตแตกต่างกันแล้ว [3] นักศึกษายังต้องปฏิบัติตามกฎระเบียบหอพักและมหาวิทยาลัยอย่างเคร่งครัด ดังนั้นนักศึกษาซึ่งอยู่ในช่วงวัยรุ่นตอนปลายจึงมีโอกาสที่จะเกิดความเครียดขึ้นจากการเปลี่ยนแปลงเหล่านี้ โดยเฉพาะนักศึกษาหญิงที่อยู่ในช่วงวัยรุ่น ซึ่งเป็นวัยของการเปลี่ยนแปงทางร่างกาย เช่น การมีหน้าอก และความรักสวย รักงามของตนเอง เมื่อนักศึกษาหญิงต้องอยู่ร่วมกับสังคมใหม่ ในช่วงแรกจึงอาจเกิดความเครียด อีกทั้งวัยรุ่นหญิงมักมีแนวโน้มที่จะเครียดจากความสัมพันธ์ระหว่างบุคคลมากกว่าวัยรุ่นชาย [4]

ดังนั้นผู้วิจัยจึงมีความสนใจที่จะศึกษาปัจจัยที่มีความสัมพันธ์กับระดับความเครียดของนักศึกษาหอพักมหาวิทยาลัยราชภัฏยะลา เพื่อประเมินระดับความเครียดของนักศึกษาหอพักมหาวิทยาลัยราชภัฏยะลา และเพื่อศึกษาปัจจัยที่มีความสัมพันธ์กับระดับความเครียดของนักศึกษาหอพักมหาวิทยาลัยราชภัฏยะลา ซึ่งการศึกษาปัจจัยที่มีความสัมพันธ์กับระดับความเครียดเป็นเรื่องที่น่าสนใจที่จะศึกษา และด้วยเหตุนี้ผู้วิจัยจึงสนใจศึกษาวิจัยเรื่องนี้เพื่อเป็นการศึกษาเรียนรู้ลักษณะความเครียด แนวโน้มของระดับความเครียด ตลอดจนหาสาเหตุต่าง ๆ ที่ก่อให้เกิดความเครียดที่เกิดขึ้นจริงในภาวะปัจจุบันของกลุ่มนักศึกษาหอพักมหาวิทยาลัยราชภัฏยะลา โดยผู้วิจัยได้นำปัจจัยในด้านการเรียน ด้านครอบครัว สิ่งแวดล้อมและเศรษฐกิจมาใช้ในการกำหนดตัวแปรที่จะศึกษา เพื่อให้ได้รับทราบข้อมูลหรือข้อเท็จจริงเพื่อประกอบการอธิบายปรากฏการณ์ความเครียดที่กลายมาเป็นปัญหาสำคัญในสังคมที่เกิดขึ้นในกลุ่มเป้าหมายนี้เป็นข้อมูลพื้นฐานสำคัญในการทำความเข้าใจ และเป็นประโยชน์ต่องานแนะแนวหรือตลอดจนเพื่อเป็นแนวทางในการหาวิธีป้องกันแก้ไขเพื่อให้เกิดความเข้าใจในปัญหาต่าง ๆ ของนักศึกษาหอพักมหาวิทยาลัยราชภัฏยะลาที่จะนำข้อมูลที่ได้ไปใช้ประโยชน์ในการป้องกันการเกิดปัญหาสุขภาพจิต หรือส่งเสริมพัฒนานักศึกษาให้สามารถเรียนรู้ได้อย่างมีความสุขจนสำเร็จการศึกษาในที่สุดและส่งเสริมให้นักศึกษามีสุขภาพจิตที่ดีต่อไป

II. ทบทวนวรรณกรรม

ความเครียดเป็นภาวะที่ร่างกายและจิตใจตอบสนองต่อสิ่งที่มาคุกคามทั้งภายในและภายนอกตัวบุคคล รวมทั้งเหตุการณ์สภาพแวดล้อมต่าง ๆ ที่ทำให้เกิดความกดดัน ความทุกข์ และความไม่สบายใจ ทำให้เกิดการปรับตัวต่อสิ่งคุกคามนั้น ๆ เพื่อรักษาสมดุลของตนไว้ โดยแสดงออกมาทางกาย จิตใจ และพฤติกรรม ซึ่งมีความแตกต่างกันไปในแต่ละบุคคล [5]

สาเหตุความเครียดอันเนื่องจากการปรับตัวของนิสิตนักศึกษา สามารถจำแนกออกเป็น 4 ด้านใหญ่ [6] ดังนี้

1. ความเครียดอันเนื่องจากการปรับตัวด้านการเรียน การปรับตัวด้านการเรียน หมายถึง ความสามารถที่นิสิตนักศึกษาปรับปรุงตนเองเกี่ยวกับการเรียนด้านต่าง ๆ ที่นิสิตนักศึกษากำลังประสบอยู่ ได้แก่ การตั้งใจและเอาใจใส่ต่อการเรียน ความพยายามที่จะเรียนให้มี ผลสัมฤทธิ์ทางการเรียนดี และความพึงพอใจในสาขาที่เลือกเรียนการเรียนการสอนมีองค์ประกอบที่สำคัญ คือ ผู้เรียน ผู้สอน สิ่งแวดล้อม และปฏิสัมพันธ์ระหว่างผู้เรียนกับผู้สอนรวมทั้งปฏิสัมพันธ์ระหว่างผู้เรียนกับผู้เรียนด้วยกัน ซึ่งเป็นส่วนสำคัญมากในการปรับตัวด้านการเรียนของนิสิตนักศึกษา และอาจก่อให้เกิดอุปสรรคต่อการปรับตัวด้านการเรียน จึงเป็นการเหมาะสมที่สถาบันการศึกษาจะมีการดูแลเอาใจใส่ หาวิธี ป้องกันและช่วยเหลือนิสิตนักศึกษาที่ประสบปัญหาดังกล่าว [7]

2. ความเครียดอันเนื่องจากการปรับตัวด้านผู้สอน อาจารย์ในมหาวิทยาลัยเป็นองค์ประกอบที่สำคัญองค์ประกอบหนึ่งที่จะช่วยให้นิสิตนักศึกษาประสบความสำเร็จด้านการเรียน และการปรับตัว ทั้งนี้เพราะอาจารย์จะมีบทบาทสำคัญต่อการจัดการเรียนการสอน ในห้องเรียน เป็นผู้ช่วยส่งเสริมพฤติกรรมด้านการสร้างสรรค์ด้วยการเปิดโอกาสให้นิสิตนักศึกษาได้แสดง ความรู้ความสามารถอย่างเต็มที่ และอาจารย์ยังเป็นผู้ที่สามารถเลือกใช้รูปแบบการเรียนการสอนให้ เหมาะสมกับเนื้อหาวิชาและคุณลักษณะของผู้เรียน อีกด้วย รูปแบบการเรียนการสอนในมหาวิทยาลัยมีหลากหลายมากมายเพียงพอที่จะให้อาจารย์เลือกมาใช้ได้ตามความเหมาะสมของวัตถุประสงค์สภาพของ นิสิตนักศึกษา และเนื้อหาวิชาโดยทั่วไปแล้ว อาจารย์ในมหาวิทยาลัยส่วนใหญ่ใช้วิธีการสอนแบบบรรยาย ในชั้นเรียนเป็นสำคัญเพราะนิสิตนักศึกษามีเป็นจำนวนมาก แต่อาจเพิ่มโอกาสให้นิสิตนักศึกษามีส่วนร่วมในภายหลัง ดังนั้นคุณลักษณะและพฤติกรรมการสอนรูปแบบต่างๆของอาจารย์จึงมีความสำคัญอย่างยิ่งต่อการจัดการเรียนการสอนในชั้นเรียนหากคุณลักษณะ และพฤติกรรมของอาจารย์เป็นไปในทางที่ ดีจะเป็นผลทำให้การเรียนการสอนดำเนินไปด้วยดี มีประสิทธิภาพ และหากนิสิตนักศึกษาสามารถปรับตัวเข้ากับอาจารย์ได้เป็นอย่างดี ย่อมส่งผลไปสู่การเรียนที่มีประสิทธิภาพสูงตามไปด้วย [8] แต่เนื่องจากอาจารย์ในมหาวิทยาลัยมีลักษณะที่แตกต่างกันมีเสรีภาพทางวิชาการในการจัดการเรียนการสอนในแต่ละวิชาที่ตนรับผิดชอบจึงอาจเป็นส่วนหนึ่งที่จะก่อให้เกิดความลำบากใจแก่นิสิตนักศึกษาในการปรับตัว

3. ความเครียดอันเนื่องจากการปรับตัวด้านเพื่อนกลุ่มเพื่อนมีความสำคัญต่อนิสิตนักศึกษาในมหาวิทยาลัยที่จะต้องเรียนร่วมกันโดยมีพื้นฐานที่ต่างกัน ความสัมพันธ์ในหมู่นิสิตนักศึกษามีความสำคัญต่อการใช้ชีวิตในมหาวิทยาลัยตลอดจนการพัฒนาการด้านต่าง ๆ ของนิสิตนักศึกษาเป็นอย่างยิ่ง หากนิสิตนักศึกษาสามารถปรับตัวเข้ากับเพื่อนได้ ได้รับการยอมรับจากกลุ่มเพื่อนจะเรียนรู้บทบาทของตนเองเกี่ยวกับการปฏิบัติตนเมื่ออยู่ในกลุ่มเพื่อน ช่วยให้เกิดความรู้สึกอบอุ่นใจ มีความมั่นคงเกิดความเชื่อมั่นในตนเอง มีสุขภาพจิตดี สามารถเล่าเรียนได้อย่างมีประสิทธิภาพ หากนิสิตนักศึกษาคนใดปรับตัวเข้ากับเพื่อนไม่ได้ เพื่อนรังเกียจ จะรู้สึกว้าเหว่ ขาดความอบอุ่น มองโลกในแง่ร้ายและเกิดความคับข้องใจ ต้องเก็บกดไว้คนเดียว เมื่อมีเรื่องทุกข์ร้อนไม่สามารถเล่าให้ใครฟังได้ จะส่งผลให้มีอารมณ์เครียดอยู่เสมอ ขาดความสุข และย่อมส่งผลไปสู่การเรียนที่ด้อยประสิทธิภาพ

4. ความเครียดอันเนื่องจากกิจกรรมนิสิตนักศึกษาเป็นการจัดกระบวนการเรียนรู้ที่สำคัญนอกห้องเรียนนับเป็นส่วนหนึ่งของการให้การศึกษาตามหลักสูตรที่มหาวิทยาลัยจัดร่วมกับนิสิตนักศึกษา เพื่อให้นิสิตนักศึกษาเสริมสร้างประสบการณ์ทางการศึกษา ส่งเสริมพลานามัย พัฒนาคุณธรรม และบุคลิกภาพอันพึงประสงค์นิสิตนักศึกษาจะได้รับการสนับสนุนให้เข้าร่วม กิจกรรมต่าง ๆ ด้วยความสมัครใจ ตามความสนใจของนิสิตนักศึกษาในด้านต่าง ๆ โดยไม่มีส่วนเกี่ยวข้องกับคะแนนการดำเนินกิจกรรมต้องได้รับความเห็นชอบจากอาจารย์ที่ปรึกษา และได้รับการสนับสนุนจากมหาวิทยาลัย

ระดับความเครียดสามารถวัดได้จากพฤติกรรมที่เป็นปฏิกิริยาตอบสนองต่อสิ่งหรือเหตุการณ์ต่าง ๆ ที่มากระทบต่อบุคคลนั้นได้มีการแสดงออกมาหลากหลายรูปแบบ ตั้งแต่ระดับที่สามารถควบคุมตนเองได้ จนถึงระดับที่ควบคุมตนเองไม่ได้ [9] ซึ่งสามารถแบ่งออกได้เป็น 5 ระดับตามระดับความเครียดของกรมสุขภาพจิต กระทรวงสาธารณสุข [10] ได้แก่

1. ระดับความเครียดต่ำกว่าเกณฑ์ปกติอย่างมาก เป็นระดับที่บุคคลอาจรู้สึกพึงพอใจกับการดำเนินชีวิตที่เป็นอยู่ โดยมีแรงกดดันหรือแรงจูงใจในการดำเนินชีวิตที่น้อยกว่าบุคคลอื่น

2. ระดับความเครียดเกณฑ์ปกติ เป็นระดับที่บุคคลสามารถจัดการกับความเครียดที่เกิดขึ้นในชีวิตประจำวัน และสามารถปรับตัวตอสถานการณต่าง ๆ ได้อย่างเหมาะสม

3. ระดับความเครียดสูงกว่าปกติเล็กน้อย เป็นระดับที่บุคคลมีความไม่สบายใจ อันอาจเกิดจากปัญหาในการดำเนินชีวิตประจำวัน หรือมีปญหาอุปสรรคหรือข้อขัดแย้งที่อาจจะยังไม่ได้รับการคลี่คลายหรือแก้ไข ซึ่งถือว่าเป็นความเครียดที่พบได้ในชีวิตประจำวัน ขณะเดียวกันความเครียดที่เกิดขึ้นในระดับนี้อาจรู้สึกได้จากการเปลี่ยนแปลงของร่างกาย อารมณ์ ความรู้สึก และพฤติกรรมบ้างเล็กน้อยแต่ไม่ชัดเจนและยังพอทนได้

4. ระดับความเครียดสูงกว่าปกติปานกลาง เป็นระดับที่บุคคลเริ่มมีความตึงเครียดในระดับค่อนข้างสูงและได้รับความเดือดร้อนเป็นอย่างมากจากปัญหาทางอารมณที่เกิดจากปัญหาความขัดแย้งและวิกฤติการณ์ในชีวิต โดยอาจสังเกตได้จากอาการแสดงถึงการเปลี่ยนแปลงทางร่างกาย อารมณ์ ความคิด พฤติกรรมการดำเนินชีวิต และสิ่งที่แสดงออกเป็นสัญญาณเตือนขั้นต้นว่าบุคคลนั้นกำลังเผชิญภาวะวิกฤติและความขัดแย้ง ซึ่งบุคคลจัดการหรือแก้ไขด้วยความยากลำบาก ตราบใดที่ความขัดแย้งต่าง ๆ ยังคงมีอยู่ ลักษณะอาการต่าง ๆ จะเพิ่มรุนแรงมากขึ้น ความเครียดระดับนี้มีผลกระทบต่อการดำเนินชีวิตได้

5. ระดับความเครียดสูงกว่าปกติมาก เป็นระดับที่บุคคลกำลังตกอยู่ในภาวะตึงเครียดหรือกำลังเผชิญกับวิกฤติการณ์ในชีวิตอย่างรุนแรง หากปล่อยให้ความเครียดในระดับนี้ยังคงมีอยู่ตอไปโดยไม่ดำเนินการแก้ไขอย่างเหมาะสมและถูกวิธี อาจนำไปสู่ความเจ็บป่วยทางจิตที่รุนแรง ซึ่งส่งผลเสียต่อตนเองและบุคคลใกลชิดต่อไปได้

ความเครียดเป็นภาวะความกดดันที่ไม่สามารถสังเกตเห็นได้ แต่เมื่อบุคคลรู้สึกเครียดจะมีปฏิกิริยาตอบสนองต่อความเครียด 4 ทาง คือ ด้านความคิด อารมณ์ พฤติกรรม และสรีระ ดังนั้นจึงสามารถประเมินความเครียดโดยการวัดจากปฏิกิริยาตอบสนองเหล่านี้ ซึ่งสรุปได้ 4 วิธี ดังนี้ [11]

1. การให้บุคคลรายงานเกี่ยวกับตนเอง (Self-report) เช่น การตอบแบบสอบถาม (Questionnaire) แบบสัมภาษณ์ แบบสำรวจ หรือแบบทดสอบมาตรฐานที่สร้างขึ้น และมีการหาคุณภาพของแบบทดสอบเหล่านั้น ทั้งในด้านความเที่ยงและความตรง แบบทดสอบความเครียดที่ใช้ เช่น

1) แบบสอบถาม SCL-90 (Symptom check list 90) ประกอบด้วยข้อคำถาม 90 ข้อ ชนิด 5 สเกล ใช้วัดความผิดปกติทางด้านจิตใจ วัดความเครียดที่แสดงออกทางร่างกาย (Somatization) อาการย้ำคิดย้ำทำ ความรู้สึกไวต่อผู้อื่น อาการเศร้า วิตกกังวล ความรู้สึกไม่เป็นมิตร ความคิดหวาดระแวง ความหลงผิดและประสาทหลอน

2) แบบสอบถาม CMI (Cornell medical index) เป็นแบบสำรวจสุขภาพจิตทั่ว ๆ ไป ประกอบด้วย ข้อคำถาม ใช่หรือไม่ใช่ จำนวน 195 ข้อ ในแบบสอบถามจะถามถึงภาวะทางจิต คือ จะถามภาวะความเศร้า ความวิตกกังวล ความรู้สึกไวต่อสิ่งเร้า ความรู้สึกโกรธ และความรู้สึกเครียด ซึ่งเป็นประเภทการวัดอาการแสดงความเจ็บป่วยทางจิต

3) แบบสำรวจ HOS (Health opinion survey) เป็นแบบสำรวจเกี่ยวกับสุขภาพกาย มีข้อคำถามจำนวน 20 ข้อ ซึ่งถามเกี่ยวกับอาการผิดปกติทางร่างกาย จำนวน 18 ข้อ อีก 2 ข้อถาม เกี่ยวกับจิตใจที่แสดงออกถึงผลของการปรับตัวต่อความเครียด

4) แบบประเมินความเครียด SOS (Symptoms of stress inventory) เป็นแบบสำรวจเพื่อประเมินระดับความเครียดของภาควิชาการพยาบาลจิตสังคม มหาวิทยาลัยวอชิงตัน ประเทศสหรัฐอเมริกา ดัดแปลงมาจาก Cornell medical index มีข้อคำถามจำนวน 107 ข้อ เหมาะกับการศึกษาในกลุ่มคนที่ปฏิบัติงานในสถานที่ทำงานที่เครียดและเป็นภาระ เช่น ผู้ปฏิบัติงานด้านธุรกิจการเงิน ธนาคาร ตำรวจ พยาบาลในหอผู้ป่วยหนัก เป็นต้น

5) แบบวัดความเครียดสวนปรุง (SPST-20) ประกอบด้วย ข้อคำถาม 20 ข้อ ชนิด 5 สเกล ในแบบสอบถามจะถามถึงภาวะทางจิต คือ ภาวะความเศร้า ความวิตกกังวล ความรู้สึกโกรธ และวัดความเครียดที่แสดงออกทางร่างกาย

6) แบบประเมินและวิเคราะห์ความเครียด (Street test) ประกอบด้วยข้อคำถาม 20 ข้อ ซึ่งถามเกี่ยวกับอาการ พฤติกรรม หรือความรู้สึกในระยะเวลา 2 เดือนที่ผ่านมา เป็นเครื่องมือที่พัฒนาขึ้นโดยกรมสุขภาพจิต เพื่อใช้วิเคราะห์หาความเครียดสำหรับประชาชนไทย

2. การใช้เทคนิคการฉายภาพ (Projective techniques) เป็นการวัดการตอบสนองของบุคคลที่มีต่อสิ่งเร้าที่กำหนดให้เป็นการฉายภาพของบุคคลนั้นผ่านการตอบสนอง เช่น แบบทดสอบ Rorschach แบบทดสอบ TAT (Thematic apperception test) การวัดโดยวิธีนี้ต้องอาศัยความเชี่ยวชาญเฉพาะในการแปลผล ซึ่งได้รับการฝึกฝนมาเป็นพิเศษ

3. การใช้การสังเกต (Observation) สามารถสังเกตได้จากพฤติกรรมที่แสดงออก เมื่อบุคคลตกอยู่ในภาวะความเครียด เช่น พูดจาเกรี้ยวกราด เบื่ออาหาร นอนไม่หลับ ไม่มีสมาธิ ประสิทธิภาพในการทำงานลดน้อยลง หรือสังเกตจากภาษาท่าทาง เช่น ถอนหายใจบ่อย ๆ สีหน้า แววตา น้ำเสียง และท่านั่ง เป็นต้น

4. การวัดการเปลี่ยนแปลงทางสรีระ (Neurophysiological change) เป็นการวัดการเปลี่ยนแปลงทางร่างกาย เช่น อัตราการเต้นของหัวใจ อัตราการหายใจ ความดันโลหิต ความตึงของกล้ามเนื้อ (EMG biofeedback) เป็นต้น การวัดด้วยวิธีนี้ต้องใช้ผู้เชี่ยวชาญและเครื่องมือที่มีประสิทธิภาพ

III. ระเบียบวิธีวิจัย

- **ประชากรและกลุ่มตัวอย่าง**

ประชากรใช้ในการศึกษาครั้งนี้ คือนักศึกษาหอพัก มหาวิทยาลัยราชภัฏยะลา ทั้งหมด 1861 คน โดยใช้วิธีกำหนดขนาดตัวอย่างตามสูตรการคำนวณของ Yamane (1973) โดยกำหนดระดับเชื่อมั่น 95% ความคลาดเคลื่อนไม่เกิน 5% ได้ขนาดกลุ่มตัวอย่างประมาณ 329 คน มาจากการเลือกตัวอย่าง โดยการสุ่มตัวอย่างแบบแบ่งพวกหรือแบ่งชั้น (Stratified Random Sampling)

- **เครื่องมือที่ใช้ในการวิจัย**

เครื่องมือที่ใช้ในการวิจัยครั้งนี้ เป็นแบบสอบถาม ซึ่งแบ่งออกเป็น 2 ส่วน ดังนี้

ส่วนที่ 1 เป็นข้อมูลทั่วไปของนักศึกษาหอพัก ได้แก่ เพศ อายุ คณะที่ศึกษา ระดับชั้นปี รายได้ที่ได้รับต่อเดือน การเป็นผู้กู้เงินกองทุนกู้ยืมเพื่อการศึกษา (กยศ.) การดื่มเครื่องดื่มประเภทแอลกอฮอล์ สถานภาพครอบครัวของบิดามารดา โรคประจำตัว

ส่วนที่ 2 เป็นข้อมูลเกี่ยวกับปัจจัยที่ส่งผลต่อความเครียดของนักศึกษาหอพัก มหาวิทยาลัยราชภัฏยะลา ได้แก่ ปัจจัยด้านการเรียน ปัจจัยด้านครอบครัว ปัจจัยด้านเศรษฐกิจและสภาพแวดล้อม และแบบวัดความเครียดกรมสุขภาพจิต (SPST)

โดยแบ่งคะแนนออกเป็น 5 ระดับ คือ (1) น้อยที่สุด (2) น้อย (3) ปานกลาง (4) มาก และ (5) มากที่สุด มีเกณฑ์ในการแปลผล คือ คะแนนเฉลี่ย 4.21-5.00 หมายถึง ระดับความเครียดมากที่สุด คะแนนเฉลี่ย 3.41-4.20 หมายถึง ระดับความเครียดมาก คะแนนเฉลี่ย 2.61-3.40 หมายถึง ระดับความเครียดปานกลาง คะแนนเฉลี่ย 1.81-2.60 หมายถึง ระดับความเครียดน้อย และคะแนนเฉลี่ย 1.00-1.81 หมายถึง ระดับความเครียด น้อยที่สุด

- **การทดสอบคุณภาพเครื่องมือ**

ผู้วิจัยมีการทดสอบความเที่ยงตรง (Validity) ของแบบสอบถาม โดยให้ผู้เชี่ยวชาญพิจารณาและตรวจสอบความเที่ยงตรงเชิงเนื้อหา (Content Validity) และความเหมาะสมของภาษาที่ใช้ (Wording) เพื่อให้อ่านเข้าใจง่าย ทำความมุ่งหมายของการวิจัยและนำไปปรับปรุงตามคำแนะนำก่อนนำไปเป็นแบบสอบถามในการเก็บข้อมูลจริง โดยใช้ดัชนีความสอดคล้องของแบบทดสอบกับจุดประสงค์ (The Index of Item Objective Congruence: IOC) และการทดสอบความเชื่อมั่น (Reliability) ผู้วิจัยได้นำแบบทดสอบที่พัฒนาขึ้นมาและปรับปรุงแก้ไขตาม คำแนะนำของผู้เชี่ยวชาญไปทำการทดลองใช้ (Try out) กับกลุ่มตัวอย่าง จำนวน 30 คน แล้วนำแบบสอบถามไป หาค่าสัมประสิทธิ์อัลฟ่าของครอนบาค (Cronbach Alpha Coefficient)

IV. ผลการทดลอง

1. ข้อมูลทั่วไป

กลุ่มตัวอย่างจำนวน 329 คน เป็นเพศชาย ร้อยละ 20.36 เพศหญิง ร้อยละ 79.63 ส่วนใหญ่มีอายุน้อยกว่าหรือเท่ากับ 19 คิดเป็นร้อยละ 44.99 สมาชิกส่วนใหญ่ศึกษาที่คณะวิทยาศาสตร์เทคโนโลยีและการเกษตร คิดเป็นร้อยละ 38.3 กำลังศึกษาชั้นปีที่ 2 ร้อยละ 40.42 รายได้ที่รับต่อเดือนต่ำกว่า 3,000 บาท/เดือน ร้อยละ 59.27 เป็นผู้กู้เงินกองทุนกู้ยืมเพื่อการศึกษา ร้อยละ 87.84 ไม่ดื่มเครื่องดื่มประเภทแอลกอฮอล์ ร้อยละ 97.87 สถานภาพครอบครัวของบิดามารดาอยู่ด้วยกัน ร้อยละ 74.47 และไม่มีโรคประจำตัว ร้อยละ 92.7

2. ปัจจัยด้านการเรียน

ปัจจัยด้านการเรียนกับระดับความเครียดของนักศึกษาหอพักมหาวิทยาลัยราชภัฏยะลา (n = 329) มีความสัมพันธ์อยู่ในระดับปานกลาง ($r = 0.437$, $p < 0.000$) เมื่อพิจารณาเป็นรายข้อ พบว่า สาเหตุที่ก่อให้เกิดความเครียดของนักศึกษาหอพัก มหาวิทยาลัยราชภัฏยะลาอยู่ในระดับปานกลาง คือ ท่านมีความกดดัน ในการเรียน ($r = 0.925$, $p < 0.000$) และผลการเรียนของท่านไม่เป็นไปตามที่คาดหวังไว้ ($r = 0.417$, $p < 0.000$) ตามลำดับ ดังตารางที่ 1

3. ปัจจัยด้านครอบครัว

ปัจจัยด้านครอบครัวกับระดับความเครียดของนักศึกษาหอพักมหาวิทยาลัยราชภัฏยะลา (n = 329) มีความสัมพันธ์อยู่ในระดับปานกลาง ($r = 0.378$, $p < 0.000$) เมื่อพิจารณาเป็นรายข้อ พบว่า สาเหตุที่ก่อให้เกิดความเครียดของนักศึกษาหอพัก มหาวิทยาลัยราชภัฏยะลาอยู่ในระดับปานกลาง คือ ผู้ปกครองมีการคาดหวังในตัวท่านมากเกินไปจนท่านรู้สึกกดดัน ($r = 0.467$, $p < 0.000$) และท่านขาดการสนับสนุนในด้านต่าง ๆ จากครอบครัว ($r = 0.453$, $p < 0.000$) ตามลำดับ ดังตารางที่ 1

4. ปัจจัยด้านเศรษฐกิจและสภาพแวดล้อม

ปัจจัยด้านเศรษฐกิจและสิ่งแวดล้อมกับระดับความเครียดของนักศึกษาหอพักมหาวิทยาลัยราชภัฏยะลา (n = 329) มีความสัมพันธ์อยู่ในระดับปานกลาง ($r = 0.473$, $p < 0.000$) เมื่อพิจารณาเป็นรายข้อ พบว่า สาเหตุที่ก่อให้เกิดความเครียดของนักศึกษาหอพัก มหาวิทยาลัยราชภัฏยะลาอยู่ในระดับปานกลาง คือ การได้ข่าวสารทางโซเชียลมีเดียมีผลต่อความเครียด ($r = 0.565$, $p < 0.000$) และรายจ่ายของท่านที่มีมากกว่ารายรับ ($r = 0.536$, $p < 0.000$) ตามลำดับ ดังตารางที่ 1

5. แบบวัดความเครียดกรมสุขภาพจิต (SPST)

ปัจจัยด้านความเครียดมีความสัมพันธ์กับระดับความเครียดของนักศึกษาหอพัก มหาวิทยาลัยราชภัฏยะลาอยู่ในระดับสูง ($r = 0.708$, $p < 0.000$) เมื่อพิจารณาเป็นรายข้อ พบว่า สาเหตุที่ก่อให้เกิดความเครียดของนักศึกษาหอพักมหาวิทยาลัยราชภัฏยะลาอยู่ในระดับสูง คือ ปวดหัวจากความตึงเครียด ($r = 0.796$, $p < 0.000$) และรู้สึกสับสน ($r = 0.781$, $p < 0.000$) และรู้สึกวิตกกังวล ($r = 0.779$, $p < 0.000$) ตามลำดับ ดังตารางที่ 2

V. อภิปรายผล

จากการศึกษาระดับความเครียดและปัจจัยที่มีความสัมพันธ์กับระดับความเครียดของนักศึกษาหอพัก มหาวิทยาลัยราชภัฏยะลา สามารถอภิปรายผลตามวัตถุประสงค์การวิจัยได้ ดังนี้

1. ระดับความเครียดของนักศึกษาหอพัก มหาวิทยาลัยราชภัฏยะลา พบว่า ระดับความเครียดของนักศึกษาหอพักมีความเครียดอยู่ในระดับสูง คิดเป็นร้อยละ 38.98 และรองลงมา คือ นักศึกษามีความเครียดอยู่ในระดับรุนแรง คิดเป็นร้อยละ 34.28 สอดคล้องกับการศึกษาของรุ่งทิวา พุขุนทด และคณะ [12] พบว่า ระดับความเครียดของนักศึกษาระดับปริญญาตรี มหาวิทยาลัยเทคโนโลยีสุรนารี จังหวัดนครราชสีมามีความเครียดอยู่ในระดับสูง คิดเป็นร้อยละ 44 ซึ่งความเครียดในระดับรุนแรงและสูงเป็นระดับที่บุคคลได้รับเหตุการณ์ที่ก่อให้เกิดความเครียดสูงถึงสูงมาก อาจไม่สามารถปรับตัวให้ลดความเครียดได้ในเวลาอันสั้น ถือว่าอยู่ในเขตอันตรายของความเครียด นอกจากนี้สอดคล้องกับการศึกษาของจุฑารัตน์ สถิรปัญญา และวิทยา เหมพันธ์ [13] พบว่า นักศึกษามหาวิทยาลัยแห่งหนึ่งร้อยละ 57.6 มีความเครียดในระดับสูง และร้อยละ 22.1 เครียดระดับรุนแรง แสดงให้เห็นว่านักศึกษามีภาวะเครียด ซึ่งควรเร่งหากลวิธีลดความเครียดให้แก่นักศึกษาที่มีระดับความเครียดรุนแรงและสูง จัดระบบดูแล ส่งเสริม และป้องกันปัญหาสุขภาพจิต เช่น การจัดให้มีหน่วยบริการให้การปรึกษาของคณะในรูปแบบพี่ช่วยน้อง เพื่อให้นักศึกษาสามารถเข้าถึงบริการ การจัดกิจกรรมการเรียนการสอนที่สอดแทรกการผ่อนคลายหรือลดความเครียด เพิ่มศักยภาพอาจารย์ที่ปรึกษาในการใช้เทคนิคการให้การปรึกษาเบื้องต้น จัดกิจกรรมผ่อนคลาย สภาพแวดล้อมที่ผ่อนคลาย และกำหนดให้มีระบบคัดกรองและเฝ้าระวังปัญหาสุขภาพจิตของนักศึกษาก่อนเข้าเรียน เพื่อลดภาวะเครียด พัฒนาคุณภาพชีวิต และป้องกันปัญหาสุขภาพจิตให้กับนักศึกษา

2. ปัจจัยที่มีความสัมพันธ์กับระดับความเครียดของนักศึกษาหอพักมหาวิทยาลัยราชภัฏยะลา พบว่า ปัจจัยด้านเศรษฐกิจและสภาพแวดล้อมของนักศึกษาหอพัก มหาวิทยาลัยราชภัฏยะลา เป็นปัจจัยที่มีความสัมพันธ์ต่อระดับความเครียดของกลุ่มตัวอย่าง ซึ่งข้อที่มีค่าเฉลี่ยมากที่สุด คือ การได้ข่าวสารทางโซเชียลมีเดียมีผลต่อความเครียด รายจ่ายของท่านที่มีมากกว่ารายรับของท่าน ค่าใช้จ่ายในด้านการเรียน เช่น ค่าหนังสือ อุปกรณ์การเรียน งานกลุ่ม และปัจจัยด้านการเรียน ซึ่งเกี่ยวข้องกับหลักสูตร และรูปแบบการเรียนการสอนของแต่ละคณะที่นักศึกษากำลังศึกษาอยู่อย่างมีนัยสำคัญทางสถิติที่ระดับ 0.05 สอดคล้องกับการศึกษาของระวิวรรณ แสงฉาย, พรวิภา เย็นใจ และล้ำศักดิ์ ชวนิชย์ [14] และสิริทรัพย์ สีหะวงษ์ และคณะ [15] พบว่า ปัจจัยที่มีผลต่อระดับความเครียดของนักศึกษา ได้แก่ ปัจจัยส่วนบุคคล ปัจจัยด้านการเรียน และปัจจัยด้านเศรษฐกิจและสภาพแวดล้อมในการดำเนินชีวิต

VI. ข้อสรุป

การวิจัยครั้งนี้สามารถนำไปประยุกต์ใช้ในการป้องกันการเกิดปัญหาทางด้านสุขภาพจิตของนักศึกษาหอพัก มหาวิทยาลัยราชภัฏยะลา และหาแนวทางที่เหมาะสมกับนักศึกษาในการผ่อนคลายความเครียด รวมถึงการจัดตั้งหน่วยงานที่ดูแลเรื่องสุขภาพจิตของนักศึกษาเพื่อให้ความรู้เรื่องสุขภาพจิต การผ่อนคลายความเครียดที่ถูกต้อง และวิธีการปรับตัวตามสภาพแวดล้อม เพื่อให้เกิดความเข้าใจในปัญหาต่าง ๆ ของนักศึกษาที่ส่งผลต่อระดับความเครียด

คำขอบคุณ

คณะผู้วิจัยขอขอบคุณกลุ่มตัวอย่างและผู้ที่มีส่วนเกี่ยวข้องทุกท่านที่มีส่วนร่วมในการให้ข้อมูล และการดำเนินการจัดทำการศึกษาวิจัยในครั้งนี้ให้สำเร็จลุล่วงและสมบูรณ์

อ้างอิง

[1] S. Phanhan, B. Panthai, and K. Srihaset, “Factors affecting learning stress of 4th - 6th year medical students. Faculty of Medicine, Ramathibodi Hospital Mahidol University,” *Veridian E-Journal, Silpakorn University*, vol. 11, no. 3, pp. 2579-2593, September-December 2018.

[2] H. Piyayodilokchai, A. Kampusiripong, M. Sawatmuang, and T. Chandrapas, *Stress and stress coping of Business Information Technology students of Rajamangala University of Technology Rattanakosin, Bophit Phimuk Chakkrawat*, Bangkok: Rajamangala University of Technoogy Rattanakosin, Bophitphimuk Chakkrawat Campus, 2014.

[3] T. Chantarasena, “Stress of freshmen at Srinakrinwirot University,” M.Ed. Thesis, Dept. Higher Education, Srinakrinwirot University, Bangkok, Thailand, 2012.

[4] S. Tantalanukul and P. Wongsawat, “Stress and stress management in nursing students,” *Boromarajonani College of Nursing, Uttaradit Journal*, vol. 9, no. 1, pp. 81-92, January-June 2017.

[5] S. Tantalanukul, “Model of stress reduction for nursing students in northern-region nursing colleges by Ministry of Public Health,” Ph.D. dissertation, Dept. Public Health, Naresuan University, Phitsanulok, Thailand, 2022.

[6] S. Terdwongworakul., “A study of adjustment and mental health of students at the Faculty of Engineering at Kampangsaen Kasetsart University,” M.Ed. Thesis, Dept. Guidance and Counseling Psychology, Srinakrinwirot University, Bangkok, Thailand, 2004.

[7] R. Pongsuvan, “A study of Ramkhamhaeng University first year students’ ploblems in learning,” M.Ed. Thesis, Dept. Development Psychology, Srinakrinwirot University, Bangkok, Thailand, 1997.

[8] S. Boonyawong, *Solving the problem of student adjustment in dormitories through group counseling*, Songkla: Department of Counseling and Educational Psychology, Srinakrinwirot University, 1996.

[9] A. Anantanatorn, *Stress and tension management of police officers in the Provincial Police Region 2*, Chon Buri: Faculty of Political Science and Law, Burapha University, 2016.

[10] U. Saelao, “Stress and adjustment of the first year undergraduate students of Srinakharinwirot University,” M.Sc. Thesis, Dept. Health Education, Srinakrinwirot University, Bangkok, Thailand, 2007.

[11] M. Tasiri, “Stress management process for Kasikornthai Bank employees, Tha Pae road branch, Mueang Chiang Mai district,” M.Ed. Thesis, Dept. Health Promotion, Chiang Mai University, Chiang Mai, Thailand, 2014.

[12] R. Pukhuntho, T. Karnjana, P. Yimchoen, A. Phutnok, N. Temsranoi, A. Chaladdee, and C. Hanchenlaksh, “The factors associated with stress level of undergraduate student,” *KKU Journal for Public Health Research*, vol. 14, no. 3, pp. 115-125, July–September 2021.

[13] C. Sathirapanya and W. hemapandha, “Stress among students in university,” *Journal of Liberal Arts, Maejo University*, vol. 1, no. 1, pp. 42-58, January-June, 2013.

[14] R. Sangchai, P. Yenjai1, and L. Chavanich, *Factor affecting stress in student, Faculty of Public Health, Bangkokthonburi University*, Bangkok: Bangkokthonburi University, 2014.

[15] S. Sihawong *et al*., "Factors causing to stress of nursing students, Ubon Ratchathani University," *Huachiew Chalermprakiet University Journal*, vol. 21, no. 42, pp. 93-106, January-June, 2018.

ตารางที่ 1 ปัจจัยด้านการเรียน ปัจจัยด้านครอบครัว ปัจจัยด้านเศรษฐกิจและสภาพแวดล้อมกับระดับความเครียดของนักศึกษาหอพักหาวิทยาลัยราชภัฏยะลา (n = 329)

ปัจจัย	ระดับความเครียด	
	r	p-value
ปัจจัยด้านการเรียน		
1. ท่านไม่ได้เรียนในคณะหรือสาขาที่ตนเองสนใจ	0.286	0.000
2. ตารางเรียนในแต่ละสัปดาห์มีเหมาะสม	0.263	0.000
3. บุคลิกภาพของผู้สอนส่งผลต่อการเข้าเรียนของท่าน	0.377	0.000
4. ท่านมีความคาดหวังสูงกับเกรดเฉลี่ย	0.357	0.000
5. ผลการเรียนของท่านไม่เป็นไปตามที่คาดหวังไว้	0.417	0.000
6. ท่านมีความกดดันในการเรียน	0.925	0.000
เฉลี่ย	**0.437**	**0.000**
ปัจจัยด้านครอบครัว		
1. ผู้ปกครองมีการคาดหวังในตัวท่านมากเกินไปจนท่านรู้สึกกดดัน	0.467	0.000
2. ตัวท่านมีการโต้เถียงกับคนในครอบครัวอยู่บ่อยครั้งเพราะความเห็นไม่ตรงกัน	0.446	0.000
3. ในครอบครัวมีการกำหนดกฎกติกาในครอบครัวอย่างเหมาะสม	0.301	0.000
4. ท่านขาดการสนับสนุนในด้านต่างๆจากครอบครัว	0.453	0.000
5. ครอบครัวของท่านเอาใจใส่ลูกเท่าๆกัน	0.300	0.000
6. ผู้ปกครองใช้อารมณ์ในการสั่งสอนท่าน	0.383	0.000
7. ผู้ปกครองยอมรับความคิดเห็นในมุมมองของท่าน	0.297	0.000
เฉลี่ย	**0.378**	**0.000**
ปัจจัยด้านเศรษฐกิจและสภาพแวดล้อม		
1. ค่าใช้จ่ายในการดำเนินชีวิต เช่น ค่าอาหาร ค่าหอ ค่าเดินทาง ค่าโทรศัพท์	0.471	0.000
2. ค่าใช้จ่ายในด้านการเรียน เช่น ค่าหนังสือ อุปกรณ์การเรียน งานกลุ่ม	0.500	0.000
3. ค่าใช้จ่ายเพื่อความบันเทิง	0.465	0.000
4. รายจ่ายของท่านที่มีมากกว่ารายรับของท่าน	0.536	0.000
5. ท่านมีความกดดันที่จะต้องหารายได้ เช่น การรับจ้างทำงานหลังเลิกเรียน	0.511	0.000
6. ค่าใช้จ่ายในการศึกษามากกว่าด้านอื่นๆ	0.481	0.000
7.ท่านมีความสะดวกในการจับจ่ายซื้อของ เช่น อาหาร เครื่องใช้ส่วนตัว เป็นต้น	0.365	0.000
8. ท่านได้กลิ่นไม่พึงประสงค์ เช่น ควันบุหรี่ กลิ่นขยะ กลิ่นท่อน้ำทิ้ง เป็นต้น	0.493	0.000
9. สภาพแวดล้อมบริเวณที่พักอาศัย ไม่เอื้ออำนวยต่อการพักผ่อน	0.478	0.000
10. ภายในมหาวิทยาลัยมีสถานที่พักผ่อนหย่อนใจ	0.390	0.000
11. สิ่งอำนวยความสะดวกยังไม่เพียงพอ เช่น ที่จอดรถไม่พอ การจราจรติดขัด	0.421	0.000
12. การได้ข่าวสารทางโซเชียลมีเดียมีผลต่อความเครียด	0.565	0.000
เฉลี่ย	**0.473**	**0.000**

ตารางที่ 2 ความสัมพันธ์ของนักศึกษาหอพักมหาวิทยาลัยราชภัฏยะลา (n = 329)

ปัจจัยด้านความเครียดกับระดับความเครียด	ระดับความเครียด	
	r	p-value
1. กลัวทำงานผิดพลาด	0.700	0.001
2. ไปไม่ถึงเป้าหมายที่วางไว้	0.708	0.000
3. ครอบครัวมีความขัดแย้งกันในเรื่องเงินหรือเรื่องงานในบ้าน	0.581	0.000
4. เป็นกังวลกับเรื่องสารพิษหรือมลภาวะในอากาศ น้ำ เสียง และดิน	0.668	0.000
5. รู้สึกว่าต้องแข่งขันหรือเปรียบเทียบ	0.678	0.000
6. เงินไม่พอใช้จ่าย	0.689	0.000
7. กล้ามเนื้อตึงหรือปวด	0.683	0.000
8. ปวดหัวจากความตึงเครียด	0.796	0.000
9. ปวดหลัง	0.653	0.000
10. ความอยากอาหารเปลี่ยนแปลง	0.725	0.000
11. ปวดศีรษะข้างเดียว	0.701	0.000
12. รู้สึกวิตกกังวล	0.779	0.000
13. รู้สึกคับข้องใจ	0.767	0.000
14. รู้สึกโกรธ หรือหงุดหงิด	0.757	0.000
15. รู้สึกเศร้า	0.746	0.000
16. ความจำไม่ดี	0.711	0.000
17. รู้สึกสับสน	0.781	0.000
18. ตั้งสมาธิลำบาก	0.740	0.000
19. รู้สึกเหนื่อยง่าย	0.728	0.000
20. เป็นหวัดบ่อยๆ	0.582	0.000
เฉลี่ย	**0.708**	**0.000**

การพัฒนาเครื่องตัดหลอดดูดน้ำจากต้นกระจูดด้วยระบบนิวแมติกส์

DEVELOPMENT OF A STRAW CUTTING MACHINE FROM KRAJOOD USING A PNEUMATIC SYSTEM

*Komkit Seepan
Program in Industrial Electrical Technology, Faculty of Science and Technology
Suratthani Rajabhat University
Suratthani, Thailand.
komkit.see@sru.ac.th

Peerapong Nuchuay
Program in Industrial Electrical Technology, Faculty of Science and Technology
Suratthani Rajabhat University
Suratthani, Thailand.
Peerapong.nuc@sru.ac.th

Mintra Trongtorkarn
Program in Industrial Electrical Technology, Faculty of Science and Technology
Suratthani Rajabhat University
Suratthani, Thailand.
Mintra.tro@sru.ac.th

Abstract— *Currently, the production of natural drinking straws is gaining increasing popularity. Many community enterprises have shown interest in utilizing hollow-stemmed plants to develop straw products, using materials such as Rapho plants, sedges, and other similar plants. Among these enterprises, the Pru Kuan Khreng Community Enterprise, located in Khuan Khreng Subdistrict, Nakhon Si Thammarat Province, has developed sedge straws for sale. Traditionally, the production process involved manual cutting, which resulted in a significant loss of raw materials, with up to 60% wastage due to cracks and uneven straw lengths.*

This issue, researchers have developed a sedge straw-cutting machine to minimize losses caused by cracks and inconsistencies during the cutting process. The cutting machine is designed with dimensions of 70 cm in width, 32 cm in length, and 110 cm in height. The machine utilizes Programmable Logic Controller for control and a pneumatic system to reduce cracking during the cutting process. This innovation allows for faster and more precise cutting, saving time and ensuring consistency in straw lengths, achieving a high-quality standard of 14.5 cm per straw. The machine effectively reduces material loss during the production of plant-based straws by up to 90%.

Keywords—Krajood Natural Tube,Tube Cutter, Natural water straw

I. บทนำ

ปัจจุบันรัฐบาลให้การสนับสนุนด้านเศรษฐกิจชีวภาพ เศรษฐกิจหมุนเวียน และเศรษฐกิจสีเขียว หรือ BCG Economy (Bio-Circular-Green Economy) เป็นโมเดลเศรษฐกิจสู่การพัฒนาที่ยั่งยืน เป็นแนวคิดการนำวิทยาศาสตร์ เทคโนโลยีและนวัตกรรมไปยกระดับความสามารถในการแข่งขันอย่างยั่งยืนให้กับ 4 อุตสาหกรรมเป้าหมาย (S-curves) [2] ได้แก่ อุตสาหกรรมเกษตรและอาหาร อุตสาหกรรมพลังงานและวัสดุ อุตสาหกรรมสุขภาพและการแพทย์ และอุตสาหกรรมการท่องเที่ยวและบริการ โดยวิทยาศาสตร์ เทคโนโลยีและนวัตกรรมจะเข้าไปช่วยเพิ่มประสิทธิภาพให้กับผู้ผลิตที่เป็นฐานการผลิตเดิม เช่น เกษตรกรและชุมชน ตลอดจนสนับสนุนให้เกิดผู้ประกอบการที่ผลิตสินค้าและบริการที่มีมูลค่าเพิ่มสูงหรือนวัตกรรม สอดคล้องกับปัญหาขยะพลาสติกที่ตกค้างอยู่ในสิ่งแวดล้อมมักเกิดจากผู้บริโภคที่ไม่ได้คัดแยกขยะมูลฝอย ไม่มีความเข้าใจในการรีไซเคิล และมีการกำจัดที่ไม่ถูกต้อง โดยขยะพลาสติกจะถูกนำไปฝังกลบรวมกับขยะมูลฝอยอื่นๆ ซึ่งขยะพลาสติกมีความคงทนและสามารถทนต่อแรงอัดได้สูง จึงใช้พื้นที่ในการฝังกลบมากกว่าขยะประเภทอื่น อีกทั้งยังใช้เวลาในการย่อยสลายนับร้อยปี ทำให้ต้องสิ้นเปลืองงบประมาณและพื้นที่ฝังกลบ [12] นอกจากนี้ ปัญหาการทิ้งขยะพลาสติกกระจัดกระจายทั่วไป มักก่อให้เกิดปัญหาการอุดตันตามท่อระบายน้ำ ทำให้เกิดปัญหาน้ำท่วม ปัญหาขยะลอยในแม่น้ำ ลำคลอง บางส่วนไหลลงสู่ทะเล ก่อให้เกิดปัญหาเศษขยะพลาสติกและไมโครพลาสติก [13] พบการแพร่กระจายในทะเลทั่วโลก ส่งผลกระทบต่อระบบนิเวศทางทะเลเมื่อการปฏิวัติอุตสาหกรรม การใช้ทรัพยากรธรรมชาติอย่างไร้ขีดจำกัด และการค้าแบบทุนนิยมส่งผลให้เกิดภาวะโลกร้อนจนทำให้ทั่วโลกต่างแสดงความกังวลและหันมาให้ความสำคัญกับเรื่องการเปลี่ยนแปลงสภาพภูมิอากาศเพิ่มมากขึ้น [11] ดังจะเห็นได้จากการที่หลายประเทศทั่วโลกได้เข้าร่วมพิธีสารเกียวโต (Kyoto Protocol) เพื่อพิจารณาหาแนวทางการลดการปล่อยก๊าซเรือนกระจก ซึ่งพิธีสารเกียวโตเองก็ได้มีการออกกฎหมายเพื่อบังคับใช้สำหรับการลดการปล่อยก๊าซเรือนกระจก นอกจากนี้ ความตกลงปารีส (Paris Agreement) ก็เป็นอีกหนึ่งความตกลงที่มีเป้าหมายในการลดการปล่อยก๊าซเรือนกระจก โดยความตกลงดังกล่าวได้มีการกำหนดหลักการซื้อขายก๊าซเรือนกระจก (Emission Trading System: ETS) และอนุญาตให้ผู้ที่ลดการปล่อยก๊าซเรือนกระจกจนอยู่ในระดับที่ต่ำกว่าเป้าหมาย [11] สามารถขายสิทธิ์การปล่อยก๊าซเรือนกระจกที่เหลือให้แก่ผู้อื่นได้ หรือที่เรียกกันว่า คาร์บอนเครดิต จากข้างต้นกล่าวได้ว่าพลาสติกเป็นสิ่งที่ย่อยสลายยากและทำลายสภาพแวดล้อม [2] ในชุมชนบางพื้นที่ได้มีการสร้างผลิตภัณฑ์จากต้นพืช [7] [8] เป็นผลิตภัณฑ์ [8] ธรรมชาติเพื่อสร้างรายได้ให้แก่ชุมชน เช่น การสานตะกร้า หมวก กระเป๋า และหลอดจากต้นกระจูด โดยกระจูดเป็นพืชที่สามารถนำมาประยุกต์ใช้กับงานได้หลายชนิดสามารถสร้างได้ทั้งอาชีพหลักและอาชีพเสริม เป็นช่องทางในการสร้างรายได้ให้กับกลุ่มชาวเกษตรกรหรือผลิตเป็นสินค้าพื้นบ้านให้มีรูปแบบที่หลากหลาย เช่น กระเป๋า ตะกร้า เบาะรองนั่ง หมวก และ หลอดดูดน้ำจากต้นกระจูด [3] [4] [8] [10]

จากเหตุผลดังกล่าวข้างต้นทั้งเรื่องของ BCG และ คาร์บอนเครดิต ผู้วิจัยเล็งเห็นถึงความสำคัญผลิตภัณฑ์จากต้นกระจูดและแปรรูปเป็นหลอดกระจูดจำเป็นอย่างยิ่งที่จะต้องสร้างเครื่องทุ่นแรงเพื่อประหยัดเวลา สะดวกรวดเร็วและปลอดภัย ในการใช้งาน ซึ่งการผลิตออกแบบและพัฒนาเครื่องตัดหลอดกระจูดและคณะผู้วิจัยได้มีการศึกษางานวิจัยเล่มสมบูรณ์ [3] โดยออกแบบและพัฒนาเครื่องตัดหลอดสำหรับการผลิตหลอดจากพืช [5] ด้วยการออกแบบตัวเครื่องให้มีขนาดความกว้าง 29 เซนติเมตร ความสูง 34 เซนติเมตร และความยาว 40 เซนติเมตร โดยใช้ Linear motor อุปกรณ์ขับเคลื่อนใบตัดระบบไฟฟ้าขนาดเล็ก แรงดันใช้งานที่ไฟฟ้ากระแสตรง 12 โวลต์ มีระยะชัก 50

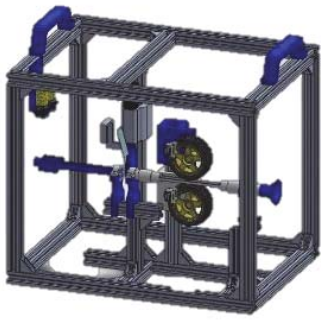
มิลลิเมตร กำลังโหลด 30 นิวตัน ความเร็วในการโหลด 30 มิลลิเมตรต่อวินาที เพื่อควบคุมใบมีดในการตัดหลอดทำงานผ่านการควบคุมโดยไมโครคอนโทรลเลอร์

คณะผู้วิจัยจึงได้ให้ขอเสนอแนะไว้ว่า อุปกรณ์ที่ใช้ในการตัด ยังคงตัดได้พืชเฉพาะที่กลวง ความหนาไม่เกิน 0.5 มม. ควรปรับปรุงให้ใช้อุปกรณ์ที่มีความแข็งแรง สามารถสร้างแรงกดได้สูง เพื่อให้ได้ใช้งานได้อย่างหลากหลายควรปรับปรุงให้ตัวเครื่องใช้งานได้แบบอัตโนมัติ เพื่อให้ได้ประสิทธิภาพที่ดียิ่งขึ้น [6] ส่วนตัวอย่างหลอดที่ตัดควรจัดทำเสนอขอมาตรฐานผลิตภัณฑ์ชุมชน (มผช.) เพื่อเพิ่มมูลค่าผลิตภัณฑ์และทำให้มีรายได้ที่มั่นคง

ด้วยเหตุนี้คณะผู้วิจัยจึงมีแนวคิดที่จะออกแบบและพัฒนาเครื่องตัดหลอดกระจูดโดยการใช้ PLC ควบคุมระบบนิวเมติกส์ในการตัดหลอดกระจูดแทนมอเตอร์ไฟฟ้าซึ่งจากเดิมเป็นมอเตอร์ไฟฟ้าลิเนียร์มอเตอร์เป็นระบบนิวเมติกส์ที่ดัดแปลงเพื่อความทนทานของเครื่องจักรและความต่อเนื่องในการทำงานเมื่อใช้งานไปนานๆ ออกแบบและพัฒนาระยะและท่านั่งทำงานตามหลักการของผู้ใช้งานอัตราเร็วในการตัดหลอดที่เหมาะสมทำให้ประหยัดเวลาในการตัดหลอดกระจูดที่เร็วขึ้นอย่างสม่ำเสมอทำให้เกิดความแม่นยำของขนาดหลอดและความเรียบร้อยของรอยตัดในขณะตัดหลอดกระจูด หากผลงานวิจัยดังกล่าวสำเร็จสามารถพัฒนาเครื่องตัดหลอดกระจูดได้ อีกทั้งเครื่องที่ออกแบบสำเร็จสามารถขยายผลไปยังวิสาหกิจชุมชนอื่นๆได้ในอนาคตซึ่งงานวิจัยนี้จะเป็นประโยชน์ต่อผู้ที่สนใจ เช่น ชุมชน ชาวบ้าน เกษตรกร และหน่วยงานทั้งภาครัฐและเอกชนที่เกี่ยวข้องสามารถนำไปใช้ให้เกิดประโยชน์ในลำดับต่อไป

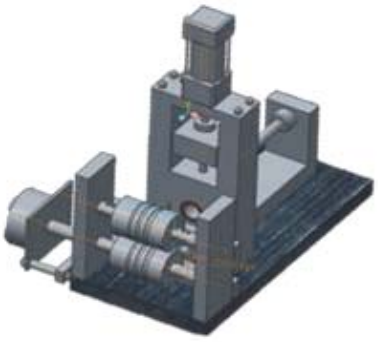
II. ทบทวนวรรณกรรม

จากการศึกษางานวิจัยที่พัฒนารูปแบบของการตัดวัสดุรูปร่างคล้ายหลอดมีรูปแบบที่หลากหลาย ดังแสดงในตัวอย่างแนวทางพัฒนาเครื่องตัดหลอดจากพืชจากการศึกษากลไกของเครื่องจักรตัดตัวอย่างแบบท่อกลวง [1] ออกแบบและพัฒนาเครื่องตัดหลอดสำหรับการผลิตหลอดจากพืชโดยใช้ลิเนียร์มอเตอร์ ดังภาพที่ 1



ภาพที่ 1 โครงสร้างและกลไกในการตัดหลอดดูดน้ำจากต้นกระจูด [3]

และการศึกษาสร้างเครื่องตัดหลอดพลาสติกโดยใช้มอเตอร์หมุนลูกกลิ้งส่งหลอดเข้าสู่ตัวกดนิวเมติกส์เพื่อตัดหลอดพลาสติก [13]



ภาพที่ 2 โครงสร้างและกลไกในการตัดหลอดดูดน้ำพลาสติก [1]

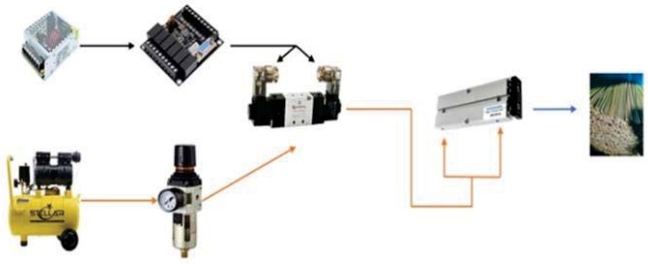
III. ระเบียบวิธีวิจัย

งานวิจัยเป็นส่วนหนึ่งของโครงการพัฒนาเครื่องตัดหลอดกระจูดโดยการเสนอวัตถุดิบจากพื้นที่ศึกษา ได้ทำการแบ่งรูปแบบการวิจัยในระยะแรกออกเป็น 3 ส่วน โดยส่วนที่หนึ่งเป็นการศึกษาค้นคว้าข้อมูล ส่วนที่สองเป็นการวางแผนและออกแบบ ส่วนที่สามเป็นการออกแบบและพัฒนาเครื่องต้นแบบ

1. พื้นที่ศึกษาและวัตถุดิบที่ใช้

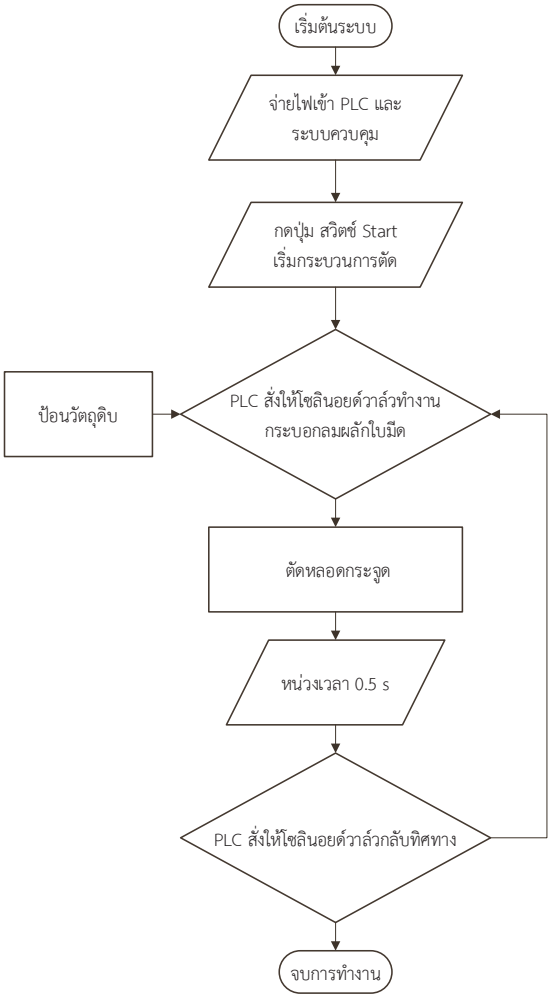
1.1 จากข้อมูลการพัฒนาผลิตภัณฑ์ทางธรรมชาติสำหรับทำหลอดดูดน้ำพบการผลิตโดยกลุ่มวิสาหกิจชุมชนพรุควนเคร็ง โดยวิสาหกิจเสนอความต้องการในการผลิตหลอดดูดน้ำจากกระจูด และผลการสืบค้นรายละเอียดเกี่ยวกับวัชพืชที่นำมาตัดเป็นหลอดพบข้อมูลที่ผลิตเชิงพานิชย์ในพื้นที่ภาคใต้ประกอบด้วย พืชราโพและพืชกระจูด โดยสอดคล้องกับความต้องการของชุมชนในการพัฒนาหลอดดูดน้ำจากพืชกระจูด จากข้อมูลพบว่ามีแหล่งวัตถุดิบพืชกระจูด 2 แหล่งใหญ่ คือ พรุควนเคร็ง ต.เคร็ง อ.ชะอวด จ.นครศรีธรรมราช และ ทุ่งกระจูด ต.ท่าสะท้อน อ.พุนพิน จ.สุราษฎร์ธานี ผู้วิจัยเลือกวัตถุดิบจากทั้ง 2 แหล่ง สำหรับทดสอบการทำงานของเครื่องต้นแบบโดยชุมชนมีส่วนร่วมในการเตรียมวัตถุดิบโดยวัตถุดิบหลักที่นำมาทดลองจะใช้จากพรุควนเคร็งเท่านั้น

1.2 ออกแบบการทำงานของเครื่องตัดหลอดกระจูดโดยศึกษาและลำดับการทำงานที่สัมพันธ์กันทั้งระบบโดยเลียนแบบการตัดแบบการตัดแบบดั้งเดิมจากวิสาหกิจชุมชนพรุควนเคร็ง อ.ชะอวด จ.นครศรีธรรมราช ดังภาพที่ 3 สำหรับควบคุมการทำงาน ประกอบด้วย PLC ปั๊มลม เครื่องกรองลม โซลินอยล์ กระบอกลม ประเมินการออกแบบที่เหมาะสำหรับเครื่องตัดหลอดจากกระจูดให้ทำงานได้อย่างประสิทธิภาพ



ภาพที่ 3 อุปกรณ์ประกอบในระบบควบคุมการตัดหลอดกระจูด

1.3 จากอุปกรณ์ในรูปที่ 3 สามารถเขียนโปรแกรมระบบควบคุมการทำงานนิวเมติกส์ ด้วย PLC สำหรับควบคุมกลไกการทำงานทั้งหมดของระบบการตัดหลอดกระจูด โดยขั้นตอนการกำหนดลำดับการทำงานในผังการทำงานของโปรแกรมในแลดเดอร์ของ PLC ดังภาพที่ 4



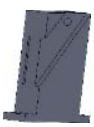
ภาพที่ 4 ลำดับการทำงานและกระบวนการควบคุมด้วย PLC

2. การวางแผนและออกแบบ

2.1 ศึกษาการเลือกอุปกรณ์ในการนำมาสร้างเครื่องตัดหลอดกระจูด มีอุปกรณ์และวัสดุในการทดลองเพื่อประสิทธิภาพในการตัด

2.2 ออกแบบชิ้นส่วนในการประกอบที่ใส่หลอด โดยใช้โปรแกรม Solidworks 2018 และผลิตชิ้นส่วนในเครื่องพิมพ์สามมิติ Flashforge2 ดังตารางที่ II

ตารางที่ II ชิ้นส่วนในการออกแบบด้วยคอมพิวเตอร์

ชื่อ	รูปภาพ	ชื่อ	รูปภาพ
ฐานรองหลอดหน้า		ตัว C ใส่ประกบท่อหลอด	
ชุดท่อนำทางหลอด		ชุดจับใบมีด	

2.3 ออกแบบโครงสร้างของเครื่องตัดหลอดกระจูด โดยกำหนดขนาดเพื่อจัดซื้อวัสดุโครงสร้างทั้งหมด ออกแบบให้มีขนาดความกว้าง 70 เซนติเมตร ความสูง 110 เซนติเมตร และความยาว 32 เซนติเมตร ภาพที่ 5



(ก.) (ข.)

ภาพที่ 5 โครงเครื่องตัดหลอดกระจูด (ก.) และเครื่องต้นแบบพร้อมใช้งาน (ข.)

3. การออกแบบและพัฒนาเครื่องตัดหลอดกระจูด

3.1 โครงสร้างหลักทรงสี่เหลี่ยมผืนผ้าประกอบจากเหล็กแผ่นและเหล็กกล่อง ผลิตชิ้นส่วนด้วยเครื่อง CNC Plasma ดังภาพที่ 6



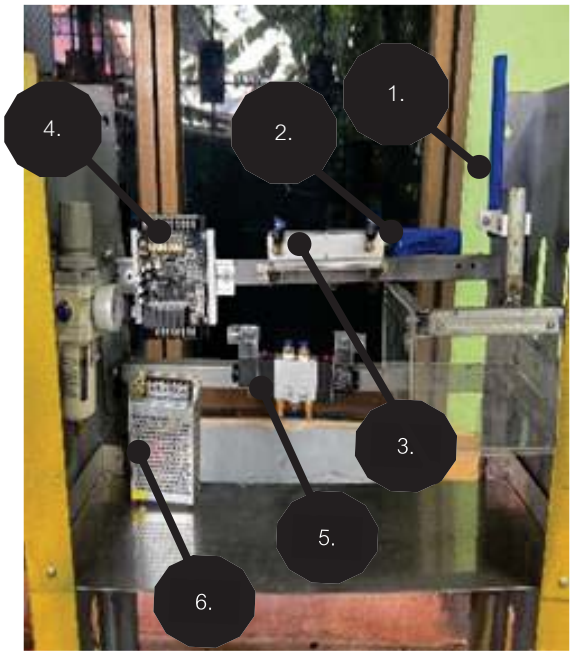
ภาพที่ 6 ตัดเหล็กด้วยเครื่อง CNC

3.2 นำเหล็กแผ่นที่ตัดด้วยเครื่อง CNC มาประกอบเข้ากับเหล็กกล้องเป็นตัวโครงเครื่องตัดหลอดกระจูด ดังภาพที่ 7



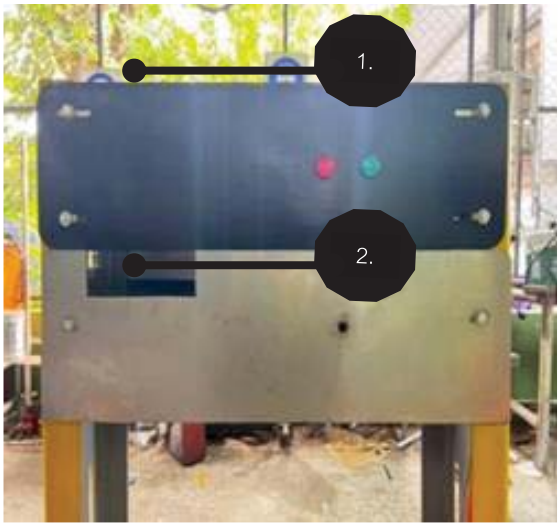
ภาพที่ 7 ประกอบโครงสร้าง

3.3 นำอุปกรณ์ทั้งหมดติดตั้งในตัวเครื่องและเดินสายไฟ ดังภาพที่ 8



ภาพที่ 8 ติดตั้งอุปกรณ์และเดินสายไฟ

3.4 ทำการหุ้มโครงป้องกันระบบการทำงาน ด้วยอลูมิเนียม ด้านหน้ากับด้านบน ขนาดความยาว 70 เซนติเมตร ความกว้าง 20 เซนติเมตร จำนวน 2 แผ่น ด้านหลัง ขนาดความยาว 70 เซนติเมตร ความกว้าง 40 เซนติเมตร จำนวน 1 แผ่น ทำการประกอบและเชื่อมต่อสายโดยหมายเลข 1 คือช่องป้อนกระจูด หมายเลข 2 คือตัวจับใบมีดทำมุม 60° โดยการเลือกใช้มุมที่เหมาะสมนี้ได้ข้อมูลมาจากเงื่อนไขของการใช้มุมใบมีดที่ 60° มาจากผลการทดสอบในงานวิจัย [3] ซึ่งมีการทดสอบการตัดที่มุมของใบมีดที่ 30° 45° 60° และ 90° พบว่าที่มุม 60° ลดความเสียหายจากการแตกได้สูงเฉลี่ย 90 เปอร์เซนต์และใบมีดมีความคมนานที่สุดเมื่อตัดซ้ำจำนวน 100 ครั้งจากการทำซ้ำ 5 ครั้งของทุกการทดสอบ หมายเลข 3 คือกระบอกสูบสองทางสำหรับสั่งตัดหลอด หมายเลข 4 คือ PLC สำหรับใช้เขียนคำสั่งควบคุมการตัด หมายเลข 5 คือ วาล์วควบคุม 4/2 สำหรับควบคุมการเคลื่อนที่เข้า-ออกของใบมีด และหมายเลข 6 คือ แหล่งจ่ายแรงดันไฟตรง 24 โวลต์ ซึ่งแสดงไว้ในภาพที่ 9



ภาพที่ 9 ภาพประกอบด้านหน้าตัวเครื่อง

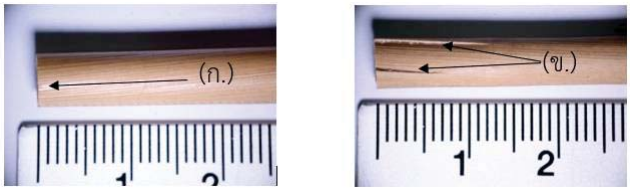
ภาพที่ 9 เป็นภาพประกอบด้านหน้าเป็นส่วนที่ออกแบบให้ปิดมิดชิดไม่มีส่วนสัมผัสใบมีดโดยตรง โดยใบมีดตัดที่ใช้ในการทดลองเป็นใบมีดคัตเตอร์รูปแบบเดียวกับที่ทางกลุ่มใช้งานปกติและสามารถหาซื้อมาใช้ทดแทนในท้องตลาด โดยความคมจะต้องเปลี่ยนทุกๆ 100 ครั้งของการตัด [3] จากภาพหมายเลข 1 คือช่องป้อนซึ่งจะใช้วิธีการป้อนแบบแนวตั้ง ซึ่งจะแตกต่างจาก [3] คือ ป้อนหลอดกระจูดในท่านอน

สำหรับการกำหนดเกณฑ์การคัดเลือกตัวอย่างในการทดสอบและเครื่องมือตรวจสอบตัวอย่าง การกำหนดเงื่อนไขการคัดเลือกและตรวจนับตัวอย่างเพื่อระบุลักษณะทางกายภาพของการแตกและไม่แตก คัดเลือกจากตัวอย่างหลอดจากพืชกระจูดจากวิสาหกิจชุมชนพรุควนเคร็ง โดยตัดที่ความยาว 46 เซนติเมตรโดยเฉลี่ยล้างทำความสะอาดภายนอกและยังไม่ทะลวงข้อ โดยใช้การตัดชิ้นงานจำนวน 50 ตัวอย่างโดยไม่เปลี่ยนใบมีด ทำซ้ำจำนวน 3 ครั้ง ดังภาพที่ 10



ภาพที่ 10 ตัวอย่างวัตถุดิบสำหรับการทดสอบ

จากนั้นใช้ภาพขยายวัตถุดิบจากการตัดโดยใช้เกณฑ์จากการแยกภาพด้วยกล้อง OLYMPUS SZ61/EO S 800D อัตราขยาย 2 เท่า เพื่อให้เห็นแนวยาวรอยแตกได้ชัดและลักษณะเส้นใยที่ผ่านการตัด โดยภาพที่ 10 แสดงตัวอย่างจากการตัดด้วยเครื่องและตัดด้วยมือ

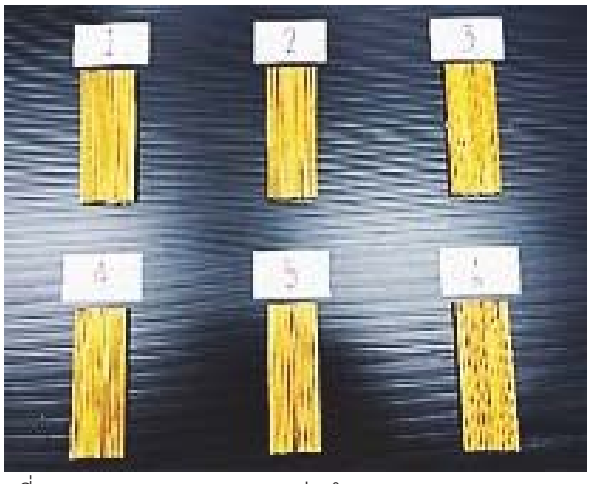


ภาพที่ 11 ตัวอย่างหลอดจากการตัดด้วยเครื่องตัดหลอดกระจูดและการตัดด้วยมือ (ก) ลักษณะทางกายภาพตัดด้วยเครื่อง (ข) ลักษณะทางกายภาพเมื่อตัดด้วยมือ

IV. ผลการทดลอง

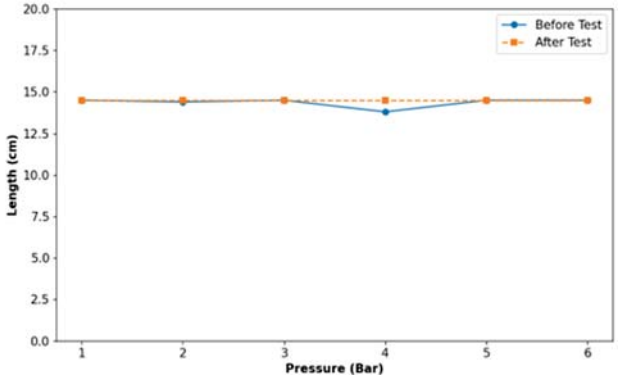
ในการดำเนินงานวิจัยตามขั้นตอนที่ได้กำหนดไว้ โดยทำการเก็บผลการทดลอง เพื่อบันทึกผลการวิจัยเครื่องตัดหลอดกระจูดที่พัฒนาจากเครื่องต้นแบบโดยใช้วัตถุดิบที่ทำการทดสอบจากพรุควนเครง ใช้เครื่องต้นแบบจำนวน 2 เครื่องคือเครื่องต้นแบบจากการทดลองในระดับปริญญานิพนธ์ [3] และเครื่องต้นแบบที่ออกแบบและพัฒนาเครื่องตัดหลอดกระจูดที่พัฒนาขึ้นใหม่ โดยใช้ ระบบควบคุมการตัด และปรับแต่งหาระดับความเร็วใบมีดให้เหมาะสมที่ให้ประสิทธิภาพการตัดสูงสุด โดยทำการทดสอบเพื่อวิจัยตามวัตถุประสงค์การวิจัย ดังนี้

4.1 ผลการทดสอบความแม่นยำของความยาวหลอดจากการตัดด้วยเครื่องตัดหลอดกระจูด



ภาพที่ 12 ผลการทดสอบความแม่นยำของความยาวหลอดจากการตัดด้วยเครื่องตัดหลอดกระจูด

จากผลการทดสอบความแม่นยำของความยาวหลอดที่ตัดด้วยเครื่องตัดหลอดกระจูดกำหนดไว้ที่ 14.5 ซม. ภายใต้ตัวแปรควบคุมคือความเร็วลมที่ 1 บาร์ 2 บาร์ 3 บาร์ 4 บาร์ 5 บาร์ 6 บาร์ ตามลำดับ แสดงดังภาพที่ 12

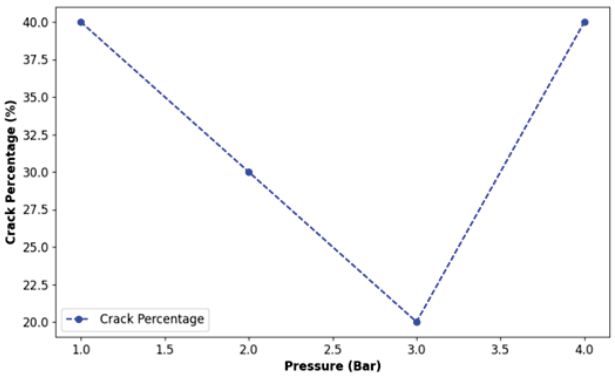


ภาพที่ 13 ค่าความแม่นยำของความยาวเฉลี่ยเมื่อปรับเปลี่ยนแรงดัน 6 ระดับ

ได้ผลการทดลองจากภาพที่ 13 ที่ความเร็วลม 1 บาร์ ความยาวเฉลี่ยของชิ้นงานอยู่ที่ 14.50 ซม. และลดลงเล็กน้อยที่ความเร็วลม 2 บาร์ โดยความยาวเฉลี่ยอยู่ที่ 14.40 ซม. อย่างไรก็ตาม เมื่อเพิ่มความเร็วลมเป็น 3 บาร์ ความยาวเฉลี่ยกลับมาอยู่ที่ 14.50 ซม. อีกครั้ง

เมื่อแรงลมเพิ่มขึ้นเป็น 4 บาร์ ความยาวเฉลี่ยลดลงมากที่สุดในข้อมูล โดยอยู่ที่ 13.80 ซม. แต่เมื่อแรงลมเพิ่มขึ้นที่ 5 บาร์ และ 6 บาร์ ความยาวเฉลี่ยกลับมาอยู่ที่ 14.50 ซม. ดังนั้น ความยาวเฉลี่ยโดยรวมของทุกแรงลมอยู่ที่ 14.50 ซม. ซึ่งเทียบเท่ากับความยาวของหลอดพลาสติกมาตรฐานที่มีจำหน่ายทั่วไปในท้องตลาดที่ขนาด 14.50 ซม. โดยแสดงถึงความคงที่และความเหมาะสมในกระบวนการผลิตที่สามารถควบคุมให้ได้ความยาวในเกณฑ์มาตรฐานที่กำหนดไว้

4.2 ผลการทดสอบความสูญเสียจากรอยแตกของหลอดจากการตัดด้วยเครื่องตัดหลอดกระจูด



ภาพที่ 14 ผลจากความสูญเสียจากการตัดเมื่อเปลี่ยนแรงดันลมที่ใช้ตัดหลอดกระจูด

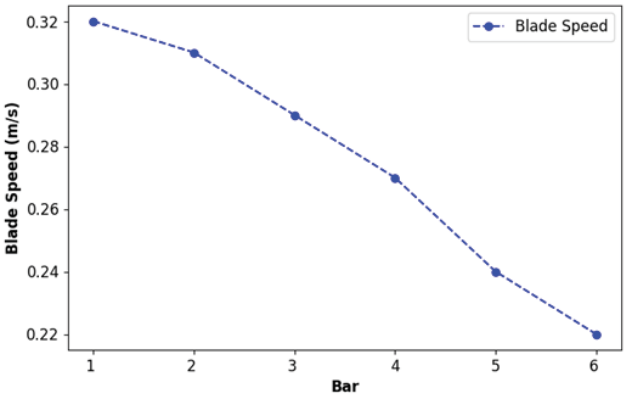
ในการพิจารณาและระบุความเสียหายเนื่องจากความสูญเสียจากรอยแตกในงานวิจัยนี้ใช้เกณฑ์การคัดแยกทางกายภาพโดยพิจารณาจากการแยกภาพด้วยกล้อง OLYMPUS SZ61/EO S

800D อัตราขยาย 2 เท่า เพื่อให้เห็นแนวยาวรอยแตกได้ชัดและลักษณะเส้นใย ตัวอย่างดังภาพที่ 10 โดยใช้การเก็บข้อมูลค่าเฉลี่ยและใช้วิธีการพิจารณาความสูญเสียรอยแตกของหลอดเป็นเปอร์เซ็นต์จากจำนวนหลอดที่แตกโดยอิงจากจำนวนหลอดที่แตกเมื่อเทียบกับจำนวนหลอดทั้งหมดที่ตัดในแต่ละรอบการทดสอบ โดยคำนวณจากสมการที่ (1)

$$\text{เปอร์เซ็นต์รอยแตก} = \left(\frac{\text{จำนวนหลอดที่มีรอยแตก}}{\text{จำนวนหลอดทั้งหมดที่ตัด}}\right) \times 100 \text{--} (1)$$

จากผลการทดสอบความสูญเสียรอยตัดของหลอดจากการตัดด้วยเครื่องตัดหลอดกระจูด ได้ผลการทดสอบแสดงในภาพที่ 14 ดังนี้ ความเร็วลมที่ทำให้เกิดรอยแตกต่ำสุดคือ 3 บาร์ โดยมีรอยแตกเฉลี่ยอยู่ที่ 10 เปอร์เซ็นต์ ซึ่งเป็นค่าที่ต่ำที่สุดในข้อมูลที่วัดได้ สำหรับความเร็วลมที่ 2 บาร์ และ 4 บาร์ มีรอยแตกเฉลี่ยเพิ่มขึ้นมาอยู่ที่ 30 เปอร์เซ็นต์ ในขณะที่ความเร็วลมที่ 1 บาร์ และ 4 บาร์ มีรอยแตกเฉลี่ยสูงขึ้นอีกเป็น 40 เปอร์เซ็นต์ ข้อมูลนี้ชี้ให้เห็นถึงความสัมพันธ์ระหว่างความเร็วลมและระดับรอยแตก โดยระดับความเร็วลมที่เหมาะสมในการลดรอยแตกคือ 3 บาร์ ซึ่งแสดงให้เห็นถึงความสำคัญของการปรับแรงดันลมให้เหมาะสมเพื่อควบคุมระดับรอยแตกให้อยู่ในเกณฑ์ที่ต่ำที่สุด

4.3 ผลการทดสอบความเร็วในการตัดของใบมีดของเครื่องตัดหลอดกระจูด



ภาพที่ 15 ผลการทดสอบความเร็วในการตัดของใบมีดของเครื่องตัดหลอดกระจูด

จากผลการทดลองความเร็วในการตัดของใบมีดของเครื่องตัดหลอดกระจูด ในภาพที่ 15 ได้ที่แรงดันลม 1 บาร์ ความเร็วใบมีดเคลื่อนที่เฉลี่ยอยู่ที่ 0.32 เมตรต่อวินาที ซึ่งเป็นค่าเดียวกับแรงดันลม 2 บาร์ ที่ยังคงความเร็วใบมีดเคลื่อนที่เฉลี่ยเท่ากับ 0.31 เมตรต่อวินาที อย่างไรก็ตาม เมื่อแรงดันลมเพิ่มขึ้นเป็น 3 บาร์ ความเร็วใบมีดเคลื่อนที่เฉลี่ยลดลงเหลือ 0.29 เมตรต่อวินาที และลดลงอีกเมื่อแรงดันลมเพิ่มขึ้นเป็น 4 บาร์ โดยความเร็วใบมีดเคลื่อนที่เฉลี่ยลดลงเหลือ 0.28 เมตรต่อวินาทีสำหรับแรงดันลมที่ 5 บาร์ ความเร็วใบมีดเคลื่อนที่เฉลี่ยลดลงอย่างต่อเนื่องอยู่ที่ 0.24 เมตรต่อวินาที และที่แรงดันลมสูงสุดในข้อมูลคือ 6 บาร์ ความเร็วใบมีดเคลื่อนที่เฉลี่ยลดลงต่ำสุดที่ 0.22 เมตรต่อวินาที ข้อมูลนี้สะท้อนให้เห็นว่าเมื่อแรงดันลมเพิ่มสูงขึ้น ความเร็วใบมีดเคลื่อนที่เฉลี่ยจะลดลงอย่างมีนัยสำคัญ โดยระยะใบมีดเคลื่อนที่ยิ่งน้อยจะส่งผลโดยตรงกับความเร็วรอบในการตัดชิ้นงานต่อชิ้นและสัมพันธ์กับความเสียหายจากการตัด ในงานวิจัยนี้มีจุดประสงค์เพื่อลดความเสียหายของชิ้นงาน ภาพที่ 14 แสดงให้เห็นว่า เมื่อแรงดันลมเพิ่มขึ้น ความเร็วใบมีดเคลื่อนที่เฉลี่ยลดลง ส่งผลให้การตัดเร็วขึ้นทำให้เวลาเฉลี่ยในการตัดต่อชิ้นลดลงเมื่อระยะตัด 10 เซนติเมตร โดยคำนวณจากความสัมพันธ์ในสมการที่ (2)

$$t = \frac{d}{v} \quad \text{----------(2)}$$

โดย t = เวลา (s)
d = ระยะทาง (m)
v = ความเร็ว (m/s)

ค่าเหมาะสมที่สุดจากการทดลองอยู่ที่แรงดันลม 3 บาร์ ซึ่งให้เวลาเฉลี่ยต่อชิ้นอยู่ที่ประมาณ 0.35 วินาที ซึ่งเป็นจุดนี้คือจุดสมดุลระหว่างความเร็วในการตัดและการควบคุมรอยแตกของชิ้นงานให้มีประสิทธิภาพสูงที่สุดที่แรงดันลม 3 บาร์ เมื่อพิจารณาที่จุดคุ้มทุน แสดงให้เห็นว่าแม้ต้นทุนต่อชิ้นจะต่ำมาก แต่ต้องผลิตจำนวนมากเพื่อคืนทุนเครื่องจักรที่ต้น 30,000 บาท เวลาเฉลี่ยในการตัดต่อชิ้นที่ 0.35 วินาที หรือ 10,440 ชิ้นต่อชั่วโมง

V. อภิปรายผล

จากการทดสอบความแม่นยำของความยาวหลอดความแม่นยำของความยาวหลอดที่ตัดด้วยเครื่องต้นแบบกำหนดไว้ที่ 14.5 ซม. ภายใต้ตัวแปรควบคุมคือความเร็วลม 1 2 3 4 5 และ 6 บาร์ ตามลำดับได้ผลการทดลอง ดังนี้ ความแม่นยำของความยาวหลอดเฉลี่ย 14.5 ซม.

การทดสอบความสูญเสียรอยแตกของหลอด พิจารณาจากเปอร์เซนต์ความเสียหายของหลอดพิจารณาจากรอยตัดของหลอดจากการตัดด้วยเครื่องตัดหลอดกระจูดจากผลการทดสอบความสูญเสียรอยแตกของหลอดจากการตัดด้วยเครื่องตัดหลอดกระจูดได้ผลการทดสอบ ดังนี้ การตัดหลอดกระจูดที่มีความสูญเสียรอย

แตกน้อยที่สุดคือ 3 บาร์ มีรอยแตกเฉลี่ย 10 เปอร์เซ็นต์ซึ่งน้อยที่สุดจากการปรับค่าทุกๆความดันลม

การทดสอบความเร็วในการตัดของใบมีด เป็นการผลการทดสอบความเร็วในการตัดของใบมีดของเครื่องตัดหลอดกระจูดขณะตัดจริง ซึ่งผลของความเร็วมีผลกับรอยแตกโดยตรง ความเร็วในการตัดของใบมีดของเครื่องตัดหลอดกระจูด ที่ได้ผลการทดสอบดังนี้ ที่ความเร็วลม 1 บาร์ ค่าเฉลี่ยของความเร็วลมเท่ากับ 0.32 เมตรต่อวินาที ซึ่งเป็นค่าเดียวกับที่ความเร็วลม 2 บาร์ ที่มีค่าเฉลี่ยความเร็วเท่ากับ 0.31 เมตรต่อวินาที เช่นกัน อย่างไรก็ตาม เมื่อความเร็วลมเพิ่มขึ้นเป็น 3 บาร์ ค่าเฉลี่ยความเร็วลมลดลงเหลือ 0.29 เมตรต่อวินาที และลดลงอีกที่ 4 บาร์ โดยค่าเฉลี่ยความเร็วลมอยู่ที่ 0.28 เมตรต่อวินาที เมื่อความเร็วลมเพิ่มขึ้นถึง 5 บาร์ ค่าเฉลี่ยของความเร็วลมลดลงเหลือ 0.24 เมตรต่อวินาที และที่ความเร็วลม 6 บาร์ ซึ่งเป็นความเร็วสูงสุดในข้อมูล ค่าเฉลี่ยความเร็วลมลดลงต่ำสุดที่ 0.22 เมตรต่อวินาที ข้อมูลนี้แสดงให้เห็นว่า โดยระยะใบมีดเคลื่อนที่ยิ่งน้อยจะส่งผลโดยตรงกับความเร็วรอบในการตัดชิ้นงานต่อชิ้นและความเสียหายจากการตัด แรงดันลม 3 บาร์ ซึ่งให้เวลาเฉลี่ยต่อชิ้นอยู่ที่ประมาณ 0.35 วินาที ซึ่งเป็นจุดนี้คือจุดสมดุลระหว่างความเร็วในการตัดและการควบคุมรอยแตกของชิ้นงานให้มีประสิทธิภาพสูงที่สุดที่แรงดันลม 3 บาร์ เมื่อพิจารณาที่จุดคุ้มทุนแสดงให้เห็นว่าแม้ต้นทุนต่อชิ้นจะต่ำมาก แต่ต้องผลิตจำนวนมากเพื่อคืนทุนเครื่องจักรที่ต้น 30,000 บาท เวลาเฉลี่ยในการตัดต่อชิ้นที่ 0.35 วินาที คิดเป็นจำนวนชิ้นต่อชั่วโมงได้ 10,440 ชิ้น ต้นทุนต่อชิ้น ประมาณ 0.012 บาท จะได้จำนวนชิ้นที่จุดคุ้มทุนหลังจากผลิตหลอดดูดน้ำจากกระจูด จำนวน 2,505,600 ชิ้น

VI. ข้อสรุป

เครื่องตัดหลอดอัตโนมัติที่ออกแบบและพัฒนาขึ้นมีความแม่นยำของความยาวหลอดที่ตัดด้วยเครื่องตัดหลอดกระจูดกำหนดไว้ที่ 14.5 ซม. มีประสิทธิภาพและความแม่นยำของการตัดที่ 99.9 เปอร์เซ็นต์ สามารถลดความเสียหายรอยตัดของหลอดจากการตัดด้วยเครื่องตัดหลอดกระจูดใน แรงดันลม 3 มีความเร็วลมอยู่ที่ 0.29 เมตรต่อวินาที ลดความเสียหายได้ 90 เปอร์เซนต์ ซึ่งดีกว่าการตัดด้วยมือซึ่งเสียหายมากกว่า 60 เปอร์เซ็นต์ ของวัตถุดิบ สำหรับข้อเสนอแนะสำหรับการพัฒนาต่อในอนาคต ด้านอุปกรณ์ที่ใช้ในการตัดยังคงตัดได้พืชเฉพาะที่กลวงความหนาไม่เกิน 0.5 มม. โดยเวลาเฉลี่ยในการตัดต่อชิ้นที่ 0.35 วินาที หรือ 10,440 ชิ้นต่อชั่วโมง ควรปรับปรุงให้ใช้อุปกรณ์ที่มีความแข็งแรง สามารถต้านทานแรงกดได้มากว่านี้ เพื่อให้ได้ใช้งานได้อย่างหลากหลาย โดยตัวอย่างหลอดที่ตัดควรจัดทำเสนอขอมาตรฐานผลิตภัณฑ์ชุมชน เพื่อได้มีรายได้ที่มั่นคงและมีมาตรฐานที่สามารถขอมาตรฐานผลิตภัณฑ์ชุมชนในอนาคต และข้อแนะนำเกี่ยวกับตัวเครื่องหลัก ควรพัฒนาให้มีตำแหน่งป้อนหลอดให้มีจำนวนมากขึ้น เพื่อที่จะเพิ่มปริมาณการตัดจำนวนของหลอดเพิ่มขึ้น

คำขอบคุณ

การวิจัยและพัฒนาเครื่องตัดหลอดดูดน้ำจากต้นกระจูดด้วยระบบนิวแมติกส์ประสบความสำเร็จอย่างดียิ่ง คณะผู้วิจัยขอแสดงความขอบคุณอย่างสุดซึ้งต่อคณะอาจารย์และเจ้าหน้าที่จากสาขาเทคโนโลยีไฟฟ้าอุตสาหกรรม ที่ให้การสนับสนุนอย่างเต็มที่ตลอดการดำเนินงาน นอกจากนี้ ขอขอบพระคุณนางสาวปิยมาศ นะแก้ว จากวิสาหกิจชุมชนพรุควนเคร็ง ที่เอื้อเฟื้อวัตถุดิบสำคัญสำหรับการทดลอง อีกทั้งอาจารย์วิโรจน์ เชาว์วิเศษ ที่เอื้อเฟื้ออุปกรณ์กล้องสำหรับการตรวจสอบพื้นผิวรอยตัดของชิ้นงาน ความสำเร็จของการวิจัยครั้งนี้เกิดขึ้นได้จากความร่วมมือและการสนับสนุนจากทุกท่าน คณะผู้วิจัยขอกราบขอบพระคุณอย่างสูงในความเมตตาและน้ำใจที่มีต่อโครงการ ซึ่งทำให้การพัฒนาครั้งนี้สำเร็จลุล่วงไปอย่างสมบูรณ์ และเป็นประโยชน์ต่อชุมชนและการพัฒนาด้านเทคโนโลยีในอนาคต

อ้างอิง

[1] Y. Y. Nandurkar, S. S. Akant, and S. L. Bankar, "Design and fabrication of automatic plastic pipe cutting machine," *International Journal of Science and Engineering Research*, vol. 3, no. 4, pp. 1–4, 2018.

[2] กันทลัส ทองบุญมา, "ขบวนการเคลื่อนไหวทางสังคมแบบใหม่เพื่อการรณรงค์ไม่ใช้หลอดพลาสติก," *วารสารประชาสัมพันธ์และการโฆษณา*, ปีที่ 12, ฉบับที่ 2, หน้า 1–15, 2562.

[3] ก้องภพ แก้วทอง และ เฉลิมเกียรติ อนันทกาญจน์, "การออกแบบและพัฒนาเครื่องตัดหลอดสำหรับการผลิตหลอดจากพืช," 2565.

[4] ตระกูลพันธ์ พัชรเมธา, "ผลิตภัณฑ์หัตถกรรมกับการพัฒนาสู่สินค้าหนึ่งตำบลหนึ่งผลิตภัณฑ์," *วารสารมหาวิทยาลัยศิลปากร ฉบับภาษาไทย*, ปีที่ 36, ฉบับที่ 1, หน้า 67–80, 2559.

[5] ยศวรรธน์ จันทนา และ นรัตว์ รัตนวัย, "ปัจจัยที่เหมาะสมเพื่อการปรับตั้งค่าเครื่องหั่นใบตะไคร้ด้วยเทคนิคออกแบบการทดลอง," *วารสารวิชาการวิทยาศาสตร์และเทคโนโลยี มหาวิทยาลัยราชภัฏนครสวรรค์*, ปีที่ 14, ฉบับที่ 19, หน้า 83–95, 2565.

[6] ศุภชัย นาทะพันธ์, *การควบคุมคุณภาพ*, กรุงเทพฯ: ซีเอ็ดยูเคชั่น, 2551.

[7] กรุงเทพธุรกิจ,"หลอดคุณหญ้าจากธรรมชาติบริสุทธิ์,"[ออนไลน์].Available: https://www.bangkokbiznews.com/social. [เข้าถึงเมื่อ: 2 ก.ย. 2566].

[8] ผู้จัดการออนไลน์, "หลอดกระจูด รักษ์โลกจากแดนไต้ ลดปัญหาไฟป่า สร้างรายได้สู่ชุมชน," [ออนไลน์]. Available: https://mgronline.com/smes/detail/9640000042762. [เข้าถึงเมื่อ: 2 ก.ย. 2566].

[9] มหาวิทยาลัยรามคำแหง, "การดำเนินการลดใช้พลาสติก," [ออนไลน์]. Available: https://mmm.ru.ac.th/MMM/IS/sun17/6114070022. [เข้าถึงเมื่อ: 2 ก.ย. 2566].

[10] สำนักงานสภานโยบายการอุดมศึกษา วิทยาศาสตร์ วิจัยและนวัตกรรมแห่งชาติ (สอวช.), "พืชโมเดลเศรษฐกิจ BCG," [ออนไลน์]. Available: https://www.nxpo.or.th/th/bcg-economy/. [เข้าถึงเมื่อ: 2 ก.ย. 2566].

[11] องค์การบริหารจัดการก๊าซเรือนกระจก (องค์การมหาชน), "ปริมาณคาร์บอน," [ออนไลน์]. Available: http://carbonmarket.tgo.or.th/. [เข้าถึงเมื่อ: 2 ก.ย. 2566].

[12] Brand Inside, "ขยะพลาสติกไทย," [ออนไลน์]. Available: https://brandinside.asia/plastic-pollution/. [เข้าถึงเมื่อ: 2 ก.ย. 2566].

[13] SciPlanet, "ผลกระทบต่อสิ่งแวดล้อมของหลอดพลาสติก," [ออนไลน์]. Available: https://sciplanet.org/content/10183. [เข้าถึงเมื่อ: 2 ก.ย. 2566].

การจำลองอพยพหนีไฟด้วยโปรแกรม Pathfinder กรณีศึกษา อาคารเฉลิมพระเกียรติ 50 พรรษา (อาคาร20) มหาวิทยาลัยราชภัฏยะลา

Simulation of Fire Evacuation Using Pathfinder Program: A Case Study of 20th Building Yala Rajabhat University

1st Hafanee Ama
Public Health Program,
Faculty of Science, Technology and Agriculture,Yala Rajabhat University
Yala Province, Thailand
Email hafanee.a@yru.ac.th

2nd Anukool Bensaard
Public Health Program,
Faculty of Science, Technology and Agriculture,Yala Rajabhat University
Yala Province, Thailand
Email 406424053@yru.ac.th

3rd Maytiya Muadchim
Public Health Program,
Faculty of Science, Technology and Agriculture,Yala Rajabhat University
Yala Province, Thailand
Email maytiya.m@yru.ac.th

4th Suradech Suwanchatree
Public Health Program,
Faculty of Science, Technology and Agriculture,Yala Rajabhat University
Yala Province, Thailand
Email Suradech.s@yru.ac.th

5th Piyaruk Pradabphetrat
Public Health Program,
Faculty of Science, Technology and Agriculture,Yala Rajabhat University
Yala Province, Thailand
Email Piyaruk.p@yru.ac.th

Abstract**—***The simulation of fire evacuation using the Pathfinder program, with a case study of the Chalerm Phra Kiat 50th Anniversary Building (Building 20) at Yala Rajabhat University, aims to study the evacuation time of this building. The research involved analyzing the building's structure, the number of occupants, and the characteristics of the occupants. These data were then input into the Pathfinder software to simulate an evacuation scenario. The simulation involved a single scenario where all occupants, totaling a maximum of 2,409 people, evacuated simultaneously. The results of the simulation indicated that the evacuation from the Chalerm Phra Kiat 50th Anniversary Building (Building 20) at Yala Rajabhat University took 34 minutes and 24.5 seconds. This duration is within the limit set by Ministerial Regulation No. 33 (1992), issued under the Building Control Act B.E. 2522 (1979), which stipulates that the fire escape system must demonstrate the ability to evacuate all occupants from the building within one hour.*

Keywords**—** *Evacuation simulation, Pathfinder program, Fire Evacuation*

I. บทนำ

ปัญหาอัคคีภัยเป็นภัยคุกคามที่ส่งผลกระทบต่อชีวิตและทรัพย์สินของประชาชนอย่างรุนแรง โดยเฉพาะอย่างยิ่งในสถานศึกษาที่มีความหนาแน่นของผู้คนสูง เช่น มหาวิทยาลัยราชภัฏยะลา ในการศึกษาครั้งนี้จึงมุ่งเน้นไปที่การประเมินประสิทธิภาพของระบบอพยพหนีไฟในอาคารเรียนรวม (อาคาร 20) มหาวิทยาลัยราชภัฏยะลา ซึ่งเป็นอาคารสูงที่มีผู้ใช้งานจำนวนมาก โดยผ่านการจำลองสถานการณ์อัคคีภัยและการอพยพหนีไฟโดยใช้โปรแกรม *Pathfinder* เพื่อระบุจุดอ่อนของระบบการหนีไฟและเสนอแนวทางปรับปรุงเพื่อให้เกิดความปลอดภัยมากยิ่งขึ้น

จากสถิติสาธารณภัยในปี พ.ศ. *2566* อัคคีภัยมีอัตราการเกิดอุบัติเหตุมากถึง 60% ซึ่งอัตราการเกิดอัคคีภัยในประเทศไทยมีแนวโน้มเพิ่มสูงขึ้นอย่างต่อเนื่อง[1] อาจเกิดจากหลายปัจจัย เช่น การกระทำที่จงใจ การประมาทเลินเล่อ หรือความบกพร่องของระบบไฟฟ้า นอกจากนี้ผู้ใช้งานส่วนใหญ่อาจขาดความรู้และประสบการณ์ในการอพยพหนีไฟ ทำให้เกิดความเสี่ยงต่อการสูญเสียชีวิตและทรัพย์สิน[2] เช่น ไฟไหม้อาคารพาณิชย์ขนาดใหญ่ในเมืองซองนัม ประเทศเกาหลีใต้ มีผู้ได้รับบาดเจ็บ 130 คน มีรายงานว่าทางหนีไฟบางจุดถูกปิดกั้นและมีสิ่งกีดขวาง ทำให้ผู้คนอพยพออกจากอาคารได้ล่าช้า ผู้คนจำนวนมากต้องอพยพอย่างยากลำบาก และมีผู้ได้รับบาดเจ็บจากการสูดควัน[3]

ดังนั้นการศึกษาครั้งนี้จึงมีความสำคัญอย่างยิ่งในการระบุจุดอ่อนของระบบอพยพหนีไฟในอาคารเรียนรวม (อาคาร 20) มหาวิทยาลัยราชภัฏยะลา และเสนอแนวทางปรับปรุง เพื่อให้มั่นใจได้ว่าผู้ใช้งานอาคารทุกคนสามารถอพยพออกจากอาคารได้อย่างปลอดภัยในกรณีเกิดเหตุฉุกเฉิน ผลการวิจัยนี้คาดว่าจะเป็นประโยชน์ต่อมหาวิทยาลัยราชภัฏยะลาและสถาบันการศึกษาอื่นๆ ในการวางแผนและดำเนินการด้านความปลอดภัยในอาคาร เพื่อลดความเสี่ยงจากเหตุการณ์อัคคีภัยและสร้างความมั่นใจให้กับผู้ใช้งานอาคาร

II. ทบทวนวรรณกรรม

1. โปรแกรม Pathfinder

เป็นโปรแกรมพื้นฐานของการอพยพหนีไฟและการจำลองการเคลื่อนไหวในการหาทางออกของมนุษย์ โดยใช้พฤติกรรมการควบคุมบังคับเลียนแบบมนุษย์ โปรแกรมมีส่วนของกราฟิกเพื่อให้ผู้ใช้งานสามารถออกแบบและจำลอง รวมถึงมีเครื่องมือในการสร้างรูปได้ทั้งแบบ 2 มิติและแบบ 3 มิติ เพื่อใช้วิเคราะห์ผล โปรแกรม Pathfinder ถูกสร้างขึ้นจากแนวคิดของการสร้างพื้นที่ทางเดินเป็นหลัก รวมถึงสิ่งกีดขวาง และบันไดต่างๆ ในแบบจำลองของโปรแกรมมีทางเลือกของพารามิเตอร์ของพฤติกรรมการเคลื่อนที่ของมนุษย์ในการอพยพหนีไฟ 2 โหมด คือโหมด SFPE และโหมด Steering โดยโหมด SFPE เป็นแบบจำลองการไหลของการเดิน โดยผู้เดินจะไม่พยายามหลีเลี่ยงกับบุคคลอื่น ๆ และจะยอมให้แทรกผ่านไปได้ความเร็วการอพยพจะขึ้นอยู่กับความหนาแน่นของผู้อาศัยในแต่ละห้อง และอัตราการไหลผ่านประตูจะขึ้นอยู่กับความกว้างของประตู ส่วนโหมด Steering อ้างอิงมาจากแนวคิดพฤติกรรมการบังคับเลี้ยงผกผัน จะมีพฤติกรรมการทำงานที่ซับซ้อนมาขึ้น เป็นผลมาจากอัลกอริทึมของการเคลื่อนไหวตามธรรมชาติ รวมถึงขจัดปัญหาการรอคิวที่ประตู ผู้อาศัยจะใช้ระบบบังคับในการเคลื่อนที่และมีปฏิสัมพันธ์ตอบโต้กับผู้อื่น ซึ่งเป็นการเลียนแบบฤติกรรมการเคลื่อนไหวของมนุษย์ได้มากที่สุดเท่าที่จะเป็นไปได้ การเคลื่อนที่มีความโค้ง โดยได้มาจากผลที่เกิดขึ้นของสมาการของเว้นระยะห่างระหว่างมนุษย์กับมนุษย์ และมนุษย์กับสิ่งกีดขวาง ซึ่งผลลัพธ์ที่ได้จะการจำลองแบบโหมด Steering จะมีความใกล้เคียงกับผลการทดลองมากกว่าการจำลองแบบโหมด SFPE [2]

2. งานวิจัยที่เกี่ยวข้อง

การจำลองการอพยพหนีไฟด้วยโปรแกรม Pathfinder กรณีศึกษาอาคาร โรงเรียนประถมศึกษาและมัธยมศึกษาโดยมีวัตถุประสงค์เพื่อศึกษาพฤติกรรมของผู้ใช้อาคารและวิเคราะห์เวลาที่ใช้ในการอพยพออกจากอาคารเรียนรวมทั้งวิเคราะห์และปรับปรุงลักษณะทางสถาปัตยกรรมอาคารเรียนเพื่อเพิ่มความปลอดภัยต่อชีวิตของผู้ใช้อาคารเมื่อเกิดเหตุเพลิงไหม้ ไม่มีกลุ่มตัวอย่างแต่จะใช้โปรแกรม Pathfinder ในการจำลองการอพยพทั้งหมด 3 สถานการณ์ สถานการณ์แรกให้ผู้ใช้อาคารอพยพพร้อมกันทั้งหมดและบันไดทางออกทั้งหมดสามารถใช้งานได้สถานการณ์ที่สองให้ผู้ใช้อาคารอพยพพร้อมกันทั้งหมด และบันไดทางออกซ้ายใช้งานไม่ได้เนื่องจากไฟไหม้ห้องเก็บของ สถานการณ์ที่สาม สมมติเกิดเหตุเพลิง ไหม้บนชั้น 3 ให้ผู้ใช้อาคารชั้น 3 อพยพก่อนชั้นอื่น และบันไดทางออกทั้งหมดสามารถใช้งานได้ผลการจำลองพบว่าสถานการณ์ที่ 1 ใช้เวลาในการอพยพผู้ใช้อาคารทั้งหมดออกจากอาคารน้อยที่สุดสำหรับแต่ละกรณี 501.6 วินาที 464.8 วินาทีและ 490.4 วินาที สถานการณ์ที่ 2 ใช้เวลาในการอพยพนานที่สุดสำหรับแต่ละกรณี 911.5 วินาที 866.3 วินาทีและ 892.3 วินาทีเนื่องจากมีความแออัดในบันไดทางออกและสถานการณ์ที่ 3 ใช้เวลาน้อยที่สุดสำหรับผู้ใช้อาคารเข้าสู่บันไดที่เป็นเส้นทางหนีไฟสำหรับแต่ละกรณีคือ คือ 553.2 วินาที 488.9 วินาทีและ 517.4 วินาที ผลการวิจัยพบว่าเวลาที่ใช้ในการอพยพออกจากอาคารเรียนในทุกสถานการณ์เกินกว่าที่กำหนดของประกาศกระทรวงอุตสาหกรรม เรื่อง การป้องกันและระงับอัคคีภัยในโรงงาน พ.ศ. 2552 ออกตามความในพระราชบัญญัติโรงงาน พ.ศ. 2535 คือต้องจัดเส้นทางหนีไฟที่อพยพคนงานทั้งหมดออกจากบริเวณที่ทำงานสู่บริเวณที่ปลอดภัย ภายใน 5 นาที (300 วินาที) [2]

การอพยพหนีไฟในสถาบันเทคโนโลยีแห่งสุวรรณภูมิโดยใช้โปรแกรมทางพลศาสตร์อัคคีภัย โดยมีวัตถุประสงค์เพื่อจำลองสถานการณ์การอพยพหนีไฟในอาคารเรียนของสถาบันเทคโนโลยีทั้งหมดออกจากบริเวณที่ทำงานสู่บริเวณที่ปลอดภัยภายใน 5 นาที (300 วินาที) ดังนั้นควรมีการปรับปรุงลักษณะทางสถาปัตยกรรมของอาคาร เพื่อเพิ่มความปลอดภัยต่อชีวิตของผู้ใช้อาคารเมื่อเกิดเหตุเพลิงไหม้แห่งสุวรรณภูมิ โดยใช้โปรแกรมจำลองทางพลศาสตร์อัคคีภัยเพื่อจำลองสถานการณ์การอพยพหนีไฟของคนที่อยู่ภายในอาคารเรียนของสถาบันเทคโนโลยีแห่งสุวรรณภูมิ ตามกฎกระทรวงกำหนดมาตรฐานในการบริหารจัดการและดำเนินการด้านความปลอดภัย อาชีวอนามัย และสภาพแวดล้อมในการทำงานเกี่ยวกับการป้องกันและระงับอัคคีภัย พ.ศ. 2553 เพื่อเปรียบเทียบสถานการณ์จำลองการอพยพหนีไฟจากโปรแกรมพลศาสตร์อัคคีภัยกับการฝึกซ้อมอพยพหนีไฟจริง ประชากรที่ใช้ในการศึกษาคือมีผู้เข้าร่วมการฝึกซ้อมอพยพหนีไฟทั้งหมด 181 คน แบ่งเป็นชาย 83 คน หญิง 98 คน เครื่องมือการวิจัย โปรแกรม Pyrosim โปรแกรม Pathfinder และการฝึกซ้อมอพยพหนีไฟ ผลคือเมื่อเปรียบเทียบผลการจำลองการอพยพหนีไฟกับการฝึกซ้อมอพยพหนีไฟประจำปี พบว่าผลการจำลองการอพยพหนีไฟใช้เวลาในการอพยพที่น้อยกว่าการฝึกซ้อมอพยพหนีไฟจริง ซึ่งผลทั้งสองเป็นไปตามกฎกระทรวงกำหนดมาตรฐานในการบริหารจัดการและดำเนินการด้านความปลอดภัยอาชีวอนามัย และสภาพแวดล้อมในการทำงานเกี่ยวกับการป้องกันและระงับอัคคีภัย พ.ศ. 2555 ที่กำหนดว่าการอพยพหนีไฟ ลูกจ้างที่ทำงานในเวลาเดียวกันทั้งหมดสู่จุดปลอดภัยได้โดยปลอดภัย ภายในเวลาไม่เกิน 5 นาที นอกจากนี้ จากการจำลองการอพยพหนีไฟพบว่าการอพยพหนีไฟที่ใช้ทางหนีไฟทางครบทั้ง 3 เส้นทาง เป็นวิธีการอพยพหนีไฟที่เหมาะสมที่สุด สามารถอพยพหนีไฟภายในเวลา 5 นาที [4]

การจำลองอพยพหนีไฟด้วยโปรแกรม Pathfinder กรณีศึกษาโรงงานผลิตชิ้นส่วนโลหะปั๊มขึ้นรูป โดยมีวัตถุประสงค์เพื่อวิเคราะห์เส้นทางหนีไฟให้สอดคล้องกับกฎหมาย และมาตรฐาน NFPA 101, Life Safety Code และเพื่อศึกษาระยะเวลาการอพยพหนีไฟ กรณีต่างๆของผู้ใช้อาคารทั้งหมดให้สอดคล้องกับกฎหมาย เครื่องมือที่ใช้ในการวิจัย เป็นงานวิจัยเชิงทดลองโดยใช้โปรแกรม Pathfinder จำลองการอพยพหนีไฟตามสถานการณ์เพลิงไหม้ที่กำหนด โดยวิธีการศึกษาแบบแปลนอาคารมีความสูงมากกว่าหนึ่งชั้น แบ่งเป็น 2 อาคาร เป็นพื้นที่ครอบครองประเภทกิจการโรงงาน มีทางออกสู่ภายนอกอาคารอยู่ 11 ทาง บันไดหนีไฟจำนวน 1 บันได และบันไดหนีไฟที่ใช้อพยพซึ่งเป็นบันไดที่ใช้สัญจรทั่วไป มีทั้งสิ้น 3 บันได รวบรวมกฎหมายและมาตรฐานที่เกี่ยวข้องกับเส้นทางหนีไฟ คำนวณจำนวนผู้ใช้อาคารตามมาตรฐาน NFPA 101, Life Safety Code มีจำนวนผู้ใช้อาคารที่คำนวณได้ตามมาตรฐาน NFPA 101, Life Safety Code มีจำนวน 1,095 คน แบ่งเป็นเพศชายร้อยละ 39.52 และเพศหญิงร้อยละ 60.48 และกำหนดรูปแบบสถานการณ์เพลิงไหม้ตามมาตรฐาน NFPA 101, Life Safety Cod ผลการศึกษา พบว่า ขีดความสามารถของประตูและบันไดที่ใช้ในการอพยพหนีไฟไม่สามารถรองรับจำนวนผู้ใช้อาคารทำให้ผู้ใช้อาคารเกิดการรอคิวที่ประตูและแออัดบริเวณบันไดจึงเสนอทำการปรับปรุงเส้นทางหนีไฟ ได้แก่ การขยายประตูหนีไฟ รื้อและสร้างบันไดหนีไฟใหม่เพิ่มเส้นทางหนีไฟ รวมถึงจำกัดจำนวนผู้ใช้อาคารที่เหมาะสมกับขีดความสามารถของอาคารไม่เกิน 766 คน เพื่อให้สามารถรองรับจำนวนผู้ใช้อาคารได้โดยผู้ใช้อาคารมีการรอคิวที่ประตู ไม่นานและไม่แออัดบริเวณบันได ส่งผลให้ผู้ใช้อาคารใช้เวลาอพยพไม่เกิน 5 นาที เป็นไปตามข้อกฎหมายกำหนด [5]

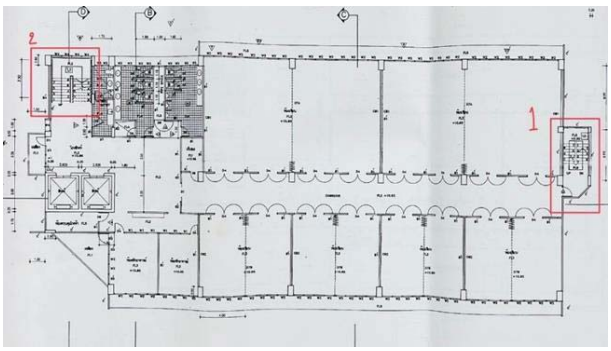
การจำลองการอพยพอัคคีภัยและการช่วยเหลือผู้ป่วยในอาคารโรงพยาบาลขนาดใหญ่ใช้โปรแกรม Pathfinder โดยมีวัตถุประสงค์เพื่อศึกษาเวลาที่ใช้อพยพเพลิงเมื่อเปรียบเทียบกับกฎหมายที่ใช้บังคับอาคารขนาดใหญ่และอาคารสูงในประเทศไทย และจำลองสถานการณ์การอพยพเพลิงโดยใช้โปรแกรม Pathfinder เพื่อจำลองการเคลื่อนไหวของมนุษย์และระบุพฤติกรรมการอพยพของผู้อาศัยอาคารรวมไปถึงสำรวจการใช้ลิฟต์ที่เป็นช่องทางการอพยพเพิ่มเติม โดยเฉพาะอย่างยิ่งสำหรับผู้ป่วยที่ป่วยหนักที่ไม่สามารถใช้ทางออกไฟได้ ผลการศึกษาการจำลองการอพยพอัคคีภัยที่ดำเนินการในอาคารโรงพยาบาลขนาดใหญ่ส่งผลให้มีเวลาอพยพ 3,048 วินาที 2,931 วินาที และ 2,958.3 วินาที ตามลำดับ ซึ่งไม่เกินขีดจำกัดเวลาที่กำหนดโดยการควบคุมอาคารสูงตามกฎหมายไทย การใช้ลิฟต์เป็นช่องทางการอพยพเพิ่มเติมสำหรับผู้ป่วยที่ป่วยหนักและทีมช่วยเหลือได้ทดสอบในสองสถานการณ์ ส่งผลให้เวลาอพยพเพลิงลดลง 2,073 วินาทีและ 1,979.5 วินาทีตามลำดับ [6]

การจำลองอพยพหนีไฟในสถานีรถไฟใต้ดินด้วยโปรแกรม Pathfinder โดยมีวัตถุประสงค์เพื่อการจำลองและวิเคราะห์กระบวนการอพยพในสถานีรถไฟใต้ดินโดยใช้ Pathfinder ทำความเข้าใจการอพยพและระบุปัจจัยสำคัญที่มีผลต่อกระบวนการอพยพเพื่อพัฒนาการอพยพให้มีประสิทธิภาพ โดยกำหนดจำนวนผู้คนสูงสุดที่สามารถอพยพได้อย่างปลอดภัยในสถานการณ์ต่างๆ ผลการวิจัยพบว่าจุดที่แออัดในการอพยพส่วนใหญ่อยู่ที่บันไดทางออกและความกว้างของทางออกมีผลต่อการลดความแออัดการอพยพ นอกจากนี้เมื่อขบวนรถไฟเต็ม จำนวนคนบนชานชาลาจะต้องจำกัดไว้ที่ 500 คน เมื่อจำนวนผู้โดยสารในรถไฟ 1,542 คน จำนวนคนบนชานชาลาจะต้องจำกัดไว้ที่ 480 คน[7]

III. ระเบียบวิธีวิจัย

1. ศึกษาโครงสร้างอาคาร

อาคารเฉลิมพระเกียรติ 50 พรรษา (อาคาร20) มหาวิทยาลัยราชภัฏยะลา อาคารเป็นแบบอาคารเดี่ยว มีแบบแปลนจากกองพัฒนาอาคารสถานที่สำนักงานสภาสถาบันราชภัฏ ภายใต้ชื่อแบบก่อสร้าง อาคารเรียนรวม 9 ชั้น ซึ่งมีจำนวนชั้น 10 ชั้น มีความสูงประมาณ 39.50 เมตร ขนาดพื้นที่รวมประมาณ 10,457 ตารางเมตร มีบันไดสำหรับหนีไฟนอกอาคารจำนวน 1 บันได มีบันไดหลัก 1 บันได รายละเอียดดังภาพที่ 1 โดยระบุหมายเลข 1 แสดงบันไดหนีไฟนอกอาคารและระบุหมายเลข 2 แสดงตำแหน่งบันไดหลัก



ภาพที่ 1 บันไดหนีไฟและบันไดหลักของอาคาร

อาคารเฉลิมพระเกียรติ 50 พรรษา (อาคาร 20) มหาวิทยาลัยราชภัฏยะลา มีการอนุมัติใช้แบบก่อสร้างเมื่อปี พ.ศ.2539 ซึ่งจัดเป็นอาคารสูงและอาคารขนาดใหญ่พิเศษตามกฎกระทรวงฉบับที่ 33 (พ.ศ. 2535) ออกตามความในพระราชบัญญัติควบคุมอาคาร พ.ศ. 2522 และตามข้อมูลในแผนกงานออกแบบและวางแผนพัฒนาอาคารทางผู้วิจัยได้ศึกษาความกว้าง ความยาว ความสูงของส่วนประกอบของอาคารแต่ละชั้น ดังตารางที่ 1

ตารางที่ 1 องค์ประกอบของอาคารเฉลิมพระเกียรติ 50พรรษา (อาคาร20) มหาวิทยาลัยราชภัฏยะลาแต่ละชั้น

องค์ประกอบของอาคาร	ขนาด (เมตร)									
	ชั้น 1	ชั้น 2	ชั้น 3	ชั้น 4	ชั้น 5	ชั้น 6	ชั้น 7	ชั้น 8	ชั้น 9	ชั้น 10
ความกว้างอาคาร	23.9	23.9	23.9	23.9	23.9	23.9	23.9	23.9	23.9	22.5
ความยาวอาคาร	46.5	46.5	46.5	46.5	46.5	46.5	46.5	46.5	46.5	46.5
ความสูง	4.1	3.1	3.1	3.1	3.1	3.1	3.1	3.1	3.1	3.1
ความกว้างของบันไดหลัก	1.6	1.6	1.6	1.6	1.6	1.6	1.6	1.6	1.6	1.6
ความกว้างของบันไดหนีไฟที่ 1	1.0	1.0	1.0	1.0	1.0	1.0	1.0	1.0	1.0	1.0
ความกว้างทางเดินร่วม(หน้าห้อง)	3.5	3.5	3.5	3.5	3.5	3.5	3.5	3.5	3.5	0
ความกว้างทางเดินร่วม(หน้าลิฟท์)	3.2	3.2	3.2	3.2	3.2	3.2	3.2	3.2	3.2	3.0
ความกว้างของประตู	0.9	0.9	0.9	0.9	0.9	0.9	0.9	0.9	0.9	0.9
ความกว้างของประตูแบบคู่	1.8	1.8	1.8	1.8	1.8	1.8	1.8	1.8	1.8	1.8

2. ศึกษาจำนวนผู้ใช้อาคารและลักษณะการใช้อาคาร

จำนวนผู้ใช้อาคารศึกษาโดยการนับจำนวนผู้ปฏิบัติงานภายในอาคารและนับจำนวนเก้าอี้ในแต่ละห้อง ซึ่งแทนจำนวนของผู้ปฏิบัติงาน และผู้เรียนทั้งในห้องสำนักงาน ห้องเรียน และห้องประชุม นำจำนวนผู้ใช้อาคารในแต่ละห้องป้อนลงในโปรแกรม Pathfinder เพื่อทำการจำลองสถานการณ์อพยพเป็นการหาเวลาที่ใช้ในการอพยพในกรณีที่คนนั่งเก้าอี้เต็มจำนวน ซึ่งรายละเอียดจำนวนผู้ใช้อาคารแสดงดังตารางที่ 2

ตารางที่ 2 แสดงจำนวนผู้ใช้อาคารมากที่สุด

จำนวนผู้ใช้อาคาร (คน)	ชั้น 1	ชั้น 2	ชั้น 3	ชั้น 4	ชั้น 5-9	ชั้น 10	ทั้งหมด (คน)
	57	72	107	63	408	70	2,409

ลักษณะการใช้อาคารของอาคารเฉลิมพระเกียรติ 50 พรรษา (อาคาร 20) มหาวิทยาลัยราชภัฏยะลา ประกอบด้วยห้องสำนักงาน ห้องประชุมห้องเรียน ห้องพักผู้บริหารและอาจารย์ รายละเอียดดังตารางที่ 3

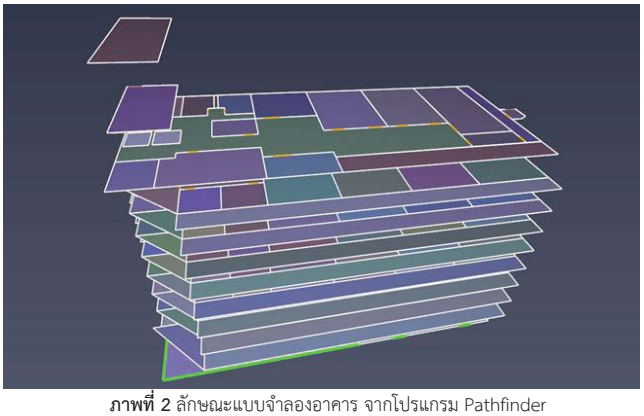
ตารางที่ 3 แสดงรายละเอียดของลักษณะการใช้งานของอาคาร

ชั้น	ลักษณะการใช้งานในแต่ละชั้น
1	ห้องสำนักงานและให้บริการติดต่อทางด้านการศึกษาจำนวน 5 ห้อง งานธุรการและสารบรรณ งานประชาสัมพันธ์ งานเจ้าหน้าที่ต่างๆ
2	มีจำนวน 13 ห้อง โดยจัดเป็นห้องผู้บริหารและเจ้าหน้าที่มหาวิทยาลัยจำนวน 9 ห้อง ห้องประชุม 1 ห้อง ห้องสำนักวิจัย 1 ห้อง ห้องสำนักงานสภาสถาบัน 1 ห้อง ประชุมย่อย 1 ห้อง
3	มีจำนวน 7 ห้อง ห้องประชุมสภามหาวิทยาลัย 1 ห้อง ห้องรับรอง 2 ห้อง ห้องประชุมกลั่นกรอง 2 ห้อง ห้องรับประทานอาหารคณะกรรมการสภามหาวิทยาลัย 1 ห้อง ห้องเตรียมเอกสารการประชุม 1 ห้อง
4	มีจำนวน 10 ห้อง ห้องประชุมแผนกต่างๆ 2 ห้อง ห้องแผนกออกแบบ 1 ห้อง ห้องหน่วยงานตรวจสอบแผนกภายใน 2 ห้อง ห้องสำหรับเจ้าหน้าที่ 2 ห้อง ห้องกองนโยบายฯ 1 ห้อง ห้องเก็บวัสดุอุปกรณ์ 2 ห้อง
5	ห้องเรียนจำนวน 8 ห้อง แต่ละห้องมีจำนวนเก้าอี้ 51 ตัว สำหรับนักศึกษา 50 ตัว สำหรับอาจารย์ 1 ตัว

ชั้น	ลักษณะการใช้งานในแต่ละชั้น
6	ห้องเรียนจำนวน 8 ห้อง แต่ละห้องมีจำนวนเก้าอี้ 51 ตัว สำหรับนักศึกษา 50 ตัว สำหรับอาจารย์ 1 ตัว
7	ห้องเรียนจำนวน 8 ห้อง แต่ละห้องมีจำนวนเก้าอี้ 51 ตัว สำหรับนักศึกษา 50 ตัว สำหรับอาจารย์ 1 ตัว
8	ห้องเรียนจำนวน 8 ห้อง แต่ละห้องมีจำนวนเก้าอี้ 51 ตัว สำหรับนักศึกษา 50 ตัว สำหรับอาจารย์ 1 ตัว
9	ห้องเรียนจำนวน 8 ห้อง แต่ละห้องมีจำนวนเก้าอี้ 51 ตัว สำหรับนักศึกษา 50 ตัว สำหรับอาจารย์ 1 ตัว
10	สำหรับนักศึกษาปริญญาโท โดยมีห้องเรียน 2 ห้อง ห้องประชุม 1 ห้อง ห้องพักอาจารย์ 1 ห้อง

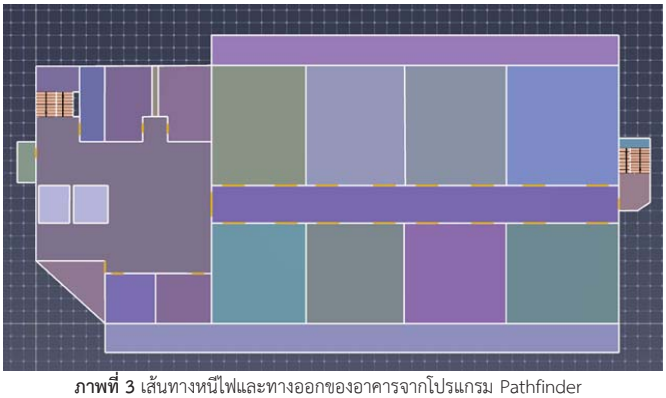
3. จำลองสถานการณ์อพยพหนีไฟโดยใช้โปรแกรม Pathfinder

3.1 สร้างแบบจำลองอาคารเฉลิมพระเกียรติ 50พรรษา (อาคาร20) มหาวิทยาลัยราชภัฏยะลา โดยใช้โปรแกรม Pathfinder จำลองตามแบบแปลนอาคารโดยกำหนดขนาดกริดเพื่อสร้างแบบจำลองตามขนาดพื้นที่จริงสร้างห้องและส่วนประกอบต่างๆของอาคารให้เทียบเท่ากับอาคารจริง ดังภาพที่ 2



ภาพที่ 2 ลักษณะแบบจำลองอาคาร จากโปรแกรม Pathfinder

3.2 สร้างเส้นทางหนีไฟโดยใช้โปรแกรม Pathfinder สร้างเส้นทางหนีไฟโดยกำหนด ขนาดความสูง ความกว้างของห้องต่างๆและของอาคาร และกำหนดเส้นทางหนีไฟ ดังภาพที่ 3



ภาพที่ 3 เส้นทางหนีไฟและทางออกของอาคารจากโปรแกรม Pathfinder

3.3 กำหนดจำนวนประชากรในแต่ละชั้นลงในโปรแกรม Pathfinder การจำลองการอพยพหนีไฟจะกำหนดจำนวนประชากรในแต่ละชั้นตามจำนวนเก้าอี้ที่ได้สำรวจ และสุ่มเพศและอายุของประชากรที่อยู่ภายในอาคาร โดยตั้งค่าให้โปรแกรม Pathfinder แยกการจำลองพฤติกรรมของบุคคลออกจากกันอย่างเป็นอิสระ ในค่าเริ่มต้นของโปรแกรมผู้อพยพแต่ละคนจะเคลื่อนที่ไปยังทางออกที่คาดว่าใช้เวลาน้อยที่สุด โดยเวลาที่ใช้จะคำนวณจากตัวแปร เช่น จำนวนผู้อพยพในบริเวณรอบๆ ระยะทางที่ใช้ในการเดินทาง โดยมีการกำหนดค่าเวลาที่ใช้ในการเตรียมการอพยพหนีไฟของผู้ใช้อาคารสำหรับงานวิจัย รายละเอียดดังตารางที่ 4 ค่าพารามิเตอร์ในโปรแกรม Pathfinder

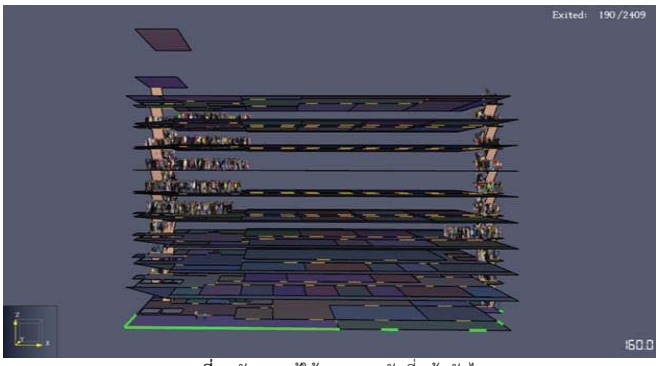
ตารางที่ 4 ความเร็วในการเคลื่อนที่ จำแนกตามเพศ และอายุ (อ้างอิงตามค่าพารามิเตอร์ในโปรแกรม Pathfinder)

เพศ	ชาย น้อยกว่า 30 ปี	หญิง น้อยกว่า 30 ปี	ชาย 30-50 ปี	หญิง 30-50 ปี
ความเร็วในการเคลื่อนที่ (เมตรต่อวินาที)	1.137	0.95	0.99	0.23

3.4 เปรียบเทียบผลกับกฎหมายตามเกณฑ์กฎกระทรวง ฉบับที่ 33 (พ.ศ. 2535) ออกตามความในพระราชบัญญัติควบคุมอาคาร พ.ศ. 2522

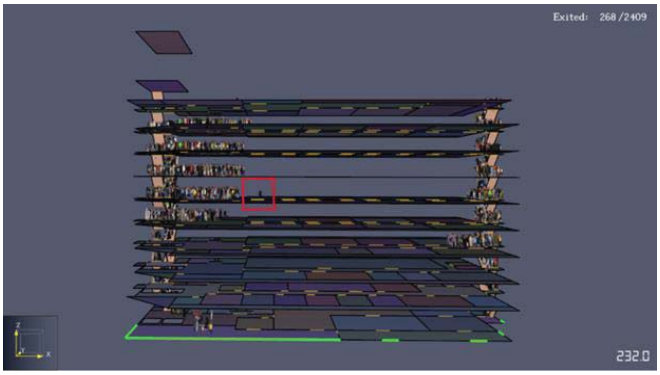
IV. ผลการทดลอง

จากการจำลองการอพยพหนีไฟโดยใช้โปรแกรมพบว่าการอพยพหนีไฟออกจากอาคารหลังจากเวลา 160 วินาที ผู้ใช้อาคารทุกชั้นออกจากห้องครบทุกคน แล้วไปรอกันที่หน้าบันไดเพื่อที่จะลงไปยังชั้นล่าง ดังภาพที่ 4



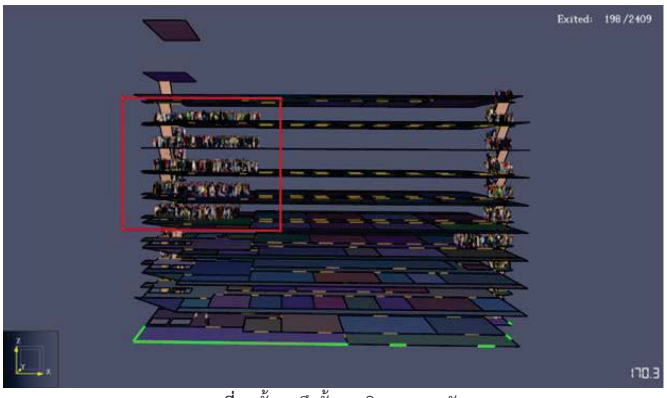
ภาพที่ 4 ลักษณะผู้ใช้อาคารรอกันที่หน้าบันได

ในช่วงวินาทีที่ 232 ผู้ใช้อาคารเริ่มเปลี่ยนเส้นทางการอพยพหนีไฟไปยังบันไดหนีไฟ เพราะบันไดหลักมีความแออัด ดังภาพที่ 5



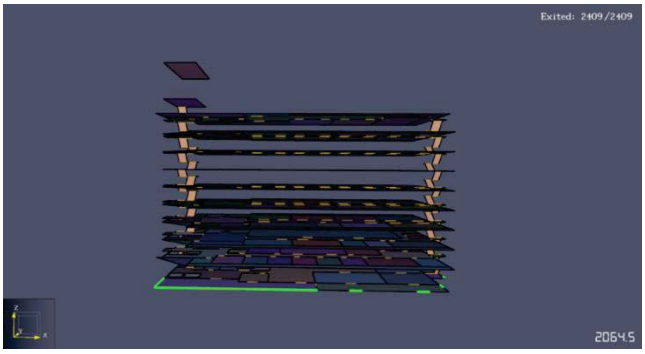
ภาพที่ 5 ผู้ใช้อาคารเปลี่ยนเส้นทางการอพยพ

ชั้นที่มีความแออัดมากที่สุดคือ ชั้น 5 ถึงชั้น 9 เพราะในแต่ละชั้นเป็นชั้นเรียนที่ใช้สำหรับการเรียนการสอนมีความจุได้สูงสุกชั้นละ 408 คน ดังภาพที่ 6



ภาพที่ 6 ชั้น 5 ถึงชั้น 9 เกิดความแออัด

จากการจำลองการอพยพหนีไฟโดยใช้โปรแกรมพบว่าการจำลองอพยพหนีไฟออกจากอาคารเวลาที่ใช้ในการอพยพจากอาคารเฉลิมพระเกียรติ 50พรรษา (อาคาร20) มหาวิทยาลัยราชภัฏยะลาใช้เวลา 2,064.5 วินาที ดังภาพที่ 7



ภาพที่ 7 ผู้ใช้อาคารออกจากตัวอาคารครบทั้งหมด

อภิปรายผล

การจำลองอพยพหนีไฟด้วยโปรแกรม Pathfinder กรณีศึกษาอาคารเฉลิมพระเกียรติ 50พรรษา (อาคาร20) มหาวิทยาลัยราชภัฏยะลา จากการสมมติฐานที่ว่า เวลาที่ใช้ในการอพยพหนีไฟของอาคารเฉลิมพระเกียรติ 50 พรรษา (อาคาร 20) มหาวิทยาลัยราชภัฏยะลา เป็นไปตามเกณฑ์กฎกระทรวง ฉบับที่ 33 (พ.ศ. 2535) ออกตามความในพระราชบัญญัติควบคุมอาคาร พ.ศ. 2522 ผลการวิจัยครั้งนี้ไม่สอดคล้องกับผลวิจัยของ กฤตพร ภักดี และ สุภัทร พัฒน์วิชัยโชต [2] ที่ศึกษาพบว่า เวลาที่ใช้ในการอพยพออกจากอาคารเรียน ในทุกสถานการณ์เกินกว่าที่กำหนดของประกาศกระทรวงอุตสาหกรรม เรื่อง การป้องกันและระงับอัคคีภัยในโรงงาน พ.ศ. 2552 ออกตามความในพระราชบัญญัติโรงงาน พ.ศ. 2535 คือต้องจัดเส้นทางหนีไฟที่อพยพคนงานทั้งหมดออกจากบริเวณที่ทำงานสู่บริเวณที่ปลอดภัย ภายใน 5 นาที (300 วินาที) ซึ่งที่ไม่สอดคล้องกันเนื่องจากผู้วิจัยใช้กฎกระทรวงฉบับที่ 33 (พ.ศ. 2535) ออกตามความในพระราชบัญญัติควบคุมอาคาร พ.ศ. 2522 ในการเทียบ ส่วนผลวิจัยของ กฤตพร ภักดี และ สุภัทร พัฒน์วิชัยโชต (2564) ใช้ประกาศกระทรวงอุตสาหกรรม เรื่อง การป้องกันและระงับอัคคีภัยในโรงงาน พ.ศ. 2552 ออกตามความใน พระราชบัญญัติโรงงาน พ.ศ. 2535 ส่วนวิธีการหาจำนวนผู้ใช้อาคารต่างกัน โดยที่ผู้วิจัยนับจำนวนผู้ปฏิบัติงานภายในอาคารและนับจำนวนเก้าอี้ในแต่ละห้อง ซึ่งแทนจำนวนของผู้ปฏิบัติงานทั้งในห้องเรียน และห้องประชุม ส่วนผลวิจัยของ กฤตพร ภักดี และ สุภัทร พัฒน์วิชัยโชต (2564) หาจำนวนผู้ใช้อาคาร เป็นการหาความจุของพื้นที่ภายในชั้นตามมาตรฐาน NFPA 101 โดยใช้ขนาดพื้นที่ของอาคารและปัจจัยความจุของผู้ใช้อาคาร เป็นค่าที่กำหนดขนาดพื้นที่ต่อคน ตามกิจกรรมของพื้นที่ใน แต่ละส่วนภายในชั้น[2]

ข้อสรุป

งานวิจัยนี้เป็นการจำลองการอพยพหนีไฟโดยใช้โปรแกรม Pathfinder กรณีศึกษาคารเฉลิมพระเกียรติ 50 พรรษา (อาคาร 20) มหาวิทยาลัยราชภัฏยะลา ผลการวิเคราะห์เส้นทางหนีไฟของอาคารจำนวน 10 ชั้น โดยจำลองจำนวนผู้ใช้อาคารสูงสุด 2,049 คน พบว่าการอพยพหนีไฟออกจากอาคารเฉลิมพระเกียรติ 50 พรรษา (อาคาร20) มหาวิทยาลัยราชภัฏยะลาใช้เวลา 2064.5 วินาที หรือ 34 นาที 24.5 วินาที ซึ่งไม่เกินที่กฎกระทรวงฉบับที่ 33 (พ.ศ. 2535) ออกตามความในพระราชบัญญัติควบคุมอาคาร พ.ศ. 2522 กำหนด เพื่อให้การอพยพหนีไฟดำเนินเป็นไปตามแบบจำลองการอพยพหนีไฟ ต้องดำเนินการตามข้อกำหนดของกฎกระทรวงฉบับที่ 33 (พ.ศ. 2535) ออกตามความในพระราชบัญญัติควบคุมอาคาร พ.ศ. 2522 ขอ ๒๒ อาคารสูงตองมีบันไดหนีไฟจากชั้นสูงสุดหรือดาดฟาสูพื้นดินอยางนอย 2 บันได ตั้งอยูในที่ที่บุคคล ไม่ว่าจะอยู ณ จุดใดของอาคารสามารถมาถึงบันไดหนีไฟไดสะดวก แตละบันไดหนีไฟตองอยูหางกันไมเกิน 60 เมตร เมื่อวัดตามแนวทางเดิน ขอ 23 บันไดหนีไฟตองทำดวยวัสดุทนไฟและไมผุกรอน ขอ 20 บันไดหนีไฟที่อยูภายในอาคารตองมีผนังกันไฟโดยรอบ และขอ 27 ประตูหนีไฟตองทำดวยวัสดุทนไฟเปนบานเปดชนิดผลักออกสูภายนอกพรอมติดตั้งอุปกรณชนิดที่บังคับใหบานประตูปดไดเอง[

คำขอบคุณ

ขอขอบคุณสาขาวิชาสาธารณสุขศาสตร์ แขนงวิชาอาชีวอนามัยและความปลอดภัย คณะวิทยาศาสตร์เทคโนโลยีและการเกษตร มหาวิทยาลัยราชภัฏยะลา และงานออกแบบและวางแผนพัฒนาอาคารและโครงสร้างพื้นฐาน กองนโยบายและแผน มหาวิทยาลัยราชภัฏยะลาที่ให้ความร่วมมือสนับสนุนข้อมูลในการทำวิจัย

อ้างอิง

[1] Department of Disaster Prevention and Mitigation. (2023). **Disaster statistics**. Ministry of Interior. [Online]. Available: https://dpmreporter.disaster.go.th/.

[2] Pakdee, K., & Patvichaichod, S. (2021). **Fire Evacuation Simulation Using Pathfinder Program: A Case Study of Primary and Secondary School Building.** TECHCON, 7, 60–69.

[3] Thai PBS. (2025). **South Korea evacuates over 300 people as building fire in Songnam South Korea**. [online]. Available: https://www.thaipbs.or.th/news/content/347838?utm_source=chatgpt.com.

[4] Sripothong, P., & Bunpheng, W. (2021). **The study of fire evacuation in Suvarnabhumi Institute of Technologyby fire dynamics program**. PTU Journal of science and technology, Vol. 2, 33-47.

[5] Thepwilai, T., & Patvichaichod, S. (2022). **Fire Evacuation Simulations using Pathfinder Program A Case Study of the Manufacturing of Metal Stamping Parts**. The 9th NEU National and 7th International Conference 2022, 395-409.

[6] Boonngam, H. & Patvichaichod, S. (2020). **Fire evacuation and patient assistance simulation in a large hospital building**. IOP Conf. Series: Materials Science and Engineering 2020, 1-6.

[7] Qin, J. Liu, C. & Huang,Q. (2020). **Simulation on fire emergency evacuation in special subway station based on Pathfinder**. Case Studies in Thermal Engineering 21.

[8] Ministerial Regulation No. 33 1992. **issued under the Building Control Act B.E. 2522 (1979)**. [online]. Available: https://www.buildinginspector1445.com/images/2.pdf.

ปัจจัยที่มีอิทธิพลต่อการถูกกลั่นแกล้งในนักศึกษามหาวิทยาลัยของรัฐ จังหวัดภูเก็ต

Factors Influencing Bullying in Public University Students Phuket Province

1th Nathanan Chatiwong
Ban Hat Khai Tao Health Promotion Hospital
Phuket,Thailand
natth07072543@gmail.com
2ndOrnruethai Aubdulla Sarychev
Faculty of Science and Technology
Phuket Rajabhat University
Phuket,Thailand
ornruethai.a@pkru.ac.th
3rd Nattida Kungthong
Krabi Provincial Public Health Office
Phuket,Thailand
Nattidakungthong@gmail.com

Abstract— This research is a cross-sectional analytical research with the aim of studying and predicting factors influencing bullying among students of state universities in Phuket Province. The sample group is 405 students of state universities in Phuket Province, randomly selected by simple random sampling. Data were collected between May and September 2023. The interview questionnaire has an acceptable reliability value higher than 0.60 and the Cronbach's alpha coefficient is 0.682, 0.698, 0.711, 0.646, and 0.857, respectively. The data were analyzed using frequency, percentage, and Multiple Regression Analysis statistics with the Enter Regression method.

The results of the research found that the relationship between students and their parents (x14) (p<.001, β=.559), self-esteem (x11) (p.<.001, β=.266), the relationship between students and their friends (x13) (p<.001, β=-.298), grade point average (x6) (p=.004, β=-.120), and educational institutions (x4) (p=.013, β=.108).

This research suggests that Other contexts should be observed initially while collecting data. Which, by context, is not from the interview, there are some limitations of information. and behavior in daily life of real students Other contextual characteristics should be assessed and in-depth observations should be made along with family interviews. or student caregivers on students' daily behavior and other relevant contexts to obtain more detailed information.

Keywords— *Factors Influencing,* ***Bullying, University Students***

บทนำ

การกลั่นแกล้ง หรือ BULLYING คือพฤติกรรมหรือการกระทำทั้งทางคำพูด ร่างกาย และสังคมทำให้ผู้อื่นเกิดความเดือดร้อน และเจ็บปวดทั้งทางร่างกายและจิตใจ โดยการกระทำหรือพฤติกรรมเหล่านี้มักเกิดขึ้นจากความตั้งใจของผู้กระทำที่ต้องการให้ผู้อื่นดูด้อยค่า เพื่อที่ตัวเองจะได้รู้สึกมีพลังอำนาจเหนือกว่า ถือเป็นการกระทำที่แสดงออกถึงความรุนแรง และความก้าวร้าว ไม่เป็นที่ยอมรับในสังคม และจะเกิดขึ้นซ้ำไปซ้ำมาอย่างต่อเนื่องจนมีผลทำให้ทั้งผู้ถูกกระทำ และตัวผู้กระทำเองต้องเจอกับปัญหาต่าง ๆ ตามมามากมาย (มูลนิธิยุวพัฒน์,2563) ผลการศึกษา สถาบันสถิติศาสตร์ (UIS) ขององค์การการศึกษา วิทยาศาสตร์ และวัฒนธรรมแห่งสหประชาชาติ หรือ UNESCO บ่งชี้ว่าเยาวชนเกือบ 1 ใน 3 ทั่วโลกเคยมีประสบการณ์ถูกล้อเลียน ถูกกลั่นแกล้งหรือถูก BULLY มาก่อน กระทรวงศึกษาธิการสาธารณรัฐเกาหลีประจำปี พ.ศ. 2558 พบว่า ร้อยละ 75.5 ของความรุนแรงในสถานศึกษาและการกลั่นแกล้งเกิดขึ้นภายในสถานศึกษาและ ร้อยละ 24.5 เกิดขึ้นนอกสถานศึกษา สถานการณ์การกลั่นแกล้งกันในสถานศึกษามีแนวโน้มทวีความรุนแรงขึ้นทั้งในประเทศไทยและต่างประเทศโดยในปี ค.ศ. 2015 จากสถิติการโดนกลั่งแกล้งในสถานศึกษาสูงสุด อันดับ 1 ประเทศออสเตรีย ด้วยค่าเฉลี่ยการถูกกลั่นแกล้ง ร้อยละ 21 ส่วนปี ค.ศ.2018 ประเทศไทยมีสถิติกลั่นแกล้งในสถานศึกษาปีละ 600,000 คน คิดเป็นอัตราส่วน ร้อยละ 40 สูงเป็นอันดับ 2 ของโลกที่มีการกลั่นแกล้งในสถานศึกษา โดยรองจากประเทศญี่ปุ่น เมื่อเกิดการกลั่นแกล้งขึ้น ผู้ถูกกลั่นแกล้งส่วนใหญ่มักจะไม่เล่าปัญหาที่เกิดขึ้นให้ใครฟัง มีเพียงร้อยละ 34 ที่จะยอมเล่า โดยร้อยละ 64.4 เลือกบอกเพื่อน รองลงมา คือ การบอกพี่น้อง ร้อยละ 37.1 ครูประจำชั้น ร้อยละ 33.8 และพ่อแม่หรือผู้ปกครอง ร้อยละ 33.8 และเหตุผลที่บอกกับผู้อื่น เพราะต้องการแก้แค้นหรือเอาคืน (กรมสุขภาพจิต,2019)

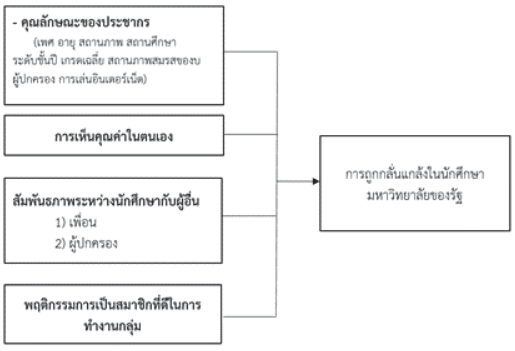
สังคมยุคปัจจุบันนี้เป็นสังคมที่เทคโนโลยีล้ำสมัย สามารถเข้าถึงเทคโนโลยีได้อย่างง่ายดาย แต่ความก้าวหน้าทางเทคโนโลยีที่เกิดขึ้นอย่างรวดเร็วนี้ ทำให้ผู้คนสามารถเชื่อมต่อและเข้าถึงกันได้ง่ายและรวดเร็ว การที่ผู้คนสามารถเข้าถึงกันได้ง่ายและรวดเร็วนี้แฝงไปด้วยอันราย เนื่องจากมีบุคคลบางกลุ่มนำความก้าวหน้าทางเทคโนโลยีเป็นช่องทางในการกลั่นแกล้งกัน (ศุภากร หวังและสมชาย เตียวกุล, 2562) โดนเฉพาะกลุ่มเยาวชนซึ่งถือเป็นกลุ่มเสี่ยง เนื่องจากข้อมูลจากสำนักงานสถิติแห่งชาติ (2558) แสดงให้เห็นว่าเยาวชนช่วงอายุ 15 - 24 ปี เป็นกลุ่มที่มีสัดส่วนในการใช้อินเตอร์เน็ตและสังคมออนไลน์มากที่สุด ในมุมมองของผู้กลั่นแกล้งนั้นถูกมองว่าเป็นเรื่องสนุกสนาน แต่บุคคลอื่นมองว่าเป็นเรื่องปกติ ซึ่งในมุมมองของผู้ที่ถูกกลั่นแกล้งนั้นได้รับผลกระทบหลายอย่าง ส่งผลต่อจิตใจ อารมณ์ และคุณภาพชีวิตในโลกจริงทั้งผู้กลั่นแกล้ง และผู้ถูกกลั่นแกล้ง เป็นความรุนแรงอย่างหนึ่งที่เป็นผลมาจากการขาดความสามารถในการจัดการปัญหา และความเครียดของผู้ถูกกลั่นแกล้งบางรายถึงขั้นพยายามฆ่าตัวตายเพื่อให้หลุดพ้นจากความเครียด และความทรมานที่ได้รับจากการกลั่นแกล้ง (PATCHIN AND HINDUJA, 2012 อ้างถึงใน นิพาดา นวนลิน ,2564)

ดังนั้นผู้วิจัยจึงสนใจที่จะศึกษาการถูกกลั่นแกล้งในนักศึกษา ในประเด็นของปัจจัยที่ส่งผลให้นักศึกษาถูกกลั่นแกล้งจากเพื่อนร่วมชั้นซึ่งอาจเกิดจากการไม่ประทับใจซึ่งกันและกันหลังทำงานกลุ่ม โดยผู้วิจัยมุ่งประเด็นของนักศึกษาที่สำคัญ ดังนี้ การเห็นคุณค่าในตนเอง พฤติกรรมการเป็นสมาชิกที่ดีในการทำงานกลุ่ม สัมพันธภาพระหว่างนักศึกษากับเพื่อน และสัมพันธภาพระหว่างนักศึกษากับผู้ปกครอง ซึ่งกลุ่มเป้าหมายที่สนใจศึกษาคือนักศึกษามหาวิทยาลัยของรัฐ จังหวัดภูเก็ต

วัตถุประสงค์การวิจัย

1. เพื่อประเมินระดับการเห็นคุณค่าในตนเอง ระดับสัมพันธภาพระหว่างนักศึกษากับผู้อื่น (เพื่อน และผู้ปกครอง) ระดับพฤติกรรมการเป็นสมาชิกที่ดี และระดับการถูกกลั่นแกล้งจากเพื่อนในการทำงานกลุ่มของนักศึกษามหาวิทยาลัยของรัฐ จังหวัดภูเก็ต
2. เพื่อวิเคราะห์ปัจจัยที่มีอิทธิพลต่อการถูกกลั่นแกล้งในนักศึกษามหาวิทยาลัยของรัฐ จังหวัดภูเก็ต

กรอบแนวคิด ดังนี้



ระเบียบวิธีวิจัย การวิจัยครั้งนี้เป็นการศึกษาแบบภาคตัดขวาง (CROSS-SECTIONAL STUDY) มีวัตถุประสงค์ เพื่อการศึกษาปัจจัยที่มีอิทธิพลต่อการถูกกลั่นแกล้งในนักศึกษามหาวิทยาลัยของรัฐ จังหวัดภูเก็ต โดยเก็บรวบรวมข้อมูลด้วยแบบสอบถามเชิงสัมภาษณ์ (INTERVIEWED QUESTIONNAIRE) ที่ผู้วิจัยพัฒนาขึ้น ระหว่าง เดือนพฤษภาคม - กันยายน พ.ศ. 2566 ประชากรที่ใช้ในการวิจัยครั้งนี้คือ นักศึกษามหาวิทยาลัยของรัฐ จังหวัดภูเก็ตประกอบด้วย 2 มหาวิทยาลัย ได้แก่ มหาวิทยาลัยราชภัฏภูเก็ต และมหาวิทยาลัยสงขลานครินทร์ วิทยาเขตภูเก็ต จำนวน 8,516 คน กลุ่มตัวอย่างที่ใช้ในการวิจัย คือ นักศึกษามหาวิทยาลัยของรัฐในจังหวัดภูเก็ต ที่ถูกคำนวณเป็นกลุ่มตัวอย่างด้วยวิธีของ เครซี่และมอร์แกน ที่ระดับความเชื่อมั่น 0.95 และที่ระดับนัยสำคัญทางสถิติ 0.05 ด้วยสูตร (KREJCIE AND MORGAN, 1970) จำนวน 405 คน การสุ่มตัวอย่างครั้งนี้ ผู้วิจัยใช้วิธีการสุ่มตัวอย่างอย่างง่าย (SIMPLE RANDOM SAMPLING TECHNIQUE) ซึ่งเป็นวิธีที่ง่ายและสะดวกต่อการนำไปใช้ในการและมีวิธีการประมาณค่าที่ง่ายและสะดวกต่อการคำนวณค่าต่าง ๆ ซึ่งเหมาะสมกับการวิจัยครั้งนี้โดยการจับสลากรายชื่อกลุ่มตัวอย่างแต่ละชั้นปี โดย มหาวิทยาลัยราชภัฏภูเก็ต ชั้นปีที่ 1 มีประชากรจำนวน 1,725 คน ถูกคำนวณเป็นกลุ่มตัวอย่าง จำนวน 82 คน ผู้วิจัยจะต้องใส่ชื่อนักศึกษา จำนวน 1,725 ชื่อ แล้วสุ่มหยิบรายชื่อขึ้นมาเป็นเป็นกลุ่มตัวอย่างจนครบจำนวน 82 รายชื่อและดำเนินการสุ่มจนครบทั้ง 9 กลุ่ม การวิจัยครั้งนี้ผู้วิจัยได้ยึดหลักจริยธรรมการวิจัยในมนุษย์ทุกขั้นตอน ซึ่งผู้วิจัยจะให้ความสำคัญและพิทักษ์สิทธิของบุคคลที่ร่วมในการศึกษาวิจัยครั้งนี้โดยยึดหลัก 3 ประการ คือหลักความเคารพในบุคคล (RESPECT FOR PERSON) หลักคุณประโยชน์และไม่ก่ออันตราย (BENEFICENCE) หลักยุติธรรม (JUSTICE) ซึ่งจะคำนึงถึงการเคารพในศักดิ์ศรีความเป็นมนุษย์ การให้คำยินยอมโดยได้รับข้อมูลที่เพียงพอและเป็นอิสระในการตัดสินใจ การเคารพในความเป็นส่วนตัวและรักษาความลับ กล่าวคือผู้ที่เกี่ยวข้องได้รับคำชี้แจงวัตถุประสงค์ของการศึกษา วิธีการเก็บข้อมูล และขอความร่วมมือในการเข้าร่วมศึกษาด้วยความสมัครใจ โดยแจ้งสิทธิ์ในการตอบรับหรือปฏิเสธการเข้าร่วมวิจัยและบอกเลิกการเข้าร่วมวิจัยได้ตลอดเวลาโดยไม่เกิดผลเสียหายต่อกลุ่มตัวอย่าง ไม่มีการบิดเบือนข้อมูลที่ได้จากการสอบถาม โดยผลการศึกษาครั้งนี้จะใช้สาหรับวัตถุประสงค์ทางวิชาการเท่านั้น และข้อมูลที่ได้ผู้วิจัยจะเก็บรักษาข้อมูลเป็นความลับ จะเผยแพร่ข้อมูลในลักษณะภาพรวมไม่ระบุถึงตัวบุคคลหรือสถานศึกษา ผู้วิจัยมีมาตรการในการรักษาความลับโดยในแบบสอบถามหรือแบบสัมภาษณ์ ไม่มีการระบุชื่อ นามสกุล ที่อยู่ สถานศึกษา หรือข้อมูลต่าง ๆ ที่จะสามารถสื่อถึงตัวบุคคลได้ ผู้วิจัยระบุเพียงรหัสชุดของแบบสอบถามเท่านั้น เครื่องมือที่ใช้ในการเก็บรวบรวมข้อมูลครั้งนี้ผู้วิจัยใช้แบบสอบถามแบบสอบถามเชิงสัมภาษณ์ (INTERVIEWED QUESTIONNAIRE) ใช้เครื่องมือสำเร็จรูปที่ถูกพัฒนาโดยสุภิศา จิตต์สม (2564) และพิชชาภา บุญณสะ (2563) ในการเก็บรวบรวมข้อมูล เครื่องมือที่ใช้ในการเก็บรวบรวมข้อมูลในการศึกษาครั้งนี้ ผู้วิจัยกำหนดเป็น 6 ส่วน ดังนี้ ส่วนที่ 1 แบบสอบถามด้านปัจจัยคุณลักษณะประชากร ประกอบด้วย เพศ อายุ สถานภาพ สถานศึกษา ระดับชั้นปี เกรดเฉลี่ยภาคเรียนครั้งล่าสุด สถานภาพสมรสของบิดา มารดา ปัจจุบันนักศึกษาอาศัยอยู่กับ ขณะที่เรียนอยู่นี้นักศึกษาพักที่ นักศึกษาใช้เวลาโดยเฉลี่ยในการเล่นอินเตอร์เน็ตประมาณวันละ ลักษณะคำถามเป็นแบบ สำรวจรายการ (CHEEK LIST) จำนวน 10 ข้อ ส่วนที่ 2 แบบสอบถามเกี่ยวกับการเห็นคุณค่าในตนเอง ประกอบด้วยข้อถามจำนวน 10 ข้อ มีข้อความทางบวก 5 ข้อ คือ 1, 2, 4, 6 และ 7 และข้อความทางลบ 5 ข้อ คือ 3, 5, 8, 9, และ 10 แบบสอบถามนี้ สุภิศา จิตต์สม (2564) ได้นำไปใช้ในการศึกษาการเห็นคุณค่าในตนเองของนักศึกษา มีค่าความเชื่อมั่นเท่ากับ 0.76 ลักษณะข้อคำถามเป็นมาตรส่วนประมาณค่า (LIKERT SCALES) ส่วนที่ 3 แบบสอบถามเกี่ยวกับพฤติกรรมการเป็นสมาชิกที่ดีในการทำงานกลุ่ม ของนักศึกษามหาวิทยาลัยของรัฐ ในจังหวัดภูเก็ต ซึ่งวัดระดับความคิดเห็นเกี่ยวกับพฤติกรรมการเป็นสมาชิกที่ดีในการทำงานกลุ่ม พิชชาภา บุญณสะ (2563) มีค่าความเชื่อมั่นเท่ากับ 1 จำนวน 10 ข้อ ซึ่งข้อคำถามแต่ละข้อได้ถูกกำหนดเกณฑ์การให้คะแนนไว้ 5 ระดับ ส่วนที่ 4 แบบสอบถามเกี่ยวกับสัมพันธภาพระหว่างนักศึกษากับเพื่อน งานวิจัยนี้วัดโดยใช้แบบสอบถามสัมพันธภาพระหว่างนักศึกษากับเพื่อนของ สุภิศา จิตต์สม (2564) ซึ่งพัฒนามาจากแบบสอบถามสัมพันธภาพระหว่างนักศึกษากับเพื่อนในนักศึกษา ในงานวิจัยของ ธิดา ฐิติพานิชยางกูร (2550) ได้ค่าความเชื่อมั่นเท่ากับ 0.91 และ สุภิศา จิตต์สม (2564) ได้มีการนำแบบสอบถามนี้ไปใช้ เพื่อศึกษาความสัมพันธ์ระหว่างปัจจัย ได้แก่ สัมพันธภาพในครอบครัว การอบรมเลี้ยงดูแบบมีเหตุผลบรรยายกาศการเรียนการสอน สัมพันธภาพระหว่างนักศึกษากับเพื่อนที่ส่งผลต่อความมั่นคงทางอารมณ์และความสามารถในการเผชิญปัญหาและฟันฝ่าอุปสรรคของนักศึกษา ได้ค่าความเชื่อมั่นเท่ากับ 0.92 แบบสอบถามนี้ประกอบด้วยข้อถามจำนวน 15 ข้อ ลักษณะข้อคำถามเป็นแบบมาตรวัดประมาณค่า (RATING SCALE) 5 ระดับ ได้แก่ จริงมากที่สุด ค่อนข้างจริง ปานกลาง ไม่ค่อยจริง ไม่จริงมากที่สุด ส่วนที่ 5 แบบสอบถามเกี่ยวกับสัมพันธภาพระหว่างนักศึกษากับผู้ปกครอง งานวิจัยนี้จะวัดโดยใช้แบบสอบถามสัมพันธภาพระหว่างนักเรียนกับผู้ปกครองของ สุภิศา จิตต์สม (2564) ซึ่งดัดแปลงมาจากแบบสอบถามระหว่างนักเรียนกับผู้ปกครองในนักเรียนระดับประกาศนียบัตรวิชาชีพการศึกษาของ ศิริวรรณ สุวินท์ (2548) มีค่าความเชื่อมั่นเท่ากับ 0.85 ประกอบด้วยข้อคำถามจำนวน 15 ข้อ เป็นข้อคำถามแบบมาตรวัดประมาณค่า (Likert scales) 5 ระดับ ได้แก่ จริงที่สุด จริง จริงบ้าง จริงน้อย จริงน้อยที่สุด ส่วนที่ 6 แบบสอบถามเกี่ยวกับการถูกกลั่นแกล้งจากเพื่อนในการทำงานกลุ่ม ของนักศึกษามหาวิทยาลัยของรัฐ ในจังหวัดภูเก็ต ซึ่งวัดระดับความคิดเห็นในเรื่องของการที่นักศึกษาได้รับการถูกกลั่นแกล้งจากเพื่อนในการทำงานกลุ่ม ถูกพัฒนาขึ้นโดย พิชชาภา บุญณสะ (2563) มีค่าความเชื่อมั่นเท่ากับ 1.00 จำนวน 14 ข้อ ซึ่งเป็นคำถามที่วัดทัศนคติในลักษณะมาตราส่วนประมาณค่าเป็นข้อคำถามแบบมาตรวัดประมาณค่า (Likert scales) ด้วยการใช้มาตราส่วนกำหนดระดับ (Rating Scale) ซึ่งข้อคำถามแต่ละข้อ ได้ถูกกำหนดเกณฑ์การให้คะแนนไว้ 5 ระดับ ได้แก่ ทุกวัน ทุกสัปดาห์ ทุกเดือน บางครั้ง ไม่เคยเลย โดยมีการตรวจสอบความเชื่อมั่น (Reliability) ของแบบสอบถาม โดยผู้วิจัยนำแบบสอบถามที่เก็บข้อมูลจากกลุ่มนักศึกษามหาวิทยาลัยของรัฐที่มีคุณลักษณะตามเกณฑ์คัดเข้าเช่นเดียวกับกลุ่มตัวอย่าง จำนวน 30 คน เพื่อนำมาวิเคราะห์หาความเชื่อมั่น (Reliability) โดยวิเคราะห์ค่าสัมประสิทธิอัลฟาครอนบาคซ์ Cronbach's Alpha ของแบบสอบถามการเห็นคุณค่าในตนเอง พฤติกรรมการเป็นสมาชิกที่ดีในการทำงานกลุ่ม ความสัมพันธภาพระหว่างนักศึกษากับเพื่อน ความสัมพันธภาพระหว่างนักศึกษากับผู้ปกครอง และการถูกกลั่นแกล้งจากเพื่อนในการทำงานกลุ่ม ซึ่งควรมีค่าความเชื่อมั่นที่ยอมรับได้สูงกว่า 0.60 (Nunnally, 1978) จึงเป็นค่าที่ยอมรับได้ว่าแบบสอบถามชุดนี้มีความน่าเชื่อถือ พบว่า มีค่าความเชื่อมัน 0.682 0.698 0.711 0.646 และ 0.857 ตามลำดับ ผู้วิจัยดำเนินการตรวจสอบความถูกต้อง และความครบถ้วนของข้อมูล หลังจากนั้นวิเคราะห์ข้อมูลด้วยโปรแกรมคอมพิวเตอร์สำเร็จรูปดังนี้ 1. วิเคราะห์ด้วยสถิติเชิงพรรณนา (Descriptive Statistics) เพื่อใช้ในการสรุปบรรยายโดยการนำเสนอการแจกแจงความถี่ (Frequencies Distribution) ค่าร้อยละ (Percentage) ค่าเฉลี่ยเลขคณิต (Mean) และส่วนเบี่ยงเบนมาตรฐาน

(Standard Deviation) ข้อมูลคุณลักษณะประชากร ระดับการเห็นคุณค่าในตนเอง ระดับพฤติกรรมการเป็นสมาชิกที่ดีในการทำงานกลุ่ม ระดับความสัมพันธภาพระหว่างนักศึกษากับเพื่อน ระดับความสัมพันธภาพระหว่างนักศึกษากับผู้ปกครอง และระดับการถูกกลั่นแกล้งจากเพื่อนในการทำงานกลุ่ม 2. วิเคราะห์ด้วยสถิติเชิงอนุมาน (Inferential Statistics) เพื่อทดสอบสมมุติฐานด้วยการวิเคราะห์ สัมประสิทธิสหสัมพันธ์พหุคูณ (Multiple regression statistic) ด้วยวิธี Enter regression

ผลการทดลอง

การวิจัยนี้ศึกษาเรื่องปัจจัยที่มีอิทธิพลต่อการถูกกลั่นแกล้งในนักศึกษามหาวิทยาลัยของรัฐ จังหวัดภูเก็ต เก็บข้อมูลจากกลุ่มตัวอย่างจำนวน 405 คน และนำเสนอผลการวิเคราะห์ข้อมูล 1. ข้อมูลทั่วไปของนักศึกษามหาวิทยาลัยของรัฐ จังหวัดภูเก็ต พบว่านักศึกษามหาวิทยาลัยของรัฐจังหวัดภูเก็ตส่วนใหญ่เป็นเพศหญิง จำนวน 252 คน คิดเป็นร้อยละ 62.22 และเพศชายมีจำนวน 153 คน คิดเป็นร้อยละ 37.78 ($\bar{x}$ = 1.62 S.D. = 0.49) มีช่วงอายุส่วนใหญ่ 18-20 ปี จำนวน 215 คน คิดเป็นร้อยละ 53.09 รองลงมา 21-23 ปี คิดเป็นร้อยละ 45.93 ($\bar{x}$ = 20.55 S.D. = 1.31) สถานภาพโสดมากที่สุด จำนวน 368 คน คิดเป็นร้อยละ 90.86 รองลงมา สถานภาพสมรส จำนวน 37 คน คิดเป็นร้อยละ 9.14 ($\bar{x}$ = 1.09 S.D. = 0.29) นักศึกษามหาวิยาลัยราชภัฏภูเก็ตมากที่สุด จำนวน 339 คน คิดเป็นร้อยละ 83.70 รองลงมา มหาวิทยาลัยสงขลานครินทร์ วิทยาเขตภูเก็ต จำนวน 66 คน คิดเป็นร้อยละ 16.30 ($\bar{x}$ = 1.16 S.D. = 0.37) เป็นนักศึกษาชั้นปีที่ 2 และ 3 มากที่สุดจำนวนชั้นปีละ 104 คน คิดเป็นร้อยละ 25.68 ($\bar{x}$ = 2.55 S.D. = 1.18) มีเกรดเฉลี่ยอยู่ในช่วง 3.00-4.00 มากที่สุด จำนวน 259 คน คิดเป็นร้อยละ 63.95 รองลงมาเกรดเฉลี่ยอยู่ในช่วง 2.00-2.99 จำนวน 146 คน คิดเป็นร้อยละ 36.05 ($\bar{x}$ = 3.13 S.D. = 0.31) นักศึกษาใช้เวลาโดยเฉลี่ยในการเล่นอินเตอร์เน็ตต่อวันอยู่ในช่วง 6-10 ชั่วโมง มากที่สุดจำนวน 324 คน คิดเป็นร้อยละ 80 รองลงมาอยู่ในช่วง 11-15 ชั่วโมง จำนวน 63 คน คิดเป็นร้อยละ 15.56 ($\bar{x}$ = 8.87 S.D. = 2.21) สถานภาพสมรสบิดามารดาของศึกษาส่วนใหญ่สมรสอยู่ด้วยกัน จำนวน 348 คน คิดเป็นร้อยละ 85.93 รองลงมาหย่าร้าง จำนวน 23 คน คิดเป็นร้อยละ 5.68 ($\bar{x}$ = 1.36 S.D. = 1.03) นักศึกษาอาศัยอยู่กับบิดามารดามากที่สุด จำนวน 340 คน คิดเป็นร้อยละ 83.95 รองลงมานักศึกษาอาศัยอยู่กับบิดาจริงและมารดาเลี้ยง จำนวน 25 คน คิดเป็นร้อยละ 6.17 ($\bar{x}$ = 1.37 S.D. = 0.98) ขณะที่นักศึกษาเรียนอยู่ส่วนใหญ่เป็นหอพัก จำนวน 359 คน คิดเป็นร้อยละ 88.64 รองลงมาบ้านของบิดามารดา จำนวน 46 คน คิดเป็นร้อยละ 11.36 ($\bar{x}$ = 1.11 S.D. = 0.32)

การเห็นคุณค่าในตนเอง

เมื่อพิจารณาเป็นรายข้อ พบว่า การเห็นคุณค่าในตนเองของนักศึกษามหาวิทยาลัยของรัฐ จังหวัดภูเก็ตที่มีค่าเฉลี่ยมากที่สุด คือ ท่านรู้สึกว่าท่านเป็นคนที่มีคุณค่าอย่างน้อยก็ทัดเทียมกับคนอื่นๆ ($\bar{\boldsymbol{x}}$ = 3.99 , S.D. = 0.86) ส่วนการเห็นคุณค่าในตนเองที่มีคะแนนเฉลี่ยน้อยที่สุด คือ บางครั้งท่านรู้สึกว่าท่านไม่มีอะไรดีเลย ($\bar{\boldsymbol{x}}$ = 3.20 , S.D. = 0.99)

ตารางที่ 1. จำนวน ร้อยละ ค่าเฉลี่ย และส่วนเบี่ยงเบนมาตรฐานของการเห็นคุณค่าในตนเองของกลุ่มตัวอย่างจำแนกตามระดับการเห็นคุณค่าในตนเอง

ระดับการเห็นคุณค่าในตนเอง	จำนวน (คน)	ร้อยละ	$\bar{\boldsymbol{x}}$	S.D.
การเห็นคุณค่าในตนเองระดับสูง	123	30.37		
การเห็นคุณค่าในตนเองระดับปานกลาง	278	68.64	3.20	0.89
การเห็นคุณค่าในตนเองระดับต่ำ	4	0.99		
รวม	405	100		

จากตารางที่ 1. พบว่าส่วนใหญ่มีการเห็นคุณค่าในตนเองอยู่ในระดับปานกลางจำนวน 278 คน คิดเป็นร้อยละ 68.64 รองลงมา คือ ระดับสูงจำนวน 123 คน คิดเป็นร้อยละ 30.37 และระดับต่ำ 4 คน คิดเป็นร้อยละ 0.99 ($\bar{\boldsymbol{x}}$ = 3.20 , S.D. = 0.89) ตามลำดับ

2. พฤติกรรมการเป็นสมาชิกที่ดีในการทำงานกลุ่ม

เมื่อพิจารณาเป็นรายข้อ พบว่า พฤติกรรมการเป็นสมาชิกที่ดีในการทำงานกลุ่ม ของนักศึกษามหาวิทยาลัยของรัฐ จังหวัดภูเก็ตที่มีค่าเฉลี่ยมากที่สุด คือ ท่านสละเวลาส่วนตัวในการพบปะเพื่อน ($\bar{\boldsymbol{x}}$ = 3.87 , S.D. = 0.83) ส่วนพฤติกรรมการเป็นสมาชิกที่ดีในการทำงานกลุ่ม ที่มีคะแนนเฉลี่ยน้อยที่สุด คือ ท่านไม่พักทานขนม ของว่างหรืองดอาหาร เพื่อทำงานกลุ่มให้เสร็จ($\bar{\boldsymbol{x}}$ = 3.24 , S.D. = 0.85)

ตารางที่ 2. จำนวน ร้อยละ ค่าเฉลี่ย และส่วนเบี่ยงเบนมาตรฐานของพฤติกรรมการเป็นสมาชิกที่ดีในการทำงานกลุ่ม

ระดับพฤติกรรม	จำนวน (คน)	ร้อยละ	$\bar{\boldsymbol{x}}$	S.D.
พฤติกรรมการเป็นสมาชิกที่ดีในการทำงานกลุ่มระดับสูง	146	36.05		
พฤติกรรมการเป็นสมาชิกที่ดีในการทำงานกลุ่มระดับปานกลาง	257	63.46		
พฤติกรรมการเป็นสมาชิกที่ดีในการทำงานกลุ่มระดับต่ำ	2	0.49		
รวม	405	100	3.55	0.81

จากตารางที่ 2. พบว่าส่วนใหญ่มีพฤติกรรมการเป็นสมาชิกที่ดีในการทำงานกลุ่มอยู่ในระดับปานกลางจำนวน 257 คน คิดเป็นร้อยละ 63.46 รองลงมา คือ ระดับสูงจำนวน 146 คน คิดเป็นร้อยละ 36.05 และระดับต่ำ 2 คน คิดเป็นร้อยละ 0.49 ($\bar{x}$ = 3.55 , S.D. = 0.81) ตามลำดับ

3. สัมพันธภาพระหว่างนักศึกษากับเพื่อน

เมื่อพิจารณาเป็นรายข้อ พบว่า สัมพันธภาพระหว่างนักศึกษากับเพื่อน ของนักศึกษามหาวิทยาลัยของรัฐ จังหวัดภูเก็ตที่มีค่าเฉลี่ยมากที่สุด คือ ท่านมีเพื่อนที่สามารถปรึกษาปัญหาได้ทุกเรื่อง ($\bar{x}$ = 3.91 , S.D. = 0.90) ส่วนสัมพันธภาพระหว่างนักศึกษากับเพื่อน ที่มีคะแนนเฉลี่ยน้อยที่สุด คือ เมื่อท่านเดือดร้อนเรื่องเงิน เพื่อนสามารถช่วยเหลือท่านได้ ($\bar{x}$ = 3.45 , S.D. = 0.82)

ตารางที่ 3. จำนวน ร้อยละ ค่าเฉลี่ย และส่วนเบี่ยงเบนมาตรฐานสัมพันธภาพระหว่างนักศึกษากับเพื่อน

ระดับสัมพันธภาพระหว่างนักศึกษากับเพื่อน	จำนวน (คน)	ร้อยละ	$\bar{x}$	S.D.
สัมพันธภาพระหว่างนักศึกษากับเพื่อน ระดับสูง	135	33.33		
สัมพันธภาพระหว่างนักศึกษากับเพื่อนระดับปานกลาง	265	65.44	3.55	0.85
สัมพันธภาพระหว่างนักศึกษากับเพื่อนระดับต่ำ	5	1.23		
รวม	**405**	**100**		

จากตารางที่ 3. พบว่าส่วนใหญ่มีสัมพันธภาพระหว่างนักศึกษากับเพื่อน อยู่ในระดับปานกลางจำนวน 265 คน คิดเป็นร้อยละ 64.44 รองลงมา คือ ระดับสูงจำนวน 135 คน คิดเป็นร้อยละ 33.33 และระดับต่ำ 5 คน คิดเป็นร้อยละ 1.23 ($\bar{x}$ = 3.55 , S.D. = 0.85) ตามลำดับ

4. สัมพันธภาพระหว่างนักศึกษากับผู้ปกครอง

เมื่อพิจารณาสัมพันธภาพระหว่างนักศึกษากับผู้ปกครองของนักศึกษามหาวิทยาลัยของรัฐ จังหวัดภูเก็ต พบว่าด้านการปฏิบัติตนของนักศึกษาต่อผู้ปกครอง เป็นรายข้อที่มีค่าเฉลี่ยมากที่สุด คือ ท่านปฏิบัติตามกฎระเบียบของผู้ปกครอง ($\bar{x}$ = 3.95 , S.D. = 0.86) ส่วนด้านการปฏิบัติตนของนักศึกษาต่อผู้ปกครองที่มีค่าเฉลี่ยมากที่สุด คือ ท่านไม่สามารถพูดคุยกับผู้ปกครอง เพื่อปรึกษาปัญหาต่างๆ ($\bar{x}$ = 3.01 , S.D. = 1.05) และด้านการปฏิบัติตนของผู้ปกครองต่อนักศึกษาเป็นรายข้อที่มีค่าเฉลี่ยมากที่สุด คือ ผู้ปกครองสอบถามเรื่องการเรียนของท่านอยู่เสมอ ($\bar{x}$ = 3.93 , S.D. = 0.90) ส่วนด้านการปฏิบัติตนของผู้ปกครองต่อนักศึกษา ที่มีคะแนนเฉลี่ยน้อยที่สุด คือ เมื่อท่านทำผิด ผู้ปกครองดุด่าโดยไม่ถามสาเหตุ ($\bar{x}$ = 2.76 , S.D. = 1.16)

ตารางที่ 4.9 จำนวน ร้อยละ ค่าเฉลี่ย และส่วนเบี่ยงเบนมาตรฐานสัมพันธภาพระหว่างนักศึกษากับผู้ปกครอง

ระดับสัมพันธภาพระหว่างนักศึกษากับผู้ปกครอง	จำนวน (คน)	ร้อยละ	$\bar{x}$	S.D.
สัมพันธภาพระหว่างนักศึกษากับผู้ปกครองระดับสูง	100	24.69		
สัมพันธภาพระหว่างนักศึกษากับผู้ปกครองระดับปานกลาง	290	71.60	3.19	0.93
สัมพันธภาพระหว่างนักศึกษากับผู้ปกครองระดับต่ำ	15	3.71		
รวม	**405**	**100**		

จากตารางที่ 4. พบว่าส่วนใหญ่มีสัมพันธภาพระหว่างนักศึกษากับผู้ปกครอง อยู่ในระดับปานกลางจำนวน 290 คน คิดเป็นร้อยละ 71.60 รองลงมา คือ ระดับสูงจำนวน 100 คน คิดเป็นร้อยละ 24.69 และระดับต่ำ 15 คน คิดเป็นร้อยละ 3.71 ($\bar{x}$ = 3.19 , S.D. = 0.93) ตามลำดับ

5. การถูกกลั่นแกล้งจากเพื่อนในการทำงานกลุ่ม

เมื่อพิจารณาเป็นรายข้อ พบว่า การถูกกลั่นแกล้งจากเพื่อนในการทำงานกลุ่มนักศึกษามหาวิทยาลัยของรัฐ จังหวัดภูเก็ต ที่มีค่าเฉลี่ยมากที่สุด คือ ท่านได้รับข้อมูลที่ไม่เพียงพอ ทำให้ส่งผลกระทบต่อผลการทำงานกลุ่ม ($\bar{x}$ = 3.25 , S.D. = 1.11) ส่วนการถูกกลั่นแกล้งจากเพื่อนในการทำงานกลุ่มที่มีคะแนนเฉลี่ยน้อยที่สุด คือ ท่านถูกคุกคาม ถูกทำร้ายร่างกาย ($\bar{x}$ = 2.25 , S.D. = 1.28)

ตารางที่ 5. จำนวน ร้อยละ ค่าเฉลี่ย และส่วนเบี่ยงเบนมาตรฐานการถูกกลั่นแกล้งจากเพื่อนในการทำงานกลุ่ม

ระดับสัมพันธภาพระหว่างนักศึกษากับผู้ปกครอง	จำนวน (คน)	ร้อยละ	$\bar{x}$	S.D.
การถูกกลั่นแกล้งจากเพื่อนในการทำงานกลุ่มระดับสูง	62	15.31		
การถูกกลั่นแกล้งจากเพื่อนในการทำงานกลุ่มระดับปานกลาง	178	43.95		
การถูกกลั่นแกล้งจากเพื่อนในการทำงานกลุ่มระดับต่ำ	165	40.74	2.68	1.18
รวม	**405**	**100**		

จากตารางที่ 5. พบว่าส่วนใหญ่มีการถูกกลั่นแกล้งจากเพื่อนในการทำงานกลุ่ม อยู่ในระดับปานกลางจำนวน 178 คน คิดเป็นร้อยละ 43.95 รองลงมา คือ ระดับต่ำจำนวน 165 คน คิดเป็นร้อยละ 40.74 และระดับสูง 62 คน คิดเป็นร้อยละ 15.31 ($\bar{x}$ = 2.68 , S.D. = 1.18) ตามลำดับ

ตารางที่ 6. เมตริกซ์สหสัมพันธ์ของปัจจัยทำนาย ปัจจัยที่มีอิทธิพลต่อการถูกกลั่นแกล้งในนักศึกษามหาวิทยาลัยของรัฐ จังหวัดภูเก็ต (n = 405)

ตัวแปร	x_1	x_2	x_3	x_4	x_5	x_6	x_7	x_8	x_9	x_{10}	x_{11}	x_{12}	x_{13}	x_{14}	x_{15}
เพศ (x_1)	1														
อายุ (x_2)	-.060	1													
สถานภาพสมรส (x_3)	.212**	.051	1												
สถานศึกษา (x_4)	-.015	-.097	-.024	1											
ระดับชั้นปี (x_5)	-.011	.920**	.035	-.102*	1										
เกรดเฉลี่ย (x_6)	-.109*	-.067	.040	.031	-.070	1									
สถานภาพสมรสของบิดา มารดา (x_7)	.042	.025	-.020	-.091	.040	-.092	1								
ปัจจุบันท่านอาศัยอยู่กับ (x_8)	.136**	-.047	-.051	.030	-.007	-.013	.685**	1							
ขณะที่เรียนอยู่นี้ท่านพักที่ (x_9)	-.026	.017	-.005	.053	.026	.001	.025	-.041	1						
ท่านใช้เวลา โดยเฉลี่ยในการเล่นอินเตอร์เน็ต (x_{10})	-.017	.161**	.034	-.078	.193**	-.007	.067	.161**	.116*	1					
การเห็นคุณค่าในตนเอง (x_{11})	-.049	.113*	-.045	-.269**	.140**	-.025	.104*	.058	-.052	.148**	1				
พฤติกรรมการเป็นสมาชิกที่ดีในการทำงานกลุ่ม (x_{12})	.116*	.060	-.003	-.253**	.100*	.133**	.155**	.170**	-.008	.087	.557**	1			
สัมพันธภาพระหว่างนักศึกษากับเพื่อน (x_{13})	.071	.103*	.020	-.273**	.123*	.112*	.189**	.169**	-.028	.067	.466**	.745**	1		
สัมพันธภาพระหว่างนักศึกษากับผู้ปกครอง (x_{14})	-.029	.082	.011	-.333**	.076	.059	.191**	.148**	-.039	.172**	.598**	.600**	.633**	1	
การถูกกลั่นแกล้งจากเพื่อนในการทำงานกลุ่ม (x_{15})	-.164**	.190**	-.013	-.069	.170**	-.152**	.050	-.001	-.011	.156**	.416**	.139**	.086	.456**	1

*p<.05 **p<.001

จากตารางที่ 6. จากการวิเคราะห์ความสัมพันธ์ระหว่างตัวแปรพบว่าปัจจัยที่มีอิทธิพลต่อการถูกกลั่นแกล้งในนักศึกษามหาวิทยาลัยของรัฐ จังหวัดภูเก็ต ได้แก่ ปัจจัยสัมพันธภาพระหว่างนักศึกษากับผู้ปกครอง มีความสัมพันธ์ทางบวกกับการถูกกลั่นแกล้งจากเพื่อนในการทำงานกลุ่ม มากที่สุดอย่างมีนัยสำคัญทางสถิติ (r = .456, p <.001) รองลงมาคือ การเห็นคุณค่าในตนเอง อายุ ระดับชั้นปี ท่านใช้เวลา โดยเฉลี่ยในการเล่นอินเตอร์เน็ต พฤติกรรมการเป็นสมาชิกที่ดีในการทำงานกลุ่ม มีความสัมพันธ์ทางบวกกับการถูกกลั่นแกล้งจากเพื่อนในการทำงานกลุ่ม อย่างมีนัยสำคัญทางสถิติ (r = .416, .190, .170, .156 และ .139 p <.001) ตามลำดับ และปัจจัยเพศมีความสัมพันธ์ทางลบกับการถูกกลั่นแกล้งจากเพื่อนในการทำงานกลุ่ม มากที่สุด อย่างมีนัยสำคัญทางสถิติ (r = -.164, p = <.001) รองลงมาคือ เกรดเฉลี่ยมีความสัมพันธ์ทางลบกับการถูกกลั่นแกล้งจากเพื่อนในการทำงานกลุ่ม อย่างมีนัยสำคัญทางสถิติ (r = -.152, p <.001)

ตารางที่ 7 การวิเคราะห์ถดถอยพหุคูณเชิงเส้นตรงของปัจจัยที่มีอิทธิพลต่อการถูกกลั่นแกล้งในนักศึกษา

ตัวแปร	b	S.E.	β	t	p - value
Constant	-1.312	1.481		-.886	.376
เพศ (x_1)	-.158	.083	-.080	-1.897	.059
อายุ (x_2)	.100	.075	.138	1.329	.185
สถานภาพสมรส (x_3)	0.43	1.36	.013	.321	.749
สถานศึกษา (x_4)	.277	.111	.108	2.495	.013
ระดับชั้นปี (x_5)	.002	.084	.002	.023	.982
เกรดเฉลี่ย (x_6)	-.364	.125	-.120	-2.922	.004
สถานภาพสมรสของบิดา มารดา(x_7)	-.001	.052	-.001	-.024	.981
ปัจจุบันท่านอาศัยอยู่กับ (x_8)	-.026	.056	-.026	-.458	.647
ขณะที่เรียนอยู่นี้ท่านพักที่ (x_9)	.004	.121	.001	.030	.976
ท่านใช้เวลา โดยเฉลี่ยในการเล่นอินเตอร์เน็ต (x_{10})	.015	.018	.034	.802	.423
การเห็นคุณค่าในตนเอง (x_{11})	.492	.099	.266	4.979	<.001
พฤติกรรมการเป็นสมาชิกที่ดีในการทำงานกลุ่ม (x_{12})	-.139	.118	-.077	-1.171	.242
สัมพันธภาพระหว่างนักศึกษากับเพื่อน (x_{13})	-.486	.105	-.298	-4.640	<.001
สัมพันธภาพระหว่างนักศึกษากับผู้ปกครอง (x_{14})	.992	.106	.559	9.377	<.001

R = .621 R^2= .385 R^2 adj = .363 F = 17.51 Prob.>F=.000

b= unstandardized beta coefficient β= unstandardized

จากผลการวิจัยสามารถเขียนสมการพยากรณ์ปัจจัยที่มีอิทธิพลต่อการถูกกลั่นแกล้งในนักศึกษามหาวิทยาลัยของรัฐ จังหวัดภูเก็ต ดังนี้

สมการพยากรณ์ในรูปแบบคะแนนดิบ Y = -1.312 + .277 (x_4) - .364 (x_6) + .492 (x_{11}) - .486 (x_{13}) + .992 (x_{14})

สมการพยากรณ์ในรูปคะแนนมาตรฐาน Z = .108 (x_4) – .120 (x_6) +.266 (x_{11}) -.298 (x_{13}) + .559 (x_{14})

อภิปรายผล

จากการวิจัยครั้งนี้พบว่าปัจจัยคัดสรรที่ศึกษาสามารถร่วมกันทำนายการถูกกลั่นแกล้งจากเพื่อนในการทำงานกลุ่มของนักศึกษามหาวิทยาลัยของรัฐ จังหวัดภูเก็ต ได้ร้อยละ 3.85 โดยตัวแปรที่สามารถทำนายได้ คือ สถานศึกษา เกรดเฉลี่ย การเห็นคุณค่าในตนเอง สัมพันธภาพระหว่างนักศึกษากับเพื่อน และ สัมพันธภาพระหว่างนักศึกษากับผู้ปกครอง โดยนักศึกษาที่มีสัมพันธภาพกับผู้ปกครองที่ดี จะถูกการกลั่นแกล้งจากเพื่อนในการทำงานกลุ่มน้อยกว่า นักศึกษาที่มีสัมพันธภาพกับผู้ปกครองที่ไม่ดี ซึ่งสอดคล้องกับ สุภิศา จิตต์สม (2564) กล่าวไว้ว่าสัมพันธภาพระหว่างนักศึกษากับผู้ปกครอง (Interpersonal relationship between students and their parents) เป็นการปฏิบัติพฤติกรรมต่างๆต่อกันของนักศึกษากับผู้ปกครอง และการปฏิบัติตนของผู้ปกครองที่มีต่อนักศึกษา เพื่อให้เกิดความสัมพันธ์ที่ดีต่อกัน ได้แก่ การให้ความเคารพ การเชื่อฟังคำสั่งสอน การประพฤติตนของนักเรียนอยู่ในกฎระเบียบของผู้ปกครอง การให้ความรัก ความอบอุ่น การให้กำลังใจซึ่งกันและกัน เพื่อกระตุ้นให้นักเรียน นักศึกษาประสบความสำเร็จทางการเรียนหรือเพื่อการพัฒนาทางด้านความคิด และสอดคล้องกับ กวินารัตน์ สุทธิสุคนธ์ (2560) อธิบายไว้ว่าสมาชิกทุกคนในครอบครัวต้องแสดงความรักความเคารพนับถือซึ่งกันและกัน ร่วมกันทำกิจกรรมสร้างสรรค์ หารือ ตัดสินใจเรื่องสำคัญๆ และครอบครัวจะต้องอยู่ร่วมกันอย่างสันติและการศึกษาความสัมพันธ์ในครอบครัวอยู่ในระดับปานกลาง การสื่อสารมีความสัมพันธ์เชิงบวกกับคุณภาพชีวิตในขณะที่บทบาทหน้าที่ไม่ใช่ความสัมพันธ์กับคุณภาพชีวิต ความสัมพันธ์ในครอบครัวเกี่ยวกับความสัมพันธ์ ความรัก และความสามัคคีในระดับปานกลาง แต่ควรติดตามอย่างใกล้ชิด เนื่องจากแนวโน้มยังคงลดลงและตามดัชนีสุขภาพครอบครัวในปี 2552 ครอบครัวไทยจำนวนมากจะละเลยการปฏิบัติที่ดีที่ช่วยสร้างความสัมพันธ์ที่ดีให้เกิดขึ้นในครอบครัว จะเห็นได้ว่าความสัมพันธ์ในครอบครัวมีความสำคัญมากต่อชีวิตของแต่ละครอบครัวให้มีความสุขและการช่วยเหลือกันในครอบครัวจึงเป็นพื้นฐานของการอยู่ร่วมกันในสังคมอีกด้วย อีกทั้งสอดคล้องกับ ภัททชฎา คำพวง (2559) การที่ครอบครัวเอาใจใส่และแสดงออกให้รู้ว่า “รัก” ผ่านพฤติกรรมต่าง ๆ เช่น การกอด การจูบหัว หรือการกล่าวด้วยวาจา และครอบครัวได้รับฟังและแนะนำ แนวทางแก้ปัญหาให้กับนักเรียน นักศึกษาทุกครั้งที่เผชิญสถานการณ์ที่เป็นปัญหา การอบรมเลี้ยงดูเหล่านี้พบว่า หากครอบครัวมีความเอาใจใส่เลี้ยงดูให้ความรักและให้ความอบอุ่น มีอิทธิพลต่อการตัดสินใจไม่ตอบโต้จากการถูกรังแกบนพื้นที่ไซเบอร์

สัมพันธภาพระหว่างนักศึกษากับเพื่อนปัจจัยที่สามารถร่วมกันทำนายการถูกกลั่นแกล้งจากเพื่อนในการทำงานกลุ่มของนักศึกษามหาวิทยาลัยของรัฐ จังหวัดภูเก็ต โดยนักศึกษาที่มีสัมพันธภาพกับเพื่อนที่ดี จะถูกการกลั่นแกล้งจากเพื่อนในการทำงานกลุ่มน้อยกว่า นักศึกษาที่มีสัมพันธภาพกับเพื่อนที่ไม่ดี ซึ่งสอดคล้องกับ

ทนง หลักคำ (2554) ระดับอุดมศึกษาทั่วทุกแห่งจัดเป็นผู้นำหรือตัวกระตุ้นเกี่ยวกับพฤติกรรมการกลั่นแกล้งในมหาวิทยาลัย เมื่อความเป็นผู้นำปล่อยให้การกลั่นแกล้งเจริญรุ่งเรือง เมื่อนักศึกษามีการทำงานกลุ่มร่วมกันเป็นเวลานานๆ ก็จะเกิดการจัดกลุ่มใหม่จากการมีปฏิสัมพันธ์ที่ไม่เป็นมิตร เนื่องจากการกลั่นแกล้งจะเกิดขึ้น เมื่อมีคนใดคนหนึ่งเก่งหรือด้วยจนเกินไป ก็จะเกิดการกลั่นแกล้ง นินทา หรือมีการแยกกลุ่มออก เป้าหมายจะมองไปที่ความเป็นผู้นำเพื่อบรรเทาความร้ายแรงหรือการเลวร้ายจากการถูกกลั่นแกล้งหลังจากเผชิญหน้ากับอีกฝ่ายหรือผู้ที่มาข่มเหงรังแก นอกจากนี้ คนที่เป็นผู้กระทำมักจะมาจากคนที่มีตำแหน่งของความเป็นผู้นำที่มีอำนาจในกลุ่มอย่างกว้างขวางผลการวิจัยมีการยืนยันว่าภาวะผู้นำสามารถกำหนดแนวทางในการปลูกฝังสภาพแวดล้อมที่ค้ำจุนหรือขจัดพฤติกรรมการกลั่นแกล้ง ด้วยการตัดออกจากกลุ่มหรือไม่คุยด้วยแค่ในช่วงระยะเวลาหนึ่ง การศึกษาในระดับอุดมศึกษาไม่สามารถจัดการเรื่องการแบ่งกลุ่มการแยกกลุ่มและการกลั่นแกล้งกันที่จะเกิดขึ้น และสอดคล้องกับ สุภิศา จิตต์สม, (2564) กล่าวไว้ว่าผลกระทบจากพฤติกรรมการกลั่นแกล้งจากเพื่อนด้านสังคม เป็นการถูกการกลั่นแกล้งมีผลกระทบทางด้านสังคมต่อเหยื่อในมิติของการสร้างสัมพันธภาพในด้านลบ ได้แก่ ผู้ที่ถูกกลั่นแกล้งโดนบีบให้อยู่คนเดียว ไม่มีใครต้องการคบหาหรือพูดคุย จนทำให้กลายเป็นคนที่กลัว ไม่กล้าเข้าสังคม ไม่กล้าคบเพื่อน ไม่กล้าพูดคุยกับใคร และอาจถึงขั้นไม่มีจุดยืนทางสังคม เนื่องจากถูกตัดสินจากข้อมูลที่บิดเบือนโดยผู้ที่กลั่นแกล้ง อีกทั้งสอดคล้องกับ ภัทรจรัส บำรุงพงษ์ และ อุนิษา เลิศโตมรสกุล (2562) ที่กล่าวว่าการนินทาหรือพูดให้เสียหายรูปแบบการกลั่นแกล้งที่พบเจอในมหาวิทยาลัยนั้น เป็นรูปแบบที่มักจะพบเห็นได้บ่อยที่สุดในสถานศึกษา ซึ่งการกลั่นแกล้งในรูปแบบดังกล่าวนี้ อาจไม่ใช่ความรุนแรงทางตรง แต่ก็สามารถส่งผลกระทบกับเหยื่อได้ไม่น้อย ไม่ว่าจะเป็นทั้งในด้านของจิตใจและการเข้าร่วมสังสม โดยพื้นที่ในการกลั่นแกล้งนั้น ไม่ได้จำกัดอยู่แต่ในห้องเรียนเท่านั้น แต่ยังรวมไปถึงสังคมภายนอกห้องเรียนในมหาวิทยาลัย อาทิเช่น การทำกิจกรรม การเข้าชมรม เป็นต้น เหล่านี้ก็สามารถพบเจอพฤติกรรมของการกลั่นแกล้ง ได้เช่นกัน ซึ่งการกลั่นแกล้งสามารถเกิดขึ้นได้ในทุกคน

การเห็นคุณค่าในตนเองเป็นปัจจัยที่สามารถร่วมกันทำนายการถูกกลั่นแกล้งจากเพื่อนในการทำงานกลุ่มของนักศึกษามหาวิทยาลัยของรัฐ จังหวัดภูเก็ต โดยนักศึกษาที่มีพฤติกรรมการเห็นคุณค่าในตนเองสูง จะมีการถูกกลั่นแกล้งจากเพื่อนในการทำงานกลุ่มน้อยกว่า นักศึกษาที่ไม่เห็นคุณค่าในตนเอง ซึ่งสอดคล้องกับ สุภิศา จิตต์สม (2564) ที่กล่าวว่าเป็นความคิด ความรู้สึกที่เกิดขึ้นภายในของแต่ละตัวบุคคลทั้งทางด้านบวกและทางด้านลบที่มีต่อตนเองและเพื่อนหรือคนรอบข้าง รวมถึงในการประเมินตนเองทั้งทางด้านบวกและด้านลบ และสอดคล้องกับ รัศมีแสง หนูแป้นทอง และคณะ (2561) ที่อธิบายว่าการเห็นคุณค่าและเชื่อมั่นในตนเอง คือ บุคคลที่มีลักษณะการเห็นคุณค่าในตนเอง โดยการเห็นคุณค่าในตนเองเกิดจากมุมมองที่มีต่อตนเองและความต้องการให้ตนเองเป็นอย่างไร หากความต้องการและมุมมองที่มีต่อตนเองสอดคล้องกันจะทำให้รู้สึกว่าตนเองมีคุณค่าและน่าภาคภูมิใจ แต่ถ้าความต้องการกับมุมมองไม่ไปด้วยกัน จะส่งผลให้บุคคลนั้นไม่รู้สึกถึงคุณค่าของตัวเอง ไม่ภาคภูมิใจในตนเอง อีกทั้งสอดคล้องกับ Stauss (2000) อธิบายว่าการเห็นคุณค่าในตนเองเป็นปัจจัยที่สำคัญต่อสุขภาพจิตและพัฒนาการของวัยรุ่นตอนกลาง ซึ่งจะมีความเกี่ยวเนื่องกันกับทั้งทางสุขภาพจิต ร่างกาย และผลกระทบทางสังคมที่ส่งผลต่อพัฒนาการของวัยรุ่นและการเปลี่ยนแปลงในการเข้าสู่วัยผู้ใหญ่ ได้แก่ ภาวะซึมเศร้า ความวิตกกังวล พฤติกรรมก้าวร้าวรุนแรง มีการใช้สารเสพติด การฆ่าตัวตาย และโรคการกิน ผิดปกติ

เกรดเฉลี่ยเป็นปัจจัยที่สามารถร่วมกันทำนายการถูกกลั่นแกล้งจากเพื่อนในการทำงานกลุ่มของนักศึกษามหาวิทยาลัยของรัฐ จังหวัดภูเก็ต โดยนักศึกษาที่มีเกรดเฉลี่ยน้อย จะมีการถูกกลั่นแกล้งจากเพื่อนในการทำงานกลุ่มน้อยกว่า นักศึกษาที่มีเกรดเฉลี่ยมาก ซึ่งไม่สอดคล้องกับ Slavin (1990, น.3) ที่กล่าวไว้ว่ากิจกรรมที่เน้นให้ผู้เรียนทำงานร่วมกันเป็นกลุ่มๆ กลุ่มละ 4-5 คน ผู้เรียนในกลุ่มจะต้องมีระดับผลการเรียนที่ต่างกัน การเรียนรู้จากการแลกเปลี่ยนความคิดเห็นร่วมกัน จะทำให้ผู้เรียนสามารถเรียนรู้แลกเปลี่ยนร่วมกัน และยังไม่สอดคล้องกับแนวคิดของ สุริยะ หาญพิชัย (2561) ที่เชื่อว่าถ้าผู้สอนใช้กิจกรรมการสอนที่ดีและเหมาะสมกับผู้เรียนก็ย่อมมีผลสัมฤทธิ์ทางการเรียนและจะบรรลุเป้าหมายทางการพัฒนาผู้เรียน วิธีการสอนในปัจจุบันนั้นมุ่งเน้นความสำคัญที่ตัวผู้เรียนโดยการเปิดโอกาสให้ผู้เรียนสามารถเลือกเรียนได้ตามความถนัดและความสนใจของตัวผู้เรียนเอง ส่งเสริมให้มีส่วนร่วมในทุกกระบวนการเรียนรู้ พัฒนาความสามารถในการแสวงหาความรู้ และการนำความรู้มาประยุกต์ใช้เพื่อพัฒนาศักยภาพของตนเองอย่างเต็มที่ รวมทั้งการปลูกฝังความมีคุณธรรม ค่านิยม และคุณ ลักษณะที่พึงประสงค์ โดยวิธีการจัดการเรียนรู้ที่จะช่วยให้ผู้เรียนเกิดการเรียนรู้และเกิดทักษะต่าง ๆ จากการเรียน อีกทั้งยังไม่สอดคล้องกับ สุภิศา จิตต์สม (2564) ได้กล่าวไว้ว่าบุคคลที่มีปัญหาผลการเรียนตกต่ำจากผลกระทบของการถูกกลั่นแกล้งจะส่งผลให้เกิดปัญหาต่างๆ ไม่ว่าจะเป็นปัญหาด้านการเรียน สุขภาพ และจิตใจ รวมถึงปัญหาทางพฤติกรรมต่างๆ ซึ่งไม่ว่าจะเป็นกลุ่มผู้รังแกผู้อื่น (Bully) กลุ่มผู้ถูกรังแก (Victim) หรือแม้แต่กลุ่มที่เป็นทั้งผู้รังแกผู้อื่นและผู้ถูกรังแก (Bully-victim) ล้วนแล้วแต่ได้รับผลกระทบจากพฤติกรรมรังแกกันทั้งสิ้น

สถานศึกษาเป็นปัจจัยที่สามารถร่วมกันทำนายการถูกกลั่นแกล้งจากเพื่อนในการทำงานกลุ่มของนักศึกษามหาวิทยาลัยของรัฐ จังหวัดภูเก็ต โดยนักศึกษามหาวิทยาลัยของรัฐ จังหวัดภูเก็ต ที่ศึกษาในมหาวิทยาลัยราชภัฏภูเก็ต จะมีการถูกกลั่นแกล้งจากเพื่อนในการทำงานกลุ่มน้อยกว่า นัก ศึกษาที่ศึกษาในมหาวิทยาลัยสงขลานครินทร์ วิทยาเขตภูเก็ต ซึ่งสอดคล้องกับผลการวิจัยของ กนกอร จันยมิตรี และกัญญ์ฐิตา ศรีภา (2020) พบว่าเด็กและเยาวชนที่โดนกลั่นแกล้งรังแกโดยเพื่อนในมหาวิทยาลัย ในสถานศึกษาต่างๆ แน่นอนว่าในสถานศึกษาทุกคนต่างมาจากแต่ละพื้นที่ ลักษณะนิสัย ความรู้ ทัศนคติต่างๆย่อมต่างกัน และเมื่อรวมตัวกันก็จะเกิดความคึกคะนอง นึกสนุก โดยที่ลืมคำนึงถึงเพื่อนผู้ที่ตกเป็นเหยื่อ ซึ่งผู้ที่ถูกกระทำหรือถูกกลั่นแกล้งนั้นอาจส่งผลร้ายแรงต่อจิตใจ สุขภาพ และการเรียนของเด็ก มากกว่าการถูกกลั่นแกล้ง และสอดคล้องกับ นันทิยา สวัสดิวิชัยโสภิต (2563) อธิบายไว้ว่าสังคมมหาวิทยาลัยหรือในชั้นเรียน ต้องมีการทำงานหรืออยู่ร่วมกันเป็นกลุ่ม ถึงแม้ว่าการกลั่นแกล้งจะไม่ใช่ในรูปแบบที่มีการปะทะโดยตรง หากแต่การกลั่นแกล้งทางวาจาหรือสังคมนั้นก็เป็นผลมาจากความแตกต่างของนักศึกษาบางรายที่มีความแตกต่างไปจากนิสิตนักศึกษาทั่วไปหรือไม่เป็นไปตามแนวทางแบบแผนของสังคม ทำให้คนในสังคมซึ่งในที่นี้หมายถึงนิสิต นักศึกษา อาจารย์ เจ้าหน้าที่ เกิดความรู้สึกปฏิเสธไม่ยอมรับ อีกทั้งสอดคล้องกับ ภัทรจรัส บำรุงพงษ์ และ อุนิษา เลิศโตมรสกุล (2019) ที่กล่าวไว้ว่าทุกโรงเรียนจะต้องมีการกำหนดนโยบายในการป้องกันการกลั่นแกล้ง รังแกทุกรูปแบบในกลุ่มนักเรียน โดยนโยบายซึ่งกำหนดขึ้นโดยทางโรงเรียนนั้น คุณครู นักเรียน รวมทั้งผู้ปกครองจะต้องรับทราบ และรับรู้อย่างทั่วถึง อีกทั้งยังหมายรวมถึงหน้าที่ของบุคลากรในสถานศึกษาในการป้องกันไม่ให้เกิดการแบ่งแยก การกลั่นแกล้งคุกคาม หรือการทำให้ผู้อื่นต้องตกเป็นเหยื่อภายในโรงเรียน

ข้อสรุป

การเห็นคุณค่าในตนเองของนักศึกษามหาวิทยาลัยของรัฐ จังหวัดภูเก็ต ที่มีค่าเฉลี่ยมากที่สุด คือ ท่านรู้สึกว่าท่านเป็นคนที่มีคุณค่าอย่างน้อยก็ทัดเทียมกับคนอื่นๆ ($\bar{X}$ = 3.99 , S.D. = 0.86) รองลงมา ท่านรู้สึกว่าท่านมีคุณสมบัติที่ดีหลายอย่าง ($\bar{X}$ = 3.80, S.D. = 0.75) ส่วนการเห็นคุณค่าในตนเองที่มีคะแนนเฉลี่ยน้อยที่สุด คือ บางครั้งท่านรู้สึกว่าท่านไม่มีอะไรดีเลย ($\bar{X}$ = 3.20 , S.D. = 0.99) ซึ่งส่วนใหญ่พบว่าการเห็นคุณค่าในตนเองอยู่ในระดับปานกลาง คิดเป็นร้อยละ 68.64 รองลงมา คือ ระดับสูง คิดเป็นร้อยละ 30.37 และระดับต่ำ คิดเป็นร้อยละ 0.99 ($\bar{X}$ = 3.20 , S.D. = 0.89) ตามลำดับ

พฤติกรรมการเป็นสมาชิกที่ดีในการทำงานกลุ่ม เมื่อพิจารณาพฤติกรรมของการเป็นสมาชิกที่ดีในการทำงานกลุ่มของกลุ่มตัวอย่างเป็นรายข้อ พบว่า พฤติกรรมในการเป็นสมาชิกที่ดีในการทำงานกลุ่มของนักศึกษามหาวิทยาลัยของรัฐ จังหวัดภูเก็ต ที่มีค่าเฉลี่ยสูงที่สุด คือ ท่านสละเวลาส่วนตัวในการพบปะเพื่อน ($\bar{X}$ = 3.87 , S.D. = 0.83) รองลงมา ท่านมีการแลกเปลี่ยนข้อมูลการเรียนให้เพื่อน ($\bar{X}$ = 3.78, S.D. = 0.73) ส่วนพฤติกรรมการเป็นสมาชิกที่ดีในการทำงานกลุ่มที่มีคะแนนเฉลี่ยน้อยที่สุด คือ ท่านไม่พักทานขนม ของว่างหรืองดอาหาร เพื่อทำงานกลุ่มให้เสร็จ ($\bar{X}$ = 3.24 , S.D. = 0.85) ซึ่งนักศึกษาส่วนใหญ่มีพฤติกรรมต่อการเป็นสมาชิกที่ดีต่อการทำงานกลุ่มอยู่ในระดับปานกลาง คิดเป็นร้อยละ 63.46 รองลงมา คือ ระดับสูง คิดเป็นร้อยละ 36.05 และระดับต่ำ คิดเป็น ร้อยละ 0.49 ($\bar{X}$ = 3.55 , S.D. = 0.81) ตามลำดับ

สัมพันธภาพระหว่างนักศึกษากับเพื่อน เมื่อพิจารณาสัมพันธภาพระหว่างนักศึกษากับเพื่อนออกเป็นรายข้อ พบว่า สัมพันธภาพระหว่างนักศึกษากับเพื่อน ของนักศึกษามหาวิทยาลัยของรัฐ จังหวัดภูเก็ต ที่มีค่าเฉลี่ยสูงที่สุด คือ ท่านมีเพื่อนที่สามารถปรึกษาปัญหาได้ทุกเรื่อง ($\bar{X}$ = 3.91 , S.D. = 0.90) รองลงมา ท่านมีเพื่อนสนิทมากกว่า 1 คน ($\bar{X}$ = 3.70, S.D. = 0.82) ส่วนสัมพันธภาพระหว่างนักศึกษากับเพื่อน ที่มีคะแนนเฉลี่ยต่ำที่สุด คือ เมื่อท่านเดือดร้อนเรื่องเงิน เพื่อนสามารถช่วยเหลือท่านได้ ($\bar{X}$ = 3.45 , S.D. = 0.82) ซึ่งจากการพิจารณาสัมพันธภาพระหว่างนักศึกษากับเพื่อน พบว่าส่วนใหญ่นักศึกษามีสัมพันธภาพระหว่างนักศึกษากับเพื่อน อยู่ในระดับปานกลาง คิดเป็นร้อยละ 64.44 รองลงมา คือ ระดับสูง คิดเป็นร้อยละ 33.33 และระดับต่ำ คิดเป็นร้อยละ 1.23 ($\bar{X}$ = 3.55 , S.D. = 0.85) ตามลำดับ

สัมพันธภาพระหว่างนักศึกษากับผู้ปกครอง เมื่อพิจารณาสัมพันธภาพระหว่างนักศึกษากับผู้ปกครองของนักศึกษามหาวิทยาลัยของรัฐ จังหวัดภูเก็ต พบว่า ในด้านของการปฏิบัติตนของนักศึกษาต่อผู้ปกครอง ที่มีค่าเฉลี่ยสูงที่สุด คือ ท่านปฏิบัติตามกฎระเบียบของผู้ปกครอง ($\bar{X}$ = 3.95 , S.D. = 0.86) รองลงมา ท่านให้ความเคารพและเชื่อฟังคำสั่งสอนของผู้ปกครอง ($\bar{X}$ = 3.85, S.D. = 0.87) ส่วนในด้านการปฏิบัติตนของผู้ปกครองต่อนักศึกษา ที่มีค่าเฉลี่ยสูงที่สุด คือ ผู้ปกครองสอบถามเรื่องการเรียนของท่านอยู่เสมอ ($\bar{X}$ = 3.93 , S.D. = 0.90) รองลงมา ผู้ปกครองแสดงความรักท่าน โดยการพูดให้กำลังใจ ($\bar{X}$ = 3.90 , S.D. = 0.85) ที่มีคะแนนเฉลี่ยต่ำที่สุด คือ เมื่อท่านทำผิด ผู้ปกครองดุด่าโดยไม่ถามสาเหตุ ($\bar{X}$ = 2.76 , S.D. = 1.16) ซึ่งจากการพิจารณาสัมพันธภาพระหว่างนักศึกษากับผู้ปกครองของนักศึกษา พบว่าส่วนใหญ่มีสัมพันธภาพระหว่างนักศึกษากับผู้ปกครอง อยู่ในระดับปานกลาง คิดเป็นร้อยละ 71.60 รองลงมา คือ ระดับสูง คิดเป็นร้อยละ 24.69 และระดับต่ำ คิดเป็นร้อยละ 3.71 ($\bar{X}$ = 3.19 , S.D. = 0.93) ตามลำดับ

การถูกกลั่นแกล้งจากเพื่อนในการทำงานกลุ่ม เมื่อพิจารณาเป็นรายข้อ พบว่า การถูกกลั่นแกล้งจากเพื่อนในการทำงานกลุ่มนักศึกษามหาวิทยาลัยของรัฐ จังหวัดภูเก็ต ที่มีค่าเฉลี่ยมากที่สุด คือ ท่านได้รับข้อมูลที่ไม่เพียงพอ ทำให้ส่งผลกระทบต่อผลการทำงานกลุ่ม ($\bar{X}$ = 3.25 , S.D. = 1.11) รองลงมา ท่านได้รับมอบหมายจากเพื่อนในกลุ่ม ($\bar{X}$ = 3.04, S.D. = 1.12) ส่วนการถูกกลั่นแกล้งจากเพื่อนในการทำงานกลุ่มที่มีคะแนนเฉลี่ยที่ต่ำที่สุด คือ ท่านถูกคุกคาม ถูกทำร้ายร่างกาย ($\bar{X}$ = 2.25 , S.D. = 1.28) ซึ่งพบว่าส่วนใหญ่มีการถูกกลั่นแกล้งจากเพื่อนในการทำงานกลุ่ม อยู่ในระดับปานกลาง คิดเป็นร้อยละ 43.95 รองลงมา คือ ระดับต่ำ คิดเป็นร้อยละ 40.74 และระดับสูง คิดเป็นร้อยละ 15.31 ($\bar{X}$ = 2.68 , S.D. = 1.18) ตามลำดับ

ปัจจัยที่มีอิทธิพลต่อการถูกกลั่นแกล้ง พบว่า นักศึกษามหาวิทยาลัยของรัฐ จังหวัดภูเก็ต ส่วนใหญ่มีปัจจัยที่มีอิทธิพลต่อการถูกกลั่นแกล้ง ซึ่งข้อที่มีคะแนนเฉลี่ยสูงที่สุด คือ ด้านสัมพันธภาพระหว่างนักศึกษากับเพื่อน ($\bar{X}$ =3.55, S.D. = 0.85) รองลงมา คือ พฤติกรรมการเป็นสมาชิกที่ดีในการทำงานกลุ่ม($\bar{X}$ = 3.55, S.D. = 0.81) การเห็นคุณค่าในตนเอง ($\bar{X}$ = 3.20, S.D. = 0.89) สัมพันธภาพระหว่างนักศึกษากับผู้ปกครอง ($\bar{X}$ = 3.19, S.D. = 0.93) และคะแนนเฉลี่ยที่ต่ำที่สุด คือ การถูกกลั่นแกล้งจากเพื่อนในการทำงานกลุ่ม ($\bar{X}$ =2.68, S.D. = 1.18) ตามลำดับ

ปัจจัยทำนาย ปัจจัยที่มีอิทธิพลต่อการถูกกลั่นแกล้งในนักศึกษาจากการวิเคราะห์ความสัมพันธ์ระหว่างตัวแปร พบว่า ปัจจัยที่มีอิทธิพลต่อการถูกกลั่นแกล้งในนักศึกษา ได้แก่ ปัจจัยเกี่ยวกับสัมพันธภาพระหว่างนักศึกษากับผู้ปกครอง พบว่า มีความสัมพันธ์ทางบวกกับการถูกกลั่นแกล้งจากเพื่อนในการทำงานกลุ่มมากที่สุดอย่างมีนัยสำคัญทางสถิติ (r = .456, p <.001) รองลงมาคือ การเห็นุณค่าในตนเอง อายุ ระดับชั้นปี ท่านใช้เวลา โดยเฉลี่ยในการเล่นอินเตอร์เน็ต พฤติกรรมการเป็นสมาชิกที่ดีในการทำงานกลุ่ม มีความสัมพันธ์ทางบวกกับการถูกกลั่นแกล้งจากเพื่อนในการทำงานกลุ่ม อย่างมีนัยสำคัญทางสถิติ (r = .416, .190, .170, .156 และ .139 p <.001) ตามลำดับ และปัจจัยเพศมีความสัมพันธ์ทางลบกับการถูกกลั่นแกล้งจากเพื่อนในการทำงานกลุ่ม มากที่สุด อย่างมีนัยสำคัญทางสถิติ (r = -.164, p = <.001) รองลงมาคือ เกรดเฉลี่ยมีความสัมพันธ์ทางลบกับการถูกกลั่นแกล้งจากเพื่อนในการทำงานกลุ่ม อย่างมีนัยสำคัญทางสถิติ (r = -.152, p <.001)

การวิเคราะห์ความถดถอยพหุคูณเชิงเส้นตรงของปัจจัยที่มีอิทธิพลต่อการถูกกลั่นแกล้งในนักศึกษา การวิเคราะห์ปัจจัยที่ทำนายปัจจัยที่มีอิทธิพลต่อการถูกกลั่นแกล้งในนักศึกษามหาวิทยาลัยของรัฐ จังหวัดภูเก็ต พบว่าตัวแปรทั้งหมดสามารถร่วมกันทำนายปัจจัยที่มีอิทธิพลต่อการถูกกลั่นแกล้งในนักศึกษามหาวิทยาลัยของรัฐ จังหวัดภูเก็ต ได้ร้อยละ 38.5 (R^2= .385) อย่างมีนัยสำคัญทางสถิติ (p<.001) โดยตัวแปรที่สามารถทำนายปัจจัยที่ทำนายปัจจัยที่มีอิทธิพลต่อการถูกกลั่นแกล้ง คือ สัมพันธภาพระหว่างนักศึกษากับผู้ปกครอง การเห็นคุณค่าในตนเอง สัมพันธภาพระหว่างนักศึกษากับเพื่อน เกรดเฉลี่ย และสถานศึกษา (β =.559, .266, และ -.298, p=<.001) (β =-.120, p=.004) และ (β =.108,p=.013) ตามลำดับ

ข้อเสนอแนะในการทำวิจัยครั้งต่อไป การศึกษารายละเอียดเพื่อให้ได้ข้อมูลเชิงลึกของกลุ่มตัวอย่างนักศึกษา ได้แก่ การเก็บข้อมูลเชิงคุณภาพ หรือการศึกษาวิจัยในรูปแบบผสมผสาน (Mixed method) เพื่อให้สามารถเข้าใจรายละเอียดของการกลั่นแกล้งของนักศึกษาโดยวิธีการหรือรูปแบบต่าง ๆ ในเชิงลึกและ

กว้างมากยิ่งขึ้นโดย ควรมีการสังเกตบริบทอื่น ๆ เบื้องต้นในขณะเก็บข้อมูล ซึ่งโดยบริบทนั้นไม่ได้เกิดจากการสัมภาษณ์จึงมีข้อจำกัดของข้อมูลบางอย่าง และพฤติกรรมในชีวิตประจำวันของนักศึกษาที่แท้จริง ควรประเมินลักษณะของบริบทอื่น ๆ และมีการสังเกตเชิงลึกควบคู่กับการสัมภาษณ์บุคคลในครอบครัว หรือผู้ดูแลนักศึกษาเกี่ยวกับพฤติกรรมในชีวิตประจำวันและบริบทอื่น ๆ ที่เกี่ยวข้องของนักศึกษาเพื่อให้ได้ข้อมูลที่ละเอียดมากยิ่งขึ้น

อ้างอิง

กนกอร จันยมิตรี และกัญญ์ฐิตา ศรีภา. (2563). การถูกรังแกผ่านโลกไซเบอร์และความเสี่ยงต่อการฆ่าตัวตายในเยาวชน.34(3).

กวินารัตน์ สุทธิสุคนธ์, จิราพร ชมพิกุล และเกรียงศักดิ์ ธรรมอภิพล. (2017). ปัจจัยที่มีผลต่อสัมพันธภาพใน ครอบครัวไทย.*Local Administration Journal*. 10(2),151-168.

กายกาญจน์ เสนแก้ว. (2558). พฤติกรรมการใช้เครือข่ายสังคมออนไลน์ของ Gen-X ใน กรุงเทพมหานคร.*หลักสูตรบริหารธุรกิจมหาบัณฑิต*,มหาวิทยาลัยกรุงเทพ. 1-104.

กรมสุขภาพจิต. (2564). ข้อมูลเกี่ยวกับการกลั่นแกล้ง สถิติของการกลั่นแกล้ง สถิติในการฆ่าตัวตายของเยาวชนในการศึกษา.

จักรกริช ปิยะ. (2557). การศึกษาการใช้สื่อสังคมออนไลน์ (Social media) เพื่อการบริหารงานก่อสร้างกรณีศึกษา ห้างหุ้นส่วนจำกัด เทคโนบิวเดอร์ (2001) อำเภอเมือง จังหวัดนครราชสีมา.*หลักสูตรปริญญาวิศวกรรม ศาสตรมหาบัณฑิต*,สาขาวิชาการบริหารงานก่อสร้างและสาธารณูปโภค,มหาวิทยาลัยเทคโนโลยีสุรนารี.1- 124.

ไชยชาญ เผือดคล้าย. (2565). แนวทางการแก้ปัญหาการกลั่นแกล้งรังแกกันในห้องเรียนชั้นประถมศึกษาด้วยการพัฒนาทักษะการเรียนรู้ทางอารมณ์และสังคม. 27(1), 223.

ไชยชาญ เผือดคล้าย. (2022). แนวทางการแก้ปัญหาการกลั่นแกล้ง รังแกกันในห้องเรียนชั้นประถมศึกษา ด้วยการพัฒนาทักษะการเรียนรู้ทางอารมณ์ และสังคม (Social and emotional learning: SEL). *วารสาร ปรัชญา ปริทรรศน์*. 27(1), 219-232.

ธันยากร ตุดเกื้อ และมาลี สบายยิ่ง. (2017). รูปแบบ ผลกระทบ และวิธีการจัดการเมื่อถูกรังแกบนโลกไซเบอร์ของนักศึกษาวิทยาลัยแห่งหนึ่งในภาคใต้ของประเทศไทย.*วารสารพฤติกรรมศาสตร์เพื่อการพัฒนา*.9(2).

นายอนันต์ วิวัฒนเดชา. (2560). ปัจจัยทางด้านเทคโนโลยีสื่อสังคมออนไลน์ต่อความรุนแรงของการกลั่นแกล้งทาง ไซเบอร์.หลักสูตรวิทยาศาสตรมหาบัณฑิต สาขาวิชานโยบายและการบริหารเทคโนโลยีสารสนเทศวิทยาลัยนวัตกรรม มหาวิทยาลัยธรรมศาสตร์.21-23.

ปวริศร์ กิจสุขจิต. (2559). ปัจจัยที่เป็นสาเหตุให้เกิดการรังแกกันในโรงเรียนมัธยมสตรี ในกรุงเทพมหานครตามแนวทฤษฎีเรียนรู้ของโรนัลด์ แอล เอเคอร์.*วารสารวิทยบริการมหาวิทยาลัยสงขลานครินทร์*. 27(1), 72-80.

พิชชาภา บุญณสะ. (2563). ผลกระทบของการกลั่นแกล้งในที่ทำงานต่อผลการปฏิบัติงาน ผ่านพฤติกรรมการเป็น สมาชิกที่ดีขององค์กร.*วิทยานิพนธ์หลักสูตรบริหารธุรกิจมหาบัณฑิต*,สาขาวิชาหลักสูตรบริหารธุรกิจ, มหาวิทยาลัยศิลปากร.

พิมพ์พลอย รุ่งแสง. (2560). ผลของกลุ่มการปรึกษาเชิงจิตวิทยาต่อการเห็นคุณค่าในตนเองของนักเรียนมัธยมศึกษาตอนต้นที่ถูกข่มเหงรังแกทางโลกไซเบอร์. *วิทยานิพนธ์ (ศศ.ม.) จุฬาลงกรณ์มหาวิทยาลัย*.

พรชนก ดาวประดับ. (2560). รูปแบบและลักษณะการมีส่วนร่วมในการกลั่นแกล้งบนพื้นที่สาธารณะออนไลน์. *วิทยานิพนธ์หลักสูตรวารสารศาสตรมหาบัณฑิต, สาขาวิชาสื่อสารมวลชน*,คณะวารสารศาสตร์และสื่อสารมวลชน ,มหาวิทยาลัยธรรมศาสตร์.1-188.

ภัททชฎา คำพวง. (2559). ปัจจัยที่มีอิทธิพลต่อพฤติกรรมตอบโต้จากการถูกรังแกบนพื้นที่ไซเบอร์ของวัยรุ่นในสถานศึกษา สังกัดสำนักงานคณะกรรมการการอาชีวศึกษาเขตกรุงเทพมหานคร.*วิทยานิพนธ์หลักสูตรวิทยาศาสตรมหาบัณฑิต,บริหารเทคโนโลยีสารสนเทศ,*คณะสถิติประยุกต์,สถาบันบัณฑิตพัฒนบริหาร ศาสตร์.

ภัทรจรัส บำรุงพงษ์ และอุนิษา เลิศโตมรสกุล. (2019). การกลั่นแกล้งในมหาวิทยาลัยกรณีศึกษานิสิตที่มีความ ต้องการพิเศษ.*วารสารคุณภาพชีวิตกับกฎหมาย*. 15(2),49-63.

ภัทรจรัส บำรุงพงษ์ และอุนิษา เลิศโตมรสกุล. (2019). การกลั่นแกล้งในมหาวิทยาลัย:กรณีศึกษานิสิตที่มีความต้องการพิเศษ BULLYING IN UNIVERSITY: A CASE STUDY OF STUDENTS WITH SPECIAL NEEDS.

รัศมีแสง หนูแป้นทอง และคณะ. (2561). การเห็นคุณค่าในตนเอง การสนับสนุนทางสังคม และพฤติกรรมรังแกกันในนักเรียนระดับมัธยมศึกษาตอนต้น.32(3).

ลักษณสุภา บัวบางพลู. (2554). ผลสัมฤทธิ์การเรียนรู้รายวิชาการประมวลผลการวิจัยทางธุรกิจด้วยคอมพิวเตอร์โดยใช้กระบวนการกลุ่มในการจัดการเรียนการสอน. กรุงเทพฯ: คณะวิทยาการจัดการ มหาวิทยาลัยราชภัฏสวนดุสิต.

วัลลี พุทโสม และจิระภา จันทร์บัว. (2021). อิทธิพลของบทบาทการทำงานกระบวนการทำงาน และแรงจูงใจใน การทำงาน ที่ส่งผลต่อประสิทธิภาพการทำงานเป็นทีม ของนักศึกษาในสถาบันการศึกษาสามแห่ง. *APHEIT JOURNAL*. 27(1), 94-112.

ศุภากร หวัง และสมชาย เตียวกุล. (2562). การถูกกลั่นแกล้งบนสื่อสังคมออนไลน์ของนักศึกษาสาขาวิทยาศาสตร์สุขภาพ.*วารสาร จิตวิทยาคลินิก*.50(2),17-28.

ศุภิศา จิตต์สม. (2564). ปัจจัยด้ายจิต สังคมที่มีอิทธิพลต่อการถูกรังแกผ่านโลกไซเบอร์ของนักเรียนชั้นมัธยมศึกษาตอนปลาย.วิทยานิพนธ์หลักสูตรพยาบาลศาสตรมหาบัณฑิต,สาขาวิชาการพยาบาลจิตเวชและสุขภาพ จิต,คณะพยาบาลศาสตร์ มหาวิทยาลัยบูรพา.

สุคนธ์ สินธพานนท์และคณะ. (2545). การจัดกระบวนการเรียนรู้: เน้นผู้เรียนเป็นสำคัญตามหลักสูตรการศึกษาขั้นพื้นฐาน.

สุภิศา จิตต์สม. (2564). ปัจจัยด้านจิตสังคมที่มีอิทธิพลต่อการถูกรังแกผ่านโลกไซเบอร์ของนักเรียนชั้นมัธยมศึกษา ตอนปลาย.*วิทยานิพนธ์หลักสูตรพยาบาลศาสตรมหาบัณฑิต*,สาขาวิชาการพยาบาลจิตเวชและสุขภาพจิต,คณะพยาบาลศาสตร์ มหาวิทยาลัยบูรพา.

สุริยะ หาญพิชัย. (2561). การพัฒนาผลสัมฤทธิ์ทางการเรียนโดยใช้การเรียนรู้แบบร่วมมือด้วยกระบวนการกลุ่มในรายวิชากลยุทธ์การวางแผนพัฒนาท้องถิ่นเชิงบูรณาการDevelopment of Learning achievement using Cooperative LearningGroups in Integrated Local Development Planning.

สุวรรณี สัคนวณิช. (2014). ความสัมพันธ์ระหว่างบุคคล พฤติกรรมการใช้ชีวิต และผลสัมฤทธิ์ทางการเรียนของ นักศึกษาที่ใช้ชีวิตในที่พักเอกชน ย่านรังสิต จังหวัดปทุมธานี.*ภาควิชาการประชาสัมพันธ์,คณะนิเทศศาสตร์,มหาวิทยาลัยกรงเทพ.*13(1),1-19.

สุฮัยณี อาหวัง,นิศริน เจ๊ะหามะ,สโรชา ชูเล่ง,นูรีดา เจะอีซอ,อับดุลคอลิก อัรรอฮีมีย์,และ ธันยากร ตุดเกื้อ (2563). ผลกระทบจากพฤติกรรมการกลั่นแกล้งของนักเรียนในจังหวัดปัตตานี.

หนึ่งฤทัย มะลาไวย์, อรพินทร์ ชูชม และนริสรา พึ่งโพธิ์สภ. (2565). การทำงานเป็นทีมของนักเรียน: ปัจจัยเชิงสาเหตุ ข้อเสนอแนะในการวิจัย StudentTeamwork : Causal Factors, Suggestions for Researchมหาวิทยาลัยศรีนครินทรวิโรฒ.

อารี ชูมณี. (2546). การศึกษาเปรียบเทียบผลสัมฤทธิ์ทางการเรียนความคิดสร้างสรรค์และมนุษยสัมพันธ์ของนักเรียนชั้นมัธยมศึกษาปีที่ 3 ที่เรียนวิชาสังคมศึกษาโดยการสอนด้วยวิธีสตอรีไลน์ และการสอนโดยใช้กระบวนการกล่มสัมพันธุ์..ปริญญานิพนธ์กศ.ม. (การมัธยมศึกษา). กรุงเทพฯ : บัณฑิตวิทยาลัย มหาวิทยาลัยศรีนครินทรวิโรฒ.คณะกรรมการควบคุม.

Fonagy.P., & Twemlow.S.W. (2005). The Prevalence of Teachers Who Bully Students in Schools With Differing Levels of Behavioral Problems.*Am J Psychiatry*.162,2387-2389.

Janyametee, Kanog-on, & Sripa.K. (2020). แนวทางการป้องกันพฤติกรรมการเบี่ยงเบนทางสังคมของวัยรุ่น จากการถูกกลั่นแกล้งทางไซเบอร์ ศึกษาเฉพาะกรณีโรงเรียนมัธยมศึกษา จังหวัดสมุทรปราการ.*วารสารพฤติกรรมศาสตร์ (Warasan Phuettikammasat)*.26(2), 16-42.

Suparp.J.,Boonyathan.W.,Kittipichai.W., & Chamroonsawasdi.K. (2010). Life Skills Development Program to Reduce Bullying and to Promote Good Practices among Primary School Students,Samut-Sakorn Province, Thailand. *Journal of Public Health*.40(1),7-15.

ความเครียดและพฤติกรรมการเที่ยวสถานบันเทิงของนักศึกษาระดับปริญญาตรี มหาวิทยาลัยแห่งหนึ่งในจังหวัดภูเก็ต

Stress and Entertainment Venue Visiting Behavior Among Undergraduate Students at a University in Phuket Province

Charinya Khanawang [1]
Phuket Rajabhat University
Phuket, Thailand
Ammyjarinya@gmail.com

Supaporn khayaikaeo [2]
Phuket Rajabhat University
Phuket, Thailand
Supaporn26253@gmail.com

Atitaya Jitjamnong [3]
Phuket Rajabhat University
Phuket, Thailand
Atitaya.j@pkru.ac.th

Abstract

This study is a survey research aimed to examine stress levels, entertainment venue visiting behaviors, and compare these behaviors across different stress levels among undergraduate students at a university in Phuket Province. The sample group consisted of 400 undergraduate students from first to fourth year, proportionately calculated and selected through accidental sampling to ensure optimal representation. A questionnaire was used as the data collection tool, with reliability tested using Cronbach's alpha coefficient, yielding a reliability value of 0.95. Data were analyzed using descriptive statistics, including percentage, frequency, mean, standard deviation, and one-way ANOVA.

The findings revealed that the majority of the participants experienced severe stress, accounting for 56.50%, and exhibited a high level of entertainment venue visiting behaviors at 45.50%. The participants reported feeling stress relief after visiting entertainment venues. It was found that participants with different stress levels displayed significantly different entertainment venue visiting behaviors at the 0.05 statistical significance level. Students with severe stress levels were more likely to visit entertainment venues than those with lower stress levels. Therefore, parents, educators, and related parties should provide guidance on stress management and systematic care to help reduce stress and promote the mental well-being of students.

Keywords: *Stress, Entertainment venue visiting behavior*

บทนำ

สภาพสังคมในปัจจุบันมีการเปลี่ยนแปลงเกิดขึ้นอย่างรวดเร็วทั้งในด้านเศรษฐกิจ ด้านการเมือง ด้านสิ่งแวดล้อม ค่านิยม และวัฒนธรรม ส่งผลทำให้การใช้ชีวิต การเรียน การทำงานของแต่ละบุคคลมีความเร่งรีบมากขึ้น ซึ่งสิ่งต่างๆ เหล่านี้ อาจเป็นสาเหตุที่ก่อให้เกิดความเครียด หากบุคคลไม่สามารถปรับตัวต่อความเครียดที่เกิดขึ้นได้ย่อมส่งผลกระทบต่อสุขภาพกายและสุขภาพจิต โดยเฉพาะในกลุ่มวัยรุ่น ซึ่งเป็นวัยที่มีการเปลี่ยนแปลงของร่างกาย จิตใจ และอารมณ์เกิดขึ้นอย่างรวดเร็ว การเปลี่ยนแปลงของสังคม และสิ่งแวดล้อมที่อยู่รอบตัววัยรุ่น หากวัยรุ่นมีความเครียดสะสมในระดับที่มากเกินไปจะส่งผลกระทบทางด้านลบต่อปัญหาสุขภาพกาย ได้แก่ นอนไม่หลับ เบื่ออาหาร อ่อนเพลีย ปวดศีรษะ ปวดท้อง ปวดหลัง ใจสั่น และส่งผลต่อสุขภาพจิต ได้แก่ หงุดหงิด โกรธง่าย เบื่อหน่าย คิดมาก วิตกกังวล เศร้าหมอง ไม่มีสมาธิ รวมทั้งทางพฤติกรรม ได้แก่ เงียบขรึม เก็บตัว สูบบุหรี่หรือดื่มสุรามากขึ้น ชวนทะเลาะ มีเรื่องขัดแย้งกับผู้อื่นบ่อยๆ มีปัญหาเรื่องการใช้สารเสพติด หากวัยรุ่นมีภาวะเครียดรุนแรงมากยิ่งขึ้น อาจถึงขั้นเกิดภาวะซึมเศร้า หรือเสี่ยงต่อการฆ่าตัวตายได้ นำมาซึ่งความสูญเสียเป็นอย่างมาก (กรมสุขภาพจิต, 2563)

ปัจจุบันสถานการณ์ภาวะเครียดในกลุ่มวัยรุ่นมีแนวโน้มสูงขึ้น ซึ่งสอดคล้องกับผลสำรวจของ Mental Health Check In พบว่า วัยรุ่นมี

แนวโน้มความเครียดสูงขึ้นมาก โดยระดับความเครียดในรอบเดือนมีนาคม 2565 ที่ผ่านมา สูงกว่าในกลุ่มวัยทำงานถึง 4 เท่า ซึ่งสาเหตุที่ทำให้เด็กเกิดความเครียด นอกจากปัญหาในเรื่องความรัก ยังมีเรื่องการเรียน ค่าใช้จ่าย รวมไปถึงการใช้เวลากับสิ่งที่เด็กสนใจ แต่ถูกตำหนิ เพราะเหมือนหมกหมุ่นในสายตาผู้ใหญ่ (กรมสุขภาพจิต, 2565) ทั้งนี้การศึกษาวิเคราะห์ปัจจัยความเครียดของเยาวชนรุ่นใหม่ อายุ 15-24 ปี และ 19-22 ปี จากแบบสำรวจเยาวชนของ คิด ฟอร์ คิดส์ ในปี 2022 จำนวน 19,034 ตัวอย่าง พบว่า การศึกษาและการทำงานเป็นสาเหตุอันดับแรกที่ทำให้เกิดความเครียด ร้อยละ 38.4 และร้อยละ 60.9 ตามลำดับ (ศูนย์ความรู้นโยบายเด็กและครอบครัว, 2565) ซึ่งนักศึกษาต้องเผชิญกับความตึงเครียดทางจิตใจ รวมกับการได้รับอิสระมากขึ้นจึงหาทางออกด้วยการพักผ่อนหย่อนใจ คลายเครียดด้วยวิธีต่างๆ โดยสถานที่ที่นิยมไปท่องเที่ยว คือ การท่องเที่ยวในยามวิกาลตามสถานบันเทิงต่าง ๆ นักศึกษามีพฤติกรรมการเที่ยวสถานบันเทิงที่ต่างไปจากเดิมเมื่อเทียบกับในช่วงมัธยม ซึ่งจากการศึกษา พบว่า ปัจจัยที่ส่งผลต่อพฤติกรรมการเที่ยวสถานบันเทิงกลางคืนของนักศึกษา คือ มูลเหตุจูงใจทางอารมณ์ด้านความเครียด (ณัชชา มณีวงศ์, 2550, อ้างถึงใน จิราภา สีเทา, 2564, น.2) โดยความเครียดเป็นภาวะที่แสดงออกมา เมื่อถูกกระตุ้นจากสิ่งแวดล้อม สังคม ภาวะอารมณ์ที่เกิดขึ้นจากจิตใจ รวมถึงสภาพร่างกาย (กรมสุขภาพจิต, 2563)

สถานบันเทิงเป็นสถานที่บริการที่กลุ่มวัยรุ่น นักเรียน นักศึกษา มักจะไปเที่ยวโดยเฉพาะในเวลากลางคืน เพื่อพบปะสังสรรค์ พักผ่อนจิตใจ หรือคลายเครียดจากเหตุการณ์ต่าง ๆ ในช่วงวันหยุดและเทศกาล ซึ่งมีการให้ความบันเทิงในรูปแบบต่าง ๆ เช่น มีนักร้อง ดนตรี แสง สี มุมนั่งเล่น เวทีสำหรับเต้นรำต่าง ๆ พร้อมกับมีการจำหน่ายเครื่องดื่มที่มีส่วนผสมของแอลกอฮอล์ อาหาร ของมึนเมาอื่น ๆ (สุภาภรณ์ อหันตะ, 2551, น. 2 อ้างถึงใน จิราภา สีเทา ,2565, น.1-2) จากการศึกษาปัจจัยการเลือกใช้บริการสถานบันเทิงของผู้บริโภคในเขตอำเภอเมืองเพชรบูรณ์ จังหวัดเพชรบูรณ์ พบว่า ส่วนใหญ่ผู้เข้าใช้บริการสถานบันเทิงเป็นเพศหญิง มีอายุเฉลี่ย 20-25 ปี เที่ยวสถานบันเทิงเฉลี่ย 1-2 ครั้งต่อเดือน และนิยมเที่ยวในวันหยุดสุดสัปดาห์ (อรอูรา ครุฑมณี, 2564) ทั้งนี้การจัดตั้งสถานบันเทิงได้รับการอนุญาต ให้จัดตั้งขึ้นตามพระราชบัญญัติสถานบริการ พ.ศ. 2509 โดยมีกฎหมายที่ควบคุมการจัดตั้ง คือ การห้ามมิให้ผู้ที่มีอายุต่ำกว่า 20 ปีบริบูรณ์เข้าไปใช้บริการ มีการกำหนดให้ปิดและเปิดตามเวลาที่กำหนด การขจัดมิให้มียาเสพติด แต่ในปัจจุบันสถานบันเทิงบางแห่งไม่ปฏิบัติตามที่กฎหมายกำหนด เช่น อนุญาตให้วัยรุ่นอายุต่ำกว่า 20 ปี เข้าไปใช้บริการ เปิดทำการเกินช่วงเวลาที่กำหนด มีการจัดตั้งสถานบริการไม่เป็นไปตามข้อกำหนด คือมีการจัดตั้งสถานบริการเพิ่มขึ้นเป็นจำนวนมาก อีกทั้งยังอยู่ใกล้สถานศึกษา ซึ่งอาจทำให้นักเรียน นักศึกษาเกิดความสนใจและมีความรู้สึกอยากรู้อยากลองถึงขั้นเข้าไปใช้บริการ โดยไม่ได้คำนึงถึงผลกระทบที่ตามมา (มติชนออนไลน์, 2566)

จังหวัดภูเก็ตเป็นแหล่งพักผ่อนชื่อดังของไทยที่ได้รับความนิยมไปทั่วโลกและมีสถานที่ท่องเที่ยวยามค่ำคืนจำนวนมาก สถานบันเทิงในจังหวัดภูเก็ตมีสถานประกอบการผับบาร์อยู่ 4 โซน ได้แก่ โซนที่ 1 ตำบล กะรน จำนวน 15 ร้าน โซนที่ 2 วงเวียนม้าน้ำ จำนวน 1 ร้าน โซนที่ 3 ที่บริเวณตลิ่งชัน ถนนกระ จำนวน 2 ร้าน และโซนที่ 4 ซอยตาเอียด ตำบลฉลอง จำนวน 7 ร้าน และบางร้านยังไม่ได้รับอนุญาตถูกต้อง นอกนั้นมีสถานบริการที่อยู่ในโรงแรม 12 ร้าน และอยู่นอกเขตโซนนิ่งที่ตั้งมาก่อนปี 2547 อีก 5 ร้าน (มติชนออนไลน์, 2566) จากเหตุผลข้างต้น ผู้วิจัยมีความสนใจที่จะศึกษาระดับความเครียดและระดับพฤติกรรมการเที่ยวสถานบันเทิงของนักศึกษาประดับปริญญาตรี มหาวิทยาลัยแห่งหนึ่งในจังหวัดภูเก็ต เนื่องจากนักศึกษายังอยู่ในวัยของการศึกษาหาความรู้ และถือว่าเป็นกำลังสำคัญในการพัฒนาสังคม ประเทศในอนาคต ซึ่งผลที่ได้จากการศึกษาจะนำเสนอผู้ที่มีส่วนเกี่ยวข้องในการหาแนวทางป้องกันและแก้ไขปัญหา เพื่อให้ปัญหาเหล่านี้ลดลง

วัตถุประสงค์การวิจัย

1. เพื่อศึกษาระดับความเครียดของนักศึกษา
2. เพื่อศึกษาระดับพฤติกรรมการเที่ยวสถานบันเทิงของนักศึกษา
3. เพื่อเปรียบเทียบพฤติกรรมการเที่ยวสถานบันเทิงของนักศึกษาตามระดับความเครียด

ระเบียบวิธีการวิจัย

รูปแบบการวิจัย เป็นการศึกษาเชิงพรรณนาแบบภาคตัดขวาง (Cross-sectional Descriptive study)

ประชากร คือ นักศึกษาระดับปริญญาตรีที่กำลังศึกษาอยู่ในปีการศึกษา 2567 ในมหาวิทยาลัยแห่งหนึ่ง จังหวัดภูเก็ต จำนวน 6,985 คน

กลุ่มตัวอย่าง คือ นักศึกษาระดับปริญญาตรีที่กำลังศึกษาอยู่ในปีการศึกษา 2567 ในมหาวิทยาลัยแห่งหนึ่ง จังหวัดภูเก็ต จำนวน 400 คน โดยผู้วิจัยได้คำนวณขนาดกลุ่มตัวอย่างโดยใช้สูตรของเครจซี่และมอร์แกน (Krejcie & Morgan,1970 อ้างถึงใน Natthakon M.,14 ก.ย 2566) ยอมรับค่าความคลาดเคลื่อนจากการสุ่มตัวอย่าง ร้อยละ 5 ระดับความเชื่อมั่นร้อยละ 95 และกำหนด ให้สัดส่วนของลักษณะที่สนใจในประชากรเท่ากับ 0.5 ได้กลุ่มตัวอย่าง จำนวน 364 คน เพื่อป้องกันความ ผิดพลาดจากการตอบแบบสอบถามไม่สมบูรณ์ ผู้วิจัยจึงเก็บข้อมูลเพิ่มขึ้น ร้อยละ 10 ได้กลุ่มตัวอย่างทั้งสิ้น จำนวน 400 คน เลือกกลุ่มตัวอย่างด้วยการสุ่มแบบสะดวก

เครื่องมือที่ใช้ในการวิจัย

เครื่องมือที่ใช้ในการศึกษาค้นคว้าวิจัยครั้งนี้ คือ แบบสอบถาม ประกอบด้วยคำถามจำนวน 3 ส่วน ดังนี้

ส่วนที่ 1 ข้อมูลส่วนบุคคล สร้างขึ้นจากการทบทวนวรรณกรรม ประกอบด้วย ได้แก่ เพศ อายุ ศาสนา คณะ ชั้นปีที่ศึกษาอยู่ เกรดเฉลี่ยสะสม สถานภาพ อาชีพเสริม รายได้ที่ได้รับต่อเดือน โรคประจำตัว การดื่มแอลกอฮอล์ การสูบบุหรี่ ระยะเวลาเฉลี่ยในการนอนหลับแต่ละวันและการออกกำลังกาย มีลักษณะเป็นข้อคำถามให้เลือกตอบและเติมคำ จำนวน 14 ข้อ

ส่วนที่ 2 ระดับความเครียด ผู้วิจัยใช้แบบสอบถามวัดความเครียดสวนปรุง (Suanprung Stress Test-20, SPST) ของกรมสุขภาพจิต (2557) โดยลักษณะแบบสอบถาม เป็นมาตราส่วนประมาณค่า (Rating Scale) 5 ระดับ ได้แก่ รู้สึกเครียดมากที่สุด (5) รู้สึกเครียดมาก รู้สึกเครียดปานกลาง รู้สึกเครียด เล็กน้อยและไม่รู้สึกเครียดเลย (1) เป็นแบบสอบถามเกี่ยวกับสาเหตุของความเครียด ผลของความเครียด พฤติกรรม และสุขภาพ จำนวน 20 ข้อ

เกณฑ์การให้คะแนนแบบสอบถามความเครียด ให้คะแนน ดังนี้ รู้สึกเครียดมากที่สุด ให้คะแนน 5 คะแนน รู้สึกเครียดมาก ให้คะแนน 4 คะแนน รู้สึกเครียดปานกลาง ให้คะแนน 3 คะแนน รู้สึกเครียดเล็กน้อย ให้คะแนน 2 คะแนน ไม่รู้สึกเครียด ให้คะแนน 1 คะแนน โดยมีแบ่งความเครียดออกเป็น 4 ระดับ ดังนี้

คะแนน 0 – 23	หมายถึง มีความเครียดน้อย
คะแนน 24 – 41	หมายถึง มีความเครียดปานกลาง
คะแนน 42 – 61	หมายถึง มีความเครียดสูง
คะแนน 62 ขึ้นไป	หมายถึง มีความเครียดรุนแรง

ส่วนที่ 3 พฤติกรรมการเที่ยวสถานบันเทิง ผู้วิจัยดัดแปลงมาจากแบบสอบถามพฤติกรรมการเที่ยวสถานบันเทิงของจิราภา สีเทา (2564) ประกอบการเตรียมตัวเพื่อไปสถานบันเทิง ประกอบด้วย การนัดหมาย การเลือกสถานที่ การแต่งตัว และการกระทำขณะอยู่ในสถานบันเทิงแห่งนั้น จนสิ้นสุดการเที่ยวสถานบันเทิง ประกอบด้วย เต้นรำ ฟังเพลง ดื่มเครื่องดื่ม รับประทานอาหาร พบปะสังสรรค์กับเพื่อนหรือบุคคลอื่น รวมไปถึงช่วงวันเวลาที่ใช้ไปกับการเที่ยวสถานบันเทิง จำนวนครั้งที่เที่ยวในแต่ละสัปดาห์/เดือน มีลักษณะเป็นข้อความให้เลือกตอบ จำนวน 24 ข้อ และเติมคำตอบ จำนวน 6 ข้อ รวมเป็น 30 ข้อ โดยลักษณะแบบสอบถามเป็นมาตราส่วนประมาณค่า (Rating Scale) 5 ระดับ ตามแนวคิดของลิเคอร์ท (Likert Scale Type) แบ่งเป็น 5 ระดับ ได้แก่ เป็นประจำ บ่อยครั้ง นานๆครั้ง บางครั้ง และไม่เคยเลย ข้อคำถามเชิงบวกให้คะแนน 5, 4, 3, 2, 1 และข้อคำถามเชิงลบ ให้ 1, 2, 3, 4, 5 ตามลำดับ การแปลผลระดับของพฤติกรรมการเที่ยวสถานบันเทิง ดังนี้

คะแนน 3.68 - 5.00 หมายถึง มีพฤติกรรมการเที่ยวสถานบันเทิงในระดับมาก

คะแนน 2.34 - 3.67 หมายถึง มีพฤติกรรมการเที่ยวสถานบันเทิงในระดับปานกลาง

คะแนน 1.00 - 2.33 หมายถึง มีพฤติกรรมการเที่ยวสถานบันเทิงในระดับน้อย

การตรวจสอบคุณภาพเครื่องมือ ตรวจสอบความเที่ยงตรงเชิงเนื้อหาโดยผู้เชี่ยวชาญ 3 ท่าน ได้ค่าดัชนีความสอดคล้องระหว่างข้อคำถามกับวัตถุประสงค์ (IOC) ของแบบสอบถาม**พฤติกรรมการเที่ยวสถานบันเทิง** เท่ากับ 0.84 และทดลองใช้แบบสอบถามกับนักศึกษาของมหาวิทยาลัยแห่งหนึ่งในจังหวัดสุราษฎร์ธานี จำนวน 30 คน ทดสอบความเชื่อมั่นของแบบสอบถามโดยใช้ สูตรสัมประสิทธิแอลฟาของครอนบาค ได้ค่าความเชื่อมั่นเท่ากับ 0.94

ขั้นตอนการเก็บรวบรวมข้อมูล

1. จัดทำหนังสือถึงมหาวิทยาลัย เพื่อขอความอนุเคราะห์ในการเก็บรวบรวมข้อมูล

2. หลังจากได้รับความอนุเคราะห์ ผู้วิจัยดำเนินการรวบรวมข้อมูลกับกลุ่มตัวอย่างที่ยินยอมให้ข้อมูล โดยใช้แบบสอบถามกระดาษ ดำเนินการแจกแบบสอบถามตามสถานที่ต่างๆในมหาวิทยาลัยและแบบสอบถามออนไลน์สำหรับกลุ่มตัวอย่างที่สะดวกให้ข้อมูลผ่านระบบออนไลน์

3. หลังเสร็จสิ้นกระบวนการเก็บรวบรวมข้อมูล ทำการตรวจสอบและบันทึกข้อมูลเข้าสู่โปรแกรมคอมพิวเตอร์ เพื่อประมวลผลและวิเคราะห์ข้อมูลทางสถิติ

การวิเคราะห์ข้อมูล

1. ข้อมูลส่วนบุคคล ระดับความเครียด พฤติกรรมการเที่ยวสถานบันเทิง วิเคราะห์โดยใช้สถิติเชิงพรรณนา ร้อยละ ความถี่ ค่าเฉลี่ย และค่าส่วนเบี่ยงเบนมาตรฐาน

2. วิเคราะห์เปรียบเทียบพฤติกรรมการเที่ยวสถานบันเทิงของนักศึกษา ตามระดับความเครียด โดยใช้สถิติการวิเคราะห์ความแปรปรวนทางเดียว (One Way ANOVA) กำหนดระดับนัยสำคัญที่ 0.05

ผลการศึกษา

1. ข้อมูลส่วนบุคคล

ผู้ตอบแบบสอบถามส่วนใหญ่เป็นเพศหญิงมากที่สุด จำนวน 212 คน คิดเป็นร้อยละ 53.00 เพศชาย จำนวน 150 คน คิดเป็นร้อยละ 37.50 และเพศทางเลือก จำนวน 38 คน คิดเป็นร้อยละ 9.50 กลุ่มตัวอย่างส่วนใหญ่มีอายุโดยเฉลี่ยเท่ากับ 20.77 ปี (S.D.= 1.14) นับถือศาสนาพุทธมากที่สุด จำนวน 326 คน คิดเป็นร้อย 81.50 กลุ่มตัวอย่างส่วนใหญ่ศึกษาในชั้นปีที่ 3 ร้อยละ 37.00 มีเกรดเฉลี่ยสะสมในช่วง 2.50 – 3.00 จำนวน 142 คน คิดเป็นร้อยละ 35.50 กลุ่มตัวอย่างส่วนใหญ่มีสถานะโสด จำนวน 395 คน คิดเป็นร้อยละ 98.75 ไม่ประกอบอาชีพเสริม จำนวน 336 คน คิดเป็นร้อยละ 84.00 สำหรับกลุ่มที่ประกอบอาชีพเสริม พบว่า ประกอบอาชีพค้าขายมากที่สุด จำนวน 28 คน คิดเป็นร้อยละ 43.75 กลุ่มตัวอย่างมีรายได้เฉลี่ยเท่ากับ 7,844.83 บาท (S.D.= 3,499.64)

ข้อมูลทั่วไปด้านสุขภาพ พบว่า กลุ่มตัวอย่างส่วนใหญ่ไม่มีโรคประจำตัว จำนวน 392 คน คิดเป็นร้อยละ 98.00 สำหรับกลุ่มที่มีโรคประจำตัว พบว่า ป่วยเป็นโรคภูมิแพ้ จำนวน 4 คน คิดเป็นร้อยละ 50.00 กลุ่มตัวอย่างส่วนใหญ่ดื่มแอลกอฮอล์นานๆครั้ง (1-2 ครั้ง/เดือน) จำนวน 285 คน คิดเป็นร้อย 71.25 รองลงมา คือ ไม่เคยดื่ม จำนวน 80 คน คิดเป็นร้อยละ 20.00 และดื่มเป็นประจำ จำนวน 28 คน คิดเป็นร้อยละ 7.00 ซึ่งในกลุ่มที่ดื่มแอลกอฮอล์เป็นประจำนั้น มีความถี่ในการดื่ม จำนวน 1 – 4 ครั้งต่อสัปดาห์ จำนวน 22 คน คิดเป็นร้อยละ 78.57 ด้านการสูบบุหรี่/บุหรี่ไฟฟ้า/ยาสูบของกลุ่มตัวอย่าง พบว่า ส่วนใหญ่ไม่เคยสูบบุหรี่ จำนวน 353

คน คิดเป็นร้อยละ 88.25 สำหรับกลุ่มที่สูบบุหรี่ ส่วนใหญ่สูบบุหรี่ จำนวน 1 – 4 มวนต่อวัน จำนวน 19 คน คิดเป็นร้อยละ 51.35 สูบบุหรี่มวนแรกภายหลังจากตื่นนอนแล้วมากกว่า 1 ชั่วโมง จำนวน 23 คน คิดเป็นร้อยละ 62.16 กลุ่มตัวอย่างมีระยะเวลาเฉลี่ยในการนอนหลับเท่ากับ 7.43 ชั่วโมง (S.D.= 1.47) ด้านการออกกำลังกายของกลุ่มตัวอย่าง พบว่า ส่วนใหญ่ไม่ออกกำลังกาย จำนวน 181 คน คิดเป็นร้อยละ 45.25

2. ข้อมูลระดับความเครียด

ผู้ตอบแบบสอบถาม พบว่า ส่วนใหญ่มีความเครียดอยู่ในระดับรุนแรง จำนวน 226 คน คิดเป็นร้อยละ 56.50 รองลงมา คือ ระดับสูง จำนวน 118 คน คิดเป็นร้อยละ 29.50 และระดับปานกลาง จำนวน 44 คน คิดเป็นร้อยละ 11.00 ดังตารางที่ 1

ตารางที่ 1 จำนวน ร้อยละ ของกลุ่มตัวอย่าง จำแนกตามระดับความเครียด (n=400)

ระดับความเครียด	ช่วงคะแนน	จำนวน (คน)	ร้อยละ
มีความเครียดน้อย	0 - 23	2	0.50
มีความเครียดปานกลาง	24 – 41	44	11.00
มีความเครียดสูง	42 – 61	129	32.25
มีความเครียดระดับรุนแรง	61 ขึ้นไป	225	56.25
รวม		400	100.00

3. ข้อมูลพฤติกรรมการเที่ยวสถานบันเทิง

กลุ่มตัวอย่างส่วนใหญ่มักไปเที่ยวเป็นประจำในวันเสาร์ ร้อยละ 48.75 กลุ่มตัวอย่างเลือกเที่ยวคาเฟ่มากที่สุด ร้อยละ 98.50 โดยส่วนใหญ่เที่ยวสถานบันเทิง จำนวน 0 - 5 ครั้งต่อเดือน ร้อยละ 83.25 ใน 1 สัปดาห์เที่ยวสถานบันเทิง จำนวน 1 – 3 วันต่อสัปดาห์ ร้อยละ 91.00 และใช้เวลาในการเที่ยวสถานบันเทิงแต่ละครั้งเฉลี่ย 4.19 ชั่วโมง (S.D.= 1.29) กลุ่มตัวอย่างมักไปเที่ยวสถานบันเทิงกับเพื่อนสนิทเพศเดียวกัน ร้อยละ 94.75 โดยกลุ่มตัวอย่าง ร้อยละ 87.50 จ่ายค่าเที่ยวสถานบันเทิง โดยใช้เงินเดือนประจำที่ได้จากผู้ปกครอง ซึ่งค่าใช้จ่ายแต่ละครั้ง เฉลี่ย 509.24 ปี (S.D.= 395.02)

ผลการวิเคราะห์ข้อมูลระดับพฤติกรรมการเที่ยวสถานบันเทิงโดยรวม พบว่า กลุ่มตัวอย่างส่วนใหญ่มีพฤติกรรมการเที่ยวสถานบันเทิงอยู่ในระดับมาก จำนวน 182 คน คิดเป็นร้อยละ 45.50 รองลงมา คือ ระดับปานกลาง จำนวน 179 คน คิดเป็นร้อยละ 44.75 และระดับน้อย จำนวน 39 คน คิดเป็นร้อยละ 9.75 ดังตารางที่ 3

ตารางที่ 3 ข้อมูลเกี่ยวกับพฤติกรรมการเที่ยวสถานบันเทิงของกลุ่มตัวอย่าง (n=400)

ระดับพฤติกรรมการเที่ยวสถานบันเทิง	ช่วงคะแนน	จำนวน (คน)	ร้อยละ
ระดับน้อย	1.00 – 2.33	39	9.75
ระดับปานกลาง	2.34 – 3.67	179	44.75
ระดับมาก	3.68 – 5.00	182	45.50
รวม		**400**	**100.00**

เมื่อจำแนกพฤติกรรมการเที่ยวสถานบันเทิงเป็นรายข้อ พบว่า กลุ่มตัวอย่างรู้สึกผ่อนคลายความเครียดหลังจากไปเที่ยวสถานบันเทิง มีค่าเฉลี่ยสูงสุด เท่ากับ 4.26 (S.D. = 1.10) รองลงมาคือ จะแต่งกายให้ดูดีที่สุดเพื่อไปเที่ยวสถานบันเทิง มีค่าเฉลี่ยเท่ากับ 4.07 (S.D. = 1.08) และใช้เวลาในการพูดคุย พบปะกับเพื่อนฝูง ขณะอยู่ในสถานบันเทิง มีค่าเฉลี่ยเท่ากับ 4.01 (S.D. = 1.08) สำหรับข้อคำถามที่มีค่าเฉลี่ยต่ำสุด คือ ไปถึงสถานบันเทิงตั้งแต่สถานบันเทิงเปิดทำการ มีค่าเฉลี่ยเท่ากับ 2.19 (S.D. = 1.00)

4. ผลการวิเคราะห์การเปรียบเทียบความแตกต่างระหว่างค่าเฉลี่ยพฤติกรรมการเที่ยวสถานบันเทิงของนักศึกษา จำแนกตามระดับความเครียด

ตารางที่ 4 ผลการวิเคราะห์ค่าสถิติที่ใช้ในการเปรียบเทียบพฤติกรรมการเที่ยวสถานบันเทิงของนักศึกษา จำแนกตามระดับความเครียด

แหล่งความแปรปรวน	df	SS	MS	F	p
ระหว่างกลุ่ม	3	6.150	2.050	4.958	.002
ภายในกลุ่ม	396	163.728	.413		
รวม	399	169.877			

$P < 0.05$

จากตารางที่ 4 ผลการวิเคราะห์ พบว่า นักศึกษาที่มีระดับความเครียดต่างกัน มีพฤติกรรมการเที่ยวสถานบันเทิงแตกต่างกันอย่างมีนัยสำคัญทางสถิติที่ระดับ 0.05 ซึ่งผลการวิเคราะห์เป็นไปตามสมมติฐานที่ตั้งไว้ จึงนำไปทดสอบความแตกต่างเป็นรายคู่ ด้วยวิธี Games-Howell

ตารางที่ 5 การเปรียบเทียบความแตกต่างระหว่างค่าเฉลี่ยพฤติกรรมการเที่ยวสถานบันเทิงของนักศึกษา จำแนกตามระดับความเครียด

ระดับความเครียด	$\bar{X}$	เครียดน้อย	เครียดปานกลาง	เครียดสูง	เครียดรุนแรง
		1.50	2.32	2.22	2.45
เครียดน้อย	1.50		-.181	-.717	-.953*
เครียดปานกลาง	2.32			.101	-.135
เครียดสูง	2.22				-.236*
เครียดรุนแรง	2.45				

*มีนัยสำคัญทางสถิติที่ระดับ 0.05

จากตารางที่ 5 เมื่อเปรียบเทียบความแตกต่างระหว่างค่าเฉลี่ยของพฤติกรรมการเที่ยวสถานบันเทิงของนักศึกษา จำแนกตามระดับความเครียด พบว่า นักศึกษาที่มีระดับความเครียดต่างกัน มีพฤติกรรมการเที่ยวสถานบันเทิงแตกต่างกันอย่างมีนัยสำคัญทางสถิติที่ระดับ 0.05 โดยนักศึกษาในกลุ่มที่มีระดับความเครียดรุนแรง มีพฤติกรรมการเที่ยวสถานบันเทิงมากกว่า ผู้ที่มีระดับความเครียดต่ำกว่า

อภิปรายผลการวิจัย

1.ระดับความเครียดของนักศึกษาระดับปริญญาตรี มหาวิทยาลัยแห่งหนึ่งในจังหวัดภูเก็ต พบว่า นักศึกษาส่วนใหญ่มีความเครียดอยู่ในระดับรุนแรง ร้อยละ 56.50 ซึ่งสอดคล้องกับผลการศึกษาของจิราภา สีเทา (2564) ที่พบว่า นักศึกษา มหาวิทยาลัยเอกชนแห่งหนึ่งในกรุงเทพมหานคร มีความเครียดอยู่ในระดับรุนแรง ซึ่งอาจสะท้อนถึงความกดดันที่เกิดจากการเรียน การดำเนินชีวิต หรือปัจจัยอื่น ๆ ที่ส่งผลกระทบต่อสุขภาพจิต และการวิจัยในครั้งนี้ยังพบว่ามีนักศึกษาที่มีความเครียดในระดับสูง ร้อยละ 29.50 และปานกลาง ร้อยละ 11.00 ซึ่งแสดงให้เห็นว่าปัญหาความเครียดในกลุ่มตัวอย่างมีความหลากหลาย ทั้งนี้ การมีนักศึกษาอยู่ในระดับความเครียดสูงและรุนแรงเป็นจำนวนมาก ชี้ให้เห็นถึงความจำเป็นในการวางแผนและพัฒนาโปรแกรมการช่วยเหลือ เช่น การให้คำปรึกษา การจัดกิจกรรมผ่อนคลาย และการส่งเสริมการดูแลสุขภาพจิตนักศึกษาให้เหมาะสม

2.พฤติกรรมการเที่ยวสถานบันเทิงของนักศึกษาระดับปริญญาตรี มหาวิทยาลัยแห่งหนึ่งในจังหวัดภูเก็ต พบว่า นักศึกษาส่วนใหญ่มีพฤติกรรมการเที่ยวสถานบันเทิงอยู่ในระดับสูง ซึ่งไม่สอดคล้องกับผลการศึกษาของจิราภา สีเทา (2564) ที่พบว่า นักศึกษามหาวิทยาลัยเอกชนแห่งหนึ่งในกรุงเทพมหานครมีพฤติกรรมการเที่ยวสถานบันเทิงอยู่ในระดับปานกลาง ซึ่งอาจอธิบายได้จากลักษณะเฉพาะของจังหวัดภูเก็ตที่เป็นเมืองท่องเที่ยวระดับนานาชาติ ภูเก็ตมีสถานบันเทิงที่ดึงดูด ทำให้ผู้คนรู้สึกสนใจและเต็มใจใช้เวลาท่องเที่ยวทั้งกลางวันและกลางคืน อีกทั้งเศรษฐกิจที่พึ่งพาการท่องเที่ยวทำให้ภูเก็ตมีสภาพแวดล้อมที่แตกต่างจากกรุงเทพฯ ซึ่งเป็นเมืองที่เน้นการทำงานและการดำเนินชีวิตประจำวันมากกว่า และในการวิจัยครั้งนี้นักศึกษาส่วนใหญ่มักเลือกเที่ยวในวันเสาร์รองลงมาคือวันอาทิตย์ นิยมไปเที่ยวที่คาเฟ่มากที่สุด ซึ่งเป็นกิจกรรมที่ช่วยให้นักศึกษารู้สึกผ่อนคลายจากความเครียด ซึ่งสอดคล้องกับการศึกษาของอรอูรา ครุฑมณี (2564) ที่พบว่า วันที่นิยมใช้บริการสถานบันเทิงส่วนใหญ่ คือ วันหยุดสุดสัปดาห์ วันเสาร์-วันอาทิตย์ นอกจากนี้ นักศึกษาส่วนใหญ่มีค่าใช้จ่ายในการเที่ยวสถานบันเทิงต่อครั้งไม่เกิน 1,000 บาท และมักไปเที่ยวกับเพื่อนสนิทเพศเดียวกัน สะท้อนให้เห็นว่าการเที่ยวสถานบันเทิงในกลุ่มนี้ไม่ได้มุ่งเน้นไปที่การใช้จ่ายสูง แต่เน้นไปที่การผ่อนคลายและการพบปะเพื่อนฝูง ซึ่งสอดคล้องกับผลการศึกษาของพันธ์ทิพย์ พระโคตร (2557, น. 51, อ้างถึงใน จิราภา สีเทา, 2564, น. 15) ที่พบว่า นักศึกษาส่วนใหญ่ที่เคยไปเที่ยวสถานบันเทิง เนื่องจากต้องการผ่อนคลาย และมักชวนเพื่อนไปเที่ยวสถานบันเทิงด้วย

3.การเปรียบเทียบระดับความเครียดกับพฤติกรรมการเที่ยวสถานบันเทิงของนักศึกษาระดับปริญญาตรี มหาวิทยาลัยแห่งหนึ่งในจังหวัดภูเก็ต พบว่า นักศึกษาที่มีระดับความเครียดต่างกัน มีพฤติกรรมการเที่ยวสถานบันเทิงแตกต่างกัน โดยกลุ่มนักศึกษาที่มีความเครียดระดับสูงหรือรุนแรง มักมีพฤติกรรมการเที่ยวสถานบันเทิงสูงกว่ากลุ่มนักศึกษาที่มีความเครียดระดับต่ำกว่า ซึ่งสะท้อนถึงการใช้การเที่ยวสถานบันเทิงเป็นวิธีการหนึ่งในการคลายเครียดของนักศึกษา อย่างไรก็ตาม นักศึกษาที่มีระดับความเครียดต่ำกว่ามักจะมีพฤติกรรมการเที่ยวสถานบันเทิงน้อยกว่า ซึ่งอาจแสดงให้เห็นว่านักศึกษามีวิธีการจัดการกับความเครียดในรูปแบบอื่นที่ไม่จำเป็นต้องอาศัยการเที่ยวสถานบันเทิง จากการวิเคราะห์นี้ สามารถสรุปได้ว่าความเครียดมีผลต่อพฤติกรรมการเที่ยวสถานบันเทิงของนักศึกษา โดยกลุ่มที่มีความเครียดสูงมักจะเที่ยวสถานบันเทิงเพื่อคลายเครียดมากกว่ากลุ่มที่มีความเครียดต่ำ

ข้อเสนอแนะ

1. สถาบันการศึกษาควรให้คำแนะนำแนวทางจัดการและดูแลอย่างเป็นระบบ เพื่อช่วยลดความเครียดและส่งเสริมสุขภาพจิตของนักศึกษา เช่น จัดตั้งศูนย์ให้คำปรึกษาโดยมีนักจิตวิทยาหรือผู้เชี่ยวชาญทางสุขภาพจิตประจำมหาวิทยาลัย พร้อมให้คำปรึกษาและสนับสนุนทางอารมณ์ หรือเสนอแนะให้นักศึกษาเข้ารับการปรึกษาทางจิตวิทยาเป็นรายบุคคล เพื่อทำความเข้าใจสาเหตุของความเครียดและหาแนวทางจัดการ

2. ผู้ปกครอง อาจารย์ หรือผู้ที่เกี่ยวข้องควรแนะนำในการเที่ยวสถานบันเทิงที่เหมาะสมและปลอดภัย เช่น ควรเลือกสถานบันเทิงที่ไม่ล่อแหลมต่อการก่อเหตุอาชญากรรม โดยตรวจสอบสภาพแวดล้อมก่อนเข้าไปในสถานบันเทิงนั้นๆ และควรตระหนักสภาพร่างกาย จิตใจของตนเอง หากมีความเครียดควรจัดการความเครียดด้วยวิธีการอื่นๆ เช่น กายออกกำลังกาย การเข้าร่วมกิจกรรมหรือการอบรมเพื่อพัฒนาทักษะใหม่ๆ การพูดคุยหรือปรึกษาผู้อื่นหรือหลีกเลี่ยงการเที่ยวสถานบันเทิงบ่อยเกินไปเพื่อรักษาสุขภาพ

ข้อเสนอแนะในการวิจัยครั้งต่อไป

1. ควรมีการศึกษาวิจัยเชิงคุณภาพ เช่น การสัมภาษณ์เชิงลึก หรือการสนทนากลุ่มเพื่อให้ได้ข้อมูลเชิงลึกเกี่ยวกับมุมมองของนักศึกษาในการจัดการความเครียด และเหตุผลที่นักศึกษาเลือกใช้การเที่ยวสถานบันเทิงเพื่อผ่อนคลายความเครียด

2. เน้นการศึกษาเกี่ยวกับผลกระด้านสุขภาพ ด้านความปลอดภัย และด้านความเสี่ยงที่อาจเกิดขึ้นจากการเที่ยวสถานบันเทิง เช่น ปัญหาสุขภาพหรือความปลอดภัย ให้ข้อมูลป้องกันแก่นักศึกษา

3. ควรเพิ่มตัวแปรปัจจัยอื่นๆ เช่น ปัจจัยทางครอบครัว เศรษฐกิจ การสนับสนุนทางสังคมหรือสุขภาพจิต เพื่อศึกษาว่าปัจจัยเหล่านี้มีความสัมพันธ์อย่างไรกับพฤติกรรมการเที่ยวสถานบันเทิงของนักศึกษา

เอกสารอ้างอิง

กิตติศักดิ์ แก้วหาวงค์ และคณะ. (2565). *พฤติกรรมการเที่ยวสถานบันเทิงกลางคืนของนักศึกษา สาขาสังคศึกษาชั้นปีที่ 4* https://online.anyflip.com/wranf/jcui/mobile/index.html

คณะทำงานจัดทำรายงานสุขภาพคนไทยเรื่องพิเศษ. (2567). *เพราะเป็นเด็กจึงเจ็บปวด? เมื่อความเครียดไม่เลือกช่วงวัย. สุขภาพคนไทย.* สืบค้นจา www.thaihealtdhreport.com/th/articles_detail.php?id=257

จิราภา สีเทา. (2564). *อิทธิพลของกลุ่มเพื่อน ความเครียด กับพฤติกรรมการเที่ยวสถานบันเทิง ของนักศึกษา มหาวิทยาลัยเอกชนแห่งหนึ่งในกรุงเทพมหานคร* (โครงงานพิเศษโครงงานพิเศษทางจิตวิทยา 2). มหาวิทยาลัยเกษมบัณฑิต. สืบค้นจาก https://psy.kbu.ac.th/wp-content/uploads/2022/09/64-61

นิตยาพร ทองเพชร และคณะ. (2563). *4 ระดับความเครียด กับ 5 เทคนิคสร้างความสมดุลตามสูตร R E L A X*. กรมสุขภาพจิต. สืบค้นจาก https://dmh.go.th/news-dmh/view.asp?id=30438

นิตยาพร ทองเพชร และคณะ. (2563). *กรมสุขภาพจิตเผยวัยรุ่นไทยปรึกษา "ปัญหาเครียด" มากสุด แนะเทคนิคจัดการความเครียด*. กรมสุขภาพจิต. สืบค้นจาก https://dmh.go.th/news-dmh/view.asp?id=30188

นิตยาพร ทองเพชร และคณะ. (2563). *ผ่า 4 กลุ่มความเครียดที่กระทบสุขภาพ เครียดแบบเราจัดอยู่กลุ่มไหน?*. กรมสุขภาพจิต. สืบค้นจาก https://dmh.go.th/news-dmh/view.asp?id=30321

ปาลิตา ปัญญาเสน และคณะ. (2562). *พฤติกรรมการเที่ยวสถานบันเทิงและความเสี่ยงต่อสุขภาพของนักศึกษาหญิงมหาวิทยาลัยราชภัฏกำแพงเพชร*.สืบค้นจาก https://search.app/SBNkLFkZL9kwYsvh

มติชน. (2566). *หนุน 4 โซนนิ่งผับบาร์ตี 4 ในเขตเมืองภูเก็ต แต่ห่วงความปลอดภัย*. มติชน. สืบค้นจากhttps://www.matichon.co.th/region

ปาณิก เวียงชัย. (2558). *การตอบสนองทางสรีรวิทยาต่อความเครียด*. สถาบันส่งเสริมการสอนวิทยาศาสตร์และเทคโนโลยี. สืบค้นจาก http://biology.ipst.ac.th/?p=2767

วิศรุต วุฒิธรรม.(2561). *พฤติกรรมการเที่ยวสถานบันเทิงในพื้นที่อำเภอหัวหินจังหวัดประจวบคีรีขันธ์*. สืบค้นจาก https://search.app/bREd1XeVnKtzKoWh8

ศูนย์ความรู้นโยบายเด็กและครอบครัว. (2565). *เด็กและเยาวชนเครียดและมีปัญหาสุขภาพจิตมากขึ้น*. สืบค้นจาก https://kidforkids.org/child-and-family-situation-report-2022/mental-health/

สมภพ จันทร์เงิน. (2558). *พฤติกรรมการเที่ยวสถานบันเทิงกลางคืนของนักศึกษาปริญญาตรีในจังหวัดชลบุรี*. สืบค้นจาก https://search.app/NsBRkvvqDzA4a7F57

แสงนภา บารมี และคณะ. (2566). *การศึกษาระดับความเครียดและแนวทางจัดการกับความเครียดของผู้ปกครองเด็กออทิสติก ที่เข้ารับการรักษาแผนกจิตเวชเด็กและวัยรุ่น โรงพยาบาลจิตเวชนครราชสีมาราชนครินทร์*.สืบค้นจาก https://he02.tci-thaijo.org/

ฤทธิไกร ไชยงาม.(2562).*มาตรวัดเจตคติแบบลิเคิร์ท(Likert rating scales)*. สืบค้นจากhttps://search.app/AfpFWsu8GPQmgDpKA

อรอุรา ครุฑมณี. (2564). *ปัจจัยการเลือกใช้บริการสถานบันเทิงของผู้บริโภคในเขตอำเภอเมืองเพชรบรูณ์ จังหวัดเพชรบรูณ์*. สืบค้นจาก http://58.181.147.25/ojsjournal/index.php/miniconference/article/view/4210

Fuad, M. D. F., Al-Zurfi, B. M. N., AbdulQader, M. A., Abu Bakar, M. F., Elnajeh, M., & Abdullah, M. R. (2015). *Prevalence and risk factors of stress, anxiety and depression among medical students of a private medical university in Malaysia in 2015*. Education in Medicine Journal, 7(2), 62-70. https://doi.org/10.5959/eimj.v7i2.362

แผ่นแบคทีเรียลเซลลูโลสโดยเชื้อ *Komagataeibacter nataicola* TISTR 975 ผสมสารสกัดหยาบจากสมุนไพรที่มีฤทธิ์ยับยั้งเชื้อ *Staphylococcus aureus*

Bacterial Cellulose produced by *Komagataeibacter nataicola* TISTR 975 in combination with Herbal Crude Extracts against *Staphylococcus aureus*

1st Rusmira Chemache
Microbiology Program, Faculty of Science Technology and Agriculture, Yala Rajabhat University, Yala, Thailand
E-mail: 406363006@yru.ac.th

2nd Dareeya Jehmu
Microbiology Program, Faculty of Science Technology and Agriculture, Yala Rajabhat University, Yala, Thailand
E-mail: 406363011@yru.ac.th

3rd Nursahirah saising
Medical and Industrial Microbiology Program, Faculty of Science Technology and Agriculture, Yala Rajabhat University, Yala, Thailand
E-mail: 406563004@yru.ac.th

4th Tajree Mingsa
Medical and Industrial Microbiology Program, Faculty of Science Technology and Agriculture, Yala Rajabhat University, Yala, Thailand
E-mail: 406563019@yru.ac.th

5th Hatsalinda Binma-ae*
Medical and Industrial Microbiology Program, Faculty of Science Technology and Agriculture, Yala Rajabhat University, Yala, Thailand
*Corresponding author, E-mail: haslinda.b@yru.ac.th

Abstract

This research aimed to study the effectiveness of bacterial cellulose produced by *Komagataeibacter nataicola* TISTR 975 in combination with herbal crude extracts against *Staphylococcus aureus*. *Komagataeibacter nataicola* TISTR 975 was cultured to produce bacterial cellulose from mature coconut water, fermented under static conditions for 10 days at room temperature (28 ± 2 °C). Three types of herbal extracts, specifically pomegranate peel (*Punica granatum* Linn.), star gooseberry leaves (*Phyllanthus acidus* (L.)), and velvet tamarind peel (*Dialium Guineense*) were assessed for their Minimal Inhibitory Concentration (MIC) and Minimal Bactericidal Concentration (MBC) against *Staphylococcus aureus.* It was found that pomegranate peel had MIC and MBC values of 3.90 and 15.62 mg/ml, star gooseberry leaves 2.50 and 5 mg/ml, and velvet tamarind peel 0.97 and 15.56 mg/ml, respectively. The effectiveness of bacterial cellulose mixed with each herbal extract was then investigated. The results revealed that bacterial cellulose mixed with velvet tamarind peel (*Dialium guineense*) crude extract exhibited the most significant inhibition against *S. aureus*, with clear zone diameters of 25.5 ± 0.55 mm. However, bacterial cellulose combined with pomegranate peel and star gooseberry leaves did not show inhibitory effects on either of the two strains. Consequently, bacterial cellulose mixed with velvet tamarind peel extract will be used to produce medical transdermal patches in the future.

Keywords **:** *Bacterial cellulose, Herbal, Bacterial inhibition, medical transdermal patches*

I. บทนำ

พลาสติกชีวภาพ เป็นแหล่งที่น่าสนใจในการทดแทนพลาสติกที่ได้จากปิโตเลียม เนื่องจากพลาสติกชีวภาพเป็นมิตรต่อสิ่งแวดล้อม โดยได้มีการนำมาใช้ในด้านต่างๆอย่างหลากหลาย อาทิเช่น สารพวกพอลิแลกติกแอซิด (PLA) พอลิไฮดรอกซิลอัลคาโน-เอท (PHAs) พอลิคาร์โปแลคโทน (PCL) พอลิบิวธิลีนซัคซิเนต (PBS) พอลิบิวธิลีนเทอเรพธาเลต (PBT) พอลิไตรเมทธิลีนเทอเรพธาเลต (PTT) และพอลิไวนิลแอลกอฮอล์ (PVA) [1] แต่มีต้นทุนในการผลิตพลาสติกชีวภาพดังกล่าวอยู่ในราคาสูง แหล่งพลาสติกชีวภาพทางจุลินทรีย์เป็นอีกทางเลือกที่น่าสนใจ โดยเฉพาะอย่างยิ่งจากเชื้อแบคทีเรีย ที่สามารถผลิตพลาสติกชีวภาพ ที่เรียกว่า ไบโอเซลลูโลส หรือ แบคทีเรียลเซลลูโลส ซึ่งเป็นเซลลูโลสที่ได้จากแบคทีเรียมีคุณสมบัติเป็นวัสดุที่มีรูพรุน มีความยืดหยุ่นสูง มีความสามารถในการอุ้มน้ำ ดูดความชื้น และย่อยสลายได้ทางธรรมชาติ แบคทีเรียลเซลลูโลสสามารถผลิตจากแบคทีเรียได้ในหลากหลายสายพันธุ์ เช่น *Acetobacter* spp., *Rhizobium* spp., *Agrobacterium* spp. และ *Sarcina* spp. แต่ที่นิยมใช้มากที่สุด ได้แก่ *Acetobacter xylinum* [2] ซึ่งแบคทีเรียบางสายพันธุ์สามารถเลี้ยงในวัตถุดิบต้นทุนต่ำจำพวกวัสดุเศษเหลือทางการเกษตรเป็นอาหารอาหารเลี้ยงเชื้อได้ เช่น

น้ำมะพร้าว เปลือกสับปะรด เปลือกแตงโม เป็นต้น [2], [3] แบคทีเรียลเซลลูโลสสามารถนำมาประยุกต์ใช้ในอย่างหลากหลายด้าน ไม่ว่าจะเป็นการแปรรูปอาหาร การผลิตบรรจุภัณฑ์พลาสติกชีวภาพ อุตสาหกรรมยา ตลอดจนการประยุกต์ใช้ในทางการแพทย์

ปัจจุบันการใช้สมุนไพรไทยในการเป็นยารักษาโรคทางเลือกมากขึ้น เนื่องจากสมุนไพรบางชนิดเป็นทั้งอาหารและยา เป็นสารที่ได้จากธรรมชาติ ไม่ต้องซื้อหา และสามารถปลูกได้เองในบ้าน อีกทั้งสมุนไพรบางชนิดมีฤทธิ์ยับยั้งยั้งเชื้อได้ โดยเฉพาะอย่างยิ่งสามารถยับยั้งแบคทีเรีย *S. aureus* ได้ ซึ่งเชื้อนี้พบบริเวณผิวหนังและเยื่อเมือกของคนและสัตว์ เป็นสาเหตุทำให้ของการเกิดฝีแผลพุพองและเกิดการติดเชื้อหลังผ่าตัดได้ สมุนไพรที่มีฤทธิ์ยับยั้ง *S. aureus* ได้ เช่น เปลือกผลทับทิม ใบทับทิม ผลอ่อนฝรั่ง ใบฝรั่ง กระทือ เปลือกผลมังคุด และรากแก่ของแตงโม [4]

งานวิจัยนี้มีวัตถุประสงค์เพื่อศึกษาการผลิตแผ่นแบคทีเรียลเซลลูโลสโดยเชื้อ *K. nataicola* TISTR 975 ผสมสารสกัดหยาบจากสมุนไพรชนิดต่างๆ เพื่อยับยั้งแบคทีเรีย *S. aureus* ในการเป็นแนวทางการประยุกต์ในเป็นแผ่นปิดแผลชีวภาพที่สามารถยับยั้งการอักเสบจากเชื้อและสามารถสมานแผลได้ อีกทั้งเป็นการสนับสนุนการนำสมุนไพรไทยมาใช้ให้เกิดประโยชน์มากขึ้นด้วย

II. ทบทวนวรรณกรรม

แบคทีเรียลเซลลูโลส (Bacterial cellulose) หรือ วุ้นสวรรค์ (Nata de coco) เป็นผลผลิตที่ได้จากการหมักโดยใช้เชื้อแบคทีเรีย โดยเส้นใยหรือชั้นของแบคทีเรียลเซลลูโลสที่เชื้อแบคทีเรียดังกล่าว ที่สร้างขึ้นมาประกอบด้วยโพลีแซคคาไรด์ที่ต่อกันด้วยพันธะ β-1,4-glycosidic- bond เป็นโพลีเมอร์ของเซลลูโลส (Cellulose) ที่สามารถผลิตจากแบคทีเรียได้นอกจากที่ได้จากพืช แบคทีเรียลเซลลูโลสมีคุณสมบัติเฉพาะ เช่น มีความบริสุทธิ์สูง สามารถดูดซับน้ำได้ดี ปริมาณของผลึก การเกิดพอลิเมอร์ไรเซชั่นและความแข็งแรงที่มากกว่าเซลลูโลสจากพืช ([5] พบได้ในแบคทีเรียหลายชนิดที่สามารถผลิตเซลลูโลส ได้แก่ *Gluconobacter xylinus, Acetobacter xylinum, A. xylinum* TISTR 975 และ *Komagataeibacter xylinus* 10245 เป็นต้น ([6], [7], [2], [8] ซึ่งการผลิตแบคทีเรียลเซลลูโลสนั้นจะต้องมีแหล่งคาร์บอนเพื่อใช้ในกระบวนการหมัก ได้แก่ น้ำตาลชนิดต่างๆ ไม่ว่าจะเป็นกลูโคส ซูโครส มอลโตส กาแลคโตส ไซโลส เป็นต้น แต่มีข้อเสียในเรื่องของราคาที่ค่อนข้างมีราคาแพง จึงมีความพยายามที่จะลดต้นทุนในการผลิตโดยการใช้วัตถุดิบที่หาได้ง่าย อย่างเช่นผลผลิตทางการเกษตรเป็นแหล่งคาร์บอน ได้แก่ แอปเปิ้ล องุ่น ส้ม เผือก แครอท มันฝรั่ง น้ำมะพร้าว [9], [2] แก้วมังกรพันธุ์เนื้อสีแดง [10] น้ำตาลโตนด [11] น้ำมะม่วง [12] เป็นต้น ซึ่งอุตสาหกรรมการผลิตแบคทีเรียลเซลลูโลสในประเทศไทยส่วนใหญ่จะใช้น้ำมะพร้าวเป็นวัตถุดิบในการผลิตหลัก [2] และในปัจจุบันทั้งในต่างประเทศและประเทศไทยมีการศึกษาการใช้วัตุดิบเศษเหลือทิ้งมาใช้การผลิตแผ่นแบคทีเรียลเซลลูโลสในการลดต้นทุน อีกทั้งเป็นการนำของเสียมาใช้ให้เกิดประโยชน์ตลอดจนสามารถกำจัดของเสียที่เกิดจากกระบวนการได้อีกด้วย เช่น น้ำคั้นเปลือกสับปะรด [2] เปลือกแตงโม [3] น้ำทิ้งจากโรงงานแปรรูปสับปะรด [13] กากน้ำตาล [14] เป็นต้น

ในประเทศไทยมีพืชสมุนไพรหลากหลายชนิดที่สามารถยับยั้งการเจริญของแบคทีเรีย โดยเฉพาะอย่างยิ่งเชื้อแบคทีเรีย *S. aureus* ซึ่งเป็นแบคทีเรียประจำถิ่นที่เจริญเติบโตบนผิวหนังและเยื่อเมือกมนุษย์ได้ *S. aureus* อยู่ในจีนัส *Staphylococcus* เป็นเชื้อแบคทีเรีย แกรมบวก มักจะสร้างโคโลนีที่มีสีเทาถึงสีเหลืองทอง ให้ผล coagulase เป็นบวกซึ่งแตกต่างกันจากสปีชีส์อื่นในจีนัสเดียวกัน และมักจะก่อโรคในมนุษย์เป็นหลัก มีความรุนแรงที่หลากหลายตั้งแต่ทำให้เกิดโรคอาหารเป็นพิษ หรือติดเชื้อที่ผิวหนัง จนกระทั่งรุนแรงถึงชีวิตได้ [15] เมื่อผิวหนังของมนุษย์เกิดบาดแผลแล้วมีการติดเชื้อจากแบคทีเรียดังกล่าวทำให้มีอาการอักเสบของแผล บวม พอง รักษาโดยการใช้ยาปฏิชีวนะได้ แต่การใช้ยาปฏิชีวนะอาจจะทำให้เกิดการดื้อยาสารตกค้างของยาในร่างกายได้ [16] จึงทำให้มีการนำสารสกัดจากสมุนไพรที่มีฤทธิ์ยับยั้งเชื้อมาใช้ในการรักษา เนื่องจากมีเป็นสารสกัดจากธรรมชาติทำให้ผู้ใช้ปลอดภัย ปัจจุบันมีการศึกษาสารสกัดจากสมุนไพรที่มีฤทธิ์ยับยั้งเชื้อมากขึ้น โดยเฉพาะเชื้อแบคทีเรีย *S. aureus* เช่น สารสกัดจากใบชะพลู [15] เปลือกและใบของผลทับทิม [4] เนื้อมะขามป้อมและใบพุดศุภโชค [17] เปลือกลูกหยี [18] ใบมะยม [19] เปลือกมังคุด [20] เป็นต้น

การรักษาบาดแผลที่เกิดขึ้นมาสามารถรักษาได้ด้วยยาและสารเคมี ซึ่งการใช้สารเคมีบางชนิดรักษามีข้อเสีย คือสามารถสะสมสารเคมีในร่างกายได้ ปัจจุบันจึงได้มีการศึกษาและพัฒนาวิธีการรักษาบาดแผลที่เกิดขึ้น โดยใช้แผ่นปิดแผลจากชีววัสดุธรรมชาติที่บรรจุสารสกัดจากธรรมชาติ เนื่องจากเป็นมิตรกับร่างกาย (Biocompatibility) และสามารถกระตุ้นการซ่อมแซมเนื้อเยื่อได้ดีกว่าชีววัสดุสังเคราะห์ [21] โดยเฉพาะอย่างยิ่งการนำแบคทีเรียลเซลลูโลสซึ่งเป็นชีววัสดุธรรมชาติมาสารสกัดจากธรรมชาติในการยับยั้งจุลินทรีย์ จากการศึกษาแบคทีเรียลเซลลูโลสจากเชื้อแบคทีเรีย *A. xylinum* ที่ประกอบด้วยสารสกัดจากเปลือกทับทิมด้วยเอธานอลร้อยละ 50 (PPE50E) ซึ่งฤทธิ์ฆ่าเชื้อแบคทีเรีย *Staphylococcus aureus*, *Staphylococcus epidermidis* และ *Propionibacterium acne* และยังมีสามารถยับยั้ง *P. acne* ได้ดีที่ความเข้มข้น 5 และ 10 มิลลิกรัมต่อมิลลิตร มีวงใสขนาด 27.7 และ 35.5 มิลลิเมตร ตามลำดับ ซึ่งใกล้เคียงกับตัวควบคุมเชิงบวกของคลินดาไมซิน (45.5 มิลลิเมตร) [22] นอกจากนี้มีการศึกษาแบคทีเรียลเซลลูโลสจากเชื้อแบคทีเรีย *G. xylinus* ผสมสารสกัดเปลือกมังคุด พบว่า มีประสิทธิภาพในการยับยั้งการเจริญเติบโตของเชื้อ *S. epidermidis* ซึ่งเป็นสาเหตุหนึ่งที่ทำให้เกิดสิวอักเสบได้ [21]

III. ระเบียบวิธีวิจัย

1. จุลินทรีย์ที่ใช้ทดสอบ

เชื้อแบคทีเรีย *Komagataeibacter nataicola* TISTR 975 กล้าเชื้อแบคทีเรียจากสถาบันวิจัยวิทยาศาสตร์และเทคโนโลยีแห่งประเทศไทย (วว.) ชื่อสายพันธุ์เดิมก่อนปี พ.ศ. 2561 คือ *Acetobacter xylinum* TISTR 975 ส่วนเชื้อ แบคทีเรีย *Staphylococcus aureus* ได้รับความ

อนุเคราะห์จากหลักสูตรจุลชีววิทยาทางการแพทย์และอุตสาหกรรม คณะวิทยาศาสตร์เทคโนโลยีและการเกษตร มหาวิทยาลัยราชภัฏยะลา

2. การสกัดสารสกัดสมุนไพร

2.1 การเตรียมตัวอย่างพืชสมุนไพร

นำสมุนไพร 3 ชนิด ได้แก่ ทับทิม (*Punica granatum* Linn.) ใช้ส่วนเปลือกผล มะยม (*Phyllanthus acidus* (L.)) ใช้ส่วนของใบ และลูกหยี (*Dialium guineense*) ใช้ส่วนเปลือกผล นำมาล้างทำความสะอาด หั่นเป็นชิ้นเล็กๆ อบให้แห้งที่อุณหภูมิ 45±2 องศาเซลเซียส ส่วนเปลือกลูกหยีนำมาผึ่งในที่ร่มให้แห้ง เป็นเวลา 7 วัน บดให้เป็นชิ้นเล็กๆ หรือจนละเอียด

2.2 การสกัดพืชสมุนไพร

นำตัวอย่างสมุนไพร 3 ตัวอย่างมาทำการสกัด โดยนำเปลือกทับทิมแช่ในเอทานอลร้อยละ 95 [4] ใบมะยมแช่ในเอทานอลร้อยละ 95 [19] และเปลือกลูกหยีมาสกัดด้วยอะซิโตน [18] จะได้สารสกัดในรูปสารสกัดหยาบ (crude extract) ของทั้งสามตัวอย่างแล้วนำมาเก็บตัวอย่างที่จะใช้ทดสอบเก็บไว้ที่ -20 องศาเซลเซียส เพื่อนำไปใช้ในการทดลองต่อไป

3. การทดสอบด้วยวิธี Broth dilution test ของสารสกัดหยาบจากสมุนไพร [20]

3.1 ความเข้มข้นต่ำสุดที่สามารถยับยั้งเชื้อ (Minimal inhibitory Concentration, MIC) นำเชื้อแบคทีเรีย *S. aureus* ทดสอบกับสารสกัดหยาบจากเปลือกทับทิม ใบมะยม และเปลือกลูกหยี โดยที่ความเข้มข้นของเปลือกทับทิมและเปลือกลูกหยี เท่ากับ 0.97, 1.95, 3.90, 7.81, 15.62, 31.25, 62.5, 125 250 และ 500 มิลลิกรัมต่อมิลลิลิตร ส่วนใบมะยมที่ความเข้มข้น เท่ากับ 0.07, 0.15, 0.31, 0.62, 1.25, 2.5, 5, 10, 20 และ 40 มิลลิกรัมต่อมิลลิลิตร ใน 96 Well Plate แล้วทำการบ่มแต่ละตัวอย่างที่อุณหภูมิ 37 องศาเซลเซียส เป็นเวลา 24 ชั่วโมง จากนั้นทำการบันทึกผลการทดลอง [20]

3.2 ความเข้มข้นต่ำสุดที่สามารถฆ่าเชื้อได้ (Minimal bactericidal Concentration, MBC) โดยสังเกตหลุมที่ไม่มีการเจริญของเชื้อข้อ 3.1 นำมา Spread plate บนอาหารเลี้ยงเชื้อ บ่มที่อุณหภูมิ 37 องศาเซลเซียส เป็นเวลา 24 ชั่วโมง ถ้าไม่พบการเจริญของแบคทีเรียแสดงว่าความเข้มข้นดังกล่าว คือ ค่า Minimum bactericidal concentration (MBC) [20]

4. การผลิตแผ่นแบคทีเรียลเซลลูโลส

4.1 เตรียมกล้าเชื้อเริ่มต้นกล้าเชื้อแบคทีเรีย *K. nataicola* TISTR ในอาหารที่ประกอบด้วยน้ำมะพร้าวแก่มากรองด้วยผ้าขาวบาง เติมน้ำตาลซูโครสร้อยละ 5 แอมโมเนียมซัลเฟตร้อยละ0.5 และกรดอะซิติกร้อยละ 1 เพื่อปรับพีเอชให้เท่ากับ 4.5 แล้วนำไปบ่มที่อุณหภูมิห้อง 28±2 องศาเซลเซียส เป็นเวลา 7 วัน จากนั้นทำการกระตุ้นการเจริญของเชื้อ โดยนำเชื้อ *K. nataicola* TISTR 975 ร้อยละ 10 โดยปริมาตรเติมลงในสูตรอาหารเดิมที่เตรียมใหม่ บ่มที่อุณหภูมิห้อง 28±2 องศาเซลเซียสเป็นเวลา 7 วัน นำ *K. nataicola* TISTR 975 ที่ได้ไปเป็นกล้าเชื้อเริ่มต้นในการทดลองต่อไป

4.2 การผลิตแผ่นแบคทีเรียลเซลลูโลส นำมะพร้าวแก่มากรองด้วยผ้าขาวบาง แล้วนำมาไปต้มจนเดือด เติมน้ำตาลซูโครสร้อยละ 5 และแอมโมเนียมซัลเฟตร้อยละ 0.5 วางทิ้งไว้ให้เย็นในถาดที่ผ่านการฆ่าเชื้อแล้ว หลังจากนั้นเติมกรดอะซิติกร้อยละ 1 โดยปริมาตร เพื่อปรับพีเอชให้เท่ากับ 4.5 เติมกล้าเชื้อ *K. nataicola* TISTR 975 ร้อยละ 10 โดยปริมาตร บ่มที่อุณหภูมิห้อง 28±2 องศาเซลเซียส ในสภาะนิ่ง เป็นเวลา 10 วัน [24] วัดความหนาของแผ่นแบคทีเรียลเซลลูโลสทุกวัน นำแบคทีเรียลเซลลูโลสที่ได้มาลอกเส้นยออกจากนั้นนำไปต้มในน้ำกลั่น และเปลี่ยนน้ำกลั่นทุกๆ 15 นาที จนกว่าจะได้ค่า pH เท่ากับ 7-8 นำแผ่นแบคทีเรียลเซลลูโลสที่ได้ไปศึกษาต่อไป

5. การทดสอบประสิทธิภาพของแบคทีเรียลเซลลูโลสผสมสารสกัดหยาบ

5.1 การเตรียมแบคทีเรียลเซลลูโลสผสมสารสกัด

ตัดแผ่นแบคทีเรียลเซลลูโลสให้เป็นวงกลมขนาดเส้นผ่านศูนย์กลาง 6 มิลลิเมตร [16] จากนั้นนำแผ่นแบคทีเรียลเซลลูโลสที่ตัดแล้วมาทำให้ปราศจากเชื้อที่อุณหภูมิ 121 องศาเซลเซียส เป็นเวลา 15 นาที และนำแผ่นแบคทีเรียลเซลลูโลสที่ได้มาหยดสารสกัดหยาบจากเปลือกทับทิม ใบมะยม และเปลือกลูกหยี โดยเลือกความเข้มข้นของสารสกัดหยาบทั้งสามมากกว่าค่า MBC เพิ่มไปอีก 5 10 15 เท่า โดยแต่ละความเข้มข้นใช้ปริมาตร 100 ไมโครลิตร หยดบนแผ่นแบคทีเรียลเซลลูโลส จากนั้นนำไปบ่มที่อุณหภูมิห้อง (28±2 องศาเซลเซียส) เป็นเวลา 24 ชั่วโมง เพื่อให้สารถูกดูดซึมเข้าไปในตัวแผ่นแบคทีเรียลเซลลูโลสก่อนนำไปทดสอบการยับยั้งแบคทีเรียในขั้นตอนต่อไป [23]

5.2 การทดสอบประสิทธิภาพของแผ่นแบคทีเรียลเซลลูโลสผสมสารสกัดหยาบด้วยวิธี disc agar diffusion

ทำการเพาะเลี้ยง *S. aureus* ในอาหาร nutrient broth (NB) บ่มที่อุณหภูมิ 37 องศาเซลเซียส เป็นเวลา 18-24 ชั่วโมง แล้วทำการปรับความขุ่นให้มีค่าเท่ากับ McFarland No. 0.5 นำไม้พันสำลีที่ปราศจากเชื้อมาจุ่มลงในเชื้อที่ปรับความขุ่นแล้ว swab ลงบนอาหารเลี้ยงเชื้อ nutrient agar (NA) จากนั้นวางแผ่นแบคทีเรียลเซลลูโลสที่ผสมสารสกัดหยาบทั้ง 3 ชนิด ได้แก่ แผ่นแบคทีเรียลเซลลูโลสที่ผสมสารสกัดหยาบเปลือกทับทิม แผ่นแบคทีเรียลเซลลูโลสที่ผสมสารสกัดหยาบใบมะยม แผ่นแบคทีเรียลเซลลูโลสที่ผสมหยาบเปลือกลูกหยี แผ่นแบคทีเรียลเซลลูโลสที่ผสมยาปฏิชีวนะให้เป็นตัวควบคุมบวก และแผ่นแบคทีเรียลเซลลูโลสที่ผสมน้ำกลั่นให้เป็นตัวควบคุมลบ จำนวนแผ่นละ 100 ไมโครลิตร วางตรงกลางอาหารเลี้ยงเชื้อ NA นำไปบ่มที่อุณหภูมิ 37 องศาเซลเซียส เป็นเวลา 24 ชั่วโมง ตรวจผลการต้านเชื้อโดยการนำมาวัดเส้นผ่านศูนย์กลางของบริเวณยับยั้ง และบันทึกผลการทดลองโดยทดสอบทั้งหมด 3 ซ้ำ [23]

IV. ผลการทดลอง

1. ร้อยละของผลผลิตของสมุนไพร

จากการสกัดสมุนไพร ได้แก่ เปลือกทับทิม, ใบมะยม และเปลือกลูกหยี พบว่า สารสกัดหยาบจากเปลือกทับทิมที่ได้มีลักษณะเหนียวหนืด มีสีน้ำตาลเข้ม มีร้อยละผลผลิต (% yield) มีค่าเท่ากับ 3.36 ส่วนสารสกัดหยาบจากใบมะยมที่ได้มีลักษณะเหนียวหนืด มีสีเขียวขี้ม้าเข้ม มีร้อยละผลผลิตเท่ากับ 4.40

และสารสกัดหยาบจากเปลือกลูกหยี ที่ได้มีลักษณะเหนียวหนืด มีสีดำน้ำตาล มีร้อยละผลผลิต เท่ากับ 1.63

2. ความเข้มข้นต่ำสุดที่สามารถยับยั้งเชื้อ (Minimal inhibitory Concentration, MIC) **และ การหาค่าความเข้มข้นต่ำสุดที่สามารถฆ่าเชื้อได้** (Minimal bactericidal Concentration, MBC) **โดยวิธี** broth dilution test

สารสกัดหยาบสมุนไพรจำนวน 3 ชนิด ได้แก่ เปลือกทับทิม ใบมะยม และเปลือกลูกหยี พบว่าค่า MIC ของเชื้อ *S. aureus* ของสารสกัดจากเปลือกทับทิม เท่ากับ 3.90 มิลลิกรัมต่อมิลลิลิตร ส่วนค่า MBC เท่ากับ 15.62 ส่วนสารสกัดใบมะยม พบว่ามีค่า MIC เท่ากับ 2.50 มิลลิกรัมต่อมิลลิลิตร และ ส่วนค่า MBC เท่ากับ 5 มิลลิกรัมต่อมิลลิลิตร และสารสกัดเปลือกลูกหยี พบว่า มีค่า MIC เท่ากับ 0.97 มิลลิกรัมต่อมิลลิลิตร ส่วนค่า MBC เท่ากับ 15.56 มิลลิกรัมต่อมิลลิลิตร ดังตารางที่ 1

TABLE 1 Minimal inhibitory concentration (MIC) and Minimal bactericidal Concentration (MBC) of herbal crude extracts against *Staphylococcus aureus*

herbal crude extracts	Part used	MIC (mg/mL)	MBC (mg/mL)
Punica granatum	peels	3.90	15.56
Phyllantus acidus	leaves	2.50	5
Dialium guineense	peels	0.97	15.56

3. การผลิตแผ่นแบคทีเรียลเซลลูโลส

จากการผลิตแผ่นแบคทีเรียลเซลลูโลสด้วยน้ำมะพร้าวแก่ โดยเชื้อ *K. nataicola* TISTR 975 พบว่า ลักษณะของแผ่นแบคทีเรียลเซลลูโลสมีลักษณะเป็นแผ่นเป็นสีขาว ผิวเรียบ มันวาว และเนื้อแผ่นแน่น เมื่อได้ทำการศึกษาความหนาของแผ่นแบคทีเรียลเซลลูโลสจากการเจริญของ *K. nataicola* TISTR 975 พบว่า ในช่วงการเจริญของเชื้อในวันที่ 1 เกิดแผ่นแบคทีเรียลเซลลูโลสบาง ความหนาเท่ากับ 2.3±0.83 มิลลิเมตร และเพิ่มขึ้นเรื่อยๆจนวันที่ 10 ของการเจริญมีความหนาเท่ากับ 13.6±0.75 มิลลิเมตร ดังภาพที่ 1

4. ประสิทธิภาพของแบคทีเรียลเซลลูโลสผสมสารสกัดหยาบ

จากการทดสอบประสิทธิภาพของแบคทีเรียลเซลลูโลสผสมสารสกัดหยาบจำนวน 3 ชนิด ได้แก่ แบคทีเรียลเซลลูโลสผสมสารสกัดหยาบเปลือกทับทิม แบคทีเรียลเซลลูโลสผสมสารสกัดหยาบใบมะยม และแบคทีเรียลเซลลูโลสผสมสารสกัดหยาบเปลือกลูกหยี ในความเข้มข้นที่มากกว่าค่า MBC พบว่า ที่ความเข้มข้น 15 เท่าของ MBC มีเส้นผ่านศูนย์กลางของวงใสเท่ากับ 25.5±0.05 มิลลิเมตร ดังภาพที่ 2 ส่วนแผ่นแบคทีเรียลเซลลูโลสผสมสารสกัดหยาบเปลือกทับทิม และแบคทีเรียลเซลลูโลสผสมสารสกัดหยาบจากใบมะยมไม่มีฤทธิ์ในการยับยั้งเชื้อ *S. aureus* ได้ สำหรับแผ่นแบคทีเรียลเซลลูโลสผสม

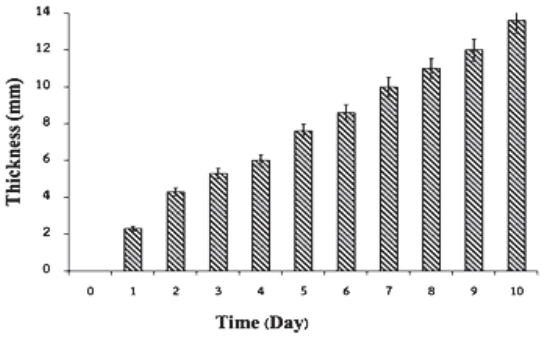


Fig. 1. Thickness of bacterial cellulose produced by *Komagataeibacter nataicola* TISTR 975 in mature coconut water at 28±2 °C for 10 days

ยาปฏิชีวนะ tetracycline ของเชื้อ *S. aureus* มีขนาดเส้นผ่านศูนย์กลางของวงใส 43.5±0.20 มิลลิเมตร และแบคทีเรียลเซลลูโลสผสมน้ำกลั่นไม่มีฤทธิ์ในการยับยั้งเชื้อ *S. aureus* เช่นกัน

V. อภิปรายผล

จากการศึกษาการสกัดสารสกัดหยาบจำนวน 3 ชนิดของสมุนไพร ได้แก่ เปลือกทับทิม ใบมะยม และเปลือกลูกหยี พบว่า มีร้อยละผลผลิต เท่ากับ 3.36 4.40 และ 1.63 ตามลำดับ จากการรายงานการสกัดเปลือกลูกหยี ด้วยอะซิโตน พบว่าค่าร้อยละผลผลิต เท่ากับ 1.04 [18] ซึ่งจะเห็นได้ว่าสารสกัดหหยาบจากเปลือกลูกหยีในการศึกษาครั้งนี้มีร้อยละผลผลิตมากกว่า และเมื่อนำสารสกัดหยาบทั้งสามสมุนไพรมาศึกษาค่าความเข้มข้นต่ำสุดที่สามารถยับยั้งเชื้อ (MIC) และ การหาค่าความเข้มข้นต่ำสุดที่สามารถฆ่าเชื้อได้ (MBC) พบว่า MIC ของเชื้อ *S. aureus* ของสารสกัดหยาบจากเปลือกทับทิม เท่ากับ 3.90 มิลลิกรัมต่อมิลลิลิตร ส่วนค่า MBC เท่ากับ 15.62 ส่วนสารสกัดหยาบใบมะยม พบว่ามีค่า MIC ของเชื้อ *S. aureus* เท่ากับ 2.50 มิลลิกรัมต่อมิลลิลิตร และส่วนค่า MBC เท่ากับ 5 มิลลิกรัมต่อมิลลิลิตร และสารสกัดหยาบเปลือกลูกหยี พบว่า มีค่า MIC เท่ากับ 0.97 มิลลิกรัมต่อมิลลิลิตร ส่วนค่า MBC เท่ากับ 15.56 มิลลิกรัมต่อมิลลิลิตร ซึ่งจากการศึกษาครั้งนี้สารกสัดเปลือกทับทิม ค่า MIC ในการยับยั้งเชื้อ *S. aureus* ต่ำกว่าจากรายงานการวิจัยที่ศึกษาฤทธิ์ยับยั้งแบคทีเรียของสารสกัดเปลือกทับทิม มีฤทธิ์ยับยั้งเชื้อ *S. aureus* มีค่า MIC และ MBC เท่ากับ 15.62 และ 31.25 มิลลิกรัมต่อมิลลิลิตร ตามลำดับ [4] ส่วนสารสกัดจากใบมะยมด้วยเอทานอลในการศึกษาครั้งนี้ มีค่า MIC และ MBC ต่ำกว่าจากรายงานการวิจัยที่ศึกษาฤทธิ์ยับยั้งแบคทีเรียของสารสกัดในมะยมด้วยเอทานอล โดยมีค่า MIC และ MBC เท่ากับ 250 และ 500 มิลลิกรัมต่อมิลลิลิตร ตามลำดับ [25] ซึ่งอาจจะเกิดจากสารสกัดสมุนไพรทั้งสามที่เอามาศึกษาต่างสายพันธุ์ หรือระยะเวลาในการเก็บต่างกัน อาจจะส่งผลทำให้ผลที่ได้ไม่สอดคล้องกัน

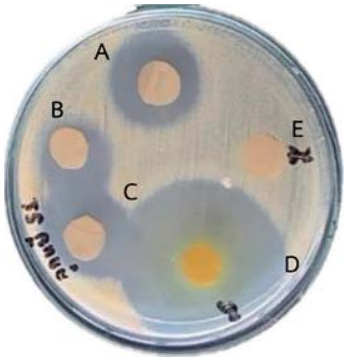


Fig. 2. An example of the inhibition zone of bacterial cellulose produced by *Komagataeibacter nataicola* TISTR 975 in combination with velvet tamarind peel (*Dialium guineense*) crude extracts against *Staphylococcus aureus*. A,B,C: Bacterial cellulose in combination with velvet tamarind peel (*Dialium guineense*) crude extracts D: Bacterial cellulose in combination with Tetracycline E: Bacterial cellulose in combination with Distilled water

หลังจากนั้นทำการผลิตแผ่นแบคทีเรียลเซลลูโลสในน้ำมะพร้าวแก่ โดยเชื้อแบคทีเรีย *K. nataicola* TISTR 975 พบว่า แผ่นมีสีขาว ผิวเรียบ มันวาว และเนื้อแผ่นแน่น เมื่อได้ทำการศึกษาความหนาของแผ่นแบคทีเรียลเซลลูโลสในวันที่ 10 ของการเจริญมีความหนาเท่ากับ 13.6±0.75 มิลลิเมตร ซึ่งมีความใกล้เคียงของการศึกษาผลิตแผ่นแบคทีเรียลเซลลูโลส โดยใช้เชื้อแบคทีเรีย *K. nataicola* TISTR 975 จากวัสดุเศษเหลือทางการเกษตรต้นทุนต่ำ ได้แก่ น้ำจากเปลือกแตงโม น้ำจากซังข้าวโพด น้ำจากซังกาบอ้อย น้ำจากผักตบชวา และน้ำมะพร้าวแก่ พบว่า ในวันที่ 10 ของการเจริญในน้ำมะพร้าวแก่ มีความหนาเท่ากับ 15.1 มิลลิเมตร และเมื่อนำแบคทีเรียลเซลลูโลสดังกล่าวมาศึกษาต่อพบว่า มีค่า Tensile strength เท่ากับ 37.8 MPa ค่าความยืดตัว ณ จุดขาด (Elongation at break) เท่ากับร้อยละ 39 และค่าการสลายทางความร้อนที่อุณหภูมิ 300 องศาเซลเซียส แล้วนำแบคทีเรียลเซลลูโลสที่ได้มาลอกเส้นยออก จากนั้นนำไปต้มในน้ำกลั่น จนกว่าจะได้ค่า pH เท่ากับ 7-8 แล้วนำไปอบที่อุณหภูมิ 50 องศาเซลเซียส เป็นเวลา 2 วันหรือจนภาชนะแห้ง ทำการตัดแผ่นแบคทีเรียลเซลลูโลสให้เป็นวงกลม จากนั้นนำแผ่นแบคทีเรียลเซลลูโลสที่ตัดแล้วมาทำให้ปราศจากเชื้อที่อุณหภูมิ 121 องศาเซลเซียส เป็นเวลา 15 นาที และนำแผ่นแบคทีเรียลเซลลูโลสที่ได้มาหยดสารสกัดหยาบจากเปลือกทับทิม เปลือกลูกหยี และการทดสอบประสิทธิภาพของแผ่นแบคทีเรียลเซลลูโลสผสมสารสกัดหยาบทั้งสามสมุนไพรด้วยวิธี agar disc diffusion พบว่า แผ่นแบคทีเรียลเซลลูโลสผสมสารสกัดหยาบเปลือกลูกหยี ที่ความเข้มข้น 250 มิลลิกรัมต่อมิลลิตร มีฤทธิ์ในการยับยั้งเชื้อ *S. aureus* ได้ มีเส้นผ่านศูนย์กลางของวงใสเท่ากับ 25.5±0.05 มิลลิเมตร ซึ่งมีความใกล้เคียงกับรายงานการศึกษาแบคทีเรียลเซลลูโลสจากแบคเรีย *G. xylinus* ผสมสารสกัดหยาบจันทร์แดง 3 สูตร ได้แก่ สูตรความเข้มข้น 5 (F1) 10 (F2) และ 15 (F3) มิลลิกรัมต่อมิลลิลิตร พบว่าสูตร F3 ที่มีความเข้มข้น 15 มิลลิกรัมต่อมิลลิลิตร มีฤทธิ์ยับยั้ง *S. aureus* ดีที่สุด มีเส้นผ่านศูนย์กลางของวงใสเท่ากับ 19±1.00 มิลลิเมตร หลังการเก็บรักษาไว้ 1 เดือน [23] ส่วนแผ่นแบคทีเรียลเซลลูโลสผสมสารสกัดหยาบเปลือกทับทิม และแบคทีเรียลเซลลูโลสผสมสารสกัดหยาบจากใบมะยมไม่มีฤทธิ์ในการยับยั้งเชื้อ *S. aureus* ได้ ดังตารางที่ 2

TABLE 2 Efficiency of bacterial cellulose produced by *Komogataeibacter nataicola* TISTR 975 in combination with herbal crude extracts against *Staphylococcus aureus*

herbal crude extracts	Part used	Times	The average Diameter of inhibition zone (mm)
Punica granatum Linn.	peels	5	NI
		10	NI
		15	NI
Phyllantus acidus	leaves	5	NI
		10	NI
		15	NI
Dialium Guineense	peels	5	NI
		10	NI
		15	25.5±0.05
Tetracycline	-	-	43.5±0.20

NI : Non-inhibition zone

VI. ข้อสรุป

งานวิจัยนี้ศึกษาเกี่ยวกับการผลิตแผ่นแบคทีเรียลเซลลูโลสโดยเชื้อ *Komagataeibacter nataicola* TISTR 975 จากน้ำมะพร้าวแก่ และศึกษาฤทธิ์ต้านเชื้อ *Staphylococcus aureus* ของแบคทีเรียลเซลลูโลสผสมสารสกัดสมุนไพร ได้แก่ เปลือกทับทิม ใบมะยม และเปลือกลูกหยี พบว่า แผ่นแบคทีเรียลเซลลูโลสผสมสารสารสกัดเปลือกลูกหยีมีฤทธิ์ในการยับยั้งเชื้อ *S. aureus* โดยมีขนาดเส้นผ่านศูนย์กลางวงใสเท่ากับ 25.5±0.55 มิลลิเมตร ส่วนแบคทีเรียลเซลลูโลสผสมสารสกัดเปลือกทับทิมและใบมะยม ไม่มีฤทธิ์ในการยับยั้งเชื้อ และควรศึกษาฤทธิ์ของสารสกัดสมุนไพรที่หลากหลาย และมาประยุกต์ผสมกับแบคทีเรียลเซลลูโลสให้มากขึ้นเนื่องจากปัจจุบันชีววัสดุธรรมชาติอย่างแบคทีเรียลเซลลูโลสได้รับความสนใจและถูกนำไปใช้เป็นชีววัสดุทางการแพทย์มากขึ้น ดังนั้นจึงมีแนวโน้มที่จะสามารถนำแผ่นแบคทีเรียลเซลลูโลสผสมสารสกัดเปลือกลูกหยีมาผลิตชีววัสดุทางการแพทย์ต่อไป

อ้างอิง

[1] Paoprasert, P. (2013). Polymers from biological sources: A Literature Review. KKU Res. J, 18(3), 536-547. (in Thai)

[2] Jaturapiree, A., Chaichana, E., Saowapark, T., Chuenpraphai, B. & Jaturapiree, P. (2019). Production and characterization of bacterial cellulose produced by *Acetobacter xylinum* TISTR 975 from pineapple peel juice. RMUTP Research Journal, 13(1), 180-192. (in Thai)

[3] Ochaikul, D. (2020). Optimization of Bacterial Cellulose Production from Watermelon Rind by *Komagataeibacte*r sp. PAP1. SWU Sci. J., 36 (1), 180-192. (in Thai)

[4] Meesup, P. & Buachard, S. (2018). Efficiency of plant extracts against *Staphylococcus aureus* and *Escherichia coli*. Agricultural Sci. J. 49(2) (Suppl.): 485-488. (in Thai)

[5] Dayal, M. S., N. Goswami, A. Sahai, V. Jain, G. Mathur & A. Mathur. (2013). Effect of media components on cell growth and bacterial cellulose production from *Acetobacter aceti* MTCC 2623. Carbohydrate Polymers. 94, 12-16.

[6] Dikshit & Kim, 2020: Dikshit, P.K. & Kim, B.S. (2020). Bacterial cellulose production from biodiesel-derived crude glycerol, magnetic functionalization, and its application as carrier for lipase immobilization. International Journal of Biological Macromolecules, 153, 902–911.

[7] Li et al., 2017: Li. G., Nandgaonkar, A. G., Habibi, Y., Krause, W.E., Wei, Q. & Lucia, L.A. (2017). An environmentally benign approach to achieving vectorial alignment and high microporosity in bacterial cellulose/chitosan scaffolds. RSC Adv.,7, 13678-13688.

[8] Schröpfer et al., 2015: Schröpfer, S.B., Bottene,M. K., Bianchin, L., Robinson, L. C. Lima, V.D., Jahno, V.D. Barud, H.D.S. & Ribeiro, S.J.L. (2015). Biodegradation evaluation of bacterial cellulose, vegetable cellulose and poly (3-hydroxybutyrate) in soil. Polímeros, 25(2), 154-160.

[9] Maichan, W., Kammanglakan, P., Sudpruek, S., Prudprom, K., Anchana, C., Pongpanich, J., & Laloknam, S.(2012). Production of bacterial cellulose by *Acetobacter xylinum* TISTR086 using agricultural products as carbon sources. J. Res. Unit Sci. Technol. Environ. 3(2), 92-97. (in Thai)

[10] Dejsungkranont, M. (2018). A study on the optimum condition for bacterial cellulose production from red dragon fruit (*Hylocereus polyrhizus* (Weber) Britton & Rose) using response surface methodology. KHONKAEN AG R.J. 46 (2), 213-226. (in Thai)

[11] Laochareonsuk, T. & Kaewtaro, S. (2005). The optimal conditions for nata production from sugar palm syrup by *Acetobacter xylinum* TISTR 107. Songklanakarin J. Sci. Technol. 27(6), 1253-1261. (in Thai)

[12] Promwongpo, C., Yokhanit, W. & Julaluk, K. (2017). A Study of the Optimal Fermentation Conditions for Nata de Coco Production by *Acetobacter xylinum* TISTR 975 from Mango Juice. KMUTT Research and Development Journal. 40(2), 271-282. (in Thai)

[13] Moukamnerd, C., Saenchang, S., Krutjan, A. & Techapun, C. (2018). Production of bacterial cellulose by *Acetobacter xylinum* using wastewater from pineapple processing as a carbon source. KHON KAEN AGR. J. 46(3), 581-590. (in Thai)

[14] Boonpan, A., Pongswat, S. & Khampha, C. (2010, 3-5 February). A study on the optimum condition for Nata production from molasses. Proceedings of 48th Kasetsart University Annual Conference: Agro-Industry. Thailand. (in Thai)

[15] Pringsulaka, O. (2013). Medical Microbiology: Pathogenic Bacteria. (2nd ed.). Charansanitwong Printing Co., Ltd. (in Thai)

[16] Masaeng, A., Suwannakae, B., Kraipasspong, S., Dumkua, T., Boomtem, R., & Piyaboon, o. (2018). Development of an effective medical transdermal patch from *Piper sarmentosum Roxb.* extract for inhibiting *Staphylococcus aureus*. Journal of Health Science. 27(1), 156-161. (in Thai)

[17] Rakkusol, S., Paerdjantuk, N., Visutthi, M. & Lohthongkam, P. (2020). Antibacterial activity of extracts mixed from *Punica granatum Phyllanthus emblica* and *Gardenia jasminoides* for control pathogenic bacteria in pets. Science and Technology Research Journal Nakhon Ratchasima Rajabhat University. 5(1), 1-9. (in Thai)

[18] Waema, S. & Benhawan, A. (2016). Antibacterial activities of crude extracts from peel velvet tamarind (*Dialium Guineense)*. (Research report). Yala: Yala Rajabhat University. (in Thai)

[19] Chanklan, R., Sittichan, S. & Kongkathip, N. (2020). Biological Activities of Crude Extract of *Phyllanthus acidus* (L.) Skeel on the Inhibition of Ca2+ Signal, Antimicrobial and Antioxidant Activity. Thai Journal of Science and Technology. 9(1), 90-104. (in Thai)
[20] Langnaradom, A., Akanimat, R. Sriracha, P., Pratuptred, J. Naksan, K. Intaked, R. & Phamchang, J. (2022). Development of Wound Dressing Hydrocolloid Patch of *Garcinia mangostana* Linn. Extracts. Koch Cha Sarn Journal of Science. 44(1), 51-61. (in Thai)
[21] Nakhawatchana, S., Srisupasitanon, S., Sukatta, U., Sukyai, P. & Piyaboon, O. (2020). Anti-*Staphylococcus epidermidis* Acnes by Bio-cellulose acne patches from mangosteen peel extracts. Journal of Health Science. 29(4), 711-718. (in Thai)
[22] Phimnuan, P., Yakew, S., Yosboonrung, A., Luangbudnak, W., Grandmottet, F. & Viyoch, J. (2019) Development of anti-acne film from bio-cellulose incorporating *Punica granatum* peel extract. Walailak J Sci & Tech, 16(10), 765-778.
[23] Chotinu-kul, T., Soingam, T., Chunhachart, O. & Srithaworn, M. (2021). Development of Natural Anti-acne Patch from Biocellulose Formulated with *Dracaena cochinchinensis* (Lour.) S.C. Chen Crude Extract. Thai Science and Technology Journal (TSTJ). 29(6), 966-976. (in Thai)
[24] Binma-ae, H., Sahoh, S., Doloh, M. & Hajiwangoh, Z. (2023). Biodegradable plant pots from bacterial cellulose production by *Komagataeibacter nataicola* TISTR 975 from agricultural waste materials. YRU Journal of Science and Technology. 8(1), 19-27. (in Thai)
[25] Chaichompoo, A. & Thongwai, N. (2011, 8-9 December 2011). Growth inhibition of some pathogenic bacteria by local medicinal plant extracts. The 8th KU-KPS conference, Kasetsart University Kamphaeng Saen Campus. (in Thai)

การศึกษาสัดส่วนพื้นที่เก็บไอน้ำในถังขับดันที่มีต่อการสูบน้ำของปั๊มสูบน้ำกำลังไอน้ำ

A Study of Steam Storage Area Ratio in Pressure Vessels Affecting Water Pumping Performance of Steam-Powered Water Pumps

Pakorn Promkaew
Industrial Technology,
Faculty of Science and Technology,
Phuket Rajabhat University
Phuket, Thailand
pakorn.p@pkru.ac.th

Goffaree Hemmin
Industrial Technology,
Faculty of Science and Technology,
Phuket Rajabhat University
Phuket, Thailand
hemmingoffaree@gmail.com

Nattapon Dadsadachan
Industrial Technology,
Faculty of Science and Technology,
Phuket Rajabhat University
Phuket, Thailand
tonza6036@gmail.com

***Abstract*— *This research aimed to examine the effects of steam storage area ratios in the pressure vessel on water pumping capacity and determine the efficiency of the steam-powered water pump via a steam-powered water pump utilizing low-temperature waste heat. The waste heat was simulated using a 6,000 W electric heater. The steam-powered pump system consists of 4 units: 1) steam generation unit, 2) water pressurization unit, 3) cooling unit, and 4) pumping unit. It works with a suction static head and discharge static head of 1 m and 2.5 m, respectively. Water volume pumped was measured under 3 operational cycles with initial steam storage area ratio in the pressure vessel at 25%, 50%, and 75% of the vessel's capacity. Results showed that both the total pumped volume and pump efficiency varied according to initial steam storage area ratio. The maximum total pumped volume was 35,000 mL, and the maximum pump efficiency was 0.005759%, which occurred with 25% initial steam storage area ratio.*

Keywords*— *pump efficiency, steam-powered pump, waste heat

I. บทนำ

ในยุคปัจจุบันที่ความต้องการใช้พลังงานเพิ่มสูงขึ้นอย่างต่อเนื่อง จากข้อมูลสถานการณ์พลังงานปี พ.ศ. 2566 การใช้ไฟฟ้าอยู่ที่ 203,923 ล้านหน่วย เพิ่มขึ้นร้อยละ 3.4 โดยมาจากการใช้ไฟฟ้าในส่วนของสาขาธุรกิจที่เกี่ยวข้องกับการท่องเที่ยวและบริการมีการขยายตัวอย่างต่อเนื่อง จากเศรษฐกิจที่ฟื้นตัวภายหลังสถานการณ์การแพร่ระบาดของโรคติดเชื้อไวรัสโคโรนา 2019 คลี่คลาย ส่งผลให้การใช้ไฟฟ้าในสาขาธุรกิจเพิ่มขึ้นร้อยละ 8.4 โดยเฉพาะอย่างยิ่งการใช้ไฟฟ้าในโรงแรมที่เพิ่มสูงขึ้นถึงร้อยละ 22.5 สอดคล้องกับอัตราการเข้าพักที่เพิ่มขึ้นจากปี พ.ศ. 2565 ร้อยละ 48 [1] การใช้พลังงานอย่างมีประสิทธิภาพและการอนุรักษ์พลังงานจึงกลายเป็นประเด็นสำคัญที่ทำให้โรงแรมให้ความตระหนักในการดำเนินการเพื่อให้เกิดการใช้ทรัพยากรและพลังงานอย่างคุ้มค่าและมีประสิทธิภาพ มีการจัดการมลพิษและสิ่งแวดล้อมที่ดีภายใต้แนวคิดโรงแรมที่เป็นมิตรต่อสิ่งแวดล้อม หรือ โรงแรมสีเขียว (Green hotel) ดังนั้นในจังหวัดที่มีโรงแรมตั้งอยู่เป็นจำนวนมาก เช่น จังหวัดภูเก็ต จึงมีการตั้งเป้าลดก๊าซเรือนกระจกเป็นเมืองคาร์บอนต่ำในปี พ.ศ. 2573 ซึ่งสอดคล้องกับแผนงานการพัฒนาการเปลี่ยนแปลงสภาพภูมิอากาศระดับจังหวัดของภูเก็ตในภาคส่วนพลังงาน โดยแผนของจังหวัดภูเก็ตตั้งเป้าไว้ที่ 440,000 tCO_2eq คิดเป็นเป้าหมายทั้งจังหวัดในการลดก๊าซเรือนกระจก คือ 9.51% ต้องทำให้ได้ในปี 2030 [2]

การสูบน้ำเป็นส่วนหนึ่งในระบบสุขาภิบาลที่มีการใช้งานในโรงแรม พื้นที่หลักที่มีการใช้น้ำของโรงแรม ได้แก่ ห้องพักแขก สระว่ายน้ำ ห้องซักรีด เป็นต้น จากการศึกษาการใช้น้ำของโรงแรมขนาดกลางและขนาดใหญ่ในเทศบาลเมืองป่าตอง จังหวัดภูเก็ต ประมาณ 450 L/Room/d [3] โดยปกติเครื่องสูบน้ำที่ใช้พลังงานไฟฟ้าถูกนำมาใช้เป็นอุปกรณ์หลักในการสูบน้ำ วิธีการอนุรักษ์พลังงานสำหรับโรงแรมประการหนึ่งที่สามารถทำได้คือ การนำความร้อนที่ถูกปล่อยทิ้งกลับมาใช้ประโยชน์ในการสูบน้ำแบบขับดันน้ำ วิธีการนี้ช่วยลดการใช้พลังงานและลดการปล่อยก๊าซเรือนกระจกได้อีกด้วย เนื่องจากไม่มีการใช้พลังงานไฟฟ้าหรือเชื้อเพลิงฟอสซิลในการสูบน้ำ

เครื่องสูบน้ำกำลังไอน้ำเป็นเทคโนโลยีที่สามารถเปลี่ยนพลังงานความร้อนเป็นพลังงานกลเพื่อใช้ในการสูบน้ำมีการวิจัยที่ใช้แหล่งพลังงานความร้อนจากแหล่งต่างๆ เช่น รังสีอาทิตย์โดยใช้ตัวรับรังสีแบบท่อสุญญากาศที่มีน้ำเป็นสารทำงาน [4] การศึกษาการปั๊มน้ำด้วยพลังงานรังสีอาทิตย์ที่มีก๊าซไฮโดรเจนเป็นสารทำงาน [5] การศึกษาการนำความร้อนเหลือทิ้งกลับมาใช้ในระบบสูบน้ำด้วยกำลังไอน้ำ [6] เครื่องสูบน้ำพลังงานความร้อนจากถ่านไม้ [7] โดยการสูบน้ำแบบขับดันน้ำด้วยกำลังไอน้ำแบ่งการทำงานเป็น 4 ช่วง ได้แก่ 1) ช่วงผลิตไอน้ำ 2) ช่วงขับดันน้ำ 3) ช่วงหล่อเย็น และ 4) ช่วงสูบน้ำ พบว่า การควบคุมความดันเกจของถังสูบน้ำช่วยให้จำนวนรอบในการสูบน้ำ และปริมาตรน้ำที่สูบได้ต่อวันเพิ่มขึ้น [8] โดยความสูงด้านดูดน้ำของระบบที่เพิ่มขึ้นมีผลทำให้ประสิทธิภาพของเครื่องสูบน้ำเพิ่มขึ้นด้วยในกรณีที่ปริมาตรน้ำที่สูบได้ในแต่ละความสูงด้านดูดน้ำใกล้เคียงกัน [7] นอกจากระดับความสูงในการสูบน้ำ อุณหภูมิภายในถังขับดัน และอุณหภูมิน้ำหล่อเย็นที่มีผลต่อการทำงานของระบบแล้ว อุณหภูมิน้ำที่สูงกว่าอุณหภูมิสิ่งแวดล้อมเมื่อเติมให้แก่ถังผลิตไอน้ำจะช่วยเพิ่มจำนวนรอบการสูบน้ำ [6]

จากเหตุผลที่กล่าวมาข้างต้น เครื่องสูบน้ำกำลังไอน้ำจากแหล่งพลังงานความร้อนมีศักยภาพที่สามารถนำมาใช้สูบน้ำ ในงานวิจัยนี้จึงมีแนวคิดในการศึกษากลไกการทำงานของปั๊มสูบน้ำที่ใช้กำลังไอน้ำที่ใช้สูบน้ำแบบขับดันน้ำโดยใช้ฮีตเตอร์ไฟฟ้าขนาด 6,000 W จำลองเป็นแหล่งพลังงานความร้อนเหลือทิ้งสำหรับผลิตไอน้ำให้กับถังขับดันที่มีน้ำในช่วงเริ่มต้นแตกต่างกัน เพื่อศึกษาผลของสัดส่วนพื้นที่ส่วนเก็บไอน้ำในถังขับดันที่มีต่อปริมาณน้ำที่สูบได้ และเพื่อหาประสิทธิภาพของปั๊มสูบน้ำกำลังไอน้ำ ซึ่งคาดหวังว่าสัดส่วนพื้นที่เก็บไอน้ำที่ต่ำจะมีปริมาณน้ำที่สูบได้และประสิทธิภาพของปั๊มสูบน้ำกำลังไอน้ำสูงที่สุด

ทบทวนวรรณกรรม

การสูบน้ำด้วยกำลังไอน้ำอาศัยหลักการเปลี่ยนแปลงอุณหภูมิและความดันของวัฏจักรทำให้เกิดการส่งความร้อนและการขับดันของเหลวด้วยไอ ระบบสามารถสูบน้ำได้โดยไม่ต้องล่อน้ำ (Self-Priming) ไม่มีการใช้ปั๊มไฟฟ้าและไม่มีการใช้ไฟฟ้าในการควบคุมวาล์วต่างๆ การวิจัยที่ผ่านมาเน้นการศึกษากลไกการทำงานของระบบสูบน้ำและตัวแปรที่มีผลต่อการสูบน้ำได้แก่ ความดันในขับดัน [4] อุณหภูมิน้ำของถังขับดันและอุณหภูมิน้ำที่เติมให้ถังผลิตไอน้ำ [6] ระดับความสูงในการสูบน้ำ [9] ปริมาณน้ำหล่อเย็น [10] นิยมใช้ฮีตเตอร์ไฟฟ้าเป็นแหล่งพลังงานความร้อน ในงานวิจัยของ [4] ศึกษาการสูบน้ำโดยใช้พลังงานความร้อนจากฮีตเตอร์ขนาด 100, 270 และ 440 W ควบคุมความดันภายในถังระเหยเท่ากับ 142, 163, 183 และ 203 kPa ทดลองที่ระดับความสูงด้านดูด 1.0, 1.5, 2.0 และ 2.5 m เครื่องสูบน้ำประกอบด้วย ถังระเหย ถังควบแน่นและแหล่งกำเนิดความร้อนจากฮีตเตอร์พบว่า ปริมาณน้ำด้านส่งเพิ่มขึ้นตามค่าความดันภายในถังขับดัน ในขณะที่ระดับความสูงด้านดูดยังมีผลไม่ชัดเจน และเมื่อระดับความสูงรวม (Total Head) เพิ่มขึ้นทำให้ปริมาณน้ำด้านส่งลดลง ถ้าพิจารณาที่ปริมาณน้ำด้านส่งเท่ากัน ประสิทธิภาพปั๊มสูงสุดเท่ากับ 0.03% จะเกิดขึ้นที่ระดับความสูงรวมมากที่สุด

ในงานวิจัยของ [6] ทดลองที่ระดับความสูงด้านส่ง 1 m และใช้ฮีตเตอร์ไฟฟ้า 3,000 W พบว่า อุณหภูมิน้ำเฉลี่ยภายในถังน้ำร้อนเท่ากับ 46.44 °C สามารถส่งน้ำไปถังเก็บน้ำได้ 47 cycle ปริมาณน้ำที่สูบได้สูงสุด 246.4 L ประสิทธิภาพความร้อน เท่ากับ 77.47% และมีประสิทธิภาพปั๊มเท่ากับ 0.023% ซึ่งจำนวนรอบการทำงานของระบบแปรผันตามอุณหภูมิน้ำที่เติมเข้าถังผลิตไอน้ำ

ในงานวิจัยของ [10] ศึกษาความเป็นไปได้ของแบบจำลองการสูบน้ำใต้ดินด้วยกำลังไอน้ำ-อากาศแบบหล่อเย็นโดยการสัมผัสทางตรง ติดตั้งฮีตเตอร์จำลองเป็นพลังงานความร้อนเหลือทิ้งสำหรับปั๊มน้ำขนาด 10 L ทดลองที่เฮดรวม 3, 4.5, 6 และ 7.5 m ใกล้เคียงกับงานวิจัยของ [11] ที่สร้างเครื่องสูบน้ำพลังงานความร้อนด้วยกำลังไอน้ำร่วมกับอากาศแบบอัตโนมัติที่กำหนดระดับความสูงด้านดูด 2-5 m พบว่า ปั๊มน้ำที่มีปริมาตรอากาศ 50% ของขนาดถังขับดันเพียงพอที่ใช้ในการสูบน้ำ อุณหภูมิในช่วงให้ความร้อนอยู่ในช่วง 100-103 °C อุณหภูมิในช่วงขับดันน้ำอยู่ในช่วง 80-90 °C และความดันอยู่ในช่วง 12-18 kPa ความดันในช่วงการดูดน้ำประมาณ -80 kPa จะมีประสิทธิภาพดีที่สุด โดยความสามารถในการสูบน้ำในเวลา 2 h พบว่าที่ระดับความสูงด้านดูด 2 m ปริมาณน้ำสูบได้สูงสุด 170 L และลดลงตามระดับความสูงด้านดูด ที่ระดับความสูงด้านดูด 3.5, 5 และ 6.5 m ปริมาณน้ำที่สูบได้สูงสุด 113 L, 96 L และ 65 L ตามลำดับ และยังสอดคล้องกับงานวิจัยของ [12] การทดลองสูบน้ำด้วยกำลังไอน้ำที่ควบคุมด้วยมือ จำลองการให้พลังงานความร้อนด้วยไฟฟ้ากระทั่งอุณหภูมิถังสูบน้ำเท่ากับ 97 °C และระบายความร้อนด้วยอากาศ พบว่าประสิทธิภาพปั๊มเพิ่มขึ้นตามระดับความสูงด้านดูด ประสิทธิภาพปั๊มสูงสุดคือ 0.15% ที่ระดับความสูงด้านดูด 5 m จึงสรุปได้ว่า การเพิ่มระดับความสูงในการสูบน้ำช่วยเพิ่มประสิทธิภาพปั๊มน้ำให้สูงขึ้น

ในงานวิจัยของ [9] ศึกษาระดับความสูงในการสูบน้ำในช่วง 2-8 m นาน 10 h พบว่า ระดับความสูงในการสูบน้ำที่เพิ่มขึ้นส่งผลให้ปริมาณน้ำที่สูบได้ลดลง แต่ประสิทธิภาพปั๊มเพิ่มขึ้น ที่ระดับความสูงในการสูบ 2 m และ 8 m ปริมาณน้ำที่สูบได้เท่ากับ 2,040 L และ 1,428 L ประสิทธิภาพปั๊มเท่ากับ 0.66649% และ 1.86619% ตามลำดับ แต่การเพิ่มระดับความสูงด้านดูดจำเป็นต้องเพิ่มความดันสุญญากาศให้มากขึ้นด้วย สอดคล้องกับงานวิจัยของ [13] ศึกษาอุณหภูมิและปริมาณน้ำหล่อเย็นที่ส่งผลต่อความดันสุญญากาศของปั๊มสูบน้ำด้วยกำลังไอน้ำ พบว่า การลดอุณหภูมิและการเพิ่มปริมาณน้ำหล่อเย็นส่งผลให้เกิดความดันสุญญากาศมากขึ้น ทำให้สามารถสูบน้ำในระดับความสูงด้านดูดที่เพิ่มขึ้น โดยที่จากการศึกษาพบว่า ปริมาณน้ำหล่อเย็นส่งผลต่อความดันสุญญากาศได้มากกว่าการลดอุณหภูมิน้ำหล่อเย็น

จากงานวิจัยที่ผ่านมา การสูบน้ำด้วยกำลังไอน้ำแบบขับดันน้ำ มุ่งเน้นการศึกษาผลของตัวแปรที่มีผลต่อจำนวนรอบการทำงานและประสิทธิภาพปั๊มสูบน้ำ เช่น ระดับความสูงด้านดูดและด้านส่งน้ำ กำลังไฟฟ้าที่ใช้ อุณหภูมิภายในถังขับดัน อุณหภูมิน้ำหล่อเย็น เป็นต้น ดังนั้น ในงานวิจัยนี้จึงได้ศึกษาผลของสัดส่วนพื้นที่ส่วนเก็บไอน้ำในถังขับดันที่มีต่อปริมาณน้ำที่สูบได้ และหาประสิทธิภาพของปั๊มสูบน้ำกำลังไอน้ำ ด้วยการจำลองแหล่งพลังงานความร้อนจากฮีตเตอร์ไฟฟ้า และกำหนดเฮดสถิตด้านดูดและเฮดสถิตด้านส่งคงที่ เพื่อมุ่งหวังในการหาเงื่อนไขเริ่มต้นการทำงานของระบบสูบน้ำที่เหมาะสมที่สุด และมีค่าพลังงานจำเพาะ (Specific Energy Consumption: SEC) ต่ำที่สุด

II. ระเบียบวิธีวิจัย

A. หลักการทำงานของระบบสูบน้ำ

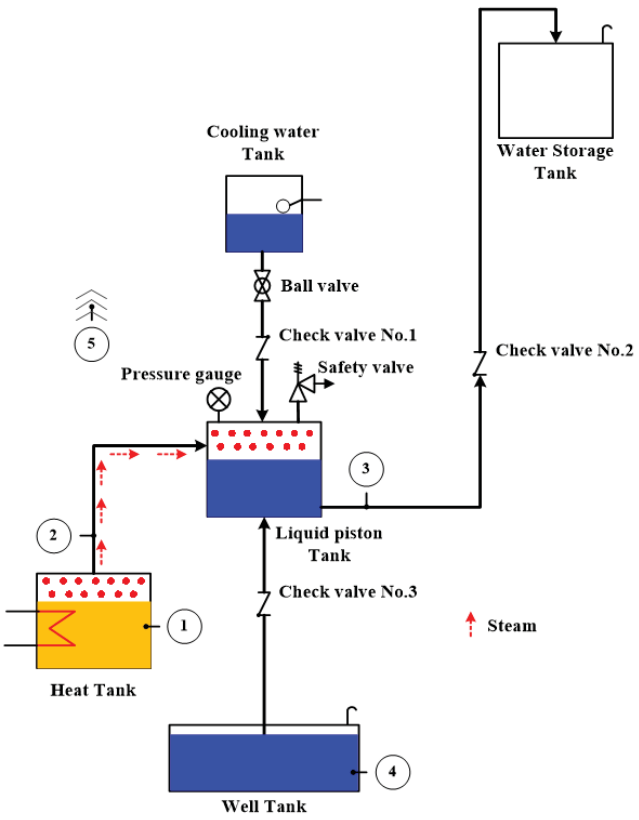
การสูบน้ำด้วยกำลังไอน้ำอาศัยหลักการสร้างสภาวะสุญญากาศในถังขับดัน (Liquid Piston Tank) เพื่อสูบน้ำและสร้างความดันที่มากกว่าความดันบรรยากาศในการผลักดันน้ำออกจากถังขับดัน แบ่งการทำงานเป็น 4 ช่วง ได้แก่ 1) ช่วงให้ความร้อน (Heating Stage) 2) ช่วงขับดันน้ำ (Water Circulating Stage) 3) ช่วงหล่อเย็น (Cooling Stage) และ 4) ช่วงสูบน้ำ (Suction Stage)

ช่วงให้ความร้อน เริ่มจากให้ความร้อนแก่น้ำในถังผลิตไอน้ำ (Heat Tank) ด้วยฮีตเตอร์ขนาด 6,000 W ที่จำลองเป็นแหล่งพลังงานร้อนเหลือทิ้งอุณหภูมิต่ำ จนกระทั่งน้ำมีอุณหภูมิเพิ่มขึ้นใกล้เคียง 100 °C ทำให้น้ำเปลี่ยนสถานะจากของเหลวกลายเป็นไอน้ำ ไอน้ำที่เกิดขึ้นจะไหลผ่านท่อเข้าสู่ถังขับดัน ดังภาพที่ 1

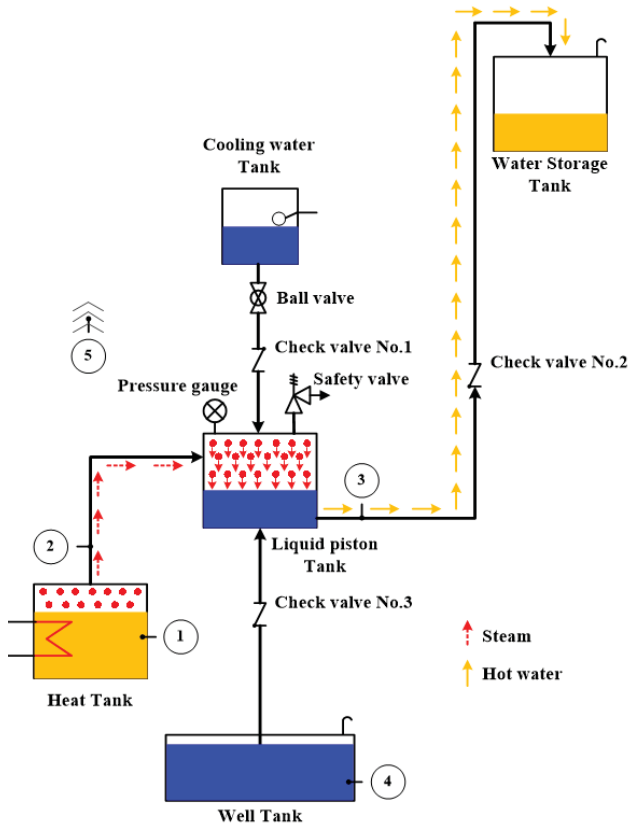
ช่วงขับดันน้ำ เมื่อไอน้ำสะสมในถังขับดันจนความดันที่เกิดขึ้นมากกว่าแรงต้านของเช็ควาล์วหมายเลข 2 ทำให้สามารถขับดันน้ำที่อยู่ในถังขับดันไหลผ่านท่อไปยังถังเก็บน้ำ (Water Storage Tank) ขนาด 50.2 L ดังภาพที่ 2

ช่วงหล่อเย็น เมื่อน้ำถูกขับดันออกจากถังขับดันจนหมด กระทั่งไอน้ำไหลออกสู่บรรยากาศภายนอกที่ปลายท่อด้านส่งน้ำ ส่งผลให้ความดันภายในถังขับดันเท่ากับความดันบรรยากาศ จึงทำให้น้ำในถังหล่อเย็น (Cooling Water Tank) สามารถไหลตามแรงโน้มถ่วงของโลกผ่านเช็ควาล์วหมายเลข 1 เข้าสู่ถังขับดันและเกิดการควบแน่นเนื่องจากผลต่างของอุณหภูมิระหว่างไอน้ำและน้ำหล่อเย็น ทำให้ไอน้ำยุบตัวเกิดสภาวะสุญญากาศ (Vacuum Stage) ชั่วขณะ ดังภาพที่ 3

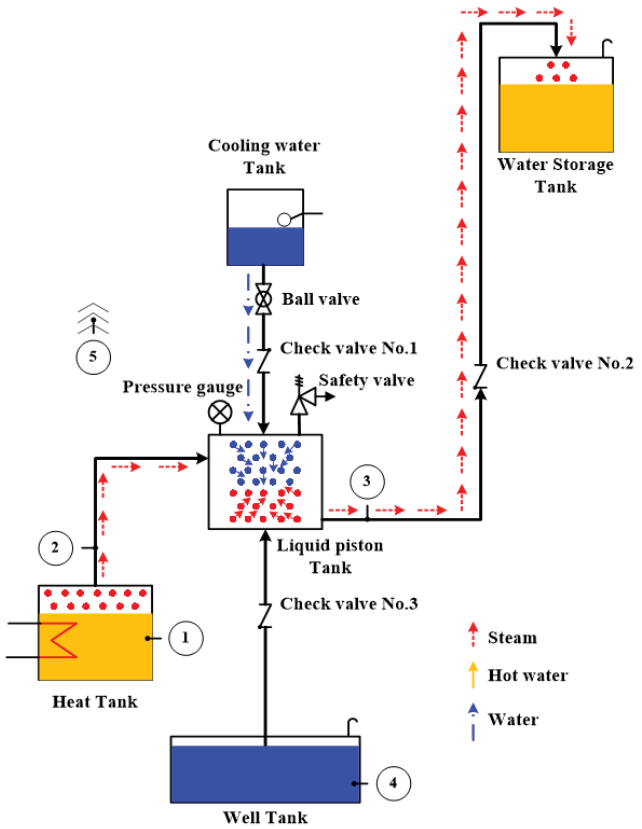
ช่วงสูบน้ำ เมื่อเกิดสุญญากาศภายในถังขับดันทำให้สามารถสูบน้ำจากแหล่งน้ำ (Well Tank) และจะหยุดก็ต่อเมื่อความดันภายในถังขับดันเท่ากับความดันบรรยากาศ น้ำที่ถูกสูบขึ้นมานั้นจะได้รับความร้อนจากไอน้ำที่มาจากส่วนผลิตไอน้ำ ดังภาพที่ 4 เพื่อเข้าสู่ช่วงขับดันน้ำต่อไป และเกิดเป็นวัฏจักรซ้ำไปเรื่อยๆ และจะหยุดก็ต่อเมื่อปริมาณความร้อนไม่เพียงพอในการสร้างสภาวะสุญญากาศและความดันของถังขับดันน้อยกว่าเฮดรวมของระบบ



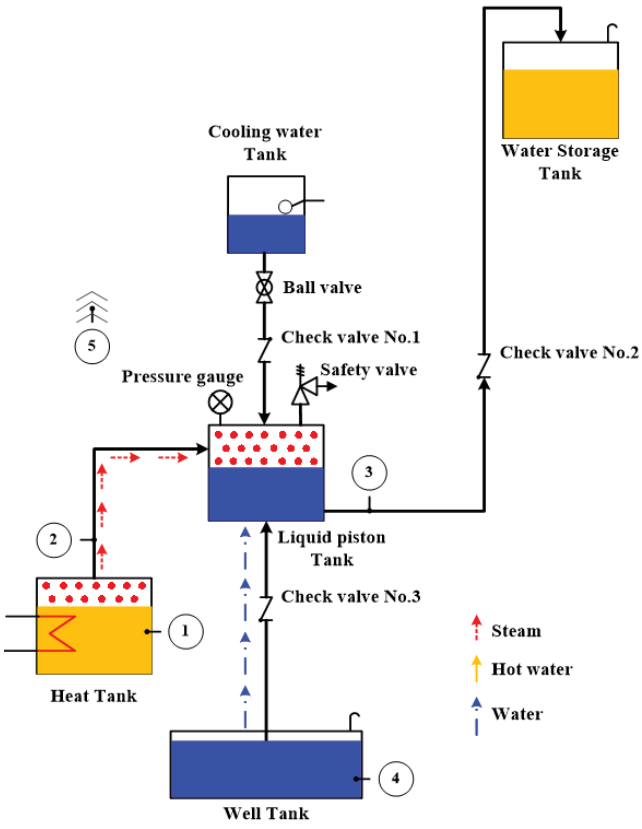
ภาพที่ 1 ไดอะแกรมระบบการทำงานของปั๊มสูบน้ำกำลังไอน้ำช่วงผลิตไอน้ำ



ภาพที่ 2 ไดอะแกรมระบบการทำงานของปั๊มสูบน้ำกำลังไอน้ำช่วงขับดันน้ำ



ภาพที่ 3 ไดอะแกรมระบบการทำงานของปั๊มสูบน้ำกำลังไอน้ำช่วงหล่อเย็น



ภาพที่ 4 ไดอะแกรมระบบการทำงานของปั๊มสูบน้ำกำลังไอน้ำช่วงสูบน้ำ

B. วัสดุอุปกรณ์

รายละเอียดของอุปกรณ์และเครื่องมือวัดที่ใช้ในงานวิจัย มีดังนี้

1) ฮีตเตอร์ชนิดแบบจุ่ม ขนาดกำลังไฟฟ้า 6,000 W ใช้เป็นแหล่งพลังงานความร้อนให้กับถังผลิตไอน้ำ

2) ถังผลิตไอน้ำ ลักษณะเป็นถังเหล็กทรงกระบอกแนวตั้ง ขนาดความจุถัง 13 L จำนวน 1 ถัง ติดตั้งฮีตเตอร์ชนิดแบบจุ่มให้ความร้อนกับน้ำเพื่อผลิตไอน้ำป้อนให้กับถังขับดัน

3) ถังขับดันน้ำ มีลักษณะเดียวกับถังผลิตไอน้ำ จำนวน 1 ถัง มีท่อขนาด ¾ in เชื่อมต่อกับถังผลิตไอน้ำ ถังน้ำหล่อเย็น ถังเก็บน้ำ และแหล่งน้ำ มีหน้าที่สูบน้ำจากแหล่งน้ำและขับดันไปยังถังเก็บน้ำ

4) ถังน้ำหล่อเย็น เป็นถังทรงกระบอกแนวตั้ง เส้นผ่านศูนย์กลาง 26 cm สูง 26 cm หนา 0.8 mm ทำมาจากสเตนเลส ขนาดความจุถัง 13.8 L มีหน้าที่บรรจุน้ำหล่อเย็นเพื่อสร้างสภาวะสุญญากาศภายในถังขับดัน

5) ถังเก็บน้ำ มีลักษณะเดียวกับถังน้ำหล่อเย็น เส้นผ่านศูนย์กลาง 40 cm สูง 40 cm หนา 0.8 mm ทำมาจากสเตนเลส ขนาดความจุถัง 50.2 L มีหน้าที่กักเก็บน้ำที่สูบได้จากระบบปั๊มสูบน้ำกำลังไอน้ำ

6) วาล์วกันกลับ (Check Valve) ทำมาทองเหลืองขนาด ¾ in ใช้ป้องกันการไหลย้อนกลับของน้ำในระบบปั๊มสูบน้ำกำลังไอน้ำ

7) เกจวัดความดัน (Pressure Gauge) ถูกติดตั้งไว้ 2 ตำแหน่งคือ ถังผลิตไอน้ำ และถังขับดันไอน้ำ ใช้สำหรับสังเกตการเปลี่ยนแปลงของความดันที่เกิดขึ้นระหว่างการทำงานของระบบปั๊มสูบน้ำกำลังไอน้ำ

8) หัววัดอุณหภูมิชนิด K (Thermocouple type K) ยาว 2 m หัววัดยาว 30 mm ช่วงการวัดอุณหภูมิ 0 °C ถึง 400 °C ใช้ตรวจวัดอุณหภูมิที่เกิดขึ้นระหว่างการทำงานของระบบปั๊มสูบน้ำกำลังไอน้ำ

9) เครื่องบันทึกอุณหภูมิ (Data logger) ใช้ไมโครคอนโทรลเลอร์ ESP32 ในการควบคุมและประมวลผลข้อมูลอุณหภูมิจาก Thermocouple type K ที่วัดอุณหภูมิได้ในช่วง 0 - 800 °C ซึ่งทำงานผ่านโมดูล MAX6675 มีจอแสดงผล LCD สำหรับแสดงผลข้อมูลอุณหภูมิและข้อมูลอื่น ๆ ที่เกี่ยวข้องแบบเรียลไทม์ และส่งข้อมูลทุก 5 sec ผ่าน Wi-Fi ไปจัดเก็บยังฐานข้อมูล MySQL ในเซิร์ฟเวอร์เพื่อแสดงผลในลักษณะตัวเลขหรือกราฟเพื่อการวิเคราะห์และประมวลผล

C. การวิเคราะห์ปั๊มสูบน้ำด้วยกำลังไอน้ำ

การวิเคราะห์ประสิทธิภาพการทำงานของปั๊มสูบน้ำกำลังไอน้ำ มีการตรวจวัดค่าอุณหภูมิ ความดันที่ถังขับดัน เฮดสถิตด้านดูดและด้านจ่าย ปริมาตรน้ำที่สูบน้ำได้ และพลังงานที่ใช้ในการสูบน้ำ โดยประสิทธิภาพปั๊มสูบน้ำกำลังไอน้ำ สามารถคำนวณได้จากพลังงานที่ได้ในการสูบน้ำต่อพลังงานที่ป้อนให้ระบบดังสมการที่ 1-3

$$\eta_p = \frac{NW_h}{Q_{input}} \times 100 \qquad (1)$$

เมื่อ η_p คือ ประสิทธิภาพปั๊มน้ำ (%) W_h คือ พลังงานที่ได้ในการสูบน้ำต่อรอบ (J) N คือ จำนวนรอบ Q_{input} คือ พลังงานที่ป้อนให้กับระบบ (J)

$$W_h = V_c \rho_w g\, h \qquad (2)$$

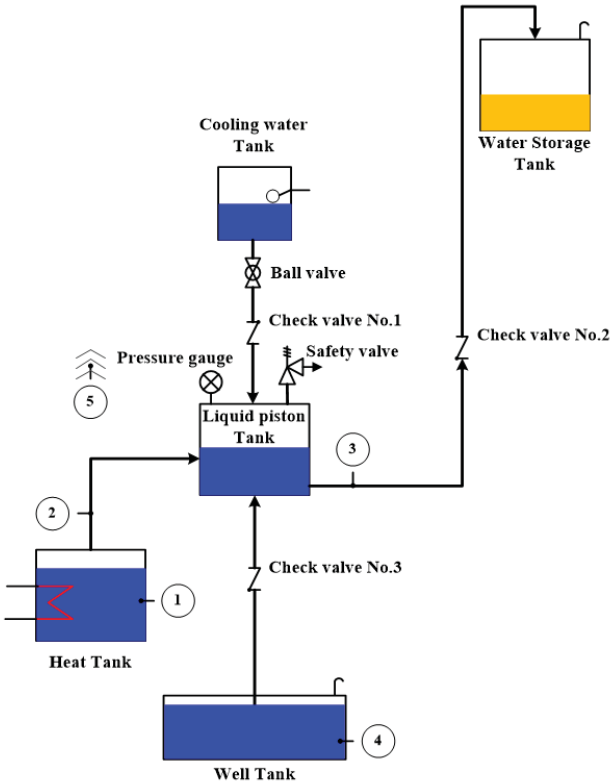
เมื่อ V_c คือ ปริมาตรน้ำที่สูบได้ต่อรอบ (m^3) ρ_w คือ ค่าความหนาแน่นของน้ำ (kg/m^3) g คือ ค่าความเร่งเนื่องจากแรงโน้มถ่วงของโลก (m/s^2) h คือ ระดับความสูงในการสูบน้ำ (m)

$$\dot{Q}_{input} = m_w C_{p,w} \frac{d(T_w)}{dt} \qquad (3)$$

เมื่อ $\dot{Q}_{input}$ คือ อัตราพลังงานที่ป้อนให้กับระบบ (kW) M_w คือ มวลน้ำในถังผลิตไอน้ำ (kg) $C_{p,w}$ คือ ค่าความจุความร้อนของน้ำ (kJ/kg °C) $\frac{D(T_w)}{dt}$ คือ ผลต่างของอุณหภูมิน้ำในถังผลิตไอน้ำที่เปลี่ยนแปลงตามเวลา (°C/sec)

D. วิธีการทดลอง

ในระหว่างกระบวนการสูบน้ำของระบบปั๊มสูบน้ำกำลังไอน้ำ อุณหภูมิภายในระบบมีการเปลี่ยนแปลงตลอดเวลา หัววัดอุณหภูมิชนิด K จึงถูกติดตั้งเพื่อใช้ตรวจวัดการเปลี่ยนแปลงของอุณหภูมิที่เกิดขึ้นระหว่างการทำงานของระบบปั๊มสูบน้ำกำลังไอน้ำทุกๆ 5 sec ตำแหน่งในการติดตั้งหัววัดอุณหภูมิมี 5 ตำแหน่ง ดังภาพที่ 5 ประกอบด้วย ตำแหน่งที่ 1 วัดอุณหภูมิน้ำภายในถังผลิตไอน้ำ (TW,HT) ตำแหน่งที่ 2 วัดอุณหภูมิไอภายในท่อที่ป้อนให้ถังขับดัน (TS,LT) ตำแหน่งที่ 3 วัดอุณหภูมิน้ำภายในท่อขาออกจากถังขับดัน (TW,LT) ตำแหน่งที่ 4 วัดอุณหภูมิน้ำจากแหล่งน้ำ (TW,WT) และตำแหน่งที่ 5 วัดอุณหภูมิบรรยากาศ (TA) โดยตลอดการทดลองอุณหภูมิสิ่งแวดล้อมอยู่ในช่วง 29-31 °C



ภาพที่ 5 ตำแหน่งติดตั้งจุดวัดค่า

เมื่อตรวจเช็คการทำงานของระบบปั๊มสูบน้ำด้วยกำลังไอน้ำแล้ว ทำการติดตั้งเครื่องมือวัดอุณหภูมิเข้ากับระบบปั๊มสูบน้ำด้วยกำลังไอน้ำ ใช้ฮีตเตอร์ขนาด 6,000 W เป็นแหล่งพลังงานความร้อน กำหนดเงื่อนไขเริ่มต้น โดย

ควบคุมอุณหภูมิน้ำภายในถังผลิตไอน้ำประมาณ 60 °C และควบคุมระดับเฮดสถิตด้านดูดและด้านจ่าย เท่ากับ 1 m และ 2.5 m ตามลำดับ หลังจากนั้น มีขั้นตอนการทดลอง ดังนี้

1) บรรจุน้ำภายในถังผลิตไอน้ำ ขนาด 13 L โดยคอยสังเกตระดับน้ำจากหลอดแก้ววัดระดับน้ำอยู่เสมอ เพื่อป้องกันไม่ให้น้ำแห้ง

2) บรรจุน้ำภายในถังขับดันตามเงื่อนไขที่กำหนด คือ ปริมาตรน้ำในถังขับดันในการทดลองกรณีที่ 1 คิดเป็น 25% ของความจุถังขับดัน การทดลองกรณีที่ 2 คิดเป็น 50% ของความจุถังขับดัน และการทดลองกรณีที่ 3 คิดเป็น 75% ของความจุถังขับดัน เมื่อถังขับดันมีความจุ 13 L

3) ทำการจ่ายไฟฟ้าให้กับฮีตเตอร์เพื่อทำการต้มน้ำในถังผลิตไอน้ำจ่ายให้กับถังขับดัน พร้อมกับเริ่มบันทึกค่าอุณหภูมิทุกๆ 5 sec

4) เมื่อความดันในถังขับดันเพิ่มขึ้นระบบปั๊มสูบน้ำด้วยกำลังไอน้ำจะสูบน้ำจากแหล่งน้ำและจ่ายไปยังถังเก็บน้ำ ถือเป็น 1 รอบการทำงาน

5) รอระบบปั๊มสูบน้ำด้วยกำลังไอน้ำจะสูบน้ำทำงานจนครบ 3 cycle แล้วบันทึกปริมาณน้ำที่สูบน้ำได้ และหยุดบันทึกค่าอุณหภูมิ

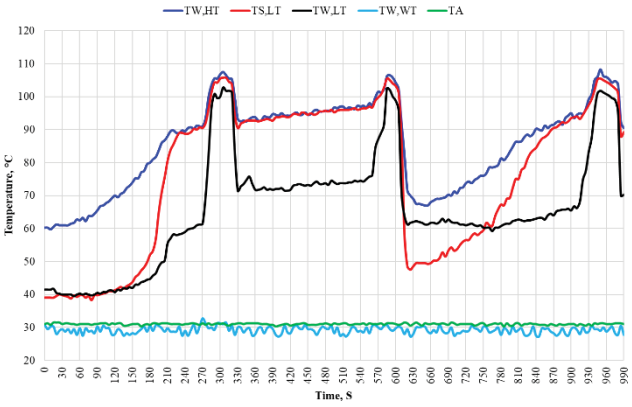
6) ทำซ้ำตามข้อ 1 ถึง 5 โดยเปลี่ยนปริมาตรน้ำในถังขับดันเริ่มต้นเป็น 50% ของความจุถังขับดัน และ 75% ของความจุถังขับดัน

7) นำข้อมูลที่ได้จากอุปกรณ์บันทึกข้อมูลมาวิเคราะห์หาประสิทธิภาพปั๊มสูบน้ำ

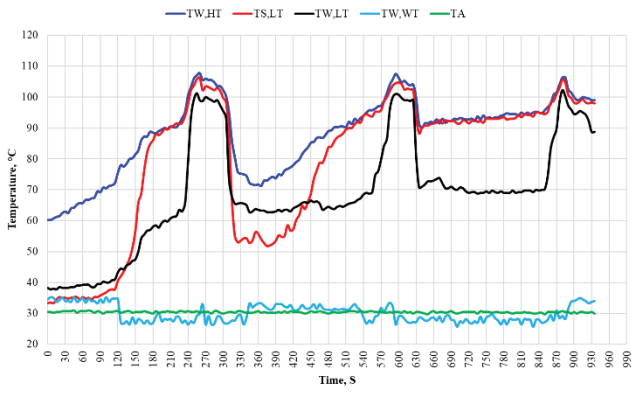
III. ผลการทดลอง

A. *การเปลี่ยนแปลงอุณหภูมิภายในระบบปั๊มสูบน้ำกำลังไอน้ำ*

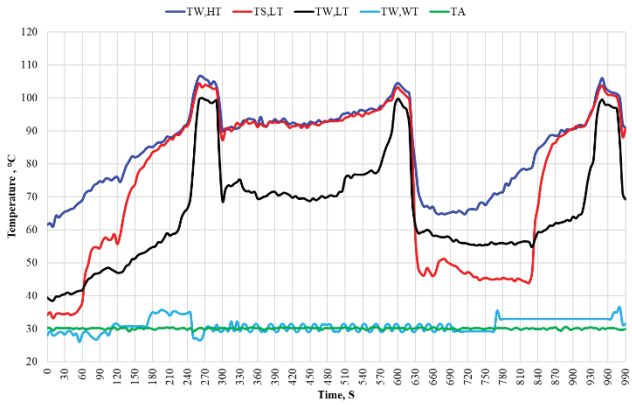
การทดลองแบ่งได้เป็น 3 กรณีตามสัดส่วนพื้นที่ส่วนเก็บไอน้ำในถังขับดันที่ 25% 50% และ 75% ของปริมาณความจุถังขับดัน เก็บข้อมูลการทำงาน 3 cycle ในแต่ละกรณีพบว่า แนวโน้มการเพิ่มขึ้นของอุณหภูมิน้ำภายในถังผลิตไอน้ำเหมือนกันทั้ง 3 กรณี โดยเริ่มให้ความร้อนจากอุณหภูมิ TW,HT เริ่มต้น 60 °C อุณหภูมิเพิ่มขึ้นอย่างช้าๆ จนกระทั่งอุณหภูมิใกล้เคียง 90 °C (อุณหภูมิน้ำและอุณหภูมิไอน้ำใกล้เคียงกัน) หลังจากนั้น อุณหภูมิ TS,LT เพิ่มขึ้นอย่างรวดเร็วเท่ากับอุณหภูมิไอน้ำอิ่มตัวที่ความดัน 0.3 bar,g คือ 108 °C (ช่วงขับดันน้ำ) สอดคล้องกับงานวิจัยของ [7] ที่ระบบจะเริ่มทำงานเมื่ออุณหภูมิ TS,LT มากกว่า 98 °C หลังจากนั้น อุณหภูมิ TS,LT จะลดลงอย่างรวดเร็ว เนื่องจากเป็นช่วงหล่อเย็นจนกระทั่งอุณหภูมิลดลงมาใกล้เคียง 90 °C ถือเป็น 1 cycle และเริ่มรับความร้อนในรอบการทำงานถัดไป ในขณะเดียวกัน อุณหภูมิ TW,LT มีแนวโน้มการเปลี่ยนแปลงเหมือนกับอุณหภูมิ TW,HT และ TS,LT แต่อุณหภูมิต่ำกว่า สอดคล้องกับงานวิจัยของ [8] ที่ควบคุมความดันเกจของถังสูบน้ำ 10 kPa อุณหภูมิ TW,HT เท่ากับ 102.9 °C และ TW,LT เท่ากับ 101.1 °C ในการทำงานรอบที่ 2 สังเกตได้ว่าหลังจากช่วงหล่อเย็นเกิดสภาวะสุญญากาศ อุณหภูมิ TW,HT และ TS,LT ลดลงมากกว่าแรก เนื่องจากน้ำที่ถูกสูบเข้าถังขับดันไหลย้อนกลับเข้าสู่ถังผลิตไอน้ำ และเวลาที่เริ่มเกิดช่วงขับดันน้ำรอบแรก ในกรณีสัดส่วนพื้นที่ส่วนเก็บไอน้ำในถังขับดันที่ 50% (ปริมาณน้ำช่วงเริ่มต้น 50%) และ 75% (ปริมาณน้ำช่วงเริ่มต้น 25%) ของความจุถังขับดัน ใช้เวลา 220 sec เร็วกว่ากรณีสัดส่วนพื้นที่ส่วนเก็บไอน้ำในถังขับดันที่ 75% (ปริมาณน้ำช่วงเริ่มต้น 25%) ของความจุถังขับดัน ประมาณ 20 sec ดังภาพที่ 7



(I) สัดส่วนพื้นที่ส่วนเก็บไอน้ำในถังขับดันที่ 75% ของความจุถังขับดัน



(II) สัดส่วนพื้นที่ส่วนเก็บไอน้ำในถังขับดันที่ 50% ของความจุถังขับดัน



(III) สัดส่วนพื้นที่ส่วนเก็บไอน้ำในถังขับดันที่ 25% ของความจุถังขับดัน

ภาพที่ 7 การเปลี่ยนแปลงอุณหภูมิภายในระบบปั๊มสูบน้ำกำลังไอน้ำ

B. *ผลของสัดส่วนพื้นที่ส่วนเก็บไอน้ำในถังขับดันที่มีต่อปริมาณน้ำที่สูบน้ำได้*

จากสัดส่วนพื้นที่ส่วนเก็บไอน้ำในถังขับดันที่ 25%, 50% และ 75% ของความจุถังขับดัน ปริมาตรน้ำที่สูบน้ำได้จากการทดลอง 3 cycle ดังตารางที่ 1

TABLE I. THE VOLUME OF PUMPED WATER

Case	*The steam storage area ratio in the pressure vessel (%)*	*The volume of pumped water (mL)*	*The rate of pumped water (lpm)*	*Specific energy consumption (kJ/mL)*
I	75	28,600	1.73	0.208
II	50	33,600	1.94	0.185
III	25	35,000	2.11	0.170

C. *ประสิทธิภาพของปั๊มสูบน้ำกำลังไอน้ำ*

จากสัดส่วนพื้นที่ส่วนเก็บไอน้ำในถังขับดันที่ 25%, 50% และ 75% ของความจุถังขับดัน ประสิทธิภาพของปั๊มสูบน้ำกำลังไอน้ำมีค่าเท่ากับ 0.004723% 0.005297% และ 0.005759% ตามลำดับ ดังตารางที่ 2 สอดคล้องกับงานวิจัยของ [14] มีประสิทธิภาพของเครื่องสูบน้ำเท่ากับ 0.00266%

TABLE II. STEAM-POWERED WATER PUMP EFFICIENCY

Case	*The steam storage area ratio in the pressure vessel (%)*	*Steam-powered water pump efficiency (%)*
I	75	0.004723
II	50	0.005297
III	25	0.005759

IV. อภิปรายผล

จากการทดลองบ่งชี้ว่าสัดส่วนพื้นที่ส่วนเก็บไอน้ำในถังขับดันมีผลต่อปริมาณน้ำที่สูบน้ำได้ เนื่องจากเมื่อพิจารณาการเปลี่ยนแปลงอุณหภูมิภายในระบบปั๊มสูบน้ำกำลังไอน้ำจะเห็นได้ว่า กรณีที่ I มีพื้นที่ส่วนเก็บไอน้ำ 75% ด้วยพื้นที่สะสมไอน้ำที่สูงกว่ากรณีที่ II และ III การเพิ่มขึ้นของความดันภายในถังขับดันจึงช้ากว่า 20 sec เพราะไอน้ำสามารถกระจายตัวในพื้นที่ที่ใหญ่กว่า ทำให้ต้องใช้ระยะเวลาในการสะสมไอน้ำและเพื่อเปลี่ยนเป็นความดันในการขับดันน้ำที่มากกว่า ขณะเดียวกันเมื่อไอน้ำเติมเข้าสู่พื้นที่เก็บไอน้ำ ไอน้ำบางส่วนจะเกิดการควบแน่นในของเหลวจนถึงจุดสมดุลระหว่างไอและของเหลว จึงทำให้ความดันสุดท้ายของกรณีที่ I ต่ำกว่าอีก 2 กรณี จากความดันสุดท้ายในการขับดันน้ำที่ต่ำกว่าจึงส่งผลต่อปริมาณน้ำที่สูบได้ต่ำที่สุดคือ 28,600 mL สอดคล้องกับงานวิจัยของ [15] ที่พบว่า สัดส่วนปริมาตรอากาศส่งผลต่อการทำงานของระบบ ปริมาตรน้ำที่สูบได้จะลดลงตามสัดส่วนของปริมาตรอากาศที่เติม ด้วยเหตุนี้จึงทำให้ประสิทธิภาพของปั๊มสูบน้ำกำลังไอน้ำต่ำที่สุด คือ 0.004723% และมีค่าการใช้พลังงานต่อหน่วยผลผลิตสูงที่สุด คือ 0.208 kJ/mL

V. ข้อสรุป

จากการทดลองระบบปั๊มสูบน้ำกำลังไอน้ำที่มีเฮดสถิตด้านดูดและด้านส่งน้ำเท่ากับ 1 m และ 2.5 m ตามลำดับ โดยวัดปริมาตรน้ำที่สูบได้จำนวน 3 cycle และควบคุมอุณหภูมิน้ำภายในถังผลิตไอน้ำ เท่ากับ 60 °C ผลการศึกษาผลของสัดส่วนพื้นที่ส่วนเก็บไอน้ำในถังขับดันที่มีต่อปริมาณน้ำที่สูบได้ สรุปได้ว่าพื้นที่ส่วนเก็บไอน้ำจะแปรผกผันกับปริมาณน้ำที่สูบได้ พื้นที่ส่วนเก็บไอน้ำที่ลดลงจะช่วยให้ประสิทธิภาพของปั๊มสูบน้ำกำลังไอน้ำเพิ่มขึ้น สามารถสูบน้ำได้ปริมาตรสูงสุด และมีค่าการใช้พลังงานต่อหน่วยผลผลิตต่ำที่สุด กรณีที่ III สามารถลดปริมาณการใช้พลังงานลงได้คิดเป็น 18% และ 8% เมื่อเปรียบเทียบกับกรณีที่ I และ II ดังนั้น จากงานวิจัยนี้กรณีที่ III จึงเป็นเงื่อนไขการทำงานที่เหมาะสมในการประหยัดพลังงาน แนวทางการวิจัยในอนาคตเพื่อเพิ่มประสิทธิภาพของปั๊มสูบน้ำกำลังไอน้ำควรศึกษาการสร้างสภาวะสุญญากาศที่สัมพันธ์กับระดับเฮดสถิตด้านดูดด้วยการติดตั้งอุปกรณ์ควบคุมการไหลของน้ำหล่อเย็นแบบอัตโนมัติเพื่อควบคุมปริมาณน้ำหล่อเย็น

คำขอบคุณ

คณะผู้วิจัยขอขอบคุณมหาวิทยาลัยราชภัฏภูเก็ตที่สนับสนุนงบประมาณในการทำวิจัย และขอขอบคุณผู้ช่วยศาสตราจารย์ ดร.ทรงเกียรติ ภาวดี ที่ให้ความอนุเคราะห์อุปกรณ์เก็บข้อมูล

อ้างอิง

[1] Energy Policy and Planning Office, “Energy situation in 2023 and trends for 2024,” [Online]. Available: https://www.eppo.go.th/images/Energy-Statistics/energyinformation/Forecast/ShorttermForecast/EnergyForecast2023.pdf. [Accessed: Jan. 26, 2025].

[2] Prachachat Business, “Phuket aims to reduce greenhouse gases and become a low-carbon city by 2030,” [Online]. Available: https://www.prachachat.net/local-economy/news-1371751. [Accessed: Jan. 26, 2025].

[3] N. Srichai, S. Kuayrakan, and C. Suwanprasit, “Water use and water demand modeling for hotel and tourism business, patong, phuket province,” the Prince of Songkla University Journal of Social Sciences and Humanities, vol. 22, no. 2, pp. 255-292, May-August 2016.

[4] S. Liengjindathawon, K. Kirtikara, P. Namprakai, and T. Kiatsiriroat, “Parametric studies of a pulsating-steam water pump,” International Journal of Ambient Energy, vol. 23, no. 1, pp. 37-46, Mar. 2011, doi: 10.1080/01430750.2002.9674867.

[5] D. Das, and M. R. Gopal, “Study on a metal hydride based solar water pump,” International Journal of Hydrogen Energy, vol. 29, no. 1, pp. 103-112, Jan. 2004, doi: 10.1016/S0360-3199(03)00044-2.

[6] K. Chalermtumrong, P. Namprakai, and N. Pratinthong, “Steam driven water pump using waste heat recovery,” in The 10th Kasetsart University Kamphaeng Saen Campus Conference, Nakhon Pathom, Thailand, December 6-7, 2013, pp. 1476-1483.

[7] P. Moonsri, P. Rakkanrane, C. Inyasree, and K. Sagulpongmalee, “A thermal water pump system from charcoal for community,” in The 8th Thailand Renewable Energy for Community Conference, Rajamangala University of Technology Thanyaburi, Pathumthani, Thailand, November 4-6, 2015, pp. 324-326.

[8] P. Salapsri, J. Sitranon, K. Witinantakit, K. Narkpiban, and P. Moonsri, “A study of the gauge pressure control that affects pumping of automatic water pump system with steam,” PSRU Journal of Industrial Technology and Engineering, vol. 5, no. 2, pp. 223–238, August 2023.

[9] J. Sitranon, K. Sutthivirode, and N. Roonprasang, “The mathematical modeling for a study of suction heads of a continuous operation thermal water pump with steam system,” SWU Engineering Journal, vol. 15, no. 3, pp. 89-100, September-December 2020.

[10] K. Sutthivirode, N. Prathinthong, P. Namprakai, N. Roonprasang, and T. Suparos, (2014). “Waste heat water pumping model with direct contact cooling,” Journal of Central South University, vol. 21, no. 10, pp. 3896-3910, Oct. 2014, doi: 10.1007/s11771-014-2377-6.

[11] S. Arunyaem, “Thermal water pump with steam and air,” M.S. thesis, Master of Science, Dept. Energy Tech., King Mongkut’s Univ. of Tech. Thonburi., Bangkok, Thailand, 2011

[12] P. Moonsri, J. Kunchornrat, and P. Namprakai, “Hybrid energy thermal water pump for producing hot water from a shallow well in Thailand,” Journal of Energy Engineering, vol. 142, no. 3, pp. 040150231-15, Jun. 2016, doi: 10.1061/(ASCE)EY.1943-7897.00002.

[13] C. Oonwised, J. Sitranon, and K. Sutthivirode, “Study of temperature and amount of cooling water affecting to vacuum pressure of steam water pump,” Journal of Renewable Energy for Community, vol. 4, no. 3, pp. 107-120, December 2021.

[14] N. Roonprasang, “A mathematical model of the solar water heater system self-circulated by a steam power,” Ph.D. dissertation, Dept. Energy Tech., King Mongkut’s Univ. of Tech. Thonburi., Bangkok, Thailand, 2008. [Online]. Available: https://dric.nrct.go.th/index.php?/Search/SearchDetail/209839

[15] J. Sitranon, C. Lertsatitthanakorn, P. Namprakai, N. Prathinthong, T. Suparos, and N. Roonprasang, “Performance enhancement of solar water heater with a thermal water pump,” Journal of Energy Engineering, vol. 141, no. 4, pp. 0401403601-10, Aug. 2014, doi: 10.1061/(ASCE)EY.1943-7897.0000216.

การยับยั้งเชื้อราก่อโรคในต้นทุเรียนด้วยสารสกัดจากสมุนไพร

Inhibition of fungi durian disease by herbal extracts

1st Angkhana Doladoi
Microbiology program
Faculty of Science technology and Agriculture
Yala Rajabhat University
Yala, Thailand
406463015@yru.ac.th

2nd Aklima Kamah
Microbiology program
Faculty of Science technology and Agriculture
Yala Rajabhat University
Yala, Thailand
Aklimas.kamah@gmail.com

3rd Afnan Domah
Medical and Industrial Microbiology program
Faculty of Science technology and Agriculture
Yala Rajabhat University
Yala, Thailand
40656301@yru.ac.th

4th Khosiya Sali*
Medical and industrial Microbiology program
Faculty of Science technology and Agriculture
Yala Rajabhat University
Yala, Thailand
Khosiya.s@yru.ac.th

ABSTRACT

The objective of this research was isolating pathogenic fungi causing anthracnose disease in durian trees, testing their ability to cause disease and the study of herbal crude extracts for inhibiting their fungal pathogens by agar diffusion method. The results showed one isolated *Colletotrichum* sp. and showed pathogenicity at level 3. The extracted herbs using 95% alcohol as solvent showed that *Alpinia galanga* (L.) Willd. had the best inhibitory effect on *Colletotrichum* sp. at a concentration of 400 mg/ml. (Inhibition percentage as 50.90±2.92), followed by *Curcumalonga* L., *Boesenbergia rotunda* (L.) Mansf. and Piper betle Linn. With percentage inhibition are 43.80±1.28 (400 mg/ml), 38.37±2.74 (400 mg/ml) and 29.20±0.73 (500 mg/ml). ml) respectively. Therefore, it is indicated that Alpinia galanga (L.) Willd. showed effective and will be studied for use in controlling certain fungi that cause disease in durian trees.

Keywords : Durian disease, Fungi, Inhibition, Herbs

I. บทนำ

ทุเรียนเป็นผลไม้เขตร้อนที่มีความสำคัญทางเศรษฐกิจของประเทศไทย โดยส่วนใหญ่จะปลูกกันมากในภาคตะวันออกและภาคใต้ จากรายงานการสำรวจในปี พ.ศ. 2565 พบว่า ภาคตะวันออกมีพื้นที่เพาะปลูกทุเรียนจำนวน 448,206 ไร่ และมีแนวโน้มเพิ่มสูงขึ้นอย่างต่อเนื่อง ส่วนภาคใต้มีพื้นที่เพาะปลูกทุเรียน จำนวน 672,330 ไร่ [1] อย่างไรก็ตาม การปลูกทุเรียนในประเทศไทยยังประสบกับปัญหากับโรคหลายชนิด โดยเฉพาะโรคที่มีสาเหตุจากเชื้อรา เช่น โรครากเน่าโคนเน่า (เชื้อ *Phytophthora palmovora*) โรคใบติดหรือใบไหม้ (เชื้อ *Rhizoctonia* sp.) โรคแอนแทรค-โนส (เชื้อ *Colletotrichum gloeosporiodes*) โรคราสีชมพู (เชื้อ *Corticium salmonicolor*) และโรคราแป้ง (เชื้อ *Oidium* sp.) โดยการเกิดโรคจะเริ่มตั้งแต่ระยะแรกของการเจริญเติบโตจนถึงระยะการเก็บเกี่ยวผลผลิต [2] สถิติการก่อโรครากเน่าโคนเน่า ปี 2565 มีพื้นที่ระบาด 12 จังหวัด ได้แก่ จังหวัดเพชรบุรี จันทบุรี ตราด ระยอง กระบี่ ชุมพร นครศรีธรรมราช นราธิวาส ปัตตานี ยะลา และจังหวัดสุราษฎร์ธานี มีเนื้อที่ระบาด จำนวน 3,083 ไร่ และในปี 2568 เนื้อที่ระบาดเพิ่มขึ้นเป็น 4,627 ไร่ และขยายพื้นที่การระบาดเป็น 16 หวัด โรคใบติดหรือใบไหม้มีพื้นที่ระบาด 9 จังหวัด ได้แก่ สงขลา ยะลา จันทบุรี ตราด ชุมพร นครศรีธรรมราช นราธิวาส สุราษฎร์ธานี และตรัง จำนวน 1,221 ไร่ โรคราดำ มีพื้นที่ระบาด 4 จังหวัด ได้แก่ จันทบุรี นครศรีธรรมราช สุราษฎร์ธานี และชุมพร จำนวน 64 ไร่ และโรคราสีชมพู มีพื้นที่ระบาด 6 จังหวัด ได้แก่ จันทบุรี ชุมพร ตราด นครศรีธรรมราช สุราษฎร์ธานี และกระบี่ จำนวน 151 ไร่ [3] ทำให้เกษตรกรมีการควบคุมโรคด้วยการใช้สารเคมี ซึ่งการใช้สารเคมีในปริมาณที่มากเกินไปส่งผลทำให้มีสารเคมีตกค้างในผลผลิต และเป็นมลพิษต่อสิ่งแวดล้อม นอกจากนั้นสารเคมีอาจมีผลทำให้เชื้อเกิดกลายพันธุ์และดื้อต่อสารเคมีที่ใช้ ทำให้การป้องกันและกำจัดเชื้อราทำได้ยากขึ้นในอนาคต จึงมีความจำเป็นที่ต้องหาแนวทางในการแก้ปัญหาดังกล่าว การใช้สารสกัดจากพืชจึงเป็นอีกหนึ่งทางเลือกในการควบคุมโรคพืชแบบชีววิธี จากรายงานวิจัย พบว่าสมุนไพรหลายชนิดมีสารสำคัญที่มีฤทธิ์ยับยั้งเชื้อรา เช่น สารสกัดจากหม่อนสามารถยับยั้งเชื้อรา *Phyllosticta* sp. และ *Colletotrichum* sp. ที่คัดแยกจากต้นทุเรียน [4] สารสกัดจากกระชาย ขมิ้นชัน หัวแห้วหมู สบู่เลือด ว่านอัคคีทวาร เปลือก มังคุด เมล็ดมะรุม และไพล มีฤทธิ์ยับยั้งการเจริญของเชื้อรา *Phytopthora* spp. [5] นอกจากนั้น กระเทียม ขิง กระชายขาว ขมิ้นข่า และตะไคร้มีผลต่อการยับยั้งการเจริญเติบโตของเชื้อรา *C. gloeosporioides* [6] ดังนั้น งานวิจัยนี้

ผู้วิจัยจึงมีความสนใจศึกษาสมุนไพรพื้นบ้าน ได้แก่ ใบพลู ข่า ขมิ้น และกระชายมาทดสอบประสิทธิภาพในการยับยั้งเชื้อราที่คัดแยกจากต้นทุเรียนในพื้นที่จังหวัดยะลา เพื่อนำมาเป็นข้อมูลพื้นฐานในการพัฒนาเป็นผลิตภัณฑ์ให้เกษตรกรนำมาใช้แทนสารเคมีต่อไปในอนาคตและเพื่อเพิ่มมูลค่าสมุนไพรในท้องถิ่น

II. ทบทวนวรรณกรรม

โรคในต้นทุเรียน

การปลูกทุเรียนในประเทศไทยประสบปัญหาเกี่ยวกับโรคที่สำคัญหลายชนิด เช่น โรครากเน่าโคนเน่าที่เกิดจากเชื้อ *P. palmivora* ซึ่งเป็นโรคที่มีความสำคัญที่สุดในการปลูกทุเรียน เนื่องจากเชื้อราชนิดนี้สามารถเข้าทำลายพืชได้ทุกส่วนของต้นทุเรียน ตั้งแต่ส่วนของราก ลำต้น กิ่ง ใบ และผล ทำให้เกิดความเสียหายกับเกษตรกรผู้ปลูกทุเรียนอย่างมาก [3] โรคแอนแทรกโนส เกิดจากเชื้อรา *Colletotrichum* spp. เชื้อราชนิดนี้ทำให้ต้นทุเรียนมีลักษณะอาการสำคัญ คือ ใบจะไหม้เป็นสีน้ำตาล ซึ่งมักเกิดบริเวณขอบใบหรือกลางใบ บริเวณเนื้อใบที่ไหม้จะเป็นสีน้ำตาลอ่อน ขอบของแผลจะเป็นสีน้ำตาลเข้มล้อมรอบแผล เนื้อใบมีลักษณะโปร่งใส โดยเชื้อ *Collectrotrichum* spp. ที่คัดแยกจากต้นทุเรียน พบว่า เป็นเชื้อ *C. gloeosporioides* [1] เช่นเดียวกับรายงานของ Sutthisa [7] โรคใบติดหรือใบไหม้ เกิดจากเชื้อ *Rhizoctonia* sp. โรคชนิดนี้ทำให้เกิดส่วนใบมีลักษณะอาการเหมือนน้ำร้อนลวกและเปลี่ยนเป็นสีน้ำตาล เชื้อราจะมีการแพร่ไปยังใบอื่น ๆ โดยการสร้างเส้นใย สุดท้ายจะทำให้เกิดอาการใบแห้งเป็นหย่อม ๆ และใบจะค่อย ๆ ร่วงหล่น ส่งผลทำให้ต้นทุเรียนเสียรูปทรง และมีการเจริญเติบโตที่ไม่สมบูรณ์ [2] โรคราสีชมพู เกิดจากเชื้อ *Erythricium salmonicolor (Corticium salmonicolor)* เชื้อราชนิดทำให้เกิดในต้นทุเรียนโดยเส้นใยสีขาวของเชื้อราเจริญคลุมกิ่งหรือลำต้น และเปลี่ยนเป็นสีครีมถึงชมพูอ่อนยึดแน่นกับกิ่ง เมื่อเฉือนดูเนื้อไม้จะเป็นแผลสีน้ำตาล กิ่งและยอดที่เป็นรอยโรคจะเหี่ยวและกิ่งจะแห้งตาย ใบเหลืองและร่วง [8] และโรคราแป้งเกิดจากเชื้อ *Oidium* sp. โดยเชื้อราชนิดนี้สามารถเข้าทำลายผลทุเรียนได้ตั้งแต่เริ่มติดผลอ่อนจนกระทั่งผลแก่ เส้นใยของเชื้อราจะเจริญปกคลุมผล หากเข้าทำลายรุนแรงในระยะติดผลใหม่ ๆ อาจทำให้ผลอ่อนร่วงหรือถ้าเป็นกับผลที่กำลังเจริญเติบโต จะทำให้สีผิวของเปลือก เป็นสีน้ำตาลแดงไม่เป็นมัน และทำให้หนามทุเรียนเป็นรอยแตกเล็ก ๆ ไม่เป็นที่ต้องการของผู้บริโภค [9]

สมุนไพร

ใบพลู (*Piper betle* L.) วงศ์ PIPERACEAE ใบพลูเป็นใบเลี้ยงเดี่ยว มีรสเผ็ด ๆ ร้อน ๆ มีกลิ่นฉุน ใบมีลักษณะกลม ๆ ปลายแหลม สารสำคัญที่พบในใบพลูขึ้นอยู่กับตัวทำละลายที่ใช้ในการสกัด [10] ใบพลูมีสาระสำคัญในกลุ่ม allypyrocatechol, eugenol [11] phenol, flavonoid และ tannin [10] และสารกลุ่ม hydroxychavicol [12] เป็นต้น จากรายงานผลการวิจัย พบว่า สารสกัดจากใบพลูมีประสิทธิภาพสูงสุดในการยับยั้งเชื้อรา *Aspergillus niger, Penicillium* sp. และ *Rhizopus* sp. [13]

ข่า (*Alpinia galanga* (L.) Willd.) วงศ์ Zingiberaceae ประกอบด้วยสารสำคัญ คือ Gingerol ที่แสดงผลการยับยั้งการเจริญของแบคทีเรียและเชื้อราหลายชนิดในการทดลองในหลอดทดลอง (*in vitro*) โดยข่ามีประสิทธิภาพสูงสุดในการยับยั้งเชื้อรา *Aspergillus niger*, *Penicillium* sp. และ *Rhizopus* sp. เช่นกัน [13] นอกจากนั้น สารสกัดจากเหง้าข่ายังสามารถยับยั้งเส้นใยเชื้อรา *Aspergillus Flavus, A. niger, Drechslera hawaiiensis and Humicola Fuscoatra* ที่เป็นสาเหตุโรคในพืช [14] สารสกัดจากข่ามีประสิทธิภาพสูงสุดในการยับยั้งเชื้อรา *Rhizoctonia solani* Kuhn. [15]

ขมิ้น (*Curcumalonga* L.) วงศ์ Zinggiberaceae สารสำคัญในขมิ้นที่มีฤทธิ์ในการยับยั้งเชื้อรา ได้แก่ Curcumin, Shikonin, Desmethoxycurcumin มีฤทธิ์ยับยั้งเชื้อรา *P. palmivora* โดยสารกลุ่ม Shikonin มีประสิทธิภาพเท่ากับสารเคมีกลุ่มเบนโนมิลและไทอะเบนดาโซล [5]

กระชาย (*Boesenbergia rotunda (L.) Mansf.*) วงศ์ Zingiberaceae ส่วนเหง้าของกระชายจะมีสารสำคัญหลายชนิด ได้แก่ สารกลุ่ม flavonoid และ chromene เป็นต้น [16] จากรายงานวิจัยพบว่า กระชายที่สกัดด้วยตัวทำละลายไดคลอโรมีเทน (CH_2Cl_2) และเมทานอล (CH_3OH) สามารถต้านการเจริญของรา *R. solani* Kuhn. เชื้อก่อโรคกาบใบแห้งในข้าวในระดับห้องปฏิบัติการ [15] นอกจากนั้นกระชายยังมีฤทธิ์ควบคุมเชื้อรา *C. gloeosporioides* ที่เป็นเชื้อสาเหตุของโรคหอมเลื้อยในห้องปฏิบัติการและในแปลงปลูก [16] จากรายวิจัย [17] พบว่า น้ำมันสกัดจากกระชายพบสาร eugenol และ linalool สามารถควบคุมการสร้างสปอร์ของเชื้อรา *Lasiodiplodia theobromae* โรคโคนเน่าของต้นกล้วย

III. ระเบียบวิธีวิจัย

1. การคัดแยกเชื้อราเป็นสาเหตุการเกิดโรคในต้นทุเรียน

เก็บตัวอย่างชิ้นส่วนจากต้นทุเรียนที่แสดงอาการของโรคจากพื้นที่จังหวัดปัตตานี และยะลาทั้งหมด 7 ตัวอย่าง โดยตัดส่วนที่เป็นรอยต่อระหว่างเนื้อเยื่อที่ดีกับบริเวณที่เกิดโรค ตัดเป็นรูปสี่เหลี่ยมจัตุรัส ขนาด 0.5 x 0.5 เซนติเมตร นำไปแช่ในสารละลายคลอร็อกซ์ (Chlorox) ความเข้มข้นร้อยละ 10 โดยปริมาตร เป็นเวลา 3 นาที แช่น้ำกลั่นปลอดเชื้อเป็นเวลา 3 นาที นำชิ้นตัวอย่างมาวางในจานอาหาร Potato Dextrose Agar (PDA) นำไปบ่มที่อุณหภูมิ 25 องศาเซลเซียส เป็นเวลา 5 วัน

สังเกตการเจริญของเส้นใย เมื่อพบการเจริญของเส้นใยเชื้อรา จะใช้เข็มปลายงอตัดส่วนปลายของเส้นใยวางบริเวณตรงกลางจานอาหาร PDA จานใหม่ จากนั้นนำไปบ่มที่อุณหภูมิ 25 องศาเซลเซียส เป็นเวลา 5 วัน แยกจนได้ลักษณะโคโลนีที่บริสุทธิ์และนำไปศึกษาลักษณะทางสัณฐานวิทยาภายใต้กล้องจุลทรรศน์แบบใช้แสง [18]

2. การทดสอบความสามารถในการทำให้เกิดโรคของเชื้อรา

นำเชื้อรา ไอโซเลท LM3 ที่แยกได้มาเลี้ยงบนอาหาร PDA เป็นเวลา 5 วัน ส่วนใบพืชเลือกใบทุเรียนหมอนทองที่สมบูรณ์ไม่มีรอยโรคนำมาจุ่มใบในสารละลาย Clorox 10% เป็นเวลา 5 นาที เพื่อฆ่าเชื้อบริเวณผิวรอบนอก จากนั้นล้างด้วยน้ำกลั่น 2 ครั้ง ผึ่งให้น้ำแห้ง จากนั้น เจาะเส้นใยเชื้อราด้วย Cork borer เบอร์ 1 เส้นผ่าศูนย์กลาง 5 มิลลิเมตร จำนวน 6 ชิ้น วางลงบนใบทุเรียนหมอนทอง โดยใบทุเรียนที่ใช้เป็นชุดควบคุมจะไม่ใส่เชื้อรา ทำทดลองทั้งหมด 5 ซ้ำ หลังจากนั้น นำใบทุเรียนที่วางเส้นใยเชื้อราใส่ในกล่องพลาสติกที่มีความชื้น โดยการฉีดน้ำใส่ลงไปในกล่องบ่มที่อุณหภูมิห้อง เป็นเวลา 3 วัน วัดเส้นผ่าศูนย์กลางการเกิดรอยโรค และนำค่าเฉลี่ยประเมินความรุนแรงของโรค โดยความรุนแรงของโรคจัดลำดับ 5 ระดับ ดังนี้ ขนาดแผล 0 = ไม่มีอาการ, 1 = ขนาดแผล 1-5 mm, 2 = ขนาดแผล 6-10 mm, 3 = ขนาดแผล 11-20 mm, 4 = ขนาดแผลมากกว่า 20 mm [19]

3. การเตรียมสมุนไพรและการสกัดสมุนไพร

นำใบพลู ข่า ขมิ้น และกระชาย มาล้างทำความสะอาด หั่นเป็นชิ้นเล็ก ๆ แล้วอบในตู้อบลมร้อนที่อุณหภูมิ 60 องศาเซลเซียส เป็นเวลา 7 วัน เมื่อสมุนไพรแห้งนำมาปั่นให้ละเอียดด้วยเครื่องปั่นแห้ง จากนั้นนำมาหมักด้วยสารละลายเอทนอลความเข้มข้นร้อยละ 95 อัตราส่วน 1 : 5 หมักที่อุณหภูมิห้องเป็นเวลา 7 วัน จากนั้นนำมากรองสารด้วยกระดาษกรอง Whatman เบอร์ 1 นำไประเหยตัวทำละลายออกด้วยเครื่อง Rotary Evaporator จะได้สารที่แข็งหนืด ชั่งน้ำหนักและเก็บสารสกัดในขวดสีชาที่อุณหภูมิ 4 องศาเซลเซียส เพื่อนำไปใช้ในการทดลองต่อไป [13] นำไปคำนวณหาร้อยละปริมาณสารสกัดหยาบคำนวณได้ดังนี้

% yield = (weight of crude extract/weight of fresh leaf) x 100

4. ทดสอบประสิทธิภาพของสารสกัดสมุนไพรต่อการยับยั้งการเจริญของเชื้อรา

การเตรียมเชื้อสำหรับทดสอบ โดยเลี้ยงเชื้อราที่คัดแยกได้มาเลี้ยงบนอาหาร PDA บ่มที่อุณหภูมิ 25 องศาเซลเซียส เป็นเวลา 5 วัน จากนั้นเจาะเส้นใยเชื้อราด้วย Cork borer ให้ได้เส้นผ่าศูนย์กลาง 4 มิลลิเมตร ตัดขอบโคโลนี วางห่างจากขอบอาหาร PDA 3 เซนติเมตร [19] จากนั้นปรับความเข้มข้นของสารสกัดที่ระดับความเข้มข้น คือ 100 200 300 400 และ 500 มิลลิกรัมต่อมิลลิลิตร ด้วยตัวทำละลาย 95% เอทานอล เพื่อให้ได้ความเข้มข้นที่ต้องการ จากนั้นเจาะอาหาร PDA ด้วย Cork borer ขนาด 4 มิลลิเมตร (วางในทิศทางตรงกันข้ามกับเชื้อรา) นำสารสกัดที่มีความเข้มข้นต่าง ๆ หยดลงในหลุม ปริมาตร 80 ไมโครลิตร ส่วนชุดควบคุมใช้ 95% เอทานอล แต่ละชุดการทดลองจะทำ 2 ซ้ำ บ่มที่อุณหภูมิห้องเป็นเวลา 7 วัน [20] บันทึกผลโดยวัดระยะการเจริญเติบโตของเชื้อรา ตรวจสอบเปอร์เซ็นต์การยับยั้งเชื้อรา คำนวณได้ดังนี้

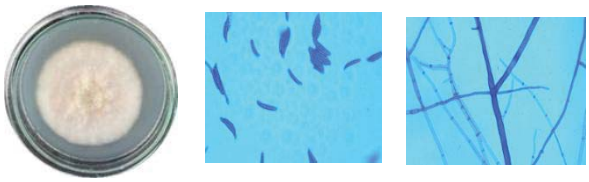
เปอร์เซ็นต์การยับยั้งการเจริญเติบโตของเชื้อ = [(A-B)/A] x 100

A = วัดรัศมีของโคโลนีเชื้อราบนจานอาหารเลี้ยงเชื้อควบคุม

B = วัดรัศมีของโคโลนีเชื้อราที่ยับยั้งด้วยสารสกัด

IV. ผลการการทดลอง

จากการคัดแยกเชื้อราจากส่วนต่าง ๆ ของต้นทุเรียนที่แสดงอาการโรคใบจุดในพื้นที่จังหวัดยะลา และปัตตานี ด้วยวิธีการเพาะเลี้ยงบนอาหาร Potato Dextrose agar สามารถคัดแยกเชื้อทั้ง 10 ไอโซเลท ที่แสดงลักษณะของเส้นใยและสปอร์ที่แตกต่างกัน เมื่อศึกษาลักษณะของเส้นใยและลักษณะภายใต้กล้องจุลทรรศน์มีเพียงไอโซเลทเดียวที่มีลักษณะที่สอดคล้องกับกลุ่มเชื้อราที่เป็นสาเหตุของโรคในต้นทุเรียน ได้แก่ ไอโซเลท LM3 มีลักษณะของเส้นใยสีขาวครีม เจริญฟูบนผิวหน้าอาหาร เมื่อตรวจสอบภายใต้กล้องจุลทรรศน์สปอร์มีลักษณะรูปร่างเป็นท่อนสั้น คล้ายพระจันทร์เสี้ยว หัวท้ายมน ไม่มีผนังกั้น ดังภาพที่ 1



ก. ข ค

ภาพที่ 1 ลักษณะของเชื้อราที่คัดแยกจากใบทุเรียน

ก. ลักษณะโคโลนีที่เลี้ยงบนอาหาร PDA

ข. ลักษณะสปอร์ภายใต้กล้องจุลทรรศน์ 400 เท่า

ค. ลักษณะเส้นใยภายใต้กล้องจุลทรรศน์แบบใช้แสง 400 เท่า

จากการทดสอบความสามารถในการทำให้เกิดโรคของเชื้อรา ไอโซเลท LM3 ที่คัดแยกได้จากต้นทุเรียน พบว่าใบทุเรียนแสดงอาการของโรคหลังการปลุกเชื้อบนใบทุเรียน โดยใบทุเรียนมีลักษณะเป็นสีน้ำตาลคล้ายโดนน้ำร้อนลวกรอบ ๆ โคโลนีของเชื้อราที่วางไว้ เมื่อนำมาคำนวณหาระดับการก่อโคพบว่า การแสดงอาการของโรคอยู่ในระดับที่ 3 ดังภาพที่แสดงในตารางที่ 1 จากการสกัดสารจากใบพลู ข่า ขมิ้น และกระชาย ด้วยตัวทำละลายเอทานอล ในอัตราส่วน 1:5 พบว่า ปริมาณของสารสกัด พบว่ากระชายให้ปริมาณของสารสกัดมากที่สุด คือ ร้อยละ 6.19 รองลงมา ขมิ้น ใบพลู และข่า ตามลำดับ ดังแสดงในตารางที่ 2 เมื่อนำสารสกัดทั้ง 4 ชนิดมาทดสอบประสิทธิภาพการยับยั้งเชื้อเรา ไอโซเลท LM3 ที่คัดแยกได้จากต้นทุเรียนระดับความเข้มข้น 100 200 300 400 และ 500 มิลลิกรัมต่อมิลลิลิตร ด้วยวิธี agar well diffusion พบว่า สารสกัดทั้ง 4 ชนิดสามารถยับยั้งการเจริญของเชื้อรา ไอโซเลท LM3 ที่ทุกความเข้มข้น โดยข่ามีร้อยละการยับยั้งการเจริญของเส้นใยเชื้อราสูงที่สุด คือ ร้อยละ 50.90 และ 49.10 ที่ระดับความเข้มข้น 400 และ 300 มิลลิกรัมต่อมิลลิลิตร ตามลำดับ ไม่แตกต่างกันอย่างมีนัยสำคัญทางสถิติ ($p<0.05$) ดังภาพที่ 2 ส่วนสารสกัดจากขมิ้น และใบพลู พบว่าทุกระดับความเข้มข้นแสดงค่าร้อย

ละการยับยั้งเชื้อราทดสอบไม่แตกต่างกันอย่างมีนัยสำคัญทางสถิติ ($p<0.05$) เช่นกัน ในขณะที่กระชาย พบว่า มีค่าการยับยั้งสูงสุดที่ระดับความเข้มข้นที่ 400 และ 500 ซึ่งแสดงค่าที่ไม่แตกต่างกันอย่างมีนัยสำคัญทางสถิติ ($p<0.05$) ดังแสดงในตารางที่ 3

ตารางที่ 1 แสดงการเปลี่ยนแปลงที่เกิดบนใบทุเรียนหมอนทองที่ทดสอบด้วยเชื้อราที่คัดแยกได้จากต้นทุเรียน

ชุดทดสอบ	ลักษณะอาการของโรค
Control	
ไอโซเลท LM3	

ตารางที่ 2 แสดงลักษณะของสารสกัดหยาบและปริมาณร้อยละของสารสกัดที่สกัดได้

สมุนไพร	ลักษณะสารสกัด	ร้อยละ
ใบพลู	สีเขียวขี้ม้า ข้นหนืด	4.21
ข่า	สีน้ำตาล ข้นหนืด	3.28
ขมิ้น	สีเหลืองส้ม ข้นหนืด	5.11
กระชาย	สีน้ำตาลเข้ม ข้นหนืด	6.19

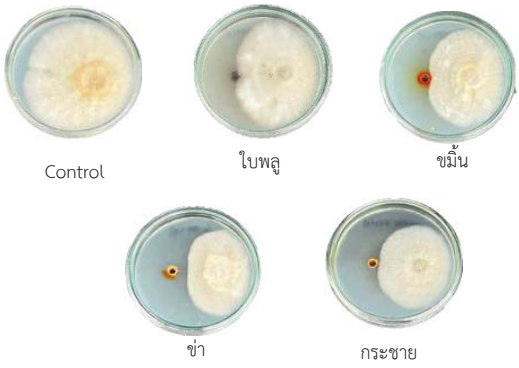
ตารางที่ 3 แสดงค่าเฉลี่ยร้อยละการยับยั้งเชื้อราของสารสกัดหยาบสมุนไพรทั้ง 4 ชนิด ด้วย วิธี agar well diffusion

ความเข้มข้น (mg/ml)	ค่าเฉลี่ยการยับยั้งเชื้อรา (%)			
	ข่า	ขมิ้น	กระชาย	ใบพลู
100	34.50^{b}±2.74	40.05^{a}±0.37	29.59^{c}±0.55	30.36^{a}±2.74
200	39.53^{ab}±0.73	40.18^{a}±0.18	31.14^{bc}±1.64	31.27^{a}±1.83
300	49.10^{a}±8.77	42.89^{a}±0.00	28.55^{c}±0.18	32.43^{a}±0.18
400	50.90^{a}±2.92	43.80^{a}±1.28	38.37^{a}±2.74	29.20^{a}±0.73
500	45.74^{ab}±2.19	40.31^{a}±3.65	35.27^{ab}±2.01	35.92^{a}±6.21

หมายเหตุ: ตัวอักษร a, b, c ที่เหมือนกันในแนวตั้งแสดงค่าเฉลี่ยของชุดทดลองไม่แตกต่างกันอย่างมีนัยสำคัญทางสถิติ ($p\leq0.05$)

V. อภิปรายผลการทดลอง

จากการคัดแยกเชื้อราจากต้นทุเรียนในพื้นที่จังหวัดยะลา และปัตตานี เมื่อนำมาเลี้ยงบนอาหาร PDA สามารถคัดแยกเชื้อทั้ง 10 ไอโซเลท ที่แสดงลักษณะของเส้นใยและสปอร์ที่แตกต่างกัน เมื่อศึกษาลักษณะของเส้นใยและลักษณะภายใต้กล้องจุลทรรศน์มีเพียงไอโซเลทเดียวที่มีลักษณะ



ภาพที่ 2 ผลของสารสกัดหยาบสมุนไพรใบพลู ข่า ขมิ้น และกระชาย ที่ระดับความเข้มข้น 500 มิลลิกรัมต่อมิลลิลิตร

สอดคล้องกับเชื้อราที่เป็นสาเหตุของโรคในต้นทุเรียน ได้แก่ ไอโซเลท LM3 มีลักษณะของเส้นใยสีขาวครีม เจริญฟูบนผิวหน้าอาหาร เมื่อตรวจภายใต้กล้องจุลทรรศน์สปอร์มีรูปร่างเป็นท่อนสั้น คล้ายพระจันทร์เสี้ยว หัวท้ายมน ไม่มีผนังกั้น ส่วนอีก 9 ไอโซเลท ที่คัดแยกได้ เมื่อนำมาศึกษาภายใต้กล้องจุลทรรศน์ ไม่พบส่วนของสปอร์ จึงทำให้ไม่สามารถระบุสายพันธุ์ของเชื้อราได้ ส่วนเชื้อรา ไอโซเลท LM3 เมื่อนำมาเทียบลักษณะของเส้นใยและสปอร์ พบว่า คล้ายกับเชื้อรา *Colletotrichum* sp. สอดคล้องกับศึกษาของธารทิพย์ รัตนะ [21] พบว่า การคัดแยกเชื้อราก่อโรคในพริกบนอาหาร PDA เมื่อตรวจสอบสปอร์ภายใต้กล้องจุลทรรศน์มีลักษณะรูปร่างเป็นท่อนสั้น หัวท้ายมน ไม่มีผนังกั้น ภายในใสไม่มีสี จำแนกเป็นเชื้อรา *C. gloeosporioides* และสอดคล้องกับรายงานของจีรนันท์ กล่อมนรา แก้วรักษา [4] พบว่า สปอร์มีลักษณะรูปร่างเป็นโค้งงอเป็นท่อนสั้น ๆ หัวท้ายมน ใสไม่มีสี จำแนกเป็นเชื้อรา *Colletotrichum* sp.

ผลการสกัดสารจากใบพลู ข่า ขมิ้น และกระชาย ด้วยตัวทำละลายเอทานอล ในอัตราส่วน 1:5 พบว่าสารสกัดสมุนไพรที่ได้ปริมาณมากที่สุด คือ กระชาย รองลงมา คือ ขมิ้น ใบพลู และข่า มีปริมาณสารสกัดร้อยละ 6.19, 5.11, 4.21 และ 3.28 ตามลำดับ ลักษณะของสารสกัดที่ได้ พบว่าใบพลูมีลักษณะสีเขียวขี้ม้า ข้นหนืด สอดคล้องกับผลการศึกษาของปาริชาติ อ้นองอาจ และคณะ [22] ข่ามีลักษณะสีน้ำตาล ข้นหนืด สอดคล้องกับผลการศึกษาของอาวุธ หงส์ศิริ และคณะ [23] ขมิ้นมีลักษณะ สีเหลืองส้ม ข้นหนืด สอดคล้องกับผลการศึกษาของธารหทัย มาลาเวช {24} กระชายลักษณะสีน้ำตาลเข้ม ข้นหนืด สอดคล้องกับผลการศึกษาของโชติรส กิจสมชีพ [25]

จากการทดสอบประสิทธิภาพของสมุนไพรทั้ง 4 ชนิด ในการยับยั้งเชื้อรา ไอโซเลท LM3 ที่คัดแยกได้จากต้นทุเรียนที่ระดับความเข้มข้น 100 200 300 400 และ 500 มิลลิกรัมต่อมิลลิลิตร ด้วยวิธี agar well diffusion พบว่า สารสกัดทั้ง 4 ชนิด สามารถยับยั้งการเจริญของเชื้อรา ไอโซเลท LM3 ที่ทุกระดับความเข้มข้น โดยข่ามีร้อยละการยับยั้งการเจริญของเส้นใยเชื้อราสูงที่สุด คือ ร้อยละ 50.90 และ 49.10 ที่ระดับความเข้มข้น 400 และ 300 มิลลิกรัมต่อมิลลิลิตร ตามลำดับ และใบพลู พบว่าทุกระดับความเข้มข้นแสดงค่าร้อยละการยับยั้งเชื้อราทดสอบไม่แตกต่างกันอย่าง

มีนัยสำคัญทางสถิติ ($p<0.05$) เช่นกัน ในขณะที่กระชาย พบว่า มีค่าการยับยั้งสูงสุดที่ระดับความเข้มข้นที่ 400 และ 500 ซึ่งแสดงค่าที่ไม่แตกต่างกันอย่างมีนัยสำคัญทางสถิติ ($p<0.05$) สอดคล้องกับงานวิจัยของภัทรภร เอื้อรักสกุล [15] พบว่า ข่าที่สกัดด้วยไดคลอโรมีเทนความเข้มข้น 1,000 มิลลิกรัมต่อลิตร (ส่วนในล้านส่วน) แสดงประสิทธิภาพในการต้านการเจริญของรา *R. solani* ได้สูงสุด (86.30%) และสอดคล้องกับงานวิจัยของวิมลศิริ สีหะวงษ์ [6] พบว่า สารสกัดข่า ขมิ้น และกระชายขาวที่สกัดด้วยเอทานอล 95 เปอร์เซ็นต์ มีฤทธิ์ยับยั้งการเจริญของเส้นใยเชื้อรา *C. gloeosporioides* ที่ระดับความเข้มข้น 1,000 มิลลิกรัมต่อลิตร โดยกระชายมีฤทธิ์การยับยั้งดีที่สุด เท่ากับร้อยละ 93.86 ซึ่งแสดงผลการยับยั้งที่ดีกว่า ทั้งนี้ อาจเกิดจากอายุและสภาพแวดล้อมในช่วงของการเก็บตัวอย่างพืชสมุนไพร เนื่องจากช่วงฤดูกาลของการเก็บตัวอย่างมีผลต่อปริมาณของสารสำคัญที่อยู่ในพืช [11] นอกจากนั้น จากการศึกษาที่ความเข้มข้น 100-500 มิลลิกรัมต่อมิลลิลิตร พบว่า สารสกัดจากข่า และกระชาย มีฤทธิ์การยับยั้งเชื้อรา *Colletotrichum* sp. โดยเมื่อเพิ่มระดับความเข้มข้นจาก 100-300 มิลลิกรัมต่อมิลลิลิตร มีเปอร์เซ็นต์การยับยั้งเชื้อราไอโซเลท LM3 แตกต่างกันอย่างมีนัยสำคัญทางสถิติ ($p<0.05$) แต่สารสกัดจากขมิ้น และใบพลู พบว่า ระดับความเข้มข้นที่เพิ่มขึ้นไม่มีผลต่อประสิทธิภาพการยับยั้ง สอดคล้องกับการศึกษาของจีรนันท์ กล่อมนรา แก้วรักษา [4] ศึกษาประสิทธิภาพของสารสกัดหยาบจากส่วนต่าง ๆ ของหม่อน ด้วยวิธี Paper Disc Diffusion ที่ระดับความเข้มข้น 300 600 900 มิลลิกรัมต่อมิลลิลิตร สามารถยับยั้งเชื้อรา *Colletotrichum* sp. ที่คัดแยกจากใบทุเรียน พบว่าความเข้มข้นที่เพิ่มขึ้นไม่ได้มีผลต่อการยับยั้งเชื้อเช่นกัน

VI. สรุปผลการวิจัย

จากการคัดแยกเชื้อราจากชิ้นส่วนต่าง ๆ ของทุเรียนที่แสดงอาการของโรคสามารถคัดแยกเชื้อราที่คุณสมบัติการเกิดโรคในต้นทุเรียน จำนวน 1 ไอโซเลท และสามารถบงชี้ว่ามีความคล้ายกับเชื้อ *Colletotrichum* sp. ผลผลการทดสอบประสิทธิภาพการยับยั้งเชื้อราจากสารสกัดหยาบจากสมุนไพรท 4 ชนิด ได้แก่ ใบพลู ข่า ขมิ้น และกระชาย พบว่าสารสกัดจากข่า ขมิ้น กระชาย และใบพลู มีร้อยละการยับยั้งดีที่สุด เท่ากับ 50.90±2.92 43.80±1.28 38.37±2.74 และ 29.20±0.73 ตามลำดับ โดยสารสกัดจากข่ามีประสิทธิภาพการยับยั้งเชื้อสูงที่สุด

อ้างอิง

[1] นิกร แสงเกตุ. (2565). *สถานการณ์ไม้ผลภาคใต้ ปี 2565*. สืบค้น 12 กันยายน 2566, จาก https://www.opsmoac.go.th/news-files441091791314?fbclid=IwAR1RP_Zz4lHDVanLud8odUoZR27OJyZQub1MV9gfpMDhPS9ktvEmlVGNoSQ.

[2] กรมวิชาการเกษตร. (2563). การผลิตทุเรียนภาคใต้ตอนล่าง. สำนักวิจัยและพัฒนาการเกษตรเขตที่ 8 กรมวิชาการเกษตร สืบค้น 20 เมษายน 2568 จาก https://www.doa.go.th/oardwp-content/uploads/2020/09/การผลิตทุเรียนภาคใต้ตอนล่างn.pdf.

[3] ศูนย์ติดตามและแก้ไขปัญหาภัยพิบัติด้านการเกษตร กระทรวงเกษตรและสหกรณ์. (2568). สถานการณ์ศัตรูพืชระบาด สืบค้น 20 เมษายน 2568 จาก https://www.moac.go.th/warning-files-471891791905.

[4] จีรนันท์ กล่อมนรา แก้วรักษา. (2562). ศึกษาประสิทธิภาพของสารสกัดหยาบจากส่วนต่าง ๆ ของหม่อนที่มีผลต่อการยับยั้งเชื้อราที่คัดแยกได้จากใบทุเรียน. วารสารวิจัยมหาวิทยาลัยเทคโนโลยีราชมงคลศรีวิชัย, 11(2), 197-20.

[5] วาสินี ธรรมสถิต, สุจิตรา สุคนธมัต และดุษณี ธนะบริพัฒน์. (2560). การคัดเลือกสมุนไพรที่มีฤทธิ์ควบคุมเชื้อรา *Phytopthora* sp. ที่ แยกจากทุเรียนในจังหวัดจันทบุรี และจังหวัด ชุมพร. *วารสารวิทยาศาสตร ลาดกระบัง*, *26*(2), 1-14.

[6] วิมลศิริ สีหะวงษ์, สายัณห์ สืบผาง และสุวิจักขณ์ อรุณลักษณ์. (2565). การควบคุมการเจริญของเชื้อรา *Collectotrichum gloeosporiodes* เชื้อสาเหตุของโรคหอมเลื้อยด้วยสารสกัดสมุนไพร. *วารสารวิทยาศาสตร์เทคโนโลยี มรย, 7*(2), 35-42.

[7] Sutthisa, W., Popranom, A., Taddeetrakool, A., & Khankhum, S. (2024). Development of *Trichoderma* formulation and application to control durian anthracnose disease. *Trends in Sciences*, *21*(1), 7276-7276.

[8] สำนักงานเกษตรและสหกรณ์ จังหวัดชุมพร. (2566). ระวังโรคราสีชมพู (เชื้อรา *Erythricium salmonicolor* (*Corticium salmonicolor*)) ในทุเรียน. สืบค้น 20 เมษายน 2568 จากhttps://www. opsmoac.go.th /chumphon-warning-preview-452791791951.

[9] สำนักงานเกษตรและสหกรณ์ จังหวัดปัตตานี. (2565). ระวัง โรคราแป้ง (เชื้อรา *Oidium* sp.) ในทุเรียน. สืบค้น 20 เมษายน 2566 จาก https://www.opsmoac.go.th/pattani-local_wisdom-preview-442891791855.

[10] Taukoorah, U., Lall, N., & Mahomoodally, F. (2016). Piper betle L.(betel quid) shows bacteriostatic, additive, and synergistic antimicrobial action when combined with conventional antibiotics. *South African Journal of Botany*, *105*, 133-140.

{11} นิรมล สิงห์ทองรัตน์, จิรดา สิงขรรัตน์ และสุมณฑา วัฒนสินธุ์. (2013). ผลของฤดูการเก็บเกี่ยวต่อลักษณะรูปแบบทางเคมีของสารสำคัญในใบพลู. *Thai Journal of Science and Technology*, *2*(3), 192-199.

[12] Ali, I., Khan, F. G., Suri, K. A., Gupta, B. D., Satti, N. K., Dutt, P., and Khan, I. A. (2010). In vitro antifungal activity of hydroxychavicol isolated from Piper betle L. *Annals of clinical microbiology and antimicrobials*, *9*, 1-9.

[13] สายสมร ลำลอง และนิตยา คำพันธ์. (2560). การยับยั้งการเจริญของเชื้อราบนยางแผ่นด้วยสารสกัดจากสมุนไพร. *Research on Modern science and Utilizing Technological Innovation Journal (RMUTI Journal)*, *10*(2), 107-118.

[14] Hanaa A. E. Attia. (2015). Anti-microbial Activity of Alpinia Galanga Rhizome Extracts Against Some Plant Phathogens. Egyptian Scientific Journal of Pesticides, 1(4), 1-5.

[15] ภัทรภร เอื้อรักสกุล, กิตติยา ศิลาวงศ์ และนิลุบล สอนแก้ว. (2024). การเปรียบเทียบประสิทธิภาพของสารสกัดจากพืชวงศ์ขิงบางชนิดต่อการ ต้านเชื้อรา *Rhizoctonia solani* Kuhn. *วารสารสถาบันวิจัยและพัฒนา มหาวิทยาลัยราชภัฏบ้านสมเด็จเจ้าพระยา*, *9*(2), 52-61.

[16] วิมลศิริ สีหะวงษ์, สายัณห์ สืบผาง และสุวิจักขณ์ อรุณลักษณ์. (2565). การควบคุมการเจริญของเชื้อรา *Collectotrichum gloeosporiodes* เชื้อสาเหตุของโรคหอมเลื้อยด้วยสารสกัดสมุนไพร. วารสารวิทยาศาสตร์เทคโนโลยี มรย, 7(2), 35-42.

[17] Rattanakreetakul, C. (2013). Fumigation with Plant Volatile Oils to Control Stem End Rot of Banana. *Acta Hortic*, *973*, 207-213.

[18] สุวรรณี แทนธานี, จารวี สุขประเสริฐ, สายจิต ดาวสุโข และโสรญา รอดประเสริฐ. (2557). การศึกษาประสิทธิภาพของว่านน้ำในการยับยั้งเชื้อราก่อโรคผลเน่าที่แยกได้จากผลลิ้นจี่. *วารสารวิทยาศาสตร์ประยุกต์*, *3*(3). *เกษตร*, 1-31.

[19] Somnuek, S., Kongtragoul, P., Jaenaksorn, T. (2023). Fungicide resistance of *Phytophthora palmivora* causing durian diseases in eastern and southern Thailand and the in vitro alternative control by cajeput leaf extracts. *International Journal of Agricultural Technology*, 19(2), 703-720.

[20] วนิดา ชื่นชัน, สมศักดิ์ อยู่บริบูรณ์ และ ศิริพร บุญส่ง. (2565). ประสิทธิภาพของสารสกัดหยาบจากสมุนไพรในการยับยั้งเชื้อรา *Phytophthora parasitica*. *วารสารสถาบันวิจัยและพัฒนา มหาวิทยาลัยราชภัฏบ้านสมเด็จเจ้าพระยา*, *7*(1), 243-252.

[21] ธารทิพย์ รัตนะ. (2559). ประสิทธิภาพของสารสกัดหยาบจากสับปะรดและมะละกอในการต่อต้านราก่อโรคแอนแทรกโนสในพริก. วารสารวิทยาศาสตร์และเทคโนโลยี, 3(24), 456-468.

[22] ปาริชาติ อ้นองอาจ, กัมปนาท คำสุข, ภรณ์ทิพย์ ชัยสว่าง, ณลิตา ไพบูลย์ และวราภรณ์ มหาทรัพย์. (2566). ผลการยับยั้งเชื้อแบคทีเรียของสารสกัดใบพลูต่อเชื้อสเตร็พโตค็อคคัสมิวแทนส์. *วารสารหมอยาไทยวิจัย, 9(1),* 89-98.

[23] อาวุธ หงส์ศิริ, อัจฉรา แก้วน้อย, อ้อมบุญ วัลลิสุต และอินทัช ศักดิ์ภักดี เจริญ. (2566). ฤทธิ์ต้านการอักเสบและต้านอนุมูลอิสระของสารสกัดตำรับยาห้าราก มะขาม และข่า. *วารสารสถาบันวิจัยและพัฒนา มหาวิทยาลัยราชภัฏบ้านสมเด็จเจ้าพระยา, 8*(2), 297-305.

[24] ธารหทัย มาลาเวช. (2559). *ผลของสารสกัดสมุนไพรขมิ้นชันต่อเชื้อ Staphylococcus aureus* (รายงานผลการวิจัย). นครศรีธรรมราช: มหาวิยาลัยราชภัฏนครศรีธรรมราช.

[25] โชติรส กิจสมชีพ. (2565). *การเตรียมนาโนอิมัลชันที่มีสารสกัดกระชายและกาแฟสำหรับผลิตภัณฑ์ชะลอวัย* (วิทยานิพนธ์ปริญญามหาบัณฑิต). กรุงเทพฯ: มหาวิทยาหัวเฉียวพระเกียรติ.

การออกแบบและพัฒนาเครื่องบรรจุน้ำผึ้งลงขวดแก้วจิ๋ว

DESIGN AND DEVELOPMENT OF A HONEY FILLING MACHINE FOR MINIATURE GLASS BOTTLES

*Komkit Seepan
Program in Industrial Electrical Technology, Faculty of Science and Technology
Suratthani Rajabhat University
Suratthani, Thailand.
komkit.see@sru.ac.th

Witchayut Srisuwan
Program in Industrial Electrical Technology, Faculty of Science and Technology
Suratthani Rajabhat University
Suratthani, Thailand.
6404335001045@student.sru.ac.th

Abstract— *The One Tambon One Product (OTOP) initiative plays a crucial role in driving Thailand's community-level economy. Honey, a natural product with high nutritional value and health benefits, is one of the most promising products under this program. Thailand ranks 36th globally in honey production, generating over 600 million baht annually in exports. Despite its economic potential, honey production at the community level faces challenges, particularly in the bottling process, which relies heavily on manual labor. This leads to inefficiencies, inconsistencies in volume, and limited daily production capacity, reducing product quality and market competitiveness.*

This study focuses on designing and developing a compact, cost-effective honey filling machine for miniature glass bottles. The machine integrates advanced technologies such as Programmable Logic Controllers (PLC) and high-performance detection devices to ensure precise and efficient bottling. The objectives are to reduce bottling time, enhance volume accuracy, and improve overall production efficiency. The expected outcomes include lower production costs, increased daily output, and higher profitability for community producers, enabling them to meet market demands effectively.

Beyond addressing practical bottling challenges, this research contributes to technological innovation in agricultural machinery and offers a model for developing similar systems for other community products. By empowering local producers with modern tools, this study promotes sustainable economic growth and strengthens the competitiveness of Thai honey products in domestic and international markets.

Keywords—Honey filling machine, PLC Mitsubishi FX3U, automation, miniature glass bottles

I. บทนำ

ในปัจจุบัน โครงการหนึ่งตำบลหนึ่งผลิตภัณฑ์ (OTOP) ได้รับการยอมรับว่าเป็นกลยุทธ์สำคัญในการขับเคลื่อนเศรษฐกิจในระดับชุมชนของประเทศไทย โครงการนี้มุ่งเน้นการเพิ่มมูลค่าผลิตภัณฑ์ท้องถิ่นผ่านการพัฒนาและส่งเสริมสินค้าให้มีคุณภาพและมาตรฐานที่สามารถแข่งขันได้ในตลาดทั้งในประเทศและต่างประเทศ ผลิตภัณฑ์จากธรรมชาติ เช่น น้ำผึ้ง ถือเป็นหนึ่งในสินค้าที่มีศักยภาพสูง โดยน้ำผึ้งไม่ได้มีเพียงความสำคัญในฐานะอาหารที่มีคุณค่าทางโภชนาการ แต่ยังมีสรรพคุณที่เป็นประโยชน์ในด้านการรักษาและบำรุงสุขภาพอีกด้วย ประเทศไทยซึ่งเป็นแหล่งผลิตน้ำผึ้งที่สำคัญ มีความโดดเด่นในด้านปริมาณการผลิต โดยติดอันดับที่ 36 ของโลก และสามารถสร้างรายได้จากการส่งออกกว่า 600 ล้านบาทต่อปี

อย่างไรก็ตาม แม้น้ำผึ้งจะเป็นสินค้าที่มีศักยภาพในเชิงเศรษฐกิจสูง แต่กระบวนการผลิตน้ำผึ้งในระดับชุมชนยังคงประสบปัญหาหลายประการ โดยเฉพาะในกระบวนการบรรจุที่ยังพึ่งพาแรงงานมนุษย์อย่างมาก ซึ่งทำให้เกิดข้อจำกัดในด้านคุณภาพและปริมาณการผลิต การบรรจุน้ำผึ้งด้วยแรงงานมนุษย์มักมีปัญหาในด้านความล่าช้า ความไม่แม่นยำในการกำหนดปริมาณน้ำผึ้งในแต่ละขวด และข้อผิดพลาดที่เกิดขึ้นจากความไม่สม่ำเสมอในกระบวนการ ทั้งนี้ ส่งผลให้ผลิตภัณฑ์ที่ได้มีความไม่สม่ำเสมอในด้านคุณภาพ และทำให้ศักยภาพในการแข่งขันในตลาดลดลง

ตัวอย่างที่ชัดเจนของปัญหานี้สามารถพบได้ในกลุ่มผู้ผลิตน้ำผึ้งชุมชนบ้านเบญจา อำเภอพนม จังหวัดสุราษฎร์ธานี ซึ่งเป็นกลุ่มผู้ผลิตน้ำผึ้งที่ยังคงใช้กระบวนการผลิตแบบดั้งเดิม แม้ชุมชนจะมีความสามารถในการผลิตน้ำผึ้งคุณภาพดี แต่กระบวนการบรรจุที่ขาดเทคโนโลยีที่เหมาะสมส่งผลให้ผลิตภัณฑ์ที่ออกสู่ตลาดขาดความสม่ำเสมอ อีกทั้งยังไม่สามารถเพิ่มปริมาณการผลิตได้ตามความต้องการของตลาด การพัฒนาเครื่องจักรที่สามารถช่วยเพิ่มประสิทธิภาพในกระบวนการบรรจุจึงกลายเป็นสิ่งจำเป็นอย่างยิ่ง โดยเฉพาะเครื่องจักรที่สามารถตอบสนองความต้องการของชุมชนได้ในด้านความคุ้มค่า ขนาดที่เหมาะสม และความแม่นยำสูง

งานวิจัยนี้จึงมุ่งเน้นไปที่การออกแบบและพัฒนาเครื่องบรรจุน้ำผึ้งที่มีขนาดกะทัดรัด ราคาประหยัด และสามารถควบคุมการบรรจุได้อย่างแม่นยำ เครื่องจักรนี้ถูกออกแบบมาเพื่อให้เหมาะสมกับบริบทของการผลิตในระดับชุมชน โดยใช้เทคโนโลยีสมัยใหม่ เช่น ระบบควบคุมอัตโนมัติด้วย Programmable Logic Controller (PLC) ซึ่งสามารถตั้งโปรแกรมให้ดำเนินการได้อย่างแม่นยำและมี

ประสิทธิภาพ ร่วมกับอุปกรณ์ตรวจจับคุณภาพที่ช่วยเพิ่มความสม่ำเสมอในกระบวนการบรรจุและลดข้อผิดพลาดที่อาจเกิดขึ้น ผลลัพธ์ที่คาดหวังจากงานวิจัยนี้ได้แก่ การลดระยะเวลาในกระบวนการบรรจุ การเพิ่มความแม่นยำในปริมาณน้ำผึ้งในแต่ละขวด และการเพิ่มประสิทธิภาพโดยรวมของกระบวนการผลิต ซึ่งจะช่วยลดต้นทุนการผลิต เพิ่มกำลังการผลิตต่อวัน และสร้างรายได้ที่เพิ่มขึ้นให้กับกลุ่มผู้ผลิตในระดับชุมชน นอกจากนี้ เครื่องจักรดังกล่าวยังช่วยให้ผู้ผลิตสามารถตอบสนองความต้องการของตลาดได้อย่างมีประสิทธิภาพ รวมถึงเพิ่มขีดความสามารถในการแข่งขันของผลิตภัณฑ์ในตลาดทั้งในประเทศและต่างประเทศ

นอกเหนือจากการประยุกต์ใช้ในเชิงปฏิบัติ งานวิจัยนี้ยังมีคุณค่าในด้านการพัฒนาองค์ความรู้และเทคโนโลยี โดยเป็นการบูรณาการความรู้ด้านวิศวกรรมระบบอัตโนมัติ และการออกแบบเครื่องจักรให้เหมาะสมกับบริบทของชุมชนไทย การพัฒนานี้ไม่เพียงช่วยยกระดับคุณภาพชีวิตของชุมชนในปัจจุบัน แต่ยังเป็นต้นแบบที่สามารถนำไปต่อยอดสำหรับการพัฒนาเครื่องจักรในอุตสาหกรรมที่มีความซับซ้อนมากยิ่งขึ้น รวมถึงการนำเทคโนโลยีมาใช้ในการพัฒนาผลิตภัณฑ์ชุมชนอื่น ๆ

ด้วยความสำคัญทั้งในมิติของการส่งเสริมเศรษฐกิจระดับชุมชน การเพิ่มศักยภาพของผู้ผลิตในระดับรากฐาน และการยกระดับมาตรฐานของผลิตภัณฑ์ งานวิจัยนี้จึงถือเป็นก้าวสำคัญในการสร้างความยั่งยืนในระบบเศรษฐกิจฐานรากของประเทศไทย อีกทั้งยังเปิดโอกาสให้ผู้ผลิตชุมชนสามารถแข่งขันในตลาดระดับโลกได้อย่างมั่นคงในระยะยาว ทั้งนี้ ความสำเร็จของงานวิจัยนี้จะไม่เพียงแค่ตอบโจทย์ในระดับชุมชน แต่ยังช่วยส่งเสริมความเข้มแข็งให้กับเศรษฐกิจในภาพรวมของประเทศ โดยวางรากฐานที่มั่นคงสำหรับการพัฒนาต่อไปในอนาคต

II. ทบทวนวรรณกรรม

ในการพัฒนาเครื่องบรรจุน้ำผึ้งลงขวดแก้วจิ๋ว การศึกษาและรวบรวมความรู้จากวรรณกรรมและงานวิจัยที่เกี่ยวข้องเป็นขั้นตอนสำคัญเพื่อสร้างความเข้าใจในกระบวนการและแนวคิดที่มีอยู่ก่อนหน้า โดยการทบทวนวรรณกรรมในหัวข้อนี้จะครอบคลุมถึงแนวทางการออกแบบเพื่อพัฒนาเครื่องจักรจาก การออกแบบและพัฒนาเครื่องบรรจุเพื่อเพิ่มประสิทธิภาพกระบวนการบรรจุน้ำพริกน้ำเงี้ยว งานวิจัยนี้เน้นการพัฒนาเครื่องบรรจุสำหรับน้ำพริกน้ำเงี้ยวโดยใช้วัสดุสแตนเลสเกรด 304 ซึ่งช่วยลดการปนเปื้อนและสามารถเลือกปริมาณการบรรจุได้หลากหลายขนาด คือ 100, 500, และ 1000 กรัม การศึกษานี้ช่วยเน้นความสำคัญของการใช้งานเครื่องจักรที่มีความแม่นยำและรองรับปริมาณที่หลากหลาย [1] การสร้างต้นแบบระบบสายพานลำเลียงสำหรับเครื่องบรรจุน้ำดื่มอัตโนมัติโดยใช้ PLC การวิจัยนี้มุ่งเน้นการพัฒนาเครื่องบรรจุที่ใช้สายพานลำเลียงร่วมกับ PLC Mitsubishi เพื่อควบคุมกระบวนการอัตโนมัติ รวมถึงการใช้ Proximity Sensor เพื่อตรวจจับตำแหน่งขวดและระดับน้ำในระบบ ข้อเด่นคือมีการควบคุมที่แม่นยำ ลดการพึ่งพาแรงงาน และเพิ่มความต่อเนื่องในกระบวนการผลิต [2] การปรับปรุงประสิทธิภาพกระบวนการผลิตน้ำดื่มบรรจุขวดด้วยเทคนิคการศึกษางาน (ECRS) การศึกษาใช้เทคนิค ECRS (Eliminate, Combine, Rearrange, Simplify) ในการปรับปรุงกระบวนการผลิตเพื่อลดขั้นตอนที่ไม่จำเป็น เพิ่มความรวดเร็ว และลดความคลาดเคลื่อน โดยเน้นการศึกษามาตรฐานเวลาและความคงที่ในกระบวนการ งานวิจัยทั้งสามชิ้นแสดงให้เห็นถึงความสำคัญของการนำเทคโนโลยีเข้ามาใช้ในการพัฒนาเครื่องจักรและกระบวนการผลิต ไม่ว่าจะเป็นการใช้วัสดุที่เหมาะสม เช่น สแตนเลสเกรด 304 ในงานวิจัยแรก หรือการพัฒนาเทคโนโลยีควบคุมอัตโนมัติ เช่น การใช้ PLC และเซ็นเซอร์ในงานวิจัยที่สอง รวมถึงการปรับปรุงกระบวนการผลิตอย่างเป็นระบบ (เช่น เทคนิค ECRS ในงานวิจัยที่สาม การออกแบบและพัฒนาเครื่องบรรจุน้ำผึ้งในงานวิจัยปัจจุบัน สามารถนำข้อดีจากทั้งสามงานวิจัยมาประยุกต์ใช้ เช่น การเลือกใช้ PLC เพื่อควบคุมกระบวนการ การออกแบบที่ลดความซับซ้อน และการเลือกวัสดุที่เหมาะสม นอกจากนี้ยังมุ่งเน้นการเพิ่มความแม่นยำ ลดเวลาการทำงาน และลดความผิดพลาด ซึ่งเป็นหัวใจสำคัญในการพัฒนากระบวนการผลิตกึ่งอัตโนมัติที่มีประสิทธิภาพ [3] การออกแบบและพัฒนาเครื่องบรรจุน้ำปลาร้ากึ่งอัตโนมัติ งานวิจัยนี้ มีเป้าหมายเพื่อแก้ปัญหาการบรรจุน้ำปลาร้าในอุตสาหกรรมขนาดเล็กและขนาดกลาง ซึ่งส่วนใหญ่มักใช้แรงงานคน ทำให้กระบวนการผลิตล่าช้า ขาดความสม่ำเสมอ และอาจมีปัญหาเรื่องสุขอนามัย เครื่องบรรจุน้ำปลาร้ากึ่งอัตโนมัติที่ถูกพัฒนาขึ้นจึงมุ่งเน้นการเพิ่มประสิทธิภาพในการผลิต ลดต้นทุนแรงงาน และควบคุมปริมาณการบรรจุให้แม่นยำยิ่งขึ้น กระบวนการออกแบบเริ่มต้นจากการศึกษาลักษณะของน้ำปลาร้า ซึ่งมีความหนืดสูงและอาจมีชิ้นส่วนของเนื้อปลาเจือปนอยู่ การออกแบบระบบจึงต้องคำนึงถึงการป้องกันการอุดตันของท่อจ่ายและการไหลของของเหลวที่สม่ำเสมอ ทีมวิจัยเลือกใช้ระบบวาล์วควบคุมการไหลแบบพิเศษ และติดตั้งกลไกการดูดจ่ายของเหลวที่เหมาะสม นอกจากนี้ เครื่องยังสามารถปรับปริมาณการบรรจุให้เหมาะกับภาชนะที่แตกต่างกันได้ โดยการพัฒนาต้นแบบเครื่องบรรจุถูกดำเนินการโดยใช้วัสดุที่ทนทานต่อการกัดกร่อน เช่น สแตนเลสเกรดอาหาร เพื่อให้มั่นใจว่าไม่มีสารปนเปื้อนลงสู่ น้ำปลาร้า การทดสอบเครื่องต้นแบบแสดงให้เห็นว่า ระบบสามารถบรรจุน้ำปลาร้าได้อย่างแม่นยำและรวดเร็ว ลดอัตราการหกเลอะเทอะ และช่วยเพิ่มกำลังการผลิตของผู้ประกอบการได้อย่างมีนัยสำคัญ [4] การออกแบบเครื่องบรรจุน้ำซุปแบบอัตโนมัติ มีวัตถุประสงค์เพื่อเพิ่มประสิทธิภาพการผลิตในอุตสาหกรรมอาหารพร้อมทาน โดยเฉพาะน้ำซุปชาบู ซึ่งแต่เดิมการบรรจุใช้แรงงานคน ทำให้มีข้อจำกัดด้านความแม่นยำและต้นทุนแรงงานสูง ได้พัฒนาเครื่องบรรจุน้ำซุปที่ทำงานอัตโนมัติ โดยใช้เทคโนโลยีที่ทันสมัย เช่น ระบบวาล์วควบคุมการไหล ระบบเซ็นเซอร์ และการทำงานร่วมกับโปรแกรม PLC (Programmable Logic Controller) เพื่อควบคุมกระบวนการบรรจุให้มีความแม่นยำและสม่ำเสมอ เครื่องบรรจุที่ออกแบบมี 6 หัวบรรจุ และสามารถจ่ายน้ำซุปในปริมาณมาตรฐานที่ 250 กรัมต่อถ้วย ±10 กรัม ผลการทดลองพบว่า เครื่องสามารถเพิ่มประสิทธิภาพการผลิตจากเดิม 1,200 ถ้วยต่อชั่วโมง เป็น 2,150 ถ้วยต่อชั่วโมง หรือเพิ่มขึ้นถึง 79.16% อีกทั้งยังช่วยลดต้นทุนแรงงานลงปีละ 316,800 บาท โดยใช้งบประมาณลงทุน 200,000 บาท และสามารถคืนทุนได้ภายในระยะเวลาเพียง 7.5 เดือน จากผลการวิจัยชี้ให้เห็นว่า เครื่องบรรจุน้ำซุปอัตโนมัติสามารถช่วยลดความผิดพลาดในการบรรจุ เพิ่มความต่อเนื่องของกระบวนการผลิต และทำให้ผลิตภัณฑ์มีมาตรฐานที่ดีขึ้น ขณะเดียวกันยังช่วยลดต้นทุนด้านแรงงาน และสามารถนำแนวคิดไปประยุกต์ใช้กับการบรรจุของเหลวประเภทอื่น ๆ ในอุตสาหกรรมอาหารได้อีกด้วย [5] นอกจากนี้แนวทางการออกแบบและสร้าง

เครื่องบรรจุผลิตภัณฑ์สำหรับผลิตภัณฑ์ที่เป็นของเหลวที่เน้นการออกแบบและสร้างเครื่องบรรจุผลิตภัณฑ์ของเหลวที่สามารถทำงานได้อย่างมีประสิทธิภาพและรวดเร็ว โดยใช้ระบบบรรจุแนวดิ่งและการผนึกซองด้วยแผ่นความร้อนควบคู่ไปกับการทำงานของมอเตอร์ไฟฟ้าสองชุด ซึ่งทำหน้าที่ในการผนึกซองทั้งด้านข้างและด้านหัว-ท้าย นอกจากนี้ ระบบลูกกลิ้งช่วยให้สามารถป้อนแผ่นพลาสติกเข้าสู่กระบวนการบรรจุและควบคุมความตึงของแผ่นพลาสติกได้อย่างแม่นยำ ผลการทดลองแสดงให้เห็นว่า เครื่องสามารถบรรจุผลิตภัณฑ์ที่มีขนาด 10 × 3 เซนติเมตร คิดเป็นปริมาตร 20 ลูกบาศก์เซนติเมตร ได้ภายในเวลา 1.5 วินาทีต่อซอง ซึ่งส่งผลให้สามารถผลิตได้ถึง 2,400 ซองต่อชั่วโมง อย่างไรก็ตาม งานวิจัยยังพบข้อจำกัดเกี่ยวกับการบรรจุผลิตภัณฑ์ที่มีความหนืดสูง เช่น แป้งผสมน้ำ ที่ทำให้เกิดปัญหาในการผนึกซอง เนื่องจากวัสดุติดค้างอยู่ระหว่างแผ่นพลาสติกขณะทำการผนึกด้วยการออกแบบที่ทันสมัยและคำนึงถึงความสะดวกในการใช้งาน งานวิจัยนี้จึงมีศักยภาพในการนำไปใช้ในอุตสาหกรรมบรรจุภัณฑ์ของเหลว เพื่อเพิ่มประสิทธิภาพการผลิต ลดต้นทุนแรงงาน และช่วยให้กระบวนการบรรจุมีมาตรฐานยิ่งขึ้น [6] การคัดแยกขนาดขวดตามความสูงและเติมน้ำในขวดด้วยพีแอลซี โตชิบ้า รุ่นT2 งานวิจัยนี้นำเสนอการออกแบบและพัฒนาระบบ คัดแยกขวดตามความสูงและเติมน้ำในขวด โดยใช้ PLC โตชิบ้า รุ่น T2 เป็นตัวควบคุมหลัก ระบบแบ่งออกเป็นสองส่วนสำคัญ ได้แก่ ระบบคัดแยกขวด และ ระบบเติมน้ำในขวด ซึ่งทำงานร่วมกันเพื่อเพิ่มความแม่นยำและประสิทธิภาพในการบรรจุ ในส่วนของ การคัดแยกขวด ระบบสามารถแยกขวดออกเป็นสองขนาด คือ 600 มิลลิลิตร และ 350 มิลลิลิตร โดยอาศัยเซ็นเซอร์ตรวจจับความสูงของขวด เมื่อขวดถูกคัดแยกเรียบร้อยแล้ว สายพานจะลำเลียงขวดไปยังจุดเติมน้ำ ซึ่งระบบจะกำหนดปริมาณน้ำที่เหมาะสมกับขนาดของขวดนั้นๆ ทำให้กระบวนการบรรจุมีความแม่นยำและลดการสูญเสียน้ำ ผลการทดลองแสดงให้เห็นว่า ระบบสามารถทำงานได้อย่างถูกต้องและแม่นยำ โดยสามารถคัดแยกขวดและเติมน้ำได้ตามที่กำหนด ซึ่งแสดงถึงศักยภาพในการนำไปประยุกต์ใช้กับระบบอุตสาหกรรมจริง การใช้ PLC โตชิบ้า รุ่น T2 ทำให้กระบวนการอัตโนมัติเป็นไปอย่างเสถียร ลดการใช้แรงงานมนุษย์ และเพิ่มประสิทธิภาพการผลิต ถือเป็นแนวทางที่ช่วยให้กระบวนการบรรจุและคัดแยกขวดมีมาตรฐานสูงขึ้น [7] การประยุกต์ใช้โปรแกรมเมเบิลลอจิกคอนโทรลเลอร์ (PLC) สำหรับเครื่องตรวจสอบ ความผิดปกติของนม ยู.เอช.ที.บรรจุกล่อง งานวิจัยนี้มุ่งเน้นการพัฒนาเครื่องตรวจสอบความผิดปกติของนมยูเอชทีบรรจุกล่อง โดยใช้โปรแกรมเมเบิลลอจิกคอนโทรลเลอร์ (PLC) แทนระบบคอมพิวเตอร์เพื่อลดขนาดและต้นทุนของอุปกรณ์ การตรวจสอบนมยูเอชทีเป็นกระบวนการสำคัญในอุตสาหกรรม เนื่องจากช่วยคัดแยกผลิตภัณฑ์ที่มีแนวโน้มเสียก่อนหมดอายุออกจากสินค้าที่มีคุณภาพดี ซึ่งช่วยสร้างความมั่นใจให้กับผู้บริโภค โดยทั่วไป วิธีการตรวจสอบมีสองรูปแบบ ได้แก่ การตรวจสอบแบบทำลาย ซึ่งต้องตัดกล่องเพื่อดูความผิดปกติภายใน และการตรวจสอบแบบไม่ทำลาย ซึ่งใช้หลักการสั่นสะเทือนแบบอิสระของของเหลวภายในกล่องนม แล้ววิเคราะห์สัญญาณการสั่นสะเทือนเพื่อแยกแยะนมดีและนมที่เสีย งานวิจัยนี้ได้พัฒนาเครื่องตรวจสอบที่ใช้ PLC แทนระบบคอมพิวเตอร์ที่ใช้การ์ด DAQ และโปรแกรม LabVIEW ซึ่งเป็นวิธีการเดิม ผลการทดลองแสดงให้เห็นว่า เครื่องตรวจสอบที่ใช้ PLC สามารถทำงานได้ในเวลาไม่เกิน 3 วินาทีต่อกล่อง และให้ผลลัพธ์ที่ถูกต้อง 100% เทียบเท่ากับระบบเดิม ดังนั้นการใช้ PLC ในการแปรผลสัญญาณจึงเป็นแนวทางที่สามารถพัฒนาให้เครื่องตรวจสอบความผิดปกติของนมยูเอชทีมีขนาดกะทัดรัดขึ้นและมีต้นทุนที่เหมาะสมกว่า [8]

III. ระเบียบวิธีวิจัย

การวิจัยนี้มุ่งเน้นการออกแบบและพัฒนาเครื่องบรรจุน้ำผึ้งลงขวดแก้วจิ๋ว โดยมีลำดับขั้นตอนที่เริ่มต้นจากการสำรวจปัญหาของการบรรจุน้ำผึ้งด้วยมือในระดับชุมชน ซึ่งพบว่ากระบวนการดังกล่าวมีความล่าช้าและขาดความแม่นยำ หลังจากนั้น ผู้วิจัยได้ศึกษาทฤษฎีและงานวิจัยที่เกี่ยวข้อง รวมถึงข้อมูลด้านเทคนิคที่จำเป็น เพื่อใช้เป็นแนวทางในการออกแบบเครื่องบรรจุน้ำผึ้งที่ตอบสนองความต้องการของชุมชนอย่างมีประสิทธิภาพ เมื่อได้ข้อมูลเพียงพอ ผู้วิจัยได้ดำเนินการออกแบบเครื่องต้นแบบ โดยเน้นให้เครื่องมีขนาดกะทัดรัดและใช้งานง่าย ทั้งนี้ ได้เลือกใช้วัสดุสแตนเลส 304 ซึ่งเหมาะสมกับมาตรฐานอาหาร และใช้ระบบควบคุมด้วย PLC Mitsubishi FX3U 14MR ที่สามารถเขียนโปรแกรมผ่านซอฟต์แวร์ GX Works2 เพื่อควบคุมการทำงานของเครื่องอย่างแม่นยำ ในขั้นตอนแรก เป็นออกแบบและงานประกอบการประกอบโครงอะลูมิเนียมโปรไฟล์เพื่อใช้เป็นโครงสร้างหลัก เนื่องจากอะลูมิเนียมโปรไฟล์นั้นสามารถถอดประกอบหรือแก้ไขได้ง่าย เพื่อลดเวลาในการสร้างชิ้นงานลง โดยออกแบบเครื่องให้มีความกว้าง 40 เซนติเมตร ความยาว 40 เซนติเมตร และความสูง 40 เซนติเมตร



ภาพที่ 1 ประกอบโครงสร้างเครื่อง

ต่อมาได้ทำการติดตั้งมอเตอร์จานหมุนขวดเข้ากับโครงอะลูมิเนียมโปรไฟล์โดยใช้ มอเตอร์ AC แบบปรับความเร็วรอบได้ ขนาด 45 W ต่อมามีการติดตั้งมอเตอร์จานหมุน ที่ทำจากสแตนเลส 304 (food grade)โดยใช้สแตนเลสหนา 2 มิลลิเมตร ตัดด้วยเครื่อง CNC Plashma



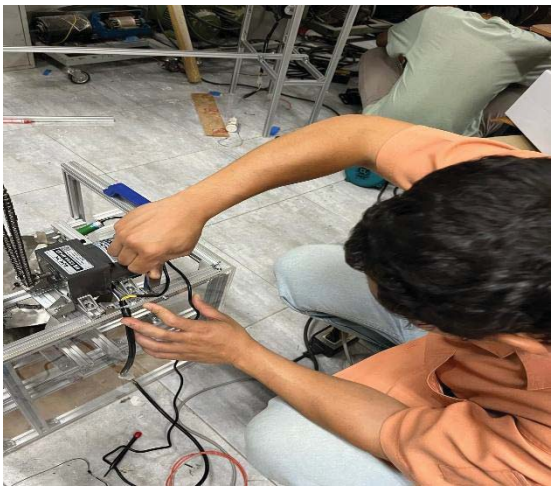
ภาพที่ 2 ตัดจานสแตนเลสด้วยเครื่อง CNC Plashma

เมื่อได้โครงสร้างเครื่องและจานหมุนแล้ว ทำการพัฒนากระบอกอัดน้ำผึ้งและติดตั้งมอเตอร์กระบอกอัดน้ำผึ้ง เพื่อให้สามารถใช้บรรจุน้ำผึ้งได้อย่างมีประสิทธิภาพ



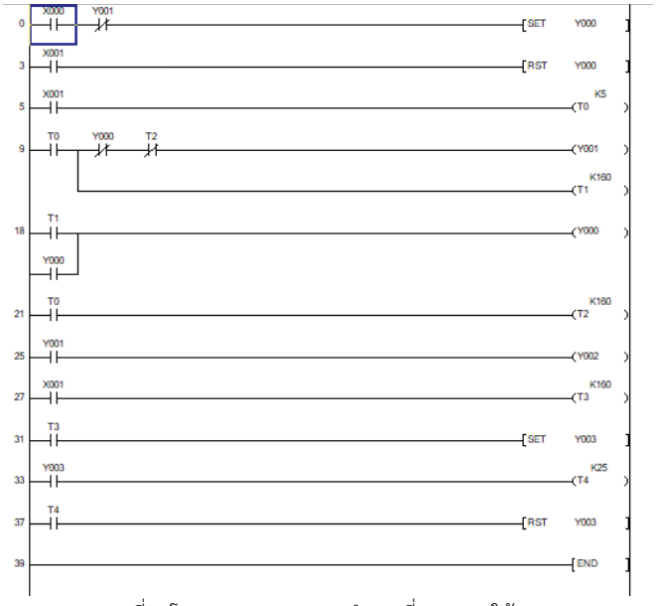
ภาพที่ 3 ติดตั้งกระบอกอัดน้ำผึ้ง

เมื่อติดตั้งกระบอกอัดน้ำผึ้งแล้ว ลำดับถัดไปคือนำมือเตอร์และชุดส่งกำลังมาประกอบกับกระบอกอัดน้ำผึ้ง เพื่อให้ใช้ PLC สั่งงานในขณะบรรจุน้ำผึ้งได้อย่างแม่นยำ



ภาพที่ 4 ติดตั้งมอเตอร์อัดน้ำผึ้ง

ขั้นตอนต่อมาทำการ ติดตั้งบอร์ด PLC และเขียนโปรแกรมควบคุมการทำงาน



ภาพที่ 5 โปรแกรมควบคุมการทำงานที่ออกแบบให้ระบบ

ตรวจสอบความสามารถของเครื่องในการบรรจุน้ำผึ้งจำนวน 6 ขวดพร้อมกัน รวมถึงปรับปรุงแก้ไขทั้งในส่วนของฮาร์ดแวร์และซอฟต์แวร์ เพื่อให้เครื่องทำงานได้อย่างมีประสิทธิภาพสูงสุด ในขั้นตอนนี้ ผู้วิจัยยังได้บันทึกข้อมูลด้านความเร็วและความแม่นยำของการบรรจุเพื่อใช้ในการวิเคราะห์ หลังจากการทดลองบรรจุน้ำผึ้งด้วยเครื่องและเปรียบเทียบกับการบรรจุด้วยมือ พบว่าการใช้เครื่องบรรจุน้ำผึ้งสามารถลดเวลาในการบรรจุลงได้อย่างชัดเจน อีกทั้งยังมีความแม่นยำในการควบคุมน้ำหนักน้ำผึ้งที่บรรจุในแต่ละขวดมากกว่า เมื่อได้ผลลัพธ์ดังกล่าว



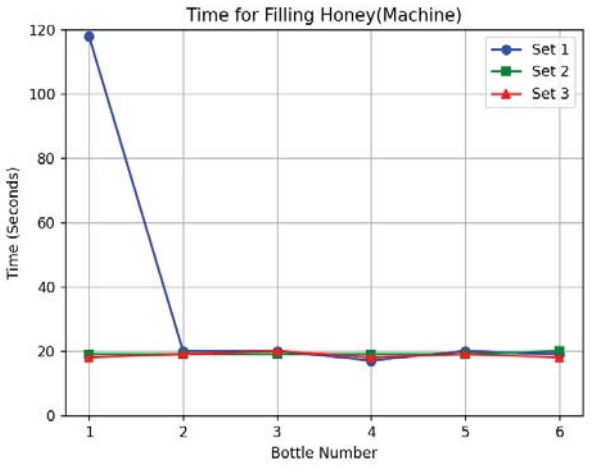
ภาพที่ 6 การเตรียมการทดสอบ

ผู้วิจัยได้นำข้อมูลที่ได้มาวิเคราะห์เพื่อเปรียบเทียบค่าความคลาดเคลื่อนของน้ำหนักน้ำผึ้งระหว่างสองวิธี พร้อมทั้งคำนวณค่าเฉลี่ยของเวลาที่ใช้ในการบรรจุ ในตอนท้ายของการวิจัยหาแนวทางสรุปผลว่าเครื่องบรรจุน้ำผึ้งที่พัฒนาขึ้นมีประสิทธิภาพและเหมาะสมกับการใช้งานในระดับชุมชน ทั้งในด้านความเร็วและความแม่นยำ รวมถึงเสนอแนะการปรับปรุงเครื่องต้นแบบในอนาคต

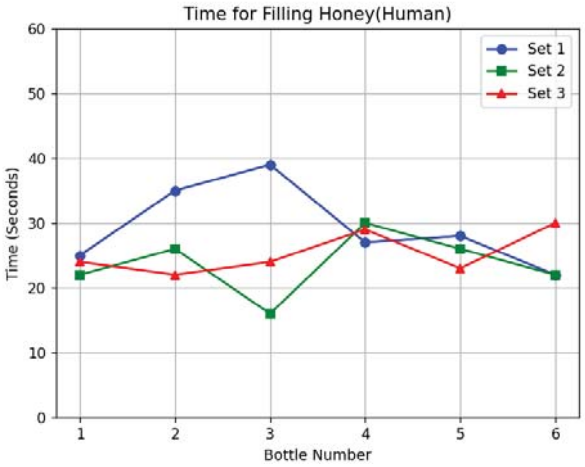
IV. ผลการทดลอง

การทดลองนี้เริ่มต้นด้วยการปรับแต่งรางป้อนขวดและจานหมุนเพื่อให้ระบบทำงานได้อย่างราบรื่นและมีประสิทธิภาพสูงสุด โดยพบว่าการตั้งองศารางป้อนขวดที่ 16 องศาทำให้ขวดไหลลงร่องจานหมุนได้ดีที่สุด จากนั้นจึงปรับความเร็วมอเตอร์จานหมุน พบว่าสเกลความเร็วที่ 5 สามารถป้องกันไม่ให้ขวดหลุดจากร่องจานหมุนในขณะเครื่องทำงาน เมื่อการปรับแต่งระบบเสร็จสิ้น ผู้วิจัยได้เริ่มการทดลองบรรจุน้ำผึ้ง โดยเปรียบเทียบระหว่างการบรรจุด้วยเครื่องและการบรรจุด้วยมือ ในการทดลองครั้งนี้วัดผลโดยใช้เวลาเฉลี่ยและน้ำหนักน้ำผึ้งในแต่ละขวดเป็นเกณฑ์หลัก

ผลการทดลองด้านเวลาแสดงให้เห็นว่าเครื่องบรรจุน้ำผึ้งมีเวลาเฉลี่ยต่อขวดสม่ำเสมอกว่า โดยใช้เวลาเฉลี่ย 21.36 วินาทีต่อขวด ซึ่งเร็วกว่าการบรรจุด้วยมือที่ใช้เวลาเฉลี่ย 26.11 วินาทีต่อขวด นอกจากนี้ การบรรจุด้วยเครื่องยังลดความผันผวนของเวลาได้อย่างชัดเจน ซึ่งแสดงให้เห็นในกราฟด้านล่าง



จากกราฟการบรรจุด้วยเครื่องสังเกตได้ว่า ชุดที่ 1 ขวดแรกใช้เวลามากถึง 120 วินาที ซึ่งเป็นค่าสูงสุด แต่หลังจากขวดแรก เวลากลับมาคงที่ประมาณ 20 วินาที ชุดที่ 2 และ ชุดที่ 3 เวลาการเติมค่อนข้างคงที่ตั้งแต่ขวดแรกจนถึงขวดที่หก โดยอยู่ที่ประมาณ 20 วินาที



จากกราฟเวลาการบรรจุด้วยมือ สังเกตได้ว่า ชุดที่ ค่าเวลาในแต่ละขวดค่อนข้างผันผวนมากที่สุด มีค่าอยู่ในช่วง 30-40 วินาที ชุดที่ 2 เวลาการเติมในแต่ละขวดมีการเปลี่ยนแปลงน้อยที่สุด อยู่ในช่วงประมาณ 20-30 วินาที และมีความสม่ำเสมอกว่า ชุดที่ 3 เวลาการเติมในแต่ละขวดมีค่าอยู่ในช่วง 20-35 วินาที

V. อภิปรายผล

ผลการทดลองในครั้งนี้แสดงให้เห็นถึงความสำเร็จในการออกแบบและพัฒนาเครื่องบรรจุน้ำผึ้งลงขวดแก้วจิ๋ว โดยผลการทดลองที่ได้ชี้ให้เห็นว่าเครื่องสามารถทำงานได้อย่างมีประสิทธิภาพเมื่อเทียบกับการบรรจุด้วยมือ ความรวดเร็วในการบรรจุของเครื่องช่วยลดระยะเวลาการทำงานลงอย่างชัดเจน ซึ่งเป็นประโยชน์อย่างมากต่อการเพิ่มกำลังการผลิต โดยเฉพาะในชุมชนที่ต้องการเพิ่มศักยภาพในการแข่งขัน

นอกจากนี้ ความแม่นยำของเครื่องในการควบคุมน้ำหนักน้ำผึ้งที่บรรจุในแต่ละขวดสะท้อนให้เห็นถึงความสามารถในการลดความผิดพลาดในกระบวนการผลิต ข้อมูลที่ได้จากการทดลองแสดงให้เห็นว่าค่าความคลาดเคลื่อนของเครื่องต่ำกว่าการบรรจุด้วยมือ ซึ่งสอดคล้องกับวัตถุประสงค์ของการวิจัยที่ต้องการเพิ่มความแม่นยำและลดความสูญเสียในกระบวนการบรรจุ

อย่างไรก็ตาม แม้ว่าเครื่องจะมีประสิทธิภาพสูง แต่ผลการทดลองยังแสดงถึงข้อจำกัดบางประการ เช่น การใช้โซลินอยด์วาล์วที่อาจต้องปรับปรุงให้รองรับการทำงานในระยะยาวได้ดียิ่งขึ้น นอกจากนี้ การปรับเปลี่ยนมอเตอร์กระบอกอัดน้ำผึ้งให้มีแรงบิดมากขึ้นอาจช่วยเพิ่มความแม่นยำในกระบวนการบรรจุอีกระดับ

โดยรวมแล้ว ผลการทดลองสะท้อนถึงความเป็นไปได้ในการพัฒนาเครื่องจักรสำหรับการใช้งานในระดับชุมชน อีกทั้งยังเป็นจุดเริ่มต้นสำคัญในการต่อยอดการวิจัยเพื่อปรับปรุงเครื่องให้เหมาะสมกับการใช้งานในอนาคต ทั้งในด้านความทนทานและการเพิ่มฟังก์ชันเพิ่มเติม เช่น การบันทึกจำนวนขวดที่บรรจุเสร็จ ซึ่งจะช่วยเพิ่มประสิทธิภาพและความสะดวกสบายให้แก่ผู้ใช้งานได้มากยิ่งขึ้น

VI. ข้อสรุป

จากการวิจัยเรื่องการออกแบบและพัฒนาเครื่องบรรจุน้ำผึ้งลงขวดแก้วจิ๋ว พบว่า เครื่องบรรจุน้ำผึ้งที่พัฒนาขึ้นสามารถเพิ่มประสิทธิภาพในการผลิตได้อย่างมีนัยสำคัญ โดยเครื่องจักรดังกล่าวช่วยลดเวลาในการบรรจุได้เฉลี่ย 14.53% เมื่อเทียบกับการบรรจุด้วยมือ นอกจากนี้ยังมีความแม่นยำสูงกว่า โดยมีค่าความคลาดเคลื่อนเพียง 1.36% ซึ่งต่ำกว่าการบรรจุด้วยมือที่มีค่าความคลาดเคลื่อนเฉลี่ย 2.57%

สิ่งที่น่าสนใจยิ่งไปกว่านั้นคือ เครื่องจักรสามารถรักษาความสม่ำเสมอของการทำงานได้ดีกว่าการใช้แรงงานคน ซึ่งช่วยลดความแปรปรวนของเวลาและน้ำหนักในการบรรจุแต่ละขวด นอกจากนี้ ผลงานวิจัยยังแสดงให้เห็นว่าเครื่องจักรนี้สามารถตอบสนองความต้องการของกลุ่มผู้ผลิตในชุมชนได้เป็นอย่างดี อีกทั้งยังมีศักยภาพที่จะพัฒนาต่อยอดเพื่อนำไปใช้ในอุตสาหกรรมอื่นที่มีลักษณะการบรรจุใกล้เคียงกัน

อย่างไรก็ตาม เพื่อให้เครื่องบรรจุน้ำผึ้งนี้มีประสิทธิภาพสูงยิ่งขึ้น ควรมีการปรับปรุงโซลินอยด์วาล์วให้มีขนาดใหญ่ขึ้นเพื่อเพิ่มความเร็วในการบรรจุ และเลือกใช้วัสดุที่สามารถรองรับการทำงานต่อเนื่องเป็นระยะเวลานานเพื่อลดปัญหาความร้อนสะสมในอุปกรณ์ ซึ่งทั้งหมดนี้จะช่วยยกระดับการใช้งานและเพิ่มความคุ้มค่าของเครื่องจักรในเชิงพาณิชย์

ดังนั้น งานวิจัยนี้ไม่เพียงแต่สร้างคุณค่าในด้านเทคโนโลยี แต่ยังส่งเสริมศักยภาพทางเศรษฐกิจของชุมชนและช่วยเพิ่มขีดความสามารถในการแข่งขันของสินค้าไทยในระดับสากลได้อย่างยั่งยืน

คำขอบคุณ

งานวิจัยเรื่อง การออกแบบและพัฒนาเครื่องบรรจุน้ำผึ้งลงขวดแก้วจิ๋ว ได้รับทุนสนับสนุนงานวิจัยจากสถาบันวิจัยและพัฒนา มหาวิทยาลัยราชภัฏสุราษฎร์ธานี

อ้างอิง

[1] นิวัฒน์ชัย ใจคำ, "การออกแบบและพัฒนาเครื่องบรรจุ เพื่อเพิ่มประสิทธิภาพกระบวนการบรรจุน้ำพริกน้ำเงี้ยว," *วารสารวิจัยเทคโนโลยีนวัตกรรม*, vol. X, pp. 68–76, 2019.

[2] ช. กิตติเดชา, "การปรับปรุงประสิทธิภาพของกระบวนการผลิตน้ำดื่มบรรจุขวดด้วยเทคนิคการศึกษางาน," *วารสารเทคโนโลยีการผลิตและการจัดการ*, June 14, 2022.

[3] ณ. แพน้อย, อ. คงประเวช, ด. เหล็กอยู่มะดัน, และ ป. ทรัพย์ทวีปัญญา, "การสร้างต้นแบบระบบสายพานลำเลียงสำหรับเครื่องบรรจุน้ำดื่มอัตโนมัติโดยใช้พีแอลซี ,"*ENGINEERING TRANSACTIONS*, vol. 24, 2021.

[4] ปวรุตม์ เปี่ยมแก้ว, อกนิษฐ์ ผดุงเรืองกิจ, กรณัฐ รัตนนท์, เมธา อึ่งทอง, & อภิชาติ ศรีประดิษฐ. (2563).การออกแบบและพัฒนาเครื่องบรรจุน้ำปลาร้ากึ่งอัตโนมัติ.*วารสารมหาวิทยาลัยธนบุรี(วิทยาศาสตร์แลเทคโนโลยี)*, 4(1), 25-43.

[5] ณัฐพงศ์ แพน้อย, อภิรักษ์ คงประเวช, เดชาธร เหล็กอยู่มะดัน, & ปฏิพล ทรัพย์ทวีปัญญา. (2564). การสร้างต้นแบบระบบสายพานลำเลียงสำหรับเครื่องบรรจุน้ำดื่มอัตโนมัติโดยใช้พีแอลซี.*ENGINEERING TRANSACTIONS*, 24(1), 28-36.

[6] ธีรภัทร หลิ่มบุญเรือง, พิสมัย พันธุ์อภัย, & สมชาย แยมไส. (2550). การออกแบบและสร้างเครื่องบรรจุผลิตภัณฑ์สำหรับผลิตภัณฑ์ที่เป็นของเหลว. *การประชุมวิชาการมหาวิทยาลัยศรีนครินทรวิโรฒ ปีการศึกษา 2550, นครนายก, ประเทศไทย, 6 สิงหาคม 2550*.

[7] นภาพร ศรีเวียง, ภารดี เพ็ชรภูมิ, & รตามณี เหลือหลาย. (2560). การคัดแยกขวดตามความสูงและเติมน้ำในขวดด้วยพีแอลซี โตชิบ้า รุ่น T2 (ปริญญานิพนธ์ปริญญาวิศวกรรมศาสตรบัณฑิต, มหาวิทยาลัยนเรศวร).

[8] จรัสพงศ์ เจษฎาเมธานนท์, กิติพงษ์ เจาจารึก, & สุวรรณ หอมหวล. (2561). การประยุกต์ใช้โปรแกรมแมเบิลลอจิกคอนโทรลเลอร์ (PLC) สำหรับเครื่องตรวจสอบความผิดปกติของนม ยู.เอช.ที.บรรจุกล่อง. *วารสารวิทยาศาสตร์และเทคโนโลยี*, 7(3), 1-10.

ผลของการเปลี่ยนแปลงการใช้ประโยชน์ที่ดินที่มีต่อปริมาณน้ำท่าในพื้นที่ลุ่มน้ำจังหวัดภูเก็ต

Impact of Land Use Changes on Discharge in Phuket Watershed

Sukanya Vongtanaboon
Faculty of Science and Technology
Phuket Rajabhat University
Phuket, Thailand
sukanya.v@pkru.ac.th

Suthathong Homya
Faculty of Science and Technology
Phuket Rajabhat University
Phuket, Thailand
suthathong.h@pkru.ac.th

Pongsakorn Kaewmanee
Faculty of Science and Technology
Phuket Rajabhat University
Phuket, Thailand
s6410951103@pkru.ac.th

Pobtham Prompen
Kajonkiet International School
Phuket, Thailand
pobthamprompen@gmail.com

Abstract

This study investigates the impact of land use changes on water discharge in the Phuket watershed, Thailand. Phuket, a rapidly growing tourist destination, faces significant water scarcity issues due to increasing urban development and tourism. The research focuses on analyzing land use changes between 2017 and 2022, categorizing land into five types: urban and built-up areas, agricultural land, forested areas, water bodies, and miscellaneous areas. The study employs land use data to assess the effects of these changes on water discharge. Results indicate a decrease in agricultural and forested areas, alongside an increase in urban and built-up areas and water bodies. These changes have led to a reduction in water discharge, highlighting the critical need for effective water resource management to mitigate the impact of land use changes and ensure sustainable water availability in the region. The findings underscore the importance of integrating land use planning with water resource management to address the growing water demands in Phuket.

Keywords*—land use change, discharge, Phuket watershed*

บทนำ

จังหวัดภูเก็ตตั้งอยู่ในเขตพื้นที่ลุ่มน้ำภาคใต้ฝั่งตะวันตก ตามการแบ่งลุ่มน้ำหลักของประเทศไทยโดยคณะกรรมการอุทกวิทยาแห่งชาติ จังหวัดภูเก็ตไม่มีแม่น้ำสายสำคัญแต่มีระบบลุ่มน้ำหลักที่สำคัญ 4 แห่ง ได้แก่ ระบบลุ่มน้ำบางเทา เกาะแก้ว กะทู้ และฉลอง [1] จังหวัดภูเก็ตเป็นเมืองหนึ่งที่ประสบปัญหาการขาดแคลนน้ำอันเนื่องมาจากการเจริญเติบโตของเมืองเพื่อรองรับธุรกิจท่องเที่ยว จำนวนนักท่องเที่ยวที่เพิ่มขึ้นในทุกปีของจังหวัดภูเก็ตเป็นเหตุในปริมาณความต้องการน้ำเพิ่มสูง ข้อมูลจากกรมชลประทานรายงานว่าจังหวัดภูเก็ตมีความต้องการน้ำต่อปีเฉลี่ย 80 ล้านลูกบาศก์เมตร ในขณะที่การผลิตน้ำสามารถผลิตได้เฉลี่ยเพียงแค่ 48 ล้านลูกบาศก์เมตรต่อปีเท่านั้น จึงมีปริมาณน้ำที่ยังขาดแคลนกว่า 32 ล้านลูกบาศก์เมตรต่อปี [1], [2] ด้วยเหตุนี้จังหวัดภูเก็ตมักประสบปัญหาขาดแคลนน้ำในช่วงหน้าแล้งของทุกปี [3] ปัจจุบันจังหวัดภูเก็ตยังประสบปัญหาทั้งด้านการขาดแคลนน้ำเป็นประจำทุกปีจากภาวะฝนทิ้งช่วงหรือฤดูแล้ง นอกจากนี้ยังมีปัญหาน้ำท่วม ซึ่งเกิดจากน้ำล้นตลิ่งจากคลองส่วนใหญ่ เนื่องจากสภาพทางภูมิประเทศในบางช่วงที่เป็นลักษณะคอขวด ทำให้ระบายน้ำได้น้อยจนเกิดน้ำสะสมล้นตลิ่ง รวมถึงมีสิ่งกีดขวางทางน้ำ น้ำทะเลหนุนบริเวณชายฝั่ง [2] และเนื่องจากการเจริญเติบโตทางเศรษฐกิจอย่างรวดเร็วของจังหวัดภูเก็ต ทั้งในส่วนของการลงทุนภาคเอกชนในการพัฒนาอสังหาริมทรัพย์และจำนวนนักท่องเที่ยวที่นิยมเดินทางเข้ามายังจังหวัดภูเก็ตอย่างต่อเนื่องทุกปี รวมทั้งการเคลื่อนย้ายประชากรเข้ามาทำงานในจังหวัดภูเก็ต ส่งผลทำให้รูปแบบการใช้ประโยชน์ที่ดิน

เปลี่ยนไป จึงทำให้มีอัตราความต้องการน้ำในแต่ละวันเพิ่มขึ้น จึงจำเป็นอย่างยิ่งที่จะต้องมีการจัดการทรัพยากรน้ำอย่างมีประสิทธิภาพ เพื่อให้เพียงพอต่อความต้องการมากที่สุด ดังนั้นการประเมินทรัพยากรน้ำจึงมีความสำคัญอย่างมากสำหรับการวางแผนการจัดการทรัพยากรน้ำให้ได้รับประโยชน์สูงสุด [4] งานวิจัยครั้งนี้จึงทำการศึกษาผลของการเปลี่ยนแปลงการใช้ประโยชน์ที่ดินที่มีต่อปริมาณน้ำท่าในพื้นที่ลุ่มน้ำจังหวัดภูเก็ต

วิธีการศึกษา

การศึกษาผลของการเปลี่ยนแปลงการใช้ประโยชน์ที่ดินที่มีต่อปริมาณน้ำท่าในพื้นที่ลุ่มน้ำจังหวัดภูเก็ต ได้ทำการศึกษาการเปลี่ยนแปลงการใช้ประโยชน์ที่ดินเพื่อวิเคราะห์ผลกระทบที่มีต่อปริมาณน้ำท่า โดยมีรายละเอียดดังนี้

การศึกษาการเปลี่ยนแปลงการใช้ประโยชน์ที่ดินในพื้นที่ลุ่มน้ำจังหวัดภูเก็ต

เตรียมชั้นข้อมูลแผนที่การใช้ประโยชน์ที่ดินจังหวัดภูเก็ตจากกรมพัฒนาที่ดิน ในการศึกษานี้ได้ใช้ข้อมูลการใช้ประโยชน์ที่ดินระหว่างปี พ.ศ. 2560 - 2565 [5] และนำข้อมูลการใช้ประโยชน์ที่ดินมาเปรียบเทียบการเปลี่ยนแปลงการใช้ประโยชน์ที่ดิน 5 ประเภท คือ พื้นที่ชุมชนและสิ่งก่อสร้าง (U) พื้นที่เกษตรกรรม (A) พื้นที่ป่าไม้ (F) พื้นที่แหล่งน้ำ (W) และพื้นที่เบ็ดเตล็ด (M) ในระหว่างปี พ.ศ. 2560 – 2565

การศึกษาผลของการเปลี่ยนแปลงการใช้ประโยชน์ที่ดินที่มีต่อปริมาณน้ำท่าในพื้นที่ลุ่มน้ำจังหวัดภูเก็ต

กำหนดพื้นที่ลุ่มน้ำ (watershed delineation) โดย (1) จำลองลักษะณะทางกายภาพโดยทั่วไปของพื้นที่ลุ่มน้ำจากแบบจำลอง DEM (2) กำหนดเส้นทางน้ำ (stream definition) (3) กำหนดรายละเอียดโครงข่ายเส้นน้ำ (stream network) (4) กำหนดจุดออกของเส้นทางน้ำ (outlet) (5) คำนวณค่าพารามิเตอร์ต่างๆ ของพื้นที่ลุ่มน้ำและเส้นลำน้ำ (calculation of basin parameters)

ประเมินน้ำท่า โดยดำเนินการรวบรวมข้อมูลปริมาณน้ำท่าในพื้นที่ลุ่มน้ำจังหวัดภูเก็ตจากศูนย์อุทกวิทยาชลประทานภาคใต้ [6] วิเคราะห์ข้อมูลปริมาณน้ำท่าในแต่ละช่วงเวลา

ศึกษาความสัมพันธ์ระหว่างการเปลี่ยนแปลงการใช้ประโยชน์ที่ดินและปริมาณน้ำท่า โดยการวิเคราะห์สมการถดถอยเชิงเส้นระหว่างการใช้ประโยชน์ที่ดินแต่ละประเภทกับปริมาณน้ำท่าในพื้นที่ลุ่มน้ำจังหวัดภูเก็ต

ผลการศึกษา

การศึกษาผลของการเปลี่ยนแปลงการใช้ประโยชน์ที่ดินที่มีต่อปริมาณน้ำท่าในพื้นที่ลุ่มน้ำจังหวัดภูเก็ต สามารถแสดงผลได้ดังนี้

การเปลี่ยนแปลงการใช้ประโยชน์ที่ดินระหว่าง พ.ศ. 2560-2565

ประเภทและพื้นที่การใช้ประโยชน์ที่ดินในพื้นที่ลุ่มน้ำจังหวัดภูเก็ต ระหว่าง พ.ศ. 2560-2565 สามารถแสดงได้ดังตารางที่ 1

ตารางที่ 1 การเปลี่ยนแปลงการใช้ประโยชน์ที่ดิน (ตร.กม.) ระหว่างปี พ.ศ. 2560 ถึง 2565

ประเภทการใช้ประโยชน์ที่ดิน	พ.ศ. 2560	พ.ศ. 2563	พ.ศ. 2565
Community areas and buildings	157.50	163.13	169.94
พื้นที่ชุมชนและสิ่งปลูกสร้าง (U)	**157.50**	**163.13**	**169.94**
Agricultural land generic	2.58	2.82	4.36
Agricultural land row crops	0.03	0.04	0.04
Orchard	147.26	146.7	143.02
Rice paddy	3.03	2.44	2.06
Pastures and barns	0.96	1.19	1.18
พื้นที่เกษตรกรรม (A)	**153.86**	**153.19**	**150.66**
Forest mixed	144.86	141.45	139.63
Range bush	24.85	26.36	26.66
พื้นที่ป่าไม้ (F)	**169.71**	**168.81**	**167.29**
Water	17.93	18.97	20.51
แหล่งน้ำ (W)	**17.93**	**18.97**	**20.51**
Wetland mixed	38.04	36.04	34.64
พื้นที่เบ็ดเตล็ด (M)	**38.04**	**36.04**	**34.64**

พื้นที่ชุมชนและสิ่งปลูกสร้างเพิ่มขึ้นจาก 157.50 ตร.กม. ในปี 2560 เป็น 169.94 ตร.กม. ในปี 2565 การเพิ่มขึ้นนี้สะท้อนถึงการขยายตัวของเมืองและการพัฒนาอสังหาริมทรัพย์เพื่อรองรับการเติบโตของภาคการท่องเที่ยวและประชากรที่เพิ่มขึ้น

พื้นที่เกษตรกรรมลดลงจาก 153.86 ตร.กม. ในปี 2560 เป็น 150.66 ตร.กม. ในปี 2565 โดยพื้นที่เกษตรกรรมทั่วไปเพิ่มขึ้นจาก 2.58 ตร.กม. เป็น 4.36 ตร.กม. ทุ่งหญ้าเพิ่มขึ้นเล็กน้อยจาก 0.96 ตร.กม. เป็น 1.18 ตร.กม. แต่สำหรับพืชสวน สวนยางพาราและสวนปาล์มลดลงอย่างมีนัยสำคัญ จาก 147.26 ตร.กม. เป็น 143.02 ตร.กม.

พื้นที่ป่าไม้โดยรวมลดลงจาก 169.71 ตร.กม. ในปี 2560 เป็น 167.29 ตร.กม. ในปี 2565 โดยป่าไม้ผสมลดลงจาก 144.86 ตร.กม. เป็น 139.63 ตร.กม.

แหล่งน้ำเพิ่มขึ้นจาก 17.93 ตร.กม. ในปี 2560 เป็น 20.51 ตร.กม. ในปี 2565 ซึ่งเป็นผลจากการจัดการน้ำเพื่อรองรับความต้องการที่เพิ่มขึ้นของชุมชนและนักท่องเที่ยว

พื้นที่เบ็ดเตล็ดลดลงจาก 38.04 ตร.กม. ในปี 2560 เป็น 34.64 ตร.กม. ในปี 2565

โดยรวมแล้วการใช้ประโยชน์ที่ดินในพื้นที่ลุ่มน้ำจังหวัดภูเก็ตมีการเปลี่ยนแปลงในช่วงหลายปีที่ผ่านมา โดยมีพื้นที่ชุมชนและแหล่งน้ำเพิ่มขึ้น ในขณะที่พื้นที่เกษตรกรรม พื้นที่ป่าไม้ และพื้นที่เบ็ดเตล็ดลดลง

การเปลี่ยนแปลงการใช้ประโยชน์ที่ดินที่มีผลต่อปริมาณน้ำท่า

ปริมาณน้ำท่าในพื้นที่ลุ่มน้ำจังหวัดภูเก็ตสามารถแสดงได้ดังตารางที่ 2

ตารางที่ 2 ปริมาณน้ำท่ารายเดือนในพื้นที่ลุ่มน้ำจังหวัดภูเก็ต ระหว่างปี พ.ศ. 2560-2565

เดือน	ปริมาณน้ำท่ารายเดือน (ล้าน ลบ.ม.)					
	พ.ศ. 2560	พ.ศ. 2561	พ.ศ. 2562	พ.ศ. 2563	พ.ศ. 2564	พ.ศ. 2565
เมษายน	1.55	1.62	1.70	1.15	2.31	1.69
พฤษภาคม	3.68	3.37	1.88	2.08	1.92	1.21
มิถุนายน	5.15	6.35	3.48	5.35	2.57	2.24
กรกฎาคม	4.25	3.11	4.14	3.81	3.16	8.13
สิงหาคม	8.22	4.43	3.01	4.85	6.05	4.93
กันยายน	12.62	6.49	4.29	10.51	5.26	6.17
ตุลาคม	8.70	5.39	4.36	8.36	5.38	4.54
พฤศจิกายน	4.63	2.79	3.06	7.35	8.38	6.61
ธันวาคม	5.82	1.49	2.72	2.81	2.85	1.52
มกราคม	2.63	1.07	1.25	1.45	1.45	1.09
กุมภาพันธ์	1.19	0.50	0.94	1.02	2.09	0.95
มีนาคม	1.12	0.42	0.84	1.04	1.44	0.81
ปริมาณน้ำท่ารายปี (ล้าน ลบ.ม.)	59.56	37.04	31.66	49.78	42.87	39.89

จากข้อมูลในตาราง พบว่า ปริมาณน้ำท่ารายเดือนสูงสุดมักเกิดขึ้นในช่วงเดือนกันยายน โดยเฉพาะในปี พ.ศ. 2560 ที่มีปริมาณน้ำท่าสูงถึง 12.62 ล้าน ลบ.ม. เดือนที่มีปริมาณน้ำท่าต่ำสุดมักเกิดขึ้นในช่วงเดือนกุมภาพันธ์และมีนาคม โดยในปี พ.ศ. 2561 ปริมาณน้ำท่าในเดือนมีนาคมอยู่ที่เพียง 0.42 ล้าน ลบ.ม.

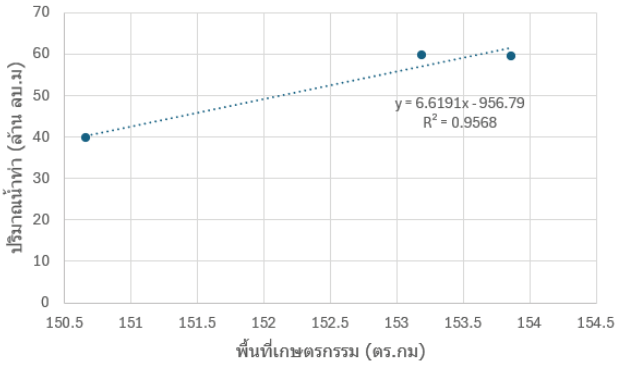
ปริมาณน้ำท่ารายปีมีค่าสูงสุดในปี พ.ศ. 2560 โดยมีปริมาณน้ำท่ารวมทั้งปีอยู่ที่ 59.56 ล้าน ลบ.ม. ปีที่มีปริมาณน้ำท่าต่ำสุดคือปี พ.ศ. 2562 โดยมีปริมาณน้ำท่ารวมทั้งปีอยู่ที่ 31.66 ล้าน ลบ.ม.

ปริมาณน้ำท่ามีแนวโน้มผันแปรในแต่ละปี โดยปี พ.ศ. 2560 มีปริมาณน้ำท่าสูงกว่าปีอื่น ๆ อย่างชัดเจน ในขณะที่ปี พ.ศ. 2562 มีปริมาณน้ำท่าต่ำที่สุดในช่วงเวลาที่ศึกษา ปริมาณน้ำท่าในปี พ.ศ. 2563 และ 2564 มีแนวโน้มเพิ่มขึ้นเล็กน้อยเมื่อเทียบกับปี พ.ศ. 2562 แต่ยังคงต่ำกว่าปี พ.ศ. 2560 ความผันแปรของปริมาณน้ำท่าสะท้อนถึงปัจจัยทางสภาพอากาศ เช่น ปริมาณฝนที่ตกในแต่ละปี ซึ่งส่งผลต่อปริมาณน้ำท่าโดยตรง

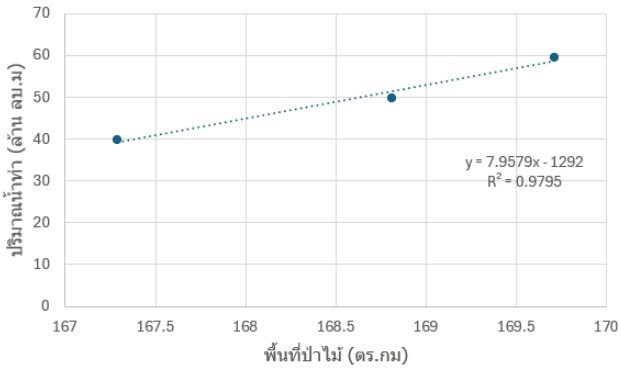
สำหรับผลของการเปลี่ยนแปลงประโยชน์ที่ดินที่มีต่อปริมาณน้ำท่า สามารถแสดงได้ดังตารางที่ 3 และภาพที่ 1-3

ตารางที่ 3 ประเภทการใช้ประโยชน์ที่ดินหลักที่เกิดการเปลี่ยนแปลงและปริมาณน้ำท่า ระหว่างปี พ.ศ. 2560 ถึง 2565

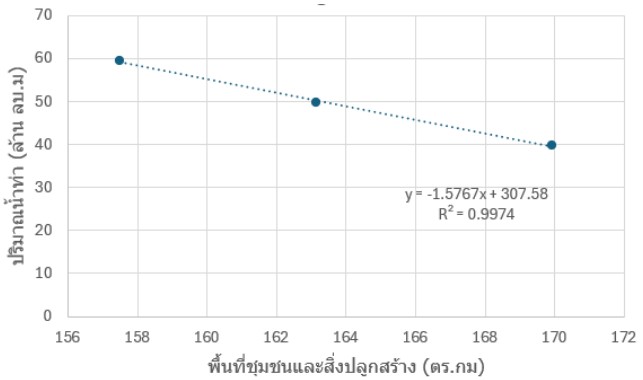
พ.ศ.	ประเภทการใช้ประโยชน์ที่ดิน (ตร.กม)			ปริมาณน้ำท่า (ล้าน ลบ.ม)
	พื้นที่เกษตรกรรม	พื้นที่ป่าไม้	พื้นที่ชุมชนและสิ่งปลูกสร้าง	
2560	153.86	169.71	157.50	59.56
2563	153.19	168.81	163.13	59.78
2565	150.66	167.29	169.94	39.89



ภาพที่ 1 การวิเคราะห์สมการถดถอยเชิงเส้นระหว่างพื้นที่เกษตรกรรมกับปริมาณน้ำท่าในพื้นที่ลุ่มน้ำจังหวัดภูเก็ต



ภาพที่ 2 การวิเคราะห์สมการถดถอยเชิงเส้นระหว่างพื้นที่ป่าไม้กับปริมาณน้ำท่าในพื้นที่ลุ่มน้ำจังหวัดภูเก็ต



ภาพที่ 3 การวิเคราะห์สมการถดถอยเชิงเส้นระหว่างพื้นที่ชุมชนและสิ่งก่อสร้างกับปริมาณน้ำท่าในพื้นที่ลุ่มน้ำจังหวัดภูเก็ต

ผลการศึกษาพบว่า การลดลงของพื้นที่เกษตรกรรมและป่าไม้ส่งผลให้ปริมาณน้ำท่าลดลง เนื่องจากพื้นที่เหล่านี้มีบทบาทสำคัญในการดูดซับและกักเก็บน้ำ การลดลงของพื้นที่ป่าไม้อาจทำให้การไหลของน้ำเพิ่มขึ้นอย่างรวดเร็วในช่วงฝนตกหนัก และลดการซึมของน้ำลงสู่ดิน [7]

การเพิ่มขึ้นของพื้นที่ชุมชนและสิ่งปลูกสร้างส่งผลให้พื้นผิวที่ปิดทึบเพิ่มขึ้น ซึ่งลดความสามารถในการดูดซับน้ำของดิน และเพิ่มปริมาณน้ำไหลบ่าหน้าดิน สิ่งนี้ทำให้ปริมาณน้ำท่าลดลงและเพิ่มความเสี่ยงต่อการเกิดน้ำท่วม

ปริมาณน้ำท่าลดลงจาก 59.56 ล้าน ลบ.ม. ในปี 2560 เป็น 39.89 ล้าน ลบ.ม. ในปี 2565 ซึ่งสอดคล้องกับการเปลี่ยนแปลงการใช้ที่ดินที่เกิดขึ้น โดยเฉพาะการลดลงของพื้นที่เกษตรกรรมและป่าไม้ และการเพิ่มขึ้นของพื้นที่ชุมชนและสิ่งปลูกสร้าง เป็นปัจจัยที่ทำให้ปริมาณน้ำท่าลดลง

ดังนั้นการเปลี่ยนแปลงการใช้ประโยชน์ที่ดินมีผลกระทบต่อปริมาณน้ำท่าในพื้นที่ลุ่มน้ำจังหวัดภูเก็ต การจัดการและการวางแผนการใช้ที่ดินอย่างยั่งยืนจึงมีความสำคัญอย่างยิ่งเพื่อให้มั่นใจว่าทรัพยากรน้ำจะเพียงพอต่อความต้องการในอนาคต

ข้อเสนอแนะ

การจัดการทรัพยากรน้ำ: ควรมีการวางแผนการจัดการทรัพยากรน้ำอย่างมีประสิทธิภาพเพื่อรองรับความต้องการที่เพิ่มขึ้นและลดผลกระทบจากการเปลี่ยนแปลงการใช้ที่ดิน

การอนุรักษ์พื้นที่ป่าไม้และเกษตรกรรม: ควรส่งเสริมการอนุรักษ์และฟื้นฟูพื้นที่ป่าไม้และเกษตรกรรมเพื่อเพิ่มความสามารถในการดูดซับและกักเก็บน้ำ

การวางแผนการใช้ที่ดิน: ควรมีการควบคุมการขยายตัวของเมืองและการพัฒนาอสังหาริมทรัพย์เพื่อลดผลกระทบต่อระบบนิเวศและทรัพยากรน้ำ

เอกสารอ้างอิง

[1] กรมชลประทาน. (2561). รายงานแผนแม่บทการพัฒนาลุ่มน้ำจังหวัดภูเก็ต.

[2] ศูนย์อำนวยการน้ำแห่งชาติ. (2566). สถานการ์น้ำจังหวัดภูเก็ตปี พ.ศ 2566.

[3] วีระพงค์ เกิดสิน. (2563). การขาดแคลนน้ำและแนวทางการแก้ไขของจังหวัดภูเก็ต.

[4] กลุ่มงานข้อมูลสารสนเทศและการสื่อสารสำนักงานจังหวัดภูเก็ต. (2561). บรรยายสรุปจังหวัดภูเก็ต.

[5] กรมพัฒนาที่ดิน กระทรวงเกษตรและสหกรณ์. (2565). ข้อมูลการใช้ประโยชน์ที่ดินจังหวัดภูเก็ตระหว่างปี พ.ศ. 2560 - 2565.

[6] ศูนย์อุทกวิทยาชลประทานภาคใต้. (2567). ข้อมูลปริมาณน้ำท่าจังหวัดภูเก็ต.

[7] เกษม จันทร์แก้ว. (2551). หลักการจัดการลุ่มน้ำ. สำนักพิมพ์มหาวิทยาลัยเกษตรศาสตร์.

ผลของลักษณะแผ่นช่องการไหลต่อประสิทธิภาพเซลล์เชื้อเพลิงชนิดเมมเบรนแลกเปลี่ยนโปรตอน

Jaruporn Saiyasupee
Department of Mechanical Engineering
Faculty of Engineering
University of Technology Lanna
128 Huay Kaew Road,
Chiang Mai, Thailand, 50300
jarupornsaiyasupee28@gmail.com

Korawat Wuttikid*
Department of Mechanical Engineering
Faculty of Engineering
University of Technology Lanna
128 Huay Kaew Road,
Chiang Mai, Thailand, 50300
korrawat_wuttikid@rmutl.ac.th

Konlayut Punyawudho
Department of Mechanical Engineering
Faculty of Engineering
Chiang Mai University
239, Huay Kaew Road
Chiang Mai ,Thailand, 50200
konlayutt.p@cmu.ac.th

Ronnachart Munsin
Department of Mechanical Engineering
Faculty of Engineering
University of Technology Lanna
128 Huay Kaew Road,
Chiang Mai, Thailand, 50300
ronnachart@rmutl.ac.th

Yottana Khunatorn
Department of Mechanical Engineering
Faculty of Engineering
Chiang Mai University
239, Huay Kaew Road
Chiang Mai ,Thailand, 50200

***Abstract*—** The proton exchange membrane fuel cell (PEMFC) is an electrical device and a highly efficient green technology. One of the most crucial factors affecting PEMFC performance is the development of the flow field configuration. This study experimentally investigates the effect of three different serpentine flow field (SFF) configurations on PEMFC performance. at the low current density, the 3-Ch_w0.8 SFF configuration provides a slightly higher performance than the others, as all three configurations use the same MEA. at medium and high current density, the 3-Ch_w0.8 SFF also delivers the best performance. Since the current demand increases, more water is generated as a byproduct of the electrochemical reaction. The 3-Ch_w0.8 SFF achieves the highest performance due to its narrower channels, which enhance reactant gas and current density uniformity. The 1-Ch 45°_w1.0 SFF configuration performs slightly worse performance comparing the 3-Ch_w0.8 SFF. Since its single-channel design results in the longest flow path, causing the highest pressure drop and reactant velocity, leading to effective water removal. In contrast, the 3-Ch_w1.0 SFF, with its wider channels and shortest flow path, characterizes the lowest pressure drop and reactant velocity, making water removal less efficient. This inefficiency is evident from its significantly lower limiting current density compared to the other configurations.

Keywords—Flow field design, Water management, Serpentine Flow field, channel width, channel length

บทนำ

เซลล์เชื้อเพลิงชนิดเมมเบรนแลกเปลี่ยนโปรตอน (proton exchange membrane fuel cell, PEMFC) เป็นอุปกรณ์ที่สามารถผลิตไฟฟ้าจากปฏิกิริยาเคมีไฟฟ้าระหว่างก๊าซตั้งต้นชนิดไฮโดรเจน (H_2) และออกซิเจน (O_2) โดยมีน้ำเป็นผลิตภัณฑ์รอง เนื่องจากเป็นการผลิตไฟฟ้าโดยไม่เกิดการสันดาป PEMFC จึงเป็นเทคโนโลยีพลังงานสีเขียวและมีประสิทธิภาพสูงสุด [1] การพัฒนาประสิทธิภาพ PEMFC ขึ้นอยู่กับหลายปัจจัย หนึ่งในปัจจัยสำคัญคือการพัฒนาส่วนประกอบชนิดแผ่นช่องไหล (Flow Field: FF) ซึ่งส่วนประกอบนี้จะมีช่องทางไหลที่ทำหน้าที่เป็นช่องนำทางของสารตั้งต้น ทั้งในฝั่งขั้วแอโนดและแคโทด ช่วยนำอิเล็กตรอนจากปฏิกิริยาไปใช้เป็นพลังงานไฟฟ้า และช่วยกำจัดน้ำออกจากระบบ [2-15] การออกแบบ FF ที่เหมาะสมช่วยให้สารตั้งต้นกระจายตัวสม่ำเสมอทั่วพื้นที่ทำปฏิกิริยา ทำให้ปฏิกิริยาเคมีไฟฟ้าและประสิทธิภาพของ PEMFC เพิ่มขึ้น การจัดการน้ำที่ดีช่วยป้องกันภาวะน้ำท่วม (Flooding) ที่ขัดขวางการเข้าถึงของสารตั้งต้นไปยังพื้นที่ทำปฏิกิริยา ซึ่งจะทำให้ประสิทธิภาพที่ลดลง นอกจากนั้นการออกแบบ FF ที่เหมาะสมยังช่วยรักษาเสถียรภาพของระบบและยืดอายุการใช้งานของเยื่อเมมเบรนอิเล็กโทรด (Membrane Electrode Assembly: MEA) [6 , 13 , 14] ในหลายทศวรรษที่ผ่านมามีการพัฒนาลักษณะ FF หลายรูปแบบ โดยหนึ่งในรูปแบบช่องการไหลที่นิยมใช้งาน คือช่องการไหลแบบคดเคี้ยว (Serpentine Flow Field: SFF) ซึ่งสามารถช่วยให้ สารตั้งต้น กระแสไฟฟ้า ความร้อน และความชื้น แพร่กระจายทั่วพื้นที่ทำปฏิกิริยาอย่างสม่ำเสมอ [3-15]

มีหลายงานวิจัยที่ประยุกต์การจำลองทางพลศาสตร์ของไหล (Computational Fluid Dynamics: CFD) เพื่อจำลองประสิทธิภาพ PEMCF ที่เงื่อนไขการเปลี่ยนแปลง SFF รูปแบบต่างๆ เช่น การศึกษาผลของจำนวนช่องการไหลใน SFF ในงานของ S. Shimpalee [14] ซึ่งได้สร้างแบบจำลองของจำนวนช่องไหลตั้งแต่ 3 ถึง 26 ช่อง ในพื้นที่ทำปฏิกิริยา 200 cm^2 โดยผลพบว่า SFF แบบ 26 ช่องให้ค่าความหนาแน่นกระแสไฟฟ้าที่เหมาะสมที่สุด มีความดันตกคร่อม (pressure drops) ของสารตั้งต้นต่ำที่สุด และมีการกระจายความชื้นที่ดี D.H. Jeon et al. [11] อธิบายว่า SFF แบบ 2 ช่อง (พื้นที่ทำปฏิกิริยา 10 cm^2) มีประสิทธิภาพสูงกว่า SFF แบบ 1 ช่อง L. Zhang et al. [6] จำลอง SFF ที่มีจำนวนช่อง, 1 ถึง 8, SFF 8 ช่องแบบซับซ้อน, และ SFF 10 ช่องแบบซับซ้อน, พบว่า SFF 8 ช่องแบบซับซ้อน มีการกระจายกระแสไฟฟ้าที่สม่ำเสมอที่สุด และให้ประสิทธิภาพสูงสุด โดยขนาดช่องไหลที่เหมาะสม คือ กว้าง 1.2 mm และลึก 0.8 mm X. Wang et al. [9,12] ได้วิเคราะห์ผลของ SFF ในพื้นที่ทำปฏิกิริยา 5.29 cm^2 ซึ่งผลพบว่า ช่องไหลที่แคบลงช่วยเพิ่มประสิทธิภาพของ PEMFC โดย SFF แบบ 1 ช่องให้ประสิทธิภาพสูงกว่ารูปแบบ 2 และ 3 ช่อง ซึ่งสอดคล้องกับผลการศึกษาของ Isikli [3] และ Y. Wu [7] ที่ให้ผลว่า SFF แบบ 1 ช่อง ช่วยเพิ่มความสม่ำเสมอของการกระจายและจัดการน้ำ เพิ่มความเร็วของก๊าซตั้งต้น อย่างไรก็ตามความดันตกคร่อมสูงขึ้นเมื่อช่องการไหลมีความยาวเพิ่มขึ้น หรือมีความกว้างลดลงซึ่งต้องใช้กำลังปั๊มสารตั้งต้นสูงขึ้นเพื่อชดเชยความดันตกคร่อมที่ตำลง

การศึกษาเชิงจำลองด้านอิทธิพลของขนาดช่องการไหล เช่น ความกว้าง ความลึก และบ่าระหว่างช่องการไหล (Rib) ใน SFF ที่มีมีต่อประสิทธิภาพของ PEMFC ได้ถูกนำเสนอ เช่น B.S. Reddy et al. [5] และ Wang et al. [9,12] รายงานว่าการลดขนาดช่องไหลช่วยเพิ่มความเร็วของก๊าซตั้งต้น ทำให้การกระจายกระแสไฟฟ้าสม่ำเสมอ Wang et al. [9,12] และ Kap-S. Choi [8] พบว่าการลดขนาด Rib มีข้อดีในการเพิ่มการพาน้ำและความร้อน ส่งผลให้ค่าความ

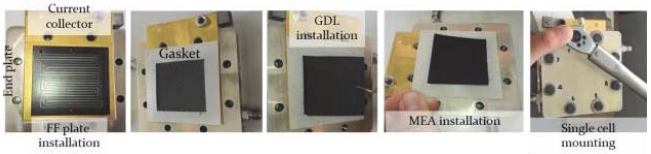
หนาแน่นกระแสไฟฟ้าสูงขึ้น อย่างไรก็ตามลดขนาด Rib มากเกินไปจะไม่เป็นประโยชน์ขึ้น การลดขนาดความกว้างช่องการไหล ส่งผลต่อความดันตกคร่อมที่สูงขึ้นแบบเอ็กซ์โปเนนเชียล โดยขนาดช่องไหลที่เหมาะสมอยู่ที่ 0.5mm (เทียบกับช่องความกว้างช่องการไหล 0.3–1.53mm) Wang et al. [12] เสนอผลวิจัยของรูปแบบ SFF แบบ 3 ช่อง ที่เปลี่ยนความกว้างช่องการไหล พบว่าการเปลี่ยนแปลงขนาด ความกว้างและ Rib ในช่วง 1mm มีผลต่อประสิทธิภาพของ PEMFC เพียงเล็กน้อย S. Shimpalee et al. [13] ให้ผลการจำลองว่าการลดขนาด SFF จาก 1.0mm เป็น 0.7mm (ความกว้างคงที่ 1.0mm) ทำให้การเพิ่มประสิทธิภาพ PEMFC มากกว่าการลดความกว้างจาก 1.0mm เป็น 0.7mm (Rib คงที่ 1.0mm) เนื่องจากการจัดการน้ำดีขึ้นเมื่อขนาด Rib ลดลง Kap-S. Choi et al. [8] ศึกษาการเปลี่ยนแปลงขนาด ความกว้าง ความลึก และ Rip ใน SFF แบบ 5 ช่อง พบว่าเมื่อเพิ่มความลึกของช่องไหล ทำให้ความดันตกคร่อมลดลงน้อย จึงเกิดการสะสมน้ำที่ช่องทางออก นำไปสู่ภาวะการแพร่กลับ (Electro osmosis Drag) ของน้ำจากแคโทดมายังแอโนดเป็นผลดีต่อการนำประจุใน MEA แต่เมื่อเพิ่มความกว้างช่องไหลให้กว้างขึ้นจะไม่เกิดปรากฏการดังกล่าว ดังนั้นประสิทธิภาพของ PEMFC จากการความกว้างช่องไหลจึงส่งผลมากกว่าการเพิ่มขนาดความลึกช่องการไหล

จากการศึกษาที่ผ่านมาพบว่า ขนาดและความยาวของช่องไหล SFF มีผลอย่างมากต่อประสิทธิภาพของ PEMFC งานวิจัยนี้จึงนำเสนอการออกแบบ SFF แบบ 1 ช่อง ที่มีความกว้างช่องไหล 1.0mm และเส้นทางไหลที่เอียง 45° ซึ่งยังไม่มีการศึกษามาก่อน (อ้างจากการทบทวนวรรณกรรมฉบับล่าสุด [2]) โดยประสิทธิภาพ PEMFC จะถูกเปรียบเทียบกับ SFF แบบ 3 ช่อง ที่มีความกว้างช่องไหล 1.0mm และ 0.8mm ผลการทดสอบในงานนี้จะเป็นเชิงทดลองซึ่งพบได้น้อยเมื่อเทียบกับงานวิจัยเชิงจำลอง งานนี้จะช่วยส่งเสริมฐานข้อมูลเชิงทดสอบที่สามารถเทียบกับผลจากแบบจำลองที่เกี่ยวข้องได้มากขึ้น

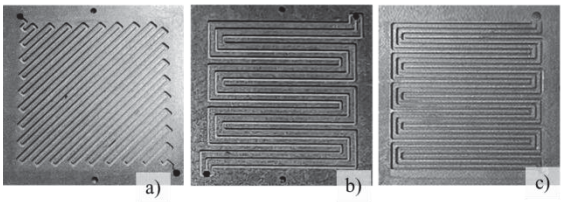
ระเบียบวิธีวิจัย

การประกอบเซลล์เดี่ยวและเงื่อนไขการทดสอบ

เยื่อแมมเบรนอิเล็กโทรด (MEA) ถูกติดตั้งอยู่ตำแหน่งแกนกลาง PEMFC แบบเซลล์เดียว ซึ่งจะถูกประกบทั้ง 2 ฝั่ง (แอโนด และแคโทด) เรียงตามลำดับด้วย 1. Gas diffusion layers (GDLs) ที่ทำจากผ้าคาร์บอน (W1S1005, CeTech) 2. ปะเก็นคอมโพสิตไฟเบอร์กลาส-ซิลิโคน 3. แผ่นช่องการไหล (FF) 4. แผ่นรวมกระแสไฟฟ้า (Current collector) และ 5. แผ่นตัวเรือน (End Plate) การทดสอบประสิทธิภาพของ PEMFC จะถูกหาจากการเปลี่ยนแปลงลักษณะ SFF 3 รูปแบบ ช่องการไหลเดี่ยว ที่ไหลเอียง 45° (1-Ch45°_w1.0) SFF แบบ 3 ช่องทางที่มีช่องทางกว้าง 1.0mm (3-Ch_w1.0) และกว้าง 0.8mm (3-Ch_w0.8) พื้นที่ทำปฏิกิริยาคือ 5 × 5 cm² MEA ผลิตจากตัวเร่งปฏิกิริยาแพลตตินัม Pt ปริมาณ 0.3 mg/cm² บนแต่ละฝั่งแอโนดและแคโทด เครื่องทดสอบประสิทธิภาพมาตรฐาน Scribner Model 890E ถูกใช้ในงานนี้ อุณหภูมิและความชื้นในการทดสอบคือ 75°C และ 85% ตามลำดับ อัตราส่วน Stoichiometry ของไฮโดรเจนต่ออากาศคือ 1.4:3.4



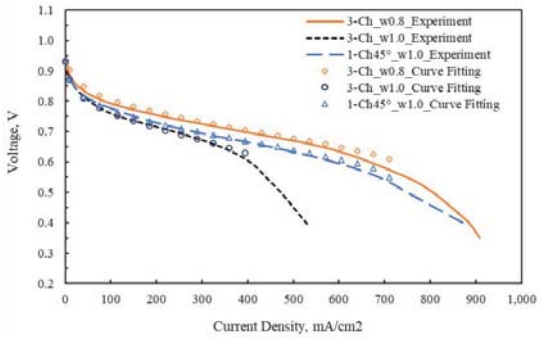
ภาพที่ 1 ขั้นตอนการประกอบเซลล์เดียวของ PEMFC



ภาพที่ 2 ลักษณะแผ่นช่องการไหล SFF แบบ a) 1-Ch45°_w1.0, b) 3-Ch_w1.0 และ c) 3-Ch_w0.8 สำหรับทดสอบประสิทธิภาพ PEMFC

ผลการทดสอบและผลการอภิปราย

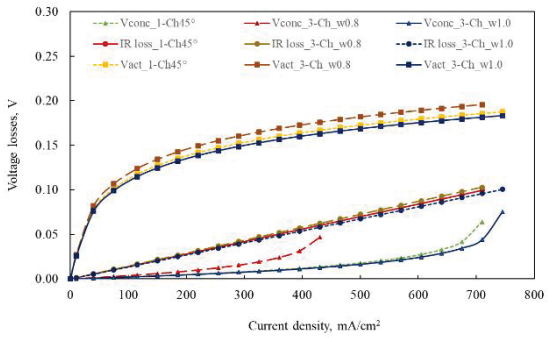
โดยทั่วไปแล้ว ประสิทธิภาพของ PEMFC จะถูกแสดงในรูปแบบของ Polarization curve หรือกราความสำพันธ์ระหว่างกระแส (mA/cm²) และแรงดัน ไฟฟ้า (V) หรือ (I-V curve) กราฟนี้ช่วยให้เราเข้าใจการตัวแปรที่สำคัญ เช่น แรงดันเริ่มต้น (open-circuit voltage หรือแรงดันไฟฟ้า ขนะที่ไม่มีการดึงกระแสไฟฟ้า) และค่าขีดจำกัดของกระแสไฟฟ้า (limiting current density) กราฟนี้ยังสามารถถูกใช้เพื่อวิเคราะห์การสูญเสียแรงดันไฟฟ้าใน PEMFC ได้แก่ การสูญเสียแรงดันไฟฟ้าจาก การกระตุ้นปฏิกิริยา (activation loss) การสูญจากความต้านทาน (ohmic loss) และการสูญเสียจากการพร่องความเข้มข้นสารตั้งต้น (concentration loss) กราฟ Polarization curve ทางทฤษฎีจะถูกสร้างขึ้นเทียบกับผลการทดลอง [1] เพื่อช่วยเสริมการวิเคราะห์ผล ผลการจำลองและผลการทดสอบแสดงในรูปที่ 3



ภาพที่ 3 ประสิทธิภาพ PEMFC ที่ได้จากการเปลี่ยนแปลงลักษณะ SFF แบบ 1-Ch 45°_w1.0, 3-Ch_w1.0, และ 3-Ch_w0.8) ที่มีการปรับ polarization curve เปรียบเทียบ

ผลการทดสอบพบว่า SFF แบบ 3-Ch_w0.8 ให้ประสิทธิภาพโดยรวมของ PEMFC ดีที่สุด รองลงมาคือ 1-Ch 45°_w1.0 และ 3-Ch_w1.0 โดยที่ 3-Ch_w0.8 มีค่า open-circuit voltage เท่ากับ 0.93 V ซึ่งสูงกว่า 1-Ch 45°_w1.0 (0.91 V) และ 3-Ch_w1.0 (0.90 V) เล็กน้อย ในช่วงความหนาแน่นกระแสต่ำ (activation loss region) 3-Ch_w0.8 ให้ประสิทธิภาพดีกว่าแบบอื่น เมื่อพิจารณาที่แรงดัน 0.8 V (ตัวแทนแรงดันไฟฟ้าของช่วง activation loss) 3-Ch_w0.8 ให้ความหนาแน่นกระแส 80 mA/cm² ซึ่งสูงกว่า 1-Ch 45°_w1.0 (42 mA/cm²) และ 3-Ch_w1.0 (31 mA/cm²) อย่างไรก็ตาม การเพิ่มหรือลดของประสิทธิภาพ PEMFC ในช่วงนี้ขึ้นอยู่กับความสามารถในการกระตุ้นปฏิกิริยาไฟฟ้าเคมีของตัวเร่งปฏิกิริยา เนื่องจากทั้ง 3 แบบ SFF ใช้ MEA แบบเดียวกัน activation loss จึงไม่มีผลกระทบอย่างมีนัยสำคัญต่อประสิทธิภาพ PEMFC เมื่อเข้าสู่ช่วงความหนาแน่นกระแสปานกลาง ohmic loss จะส่งอิทธิผลมากขึ้น เมื่อพิจารณาที่ 0.6 V (ตัวแทนแรงดันไฟฟ้าของช่วง ohmic loss) 3-Ch_w0.8 SFF ยังคงให้ประสิทธิภาพของ PEMFC ที่ดีที่สุด ด้วยความหนาแน่นกระแส 748 mA/cm² ซึ่งสูงกว่า 1-Ch 45°_w1.0 (588 mA/cm²) และ 3-Ch_w1.0 (406 mA/cm²) ในช่วงความหนาแน่นกระแสสูง (concentration loss region) เมื่อพิจารณาที่

แรงดันไฟฟ้า 0.45 V (ตัวแทนแรงดันไฟฟ้าของช่วง concentration loss) 3-Ch_w0.8 SFF ให้ค่าความหนาแน่นกระแสสูงสุดที่ 846 mA/cm² รองลงมาคือ 1-Ch 45°_w1.0 (810 mA/cm²) และ 3-Ch_w1.0 (501 mA/cm²) ในบริเวณ ohmic loss และ concentration loss ปฏิกิริยาเคมีไฟฟ้าจะสร้างกระแสที่สูงขึ้น ทำให้เกิดการผลิตน้ำมากขึ้น ซึ่งเคยถูกพิสูจน์ในงานวิจัยเชิงทดลองของ Y. Wu [7] พบว่า SFF ที่มีความดันตกคร่อมสูง เช่น SFF แบบ 1 ช่องการไหล จะมีความเร็วการไหลของก๊าซภายในช่องการไหลสูงขึ้น ซึ่งจะช่วยเพิ่มการกระจายตัวของสารตั้งต้นและความหนาแน่นกระแส พร้อมกับช่วยกำจัดน้ำออกจากระบบได้อย่างมีประสิทธิภาพ เมื่อเปรียบเทียบกับงานวิจัยนี้พบว่า 3-Ch_w0.8 SFF มีช่องทางที่แคบลง ในขณะที่ 1-Ch 45°_w1.0 SFF มีความยาวช่องการไหลที่ยาวที่สุด ซึ่งปัจจัยเหล่านี้ทำให้มีความเร็วการไหลสูงกว่า 3-Ch_w1.0 SFF ส่งผลให้ประสิทธิภาพของ PEMFC ดีขึ้น



ภาพที่ 4 ค่าการสูญเสียแรงดันไฟฟ้าทั้ง 3 รูปแบบ activation loss, ohmic loss และ concentration loss ที่ได้จากลักษณะช่องการไหลทั้ง 3 แบบ

การปรับ polarization curve ให้ใกล้เคียงกับผลการทดสอบ เพื่อช่วยเสริมการวิเคราะห์การสูญเสียแรงดันไฟฟ้าจากช่วงกระแสต่ำ กลาง และสูง ได้ถูกแสดงไว้ในรูปที่ 4 การสูญเสียแรงดันทั้ง 3 ประเภทสามารถถูกคำนวณจากสมการทางทฤษฎีของ polarization curve (1) [1]

$$E_{cell} = E - \frac{RT}{\alpha F}\ln\left(\frac{i}{i_o}\right) - \frac{RT}{nF}\ln\left(\frac{i_L}{i_L - i}\right) - iR$$

เมื่อพิจารณา activation loss, V_{act} ที่ได้จาก SFF ทั้ง 3 แบบ พบว่าการสูญเสียแรงดันเพิ่มขึ้นอย่างมีนัยสำคัญโดยเฉพาะที่ความหนาแน่นกระแสต่ำ (i < 100 mA/cm²) อย่างไรก็ตาม ค่า activation loss ของทั้ง 3 การออกแบบแตกต่างกันเพียงเล็กน้อย ซึ่งยืนยันว่าทั้งหมดใช้ MEA แบบเดียวกันและมีความสามารถในการกระตุ้นปฏิกิริยาทางเคมีไฟฟ้าที่ใกล้เคียงกัน

สำหรับ ohmic loss, IR_{loss} พบว่าทั้ง 3 การออกแบบ SFF มีค่าที่แตกต่างกันเพียงเล็กน้อย ดังนั้น การสูญเสียแรงดันที่ส่งผลต่อประสิทธิภาพ PEMFC คือ concentration loss โดยในช่วง concentration loss, V_{conc} พบว่า 3-Ch_w0.8 และ 1-Ch 45°_w1.0 SFF มีค่า limiting current density ที่แตกต่างกันเพียงเล็กน้อย ประมาณ 700 และ 680 mA/cm² ตามลำดับ ในขณะที่ 3-Ch_w1.0 SFF มีค่า limiting current density ที่ต่ำกว่าโดยมากอยู่ที่ประมาณ 400 mA/cm² โดยข้อสรุปนี้สอดคล้องกับผลการศึกษา ซึ่งชี้ให้เห็นว่ารูปแบบช่องการไหลที่มีช่องการไหลกว้างและมีความยาวสั้น เช่น แบบ 3-Ch_w1.0 SFF จะทำให้การระบายน้ำออกจากพื้นที่ทำปฏิกิริยาน้อยลง เนื่องจาก มีความดันต่ำตกคร่อมต่ำ ความเร็วในการไหล (flow velocity) ในเส้นทางไหลมีค่าลดลง ส่งผลให้ประสิทธิภาพของ PEMFC ลดลง

สรุป

การศึกษานี้ได้ทำการวิเคราะห์ประสิทธิภาพ PEMFC ที่มี SFF ลักษณะช่องการไหลต่างกัน 3 แบบคือ 1-Ch 45°_w1.0 3-Ch_w0.8 และ 3-Ch_w1.0 SFF ในช่วงการใช้กระแสไฟฟ้าต่ำ (activation loss) ช่องการไหล 3-Ch_w0.8 SFF ให้ค่าความหนาแน่นกระแสที่สูงกว่ารูปแบบอื่นเล็กน้อย เนื่องจากทั้ง 3 ช่องการไหล ใช้ MEA ชนิดเดียวกัน ในช่วงการใช้กระแสปานกลาง (ohmic loss) และช่วงกระแสสูง (Concentration loss) แผ่นช่องการไหลแบบ 3-Ch_w0.8 SFF ยังคงให้ประสิทธิภาพที่ดีที่สุด ทั้ง 2 ช่วงนี้มีความต้องการใช้กระแสไฟฟ้าเพิ่มขึ้น ทำให้น้ำที่เป็นผลิตภัณฑ์รองของปฏิกิริยาไฟฟ้าเคมีเกิดขึ้นมากตาม แผ่นช่องการไหลแบบ 3-Ch_w0.8 SFF ให้ประสิทธิภาพดีที่สุดเนื่องจากมีช่องการไหลเล็กที่สุด นอกจากนั้นจำนวนช่องการไหลที่เยอะขึ้นยังทำให้เกิดการกระจายตัวของก๊าซสารตั้งต้น และการกระจายตัวของกระแสไฟฟ้าเพิ่มขึ้น ทำให้ประสิทธิภาพสูงที่สุด แผ่นช่องการไหลแบบ 1-Ch 45°_w1.0 มีประสิทธิภาพต่ำกว่า 3-Ch_w0.8 SFF เล็กน้อย เนื่องจากช่องการไหลแบบ 1 ช่อง มีความยาวช่องการไหลยาวที่สุด ทำให้ความดันตกคร่อมสูงสุด ความเร็วการไหลของสารตั้งต้นสูงที่สุด จึงเกิดการระบายน้ำที่ดี ในขณะที่แผ่นช่องการไหลแบบ 3-Ch_w1.0 SFF มีขนาดช่องการไหลที่กว้างขึ้น และยังมีความยาวช่องการไหลสั้นที่สุด ทำให้ความดันตกคร่อมต่ำ ความเร็วก๊าซตั้งต้นต่ำ ส่งผลให้การระบายน้ำได้ไม่เต็มประสิทธิภาพ ซึ่งสังเกตุได้จากค่าการจำกัดกระแสไฟฟ้าที่ต่ำสุดเมื่อเทียบกับช่องการไหลอื่น

กิตกรรมประกาศ

ผู้เขียนขอขอบพระคุณห้องปฏิบัติการ ENERGY HARVESTING AND STORAGE LABORATORY ของมหาวิทยาลัยเชียงใหม่ ที่เอื้อเฟื้อสถานที่ในการใช้ทดสอบงานวิจัยในครั้งนี้

เอกสารอ้างอิง

[[1] Frano Barbir, “PEM Fuel cell: Theory and Practice,” Elsavier Academic Press, Burlington, USA., 2005.

[2] S. T. Bunyan, H. A. Dhahad, D. S. Khudhur, and T. Yusaf, “The Effect of Flow Field Design Parameters on the Performance of PEMFC: A Review,” *Sustainability*, vol. 15, no. 13, Art. no. 13, Jan. 2023, doi: 10.3390/su151310389.

[3] F. Işıklı, H. Işıklı, and A. Sürmen, “Effect of Number of Channels on Performance of PEM Fuel Cells for Serpentine Type Channel Configuration,” *Arab J Sci Eng*, vol. 50, no. 4, pp. 2595–2612, Feb. 2025, doi: 10.1007/s13369-024-09199-9.

[4] C. Tongsh *et al.*, “Experimental investigation of liquid water in flow field of proton exchange membrane fuel cell by combining X-ray with EIS technologies,” *Sci. China Technol. Sci.*, vol. 64, no. 10, pp. 2153–2165, Oct. 2021, doi: 10.1007/s11431-021-1815-6.

[5] S. R. Badduri, R. Siripuram, N. S. G, and S. R. S, “Effect of Width of a Serpentine Flow Channel on PEM Fuel Cell Performance,” Feb. 27, 2021, *Social Science Research Network, Rochester, NY*: 3822344. doi: 10.2139/ssrn.3822344.

[6] L. Zhang and Z. Shi, “Optimization of serpentine flow field in proton-exchange membrane fuel cell under the effects of external factors,” *Alexandria Engineering Journal*, vol. 60, no. 1, pp. 421–433, Feb. 2021, doi: 10.1016/j.aej.2020.09.007.

[7] Y. Wu *et al.*, "Effect of serpentine flow-field design on the water management of polymer electrolyte fuel cells: An in-operando neutron radiography study," *Journal of Power Sources*, vol. 399, pp. 254–263, Sep. 2018, doi: 10.1016/j.jpowsour.2018.07.085.

[8] K.-S. Choi, H.-M. Kim, and S.-M. Moon, "Numerical studies on the geometrical characterization of serpentine flow-field for efficient PEMFC," *International Journal of Hydrogen Energy*, vol. 36, no. 2, pp. 1613–1627, Jan. 2011, doi: 10.1016/j.ijhydene.2010.10.073.

[9] X.-D. Wang, W.-M. Yan, Y.-Y. Duan, F.-B. Weng, G.-B. Jung, and C.-Y. Lee, "Numerical study on channel size effect for proton exchange membrane fuel cell with serpentine flow field," *Energy Conversion and Management*, vol. 51, no. 5, pp. 959–968, May 2010, doi: 10.1016/j.enconman.2009.11.037.

[10] W.-M. Yan, H.-Y. Li, P.-C. Chiu, and X.-D. Wang, "Effects of serpentine flow field with outlet channel contraction on cell performance of proton exchange membrane fuel cells," *Journal of Power Sources*, vol. 178, no. 1, pp. 174–180, Mar. 2008, doi: 10.1016/j.jpowsour.2007.12.017.

[11] D. H. Jeon, S. Greenway, S. Shimpalee, and J. W. Van Zee, "The effect of serpentine flow-field designs on PEM fuel cell performance," *International Journal of Hydrogen Energy*, vol. 33, no. 3, pp. 1052–1066, Feb. 2008, doi: 10.1016/j.ijhydene.2007.11.015.

[12] X.-D. Wang, Y.-Y. Duan, W.-M. Yan, and X.-F. Peng, "Local transport phenomena and cell performance of PEM fuel cells with various serpentine flow field designs," *Journal of Power Sources*, vol. 175, no. 1, pp. 397–407, Jan. 2008, doi: 10.1016/j.jpowsour.2007.09.009.

[13] S. Shimpalee and J. W. Van Zee, "Numerical studies on rib & channel dimension of flow-field on PEMFC performance," *International Journal of Hydrogen Energy*, vol. 32, no. 7, pp. 842–856, May 2007, doi: 10.1016/j.ijhydene.2006.11.032.

[14] S. Shimpalee, S. Greenway, and J. W. Van Zee, "The impact of channel path length on PEMFC flow-field design," *Journal of Power Sources*, vol. 160, no. 1, pp. 398–406, Sep. 2006, doi: 10.1016/j.jpowsour.2006.01.099.

[15] Y.-G. Yoon, W.-Y. Lee, G.-G. Park, T.-H. Yang, and C.-S. Kim, "Effects of channel and rib widths of flow field plates on the performance of a PEMFC," *International Journal of Hydrogen Energy*, vol. 30, no. 12, pp. 1363–1366, Sep. 2005, doi: 10.1016/j.ijhydene.2005.04.008.

[16] K. Wuttikid, S. Shimpalee, J. W. Weidner, and K. Punyawudho, "Evaluation of Nafion with Various Pt–C Concentrations in Membrane Electrode Assemblies for PEMFCs," *Fuel Cells*, vol. 17, no. 5, Art. no. 5, Oct. 2017, doi: 10.1002/fuce.201600179.

[17] K.Wuttikid, N.Worayos, and K.Punyawudho, "Analysis of Catalyst Ink Compositions for Fabricating Membrane Electrode Assemblies in PEM Fuel Cells," *CMU Journal of Natural of Sciences*, vol. 2017, no. 16(4), Art. no. 16(4), 2017, doi: http://cmuj.cmu.ac.th/ns/full/172017100484317.pdf.

1] S. T. Bunyan, H. A. Dhahad, D. S. Khudhur, and T. Yusaf, "The Effect of Flow Field Design Parameters on the Performance of PEMFC: A Review," Sustainability, vol. 15, no. 13, Art. no. 13, Jan. 2023, doi: 10.3390/su151310389.

การพัฒนาแอปพลิเคชันบนมือถือแสดงเวลาละหมาดโดยใช้ระบบจีพีเอสสำหรับชาวไทยมุสลิม

Development of a GPS-based Prayer Times Mobile Application for Thai Muslims

Basil Salee
Faculty of Science & Technology
Phuket Rajabhat University
Phuket, Thailand
s6411423119@pkru.ac.th

Thanawat Saejia
Faculty of Science & Technology
Phuket Rajabhat University
Phuket, Thailand
s6411423116@pkru.ac.th

Nasith Laosen
Faculty of Science & Technology
Phuket Rajabhat University
Phuket, Thailand
nasith.l@pkru.ac.th

Abstract—*This paper presents the development of a mobile application providing accurate prayer times for Thai Muslims, particularly those who frequently travel across different provinces. The necessity arises because prayer times vary based on geographical coordinates and seasonal changes influenced by the sun's movement. The application's primary features include 1) precise prayer time display based on the user's current GPS location, 2) a calendar and personal note-taking system, and 3) articles and prayers related to Islamic practices. The application was developed using the Dart programming language and the Flutter framework, integrating prayer time data through the MuslimSalat API to ensure convenience, speed, and accuracy. The results of system testing indicate that the application functions correctly and effectively, meeting all specified requirements. Additionally, evaluations from actual user groups reflected high overall satisfaction, demonstrating the application's successful capability in effectively addressing user needs.*

Keywords—Muslim prayer times, mobile application, GPS-based services

I. บทนำ

ศาสนาอิสลามเป็นศาสนาหลักที่มีผู้นับถือจำนวนมากทั่วโลก และในประเทศไทยมีจำนวนประชากรที่นับถือศาสนาอิสลามประมาณร้อยละห้า หลักปฏิบัติที่สำคัญของชาวมุสลิมมีหลายอย่าง เช่น การบริโภคอาหารฮาลาล การถือศีลอด และการละหมาดวันละ 5 เวลา เป็นต้น การรู้เวลาละหมาดที่ถูกต้องเป็นสิ่งที่สำคัญมากในชีวิตประจำวันของมุสลิม เนื่องจากเกี่ยวข้องโดยตรงกับความถูกต้องในการปฏิบัติศาสนกิจ และยังส่งผลต่อกิจกรรมสำคัญทางศาสนา อื่น ๆ เช่น การละศีลอด (อิฟตาร์) และการเริ่มต้นถือศีลอด (ซูฮูร) ในเดือนรอมฎอน

เวลาละหมาดที่ถูกต้องแม่นยำจะขึ้นอยู่กับการเคลื่อนที่ของดวงอาทิตย์ ซึ่งแตกต่างกันไปตามปัจจัยทางภูมิศาสตร์ เช่น พิกัดทางภูมิศาสตร์และละติจูดของแต่ละพื้นที่ จึงทำให้เวลาละหมาดของแต่ละจังหวัดไม่เหมือนกัน การที่ต้องเดินทางไปยังจังหวัดต่าง ๆ อยู่บ่อยครั้ง ส่งผลให้ชาวมุสลิมจำนวนมากประสบปัญหาในการค้นหาเวลาละหมาดที่ถูกต้องของจังหวัดนั้น ๆ ถึงแม้จะมีเวลาละหมาดมาตรฐานจากสำนักจุฬาราชมนตรี แต่การค้นหาข้อมูลที่อาจเป็นข้อมูลเก่า ทำให้เกิดข้อผิดพลาดในการปฏิบัติศาสนกิจ ส่งผลกระทบต่อความถูกต้องและสมบูรณ์ในการปฏิบัติ เช่น การละหมาดผิดเวลา หรือการละศีลอดที่ไม่ถูกต้อง

จากปัญหาดังกล่าว ผู้วิจัยจึงได้ออกแบบและพัฒนาแอปพลิเคชันบอกเวลาละหมาดแบบเรียลไทม์ ที่สามารถคำนวณและแสดงผลเวลาละหมาดได้ตามตำแหน่งปัจจุบันของผู้ใช้งาน โดยใช้ข้อมูลพิกัดตำแหน่ง (GPS) ร่วมกับบริการ Application Programming Interface (API) จากเว็บไซต์ Muslim-Salat [1] เพื่ออำนวยความสะดวกและเพิ่มความถูกต้องในการปฏิบัติศาสนกิจให้แก่ชาวมุสลิม โดยเฉพาะผู้ที่มีความจำเป็นต้องเดินทางเป็นประจำ แอปพลิเคชันนี้ถูกพัฒนาด้วยสถาปัตยกรรมแบบบริการขนาดเล็ก (Microservices) โดยใช้ภาษา Dart และ Flutter Framework เพื่อให้มีประสิทธิภาพสูงในการใช้งานและการดูแลระบบ

II. ทบทวนวรรณกรรม

ปัจจุบันมีงานวิจัยหลายงานที่เป็นลักษณะการพัฒนาแอปพลิเคชันที่มีสถาปัตยกรรมแบบบริการขนาดเล็ก (Microservices) ซึ่งแลกเปลี่ยนข้อมูลผ่าน API และใช้ภาษา Dart และ Flutter Framework ในการพัฒนา ตัวอย่างเช่น ชนินทร์ เซ็นนันท์ และคณะ [2] ได้ทำการพัฒนาแอปพลิเคชันแจ้งเตือนกิจกรรมสำหรับมหาวิทยาลัยราชภัฏภูเก็ต เพื่อให้นักศึกษาและบุคลากรไม่พลาดการเข้าร่วมกิจกรรมของมหาวิทยาลัยซึ่งเป็นส่วนหนึ่งของการประเมินการปฏิบัติราชการ และใช้แทนงานเดิมที่เป็นเว็บไซต์ซึ่งไม่สะดวกในการใช้งาน โดยมีการพัฒนา API ในการแลกเปลี่ยนข้อมูลระหว่างแอปพลิเคชันและฐานข้อมูล รวมทั้งใช้ภาษา Dart และ Flutter Framework ในการพัฒนา

นายภัทรพล คิ้วอำไพ และคณะ [3] ได้พัฒนาแอปพลิเคชัน ณ สยาม เพื่อช่วยนักศึกษาใหม่ของมหาวิทยาลัยสยามให้เข้าถึงข้อมูลสำคัญได้สะดวกยิ่งขึ้น เนื่องจากนักศึกษาใหม่มักไม่ทราบประวัติของมหาวิทยาลัย รวมถึงตำแหน่งของอาคารสำคัญ เช่น โรงอาหาร หอประชุม และโรงยิมแอปพลิเคชันนี้แบ่งการทำงานเป็น 2 ส่วนหลัก คือ 1) ผู้ใช้งานสามารถสมัครสมาชิก ดูข้อมูลมหาวิทยาลัย และใช้ระบบนำทางไปยังอาคารต่าง ๆ และ 2) ผู้ดูแลระบบสามารถเพิ่ม แก้ไข หรือลบข้อมูลในแอปพลิเคชัน ระบบพัฒนาด้วย Flutter และภาษา Dart พร้อมระบบการจัดการฐานข้อมูลแบบ NoSQL ผ่าน Firebase แอปพลิเคชันนี้ช่วยให้การเข้าถึงข้อมูลและการสำรวจมหาวิทยาลัยเป็นเรื่องง่ายขึ้นสำหรับนักศึกษาใหม่

เวหา เกาะประเสริฐ และ สุวรรณี อัศวกุลชัย [4] ได้พัฒนา แอปพลิเคชันสำหรับการเลือกมัคคุเทศก์ โดยอ้างอิงหลักการพัฒนาซอฟต์แวร์แบบวงจรชีวิต 6 ขั้นตอน เพื่อตอบโจทย์ปัญหาของนักท่องเที่ยวที่ไม่สามารถเลือกมัคคุเทศก์ตามความต้องการได้ แอปพลิเคชันนี้ช่วยให้นักท่องเที่ยวสามารถค้นหาและเลือกมัคคุเทศก์ที่ถูกกฎหมายและตรงกับความต้องการของตนเอง โดยใช้ Flutter Framework และภาษา Dart ในการพัฒนา ระบบประกอบด้วย

การลงทะเบียนและยืนยันตัวตนเพื่อคัดกรองมัคคุเทศก์ และ ระบบแนะนำมัคคุเทศก์แบบ Collaboration Filtering ที่อิงจาก 3 ข้อมูลหลัก ได้แก่ ข้อมูลนักท่องเที่ยว คะแนนความพึงพอใจต่อมัคคุเทศก์ และข้อมูลมัคคุเทศก์ แอปพลิเคชันนี้ช่วยเพิ่มความสะดวกและความมั่นใจให้กับนักท่องเที่ยวในการเลือกมัคคุเทศก์ที่ตรงใจ

III. ระเบียบวิธีวิจัย

ผู้วิจัยได้นำหลักวิศวกรรมซอฟต์แวร์มาใช้ในการดำเนินการวิจัยเพื่อให้ได้ระบบที่มีประสิทธิภาพและตรงกับความต้องการของผู้ใช้ หลักการดังกล่าวประกอบด้วย 4 ขั้นตอนหลัก ได้แก่ การวิเคราะห์ความต้องการ การออกแบบระบบ พัฒนาระบบ และการทดสอบระบบ ซึ่งมีรายละเอียดดังนี้

A. *การวิเคราะห์ความต้องการ*

ขั้นตอนนี้เป็นการศึกษาความต้องการของผู้ใช้ โดยผู้วิจัยได้เก็บข้อมูลจากกลุ่มผู้ใช้เป้าหมายด้วยแบบสอบถามและนำมาสรุปเป็นฟีเจอร์ของระบบ เพื่อให้ได้ซอฟต์แวร์ที่ตอบโจทย์การใช้งานได้อย่างมีประสิทธิภาพ [5] กลุ่มเป้าหมายที่ใช้ในการสำรวจครั้งนี้คือชาวไทยมุสลิมที่มีความจำเป็นต้องเดินทางบ่อยครั้งภายในจังหวัดระนอง พังงา และภูเก็ต โดยทำการสุ่มกลุ่มตัวอย่างจำนวน 20 คน ผู้วิจัยได้สอบถามความคิดเห็นเกี่ยวกับปัจจัยสำคัญในการใช้งานแอปพลิเคชัน รวมถึงความต้องการของผู้ใช้ และได้สรุปความต้องการหลักของระบบ คือ 1) ความแม่นยำของเวลาละหมาด เพื่อให้ผู้ใช้สามารถปฏิบัติศาสนกิจได้ถูกต้อง 2) ปฏิทินและระบบจดบันทึก เพื่อช่วยให้ผู้ใช้บันทึกข้อมูลสำคัญระหว่างเดินทาง และ 3) บทความและบทสวดเกี่ยวกับการละหมาด เพื่อให้ความรู้และแนวทางปฏิบัติที่ถูกต้อง

B. *การออกแบบระบบ*

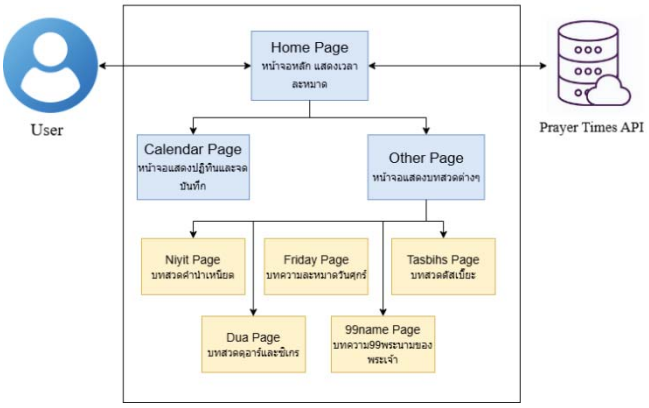
เมื่อได้ความต้องการจากผู้ใช้มาแล้ว ผู้วิจัยจึงทำการออกแบบแอปพลิเคชันให้ตรงกับความต้องการ โดยเริ่มจากการออกแบบสถาปัตยกรรมของระบบ ซึ่งแสดงได้ดังภาพที่ 1 จากภาพจะเห็นว่าแอปพลิเคชันนี้ประกอบด้วย 3 หน้าจอ (เมนู) หลัก ได้แก่

- *หน้าโฮม*: เป็นหน้าแรกเมื่อผู้ใช้เข้าสู่แอปพลิเคชัน โดยจะแสดงเวลาละหมาดของจังหวัดที่ผู้ใช้พำนักอยู่
- *หน้าปฏิทิน*: แสดงปฏิทินสากลพร้อมทั้งฟีเจอร์สำหรับบันทึกข้อมูลหรือบันทึกกิจกรรมลงในปฏิทิน
- *หน้าบทสวด*: แสดงบทสวดสำคัญที่ผู้ใช้สามารถกดเข้าไปอ่านได้ โดยในเวอร์ชันปัจจุบันจะมีทั้งหมด 5 หน้า ได้แก่ 1) บทนำและเจตนา (เหนียต) ในการละหมาด 2) ซิเกรและดุอาหลังละหมาด 3) ข้อปฏิบัติเกี่ยวกับละหมาดวันศุกร์ 4) เก้าสิบเก้าพระนามของอัลลอฮ์ และ 5) การนับตัสเบี๊ยะ (การสรรเสริญพระเจ้า)

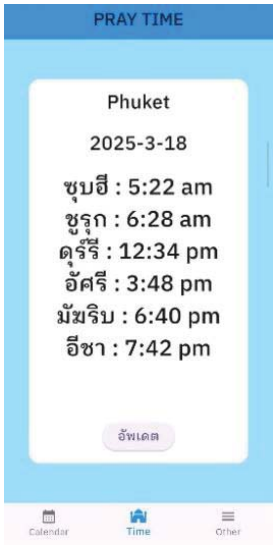
สำหรับเวลาละหมาดที่แตกต่างกันในแต่ละพื้นที่ แอปพลิเคชันจะใช้ข้อมูลจากเว็บไซต์ MuslimSalat [1] โดยจะส่งตำแหน่ง GPS ของโทรศัพท์และส่งไปให้เว็บไซต์ดังกล่าวผ่าน API เพื่อคำนวณเวลาละหมาด จากนั้นจึงนำข้อมูลที่ตอบกลับมาในรูปแบบ JSON มาแสดงผลในแอปพลิเคชัน

C. *การพัฒนาระบบ*

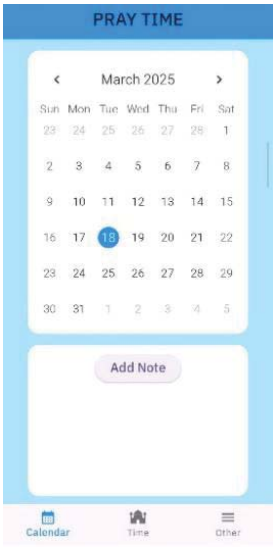
ผู้วิจัยได้ใช้ภาษา Dart และ Flutter Framework เป็นภาษาโปรแกรมมิ่ง ใช้ซอฟต์แวร์ Visual Studio Code เป็นโปรแกรมสำหรับการแก้ไขและพัฒนาซอร์สโค้ด และใช้ Emulator จาก Android Studio เป็นตัวจำลองอุปกรณ์ที่ใช้ในการทดสอบแอปพลิเคชันในสภาพแวดล้อมที่คล้ายคลึงกับอุปกรณ์จริง เพื่อให้สามารถปรับแต่งและตรวจสอบการทำงานของแอปพลิเคชันได้ก่อนนำไปใช้งานจริง ตัวอย่างหน้าจอต่าง ๆ ในแอปพลิเคชันแสดงได้ดังภาพที่ 2 ถึงภาพที่ 5



ภาพที่ 1 สถาปัตยกรรมภาพรวมของระบบ



ภาพที่ 2 หน้าจอแสดงเวลาละหมาด



ภาพที่ 3 หน้าจอแสดงปฏิทิน



ภาพที่ 4 หน้าจอแสดงบทสวดต่าง ๆ



ภาพที่ 5 หน้าจอแสดงตัวอย่างบทสวด

D. การทดสอบระบบ

ในขั้นตอนการทดสอบระบบ ผู้วิจัยได้สร้างแอนดรอยด์แอปพลิเคชันแพ็คเกจ (APK) สำหรับติดตั้งในโทรศัพท์มือถือ เพื่อทดสอบแอปพลิเคชันว่าสามารถทำงานได้ตามที่ออกแบบไว้และตอบสนองความต้องการของผู้ใช้หรือไม่ โดยจะทำการทดสอบสองแบบ คือ การทดสอบภายใน (In-house Testing) และการทดสอบภาคสนาม (Field Testing) การทดสอบแบบแรกจะเน้นไปที่การทดสอบฟังก์ชันการทำงานต่าง ๆ ของระบบ ในขณะที่การทดสอบแบบที่สองจะให้ผู้ใช้ทดลองใช้ระบบในสภาพแวดล้อมจริง รายละเอียดผลการทดสอบจะอธิบายในหัวข้อถัดไป

IV. ผลการวิจัย

A. ผลการทดสอบภายใน

การทดสอบภายในจะเป็นการทดสอบฟังก์ชันต่าง ๆ ของระบบ ได้แก่ การแสดงเวลาละหมาด การแสดงปฏิทิน การบันทึกข้อมูล และการแสดงบทความและบทสวด จากการทดสอบพบว่าแอปพลิเคชันสามารถแสดงข้อมูลต่าง ๆ ได้อย่างครบถ้วนและทำงานได้ตามที่ออกแบบไว้ทุกฟังก์ชัน นอกจากนั้นผู้วิจัยได้ทดสอบฟังก์ชันแสดงเวลาละหมาด (ซึ่งเป็นฟังก์ชันหลักของระบบ) อย่างละเอียด โดยทดสอบ 3 ประเด็น โดยมีผลการทดสอบดังนี้

- *ความถูกต้องของเวลาละหมาด*: ผู้วิจัยเปรียบเทียบเวลาละหมาดที่ได้รับจาก API กับเวลาละหมาดมาตรฐานจากสำนักจุฬาราชมนตรี พบว่าแอปพลิเคชันสามารถดึงเวลาละหมาดได้อย่างแม่นยำในพื้นที่ส่วนใหญ่ อย่างไรก็ตาม API ที่ใช้อาจให้ค่าคลาดเคลื่อนเล็กน้อยในบางจังหวัด (+/- 1 ถึง 2 นาที) เนื่องจากระบบคำนวณมุมดวงอาทิตย์แตกต่างกัน
- *ความเร็วในการดึงข้อมูล*: จากการทดสอบพบว่าแอปพลิเคชันสามารถดึงข้อมูลเวลาละหมาดผ่าน API ได้อย่างรวดเร็วภายใน 1-3 วินาที ในเครือข่ายอินเทอร์เน็ตที่เสถียร อย่างไรก็ตาม ในบางกรณีเมื่ออินเทอร์เน็ตช้า หรือ API มีปัญหา (เช่น เซิร์ฟเวอร์ของ API ล่ม) อาจใช้เวลานานขึ้นหรือไม่สามารถโหลดข้อมูลได้
- *ความแม่นยำของตำแหน่ง GPS*: จากการทดสอบระบุตำแหน่ง GPS พบว่าแอปพลิเคชันสามารถกำหนดจังหวัดของผู้ใช้ได้แม่นยำใน 90%-95% ของการใช้งาน อย่างไรก็ตาม หากผู้ใช้อยู่ในพื้นที่สัญญาณ GPS อ่อน (เช่น ในอาคารสูงหรือพื้นที่ชนบท) แอปพลิเคชันอาจดึงตำแหน่งคลาดเคลื่อนและทำให้แสดงเวลาละหมาดผิดพลาด

B. ผลการทดสอบภาคสนาม

ในการทดสอบภาคสนามจะให้ผู้ใช้ทดลองใช้งานแอปพลิเคชันและตอบแบบสอบถามเพื่อประเมินผลการใช้งาน ผู้วิจัยได้แบ่งการประเมินเป็นสองด้าน คือ ด้านการออกแบบและด้านการใช้งาน และใช้ค่าสถิติสองค่าในการประเมินผล คือ ค่าเฉลี่ยเลขคณิตและส่วนเบี่ยงเบนมาตรฐาน (S.D.) [6] โดยกำหนดเกณฑ์ดังนี้

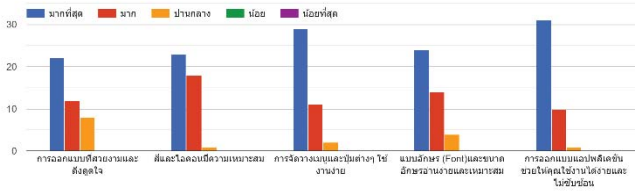
- ระดับความพึงพอใจมากที่สุด มีค่าเท่ากับ 5 คะแนน
- ระดับความพึงพอใจมาก มีค่าเท่ากับ 4 คะแนน
- ระดับความพึงพอใจปานกลาง มีค่าเท่ากับ 3 คะแนน
- ระดับความพึงพอใจน้อย มีค่าเท่ากับ 2 คะแนน
- ระดับความพึงพอใจน้อยที่สุด มีค่าเท่ากับ 1 คะแนน

จากนั้นจึงนำคะแนนไปหาค่าเฉลี่ย โดยใช้เกณฑ์ในการแปลความหมายค่าเฉลี่ย ดังนี้

- ค่าเฉลี่ย 4.51 – 5.00 หมายถึง มีความพึงพอใจในระดับมากที่สุด
- ค่าเฉลี่ย 3.51 – 4.50 หมายถึง มีความพึงพอใจในระดับมาก
- ค่าเฉลี่ย 2.51 – 3.50 หมายถึง มีความพึงพอใจในระดับปานกลาง
- ค่าเฉลี่ย 1.51 – 2.50 หมายถึง มีความพึงพอใจในระดับน้อย
- ค่าเฉลี่ย 1.00 – 1.50 หมายถึง มีความพึงพอใจในระดับน้อยที่สุด

ตารางที่ 1 ผลการประเมินด้านการออกแบบ

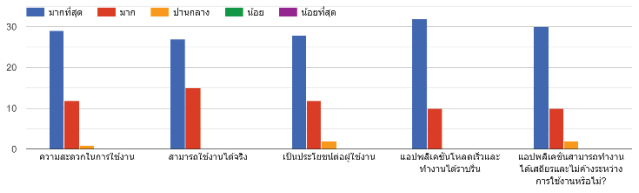
รายการประเมิน	ค่าเฉลี่ย	S.D.	แปลผล
การออกแบบที่สวยงามและดึงดูดใจ	4.35	0.80	มาก
สีและไอคอนมีความเหมาะสม	4.55	0.55	มากที่สุด
การจัดวางเมนูและปุ่มต่างๆ ใช้งานง่าย	4.65	0.57	มากที่สุด
แบบอักษร (Font)และขนาดอักษรอ่านง่ายและเหมาะสม	4.53	0.64	มากที่สุด
การออกแบบแอปพลิเคชันช่วยให้คุณใช้งานได้ง่ายและไม่ซับซ้อน	4.73	0.50	มากที่สุด
ค่าเฉลี่ยรวม	4.56	0.61	มากที่สุด



ภาพที่ 6 แผนภูมิผลประเมินด้านการออกแบบ

ตารางที่ 2 ผลการประเมินด้านการใช้งาน

รายการประเมิน	ค่าเฉลี่ย	S.D.	แปลผล
ความสะดวกในการใช้งาน	4.70	0.46	มากที่สุด
สามารถใช้งานได้จริง	4.65	0.48	มากที่สุด
เป็นประโยชน์ต่อผู้ใช้งาน	4.60	0.59	มากที่สุด
แอปพลิเคชันโหลดเร็วและทำงานได้ราบรื่น	4.78	0.42	มากที่สุด
แอปพลิเคชันสามารถทำงานได้เสถียรและไม่ค้างระหว่างการใช้งาน	4.68	0.57	มากที่สุด
ค่าเฉลี่ยรวม	4.68	0.50	มากที่สุด



ภาพที่ 7 แผนภูมิผลประเมินด้านการใช้งาน

ผู้วิจัยเก็บข้อมูลจากผู้ใช้จำนวน 40 คน ผลการประเมินด้านการออกแบบแสดงได้ดังตารางที่ 1 และภาพที่ 6 และผลการประเมินด้านการใช้งานแสดงได้ดังตารางที่ 2 และภาพที่ 7 จากผลการประเมินพบว่า ด้านการออกแบบมีค่าเฉลี่ยความพึงพอใจรวม 4.56 และมีส่วนเบี่ยงเบนมาตรฐานเท่ากับ 0.61

ในขณะที่ด้านการใช้งาน ได้ค่าเฉลี่ยรวม 4.68 และมีส่วนเบี่ยงเบนมาตรฐานเท่ากับ 0.50 ซึ่งสะท้อนถึงความพึงพอใจของผู้ใช้ที่สูงในทั้งสองด้าน

V. อภิปรายผล

จากผลการทดสอบระบบพบว่าแอปพลิเคชันสามารถทำงานได้ถูกต้องครบทุกฟังก์ชัน โดยสามารถระบุตำแหน่งของผู้ใช้ได้อย่างแม่นยำ แสดงเวลาละหมาดตามจังหวัดที่ผู้ใช้กำลังเดินทางอยู่แบบเรียลไทม์ และแสดงบทสวดได้อย่างครบถ้วน และจากผลการทดสอบกับผู้ใช้พบว่าแอปพลิเคชันสามารถใช้งานได้อย่างมีประสิทธิภาพ โดยได้รับคะแนนเฉลี่ยด้านการออกแบบและด้านการใช้งานในระดับดีมาก ซึ่งสะท้อนให้เห็นว่าแอปพลิเคชันมีศักยภาพสูงในการช่วยเหลือชาวมุสลิมในการปฏิบัติศาสนกิจได้อย่างสะดวกและแม่นยำ อย่างไรก็ตาม ยังมีบางส่วนที่สามารถพัฒนาเพิ่มเติมเพื่อเพิ่มประสิทธิภาพในการใช้งานให้ดียิ่งขึ้น เช่น การพัฒนาโหมดออฟไลน์ (Offline Mode) เพื่อให้สามารถแสดงเวลาละหมาดได้แม้ในกรณีที่ไม่มีอินเทอร์เน็ต หรือการเพิ่มฟังก์ชันบอกทิศกิบลัตที่อยู่ในทิศตะวันตกของประเทศไทย (ในประเทศซาอุดิอาราเบีย) เพื่อช่วยให้ผู้ใช้สามารถทราบทิศทางที่ถูกต้องในการละหมาดไม่ว่าจะอยู่ที่ใดก็ตาม

VI. ข้อสรุป

บทความนี้ได้นำเสนอการออกแบบและพัฒนาแอปพลิเคชันแสดงเวลาละหมาดบนโทรศัพท์มือถือสำหรับชาวไทยมุสลิม โดยเฉพาะกลุ่มผู้ที่ต้องเดินทางไปต่างจังหวัดเป็นประจำ ซึ่งต้องการทราบเวลาละหมาดที่แม่นยำของจังหวัดที่อยู่ขณะนั้น เนื่องจากเวลาละหมาดมีความแตกต่างกันไปตามพิกัดภูมิศาสตร์และฤดูกาลที่มีผลจากการเคลื่อนที่ของดวงอาทิตย์ ฟีเจอร์หลักของแอปพลิเคชันได้แก่ 1) การแสดงผลเวลาละหมาดที่แม่นยำตามตำแหน่ง GPS ของผู้ใช้ 2) ปฏิทินและระบบบันทึกข้อมูลส่วนตัว และ 3) บทความและบทสวดเกี่ยวกับการละหมาด แอปพลิเคชันดังกล่าวได้รับการพัฒนาโดยใช้ภาษา Dart และ Flutter Framework พร้อมเชื่อมโยงข้อมูลผ่านระบบ API เพื่อให้สามารถใช้งานได้อย่างสะดวก รวดเร็ว และแม่นยำ จากผลการทดสอบพบว่าแอปพลิเคชันสามารถทำงานได้อย่างถูกต้องและมีประสิทธิภาพ ครอบคลุมครบทุกฟังก์ชันตามที่ได้กำหนดไว้ อีกทั้งผลการประเมินจากกลุ่มตัวอย่างผู้ใช้งานจริงแสดงให้เห็นถึงระดับความพึงพอใจโดยรวมที่สูงมาก สะท้อนให้เห็นถึงความสำเร็จในการตอบสนองความต้องการของผู้ใช้งานได้เป็นอย่างดี

อ้างอิง

[1] MuslimSalat. “Prayer Times API for around the world.” [Online]. Available: https://muslimsalat.com/api/. [Accessed: Feb. 1, 2025].

[2] ชนินทร์ เซ็นนันท์, ธนพัฒน์ จิตต์ชะนะ และ ณสิทธิ์ เหล่าเส็น, “การพัฒนาแอปพลิเคชันแจ้งเตือนกิจกรรมสำหรับมหาวิทยาลัยราชภัฏภูเก็ต,” ใน *การประชุมวิชาการระดับชาติด้านวิทยาศาสตร์และเทคโนโลยี เครือข่ายสถาบันอุดมศึกษาภาคใต้ ครั้งที่ 9*, 2567, หน้า 206-214.

[3] ภัทรพล คิ้วอำไพ และ คุณากร กล้าอาษา, “แอปพลิเคชัน ณ สยาม (กรณีศึกษามหาวิทยาลัยสยาม),” โครงงานปริญญาตรี, คณะวิทยาศาสตร์, มหาวิทยาลัยสยาม, กรุงเทพฯ, ประเทศไทย, 2564.

[4] เวหา เกาะประเสริฐ และ สุวรรณี อัศวกุลชัย, “การพัฒนาโมบายแอปพลิเคชันสำหรับการเลือกมัคคุเทศก์,” *วารสารร่มยูงทอง*, ปีที่2, ฉบับที่ 3, หน้า 16-36, ธันวาคม 2567.

[5] I. Sommerville, *Engineering Software Products: An Introduction to Modern Software Engineering*. Hoboken, NJ, USA: Pearson Education, 2021.

[6] ชูศรี วงศ์รัตนะ, *เทคนิคการใช้สถิติเพื่อการวิจัย*, พิมพ์ครั้งที่ 14. กรุงเทพฯ, ประเทศไทย: ศูนย์หนังสือจุฬาลงกรณ์มหาวิทยาลัย, 2562.

การพัฒนาสื่อมัลติมีเดียสำหรับการเรียนรู้แบบออนไลน์ เรื่องการตัดเย็บผ้า

Development of multimedia for online learning on sewing

1st รัฐศาสตร์ เรืองศรี (Ratthasat Roungsea)
สาขาเทคโนโลยีดิจิทัล (Digital Technology Branch)
คณะวิทยาศาสตร์และเทคโนโลยี
(Faculty of Science and Technology)
ภูเก็ต,ประเทศไทย (Phuket,Thailand)
S6411423218@pkru.ac.th

2nd ธนาวุติ ชุมพล (Tanawut Chumphol)
สาขาเทคโนโลยีดิจิทัล (Digital Technology Branch)
คณะวิทยาศาสตร์และเทคโนโลยี
(Faculty of Science and Technology)
ภูเก็ต,ประเทศไทย (Phuket,Thailand)
S6411423208@pkru.ac.th

3rd อุไรรัตน์ มากจันทร์ (Urairat Makchan)
สาขาเทคโนโลยีดิจิทัล (Digital Technology Branch)
คณะวิทยาศาสตร์และเทคโนโลยี
(Faculty of Science and Technology)
ภูเก็ต,ประเทศไทย (Phuket,Thailand)
urairat.m@pkru.ac.th

Abstract*—*This research aims to develop online multimedia learning materials on sewing and examine the satisfaction of individuals interested in such materials. The study involved a sample group of 40 individuals with an interest in sewing. The research tools consisted of online multimedia learning materials on sewing and a satisfaction assessment questionnaire. The collected data were analyzed using the mean and standard deviation. The findings revealed that the online multimedia learning materials received an average satisfaction score of 4.78, which is considered very high, with a standard deviation of 0.44.

Keywords—Multimedia, AR Technology, sewing

I. บทนำ

การตัดเย็บเสื้อผ้าเป็นกระบวนการที่ต้องอาศัยความเข้าใจทั้งด้านทฤษฎีและปฏิบัติ ซึ่งมีความซับซ้อนในเรื่องของเทคนิค วิธีการ และการใช้เครื่องมือต่าง ๆ การมีความรู้ในการตัดเย็บผ้าเป็นส่วนที่เพิ่มทักษะทางด้านอาชีพ สร้างรายได้ ประหยัดค่าใช้จ่าย หรือแม้กระทั่งเป็นการอนุรักษ์และสืบสานวัฒนธรรม เนื่องจากการตัดเย็บเป็นส่วนสำคัญทางด้านวัฒนธรรมการแต่งกายของแต่ละท้องถิ่น เช่น การตัดเย็บผ้าไทย ผ้าพื้นเมือง ซึ่งช่วยอนุรักษ์ภูมิปัญญาท้องถิ่นได้ นอกจากนั้นการเรียนรู้ในงานตัดเย็บผ้าเพื่อเพิ่มทักษะจะต้องเสียค่าใช้จ่ายในราคาที่สูง และในปัจจุบันการเรียนรู้ก็ไม่ได้จำกัดเฉพาะในห้องเรียนทุกคนเรียนรู้ได้ทุกที่ ทุกเวลา จากเทคโนโลยีที่ทันสมัย สามารถสืบค้นได้บนเครือข่ายอินเทอร์เน็ต การพัฒนาสื่อมัลติมีเดียสำหรับการเรียนรู้เรื่องการตัดเย็บผ้าจึงเป็นสิ่งที่สำคัญ ช่วยให้ผู้เรียนเข้าใจเนื้อหาได้ง่ายขึ้น ลดความซับซ้อนในการเรียนรู้ สามารถศึกษาได้ด้วยตนเอง ไม่ต้องพึ่งพาผู้สอน ทำให้มีความยืดหยุ่นในการเรียนและสามารถฝึกฝนซ้ำได้ตามต้องการ ผู้วิจัยจึงมีความสนใจพัฒนาสื่อมัลติมีเดียสำหรับการเรียนรู้เรื่องการตัดเย็บผ้า โดยมีหลายรูปแบบสื่อที่หลากหลายตามลักษณะของเนื้อหา ได้แก่ สื่อวิดีโอ สื่อสามมิติ โมเดลในรูปแบบ AR ที่สามารถมองเครื่องมือได้ในรูปแบบ 360 องศาที่ช่วยผู้ให้ผู้เรียนได้ฝึกฝนเสมือนจริงก่อนลงมือปฏิบัติจริง การพัฒนาสื่อมัลติมีเดียสำหรับการเรียนรู้แบบออนไลน์เรื่องการตัดเย็บผ้า มีวัตถุประสงค์เพื่อ 1) เพื่อพัฒนาสื่อมัลติมีเดียสำหรับการเรียนรู้แบบออนไลน์เรื่องการตัดเย็บผ้า 2) เพื่อศึกษาความพึงพอใจของผู้สนใจสื่อมัลติมีเดียสำหรับการเรียนรู้แบบออนไลน์เรื่องการตัดเย็บผ้าและมีกรอบในแนวคิดในการวิจัยดังภาพที่ 1

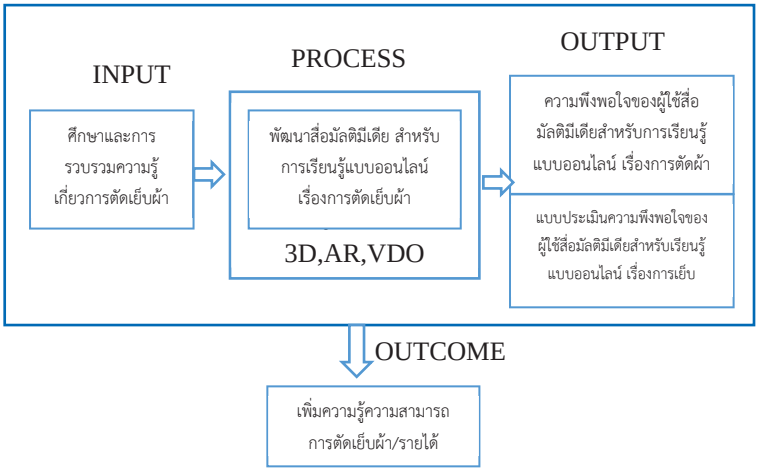


Fig. 1. กรอบแนวคิดในการวิจัยการพัฒนามัลติมีเดียการเรียนรู้แบบออนไลน์ เรื่องการตัดเย็บผ้า

II. ทบทวนวรรณกรรม

[1] วุฒิไกร พิมพขันธ์,ภัสสร ปัทวงค์ และอภิรดี เดชพงษ์สัมฤทธิ์ (2564) ได้ทำวิจัยเรื่องการออกแบบและพัฒนาสื่อแอนิเมชัน 3 มิติ โดยใช้เทคนิคการนำเสนอแบบเล่านิทานเพื่อการรณรงค์อนุรักษ์ช้างไทย มีวัตถุประสงค์ของการวิจัย 1) เพื่อออกแบบและพัฒนาสื่อแอนิเมชัน 3 มิติ โดยใช้เทคนิคการนำเสนอแบบเล่านิทานเพื่อการรณรงค์อนุรักษ์ช้างไทย 2) เพื่อประเมินประสิทธิภาพสื่อแอนิเมชัน 3 มิติ โดยใช้เทคนิคการนำเสนอแบบเล่านิทานเพื่อการรณรงค์อนุรักษ์ช้างไทย 3) เพื่อศึกษาความพึงพอใจสื่อแอนิเมชัน 3 มิติโดยใช้เทคนิคการนำเสนอแบบเล่านิทานเพื่อการรณรงค์อนุรักษ์ช้างไทย กลุ่มตัวอย่างที่ใช้ในการวิจัยโดยใช้วิธีคัดเลือกกลุ่มตัวอย่างแบ่งออกเป็น 2 กลุ่ม คือ กลุ่มที่ 1 ผู้เชี่ยวชาญด้านเนื้อหาและการออกแบบสื่อมัลติมีเดียโดยวิธีเจาะจงจำนวน 6 คน และกลุ่มที่ 2 คือนักศึกษาคณะวิทยาศาสตร์ และเทคโนโลยีมหาวิทยาลัยเซาธ์อีสท์บางกอก จำนวน 150 คน เครื่องมือที่ใช้ในการดำเนินงานวิจัย ได้แก่ 1) โปรแกรม Autodesk Maya2020 โปรแกรม Unreal Engine และโปรแกรม Adobe Premiere Pro 2002 2) แบบประเมินความพึงพอใจของผู้รับชมสื่อ สถิติที่ใช้ในการวิเคราะห์ข้อมูลประกอบด้วย ค่าเฉลี่ยและส่วนเบี่ยงเบนมาตรฐาน ผลการวิจัยพบว่าผลการประเมินความพึงพอใจของกลุ่มตัวอย่างกลุ่มที่ 1 ผู้เชี่ยวชาญอยู่ในระดับมากที่สุด ค่าเฉลี่ยโดยรวม อยู่ที่ 4.43 ส่วนเบี่ยงเบนมาตรฐานเท่ากับ 0.58 และกลุ่มที่ 2 ผู้รับชมสื่ออยู่ในระดับมากที่สุด ค่าเฉลี่ยโดยรวมอยู่ที่ 4.29 ส่วนเบี่ยงเบนมาตรฐานเท่ากับ 0.75

[2] มโนรส บริรักษ์อราวินท์, จีรวัฒน์ นาคสุวรรณ์, ชวัลรัตน์ ศรีนวลปาน (2562) ได้ทำวิจัยเรื่อง แอนิเมชัน 3D เสมือนกรณีศึกษาศูนย์วัฒนธรรมมหาวิทยาลัยราชภัฏนครศรีธรรมราช เป็นการประยุกต์ใช้โปรแกรม Autodesk 3Ds Max 2016 โดยมีวัตถุประสงค์เพื่อ 1) พัฒนาสื่อคอมพิวเตอร์มัลติมีเดีย เรื่องแอนิเมชัน 3D เสมือน กรณีศึกษา ศูนย์วัฒนธรรมมหาวิทยาลัยราชภัฏนครศรีธรรมราชในการนำเสนอข้อมูลประวัติความเป็นมาและความสำคัญของวัตถุโบราณภายในศูนย์วัฒนธรรมมหาวิทยาลัยราชภัฏนครศรีธรรมราชผ่านการจำลองการเที่ยวชมศูนย์วัฒนธรรมมหาวิทยาลัยราชภัฏนครศรีธรรมราชในรูปแบบสาม มิติ เสมือนจริง 2) ประเมินความเข้าใจในประวัติความเป็นมาและความสำคัญของวัตถุโบราณจากสื่อที่พัฒนา 3) ประเมินความพึงพอใจในรูปแบบของสื่อที่พัฒนากลุ่มตัวอย่างในการวิจัย คือ นักศึกษาสาขาวิชาวิทยาการคอมพิวเตอร์และสาขาวิชาเทคโนโลยีสารสนเทศมหาวิทยาลัยราชภัฏนครศรีธรรมราช จำนวน 60 คน เครื่องมือที่ใช้ในการวิจัยประกอบด้วย 1) สื่อแอนิเมชัน 3D เสมือน กรณีศึกษาศูนย์วัฒนธรรมมหาวิทยาลัยราชภัฏนครศรีธรรมราช 2) แบบทดสอบความรู้ และ 3) แบบสอบถามความพึงพอใจ ผลการวิจัย พบว่า สื่อแอนิเมชัน 3D เสมือนที่พัฒนาขึ้นสามารถทำให้ผู้ชมเข้าใจในประวัติความเป็นมาและความสำคัญของวัตถุโบราณ โดยค่าคะแนนทดสอบความรู้หลังชมสื่อสูงกว่าคะแนนก่อนชมสื่ออย่างมีนัยสำคัญทางสถิติที่ระดับ 01 และผู้ชมมีความพึงพอใจต่อสื่อที่พัฒนาขึ้นอยู่ในระดับมาก มีค่าเฉลี่ย 4.17 และส่วนเบี่ยงเบนมาตรฐาน 0.735

[3] ธนพงษ์ ไชยลาโภ, เอกลักษณ์ โภคทรัพย์ไพบูลย์ และ ปริญญ์ โสภา (2559)การวิจัยนี้มีวัตถุประสงค์เพื่อ พัฒนาสื่อบทเรียนออนไลน์เรื่อง : การออกแบบเพื่อการผลิตสื่อปฏิสัมพันธ์และมัลติมีเดียที่มีประสิทธิภาพ โดยใช้เครื่องมือสื่อบทเรียนมัลติมีเดีย (Multimedia Online Learning) เรื่องการออกแบบเพื่อการผลิตสื่อปฏิสัมพันธ์และมัลติมีเดีย ซึ่งประกอบด้วย 15 บทเรียน เพื่อค้นหาประสิทธิภาพและผลสัมฤทธิ์ทางการเรียนรู้ของผู้เรียนผ่านสื่อบทเรียนออนไลน์ด้วยแบบทดสอบ รวมทั้งวิเคราะห์ความพึงพอใจของผู้เรียนจากการเรียนด้วยสื่อบทเรียนออนไลน์ โดยมีกลุ่มตัวอย่างคือ นิสิตเอกการออกแบบสื่อปฏิสัมพันธ์และ มัลติมีเดีย วิทยาลัยนวัตกรรมสื่อสารสังคม มหาวิทยาลัยศรีนครินทรวิโรฒ จำนวน 40 คน ที่กำลังศึกษาในรายวิชาการออกแบบกราฟิกเบื้องต้นเพื่อสื่อปฏิสัมพันธ์ แล้วนำผล ที่ได้มาวิเคราะห์หาประสิทธิภาพและผลสัมฤทธิ์จากผลการทดลองภาคสนามมีประสิทธิภาพเท่ากับ 93.13/92.17 ซึ่งอยู่สูงกว่าเกณฑ์ที่กำหนดไว้คือ 80/80ประสิทธิผลทางการเรียนรู้ของผู้เรียน โดยมีค่าความยาก ง่าย (P) เฉลี่ยเท่ากับ 0.27 - 0.80 ค่าอำนาจจำแนก (SD) เฉลี่ยเท่ากับ 0.20 - 0.71 และค่า ความเชื่อมั่นเฉลี่ยเท่ากับ 0.96 วิเคราะห์หาผลสัมฤทธิ์ทางการเรียน โดยนำคะแนนจากการทดสอบก่อนเรียนและหลังเรียนมาเปรียบเทียบ พบว่าผลต่างของคะแนนการทดสอบหลังเรียนสูงกว่าคะแนนการทดสอบก่อนเรียน โดยมีค่าเท่ากับ 62.01 ซึ่งมีค่ามากกว่าหรือเท่ากับ 60 ผลการวิเคราะห์ความพึงพอใจผู้ขั้นมีความพึงพอใจต่อสื่อบทเรียนมัลติมีเดีย อยู่ในเกณฑ์ระดับดีมาก

จากงานวิจัยที่เกี่ยวข้อง พบว่า เป็นการพัฒนาสื่อในลักษณะที่เน้นด้านความรู้ความเข้าใจหรือจิตสำนึก ส่วนงานวิจัยที่ผู้วิจัยพัฒนาเป็นการสอนที่เน้นทักษะเชิงปฏิบัติ ที่ให้ผู้เรียนฝึกฝนและปฏิบัติตามได้ เป็นสื่อที่พัฒนาจะเป็นทั้งวีดีโอ แอนิเมชัน 3 มิติและโมเดล VR ตามลักษณะของเนื้อหาในแต่ละเรื่อง

III. ระเบียบวิธีวิจัย

ระเบียบวิธีวิจัยในการพัฒนาสื่อมัลติมีเดียสำหรับการเรียนรู้แบบออนไลน์ เรื่องการตัดเย็บผ้า ประกอบไปด้วยขั้นตอนการดำเนินการวิจัย เครื่องมือที่ใช้ในการวิจัยโดยมีรายละเอียดดังนี้

A. ขั้นตอนการดำเนินการวิจัย แบ่งออกเป็น 3 ขั้นตอนดังนี้

ขั้นตอนที่ 1 ขั้นก่อนการผลิต (Pre-production) คือศึกษาทฤษฎีที่เกี่ยวกับตัวอย่างผลงานที่เกี่ยวข้อง แนวคิดทฤษฎีและการออกแบบ เครื่องมือที่ใช้ในการสร้างสื่อมัลติมีเดีย ศึกษารวบรวมเนื้อหาการตัดเย็บผ้ามีจำนวน 3 เรื่องได้แก่ 1) ความรู้เบื้องต้นเกี่ยวกับการตัดเสื้อ 2) การวัดขนาดและการใช้งานจักรเย็บผ้า 3) การออกแบบและการวาดแบบเสื้อ รวมทั้งนำเนื้อมาสร้างสตอรี่บอร์ดตัวอย่างดังภาพที่ 2

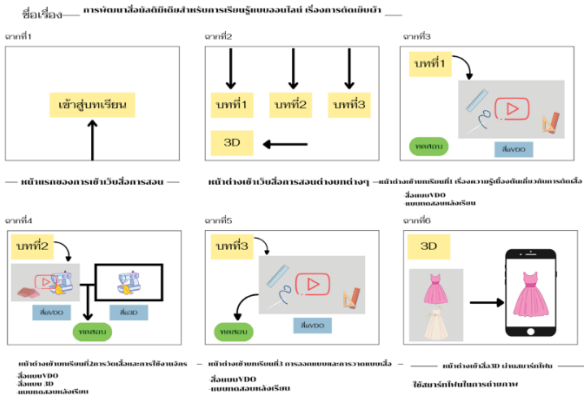


Fig.2. สตอรี่บอร์ดสำหรับการพัฒนาสื่อมัลติมีเดีย

ขั้นตอนที่ 2 ขั้นการผลิต (Production) คือขั้นตอนการลงมือสร้างสื่อมัลติมีเดีย การสร้างแบบจำลอง 3 มิติ สร้างฉาก การสร้างภาพเคลื่อนไหว การจัดแสง การประมวลผลภาพ พร้อมทั้งการใส่เทคนิคพิเศษ และมีการนำสื่อมัลติมีเดียสำหรับการเรียนรู้แบบออนไลน์ เรื่องการตัดเย็บผ้า และนำสื่อมัลติมีเดียที่แล้วเสร็จอัปโหลดขึ้นเว็บไซต์ โดยมีตัวอย่างดังภาพที่ 3



Fig.3. โมเดลแบบ 3 มิติเกี่ยวกับส่วนประกอบของจักรเย็บผ้า

ขั้นตอนที่ 3 ขั้นหลังการผลิต (Post production) นำสื่อมัลติมีเดียสำหรับการเรียนรู้แบบออนไลน์ เรื่องการตัดเย็บผ้าไปทำการทดลองกับกลุ่มตัวอย่างจำนวน 40 คน โดยใช้วิธีการเลือกกลุ่มตัวอย่างเพื่อประเมินความพึงพอใจการใช้งานสื่อมัลติมีเดียการพัฒนาสื่อมัลติมีเดียสำหรับการเรียนรู้แบบออนไลน์ เรื่องการตัดเย็บผ้า โดยใช้แบบสอบถามและมาตราส่วนประมาณค่าของลิเคิร์ท [4] (Rating Scale) โดยแบ่งออกเป็น 5 ระดับ ดังนี้

5 หมายถึง ระดับความพึงพอใจมากที่สุด

4 หมายถึง ระดับความพึงพอใจมาก

3 หมายถึง ระดับความพึงพอใจปานกลาง

2 หมายถึง ระดับความพึงพอใจน้อย

1 หมายถึง ระดับความพึงพอใจน้อยที่สุด

การแปลผลคะแนนความพึงพอใจได้ใช้ของเบสท์ [5] แบ่งระดับได้ดังนี้

ระดับความพึงพอใจมากที่สุด	คะแนนระหว่าง 4.50- 5.00
ระดับความพึงพอใจมาก	คะแนนระหว่าง 3.50- 4.49
ระดับความพึงพอใจปานกลาง	คะแนนระหว่าง 2.50- 3.49
ระดับความพึงพอใจน้อย	คะแนนระหว่าง 1.50- 2.49
ระดับความพึงพอใจน้อยที่สุด	คะแนนระหว่าง 1.00- 1.49

B. เครื่องมือที่ใช้ในการวิจัย ได้แก่

1) Hardware คือ
- เครื่องคอมพิวเตอร์ CPU RYZEN 5 5600GT, RAM 16 GB,*GPU Nvidia 1650, Solid State Drive (SSD) 512 GB*
- สมาร์ทโฟน ระบบปฏิบัติการ android 13 ขึ้นไป

2) *Software*
- โปรแกรม Adobe Photoshop ใช้สำหรับการตกแต่งภาพกราฟิก
- โปรแกรม AdobeIllustratorใช้สำหรับการวาดลายเส้นภาพกราฟิก โปรแกรม Unity ใช้ในการออกแบบเว็บไซต์
- โปรแกรม MyWebAR ใช้สำหรับรันผ่านการเปิดใช้งาน 3D model ผ่านสมาร์ทโฟน

IV. ผลการทดลอง

จากการพัฒนาสื่อมัลติมีเดียสำหรับการเรียนรู้แบบออนไลน์ เรื่องการตัดเย็บผ้าได้ผลการทดลองดังนี้

1) ผลการพัฒนาสื่อมัลติมีเดียสำหรับการเรียนการรียนรู้แบบออนไลน์ เรื่องการตัดเย็บผ้าแสดงดังตัวอย่างดังภาพ 4-7



Fig.4. แสดงเนื้อหาบทเรียนการตัดเย็บผ้า



Fig.5. แสดงเนื้อหาบทเรียนที่ 1 เรื่องความรู้เบื้องต้นเกี่ยวกับการตัดเสื้อ



Fig.6. แสดงเนื้อหาบทเรียนที่ 2 เรื่องการวัดขนาดและการใช้งานจักรเย็บผ้า

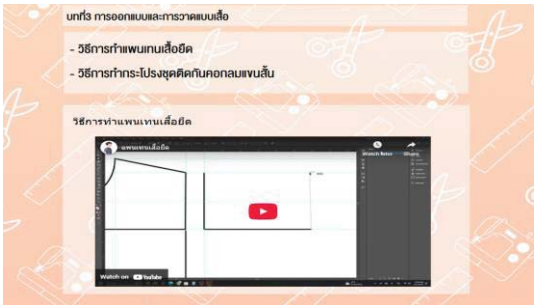


Fig.7. แสดงเนื้อหาบทเรียนที่ 3การออกแบบและการวาดแบบเสื้อ

2) แบบประเมินความพึงพอใจ

ตารางที่ 1 แสดงจำนวนและร้อยละ ข้อมูลทั่วไปของผู้ตอบแบบสอบถาม

รายการประเมิน	จำนวนผู้ตอบแบบสอบถาม	ค่าเฉลี่ยร้อยละ
1) เพศ		
ชาย	24	60.00
หญิง	16	40.00
2) ระดับการศึกษา		
ระดับประถมศึกษาชั้นปีที่ 6	4	10.00
ระดับมัธยมศึกษาตอนต้น	4	10.00
ระดับมัธยมศึกษาตอนปลายหรือ ปวช.	6	15.00
ระดับประกาศนียบัตรวิชาชีพชั้นสูง (ปวส.)	2	5.00
ระดับปริญญาตรี	23	57.50
ระดับสูงกว่าปริญญาตรี	1	2.50

จากตารางที่ 1 พบว่ามีผู้ตอบแบบประเมินความพึงพอใจเป็นเพศชายจำนวน 24 คน คิดเป็นร้อยละ 60 เพศหญิงจำนวน 16 คน คิดเป็นร้อย 40 และมีระดับการศึกษาระดับปริญญาตรีมากที่สุดจำนวน 23 คน คิดเป็นร้อยละ 57.50 รองลงมาระดับการศึกษาระดับมัธยมตอนปลายหรือ ปวช.จำนวน 6 คน คิดเป็นร้อยละ 15 รองลงมาระดับประถมศึกษาชั้นปีที่ 6 และระดับมัธยมศึกษาตอนต้น จำนวน 4 คน คิดเป็นร้อยละ 10 รองลงมาระดับประกาศนียบัตรวิชาชีพชั้นสูง (ปวส.) จำนวน 2 คิดเป็นร้อยละ 5 และระดับสูงกว่าปริญญาตรี 1 คนคิดเป็นร้อยละ 2.50 ตามลำดับ

ตารางที่ 2 แสดงค่าเฉลี่ย ค่าเบี่ยงเบนมาตรฐาน และระดับความพึงพอใจเกี่ยวกับสื่อมัลติมีเดียสำหรับการเรียนรู้แบบออนไลน์ เรื่องการตัดเย็บผ้า

รายการประเมิน	ผลการประเมินความพึงพอใจ		
	$\bar{X}$	S.D.	แปลผล
1.ด้านเนื้อหา			
ความสมบูรณ์ของเนื้อหา	4.73	0.50	มากที่สุด
ความถูกต้องของเนื้อหา	4.68	0.52	มากที่สุด
การลำดับขั้นในการนำเสนอเนื้อหา	4.68	0.57	มากที่สุด
ความชัดเจนในการอธิบายเนื้อหามีแหล่งอ้างอิงที่เชื่อถือได้	4.76	0.49	มากที่สุด
เนื้อหามีความเหมาะสมกับกลุ่มเป้าหมาย	4.80	0.46	มากที่สุด
เฉลี่ยด้านเนื้อหา	4.73	0.51	มากที่สุด

ตารางที่ 2 แสดงค่าเฉลี่ย ค่าเบี่ยงเบนมาตรฐาน และระดับความพึงพอใจเกี่ยวกับสื่อมัลติมีเดียสำหรับการเรียนรู้แบบออนไลน์ เรื่องการตัดเย็บผ้า (ต่อ)

รายการประเมิน	ผลการประเมินความพึงพอใจ		
	$\bar{X}$	S.D.	แปลผล
2.ด้านการใช้ภาษา			
ภาษาที่ใช้ มีความถูกต้องและชัดเจน	4.85	0.36	มากที่สุด
ภาษาที่ใช้มีความเหมาะสมกับวัย	4.78	0.42	มากที่สุด
มีการอธิบายและสื่อความหมายเข้าใจง่าย	4.80	0.40	มากที่สุด
เฉลี่ยด้านการใช้ภาษา	4.81	0.39	มากที่สุด
3.ด้านการออกแบบ			
การใช้รูปภาพในการประกอบสื่อมีความเหมาะสม ถูกต้อง ชัดเจน ตรงกับเนื้อหา	4.80	0.40	มากที่สุด
กราฟิกที่ใช้มีความสวยงาม และน่าสนใจ	4.88	0.33	มากที่สุด
สีสันที่ใช้ในการออกแบบสื่อมัลติมีเดียมีความเหมาะสม	4.76	0.49	มากที่สุด
สีตัวอักษร ขนาดตัวอักษร และรูปแบบตัวอักษรมีความเหมาะสม สวยงาม และอ่านง่าย	4.78	0.42	มากที่สุด
เฉลี่ยด้านการออกแบบ	4.80	0.41	มากที่สุด
เฉลี่ยรวมทุกด้าน	4.78	0.44	มากที่สุด

จากตารางที่2 ผลการประเมินความพึงพอใจของผู้สนใจสื่อมัลติมีเดียสำหรับการเรียนรู้แบบออนไลน์ เรื่องการตัดเย็บผ้า พบว่ามีความพึงพอใจอยู่ในระดับมากที่สุด มีค่าเฉลี่ย $(\bar{X})$ เท่ากับ 4.78 ส่วนเบี่ยงเบนมาตรฐาน (S.D.) เท่ากับ 0.44 โดยมีความพึงพอใจมากที่สุดคือการใช้ภาษา มีคะแนนเฉลี่ยที่ 4.80 รองลงมาเป็นด้านการออกแบบ มีคะแนนเฉลี่ยที่ 4.80 และด้านเนื้อหา มีค่าเฉลี่ยอยู่ในระดับ 4.73 ตามลำดับ

อภิปรายผล

จากผลการวิจัยการพัฒนาสื่อมัลติมีเดียสำหรับการเรียนรู้แบบออนไลน์ เรื่องการตัดเย็บผ้า ซึ่งพัฒนาและใช้ทดลองผู้ที่สนใจจำนวน 40 คน มีบทบาทที่สำคัญคือการช่วยให้ผู้เรียนมีความเข้าใจทั้งในภาคทฤษฎีและภาคปฏิบัติในการตัดเย็บผ้า ลดความซับซ้อนในการเรียนรู้ สามารถศึกษาได้ด้วยตนเองโดยไม่ต้องพึ่งผู้สอน มีความยืดหยุ่นในการเรียนรู้ ฝึกฝนได้ซ้ำ ๆ ตามที่ต้องการ มีวัตถุประสงค์เพื่อ 1) พัฒนาสื่อมัลติมีเดียสำหรับการเรียนรู้แบบออนไลน์เรื่องการตัดเย็บผ้า และ 2) ศึกษาความพึงพอใจของผู้สนใจที่มีต่อสื่อมัลติมีเดียสำหรับการเรียนรู้แบบออนไลน์เรื่องการตัดเย็บผ้า ผลการวิจัยพบว่า ผู้ใช้มีความพึงพอใจในระดับสูงมาก โดยมีค่าเฉลี่ยที่ 4.78 และค่าส่วนเบี่ยงเบนมาตรฐาน 0.44 แสดงให้เห็นว่าสื่อที่พัฒนาขึ้นสามารถตอบสนองความต้องการของผู้เรียนได้อย่างมีประสิทธิภาพ

เมื่อนำมาผลการวิจัยเปรียบเทียบกับงานวิจัยที่เกี่ยวข้อง พบว่ามีแนวโน้มที่สอดคล้องกัน โดยงานวิจัยของ วุฒิไกร พิมพขันธ์และคณะ (2564) ซึ่งพัฒนางานวิจัยเรื่องการออกแบบและพัฒนาสื่อแอนิเมชัน 3 มิติ เป็นการใช้เทคนิคการเล่าเรื่องเพื่อรณรงค์อนุรักษ์ช้างไทย พบว่าผู้เชี่ยวชาญมีความพึงพอใจในระดับสูงมากมีค่าเฉลี่ย 4.43 และผู้รับชมทั่วไปมีค่าเฉลี่ย 4.29 สะท้อนให้เห็นว่าสื่อมัลติมีเดียที่ใช้เทคนิคการเล่าเรื่องสามารถสร้างความเข้าใจและความสนใจในเนื้อหาได้เป็นอย่างดี งานวิจัยของ มโนรส บริรักษ์อราวินท์ และคณะ (2562) พัฒนาแอนิชัน 3D เสมือนกรณีศึกษาศูนย์วัฒนธรรมมหาวิทยาลัยราชภัฏนครศรีธรรมราชติ เพื่อการนำเสนอข้อมูลทางประวัติศาสตร์และวัฒนธรรม พบว่าผู้เรียนสามารถทำความเข้าใจเนื้อได้ดีขึ้นอย่างมีนัยสำคัญมีความพึงพอใจต่อสื่ออยู่ในระดับมาก มีค่าเฉลี่ยที่ 4.17 และให้เห็นว่าการใช้แอนิเมชันและเทคโนโลยี 3 มิติ ช่วยให้ผู้เรียนเข้าใจข้อมูลที่ซับซ้อนได้ดีขึ้น และงานวิจัยของ ธนพงษ์ ไชยลาโกและคณะ (2559) พัฒนาสื่อบทเรียนออนไลน์เรื่องการออกแบบเพื่อผลิตสื่อปฏิสัมพันธ์และมัลติมีเดีย พบว่ามีประสิทธิภาพสูงกว่าเกณฑ์ที่กำหนด

V. ข้อสรุป

การวิจัยนี้พบว่าสื่อมัลติมีเดียสำหรับการเรียนรู้แบบออนไลน์เรื่องการตัดเย็บผ้ามีประสิทธิภาพสูงและได้รับความพึงพอใจในระดับดีมาก โดยมีค่าเฉลี่ย 4.78 และส่วนเบี่ยงเบนมาตรฐาน 0.44 ผลการประเมินในแต่ละด้านพบว่าเนื้อหามีความถูกต้อง ครบถ้วน และมีการลำดับขั้นตอนที่ชัดเจน ได้รับคะแนนเฉลี่ย 4.73 ในขณะที่ด้านการใช้ภาษาได้รับคะแนนเฉลี่ยสูงสุดที่ 4.81 แสดงให้เห็นว่าภาษาที่ใช้มีความชัดเจน เข้าใจง่าย และเหมาะสมกับกลุ่มเป้าหมาย นอกจากนี้ ด้านการออกแบบสื่อได้รับคะแนนเฉลี่ย 4.80 โดยเฉพาะกราฟิกและสีสันที่ใช้ได้รับการประเมินว่าสวยงามและดึงดูดความสนใจ สื่อมัลติมีเดียที่พัฒนาขึ้นช่วยลดความซับซ้อนของกระบวนการเรียนรู้ ให้ความยืดหยุ่นในการศึกษา สามารถฝึกฝนซ้ำได้ตามต้องการ และช่วยให้ผู้เรียนเข้าใจทั้งภาคทฤษฎีและปฏิบัติ

สำหรับแนวทางการวิจัยในอนาคต ควรมีการพัฒนาเทคโนโลยี AR และ VR เพื่อเพิ่มองค์ประกอบเสมือนจริง ให้ผู้เรียนสามารถโต้ตอบกับโมเดล 3 มิติของจักรเย็บผ้าและวัสดุที่เกี่ยวข้องได้มากขึ้น เป็นการนำ AI มาใช้ทำเป็นระบบการเรียนรู้ส่วนบุคคล โดยการปรับแต่งบทเรียนให้เหมาะสมกับระดับทักษะของแต่ละคน

อ้างอิง

[1] วุฒิไกร พิมพขันธ์, ภัสสร ปัทวงค์, และ อภิรดี เดชพงษ์สัมฤทธิ์, "การออกแบบและพัฒนาสื่อแอนิเมชัน 3 มิติ เพื่อส่งเสริมจิตสำนึกการอนุรักษ์ช้างไทย," *วารสารวิทยาศาสตร์และเทคโนโลยี*, ปีที่ 1, ฉบับที่ 1, หน้า 53-64, ม.ค.-เม.ย., 2564.

[2] มโนรส บริรักษ์อราวินท์, จีรวัฒน์ นาคสุวรรณ์, และ ชวัลรัตน์ ศรีนวลปาน, "แอนิเมชัน 3D เสมือนกรณีศึกษาศูนย์วัฒนธรรมมหาวิทยาลัยราชภัฏนครศรีธรรมราช," ใน *การประชุมวิชาการระดับชาติ "สารสนเทศศาสตร์วิชาการ 2019"*, นครศรีธรรมราช, ประเทศไทย, 25-26 มิ.ย., 2562.

[3] ธนพงษ์ ไชยลาโก, เอกลักษณ์ โภคทรัพย์ไพบูลย์, และ ปริญญ์ โสภา, "การพัฒนาสื่อบทเรียนออนไลน์เรื่องการออกแบบเพื่อการผลิตสื่อปฏิสัมพันธ์และมัลติมีเดีย," *วารสารวิชาการนวัตกรรมสื่อสารสังคม*, ปีที่ 4, ฉบับที่ 2, หน้า 134-142, ก.ค.-ธ.ค., 2559.

[4] J. W. Best, *Research in Education*, 4th ed. New Delhi, India: Prentice Hall of India Pvt. Ltd., 1981.

A. [5] S. Likert, New Patterns of Management. *New York, NY, USA: McGraw-Hill, 1961.*

ต้นแบบเกม 3 มิติ การแนะนำขั้นตอนการเดินทางโดยสารเครื่องบิน กรณีศึกษา : ท่าอากาศยานนานาชาติภูเก็ต

3D Game Prototype Introduction to Flight Travel Procedures Case study: Phuket International Airport

1st ทนันชัย ชำนินา(Tanunchai Chamnina)
สาขาเทคโนโลยีดิจิทัล (Digital Technology Branch)
คณะวิทยาศาสตร์และเทคโนโลยี
(Faculty of Science and Technology)
ภูเก็ต,ประเทศไทย (Phuket,Thailand)
s6411423112@pkru.ac.th

2nd ธนกร แซ่หลี(Thanakorn Saelee)
สาขาเทคโนโลยีดิจิทัล (Digital Technology Branch)
คณะวิทยาศาสตร์และเทคโนโลยี
(Faculty of Science and Technology)
ภูเก็ต,ประเทศไทย (Phuket,Thailand)
s6411423113@pkru.ac.th

3rd อุไรรัตน์ มากจันทร์(Urairat Makchan)
สาขาเทคโนโลยีดิจิทัล (Digital Technology Branch)
คณะวิทยาศาสตร์และเทคโนโลยี
(Faculty of Science and Technology)
ภูเก็ต,ประเทศไทย (Phuket,Thailand)
Urairat.m@pkru.ac.th

Abstract*—*The objectives of this research were: 1) to develop a 3D prototype game introducing the air travel procedures, with a case study of Phuket International Airport, and 2) to evaluate user satisfaction with the 3D prototype game. The research process was based on the Interactive Multimedia System Design and Development (IMSDD) Model, which consists of five phases: Investigation, Design, Implementation, Application, and Evaluation.

The research results revealed that: 1) a 3D prototype game introducing the air travel procedures at Phuket International Airport was successfully developed, and 2) the user satisfaction evaluation, conducted with a sample group of 50 passengers at Phuket International Airport, showed a good level of satisfaction, with an average score of 4.25 and a standard deviation of 0.70.

Keywords—3D Game, Virtual Reality, Phuket International Airport

I. บทนำ

ท่าอากาศยานนานาชาติภูเก็ตเป็นหนึ่งในสนามบินที่อยู่ในความดูแลและรับผิดชอบของ บริษัทท่าอากาศยานไทย จำกัด (มหาชน) เป็นท่าอากาศยานที่สำคัญแห่งหนึ่งในประเทศไทย เนื่องด้วยจังหวัดภูเก็ตเป็นเมืองแห่งการท่องเที่ยวที่มีคนรู้จักและนิยมมาเที่ยวจากทั่วโลกซึ่งส่วนใหญ่ใช้การเดินทางด้วยการโดยสารเครื่องบิน [1] สถิติในปี 2023 มีจำนวนเที่ยวบินถึง 87,304 เที่ยวบิน และมีผู้โดยสาร 14 ล้านคน มีพื้นที่ 1,382 ไร่ โดยการแบ่งเป็นอาคารระหว่างประเทศและอาคารภายในประเทศ โดยที่อาคารภายในประเทศมีพื้นที่ ประมาณ 45,668 ตารางเมตร สำหรับการเดินทางโดยสารทางเครื่องบินนั้นมีขั้นตอนที่ยุ่งยากกว่าการโดยสารแบบอื่น ๆ ไม่ว่าจะเป็นการตรวจสอบเอกสาร เช็คสัมภาระ เช็คอินรับบัตรโดยสาร การโหลดสัมภาระ การให้เจ้าหน้าที่ตรวจความปลอดภัย การนั่งรอก่อนขึ้นเครื่อง หากผู้โดยสารท่านใดเดินทางครั้งแรกด้วยเครื่องบิน หรือ นาน ๆ ที่จะมีการเดินทาง อาจไม่รู้ว่าจะต้องไปตรงจุดไหนอย่างไร ดังนั้นผู้วิจัยจึงได้มีการพัฒนาต้นแบบเกม 3 มิติ การแนะนำขั้นตอนการเดินทางโดยสารเครื่องบิน กรณีศึกษา : ท่าอากาศยานนานาชาติภูเก็ต เพื่อแนะนำท่าอากาศยานนานาชาติภูเก็ต ให้กับผู้โดยสารที่ใช้บริการ ได้รับรู้ถึงขั้นตอนการเดินทางด้วยเครื่องบินของท่าอากาศยานนานาชาติภูเก็ต

โดยมีวัตถุประสงค์ในการวิจัย 1) เพื่อพัฒนาต้นแบบเกม 3 มิติ การแนะนำขั้นตอนการเดินทางโดยสารเครื่องบิน กรณีศึกษา : ท่าอากาศยานนานาชาติภูเก็ต 2) เพื่อประเมินความพึงพอใจ ต้นแบบเกม 3 มิติ การแนะนำขั้นตอนการเดินทางโดยสารเครื่องบิน กรณีศึกษา : ท่าอากาศยานนานาชาติภูเก็ต โดยมีกรอบในวิจัยดังภาพที่ 1

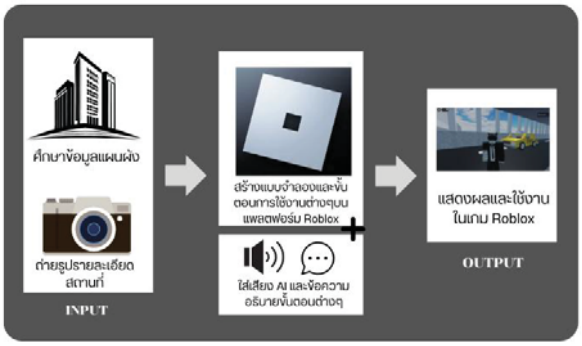


Fig.1 กรอบแนวคิดในการวิจัย เรื่องต้นแบบเกม 3 มิติ การแนะนำขั้นตอนการเดินทางโดยสารเครื่องบิน กรณีศึกษา ท่าอากาศยานนานาชาติภูเก็ต

II. ทบทวนวรรณกรรม

[2] สุรพงศ์ วิริยะ และ กิตติ์รวี พิญญาพงศ์สิน การประยุกต์ใช้สื่อเทคโนโลยีความเป็นจริงเสมือนเพื่อการแนะนำ บริษัท ยูซีไอ มีเดีย จำกัด ในรูปแบบภาพกราฟิก 3 มิติ (Application of Virtual Reality Technology for Recommendation of UCI Media Co., Ltd. In 3D Graphics) เพื่อ 1) พัฒนาสื่อโดยใช้เทคโนโลยีความเป็นจริงเสมือนในการแนะนำบริษัท ยูซีไอ มีเดีย จำกัด และ 2) ประเมินคุณภาพของสื่อเทคโนโลยีความเป็นจริงเสมือน โดยผู้วิจัยได้ใช้หลักการ IMSDD Model โดยมีวิธีการดำเนินการวิจัย คือ ขั้นตอนการศึกษาความต้องการในระบบ (System Requirements) ขั้นตอนการออกแบบ(Design) ขั้นตอนการสร้างและติดตั้งระบบ(Implementation) และขั้นตอนการประเมินผล(Evaluation) จากผลการวิจัยพบว่า 1) ได้สื่อเทคโนโลยีความเป็นจริงเสมือนเพื่อการแนะนำบริษัท ยูซีไอ มีเดีย จำกัด ที่มีการแสดงผล และการทำงานที่ถูกต้อง 2) ผลจากการประเมินคุณภาพของสื่อเทคโนโลยีความเป็นจริงเสมือน โดยผู้เชี่ยวชาญ

ทางด้านกราฟิก พบว่ามีคุณภาพของสื่อเทคโนโลยีความเป็นจริงเสมือนมีคุณภาพอยู่ในระดับดี ($\bar{x}$ = 4.41)

[3] มิตรภาพ พงษานิตร พีระศักดิ์ อัสมิมานะ และ กฤติเดช จินดาภัทร์ การพัฒนาเกมสามมิติโดยการจำลองสถานที่จริง กรณีศึกษา คณะเทคโนโลยีอุตสาหกรรม มหาวิทยาลัยราชภัฏกำแพงเพชร แม่สอด (Development of 3D games by simulating real locations: a case study of Faculty of Industrial Technology Kamphaeng Phet Rajabhat University Mae Sot) คณะผู้วิจัยได้ทำการศึกษาเกี่ยวกับการออกแบบวัตถุและสถานที่ในรูปแบบสามมิติจากสถานที่จริงด้วยโปรแกรม ออกแบบสามมิติ อีกทั้งผู้วิจัยยังได้มีความสนใจในการพัฒนาเกมด้วยโปรแกรมจำลองเกมขึ้น ทำให้มีความต้องการที่จะพัฒนารูปแบบของเกมที่มาจากการจำลองสถานที่จริงขึ้น รวมไปถึงการสร้างตัวละครในเกมที่มีปฏิสัมพันธ์กัน หรือต่อสู้กัน ภายในเกมได้ โดยคณะผู้วิจัยจึงได้ทำการออกแบบสถานที่ในเกมให้มีความเสมือนจริงด้วยโปรแกรมออกแบบสามมิติ Sketch UP และได้ทำการพัฒนาเกมจากโปรแกรม Unreal Engine ให้สามารถเป็นเกมต่อสู้และเก็บคะแนนได้ตามที่คณะผู้วิจัยได้ ทำการกำหนดรูปแบบไว้ รวมทั้งออกแบบเกมในให้มีความสามารถเล่นได้ในรูปแบบ Offline หรือ Online และสามารถ เล่นร่วมกันสูงสุดถึง 4 คนในด่านเดียวกัน เหมาะสำหรับบุคคลทั่วไปและผู้ที่สนใจเกี่ยวกับการพัฒนาเกมในรูปแบบสามมิติ ซึ่งคณะผู้วิจัยได้ทำการประเมินความพึงพอใจผู้ใช้งานจากประชากรกลุ่มตัวอย่างที่ทดลองเล่นเกมที่พัฒนาขึ้นนี้จำนวน 100 คน พบว่ามีความพึงพอใจในภาพรวมของทุกด้านเฉลี่ยอยู่ที่ 4.27 และค่าเบี่ยงเบนมาตรฐานอยู่ที่ 0.68 เกณฑ์ระดับความ พึงพอใจอยู่ที่ระดับมาก และด้านที่มีค่าระดับความพึงพอใจมากที่สุดจากภาพรวมของระบบคือด้านประโยชน์การนำไปใช้ ซึ่งมีค่าเฉลี่ยอยู่ที่ 4.43 และค่าเบี่ยงเบนมาตรฐานอยู่ที่ 0.64 ระดับความพึงพอใจอยู่ที่ระดับมากที่สุด คำสำคัญ : การพัฒนาเกมสามมิติ/ เกมสามมิติจากการจำลองสถานที่จริง

[4] อนุรักษ์ พาสวรรค , ไพรสันต์ สุวรรณศร และ พิมพ์ชนก สุวรรณศร (2567) การพัฒนาเกมสถานการณ์จำลองท่องเที่ยววิถีช้าง เพื่อพัฒนาเกมสถานการณ์จำลองท่องเที่ยววิถีช้าง กลุ่มตัวอย่างคือนักศึกษามหาวิทยาลัยราชภัฏเชียงใหม่ สาขาคอมพิวเตอร์ศึกษา ชั้นปีที่ 3 จำนวน 20 คน ได้จากการสุ่มอย่างง่าย เครื่องมือที่ใช้ในการพัฒนา ได้แก่ เกมสถานการณ์จำลองท่องเที่ยววิถีช้าง และแบบประเมินความพึงพอใจต่อ การใช้งานเกมสถานการณ์จำลองท่องเที่ยววิถีช้าง วิเคราะห์ผลด้วยค่าเฉลี่ย และส่วนเบี่ยงเบนมาตรฐาน ผลการวิจัยพบว่า ในการพัฒนาเกมด้านกราฟิก ผู้วิจัยได้ออกแบบให้มีความกึ่งเสมือนจริงใช้องค์ประกอบที่มี ความสมจริง เช่น ต้นไม้ ภูเขา แม่น้ำ เป็นต้น ผสมกับความเป็นเกมโดยใช้โมเดลที่มีอยู่แล้วภายในโปรแกรม โรบล็อกซ์สตูดิโอที่มีผู้พัฒนาอื่น ๆ สร้างไว้ ส่วนของอนิเมชั่นใช้โปรแกรมเบลนเดอร์ (Blender) ในการสร้าง อนิเมชั่นการขยับของช้าง เช่น การเดิน การแสดงโชว์ของช้าง เป็นต้น พัฒนาเกมด้วยโปรแกรมโรบล็อกสตูดิโอ ใช้ภาษาเลือ (LUA) เป็นหลักในการพัฒนาระบบภายในเกม การเล่นเกมสถานการณ์จำลองท่องเที่ยววิถีช้าง เป็นเกมที่มีการโหลดข้อมูลที่ใช้ในการแสดงผลเป็นจำนวนมาก จำเป็นอย่างยิ่งที่จะต้องใช้เครื่องคอมพิวเตอร์ หรืออุปกรณ์ที่มีประสิทธิภาพเพื่อการประมวลผลของภาพและเสียงที่สมบูรณ์ ผลการประเมินความพึงพอใจต่อ เกมสถานการณ์จำลองท่องเที่ยววิถีช้าง โดยรวมอยู่ในระดับมากที่สุด

III. ระเบียบวิธีวิจัย

A. ขั้นตอนการดำเนินงาน

การศึกษาวิจัย ต้นแบบเกม 3 มิติ การแนะนำขั้นตอนการเดินทางโดยสารเครื่องบิน กรณีศึกษา : ท่าอากาศยานนานาชาติภูเก็ต ผู้วิจัยใช้หลักการโดยใช้หลักการของ Interactive Multimedia System Design and Development IMSDD Model (Dastbaz,2003) [5] ซึ่งมีขั้นตอนดังต่อไปนี้

ขั้นตอนที่ 1 สำรวจและวิเคราะห์ความต้องการของระบบ (Investigation) เป็นการศึกษาความต้องการของท่าอากาศยานภูเก็ตและรวบรวมข้อมูลโดยการลงพื้นที่จริงเป็นการเก็บข้อมูลจากเจ้าหน้าที่เกี่ยวกับขั้นตอนการขึ้นเครื่องบินและถ่ายภาพรายละเอียดต่าง ๆ ของท่าอากาศยานภูเก็ต

ขั้นตอนที่ 2 การออกแบบ (Design) โดยการนำข้อมูลที่ได้จากการรวบรวมมาทำการวาดแผนผังของท่าอากาศยานนานาชาติภูเก็ต และนำให้เจ้าหน้าที่ท่าอากาศยานตรวจสอบความถูกต้อง

ขั้นตอนที่ 3 พัฒนาและติดตั้งระบบ (Implementation) เป็นการนำแผนผังและภาพถ่ายที่ได้มาปั้นเป็นโมเดล 3 มิติ ต้นแบบเกม 3 มิติ การแนะนำขั้นตอนการเดินทางโดยสารเครื่องบิน กรณีศึกษา : ท่าอากาศยานนานาชาติภูเก็ต

ขั้นตอนที่ 4 การนำไปใช้ (Implementation) ผู้วิจัยได้นำสื่อไปทดลองใช้งานกับผู้โดยสารทางเครื่องบินของท่าอากาศยานนานาชาติภูเก็ต จำนวน 50 คน

ขั้นตอนที่ 5 การประเมินผล (Evaluation) ทำการเก็บข้อมูลสำรวจความพึงพอใจของผู้ใช้ ต้นแบบเกม 3 มิติ การแนะนำขั้นตอนการเดินทางโดยสารเครื่องบิน กรณีศึกษา : ท่าอากาศยานนานาชาติภูเก็ต

B. เครื่องมือที่ใช้ในการศึกษา

ด้านฮาร์ดแวร์ (Hardware)

- PC MSI GF75
- Smart Phon IPhone16 Pro max
- Vr Shinecon
- คอนโทรลเลอร์ไร้สาย Dualshock4

ด้านซอฟต์แวร์ (Software)

- Roblox Studio ใช้สำหรับออกแบบจำลองสถานที่ 3 มิติ และองค์ประกอบต่างๆ
- Roblox Player ใช้ในการทดสอบควบคุมการใช้งานจริง
- Clipchamp ใช้ในการแปลงข้อความเป็นเสียงของ AI

C. วิธีการวิเคราะห์ข้อมูล

การวิเคราะห์คุณภาพของสื่อที่มีการสื่อเทคโนโลยีความเป็นจริงเสมือนสำหรับการแนะนำท่าอากาศยานแบบ เกม VR 3 มิติ เพื่อหาค่าทางสถิติได้แก่ ค่าเฉลี่ย (Mean) และส่วนเบี่ยงเบนมาตรฐาน (Standard Deviation) โดยการแปลผลระดับคุณภาพของผู้ตอบแบบประเมิน โดยใช้เกณฑ์ในการวิเคราะห์ ตามแนวคิดของเบสท์ (Best,1998) [6] แล้วนำเสนอผลการวิเคราะห์ข้อมูลดังนี้

ค่าเฉลี่ย 4.50 - 5.00 หมายถึง คุณภาพระดับดีมาก
ค่าเฉลี่ย 3.50 - 4.49 หมายถึง คุณภาพระดับดี
ค่าเฉลี่ย 2.50 - 3.49 หมายถึง คุณภาพพอใช้
ค่าเฉลี่ย 1.50 - 2.49 หมายถึง คุณภาพระดับปรับปรุง
ค่าเฉลี่ย 1.00 - 1.49 หมายถึง คุณภาพระดับควรปรับปรุง

IV. ผลการทดลอง

จากการพัฒนาต้นแบบเกม 3 มิติ การแนะนำขั้นตอนการเดินทางโดยสารเครื่องบิน กรณีศึกษา : ท่าอากาศยานนานาชาติภูเก็ตได้ผลดังนี้

1) ผลการพัฒนาต้นแบบเกม 3 มิติ การแนะนำขั้นตอนการเดินทางโดยสารเครื่องบิน กรณีศึกษา : ท่าอากาศยานนานาชาติภูเก็ต

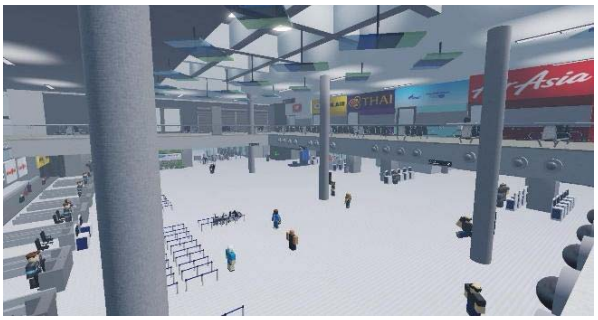


Fig.2. ตัวอย่างหน้าจอ ภาพมุมกว้างของท่าอากาศยานนานาชาติภูเก็ต



Fig.3. ตัวอย่างหน้าจอ จุดตรวจสัมภาระก่อนขึ้นเครื่อง



Fig.4. ตัวอย่างหน้าจอ จุดที่พนักงานเรียกก่อนขึ้นเครื่อง

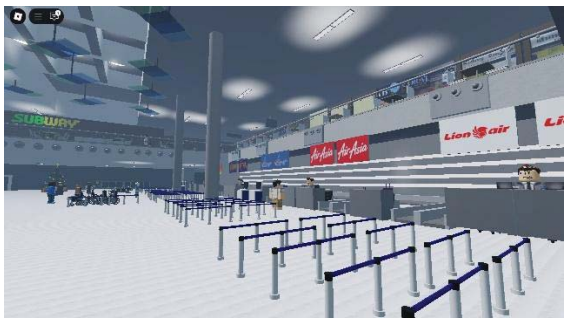


Fig.5. ตัวอย่างหน้าจอ จุดเช็คอินตามเคาน์เตอร์สายการบินต่างๆ

2) ผลการประเมินความพึงพอใจการใช้งานต้นแบบเกม 3 มิติ การแนะนำขั้นตอนการเดินทางโดยสารเครื่องบิน กรณีศึกษา : ท่าอากาศยานนานาชาติภูเก็ต

ตารางที่ 1 ข้อมูลทั่วไปของผู้ตอบแบบสอบถาม

รายละเอียดการประเมิน	จำนวน	ร้อยละ
เพศ		
ชาย	37	74
หญิง	13	26
มีสถานภาพ		
ชาวไทย	40	80
ชาวต่างชาติ	10	20
อายุของผู้ตอบแบบสอบถาม		
ต่ำกว่า 20 ปี	4	8
21-30	33	66
31-40	8	16
40 ปีขึ้นไป	5	10

จากตารางที่ 1 พบว่าผู้ตอบแบบสอบถามความพึงพอใจจำนวน 50 คน เป็นเพศชายจำนวน 37 คน คิดเป็นร้อยละ 74 เพศหญิงจำนวน 13 คน คิดเป็นร้อยละ 26 มีสถานภาพเป็นชาวไทย 40 คน คิดเป็นร้อยละ 80 ชาวต่างชาติ 10 คน คิดเป็นร้อยละ 20 มีอายุต่ำกว่า 20 ปี จำนวน 4 คน คิดเป็นร้อยละ 8 อายุระหว่าง 21-30 ปี จำนวน 33 คน คิดเป็นร้อยละ 66 มีอายุระหว่าง 31-40 ปีจำนวน 8 คน คิดเป็นร้อยละ 16 และมีอายุ 40 ปีขึ้นไป จำนวน 5 คน คิดเป็นร้อยละ 10

ตารางที่ 2 ผลการประเมินความพึงพอใจของกลุ่มตัวอย่างผู้ใช้งานที่มีต่อต้นแบบเกม 3 มิติ การแนะนำขั้นตอนการเดินทางโดยสารเครื่องบิน กรณีศึกษา : ท่าอากาศยานนานาชาติภูเก็ต

รายการประเมิน	$\bar{X}$	S.D.	แปลผล
1. ด้านประโยชน์และการนำไปใช้			
1.1 สามารถสร้างความบันเทิงให้ผู้เล่นได้	4.42	0.64	ดี
1.2 เป็นแหล่งข้อมูลที่ตรงกับความต้องการของผู้ใช้งาน	4.12	0.82	ดี
1.3 สามารถเข้าใจวิธีการใช้งานระบบได้ง่าย	4.00	0.69	ดี
1.4 สามารถนำไปเป็นแนวทางในการพัฒนาเกมต่อไปในอนาคต	4.36	0.62	ดี
รวม	4.23	0.69	ดี
2. ด้านการออกแบบ			
1.1 ความสวยงามและการจัดวางองค์ประกอบ	4.32	0.58	ดี
2.2 ความน่าสนใจและความคิดสร้างสรรค์	4.44	0.61	ดี
2.3 ความสมจริงและสิ่งแวดล้อม	4.06	0.73	ดี
2.4 ความเข้าใจง่ายของข้อความ	4.02	0.71	ดี
2.5 เสียงดนตรีประกอบเบื้องหลังและเสียงพากย์	4.18	0.77	ดี
รวม	4.20	0.68	ดี

ตารางที่ 2 ผลการประเมินความพึงพอใจของกลุ่มตัวอย่างผู้ใช้งานที่มีต่อต้นแบบเกม 3 มิติ การแนะนำขั้นตอนการเดินทางโดยสารเครื่องบิน กรณีศึกษา : ท่าอากาศยานนานาชาติภูเก็ต (ต่อ)

รายการประเมิน	$\bar{X}$	S.D.	แปลผล
3. ประสิทธิภาพและความสามารถในการใช้งาน			
3.1 ความลื่นไหลและความเสถียรของการใช้งาน	4.28	0.53	ดี
3.2 การรองรับอุปกรณ์ที่หลากหลาย (PC, Mobile, VR)	4.62	0.60	ดีมาก
3.3 ความง่ายในการควบคุมตัวละคร	4.20	0.69	ดี
3.4 ความเร็วในการโหลดและแสดงผล	4.26	0.72	ดี
รวม	4.34	0.64	ดี
รวมทั้งหมด	4.25	0.70	ดี

จากตารางที่ 2 พบว่าความพึงพอใจของกลุ่มตัวอย่างผู้ใช้งานที่มีต่อต้นแบบเกม 3 มิติ การแนะนำขั้นตอนการเดินทางโดยสารเครื่องบิน กรณีศึกษา : ท่าอากาศยานนานาชาติภูเก็ต ระดับความพึงพอใจของทุกด้านมีค่าเฉลี่ยรวมอยู่ที่ 4.25 ตามรายละเอียดคือ ด้านประโยชน์และการนำไปใช้ มีค่าเฉลี่ยอยู่ที่ 4.23 ด้านการออกแบบ มีค่าเฉลี่ยอยู่ที่ 4.20 ด้านประสิทธิภาพและความสามารถในการใช้งาน มีค่าเฉลี่ยอยู่ที่ 4.34

V. อภิปรายผล

จากผลการทดลองงานวิจัย ต้นแบบเกม 3 มิติ การแนะนำขั้นตอนการเดินทางโดยสารเครื่อง กรณีศึกษา: ท่าอากาศยานนานาภูเก็ต มีระดับความพึงพอใจที่ไม่แตกต่าง จากงานวิจัยเรื่อง การประยุกต์ใช้สื่อเทคโนโลยีความเป็นจริงเสมือนเพื่อการแนะนำ บริษัทยูซีไอ มีเดีย จำกัด ในรูปแบบภาพกราฟฟิก 3 มิติ งานวิจัยเรื่อง การพัฒนาเกมสามมิติโดยการจำลองสถานที่จริง กรณีศึกษา คณะอุตสาหกรรม มหาวิทยาลัยราชภัฏกำแพงเพชร แม่สอด โดยใช้ Sketchup และ Unreal Engine มีคะแนนความพึงพอใจเฉลี่ยที่ 4.27 และด้านที่มีการคะแนนสูงสุดคือ การนำไปใช้ประโยชน์ และงานวิจัยเรื่องการพัฒนาเกมสถานการณ์จำลองท่องเที่ยววิถีช้าง ใช้ Roblox Studio และ Blender มีความพึงพอใจในระดับมากที่สุด เช่นกัน สำหรับข้อได้เปรียบของงานวิจัยต้นแบบเกม 3 มิติการแนะนำขั้นตอนการเดินทางโดยสารเครื่อง กรณีศึกษา : ท่าอากาศยานนานาภูเก็ต คือการที่ได้ใช้กลุ่มตัวอย่างที่เดินทางจริงในสนามบินนานาชาติ ทำให้สะท้อนความคิดเห็นของผู้ใช้ที่เกี่ยวข้องโดยตรง และมีข้อจำกัดคือขนาดกลุ่มของประชากรที่ค่อนข้างเล็กเมื่อเปรียบกับงานวิจัยที่เกี่ยวข้อง

VI. ข้อสรุป

จากการวิจัยพบว่าต้นแบบเกม 3 มิติการแนะนำขั้นตอนการเดินทางโดยสารเครื่อง กรณีศึกษา: ท่าอากาศยานนานาภูเก็ต ที่พัฒนาขึ้นสามารถทำงานได้อย่างถูกต้องและตรงตามวัตถุประสงค์ โดยได้รับคะแนนความพึงพอใจจากกลุ่มตัวอย่างในระดับดี ($\bar{x}$ = 4.25, S.D. = 0.70) ซึ่งใกล้เคียงกับงานวิจัยเกี่ยวข้องอื่น ๆ แสดงให้เห็นว่าเกมนี้สามารถช่วยให้ผู้ใช้เข้าใจขั้นตอนการเดินทางโดยสารเครื่องบินได้อย่างมีประสิทธิภาพ แนวทางในการพัฒนางานวิจัยในอนาคต ควรมีการเพิ่มกลุ่มตัวอย่างให้มีการครอบคลุมกับกลุ่มผู้โดยสารที่มีความหลากหลาย เช่น นักท่องเที่ยวต่างชาติ หรือผู้ที่ไม่เคยเดินทางด้วยเครื่องบินมาก่อน หรือเป็นการวิจัยในลักษณะที่มีการเปรียบเทียบกับการให้ข้อมูลแบบอื่น เช่น การมีป้ายแนะนำ หรือแอปพลิเคชันนำทาง

อ้างอิง

[1] Airports of Thailand Public Company Limite. “CAIRPORT TRAFFIC REPORT 2023”.[ออนไลน์]. https://www.airportthai.co.th/wp-content/uploads/2024/07/ANNUAL-REPORT-2023.pdf (เข้าถึงเมื่อ: วันที่ 14 กุมภาพันธ์ 2568).

[2] สุรพงศ์ วิริยะ และ กิตติ์รวี พิญญาพงศ์สิน, “การประยุกต์ใช้สื่อเทคโนโลยีความเป็นจริงเสมือนเพื่อการแนะนำ บริษัท ยูซีไอ มีเดีย จำกัด ในรูปแบบภาพกราฟิก 3 มิติ”, วารสารวิทยาศาสตร์ วิศวกรรมศาสตร์ และเทคโนโลยี มหาวิทยาลัยราชภัฏเลย, ปีที่ 3, ฉบับที่ 1, หน้า 67-76 , มกราคม – มิถุนายน 2566.

[3] มิตรภาพ พงษานิตร พีระศักดิ์ อัสมิมานะ และ กฤติเดช จินดาภัทร์,“การพัฒนาเกมสามมิติโดยการจำลองสถานที่จริง กรณีศึกษา คณะเทคโนโลยีอุตสาหกรรม มหาวิทยาลัยราชภัฏกำแพงเพชร แม่สอด”, วารสารแม่โจ้เทคโนโลยีสารสนเทศและนวัตกรรม, ปีที่ 10, ฉบับที่ 1, หน้า 22-35 , มกราคม – เมษายน 2567.

[4] อนุรักษ์ พาสวรรค ไพรสันต์ สุวรรณศร และ พิมพ์ชนก สุวรรณศร,“การพัฒนาเกมสถานการณ์จำลองท่องเที่ยววิถีช้างเพื่อพัฒนาเกมสถานการณ์จำลองท่องเที่ยววิถีช้าง”,วารสารวิทยาศาสตร์และเทคโนโลยีสู่ชุมชน, ปีที่ 2, ฉบับที่ 4, หน้า 17-29, กรกฎาคม - สิงหาคม 2567.

[5] M. Dastbaz, *Designing Interactive Multimedia Systems*. Boston: McGraw-Hill, 2002.

[6] J. W. Best and J. V. Kahn, *Research in Education*, 8th ed. Boston: Allyn and Bacon, 1998.

การพยากรณ์การรายงานตัวของนักศึกษาระดับปริญญาตรี มหาวิทยาลัยราชภัฏภูเก็ต โดยใช้แบบจำลองการถดถอยโลจิสติกส์

Forecasting Undergraduate Student Enrollment at Phuket Rajabhat University Using a Logistic Regression Model

1st Sasina Srithong
Faculty of Science and Technology
Phuket Rajabhat University
Phuket, Thailand
s6511423128@pkru.ac.th

2nd Nissareen Sangmuaeng
Faculty of Science and Technology
Phuket Rajabhat University
Phuket, Thailand
s6511423118@pkru.ac.th

3rd Urairat Makchan
Faculty of Science and Technology
Phuket Rajabhat University
Phuket, Thailand
urairat.m@pkru.ac.th

4th Attapon Pillai
Faculty of Science and Technology
Phuket Rajabhat University
Phuket, Thailand
attapon.p@pkru.ac.th

Abstract

This research analyzes the factors influencing undergraduate student enrollment at Phuket Rajabhat University using a Logistic Regression model. These factors are crucial in students' decision-making regarding university enrollment. The study utilizes historical admission data from the academic years 2020–2024, collected from the university's admission system. The dataset includes demographic variables such as gender, faculty, major, province of high school graduation, and admission type. The analysis follows statistical processes, including data encoding (Label Encoding and One-Hot Encoding), data scaling (Standard Scaler), and Logistic Regression modeling. The dataset is split into a training set (80%) and a test set (20%) to evaluate the model's performance.

The findings indicate that the Logistic Regression model achieves an accuracy of 74.63% in predicting student enrollment. Key factors influencing enrollment include gender, faculty, major, province of high school graduation, and admission type. The ROC curve confirms the model's effectiveness in distinguishing between students likely to enroll and those who are not. Insights from this study can support admission planning, resource management, and strategic development to improve student enrollment rates.

Keywords*: Enrollment forecasting, Student enrollment, Logistic Regression, Phuket Rajabhat University*

I. บทนำ

การแข่งขันทางด้านการศึกษาเป็นปัจจัยหนึ่งที่ทำให้มหาวิทยาลัยต่าง ๆ ต้องการนักศึกษาเพื่อเข้าศึกษาต่อ ณ สถานศึกษาในสังกัด โดยมีการแข่งขันตั้งแต่ระดับประถมศึกษาจนถึงระดับอุดมศึกษา ด้วยเหตุและปัจจัยของจำนวนประชากรของประเทศที่ลดลงและมีจำนวนสถาบันการศึกษาที่เพิ่มมากขึ้น มหาวิทยาลัยราชภัฏภูเก็ตก็เป็นหนึ่งในสถาบันการศึกษาในระดับอุดมศึกษา ตั้งอยู่ในจังหวัดภูเก็ตทางภาคใต้ของประเทศไทย เป็นมหาวิทยาลัยเพื่อการพัฒนาประเทศ ผ่านการขับเคลื่อนท้องถิ่น บนพื้นฐานความรับผิดชอบต่อสังคม นักศึกษาที่เข้ามาศึกษาในมหาวิทยาลัยมาจากหลากหลายจังหวัดของประเทศส่วนใหญ่จะเป็นจังหวัดทางด้านฝั่งอันดามัน ได้แก่ ภูเก็ต พังงา กระบี่ ตรัง สตูล ซึ่งนักศึกษาที่ผ่านการรับเข้าศึกษาต่อในมหาวิทยาลัยนั้น มีกลุ่มที่ผ่านกระบวนการรับแล้วเข้าศึกษาต่อและไม่เข้าศึกษาต่อในมหาวิทยาลัย การสำรองที่นั่งให้กับนักศึกษา ก็เป็นปัจจัยหนึ่งที่ส่งผลต่อการบริหารจัดการของมหาวิทยาลัย เช่น การรับสมัคร การจัดระบบการเรียนการสอน ผู้วิจัยมีความสนใจทำการพยากรณ์การรายงานตัวของนักศึกษาระดับปริญญาตรี มหาวิทยาลัยราชภัฏภูเก็ต โดยใช้แบบจำลองการถดถอยโลจิสติกส์ (Logistic Regression) โดยนำข้อมูลผู้สมัครระหว่างปี พ.ศ. 2563-2567 จากสำนักงานส่งเสริมวิชาการและงานทะเบียน มาทำการวิเคราะห์ เพื่อนำผลการวิจัยนี้ไปใช้เป็นข้อมูลสนับสนุนเชิงนโยบายของมหาวิทยาลัยราชภัฏภูเก็ตในการการวางแผนการรับสมัคร ปรับปรุงนโยบายการบริหารทรัพยากร และออกแบบกลยุทธ์เพื่อเพิ่มอัตราการรายงานตัวของนักศึกษากลุ่มต่อไปให้สูงขึ้น

II. ทบทวนวรรณกรรม

[1] ฐิตินันท์ อนุสรณ์ และสมชาย เล็กเจริญ, "การพยากรณ์การเลือกกลุ่มคณะวิชาในการศึกษาต่อในระดับปริญญาตรี ของมหาวิทยาลัยรังสิต โดยใช้เทคนิคการทำเหมืองข้อมูล งานวิจัยนี้ศึกษาการเลือกกลุ่มคณะวิชาเพื่อพยากรณ์การเลือกเรียนในคณะต่าง ๆ ของนักศึกษามหาวิทยาลัยในประเทศไทย โดยวิเคราะห์ปัจจัยต่าง ๆ เช่น ผลการเรียน คะแนนสอบ และ

ความสนใจของนักศึกษา โดยใช้ RapidMiner Studio ในการพัฒนาและเปรียบเทียบแบบจำลอง พร้อมทั้งใช้เทคนิค ANOVA เพื่อประเมินความแตกต่างระหว่างแบบจำลอง ซึ่งแตกต่างจากงานวิจัยการพยากรณ์การรายงานตัวของนักศึกษาระดับปริญญาตรี มหาวิทยาลัยราชภัฏภูเก็ต เพราะงานวิจัยเล่มนี้จะใช้ แบบจำลองการถดถอยโลจิสติกส์ ซึ่งทั้งสองงานวิจัยก็มีทั้งดีและข้อเสีย และมีความแตกต่างกัน เริ่มต้นแต่กระบวนการรเตรียมข้อมูล งานวิจัยของมหาวิทยาลัยรังสิต ได้เก็บข้อมูลตั้งแต่ปี พ.ศ. 2559 - 2562 ในงานวิจัยของมหาวิทยาลัยรังสิต มีข้อจำกัดในแบบจำลอง ถึงแม้ว่าทั้ง 3 แบบจำลองในงานวิจัยจะมีผลใกล้เคียงกัน โดยไม่ได้วิเคราะห์ว่าแบบจำลองอื่น (เช่น Neural Networks) จะมีประสิทธิภาพดีกว่า ในขณะที่งานวิจัยของมหาวิทยาลัยราชภัฏภูเก็ต ได้ใช้เวลาในการคำนวณและทรัพยากรน้อยกว่าโมเดลที่ซับซ้อน เช่น Neural Networks ส่วนในเรื่องความแม่นยำ มีความแม่นยำสูงทั้งสองงานวิจัย แบบจำลอง Decision Tree มีค่าความแม่นยำสูง (75.79%) ซึ่งเพียงพอสำหรับการประยุกต์ใช้งานจริงในงานวิจัยของมหาวิทยาลัยรังสิต และความแม่นยำของโมเดลแบบจำลองการถดถอยโลจิสติกส์ ก็มีความแม่นยำสูง (74.63%) สามารถใช้ในการวิเคราะห์ข้อมูลที่มีความสัมพันธ์เชิงเส้นระหว่างตัวแปรอิสระและ log odds เช่นกัน

[2] อนุทิตา เล็กเพชร และธวัชชัย งามสันติวงศ์, "การพยากรณ์การพ้นสภาพของนักศึกษาระดับปริญญาตรี โดยใช้การวิเคราะห์ถดถอยโลจิสติกส์เปรียบเทียบกับวิธีตรรกศาสตร์คลุมเครือ งานวิจัยนี้พยากรณ์การพ้นสภาพของนักศึกษาที่ไม่สามารถสำเร็จการศึกษาตามเกณฑ์ เป็นการรเก็บข้อมูลจากนักศึกษามหาวิทยาลัยเทคโนโลยีราชมงคลสุวรรณภูมิตั้งแต่ปี พ.ศ. 2548 - 2551 งานวิจัยเล่มนี้ใช้การรวิเคราะห์อยู่สองแบบคือ แบบตรรกศาสตร์คลุมเคลือ และ การวิเคราะห์ถดถอยโลจิสติกส์ ซึ่งเป็นแบบเดียวกันกับงานวิจัยของมหาวิทยาลัยราชภัฏภูเก็ตเล่มนี้ ความแตกต่างระหว่างงานวิจัยของมหาวิทยาลัยเทคโนโลยีราชมงคลสุวรรณภูมิและงานวิจัยของมหาวิทยาลัยราชภัฏภูเก็ตทั้งสองเล่มนี้คือ งานวิจัยของมหาวิทยาลัยเทคโนโลยีราชมงคลสุวรรณภูมิ มีข้อจำกัดของข้อมูล ใช้ข้อมูลจากนักศึกษาเพียง 199 คน ซึ่งอาจไม่เพียงพอต่อการวิเคราะห์ทั่วไปในกลุ่มประชากรใหญ่ ความซับซ้อนของ Fuzzy Logic ใช้หลายขั้นตอนและมีความซับซ้อนสูง ส่วนวิธีแบบจำลองการถดถอยโลจิสติกส์ มีความเหมาะสมในแง่ของความแม่นยำและความง่ายต่อการใช้งาน มีความแม่นยำ 74.63% และใช้เพียงสมการเดียว ซึ่งเป็นวิธีเดียวกับงานวิจัยเล่มนี้ที่ใช้การวิเคราะห์แบบจำลองการถดถอยโลจิสติกส์ สามารถตีความค่าสัมประสิทธิ์ (Coefficients) เพื่อดูอิทธิพลของตัวแปรแต่ละตัว ค่า Odds Ratio (OR) ช่วยอธิบายผลกระทบของตัวแปรอิสระต่อเหตุการณ์สามารถปรับใช้กับข้อมูลประเภทต่าง ๆ เช่น ตัวแปรเชิงปริมาณหรือเชิงคุณภาพ นี้คือความแตกต่างของทั้งสองงานวิจัย

[3] โสภณา สำราญ และศรัญญา ทองสุข, "การวิเคราะห์การถดถอยโลจิสติกส์ทวิภาคสำหรับความสัมพันธ์ การเลือกเรียนในระดับปริญญาตรีที่มหาวิทยาลัยราชภัฏพิบูลสงครามกับปัจจัยต่าง ๆ งานวิจัยนี้ใช้แบบจำลองการถดถอยโลจิสติกส์ ในการวิเคราะห์ปัจจัยที่ส่งผลต่อแนวโน้มการเข้าเรียนของนักศึกษาในมหาวิทยาลัยราชภัฏเชียงใหม่ โดยศึกษาปัจจัยด้านสาขาวิชา คณะ จังหวัดที่จบการศึกษา และระดับผลการเรียนเฉลี่ย (GPAX) เพื่อพยากรณ์โอกาสที่นักศึกษาจะรายงานตัวต่อ ซึ่งมีแนวทางเดียวกับงานวิจัยของมหาวิทยาลัยราชภัฏภูเก็ตที่ศึกษาแนวโน้มการรายงานตัวของนักศึกษา ทั้งสองงานวิจัยใช้แบบจำลองการถดถอยโลจิสติกส์ เป็นเครื่องมือหลักในการวิเคราะห์ อย่างไรก็ตาม ความแตกต่างที่สำคัญระหว่างสองงานวิจัยนี้คือ งานวิจัยของมหาวิทยาลัยราชภัฏเชียงใหม่มุ่งเน้นไปที่การสมัครเรียน โดยใช้ข้อมูลจากระบบรับสมัครออนไลน์เป็นหลัก ในขณะที่งานวิจัยของมหาวิทยาลัยราชภัฏภูเก็ตเน้นไปที่การรายงานตัวของนักศึกษา ซึ่งใช้ข้อมูลย้อนหลังของนักศึกษาที่เคยสมัครและรายงานตัวจริง นอกจากนี้งานวิจัยของมหาวิทยาลัยราชภัฏเชียงใหม่ใช้ตัวแปรด้านผลการเรียนเฉลี่ย (GPAX) เป็นหนึ่งในปัจจัยสำคัญในการพยากรณ์ ขณะที่งานวิจัยของมหาวิทยาลัยราชภัฏภูเก็ตเน้นไปที่ปัจจัยด้านภูมิศาสตร์ เช่น จังหวัดที่ผู้สมัครสำเร็จการศึกษา แบบจำลองการถดถอยโลจิสติกส์ ในทั้งสองงานวิจัยสามารถให้ค่าความน่าจะเป็นและค่า Odds Ratio ซึ่งช่วยให้เข้าใจอิทธิพลของตัวแปรที่มีผลต่อพฤติกรรมของนักศึกษาในการสมัครและรายงานตัวได้อย่างมีประสิทธิภาพ

III. ระเบียบวิธีวิจัย



ภาพที่ 1 กรอบแนวคิดในการวิจัย

การศึกษางานวิจัยครั้งนี้มีกระบวนการในการดำเนินงาน 4 ขั้นตอน ดังนี้

1. *การเก็บรวบรวมข้อมูล (Data Collection)*

เป็นการอาศัยข้อมูลจากระบบรับสมัครของมหาวิทยาลัยราชภัฏภูเก็ต คือข้อมูลย้อนหลังเกี่ยวกับการสมัครเข้าศึกษาต่อ ประกอบด้วย รหัสผู้สมัคร ชื่อผู้สมัคร เพศ คณะ สาขาวิชาที่สมัคร ประเภทการสมัคร ปีการศึกษา จังหวัดที่ผู้สมัครสำเร็จการศึกษา และ การรายงานตัว

2. *การทำความสะอาดข้อมูล (Data Cleansing)*

การทำความสะอาดข้อมูลเป็นการเตรียมข้อมูลก่อนนำไปใช้ในการวิเคราะห์การพยากรณ์ โดยมีการจัดการค่าที่ขาดหาย การตรวจสอบและกำจัดค่าซ้ำซ้อน ในขั้นตอนนี้ได้ตัดค่าข้อมูลของ รหัสผู้สมัคร ชื่อผู้สมัคร และปีการศึกษาออก เนื่องจากว่าไม่ได้เป็นปัจจัยที่สำคัญในการพยากรณ์โดยใช้แบบจำลองการถดถอยโลจิสติกส์ และในกระบวนการทำความสะอาดข้อมูลจะใช้ Python (Google Colab) สำหรับการประมวลผลและในการดำเนินการ

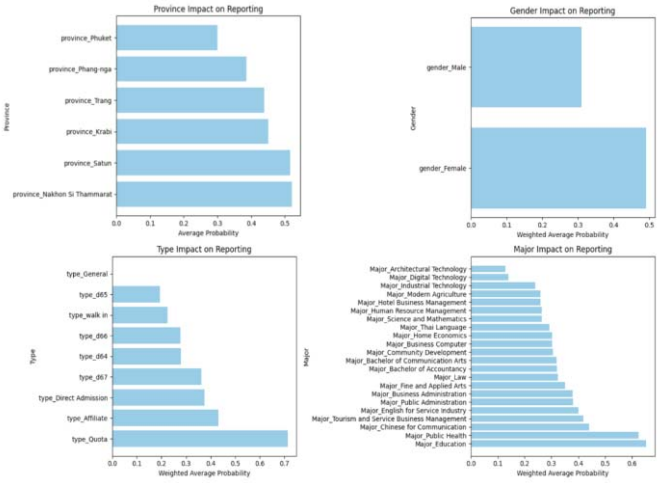
3. *การจัดเก็บข้อมูล (Data Store)*

ข้อมูลจัดเก็บไว้ในรูปแบบไฟล์ Excel ประกอบด้วยข้อมูล เพศ คณะ สาขาวิชาที่สมัคร ประเภทการสมัคร จังหวัดที่ผู้สมัครสำเร็จการศึกษา และการรายงานตัว

4. *การวิเคราะห์ข้อมูล (Data Analysis)*

กระบวนการวิเคราะห์ข้อมูลเริ่มต้นด้วยการเตรียมข้อมูล โดยใช้ Label Encoding แปลงค่าตัวแปรเป้าหมาย (การรายงานตัว) และ One-Hot Encoding สำหรับตัวแปรหมวดหมู่ เช่น เพศ จังหวัดที่จบการศึกษา คณะ สาขาวิชา และประเภทการรับสมัคร เพื่อให้โมเดลเรียนรู้ได้อย่างมีประสิทธิภาพ จากนั้นแบ่งข้อมูลเป็นชุดฝึกสอน (80%) และชุดทดสอบ (20%) พร้อมปรับขนาดข้อมูล Standard Scaler ลดความแตกต่างของช่วงค่า ก่อนสร้างแบบจำลองการถดถอยโลจิสติกส์ พร้อมจัดการกับความไม่

สมดุลของข้อมูล เมื่อโมเดลได้รับการฝึกแล้ว จะใช้พยากรณ์ผลและคำนวณค่าความน่าจะเป็น เพื่อวิเคราะห์โอกาสในการรายงานตัวของนักศึกษา ผลลัพธ์สามารถใช้ปรับปรุงการรับสมัคร นโยบายบริหารทรัพยากร และกลยุทธ์เพิ่มอัตราการรายงานตัว



IV. ผลการทดทดลอง

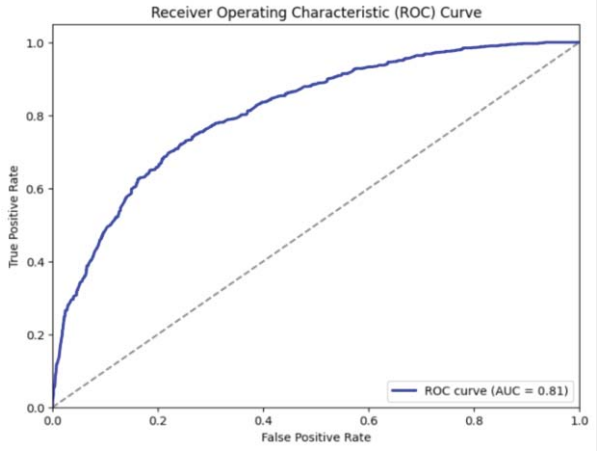
ภาพที่ 2 กราฟแสดงปัจจัยที่มีผลต่อการรายงานตัวของนักศึกษา

```
Accuracy Score: 0.7463576158940397
Confusion Matrix:
 [[1608  504]
 [ 262  646]]
Classification Report:
              precision    recall  f1-score   support

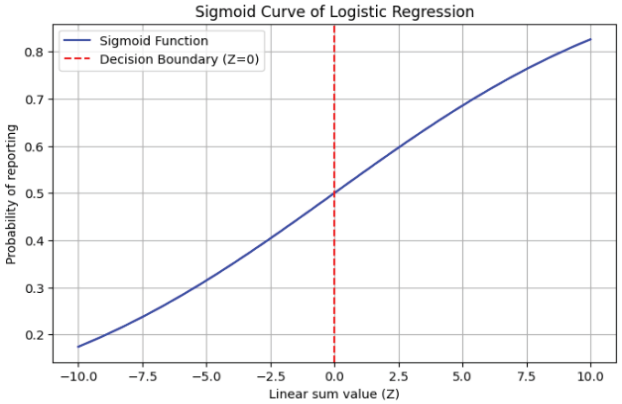
           0       0.86      0.76      0.81      2112
           1       0.56      0.71      0.63       908

    accuracy                           0.75      3020
   macro avg       0.71      0.74      0.72      3020
weighted avg       0.77      0.75      0.75      3020
```

ภาพที่ 3 ผลลัพธ์ Confusion Matrix



ภาพที่ 4 กราฟ ROC Curve



ภาพที่ 5 กราฟแบบจำลองการถดถอยโลจิสติกส์

V. อภิปรายผล

ผลการทดลองในการพยากรณ์การรายงานตัวของนักศึกษามหาวิทยาลัยราชภัฏภูเก็ตด้วยแบบจำลองการถดถอยโลจิสติกส์ พบว่าโมเดลมีความแม่นยำ 74.63% (อ้างอิงจากภาพที่ 3 ผลลัพธ์ Confusion Matrix) ซึ่งถือว่าน่าพอใจสำหรับการพยากรณ์การรายงานตัวและสามารถนำไปใช้ในทางปฏิบัติได้ ข้อมูลที่ใช้วิเคราะห์ประกอบด้วยตัวแปร เช่น เพศ จังหวัดที่ผู้สมัครสำเร็จการศึกษา คณะ สาขาวิชา และประเภทการรับสมัคร ซึ่งสะท้อนแนวโน้มการรายงานตัวของนักศึกษาได้ดี ผลลัพธ์นี้สามารถนำไปใช้ในการกำหนดกลุ่มเป้าหมายของการประชาสัมพันธ์หลักสูตรและปรับกลยุทธ์เพื่อเพิ่มอัตราการรายงานตัวในอนาคต

จาก Confusion Matrix (อ้างอิงจากภาพที่ 3 ผลลัพธ์ Confusion Matrix) โมเดลสามารถจำแนกนักศึกษาที่ไม่น่าจะรายงานตัวได้แม่นยำ โดยมีค่า True Negative (TN) 1,608 และ False Positive (FP) 504 ขณะที่ค่า True Positive (TP) 646 และ False Negative (FN) 262 แสดงให้เห็นว่าโมเดลทำนายกลุ่มที่มีแนวโน้มรายงานตัวได้ดีพอสมควร จาก Classification Report กลุ่มที่ไม่รายงานตัว (0) มีค่า Precision 0.86 และ Recall 0.76 สะท้อนความสามารถของโมเดลในการจำแนกกลุ่มนี้ได้ดี ส่วนกลุ่มที่รายงานตัว (1) มี Precision 0.56 และ Recall 0.71 โดยค่าเฉลี่ยถ่วงน้ำหนักของ F1-score อยู่ที่ 0.75 ซึ่งชี้ให้เห็นว่าโมเดลสามารถจำแนกข้อมูลได้ดีในระดับหนึ่ง

นอกจากนี้ ค่า AUC-ROC เท่ากับ 0.81 (อ้างอิงจากภาพที่ 4 กราฟ ROC Curve) แสดงว่าโมเดลสามารถแยกแยะระหว่างนักศึกษาที่จะรายงานตัวและไม่รายงานตัวได้อย่างมีประสิทธิภาพ โดยค่าที่ใกล้ 1 สะท้อนถึงศักยภาพที่ดีของโมเดลในการจำแนกกลุ่มเป้าหมาย

VI. ข้อสรุป

งานวิจัยนี้ศึกษาปัจจัยที่มีผลต่อการรายงานตัวของนักศึกษาระดับปริญญาตรีที่มหาวิทยาลัยราชภัฏภูเก็ต โดยใช้แบบจำลองการถดถอยโลจิสติกส์ ในการพยากรณ์โอกาสรายงานตัวของผู้สมัครตามปัจจัยต่าง ๆ ได้แก่ เพศ จังหวัดที่ผู้สมัครสำเร็จการศึกษา คณะ สาขาวิชา และประเภทการรับสมัคร ผลการวิเคราะห์พบว่าโมเดลมีความแม่นยำ 74.63% แสดงให้เห็นว่าสามารถใช้เป็นแนวทางสำหรับการวางแผนรับสมัครและบริหารทรัพยากรของมหาวิทยาลัยได้อย่างมีประสิทธิภาพ

จังหวัดที่ผู้สมัครสำเร็จการศึกษามีผลต่อการรายงานตัว โดยผู้สมัครจากจังหวัดนครศรีธรรมราชมีโอกาสรายงานตัวสูงสุดเป็นอันดับที่1 โดยมีความน่าจะเป็นอยู่ที่ 52.38% อันดับที่ 2 คือจังหวัดสตูล มีความน่าจะเป็นอยู่ที่ 51.17% อันดับที่ 3 จังหวัดกระบี่ มีความน่าจะเป็นอยู่ที่ 44.57% อันดับที่ 4 จังหวัดตรัง มีความน่าจะเป็นอยู่ที่ 43.06% และอันดับที่ 5 จังหวัดภูเก็ต มีความน่าจะเป็นอยู่ที่ 30.26% ตามลำดับ ในส่วนประเภทการรับสมัครพบว่าประเภทโควตามีโอกาสรายงานตัวสูงที่สุด สะท้อนถึงประสิทธิภาพของระบบโควตาในการดึงดูดนักศึกษาที่มีความสนใจในมหาวิทยาลัย ในทางตรงกันข้าม การรับสมัครแบบทั่วไปมีอัตราการรายงานตัวต่ำที่สุด อาจเป็นเพราะนักศึกษาส่วนใหญ่สมัครและยืนยันสิทธิ์ตั้งแต่รอบแรกแล้ว คณะที่เลือกเป็นอีกปัจจัยสำคัญ โดยพบว่าผู้สมัครในคณะครุศาสตร์มีแนวโน้มรายงานตัวสูงสุดเป็นอันดับที่1 โดยมีความน่าจะเป็นอยู่ที่ 65.9% อันดับที่ 2 คือคณะวิทยาศาสตร์และเทคโนโลยี มีความน่าจะเป็นอยู่ที่ 36.7% อันดับที่ 3 คือคณะมนุษยศาสตร์และสังคมศาสตร์ มีความน่าจะเป็นอยู่ที่ 34.6% อันดับที่ 4 คือคณะวิทยาการจัดการ มีความน่าจะเป็นอยู่ที่ 34.1% และอันดับที่ 5 คือคณะเทคโนโลยีการเกษตร มีแนวโน้มรายงานตัวต่ำที่สุด โดยมีความน่าจะเป็นอยู่ที่ 25.7% นอกจากนี้ พบว่าเพศของผู้สมัครมีผลต่อโอกาสรายงานตัว โดยนักศึกษาหญิงมีแนวโน้มรายงานตัวสูงกว่านักศึกษาชาย (อ้างอิงจากภาพที่ 2 กราฟแสดงปัจจัยที่มีผลต่อการรายงานตัวของนักศึกษา) ผลการวิจัยนี้สามารถนำไปใช้เป็นข้อมูลสนับสนุนเชิงนโยบายของมหาวิทยาลัยราชภัฏภูเก็ตในการการวางแผนการรับสมัคร ปรับปรุงนโยบายการบริหารทรัพยากรและออกแบบกลยุทธ์เพื่อเพิ่มอัตราการรายงานตัวของนักศึกษากลุ่มต่อไปให้สูงขึ้น

อ้างอิง

[1] ฐิตินันท์ อนุสรณ์ และสมชาย เล็กเจริญ, "การพยากรณ์การเลือกกลุ่มคณะวิชาในการศึกษาต่อในระดับปริญญาตรี ของมหาวิทยาลัยรังสิต โดยใช้เทคนิคการทำเหมืองข้อมูล," *วารสารรังสิตสารสนเทศ* 26, ฉบับที่ 1 (มกราคม – มิถุนายน 2563): 22.

[2] อนุทิตา เล็กเพชร และธวัชชัย งามสันติวงศ์, "การพยากรณ์การพ้นสภาพของนักศึกษาระดับปริญญาตรี โดยใช้การวิเคราะห์ถดถอยโลจิสติคเปรียบเทียบกับวิธีตรรกศาสตร์คลุมเครือ," *เอกสารการประชุมวิชาการแห่งชาติ มหาวิทยาลัยเกษตรศาสตร์ วิทยาเขตกำแพงแสน ครั้งที่10*, (ธันวาคม 2556): 1704.

[3] โสภณา สำราญ และศรัญญา ทองสุข, "การวิเคราะห์การถดถอยโลจิสติกส์ทวิภาคสำหรับความสัมพันธ์ การเลือกเรียนในระดับปริญญาตรีที่มหาวิทยาลัยราชภัฏพิบูลสงครามกับปัจจัยต่าง ๆ," *วารสาร Life Sciences and Environment Journal* ปีที่ 23 ฉบับที่ 2 (กรกฎาคม - ธันวาคม 2565): 306.

[4] P. Thanapatpisarn, "[Data Scientist Model EP.03] Logistic Regression โมเดลเริ่มต้นสำหรับการทำนายผลแบบ Classification Part 1," *Medium*, 1 ม.ค. 2568. [ออนไลน์]. เข้าถึงได้จาก: https://datascihaeng.medium.com/data-science-model-03-d06385d789f7

การพยากรณ์แนวโน้มจำนวนผู้สมัครเรียนระดับปริญญาตรี มหาลัยราชภัฏภูเก็ตโดยวิธีการถดถอยเชิงเส้น

Forecasting the Trend of Undergraduate Applications at Phuket Rajabhat University using the Linear regression

1st Sakuna Choochangwang
Faculty of Science and Technology
Digital Technology Program
Phuket Rajabhat University
Phuket, Thailand.
s6511423129@pkru.ac.th

2nd Aricha Tabmuenwai
Faculty of Science and Technology
Digital Technology Program
Phuket Rajabhat University
Phuket, Thailand.
s6511423133@pkru.ac.th

3rd Attapon Pillai
Faculty of Science and Technology
Digital Technology Program
Phuket Rajabhat University
Phuket, Thailand.
attapon.p@pkru.ac.th

4th Urairat Makchan
Faculty of Science and Technology
Digital Technology Program
Phuket Rajabhat University
Phuket, Thailand.
urairat.m@pkru.ac.th

Abstract

This research aims to: (1) forecast the trend of undergraduate applications at Phuket Rajabhat University and (2) support planning and resource management for the university's teaching and learning processes. The study employs linear regression analysis, utilizing historical application data from the academic years 2020 to 2024. The selected variables include the independent variable, which is the academic year, and the dependent variable, which is the number of applicants for each admission category: Walk-in, General Selection, Affiliated Programs, Direct Admission, and Quota. The model's performance is evaluated based on statistical accuracy. The findings indicate that the linear regression model accurately forecasts application trends, revealing variations across different applicant groups. Moreover, the projections for the next three years suggest a continuous increase in the number of applicants. The results of this research can serve as a guideline for policy development in student admissions and assist in the optimal allocation of resources for prospective students. Furthermore, the findings contribute to the development of more precise forecasting models in the future.

***Keywords**: Trend Forecasting, University Applications, Linear Regression, Rajabhat University*

I. บทนำ

การศึกษาระดับปริญญาตรีเป็นบทบาทสำคัญในการพัฒนาทรัพยากรมนุษย์และเสริมสร้างศักยภาพของเยาวชน ทั้งยังเป็นกลไกสำคัญในการสนับสนุนเศรษฐกิจและสังคมของประเทศไทย มหาวิทยาลัยราชภัฏภูเก็ตเป็นสถาบันการศึกษาชั้นนำในภาคใต้ของประเทศไทย มีบทบาทสำคัญในการผลิตบัณฑิตที่ตอบสนองต่อความต้องการของตลาดแรงงาน อย่างไรก็ตาม การคาดการณ์จำนวนของผู้เข้ามาสมัครเรียนเป็นส่วนหนึ่งที่มีส่วนช่วยในเรื่องของการบริหารจัดการทรัพยากรของมหาวิทยาลัยซึ่งการคาดการณ์ก็จำเป็นต้องอาศัยข้อมูลที่ถูกต้องเพื่อคาดการณ์แนวโน้มจำนวนผู้สมัครเรียนได้อย่างแม่นยำ

ปัจจุบันมหาวิทยาลัยราชภัฏภูเก็ตเผชิญกับความท้าทายในการคาดการณ์จำนวนผู้สมัครเข้าศึกษาต่อ เนื่องจากมีปัจจัยหลายประการที่ส่งผลต่อการตัดสินใจของผู้สมัคร เช่น สภาวะเศรษฐกิจ การเปลี่ยนแปลงตลาดแรงงาน และความนิยมในสาขาวิชาต่างๆ ความไม่แน่นอนที่อาจส่งผลกระทบต่อการวางแผนการบริหารจัดการทรัพยากรภายในมหาวิทยาลัย เช่น การจัดสรรจำนวนอาจารย์ ห้องเรียน และอุปกรณ์การเรียนการสอนให้มีประสิทธิภาพ งานวิจัยนี้มีวัตถุประสงค์เพื่อพยากรณ์แนวโน้มการสมัครเข้าศึกษาต่อระดับปริญญาตรีของมหาวิทยาลัยราชภัฏภูเก็ต โดยใช้วิธีการวิเคราะห์การถดถอยเชิงเส้น (Linear Regression) ซึ่งเป็นเครื่องมือที่ได้รับการยอมรับในการวิเคราะห์ความสัมพันธ์ระหว่างตัวแปรต่าง ๆ และใช้ในการคาดการณ์แนวโน้มของผู้สมัครในอนาคต การวิจัยนี้มุ่งหวังที่จะสนับสนุนการวางแผนและการจัดสรรทรัพยากรของมหาวิทยาลัยได้อย่างมีประสิทธิภาพ โดยเฉพาะในด้านการจัดสรรจำนวนอาจารย์และบุคลากรทางการศึกษา เพื่อวางแผนจำนวนอาจารย์ให้เหมาะสมกับจำนวนผู้สมัคร ห้องเรียนและอุปกรณ์การเรียนการสอน เพื่อจัดงบประมาณสำหรับการพัฒนาโครงสร้างพื้นฐานในการสนับสนุนการเรียนการสอน โดยมีกรอบแนวคิดดังภาพที่ 1



Fig.1. กรอบแนวคิดในการวิจัย

II. ทบทวนวรรณกรรม

[1] พลาพร ไชยเมือง,รัฐพล ภู่บุบผาพันธุ์.(2563) งานวิจัยนี้มีการพัฒนาแบบจำลองการถดถอยเชิงเส้นแบบพหุคูณ (Multiple Linear Regression) เพื่อคาดการณ์ปริมาณจราจรที่บริเวณทางแยกสัญญาณไฟจราจร โดยใช้ข้อมูลกิจกรรมภายในมหาวิทยาลัยเทคโนโลยีสุรนารี เช่น ตารางเรียน จำนวนผู้เรียน เวลาเข้าและเลิกเรียน รวมถึงช่วงเวลาพักระหว่างคาบเรียน ซึ่งมีผลกระทบต่อการแปรผันของปริมาณจราจรในช่วงเวลาต่าง ๆ

ของวัน ผลการวิจัยพบว่า แบบจำลองนี้สามารถคาดการณ์ปริมาณจราจรได้อย่างแม่นยำกว่าวิธีค่าเฉลี่ย (Average Method) โดยสามารถพิจารณาปัจจัยที่มีผลต่อปริมาณจราจรได้ชัดเจน เช่น จำนวนผู้เรียนที่กำลังเข้าเรียนหรือเลิกเรียนในช่วงเวลาใด ๆ และช่วงเวลาที่มีการเดินทางมากที่สุด การใช้แบบจำลองนี้ไม่เพียงแต่ช่วยเพิ่มความแม่นยำในการคาดการณ์ปริมาณจราจร แต่ยังช่วยให้การตั้งค่าระบบสัญญาณไฟจราจรในอนาคตมีความเหมาะสมมากขึ้น

[2] นางสุนันท์ มีเทศ และคณะ.(2556) การพยากรณ์ผลสัมฤทธิ์ทางการเรียน ของนักศึกษาในระดับประกาศนียบัตร ผู้ช่วยพยาบาล คณะแพทยศาสตร์ ศิริราชพยาบาล มหาวิทยาลัยมหิดล มุ่งศึกษาการพยากรณ์ผลสัมฤทธิ์ทางการเรียนของนักศึกษาในระดับประกาศนียบัตรผู้ช่วยพยาบาล คณะแพทยศาสตร์ศิริราชพยาบาล มหาวิทยาลัยมหิดล โดยเก็บข้อมูลจากนักศึกษาที่เข้าเรียนระหว่างปี 2551-2555 จำนวน 656 คน ตัวแปรที่ใช้ในการศึกษาประกอบด้วย คะแนนเฉลี่ยมัธยมปลาย (GPAM6), เพศ, ศาสนา, ภูมิลำเนา, ประเภทโรงเรียน, สาขาที่จบมัธยมปลาย, ปีการศึกษาที่เข้าเรียน, รายได้ผู้ปกครอง, และคะแนนสอบ O-NET ในวิชาต่างๆ ผลการวิจัยพบว่าปัจจัยที่สามารถพยากรณ์ผลสัมฤทธิ์ทางการเรียนได้อย่างมีนัยสำคัญมากที่สุด คือ คะแนนเฉลี่ยมัธยมปลาย (GPAM6) ซึ่งมีค่าสัมประสิทธิ์สูงสุด รองลงมาคือปีการศึกษาที่เข้าเรียน และคะแนนสอบ O-NET ในวิชาภาษาไทยและวิทยาศาสตร์ โดยปัจจัยเหล่านี้สามารถอธิบายความแปรปรวนของผลสัมฤทธิ์ทางการเรียนได้ 37.9% ในขณะที่ตัวแปรบางตัว เช่น ประเภทของโรงเรียนและรายได้ของผู้ปกครอง ไม่แสดงความสัมพันธ์อย่างมีนัยสำคัญกับผลสัมฤทธิ์ทางการเรียนในระดับประกาศนียบัตรผู้ช่วยพยาบาล คะแนนผลสัมฤทธิ์ทางการเรียนในระดับมัธยมปลายและคะแนนสอบ O-NET ในวิชาสำคัญมีบทบาทสำคัญในการพยากรณ์ความสำเร็จทางการเรียนในหลักสูตรผู้ช่วยพยาบาล ข้อมูลที่ได้จากการวิจัยนี้สามารถนำไปใช้ในการปรับปรุงกระบวนการคัดเลือกนักศึกษา รวมถึงการปรับปรุงแนวทางการสอนและการพัฒนาในอนาคตได้อย่างมีประสิทธิภาพ

[3] เปรมวดี อาวุธกรรมปรีชา.(2564) การพยากรณ์จำนวนผู้สมัครเข้าศึกษาต่อระดับบัณฑิตศึกษา กรณีศึกษามหาวิทยาลัยเทคโนโลยีพระจอมเกล้าพระนครเหนือ โดยมีวัตถุประสงค์เพื่อสร้างตัวแบบการพยากรณ์ที่เหมาะสมที่สุดสำหรับจำนวนผู้สมัครเข้าศึกษาต่อระดับบัณฑิตศึกษา โดยใช้วิธีการของบอกซ์-เจนกินส์ (Box-Jenkins) สำหรับการพยากรณ์ในระดับปริญญาโทและปริญญาเอก ในการวิจัยนี้มีจำนวนกลุ่มตัวอย่าง 38 คน ซึ่งเป็นจำนวนผู้สมัครเข้าศึกษาต่อในภาคเรียน 1 และภาคเรียนที่ 2 ของปีการศึกษา 2555-2564 ผลการศึกษาพบว่า ตัวแบบที่เหมาะสมที่สุดสำหรับการพยากรณ์จำนวนผู้สมัครระดับปริญญาโทคือ AMIRA (1,1,4) และสำหรับระดับปริญญาเอกคือ ARIMA (0,1,4) ผลการพยากรณ์ในปีการศึกษา 2565 พบว่า จำนวนผู้สมัครปริญญาโทคาดการณ์ไว้ที่ 589 คน และปริญญาเอกมีจำนวน 71 คน ผลการวิจัยแสดงให้เห็นแนวโน้มจำนวนผู้สมัครลดลง โดยเฉพาะในระดับปริญญาโทที่มีการเปลี่ยนแปลงเชิงลบชัดเจนในช่วงเวลาที่พยากรณ์ นอกจากนี้ ตัวแบบที่พัฒนาขึ้นสามารถนำไปใช้ปรับปรุงการจัดการรับสมัคร การวางแผนจัดงบประมาณ และการประชาสัมพันธ์หลักสูตรให้เหมาะสมยิ่งขึ้น ข้อเสนอแนะในการศึกษาครั้งนี้รวมถึงการเพิ่มตัวแปรภายนอกที่อาจส่งผลต่อการพยากรณ์ เช่น สภาพเศรษฐกิจหรือความต้องการแรงงานในตลาด เพื่อเพิ่มความแม่นยำของผลลัพธ์

งานวิจัยเรื่อง การพยากรณ์แนวโน้มการสมัครเรียนระดับปริญญาตรีของมหาวิทยาลัยราชภัฏภูเก็ตด้วยวิธีการถดถอยเชิงเส้น (Linear Regression) [4] มีจุดมุ่งหมายเพื่อช่วยให้มหาวิทยาลัยสามารถคาดการณ์แนวโน้มการสมัครเรียนได้อย่างแม่นยำ อันจะนำไปสู่การวางแผนจัดสรรทรัพยากรได้อย่างมีประสิทธิภาพ งานวิจัยนี้มีแนวทางคล้ายคลึงและแตกต่างจากงานวิจัยอื่น ๆ ที่ศึกษาการพยากรณ์ในลักษณะเดียวกัน โดยเฉพาะสามงานที่เกี่ยวข้อง ได้แก่ งานของพลาพร ไชยเมือง และรัฐพล ภู่บุบผาพันธุ์ (2563) งานของสุนันท์ มีเทศ และคณะ (2556) และงานของเปรมวดี อาวุธกรรมปรีชา (2564) ซึ่งแต่ละงานมีแนวทางการศึกษาที่แตกต่างกันไปตามวัตถุประสงค์ของงานวิจัย

III. ระเบียบวิธีวิจัย

การวิจัยนี้ดำเนินการตามขั้นตอนและระเบียบวิธีที่ออกแบบมาอย่างเป็นระบบ เพื่อให้ได้มาซึ่งข้อมูลที่น่าเชื่อถือและผลการวิเคราะห์ที่ถูกต้อง ในส่วนนี้ จะอธิบายถึงกระบวนการวิจัยทั้งหมด ตั้งแต่การเก็บรวบรวมข้อมูล การวิเคราะห์ข้อมูล ไปจนถึงการตีความผลการวิจัย โดยมีรายละเอียดดังนี้

1. การเก็บรวบรวมข้อมูล (Data Collection) การเก็บข้อมูลโดยเก็บจากระบบรับสมัครของมหาวิทยาลัยราชภัฏภูเก็ตและเว็บไซต์โรงเรียน ข้อมูลจากระบบรับสมัครประกอบด้วย ปีการศึกษา ประเภทการสมัคร ข้อมูลเหล่านี้ถูกนำมาวิเคราะห์เพื่อศึกษาปัจจัยที่มีผลต่อแนวโน้มการสมัครเรียนในระดับอุดมศึกษา และใช้ในการพยากรณ์และวางแผนเชิงกลยุทธ์เพื่อเพิ่มประสิทธิภาพการจัดการของมหาวิทยาลัย

2. การทำความสะอาดข้อมูล (Data Cleansing) ขั้นตอนสำคัญในการเตรียมข้อมูลก่อนนำไปใช้วิเคราะห์แนวโน้มและพยากรณ์ในวิธีการถดถอยเชิงเส้น ในงานวิจัยนี้จะใช้ Python (Google Collab) เพื่อทำความสะอาดข้อมูล และใช้ Excel เพื่อจัดเรียงข้อมูลให้เหมาะสม โดยตรวจสอบค่าที่หายไปในแต่ละคอลัมน์ของชุดข้อมูล ใช้วิธี Forward Fill หรือ Backward Fill เพื่อเติมค่าที่ขาดหาย หากมีข้อมูลที่ขาดหายมาก อาจต้องลบข้อมูลส่วนนั้นออกไป การใช้ Filter ใน Excel เพื่อตรวจสอบเซลล์ที่ว่างเปล่า และ ใช้ Sort & Filter เพื่อตรวจสอบค่าที่ซ้ำซ้อน การตรวจหาค่าผิดปกติ หากพบค่าผิดปกติ อาจใช้ Mean หรือ Median เพื่อแทนที่ หรือเลือกตัดข้อมูลทิ้ง ใช้ Sort by A-Z เพื่อเรียงลำดับรหัสผู้สมัครเข้ามหาวิทยาลัยราชภัฏภูเก็ต

3. การจัดเก็บข้อมูล (Data Store) ข้อมูลถูกจัดเก็บในรูปแบบไฟล์ Excel (.xlsx) โดยมีโครงสร้างแบบตาราง ซึ่งประกอบด้วยตัวแปรอิสระ และตัวแปรตาม ข้อมูลเหล่านี้จะถูกนำไปใช้ในกระบวนการวิธีการถดถอยเชิงเส้น เพื่อสร้างโมเดลทางสถิติที่สามารถอธิบายและพยากรณ์ความสัมพันธ์ระหว่างตัวแปรต่าง ๆ โดยใช้ไลบรารี pandas ในภาษา Python เพื่อนำเข้าข้อมูล จากนั้นทำการตรวจสอบและปรับข้อมูลให้พร้อมสำหรับการวิเคราะห์ ก่อนที่จะใช้เทคนิคการถดถอยเชิงเส้น เพื่อสร้างโมเดล ข้อมูลที่จัดเก็บในรูปแบบ Excel หรือ CSV ช่วยให้การจัดการและวิเคราะห์ข้อมูลเป็นไปอย่างมีประสิทธิภาพและแม่นยำ

4. การวิเคราะห์ข้อมูล (Data Analysis) การวิเคราะห์ข้อมูลใช้การถดถอยเชิงเส้น (Simple Linear Regression) เพื่อคาดการณ์แนวโน้มจำนวน

ผู้สมัครเรียนระดับปริญญาตรีของมหาวิทยาลัยราชภัฏภูเก็ต โดยใช้ปีการศึกษาเป็นตัวแปรอิสระ (X) และจำนวนผู้สมัครเป็นตัวแปรตาม (Y) ในช่วงปี 2563-2567 ข้อมูลถูกจัดเตรียมใน DataFrame ของ Python และใช้ฟังก์ชัน LinearRegression().fit(X, Y) เพื่อสร้างโมเดล โมเดลได้รับการประเมินความแม่นยำโดยใช้ค่า R^2 Score, ค่า Mean Absolute Error (MAE) เพื่อวัดความคลาดเคลื่อน และวิเคราะห์ค่าความชัน (Coefficient) และค่า Intercept เพื่อตรวจสอบแนวโน้มการเปลี่ยนแปลงของจำนวนผู้สมัครโมเดลที่ได้ถูกนำไปใช้ในการคาดการณ์จำนวนผู้สมัครในอนาคตสำหรับปี 2568-2570 และทำการปรับค่าพยากรณ์ให้เหมาะสมโดยกำหนดค่าต่ำสุดเป็น 0 เพื่อป้องกันค่าพยากรณ์ติดลบ ผลลัพธ์การวิเคราะห์เพื่อพยากรณ์แนวโน้มจำนวนผู้สมัครในอนาคต ใช้สมการเชิงเส้นพื้นฐาน ซึ่งมีสมการพื้นฐาน (1) ดังนี้ Y คือ จำนวนผู้สมัครที่ต้องการพยากรณ์ X คือ ปีการศึกษา (2563-2567) b0 คือ ค่า Intercept b1 คือ ค่าความชันของเส้นพยากรณ์ การพยากรณ์นี้ครอบคลุมประเภทการรับสมัคร ได้แก่ Walk-in, คัดเลือกทั่วไป, ภาคี, รับตรง, โควตา และรวมจำนวนผู้สมัครทั้งหมดในแต่ละปี ผลลัพธ์เพื่อแสดงแนวโน้มการเปลี่ยนแปลงของจำนวนผู้สมัครในแต่ละประเภท ช่วยในการวางแผนการรับสมัครนักศึกษาในอนาคตได้อย่างมีประสิทธิภาพ ผลลัพธ์การพยากรณ์ถูกแสดงในรูปแบบกราฟ Fig.3

เครื่องมือที่ใช้ในงานวิจัย

การวิเคราะห์นี้ใช้ การถดถอยเชิงเส้น(Linear Regression) เพื่อพยากรณ์แนวโน้มจำนวนผู้สมัครเรียนระดับปริญญาตรีของมหาวิทยาลัยราชภัฏภูเก็ต โดยใช้ข้อมูลจำนวนผู้สมัครในช่วงปี 2563-2567 เครื่องมือที่ใช้ในการวิเคราะห์ข้อมูล 1) เครื่องมือในการเก็บข้อมูล ระบบรับสมัครของมหาวิทยาลัยราชภัฏภูเก็ต ใช้สำหรับเก็บข้อมูลประเภทการสมัคร คณะ และสาขาวิชา ข้อมูลถูกดึงออกมาในรูปแบบ Excel (.xlsx) หรือ CSV เว็บไซต์ของโรงเรียน ใช้เพื่อเก็บข้อมูลเกี่ยวกับชื่อโรงเรียน ที่ตั้ง และจำนวนนักเรียนที่สำเร็จการศึกษาแต่ละปี 2) เครื่องมือในการทำความสะอาดข้อมูล Microsoft Excel ใช้สำหรับตรวจสอบข้อมูลที่ขาดหาย ลบข้อมูลซ้ำซ้อน และกรองข้อมูล Google Colab (Python) ใช้ ใช้เพื่อทำการทำความสะอาดข้อมูลที่ซับซ้อนกว่า โดยเฉพาะการจัดการข้อมูลที่มีขนาดใหญ่หรือมีลักษณะพิเศษ เช่น ข้อมูลที่หายไป หรือข้อมูลที่ผิดปกติ ใช้เครื่องมือ Pandas สำหรับจัดการข้อมูล และMatplotlib/Seaborn เพื่อตรวจหาค่าผิดปกติ เครื่องมือในการวิเคราะห์ 3) ข้อมูล Python ผ่าน Google Colab ใช้เทคนิค Simple Linear Regression (SLR) เพื่อวิเคราะห์แนวโน้มข้อมูล Libraries ที่ใช้ Pandas สำหรับการจัดการข้อมูล NumPy สำหรับการคำนวณทางคณิตศาสตร์ Matplotlib และ Seaborn สำหรับการสร้างกราฟ Scikit-learn สำหรับสร้างและฝึกฝนโมเดล 4) เครื่องมือในการแสดงผล Google Colab (Python) ใช้ Matplotlib และ Seaborn ในการสร้างกราฟเช่น Scatter Plot และ Line Chart เครื่องมือในการประเมินผล (Evaluation Tools) Scikit-learn ใช้สำหรับคำนวณค่าความแม่นยำของโมเดล เช่น Mean Absolute Error (MAE), Root Mean Squared Error (RMSE) และ R^2 Score สมการใช้ดังต่อไปนี้ สมการเชิงเส้นพื้นฐาน

$$Y = b0 + b1X \qquad (1)$$

IV. ผลการทดลอง



Fig.2. กราฟแสดงผลการพยากรณ์จำนวนผู้สมัครในแต่ละรอบสมัคร

จากภาพที่ 2. (Fig.2) กราฟแสดงผลการพยากรณ์จำนวนผู้สมัครในแต่ละรอบการสมัคร เป็นการวิจัยที่ใช้ Simple Linear Regression Model เพื่อพยากรณ์แนวโน้มจำนวนผู้สมัครเข้าเรียนระดับปริญญาตรีที่มหาวิทยาลัยราชภัฏภูเก็ตในระหว่างปีการศึกษา 2563-2570 โดยแบ่งผู้สมัครออกเป็น 5 ประเภท ได้แก่ Walk-in, คัดเลือกทั่วไป, ภาคี, รับตรง และโควตา ผลการวิเคราะห์พบว่า ประเภท Walk-in มีแนวโน้มเพิ่มขึ้นเล็กน้อย ประเภทคัดเลือกทั่วไปมีแนวโน้มเพิ่มขึ้นในอัตราปานกลาง ประเภทภาคีมีแนวโน้มเพิ่มขึ้นในอัตราที่สูง ประเภทรับตรงมีแนวโน้มสูงที่สุดเมื่อเปรียบเทียบกับทุกประเภท และมีอัตราการเติบโตเพิ่มขึ้นทุกปี ขณะที่ประเภทโควตามีแนวโน้มลดลงอย่างต่อเนื่อง การใช้เส้นแนวโน้มจากการพยากรณ์ทำให้เห็นได้ชัดว่าแต่ละประเภทมีการเปลี่ยนแปลงที่แตกต่างกันไป การวิเคราะห์ภาพรวมของกราฟ จุดที่อยู่บนกราฟแทนจำนวนผู้สมัครจริงที่รวบรวมมาในแต่ละปี เส้นแนวโน้มแต่ละสีเป็นเส้นที่ได้จาก Simple Linear โดย Walk-in มีแนวโน้มเพิ่มขึ้นเล็กน้อย ค่า R^2 Score อยู่ที่ 0.0165 ซึ่งหมายความว่าโมเดลไม่สามารถอธิบายแนวโน้มของข้อมูลได้ดี และคาดการณ์จำนวนผู้สมัครในปี 2568-2570 อยู่ที่ 622, 631 และ 640 คน ส่วนประเภทคัดเลือกทั่วไปมีแนวโน้มเพิ่มขึ้นในอัตราปานกลาง ค่า R^2 Score = 0.2199 และคาดการณ์จำนวนผู้สมัครในปี 2568-2570 อยู่ที่ 400, 436 และ 472 คน ขณะที่ประเภทภาคีมีแนวโน้มเพิ่มขึ้นในอัตราที่สูงกว่า Walk-in และคัดเลือกทั่วไป โดยค่า R^2 Score = 0.3830 และคาดการณ์จำนวนผู้สมัครในปี 2568-2570 อยู่ที่ 619, 705 และ 790 คน สำหรับประเภทรับตรง โมเดลสามารถอธิบายแนวโน้มได้ดี โดยค่า R^2 Score = 0.7215 ซึ่งหมายถึงมีการเติบโตของจำนวนผู้สมัครสูงสุด และคาดการณ์จำนวนผู้สมัครในปี 2568-2570 อยู่ที่ 1,281, 1,472 และ 1,664 คน ส่วนประเภทโควตามีแนวโน้มลดลง ค่า R^2 Score = 0.0146 และคาดการณ์จำนวนผู้สมัครในปี 2568-2570 อยู่ที่ 113, 95 และ 77 คน ตามลำดับ

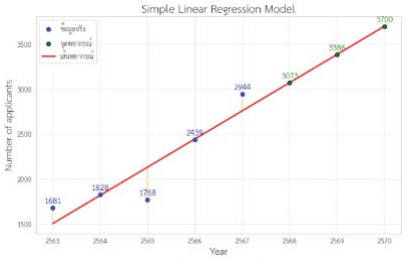


Fig.3. กราฟแสดงผลการพยากรณ์จำนวนผู้สมัครในปีการศึกษา 2563-2570

จากภาพที่ 3 (Fig3.) กราฟแสดงผลลัพธ์ของ Simple Linear Regression Model ในการพยากรณ์จำนวนผู้สมัครตั้งแต่ปี 2563-2570 จุดสีน้ำเงินแสดงจำนวนผู้สมัครจริง จุดสีเขียวแสดงค่าพยากรณ์จากโมเดล และเส้นสีแดงแสดงเส้นแนวโน้มจากการใช้ Simple Linear Regression เพื่อแสดงทิศทางในอนาคต โดยผลลัพธ์จากการพยากรณ์จำนวนผู้สมัครในปี

การศึกษา 2568 คาดการณ์จำนวนผู้สมัครที่ 3,073 คน ปีการศึกษา 2569 คาดการณ์จำนวนผู้สมัครที่ 3,387 คน ปีการศึกษา 2570 คาดการณ์จำนวนผู้สมัครที่ 3,700 คน จากการวิเคราะห์ข้อมูลพบว่า ความแม่นยำของโมเดล ค่า R^2 Score เท่ากับ 0.8326 แสดงว่าโมเดลสามารถอธิบายแนวโน้มของข้อมูลได้ประมาณ 83.26% ซึ่งถือว่าเป็นโมเดลที่มีประสิทธิภาพค่อนข้างดีค่าความคลาดเคลื่อน ค่า Mean Absolute Error (MAE) เท่ากับ 148.28 หมายความว่าค่าเฉลี่ยของข้อผิดพลาดระหว่างค่าจริงและค่าที่พยากรณ์มีค่าเบี่ยงเบนประมาณ 148 คน ค่าสัมประสิทธิ์ของโมเดลอยู่ที่ 313.7 ซึ่งหมายความว่า ทุก ๆ 1 ปีที่เพิ่มขึ้น จำนวนผู้สมัครจะเพิ่มขึ้นเฉลี่ย 313.7 คน จำนวนผู้สมัครในปี 2563 มี 1,681 คน และคาดการณ์ว่าในปี 2570 จะเพิ่มขึ้นเป็น 3,700 คน การพยากรณ์จำนวนผู้สมัครในอนาคต กราฟแสดงแนวโน้มการเติบโตของผู้สมัคร และโมเดลพยากรณ์ได้แม่นยำ แต่ค่าความคลาดเคลื่อนอาจมาจากปัจจัยอื่น ๆ ที่ไม่ได้รวมในโมเดล

V. อภิปรายผล

การวิเคราะห์การพยากรณ์จำนวนผู้สมัครเข้าเรียนระดับปริญญาตรีที่มหาวิทยาลัยราชภัฏภูเก็ตโดยใช้การถดถอยเชิงเส้น (Linear Regression) พบว่าแนวโน้มของจำนวนผู้สมัครมีการเพิ่มขึ้นอย่างต่อเนื่องในช่วงปีการศึกษา 2563–2570 ประเภท Walk-in มีแนวโน้มเพิ่มขึ้นเพียงเล็กน้อย โดยมีอัตราการเพิ่มขึ้นเฉลี่ย 9.2 คนต่อปี แต่โมเดลมีความแม่นยำต่ำ (R^2 = 0.0165) ประเภทคัดเลือกทั่วไปมีแนวโน้มเพิ่มขึ้นในระดับปานกลาง โดยจำนวนผู้สมัครเพิ่มขึ้นประมาณ 36 คนต่อปี และประเภทภาคีแสดงการเติบโตที่ชัดเจนกว่า Walk-in และคัดเลือกทั่วไป โดยเพิ่มขึ้น 85 คนต่อปี โมเดลอธิบายข้อมูลได้ในระดับปานกลาง (R^2 = 0.3830) ประเภทรับตรงมีการเติบโตสูงที่สุด โดยเพิ่มขึ้น 191 คนต่อปี และโมเดลมีความแม่นยำสูงสุด (R^2 = 0.7215) สะท้อนการรับตรงเป็นช่องทางที่ได้รับความนิยมในอนาคต ส่วนประเภทโควตาเป็นประเภทเดียวที่มีแนวโน้มลดลง โดยลดลงเฉลี่ย 18 คนต่อปี และมีค่า R^2 ต่ำ (0.0146) ซึ่งแสดงว่าอาจมีปัจจัยอื่นที่ส่งผลต่อการลดลงนี้ จากการพยากรณ์จำนวนผู้สมัครในปี 2568-2570 โดยการใช้ Simple Linear Regression พบว่าอัตราการเพิ่มขึ้นเฉลี่ยคือ 313.7 คนต่อปี และจำนวนผู้สมัครคาดว่าจะเพิ่มจาก 1,681 คนในปี 2563 เป็น 3,700 คนในปี 2570 การเปรียบเทียบกับงานวิจัยอื่นๆ เช่น งานของพลาพร ไชยเมือง และรัฐพล ภู่บุบผาพันธุ์ (2563) ที่ใช้ Multiple Linear Regression แสดงให้เห็นว่าแบบจำลองที่ใช้หลายตัวแปรจะมีความแม่นยำสูงกว่า ในขณะที่งานวิจัยนี้ใช้แค่ Simple Linear Regression ซึ่งอาจมีข้อจำกัดในการวิเคราะห์ปัจจัยที่ซับซ้อน งานวิจัยของเปรมวดี อาวุธกรรมปรีชา (2564) ที่ใช้ ARIMA Model ก็แสดงว่าการใช้ข้อมูลอนุกรมเวลาอาจช่วยเพิ่มความแม่นยำมากกว่าแบบจำลองเชิงเส้นเพียงอย่างเดียว ข้อได้เปรียบของการวิจัยนี้คือการใช้ Simple Linear Regression ที่เข้าใจง่ายและเหมาะสมกับข้อมูลที่มีแนวโน้มเชิงเส้น ช่วยสนับสนุนการวางแผนและกำหนดนโยบายรับสมัครของมหาวิทยาลัย ข้อจำกัดคือไม่ได้รวมปัจจัยอื่นๆ ที่อาจมีผลต่อจำนวนผู้สมัคร ข้อมูลย้อนหลังที่ใช้มีจำกัดเพียง 5 ปี ซึ่งอาจไม่เพียงพอสำหรับการพยากรณ์ระยะยาว

VI. ข้อสรุป

งานวิจัยนี้ใช้ แบบจำลองการถดถอยเชิงเส้น (Linear Regression) เพื่อพยากรณ์แนวโน้มการสมัครเรียนระดับปริญญาตรีของมหาวิทยาลัยราชภัฏภูเก็ต ผลการศึกษาพบว่า จำนวนผู้สมัครมีแนวโน้มเพิ่มขึ้นอย่างต่อเนื่อง ซึ่งสามารถนำไปใช้เป็นข้อมูลสนับสนุนการวางแผนการรับสมัครและบริหารทรัพยากรของมหาวิทยาลัยให้มีประสิทธิภาพมากขึ้น อย่างไรก็ตาม แบบจำลองที่ใช้ยังมีข้อจำกัด เนื่องจากพิจารณาเพียงตัวแปรปีการศึกษา โดยไม่ได้รวมปัจจัยอื่น ๆ เช่น นโยบายภาครัฐ สภาพเศรษฐกิจ และแนวโน้มตลาดแรงงาน ซึ่งอาจส่งผลกระทบต่อจำนวนผู้สมัครในอนาคต นอกจากนี้ ช่วงเวลาของข้อมูลที่ใช้มีเพียง 5 ปี ซึ่งอาจยังไม่ครอบคลุมแนวโน้มในระยะยาว แนวทางการพัฒนาในอนาคต เพื่อเพิ่มความแม่นยำของการพยากรณ์ งานวิจัยในอนาคตอาจพิจารณาใช้ Multiple Linear Regression เพื่อรวมปัจจัยเพิ่มเติมที่อาจมีผลต่อจำนวนผู้สมัคร นอกจากนี้ การใช้ Time Series Analysis เช่น ARIMA หรือ Exponential Smoothing อาจช่วยให้การพยากรณ์แนวโน้มในระยะยาวมีความแม่นยำยิ่งขึ้น ผลการศึกษานี้สามารถเป็นแนวทางในการปรับปรุงกระบวนการรับสมัครของมหาวิทยาลัย และเป็นพื้นฐานสำหรับการพัฒนาแบบจำลองที่มีประสิทธิภาพมากขึ้นในอนาคต

อ้างอิง

[1] พลาพร ไชยเมือง, รัฐพล ภู่บุบผาพันธุ์. แบบจำลองการถดถอยเชิงเส้นแบบพหุคุณสำหรับคาดการณ์ปริมาณจราจรบริเวณทางแยกสัญญาณไฟจราจรโดยใช้ข้อมูลกิจกรรมในพื้นที่. วารสารวิศวกรรมศาสตร์ มหาวิทยาลัยอุบลราชธานี. ปีที่ 14, ฉบับที่ 2, หน้า 126-134, 2563.

[2] นางสุนันท์ มีเทศ และคณะ. การพยากรณ์ผลสัมฤทธิ์ทางการเรียนของนักศึกษาในระดับประกาศนียบัตรผู้ช่วยพยาบาลคณะแพทยศาสตร์ศิริราชพยาบาล มหาวิทยาลัยมหิดล. เวชบันทึกศิริราช. ปีที่ 6, ฉบับที่ 2, หน้า 76-84, 2556.

[3] เปรมวดี อาวุธกรรมปรีชา. การพยากรณ์จำนวนผู้สมัครเข้าศึกษาต่อระดับบัณฑิตศึกษา กรณีศึกษามหาวิทยาลัยเทคโนโลยีพระจอมเกล้าพระนครเหนือ. วารสารวิจัยและพัฒนา วไลยอลงกรณ์ ในพระบรมราชูปถัมภ์. ปีที่ 6, ฉบับที่ 3, หน้า 93-103, 2564.

[4] อุตสว เดไช. การถดถอยเชิงเส้นอย่างง่าย คู่มือแบบเป็นขั้นตอน. (2566). [ออนไลน์]. เข้าถึงได้จาก: https://utsavdesai26.medium.com/linear regression-made-simple-a-step-by-step-tutorial-fb8e737ea2d9.

การพัฒนาแอปพลิเคชันแชทบอทสำหรับบริการข้อมูลนักศึกษา มหาวิทยาลัยราชภัฏภูเก็ต

Development of a Chatbot Application for Student Information Services at Phuket Rajabhat University

[1]Assada Chorraka
Faculty of Science & Technology
Phuket Rajabhat University
s6411423134@pkru.ac.th

[2] Bhurisub Dejpipatpracha
Faculty of Science & Technology
Phuket Rajabhat University
bhurisub@pkru.ac.th

[3]Poomsatit Mattajit
Faculty of Science & Technology
Phuket Rajabhat University
poomsatit.m@pkru.ac.th

Abstract

This research aims to develop a chatbot application for Rajabhat Phuket University to assist students in accessing essential academic information more efficiently. The main objective is to enable students to conveniently check academic results, class schedules, graduation status, university news, and personal profiles through the Line platform. The chatbot application is developed using HTML, CSS, and JavaScript for the frontend, while PHP Laravel is used for the backend and Firebase is utilized for hosting. The system is integrated with several Line API services, including Webhook, Message API, LIFF, and Line Business ID, to enhance interaction and user experience. To evaluate the system, a questionnaire was conducted with a sample group of 40 students. The results revealed a high level of user satisfaction. The design aspect received an average satisfaction score of 4.71, and the usability aspect received a score of 4.74, indicating that users found the system both visually appealing and practical. In conclusion, the Line Chatbot effectively fulfills its purpose by providing real-time access to academic and administrative services. The implementation significantly improves students' convenience, reduces complexity in accessing information, and enhances overall communication within the university ecosystem.

Keywords : Chatbot, Line API, Rajabhat Phuket University, student information

I. บทนำ

ในปัจจุบัน เทคโนโลยีสารสนเทศมีบทบาทสำคัญในการบริหารจัดการด้านการศึกษา โดยเฉพาะการเข้าถึงข้อมูลทางวิชาการและการให้บริการทางการศึกษาผ่านระบบออนไลน์ อย่างไรก็ตาม การเข้าถึงข้อมูลของนักศึกษาภายในมหาวิทยาลัยราชภัฏภูเก็ต ยังคงต้องดำเนินการผ่านระบบเว็บไซต์ req pkru ซึ่งแม้ว่าจะเป็นแหล่งข้อมูลที่สำคัญ แต่กระบวนการเข้าถึงข้อมูลเหล่านี้อาจใช้เวลานานและมีขั้นตอนที่ซับซ้อน ทำให้นักศึกษาประสบปัญหาในการค้นหาข้อมูลที่ต้องการ ส่งผลให้เกิดความล่าช้าและอาจก่อให้เกิดข้อผิดพลาดจากการกรอกข้อมูลหรือดำเนินการที่ไม่ถูกต้อง

จากการศึกษาพฤติกรรมการใช้งานของนักศึกษา พบว่าแอปพลิเคชัน Line เป็นแพลตฟอร์มหลักที่นักศึกษาส่วนใหญ่ใช้ในการสื่อสารและรับข้อมูลข่าวสารจากทางมหาวิทยาลัย ดังนั้น การพัฒนา Line Chatbot จึงเป็นทางเลือกที่เหมาะสมสำหรับการเพิ่มประสิทธิภาพการให้บริการข้อมูลนักศึกษา ซึ่งช่วยให้การเข้าถึงข้อมูลเป็นไปอย่างสะดวก รวดเร็ว และเป็นมิตรกับผู้ใช้งาน โดยสามารถลดขั้นตอนที่ยุ่งยากและช่วยให้นักศึกษาสามารถดึงข้อมูลที่ต้องการได้ทันทีผ่านแอปพลิเคชัน

งานวิจัยนี้มีวัตถุประสงค์ในการวิจัย 1) ออกแบบและพัฒนาแอปพลิเคชัน Line Chatbot สำหรับให้บริการข้อมูลนักศึกษา โดยใช้เทคโนโลยีที่ทันสมัย เช่น การใช้ API สำหรับดึงข้อมูลนักศึกษาแบบเรียลไทม์ การออกแบบระบบให้รองรับการสื่อสารแบบอัตโนมัติผ่าน Natural Language Processing (NLP) เพื่อเพิ่มความสามารถในการโต้ตอบของ Line Chatbot และ พัฒนาโครงสร้างฐานข้อมูลที่สามารถรองรับปริมาณผู้ใช้งานจำนวนมาก ได้อย่างมีประสิทธิภาพ พร้อมทั้งนำเทคโนโลยี ปัญญาประดิษฐ์ (Artificial Intelligence, AI) มาประยุกต์ใช้ในการเรียนรู้และปรับปรุงการตอบสนองของระบบ 2) ศึกษาผลการใช้งานแอปพลิเคชันในสถานการณ์จริง โดยทำการทดสอบระบบกับ กลุ่มตัวอย่างนักศึกษามหาวิทยาลัยราชภัฏภูเก็ต เพื่อประเมินการทำงานของ Line Chatbot โดยเน้นการออกแบบระบบที่สามารถ ใช้งานง่าย สะดวก และตอบสนองความต้องการของผู้ใช้ได้อย่างมีประสิทธิภาพ โดยแอปพลิเคชันจะมีเมนูหลัก เช่น ตรวจสอบผลการเรียน ตารางเรียน ข่าวสาร ตรวจสอบการจบ และโปรไฟล์ของนักศึกษา พร้อมทั้งทดสอบ ประสิทธิภาพของระบบ NLP ในการเข้าใจคำถามและตอบสนองได้อย่างแม่นยำ 3) วิเคราะห์คุณภาพและความพึงพอใจของผู้ใช้งาน โดยทำการเก็บรวบรวมข้อมูลผ่านแบบสอบถามและการวิเคราะห์ผลลัพธ์ในเชิงสถิติ เพื่อประเมินประสิทธิภาพของระบบ ในด้านความแม่นยำของข้อมูลที่ดึงมาแสดง ความเร็วในการตอบสนอง และความสะดวกในการใช้งานของ Line Chatbot ซึ่งจะนำไปสู่การ พัฒนาและปรับปรุงระบบให้เหมาะสมกับความต้องการของผู้ใช้ในอนาคต รวมถึงการพัฒนาความสามารถของ AI Chatbot ให้สามารถ เรียนรู้และตอบโต้ได้อย่างมีประสิทธิภาพยิ่งขึ้น

ผู้วิจัยได้ดำเนินการประยุกต์ใช้ เทคโนโลยีที่ทันสมัย โดยการพัฒนาแอปพลิเคชันแชทบอทที่สามารถ เชื่อมต่อกับฐานข้อมูลผ่าน API เพื่อให้ข้อมูลที่นำเสนอ ถูกต้อง ทันสมัย และเข้าถึงได้แบบเรียลไทม์ นอกจากนี้ ระบบยังสามารถ ทำงานอย่างมีประสิทธิภาพสูงสุด โดยใช้ (NLP) และปัญญาประดิษฐ์ (AI) เพื่อเพิ่มความสามารถในการโต้ตอบของแชทบอท

อย่างไรก็ตาม ความท้าทายสำคัญในการพัฒนา Line Chatbot ได้แก่ การออกแบบระบบให้สามารถรองรับจำนวนผู้ใช้ที่เพิ่มขึ้น (Scalability) และการปรับปรุงการสื่อสารระหว่างแชทบอทกับผู้ใช้งานให้เป็นธรรมชาติยิ่งขึ้น ตลอดจนการพัฒนา UI/UX ที่เหมาะสม กับข้อจำกัดของแพลตฟอร์ม Line ซึ่งอาจมีข้อจำกัดด้าน การแสดงผลข้อมูล ดังนั้น งานวิจัยนี้จึงมุ่งเน้นไปที่ การออกแบบและพัฒนา Line Chatbot ที่สามารถให้บริการข้อมูลนักศึกษาได้อย่างมีประสิทธิภาพ มีความแม่นยำ และสามารถต่อยอดการพัฒนาในอนาคต

II. ทบทวนวรรณกรรม

ในปัจจุบันมีงานวิจัยจำนวนมากที่เกี่ยวข้องกับการพัฒนาแชทบอทเพื่อให้บริการข้อมูล วิชัย สมบัติรักษ์ และคณะ [1] ได้พัฒนาแอปพลิเคชันแชทบอทเพื่อให้บริการข้อมูลนักศึกษาในมหาวิทยาลัยราชภัฏบุรีรัมย์ โดยแชทบอทสามารถให้บริการข้อมูลที่เกี่ยวข้องกับการลงทะเบียนเรียน การเพิ่ม-ถอนรายวิชา การชำระค่าเล่าเรียน และกิจกรรมของนักศึกษา โดยแบ่งการทำงานออกเป็น 2 ส่วนหลัก ได้แก่ ผู้ใช้งานที่เข้าถึงข้อมูลผ่าน LINE Chatbot และผู้ดูแลระบบที่จัดการข้อมูลผ่าน PHP Laravel และฐานข้อมูล MySQL ระบบนี้ช่วยลดขั้นตอนในการเข้าถึงข้อมูลและเพิ่มความสะดวกให้กับนักศึกษาได้อย่างมีประสิทธิภาพ ศักดิ์ชัย ทองเจริญ และคณะ [2] ได้เสนอการพัฒนาแชทบอทเพื่อให้บริการข้อมูลด้านสหกิจศึกษา โดยนำเทคนิค Machine Learning เช่น Decision Tree และ Multilayer Perceptron มาใช้ในการจำแนกคำถามและจัดการกับข้อความจากผู้ใช้งาน ซึ่งทำให้ระบบสามารถตอบสนองคำถามของนักศึกษาได้แม่นยำมากขึ้น และลดภาระของเจ้าหน้าที่ฝ่ายวิชาการ มหาวิทยาลัยเทคโนโลยีราชมงคลศรีวิชัย (RMUTSV) [3] ได้พัฒนาระบบสนทนาอัตโนมัติ (AI-Based Chatbot) ที่ใช้ NLP และ Machine Learning ในการตอบโต้บทสนทนาอย่างชาญฉลาด แชทบอทสามารถวิเคราะห์ข้อความของผู้ใช้และเลือกการตอบสนองที่เหมาะสมจากฐานข้อมูลที่เกี่ยวข้อง อีกทั้งยังสามารถทำงานร่วมกับหลายแพลตฟอร์ม เช่น LINE Official Account และ Facebook Messenger ซึ่งทำให้รองรับการใช้งานได้อย่างกว้างขวางในระดับสถาบันการศึกษา งานวิจัยของ รศ.ดร.พิทา จารุพูนผล, อาจารย์ ดร.ณสิทธิ์ เหล่าเส็น และอาจารย์ธนกฤษ จันทร์แสง [4] ได้พัฒนาแชทบอท “แหลงต๊ะ” โดยใช้ AI, NLP และ Machine Learning เพื่อสนับสนุนการเรียนรู้และส่งเสริมการท่องเที่ยวเชิงประวัติศาสตร์ในพื้นที่ภาคใต้ของไทย ระบบสามารถโต้ตอบบทสนทนาเกี่ยวกับข้อมูลการท่องเที่ยว การแนะนำที่พัก ร้านอาหาร และเส้นทางท่องเที่ยวโดยใช้ GPS โดยเน้นการเชื่อมโยงกับแหล่งข้อมูลประวัติศาสตร์ที่ถูกต้อง ช่วยเพิ่มประสบการณ์การเรียนรู้ที่มีความสมจริงและยั่งยืน อัครพล ลีลาวัฒน์ และจารุวรรณ จันทร์สว่าง [5] ได้นำเสนอการพัฒนาแชทบอทเพื่อให้บริการข้อมูลเบื้องต้นของหน่วยงาน โดยใช้เทคโนโลยีปัญญาประดิษฐ์ในการประมวลผลข้อความและออกแบบโครงสร้างการสนทนาเพื่อให้ตอบสนองต่อคำถามที่พบบ่อยได้อย่างแม่นยำ ช่วยลดภาระของเจ้าหน้าที่และเพิ่มความรวดเร็วในการให้ข้อมูลแก่ผู้ใช้ งานวิจัยของ อภิชัย ตระหง่านศรี [6] ได้พัฒนาแชทบอทบนแพลตฟอร์ม Line สำหรับแสดงข้อมูลการเรียนของนักศึกษา โดยใช้ Messaging API ร่วมกับ Google Chat API และ Google Apps Script เพื่อเชื่อมต่อกับข้อมูลใน Google Sheet ระบบสามารถให้ข้อมูลเกี่ยวกับคะแนน การมาเรียน และวิดีโอการสอนย้อนหลัง ซึ่งช่วยให้นักศึกษาสามารถเข้าถึงข้อมูลรายวิชาได้สะดวกยิ่งขึ้น ผลการประเมินจากนักศึกษาพบว่ามีความพึงพอใจในระดับสูง จากการทบทวนวรรณกรรมดังกล่าว แสดงให้เห็นว่าการพัฒนาแชทบอทโดยใช้เทคโนโลยี AI, NLP และ Machine Learning มีศักยภาพสูงในการให้บริการข้อมูลเชิงโต้ตอบที่รวดเร็วและแม่นยำ โดยเฉพาะในภาคการศึกษาที่ต้องการระบบสนับสนุนการเข้าถึงข้อมูลแบบอัตโนมัติและเป็นมิตรกับผู้ใช้ การออกแบบแชทบอทจึงควรคำนึงถึงทั้งประสิทธิภาพการทำงาน

III. ระเบียบวิธีวิจัย

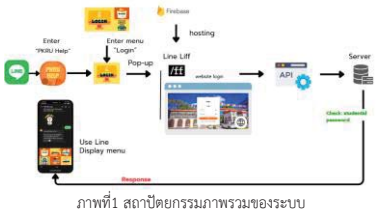
ในการพัฒนาซอฟต์แวร์ จำเป็นต้องมีกระบวนการทำงานที่ชัดเจนเพื่อให้ได้ระบบที่มีประสิทธิภาพและตรงกับความต้องการของผู้ใช้ งานวิจัยนี้ดำเนินการตามหลักวิศวกรรมซอฟต์แวร์ ซึ่งประกอบด้วย 4 ขั้นตอนหลัก

A. การวิเคราะห์ความต้องการ

ขั้นตอนนี้เป็นการศึกษาความต้องการของผู้ใช้โดยเก็บข้อมูลจากแบบสอบถามและการสัมภาษณ์นักศึกษามหาวิทยาลัยราชภัฏภูเก็ต เพื่อนำมาสรุปเป็นฟีเจอร์หลักของระบบและกำหนดขอบเขตให้ชัดเจน เพื่อให้ซอฟต์แวร์สามารถตอบโจทย์การใช้งานได้อย่างมีประสิทธิภาพ ฟีเจอร์หลักของระบบได้แก่ ารตรวจสอบผลการเรียน นักศึกษาสามารถดูผลการเรียนของตนเองผ่านแชทบอทได้ 1.ตารางเรียน นักศึกษาสามารถตรวจสอบตารางเรียนของแต่ละภาคการศึกษา 2.ข่าวสารมหาวิทยาลัย นักศึกษาสามารถรับข้อมูลข่าวสารและประกาศจากมหาวิทยาลัย 3.ข้อมูลโปรไฟล์นักศึกษา สามารถเข้าถึงข้อมูลส่วนตัว เช่น รายละเอียดการลงทะเบียน 4.ตรวจสอบสถานะการจบการศึกษา ระบบสามารถแจ้งเตือนสถานะการจบของนักศึกษาการวิเคราะห์นี้ช่วยให้การออกแบบและพัฒนาระบบตรงกับความต้องการของผู้ใช้มากที่สุด

B. การออกแบบระบบ

ขั้นตอนนี้เป็นการออกแบบระบบให้ตรงกับความต้องการของผู้ใช้ โดยแชทบอทจะดึงข้อมูลผ่าน API ของมหาวิทยาลัยเพื่อให้ข้อมูลที่ถูกต้องและแม่นยำ ระบบได้รับการออกแบบให้รองรับการทำงานผ่าน LINE Chatbot ซึ่งเป็นแพลตฟอร์มที่นักศึกษาใช้งานเป็นประจำ องค์ประกอบหลักของระบบประกอบด้วย ส่วนติดต่อผู้ใช้ (Frontend) พัฒนาด้วย HTML, CSS, และ JavaScript เชื่อมต่อกับ LINE LIFF ส่วนประมวลผล (Backend) พัฒนาด้วย PHP Laravel Framework สำหรับเชื่อมต่อ API และฐานข้อมูลระบบจัดการข้อมูล ใช้ฐานข้อมูล MySQL เพื่อจัดเก็บข้อมูลนักศึกษาและประวัติการใช้งาน



ภาพที่1 สถาปัตยกรรมภาพรวมของระบบ

C. การพัฒนาระบบ

การพัฒนาแอปพลิเคชันนี้เริ่มต้นด้วยการดำเนินการตามขั้นตอน(1)การดึงข้อมูลจากระบบมหาวิทยาลัยระบบทำการดึงข้อมูลจาก API ของมหาวิทยาลัยราชภัฏภูเก็ตเพื่อให้ข้อมูลที่ถูกต้องและแม่นยำ แชทบอทจะดึงข้อมูลต่าง ๆ เช่น ผลการเรียน ตารางเรียน ข่าวสารมหาวิทยาลัย และข้อมูลโปรไฟล์นักศึกษาเพื่อนำมาแสดงในรูปแบบที่เข้าใจง่ายสำหรับผู้ใช้ (2)การเชื่อมต่อกับ LINE

Chatbot การพัฒนาแอปพลิเคชันทำการเชื่อมต่อกับ LINE ผ่านการใช้งาน LINE Messaging API เพื่อให้ผู้ใช้งานสามารถสื่อสารกับแอปพลิเคชันได้อย่างสะดวก รวดเร็ว และสอดคล้องกับวิธีการติดต่อสื่อสารที่ผู้ใช้งานส่วนใหญ่คุ้นเคย(3) การพัฒนาระบบ Backend ระบบ Backend ถูกพัฒนาด้วย PHP และ Laravel Framework เพื่อจัดการการเชื่อมต่อ API การจัดการข้อมูลจากฐานข้อมูล API รับข้อมูลที่ตอบกลับมาในรูปแบบ JSON และการส่งข้อมูลไปยัง LINE Chatbot เพื่อให้ผู้ใช้ได้รับข้อมูลที่ต้องการได้อย่างถูกต้องและทันเวลา



ภาพที่ 2 หน้าจอ Account ID Line



ภาพที่ 3 หน้าจอ Login เข้าใช้งาน



ภาพที่ 4 หน้าจอเมนูของระบบ

D. การทดสอบระบบ

ในระหว่างการพัฒนา มีการทดสอบระบบทั้งในส่วนของการทดสอบภายใน (Unit Testing) และการทดสอบการใช้งานจริง (User Testing) เพื่อประเมินประสิทธิภาพและความถูกต้องของข้อมูลที่ระบบให้บริการ รวมถึงการทดสอบการใช้งานกับผู้ใช้งานจริง โดยใช้แบบสอบถามเพื่อเก็บข้อมูลความพึงพอใจของผู้ใช้

การพัฒนาระบบนี้ได้รับการออกแบบเพื่อรองรับการใช้งานที่สะดวกและตอบสนองความต้องการของนักศึกษามหาวิทยาลัยราชภัฏภูเก็ตอย่างครบถ้วน โดยเน้นการใช้งานผ่านแพลตฟอร์ม Line ซึ่งเป็นเครื่องมือที่นักศึกษาใช้งานเป็นประจำ

IV. ผลการทดลอง

จากผลการประเมินแบบสอบถามการใช้งานแอปพลิเคชันจากกลุ่มผู้ใช้ตัวอย่าง 40 คนนั้น ผู้วิจัยได้แบ่งการประเมินเป็นสองด้าน คือ ด้านการออกแบบและด้านการใช้งาน โดยกำหนดเกณฑ์ดังนี้

ระดับความพึงพอใจมากที่สุด มีค่าเท่ากับ 5 คะแนน

ระดับความพึงพอใจมาก มีค่าเท่ากับ 4 คะแนน

ระดับความพึงพอใจปานกลาง มีค่าเท่ากับ 3 คะแนน

ระดับความพึงพอใจน้อย มีค่าเท่ากับ 2 คะแนน

ระดับความพึงพอใจน้อยที่สุด มีค่าเท่ากับ 1 คะแนน

แล้วนำคะแนนไปหาค่าเฉลี่ย โดยใช้เกณฑ์ในการแปลความหมายค่าเฉลี่ยดังนี้

ค่าเฉลี่ย 4.51 – 5.00 หมายถึง มีความพึงพอใจในระดับมากที่สุด

ค่าเฉลี่ย 3.51 – 4.50 หมายถึง มีความพึงพอใจในระดับมาก

ค่าเฉลี่ย 2.51 – 3.50 หมายถึง มีความพึงพอใจในระดับปานกลาง

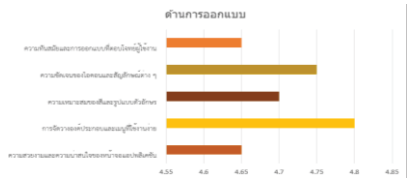
ค่าเฉลี่ย 1.51 – 2.50 หมายถึง มีความพึงพอใจในระดับน้อย

ค่าเฉลี่ย 1.00 – 1.50 หมายถึง มีความพึงพอใจในระดับน้อยที่สุด

ตารางที่ 1 ผลการประเมินด้านการออกแบบ

รายการประเมิน	ค่าเฉลี่ย	แปลผล
ความสวยงามและความน่าสนใจของหน้าจอแอปพลิเคชัน	4.65	มาก
การจัดวางองค์ประกอบและเมนูที่ใช้งานง่าย	4.80	มากที่สุด
ความเหมาะสมของสีและรูปแบบตัวอักษร	4.70	มากที่สุด
ความชัดเจนของไอคอนและสัญลักษณ์ต่าง ๆ	4.75	มากที่สุด
ความทันสมัยและการออกแบบที่ตอบโจทย์ผู้ใช้งาน	4.65	มากที่สุด
ค่าเฉลี่ยรวม	4.71	มากที่สุด

จากตารางที่ 1 พบว่าผู้ใช้งานมีความพึงพอใจในระดับที่มากที่สุด โดยมีภาพรวม ($\bar{X}$ = 4.71)

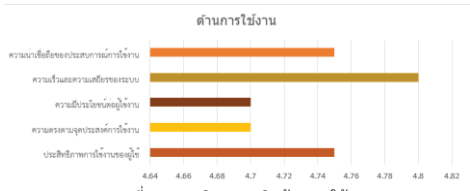


ภาพที่ 5 แผนภูมิผลประเมินด้านการออกแบบ

ตารางที่ 2 ผลการประเมินด้านการใช้งาน

รายการประเมิน	ค่าเฉลี่ย	แปลผล
ประสิทธิภาพการใช้งานของผู้ใช้	4.75	มาก
ความตรงตามจุดประสงค์การใช้งาน	4.70	มากที่สุด
ความมีประโยชน์ต่อผู้ใช้งาน	4.70	มากที่สุด
ความเร็วและความเสถียรของระบบ	4.80	มากที่สุด
ความน่าเชื่อถือของประสบการณ์การใช้งาน	4.75	มากที่สุด
ค่าเฉลี่ยรวม	4.74	มากที่สุด

จากตารางที่ 2 พบว่าผู้ใช้งานมีความพึงพอใจในระดับที่มากที่สุด โดยมีภาพรวม ($\bar{X}$ = 4.74)



ภาพที่ 6 แผนภูมิผลประเมินด้านการใช้งาน

ผู้วิจัยได้ดำเนินการสำรวจความพึงพอใจในการใช้งานแอปพลิเคชันผ่านแบบสอบถามกับกลุ่มตัวอย่างจำนวน 40 คน ผลการศึกษา พบว่าผู้ใช้มีระดับความพึงพอใจอยู่ในเกณฑ์สูง แบบสอบถามแบ่งออกเป็นสองด้าน ได้แก่ ด้านการออกแบบ และ ด้านการใช้งาน โดยผลการประเมินพบว่า ด้านการออกแบบ มีค่าเฉลี่ยความพึงพอใจรวม 4.71 ขณะที่ ด้านการใช้งาน ได้ค่าเฉลี่ยรวม 4.74 ซึ่งสะท้อนถึงความพึงพอใจของผู้ใช้ที่สูงในทั้งสองด้าน

V. อภิปรายผล

จากผลการทดลองที่ได้จากการประเมินการใช้งานของนักศึกษากับแชทบอทพบว่า ผู้ใช้งานมีความพึงพอใจในด้านการออกแบบและประสิทธิภาพการใช้งานในระดับที่สูง (ค่าเฉลี่ยด้านการออกแบบ 4.71 และด้านการใช้งาน 4.74) ซึ่งแสดงให้เห็นว่าแชทบอทสามารถตอบโจทย์ความต้องการของนักศึกษาได้เป็นอย่างดี โดยเฉพาะในแง่ของความสะดวกในการเข้าถึงข้อมูลที่สำคัญ เช่น ผลการเรียน ตารางเรียน ข่าวสาร และข้อมูลโปรไฟล์

การวิเคราะห์ผลการทดลองเปรียบเทียบกับงานวิจัยที่เกี่ยวข้องพบว่า ระบบ Line Chatbot ที่พัฒนาขึ้นในงานวิจัยนี้มีข้อได้เปรียบในเรื่องของความง่ายในการใช้งานและการเข้าถึงข้อมูลแบบเรียลไทม์ เมื่อเทียบกับระบบเดิมที่นักศึกษาต้องเข้าเว็บไซต์ req pkru ที่มีขั้นตอนซับซ้อนและใช้เวลานานกว่า นอกจากนี้ การใช้แพลตฟอร์ม Line ซึ่งเป็นแอปพลิเคชันที่นักศึกษาคุ้นเคย ช่วยเพิ่มประสิทธิภาพในการสื่อสารและทำให้การรับข้อมูลเป็นไปอย่างราบรื่น อย่างไรก็ตาม งานวิจัยนี้ยังมีข้อจำกัดอยู่บ้าง เช่น

ความสามารถในการรองรับปริมาณผู้ใช้งานที่เพิ่มขึ้นในอนาคต อาจต้องมีการปรับปรุงด้านโครงสร้างฐานข้อมูลและการจัดการ API เพื่อรองรับการใช้งานที่เข้มข้นขึ้น

ข้อจำกัดด้าน UI/UX ภายในแพลตฟอร์ม Line ที่อาจไม่สามารถปรับแต่งได้อย่างอิสระเท่ากับการพัฒนาแอปพลิเคชันบนเว็บหรือมือถือโดยตรง

จากการเปรียบเทียบกับงานวิจัยอื่น ๆ ที่ได้มีการพัฒนาแชทบอทเพื่อบริการข้อมูลในสถาบันการศึกษา พบว่าแนวทางการใช้ API และการเชื่อมต่อกับแพลตฟอร์ม Line นั้นมีความเหมาะสมและสามารถนำไปประยุกต์ใช้ได้จริง แต่การพัฒนาระบบเพื่อรองรับการใช้งานในสเกลที่ใหญ่ขึ้นและการพัฒนาความสามารถด้าน NLP ให้ครอบคลุมมากขึ้น ถือเป็นประเด็นที่ต้องได้รับการพิจารณาในขั้นตอนต่อไป

VI. ข้อสรุป

งานวิจัยนี้นำเสนอการพัฒนา Line Chatbot สำหรับให้บริการข้อมูลนักศึกษามหาวิทยาลัยราชภัฏภูเก็ต โดยมีเป้าหมายเพื่อ เพิ่มความสะดวกในการเข้าถึงข้อมูลสำคัญ เช่น ผลการเรียน ตารางเรียน ข่าวสารมหาวิทยาลัย และโปรไฟล์นักศึกษา ผ่านแพลตฟอร์มที่ใช้งานง่ายและแพร่หลาย ผลการทดลองแสดงให้เห็นว่า ระบบสามารถให้บริการข้อมูลได้อย่างถูกต้อง รวดเร็ว

เมื่อเทียบกับระบบเว็บไซต์แบบเดิม การใช้ HTML, CSS, JavaScript, PHP Laravel, Firebase และ Line API ช่วยให้ระบบสามารถตอบสนองต่อคำขอของผู้ใช้งานแบบเรียลไทม์ และผลการประเมินจากกลุ่มตัวอย่างนักศึกษา สะท้อนถึงระดับความพึงพอใจที่สูง ในด้านการออกแบบและประสิทธิภาพของระบบ

แม้ว่าระบบที่พัฒนาขึ้นจะสามารถ ปรับปรุงประสิทธิภาพการให้บริการข้อมูลได้อย่างมีนัยสำคัญ แต่ยังมีข้อจำกัดที่ควรพิจารณา เช่น การรองรับปริมาณผู้ใช้ที่เพิ่มขึ้น ซึ่งอาจต้องปรับปรุงโครงสร้างฐานข้อมูลและ API ให้มีความเสถียรยิ่งขึ้น นอกจากนี้ ข้อจำกัดด้าน UI/UX ของแพลตฟอร์ม Line อาจส่งผลต่อการแสดงผลข้อมูลที่ซับซ้อน และ การพัฒนาความสามารถในการประมวลผลภาษาธรรมชาติ NLP ยังต้องได้รับการปรับปรุงเพื่อให้แชทบอทสามารถตอบคำถามที่มีโครงสร้างซับซ้อนและเข้าใจภาษาที่เป็นธรรมชาติได้ดียิ่งขึ้น

แนวทางการวิจัยในอนาคตควรมุ่งเน้นไปที่ การพัฒนา AI-Based Chatbot ที่มีความสามารถด้าน NLP ที่ลึกขึ้น โดยใช้ Machine Learning และ Deep Learning เพื่อเพิ่มประสิทธิภาพในการโต้ตอบ นอกจากนี้ ควรพิจารณา การบูรณาการกับระบบอื่นภายในมหาวิทยาลัย เช่น ระบบแจ้งเตือนอัตโนมัติสำหรับกำหนดการลงทะเบียนเรียนและการชำระค่าเล่าเรียน เพื่อเพิ่มขอบเขตการใช้งานและศักยภาพของแชทบอท

โดยสรุป งานวิจัยนี้ได้แสดงให้เห็นถึงศักยภาพของ Line Chatbot ในการให้บริการข้อมูลแก่นักศึกษาได้อย่างมีประสิทธิภาพ และสามารถช่วยลดขั้นตอนที่ซับซ้อนในการเข้าถึงข้อมูลผ่านระบบเดิม ผลลัพธ์ที่ได้สามารถเป็นแนวทางสำคัญในการพัฒนา ระบบอัตโนมัติสำหรับบริการทางการศึกษา ในอนาคต เช่น การพัฒนาระบบแชทบอทเพื่อสนับสนุนการเรียนการสอน ซึ่งจะช่วยเพิ่มประสิทธิภาพของการบริหารจัดการทางการศึกษาและส่งเสริมการใช้เทคโนโลยีดิจิทัลในการสนับสนุนการเรียนรู้ของนักศึกษาในยุคดิจิทัลต่อไป

อ้างอิง

[1] ว. สมบัติรักษ์ และคณะ, "การพัฒนาแอปพลิเคชันแชทบอทสำหรับงานบริการนักศึกษา กรณีศึกษามหาวิทยาลัยราชภัฏบุรีรัมย์," ใน *การประชุมวิชาการระดับชาติด้านคอมพิวเตอร์และเทคโนโลยีสารสนเทศ*, กรุงเทพฯ, ประเทศไทย, ก.พ. 2565, หน้า 45-52.

[2] ศ. ทองเจริญ และคณะ, "การพัฒนาระบบแชทบอทสำหรับให้บริการข้อมูลเกี่ยวกับสหกิจศึกษาโดยใช้ Machine Learning," *วารสารวิชาการเทคโนโลยีสารสนเทศ*, ปีที่ 18, ฉบับที่ 2, หน้า 112-125, มิ.ย. 2564.

[3] มหาวิทยาลัยเทคโนโลยีราชมงคลศรีวิชัย (RMUTSV), "การพัฒนาระบบโต้ตอบการสนทนาผ่านตัวอักษรอัตโนมัติด้วยเทคโนโลยีปัญญาประดิษฐ์สำหรับให้บริการข้อมูลนักศึกษา," เอกสารเผยแพร่บนเว็บไซต์มหาวิทยาลัย, 2565. [ออนไลน์]. เข้าถึงได้จาก: https://www.rmutsv.ac.th/research/chatbot-ai-student-services.

[4] พ. จารุพูนผล, ณ. เหล่าเส็น, และ ธ. จันทร์แสง, "แหลงต๊ะ Chatbot AI สำหรับส่งเสริมการเรียนรู้และการท่องเที่ยวเชิงประวัติศาสตร์," มหาวิทยาลัยราชภัฏภูเก็ต, เอกสารเผยแพร่บนเว็บไซต์, ก.ค. 2567. [ออนไลน์]. เข้าถึงได้จาก: https://www.pkru.ac.th/th/top-news/7482-ai-chatbot-pkru-jul-2024.

[5] อ. ลีลาวัฒน์ และ จ. จันทร์สว่าง, "การพัฒนาแชทบอทเพื่อให้บริการข้อมูลเบื้องต้นของหน่วยงานด้วยเทคโนโลยีปัญญาประดิษฐ์," ใน *การประชุมวิชาการระดับชาติและนานาชาติ สถาบันพระปกเกล้า (ISSC)*, กรุงเทพฯ, ประเทศไทย, 2565. [ออนไลน์]. เข้าถึงได้จาก: https://so02.tci-thaijo.org/index.php/ISSC/article/view/256479.

[6] อ. ตระหง่านศรี, "การพัฒนาระบบสนทนาอัตโนมัติเพื่อแสดงผลข้อมูลการเรียนผ่านไลน์แชทบอท," ใน *การประชุมวิชาการระดับชาติและนานาชาติ สถาบันพระปกเกล้า (ISSC)*, มหาวิทยาลัยศรีปทุม วิทยาเขตชลบุรี, มิ.ย. 2566. [ออนไลน์]. เข้าถึงได้จาก: https://doi.org/10.14456/issc.2023.31.

การพัฒนาน้ำพริกปลาแห้งทดแทนด้วยถั่วหรั่งบางส่วน

Development of Dried Fish Chili Paste Partially Substituted with Bambara Groundnut

1st Sangrawee Napattalung
Home Economics Program
Faculty of Science and Technology
Phuket Rajabhat University
sangrawee.s@pkru.ac.th

2ndJerapat Ploykhaw
Home Economics Program
Faculty of Science and Technology
Phuket Rajabhat University
jerapat.p@pkru.ac.th

3rd Kanokwan Thongkiaw
Home Economics Program
Faculty of Science and Technology
Phuket Rajabhat University
kanokwan.h@pkru.ac.th

Chili paste is a common and popular food in Thailand, often given as a souvenir. Most long-shelf-life chili pastes belong to the dried chili paste category. Nowadays, additional ingredients are often incorporated to increase variety and enhance nutritional value. This research focuses on developing dried fish chili paste partially substituted with Bambara groundnut. The objective is to evaluate its chemical quality, including moisture content analysis, water activity (Aw) measurement, color value analysis, and microbiological testing.

The research found that the dried fish chili paste partially substituted with 25% Bambara groundnut had the following nutritional values: total energy of 2,832.27 kilocalories, protein 24.23 grams, fat 0.04 grams, carbohydrates 60.72 grams, ash content 0.17 grams, and fiber 0.04 grams.Color analysis results showed L (lightness) at 20.43, a* (redness) at 14.16, and b* (yellowness) at 24.29. The moisture content was 11.39%, Aw was 0.56, and the total microbial count was 2.5 x 10^2 colony-forming units per gram. No yeast or mold contamination was detected, complying with the community product standards (OTOP Standard for Dried Chili Paste No. 130/2556).*

Keywords *chili paste*, *Bambara Ground nut* ,*Dried fish*, *Dried chili paste*

บทนำ

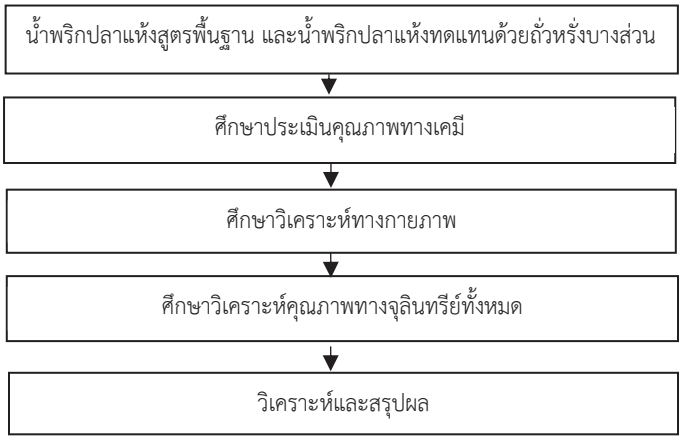
น้ำพริกเป็นอาหารอีกหนึ่งประเภทที่สามารถหาทานได้ง่าย และนิยมนำไปเป็นของฝาก ซึ่งในปัจจุบันน้ำพริกมีการเสริมส่วนประกอบอื่น ๆ เพื่อเพิ่มความหลากหลาย มีคุณค่าทางโภชนาการ เช่น เนื้อสัตว์ ผัก สมุนไพร หรือเห็ดต่าง ๆ ให้ได้รสชาติแปลกใหม่ และเป็นที่ยอมรับของผู้บริโภคมากขึ้น [1] น้ำพริกที่สามารถเก็บได้นานส่วนใหญ่เป็นกลุ่มน้ำพริกแห้ง โดยนำน้ำพริกไปผ่านกระบวนการคั่ว การผัดแบบแห้ง การอบแห้งหรือการทอด

การแปรรูปและการถนอมอาหารด้วยวิธีการคั่วเป็นการลดปริมาณน้ำในอาหาร ซึ่งช่วยลดหรือยับยั้งการเจริญเติบโตของจุลินทรีย์บางชนิด ที่มีผลต่อการเสื่อมเสียของอาหารได้ เนื่องจากปริมาณน้ำและความชื้นในอาหารมีความสัมพันธ์กับค่า aw ซึ่งค่า aw ส่งผลต่อการเสื่อมเสียของอาหาร

ถั่วหรั่งเป็นพืชที่มีโปรตีนสูง และมีคุณค่าทางโภชนาการสูงกว่าถั่วชนิดอื่น ๆ มีสีม่วงที่สวย ดูน่ารับประทาน เนื่องจากมีสารแอนโทไซยานิน และมีสารอาหารอื่น ๆ ฟลาโวนอยด์ โปรตีน คาร์โบไฮเดรต ไขมัน และวิตามินบี 1 มีฤทธิ์เป็นสารต้านอนุมูลอิสระ (antioxidant) ลดคอเลสเตอรอล อีกทั้งมีใยอาหาร กรดอะมิโนที่จำเป็นแก่ร่างกาย [2]

งานวิจัยเรื่องนี้ได้พัฒนาน้ำพริกปลาแบบแห้งทดแทนด้วยถั่วหรั่งบางส่วน โดยมีวัตถุประสงค์ในการศึกษาประเมินคุณภาพทางเคมี การวิเคราะห์ค่าความชื้น ,การวิเคราะห์หาปริมาณน้ำอิสระในอาหาร (Aw) และการวิเคราะห์ค่าสี เพื่อพัฒนาผลิตภัณฑ์อาหารสำเร็จรูปประเภทน้ำพริกให้เหมาะกับคนในยุคปัจจุบัน อำนวยความสะดวก พกพาได้ง่าย มีอายุการเก็บรักษาได้นาน และยังสามารถช่วยเพื่อเพิ่มมูลค่าของถั่วหรั่งได้

กรอบแนวคิดการวิจัย



ทบทวนวรรณกรรม

[1] จากการศึกษาการพัฒนาผลิตภัณฑ์น้ำพริกแห้งจากเม็ดบัว ก่อนและหลังการปรับปรุงการเตรียมวัตถุดิบ พบว่า น้ำพริกผัดแห้งเม็ดบัว มีปริมาณจุลินทรีย์ปนเปื้อนต่ำกว่าเกณฑ์มาตรฐานที่ มผช. กำหนด โดยมีปริมาณจุลินทรีย์ทั้งหมด 3 x 10 โคโลนี/ตัวอย่าง 1 กรัม ไม่พบการปนเปื้อนของ *E. coli.* ยีสต์และรา นอกจากนี้ยังไม่พบสารก่อมะเร็ง ในกลุ่มของสารอัลฟ่าทอกซิน

[4] การศึกษาคุณภาพของผลิตภัณฑ์น้ำพริกจากพริกไทยดำ พบว่า มีอายุการเก็บรักษาได้ไม่นาน มีค่า Aw สูง แต่เมื่อปรับปรุงการเตรียมวัตถุดิบโดยการล้าง ลวก ตากก่อน ทำให้ปริมาณค่า Aw เท่ากับ 0.447 มีปริมาณจุลินทรีย์ทั้งหมด เท่ากับ 6.30 x 10^3 โคโลนีต่อกรัม ปริมาณเชื้อยีสต์และราลดลง <10 โคโลนีต่อกรัม ซึ่งเป็นไปตามมาตรฐานผลิตภัณฑ์ชุมชน (มผช.น้ำพริกปั่นแห้ง 130/2556) ที่กำหนดไว้ดังนั้นการควบคุมคุณภาพวัตถุดิบก่อนนำมาใช้ในการผลิตน้ำพริกและการอบหลังผัดผลิตภัณฑ์เสร็จ จึงมีความสำคัญที่จะทำให้ผลิตภัณฑ์มีคุณภาพเป็นไปตามมาตรฐานผลิตภัณฑ์ชุมชน

ระเบียบวิธีวิจัย

1. กระบวนการผลิตน้ำพริกปลาแห้งทดแทนด้วยถั่วหรั่งบางส่วน

นำปลาแห้งแช่น้ำเป็นเวลา 30 นาที คั่วพริก กระเทียม หอมแดง ที่อุณภูมิ 60 ^{o}C เป็นเวลา 10 นาที นำพริก กระเทียม หอมแดง มาปั่นรวมกัน นำปลาแห้งและถั่วหรั่งปั่นรวมกันแยกไว้ ซึ่งวัตถุดิบทุกอย่างปั่น เป็นเวลา 25 วินาที จากนั้นตั้งกระทะใช้ไฟกลางที่อุณภูมิ 70 ^{o}C นำน้ำตาล น้ำมะขาม ลงไปผัดให้ละลาย ตามด้วยเนื้อปลาป่น ถั่วหรั่งป่น ผัดให้เข้ากัน ใส่พริก กระเทียม และหอมแดงที่ปั่นรวมกันไว้ ผัดให้เข้ากันเป็นระยะเวลา 15 นาที (วัตถุดิบทุกอย่างซื้อจากห้างทรัพย์สินค้าซุปเปอร์ชีป จำกัด จังหวัดภูเก็ต) โดยสูตรน้ำพริกปลาแห้งสูตรพื้นฐาน มีส่วนผสม คือ ปลาแห้ง 43.86 พริกแห้งป่น 10.96 กระเทียม 6.58 หอมแดง 17.54 น้ำมะขามเปียก 8.77 น้ำส้มสายชู 1.32 เกลือ 1.32 น้ำตาลทราย 9.65 และสูตรน้ำพริกปลาแห้งทดแทนด้วยถั่วหรั่งบางส่วน โดยมีถั่วหรั่ง ร้อยละ 25 ของปลาแห้ง มีส่วนผสม คือ ปลาแห้ง 32.9 ถั่วหรั่ง 10.96 พริกแห้งป่น 10.96 กระเทียม 6.58 หอมแดง 17.54 น้ำมะขามเปียก 8.77 น้ำส้มสายชู 1.32 เกลือ 1.32 น้ำตาลทราย 9.65

2. การวิเคราะห์คุณภาพทางเคมี

การวิเคราะห์คุณภาพทางเคมีของผลิตภัณฑ์น้ำพริกปลาแห้งทดแทนด้วยถั่วหรั่งบางส่วน นำผลิตภัณฑ์น้ำพริกที่ได้มาวิเคราะห์องค์ประกอบทางเคมี ได้แก่ โปรตีน ไขมัน คาร์โบไฮเดรต เถ้า ใยอาหาร ตามวิธีการของ AOAC (2019) และความชื้น วิเคราะห์ด้วยเครื่องวัดความชื้น Moisture Analyzer รุ่น MX-50

3. การวิเคราะห์คุณภาพทางกายภาพ

การวิเคราะห์คุณภาพทางกายภาพนำผลิตภัณฑ์น้ำพริกที่ได้มาวิเคราะห์ทางด้านกายภาพ ดังนี้ (1) ค่าสี L* a* b* วัดค่าด้วยเครื่องวัดสีแบบพกพา เครื่องวัดสีแบบพกพา ยี่ห้อ HunterLab รุ่น MiniScan EZ 45/0 (LAV) รายงานเป็นค่าความสว่าง (L*) ค่าสีแดง-เขียว (a*) และค่าความเป็นสีเหลือง-น้ำเงิน (b*) และการวิเคราะห์ค่าปริมาณน้ำอิสระ (aw) วิเคราะห์ด้วยเครื่อง water activity (Rotronic Awtherm)

4. การวิเคราะห์คุณภาพทางจุลินทรีย์

การวิเคราะห์คุณภาพทางจุลินทรีย์ เชื้อจุลินทรีย์ทั้งหมด (Total viable count) เชื้อยีสต์และรา (Yeast & Mold) ตามวิธีการของ AOAC (2000)

5. การวิเคราะห์ผลทางสถิติ

การประมวณผลโดยใช้โปรแกรมประมวลผลสำเร็จรูป โดยนำผลวิเคราะห์ต่าง ๆ มาวิเคราะห์ค่าความแปรปรวน และค่าความคลาดเคลื่อนของผลการทดลอง วางแผนการทดลองแบบสุ่มตลอด (Completely Randomized Design, CRD) การวิเคราะห์หาค่าเฉลี่ย ($\bar{X}$) การวิเคราะห์หาความแปรปรวน (Analysis of Variance, ANOVA) และวิเคราะห์หาความแตกต่างของค่าเฉลี่ยแบบ Duncan's New Multiple Range Test (Steel and Torries, 1980) โดยใช้โปรแกรมสำเร็จรูปทางสถิติ SPSS

ผลการทดลอง

ผลการศึกษาปริมาณคุณภาพด้านต่างๆ

ผลการศึกษาการวิเคราะห์คุณภาพในด้านต่าง ๆ ของน้ำพริกปลาแห้งทดแทนด้วยถั่วหรั่งบางส่วน ระหว่างสูตรพื้นฐาน กับสูตรถั่วหรั่ง ร้อยละ 25 และมีคุณค่าทางโภชนาการ ดังแสดงในตาราง มีดังนี้ โปรตีน 33.49, 24.23 ไขมัน 0.03 ,0.04 คาร์โบไฮเดรต 51.80 ,60.72 ปริมาณเถ้า 0.17 ,0.17 ไฟเบอร์ 0.03 , 0.04 ความชื้น 11.02 ,11.39 ผลค่า AW 0.52 ,0.56 ผลค่าสี L*(ความสว่าง) 25.75 ,20.43 a*(สีแดง) 14.12 ,14.16 และ b*(สีเหลือง) 27.50 ,24.29 ผลค่า aw เท่ากับ 0.52 ,0.56 ปริมาณจุลินทรีย์ทั้งหมด เท่ากับ 2.3 x10^2, 2.5 x10^2 โคโลนีต่อกรัม และไม่พบการปนเปื้อนของเชื้อยีสต์และรา

TABLE The analysis of various quality aspects of dried fish chili paste partially substituted with Bambara groundnut.

Analysis of quality	Basic formula	Bambara Groundnut 25 %
<u>Chemical qualities</u>		
Protein	33.49±0.71^{a}	24.23±1.41^{b}
Fat^{ns}	0.030±0.002	0.040±0.003
Carbohydrate	51.80±0.83^{b}	60.72±1.41^{a}
Ash^{ns}	0.17±0.002	0.17±0.002
Fiber^{ns}	0.03±0.029	0.04±0.036
Moisture^{ns}	11.02±0.02	11.39±0.03
<u>Physical quality</u>		
color		
L*^{ns}	25.75±0.73	20.43±0.12
a*^{ns}	14.12±0.14	14.16±0.31
b*^{ns}	27.50±0.49	24.29±0.19
AW (Water Activity)^{ns}	0.52±0.03	0.56±0.02
<u>Microbiological quality</u>		
Total Microbiological (CFU/G)	230	250
Yeast and Mold (CFU/G)	Not Detected	Not Detected

Data in the table are shown as mean ± standard deviation.

อภิปรายผล

การพัฒนาน้ำพริกปลาแห้งทดแทนด้วยถั่วหรั่งบางส่วน ระหว่างสูตรพื้นฐาน กับสูตรถั่วหรั่ง ร้อยละ 25 จากการวิเคราะห์คุณภาพทางเคมี พบว่า ปริมาณไขมัน เถ้า และปริมาณใยอาหาร ทั้ง 2 สูตร ไม่มีความแตกต่างกันอย่างมีนัยสำคัญทางสถิติ (<0.5) ปริมาณโปรตีน พบว่า ทั้ง 2 สูตร มีความแตกต่างกันอย่างมีนัยสำคัญทางสถิติ (<0.5) คือ 33.49±0.71 , 24.23±1.41 เนื่องจากสูตรทดแทนด้วยถั่วหรั่งมีการใช้ถั่วหรั่งทดแทนปลาแห้ง ซึ่งโปรตีนจากถั่วหรั่งเป็นประเภทโปรตีนไม่สมบูรณ์ และมีกรดอะมิโนจำเป็นไม่ครบถ้วน จึงทำให้ปริมาณโปรตีนในสูตรน้ำพริกปลาแห้งทดแทนด้วยถั่วหรั่งมีปริมาณโปรตีนต่ำกว่าสูตรพื้นฐาน ปริมาณคาร์โบไฮเดรต พบว่า ทั้ง 2 สูตร มีความแตกต่างกันอย่างมีนัยสำคัญทางสถิติ (<0.5) คือ 51.80±0.83 ,60.72±1.41 เนื่องจากการใช้ถั่วหรั่งทดแทนปลาแห้งในน้ำพริกทำให้ปริมาณคาร์โบไฮเดรต

เพิ่มขึ้น โดยถั่วหรั่งมีปริมาณคาร์โบไฮเดรตสูงกว่าเนื้อปลา (ตารางแสดงคุณค่าทางโภชนาการของอาหารไทย,2561) และด้านความชื้น พบว่า ทั้ง 2 สูตร ไม่มีความแตกต่างกันอย่างนัยสำคัญทางสถิติ (<0.5) เนื่องจากในการผลิตน้ำพริกมีการควบคุมอุณภูมิและเวลาในการคั่วแห้งทั้ง 2 สูตร

การวิเคราะห์คุณภาพทางกายภาพ ผลค่าสี L*(ความสว่าง) a*(สีแดง) และ b*(สีเหลือง) พบว่า ทั้ง 2 สูตร ไม่มีความแตกต่างกันอย่างมีนัยสำคัญทางสถิติ (<0.5) ซึ่งจะเห็นได้ว่าจากการวิเคราะห์ค่าสีน้ำพริกทั้ง 2 สูตร มีค่าสีเป็นสีแดง เนื่องจากทั้ง 2 สูตรมีส่วนประกอบปริมาณของพริกเท่ากัน ผลค่า Aw พบว่า ทั้ง 2 สูตร ไม่มีความแตกต่างกันอย่างนัยสำคัญทางสถิติ (<0.5) โดยมีผล คือ 0.52±0.03 ,0.56±0.02 ซึ่งเป็นไปตามมาตรฐานผลิตภัณฑ์ชุมชน (มผช.น้ำพริกป่นแห้ง 130/2556) ต้องไม่เกิน 0.6 และมีผลใกล้เคียงกับงานวิจัยการผลิตน้ำพริกพริกไทยดำก่อนและหลังการปรับปรุงการเตรียมวัตถุดิบเมื่อปรับปรุงโดยการล้าง ลวก ตากทำให้ ค่า Aw เท่ากับ 0.447 [4]

การวิเคราะห์คุณภาพทางจุลินทรีย์ พบว่า ทั้ง 2 สูตร ไม่มีความแตกต่างกันอย่างมีนัยสำคัญทางสถิติ โดยมีผลปริมาณจุลินทรีย์ทั้งหมดเท่ากับ 2.3×10^2 , 2.5×10^2 โคโลนีต่อกรัม และไม่พบการปนเปื้อนของเชื้อยีสต์และรา ซึ่งเป็นไปตามมาตรฐานผลิตภัณฑ์ชุมชน (มผช.น้ำพริกป่นแห้ง 130/2556) ซึ่งจุลินทรีย์ทั้งหมด ต้องไม่เกิน 1×10^4 โคโลนีต่อกรัม เชื้อยีสต์และรา 100 โคโลนีต่อ 1 กรัม โดยมีผลใกล้เคียงกับงานวิจัย การพัฒนาผลิตภัณฑ์น้ำพริกแห้งจากเม็ดบัว ที่พบว่าน้ำพริกผัดแห้งเม็ดบัว มีปริมาณจุลินทรีย์ปนเปื้อนต่ำกว่าเกณฑ์มาตรฐานที่ มผช. กำหนด โดยมีปริมาณจุลินทรีย์ทั้งหมด 3 x10 โคโลนี/ตัวอย่าง 1 กรัม ไม่พบการปนเปื้อนของ ยีสต์และรา [1]

ข้อสรุป

จากการทดลองคาดว่ามีแนวโน้มที่จะสามารถใช้ถั่วหรั่งทดแทนปลาในผลิตภัณฑ์น้ำพริก สำหรับกลุ่มคนที่รับประทานอาหารประเภทมังสวิรัติและสามารถนำถั่วหรั่งไปใช้ในกลุ่มผลิตภัณฑ์น้ำพริกอื่น ๆ ได้

คำขอบคุณ

ขอบคุณสาขาวิชาคหกรรมศาสตร์ คณะวิทยาศาสตร์และเทคโนโลยี และมหาวิทยาลัยราชภัฏภูเก็ต ที่สนับสนุนห้องปฏิบัติการ เครื่องมือและอุปกรณ์ในการทำงานวิจัย

อ้างอิง

[1] กนกวรรณ ปุณณะตระกูล, ยศพร พลายโถ, อัจจิมา มั่นทน. (2560). การพัฒนาผลิตภัณฑ์น้ำพริกแห้งจากเม็ดบัว วารสารวิจัยและพัฒนาวไลยอลงกรณ์ ในพระบรมราชูปถัมภ์ สาขาวิทยาศาสตร์และเทคโนโลยี. 11(1) , 109 – 117.

[2] จารุวรรณ์ รัตนสกุลธรรม, วิมลวรรณ วัฒนวิจิตร, ประยูร เอ็นมาก, ฉันทนา คงนคร. (2564). รายงายวิจัย เรื่อง การเก็บรักษาถั่วหรั่งในน้ำเกลือ

[3] จักรินทร์ ตรีอินทอง และ ปิยะฉัตร วิริยะอำไพวงศ์ .(2566). การพัฒนาผลิตภัณฑ์น้ำพริกปลานิลเค็ม. วารสารเกษตรพระวรุณ. 20(2) , 151 – 159.

[4] ชมพูนุช โสมาลีย์ และชาคริยา ฉลาด. (2564). รายงายวิจัย เรื่อง การควบคุมคุณภาพวัตถุดิบและศึกษาอายุการเก็บรักษาของผลิตภัณฑ์น้ำพริกพริกไทยดำเพื่อเพิ่มประสิทธิภาพการผลิตให้ได้มาตรฐานของกลุ่มแม่บ้านบ้านเขาหลัก จังหวัดตรัง. ม.ป.ท. ม.ป.พ.

[5] ผกาวดี ภู่จันทร์, โสรัจวรชุม อินเกต , ไพรวัลย์ ประมัย , สุสิตรา สิงโสม. (2563). การพัฒนาน้ำพริกผัดสมุนไพร. วารสารวิจัยรำไพพรรณี. 14(1) , 131-138

[6] สถาพร โชติช่วง. (2564). รายงายวิจัย เรื่อง การวิจัยและพัฒนาการผลิตถั่วหรั่งเพื่อเพิ่มมูลค่าและการแปรรูป. ม.ป.ท. ม.ป.พ. กรมวิชาการเกษตร.

[7] สำนักงานโภชนาการ (2561). สืบค้น กุมภาพันธ์ 21, 2568. ตารางแสดงคุณค่าทางโภชนาการของอาหารไทย, 2561, กรมอนามัย.จาก https://nutrition2.anamai.moph.go.th/th/book/194494

[8] สำนักงานมาตฐานผลิตภัณฑ์อุตสาหกรรม. (2546). สืบค้น กุมภาพันธ์ 20, 2568. มาตรฐานผลิตภัณฑ์ชุมชน น้ำพริกป่นแห้ง (มผช.130/2546). กองการบริหารมาตฐานผลิตภัณฑ์ชุมชนสำนักงานมาตรฐานผลิตภัณฑ์อุตสาหกรรม.จาก https://tcps.tisi.go.th/public/ StandardList. aspx

การพัฒนาผลิตภัณฑ์ครองแครงกรอบเสริมปลากะตักผง

Development of Crispy Snack (KrongKrang Krob) with Anchovy Fish Powder

1st Kanokwan Thongkiaw
Faculty of Science and Technology
Phuket Rajabhat University
Phuket, Thailand
Kanokwan.h@pkru.ac.th

2nd Jerapat Ploykhaw
Faculty of Science and Technology
Phuket Rajabhat University
Phuket, Thailand
Jerapat.p@pkru.ac.th

3rd Sangrawee Na pattalung
Faculty of Science and Technology
Phuket Rajabhat University
Phuket, Thailand
Sangrawee.s@pkru.ac.th

This research aims to determine the appropriate amount of anchovy powder in crispy krong krang products before coating with sauce and to study the optimal ratio of concentrated pineapple juice in the coating sauce. The study found that when adding anchovy powder at 5%, 10%, and 15% of the total weight, consumers preferred the product with 5% anchovy powder in the dough before sauce coating. This level received the highest overall sensory acceptance score (p□0.05). The product was then further analyzed for the optimal ratio of concentrated pineapple juice in the pineapple sauce, tested at three levels: 50%, 70%, and 90% of the weight of coconut sugar. Consumers showed the highest acceptance for the replacement of concentrated pineapple juice at 90%, which received the highest overall sensory acceptance score (p□ 0.05). Additionally, the moisture content and water activity (aw) values met the community product standard for crispy krong krang.

Keywords KrongKrang Krob, Anchovy Fish Powder

บทนำ

ปลากะตักเป็นปลาที่มีขนาดเล็กที่พบเผยแพร่กระจายอยู่ทั่วไปตามชายฝั่งอ่าวไทยและทะเลอันดามันซึ่งในประเทศไทยมีอยู่ ชนิด โดยสามารถ 6 เรียกชื่อตามท้องถิ่นหลายชื่อได้แก่ ปลาไส้ตัน ปลากะตักหัวแหลมปลามะลิ ปลาจิ้งจั้ง ปลาหัวอ่อน ปลายิ่วเก๊ียะ ลักษณะเด่นคือ ลำตัวค่อนข้างกลม เห็นกระดูกชัดเจน ครีบก้นมีจุดเริ่มอยู่หลังบริเวณด้านท้ายฐานครีบหลัง และมีแถบสีน้ำเงินข้างตัวชัดเจน จากการวิเคราะห์คุณค่าทางโภชนาการของปลากะตักแห้ง มิลลิกรัม 26.1333 กรัม แคลเซียม 1.70 กรัม ประกอบด้วยโปรตีน 100 ไมโครกรัม 85.304 และไอโอดีน [4] ด้วยคุณสมบัติของปลากะตักที่มีอยู่จึงสามารถนำมารับประทานหรือประกอบเป็นอาหารว่าง เพื่อเพิ่มประโยชน์ให้กับผู้บริโภคและผลิตภัณฑ์ขนมหรืออาหารได้มากขึ้น

ครองแครงกรอบเป็นอาหารว่างไทย ลักษณะคล้ายก้นหอยรสชาติหวานมันเค็ม ได้จากการผสมแป้งสาลีอเนกประสงค์ น้ำกะทิ ไข่ไก่ น้ำปูนใส น้ำมันพืช น้ำตาลทราย และเกลือ นวดจนเข้ากันนำไปรีดให้เป็นแผ่น กดด้วยพิมพ์ที่มีลักษณะเป็นซี่ๆ คล้ายก้นหอย แล้วนำไปทอดจนสุกกรอบ จากนั้นนำมาคลุกเคล้ากับน้ำเคลือบที่มีส่วนผสมของน้ำตาล น้ำเปล่า น้ำปลา เกลือ รากผักชี กระเทียม และพริกไทยโขลกรวมกัน ทำให้ครองแครงกรอบมีรสหวานและเค็ม [5] นอกจากนี้ผู้วิจัยยังใช้ผลไม้ในท้องถิ่นซึ่งเป็นสับปะรดที่เป็นพืชเศรษฐกิจโดยนิยมปลูกเพื่อใช้ในการแปรรูปได้เกือบทั้งหมด และจัดเป็นผลไม้ที่ดีต่อสุขภาพเพราะมีเอนไซม์โบรมิเลนซึ่งมีคุณสมบัติในการช่วยย่อยในระบบทางเดินอาหาร โดยสับปะรดภูเก็ตจะมีลักษณะ กรอบ มีเนื้อสีเหลืองสม่ำเสมอทั้งผล มีกลิ่นหอมเฉพาะตัว ผลขนาดเล็กทำให้มีเสน่ห์เฉพาะตัว

ดังนั้นผู้วิจัยจึงเล็งเห็นความสำคัญในการพัฒนาผลิตภัณฑ์ครองแครงกรอบเสริมปลากะตักผง โดยศึกษาปริมาณปลากะตักผงที่เหมาะสมในผลิตภัณฑ์ครองแครงกรอบ และอัตราส่วนน้ำสับปะรดเข้มข้นที่เหมาะสมในน้ำซอสเคลือบครองแครงกรอบ เพื่อเป็นการใช้วัตถุดิบในท้องถิ่นสะท้อนถึงเอกลักษณ์ของท้องถิ่น และสร้างความหลากหลายให้กับผลิตภัณฑ์ อีกทั้งยังเป็นการเพิ่มมูลค่าให้กับปลากะตักที่ตกเกรด และยังได้รสชาติจากน้ำซอสสับปะรดที่ใช้เคลือบครองแครงกรอบเพื่อให้มีรสชาติที่เป็นเอกลักษณ์เฉพาะด้วย

ทบทวนวรรณกรรม

[1] ผลของการเสริมเปลือกมะม่วงน้ำดอกไม้ในผลิตภัณฑ์ครองแครงกรอบต่อสมบัติทางเคมีกายภาพและสมบัติทางประสาทสัมผัส เป็นการนำเปลือกผลไม้มาเสริมลงในผลิตภัณฑ์ครองแครงกรอบ โดยมีความแตกต่างกันในส่วนของงานวิจัยที่ใช้ปลากะตักแทนการใช้เปลือกผลไม้ แต่มีจุดมุ่งหมายในการเพิ่มมูลค่าให้กับผลิตผลทางการเกษตรเช่นเดียวกัน

[2] การพัฒนาศักยภาพสับปะรดในผลิตภัณฑ์ซอสสำเร็จรูป มีการนำสับปะรดที่ตกเกรดนำมาผลิตซอสผัดไทย ซอสหมี่กรอบ และซอสสามรสโดยใช้น้ำสับปะรดเป็นส่วนผสมหลัก ซึ่งมีจุดเด่นที่สอดคล้องกับงานวิจัยที่ใช้น้ำซอสสับปะรดที่เคลือบครองแครงกรอบ

[4] การใช้ประโยชน์จากวัสดุเศษเหลือหัวปลากะตักเสริมโปรตีนและแคลเซียมในผลิตภัณฑ์อาหาร มีการผลิตผลิตภัณฑ์อาหารเติมหัวปลากะตักตากแห้งลงในผลิตภัณฑ์ขนมได้แก่ ขนมทองม้วน ขนมข้าวพอง และขนมกรอบพอง ซึ่งปรุงรสด้วยแกงไทย เพื่อต้องการแหล่งโปรตีนและแคลเซียม รวมถึงเพิ่มมูลค่าของอาหารไทย โดยจากงานวิจัยที่ผู้วิจัยศึกษาได้เลือกใช้ปลากะตักที่ตกเกรดนำมาผลิตผลิตภัณฑ์อาหารว่างประเภททอดคือครองแครงกรอบ จากงานวิจัยจึงมีแนวทางที่สอดคล้องกัน เพื่อต้องการเพิ่มแหล่งโปรตีนและคุณค่าทางโภชนาการให้เพิ่มจากเดิม

ระเบียบวิธีวิจัย

การผลิตปลากะตักผง

คัดเลือกปลากะตักที่ตกเกรดหรือไม่ผ่านมาตรฐาน นำมาแช่น้ำสะอาดที่อุณหภูมิห้องเป็นเวลา 6 ชั่วโมง เพื่อลดความเค็มจากปลากะตัก จากนั้นล้างด้วยน้ำสะอาด พักไว้บนตะแกรงเพื่อให้สะเด็ดน้ำประมาณ 15 นาที นำปลากะตักใส่ถาดเกลี่ยให้ทั่วเพื่อนำเข้าอบโดยอุณหภูมิความร้อนที่ระดับ

150 องศาเซลเซียสเป็นเวลา 40 นาที จากนั้นนำปลากะตักที่ได้มาปั่นให้ละเอียดด้วยเครื่องปั่นอาหาร แล้วร่อนด้วยตะแกรง 60 mesh จำนวน 3 รอบ เพื่อให้ได้ปลากะตักผงที่มีเนื้อสัมผัสที่ค่อนข้างละเอียด และเก็บรักษาด้วยถุงฟอยด์อลูมิเนียมกันความชื้น

การศึกษาปริมาณปลากะตักผงที่เหมาะสมในผลิตภัณฑ์ครองแครงกรอบก่อนเคลือบซอส

คัดเลือกและดัดแปลงสูตรครองแครงกรอบจากยศพรและคณะ [5] จากนั้นศึกษาปริมาณปลากะตักผงที่ระดับร้อยละ ของปริมาณ และ15 10 5 น้ำหนักทั้งหมด(Table 1) ดังนี้ แป้งสาลีอเนกประสงค์ร้อยละ 60 ไข่ไก่ร้อยละ 15.10 เกลือร้อยละ 1 น้ำกะทิร้อยละ 11.53 น้ำปูนใสร้อยละ12.37 โดยมีวิธีการผลิตครองแครงกรอบดังนี้ ชั่งน้ำหนักส่วนผสมตามสูตรพื้นฐาน ร่อนแป้งสาลีพักไว้และผสมส่วนผสมที่เป็นของเหลวรวมกัน จากนั้นนวดให้เข้ากัน ปั้นแป้งเป็นก้อนขนาด กรัม คลึงแป้งด้วยไ 3ม้คลึงแป้งและกดกับพิมพ์ครองแครง นำไปทอดที่อุณหภูมิ 14นาที ตักขึ้น 5 องศาเซลเซียสเป็นเวลา 0 พักให้สะเด็ดน้ำมัน เคลือบด้วยน้ำเคลือบครองแครงกรอบที่ประกอบด้วยรากผักชีร้อยละ 14 น้ำเปล่าร้อยละ 13 กระเทียมร้อยละ 5 พริกไทยดำร้อยละ 18 และน้ำตาลมะพร้าวร 2 เกลือร้อยละ้อยละ 48 ผัดให้เหนียวที่อุณหภูมิประมาณ นาที 1 องศาเซลเซียส ใส่ตัวแป้งครอบแครงที่ทอดลงคลุกให้ทั่ว 120 เทใส่ถาด เกลี่ยให้กระจาย และนำเข้าเตาอบเพื่อลดความชื้นที่อุณหภูมิ 5±60 เวลา นาที 5

Table 1 Ingredients of KrongKrang Krob with Anchovy Fish Powder

Ingredients	Content (%)		
	5%	**10%**	**15%**
Wheat Flour	60	60	60
Egg	15.10	15.10	15.10
Salt	1	1	1
Coconut milk	11.53	11.53	11.53
limewater	12.37	12.37	12.37
Anchovy Fish Powder	5	10	15

การศึกษาอัตราส่วนน้ำสับปะรดเข้มข้นที่เหมาะสมของซอสสับปะรดในผลิตภัณฑ์ครองแครงกรอบ

คัดเลือกและดัดแปลงสูตรน้ำเคลือบครองแครงกรอบจากยศพรและคณะ [5] จากนั้นศึกษาอัตราส่วนน้ำสับปะรดเข้มข้นทดแทนน้ำตาลมะพร้าวที่ระดับร้อยละ 50 70 และ90 ของปริมาณน้ำหนักน้ำตาลมะพร้าว (Table 2) ดังนี้ รากผักชีร้อยละ 18 พริกไทยดำร้อยละ 5 กระเทียมร้อยละ 13 น้ำเปล่าร้อยละ 14 เกลือร้อยละ 2 และน้ำตาลมะพร้าวร้อยละ 48 ในส่วนการผลิตน้ำสับปะรดเข้มข้นเริ่มจากการนำสับปะรดไปปั่นแล้วกรองผ่านผ้าขาวบางน้ำสับปะรดสดก่อนเคี่ยววัดปริมาณความหวาน (°Brix) ด้วยเครื่องรีแฟรกโตมิเตอร์ ได้ค่าความหวานก่อนเคี่ยวที่ 14 องศาบริกซ์ จากนั้นเคี่ยวน้ำสับปะรดที่อุณหภูมิ 80 องศาเซลเซียสเวลา 30 นาที น้ำสับปะรดเข้มข้นนำมาวัดปริมาณความหวาน (°Brix) หลังเคี่ยวได้ค่าความหวานที่ 26 องศาบริกซ์ แล้วนำไปคลุกกับแป้งครองแครงกรอบที่เตรียมไว้

Table 2 Ingredients of Sauce from Pineapple

Ingredients	Content (%)		
	50%	70%	90%
Coriander root	18	18	18
Black pepper	5	5	5
Garlic	13	13	13
Water	14	14	14
Salt	2	2	2
Coconut sugar	24	14.4	4.8
Pineapple squash	24	33.6	43.2

การศึกษาคุณภาพทางกายภาพของผลิตภัณฑ์ครองแครงกรอบเสริมปลากะตักผง

การวิเคราะห์ความชื้นในตัวอย่างด้วยเครื่องวิเคราะห์ความชื้น (A&D, Japan, MX50) โดยการชั่งตัวอย่างครองแครงกรอบปริมาณ 5 กรัม ใส่ลงในถาดอะลูมิเนียม ปรับตั้งค่าการวิเคราะห์ความชื้นที่อุณหภูมิ 100 องศาเซลเซียส

การวิเคราะห์ค่า water activity (a_w) ด้วยเครื่อง Water Activity (Rotronic Instruments, UK) โดยการชั่งตัวอย่างครองแครงกรอบปริมาณ 5 กรัม ใส่ลงในภาชนะใส่ตัวอย่าง แล้วนำมาวิเคราะห์ค่า a_w ที่อุณหภูมิ 25 องศาเซลเซียส

การศึกษาการยอมรับทางด้านประสาทสัมผัสของผลิตภัณฑ์ครองแครงกรอบเสริมปลากะตักผง

การทดสอบทางประสาทสัมผัสต่อการยอมรับผลิตภัณฑ์ครองแครงกรอบเสริมปลากะตักผง ประเมินการยอมรับของผู้บริโภคด้วยวิธีทดสอบแบบ 9-point hedonic scale (คะแนนเท่ากับ 1 คือไม่ชอบมากที่สุด และคะแนนเท่ากับ 9 คือชอบมากที่สุด) คัดเลือกโดยการสุ่มจากผู้ที่มีประสบการณ์ในการทดสอบจำนวน 50 คน

การวิเคราะห์ผลทางสถิติ

การวิเคราะห์คุณภาพทางกายภาพมีการวางแผนการทดลองแบบการวางแผนการทดลองแบบสุ่มสมบูรณ์ (completely randomized design, CRD) ส่วนการประเมินการยอมรับของผู้บริโภคจะวางแผนการทดลองแบบสุ่มในบล็อคสมบูรณ์ (Randomized complete block Design, RCBD) แล้ววิเคราะห์ความแปรปรวน ANOVA จากนั้นนำไปวิเคราะห์ความแตกต่างของค่าเฉลี่ยที่ระดับนัยสำคัญ 0.05 ด้วยวิธี Duncan's New Multiple Range Test เพื่อวิเคราะห์ข้อมูลทางสถิติโดยโปรแกรม IBM SPSS Statistic for Windows, version 22.0 (IBM, USA)

ผลการทดลอง

ผลการศึกษาคุณภาพทางกายภาพของผลิตภัณฑ์ครองแครงกรอบเสริมปลากะตักผง

จากการศึกษาผลคุณภาพทางกายภาพของผลิตภัณฑ์ครองแครงกรอบเสริมปลากะตักผงเคลือบซอสสับปะรด พบว่าปริมาณความชื้นและค่า a_w ของตัวอย่างผลิตภัณฑ์ (Table 3) มีค่าไม่แตกต่างอย่างมีนัยสำคัญทางสถิติ

(p>0.05) โดยเป็นไปตามมาตรฐานผลิตภัณฑ์ชุมชนครองแครงกรอบ (มผช.267/2552) ซึ่งเป็นคุณลักษณะที่ต้องการของผลิตภัณฑ์ [6] โดยเป็นปัจจัยสำคัญในการควบคุมและป้องกันการเสื่อมเสียของผลิตภัณฑ์อาหาร มีผลโดยตรงต่ออายุการเก็บรักษาผลิตภัณฑ์

Table 3 Physical properties of KrongKrang Krob with Anchovy Fish Powder Sauce Pineapple

Physical properties	of KrongKrang Krob with Anchovy Fish Powder Sauce Pineapple		
	50%	70%	90%
moisture (%)	3.63±0.22^{a}	3.58±0.05^{a}	3.60±0.17^{a}
a_w	0.30±0.01^{a}	0.28±0.42^{a}	0.27±0.54^{a}

ผลการศึกษาปริมาณปลากะตักผงที่เหมาะสมในผลิตภัณฑ์ครองแครงกรอบก่อนเคลือบซอส

ผลการทดสอบการยอมรับทางประสาทสัมผัสของผลิตภัณฑ์ครองแครงกรอบเสริมปลากะตักก่อนเคลือบซอสที่ระดับร้อยละ 5 10 และ 15 ของปริมาณน้ำหนักทั้งหมด (Table 4) พบว่าปริมาณปลากะตักผงที่เหมาะสมในผลิตภัณฑ์ครองแครงกรอบก่อนเคลือบซอสที่ระดับร้อยละ 5 ของปริมาณน้ำหนักทั้งหมด ได้รับคะแนนเฉลี่ยสูงสุด คุณลักษณะปรากฏ สี รสชาติ เนื้อสัมผัส และความชอบโดยรวม มีความแตกต่างกันอย่างมีนัยสำคัญทางสถิติ (p≤0.05)

Table 4 Sensory characteristics of KrongKrang Krob with Anchovy Fish Powder

Attributes	KrongKrang Krob with Anchovy Fish Powder		
	5%	**10%**	**15%**
Appearance	7.58 ± 1.05^{a}	7.30 ± 1.11^{ab}	6.94 ± 1.50^{b}
Color	7.52 ± 1.12^{a}	7.32 ± 1.28^{ab}	7.04 ± 1.65^{b}
Odor^{ns}	7.14 ± 1.40	6.96 ± 1.56	6.82 ± 1.35
Taste	7.12 ± 1.33^{a}	6.84 ± 1.64^{a}	6.26 ± 1.78^{b}
Texture	7.24 ± 1.50^{a}	6.84 ± 1.51^{a}	5.92 ± 2.24^{b}
Overall	7.70 ± 1.14^{a}	7.52 ± 1.26^{a}	6.88 ± 1.58^{b}

a-c Mean within the same column with different letters are significantly different (p≤0.05) 1/Karanda juice

ns Not significant

ผลการศึกษาอัตราส่วนน้ำสับปะรดที่เหมาะสมของซอสสับปะรดในผลิตภัณฑ์ครองแครงกรอบ

ผลการทดสอบการยอมรับทางประสาทสัมผัสของอัตราส่วนน้ำสับปะรดที่เหมาะสมของซอสสับปะรดในผลิตภัณฑ์ครองแครงกรอบที่ระดับร้อยละ50 70และ 90 ของปริมาณน้ำหนักน้ำตาลมะพร้าว (Table 5) พบว่า อัตราส่วนน้ำสับปะรดเข้มข้นที่เหมาะสมในผลิตภัณฑ์ครองแครงกรอบซอสสับปะรดเสริมปลากะตักผงที่ระดับร้อยละ 90 ของปริมาณน้ำหนักน้ำตาลมะพร้าว ได้รับคะแนนเฉลี่ยสูงสุด คุณลักษณะปรากฏ สี กลิ่น เนื้อสัมผัส และความชอบโดยรวม มีความแตกต่างกันอย่างมีนัยสำคัญทางสถิติ (p≤0.05)

Table 5 Sensory characteristics of Sauce from the Pineapple

Attributes	Sauce from the Pineapple		
	50%	**70%**	**90%**
Appearance	6.96 ± 1.51^{b}	7.34 ± 1.22^{a}	7.44 ± 1.07^{a}
Color	7.08 ± 1.51^{b}	7.32 ± 1.16^{ab}	7.48 ± 1.07^{a}
Odor	6.66 ± 1.49^{b}	7.18 ± 1.25^{a}	7.00 ± 1.27^{ab}
Taste^{ns}	6.82 ± 1.90	7.24 ± 1.57	7.26 ± 1.36
Texture	6.42 ± 1.80^{b}	6.90 ± 1.68^{ab}	7.08 ± 1.39^{a}
Overall	7.14 ± 1.27^{b}	7.52 ± 1.26^{a}	6.88 ± 1.58^{b}

a-c Mean within the same column with different letters are significantly different (p≤0.05) 1/Karanda juice

ns Not significant

อภิปรายผล

จากการทดสอบการยอมรับทางประสาทสัมผัสของผลิตภัณฑ์ครองแครงกรอบเสริมปลากะตักก่อนเคลือบซอสที่ระดับร้อยละ 5 10 และ 15 ของปริมาณน้ำหนักทั้งหมด (Table 4) พบว่าปริมาณปลากะตักผงที่เหมาะสมในผลิตภัณฑ์ครองแครงกรอบก่อนเคลือบซอสที่ระดับร้อยละ 5 ของปริมาณน้ำหนักทั้งหมด ได้รับคะแนนเฉลี่ยสูงสุด คุณลักษณะปรากฏ สี รสชาติ เนื้อสัมผัส และความชอบโดยรวม มีความแตกต่างกันอย่างมีนัยสำคัญทางสถิติ (p≤0.05) นอกจากนี้ยังมีข้อสังเกตได้ว่าปริมาณปลากะตักผงที่เพิ่มมากขึ้นทำให้คะแนนความชอบด้านกลิ่นไม่แตกต่างกันอาจเป็นเพราะปลากะตักมีกลิ่นที่เป็นเอกลักษณ์เฉพาะตัวไม่ว่าจะใส่ในปริมาณเท่าใดก็ไม่ได้ส่งผลต่อกลิ่นที่แตกต่างกัน อีกทั้งเมื่อมีการเสริมปลากะตักผงมากขึ้นจะมีลักษณะของสีผลิตภัณฑ์ที่ชัดขึ้น อีกทั้งได้มีความสอดคล้องกับการศึกษาของอรัญญาและพรหมภัสสร [7] ที่ศึกษาการผลิตและสมบัติของข้าวเกรียบปลาจากปลาเล็กปลาน้อยที่ผ่านการทอดแล้วจะมีสีเหลืองอ่อน กรอบ ฟู และมีกลิ่นปลา เนื่องจากปลากะตักที่นำมาใช้เป็นวัตถุดิบหลักมีสีน้ำตาลอ่อน และยังมีส่วนประกอบอื่นๆที่ทำให้เกิดสี และสามารถเกิดปฏิกิริยาสีน้ำตาลเมื่อได้รับความร้อนจากการทอดและการออกซิเจนของไขมันทำให้น้ำมันมีสีคล้ำลง นอกจากนี้เมื่อมีปริมาณปลากะตักผงที่เพิ่มขึ้นกลับทำให้ตัวแป้งครองแครงกรอบมีช่องว่างหรือโพรงอากาศในเนื้อผลิตภัณฑ์ที่น้อยลงจึงทำให้เนื้อสัมผัสครองแครงกรอบมีความกรอบค่อนไปทางแข็ง นอกจากนี้เมื่อเพิ่มปริมาณปลากะตักผงลงในแป้งครองแครงกรอบ ส่งผลต่อการดูดซับน้ำของเม็ดสตาร์ชและการเกิดเจลของแป้งในแป้งครองแครงกรอบให้มีลักษณะปรากฏที่ไม่พองฟู และเมื่อนำไปทอดทำให้แป้งครองแครงกรอบเกิดการพองตัวและการขยายตัวลดลงอีกด้วย

จากการทดสอบการยอมรับทางประสาทสัมผัสของอัตราส่วนน้ำสับปะรดที่เหมาะสมของซอสสับปะรดในผลิตภัณฑ์ครองแครงกรอบ โดยระดับร้อยละ 50 70 และ90 ของปริมาณน้ำหนักน้ำตาลมะพร้าว (Table 5) พบว่าอัตราส่วนน้ำสับปะรดเข้มข้นที่เหมาะสมในผลิตภัณฑ์กรอบเค็มซอสสับปะรดเสริมปลากะตักผงที่ระดับร้อยละ ของปริมาณน้ำหนักน้ำตาลมะพร้าว 90ได้รับคะแนนเฉลี่ยสูงสุด คุณลักษณะปรากฏ สี กลิ่น เนื้อสัมผัส และความชอบ

โดยรวม มีความแตกต่างกันอย่างมีนัยสำคัญทางสถิติ (p≤(05.0 เนื่องด้วยอัตราส่วนน้ำสับปะรดที่เพิ่มมากขึ้นทำให้คะแนนความชอบด้านรสชาติไม่แตกต่างกันอาจเป็นเพราะในน้ำสับปะรดมีกรดซิตริกและกรดมาลิกสูงจึงทำให้เกิดรสเปรี้ยว [8] ไม่ว่าจะใส่ในปริมาณเท่าใดก็ไม่ได้ส่งผลต่อรสชาติที่แตกต่างกัน อีกทั้งเมื่อมีการเพิ่มอัตราส่วนน้ำสับปะรดเข้มข้นมากขึ้นจะมีลักษณะของสีผลิตภัณฑ์ที่ชัดขึ้น ผลการทดลองมีแนวโน้มเช่นเดียวกับงานวิจัยของ ผกาวดี ภู่จันทร์ และคณะ [3] ที่ศึกษาผลิตภัณฑ์คุกกี้เสริมใยอาหารจากกากสับประรด ซึ่งพบว่าเมื่อมีการเติมกากสับปะรดที่มากขึ้นจะมีค่าความเป็นสีเหลืองเพิ่มมากขึ้น ทั้งนี้อาจเป็นเพราะในสับปะรดมีเอนไซม์โพลีฟีนอลออกซิเดสซึ่งเป็นสาเหตุสำคัญทำให้เกิดสีน้ำตาลแบบใช้เอนไซม์ การเกิดสีน้ำตาลแบบไม่ใช้เอนไซม์หรือปฏิกิริยาเมลลาร์ด (Maillard reaction) เกิดจากในสับปะรดมีน้ำตาลรีดิวซ์ เช่น ฟรุกโตส (Fructose)และกลูโคส (Glucose) เมื่อทำปฏิกิริยากับสารประกอบไนโตรเจนโดยมีความร้อนในระหว่างการเคี่ยวน้ำสับปะรดเข้มข้น ซึ่งเป็นตัวเร่งให้เกิดปฏิกิริยาดีไฮเดรชันได้เป็นอนุพันธ์ของฟูแรน (Furan) พอลิเมอร์ไรซ์อย่างรวดเร็วได้เป็นสารสีน้ำตาลที่มีไนโตรเจนเป็นองค์ประกอบทำให้ผลิตภัณฑ์มีสีเข้มข้น อย่างไรก็ตามผลคุณภาพทางกายภาพของผลิตภัณฑ์ครองแครงกรอบเสริมปลากะตักผงพบว่า ปริมาณความชื้นและค่า a_w ของตัวอย่างผลิตภัณฑ์ (Table 3) มีค่าไม่แตกต่างอย่างมีนัยสำคัญทางสถิติ (p>0.05) โดยเป็นไปตามมาตรฐานผลิตภัณฑ์ชุมชนครองแครงกรอบ (มผช.267/2552) ซึ่งเป็นคุณลักษณะที่ต้องการของผลิตภัณฑ์ [6] โดยเป็นปัจจัยสำคัญในการควบคุมและป้องกันการเสื่อมเสียของผลิตภัณฑ์อาหาร มีผลโดยตรงต่ออายุการเก็บรักษาผลิตภัณฑ์

ข้อสรุป

จากการวิจัยเรื่องนี้ทำให้ทราบว่าปลากะตักผงสามารถเสริมในผลิตภัณฑ์ครองแครงกรอบได้ที่ร้อยละ 5 ของปริมาณน้ำหนักทั้งหมด และอัตราส่วนน้ำสับปะรดที่เหมาะสมของซอสสับปะรดที่ร้อยละ 90 ของปริมาณน้ำตาลมะพร้าว ดังนั้นผลิตภัณฑ์ครองแครงกรอบจึงเหมาะแก่การส่งเสริมให้มีการผลิตในชุมชนเพื่อเป็นรายได้เสริม ตลอดจนยังช่วยก่อให้เกิดการใช้ประโยชน์และเพิ่มมูลค่าจากวัตถุดิบในท้องถิ่นได้

คำขอบคุณ

ขอขอบคุณสาขาวิชาคหกรรมศาสตร์ คณะวิทยาศาสตร์และเทคโนโลยี มหาวิทยาลัยราชภัฏภูเก็ต ที่สนับสนุนเครื่องมือและสถานที่ทำงานวิจัย

อ้างอิง

[1] ปานจิต ป้อมอาสา สิริมา สินธุสำราญ สามารถ สายอุต และชัยรัตน์ เตชวุฒิพร. (2566). ผลของการเสริมเปลือกมะม่วงน้ำดอกไม้ในผลิตภัณฑ์ครองแครงกรอบต่อสมบัติทางเคมีกายภาพและสมบัติทางประสาทสัมผัส. **วารสารวิทยาศาสตร์บูรพา, 28(3),** 1749-1765.

[2] เปรมระพี อุยมาวีรหิรัญ เชาวลิต อุปฐาก ลัดดาวัลย์ กลิ่นมาลัย และน้อมจิตต์ สุธีบุตร. (2562). **รายงานวิจัย เรื่อง การพัฒนาศักยภาพสับปะรดตกเกรด ในผลิตภัณฑ์ซอสสำเร็จรูป**. กรุงเทพฯ: มหาวิทยาลัยเทคโนโลยีราชมงคลพระนคร.

[3] ผกาวดี ภู่จันทร์ ปภาวรินทร์ หนูฉิม นันท์ชพร สาดอ่ำ และอารยา พรานเสือ. (2564). การพัฒนาผลิตภัณฑ์คุกกี้เสริมใยอาหารจากกากสับปะรดโดยการอบด้วยเตาถ่าน. **วารสารมหาวิทยาลัยศรีนครินทรวิโรฒ (สาขาวิทยาศาสตร์และเทคโนโลยี), 13(25),** 97-109.

[4] พรเพ็ญ อาสนศักดิ์ สุธาสินี คงทอง และ สุภาษิต ชูกลิ่น. (2564). การใช้ประโยชน์จากวัสดุเศษเหลือหัวปลากะตักเสริมโปรตีนและแคลเซียมในผลิตภัณฑ์อาหาร. **วารสารวิจัยมหาวิทยาลัยราชมงคลเทคโนโลยีราชมงคลศรีวิชัย, 13(1),** 201-215

[5] ยศพร พลายโถ กรกช เพิ่มทรัพย์ รัตนชัย ทวีวัฒนานนท์ ภาคภูมิ คูประเสริฐยิ่ง และนพรัตน์ ไวโรจนะ. (2566). การศึกษาปริมาณที่เหมาะสมของแป้งข้าวกข43 และใบชะพลูในผลิตภัณฑ์ครองแครงกรอบ. **วารสารวัฒนธรรมอาหารไทย, 5(2),** 61-72

[6] สำนักงานมาตรฐานผลิตภัณฑ์อุตสาหกรรม (สมอ.). (2558). **มาตรฐานผลิตภัณฑ์ชุมชนครองแครงกรอบ มผช.267/2552.** สืบค้น มีนาคม 8, 2568 จาก https://tcps.tisi.go.th/public/StandardList.aspx

[7] อรัญญา อำไพจิตร์ และพรหมภัสสร พรทวีโชคโภคิ. (2565). การผลิตและสมบัติของข้าวเกรียบปลาจากปลาเล็กปลาน้อย. **วารสารวิทยาศาสตร์และเทคโนโลยีนอร์ทเทิร์น, 2(4),** 99-116.

[8] Siti Rashima, R., Maizura, M., Wan Nur Hafzan, W.M., and Hazzeman, H. (2019). Physicochemical properties and sensory acceptability of pineapples of different varietis and stages of maturity. **Food Research, 3(5),** 491-500.

การพยากรณ์แนวโน้มจำนวนผู้สมัครเรียนระดับปริญญาตรี มหาวิทยาลัยราชภัฏภูเก็ต โดยใช้วิธีการวิเคราะห์อนุกรมเวลา

Forecasting Trend of Undergraduate Applications at Phuket Rajabhat University Using Time Series Analysis

1st Acharaporn Chooklam
Faculty of Science and Technology
Phuket Rajabhat University
Phuket,Thailand.
s6511423134@pkru.ac.th

2nd Nuttapon Takursuk
Faculty of Science and Technology
Phuket Rajabhat University
Phuket,Thailand.
s6511423108@pkru.ac.th

3rd Attapon Pillai
Faculty of Science and Technology
Phuket Rajabhat University
Phuket,Thailand.
attapon.p@pkru.ac.th

4th Urairat Makchan
Faculty of Science and Technology
Phuket Rajabhat University
Phuket,Thailand.
urairat.m@pkru.ac.th

Abstract

This research aims to forecast the trend of undergraduate applications at Phuket Rajabhat University using Time Series Analysis. The study utilizes enrollment data from the academic years 2020–2024 and applies the ARIMA technique to analyze and develop forecasting models. The results indicate that the most suitable ARIMA model for predicting the number of applicants at the university level is ARIMA (5,2,5) with an AIC of 50.99. At the faculty level, ARIMA (2,2,0) is the most appropriate model, with an AIC of 24.90, while at the program level, ARIMA (0,2,0) is the optimal choice, with an AIC of 50.99.

The forecast for the academic year 2025 suggests an increasing trend in the number of applicants across all levels. The projected ranking of faculties by the number of applicants is as follows: Faculty of Humanities and Social Sciences (1,278 applicants), Faculty of Management Sciences (920 applicants), Faculty of Science and Technology (766 applicants), Faculty of Education (739 applicants), and Faculty of Agricultural Technology (36 applicants).This research provides insights that can be utilized to formulate strategic enrollment plans and optimize resource allocation within the university for enhanced efficiency.

Keywords: Time Series Analysis, ARIMA, Enrollment Forecasting, Phuket Rajabhat University

I. บทนำ

ปัจจุบันการศึกษาระดับปริญญาตรีมีบทบาทสำคัญในการพัฒนาทรัพยากรมนุษย์ให้สอดคล้องกับความต้องการของตลาดแรงงานที่เปลี่ยนแปลงอย่างรวดเร็ว มหาวิทยาลัยต่าง ๆ ต้องวางแผนและบริหารจัดการทรัพยากรการศึกษาอย่างมีประสิทธิภาพ เพื่อรองรับแนวโน้มการเปลี่ยนแปลงของจำนวนผู้สมัครเรียนหากไม่มีการคาดการณ์ที่แม่นยำ อาจทำให้เกิดปัญหาในการจัดสรรอุปกรณ์การเรียนการสอน ซึ่งอาจส่งผลกระทบต่อคุณภาพทางการศึกษาและการบริหารจัดการโดยรวมของมหาวิทยาลัย อย่างไรก็ตาม จำนวนผู้สมัครเรียนมีการเปลี่ยนแปลงตามปัจจัยต่าง ๆ เช่น สภาพเศรษฐกิจ ดังนั้น การวิเคราะห์แนวโน้มจำนวนผู้สมัครเรียนจึงเป็นสิ่งสำคัญที่ช่วยให้มหาวิทยาลัยสามารถกำหนดกลยุทธ์ด้านการรับสมัครและบริหารทรัพยากรได้อย่างมีประสิทธิภาพ ผู้วิจัยจึงสนใจที่จะทำการพยากรณ์แนวโน้มจำนวนนักศึกษาที่เข้าเรียนในระดับปริญญาตรีของมหาวิทยาลัยราชภัฏภูเก็ต โดยใช้เทคนิคการวิเคราะห์อนุกรมเวลา (Time Series Analysis) ในการนำข้อมูลมาคาดการณ์เชิงลำดับเวลาเกี่ยวกับการพยากรณ์แนวโน้มจำนวนผู้สมัครเรียนระดับปริญญาตรี มหาวิทยาลัยราชภัฏภูเก็ต ซึ่งจะช่วยให้มหาวิทยาลัยราชภัฏภูเก็ตสามารถนำไปใช้วางแผน บริหารจัดการทรัพยากรและกำหนดนโยบายการรับสมัครนักศึกษาได้อย่างแม่นยำ การเป็นการวิจัยที่ใช้ข้อมูลจำนวนนักศึกษาที่สมัครเรียนระหว่างปีการศึกษา 2563 - 2567 สำหรับการพยากรณ์ โดยใช้ตัวชี้วัดทางสถิติ เช่น ค่าความคลาดเคลื่อนกำลังสองเฉลี่ย (Mean Squared Error: MSE) และค่ารากที่สองของความคลาดเคลื่อนเฉลี่ยกำลังสอง (Root Mean Squared Error: RMSE) และการแสดงข้อมูลจำนวนนักศึกษา สำหรับการวิจัยในครั้งนี้มีกรอบแนวคิดในการวิจัยดังภาพที่ 1



Fig.1. กรอบแนวคิดการวิจัย

II. ทบทวนวรรณกรรม

[1] เปรมวดี อาวุธกรรมปรีชา ได้ทำการวิจัยเรื่องการพยากรณ์จำนวนผู้เข้าศึกษาต่อระดับบัณฑิตศึกษา กรณีศึกษามหาวิทยาลัยเทคโนโลยีพระจอมเกล้าพระนครเหนือ โดยใช้วิธีการของบอกซ์-เจนกินส์ เพื่อหาค่าพยากรณ์จำนวนผู้สมัครเข้าศึกษาต่อระดับบัณฑิตศึกษา จำนวนกลุ่มตัวอย่างจำนวน 38 ค่า เป็นผู้สมัครเข้าศึกษาต่อระดับบัณฑิตศึกษา จำแนกเป็นระดับปริญญาเอก ปริญญาโท แบ่งเป็นการรับสมัครทั้งภาคการศึกษาที่ 1 และภาคการศึกษาที่ 2 ตั้งแต่ปีการศึกษา 2555-2564 เครื่องมือที่ใช้ในการวิจัย ด้วยวิธีการของ Box-Jenkins

ซึ่งผลการคัดเลือกตัวแบบเพื่อใช้ในการพยากรณ์พบว่า ตัวแบบที่เหมาะสมสำหรับพยากรณ์ผู้สมัครระดับปริญญาโท ได้แก่ ARIMA (1,1,4) ส่วนตัวแบบที่เหมาะสมสำหรับการพยากรณ์จำนวนผู้สมัครระดับปริญญาเอก ได้แก่ (0,1,4) ซึ่งผลจากการพยากรณ์ พบว่า จำนวนผู้สมัครปีการศึกษา 2565 ของระดับปริญญาโทมีจำนวน 589 คน และระดับปริญญาเอกมีจำนวน 71 คน

[2] เกศสุดา ปราสาทภิญโญปรีชา ได้ทำการวิจัยเรื่อง การสร้างตัวแบบพยากรณ์จำนวนนักเรียนนักศึกษาที่จะเข้าเรียนในระดับชั้นประถมศึกษาปีที่ 1 มัธยมศึกษาชั้นปีที่ 1 และระดับอุดมศึกษาชั้นปีที่ 1 จังหวัดสุรินทร์และทั่วราชอาณาจักร มีวัตถุประสงค์ เพื่อสร้างสมการพยากรณ์จำนวนนักเรียนและนักศึกษาของจังหวัดสุรินทร์และทั่วราชอาณาจักรในอนาคต และฉายภาพจำนวนนักเรียนที่เข้าศึกษาต่อในระดับประถมศึกษาปีที่ 1 มัธยมศึกษาปีที่ 1 และระดับอุดมศึกษาชั้นปีที่ 1 ของจังหวัดสุรินทร์และทั่วราชอาณาจักร โดยใช้เทคนิคการฉายภาพประชากร แล้วนำวิเคราะห์อนุกรมเวลาด้วยวิธีกำลังสองน้อยที่สุดและหาค่าเบี่ยงเบนมาตรฐานของค่าคลาดเคลื่อน ข้อมูลที่ใช้ในการศึกษาครั้งนี้รวบรวมมาจากรายงานการสำรวจจำนวนประชากรจากกระทรวงมหาดไทย ซึ่งมีจำนวนประชากรทั่วราชอาณาจักรและจังหวัดสุรินทร์ตั้งแต่อายุต่ำกว่า 1 ปี ถึง 99 ปี ตั้งแต่ปี พ.ศ. 2540 ถึงปี พ.ศ. 2559 เป็นข้อมูลทุติยภูมิ ผลการศึกษาพบว่า 1) การพยากรณ์จำนวนนักเรียนชั้นประถมศึกษาปีที่ 1 ทั่วราชอาณาจักรด้วยวิธีกำลังสองน้อยที่สุด ได้สมการพยากรณ์คือ Yc =678,561.13 – 28]858.16 (X) 2) การพยากรณ์จำนวนนักเรียนชั้นมัธยมศึกษาปีที่ 1 ทั่วราชอาณาจักรด้วยวิธีกำลังสองน้อยที่สุด ได้สมการพยากรณ์ คือ Yc =710.287.28 – 11,633.04 (X) 3) การพยากรณ์จำนวนนักศึกษาระดับอุดมศึกษาปีที่ 1 ทั่วราชอาณาจักรด้วยวิธีกำลังสองน้อยที่สุด ได้สมการณ์คือ Yc = 715,112.54 – 4}381.81(X) 4) การพยากรณ์จำนวนนักเรียนชั้นประถมศึกษาปีที่ 1 ในจังหวัดสุรินทร์ด้วยวิธีกำลังสองน้อยที่สุด ได้สมการพยากรณ์คือ Yc = 14,940.67 – 680.47 (X) 5) การพยากรณ์จำนวนนักเรียนชั้นมัธยมศึกษาปีที่ 1 ในจังหวัดสุรินทร์ด้วยวิธีกำลังสองน้อยที่สุด ได้สมการพยากรณ์ คือ Yc =15,750.31 – 285.85 (X) 6) การพยากรณ์จำนวนนักศึกษาระดับอุดมศึกษาปีที่ 1 ในจังหวัดสุรินทร์ด้วยวิธีกำลังสองน้อยที่สุด ได้สมการ คือ Yc = 16,336.11 – 224.70 (X)

[3] คชินทร์ โกกนุทาภรณ์ ได้ทำการวิจัยเรื่อง การเปรียบเทียบวิธีการพยากรณ์จำนวนนักศึกษาแรกเข้าคณะครุศาสตร์ มหาวิทยาลัยวไลยอลงกรณ์ ในพระบรมราชูปถัมภ์ มีวัตถุประสงค์ เพื่อศึกษาและเปรียบเทียบวิธีการพยากรณ์จำนวนนักศึกษาแรกเข้าคณะครุศาสตร์ มหาวิทยาลัยราชภัฏวไลยอลงกรณ์ ในพระบรมราชูปถัมภ์ ตั้งแต่ปีการศึกษา 2540 ถึง ปีการศึกษา 2565 จำนวน 26 ค่า ผู้วิจัยแบ่งข้อมูลออกเป็นสองชุด โดยชุดที่ 1 จำนวน 20 ค่า เริ่มตั้งแต่ปีการศึกษา 2540 ถึง 2559 สำหรับเปรียบเทียบหาตัวแบบพยากรณ์ โดยงานวิจัยนี้ใช้วิธีการพยากรณ์ คือ วิธีบอกซ์-เจนกินส์ วิธีปรับให้เรียบเอ็กซ์โพเนนเชียลแบบโฮลท์ และวิธีการทำให้เรียบแบบเอกซ์โพเนนเชียลที่มีแนวโน้มแบบแดมข้อมูลชุดที่ 2 ตั้งแต่ปีการศึกษา 2560 ถึง ปีการศึกษา 2565 จำนวน 6 ค่า สำหรับการเปรียบเทียบหาวิธีการพยากรณ์ที่เหมาะสมที่สุดโดยใช้เกณฑ์ค่ารากที่สองของความคลาดเคลื่อนกำลังสองเฉลี่ย (RMSE) และค่าเปอร์เซ็นต์ความคลาดเคลื่อนสัมบูรณ์เฉลี่ย (MAPE) ที่ต่ำที่สุด ผลการวิจัยพบว่าภายใต้เกณฑ์ค่าเฉลี่ยเปอร์เซ็นต์ความคลาดเคลื่อนสัมบูรณ์ (MAPE) วิธีการทำให้เรียบแบบเอกซ์โพแนนเชียลที่มีแนวโน้มแบบแดมเป็นวิธีการพยากรณ์ที่มีความเหมาะสมมากที่สุด ขณะที่ภายใต้เกณฑ์ค่ารากที่สองของความคลาดเคลื่อนกำลังสองเฉลี่ย (RMSE) วิธีบอกซ์-เจนกินส์ ARIMA (0,1,0) เป็นวิธีการพยากรณ์ที่มีความเหมาะสมมากที่สุด อย่างไรก็ตาม ค่าพยากรณ์ของทั้งสองวิธี มีความน่าเชื่อถือเนื่องจากไม่มีความแตกต่างกันอย่างมีนัยสำคัญทางสถิติ

III. ระเบียบวิธีวิจัย

การศึกษางานวิจัยในครั้งนี้มีระเบียบวิธีวิจัยตามขั้นตอนดังต่อไป

A. การเก็บรวบรวมข้อมูล (Data Collection)

การดำเนินการวิจัยเริ่มต้นจากการรวบรวมข้อมูลจำนวนนักศึกษาที่สมัครเข้าเรียนจากระบบการรับเข้าของงานทะเบียนมหาวิทยาลัยราชภัฏภูเก็ต และระบบกิจการการศึกษา มหาวิทยาลัยราชภัฏภูเก็ต โดยพิจารณาข้อมูลย้อนหลังตั้งแต่ปีการศึกษา 2563 - 2567 ข้อมูลดังกล่าวประกอบด้วย จำนวนผู้สมัครในแต่ละปี จำนวนผู้สมัครจากแต่ละคณะและจำนวนผู้สมัครแยกตามสาขาของมหาวิทยาลัย

B. การทำความสะอาดข้อมูล (Data Cleansing)

ภายหลังการรวบรวมข้อมูล กระบวนการทำความสะอาดข้อมูลจะถูกดำเนินการเพื่อให้มั่นใจว่าข้อมูลมีความถูกต้องและพร้อมสำหรับการวิเคราะห์ ขั้นตอนนี้รวมถึงการตรวจสอบความครบถ้วนของข้อมูล การจัดการค่าที่หายไป และการแก้ไขข้อผิดพลาดที่อาจเกิดขึ้นในชุดข้อมูลที่มีการจัดเก็บไว้ในรูปแบบไฟล์ของ Microsoft Excel เพื่อจัดเรียงข้อมูลให้เหมาะสม

C. การจัดเก็บข้อมูล (Data Storage)

ข้อมูลที่ได้รับการตรวจสอบและปรับปรุงแล้ว จะมีการนำมาจัดเก็บให้อยู่ในรูปแบบที่เหมาะสมกับการนำไปวิเคราะห์โดยใช้แบบจำลองอนุกรมเวลา (Time Series) การจัดเรียงข้อมูลโดยเรียงจาก ปีการศึกษา คณะ สาขาวิชาและจำนวนผู้สมัคร ตามลำดับเพื่อช่วยให้สามารถสังเกตแนวโน้มของจำนวนผู้สมัครเรียนได้อย่างชัดเจน จากนั้นข้อมูลจำนวนนักศึกษาที่สมัครเข้าเรียนในแต่ละปี

D. การพยากรณ์ข้อมูล (Data Forecasted)

เป็นขั้นการใช้แบบจำลอง ARIMA เพื่อพยากรณ์แนวโน้มของจำนวนผู้สมัครเรียนในอนาคต โดยมีการกำหนดและปรับค่าพารามิเตอร์ของแบบจำลองให้เหมาะสม เพื่อเพิ่มความแม่นยำในการพยากรณ์ ทั้งนี้ประสิทธิภาพของแบบจำลองจะถูกประเมินโดยใช้ตัวชี้วัด เช่น Mean Squared Error (MSE) และ Root Mean Squared Error (RMSE) เพื่อตรวจสอบความถูกต้องของผลลัพธ์ดังสมการต่อไปนี้

สมการของ ARIMA Model [4]

แบบจำลอง ARIMA ถูกกำหนดโดยใช้สัญลักษณ์ ARIMA(p,d,q) โดยที่ p, d และ q จะถูกแทนที่ด้วยค่าจำนวนเต็มเพื่อระบุแบบจำลองที่ใช้อย่างแม่นยำ

$$Y_t = c + \sum_{i=1}^{p} \phi_i Y_{t-i} + \sum_{j=1}^{q} \theta_j \varepsilon_{t-j} + \varepsilon_t \quad (1)$$

Y_t คือ ค่าปัจจุบัน
C คือ ค่าคงที่
ϕ_i คือ ค่าสัมประสิทธิ์ของ AR
θ_j คือ ค่าสัมประสิทธิ์ของ MA
ε_t คือ ข้อผิดพลาดสุ่ม

ค่าความคลาดเคลื่อนกำลังสองเฉลี่ย (Mean Squared Error : MSE)

เป็นตัวชี้วัดที่ใช้ในการประเมินประสิทธิภาพของแบบจำลองพยากรณ์ โดยคำนวณจากค่าเฉลี่ยของผลรวมกำลังสองของความคลาดเคลื่อนระหว่างค่าที่พยากรณ์ได้กับค่าจริง ซึ่งสามารถเขียนเป็นสมการได้ดังนี้

$$MSE = \frac{1}{n}\sum_{i=1}^{n}(y_i - \hat{y}_i)^2 \quad (2)$$

ค่ารากที่สองของความคลาดเคลื่อนเฉลี่ยกำลังสอง (Root Mean Square Error : RMSE)

ค่ารากที่สองของความคลาดเคลื่อนเฉลี่ยกำลังสอง (RMSE) เป็นตัวชี้วัดความแม่นยำของแบบจำลองพยากรณ์ โดยเป็นรากที่สองของค่าความคลาดเคลื่อนกำลังสองเฉลี่ย (MSE) ซึ่งคำนวณจากค่าผลต่างระหว่างค่าที่พยากรณ์ได้กับค่าจริง

$$RMSE = \sqrt{\frac{1}{n}\sum_{i=1}^{n}(Y_i - \hat{Y}_i)^2} \quad (3)$$

IV. ผลการทดลอง

ตารางที่ 1 ค่าประมาณพารามิเตอร์ ค่า AIC ของตัวแบบ ARIMA(p,d,q)

ค่าประมาณพารามิเตอร์		ตัวแบบ ARIMA(p,d,q)		
		ARIMA (5,2,5)	ARIMA (2,2,0)	ARIMA (0,2,0)
ค่าคงที่	ค่าประมาณ	0.0374	0.0041	0.0013
	p-value	0.6805	0.7312	0.8124
AR (1) ϕ_1	ค่าประมาณ	-1.4539	-0.5102	
	p-value	0.0021	0.0213	
MA (1) θ_1	ค่าประมาณ	1.1168		
	p-value	0.0032		
AIC		50.99	24.90	30.69

จากตารางที่ 1 พบว่าตัวแบบพยากรณ์ ARIMA (5,2,5) เป็นตัวแบบในระดับมหาวิทยาลัยมีค่า AIC เท่ากับ 50.99 ตัวแบบพยากรณ์ ARIMA (2,2,0) เป็นตัวแบบในระดับคณะ มีค่า AIC เท่ากับ 24.90 ตัวแบบพยากรณ์ ARIMA (0,2,0) เป็นตัวแบบในระดับสาขาวิชา มีค่า AIC เท่ากับ 30.69

จากการพยากรณ์ของข้อมูลในระดับต่าง ๆ ตัวแบบพยากรณ์ของระดับคณะเทคโนโลยีการเกษตรมีความเหมาะสมที่สุด มีความคลาดเคลื่อนน้อยที่สุด

A. *กราฟแสดงข้อมูลระดับมหาวิทยาลัยราชภัฏภูเก็ต*

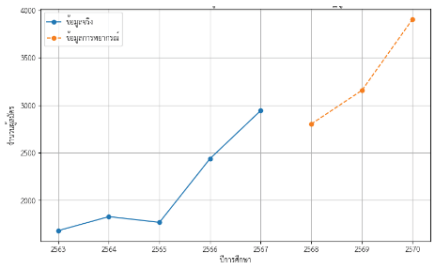


Fig.2. กราฟแสดงจำนวนผู้สมัครเข้าศึกษาภาพรวมในระดับมหาวิทยาลัย

จากรูปที่ 2 เป็นกราฟแสดงจำนวนผู้สมัครเข้าศึกษาภาพรวมในระดับมหาวิทยาลัย เป็นนำข้อมูลในอดีตคือข้อมูลการสมัครเข้าศึกษาในมหาวิทยาลัยราชภัฏภูเก็ต ตั้งแต่ปีการศึกษา 2564 – 2567 และการพยากรณ์การเข้าศึกษาในมหาวิทยาลัยราชภัฏภูเก็ตในปี 2568-2572 ในอีก 5 ปีข้างหน้า พบว่าแนวโน้มของจำนวนผู้สมัครเข้าศึกษาในมหาวิทยาลัยราชภัฏภูเก็ตมีการเพิ่มขึ้นอย่างต่อเนื่อง โดยใช้โมเดล ARIMA (5,2,5) ซึ่งให้ค่า Mean Squared Error (MSE) เท่ากับ 104.12 บ่งชี้ถึงความแม่นยำของการพยากรณ์

ตารางที่ 2 แสดงค่าพารามิเตอร์ตัวแบบ ARIMA แต่ละคณะ

สังกัดคณะ	โมเดล ที่ใช้	ค่า AIC	ค่า MSE
ครุศาสตร์	ARIMA (2,2,0)	24.90	45.00
วิทยาการจัดการ	ARIMA (0,1,0)	45.71	161.69
มนุษย์ศาสตร์และสังคมศาสตร์	ARIMA (1,2,0)	27.79	74.64
วิทยาศาสตร์และเทคโนโลยี	ARIMA (0,0,2)	55.42	93.59
เทคโนโลยีการเกษตร	ARIMA (2,2,0)	10.29	1.94

จากตารางที่ 2 พบว่ามหาวิทยาลัยราชภูเก็ตจะมีแนวโน้มจำนวนผู้สมัครในช่วงปี 2568 - 2570 มีความแตกต่างของแนวโน้มการสมัครเรียนในแต่ละคณะ ซึ่งอาจเป็นผลมาจากปัจจัยด้านความต้องการแรงงานและค่านิยมของผู้เรียนในแต่ละช่วงเวลา

B. กราฟแสดงข้อมูลระดับคณะ

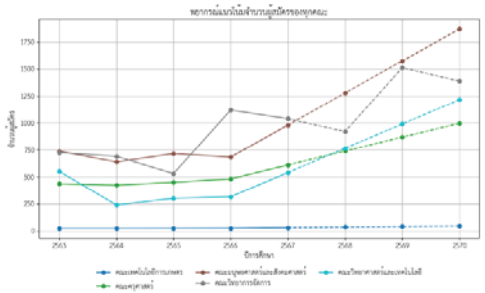


Fig.3. ขั้นตอนการนำข้อมูลจำนวนผู้สมัครเข้าศึกษาแต่ละคณะ*ในมหาวิทยาลัยราชภัฏภูเก็ต*เข้าโมเดล *ARIMA*

จากรูปที่ 3 เป็นกราฟแสดงจำนวนผู้สมัครเข้าศึกษาภาพรวมในระดับคณะเป็นนำข้อมูลในอดีตคือข้อมูลการสมัครเข้าศึกษาในมหาวิทยาลัยราชภัฏภูเก็ต ตั้งแต่ปีการศึกษา 2563 – 2567 และการพยากรณ์การเข้าศึกษาในมหาวิทยาลัยราชภัฏภูเก็ตในปี 2568-2570 ในอีก 3 ปีข้างหน้า พบว่าแนวโน้มของจำนวนผู้สมัครเข้าศึกษาในระดับคณะมีการเพิ่มขึ้นอย่างต่อเนื่อง

C. *กราฟแสดงข้อมูลระดับสาขาเทคโนโลยีดิจิทัล คณะวิทยาศาสตร์และเทคโนโลยี มหาวิทยาลัยราชภัฏภูเก็ต*

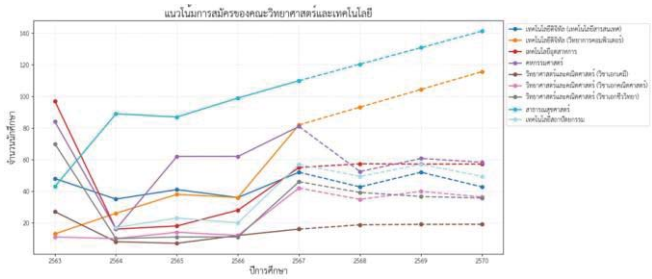


Fig.4. ตัวอย่างกราฟที่มีการแสดงแนวโน้มจำนวนผู้สมัครในระดับสาขาวิชาของคณะวิทยาศาสตร์และเทคโนโลยี โดยใช้โมเดล ARIMA

จากภาพที่ 4 เป็นตัวอย่างกราฟที่มีการแสดงแนวโน้มจำนวนผู้สมัครในระดับสาขาวิชา คณะวิทยาศาสตร์และเทคโนโลยี ซึ่งประกอบไปด้วย สาขาวิชา

เทคโนโลยีดิจิทัล (เทคโนโลยีสารสนเทศ),เทคโนโลยีดิจิทัล (วิทยาการคอมพิวเตอร์) ,เทคโนโลยีอุตสาหการ,คหกรรมศาสตร์, วิทยาศาสตร์และคณิตศาสตร์ (เคมี) วิทยาศาสตร์และคณิตศาสตร์ (คณิตศาสตร์) วิทยาศาสตร์และคณิตศาสตร์ (ชีววิทยา), สาธารณสุขศาสตร์ และเทคโนโลยีสถาปัตยกรรม พบว่าจำนวนผู้สมัครเข้าศึกษาในระดับคณะวิทยาศาสตร์และเทคโนโลยี ระหว่างปี 2563-2565 มีผู้สมัครเข้าศึกษา มีจำนวนลดลงเนื่องมีปัจจัยของโรคระบาดโควิด ระหว่างปี พ.ศ. 2566 – 2567 มีจำนวนที่เพิ่มขึ้น และพบว่าจากจากพยากรณ์ต่อไปในอนาคตระหว่างปี 2568 -2570 ในทุกสาขาวิชาของคณะวิทยาศาสตร์และเทคโนโลยี จะมจำนวนผู้สมัครเพิ่มขึ้นอย่างต่อเนื่อง

V. อภิปรายผล

การศึกษา การพยากรณ์แนวโน้มจำนวนผู้สมัครเรียนระดับปริญญาตรี มหาวิทยาลัยราชภัฏภูเก็ต โดยใช้วิธีการวิเคราะห์อนุกรมเวลา ซึ่งประกอบด้วยโมเดล ARIMA ในการพยากรณ์จำนวนผู้สมัครในภาพรวมในระดับมหาวิทยาลัย ระดับคณะ และระดับสาขาวิชา พบว่าโมเดล ARIMA (2,2,0) ซึ่งเป็นโมเดลในระดับคณะมีประสิทธิภาพสูงสุด โดยมีค่า AIC อยู่ที่ระดับ 24.90 และ MSE 1.94 สำหรับการพยากรณ์ในระดับคณะ พบว่าโมเดล ARIMA ให้ประสิทธิภาพที่แตกต่างกัน การใช้โมเดล ARIMA ในการพยากรณ์แนวโน้มจำนวนผู้สมัครเข้าเรียนระดับปริญญาตรีของมหาวิทยาลัย เป็นการช่วยให้มหาวิทยาลัยสามารถวางแผนการรับนักศึกษาอย่างมีประสิทธิภาพ ผลการวิเคราะห์พบว่าโมเดล ARIMA สามารถพยากรณ์แนวโน้มได้อย่างแม่นยำ โดยใช้ตัวชี้วัด RMSE และ MAE เป็นเกณฑ์ในการประเมินความถูกต้องของแบบจำลอง ซึ่งช่วยให้สามารถเลือกโมเดลที่เหมาะสมสำหรับข้อมูลชุดนี้ เมื่อเปรียบเทียบกับงานวิจัยที่เกี่ยวข้อง พบว่างานวิจัยก่อนหน้านี้มีความแตกต่างกันทั้งในด้านวิธีการวิเคราะห์และช่วงข้อมูลที่นำมาใช้ เช่น [1] งานวิจัยที่ใช้ Box-Jenkins Method ในการพยากรณ์นักศึกษาระดับบัณฑิตศึกษา ซึ่งใช้โมเดล ARIMA เช่นเดียวกัน แต่ไม่มีการใช้ตัวชี้วัด RMSE และ MAE ในการประเมินความแม่นยำของแบบจำลองโดยตรง ขณะที่การศึกษานี้นำตัวชี้วัดดังกล่าวมาใช้เพื่อให้ได้ผลลัพธ์ที่แม่นยำยิ่งขึ้น [2] งานวิจัยเลือกใช้ Least Squares Method เพื่อพยากรณ์แนวโน้มนักศึกษาตามข้อมูลประชากรย้อนหลัง โดยพบว่าแนวโน้มโดยรวมลดลงเนื่องจากอัตราการเกิดที่ลดลง อย่างไรก็ตาม วิธีดังกล่าวอาจไม่สามารถจับความผันผวนของข้อมูลได้ดีเท่ากับโมเดล ARIMA ที่สามารถวิเคราะห์แนวโน้มและรูปแบบของข้อมูลอนุกรมเวลาได้อย่างมีประสิทธิภาพมากกว่า นอกจากนี้ ยังมี [3] งานวิจัยที่ศึกษาเปรียบเทียบวิธีการพยากรณ์หลายรูปแบบ รวมถึง Holt's Exponential Smoothing และ Damped Exponential Smoothing ซึ่งพบว่ามีความแม่นยำในระดับที่แตกต่างกัน ขึ้นอยู่กับตัวชี้วัดที่ใช้ประเมิน อย่างไรก็ตามงานวิจัย การพยากรณ์แนวโน้มจำนวนผู้สมัครเรียนระดับปริญญาตรี มหาวิทยาลันราชภัฏภูเก็ต โดยใช้วิธีการวิเคราะห์อนุกรมเวลา เน้นการพยากรณ์ระดับมหาวิทยาลัยและคณะโดยใช้ ARIMA เป็นหลัก ซึ่งช่วยให้สามารถมองเห็นแนวโน้มของแต่ละคณะได้ชัดเจนยิ่งขึ้น ข้อได้เปรียบคือ การเลือกใช้ โมเดล ARIMA ที่สามารถปรับแต่งพารามิเตอร์ให้เหมาะสมกับลักษณะของข้อมูล ทำให้การพยากรณ์มีความแม่นยำสูงขึ้น นอกจากนี้ ยังใช้ RMSE และ MAE ในการประเมินผล ทำให้สามารถเลือกโมเดลที่ให้ค่าความคลาดเคลื่อนต่ำที่สุด ข้อจำกัดคือ การพยากรณ์อาจอาศัยข้อมูลในอดีตเพียงอย่างเดียว โดยไม่ได้รวมปัจจัยภายนอก เช่น นโยบายการศึกษา การเปลี่ยนแปลงของตลาดแรงงาน หรือปัจจัยทางเศรษฐกิจที่อาจมีผลกระทบต่อจำนวนผู้สมัครในอนาคต

VI. ข้อสรุป

ผลการวิจัยชี้ให้เห็นว่า โมเดล ARIMA เป็นเครื่องมือที่มีประสิทธิภาพในการพยากรณ์แนวโน้มจำนวนผู้สมัครเข้าเรียนระดับปริญญาตรี โดยการกำหนดพารามิเตอร์ที่เหมาะสมสำหรับแต่ละคณะและสาขาวิชา สามารถช่วยให้การวางแผนทรัพยากรของมหาวิทยาลัย ในด้านอุปกรณ์การเรียนการสอนให้เหมาะสมกับจำนวนนักศึกษา ได้อย่างมีระบบและแม่นยำมากขึ้น สำหรับแนวทางการศึกษาต่อไป อาจจะมีการพยากรณ์หรือการวิเคราะห์เชิงลึกในระดับโรงเรียน เพื่อตรวจสอบว่าผู้สมัครส่วนใหญ่มาจาก โรงเรียนเอกชนหรือรัฐบาล รวมถึงสามารถจำแนกตาม พื้นที่ภูมิศาสตร์ เช่น ตำบลหรืออำเภอ เพื่อระบุแนวโน้มการกระจายตัวของผู้สมัคร การวิเคราะห์เชิงลึกจะช่วยให้มหาวิทยาลัยสามารถกำหนดกลยุทธ์ด้านการตลาดและการประชาสัมพันธ์ เพื่อเพิ่มอัตราการสมัครจากพื้นที่ที่ยังมีจำนวนผู้สมัครน้อย หรือประยุกต์ใช้เทคนิคอื่น ๆ เช่น Machine Learning ได้แก่ Random Forest เพื่อนำมาเปรียบเทียบประสิทธิภาพกับโมเดล ARIMA และเพิ่มความแม่นยำในการพยากรณ์ โดยเฉพาะในกรณีที่ข้อมูลมีความซับซ้อนที่ ARIMA อาจไม่สามารถจับรูปแบบได้อย่างครอบคลุมในการพยากรณ์ต่อไป

อ้างอิง

[1] เปรมวดี อาวุธกรรมปรีชา, "การพยากรณ์จำนวนผู้สมัครเข้าศึกษาต่อระดับบัณฑิตศึกษา กรณีศึกษามหาวิทยาลัยเทคโนโลยีพระจอมเกล้าพระนครเหนือ", วารสารวิจัยและพัฒนา วไลยอลงกรณ์ ในพระบรมราชูปถัมภ์ สาขาวิทยาศาสตร์และเทคโนโลยี, ปีที่ 16,ฉบับที่ 3,หน้า 93-103,กันยายน-ธันวาคม 2564.

[2] เกศสุดา ปราสาทภิญโญ,"การสร้างตัวแบบพยากรณ์จำนวนนักเรียนนักศึกษาที่จะเข้าเรียนในระดับชั้นประถมศึกษาปีที่ 1 มัธยมศึกษาชั้นปีที่ 1 และระดับอุดมศึกษาชั้นปีที่ 1 จังหวัดสุรินทร์และทั่วราชอาณาจักร", วารสารก้าวทันโลกวิทยาศาสตร์,ปีที่ 21, ฉบับที่ 1,หน้า 46-62,มกราคม-มิถุนายน 2564.

[3] คชินทร์ โกกนุทาภรณ์ "การเปรียบเทียบวิธีการพยากรณ์จำนวนนักศึกษาแรกเข้าคณะครุศาสตร์ มหาวิทยาลัยราชภัฏวไลยอลงกรณ์ ในพระบรมราชูปถัมภ์",วารสารวิจัยและพัฒนา วไลยอลงกรณ์ ในพระบรมราชูปถัมภ์ สาขาวิทยาศาสตร์และเทคโนโลยี, ปีที่ 18,ฉบับที่ 3,หน้า 137-150, กันยายน-ธันวาคม 2566.

[4] G. E. P. Box, G. M. Jenkins, and G. C. Reinsel, Time Series Analysis: Forecasting and Control, 3rd ed. Englewood Cliffs, NJ: Prentice-Hall, 1994.

[5] ส. เกตุเอี่ยม, *เทคนิคการพยากรณ์*, พิมพ์ครั้งที่ 2. สงขลา: มหาวิทยาลัยทักษิณ, 2548.

การพัฒนาชุดต้นแบบราคาประหยัดเรื่องการวัดค่าความหนืดของของเหลว

Development of a cost-effective prototype for measuring the viscosity of liquids

1st Nattapong Thuedam 2nd Thitima Thanyaniti
Faculty of Science and Technology, Phuket Rajabhat University
Phuket Thailand
Email address: thittima@pkru.ac.th

Abstract.

The goal of this study is to gain a deeper understanding of the viscosity of liquids. Typically, viscosity experiments provide only a single value of viscosity at a fixed room temperature. However, in this study, we seek to investigate the relationship between viscosity and temperature. To accomplish this, we developed an experimental apparatus that collects and displays data on viscosity and temperature by using microcontroller. A microcontroller (Arduino Uno) serves as the processor for releasing the steel ball. Two methods can be used to release the ball. The first method involves an Arduino Relay Module switch and an electromagnet, which releases the object. The second method uses the DS18B20 Full Waterproof Temperature Sensor to monitor the temperature of the liquid as a signal to release steel balls. Additionally, a Photo Diode serves as a sensor for detecting the two sets of steel balls, and the time difference is calculated as the steel ball passes through the Photo Sensor to determine the object's speed. The velocity is then measured by an infrared sensor and displayed on an LCD screen. The experimental set allowed for the measurement of glycerin viscosity at a room temperature of (27.8°C ± 0.1), yielding a viscosity value of 0.786 Pa s. Hence, there exists an inversely proportional correlation between the temperature and viscosity of glycerol. In conclusion, the low-cost viscosity laboratory is cost-effective as the components are readily available and inexpensive.

Keywords: viscosity, microcontroller, low-cost laboratory

1. บทนำ

ในการจัดการเรียนการสอนปฏิบัติการเรื่องความหนืดในสถานศึกษาโดยทั่วไป จะวัดค่าความหนืดโดยการปล่อยลูกเหล็กที่มีขนาดแตกต่างกันให้ตกผ่านของเหลวที่บรรจุในท่อกระบอกใสความสูงประมาณ 50 cm ใช้นาฬิกาจับเวลาที่ลูกเหล็กเคลื่อนที่ผ่านจุดสองจุด นำค่าระยะห่างระหว่างจุดทั้งสองกับเวลามาคำนวณหาความเร็วของลูกเหล็ก แล้วนำเขียนกราฟแสดงความสัมพันธ์เชิงเส้นระหว่างเส้นผ่านศูนย์กลางของลูกเหล็ก^2 (d^2) กับความเร็ว (v) ดังความสัมพันธ์ในสมการที่ (1) หาค่าความชันของกราฟแล้วคำนวณค่าความหนืด (η) โดยใช้ความสัมพันธ์จากสมการที่ (2) [1]

$$v = \frac{g}{18\eta}(\rho_0 - \rho_f)d^2 \quad (1)$$

$$\eta = \frac{g}{18\,(\text{slope})}(\rho_0 - \rho_f) \quad (2)$$

การทดลองดังกล่าวจะมีความคลาดเคลื่อนเนื่องจากเป็นการใช้นาฬิกาจับเวลา [2] ดังนั้นผู้วิจัยจึงได้พัฒนาชุดทดลองที่สามารถเพิ่มความแม่นยำในการจับเวลา และเพิ่มความสามารถของอุปกรณ์ในการวัดค่าความหนืดที่อุณหภูมิต่าง ๆ ของของเหลว เพื่อให้ผู้เรียนได้ศึกษาความสัมพันธ์ระหว่างค่าความหนืดกับอุณหภูมิของของเหลวด้วย เนื่องจากค่าความหนืดของของเหลวจะลดลงเมื่ออุณหภูมิของของเหลวสูงขึ้น [3] จึงได้นำไมโครคอนโทรลเลอร์ Arduina Uno [4] เซ็นเซอร์วัดอุณหภูมิ Temperature Sensor และ Photo Sensor มาประยุกต์ใช้ [5] และข้อดีอีกอย่างของชุดทดลองนี้คือมีราคาถูก อุปกรณ์ต่าง ๆ สามารถหาซื้อได้ตามท้องตลาดทั่วไป ผู้สอนวิชาฟิสิกส์ในสถานศึกษาต่าง ๆ จึงสามารถผลิตขึ้นด้วยตนเองได้

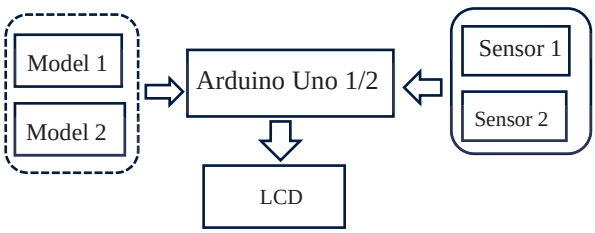
2. วิธีการ

ชุดต้นแบบเรื่องการวัดค่าความหนืดของของเหลวที่อุณหภูมิต่างๆ มีอุปกรณ์สำคัญได้แก่ ส่วนที่ 1 อุปกรณ์ในการปล่อยลูกเหล็ก โดยลูกเหล็กถูกยึดด้วย electromagnet และใช้ DS18B20 Full Waterproof Temperature Sensor เป็นตัววัดอุณหภูมิ ซึ่งจะใส่ลงในของเหลวจากส่วนบนของท่ออคริลิกใสที่มีความสูง 50 cm เส้นผ่านศูนย์กลางขนาด 4.1 cm ส่วนที่ 2 Sensor สำหรับวัดความเร็วของลูกเหล็กเมื่อเคลื่อนที่ผ่าน 2 จุด มีจำนวน 2 ตัว จะติดกับท่อ PVC ที่ผ่าครึ่ง ตัวบน เป็น Sensor ตัวที่ 1 และตัวล่างเป็น Sensor ตัวที่ 2 โดยระยะห่างระหว่าง Sensor ทั้งสองเท่ากับ 10 cm ส่วนที่ 3 หน่วยประมวลและแสดงผลจะบรรจุอยู่ในกล่องพลาสติกขนาด 12 cm x 20 cm x 7 cm ประกอบด้วย Arduino Uno Board, วงจรขยายสัญญาณ, วงจรลดสัญญาณรบกวน, จอ LCD และ ปุ่ม switch ดังแสดงในรูปที่ 1



รูปที่ 1 ชุดต้นแบบราคาประหยัดเรื่องการวัดค่าความหนืดของของเหลวที่อุณหภูมิต่างๆ

ขั้นตอนการทดลอง เริ่มต้นบรรจุของเหลวในท่ออคริลิกใสให้อยู่ต่ำกว่าขอบบนของท่อประมาณ 2 cm แล้วนำมาวางบนกล่องพลาสติก (ส่วนที่ 3) ในจุดที่กำหนดไว้ ใส่ Temperature Sensor ลงในของเหลวทางด้านบนของท่อ ค่าอุณหภูมิที่วัดได้จะแสดงบนหน้าจอ LCD เป็น T ถ้าต้องวัดค่าความหนืดของของเหลวที่อุณหภูมิห้อง คือ Model 1 ให้นำลูกเหล็กขนาดต่าง ๆ ไปยึดกับ electromagnet แล้วกด switch เพื่อปล่อยลูกเหล็กให้ตกลงในของเหลว ถ้าต้องการทดลองเพื่อศึกษาความสัมพันธ์ระหว่างค่าความหนืดกับอุณหภูมิของของเหลว คือ Model 2 เริ่มต้นให้ความร้อนกับของเหลวให้มีอุณหภูมิประมาณ 50 °C จากนั้นเทของเหลวลงในท่ออคริลิกใส่ Temperature Sensor แล้วนำลูกเหล็กขนาดใดก็ได้ไปยึดกับ electromagnet เมื่ออุณหภูมิของของเหลวลดลงจนถึงอุณภูมิที่กำหนดไว้ microcontroller จะส่งคำสั่งให้ relay ทำงาน ลูกเหล็กจะถูกปล่อยให้ตกแบบอัตโนมัติ ซึ่งทั้ง 2 Model ระบบจะจับเวลาที่ลูกเหล็กเคลื่อนที่ผ่าน Sensor ทั้งสอง แล้วนำไปคำนวณหาค่าความเร็วของลูกเหล็กจากอัตราส่วนระหว่างระยะห่างของ Sensor ทั้งสองกับเวลาที่ลูกเหล็กเคลื่อนที่ผ่าน sensor ทั้งสอง ซึ่งเป็นจุดที่ลูกเหล็กเคลื่อนที่ด้วยความเร็วคงที่ แล้วแสดงผลผ่านหน้าจอ LCD เป็น V ดังแสดงการทำงานด้วย block diagram ในรูปที่ 2



รูปที่ 2 แสดง Block Diagram of Low-Cost Viscosity Laboratory

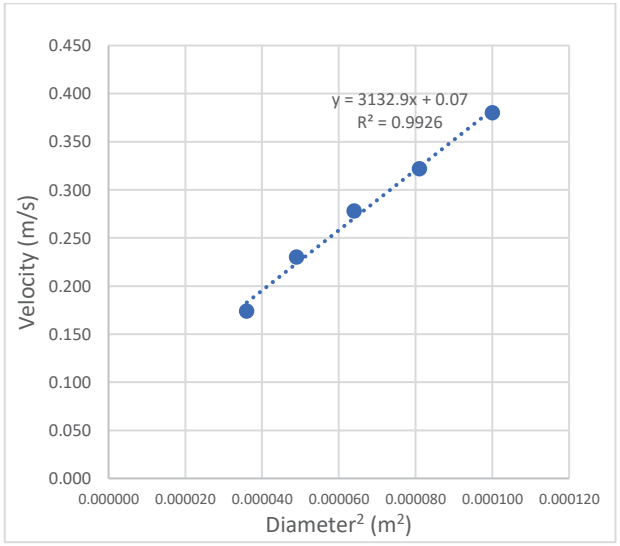
3. Results and Discussion

ตัวอย่างผลการใช้ชุดทดลองหาค่าความหนืดของกลีเซอรีล (Model 1) ที่อุณหภูมิห้อง (27.8 °C ± 0.1) โดยปล่อยลูกเหล็กที่มีเส้นผ่านศูนย์กลางแตกต่างกัน 5 ขนาด และแต่ละขนาดทำการทดลอง 3 ครั้ง นำผลค่าความเร็วทั้ง 3 ครั้งมาหาค่าเฉลี่ย ได้ผลดังตารางที่ 1

ตารางที่ 1 แสดงผลค่าความเร็วของลูกเหล็กขนาดต่างๆ

Diameter (mm)	Velocity (m/s)			
	1	*2*	*3*	*Avg*
6.0	0.174	0.174	0.175	0.174
7.0	0.231	0.229	0.231	0.230
8.0	0.276	0.277	0.281	0.278
9.0	0.324	0.322	0.321	0.322
10.0	0.387	0.373	0.379	0.380

เมื่อนำข้อมูลของ Diameter^2 (d^2) และ Velocity (v) จากตารางที่ 1 มาเขียนกราฟแสดงความสัมพันธ์เชิงเส้นดังรูปที่ 3 แล้วนำค่าความชันของกราฟมาคำนวณหาค่าความหนืดจากสมการที่ (2) ได้ค่าความหนืดเท่ากับ 0.786 Pa●s



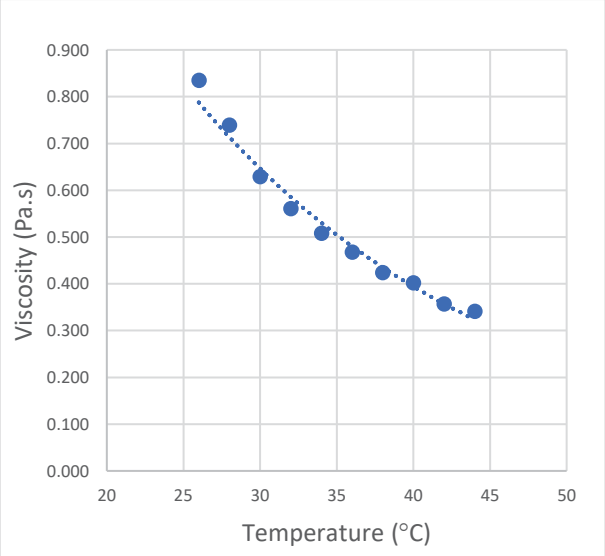
รูปที่ 3 กราฟแสดงความสัมพันธ์ระหว่าง Diameter และ Velocity ของลูกเหล็ก

ตัวอย่างผลการใช้ชุดทดลองหาความสัมพันธ์ระหว่างค่าความหนืดกับอุณหภูมิของกลีเซอรีล (Model 2) โดยใช้ลูกเหล็กขนาดเส้นผ่านศูนย์กลาง 6.0 mm เริ่มต้นปล่อยลูกเหล็กที่อุณหภูมิ 44 °C หลังจากนั้นปล่อยที่อุณหภูมิลดลงครั้งละ 2 ° C ทำการทดลองจำนวน 3 ครั้ง แล้วนำค่าความเร็วมาหาค่าเฉลี่ย จากนั้นคำนวณหาค่าความหนืดโดยใช้สมการ (1) ได้ผลดังตารางที่ 2

ตารางที่ 2 แสดงผลค่าความเร็วของลูกเหล็กและค่าความหนืดของกลีเซอรีลที่อุณหภูมิต่างๆ

Temp. (°C)	Velocity (m/s)				Viscosity (Pa•s)
	1	*2*	*3*	*Avg*	
26	0.154	0.155	0.156	0.155	0.835
28	0.174	0.176	0.176	0.175	0.739
30	0.204	0.206	0.208	0.206	0.629
32	0.231	0.230	0.232	0.231	0.561
34	0.252	0.256	0.257	0.255	0.508
36	0.275	0.278	0.277	0.277	0.468
38	0.306	0.307	0.304	0.306	0.424
40	0.311	0.330	0.326	0.322	0.402
42	0.364	0.363	0.360	0.362	0.357
44	0.386	0.371	0.381	0.379	0.341

นำข้อมูลของอุณหภูมิและความหนืดจากตารางที่ 2 มาเขียนกราฟแสดงความสัมพันธ์ระหว่างตัวแปรทั้งสองได้ดังรูปที่ 4 ซึ่งจากกราฟแสดงให้เห็นว่าเมื่ออุณหภูมิของกลีเซอรีลเพิ่มขึ้นค่าความหนืดของกลีเซอรีลจะลดลง



รูปที่ 4 กราฟแสดงความสัมพันธ์ระหว่าง Temperature และ Viscosity ของกลีเซอรีล

4. Conclusion

ชุดทดลองการวัดค่าความหนืดของของเหลวราคาประหยัด ที่สร้างขึ้นสามารถใช้ศึกษาคุณสมบัติของของเหลว เช่นกรีเซอรีน น้ำมันเครื่อง น้ำผึ้ง เป็นต้น ได้ถึง 2 เรื่องในชุดเดียวกันคือ 1) การหาค่าความหนืดของของเหลวชนิดต่าง ๆ และ 2) ศึกษาความสัมพันธ์ระหว่างค่าความหนืดกับอุณหภูมิของของเหลว ซึ่งจะช่วยให้ผู้เรียนมีความเข้าใจเรื่องความหนืดของของเหลวมากขึ้น อีกทั้งชุดทดลองนี้ยังมีราคาถูกและสามารถหาซื้ออุปกรณ์ได้ง่าย จึงมีความเหมาะสมอย่างยิ่งสำหรับนำไปผลิตใช้สำหรับจัดการเรียนการสอนในสถานศึกษาในทุกระดับชั้น

References

[1] Houari A 2011 Determining the viscosity of liquids using an extended falling ball method *Phy. Edu.* **46** 688

[2] Kurniati R 2018 Development of digital viscometer based on sensor technology and microcontroller *J. Phys.: Conf. Ser.* **1040** 012047

[3] Seeton J 2006 Viscosity-temperature correlation for liquids *Int. joint Tribol. Conf.* **42592** 131–42

[4] Kurniadi W H, Indahwati E, and Arifah F L 2018 Measurement of non-invasive blood glucose level based sensor color tcs3200 and arduino *IOP Conf. Ser.: Mater. Sci. Eng.* **336** 012019

[5] Indrasari W, Budi A S and Fadilla D P 2021 Development of a set of props for collision based on Arduino Uno Microcontroller *J. Phys.: Conf. Ser.* **1816**. 012107

การพัฒนาผลิตภัณฑ์ตะลิงปลิงผงสำเร็จรูปด้วยการทำแห้งแบบพ่นฝอย

Development of instant Bilimbi Fruit (*Averrhoa bilimbi* L.) Powder Product by Spray Drying

1st Nata-Anisong
: Home Economics
: Faculty of Science and Technology; Phuket Rajabhat University
: Phuket Thailand
: Nata.a@pkru.ac.th

2nd Pakamon-Kulnuwong
: Home Economics
: Faculty of Science and Technology; Phuket Rajabhat University
: Phuket Thailand
: pakamon.k@pkru.ac.th

3rd Unruethai-Phupornprasert
: Chemistry
: Faculty of Science and Technology; Phuket Rajabhat University
: Phuket Thailand
: Unruethai.p@pkru.ac.th

Abstract

Bilimbi (Averrhoa bilimbi L.*) is a tropical fruit recognized for its high acidity and abundance of bioactive compounds, making it a valuable ingredient for functional food products. This study focuses on developing bilimbi fruit powder through the spray drying method to enhance its stability, solubility, and shelf life while preserving its nutritional properties. The primary objectives include optimizing the spray drying process, analyzing the physical characteristics of the resulting powder, and assessing its potential applications in the food industry.*

The research involved preparing bilimbi fruit extract and subjecting it to spray drying under varying conditions, including different inlet temperatures and carrier agent concentrations. The resulting powders were evaluated for moisture content, solubility, color, water activity, and nutrient retention, particularly vitamin C and minerals. The findings indicate that an optimized inlet temperature of 150°*C combined with* 15% *maltodextrin significantly enhances the stability and flowability of the bilimbi fruit powder while effectively preserving its vitamin and mineral content. The final product demonstrated desirable properties, including improved solubility and extended shelf life, making it well-suited for use in food and beverage formulations.*

In conclusion, this study confirms that spray drying is an efficient method for producing high-quality bilimbi fruit powder. The results highlight its potential for commercialization as a functional food ingredient, offering health benefits and practical applications within the food industry.

Keywords-Bilimbi fruit, spray drying, fruit powder, functional food

I. บทนำ

ตะลิงปลิง (*Averrhoa bilimbi* L.) เป็นผลไม้เขตร้อนที่เป็นที่รู้จักอย่างกว้างขวางในด้านความเป็นกรดสูง รสชาติเปรี้ยวที่เป็นเอกลักษณ์ และความอุดมสมบูรณ์ของสารออกฤทธิ์ทางชีวภาพ ซึ่งรวมถึงวิตามินซี สารประกอบฟีนอลิก และกรดอินทรีย์ แม้จะมีคุณประโยชน์ทางโภชนาการและศักยภาพในการประยุกต์ใช้ในผลิตภัณฑ์อาหารและเครื่องดื่ม แต่ผลตะลิงปลิงสดมีอายุการเก็บรักษาสั้นและมีข้อจำกัดในการใช้ประโยชน์เชิงพาณิชย์ เนื่องจากมีปริมาณความชื้นสูงและเน่าเสียง่าย เพื่อแก้ไขความท้าทายเหล่านี้ การพัฒนาผงตะลิงปลิงผ่านเทคนิคการทำแห้งขั้นสูง จึงเป็นทางออกที่มีศักยภาพในการยืดอายุการเก็บรักษาในขณะที่ยังคงรักษาคุณสมบัติเชิงหน้าที่ของผลไม้ไว้ได้ ในบรรดาวิธีการทำแห้งต่างๆ การทำแห้งแบบพ่นฝอย (spray drying) เป็นวิธีที่นิยมใช้อย่างแพร่หลายในการแปรรูปอาหาร เนื่องจากมีประสิทธิภาพในการผลิตผงละเอียดที่ไหลได้อิสระ มีการละลายและความเสถียรที่ดีขึ้น การศึกษานี้มุ่งเน้นที่การปรับปรุงกระบวนการทำแห้งแบบพ่นฝอยสำหรับผลตะลิงปลิง เพื่อสร้างผงคุณภาพสูงที่เหมาะสำหรับการประยุกต์ใช้ในอาหารเชิงหน้าที่

วัตถุประสงค์ของการวิจัยนี้ ได้แก่: (1) เพื่อพัฒนาผงตะลิงปลิงโดยใช้วิธีการทำแห้งแบบพ่นฝอย (2) เพื่อศึกษาผลกระทบของพารามิเตอร์การทำแห้งแบบพ่นฝอยที่แตกต่างกันต่อคุณสมบัติทางกายภาพของผง และ (3) เพื่อประเมินคุณค่าทางโภชนาการ และการคงอยู่ของสารอาหาร วิตามินและแร่ธาตุ โดยการปรับปรุงสภาวะการทำแห้งแบบพ่นฝอยให้เหมาะสมที่สุด การศึกษานี้มีเป้าหมายเพื่อเพิ่มความเสถียรและความสามารถในการใช้งานของผงตะลิงปลิง ทำให้เป็นส่วนประกอบที่มีความเป็นไปได้สำหรับสูตรอาหารและเครื่องดื่มเพื่อสุขภาพ

กรอบการวิจัยมีโครงสร้างที่ครอบคลุมการเตรียมสารสกัดจากผลตะลิงปลิง การคัดเลือกปริมาณสารตัวพา (carrier agents) ที่เหมาะสม และการปรับปรุงสภาวะการทำแห้งแบบพ่นฝอย เช่น อุณหภูมิขาเข้า (inlet temperature) และความเข้มข้นของสารป้อน (feed concentration) จากนั้นจึงวิเคราะห์ผงที่ได้ในด้านปริมาณความชื้น การละลาย สี ค่าวอเตอร์แอคติวิตี้ และการคงอยู่ของสารอาหาร วิตามิน แร่ธาตุ ซึ่งแนวทางที่เป็นระบบนี้ช่วยให้มั่นใจได้ว่าจะได้ผลิตภัณฑ์ที่มีคุณภาพสูงซึ่งมีศักยภาพในการประยุกต์ใช้ในอาหารเชิงหน้าที่และผลิตภัณฑ์เสริมอาหาร

II. ทบทวนวรรณกรรม

การพัฒนาผงผลไม้ผ่านการทำแห้งแบบพ่นฝอยได้รับการศึกษาอย่างกว้างขวางเนื่องจากศักยภาพในการเพิ่มอายุการเก็บรักษา ความเสถียร และคุณสมบัติเชิงหน้าที่ของสารออกฤทธิ์ทางชีวภาพ งานวิจัยหลายชิ้นได้ศึกษากระบวนการทำแห้งแบบพ่นฝอยสำหรับผลไม้เขตร้อนต่างๆ รวมถึงมะม่วง สับปะรด และอะเซโรลา ซึ่งแสดงให้เห็นถึงประสิทธิผลของเทคนิคนี้ในการรักษาคุณสมบัติทางโภชนาการที่สำคัญ [2] อย่างไรก็ตาม มีงานวิจัยจำกัดที่มุ่งเน้นที่ผลตะลิงปลิง (*Averrhoa bilimbi* L.) ซึ่งมีองค์ประกอบที่เป็นเอกลักษณ์ของกรดอินทรีย์ วิตามินซี และสารประกอบฟีนอลิกที่สามารถเป็นประโยชน์สำหรับ

การประยุกต์ใช้ในอาหารเชิงหน้าที่ การทำแห้งแบบพ่นฝอยเป็นเทคนิคที่ใช้อย่างแพร่หลายในการแปรรูปเนื้อผลไม้หรือสารสกัดให้อยู่ในรูปของผง ซึ่งมอบประโยชน์ในด้านความเสถียรที่เพิ่มขึ้น การละลาย และความสะดวกในการเก็บรักษาและการขนส่ง กระบวนการนี้เกี่ยวข้องกับการทำให้สารสกัดผลไม้กลายเป็นละอองฝอยเข้าสู่ห้องอบแห้งซึ่งอากาศร้อนจะระเหยความชื้นออกอย่างรวดเร็ว ส่งผลให้เกิดอนุภาคผงละเอียด [1] การศึกษาต่างๆ แสดงให้เห็นว่าการเลือกสารตัวพา เช่น มอลโตเดกซ์ทรินและกัมอะราบิก มีผลอย่างมีนัยสำคัญต่อคุณสมบัติทางเคมีกายภาพของผลิตภัณฑ์สุดท้าย รวมถึงปริมาณความชื้น การละลาย และการคงอยู่ของสารออกฤทธิ์ทางชีวภาพ [7] หนึ่งในข้อกังวลหลักในการทำแห้งแบบพ่นฝอยคือการสูญเสียสารออกฤทธิ์ทางชีวภาพที่ไวต่อความร้อน เช่น วิตามินซีและสารโพลีฟีนอล เนื่องจากอุณหภูมิการอบแห้งที่สูง งานวิจัยเกี่ยวกับผงผลไม้อะเซโรลาและคามูคามูได้ชี้ให้เห็นว่าการใช้อุณหภูมิขาเข้าที่เหมาะสม (อยู่ในช่วง 130–170°C) และสารตัวพาที่เหมาะสมสามารถช่วยรักษาวิตามินซีไว้ได้ถึง 80% ของปริมาณดั้งเดิม [5] ในทางตรงกันข้าม การทำแห้งแบบแช่เยือกแข็งเป็นที่ทราบกันว่าให้การรักษาสารอาหารได้ดีกว่า แต่มีค่าใช้จ่ายสูงกว่าและใช้เวลานานกว่าเมื่อเทียบกับการทำแห้งแบบพ่นฝอย [4] การศึกษาในปัจจุบันมุ่งที่จะต่อยอดจากผลการวิจัยเหล่านี้โดยการปรับปรุงกระบวนการทำแห้งแบบพ่นฝอยสำหรับผงตะลิงปลิง เพื่อให้มั่นใจว่ามีการคงอยู่ของสารออกฤทธิ์ทางชีวภาพสูงสุดในขณะที่ยังคงรักษาคุณสมบัติทางเคมีกายภาพที่พึงประสงค์เมื่อเปรียบเทียบกับการศึกษาก่อนหน้านี้เกี่ยวกับผงผลไม้เขตร้อนอื่นๆ ความเป็นเอกลักษณ์ของงานวิจัยนี้อยู่ที่การประยุกต์ใช้การทำแห้งแบบพ่นฝอยโดยเฉพาะกับผลตะลิงปลิง งานวิจัยส่วนใหญ่ก่อนหน้านี้มุ่งเน้นที่ผลไม้ที่มีปริมาณน้ำตาลสูงกว่า ซึ่งโดยธรรมชาติช่วยเพิ่มการก่อตัวของผงและความเสถียร [3] ในทางกลับกัน ตะลิงปลิงมีความเป็นกรดสูง จึงต้องมีการเลือกพารามิเตอร์การทำแห้งและสารตัวพาอย่างระมัดระวังเพื่อให้ได้ผงที่มีคุณภาพสูง นอกจากนี้ ในขณะที่การวิจัยก่อนหน้านี้ได้ศึกษาผงผลไม้ทั่วไปเป็นหลัก การศึกษานี้เน้นย้ำถึงศักยภาพของผงตะลิงปลิงในอาหารเชิงหน้าที่ เนื่องจากมีปริมาณสารต้านอนุมูลอิสระสูงและมีศักยภาพในการประยุกต์ใช้ในผลิตภัณฑ์อาหารที่เน้นด้านสุขภาพ [6] ผลการวิจัยจากการศึกษานี้จะมีส่วนช่วยเพิ่มองค์ความรู้เกี่ยวกับเทคนิคการทำแห้งแบบพ่นฝอยและการพัฒนาอาหารเชิงหน้าที่ โดยให้ข้อมูลเชิงลึกใหม่ๆ เกี่ยวกับการแปรรูปและการประยุกต์ใช้ผงตะลิงปลิงในอุตสาหกรรมอาหาร

III. ระเบียบวิธีวิจัย

3.1 การเตรียมวัตถุดิบ

1. การคัดเลือกและทำความสะอาด: ตะลิงปลิงสดจะถูกคัดเลือก ทำความสะอาด และล้างเพื่อขจัดสิ่งสกปรกหรือสารปนเปื้อน
2. การสกัดน้ำตะลิงปลิง: ผลไม้ที่ทำความสะอาดแล้วจะถูกคั้นโดยใช้เครื่องปั่นเพื่อสกัดเนื้อผลไม้ใช้น้ำในการทำละลายอัตราส่วน 1:1
3. การกรอง: น้ำตะลิงปลิงน้ำผลไม้ที่สกัดได้จะผ่านการกรองโดยใช้ผ้าขาวบางเพื่อขจัดเนื้อหรือตะกอนที่เหลืออยู่

3.2 กระบวนการทำแห้งแบบพ่นฝอย

1. การเติมสารช่วยในการทำแห้ง: เติมมอลโตเด็กซ์ทริน (10-20%) ลงในน้ำตะลิงปลิงเพื่อเพิ่มการก่อตัวของผงและลดความเหนียว โดยปรับอัตราส่วนมวลของมอลโตเด็กซ์ทรินต่อน้ำผลไม้ ให้เหมาะสม
2. การทำแห้งแบบพ่นฝอย: ส่วนผสมจะถูกป้อนเข้าสู่เครื่องทำแห้งแบบพ่นฝอยโดยใช้อุณหภูมิลมเข้า 130-170°C อุณหภูมิลมออก 65-70°C อัตราการป้อน 50-100 มล./นาที และความเร็วของหัวฉีด 20,000-25,000 รอบ/นาที เพื่อทดสอบสภาวะที่เหมาะสม เพื่อให้ได้คุณภาพผงที่ดีที่สุด
3. การเก็บผง: ผงแห้งจะถูกเก็บจากเครื่องทำแห้งแบบพ่นฝอยโดยใช้เครื่องแยก

3.3 การเก็บรวบรวมข้อมูลและการวิเคราะห์

1. การวิเคราะห์ทางกายภาพ: ปริมาณความชื้น และความสามารถในการละลาย ของผงจะถูกวิเคราะห์โดยใช้เทคนิคมาตรฐานในห้องปฏิบัติการ
2. การวิเคราะห์คุณค่าทางโภชนาการน้ำตะลิงปลิงสดและผงตะลิงปลิงหลังผ่านการทำแห้งแบบพ่นฝอยแล้ว
3. การวิเคราะห์ทางสถิติ: ข้อมูลจะถูกวิเคราะห์โดยใช้ซอฟต์แวร์ทางสถิติ SPSS เพื่อประเมินผลของสภาวะการทำแห้งแบบพ่นฝอยที่แตกต่างกันต่อคุณสมบัติของผงตะลิงปลิง

3.4 เครื่องมือและซอฟต์แวร์

- เครื่องทำแห้งแบบพ่นฝอย: เครื่องทำแห้งแบบพ่นฝอยระดับอุตสาหกรรม ณ โรงงานต้นแบบแปรรูปอาหาร คณะเทคโนโลยีการเกษตร มหาวิทยาลัยราชภัฏภูเก็ต ซึ่งใช้สำหรับการผลิตผงตะลิงปลิงสำเร็จรูป
- ซอฟต์แวร์: SPSS สำหรับการวิเคราะห์ทางสถิติ และ Microsoft Excel สำหรับการแสดงข้อมูล

3.5 การออกแบบการทดลอง

พารามิเตอร์การทดลอง: อุณหภูมิลมเข้า อุณหภูมิลมออก อัตราการป้อน และความเข้มข้นของสารช่วยในการทำแห้งจะถูกปรับเปลี่ยนเพื่อให้ได้กระบวนการทำแห้งแบบพ่นฝอยที่เหมาะสมที่สุดและนำผลิตภัณฑ์ตะลิงปลิงผงไปวิเคราะห์คุณค่าทางโภชนาการ

IV. ผลการทดลอง

4.1 กระบวนการอบแห้งแบบพ่นฝอยสามารถเปลี่ยนสารสกัดจากตะลิงปลิงให้เป็นผงละเอียดที่ไหลลื่นได้สำเร็จ สูตรที่ปรับให้เหมาะสมนี้ใช้มอลโตเดกซ์ทรินเป็นตัวพาในความเข้มข้นที่แตกต่างกัน (10–20%) เพื่อปรับปรุงผลผลิตและความเสถียร ผลิตภัณฑ์ขั้นสุดท้ายมีสีเหลืองอมเขียวอ่อน ซึ่งเป็นลักษณะเฉพาะของรงควัตถุตามธรรมชาติของผลไม้ และแสดงให้เห็นถึงความสามารถในการละลายที่ดีในน้ำ ผลผลิตของกระบวนการจะแตกต่างกันไปขึ้นอยู่กับสภาวะการอบแห้ง โดยอุณหภูมิทางเข้า 150°C ให้ผลผลิตผงสูงสุด (16.4%) ในขณะที่อุณหภูมิที่ต่ำลงและสูงขึ้นส่งผลให้ผลผลิตลดลงเนื่องจากความชื้นที่มากเกินไปหรือการเสื่อมสภาพเนื่องจากความร้อน

4.2 คุณสมบัติทางกายภาพของผงตะลิงปลิงในสภาวะการอบแห้งแบบพ่นฝอยที่แตกต่างกัน โดยสภาวะที่อุณหภูมิ 150°C ที่มีมอลโตเดกซ์ทริน 15% มีระดับความชื้น (Moisture content) ต่ำสุด (4.4%) %) โดยอุณหภูมิการอบแห้งที่เพิ่มขึ้นส่งผลให้ปริมาณความชื้นลดลง จึงมีค่าน้ำอิสระ(Aw) อยู่ระหว่าง 0.25–0.40 ซึ่งบ่งชี้ถึงความเสถียรของจุลินทรีย์ที่ดี อุณหภูมิที่สูงขึ้นทำให้ผงสีเข้มขึ้นเล็กน้อยเนื่องจากปฏิกิริยา Maillard อีกทั้งความสามารถในการละลายที่ดีที่สุด (86.7%) ทำให้สภาวะที่อุณหภูมิ 150°C มอลโตเดกซ์ทริน 15% เหมาะสมในการช่วยปรับสมดุลระหว่างความเข้มข้นของตัวพาและประสิทธิภาพในการอบแห้งแบบพ่นฝอย ดังตารางที่ 1

ตารางที่ 1 แสดงคุณสมบัติทางกายภาพของผงตะลิงปลิงในสภาวะการทำแห้งแบบพ่นฝอยที่แตกต่างกัน

สภาวะ	ผลผลิต (% Powder Yield)	ค่าความชื้น (%)	ความสามารถในการละลาย (%)
130°C, 10% มอลโตเด็กซ์ทริน	7.2	7.3	80.3
150°C, 15% มอลโตเด็กซ์ทริน	**16.4**	**4.4**	**86.7**
170°C, 20% มอลโตเด็กซ์ทริน	2.6	6.5	75.4

4.3 ประเมินผลกระทบของการอบแห้งแบบพ่นฝอยต่อการรักษาคุณค่าทางโภชนาการ และการคงอยู่ของปริมาณสารอาหาร วิตามินและเกลือแร่ เมื่อใช้สภาวะที่อุณหภูมิ 150°C มอลโตเดกซ์ทรินร้อยละ 15 พบว่าในปริมาณผงตะลิงปลิง 100 กรัม ยังคงพบวิตามินซีในปริมาณที่สูงร้อยละ 30.2 วิตามินบี1 ร้อยละ 0.01 และวิตามินบี 2 ร้อยละ 0.02 รวมถึงแคลเซียมร้อยละ 3.91และธาตุเหล็กร้อยละ 2.32 ตามลำดับแสดง ดังตารางที่ 2

ตารางที่ 2 แสดงการเปลี่ยนแปลงคุณค่าโภชนาการก่อนและหลังขบวนการทำแห้งด้วยเครื่องพ่นฝอยในสภาวะอุณหภูมิ 150°C มอลโตเดกซ์ทรินร้อยละ 15

สารอาหาร	น้ำตะลิงปลิง (หน่วย/100 กรัม)	ผงตะลิงปลิง (หน่วย/100 กรัม)
พลังงาน (กิโลแคลอรี่)	79.91	379
โปรตีน (กรัม)	1.95	1.54
คาร์โบไฮเดรต (กรัม)	17.99	93.1
ใยอาหาร (กรัม)	2.14	1.41
วิตามินซี (มิลลิกรัม)	39.0	30.2
วิตามินบี 1 (มิลลิกรัม)	0.24	0.01
วิตามินบี 2 (มิลลิกรัม)	1.22	0.02
แคลเซียม (มิลลิกรัม)	3.66	3.91
เหล็ก (มิลลิกรัม)	1.09	2.32
โซเดียม (มิลลิกรัม)	1.83	1.49

V. อภิปรายผล

การพัฒนาผงตะลิงปลิงโดยใช้การอบแห้งแบบพ่นฝอย แสดงให้เห็นผลลัพธ์ที่มีแนวโน้มดีในแง่ของผลผลิต คุณสมบัติทางกายภาพ และการคงอยู่ของสารอาหาร สภาวะที่เหมาะสมที่สุดที่อุณหภูมิทางเข้า 150°C พร้อมมอลโตเด็กซ์ตริน 15% ทำให้ได้ผลผลิตผงสูงสุด (16.4%) และความสามารถในการละลายดีที่สุด (86.7%) ซึ่งบ่งชี้ถึงกระบวนการอบแห้งที่มีประสิทธิภาพ อุณหภูมิที่ต่ำกว่าทำให้มีปริมาณความชื้นที่สูงขึ้น ซึ่งอาจส่งผลเสียต่อเสถียรภาพในการจัดเก็บ ในขณะที่อุณหภูมิที่สูงเกินไปทำให้สารประกอบชีวภาพเสื่อมสภาพ ปริมาณความชื้นและค่าน้ำอิสระ (Aw) เป็นปัจจัยสำคัญต่อเสถียรภาพของจุลินทรีย์ สภาวะที่เหมาะสมที่สุดทำให้มีปริมาณความชื้น 4.4% และ Aw 0.30 ซึ่งต่ำกว่าเกณฑ์การเจริญเติบโตของจุลินทรีย์ ช่วยให้เก็บได้นานขึ้น การวิเคราะห์สีบ่งชี้ว่าสีเข้มขึ้นเล็กน้อยเมื่ออยู่ที่อุณหภูมิสูงขึ้นเนื่องจากปฏิกิริยา Maillard แต่สภาวะที่อุณหภูมิ 150°C ยังคงรักษาสีที่ยอมรับได้สำหรับการใช้งานเชิงพาณิชย์ ในส่วนของการรักษาคุณค่าทางโภชนาการ กระบวนการอบแห้งที่ปรับให้เหมาะสมสามารถรักษาวิตามินซีได้ 30.2% ผลลัพธ์เหล่านี้บ่งชี้ว่าการทำให้แห้งแบบพ่นฝอยสามารถรักษาคุณค่าทางโภชนาการ สารอาหารที่สำคัญไว้ได้อย่างมีประสิทธิภาพ ทำให้ผงเป็นส่วนผสมที่มีประโยชน์สำหรับการใช้งานในอาหาร

ผลการศึกษานี้สอดคล้องกับงานวิจัยก่อนหน้านี้เกี่ยวกับการผลิตผงผลไม้โดยใช้การอบแห้งแบบพ่นฝอย Tonon *et al*. (2011) รายงานว่าการอบแห้งแบบพ่นฝอยของอาซาอิ (Euterpe oleracea Mart.) ที่อุณหภูมิ 150°C ช่วยให้ผลผลิตและรักษาฤทธิ์ทางชีวภาพได้ดีที่สุด ซึ่งสอดคล้องกับผลที่ได้จากผงมะยมฝรั่ง ในทำนองเดียวกัน Marques *et al*. (2019) พบว่าการอบแห้งแบบพ่นฝอยของคามูคามู (Myrciaria dubia) ที่อุณหภูมิ 150°C ช่วยรักษาระดับวิตามินซีและโพลีฟีนอลในระดับสูง ซึ่งช่วยเสริมประสิทธิภาพของอุณหภูมินี้สำหรับผงผลไม้ที่ไวต่อความร้อน ในทางกลับกัน Kuck และ Noreña (2017) แสดงให้เห็นว่าการอบแห้งแบบแช่แข็งยังคงมีฤทธิ์ต้านอนุมูลอิสระได้สูงกว่าการอบแห้งแบบพ่นฝอยสำหรับผงสตรอว์เบอร์รี่ อย่างไรก็ตาม การอบแห้งแบบพ่นฝอยยังคงเป็นที่นิยมสำหรับการผลิตในปริมาณมาก เนื่องจากคุ้มทุนและสามารถผลิตผงละเอียดและเสถียรได้ นอกจากนี้ Gharsallaoui *et al*. (2007) เน้นย้ำว่าการเลือกตัวแทนสารตัวนำมีอิทธิพลต่อความสามารถในการละลายและความเสถียร ซึ่งสนับสนุนการค้นพบที่ว่ามอลโตเด็กซ์ตริน 15% ช่วยเพิ่มคุณสมบัติของผงในขณะที่ลดการสูญเสียสารอาหารให้น้อยที่สุด

ข้อจำกัดของการวิจัย

- จำกัดชนิดของสารพาหะในการทดสอบ: การศึกษาเน้นที่มอลโตเดกซ์ทริน การวิจัยในอนาคตอาจสำรวจสารพาหะอื่นๆ

- ขาดการประเมินทางประสาทสัมผัส: แม้ว่าจะมีการวิเคราะห์คุณสมบัติทางกายภาพแล้ว แต่ควรประเมินการยอมรับของผู้บริโภคต่อผงตะลิงปลิงที่ใช้เป็นส่วนผสมของผลิตภัณฑ์ใหม่ในการศึกษาในอนาคต

- เทคนิคการทำแห้งแบบเปรียบเทียบ: การศึกษานี้ไม่ได้เปรียบเทียบการทำแห้งแบบพ่นฝอยกับเทคนิคอื่นๆ เช่น การทำแห้งแบบแช่แข็ง ซึ่งอาจให้การคงอยู่ของสารชีวภาพที่สูงกว่า

VI. ข้อสรุป

การศึกษาครั้งนี้ประสบความสำเร็จในการพัฒนาผลิตภัณฑ์ตะลิงปลิงผงสำเร็จรูป ในการใช้กรรมวิธีทำให้แห้งแบบพ่นฝอย โดยมีการปรับสภาวะในการอบให้เหมาะสมเพื่อเพิ่มความเสถียร ความสามารถในการละลาย และการเก็บรักษาคุณค่าทางโภชนาการ ผลการวิจัยที่สำคัญสรุปได้ดังนี้:

1. สภาวะการทำให้แห้งแบบพ่นฝอยที่เหมาะสมที่สุด: ได้ผลลัพธ์ที่ดีที่สุดที่อุณหภูมิทางเข้า 150°C โดยมีมอลโตเด็กซ์ตริน 15% ซึ่งสภาวะนี้ทำให้ได้ผงละเอียดที่ไหลอิสระพร้อมคุณสมบัติการคืนตัวที่ดี

2. คุณสมบัติทางกายภาพ: ผงตะลิงปลิงมีค่าความชื้น และค่าน้ำอิสระต่ำทำให้จุลินทรีย์มีเสถียรภาพและมีอายุการเก็บรักษาที่ยาวนานขึ้น การวิเคราะห์สีบ่งชี้ว่าสีเข้มขึ้นเล็กน้อยที่อุณหภูมิสูง แต่สภาวะที่เหมาะสมที่สุดช่วยรักษาลักษณะธรรมชาติของผลไม้ไว้ได้

3. การรักษาคุณค่าทางโภชนาการและการทำงาน: สภาวะการอบแห้งที่เหมาะสมที่สุดสามารถรักษาวิตามิน และแร่ธาตุได้ ยืนยันถึงประสิทธิภาพของการอบแห้งแบบพ่นฝอยในการรักษาคุณค่าทางโภชนาการ คาดว่าส่งผลถึงคุณสมบัติทางชีวภาพของผงตะลิงปลิงที่ยังคงประสิทธิภาพ

4. การเปรียบเทียบกับงานวิจัยที่เกี่ยวข้อง: ผลลัพธ์สอดคล้องกับการศึกษาก่อนหน้านี้เกี่ยวกับการอบแห้งผงผลไม้เมืองร้อนด้วยการพ่นฝอย โดยเสริมประสิทธิภาพของอุณหภูมิการอบแห้ง 150°C ซึ่งเป็นอุณหภูมิที่เหมาะสมที่สุดสำหรับการเก็บรักษาสารออกฤทธิ์ทางชีวภาพในขณะที่ยังคงคุณภาพของผงที่สูง

ทิศทางการวิจัยในอนาคต

แม้ว่าการศึกษานี้จะแสดงให้เห็นผลลัพธ์ที่มีแนวโน้มดี แต่ควรเพิ่มเติมงานวิจัยในด้านต่อไปนี้:

- สารพาหะทางเลือก: การตรวจสอบการใช้สารห่อหุ้มอื่นๆ เช่น กัมอะราบิก (Gum Arabic) หรือโปรตีนเวย์ เพื่อปรับปรุงเสถียรภาพและการกักเก็บสารอาหาร

- เทคนิคการอบแห้งแบบเปรียบเทียบ: การประเมินการอบแห้งแบบแช่แข็ง การอบแห้งแบบสุญญากาศ หรือการอบแห้งแบบอินฟราเรด เพื่อการวิเคราะห์ที่ครอบคลุมมากขึ้นเกี่ยวกับประสิทธิภาพการอบแห้งและการกักเก็บสารอาหาร

- การศึกษาด้านการรับรู้ทางประสาทสัมผัสและผู้บริโภค: การดำเนินการทดลองประเมินทางประสาทสัมผัสเพื่อประเมินรสชาติ เนื้อสัมผัส และความชอบโดยรวมของผู้บริโภคของผลิตภัณฑ์ที่มีผงตะลิงปลิงเป็นส่วนประกอบ

- การประยุกต์ใช้ในการพัฒนาผลิตภัณฑ์ในอาหารเพื่อสุขภาพ เช่น เครื่องดื่ม ขนมหวาน และผลิตภัณฑ์เสริมอาหาร

โดยสรุปแล้ว การอบแห้งแบบพ่นฝอยเป็นเทคนิคที่มีประสิทธิภาพ ทำให้ผงตะลิงปลิงที่ได้ยังคงสภาวะเสถียรและมีประโยชน์ต่อสุขภาพ สามารถนำไปต่อยอด ใช้ในอุตสาหกรรมอาหารและอาหารเสริม การศึกษาในอนาคตควรเน้นที่การปรับปรุงการกักเก็บสารออกฤทธิ์ทางชีวภาพและการประเมินการยอมรับของผู้บริโภคเพื่อต่อยอดในเชิงพาณิชย์

คำขอบคุณ

ขอขอบคุณ คณะเทคโนโลยีการเกษตร มหาวิทยาลัยราชภัฏภูเก็ต ที่ให้ความอนุเคราะห์ในการใช้สถานที่และเครื่องมือในการทำแห้งแบบพ่นฝอย (Spray Drying) รวมถึงนักวิทยาศาสตร์ประจำคณะฯ ที่คอยแนะนำการใช้เครื่องมือและงบประมาณจากโครงการยกระดับมาตรฐานผลิตภัณฑ์ชุมชนยั่งยืนสู่แพลตฟอร์มออนไลน์ของทางมหาวิทยาลัยราชภัฏภูเก็ตรวมถึงชาวบ้านในกลุ่มตะลิงปลิง กะปงป้าเพ็ญ ต.กะปง อ.กะปง จ.พังงา ที่ให้ความร่วมมือและสนับสนุนวัตถุดิบ จนงานวิจัยสำเร็จลุล่วงไปด้วยดี

อ้างอิง

[1] A. Gharsallaoui, G. Roudaut, O. Chambin, A. Voilley, and R. Saurel, "Applications of spray-drying in microencapsulation of food ingredients: An overview," Food Res. Int., vol. 40, no. 9, pp. 1107-1121, 2007.

[2] C. Tonon, C. Brabet, and M. D. Hubinger, "Influence of process conditions on the physicochemical properties of açai (Euterpe oleracea Mart.) powder produced by spray drying," J. Food Eng., vol. 103, no. 2, pp. 152-158, 2011.

[3] F. Shishir and J. X. Chen, "Trends of spray drying: Implications for food processing," J. Food Eng., vol. 223, pp. 102-122, 2018.

[4] M. Kuck and U. Noreña, "Comparative study of spray-dried and freeze-dried strawberry powders: Physicochemical properties and antioxidant retention," LWT - Food Sci. Technol., vol. 85, pp. 158-163, 2017.

[5] R. A. C. Marques, C. M. D. Silva, and M. P. Fontes, "Effect of spray drying conditions on the physicochemical properties of camu-camu (Myrciaria dubia) powder," Powder Technol., vol. 354, pp. 793-802, 2019.

[6] S. J. Chan, H. C. Choo, and S. C. Young, "Encapsulation of bioactive compounds extracted from tropical fruits using spray drying," J. Funct. Foods, vol. 75, p. 104235, 2020.

[7] Y. Kumar, D. N. Yadav, T. Ahmad, and K. Narsaiah, "Recent trends in the encapsulation of probiotics using spray and freeze-drying techniques," Food Biotechnol., vol. 31, no. 3, pp. 231-248, 2017.

การพัฒนาผลิตภัณฑ์น้ำพริกปลาฉิงฉางส้มควายเพื่อยืดอายุการเก็บรักษา

(Development of Pla ching chang Som-Khway Chili Paste Products for Shelf Life Prolonging)

1st Pakamon-Kulnuwong
: Home Economics
: Faculty of Science and Technology; Phuket Rajabhat University
: Phuket Thailand
: pakamon.k@pkru.ac.th

2nd Nata-Anisong
: Home Economics
: Faculty of Science and Technology; Phuket Rajabhat University
: Phuket Thailand
: Nata.a@pkru.ac.th

3rd Unruethai-Phupornprasert
: Chemistry
: Faculty of Science and Technology; Phuket Rajabhat University
: Phuket Thailand
Unruethai.p@pkru.ac.th

Abstract

In the study of the production process and product development of Pla Ching Chang Som Kwai chili paste, to extend the shelf life and analyze the nutritional value of the chili paste by packing in vacuum laminated bags and storing at room temperature (30±2 ℃), the analysis was performed and the results were observed every 7 days until spoilage occurred. The analysis of physical quality, microorganisms, and nutritional value assessment were performed. It was found that when the storage period was increased, the Pla Ching Chang Som Kwai chili paste stored at room temperature had a decrease in pH, water activity (aw), and color value, but the moisture content increased. at the same time the total amount of microorganisms, mold was found to increase significantly ($p \leq 0.05$). The amount of coliform and Escherichia coli weve not found throughout the storage period at room temperature. The Pla Ching Chang Som Kwai chili paste packed in vacuum laminated bags could be stored for 1-2 weeks, respectively.

Keywords—*Som Khwai, boiled dried anchovy,Chili Paste, shelf life*

I. บทนำ

ส้มควายเป็นพืชท้องถิ่นในจังหวัดภูเก็ต มีชื่อทางวิทยาศาสตร์ว่า *Garcinia pedunculata* Roxb.เป็นไม้ยืนต้นจัดอยู่ในวงศ์ Guttiferae ผลมีลักษณะเป็นทรงกลมขนาดเส้นผ่านศูนย์กลาง 8-12 เซนติเมตร เมื่อแก่จัดสามารถนามาบริโภคหรือประกอบเป็นอาหารได้ และยังมีสรรพคุณในการรักษาโรคลักปิดลักเปิด การสมานแผล บำรุงหัวใจ (Mudoi et al., 2012) ในส้มควายมีกรดหลายชนิดซึ่งส่งผลต่อการยืดอายุของผลิตภัณฑ์น้ำพริก อีกทั้งผลแก่และผลอ่อนส่งผลต่อกลิ่นและรสชาติของส้มมีความเป็นเอกลักษณ์เฉพาะ(Apantree et al.,2016)

น้ำพริกเป็นอาหารตำรับไทยที่อยู่คู่กับสังคมไทยมาช้านาน น้ำพริกเป็นอาหารที่มีลักษณะเป็นถ้วยเล็ก ๆซึ่งน้ำพริกจะถูกปรุงแต่งรสชาติความอร่อยและวัตถุดิบที่มีความแตกต่างกันขึ้นอยู่กับภูมิภาคของไทย โดยรสชาติน้ำพริกจะมีการผสมผสานระหว่างเครื่องปรุงต่างๆ และมีพริกเป็นวัตถุดิบหลักเสมอ น้ำพริกเป็นการเชื่อมโยงฐานทรัพยากรอาหารที่สำคัญ เป็นอาหารจานเครื่องจิ้มในอาหารหลักของคนไทยที่มีวัตถุดิบเครื่องปรุงมาจากพื้นบ้านนำมารับประทานคู่กับผักพื้นบ้าน นอกจากน้ำพริกเป็นตำรับในการกินกับข้าวของคนไทยแล้ว น้ำพริกยังสร้างรายได้ให้กับคนชุมชนทั่วทั้งประเทศ ด้วยความเป็นเอกลักษณ์ตามแบบฉบับของแต่ละวัฒนธรรมของของอาหารพื้นบ้านอย่างน้ำพริก ถือได้ว่าเป็นทุนทางวัฒนธรรมของท้องถิ่นซึ่งมีการสะสมองค์ความรู้ และถ่ายทอดมาอย่างต่อเนื่อง เป็นภูมิปัญญาที่มีคุณค่าต่อยอดภูมิปัญญาไทยในน้ำพริกให้เป็นอาหารเพื่อสุขภาพ สำนักงานมาตรฐานผลิตภัณฑ์อุตสาหกรรม (2018)

ปัจจุบันพบว่า กลุ่มชุมชนในจังหวัดภูเก็ตมีหน่วยงานราชการสนับสนุนส่งเสริมให้ยกระดับมาตรฐานของพืชและผลิตภัณฑ์ในชุมชนในการสร้างรายได้เช่นเดียวกันกับน้ำพริกปลาฉิ้งฉ้างส้มควายจากชุมชนเกษตรกรรักษ์สาคู ซึ่งมีปัญหาในการเก็บรักษายืดอายุการเก็บของน้ำพริก ไม่ว่าจะเป็นกระบวนการผลิตหรือการเสื่อมเสียจากทางกายภาพเคมี ล้วนส่งผลต่ออายุการเก็บรักษา ส่งผลต่อการจัดจำหน่าย ดังนั้นหากสามารถยืดอายุการเก็บรักษาให้นานขึ้นได้ ก็สามารถเพิ่มปริมาณจำนวนยอดขายให้กับผู้ประกอบการได้ ส่วนใหญ่น้ำพริกจะเก็บรักษาได้นานแค่ 1-2 สัปดาห์ และอาจจะเก็บได้นานขึ้นเมื่อรักษาอุณหภูมิให้อยู่ในตู้เย็นหรือสภาวะสุญญากาศ (Uunop et al.,2019)

งานวิจัยนี้มีวัตถุประสงค์เพื่อศึกษาการยืดอายุการเก็บ และคุณค่าทางโภชนาการของน้ำพริกปลาฉิ้งฉ้างส้มควาย โดยกรอบของงานวิจัย ศึกษากระบวนการผลิตโดยการควบคุมเวลาและอุณหภูมิในการผลิต วิเคราะห์คุณบัติทางกายภาพเคมี จุลินทรีย์ที่ก่อให้เกิดการเสื่อมเสียที่ส่งผลต่ออายุการเก็บเพื่อผลักดันให้กลุ่มวิเสาหกิจชุมชน 2019 รักษ์สาคูได้นำไปยกระดับมาตรฐานผลิตภัณฑ์ชุมชน

II. ทบทวนวรรณกรรม

การพัฒนาผลิตภัณฑ์น้ำพริกผัดสมุนไพร งานวิจัยมีวัตถุประสงค์เพื่อศึกษาคุณค่าทางโภชนาการและคุณภาพทางกายภาพเคมีของผลิตภัณฑ์น้ำพริกผัดสมุนไพร พบว่าน้ำพริกที่ผู้ทดสอบให้คะแนนความชอบมากที่สุดคือน้ำพริกปลาย่าง เสริมกระชายดำร้อยละ 5 คุณค่าทางโภชนาการของน้ำพริกผัดอีกทั้งวิเคราะห์คุณค่าทางโภชนาการของน้ำพริก ซึ่งมีผลใกล้เคียงกับน้ำพริกปลาฉิ้งฉ้างส้มควาย อีกทั้งการทดสอบทางจุลินทรีย์พบว่า ผลิตภัณฑ์น้ำพริกผัดสมุนไพรเป็นไปตามมาตรฐานผลิตภัณฑ์ชุมชนกำหนดเป็นไปในทิศทางเดียวกันกับน้ำพริก

ปลาฉิ้งฉ้างส้มควาย [1] การควบคุมคุณภาพวัตถุดิบและศึกษาอายุการเก็บรักษาของผลิตภัณฑ์น้ำพริกพริกไทยดำเพื่อเพิ่มประสิทธิภาพการผลิตให้ได้มาตรฐานของกลุ่มแม่บ้านบ้านเขาหลัก จังหวัดตรัง ผลการศึกษาพบว่าคุณค่าทางโภชนาการของน้ำพริกพริกไทยดำมีคุณค่าทางโภชนาการด้านพลังงานทั้งหมด ไขมัน น้ำตาล มีความปริมาณที่ใกล้เคียงกัน ยกเว้น คอเลสเตอรอลซึ่งน้ำพริกปลาฉิ้งฉ้างส้มควายมีปริมาณที่ต่ำกว่าน้ำพริกพริกไทยดำ

[2] การศึกษาอายุการเก็บรักษาของผลิตภัณฑ์คั่วกลิ้งและน้ำพริกเห็ดแครง ผลการศึกษาพบว่า กระบวนการผลิตที่มีการควบคุมอุณหภูมิและเวลาและการเก็บรักษาการยืดอายุที่สภาวะต่างกันส่งผลต่ออายุการเก็บซึ่งการเก็บที่อุณหภูมิห้องและอุณหภูมิตู้เย็นมีอายุการเก็บ 1 และ3 สัปดาห์ ตามลำดับ มีความเป็นไปในทิศทางเดียวกันกับการเก็บรักษาน้ำพริกเพื่อการวิเคราะห์จุลินทรีย์ของน้ำพริกปลาฉิ้งฉ้างส้มควายที่อุณหภูมิห้องสสามารถเก็บรักษาได้ 1-2 สัปดาห์เนื่องจากความชื้นในผลิตภัณฑ์น้อยกว่าผลิตภัณฑ์คั่วกลิ้งและน้ำพริกเห็ดแครง [3]

III. ระเบียบวิธีวิจัย

1.วัตถุดิบที่ใช้ในการทดลอง

1.1 การเตรียมส้มควายที่ใช้ในการทดลองเป็นส้มควายสดที่ผลสุก ที่นำมาจากชุมชนตำบลสาคู อำเภอถลาง จังหวัดภูเก็ต โดยนำมาปอกและทำความสะอาดตากแดดในระบบปิดจนแห้ง แล้วนำมาปั่นให้ละเอียดเป็นเวลา 1 นาที และการเตรียมปลาฉิ้งฉ้างที่ใช้ในน้ำพริกโดยการนำมาแกะเอาเฉพาะส่วนเนื้อแล้วนำมาล้างทำความสะอาดหลังจากนั้นนำมาตากแดดในระบบปิด แล้วนำมาปั่นให้ละเอียดเป็นเวลา 1-2 นาที

1.2 การผลิตน้ำพริกปลาฉิ้งฉ้างส้มควาย ส่วนผสมของน้ำพริกพริกสนแห้ง ร้อยละ 5 หอมแดงร้อยละ 30 ปลาฉิ้งฉ้างร้อยละ 20 ส้มควายร้อยละ 20 กะปิกุ้งร้อยละ 10 น้ำตาลร้อยละ 5 และน้ำมันปาล์มร้อยละ 10 โดยมีขั้นตอนดังนี้คือ นำส่วนผสมทุกอย่างมาล้างทำความสะอาด ล้าง หั่น และตากแดดในระบบปิด หลังจากนั้นนำส่วนผสมส้มควายและปลาฉิ้งฉ้าง มาปั่นรวมกับส่วนผสมอื่นๆ ในน้ำพริกได้แก่ พริกสนแห้ง กระเทียม หอมแดง ตะไคร้ กะปิ น้ำมันพืช และน้ำตาล นำส่วนผสมที่ผ่านการปั่นละเอียดนำมาใส่เครื่องกวน ควบคุมอุณหภูมิในการกวน 60 องศาเซลเซียส เป็นระยะเวลา 1 ชั่วโมง 45 นาทีหรือจนแห้ง นำน้ำพริกบรรจุในถงลามิเนตสุญญากาศ หลังจากนั้นนำส่งวิเคราะห์คุณค่าทางโภชนาการและอายุการเก็บ

2.การเก็บรวบรวมข้อมูลและวิเคราะห์ผล

2.1 การวิเคราะห์ทางด้านกายภาพ ได้แก่ ความชื้น ของแข็งทั้งหมดที่ละลายได้ ค่าปริมาณน้ำอิสระ ปริมาณกรดทั้งหมด ค่าสี และความเป็นกรดด่าง

2.2 การวิเคราะห์คุณค่าทางโภชนาการ ได้แก่ ปริมาณคาร์โบไฮเดรต โปรตีน ไขมัน น้ำตาล โซเดียม เส้นใย คอเลสเตอรอล วิตามินเอ วิตามินบี 1 วิตามินบี2 แคลเซียม และเหล็ก

2.3 การวิเคราะห์จุลินทรีย์ที่ก่อให้เกิดการเสื่อมเสียในอาหาร ได้แก่ ยีสต์ (yeast) เชื้อรา (Mold) ครอสทริเดียม เพอร์ฟริงเจนส์ (Clostridium perfringens) เอสเชอริเชีย โคไล (E.coli) สตาฟิโลค็อกคัส ออเรียส(Staphylococcus aureus) ซาลโมเนลลา (Salmonella spp) บาซิลลัส ซีเรียส (Bacillus Cercus) และแบคทีเรียกลุ่มโคลิฟอร์มทั้งหมด (Total Coliform bacteria,TCB)

IV. ผลการทดลอง

จากผลการวิเคราะห์การเปลี่ยนแปลงคุณภาพด้านกายภาพ และจุลินทรีย์ พบว่าเมื่อระยะการเก็บรักษาเพิ่มขึ้นผลิตภัณฑ์น้ำพริกปลาฉิ้งฉ้างส้มควายที่เก็บรักษาที่อุณหภูมิห้องมีค่าพีเอช (pH) ค่าวอเตอร์แอคติวิตี้ (Aw)และค่าสี ลดลง แต่ความชื้นเพิ่มขึ้นในขณะที่ปริมาณเชื้อจุลินทรีย์ทั้งหมดพบเชื้อรามีปริมาณเพิ่มขึ้น สำหรับปริมาณเชื้อ coliform และ *Escherichia coli* ไม่พบตลอดระยะเวลาการเก็บรักษาที่อุณหภูมิห้อง ในขณะที่งานวิจัย (Samdaeng et al., 2015) ผลการวิเคราะห์ค่า pH ของผลิตภัณฑ์คั่วกลิ้งเห็ดแครงและน้ำพริกเห็ดแครง พบว่าค่า pH ลดลงอย่างต่อเนื่องเมื่อระยะเวลาในการเก็บรักษานานขึ้น ทั้งในผลิตภัณฑ์ที่เก็บรักษาที่อุณหภูมิห้องและ อุณหภูมิแช่เย็น เนื่องจากการเก็บรักษาผลิตภัณฑ์คั่วกลิ้งเห็ดแครงและน้ำพริกเห็ดแครงเป็นการเก็บในภาชนะปิดสนิทและจัดได้ว่าเป็นกลุ่มอาหารประเภท low acid food จึงอาจมีการเจริญของเชื้อกลุ่ม flat sour spoilage ส่งผลให้ค่า pH ในอาหารลดลง

ผลการวิเคราะห์ค่าความชื้นของผลิตภัณฑ์น้ำพริกปลาฉิ้งฉ้าง ตามตารางที่ 1 พบว่าปริมาณความชื้นมีการเปลี่ยนแปลงตลอดระยะเวลาของการเก็บรักษาในอุณหภูมิห้อง 13.37-16.81 ตามลำดับ อาจจะเป็นผลจากการเก็บรักษาผลิตภัณฑ์ที่ปิดสนิทในอุณหภูมิห้องส่งผลให้ เกิดไอน้ำในผลิตภัณฑ์ ระหว่างการเก็บรักษา

ค่า a_w เป็นปัจจัยสำคัญในการควบคุมและป้องกันการเสื่อมเสียของผลิตภัณฑ์อาหาร ตามตารางที่ 1 จึงมีผลต่อการกำหนดอายุการเก็บรักษาของผลิตภัณฑ์อาหาร (Barbosaet al.,2007) ซึ่งตามเกณฑ์มาตรฐานของสำนักงานมาตรฐานผลิตภัณฑ์อุตสาหกรรมกำหนดให้ผลิตภัณฑ์น้ำพริกปลาฉิ้งฉ้างต้องมีค่า a_w ไม่เกิน 0.6 (สำนักงานมาตรฐานผลิตภัณฑ์อุตสาหกรรม, 2549b) จากผลการทดลอง พบว่าในระหว่างการเก็บรักษา ค่า aw ของน้ำพริกปลาฉิ้งฉ้างส้มควายอยู่ในช่วง 0.78-0.82

คุณค่าทางโภชนาการของผลิตภัณฑ์น้ำพริกปลาฉิ้งฉ้างส้มควายตามตารางที่ 2 พบว่า ปริมาณ ไขมัน โปรตีน คาร์โบไฮเดรต เส้นใย และแคลเซียม ร้อยละ 11 ,20,26.6,17,และ 1.50 มิลลิกรัม/100 กรัม กับปริมาณจุลินทรีย์ทั้งหมด ไม่พบการทำให้เกิดความเสื่อมเสียยกเว้น เชื้อรา ที่มีผลมาจากความชื้นที่เพิ่มขึ้น ส่งผลให้พบเชื้อรา ในปริมาณที่ <100 (จำนวนโคโลนีต่อกรัม) ซึ่งต่ำกว่าที่มาตรฐานกำหนดตามตารางที่ 3 (เกณฑ์คุณภาพทางจุลชีววิทยาของอาหารและภาชนะสัมผัสอาหาร ฉบับที่ 3,2560)

ตารางที่ 1 คุณภาพทางกายภาพของน้ำพริกปลาฉิ้งฉ้างส้มควาย

สภาวะเก็บรักษา	คุณภาพทางกายภาพ	อายุการเก็บ (สัปดาห์)			
		1	2	3	4
อุณหภูมิห้อง	สี	9.00	8.00	8.00	7.50
	ความชื้น	15.41	13.37	14.07	16.81
	ปริมาณน้ำอิสระ	0.79	0.81	0.82	0.78
	ปริมาณของแข็งทั้งหมด	13.00	15.00	17.00	15.00
	ความเป็นกรดด่าง (pH)	4.85	4.81	4.82	4.77

ตารางที่2 คุณค่าทางโภชนาการของผลิตภัณฑ์น้ำพริกปลาฉิ้งฉ้างส้มควาย 100 กรัม

คุณภาพของคุณค่าทางโภชนาการ	ผลการทดสอบ	หน่วย(Unit)
พลังงานทั้งหมด (Total energy)	285.4	กิโลแคลอรี่
ไขมัน	11	กรัม
โคเลสเตอรอล	2.0	มิลลิกรัม
โปรตีน	20.0	ร้อยละ
คาร์โบไฮเดรต	26.6	ร้อยละ
เส้นใย	17.0	ร้อยละ
แคลเซียม	105	ร้อยละ
เหล็ก	0.50	Mg/L

ตารางที่ 3 คุณภาพจุลินทรีย์ในผลิตภัณฑ์น้ำพริกปลาฉิ้งฉ้างส้มควาย

รายการ	ผลการทดสอบ/CFU/g
รา	10-51
ยีสต์ (จำนวนโคโลนีต่อกรัม)	ไม่พบ
E. coli (จำนวนที่เป็นไปได้มากที่สุดต่อกรัม)	ไม่พบ
Clostridium perfringens	ไม่พบ
Staphylococcus aureus	ไม่พบ
Salmonella spp.	ไม่พบ
Bacillus Cereus	ไม่พบ
Total Coliform bacteria,TCB	ไม่พบ

V. อภิปรายผล

การพัฒนากระบวนการผลิตน้ำพริกปลาฉิ้งฉ้างส้มควายเพื่อยืดอายุการเก็บรักษาโดยทำการศึกษาขั้นตอนและกระบวนการผลิตที่นำวัตถุดิบผ่านทำความสะอาด และตากให้แห้งด้วยระบบปิด และมีการควบคุมอุณหภูมิและเวลาในการผลิตที่อุณหภูมิ 60 องศาเซลเซียสเป็นเวลา 1 ชั่วโมง 45 นาที เป็นไปในทิศทางเดียวกันกับงานวิจัย (Arsanahsark et al., 2021) การใช้ประโยชน์จากวัสดุเศษเหลือหัวปลากะตักเสริมโปรตีนและแคลเซียมในผลิตภัณฑ์อาหาร ได้พัฒนากระบวนการผลิตและขั้นตอนการเตรียมวัตถุดิบที่มีคุณภาพ การล้างทำความสะอาด การให้ความร้อนวัตถุดิบ รวมทั้งการควบคุมการใช้เครื่องมือและอุปกรณ์ที่สะอาดทุกขั้นตอน ช่วยลดการปนเปื้อนของเชื้อจุลินทรีย์ที่ส่งผลทำให้เกิดการเสื่อมเสียของอาหาร

อายุการเก็บรักษาผลิตภัณฑ์น้ำพริกปลาฉิ้งฉ้างส้มควายผลการศึกษาพบว่า เมื่อนำน้ำพริกในถุงลามิเนตแบบสุญญากาศและเก็บรักษาที่อุณหภูมิห้อง (30±2องศาเซลเซียส) เมื่อระยะเวลาการเก็บรักษาเพิ่มขึ้นส่งผลให้ความชื้นและค่า a_w (ปริมาณน้ำอิสระ) มีค่าเพิ่มขึ้น ส่งผลต่อการเจริญเติบโตของเชื้อราและพบปริมาณเชื้อราในสัปดาห์ที่ 2 ของการวิเคราะห์ผลแต่ไม่พบการเปลี่ยนแปลงของจุลินทรีย์อื่นๆ สอดคล้องกับ (Samdaeng et al., 2015) ผลิตภัณฑ์น้ำพริกคั่วกลิ้งเห็ดแครงและน้ำพริกเห็ดแครงที่เก็บรักษาที่อุณหภูมิห้องส่งผลต่อการเจริญเติบโตของจุลิทรีย์ที่ก่อให้เกิดความเสื่อมเสียในสัปดาห์ที่ 4

ด้านคุณค่าทางโภชนาการของผลิตภัณฑ์น้ำพริกปลาฉิ้งฉ้างส้มควายพบว่าปริมาณ ไขมัน โปรตีน คาร์โบไฮเดรต เส้นใย และแคลเซียม ร้อยละ 11 ,20,26.6,17,และ 1.50 มิลลิกรัม/100 กรัมสอดคล้องกับงานวิจัยการพัฒนาผลิตภัณฑ์ขนมทองม้วนเติมหัวปลารสแกงเขียวหวานและขนมกรอบพองเติมหัวปลาการเติมหัวปลาในผลิตภัณฑ์ทั้ง 3 ชนิด ทำให้ปริมาณโปรตีนและแคลเซียมเพิ่มขึ้นเมื่อเปรียบเทียบกับผลิตภัณฑ์ดั้งเดิมโดยขนมทองม้วนปริมาณโปรตีนและแคลเซียมเพิ่มขึ้นร้อยละ 3.76 และ 0.37 น้ำหนักต่อน้ำหนัก

ข้อจำกัดของการวิจัย

• งานวิจัยนี้ไม่ได้ทำการประเมินทางประสาทสัมผัส: แม้ว่าจะมีการวิเคราะห์คุณสมบัติทางกายภาพแล้ว แต่ควรประเมินการยอมรับของผู้บริโภค

ข้อสรุป

งานวิจัยการพัฒนากระบวนการผลิตผลิตภัณฑ์น้ำพริกปลาฉิ้งฉ้างส้มควายการศึกษาอายุการเก็บที่ใส่ถุงลามิเนตสุญญากาศที่ปิดสนิทและนำมาเก็บรักษาที่อุณหภูมิห้องเพื่อทำการวิเคราะห์คุณภาพทางกายภาพและคุณค่าทางโภชนาการตลอดจนวิเคราะห์คุณภาพจุลินทรีย์ พบว่าเมื่อระยะเวลาการเก็บรักษาเพิ่มขึ้น จะส่งผลต่อความชื้น ค่า a_w ส่งผลต่อการเพิ่มขึ้นของเชื้อรา หลังจากเก็บรักษาผลิตภัณฑ์น้ำพริกปลาฉิ้งฉ้างส้มควายไว้ 2 สัปดาห์ และเชื้อจุลินทรีย์ coliform และ *E.coli* ไม่พบตลอดระยะเวลาการทดลอง ซึ่งมีแนวโน้มอายุการเก็บรักษาได้นานยิ่งขึ้น เมื่อมีการควบคุมขั้นตอนการเตรียมวัตถุดิบที่มีคุณภาพ การล้างทำความสะอาด การให้ความร้อนวัตถุดิบ รวมทั้งการควบคุมการใช้เครื่องมือและอุปกรณ์ที่สะอาดทุกขั้นตอน ช่วยลดการปนเปื้อนของเชื้อจุลินทรีย์ที่ส่งผลทำให้เกิดการเสื่อมเสียของอาหาร

คำขอบคุณ

ขอบคุณมหาวิทยาลัยราชภัฏภูเก็ตที่ให้ทุนสนับสนุนในการลงพื้นที่ชุมชน และขอบคุณชุมชนวิสาหกิจชุมชนรักษ์สาคู 2019 ตำบลสาคู อำเภอถลาง จังหวัดภูเก็ต

อ้างอิง

[1] P. Phugan, S. Inket, P. Pramai, and S. Singsom, “Development of Stir-Fried Chilli Paste From Herb” วารสารวิจัยรำไพพรรณี ปีที่ 14 ฉบับที่ 1 เดือนมกราคม - เมษายน 2563.

[2] ชมพูนุช โสมาลีย์, ชาคริยา ฉลาด, “ ผลิตภัณฑ์น้ำพริกจำพริกไทยดำ ” การควบคุมคุณภาพของวัตถุดิบเพื่อเพิ่มประสิทธิภาพการผลิตให้ได้มาตรฐานของกลุ่มแม่บ้านเขาหลักจังหวัดตรัง” งานประชุมวิชาการระดับชาติ Engagement Thailand ครั้งที่ 8 The 8th Engagement Thailand Annual Conference 2022.

[3] W. Samdaeng, T. Maireng, B. Pimpa, and S. Lekjing, “Study on Shelf Life of Common Split Gill Mushroom (Schizophyllum commune) Roast Curry and Chili Paste Products” วารสารวิทยาศาสตร์บูรพา ปี ที่ 20 (ฉบับที่2) กรกฎาคม – ธันวาคม พ.ศ. 2558.

[4] Asish G. R., Utpala Parthasarathy, T. J. Zachariah, P. Gobinath, A Comparative Estimation of (-) Hydroxycitric acid in Different Species of Garcinia. The Hort. J., 21(1), 26-19. (2008).M. Young, The Technical Writer’s Handbook. Mill Valley, CA: University Science, 1989.

[5] **ภานุวัฒ น่ดงหนู, ดร.นนท์ธิติ เฉิศเดชา,** Propionibacterium acnes Inhibitionof Garcinia atroviridis Griff. Extract, Published Online: 4 JUN 2021.

[6] A. Meeboon, C. Puenghian, A. Sirichote, A. Voravuthikunchai, " Effects of Fruit Developmental Stages and Dehydration Times on the Physical, Chemical and Antioxidant Properties of Som Khwai (Garcinia pedunculata Roxb.), The Nationol and International Graduate Research Conference, BMP6: 2016.T. Mudoi, D C. Deka, and R. Devi, “In vitro antioxidant activity of Garcinia pedunculata, an indigenous fruit of North Eastern (NE) region of India,” International Journal of PharmTech Research

[7] T. Mudoi, D C. Deka, and R. Devi, “In vitro antioxidant activity of Garcinia pedunculata, an indigenous fruit of North Eastern (NE) region of India,” International Journal of PharmTech Research
CODEN (USA): IJPRIF, Vol.4, No.1, pp 334-342, Jan-Mar 2012.

[8] P. Arsanahsark, S. Kongthong, and S. Chooklin, “Utilization of Anchovy Head Residues Supplemented with Protein and Calcium in Food Products,” วารสารวิจัย มหาวิทยาลัยเทคโนโลยีราชมงคลศรีวิชัย, 13(1) : 201-215 (2564).I. S. Jacobs and C. P. Bean, “Fine particles, thin films and exchange anisotropy,” in Magnetism, vol. III, G. T. Rado and H. Suhl, Eds. New York: Academic, 1963, pp. 271–350.

ความรอบรู้ด้านสุขภาพและพฤติกรรมการป้องกันโรคมือเท้าปากของครูผู้ดูแลเด็กในศูนย์พัฒนาเด็กเล็ก อำเภอเมือง จังหวัดภูเก็ต

Health Literacy and Disease Prevention Behaviors Regarding Hand, Foot, and Mouth Disease Among Childhood Teachers in Child Care Centers in Mueang District, Phuket Province

1st SUPATSORN LUANKAEW
Bachelor of Public Health
Phuket Rajabhat University
Phuket Thailand
S6411166239@pkru.ac.th

2 nd NATTHAKAN WANRAEK
Bachelor of Public Health
Phuket Rajabhat University
Phuket Thailand
S6411166213@pkru.ac.th

3 rd CHAYANIT LUEVANICH
Bachelor of Public Health
Phuket Rajabhat University
Phuket Thailand
chayanit.l@pkru.ac.th

4th ORANURETHAI ABDULLA
Bachelor of Public Health
Phuket Rajabhat University
Phuket Thailand
oranurethai.a@pkru.ac.th

5th JITTIPONG SUNGTHONG
Bachelor of Public Health
Phuket Rajabhat University
Phuket Thailand
jittipong.s@pkru.ac.th

Abstract
This cross-sectional study aimed to study the level of health literacy and the prevention behavior of hand, foot, and mouth disease (HFMD) and the correlation among age, income, experience in hand, foot, and mouth disease care, length of act as childhood teacher, health literacy, and prevention behavior among childhood teachers in childcare centers in Muang District, Phuket Province. The sample consisted of 102 childhood teachers. The research tools consisted of health literacy and behavior of HFMD prevention questionnaire. Data were analyzed using frequency, percentage, mean, standard deviation, and Pearson's product-moment correlation.
The findings showed that childhood teachers had a high level of health literacy (mean = 4.41, S.D. = 0.47) and prevention behavior (mean = 4.63, S.D. = 0.55). Income, experience in hand, foot, and mouth disease care, and length of act as a childhood teacher were correlated with health literacy. Only health literacy was related to prevention behavior. Therefore, public health personnel should promote health literacy among childhood teachers and parents.

Keywords Hand, Foot, and Mouth Disease (HFMD), Teachers, Child Development Centers, Health Literacy, Prevention Behavior

I บทนำ

โรคมือเท้าปากเป็นปัญหาสาธารณสุขที่สำคัญโรคหนึ่ง เกิดจากการติดเชื้อไวรัสกลุ่มเอ็นเทอโรไวรัส(Enterovirus) โดยไวรัสที่เป็นสาเหตุและตรวจพบได้บ่อยคือไวรัสค็อกซากีชนิดเอ (Coxsackie virus A) ไวรัสค็อกซากีชนิดบี (Coxsackie virus B) และไวรัสเอ็นเทอโร 71 (Enterovirus 71) เชื้อไวรัสนี้สามารถติดต่อผ่านทางสารคัดหลั่ง เช่น น้ำมูก น้ำลาย อุจจาระ ลักษณะอาการของโรคมือเท้าปากที่พบได้บ่อย คือ มีไข้ มีแผลในปากคล้ายแผลร้อนในบริเวณลิ้นและกระพุ้งแก้ม เป็นสาเหตุทำให้เด็กไม่สามารถรับประทานอาหารได้ตามปกติ และเกิดตุ่มนูนขนาดเล็กที่ฝ่ามือ นิ้วมือ และฝ่าเท้า หากมีอาการแทรกซ้อนรุนแรงอาจทำให้เกิดอาการสมองอักเสบและเสียชีวิตได้ กลุ่มเสี่ยงต่อการเป็นโรคมือเท้าปาก ได้แก่ กลุ่มเด็ก ส่วนใหญ่พบในเด็กอายุต่ำกว่า 5 ปีซึ่งเป็นเด็กก่อนวัยเรียน ร้อยละ 45 รองลงมาคือ อายุต่ำกว่า 2 ปี ร้อยละ 44 และ 5 ปีขึ้นไป ร้อยละ 11 ตามลำดับ [1]

โรคมือเท้าปากส่งผลกระทบต่อพัฒนาการและสุขภาพโดยรวมของเด็ก คือ เด็กไม่สุขสบาย อ่อนเพลีย เบื่ออาหาร ผลที่ตามมา คือ ภาวะการขาดสารอาหาร ซึ่งการติดเชื้ออาจส่งผลให้เกิดโรคแทรก ดังนั้น ครูผู้ดูแลเด็กจะต้องมีความรอบรู้ด้านสุขภาพเกี่ยวกับโรคมือเท้าปากและพฤติกรรมการป้องกันควบคู่ไปด้วย [2] กรมควบคุมโรค กระทรวงสาธารณสุข ได้เพิ่มมาตรการในการเฝ้าระวังป้องกันโรคล่วงหน้าโดยกำหนดแนวทางมาตรการในการป้องกันควบคุมโรคมือเท้าปากในศูนย์พัฒนาเด็กเล็กเพื่อให้สามารถเฝ้าระวังคัดกรองเด็กป่วยด้วยโรคมือเท้าปากได้อย่างรวดเร็ว

สามารถแยกเด็กป่วยจากเด็กปกติ ทำให้สามารถควบคุมโรคไม่ให้แพร่ระบาดต่อไปได้ [1] ความรอบรู้เกี่ยวกับวิกฤตด้านสุขภาพ ความสามารถในการเข้าใจโรค ข้อมูลข่าวสารจะช่วยให้บุคคลมีพฤติกรรมสุขภาพที่เหมาะสมขณะเผชิญโรคติดต่อ [3] โดยองค์การอนามัยโลกกล่าวว่าความรอบรู้ด้านสุขภาพเป็นตัวกำหนดแรงจูงใจและความสามารถของบุคคลในการเข้าถึง เข้าใจและใช้ข้อมูลสารสนเทศในการเสริมสร้างและการคงไว้ซึ่งสุขภาพดี [4] และนำไปสู่การมีพฤติกรรมสุขภาพที่ดี อีกทั้งแสดงถึงผลลัพธ์ของการสร้างเสริมสุขภาพทำให้ประชาชนมีศักยภาพในการดูแลสุขภาพตนเอง [5]

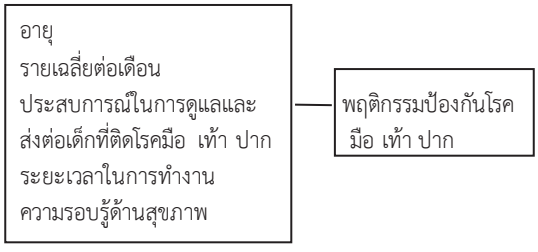
จังหวัดภูเก็ตมีรายงานจำนวนผู้ป่วยโรคมือเท้าปาก 3 ปีย้อนหลังระหว่างปี พ.ศ. 2564- 2566 พบว่าอำเภอเมืองพบผู้ป่วยสูงสุด โดยมีอัตราป่วย 36.59 169.56 และ 98.57 ต่อประชากรแสนคนตามลำดับ [6] ดังนั้น การที่จะพัฒนาครูผู้ดูแลเด็กให้สามารถดูแลเด็กได้บรรลุเป้าหมาย จึงจำเป็นที่จะต้องทราบว่าครูผู้ดูแลเด็กมีความรอบรู้ด้านสุขภาพและพฤติกรรมป้องกันโรคมือเท้าปากอย่างไร ดังนั้น คณะผู้วิจัยจึงสนใจศึกษาความรอบรู้ด้านสุขภาพและพฤติกรรมการป้องกันโรคมือเท้าปากในครูผู้ดูแลเด็กของศูนย์พัฒนาเด็กเล็กในเขตอำเภอเมือง จังหวัดภูเก็ต

วัตถุประสงค์

1. เพื่อศึกษาความรอบรู้ด้านสุขภาพและพฤติกรรมการป้องกันโรคของครูผู้ดูแลเด็กของศูนย์พัฒนาเด็กเล็ก อำเภอเมือง จังหวัดภูเก็ต
2. เพื่อศึกษาความสัมพันธ์ระหว่างอายุ รายได้ ประสบการณ์ในการดูแลและส่งต่อเด็กที่ติดโรคมือ เท้า ปาก ระยะเวลาในการทำงานดูแลเด็กในศูนย์เด็กเล็ก ความรอบรู้ด้านสุขภาพและพฤติกรรมป้องกันโรคมือเท้าปากของครูผู้ดูแลเด็กของศูนย์พัฒนาเด็กเล็ก อำเภอเมือง จังหวัดภูเก็ต

กรอบแนวคิดงานวิจัย

การศึกษาอาศัยความรอบรู้ด้านสุขภาพของกองสุขศึกษา [7] และพฤติกรรมการป้องกันโรคของโรเซนสต็อก [8] โดยความรอบรู้ด้านสุขภาพเป็นความสามารถของครูผู้ดูแลเด็กในการเข้าถึงข้อมูลสุขภาพ ในการตัดสินใจ และการใช้ข้อมูลข่าวสารเพื่อนำไปสู่การตัดสินใจมี 6องค์ประกอบตามแนวคิดของกองสุขศึกษา ประกอบด้วย 1) ด้านการเข้าถึงข้อมูล สุขภาพและบริการสุขภาพ 2) ด้านความรู้ ความเข้าใจ 3) ด้านทักษะการสื่อสาร 4) ด้านการรู้เท่าทันสื่อ 5) ด้านทักษะการตัดสินใจ และ 6) ด้านการจัดการตนเอง ส่วนพฤติกรรมการป้องกันโรค การปฏิบัติการป้องกันและควบคุมโรคประกอบด้วย 1) การรับรู้ความรุนแรงของโรค 2) การรับรู้ต่อโอกาสเสี่ยงต่อการเป็นโรค 3) ความคาดหวังในประสิทธิผลของการตอบสนอง 4) การประเมินอันตรายต่อสุขภาพ และ 5) การประเมินการเผชิญปัญหา [8] ในการศึกษาครั้งนี้ ประกอบด้วยตัวแปร ดังนี้ อายุ รายได้เฉลี่ยต่อเดือน ประสบการณ์ในการดูแลและส่งต่อเด็กที่ติดโรคมือ เท้า ปาก ระยะเวลาในการทำงานดูแลเด็กในศูนย์เด็กเล็ก ความรอบรู้ด้านสุขภาพและพฤติกรรมป้องกันโรคมือเท้าปากของครูผู้ดูแลเด็กของศูนย์พัฒนาเด็กเล็ก ดังภาพ 1



ภาพ 1 กรอบแนวคิดในการวิจัย

II ทบทวนวรรณกรรม

จากการทบทวนวรรณกรรมเกี่ยวข้องในประเด็น ความรู้และพฤติกรรมการป้องกันโรคมือ เท้า ปาก ของผู้ดูแลเด็กก่อนวัยเรียน ศูนย์พัฒนาเด็กเล็ก องค์การบริหารส่วนตำบลจัน พบว่ากลุ่มผู้ดูแลเด็กก่อนวัยเรียนมีระดับความรู้เรื่องโรคมือ เท้า ปาก อยู่ในระดับสูง เนื่องมาจากกลุ่มผู้ดูแลเด็กก่อนวัยเรียนส่วนใหญ่ให้ความสำคัญและมีความตระหนักในการป้องกันโรคมือ เท้า ปาก รวมทั้งมีโอกาสได้รับข้อมูลข่าวสารในการป้องกันโรคจากสื่อต่าง ๆ หรือได้รับความรู้จากเจ้าหน้าที่ทางสาธารณสุข จึงทำให้มีความรู้ในเรื่องโรคมือ เท้า ปาก แต่อย่างไรก็ตามยังพบว่ากลุ่มผู้ดูแลเด็กก่อนวัยเรียนที่มีระดับความรู้เรื่องโรคมือเท้า ปาก อยู่ในระดับปานกลางถึง ร้อยละ 40.00 พฤติกรรมการป้องกันควบคุมโรคมือ เท้า ปาก ในภาพรวมมีค่าคะแนนอยู่ในระดับดี ($\bar{x}$== 2.79, SD = 0.87) ผู้ดูแลเด็กเป็นอีกกลุ่มบุคคลที่มีความสำคัญในการป้องกันและควบคุมโรค มือ เท้า ปาก โดยเฉพาะในกลุ่มเด็กก่อนวัยเรียนซึ่งเป็นกลุ่มที่มีภูมิคุ้มกันต่ำ และมีโอกาสติดโรคนี้ได้ง่าย หากผู้ดูแลเด็กมีความรู้ที่ถูกต้อง มีความเข้าใจ และความตระหนักในการป้องกันโรค และมีพฤติกรรมการป้องกันโรคมือ เท้า ปาก ที่ดีและถูกต้องย่อมส่งผลดีต่อการควบคุมและป้องกันการแพร่ระบาดของโรคนี้ได้ดีมากยิ่งขึ้น [9] และการศึกษาปัจจัยที่มีความสัมพันธ์กับพฤติกรรมการป้องกันและควบคุมโรคมือเท้าปากของครูในโรงเรียนอนุบาลและศูนย์พัฒนาเด็กเล็กจังหวัดสุราษฎร์ธานี พบว่า ระดับการศึกษา ตำแหน่ง ความรู้เรื่องโรคมือ เท้า ปาก การรับรู้ความเสี่ยงโรคมือ เท้า ปาก ทัศนคติในการป้องกันโรคมือ เท้า ปาก และการรับรู้ประโยชน์ การป้องกันโรคมือ เท้า ปาก มีความสัมพันธ์กับพฤติกรรมการป้องกัน และควบคุมโรคมือ เท้า ปาก เนื่องจากครูและผู้ดูแลในโรงเรียนอนุบาลและศูนย์พัฒนาเด็กเล็กในจังหวัดสุ ราษฎร์ธานีส่วนใหญ่เห็นความสำคัญและรับรู้ความเสี่ยงของโรคมือ เท้าปาก มีความรู้และทัศนคติการป้องกันโรคมือ เท้า ปาก และการรับรู้ประโยชน์การป้องกันโรคมือ เท้าปาก เนื่องจากการมีประสบการณ์โดยตรงจากการที่มีนักเรียนของศูนย์พัฒนาเด็กเล็กเป็นโรคมือ เท้า ปาก การได้รับคำแนะนำในการปฏิบัติตัวเพื่อป้องกันโรคมือเท้าปากจากบุคคลที่เกี่ยวข้อง ไม่ว่าจะเป็นหน่วยงานที่เกี่ยวข้อง เจ้าหน้าที่สาธารณสุขหรือจากครู และผู้ดูแลด้วยกันเองส่งผลให้ครูและผู้ดูแลเด็กเกิดความรู้และทักษะในการปฏิบัติพฤติกรรมการป้องกันโรคมือ เท้า ปาก ได้อย่างถูกต้องเหมาะสม และสามารถถ่ายทอดไปยังเด็กและผู้ปกครองเพื่อป้องกันและเฝ้าระวังไม่ให้เกิดโรคมือเท้าปากได้ [10] ในขณะที่การศึกษปัจจัยทำนายพฤติกรรมการป้องกันโรคมือเท้าปากของผู้ปกครองและผู้ดูแลเด็กในศูนย์พัฒนาเด็กเล็ก อำเภอเชียงคำ จังหวัดพะเยา พบว่ากลุ่มตัวอย่าง (n=330) มีพฤติกรรมการป้องกันโรคมือเท้าปากระดับสูง อายุมีความสัมพันธ์ทางบวกกับพฤติกรรมการป้องกันโรคมือเท้าปากของผู้ปกครองและผู้ดูแลเด็ก โดยพบว่า เด็กที่มีอายุน้อยกว่า 2 ปี จะมีโอกาสเป็นโรคมือเท้าปากเป็น 6.35 เท่า เมื่อเทียบกับเด็กที่มีอายุมากกว่า 5 ปี (95% CI = 1.37–29.38) รายได้ต่อเดือน มีความสัมพันธ์ทางบวกกับพฤติกรรมการป้องกันโรคมือเท้าปากของผู้ปกครองและผู้ดูแลเด็กในศูนย์พัฒนาเด็กเล็กอย่างมีนัยสำคัญทางสถิติ ทัศนคติต่อโรคมือเท้าปากมีความสัมพันธ์ทางลบกับพฤติกรรมการป้องกันโรคมือเท้าปากของผู้ปกครองและผู้ดูแลเด็กในศูนย์พัฒนาเด็กเล็กอย่างมีนัยสำคัญทางสถิติ ปัจจัยเอื้อ มีอิทธิพลและสามารถทำนายพฤติกรรมการป้องกันโรค มือเท้าปากของผู้ปกครองและผู้ดูแลเด็ก จากการทดสอบสมมติฐาน พบว่า ปัจจัยนำ ปัจจัยเอื้อและปัจจัยเสริมสามารถร่วมทำนายพฤติกรรมการป้องกันโรคมือเท้าปากของ

ผู้ปกครองและผู้ดูแลเด็ก ตัวแปรที่มีความสัมพันธ์กับพฤติกรรมการป้องกันโรคมือเท้าปาก ได้แก่ อายุ รายได้ และทัศนคติต่อการป้องกันโรคมือเท้าปาก สามารถร่วมกันอธิบายพฤติกรรมการป้องกันโรคมือเท้าปากของผู้ปกครองและผู้ดูแลเด็กในศูนย์พัฒนาเด็กเล็กได้อย่างถูกต้อง ร้อยละ 4.5 (Adjusted R^2= 0.045, p-value <0.001) [11]

III ระเบียบวิธีวิจัย

การวิจัยในครั้งนี้เป็นการศึกษาวิจัยเชิงบรรยาย (Descriptive research) ประชากรที่ใช้ในการศึกษาครั้งนี้ คือ ครูผู้ดูแลเด็กก่อนวัยเรียนในศูนย์พัฒนาเด็กเล็ก อำเภอเมือง จังหวัดภูเก็ต จำนวนทั้งหมด 117 คน จาก 15 ศูนย์ ในอำเภอเมืองจังหวัดภูเก็ต กลุ่มตัวอย่างในการศึกษาครั้งนี้จึงใช้ประชากรทั้งหมดเป็นกลุ่มตัวอย่าง โดยมีครูผู้ดูแลเด็กปฏิเสธการเข้าร่วมวิจัย จำนวน 15 ราย คงเหลือกลุ่มตัวอย่างจำนวน 102 ราย โดยกำหนดเกณฑ์การคัดเข้า ดังนี้

1. อายุมากกว่า 18 ปีขึ้นไป
2. สามารถอ่านเขียน สื่อสารเป็นภาษาไทยได้ด้วยตนเอง และเป็นผู้ที่มีสติสัมปชัญญะครบถ้วน
3. มีประสบการณ์เป็นครูผู้ดูแลเด็กเล็กระยะเวลาตั้งแต่ 1 ปีขึ้นไป
4. ยินดีเข้าร่วมในการวิจัย

เครื่องมือในการวิจัย

เครื่องมือที่ใช้ในการเก็บข้อมูลในการวิจัยครั้งนี้แบ่งออกเป็น 3 ตอน ดังนี้

ตอนที่ 1 แบบสอบถามเกี่ยวกับข้อมูลทั่วไปประกอบด้วย เพศ อายุ ระดับการศึกษา สถานภาพสมรส รายได้ จำนวนเด็กที่ดูแลในศูนย์พัฒนาเด็กเล็ก และประสบการณ์การพบเจอเด็กติดโรคมือ เท้า ปาก จำนวน 8 ข้อ

ตอนที่ 2 แบบสอบถามเกี่ยวกับความรอบรู้ด้านสุขภาพที่เกี่ยวกับโรคมือเท้าปากสร้างโดยอาศัยแนวคิดของกองสุขศึกษา [7] ประกอบด้วยการเข้าถึงข้อมูลสุขภาพและบริการสุขภาพ ความรู้ ความเข้าใจ ทักษะการสื่อสาร การรู้เท่าทันสื่อ การตัดสินใจ การจัดการตนเอง โดยเป็นแบบสอบถามเป็นแบบมาตราส่วนประมาณค่า จำนวน 24 ข้อ แบ่งเป็น 5 ระดับ ดังนี้

มีความรอบรู้ด้านสุขภาพมากที่สุด	ให้คะแนน	5
มีความรอบรู้ด้านสุขภาพมาก	ให้คะแนน	4
มีความรอบรู้ด้านสุขภาพปานกลาง	ให้คะแนน	3
มีความรอบรู้ด้านสุขภาพน้อย	ให้คะแนน	2
มีความรอบรู้ด้านสุขภาพน้อยที่สุด	ให้คะแนน	1

สำหรับเกณฑ์ในการแปลผลความรอบรู้ด้านสุขภาพที่เกี่ยวข้องกับโรคมือเท้าปากของผู้ดูแลเด็กเล็กทั้ง 6 ด้าน แบ่งเป็น 3 ระดับดังต่อไปนี้

คะแนนเฉลี่ย 3.67 – 5.00 หมายถึง ความรอบรู้ด้านสุขภาพอยู่ในระดับสูง

คะแนนเฉลี่ย 2.34 – 3.66 หมายถึง ความรอบรู้ด้านสุขภาพอยู่ในระดับปานกลาง

คะแนนเฉลี่ย 1.00 – 2.33 หมายถึง ความรอบรู้ด้านสุขภาพอยู่ในระดับน้อย

ตอนที่ 3 แบบสอบถามเกี่ยวกับพฤติกรรมการป้องกันโรคมือเท้าปาก สร้างขึ้นโดยอาศัยแนวคิดของกองสุขศึกษา (2561) แบบสอบถามเป็นแบบประมาณค่า จำนวน 10 ข้อ แต่ละข้อมีคะแนน 1- 5 ดังนี้

5 คะแนน ปฏิบัติทุกครั้ง 6-7 ครั้งต่อสัปดาห์
4 คะแนน ปฏิบัติเกือบทุกครั้ง 4-5 ครั้งต่อสัปดาห์
3 คะแนน ปฏิบัติบางครั้ง 2-3 ครั้งต่อสัปดาห์
2 คะแนน ปฏิบัติน้อยครั้ง 1 ครั้งต่อสัปดาห์
1 คะแนน ไม่เคยปฏิบัติเลย

สำหรับเกณฑ์ในการจำแนกพฤติกรรมการป้องกันโรคมือเท้าปากในผู้ดูแลเด็กเล็ก แบ่งเป็น 3 ระดับตามเกณฑ์ ดังต่อไปนี้

คะแนนเฉลี่ย 3.67 – 5.00 หมายถึง พฤติกรรมการป้องกันโรคอยู่ในระดับสูง

คะแนนเฉลี่ย 2.34 – 3.66 หมายถึง พฤติกรรมการป้องกันโรคอยู่ในระดับปานกลาง

คะแนนเฉลี่ย 1.00 – 2.33 หมายถึง พฤติกรรมการป้องกันโรคอยู่ในระดับน้อย

คุณภาพของเครื่องมือ

เครื่องมือผ่านการตรวจความเที่ยงตรงเชิงเนื้อหาจากผู้ทรงคุณวุฒิ 3 ท่าน มีค่า IOC ระหว่าง 0.67 ถึง 1.00 และตรวจความความเชื่อมั่นของเครื่องมือโดยทดลองใช้กับกลุ่มที่มีลักษณะเหมือนกับกลุ่มตัวอย่าง ได้แก่ ครูผู้ดูแลเด็กเล็กในพื้นที่อำเภอถลาง จำนวน 30 คน แบบสอบถามความรอบรู้ด้านสุขภาพและแบบสอบถามพฤติกรรมการป้องกันโรคมือเท้าปากมีค่าสัมประสิทธิ์แอลฟ่าครอนบาค (Cronbach' Alpha Coefficient) เท่ากับ 0.95 และ 0.85 ตามลำดับ

การเก็บรวบรวมข้อมูล

1. ขออนุญาตเก็บข้อมูลจากศูนย์พัฒนาเด็กเล็กทั้ง 15 แห่ง
2. ผู้วิจัยชี้แจงวัตถุประสงค์ของการศึกษา ขั้นตอนการเก็บข้อมูล การตรวจสอบความถูกต้องของแบบสอบถาม และตรวจสอบผู้ร่วมวิจัยในการใช้แบบสอบถามเพื่อให้มีความเข้าใจตรงกัน และได้คำตอบที่ตรงกันกับผู้วิจัย และขอความร่วมมือในการเก็บรวบรวมข้อมูล

การวิเคราะห์ข้อมูล

คณะผู้วิจัยการวิเคราะห์ข้อมูลด้วยโปรแกรมคอมพิวเตอร์สำเร็จรูป ดังนี้

1. เพศ อายุ ระดับการศึกษา ประสบการณ์ดูแลเด็กที่ป่วยเป็นโรคมือเท้าปาก ระดับการศึกษา นำเสนอด้วย จำนวน ร้อยละ
2. รายได้ อายุ ระยะเวลาที่ประกอบอาชีพครูผู้ดูแลเด็ก และจำนวนเด็กในศูนย์พัฒนาเด็กเล็ก นำเสนอด้วย จำนวน ร้อยละ ส่วนเบี่ยงเบนมาตรฐาน ค่าเฉลี่ย ค่าสูงสุด และค่าต่ำสุด
3. ความรอบรู้ด้านสุภาพและพฤติกรรมการป้องกันโรคมือเท้าปาก นำเสนอด้วยค่าเฉลี่ยและส่วนเบี่ยงเบนมาตรฐาน
4. วิเคราะห์ความสัมพันธ์ระหว่างอายุ รายได้ ประสบการณ์ในการดูแลและส่งต่อเด็กที่ติดโรคมือ เท้า ปาก ระยะเวลาในการดูแลเด็กในศูนย์เด็กเล็ก ความรอบรู้ด้านสุขภาพและ พฤติกรรมป้องกันโรคมือเท้าปากของผู้ดูแลเด็กของศูนย์พัฒนาเด็กเล็กด้วยค่าสัมประสิทธิ์สหสัมพันธ์ของเพียร์สัน

IV ผลการวิจัย

จากผลการศึกษาพบว่า ครูผู้ดูแลเด็กเล็กส่วนใหญ่เป็นเพศหญิงร้อยละ 99.00 ส่วนใหญ่ส่วนใหญ่อายุ 40 ปีขึ้นไปร้อยละ 41.18 โดยมีอายุเฉลี่ย 37.46 ปี (S.D. = 9.721) สถานภาพของครูผู้ดูแลเด็กส่วนใหญ่ โสด จำนวน 52 คน คิดเป็นร้อยละ 50.98 ส่วนใหญ่สำเร็จการศึกษาระดับปริญญาตรีหรือเทียบเท่าร้อยละ 83.33 รายได้เฉลี่ยต่อเดือนของครูผู้ดูแลเด็กเล็กเฉลี่ย 16,617.75 บาท (S.D. = 7,739.98) กลุ่มตัวอย่างมีประสบการณ์ในการดูแลและส่งต่อเด็กที่ติดโรคมือเท้าปากร้อยละ 85.29 มีส่วนใหญ่มีประสบการณ์ในการดูแลเด็กเล็กน้อยกว่า 5 ปี และ 6 – 15 ปี เท่ากันกลุ่มละ จำนวน 44 คน มีเด็กเล็กในความดูแลจำนวน 21 – 25 คน ร้อยละ 38.24 ดังตารางที่ 1

ตารางที่ 1 จำนวน ร้อยละ ของข้อมูลส่วนบุคคลของกลุ่มตัวอย่าง (n=102)

ข้อมูลส่วนบุคคล	กลุ่มตัวอย่าง	
	จำนวน (คน)	ร้อยละ
1. เพศ		
ชาย	1	1.00
หญิง	101	99.00
2. อายุ		
18-23 ปี	8	7.84
24-28 ปี	13	12.74
29-33 ปี	20	19.61
34-39 ปี	19	18.63
40 ปีขึ้นไป	42	41.18

($\bar{X}$ = 37.46, S.D. = 9.721, Min = 22, Max = 56)		
3. สถานภาพ		
โสด	52	50.98
สมรส	42	41.18
หม้าย	1	0.98
หย่าร้าง	5	4.90
แยกกันอยู่	2	1.96
4. ระดับการศึกษา		
ประถมศึกษา	0	0.00
มัธยมศึกษาตอนต้นหรือเทียบเท่า	2	1.96
มัธยมศึกษาตอนปลายหรือเทียบเท่า	7	6.86
ปริญญาตรีหรือเทียบเท่า	85	83.33
สูงกว่าปริญญาตรี	5	4.90
อื่นๆ (โปรดระบุ)	3	2.94
5. รายได้เฉลี่ยต่อเดือน		
น้อยกว่า 10,000	33	32.35
10,001 – 20,001	49	48.04
20,002 – 30,002	14	13.73
30,003 – 40,003	5	4.90
40,004 บาทขึ้นไป	1	0.98
($\bar{X}$ = 16,617.75, S.D. = 7,739.98, Min = 9,500, Max = 48,000)		
6. ท่านเคยมีประสบการณ์ในการดูแลและส่งต่อเด็กที่ติดโรคมือเท้าปาก		
มี	87	85.29
ไม่มี	15	14.71
7. ท่านมีประสบการณ์การดูแลเด็กในศูนย์พัฒนาเด็กเล็กเป็นระยะเวลากี่ปี		
น้อยกว่า 5 ปี	44	43.14
6 - 15	44	43.14
16 – 25	9	8.82
มากกว่า 26 ปี	5	4.90
($\bar{X}$ = 8.54, S.D. = 7.16, Min = 1, Max = 34)		
8. ปัจจุบันท่านดูแลเด็กในศูนย์พัฒนาเด็กเล็กจำนวนกี่คน		
น้อยกว่า 15 คน	16	15.69
16 - 20	29	28.43
21 - 25	39	38.24
26 คนขึ้นไป	18	17.65
($\bar{X}$ = 21.71, S.D. = 4.86, Min = 11, Max = 30)		

จากการศึกษาความรอบรู้ด้านสุขภาพของครูผู้ดูแลเด็กเล็ก พบว่า อยู่ในระดับสูงทั้งรายด้านและโดยรวม ดังตารางที่ 2 และพฤติกรรมการป้องกันโรคพบว่าอยู่ในระดับสูงทั้งรายด้านและภาพรวมเช่นกันดังตารางที่ 3

ตารางที่ 2 ค่าเฉลี่ยและค่าเบี่ยงเบนมาตรฐานความรอบรู้ของครูผู้ดูแลเด็กเล็ก (n = 102)

ความรอบรู้ด้านสุขภาพ	$\bar{X}$	S.D.	แปลผล
ด้านการเข้าถึงข้อมูลและบริการสุขภาพ	4.44	0.51	สูง
ด้านความรู้ ความเข้าใจ	4.40	0.52	สูง
ด้านทักษะการสื่อสาร	4.34	0.56	สูง
ด้านการรู้เท่าทันสื่อ	4.27	0.55	สูง
ด้านการตัดสินใจ	4.42	0.59	สูง
ด้านการจัดการตนเอง	4.39	0.59	สูง
ภาพรวม	4.41	0.47	สูง

ตารางที่ 3 ค่าเฉลี่ยและค่าเบี่ยงเบนมาตรฐานพฤติกรรมการป้องกันโรคมือเท้าปากของครูผู้ดูแลเด็กเล็ก (n = 102)

พฤติกรรมการป้องกันโรคมือเท้าปาก	$\bar{X}$	S.D.	แปลผล
1. ท่านดูแลรักษาสิ่งแวดล้อมภายในศูนย์พัฒนาเด็กเล็กและบริเวณรอบศูนย์พัฒนาเด็กเล็กสะอาดอยู่เสมอ	4.56	0.59	สูง
2. ท่านทำความสะอาดของเล่นเด็กด้วยน้ำผสมคลอรีน น้ำยาไฮเตอร์และน้ำยาฆ่าเชื้ออื่นๆเป็นประจำ	4.57	0.57	สูง
3. ท่านทำความสะอาดห้องเรียนด้วยน้ำยาฆ่าเชื้อหลังพบเด็กเล็กป่วยด้วยโรคมือ เท้า ปาก	4.68	0.55	สูง
4. ท่านล้างมือด้วยสบู่เป็นประจำหลังทำกิจกรรมต่าง ๆ	4.62	0.55	สูง
5.ท่านให้เด็กปิดปาก ปิดจมูก ขณะไอจาม	4.48	0.63	สูง
6. หากท่านพบเจอเด็กไม่สบาย ท่านสามารถดูแลเด็กเบื้องต้น เช่นเช็ดตัว ลดไข้ โทรแจ้งผู้ปกครองมารับไปพบแพทย์	4.66	0.54	สูง
7. หากทราบว่าเด็กมีอาการป่วยเป็นโรคมือเท้าปาก ท่านจะให้เด็กหยุดเรียน เพื่อป้องกันการติดเชื้อ	4.71	0.52	สูง
8. ท่านทิ้งกระดาษหรือผ้าที่ใช้เช็ดน้ำมูก น้ำลายของเด็กที่ป่วยลงในถังขยะที่มีฝาปิดมิดชิด	4.66	0.54	สูง
9. ท่านให้เด็กแยกใช้สิ่งของส่วนตัว เช่น แก้วน้ำ ช้อน จาน ขวดนม ร่วมกับผู้อื่น	4.71	0.52	สูง
ภาพรวม	4.63	0.55	สูง

เมื่อทำการวิเคราะห์ความสัมพันธ์ พบว่า รายได้ ระยะเวลาในการดูแลเด็กในศูนย์เด็กเล็กมีความสัมพันธ์กับ ความรอบรู้ด้านสุขภาพอย่างมีนัยสำคัญทางสถิติที่ระดับ .01 ในขณะที่ประสบการณ์ในการดูแลและส่งต่อเด็กที่ติดโรคมือ เท้า ปาก มีความสัมพันธ์กับความรอบรู้ด้านสุขภาพอย่างมีนัยสำคัญทางสถิติที่ระดับ .05 และผลจากการศึกษายังพบว่าความรอบรู้ด้านสุขภาพเป็นตัวแปรเดียวที่มีความสัมพันธ์กับพฤติกรรมการป้องกันโรคมือ เท้า ปากอย่างมีนัยสำคัญที่ระดับ 0.01 (r=.520, p< .01) ดังตารางที่ 4

ตารางที่ 4 ความสัมพันธ์ระหว่างอายุ รายได้ ประสบการณ์ในการดูแลและส่งต่อเด็กที่ติดโรคมือ เท้า ปาก ระยะเวลาในการทำงานดูแลเด็กในศูนย์เด็กเล็ก ความรอบรู้ด้านสุขภาพและพฤติกรรมป้องกันโรคมือเท้าปาก (n = 102)

ตัวแปร	1	2	3	4	5	6
1. อายุ	1.00					
2. รายได้	.493**	1.00				
3. ประสบการณ์ในการดูแลและส่งต่อเด็ก	.323**	.190	1.00			
4. ระยะเวลาในการดูแลเด็ก	.724**	.599**	.249*	1.00		
5. ความรอบรู้ด้านสุขภาพ	.106	.299**	.197*	.284**	1.00	
6. พฤติกรรมป้องกันโรคมือเท้าปาก	.097	.161	.163	.157	.520**	1.00

*p<.05, ** p< .01

V อภิปราย

กลุ่มตัวอย่างส่วนใหญ่เป็นเพศหญิง ร้อยละ 99.00 อายุเฉลี่ย 37.46 ปี (SD=9.72) ส่วนใหญ่มีการศึกษาระดับปริญญาตรีหรือเทียบเท่า ร้อยละ 83.33 ระยะการทำงานในศูนย์พัฒนาเด็กเล็ก 6 – 15 ปี ร้อยละ 43.14 ดังการศึกษาที่ผ่านมา [11,12]

ความรอบรู้ด้านสุขภาพ ผลการศึกษา พบว่า ครูผู้ดูแลเด็กมีความรอบรู้ด้านสุขภาพเกี่ยวกับโรคมือ เท้า ปากทั้งในภาพรวมและรายได้ในระดับสูง โดยด้านการเข้าถึงข้อมูลมีค่าเฉลี่ยสูงสุด ($\bar{x}$ =4.44, S.D. = 0.51) รองลงมาคือ ด้านการตัดสินใจ ($\bar{x}$ = 4.42, S.D. = 0.59) อาจเนื่องจากกลุ่มตัวอย่างส่วนใหญ่ (ร้อยละ 85.29) มีประสบการณ์ในการดูแลเด็กที่ป่วยด้วยโรคมือ เท้าปากมาก่อน จึงมีโอกาสในการเข้าถึงข้อมูลได้ดี อีกทั้งส่วนใหญ่กลุ่มตัวอย่างสำเร็จการศึกษาระดับปริญญาตรี จึงสามารถเข้าถึงและทราบแหล่งสืบค้นเกี่ยวกับโรคมือเท้าปากจากแหล่งข้อมูลสุขภาพได้โดยตรงทั้งจากแหล่งข้อมูลต่าง ๆ และจากบุคลากรสาธารณสุข [9,13] ส่งผลให้กลุ่มตัวอย่างมีความรู้ความ เข้าใจอยู่ในระดับสูง โดยการศึกษาครั้งนี้พบว่ากลุ่มตัวอย่าง

ร้อยละ 49.02 ทราบถึงอาการเบื้องต้นของเด็กที่มีอาการเป็นโรคมือเท้าปาก อยู่ในระดับสูง ทั้งนี้เนื่องจากเมื่อกลุ่มตัวอย่างมีความรู้โรคมือเท้าปาก ระดับสูง ทำให้เกิดความตะหนักในการป้องกันโรค [9] สำหรับด้านทักษะการสื่อสารเมื่อพิจารณารายข้อพบว่าครูผู้ดูแลเด็กเล็กสามารถเผยแพร่ความรู้และการป้องกันโรคมือเท้าปากให้แก่ผู้ปกครองได้อยู่ในระดับสูงร้อยละ 46.08 ดังการศึกษาที่ผ่านมาพบว่าครูผู้ดูแลเด็กในศูนย์เด็กเล็กมีทักษะในการดูแลเด็กและมีความสามารถในการถ่ายทอดวิธีการดูแลแก่ผู้ปกครอง [1] การสื่อสารในงานดูแลเด็กของครูผู้ดูแลเด็กมีผลต่อพัฒนาการและสุขภาพของเด็กอย่างมาก การมีทักษะเหล่านี้จึงเป็นสิ่งสำคัญที่ควรได้รับการสนับสนุนและพัฒนาอย่างต่อเนื่อง เพื่อให้ครูผู้ดูแลเด็กสามารถให้การดูแลที่ดีที่สุดแก่เด็ก และสร้างความสัมพันธ์ที่ดีกับผู้ปกครองได้อย่างมีประสิทธิภาพในการดูแลเด็ก [14]

การรู้เท่าทันสื่อของครูผู้ดูแลพบว่า ครูผู้ดูแลเด็กสามารถซักถามเกี่ยวกับป้องกันโรคมือเท้าปากกับผู้ให้บริการสุขภาพเพื่อนำมาป้องกันโรคให้กับเด็กในศูนย์พัฒนาเด็กเล็กได้อยู่ในระดับสูง ร้อยละ 35.29 เนื่องจากการที่ครูสามารถซักถามและรับข้อมูลที่ถูกต้องจากผู้ให้บริการสุขภาพจะมีผลอย่างมากต่อการป้องกันโรคและการดูแลสุขภาพของเด็กในศูนย์พัฒนาเด็ก การมีข้อมูลที่ทันสมัยและถูกต้องช่วยให้ครูสามารถดำเนินการป้องกันและดูแลเด็กได้อย่างมีประสิทธิภาพ ส่งเสริมความมั่นใจให้กับผู้ปกครองในเรื่องการดูแลสุขภาพของบุตรหลาน

การตัดสินใจของครูผู้ดูแลเด็กพบว่า ครูผู้แลเด็กตัดสินใจให้เด็กที่ติดโรคมือเท้าปากควรหยุดเรียนและพักรักษาตัวให้หายป่วยก่อนกลับเข้ามาเรียนอยู่ในระดับสูงร้อยละ 45.10 เนื่องจากการตัดสินใจให้เด็กหยุดเรียนและพักรักษาตัวจนกว่าจะหายป่วยเป็นการให้เด็กพักรักษาตัวไม่เพียงแต่ช่วยให้เด็กฟื้นตัวได้เร็วขึ้น แต่ยังป้องกันการแพร่กระจายของโรคไปยังเด็กคนอื่น ๆ ในสถานศึกษา นอกจากนี้ การตัดสินใจแสดงให้เห็นถึงความรับผิดชอบของครูในการดูแลสุขภาพและความปลอดภัยของเด็ก รวมถึงการสร้างความเชื่อมั่นให้กับผู้ปกครองในการดูแลที่มีคุณภาพในสถานศึกษา [15]

การจัดการตนเองของครูผู้ดูแลเด็ก พบว่า ครูผู้ดูแลเด็กมีการปฏิบัติตามแผนของกระทรวงสาธารณสุขในการเฝ้าระวัง ป้องกันและควบคุมโรคติดต่อหรือโรคระบาดได้ในระดับสูง ร้อยละ 49.02 รองลงมาคือ การปรับตัวตั้งรับกับการเกิดโรค มือเท้าปากในศูนย์พัฒนาเด็กเล็กอยู่เสมออยู่ในระดับสูง ร้อยละ 47.06 เนื่องจากครูผู้ดูแลเด็กเล็กมีประสบการณ์ในการดูแลและส่งต่อเด็กที่ติดโรคมือเท้าปาก จึงมีทัศนคติที่ดีต่อการตั้งรับกับโรค และจัดการกับโรคมือ เท้า ปาก [16]

พฤติกรรมการป้องกันโรคมือเท้าปากของครูผู้ดูแลเด็กพบว่า กลุ่มตัวอย่างมีพฤติกรรมการป้องกันโรคมือเท้าปากอยู่ในระดับสูงทั้งรายข้อและภาพรวม ทั้งนี้อาจเนื่องจากกลุ่มตัวอย่างส่วนใหญ่มีการศึกษาระดับปริญญาตรี มีประสบการณ์ในการดูแลและส่งต่อเด็กที่ติดโรคมือเท้าปาก อีกทั้งนี้ความรอบรู้ด้านสุขภาพทั้งภาพรวมและรายด้านอยู่ในระดับสูง จึงส่งผลให้ครูผู้ดูแลเด็กมีพฤติกรรมการป้องกันโรคมือ เท้า ปากในระดับสูง [17-18]

การวิเคราะห์ความสัมพันธ์ ผลจากการศึกษาพบว่ารายได้ ประสบการณ์ในการดูแลและส่งต่อเด็กที่ติดโรคมือเท้าปาก และระยะเวลาในการเป็นครูผู้ดูแลเด็กมีความสัมพันธ์กับความรอบรู้ด้านสุขภาพ ดังการศึกษาของกันยา โพธิปิติ [19] และคำสงค์ ชินมาตร[20] ที่พบว่ารายได้มีความสัมพันธ์ต่อความรอบรู้ด้านสุขภาพของผู้ดูแลเด็ก ทั้งนี้ประสบการณ์ในการดูแลและส่งต่อเด็กที่ติดโรคมือเท้าปาก และระยะเวลาในการเป็นครูผู้ดูแลเด็กมีความสัมพันธ์กับความรอบรู้ด้านสุขภาพ เนื่องจากความรอบรู้ด้านสุขภาพเปรียบเสมือนสินทรัพย์ ซึ่งจะเพิ่มพูนสะสมตามประสบการณ์เดิมและทักษะที่สั่งสมมา [21] นอกจากนี้ยังพบว่าความรอบรู้ด้านสุขภาพมีความสัมพันธ์กับพฤติกรรมการป้องกันโรคมือ เท้า ปาก เนื่องจากกลุ่มตัวอย่างในการศึกษาครั้งนี้มีระดับความรอบรู้ด้านสุขภาพในระดับสูง จึงส่งให้มีพฤติกรรมการการป้องกันโรคมือเท้าปากในระดับสูง เพราะกลุ่มตัวอย่างสามารถเข้าถึงข้อมูลและบริการสุขภาพ มีความรู้ ความเข้าใจเกี่ยวกับโรคมือเท้า ปาก มีทักษะในการสื่อสาร รู้เท่าทันสื่อ สามารถตัดสินใจในการดูแลเด็กและสามารถจัดการตนเอง นั่นคือ สามารถวางแผนและปฏิบัติตามแนวทางการดูแลเด็กตามที่กรมควบคุมโรคกำหนด ผลการศึกษาเช่นเดียวกับการศึกษาของพิชัย พวงสด อมรศักดิ์ โพธิ์อ่ำและพุฒิพงษ์ มากมาย [22] ที่พบว่าความรอบรู้ด้านสุขภาพมีความสัมพันธ์กับพฤติกรรมการป้องกันโรคไข้เลือดออกของ อสม. นั่นคือ บุคคลที่มีความรอบรู้ด้านสุขภาพจะมีความสามารถในการดูแลสุขภาพของตน [23]

VI ข้อสรุป

จากการศึกษาในครั้งนี้พบว่าหากครูผู้ดูแลเด็กเล็กมีความรอบรู้และพฤติกรรมการป้องกันสุขภาพจากโรคมือ เท้า ปากที่ดี ส่งผลให้การเกิดโรคมือ เท้า ปากน้อยลงและการติดต่อของโรคน้อยลง ดังนั้น หน่วยงานที่ดูแลศูนย์พัฒนาเด็กเล็กจะต้องพัฒนาครูผู้ดูแลเด็กทุกคนให้มีความรอบรู้ด้านสุขภาพ ละมีทักษะในการสื่อสารกับผู้ปกครองและเด็กในการป้องกันตนจากโรคมือ เท้า ปาก

ข้อเสนอแนะ

จากผลการศึกษามีข้อเสนอแนะในการพัฒนางานและประเด็นในการวิจัย ดังนี้

ข้อเสนอแนะเชิงปฏิบัติการ

1. ศูนย์พัฒนาเด็กเล็ก สามารถนำผลที่ได้จากงานวิจัย ไปใช้ในสนับสนุนการดำเนินงานเสริมสร้างความรอบรู้ด้านสุขภาพและพฤติกรรมการป้องกันโรคมือเท้าปากของครูผู้ดูแลเด็กเล็กในพื้นที่ โดยเน้นความรอบรู้ด้านสุขภาพในด้านที่พบว่ามี ความรอบรู้ที่มีการตอบแบบถามน้อยแต่อยู่ในระดับสูง ได้แก่ ด้านการจัดการตนเอง ด้านทักษะการสื่อสาร และด้านการรู้เท่าทันสื่อ ให้กับครูผู้ดูแลเด็กเล็กในศูนย์พัฒนาเด็กเล็ก เพื่อให้เกิดการขับเคลื่อนไปสู่การปฏิบัติอย่างถูกต้องเป็นรูปธรรม

2. ศูนย์พัฒนาเด็กเล็ก สามารถนำผลที่ได้จากงานวิจัยไปออกแบบกระบวนการจัดการเรียนรู้ในการเสริมสร้างความรอบรู้ด้านสุขภาพและพฤติกรรมการป้องกันโรคมือเท้าปากให้กับครูผู้ดูแลเด็กในศูนย์พัฒนาเด็กเล็กที่สอดคล้องกับปัญหาและความต้องการของครูผู้ดูแลเด็กในแต่ละศูนย์พัฒนาเด็กเล็กผ่านกิจกรรมที่มีคุณภาพ และให้การสนับสนุนช่วยเหลือด้านข้อมูลความรู้สู่การปฏิบัติให้มากขึ้น

ข้อเสนอแนะในการศึกษาครั้งต่อไป

1. ควรมีการศึกษาวิจัยเชิงปฏิบัติการเพื่อสร้างความรอบรู้ด้านสุขภาพและพฤติกรรมการป้องกันโรคมือเท้าปากของครูผู้ดูแลเด็กเล็ก โดยใช้ข้อมูลจากผลการศึกษาวิจัยครั้งนี้กับข้อมูลของแต่ละพื้นที่ เพื่อให้สอดคล้องกับปัญหาและความต้องการ

2. ควรมีการศึกษาในเชิงคุณภาพ เพื่อให้ได้ข้อมูลเชิงลึกของความรอบรู้ด้านสุขภาพและพฤติกรรมการป้องกันโรคมือเท้าปากของครูผู้ดูแลเด็กเล็กในศูนย์พัฒนาเด็กเล็ก

3.ควรมีการศึกษาเพิ่มเติมเรื่องความรอบรู้ด้านสุขภาพและพฤติกรรมการป้องกันโรคมือเท้าปากในผู้ปกครองของเด็กเล็ก

คำขอบคุณ

คณะผู้วิจัยขอขอบคุณศูนย์พัฒนาเด็กเล็กและครูผู้ดูแลเด็กทั้ง 15 แห่งในการเอื้ออำนวยความสะดวกในการเก็บรวบรวมข้อมูล

อ้างอิง

[1] กรมควบคุมโรค. (2566). โรคมือ เท้า ปากแนะผู้ปกครอง สถานศึกษา คัดกรองและสังเกตอาการอย่างใกล้ชิด. [อินเตอร์เน็ต]. https://ddc.moph.go.th/odpc6/news.php

[2] วีระยุทธ ปานหล้า. (2561). *พฤติกรรมการป้องกันและควบคุมโรค มือ เท้า ปาก ของผู้ปกครองเด็ก กลุ่มชาติพันธุ์และผู้ดูแลเด็กในศูนย์พัฒนาเด็กเล็ก ตำบลแม่ขะนิง อำเภอเวียงสา จังหวัดน่าน*. การศึกษาค้นคว้าอิสระสาธารณสุขศาสตรมหาบัณฑิต สาขาการจัดการการสร้างเสริมสุขภาพ มหาวิทยาลัยธรรมศาสตร์.

[3] Abel, T., & McQueen, D. (2020). Critical health literacy and the COVID-19 crisis. *Health Promotion International*, 35(6), 1612-1613. retrieved 29 April 2020 from https://doi: 10.1093/heapro/daaa040.

[4] World Health Organization. (1998). *Health promotion glossary. Division of health promotion, education and communications, Health education and health promotion unit*. Geneva: World Health Organization.

[5] Nutbeam, D. (2000). Health literacy as a public health goal: A challenge for contemporary health education and communication strategies into the 21st century. *Health Promotion International*, 15(3), 259-267.

[6] สำนักงานสาธารณสุขจังหวัดภูเก็ต.(2567). จำนวนผู้ป่วยโรคมือ เท้า ปาก . เอกสารอัดสำเนา.

[7] กองสุขศึกษา. (2561). รายงานผลการประเมินความรอบรู้ด้านสุขภาพและพฤติกรรมสุขภาพ [อินเตอร์เน็ต]. https://hed.go.th/wp-content/uploads/2561.pdf

[8] กนกวรรณ นวนเกิด. (2563). *ปัจจัยที่มีผลต่อพฤติกรรมการป้องกันโรคมือเท้าปากของผู้ปกครองเด็ก ในศูนย์พัฒนาเด็กเล็กอำเภอวังทอง จังหวัดพิษณุโลก*. วิทยานิพนธ์ปริญญาสาธารณสุขศาตรบัณฑิต สาขาสาธารณสุขศาสตร์ มหาวิทยาลัยนเรศวร.

[9] ปาริชาติ วงษ์วริศราวิ, วิษณุ ปิ่นคำและวรัญญา หล่อพัฒนเกษม. (2564). ความรู้และพฤติกรรมการป้องกันโรคมือ เท้า ปาก ของผู้ดูแลเด็กก่อนวัยเรียนศูนย์พัฒนาเด็กเล็กองค์การบริหารส่วนตำบลจันอัด จังหวัดนครราชสีมา. *วารสารวิชาการมหาวิทยาลัยราชภัฏภูเก็ต*, 17(2), 61 – 72.

[10] กฤตภิษัช ไม้ทองงาม. (2565). ปัจจัยที่มีความสัมพันธ์กับพฤติกรรมการป้องกันและควบคุมโรคมือเท้าปากของครูในโรงเรียนอนุบาลและศูนย์พัฒนาเด็กเล็ก จังหวัดสุราษฎร์ธานี. *รายงานเฝ้าระวังทางระบาดวิทยาประจำสัปดาห์*, 54(5), 69 – 76.

[11] มัลลิกา อุตตะมา. (2565). ปัจจัยทำนายพฤติกรรมการป้องกันโรคมือเท้าปาก ของผู้ปกครองและผู้ดูแลเด็กในศูนย์พัฒนาเด็กเล็ก อำเภอเชียงคำ จังหวัดพะเยา. การศึกษาค้นคว้าอิสระสาธารณสุขศาสตรมหาบัณฑิต สาขาสาธารณสุขศาสตร์ มหาวิทยาลัยพะเยา

[12] สุพิชญา หอมทอง, ชนัญญา จิระพรกุล และ เนาวรัตน์ ภมณีนิล. (2564). ปัจจัยที่มีความสัมพันธ์กับพฤติกรรมการป้องกันโรคมือ เท้า ปาก ของผู้ปกครอง ในศูนย์พัฒนาเด็กเล็กในเขตตำบลในเมือง อำเภอเมือง จังหวัดขอนแก่น. *วารสารวิจัยสาธารณสุขศาสตร์มหาวิทยาลัยขอนแก่น*, 14(1). 57 – 66.

[13] ธนาคม คำแสน. (2560). *ปัจจัยที่มีความสัมพันธ์กับพฤติกรรมการป้องกันโรคมือเท้าปากของผู้ปกครองเด็กเล็ก ตำบลหาดล้า อำเภอท่าปลา จังหวัดอุตรดิตถ์*. วิทยานิพนธ์ปริญญาสาธารณสุขศาสตรบัณฑิต สาขาวิชาสาธารณสุขศาสตร์ มหาวิทยาลัยนเรศวร.

[14] สถาบันพัฒนาอนามัยเด็กแห่งชาติ. (2562). สรุปรายงานสถานการณ์ความรอบรู้ในการเลี้ยงดูเด็กปฐมวัย. https://nich.anamai.moph.go.th/web-upload/migrated/files/nich/330_article_file.pdf

[15] เปมิกา ไทยชัยภูมิ. (2561). *การศึกษาบทบาทครูในการส่งเสริมพฤติกรรมความปลอดภัยของเด็กอนุบาลในโรงเรียนในสังกัดคณะกรรมการการศึกษาขั้นฐานพื้น*. วิทยานิพนธ์ครุศาสตรมหาบัณฑิต สาขาวิชาการศึกษาปฐมวัย จุฬาลงกรณ์มหาวิทยาลัย.

[16] แสงดาว เกษตรสุนทร, นงเยาว์ เกษตร์ภิบาล, และ จิตตาภรณ์ จิตรีเชื้อ. (2558). ปัจจัยทำนายความตั้งใจในการคัดกรองโรคมือ เท้าและปาก ของครูพี่เลี้ยงของศูนย์พัฒนาเด็กเล็กในภาคใต้. *พยาบาลสาร*, 42(1), 74-85.

[17] รำพึง นุ่มสารพัดนึก. (2565). ความรอบรู้ด้านสุขภาพและพฤติกรรมการป้องกันโรคโควิด 19 ของนักเรียนมัธยมศึกษา จังหวัดนครนายก. *สรรพสิทธิเวชสาร*, 43(3), 91-110.

[18] Kinoshita, S., Hirooka, N., Kusano, T., Saito, K., & Aoyagi. R. (2024). Does health literacy influence health-related lifestyle behaviors among specialists of health management? A cross-sectional study. BMC Primary Care, 25(29),1-9.

[19] กันยา โพธิปิติ. (2565). ความรอบรู้ด้านสุขภาพในการเลี้ยงดูเด็กปฐมวัยของผู้เลี้ยงดูหลักและครูผู้ดูแลเด็ก ในเขตสุขภาพที่ 5. *วารสารศูนย์อนามัยที่ 7 ขอนแก่น*. 15(1). 28 – 50.

[20] คำสงค์ ชินมาตร. (2567). ปัจจัยที่มีความสัมพันธ์กับความรอบรู้ด้านสุขภาพและความสัมพันธ์ระหว่างความรอบรู้ด้านสุขภาพกับภาวะโภชนาการและพัฒนาการเด็กปฐมวัยในผู้เลี้ยงดูเด็ก. *วารสารวิจัยและพัฒนาระบบสุขภาพ*. 17(2). 140 – 153.

[21] วิมลรัตน์ บุญเสถียร และ อรทัย เหรียญทิพยะสกุล. (2563). ความรอบรู้ด้านสุขภาพ: สถานการณ์และผลกระทบต่อสภาวะสุขภาพของผู้สูงอายุ. *วารสารพยาบาลและสุขภาพ สสอท*. 2(1), 1-19.

[22] พิชัย พวงสด, อมรศักดิ์ โพธิ์อ่ำและพุฒิพงษ์ มากมาย. (2563). ความรอบรู้ด้านสุขภาพที่มีความสัมพันธ์กับพฤติกรรมการป้องกันและควบคุมโรคไข้เลือดออกของอาสาสมัครสาธารณสุขประจำหมู่บ้านเขตอำเภอปราสาท จังหวัดสุรินทร์. *วารสารวิทยาศาสตร์และเทคโนโลยีนอร์ทเทิร์น*. 1(3), 1-11.

[23]. ขวัญเมือง แก้วดำเกิง. (2561). *ความรอบรู้ด้านสุขภาพ เข้าถึง เข้าใจ และการนำไปใช้*. นนทบุรี: อัมรินทร์พริ้นติ้ง แอนด์ พลับลิชชิง จำกัด มหาชน.

การเปรียบเทียบชนิดและองค์ประกอบทางกายภาพขยะมูลฝอย จากการย้อมผ้าด้วยเทคนิค Eco Printing

Types and Physical Composition of Solid Waste from Textile Dyeing with Eco-Printing Technique

Suthathong Homya
Faculty of Science and Technology
Phuket Rajabhat University
Phuket, Thailand
suthathong.h@pkru.ac.th

Sukanya Vongtanaboon
Faculty of Science and Technology
Phuket Rajabhat University
Phuket, Thailand
sukanya.v@pkru.ac.th

Phurinat Paladsongkhram
Faculty of Science and Technology
Phuket Rajabhat University
Phuket, Thailand
phurinat.p@pkru.ac.th

Pahol Rongkul
Faculty of Science and Technology
Phuket Rajabhat University
Phuket, Thailand
pahol.r@pkru.ac.th

Siri Jaroenjai
Faculty of Science and Technology
Phuket Rajabhat University
Phuket, Thailand
siri.j@pkru.ac.th

Kanokporn Tangsabpaiboon
Faculty of Science and Technology
Phuket Rajabhat University
Phuket, Thailand
kanokporn.t@pkru.ac.th

***Abstract*—*The Eco Printing dyeing technique, which utilizes natural, environmentally friendly colors to create fabric patterns, is currently gaining significant popularity. This study aims to compare the types and physical composition of waste generated from two Eco Printing techniques: the Basic method and the Blanket method. Waste samples were collected at the source over two days in October 2024, from 8:30 AM to 5:00 PM. The results revealed a total waste generation of 17.90 kg from Eco Printing. Specifically, the Basic Eco Printing method produced 6.65 kg of waste (37.13%), equivalent to 0.74 kg per dyed fabric piece, while the Blanket Eco Printing method generated 11.25 kg of waste (62.87%), equivalent to 0.66 kg per dyed fabric piece. Organic waste constituted the majority of the waste composition in both techniques, attributed to the use of natural materials in the dyeing process. This study highlights differences in waste output between the two methods and underscores the predominance of biodegradable waste in Eco Printing practices.*

Keywords*—*Eco Printing, Solid Waste Management, Eco-friendly, Natural dyes

บทนำ

เครื่องนุ่งห่มเป็นหนึ่งปัจจัยในสี่ที่มีความสำคัญต่อการดำรงชีวิตของมนุษย์ ซึ่งในการผลิตสิ่งทอและเครื่องนุ่งห่มที่ใช้สีสังเคราะห์ในการพิมพ์สิ่งทอนั้นอาจส่งผลเสียต่อผิวหนังของผู้สวมใส่ และไม่เป็นมิตรกับสิ่งแวดล้อม ในปัจจุบันผู้บริโภคมีความตระหนักผลกระทบต่อสิ่งแวดล้อมและการเปลี่ยนแปลงสภาพภูมิอากาศเพิ่มมาก ทำให้สิ่งทอที่ผลิตด้วยสีย้อมธรรมชาติและเป็นมิตรกับสิ่งแวดล้อมมีความต้องการของผู้บริโภคเพิ่มมากขึ้นเช่นกัน [1] ซึ่งการย้อมผ้าด้วยเทคนิค Eco Printing เป็นการสร้างสรรค์ผ้าพิมพ์ลายพืชพรรณธรรมชาติ โดยอาศัยความร้อนจากไอน้ำเป็นตัวกลางช่วยในการสกัดและถ่ายเทสารสีจากพืชให้แพร่กระจายติดเส้นใยผ้า ในการถ่ายโอนสีและการประทับโครงสร้างของวัสดุธรรมชาติลงบนผ้าทอจากเส้นใยธรรมชาติ [2] ซึ่งสามารถทำได้ง่ายโดยใช้วัสดุในท้องถิ่นและมีอุปกรณ์ที่ไม่ยุ่งยากซับซ้อน ทำให้มีการย้อมผ้าและสร้างสรรค์ผลิตภัณฑ์จากผ้าที่ย้อมสีธรรมชาติด้วยเทคนิค Eco Printing เพิ่มขึ้นในพื้นที่ของจังหวัดต่างๆ ของประเทศไทยเพิ่มมากขึ้น จากข้อมูลดังกล่าวทำให้เกิดการพัฒนาการวิจัยนี้ขึ้นโดยวัตถุประสงค์เพื่อเปรียบเทียบชนิดและองค์ประกอบทางกายภาพขยะมูลฝอยจากการย้อมผ้าด้วยเทคนิค Eco Printing เพื่อเพิ่มประสิทธิภาพการใช้ทรัพยากรในท้องถิ่นและลดการเกิดขยะมูลฝอย โดยทำการศึกษาข้อมูลจากดำเนินงานของโครงการศูนย์อัจฉริยะเพื่อการพัฒนาท้องถิ่นภาคใต้ กิจกรรมสร้างแบรนด์ผลิตภัณฑ์พิมพ์ลายพฤกษา มัดย้อมและบาติกสีธรรมชาติ มหาวิทยาลัยราชภัฏภูเก็ต โดยการร่วมบูรณาการระหว่างเทศบาลตำบลฉลองและมหาวิทยาลัยราชภัฏภูเก็ต

ทบทวนวรรณกรรม

การย้อมผ้าด้วยเทคนิค Eco Printing เป็นวิธีการหนึ่งที่สามารถลดผลกระทบต่อสิ่งแวดล้อมได้เป็นอย่างดี ดังเช่นงานวิจัยของ Batham and Mandhary (2023) [3] ที่ได้ย้อมผ้าด้วยเทคนิค Eco Printing โดยใช้การสกัดสีธรรมชาติจากดอกดาวเรืองและดอกกุหลาบที่ใช้บูชาในวัดของประเทศอินเดีย และมีการทดสอบพบว่ามีความคงทนการซักและการขัดถูอยู่ในระดับดี

งานวิจัยของ Manuja et al., (2023) [4] ทำการศึกษาการพิมพ์แบบ Eco Printing โดยใช้ใบกุหลาบ พบว่า เป็นวิธีการพิมพ์สิ่งทอในครัวเรือนที่ง่ายและประหยัด เป็นมิตรต่อสิ่งแวดล้อม และมีความคงทนของสีต่อการซักสูงแต่มีความคงทนของสีที่ไม่ดีเมื่อสัมผัสแสงแดด และงานวิจัยของ Šabarić et al.,(2024) [5] มีการศึกษาทางด้านเคมีสิ่งทอ ส่งเสริมการการย้อมผ้าด้วยเทคนิค Eco Printing สู่การออกแบบที่ยั่งยืน

นอกจากนี้งานวิจัยของ วราภรณ์ บันเล็งลอย และคณะ (2565) [6] ได้ทำการออกแบบเสื้อผ้าจากการพิมพ์ลวดลายด้วยพืชพรรณไม้ พบว่ากระบวนการพิมพ์ลายผ้าด้วยพืชพรรณไม้มี 2 ขั้นตอนหลัก คือ ขั้นแรกการเตรียมผ้าและใบไม้ และขั้นที่สองการพิมพ์ลายธรรมชาติด้วยพรรณไม้ และทำการออกแบบเสื้อผ้าจำนวน 1 คอลเลคชั่น จำนวน 5 ชุด โดยผลการประเมินความพึงพอใจของผู้บริโภคที่มีต่อเสื้อผ้าในภาพรวมมีความพึงพอใจในระดับมากที่สุด

และงานวิจัยของ วีระศักดิ์ ศรีสารัตน์ และคณะ (2565) [1] ได้ทำการศึกษาการพิมพ์สีธรรมชาติจากใบเพกาด้วยเทคนิคการถ่ายโอนสีสู่ผ้าฝ้าย เพื่อหาวิธีการพิมพ์สีธรรมชาติที่ดีที่สุด โดยเปรียบเทียบความแตกต่างของปัจจัยต่างๆ ได้แก่ สารที่ช่วยกระตุ้นเม็ดสี และระยะเวลา รวมถึงประเมินความพึงพอใจของกลุ่มตัวอย่างต่อการวางลวดลาย ทำให้ทราบว่าการพิมพ์ผ้าด้วยเทคนิคที่เป็นธรรมชาติสามารถทำให้สีใบเพกามีความชัดเจน และมีลวดลายทันสมัย โดยสามารถดึงสีสันจากสีใบเพกาให้มีสีเหลืองเข้ม ลวดลายมีความคมและประณีตอีกด้วย

แต่อย่างไรก็ตามจากการทบทวนวรรณกรรมของผู้วิจัยพบว่างานวิจัยที่ผ่านมาในอดีตไม่มีการศึกษาปริมาณขยะมูลฝอยจากกิจกรรมการย้อมผ้าEco Printing จึงนำไปสู่การวิจัยเพื่อทราบถึงชนิดและองค์ประกอบทางกายภาพขยะมูลฝอยจากการย้อมผ้าด้วยเทคนิค Eco Printing ขึ้น

ระเบียบวิธีวิจัย

A. *ศึกษากระบวนการย้อมผ้าด้วยด้วยเทคนิค Eco Printing แบบเทคนิคพื้นฐาน (Basic methods) และเทคนิคการห่มผ้า (Blanket method) ทบทวนเอกสารและงานวิจัยที่เกี่ยวข้อง และกำหนดขอบเขตการศึกษา รวมถึงออกแบบวิธีการศึกษา*

B. *ทำการศึกษาชนิด และองค์ประกอบทางกายภาพขยะมูลฝอยจากการย้อมผ้าโดยใช้สีธรรมชาติด้วยเทคนิค Eco Printing ซึ่งดำเนินกิจกรรมภายในพื้นที่เทศบาลตำบลฉลอง ในเดือนตุลาคม พ .ศ.2567 จำนวน 2 วัน โดยทำการสำรวจและเก็บตัวอย่างในช่วงเวลา 08.30 - 17.00 น .โดยทำการเก็บตัวอย่างขยะที่เกิดขึ้นทั้งหมด]7จากการ [ย้อมผ้าใช้สีธรรมมชาติด้วยเทคนิค Eco Printing แบบเทคนิคพื้นฐาน (Basic methods) และเทคนิคการห่มผ้า (Blanket method) โดยมีอุปกรณ์ ได้แก่ เครื่องชั่งน้ำหนัก ที่คีบ ถุงดำ ถุงพลาสติกใส ปากกา เทป กล้องถ่ายรูป และแบบบันทึกข้อมูล*

C. *นำข้อมูลที่ได้วิเคราะห์ข้อมูลและสรุปผลชนิด ปริมาณ และองค์ประกอบทางกายภาพขยะมูลฝอยจากการย้อมผ้าด้วยเทคนิค Eco Printing โดยใช้สถิติเชิงพรรณนา คือ ค่าร้อยละ และค่าเฉลี่ย*

ผลการทดลอง

จากการศึกษากระบวนการย้อมผ้าด้วยเทคนิค Eco Printing จำนวน 2 รูปแบบเทคนิค คือ เทคนิคพื้นฐาน และเทคนิคการห่มผ้า พบว่า การย้อมผ้าด้วยเทคนิค Eco Printing ประกอบด้วย 5 ขั้นตอน ดังนี้

1) การเตรียมใบไม้และดอกไม้



2) การเตรียมผ้าก่อนย้อม



3) การเตรียมสารช่วยติดสี



4) การออกแบบลวดลาย



5) การย้อมผ้า



เมื่อพิจารณาในแต่ละรูปแบบเทคนิคการย้อมผ้า พบว่าการย้อมผ้าด้วยเทคนิค Eco Printing แบบพื้นฐาน มีปริมาณขยะมูลฝอยรวม 6.65 กิโลกรัม โดยเกิดจากการย้อมผ้า จำนวน 9 ผืน คิดเป็นปริมาณขยะมูลฝอยเฉลี่ยต่อการย้อมผ้า 1 ผืน เท่ากับ 0.74 กิโลกรัม โดยขั้นตอนการออกแบบลวดลายและการย้อมผ้ามีปริมาณขยะมูลฝอย 5.62 กิโลกรัม ซึ่งเป็นขั้นตอนที่พบขยะมูลฝอยมากที่สุด

สำหรับการย้อมผ้าด้วยเทคนิค Eco Printing แบบการห่มผ้า มีปริมาณขยะมูลฝอยรวม 11.25 กิโลกรัม โดยเกิดจากการย้อมผ้า จำนวน 17 ผืน คิดเป็นปริมาณขยะมูลฝอยเฉลี่ยต่อการย้อมผ้า 1 ผืน เท่ากับ 0.66 กิโลกรัม โดยขั้นตอนการออกแบบลวดลายและการย้อมผ้ามีปริมาณขยะมูลฝอย 8.27 กิโลกรัม ซึ่งเป็นขั้นตอนที่พบขยะมูลฝอยมากที่สุดเช่นเดียวกับเทคนิค Eco Printing แบบพื้นฐาน รายละเอียดดังตาราง 1

ตาราง 1 ปริมาณขยะมูลฝอยจากการย้อมผ้าด้วยเทคนิค ECO PRINTING

ขั้นตอนการย้อมผ้า	ปริมาณขยะมูลฝอยจากการย้อมผ้าด้วยเทคนิค Eco Printing (กิโลกรัม)		
	รูปแบบพื้นฐาน	รูปแบบการห่มผ้า	รวม
การเตรียมใบไม้และดอกไม้	0.97	2.76	3.73
การเตรียมผ้าก่อนย้อม	0.00	0.00	0.00
การเตรียมสารช่วยติดสี	0.06	0.22	0.28
การออกแบบลวดลายและการย้อมผ้า	5.62	8.27	13.89
รวม	6.65	11.25	17.90

ข้อสรุป

การศึกษาและวิจัยนี้จึงมีวัตถุประสงค์เพื่อเปรียบเทียบชนิดและองค์ประกอบทางกายภาพขยะมูลฝอยจากการย้อมผ้าด้วยเทคนิค Eco Printing ด้วยเทคนิคที่แตกต่างกัน คือเทคนิคพื้นฐาน (Basic methods) และเทคนิคการห่มผ้า (Blanket method) โดยทำการเก็บตัวอย่างขยะมูลฝอยที่เกิดขึ้นทั้งหมด ณ แหล่งกำเนิด จำนวน 2 วัน ในเดือนตุลาคม พ.ศ. 2567 ช่วงเวลา 08.30 - 17.00 น. จากผลการศึกษาพบว่าการย้อมผ้าด้วยเทคนิค Eco Printing มีปริมาณขยะมูลฝอยรวม 17.90 กิโลกรัม โดยมีปริมาณขยะมูลฝอยจากการย้อมผ้าด้วยเทคนิค Basic Eco Printing methods มีปริมาณรวม 6.65 กิโลกรัม (ร้อยละ 37.13) คิดเป็นปริมาณขยะมูลฝอยต่อการย้อม จำนวน 1 ผืน เท่ากับ 0.74 กิโลกรัม และปริมาณขยะมูลฝอยจากการย้อมผ้าด้วยเทคนิค Blanket Eco Printing methods มีปริมาณรวม 11.25 กิโลกรัม (ร้อยละ 62.87) คิดเป็นปริมาณขยะมูลฝอยต่อการย้อมผ้า 1 ผืน เท่ากับ 0.66 กิโลกรัม ซึ่งมีองค์ประกอบของขยะมูลฝอยส่วนใหญ่เป็นขยะอินทรีย์มากที่สุดทั้งสองเทคนิควิธีการย้อม เนื่องจากเป็นการย้อมผ้าโดยการใช้วัสดุธรรมชาติ และอาศัยความร้อนเพื่อถ่ายโอนสีและการประทับโครงสร้างจากพืชลงบนผ้า โดยจะเห็นได้ว่าการย้อมผ้าด้วยเทคนิค Eco Printing แบบพื้นฐานและแบบการห่มผ้า มีปริมาณขยะมูลไม่แตกต่างกันมาก แต่ปริมาณสีที่ติดยึดแน่นกับเส้นด้ายของผ้าและความคมชัดของลวดลายจะมีความแตกต่างกัน จึงควรมีการวางแผนออกแบบลวดลายให้ตรงกับความต้องการของลูกค้าเพื่อช่วยลดการเกิดขยะมูลฝอยในขั้นตอนการย้อมให้เกิดขึ้นน้อยที่สุด

คำขอบคุณ

ขอขอบคุณเทศบาลตำบลฉลอง จังหวัดภูเก็ต กลุ่มเครือข่ายสมาชิกชมรมผู้สูงอายุเทศบาลตำบลฉลอง สมาชิกกลุ่มสตรีเทศบาลตำบลฉลอง รวมถึงกลุ่มอาชีพในตำบลฉลอง และคณะวิทยาศาสตร์และเทคโนโลยี มหาวิทยาลัยราชภัฏภูเก็ตและเจ้าหน้าที่บุคลากรที่เกี่ยวข้องทุกท่านที่ร่วมขับเคลื่อนโครงการศูนย์อัจฉริยะเพื่อการพัฒนาท้องถิ่นภาคใต้ กิจกรรมสร้างแบรนด์ผลิตภัณฑ์พิมพ์ลายพฤกษา มัดย้อมและบาติกสีธรรมชาติ ซึ่งส่งผลให้การวิจัยนี้สำเร็จลุล่วงไปได้ด้วยดี

อ้างอิง

[1] วีระศักดิ์ ศรีลารัตน์. (2565). การพิมพ์สีธรรมชาติจากใบเพกาด้วยเทคนิคการถ่ายโอนสีสู่ผ้าฝ้าย. วารสารวิจัยและพัฒนา วไลยอลงกรณ์ ในพระบรมราชูปถัมภ์, 17(1), 45-55.

[2] สุธาทอง หอมยา สุกัญญา วงศ์ธนะบูรณ ภูริณัฐ ปลัดสงคราม และกิตติศักดิ์ จิตต์เกื้อ. (2567). การจัดการขยะมูลฝอยจากการพิมพ์ผ้าลายพฤกษา. ใน การประชุมวิชาการเทคโนโลยีสิ่งแวดล้อมประจำปี ครั้งที่ 36 สวสท. '67 วันที่ 22 พฤศจิกายน 2567 (หน้า 139-144). กรุงเทพมหานคร: สมาคมวิศวกรรมสิ่งแวดล้อมแห่งประเทศไทย.

[3] Batham, M., & Mandhary, S. (2023). Recycling floral waste from temple using different techniques of eco-printing on cotton fabric. International Journal of Science and Research Archive, 9(1), 118–125. https://doi.org/10.30574/ijsra.2023.9.1.0351

[4] Manuja, A., Ojha, I., & Singh, D. M. (2023). Eco-Printing: Domestic technique of textile printing using the leaves of Rose Indica. International Journal of Engineering Technology and Management Sciences, 7(3), 116–121. https://doi.org/10.46647/ijetms.2023.v07i03.016

[5] Šabarić, I., Sutlović, A., Filipčić, J., & Karin, F. (2024). Contribution of Plant Transfer Printing to Sustainable Fashion. Sustainability, 16(11), 4361. https://doi.org/10.3390/su16114361

[6] วราภรณ์ บันเล็งลอย, กัญญาณัฐ ทรวงถูก และ พรพิริยา ลาดหนองขุ่น. (2565). การออกแบบเสื้อผ้าจากผ้าพิมพ์ลวดลายด้วยพืชพรรณไม้. วารสารเทคโนโลยีคหกรรมศาสตร์และนวัตกรรม, 1(1), 32-42.

[7] กรมควบคุมมลพิษ. 2565. การศึกษาองค์ประกอบขยะมูลฝอย ปี 2564. สืบค้นได้จาก :https://www.pcd.go.th/wp-content/uploads/2022/08/pcdnew-2022-08-09_08-58-28_103322.pdf

ปัจจัยที่มีความสัมพันธ์กับความรอบรู้ด้านสุขภาพและพฤติกรรมการป้องกันโรคมือเท้าปากของครูผู้ดูแลเด็ก ในศูนย์พัฒนาเด็กเล็ก อำเภอเมือง จังหวัดภูเก็ต

Factors Associated with Health Literacy and Disease Prevention Behaviors Regarding Hand, Foot, and Mouth Disease Among Childhood Teachers in Child Care Centers in Mueang District, Phuket Province

1st SUPATSORN LUANKAEW
Bachelor of Public Health
Phuket Rajabhat University
Phuket Thailand
S6411166239@pkru.ac.th

2 nd NATTHAKAN WANRAEK
Bachelor of Public Health
Phuket Rajabhat University
Phuket Thailand
S6411166213@pkru.ac.th

3 rd CHAYANIT LUEVANICH
Bachelor of Public Health
Phuket Rajabhat University
Phuket Thailand
chayanit.l@pkru.ac.th

4 th ORANURETHAI ABDULLA
Bachelor of Public Health
Phuket Rajabhat University
Phuket Thailand
oranurethai.a@pkru.ac.th

5th JITTIPONG SUNGTHONG
Bachelor of Public Health
Phuket Rajabhat University
Phuket Thailand
jittipong.s@pkru.ac.th

Abstract
This cross-sectional study aimed to study the level of health literacy and the prevention behavior of hand, foot, and mouth disease (HFMD) and the correlation among age, income, experience in hand, foot, and mouth disease care, length of act as childhood teacher, health literacy, and prevention behavior among childhood teachers in childcare centers in Muang District, Phuket Province. The sample consisted of 102 childhood teachers. The research tools consisted of health literacy and behavior of HFMD prevention questionnaire. Data were analyzed using frequency, percentage, mean, standard deviation, and Pearson's product-moment correlation.
The findings showed that childhood teachers had a high level of health literacy (mean = 4.41, S.D. = 0.47) and prevention behavior (mean = 4.63, S.D. = 0.55). Income, experience in hand, foot, and mouth disease care, and length of act as a childhood teacher were correlated with health literacy. Only health literacy was related to prevention behavior. Therefore, public health personnel should promote health literacy among childhood teachers and parents.

Keywords Hand, Foot, and Mouth Disease (HFMD), Teachers, Child Development Centers, Health Literacy, Prevention Behavior

I บทนำ

โรคมือเท้าปากเป็นปัญหาสาธารณสุขที่สำคัญโรคหนึ่ง เกิดจากการติดเชื้อไวรัสกลุ่มเอ็นเทอโรไวรัส(Enterovirus) โดยไวรัสที่เป็นสาเหตุและตรวจพบได้บ่อยคือไวรัสค็อกซากีชนิดเอ (Coxsackie virus A) ไวรัสค็อกซากีชนิดบี (Coxsackie virus B) และไวรัสเอ็นเทอโร 71 (Enterovirus 71) เชื้อไวรัสนี้สามารถติดต่อผ่านทางสารคัดหลั่ง เช่น น้ำมูก น้ำลาย อุจจาระ ลักษณะอาการของโรคมือเท้าปากที่พบได้บ่อย คือ มีไข้ มีแผลในปากคล้ายแผลร้อนในบริเวณลิ้นและกระพุ้งแก้ม เป็นสาเหตุทำให้เด็กไม่สามารถรับประทานอาหารได้ตามปกติ และเกิดตุ่มนูนขนาดเล็กที่ฝ่ามือ นิ้วมือ และฝ่าเท้า หากมีอาการแทรกซ้อนรุนแรงอาจทำให้เกิดอาการสมองอักเสบและเสียชีวิตได้ กลุ่มเสี่ยงต่อการเป็นโรคมือเท้าปาก ได้แก่ กลุ่มเด็ก ส่วนใหญ่พบในเด็กอายุต่ำกว่า 5 ปีซึ่งเป็นเด็กก่อนวัยเรียน ร้อยละ 45 รองลงมาคือ อายุต่ำกว่า 2 ปี ร้อยละ 44 และ 5 ปีขึ้นไป ร้อยละ 11 ตามลำดับ [1]

โรคมือเท้าปากส่งผลกระทบต่อพัฒนาการและสุขภาพโดยรวมของเด็ก คือ เด็กไม่สุขสบาย อ่อนเพลีย เบื่ออาหาร ผลที่ตามมา คือ ภาวะการขาดสารอาหาร ซึ่งการติดเชื้ออาจส่งผลให้เกิดโรคแทรก ดังนั้น ครูผู้ดูแลเด็กจะต้องมีความรอบรู้ด้านสุขภาพเกี่ยวกับโรคมือเท้าปากและ

พฤติกรรมการป้องกันควบคู่ไปด้วย [2] กรมควบคุมโรค กระทรวงสาธารณสุข ได้เพิ่มมาตรการในการเฝ้าระวังป้องกันโรคล่วงหน้าโดยกำหนดแนวทางมาตรการในการป้องกันควบคุมโรคมือเท้าปากในศูนย์พัฒนาเด็กเล็กเพื่อให้สามารถเฝ้าระวังคัดกรองเด็กป่วยด้วยโรคมือเท้าปากได้อย่างรวดเร็ว สามารถแยกเด็กป่วยจากเด็กปกติ ทำให้สามารถควบคุมโรคไม่ให้แพร่ระบาดต่อไปได้ [1] ความรอบรู้เกี่ยวกับวิกฤตด้านสุขภาพ ความสามารถในการเข้าใจโรค ข้อมูลข่าวสารจะช่วยให้บุคคลมีพฤติกรรมสุขภาพที่เหมาะสมขณะเผชิญโรคติดต่อ [3] โดยองค์การอนามัยโลกกล่าวว่าความรอบรู้ด้านสุขภาพเป็นตัวกำหนดแรงจูงใจและความสามารถของบุคคลในการเข้าถึง เข้าใจและใช้ข้อมูลสารสนเทศในการเสริมสร้างและการคงไว้ซึ่งสุขภาพดี [4] และนำไปสู่การมีพฤติกรรมสุขภาพที่ดี อีกทั้งแสดงถึงผลลัพธ์ของการสร้างเสริมสุขภาพทำให้ประชาชนมีศักยภาพในการดูแลสุขภาพตนเอง [5]

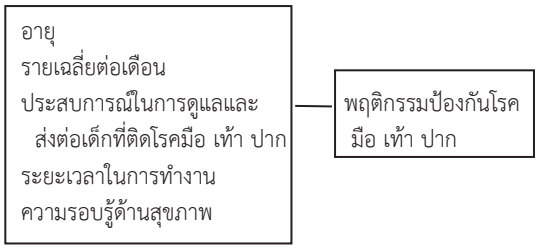
จังหวัดภูเก็ตมีรายงานจำนวนผู้ป่วยโรคมือเท้าปาก 3 ปีย้อนหลังระหว่างปี พ.ศ. 2564- 2566 พบว่าอำเภอเมืองพบผู้ป่วยสูงสุด โดยมีอัตราป่วย 36.59 169.56 และ 98.57 ต่อประชากรแสนคนตามลำดับ [6] ดังนั้น การที่จะพัฒนาครูผู้ดูแลเด็กให้สามารถดูแลเด็กได้บรรลุเป้าหมาย จึงจำเป็นที่จะต้องทราบว่าครูผู้ดูแลเด็กมีความรอบรู้ด้านสุขภาพและพฤติกรรมป้องกันโรคมือเท้าปากอย่างไร ดังนั้น คณะผู้วิจัยจึงสนใจศึกษาความรอบรู้ด้านสุขภาพและพฤติกรรมการป้องกันโรคมือเท้าปากในครูผู้ดูแลเด็กของศูนย์พัฒนาเด็กเล็กในเขตอำเภอเมือง จังหวัดภูเก็ต

วัตถุประสงค์

1. เพื่อศึกษาความรอบรู้ด้านสุขภาพและพฤติกรรมการป้องกันโรคของครูผู้ดูแลเด็กของศูนย์พัฒนาเด็กเล็ก อำเภอเมือง จังหวัดภูเก็ต
2. เพื่อศึกษาความสัมพันธ์ระหว่างอายุ รายได้ ประสบการณ์ในการดูแลและส่งต่อเด็กที่ติดโรคมือ เท้า ปาก ระยะเวลาในการทำงานดูแลเด็กในศูนย์เด็กเล็ก ความรอบรู้ด้านสุขภาพกับพฤติกรรมป้องกันโรคมือเท้าปากของครูผู้ดูแลเด็กของศูนย์พัฒนาเด็กเล็ก อำเภอเมือง จังหวัดภูเก็ต

กรอบแนวคิดงานวิจัย

การศึกษาอาศัยความรอบรู้ด้านสุขภาพของกองสุขศึกษา [7] และพฤติกรรมการป้องกันโรคของโรเซนสต็อก [8] โดยความรอบรู้ด้านสุขภาพเป็นความสามารถของครูผู้ดูแลเด็กในการเข้าถึงข้อมูลสุขภาพ ในการตัดสินใจ และการใช้ข้อมูลข่าวสารเพื่อนำไปสู่การตัดสินใจมี 6องค์ประกอบตามแนวคิดของกองสุขศึกษา ประกอบด้วย 1) ด้านการเข้าถึงข้อมูล สุขภาพและบริการสุขภาพ 2) ด้านความรู้ ความเข้าใจ 3) ด้านทักษะการสื่อสาร 4) ด้านการรู้เท่าทันสื่อ 5) ด้านทักษะการตัดสินใจ และ 6) ด้านการจัดการตนเอง ส่วนพฤติกรรมการป้องกันโรค การปฏิบัติการป้องกันและควบคุมโรคประกอบด้วย 1) การรับรู้ความรุนแรงของโรค 2) การรับรู้ต่อโอกาสเสี่ยงต่อการเป็นโรค 3) ความคาดหวังในประสิทธิผลของการตอบสนอง 4) การประเมินอันตรายต่อสุขภาพ และ 5) การประเมินการเผชิญปัญหา [8] ในการศึกษาครั้งนี้ประกอบด้วยตัวแปร ดังนี้ อายุ รายได้เฉลี่ยต่อเดือน ประสบการณ์ในการดูแลและส่งต่อเด็กที่ติดโรคมือ เท้า ปาก ระยะเวลาในการทำงานดูแลเด็กในศูนย์เด็กเล็ก ความรอบรู้ด้านสุขภาพและพฤติกรรมป้องกันโรคมือเท้าปากของครูผู้ดูแลเด็กของศูนย์พัฒนาเด็กเล็ก ดังภาพ 1



ภาพ 1 กรอบแนวคิดในการวิจัย

II ทบทวนวรรณกรรม

จากการทบทวนวรรณกรรมเกี่ยวข้องในประเด็นความรู้และพฤติกรรมการป้องกันโรคมือ เท้า ปาก ของผู้ดูแลเด็กก่อนวัยเรียน ศูนย์พัฒนาเด็กเล็ก องค์การบริหารส่วนตำบลจัน พบว่ากลุ่มผู้ดูแลเด็กก่อนวัยเรียนมีระดับความรู้เรื่องโรคมือ เท้า ปาก อยู่ในระดับสูง เนื่องมาจากกลุ่มผู้ดูแลเด็กก่อนวัยเรียนส่วนใหญ่ให้ความสำคัญและมีความตระหนักในการป้องกันโรคมือ เท้า ปาก รวมทั้งมีโอกาสได้รับข้อมูลข่าวสารในการป้องกันโรคจากสื่อต่าง ๆ หรือได้รับความรู้จากเจ้าหน้าที่ทางสาธารณสุข จึงทำให้มีความรู้ในเรื่องโรคมือ เท้า ปาก แต่อย่างไรก็ตามยังพบว่ากลุ่มผู้ดูแลเด็กก่อนวัยเรียนที่มีระดับความรู้เรื่องโรคมือ เท้า ปาก อยู่ในระดับปานกลางถึง ร้อยละ 40.00 พฤติกรรมการป้องกันควบคุมโรคมือ เท้า ปาก ในภาพรวมมีค่าคะแนนอยู่ในระดับดี ($\bar{x}$== 2.79, SD = 0.87) ผู้ดูแลเด็กเป็นอีกกลุ่มบุคคลที่มีความสำคัญในการป้องกันและควบคุมโรค มือ เท้า ปาก โดยเฉพาะในกลุ่มเด็กก่อนวัยเรียนซึ่งเป็นกลุ่มที่มีภูมิคุ้มกันต่ำ และมีโอกาสติดโรคนี้ได้ง่าย หากผู้ดูแลเด็กมีความรู้ที่ถูกต้อง มีความเข้าใจ และความตระหนักในการป้องกันโรค และมีพฤติกรรมการป้องกันโรคมือ เท้า ปาก ที่ดีและถูกต้องย่อมส่งผลดีต่อการควบคุมและป้องกันการแพร่ระบาดของโรคนี้ได้ดีมากยิ่งขึ้น [9] และการศึกษาปัจจัยที่มีความสัมพันธ์กับพฤติกรรมการป้องกันและควบคุมโรคมือเท้าปากของครูในโรงเรียนอนุบาลและศูนย์พัฒนาเด็กเล็กจังหวัดสุราษฎร์ธานี พบว่า ระดับการศึกษา ตำแหน่ง ความรู้เรื่องโรคมือเท้า ปาก การรับรู้ความเสี่ยงโรคมือ เท้า ปาก ทัศนคติในการป้องกันโรคมือ เท้าปาก และการรับรู้ประโยชน์ การป้องกันโรคมือ เท้า ปาก มีความสัมพันธ์กับพฤติกรรมการป้องกัน และควบคุมโรคมือ เท้า ปาก เนื่องจากครูและผู้ดูแลในโรงเรียนอนุบาลและศูนย์พัฒนาเด็กเล็กในจังหวัดสุ ราษฎร์ธานีส่วนใหญ่เห็นความสำคัญและรับรู้ความเสี่ยงของโรคมือ เท้าปาก มีความรู้และทัศนคติการป้องกันโรคมือ เท้า ปาก และการรับรู้ประโยชน์การป้องกันโรคมือ เท้าปาก เนื่องจากการมีประสบการณ์โดยตรงจากการที่มีนักเรียนของศูนย์พัฒนาเด็กเล็กเป็นโรคมือ เท้า ปาก การได้รับคำแนะนำในการปฏิบัติตัวเพื่อป้องกันโรคมือเท้าปากจากบุคคลที่เกี่ยวข้อง ไม่ว่าจะเป็นหน่วยงานที่เกี่ยวข้อง เจ้าหน้าที่สาธารณสุขหรือจากครู และผู้ดูแลด้วยกันเองส่งผลให้ครูและผู้ดูแลเด็กเกิดความรู้และทักษะในการปฏิบัติพฤติกรรมการป้องกันโรคมือ เท้า ปาก ได้อย่างถูกต้องเหมาะสม และสามารถถ่ายทอดไปยังเด็กและผู้ปกครองเพื่อป้องกันและเฝ้าระวังไม่ให้เกิดโรคมือเท้าปากได้ [10] ในขณะที่การศึกษปัจจัยทำนายพฤติกรรมการป้องกันโรคมือเท้าปากของผู้ปกครองและผู้ดูแลเด็กในศูนย์พัฒนาเด็กเล็ก อำเภอเชียงคำ จังหวัดพะเยา พบว่ากลุ่มตัวอย่าง (n=330) มีพฤติกรรมการป้องกันโรคมือเท้าปากระดับสูง อายุมีความสัมพันธ์ทางบวกกับพฤติกรรมการป้องกันโรคมือเท้าปากของผู้ปกครองและผู้ดูแลเด็ก โดยพบว่า เด็กที่มีอายุน้อยกว่า 2 ปี จะมีโอกาสเป็นโรคมือเท้าปากเป็น 6.35 เท่า เมื่อเทียบกับเด็กที่มีอายุมากกว่า 5 ปี (95% CI = 1.37–29.38) รายได้ต่อเดือน มีความสัมพันธ์ทางบวกกับพฤติกรรมการป้องกันโรคมือเท้าปากของผู้ปกครองและผู้ดูแลเด็กในศูนย์พัฒนาเด็กเล็กอย่างมีนัยสำคัญทางสถิติ ทัศนคติต่อโรคมือเท้าปากมีความสัมพันธ์ทางลบกับพฤติกรรมการป้องกันโรคมือเท้าปากของผู้ปกครองและผู้ดูแลเด็กในศูนย์พัฒนาเด็กเล็กอย่างมีนัยสำคัญทางสถิติ ปัจจัยเอื้อ มีอิทธิพลและสามารถทำนายพฤติกรรมการป้องกันโรค มือเท้าปากของผู้ปกครองและผู้ดูแลเด็ก จากการทดสอบสมมติฐาน พบว่า ปัจจัยนำ ปัจจัยเอื้อ

และปัจจัยเสริมสามารถร่วมทำนายพฤติกรรมการป้องกันโรคมือเท้าปากของผู้ปกครองและผู้ดูแลเด็ก ตัวแปรที่มีความสัมพันธ์กับพฤติกรรมการป้องกันโรคมือเท้าปาก ได้แก่ อายุ รายได้ และทัศนคติต่อการป้องกันโรคมือเท้าปาก สามารถร่วมกันอธิบายพฤติกรรมการป้องกันโรคมือเท้าปากของผู้ปกครองและผู้ดูแลเด็กในศูนย์พัฒนาเด็กเล็กได้อย่างถูกต้อง ร้อยละ 4.5 (Adjusted R^2= 0.045, p-value <0.001) [11]

III ระเบียบวิธีวิจัย

การวิจัยในครั้งนี้เป็นการศึกษาวิจัยเชิงบรรยาย (Descriptive research) ประชากรที่ใช้ในการศึกษาครั้งนี้ คือ ครูผู้ดูแลเด็กก่อนวัยเรียนในศูนย์พัฒนาเด็กเล็ก อำเภอเมือง จังหวัดภูเก็ต จำนวนทั้งหมด 117 คน จาก 15 ศูนย์ ในอำเภอเมืองจังหวัดภูเก็ต กลุ่มตัวอย่างในการศึกษาครั้งนี้จึงใช้ประชากรทั้งหมดเป็นกลุ่มตัวอย่าง โดยมีครูผู้ดูแลเด็กปฏิเสธการเข้าร่วมวิจัย จำนวน 15 ราย คงเหลือกลุ่มตัวอย่างจำนวน 102 ราย คิดเป็นร้อยละ 87.18 ของกลุ่มตัวอย่าง โดยกำหนดเกณฑ์การคัดเข้า ดังนี้

1. อายุมากกว่า 18 ปีขึ้นไป
2. สามารถอ่านเขียน สื่อสารเป็นภาษาไทยได้ด้วยตนเอง และเป็นผู้ที่มีสติสัมปชัญญะครบถ้วน
3. มีประสบการณ์เป็นครูผู้ดูแลเด็กเล็กระยะเวลาตั้งแต่ 1 ปีขึ้นไป
4. ยินดีเข้าร่วมในการวิจัย

เครื่องมือในการวิจัย

เครื่องมือที่ใช้ในการเก็บข้อมูลในการวิจัยครั้งนี้แบ่งออกเป็น 3 ตอน ดังนี้

ตอนที่ 1 แบบสอบถามเกี่ยวกับข้อมูลทั่วไปประกอบด้วย เพศ อายุ ระดับการศึกษา สถานภาพสมรส รายได้ จำนวนเด็กที่ดูแลในศูนย์พัฒนาเด็กเล็ก และประสบการณ์การพบเจอเด็กติดโรคมือ เท้า ปาก จำนวน 8 ข้อ

ตอนที่ 2 แบบสอบถามเกี่ยวกับความรอบรู้ด้านสุขภาพที่เกี่ยวกับโรคมือเท้าปากสร้างโดยอาศัยแนวคิดของกองสุขศึกษา [7] ประกอบด้วยการเข้าถึงข้อมูลสุขภาพและบริการสุขภาพ ความรู้ ความเข้าใจ ทักษะการสื่อสาร การรู้เท่าทันสื่อ การตัดสินใจ การจัดการตนเอง โดยเป็นแบบสอบถามเป็นแบบมาตราส่วนประมาณค่า จำนวน 24 ข้อ แบ่งเป็น 5 ระดับ ดังนี้

มีความรอบรู้ด้านสุขภาพมากที่สุด	ให้คะแนน	5
มีความรอบรู้ด้านสุขภาพมาก	ให้คะแนน	4
มีความรอบรู้ด้านสุขภาพปานกลาง	ให้คะแนน	3
มีความรอบรู้ด้านสุขภาพน้อย	ให้คะแนน	2
มีความรอบรู้ด้านสุขภาพน้อยที่สุด	ให้คะแนน	1

สำหรับเกณฑ์ในการแปลผลความรอบรู้ด้านสุขภาพที่เกี่ยวข้องกับโรคมือเท้าปากของผู้ดูแลเด็กเล็กทั้ง 6 ด้าน แบ่งเป็น 3 ระดับดังต่อไปนี้

คะแนนเฉลี่ย 3.67 – 5.00 หมายถึง ความรอบรู้ด้านสุขภาพอยู่ในระดับสูง

คะแนนเฉลี่ย 2.34 – 3.66 หมายถึง ความรอบรู้ด้านสุขภาพอยู่ในระดับปานกลาง

คะแนนเฉลี่ย 1.00 – 2.33 หมายถึง ความรอบรู้ด้านสุขภาพอยู่ในระดับน้อย

ตอนที่ 3 แบบสอบถามเกี่ยวกับพฤติกรรมการป้องกันโรคมือเท้าปากสร้างขึ้นโดยอาศัยแนวคิดของกองสุขศึกษา (2561) แบบสอบถามเป็นแบบประมาณค่า จำนวน 10 ข้อ แต่ละข้อมีคะแนน 1- 5 ดังนี้

5 คะแนน ปฏิบัติทุกครั้ง 6-7 ครั้งต่อสัปดาห์

4 คะแนน ปฏิบัติเกือบทุกครั้ง 4-5 ครั้งต่อสัปดาห์

3 คะแนน ปฏิบัติบางครั้ง 2-3 ครั้งต่อสัปดาห์

2 คะแนน ปฏิบัติน้อยครั้ง 1 ครั้งต่อสัปดาห์

1 คะแนน ไม่เคยปฏิบัติเลย

สำหรับเกณฑ์ในการจำแนกพฤติกรรมการป้องกันโรคมือเท้าปากในผู้ดูแลเด็กเล็ก แบ่งเป็น 3 ระดับตามเกณฑ์ ดังต่อไปนี้

คะแนนเฉลี่ย 3.67 – 5.00 หมายถึง พฤติกรรมการป้องกันโรคอยู่ในระดับสูง

คะแนนเฉลี่ย 2.34 – 3.66 หมายถึง พฤติกรรมการป้องกันโรคอยู่ในระดับปานกลาง

คะแนนเฉลี่ย 1.00 – 2.33 หมายถึง พฤติกรรมการป้องกันโรคอยู่ในระดับน้อย

คุณภาพของเครื่องมือ

เครื่องมือผ่านการตรวจความเที่ยงตรงเชิงเนื้อหาจากผู้ทรงุณวุฒิ 3 ท่าน มีค่า IOC ระหว่าง 0.67 ถึง 1.00 และตรวจความความเชื่อมั่นของเครื่องมือโดยทดลองใช้กับกลุ่มที่มีลักษณะเหมือนกับกลุ่มตัวอย่าง ได้แก่ ครูผู้ดูแลเด็กเล็กในพื้นที่อำเภอถลาง จำนวน 30 คน แบบสอบถามความรอบรู้ด้านสุขภาพและแบบสอบถามพฤติกรรมการป้องกันโรคมือเท้าปากมีค่าสัมประสิทธิ์แอลฟ่าครอนบาค (Cronbach' Alpha Coefficient) เท่ากับ 0.95 และ 0.85 ตามลำดับ

การเก็บรวบรวมข้อมูล

1.ขออนุญาตเก็บข้อมูลจากศูนย์พัฒนาเด็กเล็กทั้ง 15 แห่ง

2.คณะผู้วิจัยชี้แจงวัตถุประสงค์ของการศึกษา ขั้นตอนการเก็บข้อมูลและขอความร่วมมือในการเก็บรวบรวมข้อมูล

3.คณะผู้วิจัยเก็บรวบรวมข้อมูลรหะว่าง 1 สิงหาคม 2567 30 กันยายน 2567

การวิเคราะห์ข้อมูล

คณะผู้วิจัยการวิเคราะห์ข้อมูลด้วยโปรแกรมคอมพิวเตอร์สำเร็จรูป ดังนี้

1. เพศ อายุ ระดับการศึกษา ประสบการณ์ดูแลเด็กที่ป่วยเป็นโรคมือเท้าปาก ระดับการศึกษา นำเสนอด้วย จำนวน ร้อยละ

2. รายได้ อายุ ระยะเวลาที่ประกอบอาชีพครูผู้ดูแลเด็ก และจำนวนเด็กในศูนย์พัฒนาเด็กเล็ก นำเสนอด้วย จำนวน ร้อยละ ส่วนเบี่ยงเบนมาตรฐาน ค่าเฉลี่ย ค่าสูงสุด และค่าต่ำสุด

3. ความรอบรู้ด้านสุขภาพและพฤติกรรมการป้องกันโรคมือเท้าปาก นำเสนอด้วยค่าเฉลี่ยและส่วนเบี่ยงเบนมาตรฐาน

4. วิเคราะห์ความสัมพันธ์ระหว่างอายุ รายได้ ประสบการณ์ในการดูแลและส่งต่อเด็กที่ติดโรคมือ เท้า ปาก ระยะเวลาในการดูแลเด็กในศูนย์เด็กเล็ก ความรอบรู้ด้านสุขภาพกับพฤติกรรมป้องกันโรคมือเท้าปากของผู้ดูแลเด็กของศูนย์พัฒนาเด็กเล็กด้วยค่าสัมประสิทธิ์สหสัมพันธ์ของเพียร์สัน

IV ผลการวิจัย

จากผลการศึกษาพบว่า ครูผู้ดูแลเด็กเล็กส่วนใหญ่เป็นเพศหญิงร้อยละ 99.00 ส่วนใหญ่ส่วนใหญ่อายุ 40 ปีขึ้นไปร้อยละ 41.18 โดยมีอายุเฉลี่ย 37.46 ปี (S.D. = 9.721) สถานภาพของครูผู้ดูแลเด็กส่วนใหญ่ โสด จำนวน 52 คน คิดเป็นร้อยละ 50.98 ส่วนใหญ่สำเร็จการศึกษาระดับปริญญาตรีหรือเทียบเท่าร้อยละ 83.33 รายได้เฉลี่ยต่อเดือนของครูผู้ดูแลเด็กเล็กเฉลี่ย 16,617.75 บาท (S.D. = 7,739.98) กลุ่มตัวอย่างมีประสบการณ์ในการดูแลและส่งต่อเด็กที่ติดโรคมือเท้าปากร้อยละ 85.29 มีส่วนใหญ่มีประสบการณ์ในการดูแลเด็กเล็กน้อยกว่า 5 ปี และ 6 – 15 ปี เท่ากันกลุ่มละจำนวน 44 คน มีเด็กเล็กในความดูแลจำนวน 21 – 25 คน ร้อยละ 38.24 ดังตารางที่ 1

ตารางที่ 1 จำนวน ร้อยละ ของข้อมูลส่วนบุคคลของกลุ่มตัวอย่าง (n=102)

ข้อมูลส่วนบุคคล	กลุ่มตัวอย่าง	
	จำนวน (คน)	ร้อยละ
1. เพศ		
ชาย	1	1.00
หญิง	101	99.00
2. อายุ		
18-23 ปี	8	7.84
24-28 ปี	13	12.74
29-33 ปี	20	19.61
34-39 ปี	19	18.63
40 ปีขึ้นไป	42	41.18

($\bar{x}$= 37.46, S.D. = 9.721, Min = 22, Max = 56)		
3. สถานภาพ		
โสด	52	50.98
สมรส	42	41.18
หม้าย	1	0.98
หย่าร้าง	5	4.90
แยกกันอยู่	2	1.96
4. ระดับการศึกษา		
มัธยมศึกษาตอนต้นหรือเทียบเท่า	2	1.96
มัธยมศึกษาตอนปลายหรือเทียบเท่า	7	6.86
ปริญญาตรีหรือเทียบเท่า	85	83.33
สูงกว่าปริญญาตรี	5	4.90
อื่นๆ (โปรดระบุ)	3	2.94
5. รายได้เฉลี่ยต่อเดือน		
น้อยกว่า 10,000	33	32.35
10,001 – 20,001	49	48.04
20,002 – 30,002	14	13.73
30,003 – 40,003	5	4.90
40,004 บาทขึ้นไป	1	0.98
($\bar{x}$= 16,617.75, S.D. = 7,739.98, Min = 9,500, Max = 48,000)		
6. ท่านเคยมีประสบการณ์ในการดูแลและส่งต่อเด็กที่ติดโรคมือเท้าปาก		
มี	87	85.29
ไม่มี	15	14.71
7. ท่านมีประสบการณ์การดูแลเด็กในศูนย์พัฒนาเด็กเล็กเป็นระยะเวลากี่ปี		
น้อยกว่า 5 ปี	44	43.14
6 - 15	44	43.14
16 – 25	9	8.82
มากกว่า 26 ปี	5	4.90
($\bar{x}$ = 8.54, S.D. = 7.16, Min = 1, Max = 34)		
8. ปัจจุบันท่านดูแลเด็กในศูนย์พัฒนาเด็กเล็กจำนวนกี่คน		
น้อยกว่า 15 คน	16	15.69
16 - 20	29	28.43
21 - 25	39	38.24
26 คนขึ้นไป	18	17.65
($\bar{x}$ = 21.71, S.D. = 4.86, Min = 11, Max = 30)		

จากการศึกษาความรอบรู้ด้านสุขภาพของครูผู้ดูแลเด็กเล็ก พบว่า อยู่ในระดับสูงทั้งรายด้านและโดยรวม ดังตารางที่ 2 และพฤติกรรมการป้องกันโรคพบว่าอยู่ในระดับสูงทั้งรายด้านและภาพรวมเช่นกันดังตารางที่ 3

ตารางที่ 2 ค่าเฉลี่ยและค่าเบี่ยงเบนมาตรฐานความรอบรู้ของครูผู้ดูแลเด็กเล็ก (n = 102)

ความรอบรู้ด้านสุขภาพ	$\bar{x}$	S.D.	แปลผล
ด้านการเข้าถึงข้อมูลและบริการสุขภาพ	4.44	0.51	สูง
ด้านความรู้ ความเข้าใจ	4.40	0.52	สูง
ด้านทักษะการสื่อสาร	4.34	0.56	สูง
ด้านการรู้เท่าทันสื่อ	4.27	0.55	สูง
ด้านการตัดสินใจ	4.42	0.59	สูง
ด้านการจัดการตนเอง	4.39	0.59	สูง
ภาพรวม	4.41	0.47	สูง

ตารางที่ 3 ค่าเฉลี่ยและค่าเบี่ยงเบนมาตรฐานพฤติกรรมการป้องกันโรคมือเท้าปากของครูผู้ดูแลเด็กเล็ก (n = 102)

พฤติกรรมการป้องกันโรคมือเท้าปาก	$\bar{x}$	S.D.	แปลผล
1. ท่านดูแลรักษาสิ่งแวดล้อมภายในศูนย์พัฒนาเด็กเล็กและบริเวณรอบศูนย์พัฒนาเด็กเล็กสะอาดอยู่เสมอ	4.56	0.59	สูง
2. ท่านทำความสะอาดของเล่นเด็กด้วยน้ำผสมคลอรีน น้ำยาไฮเตอร์และน้ำยาฆ่าเชื้ออื่นๆเป็นประจำ	4.57	0.57	สูง
3. ท่านทำความสะอาดห้องเรียนด้วยน้ำยาฆ่าเชื้อหลังพบเด็กเล็กป่วยด้วยโรคมือ เท้า ปาก	4.68	0.55	สูง
4. ท่านล้างมือด้วยสบู่เป็นประจำหลังทำกิจกรรมต่าง ๆ	4.62	0.55	สูง
5.ท่านให้เด็กปิดปาก ปิดจมูก ขณะไอจาม	4.48	0.63	สูง
6. หากท่านพบเจอเด็กไม่สบาย ท่านสามารถดูแลเด็กเบื้องต้น เช่นเช็ดตัว ลดไข้ โทรแจ้งผู้ปกครองมารับไปพบแพทย์	4.66	0.54	สูง
7. หากทราบว่าเด็กมีอาการป่วยเป็นโรคมือเท้าปาก ท่านจะให้เด็กหยุดเรียน เพื่อป้องกันการติดเชื้อ	4.71	0.52	สูง
8. ท่านทิ้งกระดาษหรือผ้าที่ใช้เช็ดน้ำมูก น้ำลายของเด็กที่ป่วยลงในถังขยะที่มีฝาปิดมิดชิด	4.66	0.54	สูง
9. ท่านให้เด็กแยกใช้สิ่งของส่วนตัว เช่น แก้วน้ำ ช้อน จาน ขวดนม ร่วมกับผู้อื่น	4.71	0.52	สูง
ภาพรวม	4.63	0.55	สูง

เมื่อทำการวิเคราะห์ความสัมพันธ์ พบว่า รายได้ ระยะเวลาในการดูแลเด็กในศูนย์เด็กเล็กมีความสัมพันธ์กับความรอบรู้ด้านสุขภาพอย่างมีนัยสำคัญทางสถิติที่ระดับ .01 ในขณะที่ประสบการณ์ในการดูแลและส่งต่อเด็กที่ติดโรคมือ เท้า ปาก มีความสัมพันธ์กับความรอบรู้ด้านสุขภาพอย่างมีนัยสำคัญทางสถิติที่ระดับ .05 และผลจากการศึกษายังพบว่าความรอบรู้ด้านสุขภาพเป็นตัวแปรเดียวที่มีความสัมพันธ์กับพฤติกรรมการป้องกันโรคมือ เท้า ปากอย่างมีนัยสำคัญที่ระดับ 0.01 (r=.520, p< .01) ดังตารางที่ 4

ตารางที่ 4 ความสัมพันธ์ระหว่างอายุ รายได้ ประสบการณ์ในการดูแลและส่งต่อเด็กที่ติดโรคมือ เท้า ปาก ระยะเวลาในการทำงานดูแลเด็กในศูนย์เด็กเล็ก ความรอบรู้ด้านสุขภาพและพฤติกรรมป้องกันโรคมือเท้าปาก (n = 102)

ตัวแปร	1	2	3	4	5	6
1. อายุ	1.00					
2. รายได้	.493**	1.00				
3. ประสบการณ์ในการดูแลและส่งต่อเด็ก	.323**	.190	1.00			
4. ระยะเวลาในการดูแลเด็ก	.724**	.599**	.249*	1.00		
5. ความรอบรู้ด้านสุขภาพ	.106	.299**	.197*	.284**	1.00	
6. พฤติกรรมป้องกันโรคมือเท้าปาก	.097	.161	.163	.157	.520**	1.00

*p<.05, ** p< .01

V อภิปราย

ตารางที่ 1 กลุ่มตัวอย่างส่วนใหญ่เป็นเพศหญิง ร้อยละ 99.00 อายุเฉลี่ย 37.46 ปี (SD=9.72) ส่วนใหญ่มีการศึกษาระดับปริญญาตรีหรือเทียบเท่า ร้อยละ 83.33 ระยะการทำงานในศูนย์พัฒนาเด็กเล็ก 6 – 15 ปี ร้อยละ 43.14 ดังการศึกษาที่ผ่านมา [11,12]

ตารางที่ 2 ความรอบรู้ด้านสุขภาพ ผลการศึกษา พบว่า ครูผู้ดูแลเด็กมีความรอบรู้ด้านสุขภาพเกี่ยวกับโรคมือ เท้า ปากทั้งในภาพรวมและรายด้าน ในระดับสูงโดยด้านการเข้าถึงข้อมูลมีค่าเฉลี่ยสูงสุด ($\bar{x}$ =4.44, S.D. = 0.51) รองลงมาคือ ด้านการตัดสินใจ ($\bar{x}$ = 4.42, S.D. = 0.59) อาจเนื่องจากกลุ่มตัวอย่างส่วนใหญ่ (ร้อยละ 85.29) มีประสบการณ์ในการดูแลเด็กที่ป่วยด้วยโรคมือเท้าปากมาก่อน จึงมีโอกาสในการเข้าถึงข้อมูลได้ดี อีกทั้งส่วนใหญ่กลุ่มตัวอย่างสำเร็จการศึกษาระดับปริญญาตรี จึงสามารถเข้าถึงและทราบแหล่งสืบค้นเกี่ยวกับโรคมือเท้าปากจากแหล่งข้อมูลสุขภาพได้โดยตรงทั้งจากแหล่งข้อมูลต่าง ๆ และจากบุคลากรสาธารณสุข [9,13] ส่งผลให้กลุ่มตัวอย่างมีความรู้ความเข้าใจอยู่ในระดับสูง โดยการศึกษาครั้งนี้พบว่ากลุ่มตัวอย่างร้อยละ 49.02 ทราบถึงอาการเบื้องต้นของเด็กที่มีอาการเป็นโรคมือ

เท้าปากอยู่ในระดับสูง ทั้งนี้เนื่องจากเมื่อกลุ่มตัวอย่างมีความรู้โรคมือเท้าปากระดับสูง ทำให้เกิดความตะหนักในการป้องกันโรค [9] สำหรับด้านทักษะการสื่อสารเมื่อพิจารณารายข้อพบว่าครูผู้ดูแลเด็กเล็กสามารถเผยแพร่ความรู้และการป้องกันโรคมือเท้าปากให้แก่ผู้ปกครองได้อยู่ในระดับสูงร้อยละ 46.08 ดังการศึกษาที่ผ่านมาพบว่าครูผู้ดูแลเด็กในศูนย์เด็กเล็กมีทักษะในการดูแลเด็กและมีความสามารถในการถ่ายทอดวิธีการดูแลแก่ผู้ปกครอง [1] การสื่อสารในงานดูแลเด็กของครูผู้ดูแลเด็กมีผลต่อพัฒนาการและสุขภาพของเด็กอย่างมาก การมีทักษะเหล่านี้จึงเป็นสิ่งสำคัญที่ควรได้รับการสนับสนุนและพัฒนาอย่างต่อเนื่อง เพื่อให้ครูผู้ดูแลเด็กสามารถให้การดูแลที่ดีที่สุดแก่เด็ก และสร้างความสัมพันธ์ที่ดีกับผู้ปกครองได้อย่างมีประสิทธิภาพในการดูแลเด็ก [14]

การรู้เท่าทันสื่อของครูผู้ดูแลพบว่า ครูผู้ดูแลเด็กสามารถซักถามเกี่ยวกับป้องกันโรคมือเท้าปากกับผู้ให้บริการสุขภาพเพื่อนำมาป้องกันโรคให้กับเด็กในศูนย์พัฒนาเด็กเล็กได้อยู่ในระดับสูง ร้อยละ 35.29 เนื่องจากการที่ครูสามารถซักถามและรับข้อมูลที่ถูกต้องจากผู้ให้บริการสุขภาพจะมีผลอย่างมากต่อการป้องกันโรคและการดูแลสุขภาพของเด็กในศูนย์พัฒนาเด็ก การมีข้อมูลที่ทันสมัยและถูกต้องช่วยให้ครูสามารถดำเนินการป้องกันและดูแลเด็กได้อย่างมีประสิทธิภาพ ส่งเสริมความมั่นใจให้กับผู้ปกครองในเรื่องการดูแลสุขภาพของบุตรหลาน

การตัดสินใจของครูผู้ดูแลเด็กพบว่า ครูผู้แลเด็กตัดสินใจให้เด็กที่ติดโรคมือเท้าปากควรหยุดเรียนและพักรักษาตัวให้หายป่วยก่อนกลับเข้ามาเรียนอยู่ในระดับสูงร้อยละ 45.10 เนื่องจากการตัดสินใจให้เด็กหยุดเรียนและพักรักษาตัวจนกว่าจะหายป่วยเป็นการให้เด็กพักรักษาตัวไม่เพียงแต่ช่วยให้เด็กฟื้นตัวได้เร็วขึ้น แต่ยังป้องกันการแพร่กระจายของโรคไปยังเด็กคนอื่น ๆ ในสถานศึกษา นอกจากนี้ การตัดสินใจแสดงให้เห็นถึงความรับผิดชอบของครูในการดูแลสุขภาพและความปลอดภัยของเด็ก รวมถึงการสร้างความเชื่อมั่นให้กับผู้ปกครองในการดูแลที่มีคุณภาพในสถานศึกษา [15]

การจัดการตนเองของครูผู้ดูแลเด็ก พบว่า ครูผู้ดูแลเด็กมีการปฏิบัติตามแผนของกระทรวงสาธารณสุขในการเฝ้าระวัง ป้องกันและควบคุมโรคติดต่อหรือโรคระบาดได้ในระดับสูง ร้อยละ 49.02 รองลงมาคือ การปรับตัวตั้งรับกับการเกิดโรคมือเท้าปากในศูนย์พัฒนาเด็กเล็กอยู่เสมออยู่ในระดับสูง ร้อยละ 47.06 เนื่องจากครูผู้ดูแลเด็กเล็กมีประสบการณ์ในการดูแลและส่งต่อเด็กที่ติดโรคมือเท้าปาก จึงมีทัศนคติที่ดีต่อการตั้งรับกับโรค และจัดการกับโรคมือ เท้า ปาก [16]

ตารางที่ 3 พฤติกรรมการป้องกันโรคมือเท้าปากของครูผู้ดูแลเด็กพบว่ากลุ่มตัวอย่างมีพฤติกรรมการป้องกันโรคมือเท้าปากอยู่ในระดับสูงทั้งรายข้อและภาพรวม ทั้งนี้อาจเนื่องจากกลุ่มตัวอย่างส่วนใหญ่มีการศึกษาระดับปริญญาตรี มีประสบการณ์ในการดูแลและส่งต่อเด็กที่ติดโรคมือเท้าปาก อีกทั้งนี้ความรอบรู้ด้านสุขภาพทั้งภาพรวมและรายด้านอยู่ในระดับสูงจึงส่งผลให้ครูผู้ดูแลเด็กมีพฤติกรรมการป้องกันโรคมือ เท้า ปากในระดับสูง [17-18]

ตารางที่ 4 การวิเคราะห์ความสัมพันธ์ ผลจากการศึกษาพบว่ารายได้ ประสบการณ์ในการดูแลและส่งต่อเด็กที่ติดโรคมือเท้าปาก และระยะเวลาในการเป็นครูผู้ดูแลเด็กมีความสัมพันธ์กับความรอบรู้ด้านสุขภาพ ดังการศึกษาของกันยา โพธิปิติ [19] และคำสงค์ ชินมาตร[20] ที่พบว่ารายได้มีความสัมพันธ์ต่อความรอบรู้ด้านสุขภาพของผู้ดูแลเด็ก ทั้งนี้ประสบการณ์ในการดูแลและส่งต่อเด็กที่ติดโรคมือเท้าปาก และระยะเวลาในการเป็นครูผู้ดูแลเด็กมีความสัมพันธ์กับความรอบรู้ด้านสุขภาพ เนื่องจากความรอบรู้ด้านสุขภาพเปรียบเสมือนสินทรัพย์ ซึ่งจะเพิ่มพูนสะสมตามประสบการณ์เดิมและทักษะที่สั่งสมมา [21] นอกจากนี้ยังพบว่าความรอบรู้ด้านสุขภาพมีความสัมพันธ์กับพฤติกรรมการป้องกันโรคมือ เท้า ปาก เนื่องจากกลุ่มตัวอย่างในการศึกษาครั้งนี้มีระดับความรอบรู้ด้านสุขภาพในระดับสูง จึงส่งให้มีพฤติกรรมการการป้องกันโรคมือเท้าปากในระดับสูง เพราะกลุ่มตัวอย่างสามารถเข้าถึงข้อมูลและบริการสุขภาพ มีความรู้ ความเข้าใจเกี่ยวกับโรคมือ เท้า ปาก มีทักษะในการสื่อสาร รู้เท่าทันสื่อ สามารถตัดสินใจในการดูแลเด็กและสามารถจัดการตนเอง นั่นคือ สามารถวางแผนและปฏิบัติตามแนวทางการดูแลเด็กตามที่กรมควบคุมโรคกำหนด ผลการศึกษาเช่นเดียวกับการศึกษาของพิชัย พวงสด อมรศักดิ์ โพธิ์อำและพุฒิพงษ์ มากมาย [22] ที่พบว่าความรอบรู้ด้านสุขภาพมีความสัมพันธ์กับพฤติกรรมการป้องกันโรคไข้เลือดออกของ อสม. นั่นคือ บุคคลที่มีความรอบรู้ด้านสุขภาพจะมีความสามารถในการดูแลสุขภาพของตน [23]

VI ข้อสรุป

จากการศึกษาในครั้งนี้พบว่าหากครูผู้ดูแลเด็กเล็กมีความรอบรู้ด้านสุขภาพและพฤติกรรมการป้องกันโรคมือ เท้า ปากที่ดี ส่งผลให้การเกิดโรคมือ เท้า ปากน้อยลงและการติดต่อของโรคน้อยลง ดังนั้น หน่วยงานที่ดูแลศูนย์พัฒนาเด็กเล็กจะต้องพัฒนาครูผู้ดูแลเด็กทุกคนให้มีความรอบรู้ด้านสุขภาพ ละมีทักษะในการสื่อสารกับผู้ปกครองและเด็กในการป้องกันตนจากโรคมือ เท้า ปาก

ข้อเสนอแนะ

จากผลการศึกษามีข้อเสนอแนะในการพัฒนางานและประเด็นในการวิจัย ดังนี้

ข้อเสนอแนะเชิงปฏิบัติการ

1. ศูนย์พัฒนาเด็กเล็ก สามารถนำผลที่ได้จากงานวิจัย ไปใช้ในสนับสนุนการดำเนินงานเสริมสร้างความรอบรู้ด้านสุขภาพและพฤติกรรมการป้องกันโรคมือเท้าปากของครูผู้ดูแลเด็กเล็กในพื้นที่ โดยเน้นความรอบรู้ด้านสุขภาพในด้านที่พบว่ามี ความรอบรู้ที่มีการตอบแบบถามน้อยแต่อยู่ในระดับสูง ได้แก่ ด้านการจัดการตนเอง ด้านทักษะการสื่อสาร และด้านการรู้เท่าทันสื่อ ให้กับครูผู้ดูแลเด็กเล็กในศูนย์พัฒนาเด็กเล็ก เพื่อให้เกิดการขับเคลื่อนไปสู่การปฏิบัติอย่างถูกต้องเป็นรูปธรรม

2. ศูนย์พัฒนาเด็กเล็ก สามารถนำผลที่ได้จากงานวิจัยไปออกแบบกระบวนการจัดการเรียนรู้ในการเสริมสร้างความรอบรู้ด้านสุขภาพและพฤติกรรมการป้องกันโรคมือเท้าปากให้กับครูผู้ดูแลเด็กในศูนย์พัฒนาเด็กเล็กที่สอดคล้องกับปัญหาและความต้องการของครูผู้ดูแลเด็กในแต่ละศูนย์พัฒนาเด็กเล็กผ่านกิจกรรมที่มีคุณภาพ และให้การสนับสนุนช่วยเหลือด้านข้อมูลความรู้สู่การปฏิบัติให้มากขึ้น

ข้อเสนอแนะในการศึกษาครั้งต่อไป

1. ควรมีการศึกษาวิจัยเชิงปฏิบัติการเพื่อสร้างความรอบรู้ด้านสุขภาพและพฤติกรรมการป้องกันโรคมือเท้าปากของครูผู้ดูแลเด็กเล็ก โดยใช้ข้อมูลจากผลการศึกษาวิจัยครั้งนี้กับข้อมูลของแต่ละพื้นที่ เพื่อให้สอดคล้องกับปัญหาและความต้องการ

2. ควรมีการศึกษาในเชิงคุณภาพ เพื่อให้ได้ข้อมูลเชิงลึกของความรอบรู้ด้านสุขภาพและพฤติกรรมการป้องกันโรคมือเท้าปากของครูผู้ดูแลเด็กเล็กในศูนย์พัฒนาเด็กเล็ก

3.ควรมีการศึกษาเพิ่มเติมเรื่องความรอบรู้ด้านสุขภาพและพฤติกรรมการป้องกันโรคมือเท้าปากในผู้ปกครองของเด็กเล็ก

คำขอบคุณ

คณะผู้วิจัยขอขอบคุณศูนย์พัฒนาเด็กเล็กและครูผู้ดูแลเด็กทั้ง 15 แห่งในการเอื้ออำนวยความสะดวกในการเก็บรวบรวมข้อมูล

อ้างอิง

[1] กรมควบคุมโรค. (2566). โรคมือ เท้า ปากแนะผู้ปกครอง สถานศึกษา คัดกรองและสังเกตอาการอย่างใกล้ชิด. [อินเตอร์เน็ต]. https://ddc.moph.go.th/odpc6/news.php

[2] วีระยุทธ ปานหล้า. (2561). *พฤติกรรมการป้องกันและควบคุมโรค มือ เท้า ปาก ของผู้ปกครองเด็ก กลุ่มชาติพันธุ์และผู้ดูแลเด็กในศูนย์พัฒนาเด็กเล็ก ตำบลแม่ขะนิง อำเภอเวียงสา จังหวัดน่าน.* การศึกษาค้นคว้าอิสระสาธารณสุขศาสตรมหาบัณฑิต สาขาการจัดการการสร้างเสริมสุขภาพ มหาวิทยาลัยธรรมศาสตร์.

[3] Abel, T., & McQueen, D. (2020). Critical health literacy and the COVID-19 crisis. *Health Promotion International*, 35(6), 1612-1613. retrieved 29 April 2020 from https://doi: 10.1093/heapro/daaa040.

[4] World Health Organization. (1998). *Health promotion glossary. Division of health promotion, education and communications, Health education and health promotion unit*. Geneva: World Health Organization.

[5] Nutbeam, D. (2000). Health literacy as a public health goal: A challenge for contemporary health education and communication strategies into the 21st century. *Health Promotion International*, 15(3), 259-267.

[6] สำนักงานสาธารณสุขจังหวัดภูเก็ต. (2567). จำนวนผู้ป่วยโรคมือ เท้า ปาก . เอกสารอัดสำเนา.

[7] กองสุขศึกษา. (2561). รายงานผลการประเมินความรอบรู้ด้านสุขภาพและพฤติกรรมสุขภาพ [อินเตอร์เน็ต]. https://hed.go.th/wp-content/uploads/2561.pdf

[8] กนกวรรณ นวนเกิด. (2563). *ปัจจัยที่มีผลต่อพฤติกรรมการป้องกันโรคมือเท้าปากของผู้ปกครองเด็ก ในศูนย์พัฒนาเด็กเล็กอำเภอวังทอง จังหวัดพิษณุโลก.* วิทยานิพนธ์ปริญญาสาธารณสุขศาตรบัณฑิต สาขาสาธารณสุขศาสตร์ มหาวิทยาลัยนเรศวร.

[9] ปาริชาติ วงษ์วริศราวิ, วิษณุ ปิ่นคำและวรัญญา หล่อพัฒนเกษม. (2564). ความรู้และพฤติกรรมการป้องกันโรคมือ เท้า ปาก ของผู้ดูแลเด็กก่อนวัยเรียนศูนย์พัฒนาเด็กเล็กองค์การบริหารส่วนตำบลจันอัด จังหวัดนครราชสีมา. *วารสารวิชาการมหาวิทยาลัยราชภัฏภูเก็ต*, 17(2), 61 – 72.

[10] กฤตภิษัช ไม้ทองงาม. (2565). ปัจจัยที่มีความสัมพันธ์กับพฤติกรรมการป้องกันและควบคุมโรคมือเท้าปากของครูในโรงเรียนอนุบาลและศูนย์พัฒนาเด็กเล็ก จังหวัดสุราษฎร์ธานี. *รายงานเฝ้าระวังทางระบาดวิทยาประจำสัปดาห์,* 54(5), 69 – 76.

[11] มัลลิกา อุตตะมา. (2565). ปัจจัยทำนายพฤติกรรมการป้องกันโรคมือเท้าปาก ของผู้ปกครองและผู้ดูแลเด็กในศูนย์พัฒนาเด็กเล็ก อำเภอเชียงคำ จังหวัดพะเยา. การศึกษาค้นคว้าอิสระสาธารณสุขศาสตรมหาบัณฑิต สาขาสาธารณสุขศาสตร์ มหาวิทยาลัยพะเยา

[12] สุพิชญา หอมทอง, ชนัญญา จิระพรกุล และ เนาวรัตน์ ภมณีนิล. (2564). ปัจจัยที่มีความสัมพันธ์กับพฤติกรรมการป้องกันโรคมือ เท้า ปาก ของผู้ปกครอง ในศูนย์พัฒนาเด็กเล็กในเขตตำบลในเมือง อำเภอเมือง จังหวัดขอนแก่น. *วารสารวิจัยสาธารณสุขศาสตร์มหาวิทยาลัยขอนแก่น*, 14(1). 57 – 66.

[13] ธนาคม คำแสน. (2560). *ปัจจัยที่มีความสัมพันธ์กับพฤติกรรมการป้องกันโรคมือเท้าปากของผู้ปกครองเด็กเล็ก ตำบลหาดล้า อำเภอท่าปลา จังหวัดอุตรดิตถ์*. วิทยานิพนธ์ปริญญาสาธารณสุขศาสตรบัณฑิต สาขาวิชาสาธารณสุขศาสตร์ มหาวิทยาลัยนเรศวร.

[14] สถาบันพัฒนาอนามัยเด็กแห่งชาติ. (2562). สรุปรายงานสถานการณ์ความรอบรู้ในการเลี้ยงดูเด็กปฐมวัย. https://nich.anamai. moph. go.th/web-upload/migrated/files/nich/330_article_file.pdf

[15] เปมิกา ไทยชัยภูมิ. (2561). *การศึกษาบทบาทครูในการส่งเสริมพฤติกรรมความปลอดภัยของเด็กอนุบาลในโรงเรียนในสังกัดคณะกรรมการการศึกษาขั้นฐานพื้น.* วิทยานิพนธ์ครุศาสตรมาหบัณฑิต สาขาวิชาการศึกษาปฐมวัย จุฬาลงกรณ์มหาวิทยาลัย.

[16] แสงดาว เกษตรสุนทร, นงเยาว์ เกษตร์ภิบาล, และ จิตตาภรณ์ จิตรีเชื้อ. (2558). ปัจจัยทำนายความตั้งใจในการคัดกรองโรคมือ เท้าและปาก ของครูพี่เลี้ยงของศูนย์พัฒนาเด็กเล็กในภาคใต้. *พยาบาลสาร*, 42(1), 74-85.

[17] รำพึง นุ่มสารพัดนึก. (2565). ความรอบรู้ด้านสุขภาพและพฤติกรรมการป้องกันโรคโควิด 19 ของนักเรียนมัธยมศึกษา จังหวัดนครนายก. *สรรพสิทธิเวชสาร*, 43(3), 91-110.

[18] Kinoshita, S., Hirooka, N., Kusano, T., Saito, K., & Aoyagi. R. (2024). Does health literacy influence health-related lifestyle behaviors among specialists of health management? A cross-sectional study. BMC Primary Care, 25(29),1-9.

[19] กันยา โพธิปิติ. (2565). ความรอบรู้ด้านสุขภาพในการเลี้ยงดูเด็กปฐมวัยของผู้เลี้ยงดูหลักและครูผู้ดูแลเด็ก ในเขตสุขภาพที่ 5. *วารสารศูนย์อนามัยที่ 7 ขอนแก่น*. 15(1). 28 – 50.

[20] คำสงค์ ชินมาตร. (2567). ปัจจัยที่มีความสัมพันธ์กับความรอบรู้ด้านสุขภาพและความสัมพันธ์ระหว่างความรอบรู้ด้านสุขภาพกับภาวะโภชนาการและพัฒนาการเด็กปฐมวัยในผู้เลี้ยงดูเด็ก. *วารสารวิจัยและพัฒนาระบบสุขภาพ*. 17(2). 140 – 153.

[21] วิมลรัตน์ บุญเสถียร และ อรทัย เหรียญทิพยะสกุล. (2563). ความรอบรู้ด้านสุขภาพ: สถานการณ์และผลกระทบต่อสภาวะสุขภาพของผู้สูงอายุ. *วารสารพยาบาลและสุขภาพ สสอท.* 2(1), 1-19.

[22] พิชัย พวงสด, อมรศักดิ์ โพธิ์อ่ำและพุฒิพงษ์ มากมาย. (2563). ความรอบรู้ด้านสุขภาพที่มีความสัมพันธ์กับพฤติกรรมการป้องกันและควบคุมโรคไข้เลือดออกของอาสาสมัครสาธารณสุขประจำหมู่บ้านเขตอำเภอปราสาท จังหวัดสุรินทร์. *วารสารวิทยาศาสตร์และเทคโนโลยีนอร์ท เทิร์น*. 1(3), 1-11.

[23]. ขวัญเมือง แก้วดำเกิง. (2561). *ความรอบรู้ด้านสุขภาพ เข้าถึง เข้าใจและการนำไปใช้*. นนทบุรี: อัมรินทร์พริ้นติ้ง แอนด์ พลับลิชชิง จำกัดมหาชน.

การยับยั้งเชื้อราก่อโรคในต้นทุเรียนด้วยสารสกัดจากสมุนไพร

Inhibition of fungi durian disease by herbal extracts

อัฟนาน ดอมะ, อัคลีมาร์ กาหมัะ, อังคณา ดอล่าโดย, คอสียาห์ สะลี*

Aklima Kamah, Angkhana Doladoi, Khosiya Sali

หลักสูตรจุลชีววิทยาทางการแพทย์และอุตาหกรรม คณะวิทยาศาสตร์เทคโนโลยีและการเกษตร มหาวิทยาลัยราชภัฏยะลา

40656301@yru.ac.th, *Khosiya.s@yru.ac.th

บทคัดย่อ

งานวิจัยนี้มีวัตถุประสงค์เพื่อคัดแยกเชื้อราก่อโรคใบจุดในทุเรียน การทดสอบความสามารถในการก่อโรคในใบทุเรียน และศึกษาประสิทธิภาพของสารสกัดหยาบจากสมุนไพรด้วยวิธี Agar well diffusion ต่อการยับยั้งเชื้อราก่อโรคในต้นทุเรียนที่ระดับความเข้มข้น 100, 200, 300, 400 and 500 mg/ml ผลการศึกษาสามารถคัดแยกเชื้อรา *Colletotrichum* sp. จำนวน 1 ไอโซเลท ที่แสดงอาการก่อโรคบนใบทุเรียนอยู่ในระดับที่ 3 และผลการศึกษาประสิทธิภาพการยับยั้งเชื้อและความเข้มข้นของสารสกัดสมุนไพรที่สกัดด้วยเอทานอล 95% ด้วยวิธี Agar well diffusion พบว่าสารสกัดจากข่ามีผลการยับยั้งดีที่สุดที่ระดับความเข้มข้น 400 มิลลิกรัมต่อมิลลิลิตร (ร้อยละการยับยั้ง เท่ากับ 50.90±2.92) รองลงมาขมิ้น กระชาย และใบพลู มีร้อยละการยับยั้งเท่ากับ 43.80±1.28 (400 mg/ml) 38.37±2.74 (400 mg/ml) และ 29.20±0.73 (500 mg/ml) ตามลำดับ ดังนั้นแสดงให้เห็นว่าเหง้าจากข่ามีประสิทธิภาพที่จะนำไปศึกษาต่อเพื่อนำมาใช้ในการควบคุมเชื้อราบางชนิดที่เป็นสาเหตุการเกิดโรคในต้นทุเรียน

คำสำคัญ : โรคในทุเรียน เชื้อรา ยับยั้ง สมุนไพร

ABSTRACT

The objective of this research was isolating pathogenic fungi causing anthracnose disease in durian trees, testing their ability to cause disease and the study of herbal crude extracts for inhibiting their fungal pathogens by agar diffusion method at concentrations of 100, 200, 300, 400 and 500 mg/ml. The results showed one isolated *Colletotrichum* sp. and showed pathogenicity at level 3. The extracted herbs using 95% alcohol as solvent showed that *Alpinia galanga* (L.) Willd. had the best inhibitory effect on *Colletotrichum* sp. at a concentration of 400 mg/ml. (Inhibition percentage as 50.90±2.92), followed by *Curcumalonga* L., *Boesenbergia rotunda* (L.) Mansf. and Piper betle Linn. With percentage inhibition are 43.80±1.28 (400 mg/ml), 38.37±2.74 (400 mg/ml) and 29.20±0.73 (500 mg/ml). ml) respectively. Therefore, it is indicated that Alpinia galanga (L.) Willd. showed effective and will be studied for use in controlling certain fungi that cause disease in durian trees.

Keywords : Durian disease, Fungi, Inhibition, Herbs

I. ทนำ

ทุเรียนเป็นผลไม้เขตร้อนที่มีความสำคัญทางเศรษฐกิจของประเทศไทย โดยส่วนใหญ่จะปลูกในภาคตะวันออกและภาคใต้ (สุมิตร คุณเจตน์, 2560) จากผลการสำรวจในปี พ.ศ. 2565 ภาคตะวันออกมีพื้นที่เพาะปลูกทุเรียนจำนวน 448,206 ไร่ และมีแนวโน้มเพิ่มสูงขึ้นอย่างต่อเนื่องส่วนภาคใต้มีพื้นที่เพาะปลูกทุเรียนจำนวน 672,330 ไร่ (นิกร แสงเกตุ, 2565) อย่างไรก็ตาม การปลูกทุเรียนในประเทศไทยยังประสบกับปัญหาเกี่ยวกับโรคหลายชนิด เช่น โรครากเน่าโคนเน่า โรคผลเน่า โรคใบจุด โรคใบติดหรือใบไหม้ โรคจุดสนิม โรคราสีชมพู และโรคราแป้ง โดยมีการเกิดโรคจะมีตั้งแต่ระยะแรกของการเจริญเติบโตจนถึงระยะการเก็บเกี่ยวผลผลิต (สุมิตร คุณเจตน์, 2560) สถิติการก่อโรครากเน่าโคนเน่าพื้นที่ระบาด 12 จังหวัดในปี 2565 ได้แก่ จังหวัดเพชรบุรี จันทบุรี ตราด ระยอง กระบี่ ชุมพร นครศรีธรรมราช นราธิวาส ปัตตานี ยะลา และจังหวัดสุราษฎร์ธานี จำนวน 2,291 ไร่ พื้นที่ระบาดเพิ่มขึ้นจากปี 2564 จำนวน 251 ไร่ (กระทรวงเกษตรและสหกรณ์, 2565) เชื้อที่เป็นสาเหตุการเกิดโรคในทุเรียนส่วนใหญ่จะเป็นกลุ่มเชื้อรา ได้แก่ เชื้อ *Phytophthora* sp., *Rhizoctonia* sp., *Phyllosticta* sp., *Colletotrichum* sp., *Cortricium* sp. และ *Oidium* sp. ซึ่งเชื้อแต่ละชนิดจะก่อโรคในตำแหน่งที่แตกต่างกัน โดยเชื้อ *Phytophthora* sp. ก่อโรครากเน่าโคนเน่าและโรคผลเน่าเชื้อ *Phyllosticta sp.* และเชื้อ *Colletotrichum sp.* ก่อโรคใบจุด เชื้อ *Rhizoctonia sp.* ก่อโรคใบติดหรือใบไหม้ เชื้อ *Cortricium sp.* ก่อโรคราสีชมพู และเชื้อ *Oidium* sp. ก่อโรคราแป้ง (จีรนันท์ กล่อมนรา แก้วรักษา, 2562)

การควบคุมโรคในปัจจุบันนิยมใช้กสารเคมี เช่น สารเมตาแลกซิล ซึ่งการใช้สารเคมีในปริมาณที่มากเกินไป ทำให้มีผลต่อผู้บริโภคทั้งทางตรงและทางอ้อม นอกจากนั้นสารเคมีอาจมีผลทำให้เชื้อเกิดกลายพันธุ์และดื้อต่อสารเคมีที่ใช้ ทำให้การป้องกันและกำจัดเชื้อราก่อโรคทำได้ยากขึ้นในอนาคต (สุมิตร คุณเจตน์, 2560) จึงมีความจำเป็นที่ต้องหาแนวทางในการแก้ปัญหาดังกล่าว การใช้สารสกัดจากพืชจึงเป็นอีกหนึ่งทางเลือกในการควบคุมโรคพืชแบบชีววิธี ซึ่งจากรายงานวิจัย พบว่า สมุนไพรหลายชนิดมีสารสำคัญที่มีฤทธิ์ยับยั้งเชื้อรา เช่น *Phytophthora palmivora* (วาสินี ธรรมสถิต และคณะ, 2560), *Aspergillus niger*, *Penicillium* sp., *Rhizopus* sp. (สายสมร ลำลอง และคณะ, 2560) และ *Colletotrichum gloeosporioides* (วิมลศิริ สีหะวงษ และคณะ,

2065) ดังนั้นงานวิจัยครั้งนี้ผู้วิจัยจึงมีความสนใจศึกษาสมุนไพรพื้นบ้านมาทดสอบประสิทธิภาพในการยับยั้งเชื้อรา *Colletotrichum* sp. ที่เป็นสาเหตุก่อโรคใบจุดในต้นทุเรียน เพื่อนำมาเป็นข้อมูลพื้นฐานในการพัฒนาเป็นผลิตภัณฑ์ให้เกษตรกรนำมาใช้แทนสารเคมีต่อไปในอนาคตและเพื่อเพิ่มมูลค่าสมุนไพรในท้องถิ่น

II. ทบทวนวรรณกรรม

เชื้อรา *Colletotrichum* sp.

เชื้อรา *Colletotrichum* sp. เจริญบนอาหาร PDA มีลักษณะเส้นใยเป็นสีขาว อมเทา คล้ายสำลี ฟู เจริญเต็มผิวหน้าอาหาร (รัมม์พัน โกศลานันท์ และคณะ, 2557) และรูปร่างภายใต้กล้องจุลทรรศน์สปอร์มีลักษณะรูปร่างโค้งงอ เป็นท่อนสั้น ๆ หัวท้ายมน ลักษณะเส้นใยมีผนังกั้น เชื้อรา *Colletotrichum* spp. เป็นสาหตุของโรคใบจุดในต้นพืชหลายชนิด โดยลักษณะอาการทำให้ใบไหม้เป็นรอยแห้งจากปลายใบและใบจะร่วงหล่น และจะทำลายดอกทำให้ดอกเน่า ดำแห้งและร่วงหล่น จากรายงานของ Armand et al., (2023) ได้วิเคราะห์ลักษณะทางสัณฐานวิทยาและวิวัฒนาการ พบว่า Colletotrichum 4 ชนิด ที่มีความสัมพันธ์กับโรคเน่าของผลทุเรียนในภาคเหนือของประเทศไทย ได้แก่ *C. durionigenum, C. gigasporum, C. pandanicola* และ *C. truncatum* ปัจจุบัน เกษตรกรจะนิยมใช้สารเคมีในการควบคุมโรคเนื่องจากสะดวก รวดเร็ว และมีประสิทธิภาพสูงเมื่อเทียบกับวิธีการอื่น ๆ โดยมีการใช้สารเคมีในกลุ่ม Benzimidazole เช่น เบนโนมิล (Benomyl) ไทอะเบนดาโซล (Thiabendazole) เป็นต้น ทำให้มีอากาสพบสารพิษตกค้างที่เกินค่าปลอดภัย ดังนั้นปัจจุบันนักวิจัยเริ่มให้สนใจทดลองใช้สารสกัดจากธรรมชาติ เช่น สารสกัดจากพืชสมุนไพร สารสกัดจากจุลินทรีย์ มาใช้ในการยับยั้งกลุ่มเชื้อราก่อโรคในพืช เนื่องจากในพืชสมุนไพรมีสารสำคัญหลายชนิดที่มีฤทธิ์ในการยับยั้งการเจริญของเชื้อรา

สมุนไพร

ใบพลู และข่า มีสารสำคัญกลุ่ม Eugenol เป็นสารกลุ่มที่มีฤทธิ์ยับยั้งเยื่อหุ้มของเชื้อราและเอนไซม์ที่เร่งปฏิกิริยา โดยใบพลูมีประสิทธิภาพสูงสุดในการยับยั้งเชื้อรา *Aspergillus niger*, *Penicillium* sp. และ *Rhizopus* sp. ที่เจริญบนยางแผ่นได้สูงที่สุด (สายสมร ลำลอง และคณะ, 2560) นอกจากนั้น ข่ายังสามารถยับยั้งเส้นใยของเชื้อรา *Curvularia* sp. (สุภัทรา จามกระโทก และคณะ, 2547) และสารสกัดพลูที่สกัดด้วยตัวทำละลายเอทานอล สามารถยับยั้งการเจริญของเชื้อ *Aspergillus flavus* (คอสียาห์ สะลี และคณะ, 2564)

ขมิ้น สาระสำคัญในขมิ้น ได้แก่ Curcumin, Shikonin, Desmethoxycurcumin มีฤทธิ์สามารถยับยั้งเชื้อรา *Phytophthora palmivora* โดยสารกลุ่ม Shikonin มีประสิทธิภาพเท่ากับสารเคมีกลุ่มเบนโนมิลและไทอะเบนดาโซล (วาสินี ธรรมสถิต และคณะ, 2560)

กระชาย สารกลุ่ม Phytochemicals และ Shikonin ในกระชายมีฤทธิ์ในการยับยั้งเชื้อรา (สุดารัตน์ หอมหวล, 2010) นอกจากนั้น กระชายยังมีฤทธิ์ยับยั้งการเจริญของเส้นใยของรา *Rhizopus* sp. (สุภัทรา จามกระโทก และคณะ, 2547) และมีประสิทธิภาพในการควบคุมเชื้อรา *Collectotrichum gloeosporioides* ที่เป็นเชื้อสาเหตุของโรคหอมเลื้อยในห้องปฏิบัติการและในแปลงปลูก (วิมลศิริ สีหะวงษ์ และคณะ, 2565) จากการศึกษาของ Oranun & Jiraungkoorskul (2017) แสดงให้เห็นว่ากระชายมีการแสดงฤทธิ์ในการควบคุมแบคทีเรียและเชื้อรา Kittika et al. (2017) พบว่าสารสกัดจากกระชายมีผลยับยั้งเชื้อรา *Aspergillus flavus* ในฝักของถั่วลิสง นอกจากนั้น Rattanakreetakul (2013) ยังพบว่าน้ำมันสกัดจากกระชายพบสาร eugenol linalool และ geraniol สามารถควบคุมการสร้างสปอร์ของเชื้อรา *Lasiodiplodia theobromae* โรคโคนเน่าของต้นกล้วย

III. ระเบียบวิธีวิจัย

1. การคัดแยกเชื้อรา *Colletotrichum* sp. ที่เป็นสาเหตุการเกิดโรคในทุเรียน

เก็บตัวอย่างชิ้นส่วนของทุเรียนที่แสดงอาการของโรคใบจุด จากพื้นที่จังหวัดปัตตานี และยะลาทั้งหมด 7 ตัวอย่าง มาตัดส่วนที่เป็นรอยต่อระหว่างใบที่ดีกับใบที่เกิดโรค ให้เป็นรูปสี่เหลี่ยมจัตุรัส ขนาด 0.5 x 0.5 เซนติเมตร นำไปแช่ในสารละลายคลอร็อกซ์ (Chlorox) ความเข้มข้นร้อยละ 10 โดยปริมาตร เป็นเวลา 3 นาที แช่น้ำกลั่นปลอดเชื้อ เป็นเวลา 3 นาที นำชิ้นตัวอย่างมาวางในจานอาหาร Potato Dextrose Agar (PDA) นำไปบ่มที่อุณหภูมิ 25 องศาเซลเซียส เป็นเวลา 5 วัน สังเกตการเจริญของเส้นใย เมื่อพบการเจริญของเส้นใยเชื้อรา ใช้เข็มปลายงอ ตัดส่วนปลายของเส้นใยวางบริเวณตรงกลางจานอาหาร PDA บ่มที่อุณหภูมิ 25 องศาเซลเซียส เป็นเวลา 5 วัน แยกจนได้นทีกลักษณะโคโลนีและนำไปศึกษาลักษณะทางสันฐานวิทยาและเลี้ยงเชื้อราที่บริสุทธิ์ (สุวรรณี แทนธานี และคณะ, 2557)

2. การทดสอบความสามารถในการทำให้เกิดโรคของเชื้อรา

ใบทุเรียนที่สมบูรณ์ไม่มีรอยโรคนำมาจุ่มใบในสารละลาย Clorox 10% เป็นเวลา 5 นาที เพื่อฆ่าเชื้อบริเวณผิวรอบนอก จากนั้นล้างด้วยน้ำกลั่น 2 ครั้ง ผึ่งให้น้ำแห้ง จากนั้นนำเชื้อรา *Colletotrichum* sp. ที่แยกได้มาเลี้ยงบนอาหาร PDA เป็นเวลา 5 วัน เจาะเส้นใยราด้วย Cork borer เบอร์ 1 เส้นผ่าศูนย์กลาง 5 มิลลิเมตร จำนวน 6 ชิ้น วางบนใบทุเรียนหมอนทอง โดยชุดควบคุมไม่ใส่เชื้อรา ทำทดลองทั้งหมด 5 ซ้ำ นำใบทุเรียนใส่ในกล่องพลาสติกที่มีความชื้น โดยการฉีดน้ำใส่ลงไปในกล่อง บ่มที่อุณหภูมิห้อง เป็นเวลา 3 วัน วัดเส้นผ่าศูนย์กลางการเกิดรอยโรค และนำค่าเฉลี่ยประเมินความรุนแรงของโรค โดยความรุนแรงขอโรคจัดลำดับถึง 5 ระดับ ขนาดแผล 0 = ไม่มีอาการ 1 = ขนาดแผล 1-5 mm, 2 = ขนาดแผล 6-10 mm, 3 = ขนาดแผล 11-20 mm, 4 = ขนาดแผลมากกว่า 20 mm (Somnuek *et al*., 2023)

3. การเตรียมสมุนไพรและการสกัดสมุนไพร

นำใบพลู ข่า ขมิ้น และกระชาย มาล้างทำความสะอาด หั่นเป็นชิ้นเล็ก ๆ แล้วอบให้แห้งโดยใช้ตู้อบลมร้อนที่อุณหภูมิ 60 องศาเซลเซียส เป็นเวลา 7 จากนั้นนำมาหมักด้วยสารละลายเอทนอลความเข้มข้นร้อยละ 95 อัตราส่วน 1 : 5 หมักแช่ที่อุณหภูมิห้องเป็นเวลา 7 วัน จากนั้นกรองสารสกัดด้วยกระดาษกรองเบอร์ 1 นำไประเหยตัวทำละลายด้วยเครื่อง Rotary

Evaporator จะได้สารที่แข็งหนืด ชั่งน้ำหนักและเก็บสารสกัดในขวดสีชาที่อุณหภูมิ 4 องศาเซลเซียส เพื่อนำไปใช้ในการทดลองต่อไป (สายสมร ลำลอง และนิตยา คำพันธ์, 2560) นำไปคำนวณหาร้อยละปริมาณสารสกัดหยาบคำนวณได้ดังนี้

% yield = (weight of crude extract / weight of fresh leaf) x 100

4. ทดสอบประสิทธิภาพของสารสกัดสมุนไพรต่อการยับยั้งการเจริญของเชื้อรา

เชื้อราที่คัดแยกจนได้เชื้อบริสุทธิ์มาเลี้ยงบนอาหาร PDA บ่มที่อุณหภูมิ 25 องศาเซลเซียส เป็นเวลา 5 วัน จากนั้นเจาะเส้นใยเชื้อราด้วย Cork borer ให้ได้เส้นผ่าศูนย์กลาง 4 มิลลิเมตร ตัดขอบโคโลนี วางห่างจากขอบอาหาร PDA 3 เซนติเมตร (Somnuek *et al*., 2023) จากนั้นปรับความเข้มข้นของสารสกัดที่ระดับความเข้มข้น คือ 100 200 300 400 และ 500 มิลลิกรัมต่อมิลลิลิตร ด้วยตัวทำละลาย 95% เอทานอล เพื่อให้ได้ความเข้มข้นที่ต้องการ จากนั้นเจาะอาหาร PDA ด้วย Cork borer ขนาด 4 มิลลิเมตร (วางในทิศทางตรงกันข้ามกับเชื้อรา) นำสารสกัดที่มีความเข้มข้นต่าง ๆ หยดสารสกัดลงในหลุม ปริมาตร 80 ไมโครลิตร ส่วนชุดควบคุมใช้ 95% เอทานอลหยดแทนสารสกัด ทำการทดลองทั้งหมด 2 ซ้ำ บ่มที่อุณหภูมิห้อง เป็นเวลา 7 วัน (วนิดา ชื่นชวน และคณะ, 2565) บันทึกผลวัดระยะการเจริญเติบโตของเชื้อรา ตรวจสอบเปอร์เซ็นต์การยับยั้งเชื้อราคำนวณได้ดังนี้

เปอร์เซ็นต์การยับยั้งการเจริญเติบโตของเชื้อ = [(A-B) / A] x 100

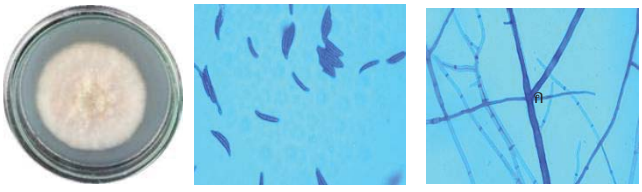
A = วัดรัศมีของโคโลนีเชื้อราบนจานอาหารเลี้ยงเชื้อควบคุม

B = วัดรัศมีของโคโลนีเชื้อราที่ยับยั้งด้วยสารสกัด

IV. ผลการการทดลอง

1. การคัดแยกเชื้อรา *Colletotrichum* sp. ที่เป็นสาเหตุการเกิดโรคใบจุดในต้นทุเรียน

จากการคัดแยกเชื้อรา *Colletotrichum* sp. จากใบทุเรียนที่แสดงอาการโรคใบจุดในพื้นที่จังหวัดยะลา และปัตตานี เมื่อนำมาเลี้ยงบนอาหาร Potato Dextrose agar พบเส้นใยสีขาวอมเทา คล้ายสำลี ฟู เจริญเต็มผิวหน้าอาหาร เมื่อดูลักษณะของสปอร์ภายใต้กล้องจุลทรรศน์มีลักษณะเป็นท่อนสั้น ๆ คล้ายจันทร์เสี้ยว หัวท้ายมน เส้นใยแบบมีผนังกั้นและมีการแตกกิ่งก้าน (ภาพที่ 1)



ก. ข. ค

ภาพที่ 1 ลักษณะของเชื้อรา *Colletotrichum* sp. ที่คัดแยกจากใบทุเรียน

ก. ลักษณะโคโลนีที่เลี้ยงบนอาหาร PDA

ข. ลักษณะ ascospores ภายใต้กล้องจุลทรรศน์ 400 เท่า

ค. ลักษณะเส้นใยภายใต้กล้องจุลทรรศน์ 400 เท่า

2. ทดสอบความสามารถของเชื้อรา *Colletotrichum* sp. ในการทำให้เกิดโรคบนใบทุเรียน

จากการทดสอบความสามารถในการทำให้เกิดโรคของเชื้อรา พบว่า เชื้อรา *Colletotrichum* sp. ที่คัดแยกได้แสดงอาการของโรคใบบนใบทุเรียนหลังการปลุกเชื้อบนใบทุเรียน โดยใบมีลักษณะเป็นสีน้ำตาลคล้ายโดนน้ำร้อนลวกรอบ ๆ โคโลนีของเชื้อราที่วางไว้ เมื่อนำมาคำนวณระดับการก่อโคพบว่า การแสดงอาการของโรคอยู่ในระดับที่ 3 ดังตาราง 1

ตารางที่ 1 ทดสอบความสามารถของเชื้อรา *Colletotrichum* sp. ในการทำให้เกิดโรคบนใบทุเรียน

ชุดทดสอบ	ลักษณะอาการของโรค
Control	
Colletotrichum sp.	

3. ผลการสกัดสารสกัดจากพืชสมุนไพร

ผลการสกัดสารจากใบพลู ข่า ขมิ้น และกระชาย ด้วยตัวทำละลายเอทานอล ในอัตราส่วน 1:5 พบว่าสารสกัดสมุนไพรที่ได้ปริมาณมากที่สุด คือ กระชาย รองลงมา คือ ขมิ้น ใบพลู และข่า มีปริมาณสารสกัดร้อยละ 6.19, 5.11, 4.21 และ 3.28 ตามลำดับ ลักษณะของสารสกัดที่ได้ พบว่า ใบพลูมีลักษณะสีเขียวขี้ม้า ข้นหนืด สอดคล้องกับผลการศึกษาของ ปาริชาติ อ้นองอาจ และคณะ (2566) ข่ามีลักษณะสีน้ำตาล ข้นหนืด สอดคล้องกับผลการศึกษาของ อาวุธ หงส์ศิริ และคณะ (2566) ขมิ้นมีลักษณะ สีเหลืองส้ม ข้นหนืด สอดคล้องกับผลการศึกษาของ ธารหทัย มาลาเวช (2559) กระชายลักษณะสีน้ำตาลเข้ม ข้นหนืด สอดคล้องกับผลการศึกษาของ โชติรส กิจสมชีพ (2565) ดังแสดงในตารางที่ 2

ตารางที่ 2 แสดงลักษณะของสารสกัดหยาบจากสมุนไพรและปริมาณร้อยละของสารสกัดที่สกัดได้

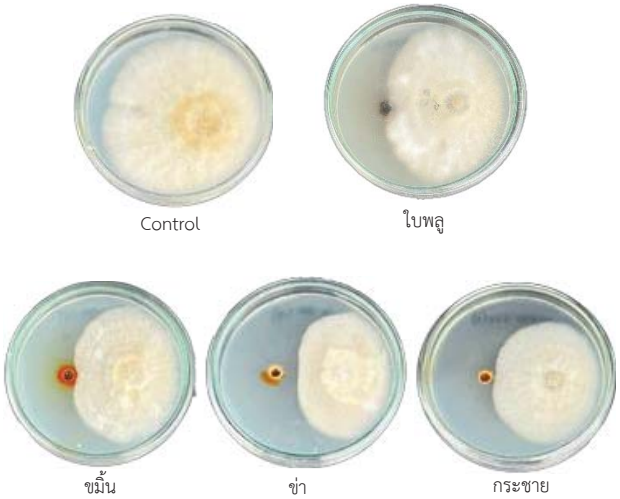
สมุนไพร	ลักษณะสารสกัด	ร้อยละ
ใบพลู	สีเขียวขี้ม้า ข้นหนืด	4.21
ข่า	สีน้ำตาล ข้นหนืด	3.28
ขมิ้น	สีเหลืองส้ม ข้นหนืด	5.11
กระชาย	สีน้ำตาลเข้ม ข้นหนืด	6.19

4. การทดสอบประสิทธิภาพของสารสกัดสมุนไพรต่อการยับยั้งการเจริญของเชื้อรา *Colletotrichum* sp

จากการทดสอบประสิทธิภาพสารสกัดหยาบทั้ง 4 ชนิด คือ ใบพลู ข่า ขมิ้น และกระชาย ในการยับยั้งเชื้อรา *Colletotrichum* sp. ที่ระดับความเข้มข้น 100 200 300 400 และ 500 มิลลิกรัมต่อมิลลิลิตร ด้วยวิธี agar well diffusion พบว่า สารสกัดข่า ขมิ้น และกระชาย สามารถยับยั้งดีที่สุดที่ระดับความเข้มข้น 400 มิลลิกรัมต่อมิลลิลิตร โดยมีค่าร้อยละการยับยั้งดีที่สุด เท่ากับ 50.90 43.80 และ 38.37 ตามลำดับ ส่วนสารสกัดใบพลู มีค่าร้อยละการยับยั้งดีที่สุด เท่ากับ 35.92 ที่ระดับความเข้มข้น 500 มิลลิกรัมต่อมิลลิลิตร ดังตารางที่ 3 (ภาพที่ 2) สารสกัดจากข่า และกระชาย ระดับความเข้มข้นที่เพิ่มขึ้นมีผลต่อร้อยละการยับยั้ง แสดงค่าแตกต่างอย่างมีนัยสำคัญทางสถิติ ($P<0.05$) แต่สารสกัดจากขมิ้น และใบพลู ระดับความเข้มข้นที่เพิ่มขึ้นผลไม่แตกต่างกันอย่างมีนัยสำคัญทางสถิติ ($P<0.05$)

ตารางที่ 3 แสดงค่าเฉลี่ยร้อยละการยับยั้งเชื้อราของสารสกัดหยาบสมุนไพรทั้ง 4 ชนิด ด้วยวิธี agar well diffusion

ความเข้มข้น (mg/ml)	ค่าเฉลี่ยการยับยั้งเชื้อรา (%)			
	ข่า	ขมิ้น	กระชาย	ใบพลู
100	$34.50^{b}\pm2.74$	$40.05^{a}\pm0.37$	$29.59^{c}\pm0.55$	$30.36^{a}\pm2.74$
200	$39.53^{ab}\pm0.73$	$40.18^{a}\pm0.18$	$31.14^{bc}\pm1.64$	$31.27^{a}\pm1.83$
300	$49.10^{a}\pm8.77$	$42.89^{a}\pm0.00$	$28.55^{c}\pm0.18$	$32.43^{a}\pm0.18$
400	$50.90^{a}\pm2.92$	$43.80^{a}\pm1.28$	$38.37^{a}\pm2.74$	$29.20^{a}\pm0.73$
500	$45.74^{ab}\pm2.19$	$40.31^{a}\pm3.65$	$35.27^{ab}\pm2.01$	$35.92^{a}\pm6.21$
หมายเหตุ: a, b, c แสดงความแตกต่างในแนวตั้ง				



ภาพที่ 2 ผลของสารสกัดหยาบสมุนไพรใบพลู ข่า ขมิ้น และกระชาย ที่ระดับความเข้มข้น 500 มิลลิกรัมต่อมิลลิลิตร

V. อภิปรายผลการทดลอง

จากการคัดแยกเชื้อรา *Colletotrichum* sp. จากใบทุเรียนที่แสดงอาการโรคใบจุดในพื้นที่จังหวัดยะลา และปัตตานี เมื่อนำมาเลี้ยงบนอาหาร Potato Dextrose agar พบเส้นใยสีขาวอมเทา คล้ายสำลี ฟู เจริญเต็มผิวหน้าอาหาร เมื่อดูลักษณะของสปอร์ภายใต้กล้องจุลทรรศน์มีลักษณะเป็นท่อนสั้น ๆ คล้ายจันทร์เสี้ยว หัวท้ายมน เส้นใยแบบมีผนังกั้นและมีการแตกกิ่งก้าน (ภาพที่ 1) ซึ่งมีคุณสมบัติสอดคล้องกับการศึกษาของรัมม์พันโกศลานันท์ และคณะ (2557) และจีรนันท์ กล่อมนรา แก้วรักษา (2562) ผลการสกัดสารจากใบพลู ข่า ขมิ้น และกระชาย ด้วยตัวทำละลายเอทานอลในอัตราส่วน 1:5 พบว่าสารสกัดสมุนไพรที่ได้ปริมาณมากที่สุด คือ กระชาย รองลงมา คือ ขมิ้น ใบพลู และข่า มีปริมาณสารสกัดร้อยละ 6.19, 5.11, 4.21 และ 3.28 ตามลำดับ ลักษณะของสารสกัดที่ได้ พบว่าใบพลูมีลักษณะสีเขียวขี้ม้า ข้นหนืด สอดคล้องกับผลการศึกษาของ ปาริชาติ อ้นองอาจ และคณะ (2566) ข่ามีลักษณะสีน้ำตาล ข้นหนืด สอดคล้องกับผลการศึกษาของ อาวุธ หงส์ศิริ และคณะ (2566) ขมิ้นมีลักษณะ สีเหลืองส้ม ข้นหนืด สอดคล้องกับผลการศึกษาของ ธารหทัย มาลาเวช (2559) กระชายลักษณะสีน้ำตาลเข้ม ข้นหนืด สอดคล้องกับผลการศึกษาของ โชติรส กิจสมชีพ (2565) จากการศึกษาความเข้มข้น 100-500 มิลลิกรัมต่อมิลลิลิตร ต่อฤทธิ์การยับยั้งเชื้อรา *Colletotrichum* sp. พบว่า สารสกัดจากข่า และกระชาย เมื่อระดับความเข้มข้นเพิ่มขึ้นมีร้อยละการยับยั้งแตกต่างกันอย่างมีนัยสำคัญทางสถิติ ($P<0.05$) แต่สารสกัดจากขมิ้น และใบพลู ระดับความเข้มข้นที่เพิ่มขึ้นไม่มีผลต่อร้อยละการยับยั้ง สอดคล้องกับการศึกษาของจีรนันท์ กล่อมนรา แก้วรักษา (2562) ศึกษาประสิทธิภาพของสารสกัดหยาบจากส่วนต่าง ๆ ของหม่อน ด้วยวิธี Paper Disc Diffusion ที่ระดับความเข้มข้น 300 600 900 มิลลิกรัมต่อมิลลิลิตร สามารถยับยั้งเชื้อรา *Colletotrichum* sp. ที่คัดแยกจากใบทุเรียน ที่ระดับความเข้มข้น 600 มิลลิกรัมต่อมิลลิลิตร มีร้อยละการยับยั้งดีที่สุด ซึ่งพบว่าความเข้มข้นที่เพิ่มขึ้นไม่ได้มีผลต่อการยับยั้งเชื้อเช่นกัน สารสกัดจากข่า และกระชาย ระดับความเข้มข้นที่เพิ่มขึ้นมีผลต่อร้อยละการยับยั้ง แสดงค่าแตกต่างอย่างมีนัยสำคัญทางสถิติ ($P<0.05$) แต่สารสกัดจากขมิ้น และใบพลู ระดับความเข้มข้นที่เพิ่มขึ้นผลไม่แตกต่างกันอย่างมีนัยสำคัญทางสถิติ ($P<0.05$) สอดคล้องกับการศึกษาของจีรนันท์ กล่อมนรา แก้วรักษา (2562) ศึกษาประสิทธิภาพของสารสกัดหยาบจากส่วนต่างๆ ของหม่อน ด้วยวิธี Paper Disc Diffusion ที่ระดับความเข้มข้น 300 600 900 มิลลิกรัมต่อมิลลิลิตร สามารถยับยั้งเชื้อรา *Colletotrichum* sp. ที่คัดแยกจากใบทุเรียน ที่ระดับความเข้มข้น 600 มิลลิกรัมต่อมิลลิลิตร มีร้อยละการยับยั้งดีที่สุด ซึ่งพบว่าความเข้มข้นที่เพิ่มขึ้นไม่ได้มีผลต่อการยับยั้งเชื้อ ส่วนฤทธิ์การยับยั้งเชื้อของสมุนไพรทั้ง 4 ชนิด พบว่า สมุนไพรทั้ง 4 ชนิดสามารถยับยั้งการเจริญของเส้นใยรา *Colletotrichum* sp. โดยข่ามีร้อยละการยับยั้งดีที่สุด ทั้งนี้แสดงให้เห็นว่าสมุนไพรทั้ง 4 นี้มีสารสำคัญที่มีฤทธิ์ยับยั้งการเจริญของเชื้อราได้

VI. สรุปผลการวิจัย

การคัดแยกเชื้อราจากชิ้นส่วนต่าง ๆ ของทุเรียนที่แสดงอาการของโรคสามารถคัดแยกเชื้อรา *Colletotrichum* sp. จำนวน 1 ไอโซเลท ผลการทดสอบประสิทธิภาพการยับยั้งเชื้อราจากสารสกัดหยาบจากสมุนไพรทั้ง 4 ชนิด ได้แก่ ใบพลู ข่า ขมิ้น และกระชาย พบว่าสารสกัดจากข่า ขมิ้น กระชาย และใบพลู มีร้อยละการยับยั้งดีที่สุด เท่ากับ 50.90 ± 2.92 43.80 ± 1.28 38.37 ± 2.74 และ 29.20 ± 0.73 ตามลำดับ

อ้างอิง

จีรนันท์ กล่อมนรา แก้วรักษา. (2562). ศึกษาประสิทธิภาพของสารสกัดหยาบจากส่วนต่างๆ ของหม่อนที่มีผลการยับยั้งเชื้อราที่คัดแยกได้จากใบทุเรียน. *วารสารวิจัยมหาวิทยาลัยเทคโนโลยี ราชมงคลศรีวิชัย*, *11*(2), 197-207.

ปาริชาติ อ้นองอาจ, กัมปนาท คำสุข, ภรณ์ทิพย์ ชัยสว่าง, ณลิตา ไพบูลย์ และวราภรณ์ มหาทรัพย์. (2566). ผลการยับยั้งเชื้อแบคทีเรียของสารสกัดใบพลูต่อเชื้อสเตร็พโตค็อคคัสมิวแทนส์. *วารสารหมอยาไทยวิจัย, 9(1),* 89-98.

รัตนาภรณ์ สมฤทธิ์, วรุตม์ คุณสุทธิ์, ธีระวิทย์ พลโคกก่อง, อารีรัตน์ เมืองแสน, ปัฐพงศ์ เทียมตรี, ชนิตา บุตรรัตนะ, นิรันดรไชนันท์ ชาญชาติ และณัฐฐิญา สุดชารี. (2566). ประสิทธิภาพการยับยั้งเชื้อราก่อโรคราน้ำค้างในเมล่อนด้วยซิงค์ออกไซด์ผสมสารสกัดจากขิง ข่า และไพล. *วารสารเกษตรศาสตร์และเทคโนโลยี,* 4(1), 60-89.

วนิดา ชื่นชัน, สมศักดิ์ อยู่บริบูรณ์ และ ศิริพร บุญส่ง. (2565). ประสิทธิภาพของสารสกัดหยาบจากสมุนไพรในการยับยั้งเชื้อรา *Phytophthora parasitica*. *วารสารสถาบันวิจัยและพัฒนามหาวิทยาลัยราชภัฏบ้านสมเด็จเจ้าพระยา*, *7*(1), 243-252.

วาสินี ธรรมสถิต, สุจิตรา สุคนธมัต และดุษณี ธนะบริพัฒน์. (2560). การคัดเลือกสมุนไพรที่มีฤทธิ์ควบคุมเชื้อรา *Phytopthora* sp. ที่แยกจากทุเรียนในจังหวัดจันทบุรีและจังหวัดชุมพร. *วารสารวิทยาศาสตร์ลาดกระบัง*, *26*(2).

วิมลศิริ สีหะวงษ์, สายัณห์ สืบผาง และสุวิจักขณ์ อรุณลักษณ์. (2565). *การควบคุมการเจริญของเชื้อรา Collectotrichum gloeosporiodes เชื้อสาเหตุของโรคหอมเลื้อยด้วยสารสกัดสมุนไพร. วารสารวิทยาศาสตร์เทคโนโลยี มรย, 7*(2), 35-42.

สมศิริ แสงโชค และปัจจามา กวางติ๊ด. การจัดการเชื้อรา *Phytophthora palmivora* (Butler) สาเหตุโรครากเน่า และผลเน่าของทุเรียนในจังหวัดจันทบุรี. *ภาควิชาโรคพืช คณะเกษตร* (รายงานผลการวิจัย). มหาวิทยาลัยเกษตรศาสตร์.

สายสมร ลำลอง และนิตยา คำพันธ์. (2560). การยับยั้งการเจริญของเชื้อราบนยางแผ่นด้วยสารสกัดจากสมุนไพร. *วารสารมหาวิทยาเทคโนโลยีราชมงคลอีสาน*, *10*(2).

สุมิตร คุณเจตน์. (2560). *การผลิตต้นกล้าทุเรียนพันธุ์หมอนทองเพื่อลดการติดเชื้อ Phytopthora palmivora โดยวิธีการควบคุมอุณหภูมิและความชื้นสัมพัทธ์ในโรงเรือนเพาะชำด้วยระบบควบคุมฟัซซี่* (รายงานผลการวิจัย). จันทบุรี : มหาวิทยาลัยบูรพา.

สุรวีร์ จิตรพิลา. (2563). การพัฒนาการแสดงผลภาพเพื่อให้ความรู้เกี่ยวกับเรื่องสมุนไพรในประเทศไทย. มหาวิทยาลัยศรีปทุม.

สุวรรณี แทนธานี, จารวี สุขประเสริฐ, สายจิต ดาวสุโข และโสรญา รอดประเสริฐ. (2557). การศึกษาประสิทธิภาพของว่านน้ำในการยับยั้งเชื้อราก่อโรคผลเน่าที่แยกได้จากผลลิ้นจี่. *วารสารวิทยาศาสตร์ประยุกต์*, *3*(3). *เกษตร*, 1-31.

11th iCeast 2025

Phuket, Thailand















IEEE Thailand Section

IEEE BT Society Thailand Chapter